



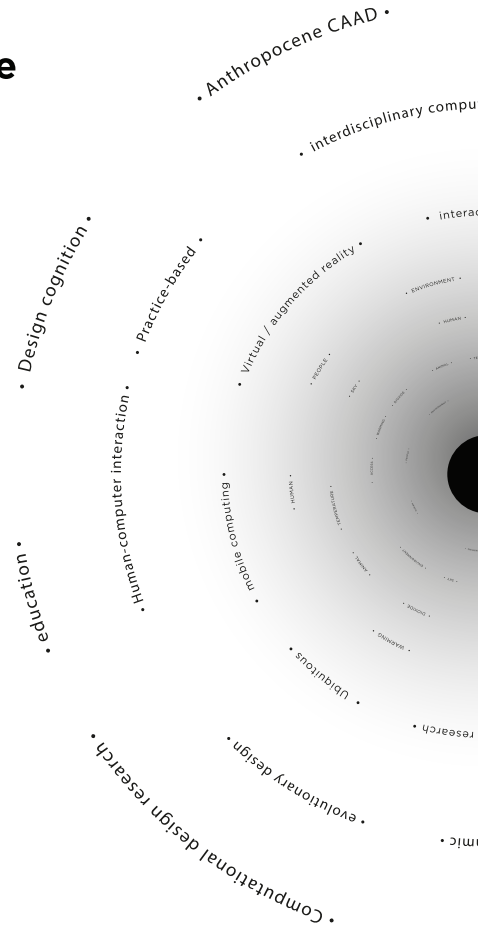
# CAADRIA2020

## RE: ANTHROPOCENE

Design in the Age of Humans

25th International Conference  
of the Association for  
Computer-Aided  
Architectural Design  
Research in Asia

**VOLUME 1**



EDITED BY:

Dominik Holzer  
Walaiporn Nakapan  
Anastasia Globa  
Immanuel Koh

# **RE: Anthropocene, Design in the Age of Humans**

Proceedings of the 25th International Conference on Computer-Aided  
Architectural Design Research in Asia (CAADRIA 2020)

**Volume 1**

**Edited by**

**Dominik Holzer**

*The University of Melbourne, Australia*

**Walaiporn Nakapan**

*Rangsit University, Thailand*

**Anastasia Globa**

*The University of Sydney, Australia*

**Immanuel Koh**

*Singapore University of Technology and Design, Singapore*

RE: Anthropocene, Design in the Age of Humans

25th International Conference on Computer-Aided Architectural Design  
Research in Asia (CAADRIA 2020)

5 – 6 August 2020

Faculty of Architecture

Chulalongkorn University Bangkok, Thailand

© 2020 *All rights reserved and published by*

The Association for Computer-Aided Architectural Design Research in Asia  
(CAADRIA), Hong Kong

ISBN: 978-988-78917-3-4

Cover design and cover image: The supersub Co., Ltd

## Foreword

The annual CAADRIA (Association for Computer-Aided Architectural Design Research in Asia) conference provides an international community of researchers and practitioners with a venue to exchange, to discuss and to publish their latest ideas and accomplishments. The proceedings have two volumes containing the research papers that were accepted for presentation at the *RE: Anthropocene, Design in the Age of Humans* – 25<sup>th</sup> International CAADRIA Conference, hosted and organised by the Faculty of Architecture at Chulalongkorn University Bangkok, Thailand. The papers are also available online at the open access cumulative database CumInCAD {<http://papers.cumincad.org>}. The proceedings are the outcome of an extensive collaborative effort of a team of volunteers and CAADRIA's international Academic Review Committee.

Against the backdrop of a year that many count among the most difficult in recent history, the conference organisers and the broader CAADRIA community have shown great resolve, passion, and commitment, resulting in a body of work of highest international standards. Calls for papers in July 2019 led to the submission of 466 abstracts. These were blind reviewed by the Paper Selection Committee, which invited 311 abstracts for further development. Of these, 233 full papers were submitted to the full paper review stage. A team of 91 international reviewers assisted us in this stage. Two-to-three international reviewers carried out a double-blind review of each submitted paper. Following the reviewers' recommendations, we were fortunate to be able to accept 183 papers. The travel restrictions caused by the global pandemic required changes, both to the conference date, as well as its format. We are very pleased that 158 papers ultimately got included in these conference proceedings, in particular given the fact that CAADRIA 2020 is being run as a virtual conference. We congratulate the authors for their accomplishment.

Next to the authors, the reviewers, who volunteered valuable time and effort, deserve our sincere thanks and acknowledgements. We thank the Organising Team and hosts at Chulalongkorn University in Bangkok for hosting the 25th International CAADRIA Conference online.

We extend absolute special thanks the ProceeDings team, and in particular Gabriel Wurzer, for his relentless support with customizing the submission and review system to the needs of CAADRIA from the full-paper submission stage all the way to production. On the following pages, we acknowledge and thank those who contributed to the production of this volume. In closing, we sincerely like to thank the CAADRIA community for offering us the honour to serve as members of the Paper Selection Committee for *RE: Anthropocene, Design in the Age of Humans, the 25th International CAADRIA Conference 2020*.

*Dominik Holzer (Chair), The University of Melbourne  
Walaiporn Nakapan, Rangsit University  
Anastasia Globa, The University of Sydney  
Immanuel Koh, Singapore University of Technology and Design*

**CAADRIA 2020 Theme**

RE: Anthropocene, Design in the Age of Humans

What if we are already in the Anthropocene epoch where the function of the Earth system is being impacted by human activities? What if our actions indeed are significant enough to have a critical force on the Earth as a system? The term Anthropocene (the Age of Humans) has gained increasing recognition as a description of a crucial geological stage of our planet as we face the consequences of our own events on the earth's ecosystem. While we are beginning to address the predominant challenges of sustainability and ecology, the environments we built have also shaped our behaviors.

To celebrate CAADRIA's 25th Anniversary, we challenge ourselves with these questions, asking what we want our future to look like in the next 25, 50, or even 100 years from now? If human creations are substantial enough to start a new geological epoch, what does this imply for our explorations of the realm of computational design and how will advanced technologies shape our future?

With the theme of RE: Anthropocene, we ask our contributors to REgard this new geological age as the main meaningful site for exploration into the future, REthink what our planet could become, REvisit our actions and behaviors to foster the REsponsibilities for the planet existence, and perhaps & importantly, REspond to whatever magnitudes happen to the built-environments and other planetary beings.

As the CAADRIA 2020 organizing committee, the beginning of 2020 has been quite challenging as we faced the COVID-19 pandemic in midst of conference preparations. We too, have been faced with disruptions and had to REthink, REvisit and REspond to the original format of the conference as we explored virtual possibilities. The resilience of people has never seized to surprise us and we are proud to present CAADRIA 2020 as the very first virtual conference in CAADRIA history. The essence of CAADRIA has always been and will forever be centered around the community and for that we thank all contributors for making this possible.

*Organizing Committee  
International Program in Design and Architecture  
Faculty of Architecture, Chulalongkorn University  
Surapong Lertsithichai  
Sorachai Kornkasem  
Walaiporn Nakapan  
Thanatcha Pojthaveekiat*

## About CAADRIA

The *Association for Computer-Aided Architectural Design Research in Asia* (CAADRIA) promotes teaching and research in CAAD in the larger Austral-Asian and Pacific region supported by a global membership.

CAADRIA was founded in 1996 with the following objectives:

- To facilitate the dissemination of information about CAAD among Asian schools of architecture, planning, engineering, and building sciences.
- To encourage the exchange of staff, students, experience, courseware, and software among schools.
- To identify research and develop needs in CAAD education and to initiate collaboration to satisfy them.
- To promote research and teaching in CAAD that enhances creativity rather than production.

CAADRIA organizes among others an annual conference, the first of which was held in 1996 in Hong Kong. Since then, 24 conferences have been held in Australia, China, Hong Kong, India, Japan, Korea, Malaysia, New Zealand, Singapore, Taiwan, and Thailand. The annual CAADRIA conferences provide an opportunity to meet, to learn about the latest research, and to continue the discourse in the field. The 25<sup>th</sup> anniversary conference, in 2020, is hosted by Chulalongkorn University in Bangkok, Thailand. CAADRIA2020 is held as a virtual conference for the first time in the history of the Association to bring together researchers, practitioners and schools of the Pacific region even at a time of global Covid-19 related travel restrictions.

Proceedings of CAADRIA conferences are available online at the open access cumulative database *CumInCAD* (<http://papers.cumincad.org>). CAADRIA is one of the four founding organizations of the *International Journal of Architectural Computing* (IJAC), and co-edits one issue each year. IJAC is published by SAGE in both paper and electronic versions.

*Christiane M. Herr*  
*President, CAADRIA*

### **CAADRIA Officers**

President: Christiane M Herr

*Xi'an Jiaotong-Liverpool University, China*

Secretary: Walaiporn Nakapan

*Rangsit University, Thailand*

Treasurer: Wei Xin Huang

*Tsinghua University, China*

Membership Officer: Sky Lo Tian Tian

*Harbin Institute of Technology (ShenZhen), China*

Web Master: Kyung Hoon Hyun

*Hanyang University, South Korea*

Administrative Officer: Marc Aurel Schnabel

*Victoria University of Wellington, New Zealand*

### **CAADRIA 2020 Conference Committees**

Organisers & Hosts *Chulalongkorn University, Thailand*

*Surapong Lertsithichai, Chair (Chulalongkorn University)*

*Sorachai Kornkasem (Chulalongkorn University)*

*Walaiporn Nakapan (Rangsit University)*

*Thanatcha Pojthaveekiat, Coordinator (Chulalongkorn University)*

Award Committee:

*Sky Lo Tian Tian (Chair), Anastasia Globa, Tane Moleta*

Paper Selection Committee:

*Dominik Holzer (Chair), Anastasia Globa, Immanuel Koh and Walaiporn Nakapan*

PG Students Consortium:

*Christiane M Herr (Chair), Dagmar Reinhardt and Sky Lo Tian Tian*

Sasada Prize Committee:

*Tom Kvan (Chair), Christiane Herr, Atsuko Kaga*

Young CAADRIA Award Committee:

*Christiane M Herr (Chair), Jin-Kook Lee and Per Stefan Svedberg*

## International Review Committee

- Wael Abdelhameed  
*Norseen Consultancy Company*
- Henri Achten  
*Czech Technical University in Prague*
- Suleiman Alhadidi  
*MIT Media Lab*
- Pedro Azambuja Varela  
*University of Porto*
- Jose Beirao  
*University of Lisbon*
- Chitraj Bissoonauth  
*Xi'an Jiaotong-Liverpool University*
- Johannes Braumann  
*UJG Linz - Robots in Architecture*
- Michael Budig  
*Singapore University of Technology and Design*
- Inês Caetano  
*University of Lisbon*
- Tilanka Chandrasekera  
*Oklahoma State University*
- Teng-Wen Chang  
*National Yunlin Univ. of Scie. and Technology*
- Jia-Yih Chen  
*CSCA Architects & Partners*
- Sheng-Fen Chien  
*National Cheng Kung University*
- Kristof Crolla  
*Chinese University of Hong Kong*
- Wowo Ding  
*Nanjing University*
- Ben Doherty  
*Notion Parallax*
- Theodoros Dounas  
*Robert Gordon University*
- Halil Erhan  
*Simon Fraser University*
- Alberto T. Estevez  
*iBAG-UIC Barcelona/Univ. Int. de Catalunya*
- Ruwan Fernando  
*Griffith University*
- Paolo Fiamma  
*University of Pisa*
- Thomas Fischer  
*Xi'an Jiaotong-Liverpool University*
- Tomohiro Fukuda  
*Osaka University*
- Fernando García Amen  
*University of La República*
- Aanastasia Globa  
*The University of Sydney*
- Ning Gu  
*University of South Australia*
- Yinghsiu Huang  
*National Kaohsiung Normal University*
- M. Hank Haeusler  
*UNSW*
- Oliver Heckmann  
*Singapore University of Tech. and Design*
- Christiane Herr  
*Xi'an Jiaotong-Liverpool University*
- Pablo Herrera  
*Universidad Peruana de Ciencias Aplicadas*
- Dominik Holzer  
*The University of Melbourne*
- June-Hao Hou  
*National Chiao Tung University*
- Jie-Eun Hwang  
*University of Seoul*
- Aswin Indraprastha  
*Institut Teknologi Bandung*
- Patrick Janssen  
*NUS*
- Taysheng Jeng  
*National Cheng Kung University*
- Guohua Ji  
*Nanjing University*
- Sam Joyce  
*SUTD*
- Mine Kabakcioglu  
*Istanbul Technical University*
- Keita Kado  
*Chiba University*
- Chin Koi Khoo  
*Deakin University*
- Joachim Kieferle  
*RheinMain University of Applied Sciences*
- Sung-Ah Kim  
*Sungkyunkwan University*
- Mi Jeong Kim  
*Hanyang University*
- Michael Kleiss  
*Clemson University*
- Christoph Klemmt  
*University of Cincinnati*
- Immanuel Koh  
*Singapore University of Tech. and Design*



- Thomas Kvan  
*SUSTech*
- Dennis Lagemann  
*ETHZ*
- Ih-Cheng Lai  
*Tamkang University*
- Ji-Hyun Lee  
*KAIST*
- Hyunsoo Lee  
*Yonsei University*
- António Leitão  
*Instituto Superior Tecnico*
- Surapong Lertsithichai  
*Chulalongkorn University*
- Andrew Li  
*Kyoto Institute of Technology*
- Biao Li  
*Southeast University*
- Yuezhong Liu  
*Nanyang Technological University*
- Tian Tian Sky Lo  
*Harbin Institute of Technology*
- Paul Loh  
*The University of Melbourne*
- Thorsten Lomker  
*Zayed University*
- Russell Loveridge  
*NCCR Digital Fabrication / ETH Zurich*
- Mohammed Makki  
*University of Technology Sydney*
- Michio Matsubayashi  
*National Institute of Tech., Kushiro College*
- Tane Moleta  
*Victoria University Wellington*
- Jules Moloney  
*RMIT University*
- Hugo Mulder  
*University of Southern Denmark*
- Rizal Muslimin  
*The University of Sydney*
- Walaiporn Nakapan  
*Rangsit University*
- Alberto Pugnale  
*The University of Melbourne*
- Ahmad Rafi  
*Multimedia University*
- Dagmar Reinhardt  
*Aarhus School of Architecture*
- Luís Romão  
*Universidade de Lisboa*
- Guillermo Sánchez Soté  
*Xi'an Jiaotong-Liverpool University*
- Yasushi Sakai  
*MIT Media Lab*
- Marc Aurel Schnabel  
*Victoria University Wellington*
- Gerhard Schubert  
*Technical University of Munich*
- Rudi Stouffs  
*National University of Singapore*
- Peng Tang  
*Southeast University*
- Ziyu Tong  
*Nanjing University*
- Jin Tsou  
*City University of HK*
- Bigge Tuncer  
*Singapore University of Tech. and Design*
- Tsung-Hsien Wang  
*Sheffield School of Architecture*
- Glen Wash  
*Xi'an Jiaotong Liverpool University*
- Claudia Westermann  
*Xi'an Jiaotong-Liverpool University*
- Albert Wiltsche  
*Graz University of Technology*
- Andrew Wit  
*Temple University*
- Thomas Wortmann  
*Xi'an Jiaotong Liverpool University*
- Yen-Liang Wu  
*National Taichung Univ. of Scie. and Tech.*
- Satoshi Yamada  
*Ritsumeikan Univ.*
- Rongrong Yu  
*Griffith University*
- Chao Yuan  
*National University of Singapore*
- Philip F Yuan  
*Tongji University*

**Keynote Speakers**

Making Magic with Creative Technology and Design

*Ellen Yi-Luen Do*

Cumulative, Collaborative, Disruptive: Architectural geometry in research and practice and its imminent mainstream future.

*Shajay Bhooshan*

Relationship Among People.

*Takeshi Yamada*

## **Making Magic with Creative Technology and Design**

Ellen Yi-Luen Do

*Director of Partnership and Innovation, ATLAS Institute*

Now is an exciting time to engage in creative design computing, to implement physically and computationally enhanced environment, to explore experience media and interactive computing projects, towards a smart living environment. Advancing technology offers new ways to solve problems, discover opportunities, and create new objects and experience that delight our senses and improve the way we live and work. With a spark of creativity and enthusiasm, followed up with design and computational thinking, we can create objects of various scales and target digital innovation, interactive artifacts or mobile apps, to support happy, healthy living. In this talk, Ellen will introduce projects from the ATLAS Institute at the University of Colorado Boulder.

### BIOGRAPHY

**Ellen Yi-Luen Do** is a Professor and Director of Partnership and Innovation in the ATLAS Institute, at the University of Colorado Boulder. She invents at the intersections of people, design, and technology. She holds a Ph.D. from Georgia Tech, a MDesS from the Harvard GSD, and a BArch from NCKU in Taiwan. She has served on the faculties of the University of Washington, Carnegie Mellon University and Georgia Tech, and co-director of the Keio-NUS CUTE Center in Singapore before joining CU Boulder.

**ATLAS** is an interdisciplinary institute for radical creativity and invention. Our synthesis of design and technology amplifies innovation in engineering and the arts. We believe the best way to shape the future is to invent it. We promote rigorous, curiosity-driven investigation in a thriving academic community that is supportive, energetic, and playful.

**Cumulative, Collaborative, Disruptive: Architectural geometry in research and practice and its imminent mainstream future.**

Shajay Bhooshan

*Senior Associate of Zaha Hadid Architects*

Solutions to the significant social, ecological and economic opportunities and problems of 21st-century architecture and urbanism involve a vast number of variables. These solutions will require the use of data-driven technologies to acquire physical and social information of sites and consumer communities, digital technologies to design for the briefs so acquired and robotic manufacturing to deliver the designed solutions effectively.

In this context, Architectural Geometry (AG) is a highly relevant design technology paradigm. AG focuses on the synthesis of shapes that guarantee structural and fabrication optimality. It is also closely aligned with and complementary to the development of robotic and digital fabrication (RDF). Further, in combining historical geometry-based methods of structural analysis, modern mathematics as used in computer graphics (CG) and computational technologies, the field is opening up several rich shape-possibilities that are also economically viable. Design that is so digitally empowered is proving to be significantly more effective in terms of spatial expressivity and user experience, ecologically, preservation of building trades, etc.

The lecture will cover the benefits of AG in research and practice and its imminent mainstream future as strikingly innovative solutions to the problems and opportunities of the 21st century.

BIOGRAPHY

**Shajay** is a Senior Associate at Zaha Hadid Architects where he co-founded and heads the research activities of the Computation and Design (CODE) group. He also works as a studio master at the AA DRL Master's program in London. He pursues his research in structure and fabrication aware architectural geometry as a PhD Candidate at the Block Research Group, ETH Zurich. Previously, he has worked at Populous, London and completed his M.Phil from the university of Bath and M. Arch from the AA School of Architecture, London

**Shajay** has published in scientific journals and conferences, along with contributions to architectural discourse through Architectural Design and other magazines. He has taught and presented work at various professional conferences, events and institutions across the world including Architectural Association London, ETH Zurich, Poly-technic of Milan and Bari, Tongji University Shanghai, SIGGRAPH, Autodesk University etc. He has also made curatorial contributions to various exhibitions of Zaha Hadid Architects, including Venice Biennale 2012 and Zaha Hadid memorial exhibition in Venice 2016, apart from shows in Mexico, UK, USA, Taiwan etc.

## Relationship Among People

Takeshi Yamada

*Management Team, teamLab*

teamLab aims to explore a new relationship between humans and nature, and between oneself and the world through art. Digital technology has allowed art to liberate itself from the physical and transcend boundaries. teamLab sees no boundary between humans and nature, and between oneself and the world; one is in the other and the other in one. Everything exists in a long, fragile yet miraculous, borderless continuity of life.

## BIOGRAPHY

**Takeshi Yamada** has been working for teamLab's management team in Tokyo, Japan, since 2017. Before joining teamLab, he worked as a marketer for a tourist industry at Zurich.

**teamLab** is an art collective, whose collaborative and interdisciplinary practice seeks to navigate the confluence of art, science, technology, design and the natural world. Various specialists such as artists, programmers, engineers, CG animators, mathematicians and architects form teamLab. The artwork of the collective has been the subject of numerous exhibitions at venues worldwide and is also in permanent collections of art galleries and museums all around the globe.

## TABLE OF CONTENTS

Foreword	v
Conference Theme: RE: Anthropocene, Design in the Age of Humans	vi
About CAADRIA	vii
CAADRIA Officers	viii
CAADRIA 2020 Conference Committees	viii
International Review Committee	ix
Keynote Speakers	xi
Making Magic with Creative Technology and Design, Keynote 1	xii
Cumulative, Collaborative, Disruptive: Architectural Geometry in Research and Practice and its Imminent Mainstream Future, Keynote 2	xiii
Relationship Among People, Keynote 3	xiv
<b>Digital Fabrication &amp; Construction</b>	<b>11</b>
Research on Voxel-based Aggregation Design and its Fabrication <i>Kai Xiao, Chen-cheng Chen, Zhe Guo, Xiang Wang, Chenyun Yan</i>	13
Double Loops Parametric Design of Surface Steel Structure Based on Performance and Fabrication <i>Chenjun Liu</i>	23
Thermo-Shading <i>Jungwon Yoon, Seok-won Choi</i>	35
Digital Architextiles <i>Joann Wang</i>	45

Knitted Composites Tower <i>Yige Liu, Hua Chai, Philip F. Yuan*</i>	55
Managing Risk in a Research-Based Practice as Projects Scale To Construction <i>Stan Carroll</i>	65
Funicular Structures using Topological Assemblies <i>Urvi Sheth, Aysha Fida</i>	75
Connecting Timber Sheet Materials to Create a Self-Supporting Structure using Robotic Fabrication and Computational Tools <i>Celine Cheng, Antony Pelosi</i>	85
Web-Based Distributed Design to Fabrication Workflows <i>Paul Poinet, Dimitrie Stefanescu, Eleni Papadonikolaki</i>	95
A Co-existing Interactive Approach to Digital Fabrication Workflow <i>Chi-Fu Hsiao, Ching-Han Lee, Chun-Yen Chen, Teng-Wen Chang</i>	105
Sewing Pneumatic Textures <i>Virginia Melnyk</i>	115
Digital Workflows for Natural Wood in Constructions <i>Niels Martin Larsen, Anders Kruse Aagaard, Lynn Hyun Kieffer</i>	125
Closing the Loop - Recycling Waste Plastic <i>Caitlin Bruce, Kevin Sweet, Jeongbin Ok</i>	135
Digital Planting <i>Sihan Wang, Chi Liu, Guo Li Zhang, Qi Huan Luo, Weishun Xu, Felix Raspall</i>	145
Detailing the Configuration to Perform Better Clay Printing <i>Sihan Wang, Hui Ping Toh, Felix Raspall, Carlos Banon</i>	153
A Computational Approach for the Mass Customization of Materially Informed Double Curved Façade Panels <i>Sherif Abdelmohsen, Ahmed Hassab</i>	163

3D Printed Monolithic Joints	173
<i>Shiyu Feng, Mengzeshan Du, Weiyi Wang, Heng Lu, Daekwon Park, Guohua Ji</i>	
Large-Scale 3D Printing for Functionally-Graded Facade	183
<i>Yoana Taseva, Nik Eftekhar, Hyunchul Kwon, Matthias Leschok, Benjamin Dillenburger</i>	
4D printing: Computational Mechanical Design of Bi-dimensional 3D Printed Patterns over Tensioned Textiles for Low-energy Three-dimensional Volumes.	193
<i>Tomas Vivanco, Antonia Valencia, Philip F. Yuan</i>	
Horizontal Forming in Additive Manufacturing: Design and Architecture Perspective	203
<i>Alexander Geht, Michael Weizmann, Yasha Jacob Grobman, Ezri Tarazi</i>	
Knit Concrete Formwork	213
<i>Abhipsa Pal, Wi Leen Chan, Ying Yi Tan, Pei Zhi Chia, Kenneth Joseph Tracy</i>	
Hygro-Compliant: Responsive Architecture with Passively Actuated Compliant Mechanisms	223
<i>Stella Yi Ning Loo, Dhileep Kumar Jayashankar, Sachin Gupta, Kenneth Tracy</i>	
Circular Concrete Construction Through Additive FDM Formwork	233
<i>Roberto Naboni, Giulio Paparella</i>	
CAM as a Tool for Creative Expression	243
<i>Ozguc Bertug Capunaman</i>	
<b>Generative, Algorithmic &amp; Evolutionary Design/Techniques</b>	<b>253</b>
Enabling Optimisation-based Exploration for Building Massing Design	255
<i>Likai Wang, Kian Wee Chen, Patrick Janssen, Guohua Ji</i>	
Spatial Metaphors for Multi-Dimensional Design Gallery Interfaces	265
<i>Naghmi Shireen, Halil Erhan, Robert Woodbury, Alissa N. Antle</i>	



Architectural Layout Design through Simulated Annealing Algorithm <i>Hao Zheng, Yue Ren</i>	275
Generation of Public Space Structure Based on Digital Multi-agent System <i>Zhuoxing Gu, Chunxia Yang</i>	285
Escaping Evolution <i>Inês Pereira, Catarina Belém, António Leitão</i>	295
Towards a Finer Heritage Management <i>Nan Bai, Pirouz Nourian, Anping Xie, Ana Pereira Roders</i>	305
Construction of Architectural Floor Plans for Given Adjacency Requirements <i>Krishnendra Shekhawat, Pinki pinki</i>	315
The Evolution of CAADRIA Conferences <i>Tomo Cerovsek, Bob Martens</i>	325
Optimization of Public Space Design Based on Reconstruction of Digital Multi-Agent Behavior <i>Chunxia Yang, Zhuoxing Gu</i>	335
A Comparison of Design Impact and Creativity in the Early Stage of Complex Building Design Processes <i>Yuan Sung (Kris) Hsiao</i>	345
Fantastic Facades and How to Build Them <i>Surapong Lertsithichai</i>	355
Does Architectural Design Optimization Require Multiple Objectives? <i>Thomas Wortmann, Thomas Fischer</i>	365
Visual Meets Textual <i>Renata Castelo-Branco, António Leitão</i>	375
Algorithmic generation of architectural Massing Models for building design optimisation <i>Likai Wang, Kian Wee Chen, Patrick Janssen, Guohua Ji</i>	385

A Method for Load-responsive Inhomogeneity and Anisotropy in 3D Lattice Generation Based on Ellipsoid Packing <i>Yao Lu, Eda Begum Birol, Colby Johnson, Christopher Hernandez, Jenny Sabin</i>	395
Revisiting Packing Algorithm <i>Beatricia Beatricia, Aswin Indraprastha, M. Donny Koerniawan</i>	405
The Taikoo Shing Superblock: Addressing urban stresses through sequential evolutionary simulations <i>Madison Randall, Tina Kordrostami, Mohammed Makki</i>	415
An Informed Method - Visualization for Multi-objective Optimization in Conceptual Design Phase <i>Zhu Shuyan, Ma Chenlong</i>	425
From Geometrically to Algebraically Described Hyperbolic Paraboloids <i>Thomas Fischer, Thomas Wortmann</i>	435
Generative Modelling with Design Constraints <i>Yuta Akizuki, Mathias Bernhard, Reza Kakooee, Marirena Kladeftira, Benjamin Dillenburger</i>	445
A Reconfigurable Joint Based on Extruded Polyhedrons <i>Huadong Yan, Ziyu Tong, Daekwon Park, Heng Lu</i>	455
Building from Waste Cardboard <i>Julio Diarte, Elena Vazquez</i>	465
FlowUI: Combining Directly-Interactive Design Modeling with Design Analytics <i>Halil Erhan, Maryam Zarei, Ahmed M. Abuzurairq, Alyssa Haas, Osama Alsalman, Robert Woodbury</i>	475
The Many Faces of Similarity <i>Ahmed M. Abuzurairq, Halil Erhan</i>	485

<b>Simulation &amp; Analysis</b>	<b>495</b>
Influence of Uncertainties in Envelope and Occupant Parameters on the Reliability of Energy-Based Form Optimization of Office Buildings <i>Chunxiao Wang, Shuai Lu</i>	497
Insulating with Geometry <i>Cheli Hershcovich, RENÉ van Hout, Vladislav Rinsky, Michael Laufer, Yasha J. Grobman</i>	507
Establishing a Prediction Model for Better Decision Making Regarding Urban Green Planning in a High-density Urban Context <i>Jia Ding Zhong, Ming Chun Chao, Sara, Jin Yeu Tsou</i>	517
An Investigation on the Deviation of Microclimate Simulation Based on ENVI-met <i>Hainan Yan, Guohua Ji</i>	527
Research on Spatial Distribution and Performance Evaluation of Mass Sports Facilities Based on Big Data of Social Media <i>Qi Guo, Hongyuan Mei</i>	537
How to Share a Home <i>Djordje Stojanovic, Milica Vujovic</i>	547
What do Design Data say About Your Model? <i>Halil Erhan, Ahmed M. Abuzurairq, Maryam Zarei, Osama AlSalman, Robert Woodbury, John Dill</i>	557
Optimizing Tensile Membrane Architecture for Energy Harvesting <i>Hoyoung Maeng, Kyung Hoon Hyun</i>	569
Parametric Modelling and Simulation of an Indoor Temperature Responsive Rotational Shading System Design <i>Jiahui Cheng, Zhuoqun Zhang, Chengzhi Peng</i>	579
Research on Commercial Space Vitality of Airport Terminal Based on 3D Vision Field Simulation of Pedestrian Flows <i>Zhichao Ma, Yiqiang Xiao, Xiong Chen</i>	589

Creativity Inspired by Analysis	599
<i>Inês Caetano, Sara Garcia, Inês Pereira, António Leitão</i>	
Representation of Sound in 3D	609
<i>Li-Min Tseng, June-Hao Hou</i>	
Immersive Simulations of Acoustics for Building Analysis	619
<i>Michael Yeow, Kenneth Tracy, Christine Yogiama</i>	
<b>Virtual/Augmented/Mixed/Interactive-Environments</b>	<b>629</b>
Visual Attention in Retail Environments	631
<i>Nayeon Kim, Hyunsoo Lee</i>	
The Impact of Moving through the Built Environment on Emotional and Neurophysiological State	641
<i>Mitra Homolja, Sayyed Amir Hossain Maghool, Marc Aurel Schnabel</i>	
VR Unmatched	651
<i>Marc Aurel Schnabel, Shuva Chowdhury</i>	
Urban Wellbeing, As Influenced by Densification Rates and Building Typologies	661
<i>Yaala Trossman Haifler, Dafna Fisher-Gewirtzman</i>	
The Guidance System of Gamification and Augmented Reality in a Museum Space	671
<i>Zi-Ru Chen</i>	
Mobile Mixed Reality for Environmental Design Using Real-Time Semantic Segmentation and Video Communication	681
<i>Daiki Kido, Tomohiro Fukuda, Nobuyoshi Yabuki</i>	
Holonavi	691
<i>Takaharu Suzuki, Hikaru Ikeda, Issei Takeuchi, Fumiya Matsunaga, Eri Sumitomo, Yasushi Ikeda</i>	
sensMOD	701
<i>Robert Doe</i>	

The Association Study Between Residential Building Interface and Perceived Density based on VR Technology <i>Yan LI, Hongwu DU, Qing WANG</i>	711
Multi-sensory Materiality <i>Marcus Farr, Andrea Macruz</i>	721
Feng-Shui and Computational Fluid Dynamics (CFD) <i>Bin Li, Weihong Guo, Marc Aurel Schnabel, Tane Moleta</i>	731
A Machine-Learning driven Design Assistance Framework for the Affective Analysis of Spatial Enclosures <i>Rohit Priyadarshi Sanatani</i>	741
User-driven Parcellation of High-rise Units for Future Urban Habitation <i>Oliver Heckmann, Michael Budig, Zack Xuereb Conti, Ray Chern Xi Cheng, Sky Lo Tian Tian</i>	751
A Light-weight CAAD-VR Bridge <i>Sheng-Fen Chien, Chieh-I Lin, Kuan-Ling Lin</i>	761
<b>Building/City/Region Information Modelling/Management</b>	<b>771</b>
OGOS+ <i>Anna-Maria Chatzi, Lisa-Marie Wesseler</i>	773
Development of an Urban Greenery Evaluation System Based on Deep Learning and Google Street View <i>Yixi Xia, Nobuyoshi Yabuki, Tomohiro Fukuda</i>	783
Geo-computation for District Planning <i>Pradeep Alva, Han Jie Lee, Zhuoli Lin, Palak Mehta, Jielin Chen, Patrick Janssen</i>	793
Irradiance Mapping for Large Scale City Models <i>Han Jie Lee, Zhuoli Lin, Ji Zhang, Patrick Janssen</i>	803
FLÄVIZ in the rezoning process <i>Wolfgang E. Lorenz, Gabriel Wurzer</i>	813

Spatial Characteristics Analysis of Urban Form at the Macroscale Based on Landscape Pattern Indices <i>JueLun Zhou, ZiYu Tong</i>	823
Spatial Elements of Commercial Streets and Pedestrian Perceptions via a Multi-scale Perspective <i>Zhen Zhang, Hong Wu Du, Yan Li</i>	833
Automatic Recognition and Segmentation of Architectural Elements from 2D Drawings by Convolutional Neural Network <i>Yahan Xiao, Sen Chen, Yasushi Ikeda, Kensuke Hotta</i>	843
Computational Methods for Examining Reciprocal Relations between the Viewshed of Planned Facilities and Historical Dominants <i>Klara Czynska</i>	853
Sustainable development of a cityscape using the Visual Protection Surface method - optimization of parameters for urban planning <i>Pawel Rubinowicz</i>	863
Environmental Performance-based Community Development <i>Jong Bum Kim, Bimal Balakrishnan, Jayedi Aman</i>	873
Four Approaches for Integration of Digital BIM Practices in AEC Projects <i>Gilles Halin, Veronika Bolshakova, Elodie Hochsheid, Henri-Jean Gless, Siala Aida</i>	883



# **Digital Fabrication & Construction**





# RESEARCH ON VOXEL-BASED AGGREGATION DESIGN AND ITS FABRICATION

KAI XIAO<sup>1</sup>, CHEN-CHENG CHEN<sup>2</sup>, ZHE GUO<sup>3</sup>, XIANG WANG<sup>4</sup>  
and CHENYUN YAN<sup>5</sup>

<sup>1,5</sup>*Huaqiao University*

<sup>1,5</sup>{17014085035|18014085036}@stu.hqu.edu.cn

<sup>2</sup>*TamKang University*

<sup>2</sup>097016@mail.tku.edu.tw

<sup>3,4</sup>*CAUP, Tongji University*

<sup>3,4</sup>{1732143|18310021}@tongji.edu.cn

**Abstract.** The application of aggregation structure in architecture has a long history, such as a stone wall and bucket arch. With the development of digital design technology, the aggregation structure has become more possibilities in terms of form design and rationality. However, many types of research on aggregation structure focus on a specific form or fabrication process, only a few discuss the simple design method of the discrete structure in the digital platform. Here we show an approach of aggregation structure design and fabrication based on voxel. Within the framework of six voxels, a group of “aggregation units” are designed, which are used in different parts of the aggregation structure according to the structural requirements. Finally, part of the structure is made by digital tools. We anticipate that the morphology and fabrication method of aggregation structure based on voxel framework able to provide more convenience, which not only reflected in the design process of the unit but the generation operation and optimization process of the overall structure.

**Keywords.** Aggregation; Voxel; Digital Fabrication; Generative Design.

## 1. Introduction

Aggregation structure is a kind of structure composed of discrete units, which has a long history in architecture. With the development of digital technology, the design and fabrication of aggregation structures are more diverse. (Gilles Retsin, 2019a) In previous studies, the “aggregation unit” was designed as the shape of some kind of organism which is to study the structural form formed by spontaneous aggregation of organisms in nature. For example, the research on the spontaneous combination of ants to form an “ant bridge” (Michael James Rogers, 2013). Some non-convex units (S-shaped, space star, space Z-shaped) are in loose contact and form a stable whole with the interaction between particles (Karola Dierichs, 2013), (Kieran Murphy, 2017). The study of “aggregation structure”

also focuses on the characteristics of materials and aggregation methods. The units with rough surface contact closely in the vacuum film, which can form a stable structure (Andrew Borgart, 2008). However, most of the current researches focus on a kind of “aggregation structure” formal logic or fabrication mode. There is little research on the methodology of unit shape design. In this study, “voxel” is the basic design method. The research of “aggregation structure” includes “unit shape”, “aggregation connection design” and “aggregation structure operation design”. The shape of the “aggregation unit” is based on “voxel”. In the aggregation operation or topology optimization, the voxel is also used to replace “unit” to reduce the consumption of operation. This is necessary for the design and fabrication of “aggregation structure”.

## 2. Voxel

### 2.1. VOXEL-BASED DESIGN

Voxels, also known as three-dimensional pixels, are a tool to represent space numerically on three-dimensional meshes. The basic shape of a voxel is a cube, which represents space numerically in a computer model. Because of these characteristics, it is used in highly space-sensitive disciplines, such as meteorology, medical imaging, and digital architectural design (Roberto Bottazzi, 2018). Voxel-based aggregation is designed by the shape of voxels. At least one part of the shape of the aggregation unit should be connected with the boundary of the voxel, to ensure the connection of the unit in the aggregation structure. These connections can be classified into connection point, connection line and connection surface according to different geometry. Different types of connections mean different degrees of stability.

### 2.2. VOXEL SHAPE DEVELOPMENT

The shape of the aggregation unit is restricted by the voxel boundaries. When the voxel changes from a cubic form to a more complex form, the shape of the aggregation unit will be more diverse, and the aggregation structure complexity will increase. To achieve this, the cube voxel changes shape by moving a horizontal edge and a vertical edge outward. This operation is based on subjective judgment. The new voxel shape is more versatile than the cube. (Figure 1)

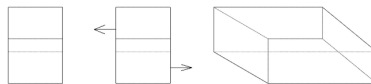


Figure 1. Changes in cube voxel morphology.

To increase the rationality and complexity of aggregation structure, voxel types in aggregation structure have developed from one to many. There are two steps in this process: the first step, voxel elongation, is to adapt different length units to different structural parts. The second step, voxel amplification, is to improve the morphology and enhance the structure by using the fractal method. ( Gilles Retsin, 2019) The dimensions of the six voxels are shown in the figure. (Figure

2)The aggregation units of different scale voxels played different roles in the aggregation composed of voxels. Large-scale voxels are usually used as the main part of the aggregation, because of its integrity; small-scale voxels are usually used as the non-main part of the aggregation where to reduce the self-weight of the aggregation or increase the structural strength. (Figure 3)

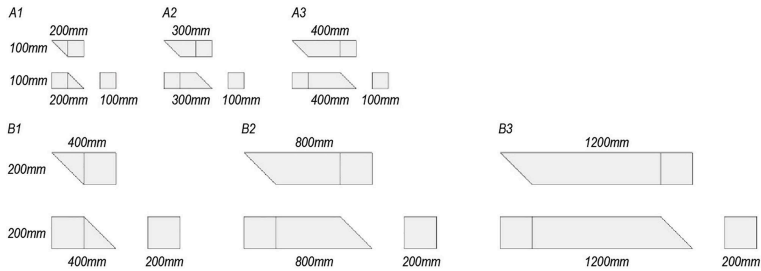


Figure 2. Six voxel shapes formed from cube voxels.

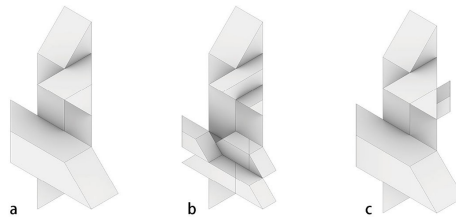


Figure 3. a. One of the large voxel combinations b. Replace large voxels with small voxel combinations c. Reinforce large voxels with small voxels.

### 3. Aggregation Structure Units

#### 3.1. UNITS DESIGN

Aggregation unit is the fundamental of aggregation structure. The design of aggregation units requires a comprehensive consideration of connection methods and fabrication methods (fabrication methods and materials). The characteristics of different fabrication methods and materials will affect the shape of discrete units. For example, a line pattern formed by bending a metal, which is connected by a joint; 3D printed surfaces, with units connected by boundary lines; The body shape formed by cement pouring, the masses are connected through the contact surface.

In this study, the face-to-face connection is used as the basic connection method. This is a stable connection method (large contact area), which is suitable for structures or building components with structural strength. Among the six forms of voxels, there are three face shapes, square, rectangle, and triangle, which can be connected to faces of the same type. The connecting surface of the aggregation is the same as the corresponding voxel. At this time, the

basic morphology of the aggregation unit is still uncertain. Aggregation unit morphology is related to fabrication methods and materials. Therefore, the next step consideration is the design of fabrication methods, materials, and joint details.

### 3.2. FABRICATION METHODS AND MATERIALS

The physical model is different from the scaleless model on the computer. The fabrication is restricted by many factors, including material characteristics, fabrication methods, structural strength, fabrication difficulty, time-consuming and economical. According to the size of the aggregation unit, it can be roughly classified into “small scale model”, “decorative component size” and “building component size”. Different fabrication methods and materials are suitable for unit research at different scales. For small-scale aggregation models, 3D printing units are a suitable research method in the study of geometric shapes. 3D printing can make complex unit shapes, and the aggregation is achieved by the powerful magnets embedded in the units; These fabrication methods are characterized by short fabrication time and low cost, but their connections are weak. For the study of larger size aggregation structure, magnetic attraction is not suitable as a connection because this type of aggregation structure requires a certain loading capacity (self-weight and external force). Generally, the materials of the aggregation unit include cement, wood, steel, clay, hard plastic, etc., which are aggregation in a higher strength connection. For example, connecting units with embedded components in welded cement; Joining wood units by mortise and tenon; (Fei-Fan Sung 2018)Welding connection between metalworking (Lin Chin-Ying 2019).

After considering the constraints, we choose an appropriate way to fabricate. Some of these materials and fabrication methods are compared (Figure 4). The design study includes six different methods, including EPS, 3D printing, MDF (medium-density fibreboard) enclosure, timber milling, MDF stacking, and cement infusion. Comprehensively judge from five aspects of their unit structure strength, fabrication time per unit, fabrication price per unit, fabrication difficulty, and unit freedom of combination. The higher the score, the more advantageous it is. First, structural strength and combinational diversity are the two most important factors for discrete units and structural aggregation. The strength of the unit and the connection method determines the upper limit of the strength of the aggregation structure; The combinational diversity is the basic advantage of aggregation structure. Firstly, based on the above two points, the EPS unit, MDF enclosure unit and cement pouring unit are not selected. Secondly, considering the time and price of unit fabrication, the price of the 3D printing unit is too high, and the solid wood milling unit takes more time. In the end, discrete units are made by method *e*.

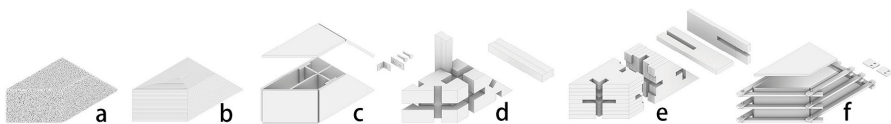


Figure 4. Comparison of several unit fabrication methods and materials (a. EPS b. 3D printing c. MDF enclosure d. timber milling e. MDF stack f. Cement pouring).

Table 1. A comprehensive comparison of six units of fabrication methods from five aspects.

(Score 1-6)	Unit Strength	Fabrication Time	Fabrication Price	Fabrication Difficulty	Freedom of Aggregation
EPS	1	6	6	5	6
3D printing	4	1	1	6	5
MDF enclosure	3	4	5	3	3
timber milling	5	2	2	3	5
MDF stack	5	5	5	4	6
Cement pouring	6	4	5	2	3

### 3.3. CONNECTOR DESIGN

The key point of the connection is the stability and the combination freedom of the connection method (Some connections are directional ). For wooden constructions, connection can usually be made with mortise, screws or nails. Sometimes unit aggregation is a trial and error process. The advantage of mortise and tenon compared with the latter is that the connection is detachable, which is very important when combining units.

Another issue to be solved is the connection between aggregation units of different sizes. Hence, each connecting surface of the large-scale unit is divided into four parts, and the shape of these four parts is the same as that of the small-scale unit. Cross-shaped slots are provided on these faces. These slots are of equal size and are presented in a cross shape. When the two units are connected, an additional accessory pin passes through the two units and acts as a fixture. The cruciform shape prevents mutual rotation between the units. (Figure 5)

### 3.4. FABRICATION DESIGN OPTIMIZATION

Because of the thickness of MDF, a unit needs to be divided into two parts to fabricate. The purpose is to avoid the appearance of stepped shapes on a certain line surface and thus affect the connection between the units. Furthermore, the optimization process includes weight reduction and units of structure enhancement. Specifically, calculate the number of MDF boards required for a discrete unit, and use a laser cutter to cut the outline and slot position of the unit on a 6 mm thick MDF board; remove some of the internal units that do not affect the strength The MDF board reduces the weight of the unit; try to use the tenon to combine the two parts of the unit body. The greater the number of tenons, the deeper the unit, the more stable the internal structure of the unit.

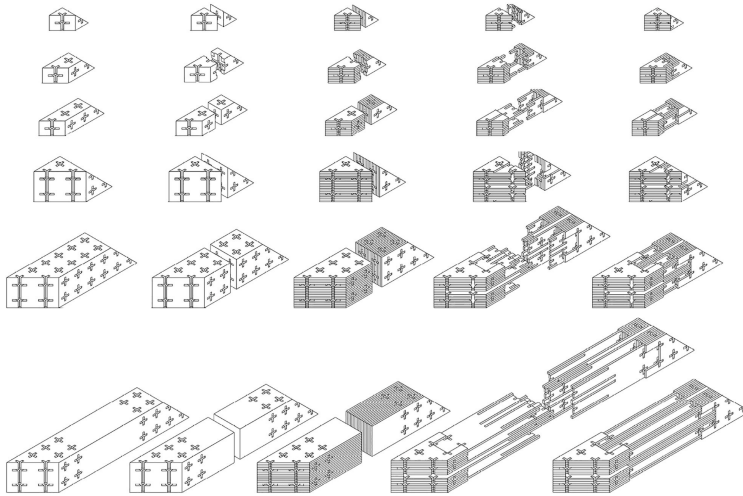


Figure 5. Aggregation Unit Optimized Design for Fabrication of MDF Board Stacks.

#### 4. Aggregation Logic and Optimization

After discussing the morphological design of aggregation units based on voxels, this section further studies how to realize the generation of aggregations based on the characteristics of voxels. Generally speaking, there are two ways, one is to convert the existing form into a form composed of voxels through a top-down voxelization method; the other is to set the Combine the rules, and later generate them by computer operation according to these rules.

##### 4.1. VOXELIZATION-TOP DOWN

The top-down aggregation structure design is a process from concrete shape to voxelized shape and then to aggregation structure. The advantage of this method is that the designer can control the outline of the final aggregation structure. Some plug-ins in grasshopper, such as yellow, can easily execute the voxelization operation (cube voxel). The method for nonstandard voxels needs further study. There are four steps: 1. Determine the shape; 2. Cube voxelization; 3. Randomly combine all cube voxels into the shape of deformed voxels. 4. Voxels are replaced by aggregation unit entities. (Figure 6)

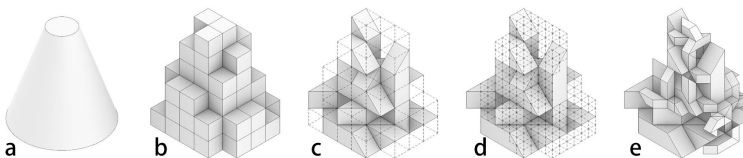


Figure 6. Top-down voxelization process using a cylinder as an example (a. Cylinder b. Cube voxelization c. Voxel replacement d. Voxelization again e. Small voxel insertion).

#### 4.2. VOXEL AGGREGATION GENERATION-BOTTOM UP

For the bottom-up voxel generation method, the key lies in how to abstract the relatively complex units aggregation process into a voxel aggregation process. The design of the unit is based on the voxel framework. Voxels have different characteristics given by the unit shape on different interfaces. For this case, due to the units that have the feature that it can be connected at all faces of the same geometric type, the iterative growth regularization of voxels must correspond to it, that is, the iterative generation of voxels.

The generation process of the voxel group can be performed in a pre-defined field range or an unlimited range, which means that the possibility of artificially controlling the voxel generation form (by controlling the field) to a certain extent. Unlike top-down voxelization, the morphological design of this aggregation is between “top-down” and “bottom-up”. The preset generation field can be generated by linear or planar objects. It can be understood that the area closer to the object in space becomes the place where the aggregation unit appears first. The result is that the aggregation roughly forms the shape of the object. The voxel group generation process in the figure below is performed in a limited field, which is generated based on two shapes: “line” and “surface”.(figure 7)

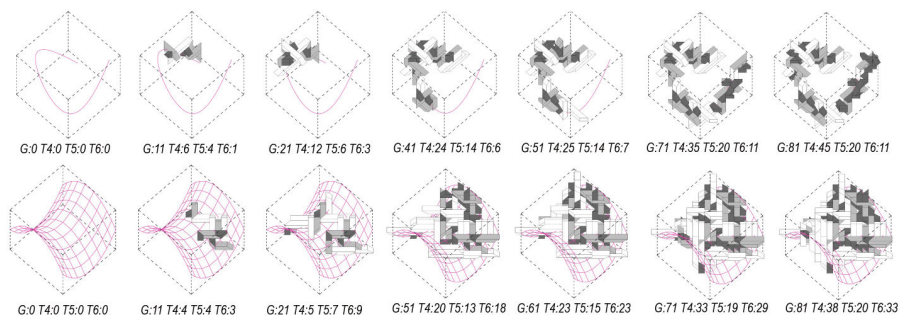


Figure 7. Voxels are aggregated by “line” and “surface”.

#### 4.3. FORM FINDING

Fields generated based on “lines” or “surfaces” are not mechanically optimized. How to make the force reasonable in the setting of the field? Continuous topology optimization is a better method for field generation of reasonable force patterns. Continuous topology optimization and aggregation structure have the same premise. In short, continuum topology optimization is to divide the material of optimization space into finite units (shell units or body units)(Li Zhuyu, 2017).

The *topos* plug-in of Grasshopper is used to optimize the field topology. aggregation structure is defined to be generated in a cube space, which is subdivided into a finite number of small parts with a numerical resolution. The top of the space receives downward pressure and the bottom is diagonally supported by two upward forces. In this case, the part less than a certain value in cube space is deleted, to obtain the most suitable space location for aggregation structure (Figure



8b). Different colors in the field indicate different stress intensity (red is the highest and green is the lowest). Aggregation structure units will aggregate in areas with high-stress intensity.

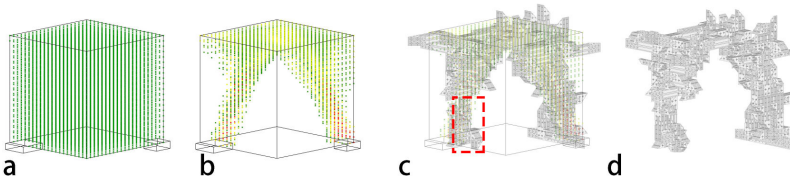


Figure 8. Generation of aggregate pavilions (a. Original field b. Topology optimization field c. Aggregate body generation d. Small unit placement or replacement for optimization).

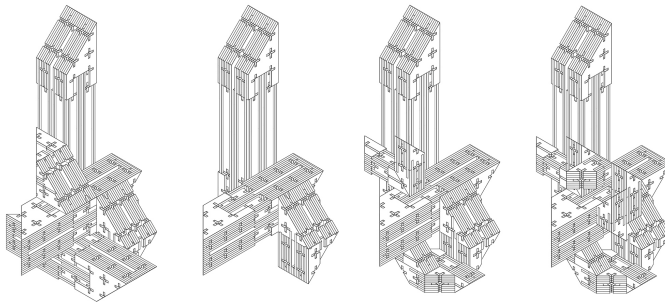


Figure 9. The optimization process of small size units aggregation (part).

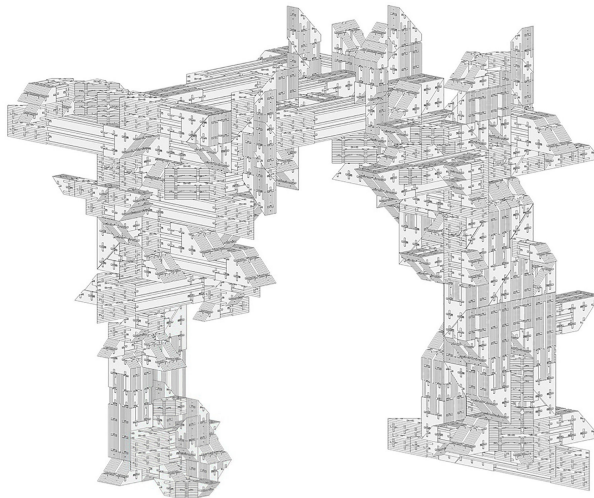


Figure 10. Final aggregation pavilion .

The new field limits the bottom-up generation of aggregation structures. This process will be completed according to the set generation quantity and generation rules. It should be noted that after the aggregation of three large-size aggregation structural units, the small-size aggregation structural units aggregate in the vulnerable parts of the structure, such as the cantilever, forming a “Topological Triangle” of stable structural relationship. Small size aggregation structural units are also used to replace large size aggregation units in places with small stress to reduce structural weight, such as at the edge of the pavilion roof. This is a partial demonstration for the local small-size aggregation structural units to aggregate and optimizes the structure (Figure9). The part of the pavilion of aggregation structure is made in the proportion of 2:1. (Figure 11)

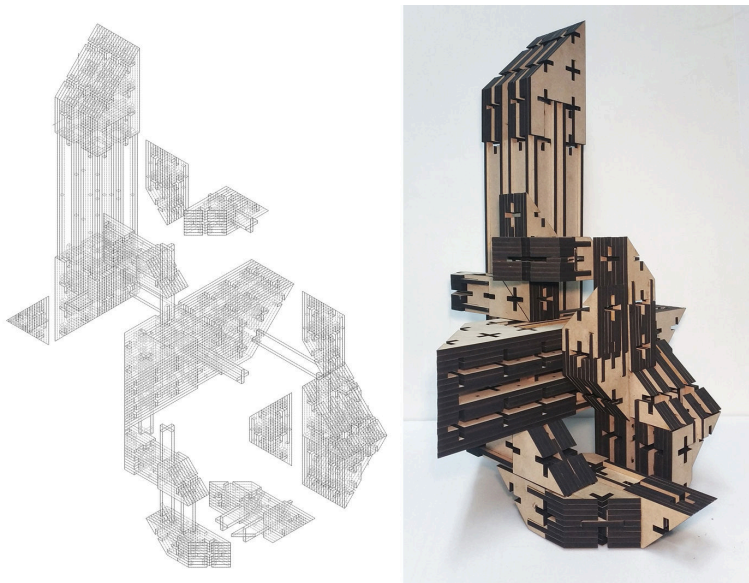


Figure 11. Fabrication details and results.

## 5. Conclusions

This article presents a voxel-based aggregation design and fabrication method. Variations in voxel morphology have developed diverse aggregation design possibilities. The aggregation units are made of MDF and connected by tenon and mortise. This structure has the characteristics of diverse combinations and detachability and also has certain structural stability. In this study, the optimization of aggregation mechanical model is completed in a certain range of experiences. The difference in the internal structure of the units is not fully considered in the process of stress optimization. In future research, we should make targeted optimization design for the formation field of aggregation and the local vulnerable points of aggregation in a more targeted way. At the same time, there are more forms of possibility in voxel-based aggregation design. For example, the form of

voxel unit, the form of aggregation unit (line, surface, body), and the connection mode of the aggregation units. In the future, the design of voxel-based aggregates will have more development prospects.

\* Subsidized Project for Postgraduates' Innovative Fund in Scientific Research of Huaqiao University.

## References

- Borgart, A.: 2008, *Imagine No. 02: Deflateables*, nai010 publishers.
- Bottazzi, R.: 2018, *Digital Architecture Beyond Computers: Fragments of a Cultural History of Computational Design.*, Bloomsbury Publishing, London.
- Dierichs, K.: 2013, Aggregate Architecture: Simulation Models for Synthetic Non-convex Granulates, *Proceedings of ACADIA 2013*.
- Li, Z.Y.: 2017, *Level Set-based Topology Optimization Method for Architectural Structure Design*, Master's Thesis, South China University of Technology.
- Lin, C.Y.: 2019, *Application Robot Arm Digital Fabrication and Tectonic-Take Metalworking as an Example*, Master's Thesis, Tamkang University.
- Murphy, K.: 2017, Aleatory Construction Based on Jamming: Stability Through Self-Confinement, *architectural design*, **87(4)**, 74-81.
- Retsin, G.: 2019a, Discrete Architecture in The Age of Automation, *Architectural Design*, **258**, 7-13.
- Retsin, G.: 2019b, Digital Assemblies: From Craft to Automation, *Architectural Desig*, **258**, 38-45.
- Rogers, M.J.: 2013, Formicis: A Study in Behavioral Componentry, *Proceedings of ACADIA 2013*.
- Sung, F.F.: 2018, *A Study of Architextiles for Timber Structure Design*, Master's Thesis, Tamkang University.

# DOUBLE LOOPS PARAMETRIC DESIGN OF SURFACE STEEL STRUCTURE BASED ON PERFORMANCE AND FABRICATION

CHENJUN LIU

<sup>1</sup>*Studio DeepMesh*

<sup>1</sup>*liuchenjun0@gmail.com*

**Abstract.** In intelligent epoch, automatic parameter design systems reduce the requirements of the skills needed to create objects. The creator only needs to select the most perceptual primitive form to automatically generate the data system that iterates to the most efficient solution. In this paper, a method of combining performance driven optimization with parametric design is proposed. The iterative evolution is under the control of performance loop and fabrication loop, which makes all the data provided by parametric design in a practical project available for exploring structural analysis and digital prefabrication. Related to the case of surface steel structure, parametric optimization is not limited to a set of shape types or design problems, it would be based on the generality and built-in characteristics of parametric modelling environment in the most convenient and flexible way. (Rolvink et al. 2010) And the given parameters would be fed back on geometric structure, performance indicators, and design variables, so that designers can easily and effectively coordinate and try different solutions. The system transforms the generated data into machine language so that the process including design, analysis, manufacturing, and construction can maintain the orthogonal persistence of the data.

**Keywords.** Parametric design; component prefabrication; curved steel structure; performance driven.

## 1. Introduction

The combination of parametric modeling and optimization algorithm has become one of the most widely used calculation methods in conceptual design. Designers and engineers are committed to finding an operating system platform with orthogonal persistence, so that the combination of project attributes and data can be operated consistently when modifying the component. In this project, the parametric platform offers designers write complex generation algorithm scripts without prior programming knowledge, and help to guide the exploration of free form space. This approach is not only dedicated to computer-aided drawing, but also benefits from several plugins available to evaluate the performance of architectural design according to a wide range of criteria, from the mechanical performance of buildings to the physical performance of buildings (Danhaive and Muelle 2015).

The practical project is an auxiliary structure of a hospital building, whose functional form is mainly based on the combination of the ramp and the entrance surface (see figure 1). It drives the team to build a compatible parameter workflow under the high reduction requirements of components and nodes, together with the designer's demand for project adjustment and performance driven structure optimization. To achieve data consistency in the whole process, data working interfaces are established in one platform with input data from different plugins. The project takes advantage of the software platform in data processing:

1. Unified processing of data structure
2. Accurate independence of location
3. Data encapsulation and reuse

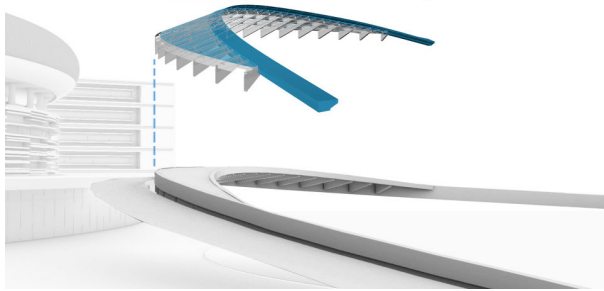


Figure 1. the Relationship between Surface Steel Structure and the Main Building.

## 2. Double Loop Parametric Design System

In this project, the team has established a set of parametric model framework discussing the influence of the designer's intervention on the whole closed-loop process. Architects and engineers face two factors: conceptual knowledge (three-dimensional geometry, shape-finding technology, nonlinear behavior, large-scale deformation, permanent bending stress, etc.) and design tools. (Peloux et al. 2013) So that our team builds an interactive system and feedback platform which runs from initial shape to prefabricated construction on the parametric plugin Grasshopper of modelling software-Rhinoceros. In the process of project evolution, the prototype is controlled by two factors: structural performance and prefabricated construction. By setting two conditional optimization statements in the original design programming, it is found in multiple iteration optimization called the double loop that the optimal solution of conforming to the requirements of structural performance, manufacturing accuracy and cost-performance ratio. The finite element analysis software Karamba3D and Millipede are used to iterate the performance evolution, and the self-programmed script is used to select optimal prefabricated parameters (see figure 2).

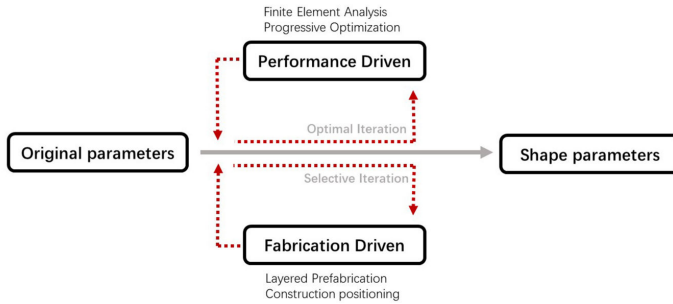


Figure 2. Double Loop Parametric Design System.

### 2.1. THE LOOP OF FABRICATION DRIVEN

The parametric definition of external geometry enables the team to effectively explore design alternatives and change joint shape within conceptual constraints. The parameters are used to manipulate the point cloud (sorting, transformation) which allows the designers to study the different characteristics of the outer surface. In the loop of fabrication driven (see figure 3), the data stream flows from point cloud to the final layer data through three self-programmed script plugins whose function is linear selection, constraint adaptation and deliver layered construction data. In this loop, the feedback component offers a self-form point cloud operates on the cycle of optimization.

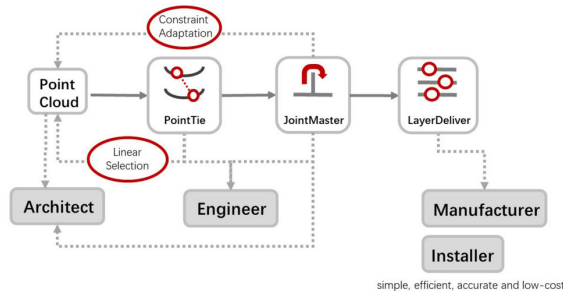


Figure 3. The Loop of Fabrication Driven (Select Iteration and Optimize Construction).

In the initial design of the project, the self-programming plugin “PointTie” is used to explore the prototype (see figure 4), under the cooperation rule of shared information platform which is conducive to the real-time communication of the scheme. After confirming the rule of the original shape, the design proceeds to the parameter fine-tuning stage. Based on determining the two-dimensional parametric curve, the undulation height parameters controlled by point cloud are added, and the scheme could be further selected and adjusted.

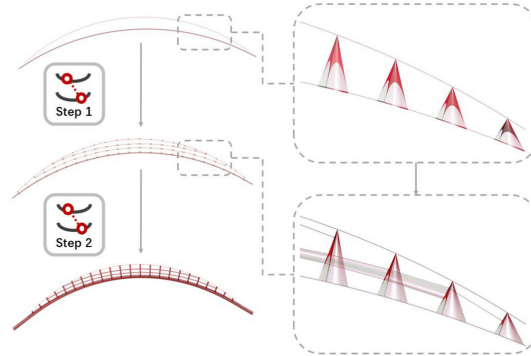


Figure 4. PointTie—Self-form point cloud related to fabrication driven constraint.

In the second stage of design, the self-programming plugin “JointMaster” which contains different solutions to solve the joint problem, is used to set the intersection relationship of the structure under the guidance of the parametric point cloud data. On the framework of setting constraints, the hierarchical relationship between data is accurately reflected in the body’s relative position. The whole design process is programmed in the compression package in the intensive scheme so that the scheme can be switched and adjusted flexibly. The most suitable beam formation and joint connection mode will be obtained after three parallel constraints solution (see figure 5).

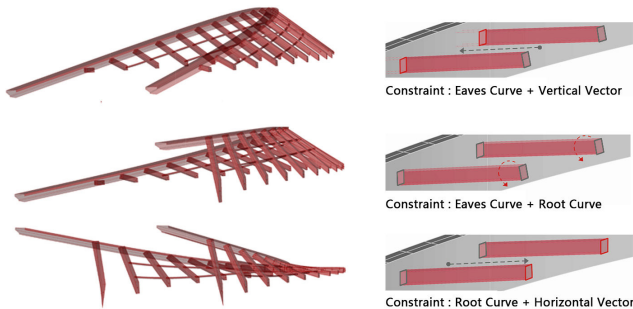


Figure 5. JointMaster—Adaptive variable beam joints related to fabrication driven constraint.

Threshold constraints are set in the design process of articulated joints, which leads to a simple, efficient, accurate and low-cost environment. The information includes angle and length is imported into the machine automatically and accurately through the parametric process, which transfers the positioning problem (human error on-site) to the prefabrication problem (machine error in factory).

2.2. THE LOOP OF PERFORMANCE DRIVEN

In recent years, the development of initial geometry analysis (IGA) has paved the way for the close combination of engineering design and calculation analysis. The core idea of IGA is to use the same basic function to represent geometry in CAD and approximate solution field in finite element analysis (FEA). (Hsu et al. 2015) In this part, an interactive parametric design method based on the analysis platform is used to help design engineers and analysts make more effective use of geometric analysis methods to improve product design and performance.

Performance driven architecture design emphasizes the comprehensive optimization of various quantifiable properties of buildings. It is necessary to develop effective technology for performance driven design and optimization from the perspective of architects. (Shi and Yang. 2013) Karamba3D and Millipede are fully embedded in Grasshopper’s parametric design environment, and the parametric workflow platform is reasonably structured for data support and interactive optimization. This makes it easy to combine parametric geometric models, finite element calculations and optimization algorithms (such as Galapagos). The process has four stages:

1. gridding the conceptual three-dimensional volume
2. dynamic force adaptation analysis of homogeneous grid
3. generating mechanical model and data
4. machine learning and dynamic design

In the loop of performance driven, the data stream flows from line data to the final component data through two grasshopper plugins whose function is statement iteration and dynamic evolution (see figure 6). The feedback component offers a self-form line operated on the cycle of optimization. In the first step, it is to build beams with the same section by default line segment, analyze the stress of a single beam, and then integrate the whole grid structure to find the most stable component changing. In the second step, it explores the force evolution of the whole grid structure and the individual performance of beams in different positions for the standardized structure manufacturing that meet the mechanical characteristics. Three groups of data interact and interfere with each other in iterative evolution, and finally form an optimal solution of dynamic balance.

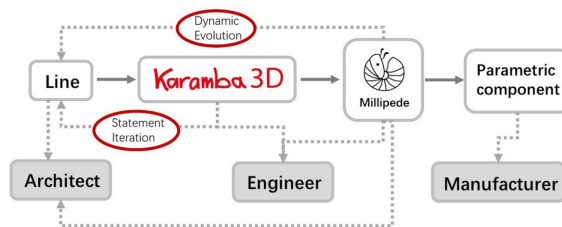


Figure 6. The Loop of Performance Driven (Finite Element Analysis Progressive Optimization) .

The finite element analysis (FEA) software Karamba3d is used in the



mechanical analysis of the preliminary steel structure. The interactive geometric modeling and parametric design platform proposed by the design team hides the complex CAD functions in the background through the generation algorithm, and allows users to control the design through key design parameters. Because of the combination of design concept and analysis, design parameters can include not only geometric parameters, but also material properties, loads and boundary conditions. (Hsu et al. 2015) Karamba3d is completely embedded in the parametric design environment of grasshopper, which also reasonably supports and optimizes our parametric workflow platform in terms of structural data and interaction.

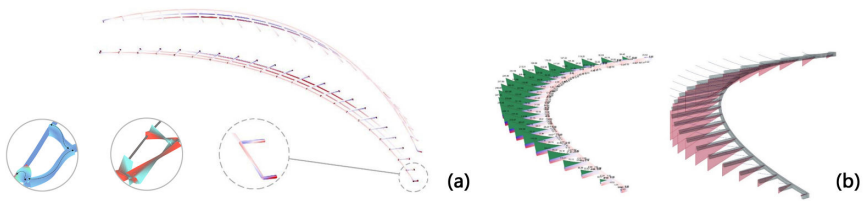


Figure 7. Karamba3D—Mechanics Analysis and Adaptive Interactive Design (a) Mechanics Analysis and Adaptive Interactive Design (b).

By combining the utilization rate and bending moment analysis of the curved steel structure girder (see figure 7a), the team transformed the force data on the unit length node of the girder into the dimension data of section and relative position of unit beam, realizing the data flow of the linkage between the curved surface's modeling curvature and the structural thickness of the girder (see figure 7b).

Millipede is a plugin of the grasshopper parametric design platform, focusing on structural analysis and dynamic optimization. In the project, we use millipede algorithm to demonstrate the collapse model comparison of the designed structure and the topology optimization of the steel structure members. It helps us to embed the parametric modeling method into the structural design process to quickly build structural alternatives, generate structural models and re-analyze the structure.

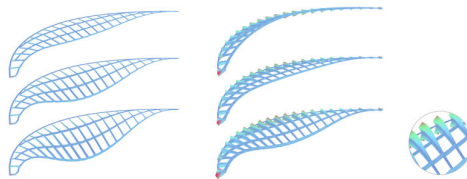


Figure 8. Millipede—Collapse analysis and optimization comparison .

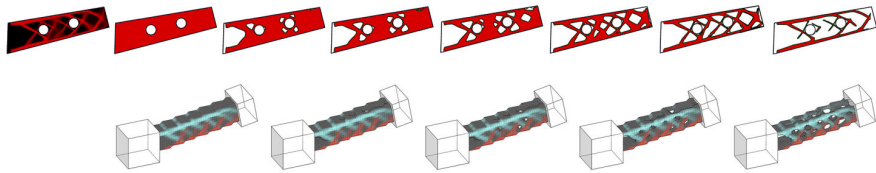


Figure 9. Millipede—Progressive optimization of finite element method.

In the model preview, the pressure deformation value is increased to evolve the collapse model under different pressure conditions (see figure 8). This collapse shows the deformation of specific parts with exaggerated effect, and guides those parts of the structure to be strengthened. In the previous step, we realized the real-time adjustment and optimization of the structure through the parameters of the structural thickness and curvature of the main beam. In the collapse model, it can be shown that the collapse degree of the optimized structure is significantly less than that of the homogeneous structure.

In the progressive optimization of steel structure components by finite element design, the project team gets different degrees of topology optimization model (see figure 9). The purpose of this analysis is to compare the relationship between the material characteristics and the mechanical load, to do the preliminary research for the future project deepening.

### 3. Fabrication of Hierarchical System

The prefabrication design is based on a modular integrated parametric system. Programming scripts are used to establish an automated communication flow among engineer teams. (Hsu et al. 2015) After the previous stage of design selection and performance optimization, the whole curved steel frame gradually becomes a multi-level frame system customized and quantified under the guidance of the intensive programming plugin package (see figure 10). On this basis, we decompose and classify the component data according to the specific prefabrication process and construction requirements.

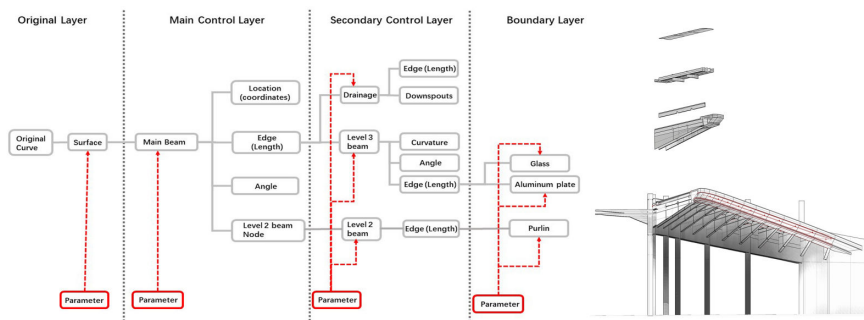


Figure 10. Layered affiliated component in Hierarchical System.

In the process of data encapsulation and reuse, linked data is processed continuously. With this feature, it can be extract the accurate hierarchical shape with position data during the process of parametric split. These data levels are closely related and originate from the initial data, so that the self-programming plugin has real-time linkage and orthogonal persistence, which means that all components of the project can be effect interactively and change in linkage before the process of prefabrication. It provides efficiency and accuracy guarantee for project coordination and adjustment (see figure 11).This parametric platform can be widely used as a set of strong adjustable products in different projects.

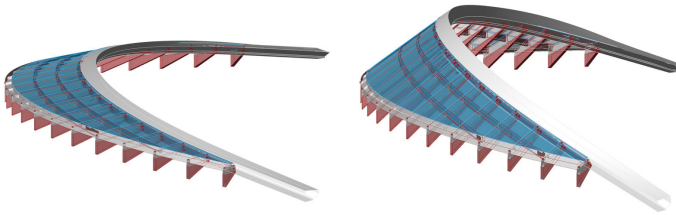


Figure 11. The dynamic system of all layer component related to adjusting the initial parameters.

In the process of document preparation, we have established a parametric workflow system to connect different levels of design and document environment (Miller 2011), so as to achieve a seamless team collaboration:

- Geometry Design: Building parametric framework and applying the initial geometry
- Form Iteration: Rapid optimization of the building form and testing alternatives.
- Structural Selection: Systems for producing prefabrication driven models.
- Mechanical optimization: Classifying physics simulation for an intuitive understanding of performance driven structures.
- Hierarchical System: Affiliated component property depends on layered parameter.
- Coordination and Documentation: Organizing and transforming the component parameter for CNC pre-manufacturing

The basic geometry is used to generate ancillary systems such as flume, aluminum plate and glass, creating a group of prototype linkages under the guidance of the main system frame data (see figure 12).

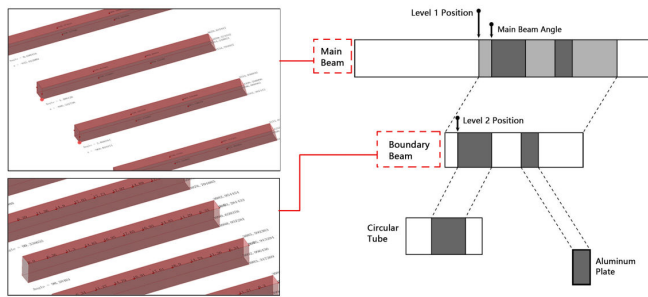


Figure 12. Multi-layer Associated Data and Digital prefabrication.

During the stage of steel prefabrication, the construction component is shaped by a series of CNC machine system whose analog signals and digital signals are related to the hierarchical analysis from construction layers (see figure 13). The first step is to use a mechanical bending machine bend the standard straight steel to two-dimensional curve steel. After that, the manufacturing team uses induction bending technology and robotic technology to do the free form three-dimensional bending. Finally, the section of joint is cut at accurate angle by the cutting machine. During the induction bending, the system is operated by the position and angle data of the robotic technology, to achieve the free form shape of the three-dimensional curve steel pipe (see figure 14).

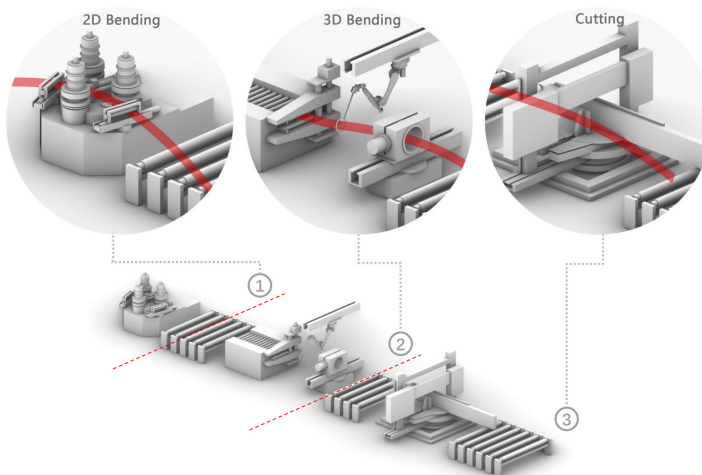


Figure 13. Steel bending and cutting system.

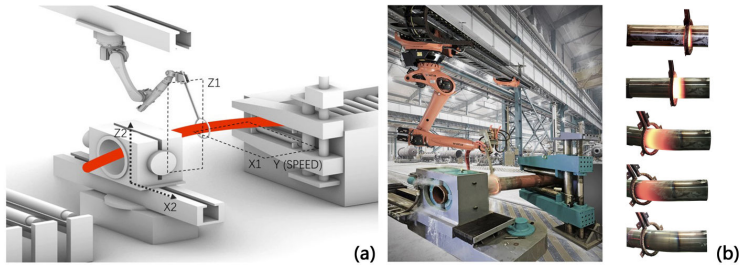


Figure 14. Steel three-dimensional Bending Rendering Diagram (Induction Bending and Robotic Technology) (a) Induction Pipe Bending Test by Kubes Steel (b).

#### 4. Conclusion

The development of digital technology and electronic technology has liberated buildings from the traditional situation. The ecosystem of construction combines with the optimization and iteration of the social data structure in the same programming language. In this paper, parametric thinking about sub-package data achieves the goals of efficient and precise coordination and intelligent optimization iteration in the process of architectural design, analysis and construction, which in the framework of continuous interactive feedback. After a series of processing through the structural intelligent selection and physical performance optimization, it converts the physical shape into digital dataset in the stage of design, which will be transferred to the digital signal and analog signal of CNC machine in the manufacturing stage. The traditional way of drawing design - human eye recognition - on-site construction will convert into the way of cloud platform design - electronic computing optimization - signal conversion construction.

The relationship between humans and architecture has been upgraded. The subjective parameter is input as the role of the original form and environmental factors. It contributes that the automation capability is stronger, the teamwork is closer, and the impact of personnel decisions on the building is more direct and profound. It develops a semi-autonomous system in which people and machines are coordinated.

#### References

- “Kubes Steel:Induction Bending Stainless Steel Pipe” : 2019. Available from <<https://kubesteel.com/article/20190703-induction-bending-stainless-steel-pipe>> (accessed 25 October 2019).
- Danhaive, R.A.: 2015, Combining parametric modeling and interactive optimization for high-performance and creative structural design, *Proceedings of IASS Annual Symposia 2015*.
- Hsu, M.C., Wang, C. and Herrema, A.J.: 2015, An interactive geometry modeling and parametric design platform for isogeometric analysis, *Computers & Mathematics with Applications*, **70(7)**, 1481-1500.
- Miller, N.: 2011, “The Hangzhou tennis center: a case study in integrated parametric design, *Proceedings of ACADIA 2011*.
- Du Peloux, L., Baverel, O., Caron, J.F. and Tayeb, F.: 2013, From shape to shell: a design tool to materialize freeform shapes using gridshell structures, *Proceedings of Design Modelling*

*Symposium Berlin 2013.*

- Preisinger, C.: 2019, "Karamba3D parametric engineering" . Available from <<https://www.karamba3d.com/download/#manual>> (accessed 29 August 2019).
- Rolvink, A., van de Straat, R. and Coenders, J.: 2010, Parametric structural design and beyond, *International Journal of Architectural Computing*, **8(3)**, 319-336.
- Sawako, K. and Panagiotis, M.: 2014, "Millipede March 2014 release : A Finite Element Analysis Software" . Available from <<http://www.sawapan.eu/>> (accessed 29 August 2019).
- Shi, X. and Yang, W.: 2013, Performance-driven architectural design and optimization technique from a perspective of architects, *Automation in Construction*, **32**, 125-135.



# THERMO-SHADING

## *Digital Design and Additive Manufacturing of SMP Prototypes*

JUNGWON YOON<sup>1</sup> and SEOK-WON CHOI<sup>2</sup>

<sup>1</sup>*University of Seoul*

<sup>1</sup>*jwyoona@uos.ac.kr*

<sup>2</sup>*B.Arch, University of Seoul*

<sup>2</sup>*csw951120@gmail.com*

**Abstract.** We present results on the development of an intelligent and informed SMP prototypes, as proof-of-concept models to assess applicability of thermo-responsive materials in adaptive façades. SMP has the intrinsic properties to detect environmental heat changes and react by changing its form into memorized shapes. Among different morphology and deformation behaviours of SMP components, this design-to-fabrication study focuses on design and 3D printing fabrication of prototypes. Additionally, casting was tested to validate the rapid prototyping of additive manufacturing. Furthermore, two different activation systems of SMP were presented to compare mechanisms between a surface-active system and an actuator system.

**Keywords.** SMP; AM; thermo-responsive.

### 1. Introduction

Building elements that offer adaptive features adjusting to environmental changes or external stimuli are termed responsive (Chang et al., 2019). Responsive building elements maintain high performance levels in fluctuating environmental conditions through programmed changes in their physical properties, surface features, or forms (Loonen et al., 2013). The responsive elements require integration across geometric, structural, material and electronic subsystems (Chang et al., 2019) in addition to energy-intensive actuation mechanisms that contradict the intended goal of energy-efficient performance (Gupta et al., 2019).

However, material-based actuated systems such as smart shape-changing material mechanisms (Gupta et al., 2019) reduce energy demand and simplify the assembly design (Correa et al., 2015). Thermo-responsive shape memory polymer (SMP) is studied for climate-adaptive responsive façades due to the internal shape-changing properties stimulated by specific glass-transition temperature (T<sub>g</sub>) (Yoon, 2018). SMP is preferred (Arun et al., 2018) to approach the digital fabrication combining material embedded system, due to its manufacturing methods and extensive design interpretations (Ge et al., 2016). Among different morphology and deformation behaviours of SMP components, this study focuses



on design and fabrication of thermo-responsive shading devices with flapping mechanism as façade elements. The design process of an adaptive prototype involves human intuitive design propositions with digital tools, their empirical verification through reiterative experiments by Additive Manufacturing (AM), and revisiting the research after reconsideration of experiment results. AM allows rapid assembly and prototyping, innate ability for customization, functional integration and improved resource utilization (Chang et al., 2019; Garcia Rosales et al., 2019; Kolarevic, 2004; Tofail et al., 2018; Yoon, 2019a), at the centre of research across disciplines (Dritsas et al., 2019; Thompson et al., 2016), gaining significant ground (Mitchell et al., 2018), and allowing researchers to create complex shapes (Zhang et al., 2019). The concept has evolved into 4D printing by incorporating smart materials (Tibbits, 2014) which can transform in response to an external stimulus (Mitchell et al., 2018; Zhang et al., 2019). By adopting the commercially available SMP pellet as the main material, we present a method to utilize SMP and rationalize the responsive shading system using a combination of material properties and digital fabrication.

## 2. Methodology

### 2.1. DIGITAL DESIGN

Among various morphology and deformation behaviours of SMP components, this study focuses on the flapping prototypes. Initially, a folded blade was designed and fabricated, from the biomimetic design approach with a reference to Flectofin (Lienhard et al., 2011), but by adjusting the flapping mechanism into SMP bending deformation, with variations. As proofs-of-concept, 100mm-long models were tested to recalibrate the 3D printing setting for SMP filament in addition to formal factors to be considered. To continuing the study into more complicated geometric models (Yoon, 2019b), a swirl-shaped design was selected for a larger-scale proof-of-concept prototype after considering the simple one-directional reversing mechanism. In the design, the circular disc has flapping wings to have openings by pulling force while being closed by shape memory effect. However, scale of models and constructability of prototypes in building scale were pointed out as problematic. To overcome the issues, the models were resized to demonstrate 3D printing feasibility of SMP.

### 2.2. MANUFACTURING PROTOTYPES

#### 2.2.1. Additive Manufacturing

To evaluate 3D printability and to demonstrate deformation, the only commercially available MM5520 filament with  $T_g$  at 55°C was applied in the first-stage experiments (Yoon, 2019a). The lower  $T_g$  would be more preferred for a climate-adaptive façade in Seoul. Therefore, custom filaments were made by material extrusion of SMP pellets with  $T_g$  at 35°C. Consequently, the 3D printing settings and environmental conditions were recalibrated, while shape deformations and recoveries of models at the  $T_g$  as well as geometric and formal complexity and sizes were tested.

### 2.2.2. Casting

3D printing is considered as not yet ready to be used for large scale manufacturing due to its slow cycle time and the undesirable trade-off between quality and scale (Gao et al., 2015; Zhang et al., 2019). To validate AM in rapid prototyping and to assess better manufacturing method for larger SMP elements, casting was experimented for comparison. SMP models are produced in four steps: (1) mould production, (2) solution preparation, (3) casting, and (4) drying. The SMP consists of resin and hardener, which should be dried for more than 1 hour at less than 50 Torr according to instruction provided by SMP Technologies. Resin and hardener are mixed, stirred for 30 seconds at 60 rpm and potted to the mould. In spite of the recommended 2-hour-curing at 70°C, they were cured for additional 24 hours and dried for 6 days at the room temperature.

## 3. Experiment

### 3.1. DESIGN OF THE PROTOTYPE

#### 3.1.1. Blade

The design process is driven by inspiration from references and intuitive modification to achieve the aesthetically acceptable, but suitable shapes for production and expected deformation. From earlier fabrication studies, it was noted that the thickness along the bending axis would affect deformation ratio, in addition to weakening and damage of the bending axis. However, the influence of curvature in addition to the thickness along the bending axis upon the SMP deformation and response has not been studied as main factors to lead design variations. Therefore, three types were tested as shown in Figure 1. Type 1 is relatively easier to be 3D printed due to its simpler form, but the model is weaker at the bending area due to the thinner surface thickness which is assumed to help bending. Therefore, a spine was added on the opposite side of surface from the bending direction to increase strength in Type 2. In case of Type 3, the curvature in the opposite direction from bending was added to verify the deformation effect.

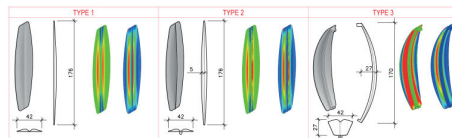


Figure 1. Design Variations with curvature mappings of SMP Folded Blades.

#### 3.1.2. Swirl-shaped Porous Folding

Three porous folding prototypes: (1) lattice, (2) blossom, and (3) swirl were designed for deployable SMP elements (Yoon, 2019b). In programming 3D printed objects from the memorized shape into open position, lattice and blossom models needed more delicate force handling, while the swirl model could be controlled with one central pulling force to deform flaps.



Figure 2. Three design alternatives for deployable elements: (1) lattice; (2) blossom; (3) swirl.

## 3.2. FABRICATION

### 3.2.1. 3D Printing of the Blade Prototype

Due to subtle complexity of curvature and projected spine structures as well as the pliable materiality of SMP, printing directions and support settings were important factors to determine. In the end, the printing paths of Type 2 and 3 were defined, and fabricated in MM5520. Type 2 was made without failure, and bending test demonstrated the expected responses. In the heat test, Type 2 was successfully recovered to the open position after the closing programming. However, Type 3 required longer time to be printed, due to the amount of supports. After the first closing programming, the shape was not recovered to the initial position. This experiment indicates that the curvature in a flexible SMP element works in the unexpected way and should be carefully considered for design. Therefore, for the further experiment to fabricate the model with MM3520, only Type 2 was applied.

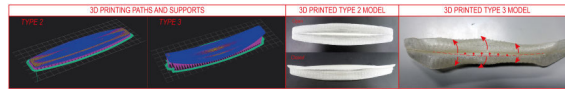


Figure 3. 3D Printing Paths and Outcomes of Type 2 and 3.

Table 1. Primary parameter setting for 3D printing with SMP filaments .

Primary parameter	MM5520	MM3520
Extruder Temperature	215~220 ° C	210 ° C
Bed Plate Temperature	50 ° C	Unheated
Extruding Speed	50 mm/s	50 mm/s
Speed without Extruding	150 mm/s	100 mm/s
Retraction Speed	-	40 mm/s
Retraction Distance	3~10 mm	1.5mm

MM3520 filament requires recalibration of 3D printing parameter settings, as exhibited in Table 1. As shown in the last model in the Figure 4, the Type 2 in MM3520 could be successfully made.

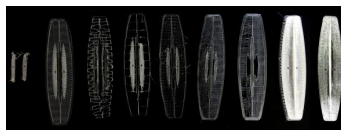


Figure 4. 3D printing results with MM3520 filament and final product.

### 3.2.2. 3D Printing of Swirl-shaped Porous Folding with MM3520 Filament

The swirl-shaped porous folding model was 3D printed in MM3520 filament. Due to sensitivity of the 3D printer to the filament thickness, and strong viscosity of the hot melt SMP, many fabrication tests failed. By handling all the issue during the 3D process by human actions, the swirl-shape model could be produced.

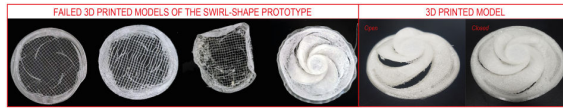


Figure 5. Failure in 3D printing of Swirl-shaped models, and Final 3D printed model.

To enlarge the scale, the model was simply scaled up to 150mm in diameter. The digital model was rechecked and revised to compact and precise geometry with surface attachment points. For a quick examination of 3D printability of the designed shape and size, the model was 3D printed in ABS and TPU. However, in spite of similar properties of TPU and SMP and success in TPU fabrication, SMP couldn't be successfully 3D printed, as in Figure 6. There are several issues to resolve: 1) mounting method of the model to the bed plate; 2) replacement of support materials to other stable plastics and phased 3D printing; and 3) replace of the machine. 10-hour-surveillance on the 3D printer to handle the SMP clog in the nozzle is required for successful 3D printing. Also, the filament thickness, the flow amount of extruded material and printing speed should be optimized to fit for SMP prototype sizes.

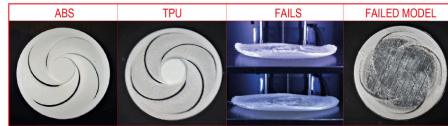


Figure 6. 3D Printed Models of 150mm-long Prototype in ABS, TPU and SMP.

### 3.2.3. Casting of Swirl-shaped Porous Folding with MP3520 Resin

To compare manufacturing processes and outcomes between AM and casting, the same swirl-shape prototype was tested for resin casting. In the first phase of casting, ABS mould was easily made by 3D printing with detailed considerations. However, after casting process, SMP components couldn't be detached from the mould. In the second phase, silicon mould was made by using ABS 3D printed model as the master. Due to the volume of the prototype, the curing time for SMP increased significantly than the expected. As in Figure 8, the complicated geometry with wings was not adequate for casting.

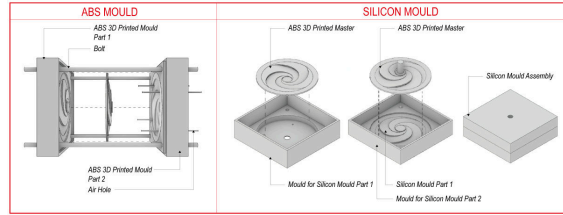


Figure 7. Mould Designs.



Figure 8. Moulds and Casting Results of SMP Prototypes.

### 3.2.4. Comparison of Fabrication Methods

After numerous failures in SMP 3D printing, validity of the method was doubted. To demonstrate the efficacy of SMP AM, two step moulding techniques were tested and compared. As in the early design-to-fabrication research process, rapid prototyping and validation is very critical. To compare the production time, for the tested model, it took 10 hours in 3D printing while it took more than 3 days in casting. Other than production, more complicated equipment and procedures in addition to materials are required for casting. In AM, except for SMP support materials, there is no by-product, while casting needs a master, fillings, and formworks. In a long-term and mass production, casting may be advantageous by reusing masters and formworks. However, it is hinted that the unstable 3D printing supports may be replaced with partial formworks which will combine advantages of two fabrication methods, if the coding method for 3D printing is provided.

## 3.3. MECHANISM

### 3.3.1. Surface-active System

The operational functionality of the responsive façades can be controlled on material level and through design of skin configurations and supporting structure. Meanwhile, reversible reiteration of shape-changing and recovery is the main hurdle for such an installation. In applying the SMP elements for shading elements, simply the surface-active system was assumed in design and tested for digital fabrication. However, from complications which we faced in experiments to scale up the proof-of-concept models, the appropriateness of surface-active system in SMP is doubted. Also, obsession with the aesthetically pleasing outcomes misguided more complicated forms requiring more supports in 3D printing. Therefore, revisiting of the SMP system has led developing SMP elements into actuators for the same device.

3.3.2. Actuator System

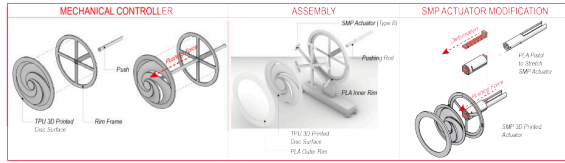


Figure 9. Design of SMP Actuator System.

In designing the simple mechanical device to revert shape changing for the swirl-shaped prototype, SMP actuators were introduced, to make easier 3D printing. To achieve the flexibility and stiffness of shading element surfaces, TPU was applied in thinner thickness than the SMP surface model. For SMP actuators, two different variations were tested in the first stage: (1) Type A - Spiral; (2) Type B - Radial. Each actuator was 3D printed rapidly, without a 3D printing support. However, the advantages of simple planar actuator designs cause fundamental questions on the reason for SMP 3D Printing productions and technology-led design directions. To improve operation and performance of the actuator, the shape was revised to a right-angled spring as the optimum form to be rapidly 3D printed, as in Figure 9. The final assembly clearly exhibits the opening and closing mechanism of the prototype, by the SMP deformation, as in Figure 10.

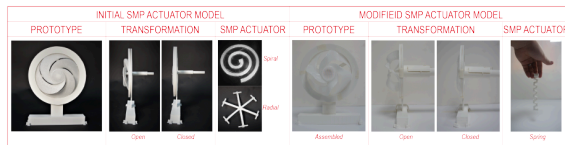


Figure 10. Prototype Model and Variations of SMP Actuators.

4. Results & Discussion

4.1. SHAPE-CHANGING AND REVERSIBILITY OF MM3520 PROTOTYPE

The actuation time for the response from the initial shapes to the programmed shapes was found to range widely based on  $T_g$ , thickness and manner of deformation. The SMP folded blade and swirl-shaped model in MM3520 showed very prompt response, transforming smartly in reaction to the temperature at 35°C. This makes the SMP prototype as convincing to be applied in a climate-adaptive building skin.

However, the reverse programming of shape-changing needs a different solution other than intrinsic behavior of SMP, with the current technological advances. The studied swirl-shaped deployable shading will be rational to have a simple mechanical pushing device with the minimum power demand. In the end, the autonomous system of the responsive building façade mechanism with no power supply such as the two-way SMP or renewable energy system combination

would be desirable in the future. As an alternative way to the two-way SMP, composite materials are worth of challenging to achieve the reversibility and to improve material properties.

The performative and environmental effect of such a shading element should be scrutinized by simulating thermal radiance and daylight as well as by building a mock-up and measure actual data. And comprehensive evaluation of sustainability related to the material, fabrication process and the application should be conditioned to determine our action on the SMP system.

#### 4.2. SELECTION OF FABRICATION METHODS

AM is a powerful process to combine the digital design process with the fabrication and test process, and to responsively provide feedback for improvement of a design. Yet many challenges in this field are to be overcome. One major challenge is the limitations of current equipment to address fundamental 3D printing issues such as avoiding support structures, especially for inaccessible internal structures, simultaneously printing different material groups, the lack of low-cost printable materials, and short printing time (Zhang et al., 2019). When the prototype has a very complicated shape requiring additional supports for 3D printing process, it is neither environment-friendly nor productive to fabricate. Also, in scaling up the 3D printed outcomes, the required time and human attention gets amplified to doubt effectiveness of digital fabrication. Therefore, it needs to be evaluated which fabrication method would be most optimal for a designed prototype by human response to the technological surroundings, or a design prototype shall be revisited to present the compelling fabrication and system. Therefore, it is rational to consider design optimization which can be best suitable for 3D printing without missing the design intention and concept. From our experiments comparing AM and casting in prototyping process, it is obvious that applying 3D printing at the early stage of design and research is a very efficient and cost-saving process in novel material explorations.

#### 4.3. DEVELOPMENT OF ASSEMBLY

To make the full-scale components or an installation, it is necessary to consider the collective assembly of individual SMP components. Differently from the fabrication study of a single SMP prototype, arrangements, assembly methods and principles in addition to forms of all the elements should be considered and designed. This approach is a scale-up process of the fragments without scaling up the fragment sizes. Differently from the fabrication study of single SMP components, design and manufacturing of all the supports and connectors is also critical for the scale-up installation. Joints and connectors are among the most critical components affecting the overall performance of building assemblies and systems (Chun et al., 2018). In our SMP actuator system, the SMP actuator was chemically bonded to the pistol components. However, many of the mechanical failures occur at joints as the stresses, loads, vibrations, and movements tend to concentrate at these locations (Chun et al., 2018). As Gupta et al (2019) fabricated shape-changing structures, to ensure the balance between the limits of forces of SMP and weights of other elements, other members can be considered to be

fabricated from other materials to improve strength-to-weight ratio and achieve various sizes. Furthermore, the simulation could be augmented to include analysis steps considering mechanical properties of the assembly components. But in the end, human-led testing to see if the strength of the SMP elements is adequate to lift other connected parts to act as actuators is inevitable to bring the materialistic and human design approach into the realm of digital design..

## 5. Conclusion

In summary, of the numerous issues to be tackled to evaluate and apply SMP products for the climate-adaptive building façade, this paper focuses on very specific forms and mechanisms to experiment and understand the SMP additive manufacturing. By trial and error, the final assembly, a kit-of-parts comprised of passive plastic elements with the active SMP actuator presented a promising shape-changing behaviour and deploying performance. Although, the early approach to design a form directly inspired from biological creatures or principles helped us to immediately commence hands-on fabrication studies, the human obsession to exhibit the main material and its behavior more visibly misled the investigation into form-findings which apparently caused main issues and failures. However, by rethinking all the issues which we faced throughout the study and revisiting the SMP prototype shape and behaviour, the responsive SMP prototype could be successfully achieved in fabrication, although it is not the most optimal and persuasive form to state the necessity of SMP additive manufacturing. Nevertheless, we have learned that to further develop SMP prototypes, it would be promising to examine composite systems of SMP and other materials as well as to design SMP shapes to inherently prevent additive manufacturing failure. With the bottom-up approach by researchers' human interpretation and actions on the thermo-responsive smart materials, we expect someday the building façade system to be impacted, thus the built-environment to autonomously respond to its changing thermal climate.

## Acknowledgement

This research was supported by the Basic Science Research Program through the National Research Foundation of Korea (NRF) funded by the Ministry of Science, ICT, and Future Planning (NRF-2017R1C1B5015080).

## References

- D.I. Arun, P. Chakravarthy, R. Arochia Kumar and B. Santhosh (eds.): 2018, *Shape Memory Materials*, CRC Press.
- Chang, T.W., Huang, H.Y. and Datta, S.: 2019, Design and fabrication of a responsive carrier component envelope, *Buildings*, 9(84), 1-14.
- Chun, J., Lee, J. and Park, D.: 2018, TOPO-JOINT: Topology Optimization Framework for 3D-Printed Building Joints, *Learning, Adapting and Prototyping, Proceedings of the 23rd International Conference of the Association for Computer-Aided Architectural Design Research in Asia (CAADRIA) 2018*, 205-214.
- Correa, D., Papadopoulou, A., Guberan, C., Jhaveri, N., Reichert, S., Menges, A. and Tibbits, S.: 2015, 3D-Printed Wood: Programming Hygroscopic Material Transformations, *3D Printing and Additive Manufacturing*, 2(3), 106-116.



- Dritsas, S., Vijay, Y., Teo, R., Halim, S., Sanandiya, N. and Ferenandez, J.G.: 2019, Additive manufacturing with natural composites: From material intelligence to informed digital fabrication, *Intelligent \& Informed, Proceedings of the 24th International Conference of the Association for Computer-Aided Architectural Design Research in Asia (CAADRIA) 2019*, 263-272.
- Gao, W., Zhang, Y., Ramanujan, D., Ramani, K., Chen, Y., Williams, C.B., Wang, C.C., Shin, Y.C., Zhang, S. and Zavattieri, P.D.: 2015, The status, challenges, and future of additive manufacturing in engineering, *CAD Computer Aided Design*, **69**, 65-89.
- Ge, Q.i., Sakhaei, A.H., Lee, H., Dunn, C.K., Fang, N.X. and Dunn, M.L.: 2016, Multimaterial 4D Printing with Tailorable Shape Memory Polymers, *Scientific Reports*, **6**(July), 1-11.
- Gupta, S.S., Jayashankar, D.K., Sanandiya, N.D., Ferenandez, J.G. and Tracy, K.: 2019, Prototyping of chitosan-based shape-changing structures, *Intelligent \& Informed, Proceedings of the 24th International Conference of the Association for Computer-Aided Architectural Design Research in Asia (CAADRIA) 2019*, 441-450.
- Kolarevic, B.: 2004, Back to the Future: Performative Architecture, *International Journal of Architectural Computing*, **2**(1), 43-50.
- Lee, A.Y., An, J. and Chua, C.K.: 2017, Two-Way 4D Printing: A Review on the Reversibility of 3D-Printed Shape Memory Materials, *Engineering*, **3**(5), 663-674.
- Lienhard, J., Poppinga, S., Masselter, T., Milwisch, M., Speck, T. and Knippers, J.: 2011, Flectofin: A hingeless flapping mechanism inspired by nature, *Bioinspiration and Biomimetics*, **6**(4), 1-7.
- Loonen, R., Trcka, M., Costola, D. and Hansen, J.L.M.: 2013, Climate adaptive building shells: State-of-the-art and future challenges, *Renewable and Sustainable Energy Reviews*, **25**, 483-493.
- Mitchell, A., Lafont, U., Holynska, M. and Semprimoschnig, C.: 2018, Additive manufacturing — A review of 4D printing and future applications, *Additive Manufacturing*, **24**(October), 606-626.
- Garcia Rosales, C.A., Kim, H., Garcia Duarte, M.F., Chavez, L., Castañeda, M., Tseng, T.L.B. and Lin, Y.: 2019, Characterization of shape memory polymer parts fabricated using material extrusion 3D printing technique, *Rapid Prototyping Journal*, **25**(2), 322-331.
- Thompson, M.K., Moroni, G., Vaneker, T., Fadel, G., Campbell, R.I., Gibson, I., Bernard, A., Schulz, J., Graf, P., Ahuja, B. and Martina, F.: 2016, Design for Additive Manufacturing: Trends, opportunities, considerations, and constraints, *CIRP Annals - Manufacturing Technology*, **65**(2), 737-760.
- Tibbits, S.: 2014, 4D printing: Multi-material shape change, *Architectural Design*, **84**(1), 116-121.
- Tofail, S.A., Koumoulos, E.P., Bandyopadhyay, A., Bose, S., O'Donoghue, L. and Charitidis, C.: 2018, Additive manufacturing: scientific and technological challenges, market uptake and opportunities, *Materials Today*, **21**(1), 22-37.
- Yoon, J.: 2018, Climate-adaptive Facade Design with Smart Materials : Evaluation and Strategies of Thermo-Responsive Smart Material Applications for Building Skins in Seoul, *PLEA 2018 HONG KONG*, 620-626.
- Yoon, J.: 2019a, SMP Prototype Design and Fabrication for Thermo-responsive Facade Elements, *Journal of Facade Design and Engineering*, **7**, 41-61.
- Yoon, J.: 2019b, Additive Manufacturing of SMP for deployable structures, *Proceedings of International Conference on Emerging Technologies In Architectural Design (ICETAD2019)*, Toronto, Canada, 64-71.
- Zhang, Z., Demir, K.G. and Gu, G.X.: 2019, Developments in 4D-printing: a review on current smart materials, technologies, and applications, *International Journal of Smart and Nano Materials*, **10**(3), 205-224.

# DIGITAL ARCHITEXTILES

## *Nonwoven textile thermoforming in robotic fabrication*

JOANN WANG

<sup>1</sup>*Interactive Architecture Laboratory, Department of Architecture,  
National Cheng Kung University, Taiwan*

<sup>1</sup>*joa5130666@gmail.com*

**Abstract.** This paper includes an experimental study of parametric design, which is combined with digital fabrication and weaving techniques for Digital Architextiles. Digital Architextiles is a way of combining circular material of PET (Polyethylene Terephthalate) winding and thermoforming fabrication with robot collaboration for circular economy. In addition, combined with the concept of circular economy, mass customization with tailor-made material can effectively reduce unnecessary waste. Collaborating with parameterized tools, the research work has developed lightweight structures in different winding patterns. Therefore, starting from the exploration of the material system, the paper studies the circular PET material fiber in the digital process assisted by the robot arms, and proposes a circular-based system with high adaptability and freedom, which can be used for the production tool in the multi-stage manufacturing, and to produce a building winding unit responding to various needs in circular economy to various surface shapes.

**Keywords.** PET material of Circular Economy; Parametric Design; Winding Fabrication; Thermoforming Fabrication; Robotic Fabrication.

## 1. Introduction

With the development of material science, design and engineering revolutions, the architecture theoretical proposes the concept of Architextiles, which is in the perspective of textile as a guide to create a new way for the architecture space. The soft material turns to be a stable surface structure by weaving and knitting it, making the architecture gain more properties in surface continuities, lightness, temporary, flexibility and self-structural (Mark Garcia, 2006).

Since the increasing investigating of materials science and robotic fabrication, the advances in winding fabrication has developed lots of studies of CFRP winding in robotic arms. Most work in winding fabrication focuses on producing optimized and repeatable systems. Using the robotic arm to wind CFRP with module frames to explore different types of winding structure, and it would be cured in

a pre-impregnated system with the low temperature controlling instead of using wet-wound CFRP (Wit, Andrew & Kim, Simon, 2016). In addition, the CFRP winding fabrication has also studied into variable fabric formwork, which could reduce waste in the procedure and represents a production method for flexibility in the form, lightness of material, and quick deployment (Xuyou Yang, Paul Loh, & David Leggett, 2017).

With the development of Circular Economy, the paper is focus on nonwoven textile, which is made of PET material of Circular Economy, in replacement of CFRP, which is of higher pollution to the environment to study the digital fabrication. Recent work on digital fabrication in nonwoven textile has explored the needle felting. In the concept of additive manufacturing to lay up materials and create the complex geometric forms, the process is seamless and does not require the addition of thread or adhesives. Then it would be heated in an oven to be cured (Wes Mcgee, Tsz Yan & NgAsa Peller, 2018). However, there are many extensible discussions on the practice of thermoforming in this study. A few research also work on PET panel thermoforming fabrication, change the material property after heating and make the material malleable. Deformed the PET surface with deformer tools to create different sizes and shapes of apertures in controlling the point and depth of deformation, to test the limits and feedback of material, as well as the control of geometric shape (Renate Weissenböck, 2017).

As a result, the objective of this paper is to develop nonwoven textile in winding fabrication with robotic arms and angle changed frames before the thermoforming fabrication in thermal single point incremental forming. With the exploration of surface structural and cumulative heating path, the thermal storage of nonwoven textile is enabling the capacity of working with complex geometric forms. Therefore, this research work is divided into two main parts: "Construction of digital winding pattern" and "Fabrication system of thermoforming" in digital fabrication with robotic arms. The research work is conducted as following:

1. Study the material properties of thermoplastics (PET) : The thermoplastic process will use the high-temperature yarn and the low-temperature yarn made of PET, and the two melting points have different characteristics. At a temperature of about 200 degrees, the effect of only dissolving the low-temperature yarn and retaining the high-temperature yarn fiber is presented. The low temperature yarn is used as an auxiliary filler for the fabric; and the high temperature yarn is reinforced as a structure of the skeleton.
2. Construction of the digital winding pattern : It combines the technology of weaving and the robotic arm fabrication to study the fabric properties in its toughness and multi-dimensional performance.
3. The fabrication system of thermoforming : Based on the development of digital weaving technology, the research investigates the PET material properties and the workflow of thermoforming fabrication. In order to achieve the partial heating press, it takes the advantage of the coding path in robotic arm. Therefore, it can de-molding and reduce unnecessary production waste, and also strengthen the structural strength of the node by heating the PET. The fabrication process is to make PET material heat treated and use the heating press way to reach a malleable state, which behaves like stretchable fabric.

This research includes an experimental study by exploring the formation of design in robotic fabrication workflow, including cyclic PET material and mechanically assisted production processes, as well as parametric programming simulations and physical execution of unit products. In this research, the result has improved the efficiency of using robotic fabrication in architecture construction. The experiment is conducted towards the goal of "One material, One machine".

## 2. Material Performance of PET

In addition, PET, as a common plastic waste in daily life, can be recycled and turned into yarn in fiber state, and then reused into fabric. Through the temperature control, the material can reach two different properties between "fabric" and "plastic". It can be developed for more applications and be turned into valuable circular materials.

Therefore, the project explores the possibility of PET fiber being used for architecture, and studies in digital fabrication by PET non-woven materials.

### 2.1. MATERIALITY

The PET non-woven material used in this project is made of lots of fibers with different melting points. The effect of melting state can be controlled by a temperature of about 200°. As the temperature rises, it will get closer to the material properties of a plastic. As a result, it is possible to achieve the goal of "using a material, but attaining more properties."

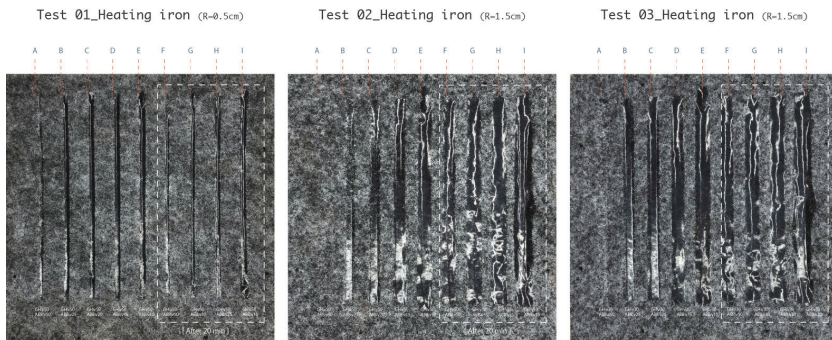


Figure 1. Temperature test of customized heating iron in robotic arm operation.

### 2.2. COMPRESSION AND MOTION PATH

In the existing thermoforming fabrication, the PET material is shaped by the press of mold after it is softened by heat. In response to variable needs of shapes, it costs a lot to make different metal molds. Thus, to avoid the waste of material and to reduce cost, this project promotes the idea of solving these problems by pressing. With the heating motion path in a single point at incremental forming (SPIF), it can produce a variety of shapes without a mold.

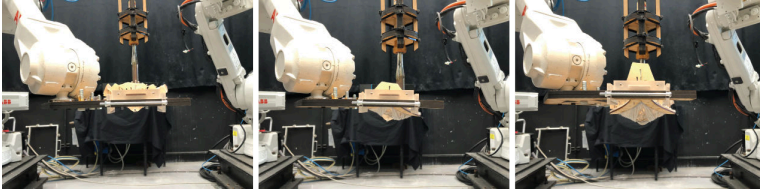


Figure 2. Process of robotic arm force on jig.

### 3. The System of Digital fabrication

With parametric and computational designs, the traditional weaving technique and plastic compression molding can be reinterpreted. Combining winding fabrication and thermoforming fabrication, these two manufacturing methods create variable concave surface units for building skin. The robotic arm used on these fabrication system has the advantage of its 6-axis to achieve higher degrees of freedom in three-dimensional space.

#### 3.1. WINDING FABRICATION

In the overall digital manufacturing system, the winding fabrication is used to study the generation of the mesh surface as a preliminary preparation for the next stage of thermoforming fabrication. By controlling the weaving pattern technology, the researcher uses computational design to parameterize the weaving technique, and then investigates the situation of winding PET fiber and the thickness of material overlapping after operating winding fabrication by a robotic arm. Based on that, it can control the subsequent thermoforming fabrication in hot strength, hot elongation, and the influence of thermal deformation.

In order to improve the accuracy in the execution process and the stability in the winding fabrication, the researcher needs to constantly adjust the component of the end-effector weaver and the diameter of the pipe to avoid the robotic arm from pulling too hard or the angle of the operation being not smooth.

Besides, in the construction method of Bottom-up, the assembly method of the generated units will need to generate winding units of various sizes. Therefore, a set of variable mold system is necessary. By adjusting the angle change of the jig, it can create different width of unit with improved weavers.

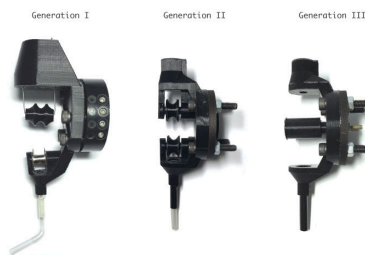


Figure 3. End-effector design of weaver.

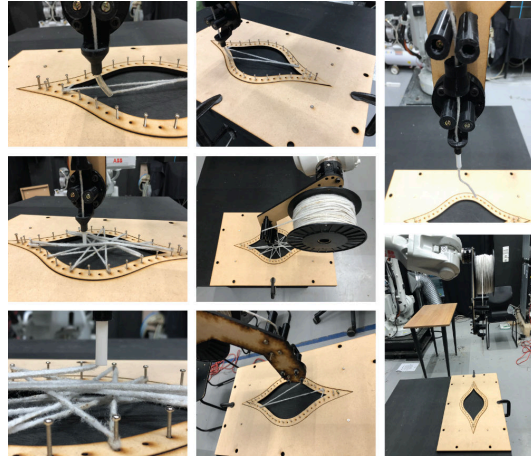


Figure 4. Process of Winding fabrication.

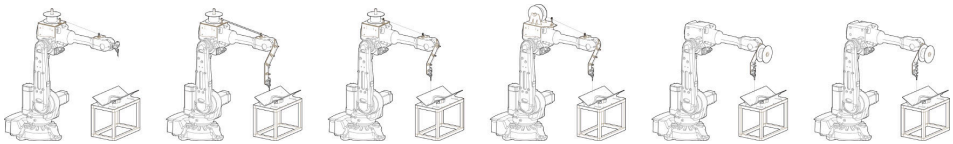


Figure 5. Development of Winding fabrication system.

### 3.2. THERMOFORMING FABRICATION

Since the material studied in this project is PET, the material needs thermoforming fabrication for fixing forming after the winding fabrication, just like the carbon fiber winding fabrication takes epoxy to finalize the shape. In order to achieve the best heat pressing effect and operation method, the project is customized into two sizes of heating iron with a radius of 0.5 cm and 1.5 cm for testing.

In order to solve the problem of material sticking, there are two develop directions. One of them is making the point pattern in motion path, while the other is covering the Teflon paper as the barrier. Finally, the most efficient method is overlapping the Teflon paper on PET surface and heat pressing it.

The variable mold system at this stage explores the design of lightweight and repetitive collocation. After iterative changes, the jig system, which is shared with both fabrication, lightens the weight of jig on end-effector to get operation accuracy. The jig of thermoforming fabrication is easily disassemble and made of wood board. In this way, the jig gets well material toughness to absorb the force from the robotic arm in case of the breakage and damage.

Through the robotic collaboration the researcher can explore the factors to operate the affecting parameters in PET surface forming, including the programming of heating path, temperature control, speed and dwell time, as well as the different combination of angle with moving position in each robotic

arm. In addition, the researcher also tests the environment restriction of robotic arm operation under the interaction mode to avoid the singularity, and takes the collision tests. As a result, the researcher explores the limits of robotic arm flexibility and load to achieve the most efficient operation.

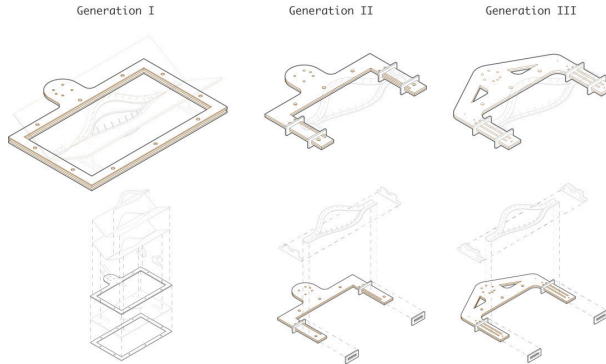


Figure 6. Development of lightweight the jig.

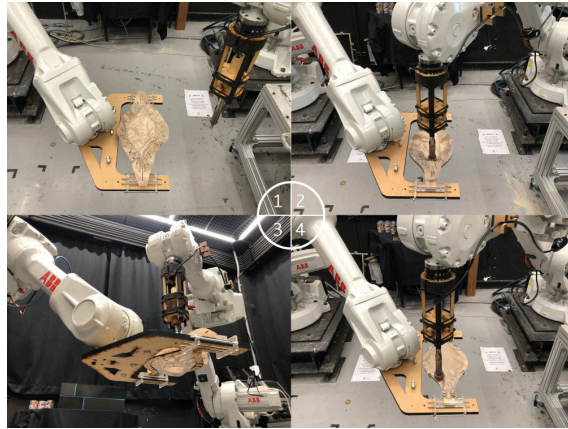


Figure 7. Process of Thermoforming fabrication.

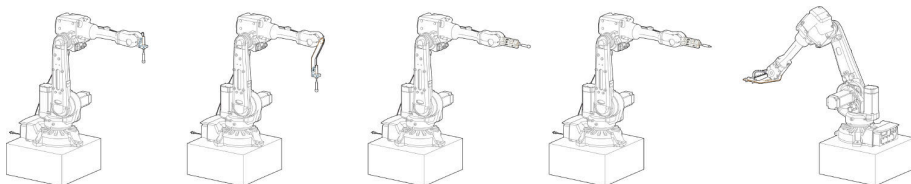


Figure 8. Development of Thermoforming fabrication system.

#### 4. Simulation and Practice

In the programming simulation, the researcher uses TACO, which is a plug-in in Grasshopper, to simulate the motion path of ABB brand robotic arm and adjust the calibration error between software simulation and implementation iteratively, and test the limit values of materials. In the thermoforming path simulation, the attempts and control of different hot-pressure paths are compared.

However, the expecting surface forming would be affected by the following factors: the material superimposed thickness in actual operation, the barrier of Teflon paper reduces the force from the robotic arm, the direction of motion path, the heat strength and heat elongation caused by the temperature, and the material behavior which makes PET surface rebound caused by winding fiber.



Figure 9. Winding PET fiber with robotic arm.

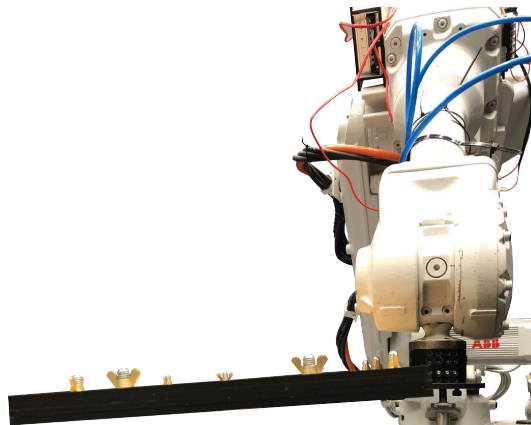


Figure 10. Problem of overweight jig.



#### 4.1. FABRICATION ACCURACY

In response to the demand for compression molding, the surface needs another force response to achieve the effect of compression in addition to using customized heating iron to perform single point incremental forming (SPIF). In view of the winding fabrication method used in the early stage, the structural force caused by the winding mesh surface can generate the rebound force naturally during the robotic arm operation, just as the compressing action. Therefore, the winding pattern is related to the direction of heating path.

In addition, the motion path is also an important affecting factor. In the study we can find that, the initial point of end-effector is the heaviest, and the final point is the lightest during the motion path. As a result, even if the programming of the path is linear, the forces on the two end points of curve will be uneven. Accordingly, the optimal heat pressing path is programmed as a continuous linear, to avoid causing the breakpoints and being raised in midway. Otherwise, the PET surface will be biased to one side, and will also affect the expected forming effect.

The heat storage is also one of the key points. Apart from preventing the material from sticking after contacting the heating source, the Teflon paper can also maintain the thermal storage property of the heating before the PET surface cool down and shape. Additionally, the effect of heat storage is also related to the speed and number of times of the robotic arm manipulation. While the operate speed sets up in v50, increasing the number of motion paths will help to get expected forming. Different from the expected, increasing the temperature and speeding up during the operation will lead to PET surface break and get the material into limit. However, taking a slow and repetitive operation speed with the temperature of about 180 ~ 190 °C, and increasing the force on it will be able to get a better heat elongation and achieve a more stable state.

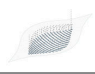




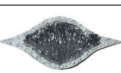


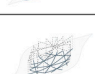
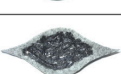
Type	Path Coding	Radius of the iron rod	Temperature	Speed		Physical Model
				GH	ABB	
Type-A Parallel movement-I		r: 1.5cm	180°C	v50	Twice:v50	
Type-B Parallel movement-II		r: 0.5cm	180°C	v50	Twice:v50	
Type-C Parallel variable movement		r: 1.5cm	190°C	v50	Once:v50 Once:v25	
Type-D Spiral		r: 1.5cm	190°C	v50	Twice:v50	
Type-E Pattern		r: 1.5cm	190°C	v50	Twice:v50	

Figure 11. Test record of thermoforming fabrication.

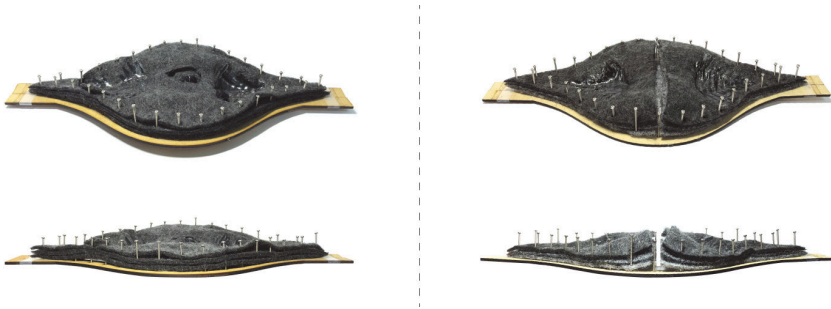


Figure 12. Comparison of whole nonwoven and cutted nonwoven in thermoforming.

#### 4.2. SURFACE AND STRUCTURE

In the assembly and distribution of the units, each unit is made of winding PET fiber combined with broadside in heat pressing. The broadside is also made of PET non-woven, as a component to connect other units. In the composition of units, it takes hard PET board as structure of bottom foundation. It defines the material properties between softness and hardness, which tends to be fabric or plastic, surface or structure, by temperature control and thermoforming pressing. And it makes the PET mesh surface integrate with PET hardboard by heat pressing, and strengthens a unit's unity, which further shows that "getting more properties that are exhibited by one material".



Figure 13. Production of PET nonwoven thermoforming.

#### 5. Conclusion

With the development of material innovation, improving the existing fabrication in AEC industry advances the Circular Economy. The setup of adaptive machines, such as robotic arms, combining with parametric design will increase the productivity of Mass Customization. The project suggests that the digital

fabrication of circular material PET be a novel manufacturing technique.

In addition, the nonwoven textile takes a certain proportion of existing textile market. It is necessary to explore the application of it. Research on PET thermoforming fabrication will help to explore the topic of "partial-integration," which reduces the amount of excess material waste and the number of joined parts when the material can be controlled with temperature. Either the impact on environment or the optimization of the surface shape can improve the efficiency of the assembly in the construction, and replace the existing splicing method of the minimize planar units. The fabrication studies also proposes a set of system of variable molds to reduce the development of specific molds, and to respond to the generation of multi-forms in a path-based operation mode.

In this research, by controlling the behavior of the material, the characteristics of the material can be changed. By winding the material before the heating, it can enhance the extensibility of the material and avoid the cracking of the curved surface. The maintenance of heat storage determines the degree of adhesion between the materials and the control of the surface. The future work will focus on exploration of scale in thermoforming fabrication. In order to achieve the properties of material consistency and overall stability, the author suggests using the winding and thermoforming way as the connecting methods between materials. Further testing will include the thickness of material layup and limits of materials' heat elongation.

### **Acknowledgement**

The author would like to thank her thesis advisor Dr. Taysheng Jeng for his helpful advice and comments, MiniWiz company for support of PET material and techniques, and IDF YunTech for assistance of ABB brand robotic arms.

### **References**

- Garcia, M.: 2006, Architecture + Textiles = Architextiles, *Architectural Design*, **76**, 5-11.
- Mcgee, W.e.s., Yan, T.s.z. and Peller, N.: 2018, Hard+Soft: Robotic Needle Felting for Nonwoven Textiles, *ROBARCH 2018*, Zurich, 192-204.
- Weissenböck, R.: 2017, ROBOTRACK - Linking manual and robotic design processes by motion-tracking, *eCAADe 2017*, Rome, Italy, 651-660.
- Wit, A. and Kim, S.: 2016, rolyPOLY - A Hybrid Prototype for Digital Techniques and Analog Craft in Architecture, *eCAADe 2016*, Oulu, 631-638.
- Yang, X., Loh, P. and Leggett, D.: 2017, Robotic Variable Fabric Formwork, *CAADRIA 2017*, China, 873-882.

# KNITTED COMPOSITES TOWER

## *Design Research for Knitted Fabric Reinforced Composites Based on Advanced Knitting Technology*

YIGE LIU<sup>1</sup>, HUA CHAI<sup>2</sup> and PHILIP F. YUAN\*<sup>3</sup>  
<sup>1,2,3</sup> *Tongji University*  
<sup>1,2,3</sup> {yige.liu|chaihua|philipyuan007}@tongji.edu.cn

**Abstract.** Faced with growing urbanization demands of developing countries and global shortages of construction materials, this research looks for an innovative light-weight high-performance material system for architectural applications. The knitted composites tower is a 7.2-meter, 260-kilogram and self-supported prototype that uses 2mm thick knitted fabric reinforced composites. The result is lightweight and strong. It demonstrates the design potentials of knitted fabric reinforced composites. This article takes knitted composites tower as an example to illustrate a design method for knitted fabric reinforced composites. The design method covers three aspects of structural form selection, structure arrangement, and microscopic configuration. At last, the complete fabrication and construction process will be discussed with a full-scale physical prototype.

**Keywords.** Knitting; Composites; Architectural Design.

### 1. Introduction

Faced with growing urbanization demands of developing countries and global shortages of construction materials, this research looks for an innovative light-weight high-performance material system for architectural applications. We test knitted fabric reinforced composites material using advanced knitting technology and set up related design methods.

Flat knitting is highly potential for creating light-weight and high-performance structures. Flat knitting allows complex properties and details to be integrated into one single piece of fabric using a minimum amount of materials, it also allows flexible material manipulations in response to complex structural and environmental conditions. Moreover, flat knitting allows high-speed and low-cost mass customization, which is crucial for architectural production. And when combined with polymers, textiles can become structural.

Numerous researches have been carried out to explore the design potentials of knitting. Advanced flat knitting machines and related computer-aided design systems have enabled designers to custom architectural products with flexible definitions of reinforcement, porosity, density, yarn combinations, joints, etc.

(Thomsen et al. 2016, Sabin 2013, Ahlquist 2015). Knitted textiles have been integrated with pneumatic or bending-active elements to become light-weight hybrid structures (Thomsen et al. 2015, La Magna et al. 2018, Ahlquist et al. 2013, Ahlquist et al. 2017), or with functional elements for lighting, heating, sensing, monitoring, etc. (Dias 2015). Automatic knitting information generation methods (Wu et al. 2019, Popescu et al. 2017, Narayanan et al. 2018, Liu et al. 2019) have enabled designers to customize 3D fabrics with complex geometry.

## 2. Design Method

This article takes a knitted composites tower as an example and proposes a design method for knitted fabric reinforced composites to give full play to the advantages of the material. The design method proposed by this article covers three aspects, including structural form selection, structural arrangement, and microscopic configuration. Structural form selection searches for an appropriate structural form for the material system. Structural arrangement establishes distribution patterns of structural elements, such as fabric patches, reinforcements, holes, and connections. Microscopic configuration generates distribution patterns of knitting stitches and stitches' internal structures.

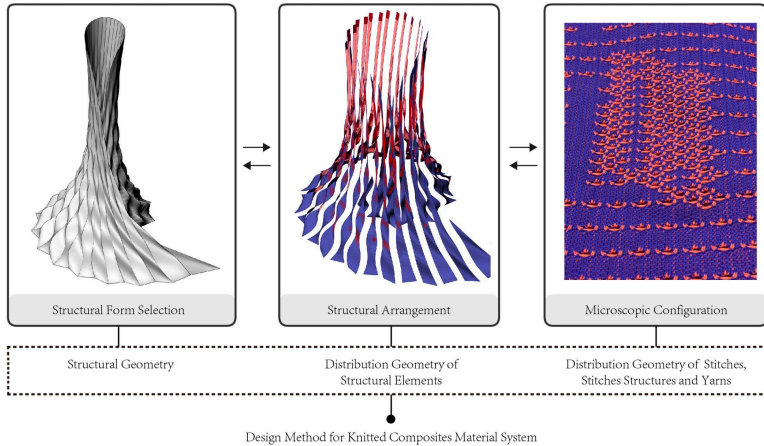


Figure 1. The design method covers three aspects of structural form selection, structure arrangement, and microscopic configuration.

### 2.1. STRUCTURAL FORM SELECTION

In structural form selection, major challenges are, first, knitted composites tower belongs to fabric-formed shells, so its structural form should allow uncured fabrics to get balanced under weight loads, second, knitted composites material is only 2-3mm thick, but is required to support a 7-meter tower. In response to those challenges, knitted composites tower uses a spiral anticlastic surface as the basic geometry since anticlastic surfaces are very common equilibrium forms in membrane structures. Furthermore, creases are introduced to help increase

structural effective thickness as well as stability.

The final surface of the tower is controlled by a series of horizontal spirals and 36 vertical crease curves. The wavy surface is created by lofting the crease curves in pairs. Geometry variables of the structural surface include spirals' diameter, creases' depth and creases' quantity. To determine the parameters of those variables, we used finite element analysis plug-in Karamba3D (Preisinger 2013) to compare the performance of structural forms with different surface curvature, diameters and crease modes. Elastic energy, max displacement and max Von Mises stress are major indicators for evaluation. Elastic energy reflects overall stability, max displacement and max Von Mises stress illustrate local stability. And the smaller the values are, the more stable is the structure. The analysis result shows that better structural stability can be achieved when diameters of horizontal spirals are in a linear relationship, or the diameter of top or bottom becomes smaller. Moreover, increased crease depth enhances local stability, smoother upper parts of creases enhance overall stability. At last, it should be noted that, though structural performance is the most important criteria for choosing a good structural form for knitted composites, the final result is not necessarily of the best structural performance, instead, it is a balanced result, which has a relatively good structural performance while balancing all other criteria, such as fabrication time, spatial perception and aesthetic preferences.

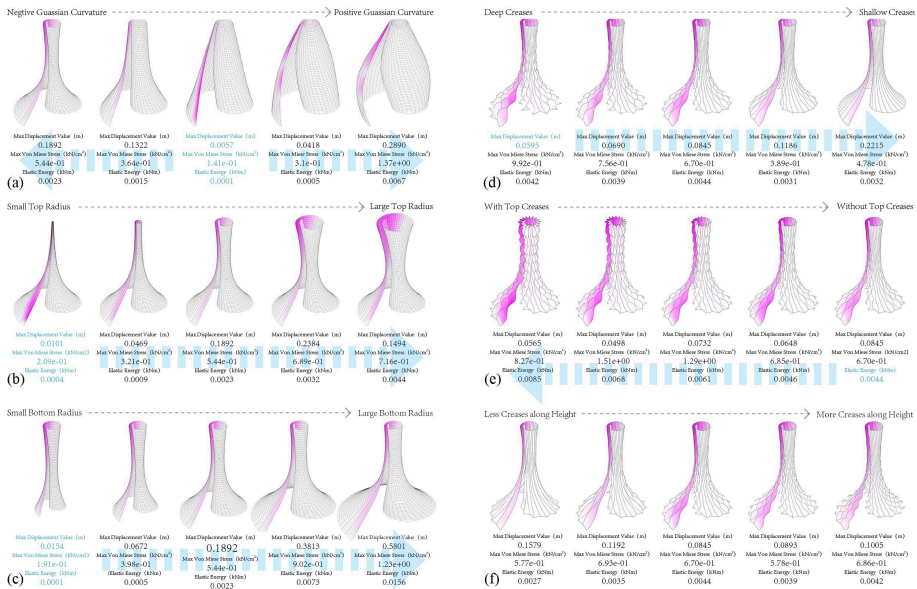


Figure 2. The structure is more stable when diameters of horizontal spirals are in a linear relationship (a), or the top (b) or the bottom(c) is small. Increased crease depth reduces local displacement (d), smoother upper parts of creases increase overall stability (e), quantity of creases doesn't show clear influence over structural performance.

## 2.2. STRUCTURAL ARRANGEMENT

Structural arrangement determines distribution patterns of fabric patches, connections, reinforcements and porosity. Major challenges in structural arrangement include, how to divide the structural surface into fabric patches that are beneficial to structural performance, knitting process as well as construction convenience, how to appropriately extract stress concentrated area or material redundant area from the structural surface to add reinforcements or porosity.

In the tower project, the seams of fabric patches follow longitude crease curves. In this manner, we can fully take advantage of automatic knitting machines, and make fabric patches as large as possible, eliminating unnecessary connections. Besides, this division pattern enables the geometry of each fabric to be easily controlled by inserting curved steel plates along its two edges. Moreover, arranging seams in a vertical direction is beneficial to enhance structural stability against weight load, since seams have a greater stiffness than other parts of the fabric. Finally, the structural surface of the tower is divided into 35 pieces of fabric. The quantity makes sure that the width of each fabric is within the width limitation of a knitting bed, yet still making the most use of it.

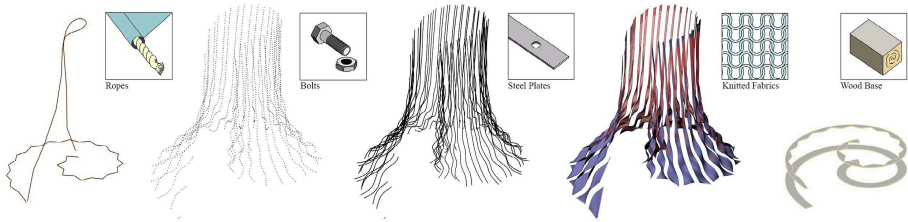


Figure 3. Major structural elements of the knitted composites tower.

The distribution patterns of holes and reinforcement are informed by stress conditions within the structural surface. We used Millipede (Michalatos and Kaijima 2014) plug-in and its built-in topology optimization algorithm. The algorithm reduces material mass to a prescribed percentage and shows the stressful area in a thickness map after optimization. Following this thickness diagram, we can easily extract less stressful area from the structural surface and adjust local porosity according to thickness value. With increased porosity, local polymer materials are reduced in the related area. Moreover, we used a deformation analysis model generated by Karamba3D (Preisinger 2013) to inform the distribution of reinforcement. At places that tend to show obvious deformation, such as free edges, holes are removed and an extra rope is added to increase local thickness and fiber content.

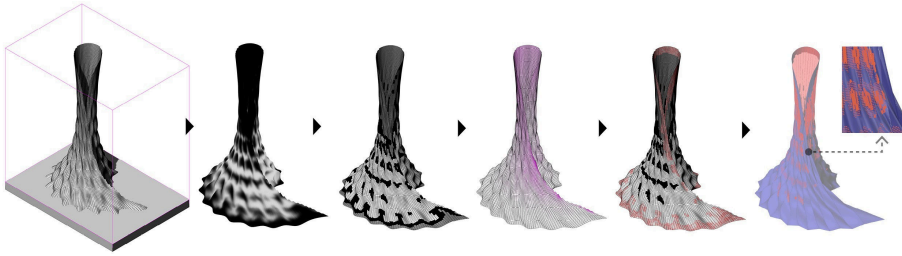


Figure 4. Distribution of porosity over the structure is informed by stress distribution within the structure.

### 2.3. MICROSCOPIC CONFIGURATION

Microscopic configuration discusses distribution patterns of stitches over fabrics, stitches' internal structures and choices of yarns. Challenges in designing the microscopic configuration of knitted composites structures lie in three aspects. First, how to generate a stitch distribution pattern that not only responds to the 3D geometry, pattern and connection details of a fabric but also obeys knitting logic, since a stitch is a fabrication unit of a fabric? Second, how to determine the combination of stitch structures? Third, how to evaluate yarn choices?

To generate a stitch distribution pattern, we developed a program in Grasshopper (Rutten 2019). Each fabric model with bespoke shape, pattern and connection details can be automatically translated into a stitch model. The inputs of the program include a fabric surface, models of patterns and details and stitch size parameters. The output of the program is a multi-color bitmap containing stitch distribution data and stitch structure data. The bitmap can be directly used for production.

The generation process of stitch information includes flattening, defining patterns and details, defining stitch structures, rasterization, knittability optimization, translation into machine actions and non-uniform scale. Compared with computing stitch distribution directly on 3D surfaces, flattening simplifies calculations, which is beneficial for large fabrics with millions of stitches. After flattening, an automatic rotation is made to make sure the maximum width of a flattened surface is within the width limitation of a knitting machine. Then, patterns and details are represented as lines and dots, they are created either by unfolding models from 3D or by drawing directly on the flattened surface. Colors are also added to define different stitch structures. To get the exact location of each stitch over the surface, rasterization is carried out. During rasterization, each stitch is represented as a rectangle, whose width and height are identical to the input stitch size parameter. To make the stitch distribution pattern knittable, the program optimizes the layout of stitches to make sure that each knitting row can be smoothly connected with its next row, and all stitches can be linked by a continuous zigzag curve, which represents the knitting path. Finally, the program translates stitch structures into symbols of machine actions and uses a non-uniform scale to transform stitch drawings into a knitting diagram. In the knitting diagram, each



pixel represents a stitch, each color represents a series of machine actions. In knitted composites tower, each fabric is translated into a 18-color bitmap. The bitmaps can be directly imported to Stoll's M1 plus Software and production can begin soon after defining machine actions for each color and adding a cast-on template.

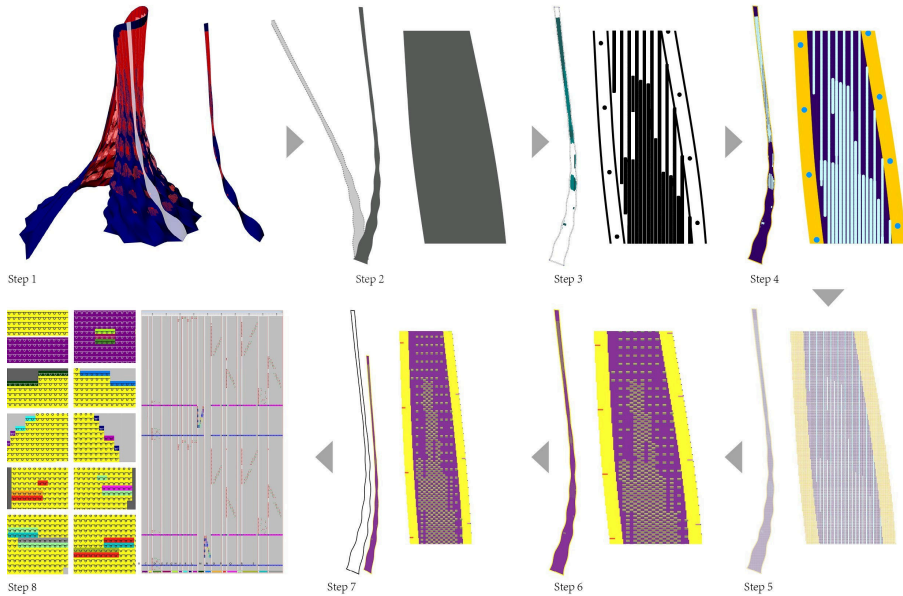


Figure 5. Generation steps of stitch information include flattening(step 2), defining patterns and details(step 3), defining stitch structures(step 4), rasterization and knittability optimization(step 5), translation into machine actions(step 6) and non-uniform scale(step 7).

The combination of stitch structures is determined by designers and technicians together according to required effect, details, knitting constraints and performance. A double-sided tuck structure is chosen as the major stitch structure for the tower project. This type of stitch structure can achieve the effect of red and blue on each fabric side, it also allows arbitrary connection status of a fabric's two sides in one knitting row. The two sides can be either interlocked or separated at random places, and when they are separated, a hollow sleeve is created, allowing for inserting steel plates or reinforcing ropes. In addition, we also introduced lace structure to form lace holes, and increase, decrease, cast-on, cast-off stitches to shape irregular contours of fabrics, openings and bolt holes.

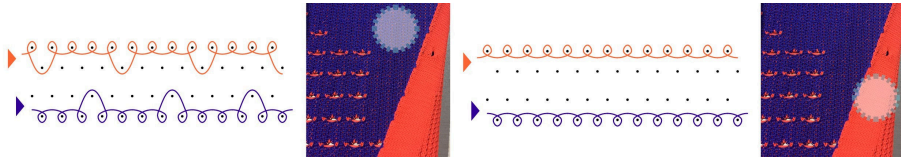


Figure 6. Major stitch structures for the knitted composites tower.

To find an appropriate type of yarn, we compared engineering yarns and common yarns. Engineering yarns, such as yarns made of carbon fiber, glass fiber, aramid fiber, are of high modulus, but very few of them are flexible enough for knitting, especially when required stitch structures are complicated. Moreover, engineering yarns often have limited choices of thickness and color. Compared with engineering yarns, polyester yarns offer a wider range of colors and thickness, but tests have to be made to prove their structural capability for this project. Our tests follow Chinese national standards GBT1447-2005 for testing the tensile performance of fiber-reinforced polymer composites. Given material mechanical properties and estimated weight, we evaluated the deformation status of the structure and concluded that polyester yarns were sufficient for the tower project. The choice of polyester yarn is also affected by the issue that knitted fabrics may become darker when saturated with polymers. Such a problem can be solved by using yarns with fluorescent colors since they can maintain brightness when immersed in polymers. However, such color cannot be found in engineering yarns.

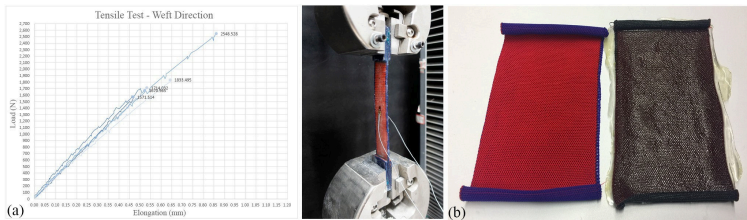


Figure 7. Tensile tests for knitted composites(a), and the color of knitted fabrics(c) get dark when saturated with polymers.

### 3. Fabrication and Assembly

In the tower project, we used four Stoll CMS 502HP automatic knitting machines to fabricate 35 pieces of fabric. There are over 200,000 knitting rows in total and the knitting time is more than 137 hours excluding time spent on tests and errors. For each piece of fabric, knitting time varies from 50 minutes to 5 hours, depending on the size of the fabric and the complexity of the craft. Wooden base, wooden top panel and steel plates are cut by CNC machines. Grooves are left on wooden panels for positioning steel plates, holes are drilled on steel plates for connection.

The 3D geometry of the fabric is controlled by steel plates, therefore positioning the steel plates becomes the key aspect of positioning the tower. One

centimeter wide steel plates were first inserted into the sleeves on fabrics' edges. Both steel plates and edge sleeves have pre-set bolt holes, so that neighboring fabrics can be connected by fastening bolts through adjacent steel plates and fabric sleeves. After connecting neighboring fabrics, upper ends of steel plates are tied to top panels using 3mm steel cables with predefined lengths. Then, top panels are raised to the top of scaffolds and the whole structure is suspended from top panels. After fixing the bottom of steel plates and fabrics to the grooves on base panels, the structure is ready for adding polymers.

We used EL2 laminate epoxy from Easy Composites and took one kilogram as an operation unit. Since the interior of the tower is not wide enough to put a scaffold, epoxy is mainly used on the outside of the tower, except for areas within reach of students and workers. The application of polymer materials takes two times for the tower. However, we find that multiple applications of epoxy results in glue stains and uneven gloss on the surface. In response to this issue, we used matte varnish on the surface to reduce unwanted luster.

#### 4. Result and Discussions

The final knitted composites tower is 7.2 meters high, 260 kilograms and is self-supported. The effective structure is achieved by using a small amount of material compared with conventional structures. This light-weight and high-performance tower pushes the limit of knitted composites and demonstrates the design potential of the material.



Figure 8. Perspective(a) and interior detail(b) of the tower.

The major limitation of this research lies in the issue of wrinkles. Wrinkles are caused by the following reasons: 1. Steel plates are slender and easy to deform even though its two ends are fixed. Extra position points in the middle should be added, however, during construction, positioning points for the middle are not sufficient and accurate, so the actual shape of steel plates are not identical as the design model. 2. During generating knitting information, a uniform stitch size parameter input is used. However, stitch sizes of different stitch structures are different, such as the stitch size of lace holes is larger than that of plain stitches. It causes the calculated number of stitches to exceed actual demands, and redundant stitches result in wrinkles. 3. The equilibrium form of a fabric-formed structure is also affected by internal force distribution. To further control the realization of structural form, the design process should consider a method to accurately control the distribution of force within the structure. 4. The structure surface is simply suspended rather than properly tensioned, so the fabric don't have enough inherent stress as well as stiffness. As a result, the weight of epoxy can easily lead to deformations of fabric, causing more wrinkles.

In the future, the design method for knitted composites will be further improved. We look forward to integrating form-finding and tension force control with current methods. Future improvements on stitch placement generation will focus on robust computation methods to generate stitch information directly from large-scale 3D surfaces, to allow multiple stitch size inputs and alignment with principal force fields.

### Acknowledgment

The knitted composites tower was developed by Yige Liu, Hua Chai, Jia Hu, Ailing Zhang, Yiwei Zhang, Qi Chen from Group 12 led by Prof. Philip F. Yuan during 2019 DigitalFUTURES Summer School. Knitting process was done in collaboration with Stoll, Chemax Industrial Co., Ltd. and Zheng Xing Yuan Knitting Garment Co., Ltd.

### References

- Ahlquist, S., Lienhard, J., Knippers, J. and Menges, A.: 2013, Exploring Materials Reciprocities for Textile-Hybrid Systems as Spatial Structures, *Prototyping Architecture*, 187-210.
- Ahlquist, S., McGee, W. and Sharmin, S.: 2017, PneumaKnit: Actuated Architectures Through Wale-and Course-Wise Tubular Knit-Constrained Pneumatic Systems, *Proceedings of ACADIA 2017*, Cambridge, 38-51.
- Dias, T.: 2015, *Electronic Textiles: Smart Fabrics and Wearable Technology*, Elsevier Science.
- Liu, Y., Li, L. and Yuan, P.F.: 2019, A Computational Approach for Knitting 3D Composites Preforms, *Proceedings of The International Conference on Computational Design and Robotic Fabrication*, 232-246.
- La Magna, R., Fragkia, V., Längst, P., Lienhard, J., Noël, R., Šinke Baranovskaya, Y., Tamke, M. and Thomsen, M.R.: 2018, Isoropia: an Encompassing Approach for the Design, Analysis and Form-Finding of Bending-Active Textile Hybrids, *Proceedings of IASS Annual Symposia*, 1-8.
- Michalatos, P. and Kajjima, S.: 2014, "Millipede". Available from <<http://sawapan.eu/>>.
- Narayanan, V., Albaugh, L., Hodgins, J., Coros, S. and McCann, J.: 2018, Automatic Machine Knitting of 3D Meshes, *ACM Transactions on Graphics (TOG)*, **37(3)**, 35.

- Popescu, M., Rippmann, M., Van Mele, T. and Block, P.: 2017, Automated Generation of Knit Patterns for Non-developable Surfaces, *Humanizing Digital Reality - Design Modelling Symposium*, 271-284.
- Preisinger, C.: 2013, Linking structure and parametric geometry, *Architectural Design*, **83(2)**, 110-113.
- Rutten, D.: 2019, "Grasshopper". Available from <<http://www.rhino3d.com>>.
- Sabin, J.E.: 2013, myThread Pavilion: Generative Fabrication in Knitting Processes, *Proceedings of ACADIA 2013*, Cambridge, 347-354.
- Thomsen, M.R., Tamke, M., Deleuran, A.H., Tinning, I.K.F., Evers, H.L., Gengnagel, C. and Schmeck, M.: 2015, Hybrid tower, designing soft structures, *Modelling behaviour*, 87-99.
- Thomsen, M.R., Tamke, M., Karmon, A., Underwood, J., Gengnagel, C., Stranghoner, N. and Uhlemann, J.: 2016, Knit as bespoke material practice for architecture, *Proceedings of ACADIA 2016*, Ann Arbor, 280-289.

# MANAGING RISK IN A RESEARCH-BASED PRACTICE AS PROJECTS SCALE TO CONSTRUCTION:

*A Case Study*

STAN CARROLL

<sup>1</sup>*Tongji University, Digital Futures PhD Program, Shanghai, China*

<sup>1</sup>*scarroll@beyondmetal.com*

**Abstract.** Research-based architectural practices often experiment along the bleeding edge of the new frontier of design and include developing methodologies unfamiliar to the construction industry. Successfully implementing the resulting research methodologies to an architectural scale requires careful consideration of risk management within a Design-Bid-Build construction project. How a firm manages the risk when scaling a research conclusion to an architectural scale is an essential aspect of assuring the success of the project. These considerations are particularly acute within firms whose research involves convoluted geometry. In the field of doubly-curved geometric material systems, the level of precision required to manage professional risk is commensurate with the level of geometric complexity. Adopting the mindset of a Medieval master mason's process within the context of twenty-first-century materials and processes can be a method toward a successful project. By performing well thought-out transfer procedures of digital data, resolving the fundamental challenges of fabrication, and including structural analysis as a part of the early design phases, experimental architectural expressions can be realized without extra financial risk to the designer.

**Keywords.** Risk Management; Research-Based Practice; Complex Geometry; Digital Fabrication; Computational Design.

## 1. Risk Management

Construction projects contain many risks to stakeholders that require careful management throughout the design and construction process. Designers, engineers, contractors, financiers, public regulatory bodies, and clients all assume various significant risks throughout the development of a project. Each party involved must take responsibility for identifying and managing their specific exposure as defined by the project's scope and conditions. Typical risks include broad range issues spanning from public health and safety to financial aspects. The primary considerations in determining one's risk require careful consideration of exposure, capability, responsibility, and power. The scope of this case study is

limited to the financial threats designers assume when designing untried building elements or utilizing unconventional construction methods.

Financial risk can be effectively managed if the designer adopts a mindset from the past to engage structural analysis earlier, resolve fabrication challenges during the design phase, and devise a well-reasoned transfer of digital data. This paper establishes the context for three specific areas of financial risk management germane to scaling design research findings to an architectural scale through the involvement of outside contracted constructors. Finally, each of the three risk management strategies are discussed related to a case study project recently completed for a war hero memorial located in Texas.

There has been extensive writing on evaluating risk within the domain of conventional construction and include consideration of aspects regarding exposure, capability, responsibility, and power. Project risk assessment, analysis, and monitoring can be evaluated by answering four questions recommended by The American Institute of Architects: “What is the exposure inherent in this duty? Who is most capable of handling that exposure? Who has responsibility for that exposure? Who has the power to make sure that the responsibility is carried out?” (The AIA Trust, 2019).

Research-based architectural practices assume additional financial liability as they experiment along the bleeding edge of the new frontier of design and include developing methodologies unfamiliar to the construction industry. How a firm addresses these additional financial liabilities when scaling a research advancement to the larger architectural scale is an essential aspect of assuring the success of the project. These considerations are particularly acute within firms whose research involves convoluted geometry. In the field of novel doubly-curved geometric material systems, the level of precision required to manage professional risk is commensurate with the level of geometric complexity.

During architectural research, the investigation is often performed within complete control of the firm’s management and at low economic risk due to the small experimental scale of a research pavilion or mock-up. To upsize a research ambition to an architectural scale, often the engineering, fabrication, and a portion of the economic risk of the work are transferred to an outside engineer or general contractor. Transferring that risk to the engineer or contractor requires careful attention by the designer in order to avoid unnecessary cost escalation.

The primary strategy an architect can use to manage risk is to limit the engineer’s and contractor’s effort by clearly defining the division of work between the architect, engineer, and contractor. Engineering costs can be minimized by limiting the engineer’s effort to only confirming the viability of a solution the designer has proven works, rather than engineering several iterations of an unproven idea. The contractor’s effort can be minimized by limiting their work to only pre-proven construction methods. Performing exhaustive, comprehensive coordination with the contractor’s digital and physical workflow, resolving fabrication methodologies, and performing quantitative structural analysis are traditionally outside the architect’s purview. However, assuming responsibility for these aspects is critical to effectively managing financial risks when scaling research findings to an architectural scale. The primary instruments used to

successfully control risk management are precise and succinct digital 3D files derived through practical, hands-on prototyping and structural finite element analysis. By taking a proactive position in these aspects, the designer's financial exposure can be reduced. This paper is a case study in defining an effective risk management strategy for a material system involving a tessellated complex doubly-curved global form.

### 1.1. RISK BY PHASE AND TYPE

The overarching financial dangers for the designer are associated throughout the entire project. Through centuries of general contractor built projects, the design process has evolved based on finding a successful balance between design quality and financial liability. Research-based design processes amplify the need to follow a finer-grained risk management approach. The level of the designer's risk can be minimized by promptly resolving the various issues within the appropriate phase of the project. The primary disciplines of the contracted procurement process particularly vulnerable to financial risks within the case study project feature wall were structural engineering and fabrication. Both aspects required the process to be broadened beyond the typical designer's role to resolve the challenges posed to these disciplines.

### 1.2. MASTER MASONS

An experimental research-based architect must develop a master mason's mindset. From the medieval period of architecture, master masons are considered the precursor of the architect. According to Coldstream, "Unlike a modern architect, whose main job is to provide drawings, the master mason was also the structural engineer and building contractor...he became a master, not through academic study, but by training within the building industry" (2002, p. 97). Master masons were experimental multidisciplinary technically knowledgeable experts at the cutting edge of construction during the medieval period whose most notable mark on the profession was the stone masonry vault (Rossi, 2012). Stone masonry vaults were quite risky from a structural perspective, extremely challenging from a constructor's perspective, and "who directly calculated constructional methods according to their practical needs" (Feher et al, 2019). As Foyle noted, "Medieval master-masons conceived buildings according to resolved structural geometries that depended on firm control of the constituent parts" (Foyle, 2006). Master masons historically oversaw the roles of design, structural engineering, geometric detailing, and fabrication (see Figure 1) (Irwin, 2019).





Figure 1. Medieval stone vault, Notre Dame Cathedral.

### 1.3. DESIGN RISKS

Financial risk management is most effective if applied throughout every phase of the project and across several of the associated disciplines. Maintaining control of outside consultants' fees and fabrication costs is an essential tactic in minimizing the designer's financial exposure. Addressing the various pitfalls throughout the process will prove to be the most efficient method as compared to addressing risk only at a singular moment in the project. Addressing potential financial hazards during the design phase involves finding efficient methods to quickly and effectively study form, understand structural performance, overcome fabrication challenges, and define project communication protocols.

## 2. The Case Study Project

In a research based architectural practice, working with complex geometry exposes the designer to higher levels of risk than a conventional construction project. Below is a project case study constructed from a research-based material system which exposed a high level of financial risk to the designer. Below is a detailed description of how the designer addressed each of the three primary risk exposures involved in the project: Data Production and Transfer, Structural Analysis, Fabrication Process Definition.

### 2.1. THE CASE STUDY WALL

A doubly curved wall made of 12-gauge sheet metal acts as the project's focal point, as well as the primary focus of this case study. The ship hull shaped wall is 140 feet long, seventeen feet tall at the bow, and four feet tall at the stern. The global geometric form of the wall is a doubly curved, tapered torus patch shape. The torus continually varies in radius along both its toroidal and its poloidal directions. (see Figure 2)



Figure 2. Doris Miller Memorial, Waco, Texas.

The wall is a material system assembly constructed entirely of stainless steel sheet metal approximately 0.1” thick. The wall tectonics is a tessellation of 258 modules, forty-three modules long, and six modules high. The continuous dimensional variation of the modules along the entire length and height of the wall is responsible for producing the tapering of the torus shape. The part configuration is solely responsible for producing the necessary structural stiffness and was required to withstand a 100 mile per hour wind force. There is no internal structure. The wall is fabricated from over 1,500 unique parts and fastened together with over 9,000 bolts requiring precise placement of over 30,000 bolt holes. Each unique laser-cut part was precisely bent to create a flange-to-face bolted connection to its adjacent neighbor. A parametric algorithm was built in McNeel’s Rhino/Grasshopper capable of generating infinite variations of geometric solutions for every plate and bolt hole within a few quick computer mouse clicks.

## 2.2. GENERAL

The designer employed three imperative processes to control financial risks during the design process. Procedures were developed to improve how data was produced and transferred to the engineer and the fabricator, how structural decisions were made in the early design process, and how realistic fabrication configurations were confirmed. Below is a summary of the details of each of the procedures used during this project.

### 2.3. DATA PRODUCTION AND TRANSFER

During a complex geometric project such as this one, data generated by the designer for geometric control is shared with both the engineer and the fabricator. Current state of the art software platforms remains particular to each party involved. There is no single software ideally suited for all the players along the Design-Engineering-Fabrication workflow so it remains a key responsibility for the designer to establish an agreeable data transfer process that assures accurate data transfer for the particular players involved. Devising a successful data transfer process provides a major benefit toward mitigating unnecessary risk. The information shared with the engineer was different from the information transmitted to the fabricator. Each version contained only the critical information for that discipline. Each party's data file was formatted based on mutual convenience. The designer sent the structural engineer a RISA file containing the FEA, an AutoCAD File with the pure geometry, and a Sketch-Up file for their visual reference. The engineer was able to utilize the data to perform the formal engineering analysis using the software he was accustomed to using.

The designer sent drawings to the fabricator in a format easily translated to the software they used. The designer generated the geometry in Rhinoceros software. Solidworks software was the fabricator's preferred software for generating shop drawings and Computer Numeric Controlled (CNC) laser cut files. The data was transferred from Rhino to Solidworks via an intermediate file format called .stp file (Standard for the Exchange of Product File). This file format is a standard 3D format readable by both Rhino and Solidworks software.

The specialized configuration of the digital information produced by the designer was governed by the fabrication methods and particular materials anticipated. With the advent of parametric mass customization involving hundreds or even thousands of bespoke parts, the fabricator was not typically equipped to generate such geometrically complex data. Therefore, the designer provided the fabricator with precise digital data suitable for the specific material and fabrication methods. Accurately determining the information needed by the fabricator was possible as a result of a precise Data Transfer Protocol DTP effort. In this case, it was important the primary plates and their bolt holes were positioned in 3D space exactly as the designer intended in order for the global geometry to be produced.

Stainless steel sheet metal's potential to be quickly configured to form simple and effective flange connections and its ability to be geometrically configured through bending to achieve specific structural stiffness properties are offered due to the ductility and malleability of steel. When using methods involving laser cut, laser bent sheet metal parts, the fabricator made dimensional modifications to account for the bending effects of the material caused by their own proprietary processes and machinery tooling used but with the goal of achieving the designer's intended flange-hole-to-plate relationships. The yield region of the parts involving the flange bends was less important as long the holes were positioned correctly relative to the primary plate surfaces. This freedom within the bend yield region allowed the fabricator significant latitude regarding the exact radius profile as long as the holes were in placed correctly in 3D space. The fabricator was given the

freedom to configure the bend yield region however they needed as long as the flange holes-to-plate relationship remained as designed.

This aspect was the primary determination of what data the designer transferred to the fabricator in the DTP. In this case, the designer produced digital files consisting of surfaces with zero thickness representing the center plane of the primary plates and flanges. At the bend regions, the zero thickness surfaces met at corners with zero radii. This data was transferred in a .stp file of the entire wall so either party could open and visually confirm every part was positioned correctly, that all the holes aligned, and the global surface would be the result. (see Figure 3) If the primary plates and the flange bolt holes were placed precisely, the global geometry was assured to occur. This verifiable data assured the designer's data was correct.

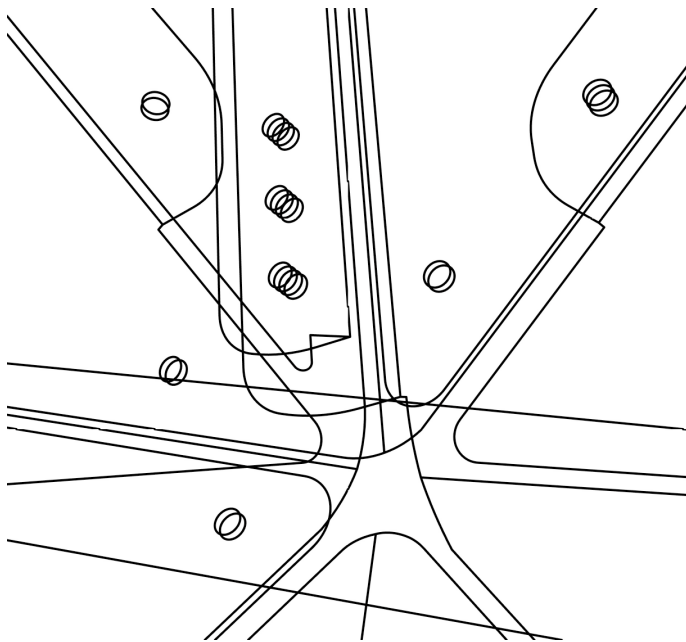


Figure 3. Visually confirmable hole alignment, offset by material thickness.

#### 2.4. STRUCTURAL ANALYSIS

Early in the design development phase, the designer performed structural finite element analysis using Risa-3D Software by Nemetschek Group. The principal purpose of the analysis was to determine the amount of deflection caused by extreme wind conditions.

The drawing exchange file (.dxf) format containing the geometry proved to be a precise method to quickly transfer the geometric data from the parametric design software to the FEA software. The designer imported the geometry into the FEA software, applied wind loads, defined supports, material properties, and

performed the analysis. It took approximately twenty minutes to export the revised data to RISA-3D, set up the analysis, and to receive the results. Initially, the deflection due to 100 mile-per-hour wind loads measured twelve inches, which far exceeded acceptable limits. The designer made modifications to the geometry to try to reduce the deflection by only making geometric changes. The changes made included thickening the wall where it contacted the ground, increasing the curvature in plan (toroidal direction), and increasing the curve of the wall in its vertical section (poloidal direction). The refinement process involving deflection analysis, algorithmic shape modification, and deflection re-analysis took approximately forty-five minutes.

The parametric algorithm provided a fast method to revise the 1500 parts' geometry of the entire wall in a few minutes. The analysis/modification/analysis process resulted in the designer reducing the deflection from twelve inches to one inch after only six iterations and only a few hours. The designer was able to resolve the wall structure quickly and without enduring additional structure engineering costs for quantitative early design phase calculations. Detailed deflection analysis calculations are outside of the scope of the early design development phase of a typical engineering contract. The design was passed on to the structural engineer where he conducted his analysis which resulted in only ½" of deflection. The deflection varied because the designer made more conservative assumptions than the structural engineer.

## 2.5. FABRICATION DEFINITION THROUGH PROTOTYPING.

The designer explored the construction methods for the wall by producing the architectonic prototyping models in three progressive phases. The initial architectonic prototype paper model contained twelve adjacent modules at ¼ actual scale. The tasks to produce this paper prototype included 3D modeling, laser cutting, hand folding, and hand assembly. During this phase of the process, the designer was able to begin to decide how to subdivide the modules into individual parts and where to place flanges for the part-to-part connections. Valuable observations made during this phase included bending logics. Paper folds involving adjacent highly acute triangles created a condition at the end of the fold that is not possible in sheet metal due to the higher stiffness. As a result, corners were rounded to minimize acute triangles and avoid sharp points.

Armed with the knowledge gained from the paper prototype results, modifications to the digital model were made and a half-scale prototype containing six modules was fabricated using thin sheet metal bolted together. (see Figure 4) For this prototype, the designer increased the stiffness of the sheet metal well beyond that of the first paper prototype; however, its stiffness remained less than the final material stiffness. The designer built the prototype with sheet metal machinery. Several other practical modifications had to be made to the design as a result of using sheet metal fabrication equipment. The designer made valuable refinements to the connection location configuration. The metal prototype also forced the designer to resolve how bend lines would be marked efficiently. This prototype revealed limits of the bend angles that could be achieved at each condition. These conclusions increased the designer's level of confidence that

the parts could be fabricated economically. Costs were effectively controlled by assuring constructability prior to obtaining pricing from the final commissioned fabricator.

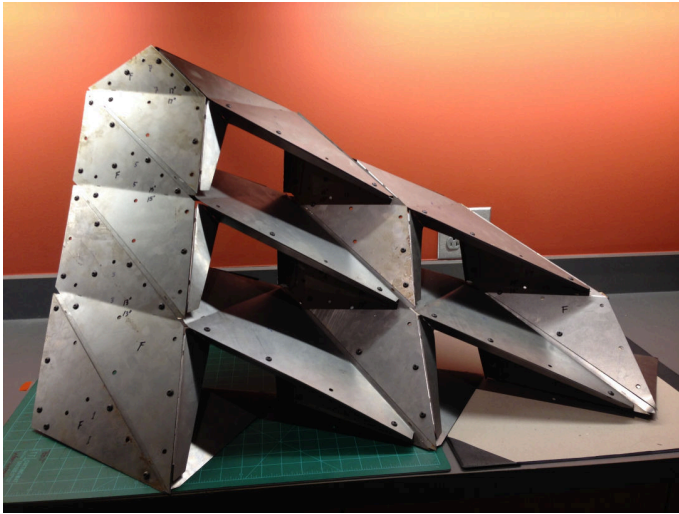


Figure 4. Thin sheet metal prototype.

If the commissioned fabricator had made these discoveries after pricing, there would have been significant unexpected fabrication cost increases, redesign costs, and schedule delays.

It was important to involve the fabricator as soon as the designer had confidence in the fabrication process. The designer specified the commissioned fabricator be responsible for building the final prototype using the actual materials and at full scale. (see Figure 5) The purpose of this final prototype simulated the entire build process, including digital file data transfer, generation of shop drawings, shop drawing review, and fabrication. By performing the previous prototype efforts, the design of the material system got flushed out prior to bringing the fabricator on-board. The final prototype went together flawlessly. As a result, the designer was not required to make any additional modifications to the design. Since no changes were required, the fabricator was able to include the final prototype as part of the final wall. The reuse of the prototype in the final wall resulted in time savings and cost savings for the owner as well as the designer and fabricator.



Figure 5. Prototype with actual material at full scale.

## 2.6. CONCLUSION

Implementing an intentional risk management process can provide an experimental designer with a path toward building never tried methods of construction at an architectural scale. By avoiding unnecessary financial risks through a carefully planned process, the designer of experimental material systems can scale research findings to an architectural scale. Adopting the mindset of a Medieval master mason process within the context of twenty-first-century materials and processes can be a method toward a successful project. By performing well thought-out transfer procedures of digital data, resolving the fundamental challenges of fabrication, and including structural analysis as a part of the early design phases, experimental architectural expressions can be realized without extra financial risk to the designer.

## References

- The AIA, T.: 2019, “Back to Basics: An Effective Risk Management Program” . Available from <<https://www.theaiatrust.com/basic-risk-management-program/>> (accessed 10 December 2019).
- Coldstream, N.: 2002, *Medieval Architecture*, New York: Oxford University Press.
- Feher, K., Szilagya, B., Bolcskei, A. and Halmos, B.: 2019, “Pentagons in Medieval Sources and Architecture, Nexus Network Journal” . Available from <<https://link.springer.com/article/10.1007%2Fs00004-019-00450-7>> (accessed 2 February 2020).
- Foyle, J.: 2006, “The Architecture of Inigo Jones Was the Flat-Pack of Its Day, Architects’ Journal, vol. 223” . Available from <[search.ebscohost.com/login.aspx?direct=true&db=vt&AN=20363049&site=ehost-live](http://search.ebscohost.com/login.aspx?direct=true&db=vt&AN=20363049&site=ehost-live)> (accessed 2 February 2020).
- Irwin, A.: 2019, “Notre Dame: Medieval Stonemasons Built Vaulted Ceilings to Protect Against Fires” . Available from <<https://horizon-magazine.eu/article/notre-dame-medieval-stonemasons-built-vaulted-ceilings-protect-against-fires.html>> (accessed 11 December 2019).
- Rossi, A.: 2012, “From Drawing to Technical Drawing”, Nexus Network Journal” . Available from <<https://link.springer.com/article/10.1007%2Fs00004-011-0102-4>> (accessed 2 February 2020).

# FUNICULAR STRUCTURES USING TOPOLOGICAL ASSEMBLIES

URVI SHETH<sup>1</sup> and AYSHA FIDA<sup>2</sup>

<sup>1,2</sup>CEPT University

<sup>1</sup>urvi.sheth@cept.ac.in <sup>2</sup>ayshafida.p@gmail.com

**Abstract.** Presented work is inspired by the research on funicular structures by Block Research Group and customising bricks by the first author. The research is focused on developing a mortarless construction system for funicular structures using topological assemblies on site. To make the proposed system financially viable in the India, it is suggested to limit the customisation of the topological modules. Topological assemblies interlock with its contact surfaces (Tessman, 2012). Further these force locked elements are kinematically constrained using an extrados post tensioning. As a result, the system is stable not only in complete compression, but it can also withstand lateral loads and vertical upliftment. Additionally, it is quick to assemble and dismantle the structure without foundation and by using minimum scaffolding. Therefore, the construction system can be used to build a range of temporary as well as permanent structures like temporary exhibition halls, emergency shelters, earthquake resistant structures, etc.

**Keywords.** Funicular structures; Mortarless masonry; Topological assembly; Interlocking modules; Limited customisation.

## 1. Introduction

Advancements in computational design and digital fabrication techniques opened immense possibilities of generating forms through structural concepts, integration of material behaviour and construction of funicular vaults. Several studies are conducted on form finding of funicular structures of both types, symmetrical and asymmetrical. In the last decade researches by organisations like Block Research Group has developed interactive digital tools which establish the relation between force and form in compression curved surface structures. These tools offer an intuitive and playful interface (Rippman M, 2016). Researches using these tools have demonstrated examples of designed and built projects.

RhinoVault plugin for Rhinoceros 5 is one such plugin that works on the principle of Thrust network Analysis (TNA) for funicular form generation (Rippman M, 2016). The generated forms are being constructed using a variety of techniques and materials. For example, traditional Catalan vaulting with thin brick shells, advanced stereotomic design with stone, ceramic tile construction, etc. (Rippman, Block 2013). Presented work uses RhinoVAULT to generate forms and investigate the construction possibility using topological assemblies



## 2. Topological Assemblies

Topological assemblies are a type of interlocking system with solid and repetitive blocks which are kinematically constrained. The assemblies interlock with its contact surfaces. The planer topological assemblies were developed by the Institute of Material Science, Technical University Clausthal, Germany Tessmann (2012). These solids interlock three dimensionally, purely based on their geometric shapes. These assemblies are made of repetitive polyhedrons (Fig 1a) and osteomorphic blocks (Fig 1b). There are two types of topological interlocking, platonic solids and osteomorphic blocks. The first is interlocked with planar surfaces while the second has non-planar interlocking faces. Osteomorphic blocks interlock due to their matching concavo-convex surfaces. Given fixed boundary conditions the assemblies are able to resist high bending forces and even tension without any additional binding material like mortar (Fig 1c) (Dyskin et al. 2003).

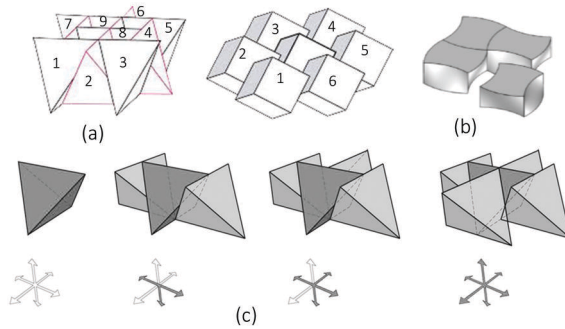


Figure 1. (a) Assembly of repetitive polyhedrons (Belenov - kernel et al. 2009), (b) Assembly of Osteomorphic blocks (Weizmann et al. 2011). (c) Tetrahedron configuration with interlocking properties (Tessmann 2012).

## 3. Module Design

### 3.1. FORM

Based on the osteomorphic topological assembly, a module is proposed. The module design is based on a Cosine/Sine trigonometric identity that resembles an osteomorphic block by D A Robinson. The proposed module has following curve character,

$$z(x, y) = 0.5h \cos\left(\pi \frac{x}{B}\right) \sin\left(\pi \frac{y}{B}\right), \text{ where } B \leq x < 3B, 0 \leq y < 2B, h = B \quad (1)$$

The proportions of the module are maintained as  $2B \times 2B \times B$ , where  $B$  is a variable value that determines the height of the block (Fig 2b).

The geometry of module is symmetrical along the central axis (Fig 2c, 2d). Thus, when the module is rotated by 180 degrees, the non-planar surfaces of the rotated module matches with the original module (Fig 2e) which ensures the

interlocking of modules in two dimensional plane. These modules are defined as “standard module” here.

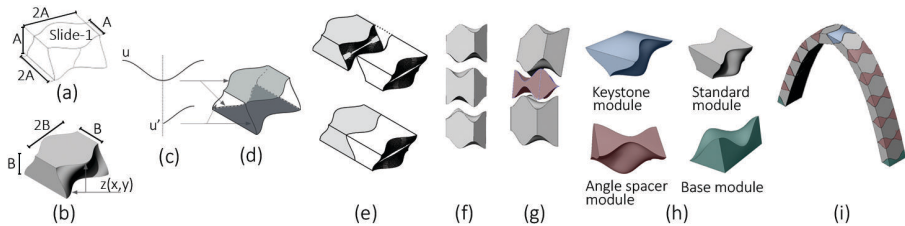


Figure 2. (a) Osteomorphic block by D A Robinson, (b) Proposed module, (c) Curves  $u$  and  $u'$  that defines the geometry (d) Top and bottom surface of the geometry. (e) Interlocking of modules (f) Linear assembly of modules. (g) Module assembly with angle spacers to achieve a curvature. (h) Types of modules (i) Assembly of modules along a catenary arch.

Unlike planer assembly (Fig 2f), to build curved geometry like centenary arch, funicular barrel vaults and symmetrical funicular forms, the system either demands 100% customisation or a limited customisation. A sequence of alternate standard module and “angle spacer” is proposed for the curved geometry (Fig 2g). The wedge shaped modules corresponding to the range of angles between two standard modules are called “angle spacers”. The size and geometry of angle spacer varies with reference to the span, rise and curvature (single or double curvature) of the forms. Among the angle spacers, “Base module” and “Key stone” are named specifically (Fig 2h). These four types of modules make an interlocking system resulting in the elimination of mortar as well as limiting customisation of modules for construction (Fig 2i).

### 3.2. SIZE

To fix the size of the proposed form, a structural simulation was done using Scan-and-Solve plugin to Rhinoceros 5.0. The plugin allows structural simulation of bonded assemblies consisting of any collection of solid geometry using Finite Element Method (FEM). Total displacement, principle compression and tension were calculated for catenary arches using different module sizes. Following parameters are considered to run the simulation:

1. As generated in RhinoVAULT, structure is in complete compression.
2. Dynamic parameter 1: Size of module (Module 1: 10cm x 10cm x 5cm; Module 2: 15cm x 15cm x 7.5cm; Module 3: 20cm x 20cm x 10cm)
3. Dynamic parameter 2: Span and Rise (Case 1:  $x_1=x_2= x$ ; Case 2:  $x_1=x_2= 2x$ ; Case 3:  $x_1= x_2= 4x$ ; where  $x_1$  is span,  $x_2$  is rise and  $x= 75$ cm)
4. Material: M20 concrete

Simulation showed similar behaviour for total displacement in all three cases and it was negligible for all the cases (Fig 3a). Therefore, it is not considered while determining the size. Based on the simulation results of principle compression and tension (Fig 3b), maximum span and height up to 150cm was achieved safe with Module 3.

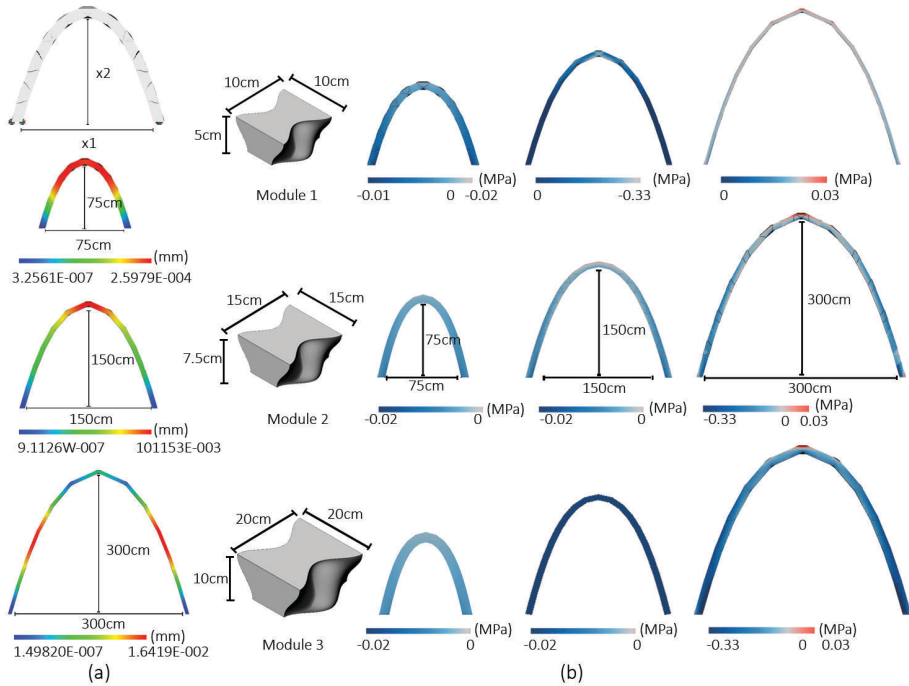


Figure 3. (a) Total Displacement in arch with respect to Case 1, Case 2 and Case 3 (b) Principle Compression and Tension in Catenary arch for Case 1, 2 and 3 using Module 1, 2 and 3.

Module 3 of size 20cm x 20cm x 10cm was used for further research.

#### 4. Test Cases

##### 4.1. CATENARY ARCH & FUNICULAR BARREL VAULT

Catenary arches of span 300cm are simulated using module size 20cm x 20cm x 10cm to calculate total displacement and principle compression and tension (Fig 4). Rise of these arches are defined as, Case 1a ( $x_1 = 4x, x_2 = x$ ); Case 1b ( $x_1 = 4x, x_2 = 2x$ ); Case 1c ( $x_1 = 4x, x_2 = 3x$ ), where  $x_1$  is span,  $x_2$  is rise and  $x = 75$ cm.

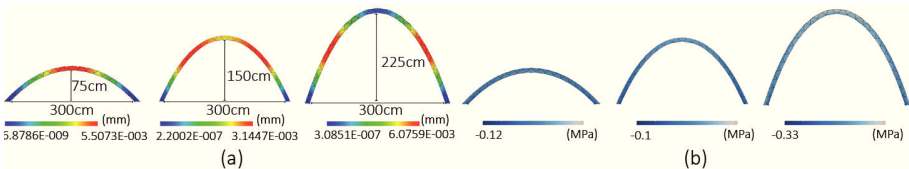


Figure 4. (a) Total displacement (b) Principle Compression and Tension in Catenary arch.

These catenary arches were repeated horizontally for 5 and 10 times to create funicular barrel vaults. Principle compression and tension of the same are shown below (Fig 5a to 5b)

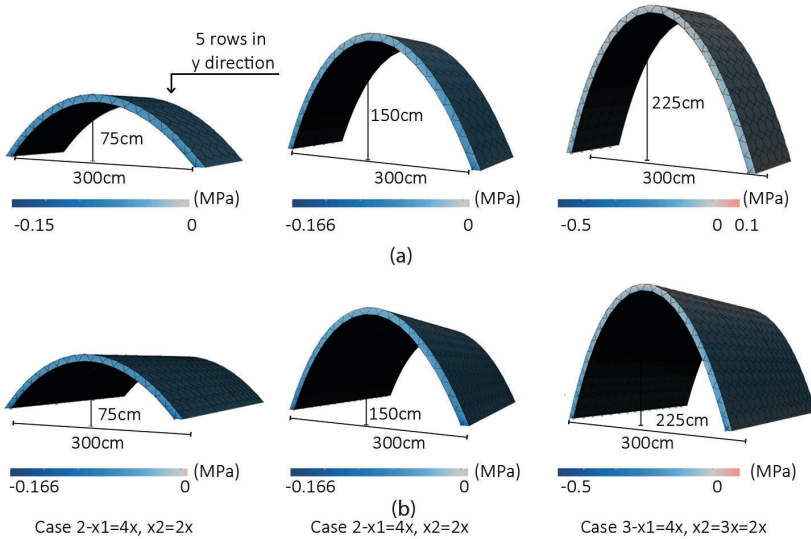


Figure 5. Principle compression and tension (a) Barrel Vault with 5 rows of catenary arches (b) Barrel Vault with 10 rows of catenary arches.

Inference: Height of the catenary arch should be less than 3/4 of the span. Barrel vault is in complete compression for the span 300cms and maximum rise 150cm. Tension zone is observed at the top of the vault for 225cm rise. Hence the rise of the structure should be equal to or less than 1/2 of the span. The behavior of vault is independent of the number of horizontal repetition.

#### 4.2. FUNICULAR FORM WITH TWO PARALLEL SUPPORTS

Funicular form is generated with two parallel supports measuring 180cms. The module size is 20cm x 20cm x 10cm and span 300cm. Rise varies as, Case 2a ( $x_1 = 4x$ ,  $x_2 = x$ ); Case 2b ( $x_1 = 4x$ ,  $x_2 = 2x$ ), where  $x_1$  is span,  $x_2$  is rise and  $x = 75$ cm. Two alternative assembly methods, one where modules are assembled vertically and the other with horizontal assembly, were tested for total displacement (Fig 6) and principle compression and tension (Fig 7).

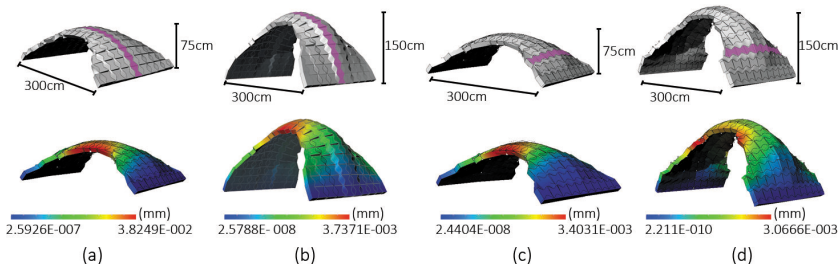


Figure 6. Total displacement (a, b) Modules assembled vertically (c, d) Modules assembled horizontally.

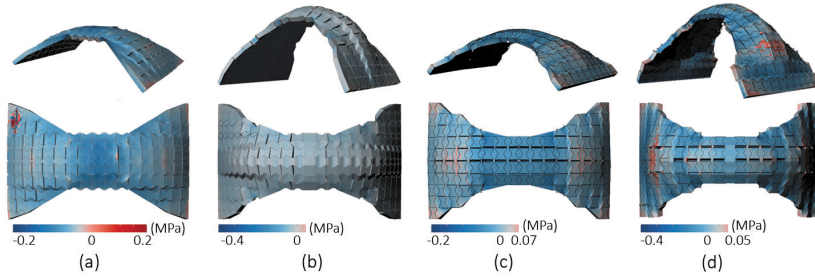


Figure 7. Principle compression and tension in funicular form with two parallel supports (a, b) Modules assembled vertically (c, d) Modules assembled horizontally.

Inference: For the span of 300cm, structure is in complete compression using horizontal assembly for the rise of 75cm and using vertical assembly for the rise of 150mm. Therefore, for such forms, assembly logic would vary case wise.

#### 4.3. FUNICULAR FORM WITH FOUR LINEAR SUPPORTS

Funicular form is generated with four linear supports, each measuring 300cms. The module size, span and varying rise same as the previous case. Figure 8 show principle compression and tension.

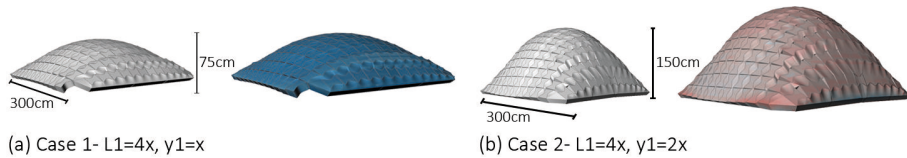


Figure 8. Principle compression and tension in funicular form with four linear supports .

Inference: Vault is in complete compression for the span of 300cm and rise of 75cm. For the rise of 150cm, the entire assembly had several gaps between modules which led to tension in the structure. Therefore, further simulations were done by filling these gaps for a range of span 300cm to 450cm and rise 75cm to 150cm (Fig 10)

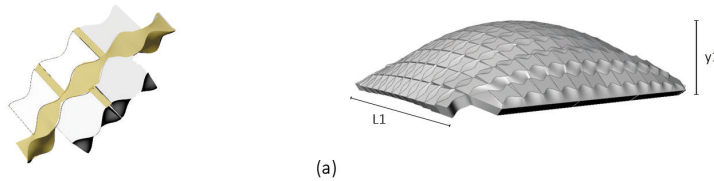


Figure 9. (a) Detail of filling the gaps between standard modules.

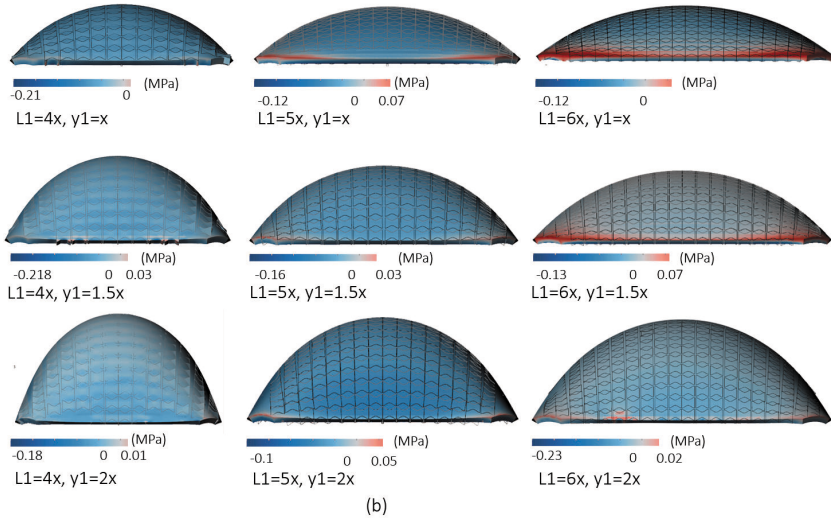


Figure 10. Principle compression and tension in funicular form with four side supports.

By filling the gaps, the assembly is bonded and the performance of the structure improved. It is in complete compression for the maximum span of 450cm and rise 150cm. Filler material is yet to be decided.

## 5. Construction logic

### 5.1. BARREL VAULT

Two methods of construction are visualised through scale 1:10 prototypes for Funicular barrel vault. Method 1, without scaffolding and Method 2, with limited scaffolding. In both the cases, modules were assembled by staggering standard modules and angle spacers alternatively. The staggering of block ensures that the modules are mutually locked with each other and construction joints are not continuous. It also eliminates the need of a continuous scaffolding. The entire assembly is kinematically constrained by extrados post tensioning.

Construction method 1 (Fig 11a to 11d): A catenary arch is drawn on ground along which modules were assembled horizontally. Once the first arch is completed, it is kinematically constrained with the tension cable fixed at its base before the next layers are assembled. The process is repeated for successive layers. On completion of the required number of layers, entire assembly is turned vertical and placed in its position with the help of a crane or a mechanical system.

Construction method 2 (Fig 11e to 11h): Scaffolding is required to assemble the first catenary arch in its position on site. Once the first arch is assembled, it is kinematically constrained with the tension cable fixed at its base before the next layers are assembled. The scaffolding can now be removed and the next rows of arches can be built without scaffolding. Staggering of modules create a pocket for the next block and ensures interlocking. The process is repeated for the required

number of rows for the vault.

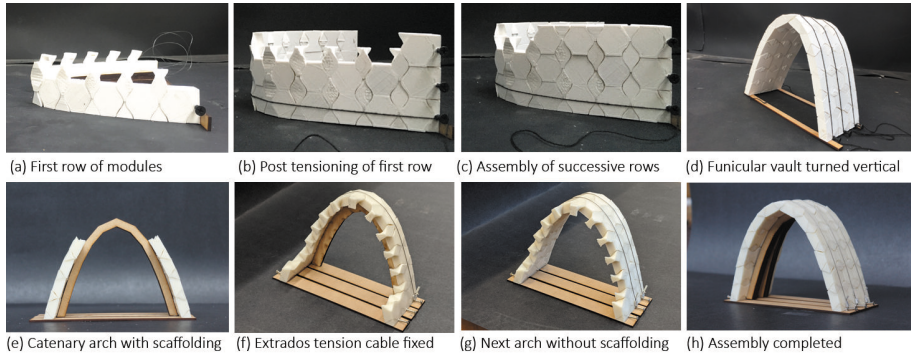


Figure 11. Construction method 1 and 2 for barrel vault.

## 5.2. FUNICULAR FORM WITH FOUR LINEAR SUPPORTS

For such symmetrical form having a square plan, the assembly begins from the outer edge having two parallel supports for the first arch. In case the base plan was rectilinear with similar support condition, the assembly would follow the line diagram of the trust network to ensure force flow through the structure. Similar to construction method 2 of barrel vault, modules are staggered and the first arch requires scaffolding. The rest can be assembled without continuous scaffolding. Supports can be provided at strategic locations. Refer Fig 12

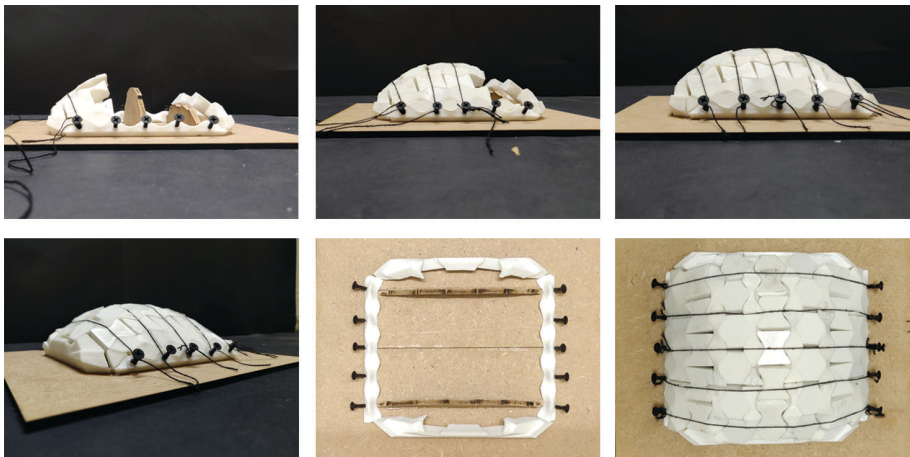


Figure 12. Construction method for funicular form with four sides support.

## 6. Conclusion

The construction system developed is **self-supporting, dry construction for symmetrical funicular forms using topological assemblies**. These are force locked elements which are kinematically constrained using an extrados post tensioning. Because of this, the system is stable not only in complete compression but **it can also withstand lateral loads and vertical upliftment**. The modules can be assembled and dismantled as required and transported to various locations. Therefore, the construction system can be used to build a range of temporary as well as permanent structures like temporary exhibition halls, emergency shelters, earthquake resistant structures, etc.

By **limiting customisation, minimising on scaffolding and layers of construction**, the proposed system is a value addition to the construction industry like India, where 100% customisation is not yet affordable. Customisation is reduced by 45-55% for symmetrical funicular forms and up to 68% for barrel vaults. The construction system also ensures minimising on scaffolding which results in saving cost and time to build curved forms. This system also helps avoiding layers of construction as compared with the Catalan tile vaulting construction. Here the construction is completed in single layer without requirement of skilled labour which in turn saves the cost of craftsmanship and time.

## 7. Way forward

### 7.1. CHOICE OF MATERIAL

Three materials were chosen to prototype the modules. M20 concrete, burnt clay and fly-ash. Two primary reasons to choose these materials were, local availability and conventional practices. Other factors considered were, compressive strength of the module and production cost. Based on the analysis done in scan and solve plugin, the maximum compressive strength required is less than 1 MPa. Compressive strength of M20 Concrete is 20 Mpa, burnt clay bricks is 7.35 Mpa and fly-ash bricks is 7.5 Mpa. Hence used for prototyping the module. Although materials like sandstone and limestone has high compressive strength, the cost required for CNC milling them is much higher than the chosen materials.

#### *7.1.1. M20 concrete block*

All four types of the blocks, standard, angle spacer, base and key stone were prototyped. Fibre reinforce plastic (FRP) is chosen as material to make moulds of each of them. Scale 1:1 3D printed blocks (Fig 13a) were used to make FRP mould (Fig 13b). A standard M20 mix was made in the laboratory (Fig 13c) and cast in the moulds (Fig 13d). The block was removed from the block after 24 hours and cured for 21 days. Fig 13e to 13h shows final blocks. Structural test, handling and prototyping full scale structure is an ongoing research.



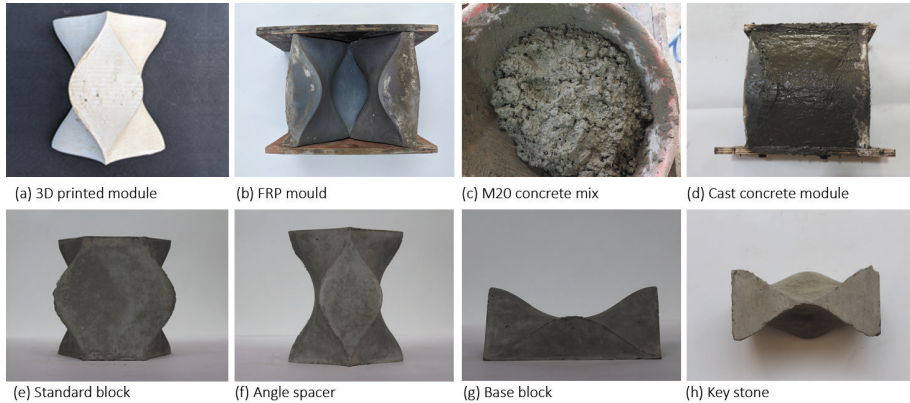


Figure 13. Making of M20 concrete block.

## 7.2. FREE-FORM FUNICULAR VAULTS

Further an inquiry into the possibility of this construction system to be used to build free form funicular vaults can be explored.

### Acknowledgement

Ketan Solanki, Tanvir Khorajiya, Nikunj Dave and Sameera Bommisetty

### References

- “OsteoMorphing” : 2019. Available from <<http://www.architetturadi Pietra.it/wp/?p=7080>> (accessed 15th March 2019).
- Belov, K., Dyskin, A. and Eslein, Y.: 2009, Interlocking of convex polyhedra: Towards a geometric theory of fragmented solids, *Moscow Mathematical Journal*.
- Block, P.: 2009, *Thrust Network Analysis: Exploring Three-dimensional Equilibrium*, Ph.D. Thesis, Massachusetts Institute of Technology..
- Dallinger, S. and Kolinger, J.: 2008, *Thin post tensioned concrete shell structures*, *Tailor Made Concrete Structures*, Walraven & Stoelhorst (eds) Taylor & Francis Group, London.
- Dyskin, A., Estrin, Y., Pasternak, E., Khor, H.C. and Kanel-Belov, A.: 2003, *Fracture Resistant Structures Based on Topological Interlocking with Non-planar Contacts*, *Advanced Engineering Materials*.
- Rippman, M.: 2016, *Funicular Shell Design: Geometric approaches to form finding and fabrication of discrete funicular structures*, Ph.D. Thesis, University of Stuttgart.
- Rippmann, M. and Block, P.: 2013, Funicular Shell Design Exploration, *Proceedings of ACADIA 2013*.
- Tessmann, O.: 2012, Topological interlocking assemblies, *Proceedings of eCAADe 2012*, 211-219.
- Vella, I. M. and Kotnik, T.: 2016, Geometric Versatility of Abeille Vault - A Stereotomic Topological Interlocking Assembly. Complexity & Simplicity, *Proceedings of the 34th eCAADe - Volume 2*, Finland, 391-397.
- Weizmann, M., Amir, O. and Grobman, J.: 2017, Topological interlocking in architecture: A new design method and computational tool for designing building floors, *International journal of architectural computing*.

# CONNECTING TIMBER SHEET MATERIALS TO CREATE A SELF-SUPPORTING STRUCTURE USING ROBOTIC FABRICATION AND COMPUTATIONAL TOOLS

CELINE CHENG<sup>1</sup> and ANTONY PELOSI<sup>2</sup>

<sup>1,2</sup>*Victoria University of Wellington*

<sup>1</sup>*celinecheng5@gmail.com* <sup>2</sup>*antony.pelosi@vuw.ac.nz*

**Abstract.** The research developed in this paper is the workflow to create a self-supporting structure from sheet materials using robotic fabrication and computational tools. This research focuses on timber sheet materials, as timber is a material that can be altered in a variety of ways. Japanese timber connections were a strong influence for this research, due to its prolonged lifespan and sustainable advantages. In the past, timber fabrication techniques have been limited due to design limitations. This research explored how current technology, specifically parametric software combined with robotic fabrication, can create timber connections to connect sheet materials at different angles. This method was utilised to repurpose the concept of sheet materials towards a complex structure, which adopted the idea of mass customisation over mass production. This can help reshape the future of architecture through the use of advancing technology and sustainable assembly techniques using timber to timber joints.

**Keywords.** Architecture; Robotic Fabrication; Timber; Parametric Design.

## 1. Introduction

Sheet materials have been used in the construction industry since 1905 (APA Wood, 2010). Such materials include plywood, MDF, laminated timber and many more. These flat surfaces were created for the purpose of mass production, which allows for efficiency and repetition. This causes many surfaces seen in the building industry today to be constructed in a similar manner. These materials are often not structurally stable alone, instead often relying on another structural element such as steel fixings. With the increasing concerns of environmental issues, timber is a beneficial material to use because it is a renewable source and a promising building material that should be used more frequently. It is a material that can be modified in a number of ways, allowing it to be a multifunctional material.

To date, a number of studies have created a structure using robotic fabrication and computational tools. A key example is the Landesgartenschau Exhibition Hall. It showcases the opportunities of timber structures that lie outside of the scope of conventional timber designs. The robot was also used to mill the timber to create finger joints. 243 unique beech plates were locked together with 7356 individual

finger joints (Schwinn, 2017). Although this was a successfully built structure, it still relied on nails to hold the finger joints in place.

Engineered timber connections today tend to rely on fasteners, which faces many challenges ranging from the behaviour of the materials to the point of recycling (Schwinn, Krieg, & Menges, 2013). Current timber building designs lacks a sustainable design approach, as many timber construction methods produce a lot of waste and disregards how the timber in buildings can be reused. Alternative methods of construction can be implemented than the ones that are currently used today. Timber is an above average insulator compared to other inorganic building materials. Due to metal fasteners being a good conductor of heat, issues arise when the fasteners are inserted into the timber. This is because metal cools faster than timber when there is a change in temperature. Therefore, condensation occurs on the metal, causing the metal fasteners where their galvanised coating has been damaged due to abrasion from penetrating the timber. Furthermore, timber surrounding the fasteners tend to rot due to the dampness. This causes the bolt to no longer to be fully secure and they lose their load bearing. To set back the process of decay, large quantities of non-environmentally friendly chemical wood preservatives are used. Therefore, in buildings with wood to wood joints, these chemical wood preservatives would not be needed (Graubner, 1992). Joints are made where supporting and supported elements meet, where timber must be spliced, supported or braced together. Looking into traditional Japanese joinery techniques can help lead to a sustainable design approach.

Historical Japanese architecture is renowned for their unique use of timber connections, which has allowed many of their timber only structures to remain standing after centuries. However, these connections were manually created and was a time-consuming process to learn the proper techniques to create them. Current technology, specifically parametric software combined with the robotic arm, can be utilised to repurpose the concept of sheet materials towards complex structures. This saves time compared to creating the connections manually. This research focuses on fabricating with the 6-axis industrial robotic arm. Advances in computer- aided design (CAD) and computer- aided manufacturing (CAM) are creating a strong impact in the architectural design process (Kolarevic, 2003). They have allowed the production and construction of complex forms that were until recently, challenging and expensive to design, fabricate and assemble using traditional construction methods. The use of a digitally controlled fabrication process broadens the boundaries which offer the opportunity to create complex designs and inform new construction techniques. Instead of a limited choice of possible construction options, every surface can be customised based on design parameters. Therefore, the aim of this research is to investigate a way to combine the flat materials and integrate structural stability within it, to create a self-supporting structure.

The robotic arm is a tool that is not restricted to a particular application or optimised for a specific disciplinary focus, however it is a tool that is becoming relevant in architecture. The difference between contemporary industrial robots and their industrial predecessors and other computer controlled devices is their versatility (Willma, Block, Hutter, Byrne, & Schork, 2018). The robotic arm is

an efficient machine that can achieve a variety of tasks dependent on the tool that is attached to it. Some examples include milling, 3D printing, picking up objects and cutting (Owen-Hill, 2018). In order for these manoeuvres to occur, a toolpath created from visual programming software such as Grasshopper, is sent as a code to the robotic arm. The versatility of the robotic arm allows it to be programmed to achieve a wide range of specific tasks both at a small and large scale.

Grasshopper has made robotic fabrication accessible to architects and designers as it can fabricate parametric components easily. Despite being an accessible programme, a lot of testing and checking needs to be done to ensure it makes no mistakes with the robotic arm. This process can take up more time compared to setting up on software used by traditional CNC machines (Dunn, 2012). The main advantage of the robotic arm compared to other fabrication machines is that the robotic arm has the ability to move around 6-axis. This enables it to rotate and mill around different angles in one tool path, giving the option to create complex components. Having the capability to rotate upside down and around a three-dimensional object prevails over conventional machines. This advantage gives the opportunity to showcase how the robotic arm can give designers the freedom to design outside the scope of conventional designs.

## **2. Methodology**

This research required a feedback loop for after each stage where a critical analysis was completed to identify the outcomes, strengths and weaknesses. This was important to see what areas needed to be improved. Prototypes of timber connections were created to develop an outcome that will structurally support itself. The outcome of each prototype was evaluated and compared with one another to establish which connection would be most suited to bring forward to the self-supporting structure. Computational simulations were used to explore individual structures which created panels that were automatically flattened in the software. This allowed the digital file to be transferred to the robotic arm to be milled.

The advantages of computational simulations is that it allows for an iterative process to examine which design will work best for the environment it has been placed in. In the paper, Simulation research methods, Dooley claims that “Simulation enables studies of more complex systems because it creates observations by ‘moving forward’ into the future, whereas other research methods attempt to look backwards across history to determine what happened and how” (Dooley, 2002). This is relevant to this study as computational simulations highlighted the design possibilities and captured the behaviour of the panels. The iterative process means different outputs occurred depending on what rules were given to the code. The iterations were built on previous simulations which allowed the outputs to be compared. These simulations are also important because they acted as a substitute for the actual physical prototyping which minimised the time needed to achieve it. Furthermore, simulations educated and helped us understand how the complex panel system could work. However, some limitations that occurred with this research method is that multiple parameters existed within computational simulations. This allowed for an unlimited amount of times that

the simulation can be run, which always gave the ‘what if’ question each time a simulation is finished. Although this allows for multiple possibilities, a stop point was called to allow us to move forward with this research.

The aim of this research is to develop a workflow through designing panels and connections to create a self-supporting structure created from sheet materials using robotic fabrication and computational tools. This research involved the design, fabrication and assembly of the sheet materials to connect at different angles. This involved a process to design a connection and create a toolpath to enable it to be fabricated by the robotic arm. This toolpath is parametric, allowing customisation based on each individual’s preferences. This required testing many iterations with the robotic arm to see if they can fit in and hold each panel. However, structural testing of these panels fall outside the scope of this research due to software constraints. Since this research focused on the development of a workflow to get to a self-supporting structure, a full-scale physically fabricated and assembled structure also falls outside the scope of this research. Instead, a part of the structure was physically fabricated and assembled to prove the connections work and can hold itself together without needing nails or screws.

### **3. Process**

#### **3.1. TOOLPATH**

To commence the project, a toolpath was created with the robotic arm. Due to there being no set software for robotic milling, toolpaths were created on Grasshopper, which is a visual scripting language add on for Rhinoceros 3D. HAL Robotics is a grasshopper plugin that was used to create the toolpath. These programmes combined, provided a way to view the toolpath as a 3D graphic in the Rhino interface. This was an efficient way to generate computational simulations with the toolpath as visual feedback indicated where the toolpath would mill through the timber and show where the spindle would clash with it. This led to reworking the code until the toolpath was going in the right direction.

Creating the toolpaths involved many parameters such as speed, planes, router size and amount of passes to ensure it can be outputted correctly as the robotic arm’s Rapid Code. The toolpath created in this process goes beyond the limitations of a traditional CNC machine’s CAM (Computer Aided Manufacturing) toolpath generator. Customisation of the toolpath was a key benefit as it creates greater design freedom and allows the fabrication of bespoke designs.

#### **3.2. FABRICATION**

Mortise and tenon joints have been widely used for centuries especially in building and furniture making (Tankut & Tankut, 2004). It consists of two components, the mortise hole and the tenon tongue (Figure 1). The tenon is cut to fit perfectly into the mortise hole. An advantage of the mortise and tenon joint system is that it is a strong joint. The mortise and tenon is generally used when corner joints need a sturdy frame.

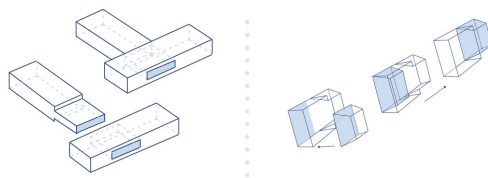


Figure 1. Mortise and Tenon Joint on left & Sliding Mortise and Tenon on right.

A locking system that was based off the traditional mortise and tenon joint system was created (Figure 1). Iterations of this joint was designed to establish how the panel with the tenon could lock in and hold itself together with just this connection. Following on, a sliding mortise and tenon square joint system was established that locks in and prevents it from falling apart. This system was more successful compared to the initial finger joint that was planned on being used. This new system allowed the model to be parametric and simplified the grasshopper code compared to figuring out each angle the finger joint needed on the surface. The finger joint was unsuccessful, as although it can fit into each other like a puzzle to lock together, it would still require many screws as shown by the Landesgartenschau Exhibition Hall Precedent. The implication with the use of these screws lowers the sustainable quality of the joint system and makes it difficult to take apart.

This sliding mortise and tenon system square system was first milled on gold foam to identify and resolve the issues found with the robotic arm environment, spindle tool and material used before continuing on with the milling of more timber connections. This enabled a faster setup for the cuts following on from this first set.

A limitation with the first design was that it can't have sharp corners due to the size of the router bit used. As the 6mm straight router tool cannot plunge deep into the timber in one go, multiple passes were created to cut the mortise out, which cuts the timber only a few millimeters at a time. Due to the amount of passes required, the interior of the mortise is rough, which caused some difficulty for the tenon to slide in smoothly. This led to a rework in design to resolve the issues that were found from this design.

### 3.3. TOOL CHANGE

To solve this issue, the tool used was changed to a 13mm dovetail shaped router that can be attached to the end of the spindle (Figure 2). This created a design change to best optimise the execution of the dovetail router, causing the shape of the mortise and tenon to be a circle instead of a square. This allowed the dovetail tool to plunge itself straight into the plywood and move across and out. This was a beneficial decision because it allowed the grasshopper code to be simpler, because there is now only one curve instead of four separate curves to create the shape. This also ensured the cut was faster as the robot only had to make two moves instead of making four moves and having to repeat the four moves each time it went deeper into the plywood.

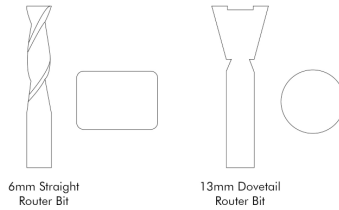


Figure 2. Router Bits.

Due to the 13mm tenon not being strong enough to hold the weight of the panel, the 16mm dovetail router was tested on the spindle to examine whether it would be stronger. This enabled the tenon to be thicker and the mortise to be wider (Figure 3). Instead of only having three tenons on the edge of the panel, a fourth one was also added to further increase the strength of the connection. The joint was tested on a scrap piece of LVL (Laminated Veneer Lumber), which caused the joint to break off when the dovetail router was halfway cutting through the circular shape of the tenon. This indicated the joint was not strong enough and the cut should have been tested on plywood, as LVL is a type of timber where thin layers of wood are oriented together in the same direction. This caused the timber to be initially weak, and if tested on plywood where adjacent layers are rotated up to 90 degrees, it may not have broken off as it would have been stronger. Regardless, the joint still needed to be stronger to ensure it would not break off no matter what timber was used.



Figure 3. 13mm Mortise vs 16mm Mortise.

#### 3.4. ANALYSIS OF FIRST SET

Plywood that was 25mm thick was used for the panels. Once the joints were cut, the panels were able to slide in and hold itself. Only three panels with joints were first cut, to analyse whether it could join together (Figure 4). This reduced wastage of plywood, as this was not the final set and was only cut to analyse the strength and success of the connection. This set was not successful because two out of the three joints on one edge eventually broke off after sliding it in and out a few times. This led to a redesign of the joints to ensure it can hold itself together without snapping off.

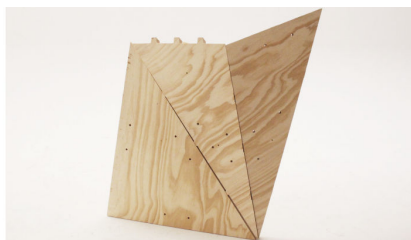


Figure 4. First Three Panels.

### 3.5. STRONGER JOINTS

From re-evaluating the current joints created, the joints needed to be a lot stronger to successfully hold itself together. The tenon needed to be wider to have a greater amount of surface area between the tenon and the panel. Therefore, a wider joint was designed, which used the 6mm straight router to initially cut the mortise. Following on, the 16mm dovetail router was used to plunge into the timber and move across to create the keyhole of the mortise. The same width was used to cut the tenon and it did not snap off during the cutting process (Figure 5). The same LVL timber was used which showed that the wider joint was a lot stronger and it can be used to further progress into the actual plywood panel connections (Figure 8).

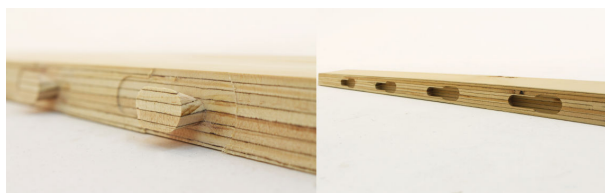


Figure 5. Wider Joints.

### 3.6. CUTTING PROCESS

When using the robotic arm, a cutting process was established to ensure it would be precise (Figure 6). The cutting process started with two holes were drilled 40mm apart and spaced 40mm from the edge of the table. The same holes were drilled 40mm from the center of each edge of each panel that would be cut (Figure 6). This was done to ensure when the panels were once cut, they were able to be manually lined up with the 2 holes drilled into the edge of the table. Lining the holes up to the center of the table surface allowed the mortise and tenon to be cut precisely from the y axis. There were some issues with this method as sometimes it would be half a millimeter off. To solve this accuracy issue, when cutting with the dovetail tool, it would get paused just before it gets cut, and checked to see if it was touching the timber perfectly, where it would be cut. Most of the time it was accurate, however during the times when it was not accurate, the timber panel



would be manually moved to touch the tip of the router.

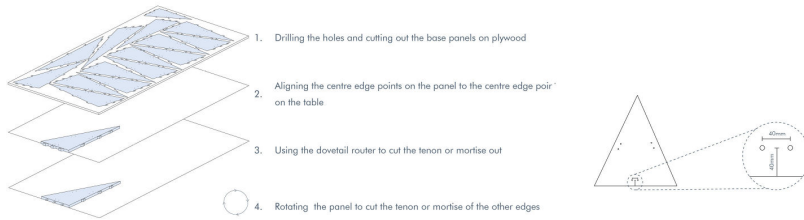


Figure 6. Cutting Process.

### 3.7. PANELS

Five panels were able to be robotically fabricated using the cutting process (Figure 7). The wider joints worked successfully as the panels were able to be slotted in together without the use of any metal fixings or glue. This method can be brought forward to create a self-supporting structure, however further structural testing will be needed to prove the structural stability of this method.

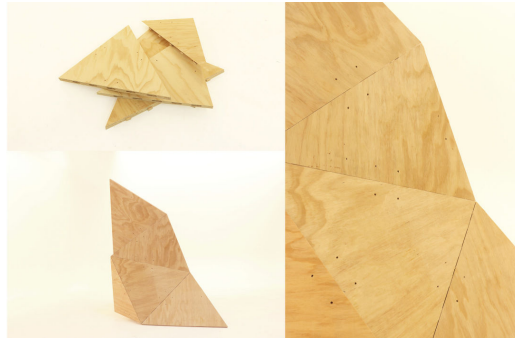


Figure 7. Final Panels Assembled & Disassembled.

## 4. Discussion

### 4.1. ERRORS

Double checking the points are in the right place is an important step before exporting the code to the robotic arm. At the step of routing the holes 40mm from the center of each edge of each panel that would be cut, a point for one of the holes was under the work table (Figure 8). This caused the router to go through the plywood and work table (Figure 8). This caused the router to go through the plywood and work table, causing the need to use the emergency stop button for the machine. Safety was an important issue that was discovered in this process due to the robotic arm being unable to recognise any obstacles. Similar to most machinery, this is a drawback of the robotic arm. Other machinery such as woodworking machines are unable to move around 6-axis and can only move to a

certain degree, therefore safety is not a big issue for those machines. However, the robotic arm does have the ability to move around 6-axis. Therefore, if a point is in the wrong spot, the robotic arm will still go to that point regardless if there are any obstacles in the way. This highlights the need to ensure the points are accurately placed in the correct spot to ensure safety, prevent errors and save time.

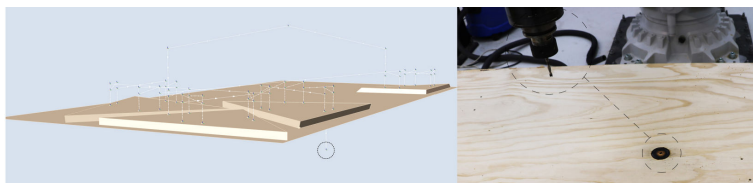


Figure 8. Point Underneath Work Table Causing Router Bit to get through Plywood.

An issue with the sliding mortise and tenon system was that not every panel was able to slide in to create the structure, therefore a build sequence was established for the base form. As once a certain point was reached, the sliding method became impossible and a new method would need to be explored to fit in the remaining pieces. This meant that some panels had a sliding mortise and tenon joint and some other panels would just be a mortise and tenon that does not slide and instead slot into place and hold itself together. This allowed the panels to still be able to be slotted into the difficult positions. Openings in the structure will be created, to enable more panels to use the sliding system and help aid in the construction of the structure.

The fabrication of the panels were not as straightforward as anticipated, as many issues had risen. Such as points not being in the correct place, and placement of the panels not being as accurate. The fabrication involved a fabricating, re-coding, and re-fabrication process to ensure the panels were cut correctly. The need to rework the code was time consuming and does not necessarily entail a 100% success rate. This is because the cutting process involved a manual placement of the panels which does not involve the robotic arm when preparing for the mortise and tenon to be cut. This caused the mortise to be 1.5mm shallower than needed, which led to the mortise not being wide enough for the tenon to fit through. This meant that the panel had to be moved 1.5 mm closer to the edge of the table and re-cut to allow the tenon to fit.

#### 4.2. IMPROVEMENTS

For this research to develop further, there are several improvements that could be implemented to address the issues found. To reduce errors, the manual placement of the panels would be removed and the use of the robotic suction gripper tool would be attached to the end of the arm, and used to place the panels in the right position. Automated tool switching such as switching from the 6mm router to the 16mm dovetail router could be implemented to speed up the process. The design of the joints relied on the tools that were readily available, however other tools could have been explored that were not a straight or a dovetail router. Lastly, collaboration with structural engineers, will increase the structural stability of

this system and also increase the potential of this research to be used in future structures.

## 5. Conclusion

Robotic fabrication is still developing in architecture, however it is opening up new opportunities in the industry. Preliminary research showed that prototypes of robotically fabricated structures still relied on fasteners to hold it into place. This research was undertaken to develop a workflow to create a self-supporting structure from sheet materials using robotic fabrication and computational tools. This study aided in the growth of knowledge in the design and fabrication with the robotic arm. Computational simulations was the methodology adopted for this research, enabling us to run an iterative process to act as a substitute for the actual physical prototyping and highlight the issues found.

Five panels were fabricated with the robotic arm. The five panels all consisted of the sliding mortise and joint system. The creation of these panels broadened the understanding of bringing a design from the digital world to the physical world. When designing the toolpath on Grasshopper and running the simulations, it was difficult to predict the errors that can occur until the prototypes are physically fabricated. This method of going from digital to physical was successful as only some parameters needed to be changed to resolve the issues found. The resolution of the issues created part of a structure that was able to hold itself with the joints that were designed. No glue nor screws were needed, which showcased the success of these joints. Although this research did not create a full structure, it did substantiate that parametric software combined with robotic fabrication, can create timber connections to connect sheet materials at different angles. A full scale structure will establish a greater degree of accuracy, thus a full scale structure based on this workflow can be explored in further research.

## References

- “A Guide to Engineered Wood Products” : no year given. Available from <<https://www.apawood.org/publication-search?q=c800&tid=1>> (accessed 11th May 2019).
- Dooley, K. 2002, Simulation Research Methods, in J. Baum (ed.), *Companion to Organisations*, Blackwell, London, 1-39.
- Dunn, N.: 2012, *Digital Fabrication in Architecture*, Laurence King Publishing, London.
- Graubner, W.: 1992, *Encyclopedia of Wood Joints*, The Taunton Press, Germany.
- Owen-Hill, A.: 2018, “Can a Robot Outperform a CNC Machine for Robot Machining?” . Available from <<https://robotk.com/blog/robot-machining-vs-cnc/>> (accessed 10th April 2019).
- Schwinn, T., Krieg, O.D. and Menges, A. 2012, Robotically Fabricated Wood Plate Morphologies, in S. Brell-Cokcan and J. Braumann (eds.), *Robotic Fabrication in Architecture, Art, and Design*, Springer , Vienna, 48-61.
- Schwinn, T. 2017, Landesgartenschau Exhibition Hall, in A. Menges, T. Schwinn and O.D. Krieg (eds.), *Advancing Wood Architecture*, Routledge, New York, 111-124.
- Tankut, A.N. and Tankut, N.: 2004, The Effects of Joint Forms (Shape) and Dimensions on the Strengths of Mortise and Tenon Joints, *Turkish Journal of Agriculture and Forestry*, **29**, 493-498.
- Willma, J., Block, P., Hutter, M., Byrne, K. and Schork, T.: 2018, *Robotic Fabrication in Art Architecture, Art and Design 2018*, Springer Nature, Switzerland.

# WEB-BASED DISTRIBUTED DESIGN TO FABRICATION WORKFLOWS

PAUL POINET<sup>1</sup>, DIMITRIE STEFANESCU<sup>2</sup> and  
ELENI PAPADONIKOLAKI<sup>3</sup>

<sup>1,2,3</sup>*University College London - Bartlett School of Construction and  
Project Management*

<sup>1,2,3</sup>*{p.poinet|d.stefanescu|e.papadonikolaki}@ucl.ac.uk*

**Abstract.** As architectural design projects tend to tackle larger scales and become more complex, multiple involved actors often need to work from different remote locations. This increased complexity impacts the digital design-to-fabrication workflows that become more challenging, as each actor involved in a project operates on different software environments and needs to access precise fabrication data of specific design components. Consequently, managing and keeping track of design changes throughout the design-to-fabrication workflow still remains a challenge for all actors involved. This paper discusses how this challenge can be tackled through both Speckle, a complete open source data platform for the Architecture, Engineering and Construction (AEC), and SpeckleViz, a custom web-based interactive Activity Network Diagram (AND) built upon Speckle. SpeckleViz continuously maps data transfers across design and building processes, enabling the end-users to explore, interact and get a better understanding of the constantly evolving digital design workflows. This is demonstrated in this paper through a computational design and digital fabrication workshop conducted at the Centro de Estudios Superiores de Diseño de Monterrey (CEDIM), during which an integrative, file-less collaborative design workflow has been set through Speckle, connecting different Rhino-Grasshopper sessions acting as discrete computational design pipelines.

**Keywords.** Collaborative Workflows; Distributed Design; Activity Network Diagram; Data Flow.

## 1. Introduction

Design is a key phase across projects' lifecycle and collaboration among design actors is complex and crucial for project success. A recent report released by the Association of Project Management (APM) emphasizes the need for developing custom specific solutions to tackle contemporary large-scale and complex projects: *"Many infrastructure projects in the UK now recognize the need for solutions that are designed to deal with the specific challenges involved in planning and executing large, complex projects. (...) Over the past decade,*

*many of the UK's largest and most complex infrastructure projects have abandoned traditional delivery models*" (Davies 2019). Indeed, contemporary design to manufacture process of large-scale and geometrically complex architectural projects remains a significant challenge, even though digital literacy keeps improving and computational design knowledge becomes widely available.

Apart from being able to model complex geometry, the design process must also be curated, shared and understood in more simple, transparent and intuitive ways than it is currently taking place within the Architecture, Engineering and Construction (AEC) industry. In the AEC sector, current design processes are still segregated, and laborious manual interventions sometimes become a daily routine (Burry and Holzer 2009). To tackle this issue, custom management and visualization tools enabling better understanding and curation of complex projects Activity Network Diagrams (AND) have been proposed by different firms and individuals. Those proposed solutions converge towards the need for defining low level open-source infrastructures enabling more transparent collaborative workflows. To this end, this study aims to address this need by presenting a web-based open-source interoperability framework Speckle (2020) that increasingly gains traction in the AEC. Built upon Speckle, SpeckleViz (2020) an interactive AND, helps end users to get an overview of data flows in a specific Speckle Project. This paper is divided into five sections after this introduction: description of Speckle framework, description of SpeckleViz interface, empirical testing in a case study of "Piped Assemblies" workshop, where both Speckle and SpeckleViz were deployed, discussion section and section with concluding remarks.

## **2. Speckle open-source data framework**

Speckle (2020) is a unique, complete open-source data framework for the AEC that differs from commercial web-based interoperability platforms. It was originally developed at University College London (UCL) in 2016 by Dimitrie Stefanescu (Stefanescu 2020). Unlike the existing AEC standard Industry Foundation Classes (IFC) that characterizes most of Building Information Modelling (BIM) software available today, Speckle does not impose a predefined topology of communication patterns (or specific object model), but rather allows for the emergence of meaningful data-driven dialogue amongst different actors involved in the design process. Contrary to the current single monolithic BIM model paradigm that argues in favor of centralizing all data coming from different trades involved in the design process of an architectural project, Speckle embraces and acknowledges the existing decentralized design processes by providing an open source infrastructure to better manage and curate them.

Practically, Speckle currently offers a set of Computer Aided Design (CAD) application integrated clients (Grasshopper, Dynamo, Rhino, Blender, Revit and GSA), which support seamless data exchanges through "Streams". In Speckle, a Stream is essentially a collection of geometrical objects that has been sent to or received from a Speckle client. As the data exchanges happen informally across users working remotely from the different mentioned software platforms, SpeckleViz - a web application for Speckle - has been implemented, in order to

obtain a clear visual representation of the overall data flow for a specific project.

### 3. SpeckleViz data flows visualization interface

SpeckleViz is an AND developed in Speckle to get a better understanding of data flows in a Speckle Project across multiple Speckle Users (users logged in the Speckle Admin interface), Speckle Streams (collections of Speckle Objects shared across multiple users) and documents (the software environments from which data has been sent or received via Speckle). The interface is situated at the bottom of a Speckle Project page and directly reflects how Speckle Streams are organized and relate to each other within a same Speckle Project. The SpeckleViz interface (see Figure 1) is divided into two main parts: the control interface, composed of the main toolbar, the time range slider and the tag query selector, and the graph canvas. The next paragraphs summarize the main visualization and interaction features of SpeckleViz and the complete documentation of the interface is available on its dedicated documentation page available within the main Speckle website (SpeckleViz 2020).

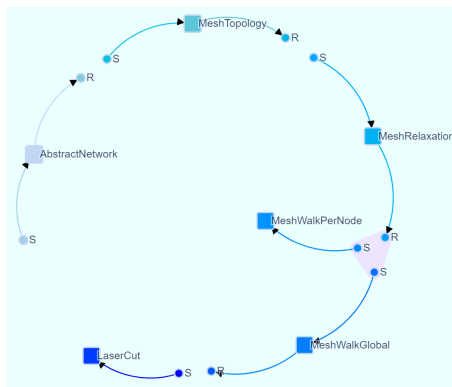


Figure 1. The SpeckleViz interface can be found at the bottom of a Speckle Project page.

#### 3.1. SPECKLEVIZ VISUALIZATION FEATURES

Similarly to any graph (Biggs et al., 1976), SpeckleViz consists of nodes and edges. First, circle nodes represent Speckle Senders or Speckle Receivers, square nodes represent Speckle Streams. Second, graph edges represent either data that has been shared to a stream by the user (Receiver to Stream) or data that has been retrieved by a user from a stream (Stream to Sender). The edges' thickness is proportional to the number of exchanged geometrical objects. Generally, both nodes and edges are colored according to their respective *createdAt* timestamp: dark blue for the newest created, and light grey for the oldest. Senders and Receivers can be grouped either by identical Document GUID (Globally Unique Identifier) or identical Client's owner ID. While the latter is represented by a blue convex hull, the former is visualized by a pink convex hull.

### 3.2. SPECKLEVIZ INTERACTION FEATURES

Multiple interaction features have been implemented on the front-end in order to give the end-user a more granular control over the data exposed by SpeckleViz:

- **Dragging nodes:** Nodes can be dragged through the canvas by holding left click on a specific node.
- **Zooming/Panning:** It is possible to zoom in or zoom out by using the scroll wheel, and pan by holding left click on the background canvas and moving the mouse around it. If the graph disappears, clicking on the GPS button situated on the toolbar will re-center the graph.
- **Switching between data flow types:** The clients are grouped either by Document GUID or User GUID. The SpeckleViz toolbar exposes a toggle button enabling users to choose between the “*Data flow per user*” and “*Data flow per document*” modes. Thus, SpeckleViz provides users with illustrations of data flows among the Social Network, as described by Wasserman and Faust (1994), and the inherent AND, as defined by Bauke de Vries (1995). Switching between these two modes dynamically updates the graph that reorganizes its nodes according to chosen data flow perspective.
- **Expanding/Collapsing clusters:** The slider located on the right side of the toolbar enables the user to expand or collapse the clusters described above. This might be useful to disentangle the wires and zoom in on a particular cluster.
- **Inspecting a specific stream:** Right clicking on a Stream will trigger a context menu from which it is possible to: (1) inspect the Stream within the Speckle Viewer, (2) inspect the Stream within the Speckle Admin, (3) inspect the Stream’s raw data and (4) inspect the Stream’s related client’s raw data.
- **Inspecting a time frame:** As specified above, both Streams and Clients expose the *createdAt* property informing on when the Stream or Client was created. This data has been brought to the front-end of SpeckleViz by integrating a slider within the application, enabling the end-user to select a specific time frame of the project. When dragging the slider, the graph’s nodes and links fade out when they are out of range and fade back in when they are in range. Furthermore, the Streams created within the selected time frame are continuously collated and can be visualized altogether inside the Speckle viewer through a dedicated button.
- **Refreshing the graph:** If the project is modified (e.g. through the addition or removal of a Speckle Stream), the user will need to hit the refresh button situated on the left side of the toolbar, as the graph won’t listen for changes and therefore won’t update automatically.
- **Tag-based queries:** In Speckle, Streams can be tagged by the end-user through the web management admin interface. In SpeckleViz, streams can be selected by tag(s) - which were previously set through the management interface - within the search bar situated below the time range slider. The selection dynamically updates the display of the Stream nodes within the graph by highlighting the ones containing at least one tag present within the current selection. Furthermore, the selected tagged Streams are continuously collated and can be visualized altogether inside the Speckle viewer through a dedicated button.

#### 4. Case study: “Piped Assemblies” Workshop at CEDIM

This study uses a case study to provide empirical data on the operation of Speckle and SpeckleViz and illustrate their function. SpeckleViz has been tested against data generated from design to fabrication during the “Piped Assemblies” Workshop conducted at CEDIM during 26 November to 7 December 2018. This workshop addressed the challenge of introducing state of the art web-based collaborative computational design workflows to undergraduate students in architecture, through the design and fabrication of a free-form networked structure made of laser-cut polypropylene plastic strips.

##### 4.1. CASE STUDY DATA COLLECTION AND ANALYSIS

Through the Grasshopper Speckle client, both Speckle Senders and Receivers were used to seamlessly share design data across all the phases of the design process. The data collected originated directly from the different Rhino-Grasshopper sessions manipulated by the students, and could serve three different purposes:

- **Exchanging design ideas:** data could be shared in the sole purpose of exchanging design ideas. This way, students could always log in to the admin interface and explore and be inspired by the different models shared by their classmates.
- **Keeping track of the project’s timeline history:** data could also be gathered in order to keep track of the chronological evolution of the design process, from the lowest level of detailing to the highest (as defined in sections 4.2.1 and 4.2.2). In this specific case, SpeckleViz helped the users to visualize and inspect the evolutionary process of the data flow which is passed from one Stream to another, through time.

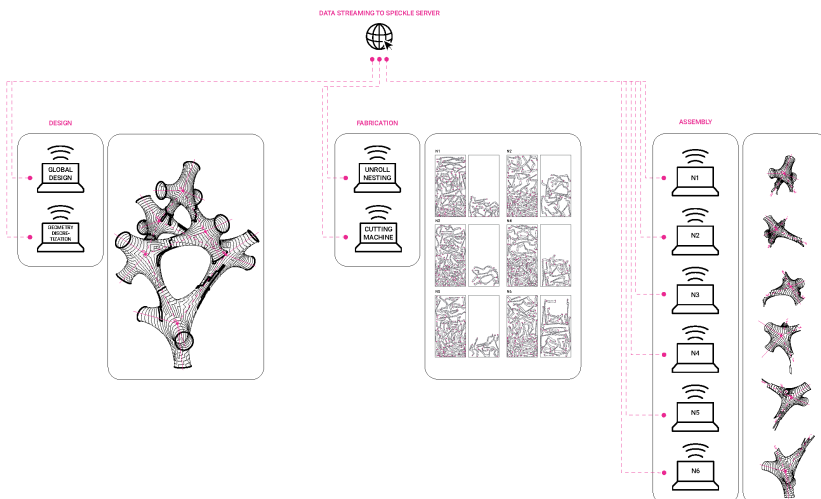


Figure 2. Overall design to fabrication workflow of the Piped Assemblies workshop.



## 4.2. DESIGN-TO-FABRICATION WORKFLOW

The design-to-fabrication workflow of the Piped Assemblies workshop had to be both flexible enough to let the students explore different design options, and to embed rationality (Attar et al. 2010) as well as multiple constraints for further fabrication and assembly feasibilities. While the students were subdivided into three different groups responsible respectively for design, fabrication and production, the overall design to fabrication workflow (see Figure 2) has been segregated into 7 distinct computational pipelines - or remote concurrent shared parametric models (Burry and Holzer 2009) - which are all connected through Speckle Streams:

### 4.2.1. Design Generation and Embedded Rationality

- **(1) Definition of the overall abstract network.**
- **(2) Base mesh generation.** This step was particularly crucial to generate a design which had to be consistent enough to be fabricated and assembled with differentiated polypropylene strips. The mesh resolution, the curvature relaxation and the planarity of each mesh face all had to be considered to evaluate the feasibility of the design.
- **(3) Mesh relaxation and planarization.** Once a consistent global mesh has been generated in the previous step, a dynamic relaxation has been performed using Kangaroo 2 (Piker 2020), a live physics engine for interactive simulation, form-finding, optimization and constraint solving. The relaxation used here constrained all the mesh quads to remain planar, ensuring further developability for laser cut fabrication.

### 4.2.2. Data Generation for Fabrication

- **(4) Strips generation.** Here, a mesh-walk algorithm has been developed. The python library NetworkX (2020) allowed to convert the relaxed mesh into a graph, and run the Dijkstra's Shortest Path First algorithm which could find the shortest path between two mesh face center points. Although not perfectly geodesic, such path tends to minimize the curvature of each strip. This particular design process was iteratively computed through a feed-back loop: after the generation of one strip, the latter was "removed" from the global mesh, and the Dijkstra's Shortest Path First was re-computed onto the "remaining" global mesh. The feedback loop stopped once the global mesh was completely transformed into individual strips. From this step, the overall discretized structure has been segregated into six different nodes.
- **(5) Labelling, unrolling and sorting of the strips.** From this step, the students had to orchestrate themselves into six different teams to Separate the Concerns (Dijkstra 1970) and fabricate separately the six different nodes of the structure, thus reducing complexity of the future assembly process. For each node, the processes described from (5) to (7) intertwined themselves in order to optimize the timeline of the fabrication process. Indeed, while a team focuses on the laser cutting process, another team does not have to wait for all the pieces of the entire structure to be ready and can start assembly as soon as a set of strips

necessary to form a node is ready. The same goes for the assembly process between multiple nodes, which can start as soon as two neighboring nodes are ready to be connected.

- **(6) Nesting of the strips** through OpenNest (Vestartas 2020) - a plug-in for Grasshopper - and generation of their respective connection tabs around the edges. During the nesting process, the strips were distributed amongst 12 boards of 122\*244 centimeters. Finally, the tabs for the rivet connections were generated by means of custom offsets.
- **(7) Exporting the fabrication data** via .dxf files for machine-ready deliverables and wireless transfer to the laser cutter at STM Robotics (laser cutter fabricator and sponsor of the workshop).

#### 4.2.3. Fabrication and Assembly

After being laser cut at STM Robotics, all the polypropylene plastic strips had to be manually sorted both by their respective length and index number (engraved into which element) to ease the further fabrication process. This design-to-fabrication workflow described above enabled the participants to track each strip and detect their neighboring pieces, within and between each node. The six nodes have been constructed parallelly but assembled one after the other (one neighbor at a time), facilitating the reach of the connecting tabs from both inside and outside the nodes during the manual placement of the rivets. The final assembled physical prototype has been hanged with nylon threads in the main entrance of CEDIM, between the first and the ground floor through the mezzanine aperture (see Figure 3). The tension of the structure was adjusted manually and empirically by calibrating the tensile force and anchor location of each thread.



Figure 3. Final installation suspended above the main entrance of CEDIM.

#### 4.3. WEB-BASED COLLABORATION THROUGH SPECKLE STREAMS AND SPECKLEVIZ

After describing the design-to-fabrication workflow deployed in the workshop, reflection on the communicative and collaborative strategies deployed throughout

the project follows. Using a Speckle server to gather geometrical data allowed flexibility in the design and fabrication process as team members were not required to collocate, but could instead spread across the various locations to support design, fabrication and assembly of the structure, and work remotely from those: (1) the laser cutter at STM Robotics for fabrication, (2) the university's workshop for assembly and (3) the exhibition space for installation. Through the Grasshopper Speckle clients, both Senders and Receivers were used to seamlessly share design data across all design actors, software platforms and across pipelines.

During each design transaction, and via Speckle and SpeckleViz, the students were able to inspect and enrich geometric information with metadata needed for their specific subtasks, thus maintaining a high degree of information efficiency and little overhead in terms of data payload, as the minimum required information could be seamlessly shared via Speckle Streams, without the need of converting and exporting entire files. Multiple informational Streams were created, aggregated and throughout the process (see Figure 4). In the present case study, each Stream geometrically depends on each other, and the overall workflow goes from the lowest level of detailing to the highest:

- 1. Definition of the overall abstract network (generated by the design group).
- 2. Base topological mesh design generation (generated by the design group).
- 3. Mesh relaxation (generated by the design group).
- 4. Strip segments generation (inspected by the fabrication groups).
- 5. Unrolling and nesting (generated and inspected by the fabrication groups).

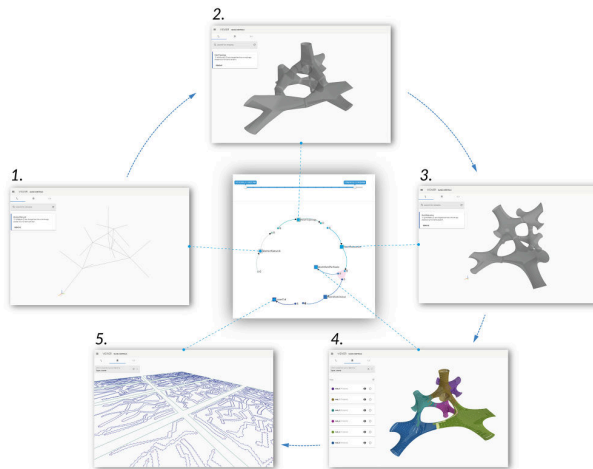


Figure 4. Through the SpeckleViz interface, the user can visualize the data exchanges and access each Stream within the Speckle viewer, from the design to the fabrication stages.

Here, the design Streams in Speckle maintained their relevance and usefulness both in the later fabrication stages, during laser cutting and labelling processes, as well as during assembly, by being able to visually relate parts to the whole, interactively, and on-site.

## 5. Discussion

The present case study demonstrated that Speckle could orchestrate a complete workflow, in which data are sent seamlessly from and to different Streams, and thus throughout the whole design process of an architectural project in an academic context. Furthermore, SpeckleViz enhances design collaboration at the project by allowing Speckle users to visualize and inspect the data flow taking place at any stage in the design process through AND. The workshop case described above, demonstrated that users could easily use SpeckleViz to trace back the project timeline history and retrieve specific Streams that were previously created and shared.

Both Speckle and SpeckleViz enable a seamless flow of data across different design processes that were previously segregated (Burry and Holzer 2009) and offers new perspectives for the design to fabrication workflows of large-scale and complex architectural design projects. This is particular important for contemporary projects that lack custom solutions (Davies 2019). Whereas the present case study happened in the context of an academic workshop for undergraduate students in architecture, the authors believe that these particular design methodologies and new ways of sharing data through the Speckle platform could also be deployed in practice, as they present great potential for seamless collaboration strategies. Such design methodologies offer new ways of sharing data through the Speckle platform and present great potential for seamless collaboration strategies. For example, the Building Information Generation (Van der Heijden et al. 2015) workflow, a modelling strategy deployed by Front Inc., that consists of a strategic alternation between the generation of objects in Grasshopper and their subsequent storage and classification within staged Rhino3D models, could largely benefit of the Speckle platform which would enable a live connection between the different deployed Rhino3D and Grasshopper clients, as well as SpeckleViz which would enable the Speckle users to visualize and inspect the data flow throughout the whole design process.

## 6. Conclusion and Outlook

This paper puts forward a new, prototypical way through which information modelling can be employed in an agile manner in fabrication processes. Through the design process and physical outcome of the digital fabrication workshop conducted at CEDIM, we show that a distributed, informal communication process can evolve into a highly efficient and lean workflow that maintains the necessary precision and coordination for precision manufacturing and assembly. Future work will look more particularly at how SpeckleViz could represent data flows beyond a single project environment. Visualizing data exchanges across multiple projects, companies and/or servers would be next steps towards streamlining design and fabrication in the AEC.

## Acknowledgements

The authors would like to thank Djordje Stanojevic, Yessica Mendez, David Durán, the workshop sponsors and the students involved in the Piped Assemblies

workshop at CEDIM. The SpeckleViz interface has been developed during the “AEC Delta Mobility” project which has received funding from InnovateUK under the competition “Increase Productivity, Performance and Quality in UK Construction” (proj. no. 104799). Speckle was originally developed at The Bartlett School of Architecture as part of the InnoChain project, which received funding from the European Union’s Horizon 2020 research and innovation programme under the Marie-Sklodowska-Curie grant agreement No 642877.

## References

- “Piped Assemblies” : 2019. Available from <<http://blog.cedim.edu.mx/arquitectura/piped-assemblies/>> (accessed 28th of January 2020).
- “Rhinoceros (typically abbreviated Rhino, or Rhino3D) is a commercial 3D computer graphics and computer-aided design (CAD) application software developed by Robert McNeel & Associates” : 2020. Available from <<https://www.rhino3d.com/>> (accessed 28th of January 2020).
- “Grasshopper is a visual programming language and environment that runs within the Rhino3D.” : 2020. Available from <<https://www.grasshopper3d.com/>> (accessed 28th of January 2020).
- “SpeckleViz documentation page” : 2020. Available from <<https://speckle.systems/docs/web/speckleviz/>> (accessed 28th of January 2020).
- “NetworkX homepage” : 2020. Available from <<https://networkx.github.io/>> (accessed 28th of January 2020).
- Balaji, S.B. and Murugaiyan, S.M.: 2012, Waterfall vs V-Model vs Agile: A Comparative Study on SDLC, *International Journal of Information Technology & Business Management*, **2**(1), 26-30.
- Biggs, N., Lloyd, E.K. and Wilson, R.J.: 1976, *Graph Theory 1736-1936*, Oxford University Press, New York, USA.
- Burry, J.B. and Holzer, D.H.: 2009, Sharing Design Space: Remote Concurrent Shared Parametric Modeling, *Proceedings of eCAADe 2009*, Istanbul Technical University, Faculty of Architecture, 333-340.
- Davies, A.D.: 2019, *Project management for large, complex projects*, Association for Project Management, Princes Risborough.
- Dijkstra, E.W.D.: 1970, Notes on Structured Programming, *EUT report. WSK, Dept. of Mathematics and Computing Science*, **70**(3), 1-84.
- Van Der Heijden, R., Levelle, E.L. and Reise, M.R.: 2015, Parametric Building Information Generation for Design and Construction, *Proceedings of ACADIA 2015*, Cincinnati, Ohio, United States, 417-430.
- Mirtschin, J.M.: 2019, “Revit IFC User Meeting” . Available from <<https://www.youtube.com/watch?v=1fJbQ2PmhqA>> (accessed 28th of January 2020).
- Neijur, A.N. and Seinfeld, K.S.: 2016, Ivy: Bringing a Weighted-Mesh Representation to Bear on Generative Architectural Design Applications, *Posthuman Frontiers: Data, Designers, and Cognitive Machines, Proceedings of the 36th Annual Conference of the Association for Computer Aided Design in Architecture (ACADIA)*, Ann Arbor, 140-151.
- Piker, D.P.: 2020, “Kangaroo2 download page” . Available from <<https://www.food4rhino.com/app/kangaroo-physics/>> (accessed 28th of January 2020).
- Stefanescu, D.S.: 2020, *Alternate Means of Digital Design Communication*, Ph.D. Thesis, UCL.
- Vestartas, P.V.: 2020, “OpenNest homepage” . Available from <<https://www.food4rhino.com/app/opennest/>> (accessed 28th of January 2020).
- De Vries, B.D.V.: 1995, Message Development in the Building Process, “*Modeling of Buildings through their Life-Cycle*”, *Proceedings of the CIB w78 Conference*, Stanford, 467-479.
- Wasserman, S.W. and Faust, K.F.: 1994, *Social network analysis: Methods and applications*, Cambridge University Press, Cambridge, United Kingdom.

# A CO-EXISTING INTERACTIVE APPROACH TO DIGITAL FABRICATION WORKFLOW

CHI-FU HSIAO<sup>1</sup>, CHING-HAN LEE<sup>2</sup>, CHUN-YEN CHEN<sup>3</sup> and TENG-WEN CHANG<sup>4</sup>

<sup>1,3,4</sup>*National Yunlin University of Science and Technology*

<sup>1</sup>*chifu.research@gmail.com* <sup>3,4</sup>*{m10635013|*

*tengwen}@gmail.yuntech.edu.tw*

<sup>2</sup>*Dept. of Architecture, Tamkang University*

<sup>2</sup>*chinghanglee@gmail.com*

**Abstract.** In recent years, digital fabrication projects have explored how to best present complex spatial patterns. These patterns are generated by a series of function clusters and need to be separated into reasonable working sequences for workers. In the stage between design and fabrication, designers and workers typically spend considerable time communicating with each other and prototyping models in order to understand the complex geometry and joint methods of fabrication works. Through the potential of mixed reality technology, this paper proposes a novel form of co-existing interactive workflow that helps designers understand the morphing status of material composition and assists workers in achieving desired results. We establish this co-existing workflow mechanism as an interface between design and reality that includes a HoloLens display, a parametric algorithm, and gesture control identification. This paper challenges the flexibility between the virtual and reality and the interaction between precise parameters and natural gestures within an automation process.

**Keywords.** Co-existing interactive workflow; Digital fabrication; HoloLens; Digital twin; Prototype.

## 1. Introduction

Digital fabrication is a recursive process that interacts with a designer's ideas, fabrication tools, and the need for alignment with a ductility remapping system from the virtual database to the real space (Chen et al. 2019). This paper proposes a co-existing, interactive, and immersive method that combines a digital visual model with physical materials and surrounding space. Although the enhancement of digital software has enabled designers to create more projects with complex form, the thoughtlessness of practical experiences and armature construction technology have presented certain challenges. Pure digital modeling is not sufficiently clear when designers are attempting to implement their work in the physical world.

Based on the “seeing-moving-seeing design-thinking model” (Schon and Wiggins 1992), a co-existing interface provides real-time feedback, allows

designers to refine their ideas, and makes it easier for participants to exchange their ideas, patterns, and experimental prototypes with each other. As the study by Lai and Chang confirmed, a co-existing environment of interactive representation can help the interplay move from virtual to reality via visual display processes (Lai and Chang 2003). Waseda university team proposed the “Interactive Spatial Copy Wall” (ISCW), a system that interactively manages hundreds of moving pipes so that remote participants can interact with each other in visual representation (Wesugi et al.2004).

Thus, an effective process of prototyping that constructs a bridge between designers and work-team is important in digital fabrication workflows. In order to lower the fabrication threshold and ensure the flexibility of the digital design subject, a collective-fabrication team in 2017 CAADRIA workshop proposed a “Design Fabrication Assembly” (DFA) system, which is an integrated prototyping workflow (Huang et al. 2017). The DFA uses a framework that helps every participant, including designers and armature workers, partake in the entire project, understand the process of each complex fabrication state, and identify any potential design mistakes.

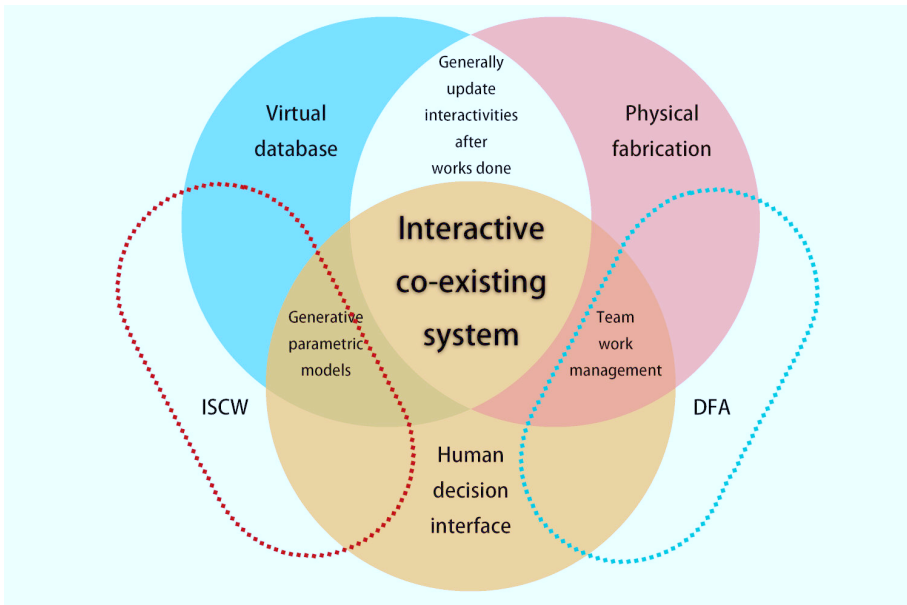


Figure 1. A comparison between the ISCW and DFA frameworks and the lack of real-time co-existing interactions.

On the basis of the DFA framework, the fabrication workflow would become fragmentary for armature work mates would need to stop assembling several times to discuss the misunderstanding of 2D drawings or unclear construction notes, however. Thus, this paper also proposes a HoloLens display as an interactive fabrication interface to facilitate communication between the parametric digital

model and physical construction so as to enhance the management quality of the team-based digital fabrication process. A HoloLens is a head-mounted mixed reality display that integrates the physical and digital environment to create an immersive world where real and virtual objects co-exist and can instantly reflect the user’s gestures. A mixed reality system such as this expands design possibilities, integrating tools, and designer behavior within a more immersive interplay system.

**2. Co-existing fabrication system method**

We implement this mixed reality interactive process as a “co-existing fabrication system” (Cofabs) to support manufacturing workflow. Cofabs is composed of three aspects: designer behavior, digital data flow, and physical entities. Each thread is separated into gestures, parameter morphing, and design decisions in a recursive manner. These threads are automatically connected to each other in the fabrication workflow to reduce the technical threshold (as shown in Figure 2).

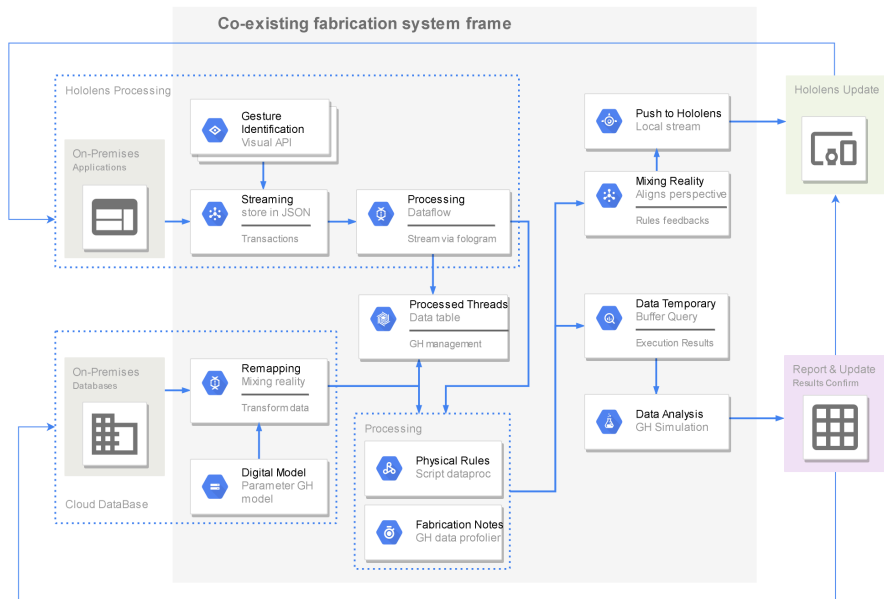


Figure 2. Cofabs workflow structure.

In comparison to the DFA, the Cofabs integrates both real-world and virtual environments based on the “Digital Twin” (DT) concept, which proposes a system where physical entities and virtual information are referenced to each other in a recursive way through a series of physical changes, information analysis, and generative fabrication suggestions. In this way, the workflow is optimized (Grieves and Vickers 2016). We divide the workflow of the Cofabs into three stages: the physical prototype stage, the digital/virtual DT model stage, and the



stage that as the interface to deals with these two elements. The execution of these stages is described below.

- First, we build a cloud database to record the environment's static background and the parametric geometry DT model.
- In order to simplify the process of the DT model, the assembly steps, and the fabrication decision, we build the DT model as a design subject and immerse the model scale in the real-world environment.
- We then connect the parametric geometry model to the HoloLens through Fologram, a plug-in to connect 3D software and HoloLens, (Jahn et al. 2018) and merge this changing DT model with the users' perspectives.
- The team leader use HoloLens as the bridge interface, constantly update the DT model and supervise the progression of the project while the work-team assemble their fabrication project.
- Certain physical factors can influence the representation of the simulated DT model, depending on the material chosen. Thus, we need to code several scripts, such as gravity, inner tension, and deformation quantity, to calculate the difference between the designing algorithm and the real fabrication situations.
- The Cofabs then arranges the buffering information of the DT model and its physical states in real time to guide designers through the steps of the fabrication workflow.

### **3. Fabrication experiment workflow**

Cofabs presents a framework that prototypes designers' ideas in a rapid, interactive, and visually understandable way. We apply this interactive system to re-fabricate a practical weaving structure constructed (Huang et al. 2016) from flexible linear material (we use 5mm diameter acrylic rod in this case) as an experiment to improve the possible use of Cofabs. In order to enhance the effect of interactive operations, we simplify the form-finding process into a systematic modular system during the design stage. The weaving project is generated in mesh-type parametric model, and it permits designers to change the shape of project by controlling its weaving intersection nodes.



Figure 3. Traditional fabrication methodology with handwritten markers and a rough weaving curvature.

In the traditional experiment workflow, the work-team need to spend considerable time preparing the material and mark the exact position of the intersection points via tapes and stickers (Huang et al. 2018). For the work-team, an expert leader should manage the entire fabrication process and ensure that all of the details are taken care of, including confirming whether the site has been cleared, the material located, and the marker prepared (as shown in Figure 3).

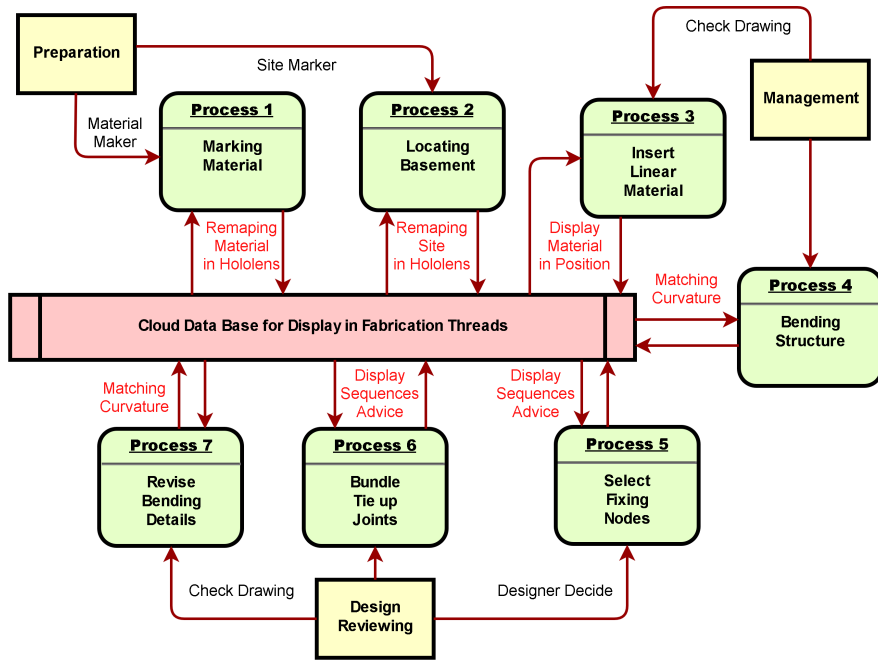


Figure 4. A comparison between the traditional process and the Cofabs fabrication process.

Following the preparation phase, decisions need to be made regarding the different aspects of the construction process, including basement locating, extends weaving, and units jointing. Within this complex and synchronized fabrication workflow, only some participants can transcribe the design schedule into reality, and even fewer participants can supervise the progress of the fabrication, highlight mistakes, or propose emergency solutions. A comparison between the traditional process and the Cofabs fabrication process is shown in Figure 4, with the traditional method highlighted in black and the Cofabs method highlighted in red (shown in Figure 4).

#### 4. Physical and virtual interaction

Since the Cofabs process uses HoloLens as the interface to represent the co-existing DT model of the weaving structure, we focus on how to use this interactive interface to aid users in making decisions. First, we upload the DT model to HoloLens and establish a mixed reality environment. In order to make the fabrication easier, HoloLens can align users' perspectives, identify gestures through UI events listening, and simulate the consequences of decisions during the fabrication process.

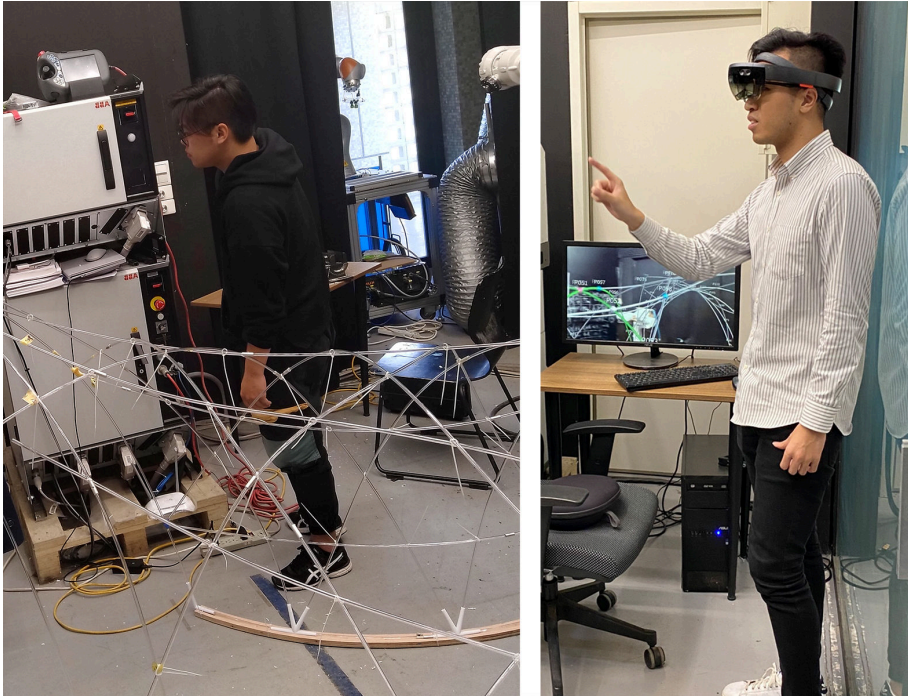


Figure 5. The Cofabs workflow, cooperate with HoloLens user and armature worker.

In order to effectively manage the decisions and feedback of the users, we organize their reflecting threads into four threads: selector identification, data retrieval, custom-method use, and gesture confirmation.

1. In the selector identification thread, a ray-casting pointer projects from the center of the user's sight and applies the selector category in the background thread, catching up the event if there has been collider callback from the virtual object.
2. In the data retrieval thread, active internalize view constantly listening to the selector's selected event. The HoloLens will display the information from the selected object to help users understand the status of the subject and make design decisions.
3. In the custom method thread, designers can script their own reflecting method according to the fabrication methodology. For example, with the weaving structure, we code our custom interactive function via different forms of gesture and behavior identification, such as anchor, de-anchor, pull, push, or rotate, to classify the normal vector of nodes on the weaving structure.
4. In the gesture confirmation thread, the active internalized view constantly identifies the index and thumb gestures as clicks, or dragging is performed. The Cofabs system also renders the subjects transparent before helping the user decide on their fabrication order.

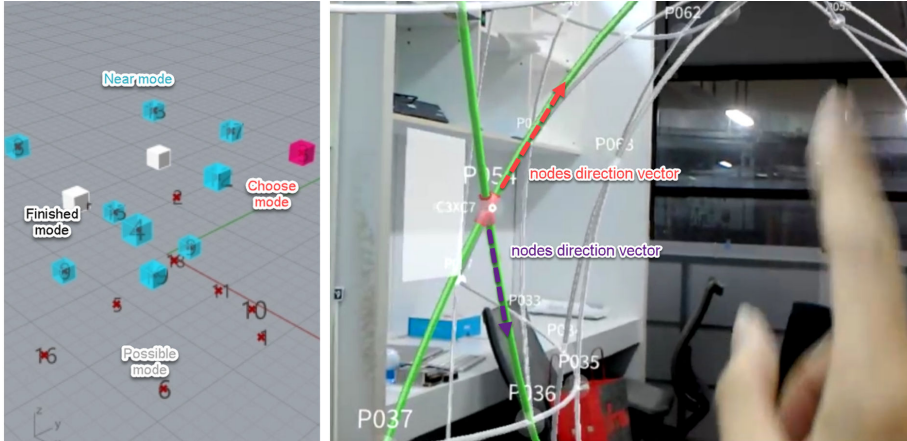


Figure 6. The setting of the experimental rendering mode used in this study.

Cofabs renders each digital node as having four understandable modes: (1) Choose, (2) Near, (3) Finished, and (4) Possible (shown in Figure 6)

1. The Choose mode refers to the focus of the fabrication thread. The node will render to red and list the information within the GUI panel. Executable activities, such as pull, push, move, or rotate, will control the normal direction of mesh surface via gestures.
2. The Near mode will appear when the Choose node is close by. It renders to blue and refers to the next possible node.
3. The Finished mode indicates that the fabrication is finished, renders to white, and helps the user track the progress of the fabrication schedule.
4. The Possible mode expresses the quantum state of any uncertain nodes. The Cofabs permits users to set the render type as transparent in order to confirm the design model or hide the possible mode nodes themselves for more clearly executed scenery.

Within this framework of feedback and render, the work-team members can deal with the complex structures of assembly in an asynchronous manner. While the leader of the project oversees the progression of the fabrication intuitively under an immersive mixed reality environment, every team member can also supervise the progress of the fabrication by simultaneously sharing the leader's perspective.

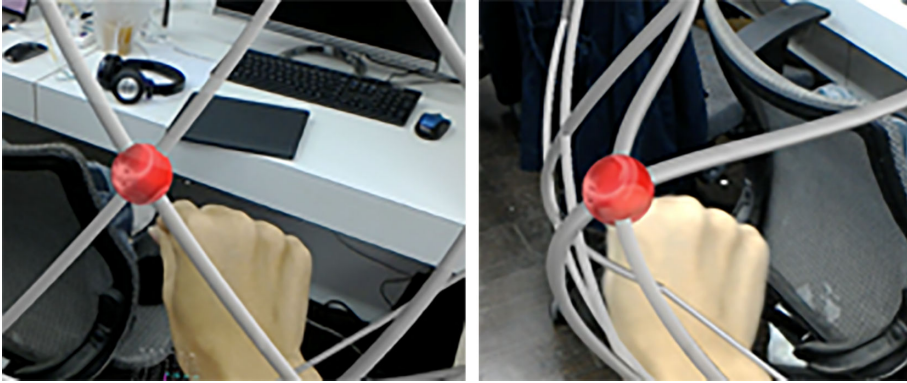


Figure 7. The variable parameter ( $P_a$ ) at various degrees of bending in the same weaving structure DT model (Left  $P_a = 1$ ; Right  $P_a = 1.5$ ).

Following the fabrication process, we discovered that the weaving structure changes every time we change the position of a node due to a waving structure is connected each other. Thus, we add a variable parameter ( $P_a$ ) to express the degree of bending. Inputting this parameter helps us identify the most reliable design decision, and users can use the same gesture to move the node according to different  $P_a$  values and compare the DT model with real material morphing states (shown in Figure 7).

Under the Cofabs framework, fabrication threads can operate clearly matching, adjusting, limited problem space and are able to share the progress of the design prototype and fabrication in an easy and clear manner. We are not only able to retrieve a real-time DT model with an immersive perspective, but we can also manage and modernize the entire fabrication workflow through the Cofabs method.

## 5. Discussion and Conclusions

This paper is based on the DT concept and proposes a co-existing fabrication system that helps designers make decisions with perceived immersive co-existing mixed reality environments and manage fabrication threads by sharing the team leader's real time perspectives. As well as this, Cofabs executes a generative co-existing mechanism of parameter control, where designers can inspect and compare the consequences of functional DT results in comparison to real material. The final analytical process helped the work-team improve the effectiveness of the system's optimization. This paper proposes the possibility and flexibility of the immersive interactive environment. This team-based fabrication methodology could help designers work in teams, as it represents a new type of co-existing interaction that bridges the gap between virtual and reality, reflection and automation, and humans and machines.

## Acknowledgement

This paper was partly supported by the Ministry of Science and Technology, R.O.C and under the research project on “Developing an interactive co-existing system and fabrication process of maker based on ”seeing-moving-seeing“ model” (108-2410-H-224-012-MY2 ).

## References

- Chen, C.-Y., Chang, T.-W., Hsiao, C.-F. and Huang, H.-Y.: 2019, Developing an Interactive Fabrication Process of Maker Based on “Seeing-Moving-Seeing” Model, *Proceedings of CDRF 2019*.
- Grieves, M. and Vickers, J. 2016, Digital Twin: Mitigating Unpredictable, Undesirable Emergent Behavior in Complex Systems, in F.-J. Kahlen, S. Flumerfelt and A. Alves (eds.), *Trans-Disciplinary Perspectives on System Complexity*, Springer, Switzerland, 85-114.
- Huang, H.-Y., Chang, T.-W., Wu, Y.-S. and Chen, J.-Y.: 2017, Collective Fabrication: A Responsive Dynamic Skin Design Case, *Proceedings of CAADRIA 2017*.
- Huang, W., Williams, M., Luo, D., Wu, Y. and Line, Y.: 2018, Rsu X Tsinghua X Yuntech Weaving Structure and Interactive Space Workshop, *Proceedings of CAADRIA 2018*.
- Huang, W., Yan, D., Luo, P. and Li, X.: 2016, Digital Design and Construction of a Weaving Structure, *Proceedings of CICE 2016*.
- Jahn, G., Newnham, C., van den Berg, N. and Beanland, M.: 2018, Making in Mixed Reality: Holographic Design, Fabrication, Assembly, and Analysis of Woven Steel Structures, *Proceedings of ACADIA 2018*.
- Lai, I.-C. and Chang, T.-W.: 2003, Companing Physical Space with Virtual Space: A Co-existence Approach, *Proceedings of eCAADe 2003*.
- Schon, D.A. and Wiggins, G.: 1992, Kinds of Seeing and their Functions in Designing, *Design studies*, **13(2)**, 135-156.
- Wesugi, S., Ishikawa, K., Suzuki, N. and Miwa, Y.: 2004, Interactive Spatial Copy Wall for Embodied Interaction in a Virtual Co-existing Space, *RO-MAN 2004. 13th IEEE International Workshop on Robot and Human Interactive Communication*, Kurashiki, Okayama, Japan.

# SEWING PNEUMATIC TEXTURES

*Three-dimensional digital design based on the craft of dressmaking*

VIRGINIA MELNYK

<sup>1</sup>*Tongji University International Digital Futures PhD program*

<sup>1</sup>*vemelnyk@gmail.com*

**Abstract.** This project explores a novel approach to digitally designing pneumatic membrane structures, utilizing traditional sewing methods from dressmaking. These sewn fabric manipulation techniques are commonly used to fit flat non-stretchy fabrics around the curvature of the body. The goal is to adapt these methods to create, shape, texture, and articulation on the pneumatic surfaces. This is in contrast with other research that is interested in creating smooth minimal surfaces with complex paneling patterns. The expression of textures explore engagement with tactility, addressing desires of playful touch and comfort within the built environment. Computer software for the fashion industry is used in the design process. The software has built in simulations and works with CAD-CAM software to produce patterns, which streamlines production and fabrication. The prototypes produced test the possibilities of these methods of sewing and the physical outputs for shape, tactility, and aesthetics.

**Keywords.** Textiles; Engagement; Computation; Interdisciplinary; Texture.

## 1. INTRODUCTION

Utilizing sewing techniques from the traditional craft of dressmaking, this project is inspired by contrasting the materiality and texture of typical pneumatic textiles. Dressmaking techniques transform flat fabrics through a variety of different ways of manipulating and sewing that shape the fabric around the three dimensional curvatures of the human form. Clo3D, a computer program from the fashion industry, is adapted in this project to digitally design the pneumatic structures. The software allows for a streamlined process between digital simulations to fabrication. The built in physics simulations have encoded properties of standard textiles, which computationally calculate the appearance of drape and flow of a fabric under forces. The sewing methods used to make clothes fit to the complex curvature of the human body are also built in tools within the software. In this project a few specific techniques are looked at individually for their different qualities and results. These techniques include darts, gathers, pleats, tucks, and ruching. Three prototypes are ultimately created which each



explore a different way of using the sewing techniques as a test set. The resultants are small scale pneumatic structures which are abstract three-dimensional bulbous shapes. In this case, the overall form is less important than the interest in the resulting textures. Wrinkles, bulges, flaps, and crenulation, are part of the aesthetic textures that are explored. These textures are similar to those found on the skin of our bodies. The project ultimately adapts techniques from the discipline of dressmaking and utilizes the computational software from that field to design and fabricate a speculative architectural pneumatic structures which results in novel textured surfaces.

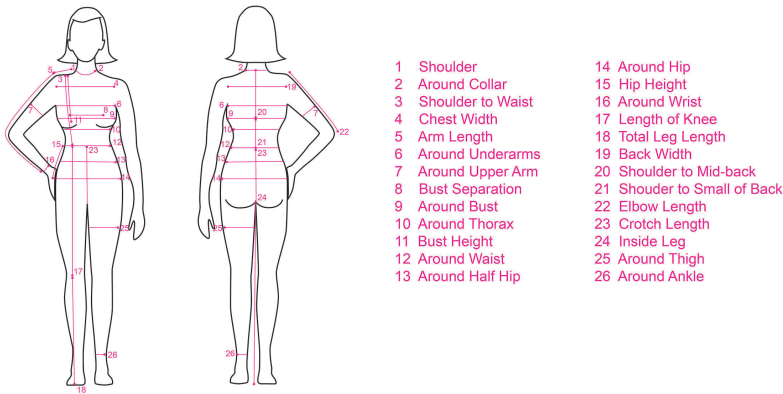


Figure 1. Image of measurement locations for dressmaking: (Melnyk 2019).

## 2. THE BODY

### 2.1. CURVATURE

The human body is a mixture of convex and concave curvatures that vary in steepness and scale. This project explores the sewing techniques from dressmaking that are used to create curvature that fits flat fabrics around the body. In architectural graphic standards *Neufert*, the body is explored through lengths and heights of standard bodies, and in different positions such as sitting, standing, lying down, and reaching (Neufert, 2012). Dressmaking measures the body at its peaks and valleys, to define areas where more or less fabric needs to create a good fitting garment (Talbot, 1943). Common measurements include waist, hips, shoulders, and bust size. See Figure 1. Often women's clothing is designed as one size, and then graded by offsetting the measurements to get the various larger and smaller sizes, which can result in ill-fitting clothing. Companies such as Alvanon, which provides digital avatars for computer programs like Clo3D, have been collecting new data of bodies through three-dimensional scanning and data analysis. They have provided more specified sizing for different ages, genders, races and body types. This is useful as the human body has changed over time to due to diet, health, and lifestyle. For example, this new data was used for a plus-sized women's clothing line at JCPenney stores, which resulted in better sales

and less clothing being left over to be put on sale rack at the end of the season (Keiser, 2017).

## 2.2. TOUCH

“Seeing’s believing, but feeling’s the truth.” - Thomas Fuller (Fuller, 1817).

Our embodied consciousness is dependent on our multi-sensory inputs to understand our existence. The hands are one of our main sense organs, we feel with our hands in several different ways. “Surface sensations” are the sensations of textures on a surface (Alpenfels, 1955). See figure 2. Meanwhile, “space-like sensations” sense the overall forms and shapes of things, by running the hand over a form in space (Alpenfels, 1955). The way that we perceive architecture is often more visual than tactile. Juhani Pallasmaa makes the case that the sense of touch is not only literally through touching, but the basis of how we can associate the senses together. Seeing textures on a surface can be an extension of this tactile sense as we can perceive how that texture feels through our senses of sight (Pallasmaa, 2012).



Figure 2. Hands touching and feeling the textures of sewn prototypes: (Melnyk 2019).

## 2.3. NEED FOR TOUCH

Loneliness is on the rise in contemporary culture as people are more isolated by the technological devices we have created. The need for tactile connection is explored through the art work of Lucy McRae. Her piece *Future Day Spa*, is a machine that synthesizes hugs for participants, making them feel safe and comforted (McRae, 2019). Hugs and other forms of human touch have been proven to release beneficial oxytocin in our bodies. Research in neuroscience has found evidence of neural connections between the somatosensory cortex (the region of the brain involved in the processing of tactile information) and the insular cortex (the brain regions involved in the processing of emotions) (Nicholas, 2010). Patients with certain types of synesthesia have been studied for their connections between different textures such as sandpaper, denim, and wax, having different

emotions related to them (Nicholas, 2010). Although there is very little known in this field of study, this project speculates on the possibilities of feeling soft skin like textures in our built environments as a way to create deeper connections, experiences, and human emotional responses.

### 3. PROTOTYPES

The sewing techniques chosen for the prototypes are typically used create compression and expansion of fabric where needed to conform to the curvature of the body. This results in a shaping of the overall forms that is experienced through the space-like sensations. Another result of the sewing techniques are different textures from wrinkling, puckering, folding, creasing, and bluing of the fabric. These qualities are the focus for the research and are experienced through surface sensations. The wrinkles visually appear similar to the creasing, folds, and wrinkles that exist on the skin of our bodies. See Figure 3. In developing the following prototypes, the sewing techniques were used explicitly per prototype to isolate the results of form, texture and tactile experiences resulting from the manipulation the fabric. The techniques used are pleats and tucks, gathers and ruching, and darts. Each prototype implemented variations on the different sewing techniques by manipulating the size, spacing and repetition of the sewing methods.



Figure 3. Body wrinkles with wrinkles and forms of prototypes: (Melnyk 2019).

### 4. SEWING TECHNIQUES

#### 4.1. PLEATS AND TUCKS

Pleats are used to create expansions in fabric through folding fabric and sewing it at one end, often used around skirts and waistlines. To create a pleat, the fabric is folded over itself in repeating layers. Different types of pleats are made depending on how the fabric is folded, whether it is in one direction or switching back and forth, determines a box pleat or knife pleat. See Figure 4. There are three layers of fabric produced once folded; a top, a middle and a bottom layer. The amount of overlap between these layers can vary in different lengths, but the most common

pleat is the full pleat, where all the layers are folded to the same length (Shoben, 1980). This creates a proportion of thirds as the end result of the pleated fabric is one third the original length. Pleats can also be given a top stitch along the fold line to emphasize the folds or keep the folds together down the length of the fold.

Tucks are similar to pleats, they fold and overlap fabric which is stitched it together, but occur in the middle of the fabric rather than at the ends. This reduces the surface area of the fabric in a region not necessarily along a seam (Talbot 1943). It is used decoratively and functionally to create a thickness of the material adding structure in areas. Tucks are often seen used on more delicate sheer fabrics, as they can play with light and the opacity of fabrics, as in undergarments, necklines, yolks, and blouses.

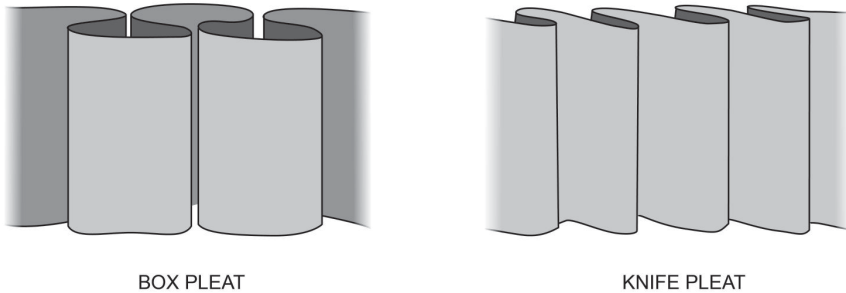


Figure 4. Diagram of knife pleat and box pleat. Source: (Melnyk 2019).

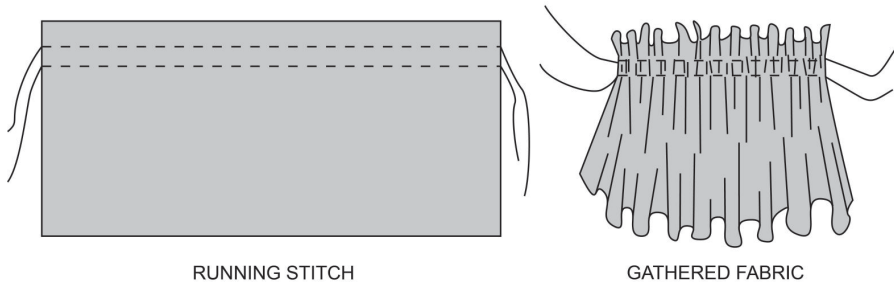


Figure 5. Diagram of gathering. Source: (Melnyk 2019).

#### 4.2. GATHERING AND RUCHING

Gathers are a more organic technique of contracting fabric length. Resulting in a softer ruffled look, compared to the ordered folding of tucks or pleats. Used commonly on skirts, necklines, and puffed sleeves (Talbot 1943). A running stitch is sewn through the fabric, then the thread is pulled to naturally bunch up the fabric along the stitch, until the desired length is achieved to match a shorter edge of fabric at a seam (Talbot 1943). See figure5.

Ruching uses the same running stitch technique to cinch fabric along a line, but occurs in the middle of the fabric. It can also include elastic to have more flexibility for movement. Ruching creates fullness and wrinkles in fabric that are used decoratively such as on a bodice of a dress or to give subtle modesty and elasticity on typically tight-fitting clothing such as bathing suits. Because it occurs in the middle of the fabric, several parallel lines of stitching may be used to create repetition and visual appeal (Shoben 1980).

#### 4.3. DARTS

Darts are commonly used in the small of the back or under the bust. Darts are made of small triangles of fabric that can be cut away and then by stitching back together the two remaining edges to create a pinch in the fabric (Talbot 1943). Darts are not typically used decoratively, but more functionally to create fitting. Darts can be done singularly (as in under a bust or on the small of the back) or in repetition (as long a waistline of a dress).

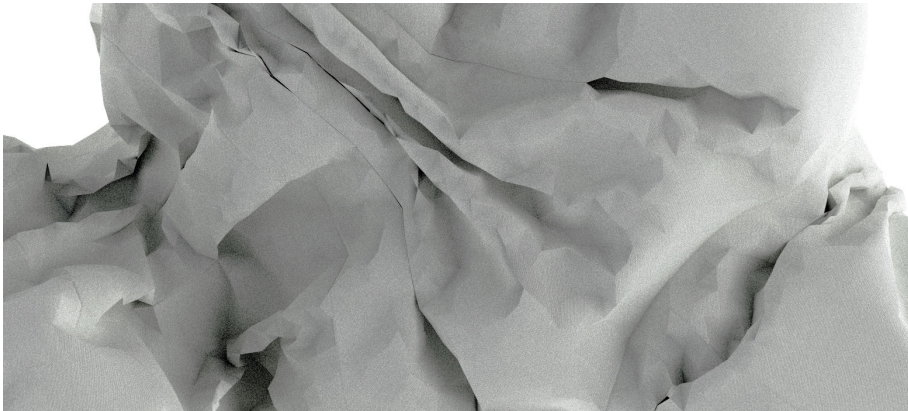


Figure 6. Clo3D rendered image of simulated wrinkled fabric. Source: (Melnik 2019).

## 5. COMPUTATION

### 5.1. CLO3D

The fashion industry has developed CAD-CAM computer software for faster design development and streamlined production. For this project, Clo3D was used; it uses meshes to model and simulate designs with material properties and forces like wind and gravity. These physics simulations are more specific to the textile properties than those in other physics simulations in programs such as Kangaroo or MAYA. A variety of environmental simulations such as gravity and wind are available, as well as features to add other forces like pressure to simulate inflation, which is useful for this research in pneumatic forms. The virtual model can show the potential outcomes of an inflated form and the resulting wrinkles that are generated in the process. See figure 6. The built in tools can apply different sewing techniques such as the ones mentioned above. Clo3D works in a

two viewport mode where you can simultaneously preview the three-dimensional model and the two-dimensional pattern. This mode allows you to design from the pattern and preview the results rather than the pattern being an end result of the three-dimensional design process.

## 6. INFLATABLE SKINS

### 6.1. PNEUMATICS IN HISTORY

Inflatable structures have beginnings with hot air balloons from the mid-eighteenth century in France (Topham 2002). During the 1960's, pneumatic designs were popular with architecture groups such as Archigram, Ant-farm, and Utopie. These architectural activists rejected the hard concrete of Brutalism and in turn making proposals for softer, mobile, temporal and ephemeral designs (Dessauce, 1999). These qualities are part of the researching interest today, as their lightness and deployability can also provide ecological benefits by reducing amounts of materials needed and weight during transportation.

### 6.2. RESEARCH IN PNEUMATICS

Frei Otto and Walter Bird were interested in membrane structures for their efficiency and minimal surfaces (Topham 2002). This continues to be one of the main interests of current architectural research in pneumatics, which focuses on form finding and optimization of paneling to create smooth membranes. *Inflated Restraint* by CITA in 2016, develops on new complex panelization methods using grasshopper relaxation tools in Kangaroo to create a large, smooth membrane (Thomsen, 2019). As a result, this method generates a large number of complex pieces. This project rejects these smooth models of pneumatic design and complex paneling, and desires to generate a unique textural surfaces and forms with more simplified pattern pieces.

## 7. THE PROTOTYPES

Using the sewing methods and computer program Clo3D, three prototypes were designed. Each prototype focuses on a type of sewing technique pleats with tucks, gathers with ruching, and darts on its own. The designs were first generated in the computer using Clo3D. Simulations were done to preview the possible design outcomes and patterns. The patterns were printed on a plotter, and then cut from rip-stop nylon fabric, which was used for its lightness and air tight qualities. The variations of the types of sewing were tested on each prototype by manipulating scale, density, and repetition of the technique. The final sewing was done by hand on a standard Pfaff sewing machine. The resulting prototypes were then photographed to show the different textural results of the sewing variations, as well as the engagement with the body. The overall shape of the prototype was not necessarily as important, as the exploration into the resulting textural qualities was the main focus. But because the methods of sewing are adapted from dressmaking and fitting, the results are expansions and contractions of fabric, which when the forces of pneumatic pressure results in abstract bulbous forms.

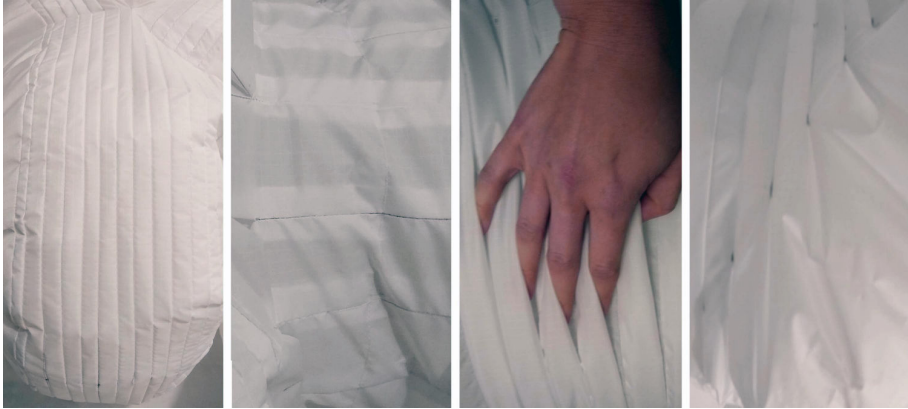


Figure 7. Variations on pleated prototype. Source: (Melnyk 2019).

### 7.1. PLEATED PROTOTYPE

The pleated model folds the fabric and stitches it together in various ways. Different spacing and amounts of overlap were tested throughout the prototype. Box pleats and knife pleats were also being used at various points of the design. One result is that folded characteristic of the tucks and pleats creates small pockets of fabric that you can slip your fingers within. See figure 2. Overall, the proportions relating to thirds allowed for fabric to expand and contract in the form quite drastically, which created cozy volumes of space between the geometry to rest body parts in, such as an arm or a foot. See figure 3. The smaller tighter pleats and tucks resulted in more rigid textures and stiffening of fabric. This could be felt when rubbing your hand over the over the ribbed texture, and in the appearance of the overall inflated shape. Some tucks were done in a graduating length which created large wrinkles in the fabric. Other tucks exposed the folded fabric to create long strips of excess fabric that were expressed rather than hidden within the form. These pieces of extra fabric were opportunities where the fingers desired to play and touch. The result of the overlapping of fabric also created variation in visual color as the rip-stop nylon has a slight translucent quality, resulting in more opacity when layered. See figure 7.

### 7.2. GATHERED PROTOTYPE

The gathered model resulted in more natural wrinkles, as the fabric is cinched together rather than folded. Ruching was explored with parallel and unparallel stitch lines, as well as with different spacing and lengths on the fabric. Unlike the pleats, the proportions of the resulting gathers were explored as the length of the gathered fabric could be 2:1 or 3:1 or 1.5:1, from the original length to the gathered length. These resulted in less extreme deviation between the fuller areas and contracted areas of the fabric. The outcome was a form that was less bulbous and has smoother shifts in shape. Overall, the gathered model's texture had many smaller wrinkles. See figure 8



Figure 8. Variations on gathered prototype. Source: (Melnyk 2019).

### 7.3. DARTED PROTOTYPE

On the darted prototype, instead of removing the triangle of fabric, it was kept and sometimes exposed and other times hidden inside the pneumatic form. Larger and smaller darts were tested as well as the proportions of the triangular shapes that create the dart. Several small darts versus one large dart, or more acute darts versus isosceles shaped darts. When excess fabric from the darts were hidden inside the form they created a smoother outer texture only noticeable by a small bump from stitched seam. Alternatively, when the left over fabric was exposed, this created an opportunity for engagement as hands and other body parts could play with this extra piece of material. See Figure 9. These pieces were much larger and flapped around more than those that were exposed on the pleated prototype. the darted models shape was overall less bulbous, as the triangular cuts from the darts created smoother transitions in form, but the textures produced were larger and not as articulate as those seen in the previous prototypes.



Figure 9. Variation on the darted prototype. Source: (Melnyk 2019).



## 8. CONCLUSION

This project shows that the method of making pneumatic structures does not need to be a smooth form membrane, but can take inspiration from traditional dressmaking sewing techniques to generate decorative and tactile textures. The prototypes are experienced through space-like sensations and through touch with surface sensations. These sensations could potentially engage with the neuroreceptors to create emotional effects, but more study will have to be done to really understand the results. At this point, we can conclude that some of the resulting elements from the stitching were more interesting to touch and offered different moments where the hands desired to play with the materiel. Clo3D was used for its advanced three-dimensional modeling simulations and design tools that directly implemented the dressmaking techniques into patterns that could easily be fabricated on a sewing machine. Each pneumatic prototype individually explores variations of the sewing techniques; pleats, tucks, gathers, ruching, and darts. The results show different results for these techniques which, in the next phase, could be explored further by combining the different methods into one singular prototype, giving more control to shaping and enhancing textured design. The project is ultimately speculative, but results in new thoughts on texture, tactility, fabrication, and design process, for pneumatic membranes, which is inspired by dressmaking.

## References

- Alpenfels, E.J.: 1955, *The Anthropology and Social Significance of the Human Hand, Artificial Limbs: A Review of Current Developments*.
- Dessaube, m.: 1999, *The Inflatable Moment: Pneumatics and protest in 68*, Princeton Architectural Press and The Architectural League of New York, New York.
- Fuller, T.: 1817, *Gnomologia: adages and proverbs, wise sentences, and witty sayings*, T. and J. Allman, London.
- Keiser, S.J., Garner, M.B. and Vandermar, D.A.: 2017, *Beyond Design: the Synergy of Apparel Product Development*, Fairchild Books, New York.
- McRae, L. and Amon, S.L.: 2019, *Lucy McRae: body architect*, National Gallery of Victoria, Melbourne.
- Neufert, E., Neufert, P. and Kister, J.: 2012, *Neufert*, Wiley-Blackwell, Oxford.
- Nicholas, J.: 2010, *From Active Touch to Tactile Communication: What's Tactile Cognition Got to Do with It?*, Danish Resource Centre on Congenital Deafblindness.
- Pallasmaa, J.: 2014, *The eyes of the skin: architecture and the senses*, Wiley, Chichester.
- Shoben, M. and Ward, J.: 1980, *Pattern Cutting and Making Up: The Professional Approach*, Batsford Academic and Educational Limited, London.
- Talbot, C.: 1943, *The Complete Book of Sewing; Dressmaking and Sewing for the Home Made Easy*, Book Presentations, New York.
- Thomsen, M.R., Tamke, M., Ayres, P. and Nicholas, P.: 2019, *CITA Complex Modeling*, Riverside Architectural Press, Toronto.
- Topham, S.: 2002, *Blowup: Inflatable Art, Architecture, and Design*, Prestel, New York.

# DIGITAL WORKFLOWS FOR NATURAL WOOD IN CONSTRUCTIONS

NIELS MARTIN LARSEN<sup>1</sup>, ANDERS KRUSE AAGAARD<sup>2</sup> and LYNN HYUN KIEFFER<sup>3</sup>  
<sup>1,2,3</sup>*Aarhus School of Architecture*  
<sup>1,2,3</sup>{nml|akaa|lhk}@aarch.dk

**Abstract.** This research challenges current linear processing methods for standardised timber. The current industry does not leave room for irregular shapes of naturally grown wood. This paper describes a bespoke design and fabrication method that leverages these natural irregularities of the wood. The customised development of a digital tool allows the distribution of the non-standard material to form a structure and the associated robotic machining processes of the individual logs. This research seeks to motivate a more inclusive, diverse and sensitive culture of processing and building with wood while exploring the unique aesthetic qualities of non-standardised wood.

**Keywords.** Robotic fabrication; digital workflows; wood processing.

## 1. Wood as a potentially sustainable resource

The recent years have indicated that wood buildings can compete with concrete and steel constructions in terms of volume and height. More and higher wood buildings are being built and planned, and studies point to modern uses of wood as feasible alternatives to concrete-based construction methods (Laguarda-Mallo and Espinoza 2016; Østnor, Faanes, and Lædre 2018). Wood is absorbing CO<sub>2</sub> during the growth of the tree (Gustavsson et al. 2006), thereby gaining the status of sustainable material. However, building with wood must be thought through and done holistically.

We are living in the age of the Anthropocene. Humans are dominating the world, and our will and behaviours change the ecosystems of the earth. Our cities and industry of construction show this clearly. To build, we excavate, mine, harvest and transform large areas of land. The consequence is the creation of biological uniformity, dying species and the vast regions of monoculture. Swapping steel and concrete for wood will reduce CO<sub>2</sub>; however, scaling up the current wood and timber industry to meet the demands equivalent to concrete could have unpredictable consequences for the forest areas of the world. In the shift towards more sustainable buildings, supply chains for raw materials and natural resources will need to be rethought.

Today the timber industry is an optimised machine that delivers wood to an industry defined by standardisation. Prefab and montage construction principles

require standard-sized materials, and engineered wood solutions such as glulam, CLT, LVL and other timber-based products meet these requirements. These products require straight equal-sized boards, veneer sheets or similar, and the best way to obtain such specifications is through straight- grown trees. Managing tree growth is easiest done through controlled plantation forestry; however, these forests are not without sustainable challenges. Research shows that plantation forestry impacts biodiversity (Bremer and Farley 2010) and that the current practice of timber production is often degrading the forests (Dudley, Jeanrenaud, and Sullivan 2014). The details are intricate, but, to be able to position wood truly as a sustainable resource for buildings, the current industry would have to change. The building design needs to adapt to both the natural properties of wood and accommodate a more sustainable timber production.

The work unfolded in this paper takes on the challenge of rethinking the way we use timber in construction. A new-developed workflow combining natural properties of wood and digital technology serves as an example of how trees could be utilised more focussed. It is the hope that this research can make an example that can provoke and inspire a radical reconsideration of the relation between architectural design and building materials. This paper is part of a longer research trajectory (Larsen and Aagaard, n.d.). It focuses mainly on the recent developments, such as the algorithmic distribution of stock material in the design and the integrated toolpath generation.

## **2. Research in wood construction and robotic fabrication**

Besides a long history of research in wood as a construction material, the method presented here is inspired by a growing research field addressing new ways of using scanning technology and robotic fabrication for wood processing and construction. For instance, Helen Hard architects have used 3D scanning and CNC fabrication for the Ratatosk Pavillon (Stangeland and Kropf 2012). In the HygroScope and HygroSkin projects at ICD/ITKE in Stuttgart, the behaviour of wood fibres was investigated (Menges 2012; Krieg et al. 2014), and later developed into building scale in the Urbach Tower project. The research is directly inspired by projects carried out at Architectural Association's Hooke Park facilities, such as the Wood Chip Barn, where Y-shaped tree trunks are used directly in construction. Our goal is to present a method that is less specific in terms of the stock material and allows a higher degree of control over the manufacturing and placement of the construction components. The research takes the starting point in technologies that are present in the wood industry, which we have studied on field trips to Finnish sawmills and manufacturers of timber products. Here, both exterior laser scanning and interior X-ray scanning methods are used for harvesting, sorting and processing the sawlogs as well as quality control. The research is influenced by traditional crafts (Zwerger 2011; Andersen 1997) and general knowledge about wood species and their properties (Hoadley 2000). There exist a number of historical typologies for using crooked wood, for instance, in construction of ships (Matthew et al. 1831) and in vernacular farm buildings, and the research seeks to reinstate some of the qualities of these examples through the use of the technologies available today. The lamella roof principle used here has

been explored in relation to digital form generation and CNC fabrication in earlier projects (Tamke, Riiber, and Jungjohann 2010), but not combined with the use of irregular sawlogs, which opens for new possibilities.

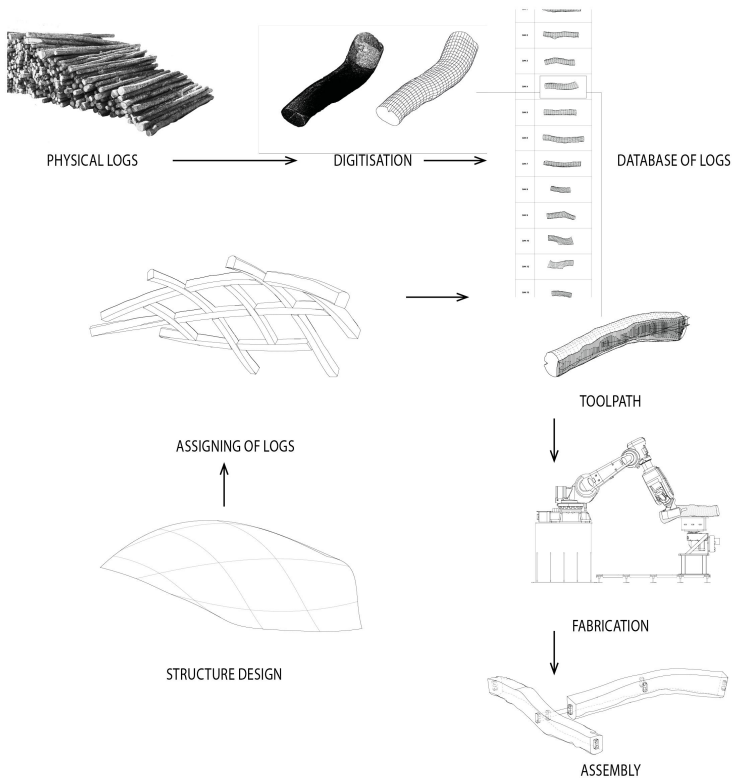


Figure 1. diagram of the workflow.

### 3. Overall concept

This paper unfolds bespoke design to production methods for non-standard wood logs using an industrial robot. The research is based on technologies for data-handling and wood processing that are already present in the wood industry. For this research only lab equipment, such as a Faro Focus scanner and a robotic arm with a spindle for milling, was available. Compared to industrial standards, the equipment is quite flexible to use but much less efficient. The goal is to suggest workflows that would be possible to implement in a well-known production workflow without significant changes. The general concept is to digitise each sawlog and create a database that can function as the basis for specific design solutions where it can be an advantage the material is already curved before machining it. A bespoke algorithm can select and place the material efficiently in

the structure design, and toolpaths for machining of the sawlogs are automatically generated.

#### 4. The workflow

The method consists of a series of steps that are closely connected as shown in Figure 1. The first part is the establishment of a database of sawlogs. Each sawlog is scanned and analysed through the use of bespoke algorithms into a NURBS representation of the log's centre curve and surface, which is saved with information about location, quality, species and dimensions. An overall design solution is defined, here in the form of a lamella roof structure. A customised script is used for the automatic distribution of the material in the structure. The script searches through the database and compares each segment of the roof structure with the shape of the available logs, and selects the best fit for each component. A set of information about joints, cutting directions is attached to each component. For the robotic fabrication, the toolpaths needed for the machining of the logs are generated, and motion capture technology is used for positioning.

#### 5. Laser scanning the logs

Before the scanning, the unprocessed wood logs are marked with three equally sized red dowels, for later positioning, as seen in Figure 2. These logs are then, while elevated from the ground on thin stands, scanned using a Faro laser scanner. The lifting of the elements away from the floor allows for better visibility of their surface area and therefore enables the creation of high-quality point clouds through less individual scanning processes.



Figure 2. Figure 2 Scanning of the logs are currently performed using a lidar scanner; however, multiple techniques have been tested and tried. These logs are scanned on the ground, while later tests showed that the scan data was improved when placing the logs on stands.

#### 6. From point cloud to rationalised geometry

The point cloud from the scanning of the sawlog is translated into rationalised geometry through the use of the Volvox plugin and custom scripts for Grasshopper

in Rhino. The main task is to define a centre curve since this is used for the selection and placement of logs, toolpath generation, and visual representation. The end planes identified during the scanning are used for setting the general direction of the log. (Fig. 4A) Along this straight line, a series of sections are defined where rings of points on the log's surface are extracted. (Fig. 4B) The centroid, or average point position, of each ring, is then found to have an ordered set of points that lies inside the periphery of the sections. (Fig. 4C). From each of these points, a set of radial lines is generated. For every line, the closest points in the corresponding point ring are found, thereby creating a new set of point rings. These new points are well-ordered, as the hours on a dial, and therefore allows the construction of rationalised NURBS curves, describing sections through the log. The area centroid of each section is then used for defining the centre curve. (Fig. 4D) To get an even distribution of isocurves, a new set of radial lines and corresponding sections are constructed from the centre curve, and these are used for defining the NURBS surface representation of the log (Fig 4E). This light-weight geometric information is saved in the database together with information about the quality, storage place and overall dimensions. For the experiments shown here, the database consists of block references in Rhino, where data is attached to each log through the use of the Elefront plugin for Grasshopper.

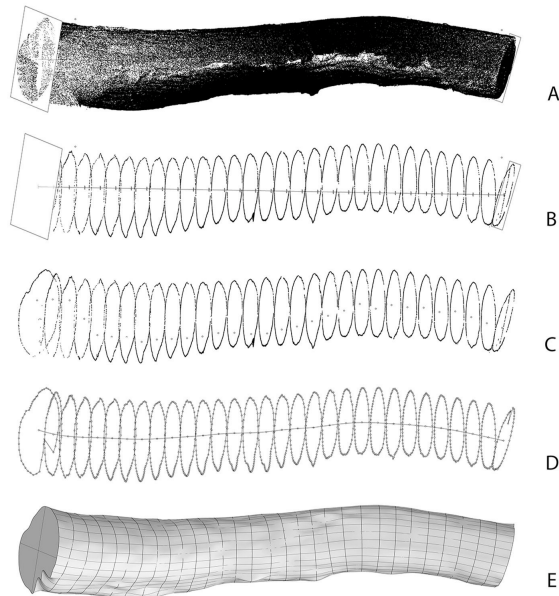


Figure 3. Figure 3 A) Point Cloud. B) Sections through the point cloud. C) Average point position for each section. D) Ordered point rings are used for drawing section curves, which then suggests a centreline based on the area centroid. E) NURBS surface representation.

## 7. Selection and distribution of logs in the construction

The structure design is constituted as a digital model, where geometric information about the building components can be extracted and used for searching through the database of available sawlogs to find the best match. Here, we are using a lamella roof principle, based on a predefined NURBS surface where the isocurves define the segments in the lamella structure. A customised algorithm compares each segment with the centre curves of the available sawlogs in the database and registers the deviations. The analysis is done by placing the centre curve of each potential sawlog in the position of the isocurve segment in the digital model. A series of positions and rotations are tested, and for each segment, the sawlog with the best match is assigned for the fabrication of the building component. Figure 6 visualises a sawlog assigned to a curve segment after being selected. To minimise the deviations, the components with the largest deviations are the first to have a sawlog assigned. The selection process is here simplified, but could eventually include a series of weighted parameters, such as material strength, distance to the storage, drying time, and amount of excess material.

Through the selection process, each member in the structure ends up with a log assigned to it. The next step is to define the trimming procedure, which depends on which components, and their sawlogs are connected. This is done as part of the algorithmic workflow. First, the topology is analysed, to define all the nodes and connections in the structure. These are used for defining the position and orientation of the joints. Then, the cut surfaces that define the trimming of the sides of each log is generated. The cut follows the centreline, so the component maintains a constant cross-section, but it is oriented to follow the surface normal, defined by the overall shape of the construction, i.e., the control surface. This ensures that the components meet at the joints with a relatively smooth transition since they share the normal of the control surface at the node. The information about cut surfaces is saved with each member and the assigned log.

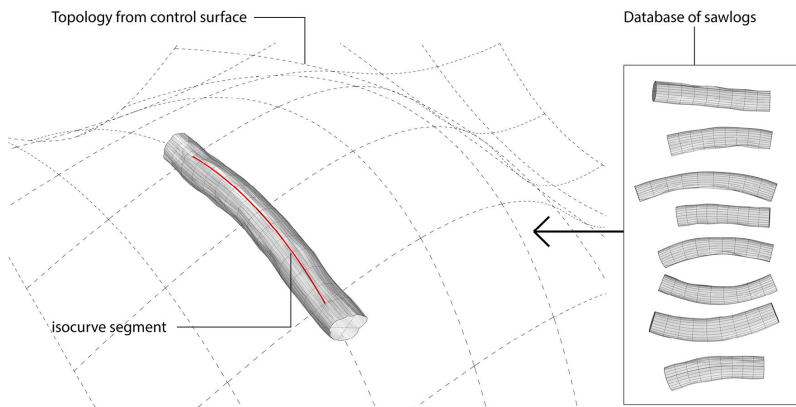


Figure 4. For each segment in the structure, a sawlog in the database is assigned.

### 8. Toolpath generation and processing of the logs

Based on the information attached to each component and its related sawlog, an individualised set of instructions for machining can be generated. The toolpaths are informed by the curvature described by the individual wood log. This process enables the preservation of the wood's natural anisotropic qualities and aims the forming of building elements that can be applied to larger structures, without weakening the material through the breaking of its fibres (Devadass 2016). Each of the previously defined cut surfaces allows identifying the orientation of every target of the toolpath. The position of these is defined through the offsetting of the initial cutting surface towards the external border of the log surface, while tested for its furthest translation possible without enlarging the given incremental cutting size of the layers. See Figure 5. The other layers are defined by a variable overall cutting depth and the incremental size of each layer.

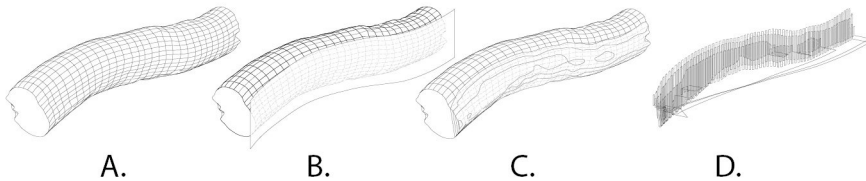


Figure 5. A) NURBS surface representation, B) position of the external cutting surface, C) slicing of the geometry and extraction of the minimal cutting area, D) generation of a toolpath that has a minimal length.

The physical logs are positioned on a rotary table, which allows the rotation of the material and thereby avoid 'out of reach' situations for the robot and enables the processing of the whole piece. After the fixation of the log, the earlier mentioned three orientation points are probed using the real-time tracking systems OptiTrack. Through camera calibration, these give high accuracy spatial representations, which are then translated for digital placement from Motive to Grasshopper for Rhino.





Figure 6. Two curved logs joined together using the developed workflow. The two logs describe a part of a larger surface.

The first experiment investigates the generation of horizontally oriented toolpaths, cutting in both directions of the log and following the curvature of this. This cutting method showed rapidly that in order to achieve a smooth surface, the tool should cut only in one direction. The second experiment uses vertical raster patterned toolpath, which is prolonged by 20mm at every end of a cutting line. Increased material vibrations through milling in the wrong direction led to a third iteration. This ran a toolpath that retracted from the material and only allowed one-directional cutting. The joints are incorporated directly into the wood logs as groove and tongue connections, as shown in Figure 6.

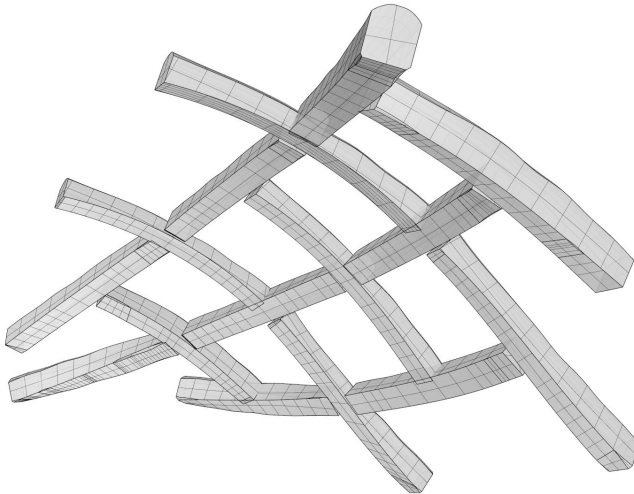


Figure 7. Fabrication of a prototype with 15 components could reveal more aspects of the system's viability. .

## 9. Use of irregular wood in construction

The main components to establish a continuous design-to-production workflow for scanning, analysis, selection, distributing and processing of irregular sawlogs have been developed and preliminarily tested. A few components have been produced and begin to reveal important parameters to consider. For instance, an unpredictable breaking of joints along the fibres has occurred after finishing some of the pieces. This is resulting from the discarding of the irregular logs by the sawmill as waste material and hence the lack of continuously adjusted drying climates. This internal movement of the material could be reduced through a controlled drying environment. To uncover challenges related to construction, it is necessary to carry out the building of larger prototypes with multiple components, as shown in Figure 7. Then, it will be possible to study the viability of the coupling of sawlogs with the overall design and the precision of the fabrication workflow. Another level of complexity will arise from the handling of many discrete building components, and solutions for anchoring and connection to other materials will need to be developed. The method described here is based on a lamella roof principle, but it will be relevant to study how the irregular wood can become relevant for many other construction types, such as roof trusses or cladding types.

## 10. Conclusion

The research described in this paper demonstrates a concrete input to a growing debate regarding sustainable building solutions. While the current workflow needs further refinement and physical testing on a larger scale, it points towards a future scenario where better utilisation of materials is key to architectural design. Currently, the workflow lives inside a lab environment but is built by replicating or mimicking technologies already used and implemented in the wood industry. Consequently, the suggested workflow or a similar method should be scalable within the existing context of wood production. The limiting factor seems instead to be the current building culture. At this point, highly deviating building components, such as the ones suggested in this paper, do not fit easily within today's standardised construction methods. The challenges of scaling up are much more related to current practice than to technological limitations. The design-to-production method suggested and unfolded in this paper consist of several technical contributions. The research is anchored in an existing field but expands the scope for using natural sawlogs through the custom-made digital tools and fabrications workflows explained in this paper. The full-machining of sawlogs in this project has required the overcoming of a series of challenges such as highly accurate, but low weight, representations of the entire sawlog surface. This is done through the bespoke evaluation of the physical log and rationalisation of scanned data. This contributes to the field through a fully adaptable method for the unique machining of the whole logs, going beyond the machining of custom details. This parameter has, as detailed in the paper, resulted in innovations both regarding tools for analysis and the generation of bespoke toolpaths, and the actual fabrication setup. The work presented in this paper should be seen as both actual technical innovations and as a polemic input to a current discourse of sustainability where wood construction is positioned as the successor of our current buildings practice.

## References

- E. Andersen (ed.): 99, *Roar Ege: skuldelev 3 skibet som arkaeologisk eksperiment*, Vikingeskibshallen, Roskilde.
- Bremer, L.L. and Farley, K.A.: 01, Does plantation forestry restore biodiversity or create green deserts? A synthesis of the effects of land-use transitions on plant species richness, *Biodiversity and Conservation*, 3893-3915.
- Dudley, N., Jeanrenaud, J.P. and Sullivan, F.: 01, *Bad harvest: The timber trade and the degradation of global forests*, Routledge.
- Gustavsson, L., Madlener, R., Hoen, H.F., Jungmeier, G., Karjalainen, T., Kloehn, S., Mahapatra, K., Pohjola, J., Solberg, B. and Spelter, H.: 00, The Role of Wood Material for Greenhouse Gas Mitigation, *Mitigation and Adaptation Strategies for Global Change*, 1097-1127.
- Hoadley, R.B.: 00, *Understanding Wood: A Craftsman's Guide to Wood Technology*, The Taunton Press, Newtown, CT : Emeryville, CA.
- Krieg, O., Christian, Z., Correa Zuluaga, D., Menges, A., Reichert, S., Rinderspacher, K. and Schwinn, T. 01, HygroSkin – Meteorosensitive Pavilion, in F. Gramazio, M. Kohler and S. Langenberg (eds.), *Fabricate 2014*, UCL Press, London, 272-279.
- Laguarda-Mallo, M. and Espinoza, O.: 01, *Cross-laminated Timber vs. Concrete/Steel: Cost Comparison Using a Case Study*.
- Matthew, P., Andrews, U.o.S., ibrary, initials missing and Collection, C.D.: 83, *On Naval Timber and arboriculture ; with critical notes on authors who have recently treated the subject of planting. by Patrick Matthew.*, Longman, Rees, Orme, Brown, and Green ;, London; and Adam Black, Edinburgh.
- Menges, A. 01, HygroScope – Meteorosensitive Morphology, in N. Gattegno, B. Price, A. Architecture and A. (Conference) (eds.), *ACADIA 2012*, ACADIA, New York, N.Y..
- Stangeland, S.H. and Kropf, R. 01, Relational Practice, in M. Hensel (ed.), *Design innovation for the built environment: research by design and the renovation of practice*, Routledge, Abingdon, Oxon; New York, 171-188.
- Tamke, M., Riiber, J. and Jungjohann, H.: 2010, Generated Lamella, *LIFE in: formation. On responsive information and variations in architecture: ACADIA 2010*, 340-347.
- Zwerger, K.: 01, *Wood and wood joints*, Birkhäuser, Basel.
- Østnor, T., Faanes, S. and Lædre, O.: 01, *Laminated Timber Versus on-Site Cast Concrete: A Comparative Study*.

# CLOSING THE LOOP - RECYCLING WASTE PLASTIC

CAITLIN BRUCE<sup>1</sup>, KEVIN SWEET<sup>2</sup> and JEONGBIN OK<sup>3</sup>

<sup>1,2,3</sup>Victoria University of Wellington

<sup>1</sup>caitlinbruce@outlook.com <sup>2,3</sup>{kevin.sweet|jeongbin.ok}@vuw.ac.nz

**Abstract.** Worldwide we produce billions of tonnes of waste per year, including a million tonnes of plastic waste. Currently, there are methods for recycling plastic, but these methods can be expensive and time-consuming, resulting in most of the plastic being thrown into the landfill. Because plastic does not fully degrade, it ends up in the ocean and other waterways, poisoning the water with toxins. The purpose of this research is to provide a solution to reducing plastic waste by creating an alternative method of recycling that utilises new technologies such as additive manufacturing, to create a building material that fits into the concept of the circular economy. The findings of this research explored the recycling of plastic by collecting plastic waste such as PLA (Polylactic Acid) from old 3D printed models and other sources. The plastic was recycled into filament for additive manufacturing (AM) and used to print a building component, establishing a foundational proof of concept for the use of recycled plastic as a potential building material.

**Keywords.** Additive Manufacturing; 3D Printing; Recycling Plastic; Recycled Filament; Waste Plastic.

## 1. Introduction

Worldwide our annual waste generation in 2016 reached 2.01 billion tonnes of waste (0.74 kilograms per person per day) with 242 million tonnes of this waste being plastic waste. It is now estimated that our waste generation is set to reach 3.40 billion tonnes in 2050 (McCormick et al., 2019). According to Thompson, Moore, vom Saal, & Swan (2009), current reliance on plastic is simply not sustainable. The reserves where raw materials such as ethane are taken to make plastic are declining. The short-lived one-use products created are accumulating. Since 1950 to 2015 only 9% of waste was recycled, 12% incinerated and the rest either ended up in landfills or the natural environment (Rhodes, 2018). This resulted in physical problems for wildlife and humans' through ingestion, entanglement in plastic, the leaching of chemicals from plastic products and the transfer of chemicals to natural habitats (Thompson et al, 2009). Current methods for recycling plastic have flaws. Laura Parker (2018) states that 'of the 8.3 billion metric tons (of plastic) that have been produced, 6.3 billion metric tons have become plastic waste. Of that, only nine percent has been recycled'. This is where adopting a circular economy model for plastic waste is critical. If waste plastic was designed with its end use in mind, then products can be reused, and

recycled efficiently. This eventually reduces or eliminates the use of raw materials and waste sent to the landfill by relying on the material already in circulation. Plastic waste has become an object of research to help people find solutions to the issue. Previous studies have reported that there are possible solutions, some easier to achieve than others. These include material reduction, design for end-of-life recyclability, increased recycling capacity, development of bio-based feedstocks, strategies to reduce littering, and revised risk assessment approaches (Thompson et al, 2009). New methods such as additive manufacturing can play an important role in addressing how waste materials such as plastic can be recycled. It has become a tool for creating designs that were not possible with traditional tools by using materials ranging from concrete, resins, clay, plastic, and even biomaterials. Entire buildings, walls or elements, such as facade panels or bricks can be printed through this process (e.g. XtreeE, 2017). The presented research investigates how an alternative recycling system be created for waste plastic to create a circular economy using additive manufacturing

## **2. Background**

On the surface, plastic may seem like a game-changer but its use of raw materials such as cellulose, coal, petroleum and natural gases has a detrimental effect on the environment. Obtaining these raw materials to produce the plastic creates greenhouse gases, contributing to climate change. To produce 28 grams of polyethylene (PET) it produces 28 grams of carbon dioxide. These emissions can be reduced by 30% through recycling (Staley, 2009). Most plastics can be recycled. However, many are thrown into landfills following a linear, single-use approach to waste instead of a circular model. In the UK alone 3.7 million tonnes of plastic are thrown away each year. A single-use water bottle can take 400 years or more to degrade, and these pieces do not fully degrade but instead get smaller and smaller (Parker, 2018). Not all plastics thrown into landfills are easily recyclable. PET (1) and HDPE (2) are the easiest, unless they are contaminated with food waste which makes them harder to recycle. Other plastics such as PVC (3), polyethylene (4 & 5), polystyrene (6) and everything else (7) are either not recyclable or too expensive to process (Recycle.co.nz, 2018).

### **2.1. CURRENT PLASTIC RECYCLING**

The idea of recycling first came about in 1994, when plastic packaging was seen as a waste product (Hita, Pérez-Gálvez, Morales-Conde, & Pedreño-Rojas, 2018). Recycling the materials meant extending the life cycle of it.

Developed countries such as New Zealand and the United States are sending their plastic waste to facilities in some of the world's poorest countries such as Bangladesh, Laos, Ethiopia, Senegal, Thailand, Indonesia, Vietnam, Malaysia, and Sri Lanka (Rhodes, 2018) rather than recycling it themselves. These places offer cheap labour and limited environmental regulation making them an ideal immediate solution without considering the long term consequences (McCormick et al, 2019). Interestingly, the five heaviest polluters of plastic waste are China, Indonesia, Philippines, Vietnam and Sri Lanka, which between them contribute

56% of global plastic waste (Rhodes, 2018).

## 2.2. ADDITIVE MANUFACTURING

The Economist (Kafka, 2012) is calling additive manufacturing the third industrial revolution. It is a 'game-changer' and has energized the world of manufacturing (Badiru, Valencia, & Liu, 2017). Each method of additive manufacturing has its own capabilities, advantages, and limitations that are driven by the materials and qualities of the process involved. Researchers have spent almost a decade investigating and refining 3D printing technologies. A common advantage and major incentive to many industries who have adopted additive manufacturing is the increase in freedom of design. The technology has the ability to bring complex forms to life suggesting that 'if you can't build it, print it' (de Laubier, Wunder, Witthoft, & Rothballer, 2018). This new technology can provide capabilities beyond that of traditional builders. Digital models of the designs allows designers to get an idea of what the object will look like before it is printed, as the printed model is nearly identical to the virtual version.

## 3. Circular Economy

The circular economy has been a term that's been used since the late 1970s by academics and businesses, making it difficult to track back to one single date or author. The circular economy model incorporates and integrates ideas from a range of authors to produce principles for this new system. William McDonough and Michael Braungart who established the 'cradle to cradle' model focuses on products and materials that are safe for human health and the environment (Braungart & McDonough, 2002). They introduced the idea of classifying materials as either biological or technical nutrients instead of been thrown to the 'grave'. An example of biological nutrients is when the 'waste' of an animal becomes the nutrients for fungi and plants. Technical nutrients are when a product such as metal and plastic can become 'food' for another product/s. Another author, architect Walter Stahel pursues four main goals of product life extension, long-life goods, reconditioning activities, waste prevention and the selling of services rather than a product. (Winans, Kendall, & Deng, 2017). Biomimicry is an idea that author Janine Benyus defines as 'a new discipline that studies nature's best ideas, and then imitates these designs and processes to solve human problems'. The circular economy takes these ideas and uses nature as a model to follow its processes to help solve ours. Finally, author John T. Lyle suggests an idea of regenerative design, which is said to be the foundation to which the circular economy is built on (Lyle, 1996). From these key authors and others, three key foundations to the concept of a circular economy have been developed; design out waste and pollution, keep products and materials in use, and regenerate natural systems. While all three foundations are import to the circular economy, this research focuses on using waste plastic to help design out waste. The idea is to keep plastic in use, whether a product is recycled and re-grinded at the end of its use or an element is reused. By using recycled plastic, the need for raw materials to produce new plastic becomes unnecessary.

The Ellen Macarthur Foundation strongly follows and advocates for the circular economy system. They have adapted a calculator that allows users to work out the circularity of a material called a Material Circularity Indicator (MCI). As plastic can be recycled and reused it reached an overall MCI level of 1.0. The MCI calculator follows the assumptions that the material recovered for recycling does not have to go back to the manufacturer. This element is useful to consider as this research does not follow this model. The model also assumes that the recovered material at the end of its use can be processed to a similar quality as the original virgin material. It is also assumed that there is no material loss or damage.

Through this research, using waste plastic will help to design out waste. This will then keep plastic in use, whether a product is recycled and re-grinded at the end of their use or an element reused. This will then allow the regeneration of natural system. Using recycled plastic the need for raw materials to produce new plastic is unnecessary. The circular economy is vast and full of multiple strategies. This research only covered a small portion of the circular economy. Where it focused on the lifecycle of an element. Rather than considering aspects such as whether the material is toxic, as this was outside the scope of this research.

#### **4. Recycling Plastic Waste**

Around 300 million tons of plastic are produced globally each year (Wassener, 2011). Once this plastic is served its purpose/use then its considered as 'waste', where the 'cradle to grave' model will be adopted. To turn this into a circular model the plastic must be recycled and reused at the end of its life cycle to produce a new product. One example is collecting plastic waste and turning it into usable 3D printing filament. Currently there are a limited amount of companies developing recycled plastic filament. The company REFIL in Germany takes plastic bottles, refrigerators and car dashboards, shreds them to be made into 3D printing filament (Refil, 2015). Another company is 3DEVO who strive to 'close the circle' by converting waste plastic into 3D printing filament, "Shred-it, melt it, spool it, and print it" (3devo, 2018). The University of New South Wales has taken a different approach and has created an e-waste micro-factory. They can turn old cellular phones, laptops, and electrical devices into 3D printing filament. They have taken these difficult to recycle materials and created a new life for them (UNSW, 2018). The scope of this research will focus on the waste material of plastic, and whether it be upcycled and used to additive manufacture wall tiles.

To begin the process of creating a recycled plastic filament, plastic such as PLA is collected from plastic cups, milk bottles and ice cream containers. These are then cleaned and shredded into tiny pieces, or made into pellets (Fig. 03). The ground plastic/or pellets are then placed into a machine where it is melted and extruded into a filament (Fig. 03). The extrudate is collected and spun onto a spool, where it can then be used to 3D print.

A limitation that needs to be considered throughout this research is that the process of turning the plastic into filament may not be very sustainable at this stage. This research does not cover the carbon emissions or energy use of the processes as this is outside the scope of the research. The recycling process allows material

that would have been thrown out to be rescued and made into a usable product creating a new life cycle for it. The use of raw materials is also then eliminated.

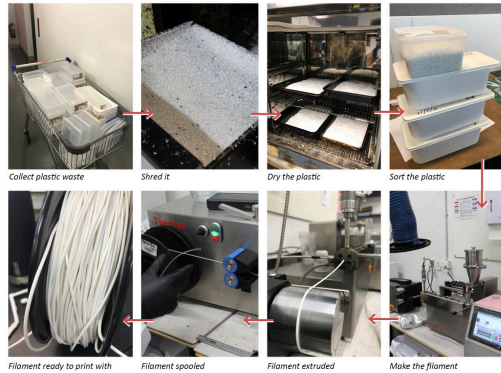


Figure 1. Recycling waste plastic into filament.

## 5. Design Output

### 5.1. WALL TILES

To test the performance of the plastic recycling system, a building element was chosen to design and print. The chosen element were wall tiles. The tiles are made of recycled plastic and are part of a system that can be attached to an existing wall then taken off at the end of its life-cycle and either reused or recycled into another plastic product. The performance of the system was measured against criteria that was created to test the mechanical and aesthetic properties of the tiles to determine the level of success of the output.

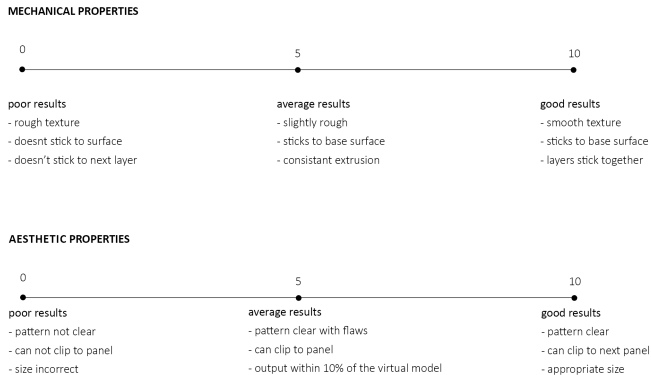


Figure 2. Performance Criteria .



5.2. ITERATIONS

The initial iteration as seen in Fig.05. demonstrates the design concept of a wave pattern that is influenced by a sound wave. The design concept was important to generate unique tiles that took advantage of the customised additive manufacturing system. The workflow for producing this was created in Grasshopper and uses a sine wave equation to create the smooth curves on the surface. The size of the area on the wall is made into one large panel which is then divided into smaller pieces to print.

The addition of the ‘clip’ as seen in Fig.05. allowed the tile to be clipped onto a wall and provided the surface area for the plastic to adhere to the printing surface more effectively. As the filament cools it begins to shrink, causing the print to lift from the surface. The addition of an adhesive to the surface helped to mitigate this issue so the print could be completed.

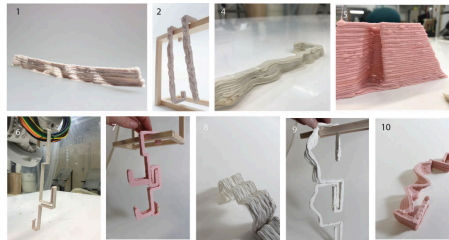


Figure 3. Wall Tile Iterations.

Table 1. Iterations and Performance Criteria.

ITERATION	PERFORMANCE	
	MECHANICAL	AESTHETIC
1	4	5
2 & 3	7	7
4	7	8
5	6	8
6	5	6
7	6	8
8	7	7
9	7	8.5
10	8	8
11	8	9

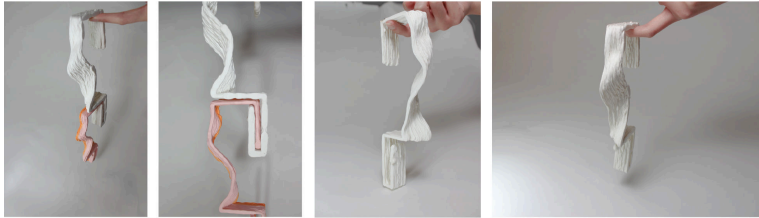


Figure 4. Final Design Printed Tiles.

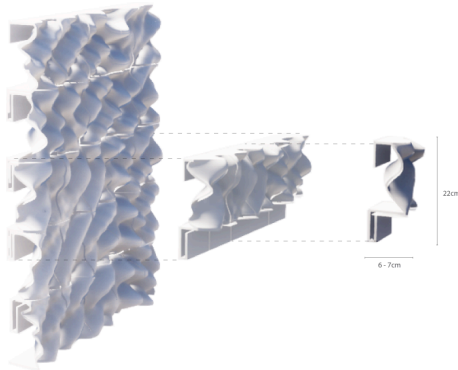


Figure 5. Final Design.



Figure 6. Final Design Example.

### 5.3. A CLOSED LOOP SYSTEM FOR WASTE PLASTIC

A recycling plastic waste process through additive manufacturing is now possible and adapts a circular economy. Following are the steps taken throughout the

process:

- STEP ONE - Waste plastic is collected, cleaned, sorted, shredded and dried.
- STEP TWO - The waste plastic shreds are put into a twin-screw extruder which is used to make the recycled plastic filament.
- STEP THREE - A design is developed digitally and then is printed using additive manufacturing.
- STEP FOUR - The new material is used, then at the end of its lifecycle its either reused, send to composting facility or shredded to create a new product and begin a new lifecycle.

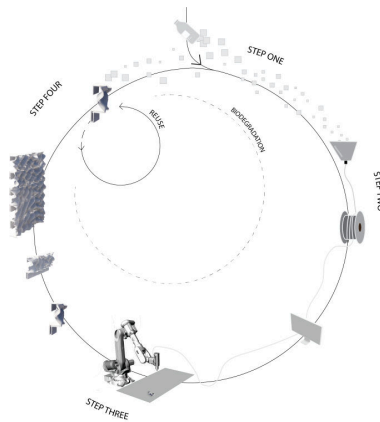


Figure 7. A Closed Loop System for Waste Plastic .

## 6. Conclusion

### 6.1. FINDINGS AND REFLECTION

The research concludes that additive manufacturing can be used to recycle waste plastic. Suitable waste plastics were collected, shredded, dried and turned into filament. A design system was generated to create unique parametric designs to print. The filament was then used to additive manufacture wall tiles. The identified system has the possibility to be used as an alternative recycling system to contribute to the circular economy of plastic. This closes the loop on waste plastic and creates a material that can be used to produce new building elements. Products made from recycled plastic now have the possibility to be ground up and used again in the built environment. This prevents plastic from entering the waste stream and polluting the planet, further reducing our reliance on raw materials. It requires less energy to recycle plastic than it does to make it from raw materials. This study has found a way to change the future of plastic waste by redesigning, reusing and recycling waste plastic, but it also helps to create awareness of the issue.

The research has provided a deeper insight into additive manufacturing. 3D printing now has the possibility to shape our future through the use of alternative

materials, adding value to a once valueless waste product. Providing insight into a different method of recycling plastic waste to produce into a usable product, extending and contributing to our knowledge in this area. A significant finding is that similar plastics had to be used together to produce consistent prints. Because different plastics have different melting points, therefore affecting the quality of the overall material produced. This indicates that the condition of the end product made from the mixed plastic will be poor quality if like plastics are not used. A strength of this study is the development of a workflow to produce a viable method of recycling waste plastic.

## 6.2. LIMITATIONS AND FUTURE RESEARCH

The creation of the plastic filament was problematic for the research. The overall process of collecting, shredding, making the filament and printing with it is a highly volatile (intensive) process. Observation, care, and patience must be practiced at each stage to achieve a desirable outcome. The plastic must be collected and sorted appropriately. Failure to do so will result in unpredictable formulas for the filament. Care must be taken during the extrusion process to ensure that the filament is consistent. If the filament is inaccurate, it creates problems for the extruder that delivers the plastic to the surface. If the filament is too thick or thin then it will not extrude at a consistent rate. The research was limited by an inconsistent output of recycled filament that made repetition in experiments difficult. There are new filament extruders that can help to solve these issues, giving more time to focus on experimenting with materiality.

This research has thrown up many questions in need of further investigation. Limitations provide evidence that more research is needed in terms of additive manufacturing with waste plastic to gain knowledge in this area. A key area that needs development is the quality of the extruded material. Due to the constraints of the twin-screw extruder, getting a consistent diameter thickness of filament was hard to maintain. As technologies develop improvements in this area can help to resolve this issue and provide better quality filament resulting in better quality printed products.

Resolution of this issue also means that there is potential for exploration in the use of additives to plastic or the use of other materials. There is then also the opportunity to explore the additive manufacturing tool of freeform 3D printing to its full potential, looking into the structural strength of the material.

## References

- “Filabot - The Misleading Biodegradability of PLA” : 2015. Available from <<https://www.filabot.com/blogs/news/57233604-the-misleading-biodegradability-of-pla>> (accessed 9 December 2019).
- “Refil” : 2015. Available from <<https://www.re-filament.com/>> (accessed 27 May 2019).
- “Sources of Greenhouse Gas Emissions” : 2016. Available from <<https://ghgemissions/sources-greenhouse-gas-emissions>> (accessed 14 October 2019).
- “XtreeE” : 2017. Available from <<https://www.xtreee.eu/projects/>> (accessed 7 May 2019).
- “Desktop Filament Maker and Shredder” : 2018. Available from <<https://3devo.com/>> (accessed 8 November 2019).
- “Plastic Container Recycling” : 2018. Available from <<http://www.recycle.co.nz/page.php?ref>>

- =recycled-waste&id=edit4cf831d8d2d96> (accessed October 14, 2019).
- “World first e-waste microfactory launches at UNSW” : 2018. Available from <<https://www.youtube.com/watch?v=INSUR8et87A>> (accessed 8 November 2019).
- Badiru, A.B., Valencia, V.V. and Liu, D.: 2017, *Additive Manufacturing Handbook*, CRC Press.
- Braungart, M. and McDonough, W.: 2002, *Cradle to Cradle: Remaking the way we make things*, Farrar, Straus and Giroux, New York.
- Chanda, M.: 2017, *Plastics Technology Handbook*, CRC Press.
- Hita, P.R., Pérez-Gálvez, F., Morales-Conde, M.J. and Pedreño-Rojas, M.A.: 2018, Reuse of plastic waste of mixed polypropylene as aggregate, *Journal of Cleaner Production*, **198**, 1515–1525.
- Kafka, A.: 2012, *A third industrial revolution*, The Economist.
- de Laubier, R., Wunder, M., Witthoft, S. and Rothballer, C.: 2018, Will 3D Printing Remodel the Construction Industry?, *Boston Consulting Group*, **1**, 1- 10.
- Lyle, A.: 1996, *Regenerative Design for Sustainable Development*, John Wiley & Sons.
- McCormick, E., Gee, A., Simmonds, C., Murray, B., Fonbuena, C. and Saraçoğlu, G.: 2017, Where does your plastic go?, *The Guardian*, **1**, 1 - 15.
- Parker, L.: 2018, A whopping 91% of plastic isn't recycled, *National Geographic News*, **2**, 1-3.
- Rhodes, C.J.: 2018, Plastic pollution and potential solutions, *Science Progress*, **101**, 207–260.
- Thompson, R.C., Moore, C.J., vom Saal, F.S. and Swan, S.H.: 2009, Plastics, the environment and human health, *Biological Sciences*, **364**, 2153–2166.

# DIGITAL PLANTING

## *Fabrication of Integrated Concrete Green Wall via Additive Manufacturing*

SIHAN WANG<sup>1</sup>, CHI LIU<sup>2</sup>, GUO LI ZHANG<sup>3</sup>, QI HUAN LUO<sup>4</sup>,  
WEISHUN XU<sup>5</sup> and FELIX RASPALL<sup>6</sup>

<sup>1</sup>*Singapore University of Technology and Design*

<sup>1</sup>*sihan\_wang@mymail.sutd.edu.sg*

<sup>2,3,4,5</sup>*Zhejiang University*

<sup>2</sup>*kiki19970310@gmail.com* <sup>3</sup>*1303162279@qq.com*

<sup>4</sup>*qhuanluo@outlook.com* <sup>5</sup>*xuweishun@zju.edu.cn*

<sup>6</sup>*Universidad Adolfo Ibáñez*

<sup>6</sup>*felix.raspall@uai.cl*

**Abstract.** Green walls are becoming a symbol of modern architecture representing sustainability and aesthetics. However, the fabrication of wall components that can nurture the growth of plants and other living creatures requires components to locate soil and other substrates, a controlled rugosity for plants and moss to grip, and conduits to distribute water and nutrients. This is normally done by adding extra attachments to the façade. In this paper, we introduce a digital approach to design and produce architectural components that can integrate green wall's functional requirements into the wall itself. Such components are fabricated via Additive Manufacturing (AM) extrusion with the assists of robotic arms.

**Keywords.** Green Wall; Additive Manufacturing; Robotic Fabrication; Clay Printing.

### 1. Introduction

Green wall is a general category in architecture that refers to varies types of vegetated wall components. Its history can be traced back to the Hanging Gardens of Babylon. Up to date, the green wall is divided into two types, the direct green façades, and the living walls. A direct green façade usually relies on the capability of climbing plants to attach themselves on the surface of vertical walls without support structures. On the contrary, living walls introduce frames as supports to hold soil and substrates for plants to grow upon (Manso & Castro-Gomes, 2015). Many examples could be found on Growing Green Guide. Our research focuses on the living wall system to sidestep the limitation of a direct green wall in which plants must have the self-clinging ability.

To facilitate the plants to grow, the living wall system always contains necessary elements such as supporting structure, growing media, irrigation, and

drainage. The efficiencies of installation, maintenance and replacement are also considered to improve the performance in all building phases (Manso & Castro-Gomes, 2015). However, such a green wall system has always been constructed as an attachment over the architectural envelope. To respond, we propose this green wall fabrication approach which integrates the functional elements that nurture the growth of plants into concrete walls.

## 2. Methodology

Our approach takes advantage of Clay Robotics (Wang et al., 2017), a digital fabrication method to produce clay moulds for concrete casting via AM extrusion. Such an AM process can not only fabricate the mould envelope but also realizes the interior growing media inside the envelope by spatially printing clay following a designated path. After the concrete casting and dehydration, the exterior clay envelope will be demoulded, recycled for reuse. In this scenario, the designed concrete component will allocate cavities for plants to root and grow, where clay may be left, serving as the substrate for plants, rather than removed.

### 2.1. EXPERIMENT SETUP

We utilized a KUKA KR 90 R3100 robot arm to control the motion of material deposition (Figure 1, left), with a bespoke end effector. Regarding the extruded clay which represents the outline of the wall and the geometries of cavities for plants to grow must have sufficient stiffness to maintain the shape when sustaining concrete casting, we considered two main factors of the clay extrusion mechanism: the necessary torque to extrude rather viscous material and the precise material deposition rate. In this scenario, we opted the ram pump mechanism to execute a constant clay extrusion (Figure 1, right). This extrusion system consisted of a NEMA 34 stepper motor, a 1: 40-reduction gearbox with cylinder, piston with frames.

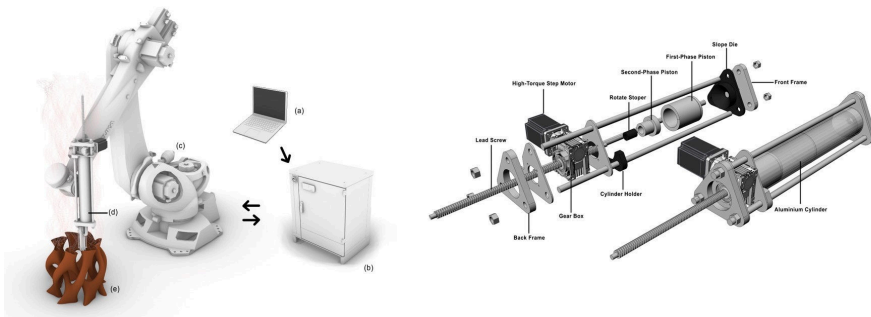


Figure 1. Workcell Setup. Left: Diagram of Setup, (a) Personal computer, (b) Robotic arm controller, (c) Robotic arm as positioning apparatus, (d) Extrusion system & End effector, (e) Printed clay mould. Right: Assembly of Clay Pump.

The printing material remained the same from the authors' previously research:

terracotta clay with 35-40% water ratio through extrusion. We first calibrated the clay AM system to match the extrusion velocity with the nozzle movement speed that facilitated a constant filament deposition. In the case of our pump, each round per minute (rpm) of the motor rotation could extrude 1/90 ml of clay. In this case, to match up a 15.6 mm/s nozzle movement speed, we set the rpm as 90 for 16 mm extrusion nozzle diameter.

## 2.2. GREEN WALL GEOMETRY

Our objective is to initiate a double-curved green wall prototype with the dimension of 1200\*900 mm (length \* height) and an average 130 mm thickness as shown in Figure 2. The green demonstrates the designated flat pattern of plants to grow and grey represents the double-curved concrete surface. Considering the fabrication efficiency and the possibility of success, we segmented the wall into 20 sections and printed each block respectively.

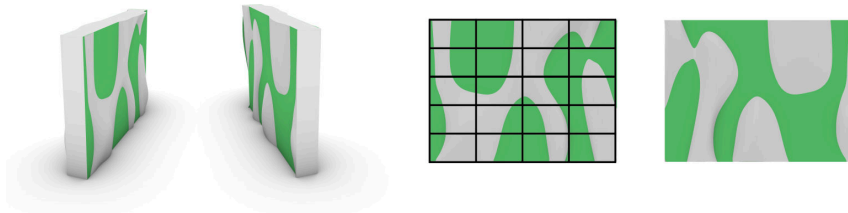


Figure 2. The design of green wall prototype. From the left: The perspectives of front and back of the wall; the segmentation of wall on front view; the back view. .

## 2.3. PRINTING TOOL PATH DESIGN

The printing path of each block's mould envelop was given by the contour lines. As for the internal cavity printing, we considered three key factors: 1. The continuity of cavities that enables sufficient room for plants to root in and eases irrigation and drainage, 2. The controllability of the positions on the surface where plants grow and 3. Adequate space among cavities which implements a successful concrete casting.

To respond, we applied the spatial printing strategy that vertically layered zigzag lines as interior printing path with the same height and number as envelop printing layers. Every two adjacent layers of zigzags interlaced to accomplish the continuities of the extruded clay through the intersections between layers. This also introduced a coherent mould space for concrete casting (Figure 3a).

As for the positioning of plants, we applied two scenarios on the relations of zigzag paths and envelop paths. When the zigzag path came across the envelope, the interior clay would expose on a concrete surface at the intersections (Scenario I). Such exposures implemented the planting of vegetations. On the contrary, the detachment of zigzag to envelop resulted in a solid concrete surface (Scenario II, Figure 3b).

In relation to the ease of concrete casting, the minimal length of the shorter



diagonal of each quadrangular interspace should no less than 22 mm (Figure 3c). Due to the two scenarios whether interior zigzags intersect with envelope, each segment on zigzag lines underwent cantilever and span. According to (Im, AlOthman, & Del Castillo, 2018), longer span of clay printing would cause a larger deflection. In this situation, we restricted the largest span and cantilever distance as 50 mm.

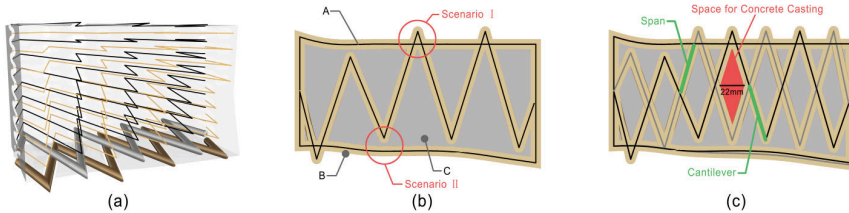


Figure 3. Printing Path Design. (a) The layout of zigzag printing path within a block boundary. (b) The plan view of a single layer: A in black is the printing path that followed by the nozzle centroid, B in khaki represents the width of clay filament, C in gray stands for concrete. (c) The span and cantilever in clay printing due to Scenario 1 and 2, respectively.

To realize the plant's pattern of the whole green wall, we first divided the projection of the wall into two  $30 \times 90$  grids with  $40 \text{ mm} \times 10 \text{ mm}$  cells on both front and back sides. Such cell size would restrict the maximum span distance under 50 mm. The nodes of two grids functioned as the control points of zigzag lines. Each node on the grid represented a checkpoint to identify whether it is Scenario I (Plants) or Scenario II (Concrete). For example, the checkpoints fell in the range of designated plants area (green color in Figure 4) belonged to Scenario I that plants should grow, vice versa. In this scenario, combined with the outlines of each block, we could generate the printing path for 20 segments.

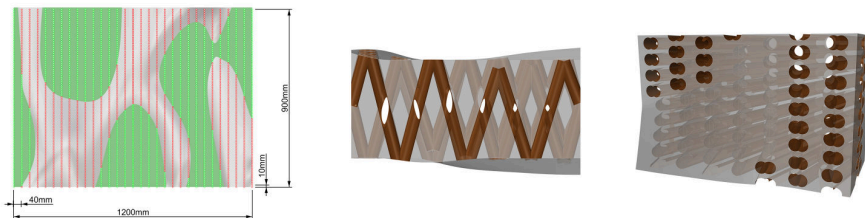


Figure 4. (a) Checkpoints on the front of wall: green points represent Scenario I and red points stand for Scenario II. (b) & (c) The rendered distributions of cavities from top & perspective views.

## 2.4. FABRICATION

During the printing process, one limitation was revealed that the 50mm span distance resulted in a huge downward deformation, even fracture. In this scenario, we applied a middle point acceleration which was to increase the nozzle movement

speed to double when the nozzle met the middle point of a span while maintaining the extrusion speed. In this case, all of the moulds for 20 blocks were successfully printed with continues interior lattice distribution.



Figure 5. Fabrication Procedures. (a) Printed clay mould. (b) Sandbox reinforce the concrete casting. (3) Demoulded concrete block.

In regard to the concrete casting, we proceeded the casting within 6 hours after the clay mould been printed. The intention was to cast concrete into humid clay mould to avoid the potential surface crack and structural fracture due to dried clay mould absorbing water from concrete (Wang et al., 2019). Firstly, we built sandbox support for wet clay mould to sustain the concrete pressure (Figure 5b). Subsequently, we cast concrete with the paste of fine aggregates, cement, water and plasticizer (3:2:1:0.005). After 24 hours of dehydration, we peeled off and recycled the clay envelope for succeeding the vegetation planting (Figure 5c).

### 3. Result

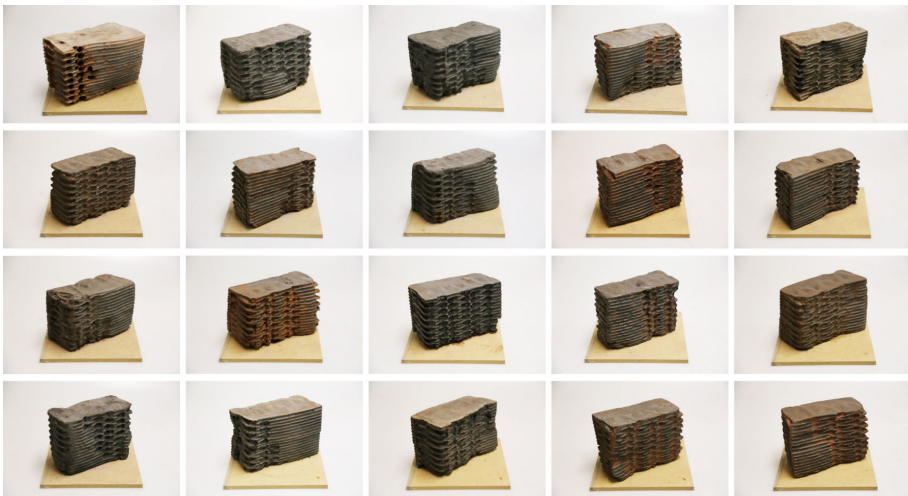


Figure 6. 20 segments of the green wall.

The twenty finished concrete blocks were successfully cast and demoulded as presented in Figure 6. We chose mosses, pileas, and ferns as vegetations for our

green wall system. The planting was carefully executed that we wet the clay in the cavities and gently inserted the roots of plants in. Finally, we layered the vegetative blocks as the layout shown in the cover photo (Figure 7).



Figure 7. Integrated concrete green wall made of twenty segments.

#### 4. Conclusion and Further Development

This paper proposed a digital fabrication approach that integrates green wall's functional requirements such as growing media for plants, irrigation, and drainage into the concrete components without the necessity of extra attachments as support structures. It takes advantage of AM which enables the design freedom of building envelopes from a vast geometrical variety and also facilitates the precise vegetative pattern. Furthermore, during the fabrication process, almost all the clay as mould envelopes can be recycled for subsequent prints, that contributes to environmental sustainability. However, it has to be pointed out that the upscaling that fabricating the façade in a monolithic piece other than segmented is still a challenge.

In a material context, we propose to further develop the mould material (clay paste) and the casting material (concrete) respectively. For clay, researches will follow two aspects that to increase its mechanical performance as a mould material and to hybrid necessary nutrition to facilitate plants' growth. For concrete, we will improve the mixture on its fluidity which enables ease of casting to small spaces while maintaining the structural strength.

Moreover, different types of printing paths for interior cavities can be investigated. Although zigzag-strategy offers a valid solution, the size and dimension of each cavity are unified, meaning the amount of earth in each cavity

is nearly equal. This might not be suitable for the varieties of plants since some might require larger room to root in. Additionally, an optimization to enhance the drainage along cavities has also been concerned.

Finally, concerning the challenge of transplanting the whole plants, we propose to investigate an automatically seeding approach that either seeding after demoulding or mix a certain amount of seeds into clay mixture.

## References

- “Growing Green Guide” : 2014. Available from <<http://www.growinggreenguide.org/>> (accessed 13th December 2019).
- Im, H. C., AlOthman, S. and Del Castillo, J.L.G.: 2018, Responsive spatial print: Clay 3D printing of spatial lattices using real-time model recalibration, *Acadia*.
- Manso, M. and Castro-Gomes, J.: 2015, Green wall systems: A review of their characteristics, *Renewable and Sustainable Energy Reviews*, **41**, 863-871.
- Wang, S., Conti, Z.X. and Raspall, F.: 2019, Optimization of Clay Mould for Concrete Casting Using Design of Experiments, *Intelligent & Informed - Proceedings of the 24th CAADRIA Conference*.
- Wang, S., Dritsas, S., Morel, P. and Ho, K.: 2016, Clay robotics: A hybrid 3D printing casting process, *Proceedings of the International Conference on Sustainable Smart Manufacturing*.



# DETAILING THE CONFIGURATION TO PERFORM BETTER CLAY PRINTING

SIHAN WANG<sup>1</sup>, HUI PING TOH<sup>2</sup>, FELIX RASPALL<sup>3</sup> and CARLOS BANON<sup>4</sup>

<sup>1,2,4</sup>*Singapore University of Technology and Design*

<sup>1</sup>*sihan\_wang@mymail.sutd.edu.sg* <sup>2,4</sup>*{huiping\_toh|*

*carlos\_banon}@sutd.edu.sg*

<sup>3</sup>*Universidad Adolfo Ibáñez*

<sup>3</sup>*felix.raspall@uai.cl*

**Abstract.** In this paper, we introduce an in-depth study on the performance of clay Additive Manufacturing (AM) process under various printing configurations. Our objective is to examine the filament behavior through clay extrusion with the focus on its printability, geometrical accuracy, and mechanical performance. Such research contributes to AM clay and ceramic artefacts in terms of the shaping and durability. The tests initiate with single layer extrusion which intends to investigate the relations between filament profile and input parameters, such as: Extrusion configurations (Layer height  $H$ , nozzle diameter  $D$ , velocity ratio  $R$  between extrusion and nozzle movement) and Printing-path parameters (Curvature). Subsequently, we apply the configurations from single layer extrusion on multiple layers printing test. The benchmark is based on the consistency of filament in each layer, the bonding strength between layers and the maximum flexural stress along build-up direction.

**Keywords.** Additive Manufacture; Robotic Fabrication; Clay Printing.

## 1. Introduction

As a natural composite of rock, soil mixed with water and other minerals with organics, clay is known as one of the earliest building construction material. In the practices of AM clay extrusion, various applications could be found as tableware (Herpt, 2018), arts & crafts (Pacelli, 2016), and architectural installations (Friedman et al., 2010; Ceramic Constellation Pavilion, 2017). The researches approach assorted aspects such as fine detailing with 0.4 millimeter layer height (Herpt, 2018; Pacelli, 2016), large-scale printing works up to 2 meters in height (WASP, 2016) and small robots' application in large artifact (IAAC, 2013).

In the AM process of clay extrusion, the dimension of the nozzle determines the shape and size of filaments. The diameter of a nozzle represents the minimal feature size as known as the resolution of printing work (Gibson, Rosen, & Stucker,

2015). Various filaments profile also results in different bonding surface area between layers which affects the mechanical performance of overall artifact. It is necessary to study the effects of orifice shape with other fabrication parameters such as extrusion velocity and nozzle speed (Kwon et al., 2002). Calvert & Crockett investigated the correlation between extrusion and nozzle speed with epoxy slurry. They indicated that with a given nozzle set and extrusion velocity, the cross-section of extruded filament changes with nozzle movement speed. By setting nozzle speed to 50% and 200% of the ideal speed, barrel distortion and pincushion distortion of filament profiles could be observed respectively (Calvert & Crockett, 1997).

In this paper, our aim is to explore the effects of clay printing configurations, the nozzle size, extrusion flow rate, and nozzle velocity on the appearance and mechanical performance of the printing work. The structure of this paper is as follow. In section 2, we introduce the experimental set-up including the design of work cell, testing material, and printing configurations. Section 3 demonstrates the single layer printing test with a focus on the filament appearance and adhesion under straight and curvilinear printing path. Section 4 discusses the mechanical performance of multi-layer printing work under various printing configuration. In the end, we address our conclusion and further research plans.

## **2. Experimental set-up**

### **2.1. PRINTING HARDWARE AND MATERIAL**

We utilized a ram pump mechanism to execute the constant clay extrusion through a rounded nozzle as shown in Figure 1. A combination of NEMA 34 stepper motor with a 1:40 reduction gearbox was opted as the actuator which provided enough torque to extrude rather viscous clay. This worked with a lead screw, a cylinder, a piston and frames as the extrusion end effector. The clay extruder was mounted on an ABB IRB 6620 robotic arm which serves as positioning apparatus enabling the accurate movement with our heavy end effector up to 30 kg when fully loaded with clay. The printing material remained the same from the authors' previously research: terracotta clay with a water ratio between 35-40%.

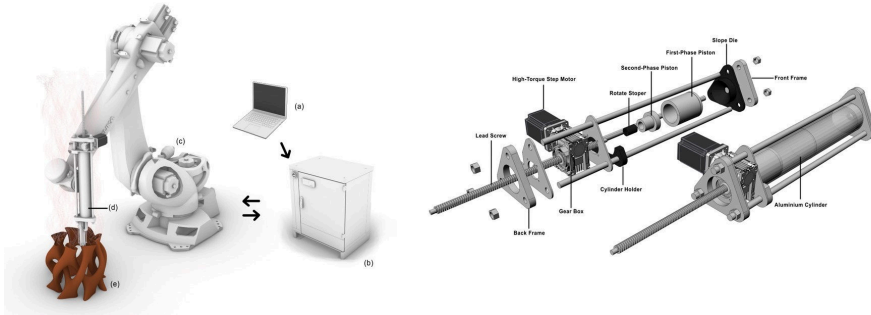


Figure 1. Schematic of work cell. Left: Diagram of printing system, (a) Personal computer, (b) Robotic arm controller, (c) Robotic arm, (d) End effector. Right: The assembly of the end effector.

As for the aforementioned ram extrusion end effector, each round per minute (rpm) of the motor extruded out 1/90 ml clay. We first investigated the rpm setup for optimal extrusion. The optimal extrusion represents that with a given nozzle movement velocity and printing layer height, the filament width equals the nozzle diameter. In this scenario, for a 4 mm nozzle with 50 mm/s speed, the rpm was set as 18. In a similar fashion, rpm 36 for 8 mm nozzle.

## 2.2. SINGLE LAYER PRINTING CONFIGURATION

Our single layer printing experiments initiated with determining the correlation of filament width and nozzle movement velocity for constant linear extrusion. A set of nozzles in 4 mm and 8 mm diameter were employed for the tests on a flat Medium Density Fiberboard. Each nozzle set underwent three printing tests targeting on linear and curved performance. The extrusion followed a sinuous printing path with a 250 mm long-side, that exams seven configurations with 1 mm printing layer height and nozzle velocity at 50, 45, 40, 35, 30, 25, and 20 mm/s with the ratio at 100, 90, 80, 70, 60, 50, and 40% of optimal extrusion speed. The performance of each filament was examined in terms of the smoothness, fluctuation on filament edges, and the adhesion.

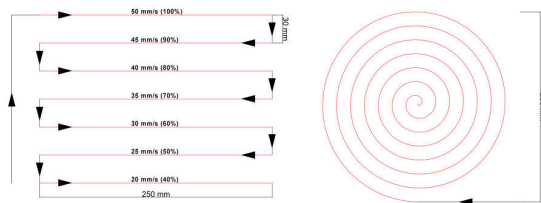


Figure 2. Single layer printing path, linear printing on the left and curvilinear on the right.

Subsequently, the extrusion was performed with a flat spiral path to analysis its performance under different local curvatures. Observation of curvature printing



will be focused on the smoothness of filament and the adhesion that whether filament detaches with printing base or the former layer.

### 2.3. MULTI-LAYER PRINTING CONFIGURATION

As introduced above, the filament width could change due to the nozzle movement velocity variation, indicating that there could be various combinations of nozzle diameter and velocity to achieve a given width. Therefore, our objective of the multi-layer printing test was to verify the mechanical performance of the samples printed with various nozzle diameters through bending tests. We printed out specimens with a dimension of 100 mm (height) X 100 mm (width) X 8 mm (thickness). There were 20 pieces of samples printed with a 4 mm nozzle and another 20 with an 8 mm nozzle. All the samples were printed with a fixed extrusion flow rate with the motor set at 36 rpm and a constant nozzle velocity at 50 mm/s to ensure the same amount of clay distribution. We sealed 10 samples of each nozzle setup with double-layer plastic bags immediately after the printing work to maintain the humidity to study the mechanical performance in the printing process. The rest were exposed in the lab condition for the natural air drying process over 120 hours. Before the bending test, half of the specimens were cut into half along the printing layer direction the rest were along the cross-layer direction. Subsequently, we measured the bonding width between layers to calculate the bonding area. Furthermore, the specimens underwent the 3-point bending test with Instron 5943 series electromechanical universal testing system. The aim was to analyze the adhesion between the bonded layers as well as the along layer direction. This experiment determines the suitable configuration to perform different printing thickness of clay artifacts.

Table 1. The setup of testing specimens.

Nozzle Diameter (mm)	Condition	Bending Test Direction	Number of Samples
4	Dry	Along Layers	10
8	Humid	Along Layers	10
4	Humid	Along Layers	10
8	Dry	Along Layers	10
4	Dry	Cross Layers	10
8	Humid	Cross Layers	10
4	Humid	Cross Layers	10
8	Dry	Cross Layers	10

### 3. Result and Discussion

#### 3.1. SINGLE LAYER PRINTING RESULT

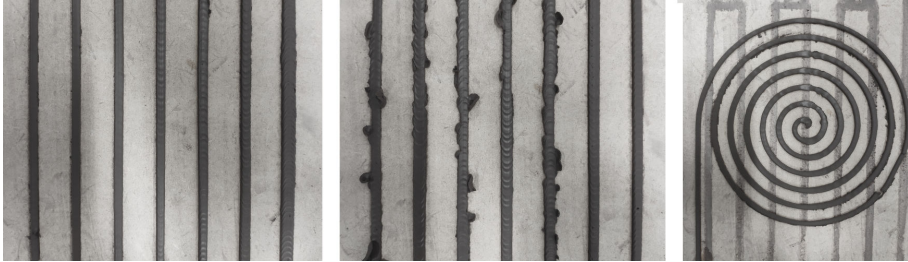


Figure 3. Single layer extrusion tests. On the left: Printing with decreasing speeds from left to right; In the middle: Printing with increasing speeds from left to right; On the right: Printing in flat spiral.

We executed the single-layer linear extrusion test over ten times to monitor the filament behavior. As expected, by reducing the nozzle movement speed while maintaining the extrusion flow rate, the deposited filament could become wider. The average width of the filaments increased gradually from 4 mm to 8 mm when changing the nozzle speed from 100% to 50% of the optimal (Figure 3). When reducing the nozzle speed to 40%, the extrusion became unstable which means the variation of width and texture was unpredictable. Besides printing in the manner of decreasing the nozzle speed in sequence, we also tested the extrusion with increasing speed from 40% to 100% as shown in the middle image of Figure 3. This was followed by the flat spiral printing test. Our observation on the printing samples included:

- The reduction of nozzle speed increases the variability of the filament. The more the nozzle speed be decreased, the more variation on the width of the filament can be spotted through the extrusion.
- There is no obvious challenge when printing under various local curvatures and radius.
- The adhesion between filament and printing base increases with a decreasing nozzle speed.
- When constant print with a low nozzle speed, the redundancy of extrusion material can be monitored and it accumulates.
- Printing starts with low nozzle speed instantly result in a messy edge condition and will transmit it until nozzle speed reaching 90% of the optimal as shown in the middle image of Figure 3. On the contrary, printing starts with high nozzle speed does not have the same effect.

### 3.2. MULTI-LAYER PRINTING RESULT

#### 3.2.1. Overall observation

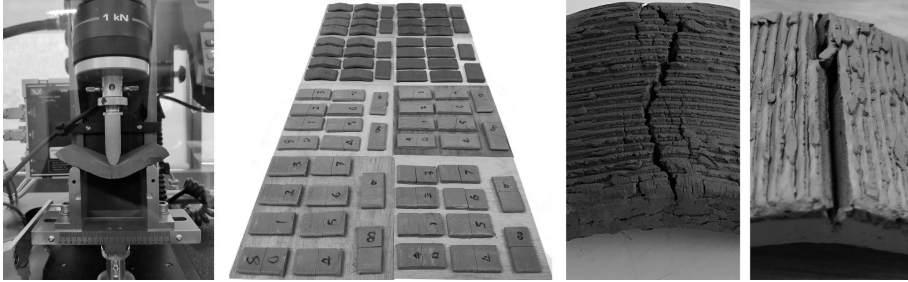


Figure 4. Images of bending tests. From the left: Testing environment, 80 specimens after testing, crack on the cross-layer direction, and crack between layers.

We first observed the flexure from the appearances of the specimens through and after the bending processes (Figure 4). Afterward, we had a glance at the general bending results data as well as the flexure curves to further understand such phenomenons (Figure 5). In the end, we compared and contrasted the distinctions between specimens printed with 4 mm and 8 mm nozzle as well as different results in along-layer and cross-layer directions. We picked up the mean value of every test group in ten and listed them in Table 2. The summary of our glancing is as:

- For the tests of humid samples, flexural cracks happen as winding curves around loading area when force been applied in the cross-layer direction. In the along-layer direction, the clay specimens fail at their bonding between layers.
- Clay printing work gains stiffness and yield strength through the air-drying process in both along and cross-layer directions. This effect comes along with a deformation type change from elastic (humid) to plastic (dry) as shown in Figure 5.
- The flexure stress at maximum load has a huge standard deviation as 1.20816 Mpa (28.7%) for 8 mm printing dry samples when force been applied across layers. Such a huge deviation also happens at other cross-layer loading tests, see Table 2.

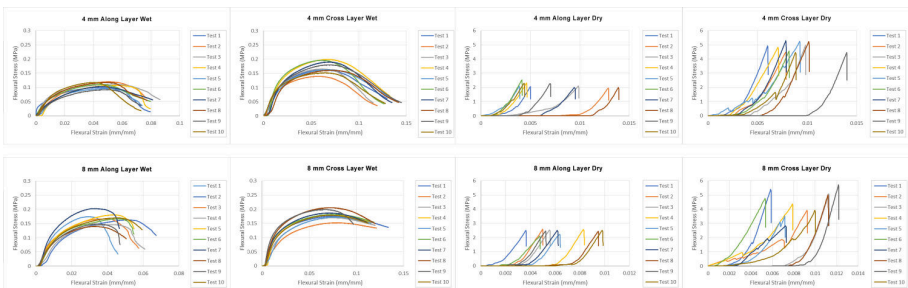


Figure 5. Bending test results of all eighty specimens in curve charts.

Table 2. Mean value and standard deviation of all bending tests.

Final thickness	8 mm				
Final width	50 mm				
		Extension at Maximum Load	Flexure extension at Maximum Load	Flexure strain (Extension) at Maximum Load	Flexure stress at Maximum Load
		(mm)	(mm)	(mm/mm)	(MPa)
4 mm Along-Layer Wet	Mean	4.89075	4.89075	0.04791	0.10763
	Standard deviation	0.42738	0.42738	0.00419	0.00963
4 mm Cross-Layer Wet	Mean	6.65281	6.65281	0.06517	0.17098
	Standard deviation	0.49628	0.49628	0.00486	0.01975
4 mm Along-Layer Dry	Mean	0.77661	0.77661	0.00761	2.168377
	Standard deviation	0.39126	0.39126	0.00383	0.84863
4 mm Cross-Layer Dry	Mean	0.90832	0.90832	0.0089	4.84651
	Standard deviation	0.22293	0.22293	0.00218	0.34091
8 mm Along-Layer Wet	Mean	4.06759	4.06759	0.03985	0.16593
	Standard deviation	0.73392	0.73392	0.00719	0.01849
8 mm Cross-Layer Wet	Mean	7.51862	7.51862	0.07365	0.18035
	Standard deviation	0.39629	0.39629	0.00388	0.01484
8 mm Along-Layer Dry	Mean	0.65596	0.65596	0.00643	2.44382
	Standard deviation	0.21256	0.21256	0.00208	0.15647
8 mm Cross-Layer Dry	Mean	0.84533	0.84533	0.00828	4.20501
	Standard deviation	0.27664	0.27664	0.00271	1.20816

3.2.2. Comparisons on along-layer and cross-layer directions

The flexure test comparisons in this section indicate the differences in the mechanical performances of 3D printed clay artifacts on along-layer and cross-layer direction. The along-layer represents that forces been applied along the layer printed direction which aims at testing the bonding strength between layers. The cross-layer tests are intended to study the flexure across the filament layers when load been applied across layers. Here, we choose the mean value of every testing group to make the comparison diagrams in curve charts as in Figure 6.

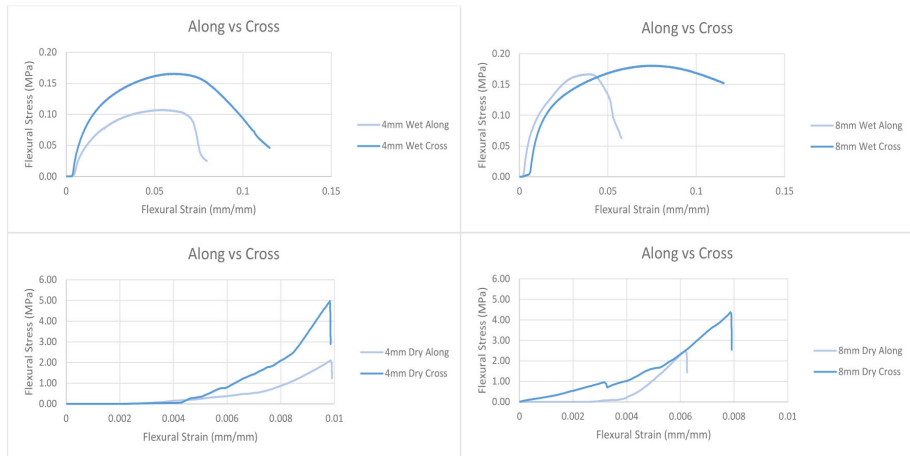


Figure 6. Flexure tests comparisons between along-layer and cross-layer directions.

At first glance, all the results directly show that the specimens survive larger flexural stress when loads been applied across layers in both humid and dry conditions. These indicate the bonding adhesion between layers is always the weaker portion in the clay printing work. In this scenario, the layer bonding strength has to be key criteria to concern about, especially when bending moments happen crossing layers. When printing with an 8 mm nozzle, the maximum flexural stresses of the printing work do not have significant differences in each direction in humid condition (Figure 6, top right). However, when beyond the maximum, the layer bonding tends to fail immediately other than the progressively deform in the other direction.

### 3.2.3. Comparisons of printing work with 4 mm and 8 mm nozzles

The bending test results of printing works via 4 mm and 8 mm nozzles show opposite performances on along-layer and cross-layer directions. 8 mm samples have larger maximum flexural stresses when testing the adhesion between layers with along-layer loads. However, referring to the other direction, printing with 4 mm and 8 mm nozzles have similar performances in humid conditions. 4 mm samples even perform better in terms of their higher peak of flexural stress when dried (Figure 7, bottom right). Our conclusion of such behavior is when printing with 4 mm, although extrusion could produce 8 mm filament layers, the bonding strength between layers highly depends on the original size of the nozzle. On the other hand, a smaller nozzle size does not reduce the performance on the along layer direction.

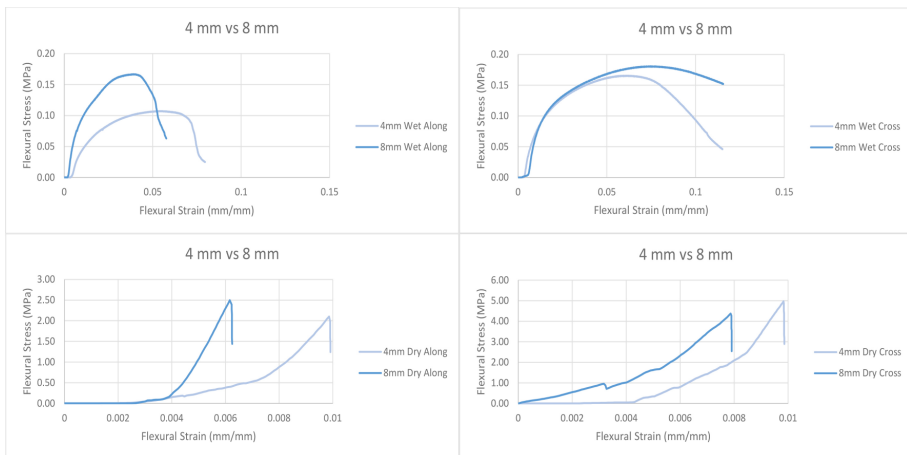


Figure 7. Flexure tests comparisons between specimens printed via 4 mm and 8 mm nozzles.

## 4. Conclusion

In this paper, we took upon a systematic approach for studying the impacts of AM clay configurations on the filament appearance, extrusion compacity and mechanical characteristics of printing work. We would like to exam the maximum

width of filament a nozzle could produce without losing the extrusion constancy as well as how was the mechanical performance compared with printing with a larger nozzle. In this scenario, we employed a pair of nozzles with 4 mm and 8 mm diameters as a case study. The results revealed that when printing with a 4 mm nozzle, by reducing the nozzle movement speed to 50% of the optimal speed which produced 4 mm wide filament while maintaining the extrusion flow rate, it enabled a constant extrusion of 8 mm filament. This offered us an opportunity that by manipulating nozzle movement speed, clay printing work could be built with various thicknesses without the necessity of changing nozzle sets.

Subsequently, we asked a derived question from the nozzle effect listed above that how was the mechanical performance of a clay printing work done with a small nozzle compared with a larger one. To respond to this question, we examined 80 pieces of specimens through bending tests in humid and dry conditions to study the flexural stress in along-layer and cross-layer directions. The results indicated that the ones printed with a smaller nozzle had weaker performance in their layer adhesions in the humid condition. However, after the air-drying process, clay gained stiffness and maximum flexural stress resulted in an enhanced bonding strength that closed the gap of layer adhesion differences between two nozzle sets. This offered us the confidence to keep practicing researches about these printing configurations to produce end products.

Furthermore, we propose follow-up researches by investigating the mechanical performance of clay printing after kilning. Extra sets of nozzle diameter combinations are also expected to further understand the impacts of the printing configurations.

## References

- “IAAC Minibuilders” : 2013. Available from <<http://robots.iaac.net/>> (accessed 13th December 2019).
- “WASP” : 2016. Available from <<http://www.wasproject.it/w/en/il-muro-di-terra-e-paglia-alle-soglie-dei-3-metri/>> (accessed 13th December 2019).
- “Ceramic Constellation Pavilion” : 2017. Available from <[http://www.arch.hku.hk/research\\_project/ceramic-constellation-pavilion/](http://www.arch.hku.hk/research_project/ceramic-constellation-pavilion/)> (accessed 13th December 2019).
- Calvert, P. and Crockett, R.: 1997, Chemical Solid Free-Form Fabrication: Making Shapes without Molds, *Chemistry of Materials*, **9**, 650-663.
- Friedman, J., Kim, H. and Mesa, O.: 2014, Woven Clay, *Acadia*.
- Gibson, I., Rosen, D. and Stucker, B.: 2015, . *Additive Manufacturing Technologies. Additive Manufacturing Technologies: 3D Printing, Rapid Prototyping, and Direct Digital Manufacturing, Second Edition*, Springer.
- Herpt, O.V.: 2018, “Clay printing work” . Available from <<http://oliviervanherpt.com/functional-3d-printed-ceramics/>> (accessed 9th February 2018).
- Kwon, H., Bukkapatnam, S., Khoshnevis, B. and Saito, J.: 2002, Effects of orifice shape in contour crafting of ceramic materials, *Rapid Prototyping Journal*, **8**, 147-160.
- Pacelli, F.: 2016, “Ceramic art and 3d printing” . Available from <<http://www.wasproject.it/w/en/ceramic-art-and-3d-printing/>> (accessed 13th December 2019).
- Wang, S., Dritsas, S., Morel, P. and Ho, K.: 2016, Clay robotics: A hybrid 3D printing casting process, *Proceedings of the International Conference on Sustainable Smart Manufacturing*, Lisbon, 83-89.



# A COMPUTATIONAL APPROACH FOR THE MASS CUSTOMIZATION OF MATERIALLY INFORMED DOUBLE CURVED FAÇADE PANELS

SHERIF ABDELMOHSEN<sup>1</sup> and AHMED HASSAB<sup>2</sup>

<sup>1</sup>*American University in Cairo; Ain Shams University*

<sup>1</sup>*sherifmorad@aucegypt.edu*

<sup>2</sup>*American University in Cairo*

<sup>2</sup>*ahmedhassab@aucegypt.edu*

**Abstract.** Despite recent approaches to enable the mass customization of double curved façade panels, there still exist challenges including waste reduction, accuracy, surface continuity, economic feasibility, and workflow disintegration. This paper proposes a computational approach for the design and fabrication of materially informed double curved façade panels with complex geometry. This approach proposes an optimized workflow to generate customizable double curved panels with complex geometry and different material properties, and optimize fabrication workflow for waste reduction. This workflow is applied to four different fabrication techniques: (1) vacuum forming, (2) clay extrusion, (3) sectioning, and (4) tessellation. Four experiments are introduced to apply surface rationalization and optimization using Rhino and Grasshopper scripting. Upon simulating each of the four design-to-fabrication techniques through different iterations, the experiment results demonstrated how the proposed workflows produced optimized surfaces with higher levels of accuracy and reduced waste material, customized per type of material and surface complexity.

**Keywords.** Digital fabrication; Double curved facades; Mass customization; Design-to-fabrication.

## 1. Introduction

Recent approaches to enable the mass customization of double curved façade panels have included applying techniques such as cold bending, forming, sheet metal processing, material deposition, robotic milling, flexible modular systems, and others (Shelden, 2002; Li et al., 2002; Buswell, 2007; Hauschild and Karzel, 2011; Lee and Kim, 2012; Castañeda et al., 2015; Abdelmohsen and Tarabishy, 2017). Despite these recent advances, challenges still exist for the mass customization process of double curved façades, including waste reduction, accuracy, surface continuity, economic feasibility, and generating complex geometries for panels with varying materials and material properties. One of the primary challenges is the disintegration in workflow for this process for different materials and processes, leading typically to a waste in resources and materials.



This paper proposes a computational approach for the design and fabrication of materially informed double curved façade panels with complex geometry. This approach proposes an optimized workflow that focuses on (1) generating customizable double curved panels with complex geometry and different material properties; and (2) optimizing fabrication workflow, where waste material is reduced compared to other conventional workflows. This workflow is applied to four different fabrication techniques: (1) vacuum forming, (2) clay extrusion, (3) sectioning, and (4) tessellation.

The paper introduces four experiments that apply surface rationalization and optimization using Rhino and Grasshopper scripting, and devise design-to-fabrication workflows to produce optimized and accurate double curved panel prototypes based on different materials, such as acrylic, clay, and medium density fibers. Upon simulating each of the four design-to-fabrication techniques through different iterations, the results demonstrated how the proposed workflows produced optimized surfaces with higher levels of accuracy and reduced waste material, customized per type of material and surface complexity.

## 2. Experiment 1: Vacuum Forming

Vacuum forming is typically the process of heating a thermoplastic material and shaping it in a mold (Throne, 1999), where a sheet of plastic is heated to a forming temperature, stretched onto a single-surface mould, and forced against the mould by vacuum. Attempts to utilize vacuum forming for fabricating double curved façades have faced challenges related to attainability, surface congruity, precision, waste reduction, and economic challenges, due to the need to fabricate surfaces using custom moulds to vacuum every single piece.

Our approach couples multipoint forming together with automated free form material deposition to create mass adjustable double curved façade panels. We developed a vacuum forming simulation workflow script in Grasshopper to rationalize acrylic panel surfaces and extract Z-values for fabrication. We developed a vacuum forming machine where a cast silicon sheet connecting a set of vertically displaced metal rods regulate the desired geometry of the heated acrylic panel using a vacuum forming process (figure 1).

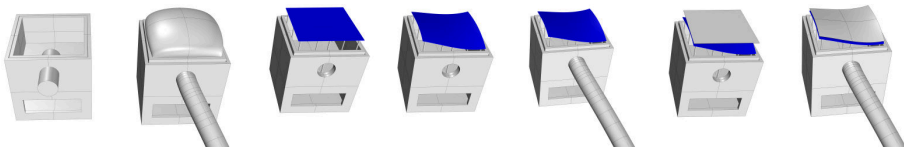


Figure 1. Vacuum forming machine simulated workflow .

The inputs for the vacuum forming core component in Grasshopper are the double curved surface to be fabricated, the number of sub-surfaces in the U-direction and V-direction, and the number of rods in the U-direction and V-direction. The main outputs include the selected item for data extraction, the double curved surface and its projection on the XY plane, the travel distances that the rods will move in the Z-direction to push the acrylic sheets to a specific location

on the new surface 3D location (figure 2).

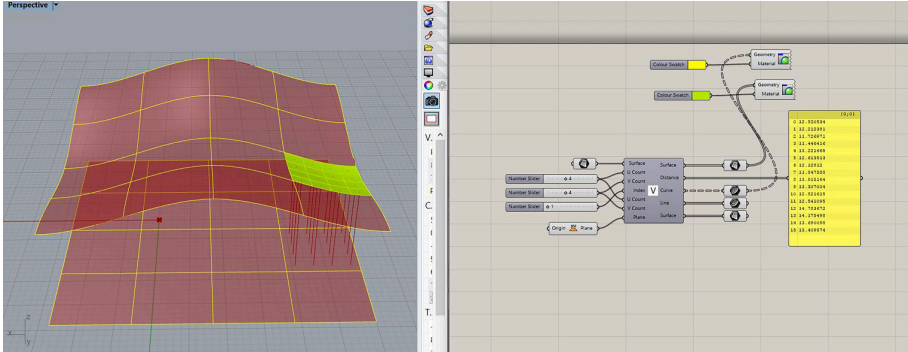


Figure 2. Surface subdivision and fabrication workflow (Left: Subdividing the surface, and preparing tiles for fabrication, Right: Grasshopper workflow for vacuum forming).

The fabrication process using the vacuum machine involves the following: (1) casting the silicon sheet based on the dimensions of the machine workspace, (2) sending Z-coordinates to the adjustable mould, (3) preparing an acrylic tile to be heated in the oven till it reaches elasticity, (4) loading the acrylic sheet on the adjustable mould and closing the machine using the fabric, (5) initiating the vacuum process, and (6) repeating the same process with remaining tiles. Figure 3 shows the vacuum forming device used and the fabricated acrylic tiles.



Figure 3. Vacuum forming output (Left: Vacuum forming device based on multipoint forming and material deposition, Right: Fabricated acrylic tiles).

### 3. Experiment 2: Clay Depositing

In this experiment, a clay extrusion script was developed in Grasshopper to deposit subsequent vertical layers of clay using an extruder attached to a CNC machine. The script defines the form height, clay mixture composition based on air pressure values, Z-value for form expansion, direction and angle of movement, the printing path for the CNC machine, and simulation workflow for material deposition.

The digital process of modeling and clay depositing involved the following procedures. First, a Grasshopper script was developed to create the surface for clay printing (figure 4). This involved defining a base curve component, a Z-direction for form expansion, a movement component to proceed in the sequential vertical movement direction to create the final base curve for the form, an area component to define the center of the base curves, in addition to a loft form for surface printing and a rotation definition for the vertical surface curvature along the axis of rotation.

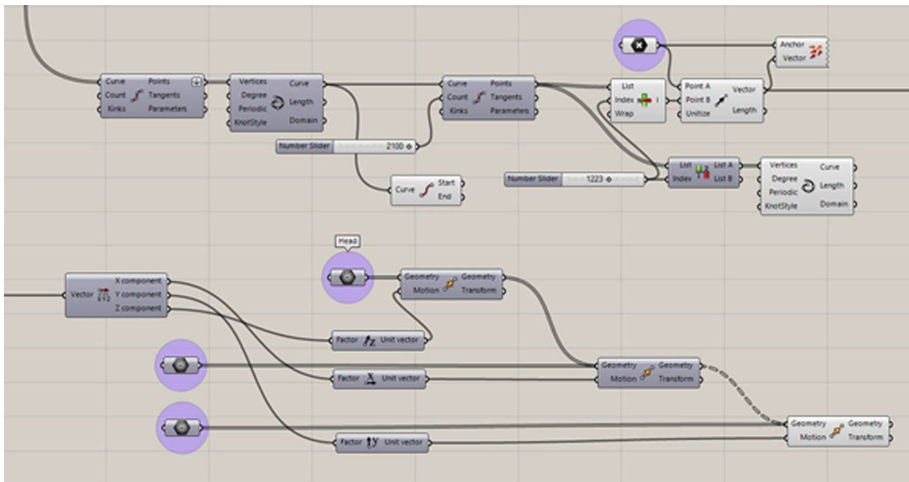


Figure 4. Extract from clay deposition Grasshopper script (Top: creating printing path for CNC router machine, Bottom: Clay printing).

The surface was then rationalized and its fabrication printing path for the CNC router machine was prepared. This involved dividing the base curves, defining the printing path curve, dividing the printing path to define points, and defining the movement vector to follow the path connected to the CNC router machine. Another script involved simulation of the clay printing process, including modifiers to the CNC router machine, deconstructing the vector to synchronize the movement, and transferring the movement in X, Y and Z to the machine head. Figure 5 illustrates the process of modeling, clay depositing simulation, and the developed extruder device.

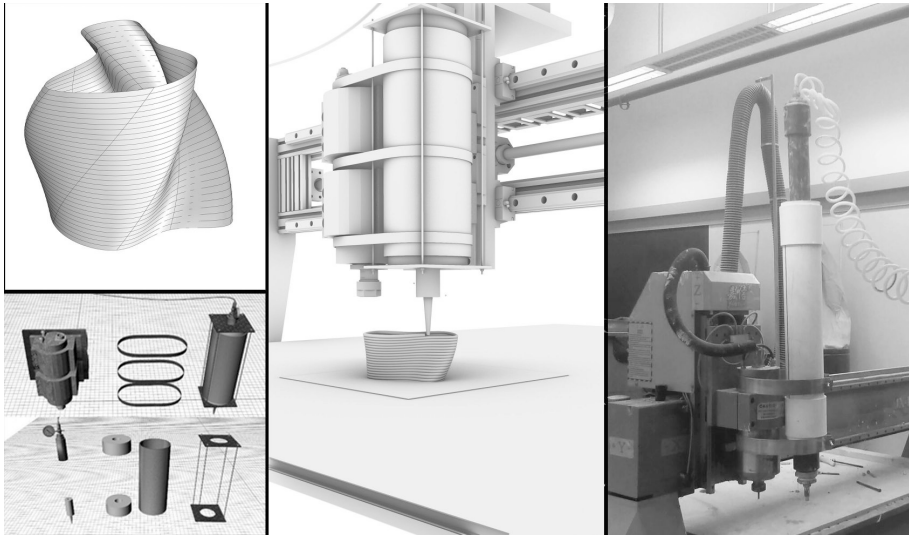


Figure 5. Upper left: Creating the model surface, Bottom left: Components of clay depositing setup including air pressure flow, extruder, CNC motor, clay mixture container, Middle: Grasshopper simulation preview for clay depositing experiment, Right: Developed extruder device added to CNC router machine.

#### 4. Experiment 3: Sectioning

Sectioning is generally a method of profiling components in relation to surface geometry by means of a series of sectional cuts through a digital model (Dunn, 2012). In this experiment, a sectioning workflow script was developed in Grasshopper to rationalize poly surfaces, prepare planar cuts for the fabrication of MDF sheets, apply the desired angle of sectioning technique, and define an optimized method for assembly for the resulting complex double curved geometry.

The objective of this experiment was to generate a double curved surface using a planar material, simulate its fabrication process, and increase the accuracy of the generated surface by linking extracted data directly to the CNC router machine. Planar MDF (14mm) sheets and vertical metal rods were used for stiffness. A surface was first created based on a sweep and was converted to a poly surface which was then rationalized and prepared for fabrication using a Grasshopper script, as shown in figure 6. This was applied for both a horizontal and vertical sectioning process, as shown in figure 7.

The workflow for the Grasshopper script was as follows. The input variables consisted of the poly surfaces (B-reps), the material thickness, the metal rod coordinates in both X and Y directions, the grid size for arranging planar cuts, and coordinate tags in X and Y directions. The outputs included the 2D geometry for CNC subtractive fabrication, and the number and position tagging for the fabrication engraving, cutting and simulation.

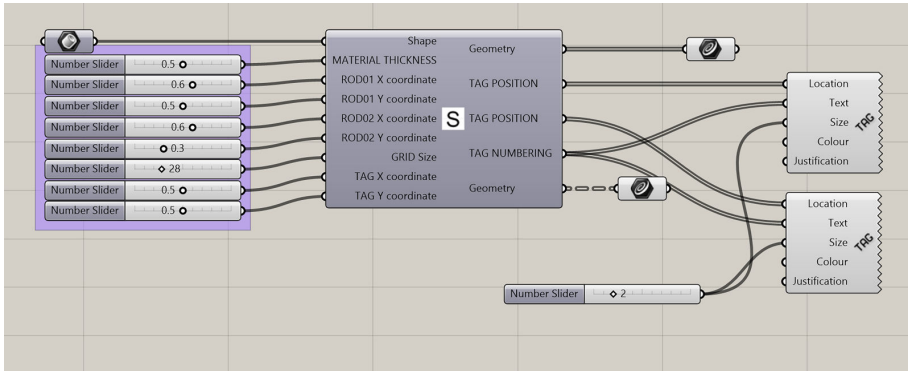


Figure 6. Workflow for Grasshopper sectioning plugin .

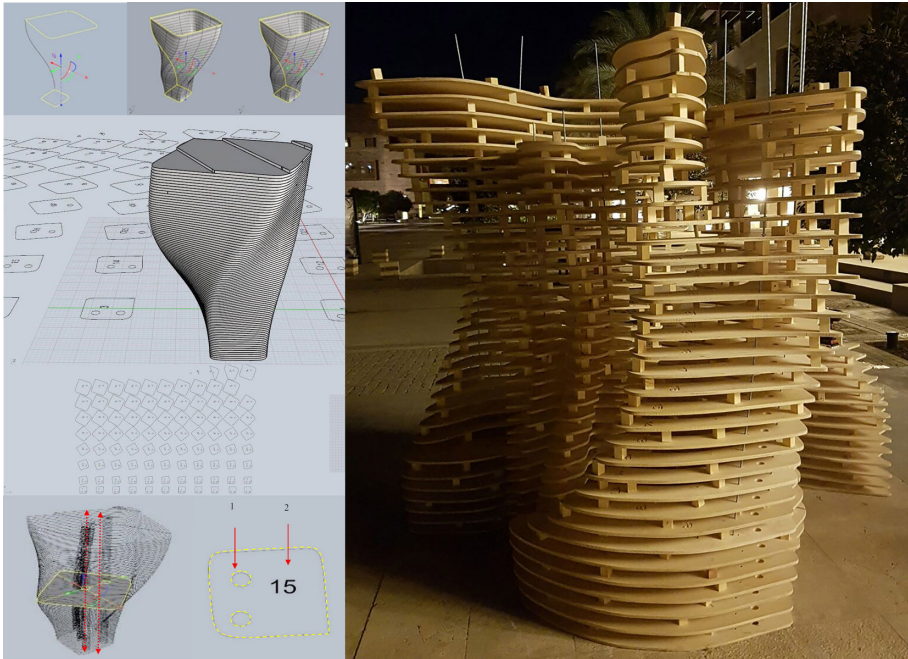


Figure 7. Output of sectioning process (Left: Process of rationalization of poly surface and preparing planar cuts for fabrication using sectioning plugin for a vertical sectioning process, Right: Fabricated outcome).

## 5. Experiment 4: Tessellation

Tessellation is a well-known fabrication technique that describes a collection of pieces that fit together without gaps to form a plane or surface. Tessellations can represent in essence any shape as long as they fit together in tight puzzle-like

formation (Iwamoto, 2009). Similar to panelized facades and brick walls, tessellated panels can refer to approximated surfaces, often singly or doubly curved, with polygonal meshes. There is typically an emphasis in freeform design on meshing arbitrary surfaces into discrete building components, where each component is procedurally constructed from a base polygonal (triangular or quadrilateral) pattern (Wang, 2009).

In this experiment, the objective was to generate a double curved surface using metals, and increase the accuracy of the surface using tessellation as a technique while linking the extracted data directly to the CNC router machine. A tessellation workflow script was developed in Grasshopper (figure 8) to define and control the resolution and number of multi-directional subdivisions of the desired metal sheet surface, surface depth, surface tagging, tile assembly, cut sheet geometry, and vertical and horizontal assembly.

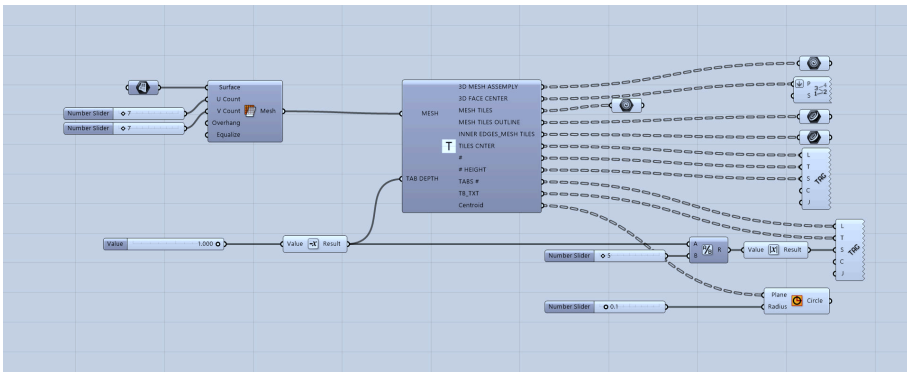


Figure 8. Grasshopper tessellation script.

Input variables of this script include the double curved surface to be fabricated, a mesh surface component that converts Rhino NURBS to a mesh surface to induce the basic surface tessellation, and the number of subdivisions in the U-direction and V-direction, the tab depth used to lock the tiles together. Outputs include the geometric component representing the tessellated mesh, tagging of the tessellated mesh panels, output curves, panel and tab tagging, and control of the diameter for pin cuts.

The core component of the script comprises sub-components for 3D mesh assembly to represent 3D surface upon tessellation, 3D face center to represent the numbering annotation in the 3D surface as a reference for fabrication, mesh tiles to represent the generated tiles for the fabrication simulation process, mesh tile outlines which represent the position for the 2D tagging on the 3D curve simulation, inner edge mesh tiles which represent inner edges for fabrication engraving, tiles center which denote tag positions for engraving, the number of tile tags and height for engraving, and the centroids for pin cuts. The plugin was applied to the surface (figure 9), and the CAD fabrication file was extracted. The panels were then folded for tighter assembly. Figure 10 illustrates the output of the tessellation script, showing the surface tags, 2D cutting sheets for panels and

3D assembly, panel engraved boundaries and cuts for connection pins.

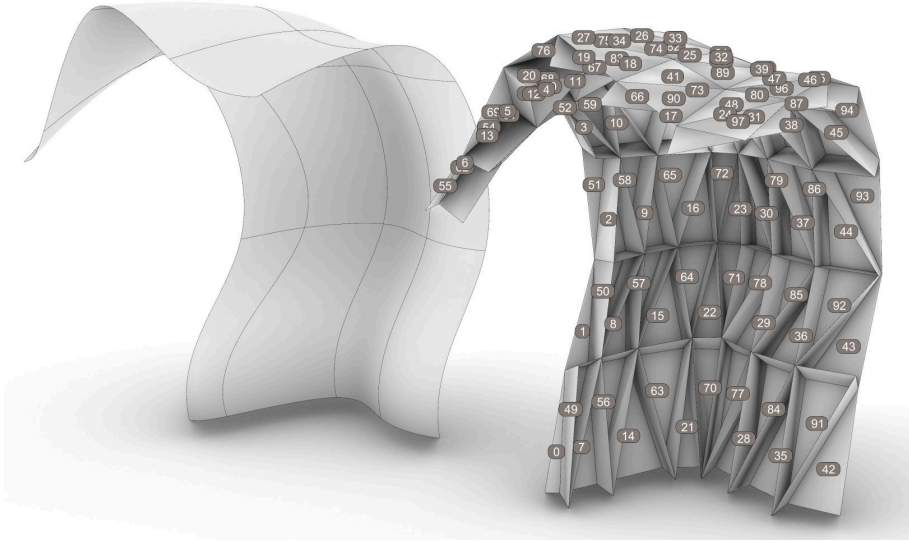


Figure 9. Automated surface tessellation and fabrication tagging of double curved surface using tessellation Grasshopper script.

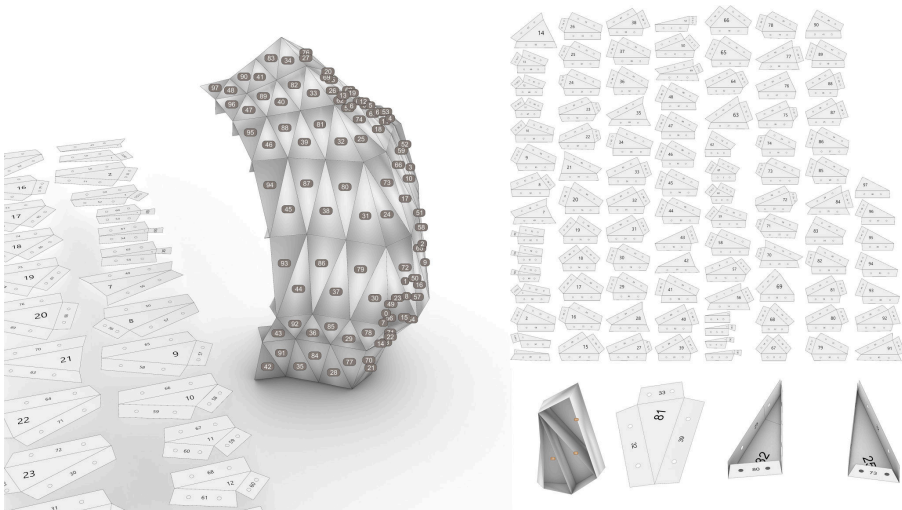


Figure 10. Output of tessellation script (Left: Tessellation script output showing surfaces tags and 2D cutting sheets for panels, Right: 2D cutting sheets showing 3D assembly, panel engraved boundaries and cuts for connection pins).

## 6. Discussion

For each of the modeling-to-fabrication experiments above, the objective was primarily the efficient and accurate representation of double curved surface geometrical data extracted for fabrication based on a variety of materials, including acrylic, clay, MDF and metal. The purpose of the proposed scripts was to streamline and partially automate the process of data extraction for fabrication of double curved surfaces while considering material properties and configurations.

In the vacuum forming experiment, the implemented device increased the accuracy of the total double curved geometry in comparison to conventional vacuum forming devices, where the overall surface subdivision and the combined use of multipoint forming and material deposition approach allowed for a coherent surface geometry based on the adjustable mould concept, which also contributed to waste reduction and reuse. Based on a preliminary comparison to different acrylic sheet thicknesses (5mm, 3mm and 2mm), the thickness of the sheets used was 2mm, which allowed for quick elasticity (50 seconds) under 200 degrees Celsius, making the fabrication process faster and more reliable. The experiment was originally implemented using 9 metal rods to easily manipulate the resulting acrylic panel based on the initial surface geometry in the Rhino model. By increasing the density of the rods in the digital simulation (starting initially at 4 rods and extending to test using 16 rods), it was observed that the fabricated surface resolution further increased by 200% upon doubling the number of rods.

In the clay depositing experiment, a low-cost approach was adopted, where a 3D clay extruder was developed and attached to a CNC router machine. Local materials and clay mixture were purchased from a local provider. In addition to developing a script to simulate the double curved vertical surface printing process, the CNC machine was used effectively for a sequential additive manufacturing process by automatically linking data extracted from the double curved geometry of the model to the material deposition in the attached extruder. As opposed to more sophisticated methods such as robotic fabrication and depositing using extruder tool heads, this approach utilized a conventional CNC router machine and a locally developed clay extruder to economically generate and fabricate double curved surfaces with similar surface continuity and precision while minimizing waste, where the double curved geometrical data was linked directly to the pumping and depositing mechanism of the extruder.

In the sectioning experiment, as opposed to tools similar to Slicer for Autodesk Fusion 360 or RhinoNest which are characterized by the capability to slice and convert 3D models into 2D patterns that can be cut out of any flat material, the added value in the developed script was the ability to directly extract fabrication data, simulate the sectioning process, and identify accurately the location of any vertical or horizontal structural stiffening, as in the metal rods described in the experiment. This allows for an element of structural integrity with complex double curved surfaces in both horizontal and vertical sectioning directions, in addition to reducing the preparation time and enhancing the accuracy of the fabricated model. It was also observed from the experiment attempts that the number of sectional cuts is directly proportional to surface resolution and accuracy, while layer thickness is



inversely proportional. Using the developed script, the density of the sectioning layers can be controlled to regulate surface resolution.

In the tessellation experiment, as opposed to methods similar to RhinoNest pre-fabrication nesting and optimization techniques, the developed script directly extracts the required data for fabrication and simulates the tessellation as well as the assembly process for metal double curved panels. It was also observed that the surface resolution and accuracy is almost 200% upon doubling the number of surface U/V subdivisions. By controlling the number of subdivisions and tiles rationalizing the surface, and simulating the full process of design, tessellation and assembly, the surface resolution and fabrication time can be effectively controlled.

## 7. Conclusion

We introduced a computational approach for the design and fabrication of double curved façade panels with complex geometry and different material configurations and properties, with focus on optimized fabrication workflow and waste reduction. We developed scripts using Grasshopper to apply surface rationalization and optimization, automated data extraction for fabrication, and simulation of fabrication process, for four different techniques; vacuum forming, clay depositing, sectioning, and tessellation. We demonstrated how the developed approach can further achieve higher levels of surface resolution and reduce waste material per type and surface complexity.

## References

- Abdelmohsen, S. and Tarabishy, S.: 2017, Optimized Design to Robotic Production: Integrating Multipoint Forming and Free Form Material Deposition in the Mass Customization of Double Curved Facades, *International Journal of Parallel, Emergent and Distributed Systems (IJPEDS)*, **32**, 180-189.
- Buswell, R.A., Soar, R.C. and Gibb, A.G.F.: 2007, Freeform construction: Mega-scale rapid manufacturing for construction, *Automation in Construction*, **16**(2), 224-231.
- Castañeda, E., Lauret, B. and Lirola, J.M.: 2015, Free-form Architectural Envelopes: Digital Processes Opportunities of Industrial Production at a Reasonable Price, *Journal of Façade Design and Engineering*, **3**(1), 1-13.
- Dunn, N.: 2012, *Digital Fabrication in Architecture*, Lawrence King Publishing Ltd, London.
- Hauschild, M. and Karzel, R.: 2011, *Digital processes: planning, design, production*, Birkhauser, Munich, Germany.
- Iwamoto, L.: 2009, *Digital Fabrication Material and Architecture*, Princeton Architectural Press.
- Lee, G. and Kim, S.: 2012, Case Study of Mass Customization of Double-Curved Metal Façade Panels Using a New Hybrid Sheet Metal Processing Technique, *Journal of Construction Engineering and Management*, **138**, 1322-1330.
- Li, M.Z., Cai, Z.Y. and Sui, Z.: 2002, Multi-point Forming Technology for Sheet Metal, *Journal of Materials Processing Technology*, **129**, 333-338.
- Shelden, D.R.: 2002, *Digital surface representation and the constructability of Gehry's architecture*, Ph.D. Thesis, Massachusetts Institute of Technology.
- Throne, J.L.: 1999, *Understanding Thermoforming*, Hanser Gardner Publications, Inc, Cincinnati, OH.
- Wang, T.H.: 2009, Procedural Reconstruction of NURBS Surfaces for Architectural Exploration, *Proceedings of the 14th International Conference on Computer-Aided Architectural Design Research in Asia (CAADRIA)*, Yulin, Taiwan, 597-606.

# 3D PRINTED MONOLITHIC JOINTS

## *A Mechanically Bistable Joint*

SHIYU FENG<sup>1</sup>, MENGZESHAN DU<sup>2</sup>, WEIYI WANG<sup>3</sup>, HENG LU<sup>4</sup>,  
DAEKWON PARK<sup>5</sup> and GUOHUA JI<sup>6</sup>

<sup>1,2,3,4,6</sup>*Nanjing University School of Architecture and Urban Planning*

<sup>1,2,3</sup>{286507275|262434307|729605034}@qq.com

<sup>4</sup>*childswim@gmail.com* <sup>6</sup>*jgh@nju.edu.cn*

<sup>5</sup>*Syracuse University School of Architecture*

<sup>5</sup>*dpark103@syr.edu*

**Abstract.** This paper describes the design and fabrication process of an adaptive joint using 3D printed mono-material bistable mechanisms. The proposed joint deforms when external forces are applied, achieving two stable states. An x-shaped microstructure (simul-SLE) is designed for the connection portion of the bistable structure inside the joint. 3D-Printing experiments is conducted to explore the possibility of various forms of simul-SLE, which realize bistable by a single material. The experiment primarily solved two problems, namely the selection of materials and how to make the rigid 3D printed material acquires properties of flexibility and softness. Finally, practical applications are shown to prove the future of this joint.

**Keywords.** 3D printing; adaptive joint; mechanically-bistable joint.

## 1. Introduction

Bistability is a buckling-induced mechanical phenomenon(Hu et al.,2015) which shows that a mechanism is capable of steadily staying at two distinct positions without power inputs (Chen et al.,2011). Compliant multistable mechanisms can be synthesized through the use of a single bistable mechanism. The bistable shell structure of composite materials invented by Daton-Lovett in 1996 is the first application (Iqbal et al.,2000).

Bistable mechanisms are an economical and effective way for designers to achieve multistability, and they have been increasingly researched in engineering field especially in aerospace engineering and micro electro mechanical system. Origami-based bistable mechanism, which can accommodate thickness, is a solution for latching or deploying space systems such as deployable solar arrays in space (Shannon et al.,2013). It has the advantage of increased performance, reduced or eliminated assembly, no friction or wear, fewer parts, lower cost, and lower weight(Zirbel et al.,2016). As for space applications such as in MEMS field, Matsunaga from Tohoku University developed a bulk micromachined silicon

mechanical acceleration switch that using squeeze film effect to install for side airbag systems with extended holding time (Tadao et al.2002), which shows bistable mechanism could be responded effectively to the change of external factors .

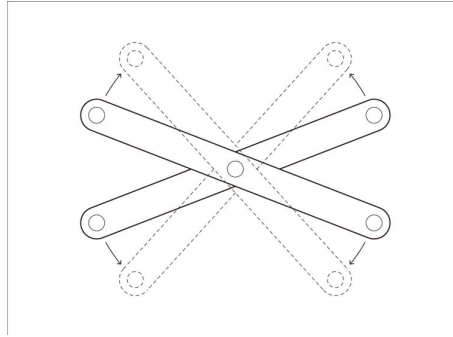


Figure 1. Scissor-like element (SLE).

Scissor-like element (SLE) is a type of structure which could achieve deformation(Fig.1). The simplest form of SLE is composed of two rod-shaped components and a joint. The rod hinged through the joint can rotate in the plane.

SLE had been applied in architecture structure from last century. By using simple planar SLE, Spanish engineer Piñero designed a movable light architecture, involved the foldable space grid, in which the covering was attached to the structure(Chilton,2000)(Fig.2). Following the development of the angulated element, which is a variation of the simple SLE, Hoberman designed various deployable dome. These new architecture structures based on SLE all have the properties of flexibility and adaptability.

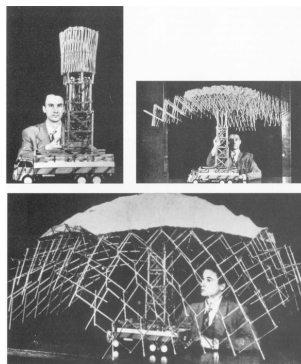


Figure 2. Folding structure of movable theatre[from:keywordbasket.com].

This study utilizes 3D-Printing technology to conduct experiments with different materials, and explore the possibility of various forms of simul-SLE, which realize bistable by a single material. Furthermore, the combination of the

joints and other components are also investigated. With the benefits mentioned above, we introduce the bistable mechanical system into the shading system of the building glass curtain wall to design a variety of dynamic joints with high efficiency, low cost and capability to interact with the environment or users. The following describes the analysis and design of a single joint, the combination of the joints and its practical application.

## 2. Mechanically Bistable Joint

The prototype of the mechanically bistable joint is a triangle structure composed of one bent bar and two linear bars. Two stable states - opening and closing - could be transferred through pressing and pulling the connection part between the linear bars. The three bars can be abstracted into rigid bodies. Adjacent bars are connected by thin sheets with a certain flexibility of the same material, which is suitable for integrated manufacturing technologies, such as 3D printing. The three rigid members constitute the two stable states of geometrical forms, and the flexible connection confirms the deformation of the joint (Fig. 3). In the experiment, the size of the two stable states of the joint is  $40 \times 24 \times 6 \text{mm}$  and  $40 \times 20 \times 6 \text{mm}$ .

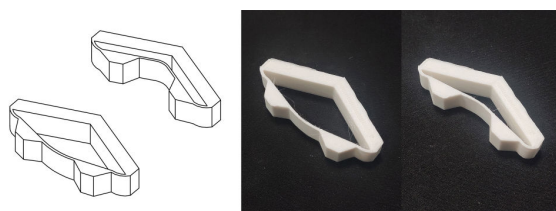


Figure 3. Two stable states of the prototype of the joint.

In the prototype of the mechanically bistable joint, the bent bar fixes one end of each of the two straight bars. Considering the length of the straight bar itself cannot change when the joint switches between two stable states, the distance between the other end of each of the two straight bars changes leading to the deformation of the thin sheets between adjacent bars. Elasticity produced by the deformation blocks the joint from the switch between two stable states, which ensures the stability of the joint.

### 2.1. CONNECTION MODE BETWEEN JOINT AND COMPONENTS

The prototype of the joint has at least two main ways of connecting with other components. Different ways of connecting lead to different displacements between components connected to the joint. In the first way, the corner point of the folded bar and the connection point of the two linear bars are regarded as the connection point with other components. When the joint switches between the two stable states, the two components connected by the joint move perpendicularly along the center line of the folded bar, and there is no relative rotation between the two components (Fig. 4).

In the second way, the midpoint of two straight bar is connected with other

components by a circular hole in each direction perpendicular to the bar and coplanar with the joint. When the joint switches between the two stable states, there is almost no relative displacement between the two connected components. Different from the first way of connection, the two connected components form relative rotation. The relative rotation angle is equal to twice the supplementary angle of the angle between the two straight bars in any stable state of the joint. In this part of the experiment, the size of the two stable states of the joint is the same as the last part.

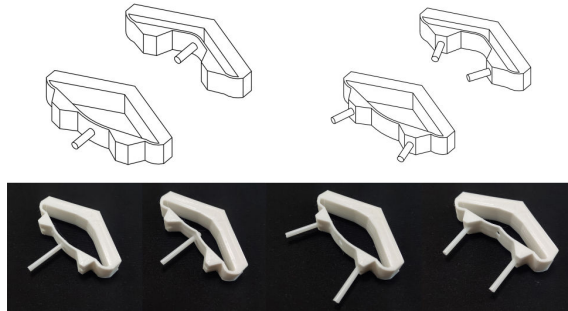


Figure 4. Connection mode between joint and components.

## 2.2. STRETCHING MOTION JOINT

The basic connection mode connect the connection point of two linear bars of one the prototype joint to the corner point of the folding bar of the other prototype joint. This connection mode realizes the linear scaling of the whole joint along the connection direction. The scaling ratio is related to the Angle between two linear bars in the prototype joint.

In order to realize the whole joint scaling in two-dimensional direction, we design the following joint unit, which is more complex. The corner points of the two prototype joints are connected to form a symmetric structure as part A of the new joint unit.

The part B of the joint is a closed loop. The difference between the two parts is the part B don't have the x-shaped part in the middle of part A, and add two linear bars to connect the rest part into a closed loop. The final joint unit is the result of connecting two parts in a direction perpendicular to each other, and the connection point is the connection point of their respective linear bars. When an external force is applied to one of the parts to open it up, the other part closes, which achieves the new stable state, and vice versa.

The stretching motion joint connects connection point of two linear bars of part A of one unit to the same part of another unit in one direction, then connect the part B of each unit in the similar way in the perpendicular direction. If we squeeze the combination in one direction, it will stretch in the other direction(Fig.5). In this part of the experiment, the size of each joint of the two stable states is  $40 \times 32 \times 48 \text{mm}$  and  $32 \times 40 \times 48 \text{mm}$ .

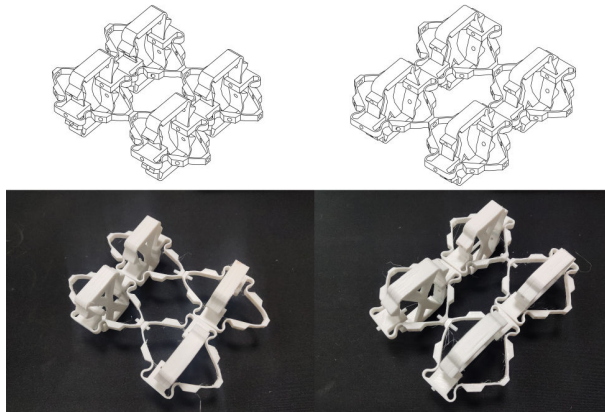


Figure 5. Stretching Motion Joint.

### 2.3. BENDING MOTION JOINT

The stretching motion joints is developed from the first connection mode of the prototype joint. If we change the connection point above from the connection point of the linear bar to the midpoint of the linear bar, the rotation effect similar to that of the second connection mode of the prototype joint will be generated. By adding a linear bar between two connection points, the collision between joint units can be avoided when the joint is switched between two stable states (Fig.6). In this part of the experiment, the size of each joint of the two stable states is the same as the last part.

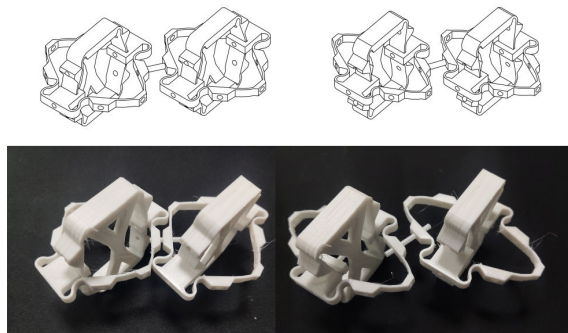


Figure 6. Bending Motion Joint.

### 2.4. COMPOUND MOTION JOINT

Compound motion joint is a hybrid of the above two joint unit connection modes, which makes it can realize most of the bending and stretching changes when it switches between the two stable states. More abundant deformation requires each

joint unit to be as small as possible, which also puts forward requirements for the manufacturing process of the joint(Fig.7).In this part of the experiment, the size of each joint of the two stable states is the same as the last part.

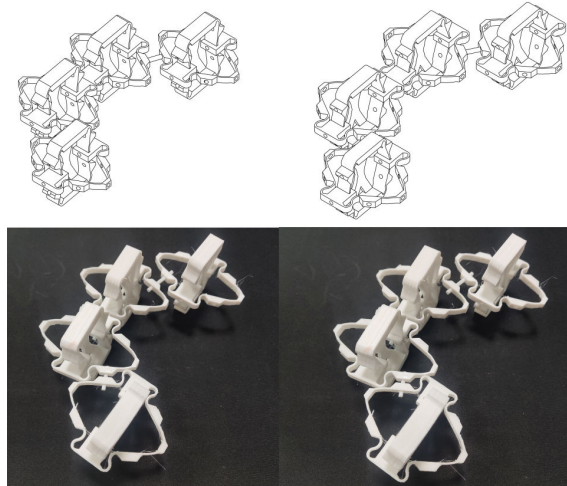


Figure 7. Compound Motion Joint.

### 3. Fabrication

#### 3.1. ADDITIVE MANUFACTURE TECHNOLOGY

The joints are fabricated by additive manufacture technology, which has the following advantages. Firstly, for traditional manufacturing processes, the increase in the complexity of the joint combination will lead to the increase in the manufacturing cost. The manufacturing cost of additive manufacture technology is only related to the volume of the product, which makes it very suitable for the manufacturing of the complex joint combination. Secondly, additive manufacture technology can ensure the uniformity of physical properties of the product. Finally, the volume of the joint unit in some applications should be as small as possible, and additive manufacture technology has advantages in this respect.

#### 3.2. MATERIAL EXPERIMENTS

It is not difficult to fabricate the bars of the joint and ensure its strength by additive manufacture technology. The difficulty lies in the flexible connection between the bars. The design of this part includes material selection and the experiments of specific geometric dimensions.

Through material experiments, lifespan and stability are two main standards for the selection of 3D printing material. ABS, PLA and TPU are three most common 3D printing consumables, the experiment compares them by above standards. Firstly, the fracture elongation of PLA material is less than 5%, which makes it

unable to meet the requirements of the flexibility. Secondly, the bending modulus of TPU material is less than 35MPa, which is hard to suit the requirements of the member bar's strength. Finally, ABS have a fracture elongation of more than 10% and a bending modulus of more than 60MPa, therefore can be better adapted to the standards of the member bar in both flexibility and intensity.

In the part A of the more complex joint unit, experimental results indicate that the optimum thickness of the bending section was 3 layers (about 1mm). The same part of the part B of the joint unit need to be softer so that part B becomes the slave of part A. Considering that further reduction of thickness will affect the strength of the bending section, the design elongates the corresponding part and bend it in the S-shape to make it softer without reducing its strength(Fig.8).

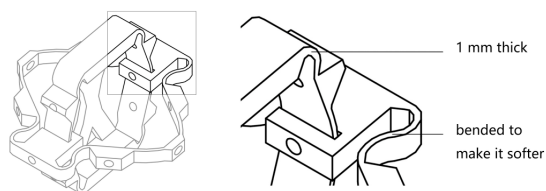


Figure 8. Bending section.

#### 4. Application fields

Bistable composite structures have been used in aerospace, bionics, isolators, energy harvesting and other fields, meanwhile received considerable attention. Based on previous research, the novel joints can be adopted in many ways.

##### 4.1. FOLDING FURNITURE

When the component is linear, it will be connected with the connection points of the joint, and the whole structure can be transformed from a plane to a 3D state only though the control of the joint, which can be actually applied to foldable furniture, such as tables and tents(Fig.9). The final volume can be changed by adjusting the length of the connecting rod. Compared with the traditional folding furniture, the overall printing material node is easier to operate and more robust, and it has a regular geometric shape before and after folding, which has a strong adaptability.



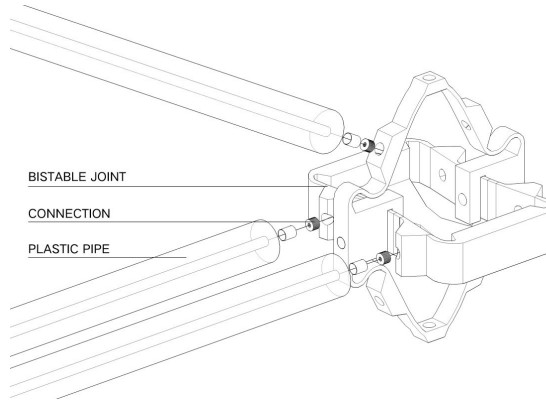


Figure 9. Bistable joint axonometry.

#### 4.2. INTERACTIVE FAÇADE

The difference between the standard unit of the interactive façade and the joint above is that the part B of the interactive façade is scaled in the direction perpendicular to itself, and half of Part B which is on the other side of part A is cancelled. (Fig.10)

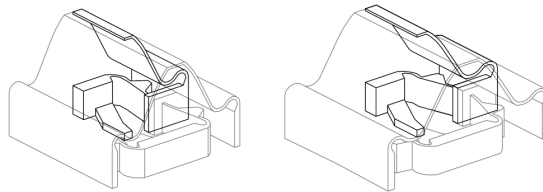


Figure 10. Standard unit of the interactive façade.

By pressing or pulling part B of the curtain wall unit, the curtain wall unit switches between two different widths, which achieves the opening and closing of the curtain wall. Because of the advantage of 3D printing technology in the manufacture of small-scale structures, the opening and closing state of the curtain wall can be more accurately responded to the contour of the pressed object by making the curtain wall unit smaller. (Fig.11)

This kind of joints can bring many advantages compared with current wall systems. The opening and closing of the curtain wall/sunshade system can be regulated automatically influenced by temperature, day lighting, ventilation or even human actions, thus producing a pleasant internal environment and interesting building façade.

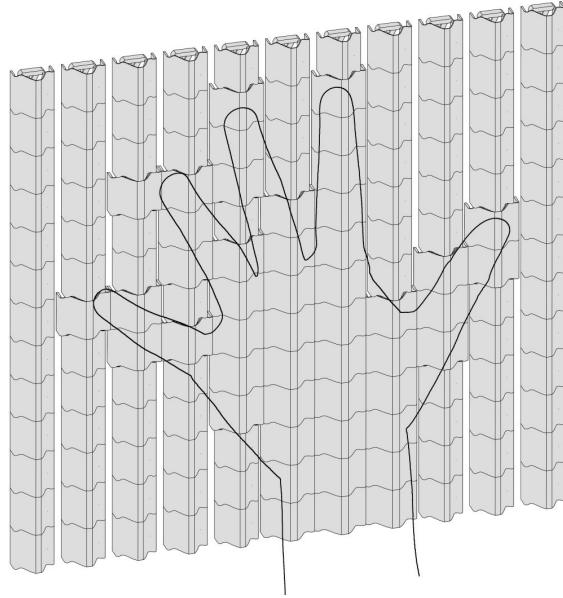


Figure 11. Interactive façade.

## 5. Discussion

Bistable mechanisms have attracted extensive attention due to their excellent mechanical properties and flexible structural characteristics. By using the structural characteristics of bistable state itself, the complex realization process in the future interaction between buildings and people can be greatly simplified. Therefore, the building's ability to perceive and respond to users' needs will be greatly enhanced. If appropriate sensors are put into the corresponding control system of this joint, it can even actively adjust the light, sound and thermal environment, or realize the opening and closing of the main structure according to the requirements. The opening and closing effect can be realized through the operation form of 3D integrated printing, which will replace the complex mechanical mechanism in traditional design. In addition, compared with the traditional switch operating on a two-dimensional plane, this joint finally realizes the opening and closing of the horizontal plane through the stretching of the vertical bar with which it is perpendicular. This breakthrough of the principles will bring more possibilities to the form of interaction between human beings and buildings.

Although the model has many possibilities in the application level, the practical application scope of the theoretical model remains to be verified due to the influence of the laboratory simulation environment. In addition, this joint is feasible in practical application. In practical operation, materials with sufficient strength and deformation capacity must be found, and the durability of materials at the junction of joints must be improved. At the same time, if the theoretical model

is scaled up, whether the mechanical properties of materials will change when applied to different scales, and the structural rationality caused by scale difference will be taken into further consideration.

## 6. Conclusion and Future Work

In this paper, by analyzing the physical properties of materials in the bistable mechanism, the structure transformation from two-dimensional plane to three-dimensional space is realized by single point manipulation. Starting from the three different properties of connection, the research uses these principles to design a series of adjustable facilities and interactive building structures of the different scales. For example, when connecting rods, it can be used as a fold furniture, when connecting glass (rigid material), or shutter (flexible material), it can form curtain wall, shading system respectively, and their mutual connection can form stable structure, etc. Although their scale varies, but has the strong interactive performance, therefore has the widespread application prospect.

Due to the operational convenience brought by this theoretical model, it will be applicable not only in the field of architecture, but also in the field of mechanical and medical applications. Given that the theoretical model is still lacking in the final realization way, subsequent studies will focus on how to realize the overall linkage of joints and make the design more ergonomic.

## References

- Chen, G., Gou, Y. and Zhang, A.: 2011, Synthesis of Compliant Multistable Mechanisms Through Use of a Single Bistable Mechanism, *Journal of Mechanical Design*, **133**(8), 081007.
- Chilton, J.: 2000, *Space grid structures*, Oxford: Architectural Press.
- Hu, N. and Burgueño, R.: 2015, Buckling-induced smart applications: recent advances and trends, *Smart Materials and Structures*, **24**(6), 063001.
- Iqbal, K., Pellegrino, S. and Daton, L.: 2000, *A Bi-stable composite slit tubes*, IUTAM-IASS Symposium on deployable structures: Theory and Applications, Springer Netherlands.
- Matsunaga, T. and Esashi, M.: 2002, Acceleration switch with extended holding time using squeeze film effect for side airbag systems, *Sensors and Actuators A: Physical*, **100**(1), 10-17.
- Zirbel, S.A., Tolman, K.A., Trease, B.P. and Howell, L.L.: 2016, Bistable Mechanisms for Space Applications, *PLoS ONE*, **11**(12), e0168218.

# LARGE-SCALE 3D PRINTING FOR FUNCTIONALLY-GRADED FACADE

YOANA TASEVA<sup>1</sup>, NIK EFTEKHAR<sup>2</sup>, HYUNCHUL KWON<sup>3</sup>,  
MATTHIAS LESCHOK<sup>4</sup> and BENJAMIN DILLENBURGER<sup>5</sup>  
<sup>1,3,4,5</sup>*Digital Building Technologies (DBT), ITA, D-ARCH, ETH Zurich*  
<sup>1,3,4,5</sup>{taseva|kwon|leschok|dillenburger}@arch.ethz.ch  
<sup>2</sup>*Gramazio Kohler Research (GKR), ITA, D-ARCH, ETH Zurich*  
<sup>2</sup>eftekhar@arch.ethz.ch

**Abstract.** Additive manufacturing (AM) technologies such as fused deposition modeling (FDM) have been gaining ground in architecture due to their potential to fabricate geometrically complex building components with integrated functionality. With that in mind, this paper showcases a novel design and fabrication strategy for the production of functionally graded façade elements. Three functional integrations are investigated: gradient infill structures (Figure 1), a non-orthogonal discretization approach for 3D-printed façade elements, and an integrated snapping panel-to-panel connection system. The presented process is then incorporated into a large-scale demonstrator consisting of eight individual façade-panel elements. This paper first presents a prototypical approach for a large-scale, graded 3D-printed facade system with non-standard discretization and then opens the discussion to further related challenges.

**Keywords.** Large-scale 3D Printing; Freeform Façade; Functional Integration; Complex 3D Assembly Connection.

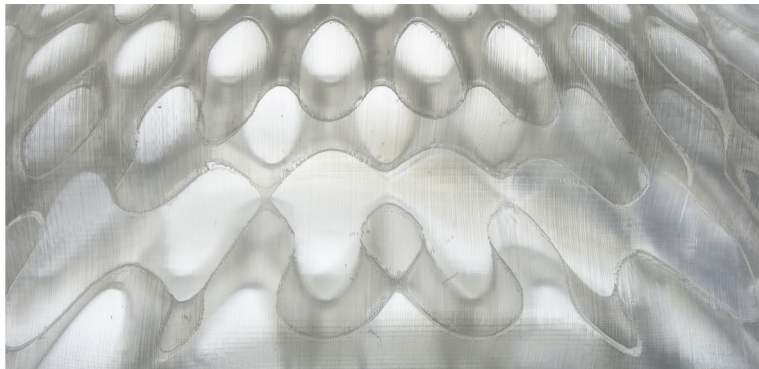


Figure 1. Graded infill microsurface.

## 1. Introduction

### 1.1. BACKGROUND

The primary function of a façade is to serve as an interface between the interior and exterior environments of a building while sheltering its occupants (Zaera-Polo 2014). Thus, façade design needs to be site-specific in order to address particular climate challenges, such as inclement or arid weather (Zaera-Polo 2014). These design constraints, along with the fact that façades account for 70% of a building's energy performance (Yang and Choi 2015), make façade design vital for sustainable architecture. Furthermore, often the façade is the first and sometimes only impression of a building, being its most prominent component (Zaera-Polo 2014); and as such, it needs to meet certain architectural design criteria, in addition to the primary functional requirements.

While complex façade design requirements are currently addressed with conventional fabrication strategies, AM technologies are gaining ground in architecture and expanding the design space of façade elements. AM enables the fabrication of building components with high geometric complexity and holds the potential to materialize the unprecedented integration of multi-functionality (Aghaei-Meibodi et al. 2017; Kwon et al. 2019). 3D printing (3DP) can offer the opportunity to integrate functional geometric features of complex assembly details as well as functional layers such as insulation, internal channels for conduits and ventilation, and/or electric infrastructure in a single fabrication process. Moreover, the unique geometries of every façade element can accommodate views, shading, and other site-specific requirements due to the customizability of 3DP. Unlike internal building components such as slabs and walls, which are designed universally, often regardless of building location, façade elements are relevant for the investigation of site-specific adaptability. Achieving such functional integration and site-responsive designs is challenging, time-consuming, and expensive for conventional fabrication methods because it requires the use of unique, single-use molds (Strauss 2013). However, AM technologies can accommodate these complexities and functionalities without added time or cost.

Therefore, this research stems from the interest to integrate multiple functional and design aspects of a façade into a coherent computational design and fabrication process.

### 1.2. STATE-OF-THE-ART

In line with the increased application of AM in architecture, recently a few projects have been investigating 3D-printed façades (Strauss 2013), mostly by using FDM as a fabrication method (Snooks 2018). FDM is an AM fabrication method that creates three-dimensional objects from thermoplastic materials, by depositing material layer by layer. In contrast to other AM technologies, FDM offers the freedom to produce geometrically complex shapes at a faster rate of production and lower cost (Ryder et al. 2002).

Several research projects which used FDM 3DP are considered as precedents for this paper. SensiLab Studio (Snooks 2018) and Fluid Morphology (Mungenast 2017), both utilize large-scale FDM 3DP for full-scale building elements. Two

other research projects combine the use of multiple materials for functionally graded performance of 3D-printed façade elements. In *Digital Composites* (Kwon et al. 2018), carbon fiber is 3D-printed laterally to the FDM layers of the façade panel along the stress lines to provide structural stability. Similarly, *Electric Skin* integrates the fabrication of electric infrastructure simultaneously with the building skin in a custom, multi-material 3DP process (Kwon et al. 2019).

## 2. Complex Snap-Fit Graded Façade

Although these precedents show the possibilities of FDM to innovate the design approach for façade elements, they also raise new questions. While the geometries presented by the projects are rather complex, the discretization systems remain orthogonal. The freedom offered by 3DP could enable an alternative and more integrated, non-orthogonal discretization procedure, specifically for complex geometries. Furthermore, while the exterior of these digitally designed elements has been investigated to a certain extent (Mungenast 2017; Snooks 2018), the internal geometries and their capacity for functional integration have not yet been widely explored.

A 3D-printed façade is not only defined by its inner and outer shell, but also by its internal geometries, or infill structures (Kwon and Dillenburger 2019). In contrast to conventional manufacturing, AM enables the creation of complex interior structures at no additional costs and has the capacity to create unprecedented functionally-graded inner cores. Therefore, the design space of inherent site-specific façade characteristics could benefit from the freedom gained through AM design and fabrication.

Accordingly, the research aims to develop these topics beyond the state-of-the-art of FDM 3D-printed façades by focusing on three main aspects of façade elements: gradient infill structures, a new discretization method and integrated snapping connection details between elements. In addition, two design aspects are explored: façade element topology and translucency.

## 3. Approach

FDM is used for this research and polylactic acid (PLA) is chosen as the 3DP material, due to its ubiquity, ease of 3DP, and interchangeability by other kinds of polymers. Functional and design criteria are investigated through a series of test prints. Initially, connection details and material properties are tested through small-scale prints, while infill patterns and an exterior shell design method are developed through medium-scale experiments. As a final step, full-scale elements are 3D-printed, achieving precise tolerances of assembly connections. The results, which are explained throughout the following sections, were applied on a one-to-one scale demonstrator.

### 3.1. FUNCTIONALLY GRADED INFILL STRUCTURES

The 3DP infill patterns investigated in this research create a gradient inner structure that varies the opacity and translucency of the facade panel, dependent on the size of the inner geometries. It is influenced by external inputs such as light

directionality and its location on the building as well as the overall façade itself. The infill geometry is a minimal surface generated through volumetric modeling, a digital design process that utilizes distance functions to generate geometry (Bernhard et al. 2018). The size of these internal geometries is controlled by the function of the minimal surface through parameters such as wavelength and amplitude, and the gradient is generated through external control inputs, such as curves or points (Figure 2.a).

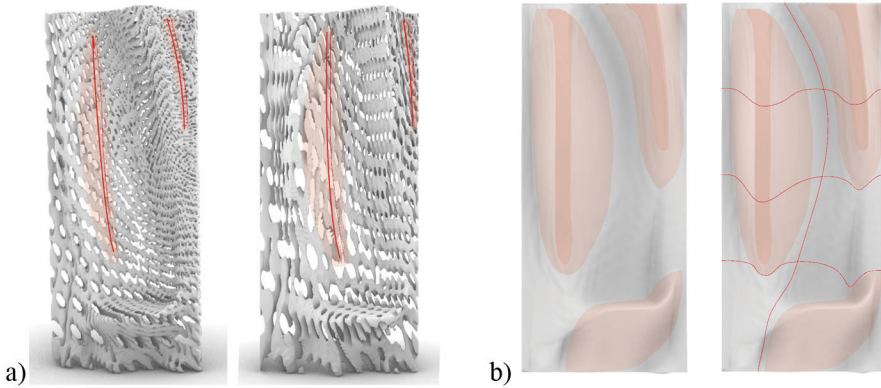


Figure 2. a) Investigated minimal surface internal gradient geometries with wavelengths of 10 and 5. b) Zones and lines of discretization.

### 3.2. DISCRETIZATION METHOD FOR NON-ORTHOGONAL FAÇADE ELEMENTS

In order to improve transportability and human-scale operability, a computational discretization method is implemented, improving time-effectiveness in on-site assembly. The overall façade can be subdivided through horizontal and vertical curved seams, creating efficiently discretized non-orthogonal panels (Figure 2.b). The vertical seam is located in the façade thinnest section area in order to achieve the lowest seam section variability and ease of assembly. This is calculated by conducting closest point analysis on curves obtained from slicing the exterior and interior surfaces. Horizontal seams are placed at equidistant heights, taking into consideration the maximum 3DP volume of the fabrication setups. These seam curves are used as a reference in generating the horizontal connection tabs (Figure 3.b). These two different strategies prioritize the vertical seams over the horizontal seams so as to establish a predefined assembly sequence. All pieces are oriented in such a way that all 3D-printed supports are minimized and their removal eased.

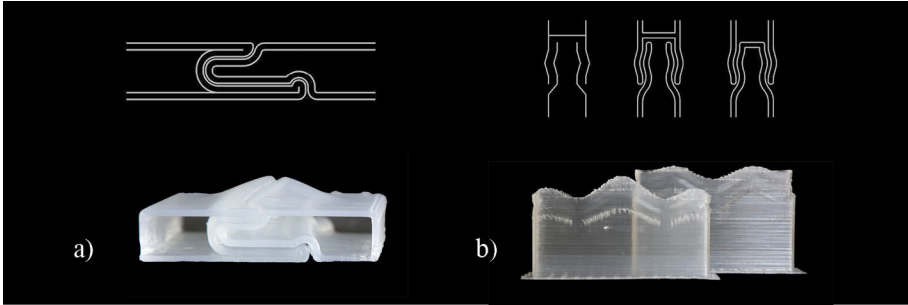


Figure 3. a) Vertical connection with a tolerance of 1mm. b) Horizontal connection with a tolerance of 2mm.

### 3.3. DESIGN METHOD FOR NON-ORTHOGONAL FAÇADE PANEL CONNECTIONS

Implementing AM techniques allows for more design flexibility and the fabrication of non-conventional complex façade designs. Standard connection systems need to be rethought by incorporating the benefits of 3DP. This will result in improved connection functionality and a new connection appearance.

In order to understand conventional connection systems, metal or foam-cored sandwich panel connection details are analyzed (Koschade 2011) and snap-fit connection strategies are studied (Bonenberger 2016). Snapping features are integrated into the connection design to take advantage of the bending properties of the PLA (Klahn et al. 2016).

3DP tolerances and offsets are an important factor in the design of the snapping connection and have to be calibrated for each snapping feature. Two lateral snapping tabs with a 2mm tolerance constitute the horizontal seams, whereas a snapping hook with 1mm tolerance locks the elements together in the vertical seams (Figure 3).

### 3.4. THREE DISTINCT FABRICATION SETUPS

For FDM 3DP to be applicable at an architectural scale with reasonable fabrication time, the 3DP process for the large-scale demonstrator is parallelized, and three different setups are used (Table 1). For all setups, a custom low-resolution tool head is implemented. In general, the layer height of a conventional desktop 3D printer is approx. 0.1mm-0.25mm, allowing high 3DP resolution. In this research, low-resolution/high-volume 3DP setups are used, with a layer height of 1mm and a layer width of 2.7mm, which delivers more robust prints at a much faster 3DP time.



Table 1. Comparison of three different setups.

Printing Setup	Build Volume	Print Speed	Benefits / Quality
<b>BigRep One</b>	100x100x100cm	20mm/s	The largest available 3DP volume.
<b>Custom Multi-Head 3D Printer</b>	95x65x100cm	25mm/s	The fastest available 3DP speed.
<b>ABB IRB1600 With Custom FDM 3DP Tool</b>	100x70x82cm	23mm/s	Robust control of 3DP parameters with the highest quality.

## 4. Results

The following experiments incorporate optimal parameters derived from early-stage 3DP tests. The highest PLA translucency is achieved by 3DP with a nozzle temperature of 230°C and reducing print speed by 30%. 3DP time is reduced by limiting overhangs to 50° to eliminate the need for supports but maintain 3DP quality.

### 4.1. INITIAL TEST RESULTS

#### 4.1.1. Infill Gradients

Medium-scale experiments are conducted to investigate certain infill inherent functionalities, such as light control, structural enhancement or graded transitions (Figure 4).



Figure 4. Investigated infill geometry types: circular gradient, truss-gradient, ShwartzP minimal surface gradient.

#### 4.1.2. Connection Experiments

Different connection typologies such as compression, notches, and snapping are tested in small-scale. The connections that show the best performance horizontally and vertically are identified and subsequently, the cross-point between them is designed, introducing a hierarchy of vertical seam over the horizontal seams

(Figure 5).

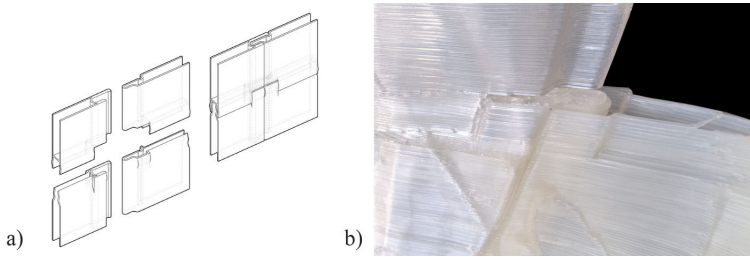


Figure 5. a) Assembly system connection crosspoint. b) Crosspoint in large-scale demonstrator.

#### 4.2. LARGE-SCALE DEMONSTRATOR

The final demonstrator is a facade with a height of 3.0m and a width of 1.3m (Figure 6). In order to design it, a computational tool is developed with three main stages. As an initial step, daylighting studies inform the design of the overall facade geometry. The facade element has two major sections: the bottom, which incorporates an integrated functional seat, while the top is angled in such a way to receive direct light for most of the year. Attractor lines are used to apply sine wave functions that generate micro-patterns on the exterior and interior shell in order to improve surface rigidity (Jipa et al. 2019). As a second step, the infill geometries are generated, and finally, the full facade is discretized and smart connection details are applied.



Figure 6. Final 3DP facade demonstrator.

In order to allow for faster fabrication, the facade thickness varies between 2cm to 6cm and the volume of the seat is reduced, by incorporating an interior hollow pocket (Figure 7).

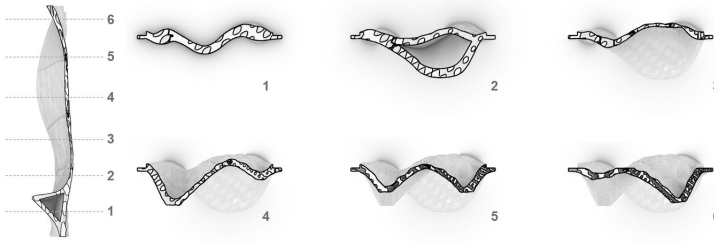


Figure 7. Façade vertical and horizontal sections.

Figure 8 shows the individual units discretized by one vertical seam and three horizontal through the above-mentioned computational method (see section 3.2). Each of the eight discretized panels is less than 10kg, except for the biggest piece (12kg). According to the size of pieces and each 3DP setup, pieces 1, 2, and 8 are 3D-printed on BigRep One; 4 and 5 with the ABB IRB1600; and 3,6 and,7 with the custom-built Multi-Head 3D Printer. The shortest 3DP time is 27 hours and the longest is 68 hours. The whole façade was simultaneously 3D-printed on these three setups in five days and post-processed (support removal, surface finish, etc.) in 4.5 hours, while the assembly was done within a few minutes only.

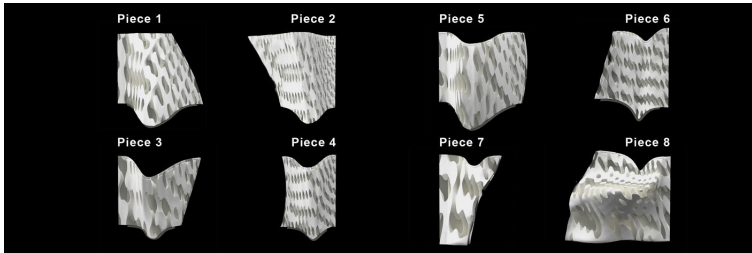


Figure 8. Volumetry of façade final pieces.

## 5. Discussion and Outlook

This research needs to be considered as a first prototypical approach to develop design and fabrication methods for bespoke façade elements. However, relevant aspects, such as insulation, wind loads, transparency, airtightness, and aging or deformation have not been evaluated yet, which is needed to make this façade system feasible to create an actual architectural component. As further topics of investigation, specialized testing facilities can be used providing the opportunity to simulate wind loads or heavy rain on a façade prototype allowing to study and to improve its behavior. Heat exposure and UV light overexposure experiments are considered to test material strength and to analyze PLA deterioration.

### 5.1. STRUCTURAL INTEGRATION: FOAMED COMPOSITES

Façade panels could be transformed easily into insulating composites, using the 3D-printed object as a mold for foam or other infill materials. There are

several issues which should be considered: type of foam/material (particle-based, expansive, etc.); to what extent does this influence its recyclability; how to 3DP an airtight object in order to prevent leaks due to expansion forces of foam; effective material bonding between PLA and selected foam.

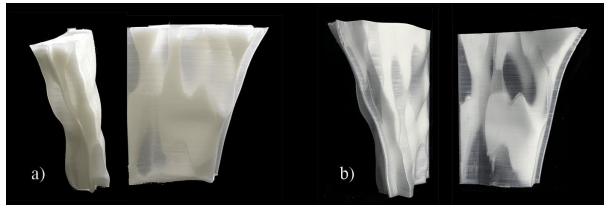


Figure 9. Initial tests of polyurethane foam infilled façade elements.

## 5.2. LOGIC OF DISCRETIZATION: FURTHER DEVELOPED

A more coherent design can be achieved with an improved discretization logic. Ideally, it should be programmed to not only follow the thinnest sections of the façade but also take into account the internal geometries. For the large-scale demonstrator, this is not taken into consideration, as seams and infill structures were not correlated. Prospectively, placing seams where there is less quantity of infill structures can create a more robust connection system and a consistent design.

## 5.3. CONNECTIONS FAÇADE-CEILING / FLOOR SLAB

The main focus of this research, regarding assembly strategies, is the panel-to-panel connections. For now, those connections are designed for fast 3DP and simple assembly. What still needs to be investigated is how water and airtight those connections are. Moreover, there are connections that have not been developed yet, such as panel-to-slab or panel-to-ceiling. These connections would have to hold the tributary weight of the façade applied linearly/punctually on the connection, plus wind loads.

## 6. Conclusion

This research demonstrates the potential of using 3DP to fabricate freeform customized façades elements where complexity can be added without increasing the cost of production. The developed assembly/connection system enables a non-orthogonal discretization approach, allowing for a more coherent overall design, which takes advantage of 3DP and its material properties. Currently, the developed gradient infill structure mainly serves visual and shading aspects, but additional functionalities can be imagined and integrated, such as inner channels to collect rainwater, and to heat and/or cool the façade, as well as insulation properties.

As AM holds the potential to customize façade elements adaptively, the authors strongly believe that 3D-printed façades can have a positive impact on the

performance of buildings in the near future regarding integration, functionality, aesthetics, and sustainability.

### Acknowledgments

The research was developed for a thesis of the 2018/19 MAS ETH DFAB. The MAS ETH DFAB is a one-year full-time educational program of the NCCR Digital Fabrication, jointly organized by Digital Building Technologies (DBT) and Gramazio Kohler Research. The authors would like to thank a number of partners and collaborators whose dedication helped fulfill the research described in this paper, including Mathias Bernhard, Andrei Jipa (DBT, ETH Zurich), FormFutura, Extrudr, Kaupo (industrial partners), Victoria Scoville and Loren Rapport.

### References

- Aghaei-Meibodi, M., Bernhard, M., Jipa, M. and Dillenburger, B.: 2017, The Smart Takes from the Strong, *Proceedings of Fabricate*, Stuttgart, Germany, 210–217.
- Bernhard, M., Hansmeyer, M. and Dillenburger, B.: 2018, Volumetric modelling for 3D printed architecture, *Advances in Architectural Geometry 2018*, Gothenburg, Sweden, 392-415.
- P. R. Bonenberger (ed.): 2016, *The First Snap-Fit Handbook: Creating and Managing Attachments for Plastics Parts*, Hanser Publishers, Munich.
- Jipa, A., Giacomarra, F., Giesecke, R., Chousou, G., Lomaglio, M. and Leschok, M.: 2019, 3D-printed formwork for bespoke concrete stairs: from computational design to digital fabrication, *Proceedings of the ACM Symposium on Computational Fabrication*, Pittsburg, PA.
- Klahn, C., Singer, D. and Meboldt, M.: 2016, Design Guidelines for Additive Manufactured Snap-Fit Joints, *Proceedings of CIRP 50*, 264–269.
- R. Koschade (ed.): 2011, *Sandwichbauweise : Konstruktion, Systembauteile, Ökologie*, München: Institut für internationale Architektur-Dokumentation, pp. 50-65 and 110-131.
- Kwon, H. and Dillenburger, B.: 2019, Optimized Internal Structures for 3D-Printed Sandwich Elements, *Proceedings of IASS Annual Symposia*, Barcelona, Spain, 1278 - 1285.
- Kwon, H., Eichenhofer, M., Kyttas, T. and Dillenburger, B.: 2018, Digital Composites: Robotic 3D Printing of Continuous Carbon Fiber-Reinforced Plastics for Functionally-Graded Building Components, *Proceedings of RobArch*, Zurich, Switzerland.
- Kwon, K., Kyttas, T. and Dillenburger, B.: 2019, Electrical skin: 3D-printed façade panel with integrated electric infrastructure, *Proceedings of Conference on Advanced Building Skins 2019*, Bern, Switzerland, 794-804.
- Mungenast, M.: 2017, Fluid Morphology – 3D-printed functional integrated building envelope, *Proceedings of 12th Conference of Advanced Building Skins*, Bern, Switzerland, 110-124.
- Ryder, G., Ion, B., Green, G., Harrison, D. and Wood, B.: 2002, Rapid design and manufacture tools in architecture., *Automation in Construction*, **1**, 279-290.
- Snooks, R. 2018, Sacrificial Formation, in M. Daas and A.J. Wit (eds.), *Towards a Robotic Architecture*, Applied Research + Design Publishing, Novato, CA, 100-113.
- Strauss, H.: 2013, *AM Envelope: The potential of Additive Manufacturing for façade construction*, Delft University of Technology, Faculty of Architecture, Architectural Engineering Technology Department., Delft, The Netherlands, pp. 95-101, 142-159.
- Yang, C. and Choi, J.-H.: 2015, Energy Use Intensity Estimation Method Based on Façade Features., *Procedia Engineering*, **118**, 842–852.
- Zaera-Polo, A., Trüby, S., Koolhaas, R. and Boom, I.: 2014, *Elements of Architecture: Facade*, Marsilio.

# 4D PRINTING: COMPUTATIONAL MECHANICAL DESIGN OF BI-DIMENSIONAL 3D PRINTED PATTERNS OVER TENSIONED TEXTILES FOR LOW-ENERGY THREE-DIMENSIONAL VOLUMES.

TOMAS VIVANCO<sup>1</sup>, ANTONIA VALENCIA<sup>2</sup> and PHILIP F. YUAN<sup>3</sup>

<sup>1</sup>*Tongji University, Pontificia Universidad Católica de Chile*

<sup>1</sup>*tvivanco@uc.cl*

<sup>2</sup>*Pontificia Universidad Católica de Chile*

<sup>2</sup>*arvalencia@uc.cl*

<sup>3</sup>*Tongji University*

<sup>3</sup>*philipyuan007@tongji.edu.cn*

**Abstract.** From the distribution of the embedded energy in materials, can be operated in order to design and produce optimized material systems with minimum use of external energy to achieve its maximum three-dimensional capacity within their mechanical constraints. This research studies the process of 3D printing bidimensional layers over a tensioned fabric to generate three-dimensional shapes. After the tension of the fabric is released, the printed pattern generates tension and compression over the textile, which conduce and distribute the internal forces generating a controlled deformation with a final form. Digital simulation of finite anticlastic shapes and parametric design under mechanical constraints of the material used to predict and compare both physical and digital forms. These allow us to evaluate and optimize the printed pattern in order to decrease the amount of used energy and material to produce a performative shape.

**Keywords.** 4d printing; material computation; digital fabrication.

## 1. Introduction

Material Computation doesn't require the use of computers (Vivanco, Yuan, 2019) to compute physical forms, nevertheless, computational tools might be needed to explore, evaluate and simulate formal, behavioural and mechanical properties (Terzidis, 2006), of the potential outcomes.

Understanding and controlling the distributed forces of different materials allows computing its mechanical and formal behaviours pursuing performativity. Formal reactions, transitions and variations led by the information embedded in materials are conditioned to environmental, structural and/or mechanical constraints that affect matter in different interactions. Giving it a gradient continuity, promoting heterogeneity and fluidity instead of rigid and static development (Oxman, 2010). A material entity embeds its material characteristics, geometric behaviour, and manufacturing processes by integrating a wide understanding of form, structure and behaviour (Mengues, 2011).

Computational tools enable the incorporation of mechanical constraints into the formal exploratory process, which can be categorized into a morphogenetic space where all the possible and probable geometries that the internal and external systems allow (Mengues, 2018) are located. The selection of forms within the morphogenetic space must be accompanied by an evaluation process of the formal objectives and mechanical behaviours that might be required (Hensel, Mengues, 2008), associated to the physical representation capacity of those forms, conditioned by the available tools that and material properties. Overall, it is determined as a deterministic selection process (Leach, 2019) in which constructive viability is critical.

By activating the information of material through mechanical stimuli (Tibits, 2017), such as stretching, new formal compositions can be explored under the conditions of physical and mechanical constraints. These activated forms can be stabilized by the use of a second material or element, achieving an equilibrium state of the tension. Allowing to decrease the amount of energy invested into the configuration of three-dimensional forms by operating the material in two dimensions, in this case, the use of horizontal forces to create vertical deformations.

Previous studies in the three-dimensional behaviour of bi-dimensional patterns to create 3D forms by applying a resin pattern over pre-stretched latex sheets (Oxman, Rossemberg, 2007) have led to the development of digital simulators to study the relationship between geometry and material behaviour in both digital and physical prototypes. Defining the transitional process from a bidimensional to three-dimensional form as four-dimensional. Due to the self, but a controlled material changes, in this case, the latex sheet.

A similar research, but based on external forces to keep the three-dimensional material activation in position, an exploration into 3D printing over the pre-stretched fabric, based on the analysis of 2D patterns that provide relief with 3D printing, generating volumes of figures (Nervous Systems, 2018). Where an algorithm (Rohan Sawhney and Keenan Crane, 2018) is used to flatten a 3D model to generate a bi-dimensional figure. Then, the figure was processed to generate patterns with areas of contraction and compression of different points, printed over a sheet of pre-stretched fabric to create volumes.

## **2. Aims and objectives.**

The concept of operating materials through their information raises the question of which could be the minimum energy (information and/or material) invested to maximize three-dimensional performativity. At the same time, how much control of the physical final form could be achieved and how the mechanical constraints can be incorporated into the design and digital production process to predict the outcome.

The aim of this research is to study both physical and digital prototypes through the develop a simulator tool to predict three-dimensional forms working only in two dimensions in order to decrease the amount of energy (and material) invested. The main function of the simulator is in first instance, to predict the resultant

three-dimensional shapes designed in two dimensions. In a second instance, to study the deflection digital and physical prototypes, and last to compare both physical and digital prototypes.

### 3. Methods and Design Process.

The design methodology developed in this research is primarily divided into five steps (Figure 1). The first step is to define the input pattern by form-finding studies using physical prototypes with both analogue and digital fabrication processes. Second, the application of the mechanical theory of buckling columns. Third, the development of a digital simulator that makes visible an approximation to the form generated from the input pattern and the output form. Fourth, the generation of the physical outcome form. As last, the mechanical analysis of both digital and physical outcomes, a critical step for the detection of patterns and discoveries will serve for further developments.



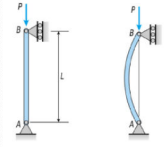



Input Pattern Experiments		Mechanical Principle	Simulation		Outcome physical form	Mechanical analysis of the digital and physical forms
Resin	Digital		Input	Output		
 3.1	 3.2	 3.3	 3.4	 3.4	 3.5	4

Figure 1. Summary table of the 5 steps of the design methodology developed in this research.

#### 3.1. INPUT PATTERN

As the elastic membrane is horizontally pre-stretched to distribute the force which creates a volume once is released, the input pattern is a stiff flat geometry that will work in compression when the tension is released. Through this, the membrane will contract to generate a three-dimensional deformation (Figure 2).

Firsts prototypes were done with latex sheets and epoxy resin patterns. By the end of these tests, two issues stood out:

- A large amount of time invested in the preparation of the materials to tests the prototypes.
- The latex sheets weren't homogeneous in their height and size, making the prototypes not comparable with others.

To have standardized measurements of deformed latex sheets were replaced by elastic textiles. Also, a form-finding process lead to define basic patterns geometries (crosses, squares, circles and parallel lines) with different widths and orientations over the tension of the fabric. Where the density and rigidity of the resin played a key role in setting the final shape due to the compression stress which is subjected, considering a prestretch length of 50% of the textile sheet size was considered for the development of initial prototypes.



### 3.2. DIGITAL INPUT PATTERN

Based on the previous step, 3D printed patterns with precise control over the printing variables of thickness, linearity and height of the input-form needed to refine. Initial forms are generated to contrast or validate the behaviour of the previous prototypes. After several tests, the configuration of the 3D printing machine presets for ABS plastic with Infill: 80%; Number of shells: 3; Shell Height: 0,1 mm; Speed while Extruding: 70 mm/s.

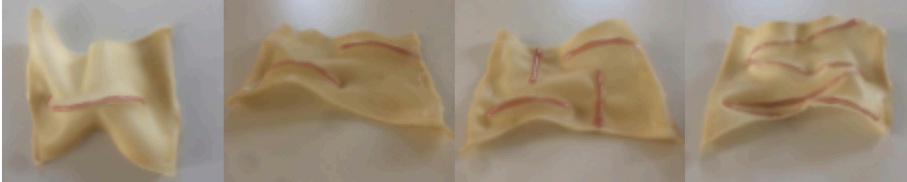


Figure 2. Firsts Latex prototypes.

### 3.3. MECHANICAL PRINCIPLES

3D printed patterns in shrunken flexible textiles have similar mechanical behaviour as deflected buckled columns. The analysis of the column's deflection based on how a finite linear element with known mechanical properties, like density, elastic or Young's modulus and geometric dimensions, is influenced by restrictive forces bent buckling principle. Conditioned by the freedom of the ends of the column, defined as pivoted, fixed or free (Gere, 2009). The bending columns theory is based on the solutions of the differential bending moment equation:

$$EIvPv = 0 \quad (1)$$

Where EI represents the flexural rigidity of the column, in which E is the material's Young's Modulus and I its inertia, v is the lateral deformation of the column and P the bucking pressure associated with its deflection. Also:

$$k^2 = \frac{P}{E}I \quad (2)$$

Which is a factor that relates the bending pressure to the flexural rigidity of the column. The main equation is a homogeneous, linear, second order differential equation with constant coefficients, which allows to determine the magnitude of the critical load and the deflected shape of the buckled column. With this in mind, the solution to the bending moment equation can be written as:

$$v = C_1 \sin(kx) + C_2 \cos(kx) \quad (3)$$

With  $C_1$  and  $C_2$  the constant parameters of the solution. Fixing the border conditions (deformation in the ends of the columns are equal to 0) it's obtained that  $C_2=0$ . This leads to the main buckling equation:

$$C_1 \sin(kL) = 0 \quad (4)$$

That has 2 cases for solving. The first one, being the mathematical trivial scenario, is  $C_1$  be equal to zero, physically relevant in order to explain the equilibrium state

of the column, thus it has not been deformed. The second scenario is  $\sin(kL)=0$ , which will occur when

$$kL=n\pi, n=1,2,3,\dots$$
 Defining  $n$  as buckling mode,  $P_{cr}=n^2 \pi^2 EI / L^2$

$P_{cr}$  is called critical bending pressure and becomes relevant for design, since determines the material to be used and the wanted deformation, related to flexural rigidity and the cross-sectional area of inertia, respectively.

Compared with the central buckling equation, it can be noticed that this theoretical value will only describe the column's behaviour when the bending pressure is equal to  $P_{cr}$ . Thus, for higher or lower values, the bending equilibrium will be present only if the column remains with no external perturbations, except the bending pressure.

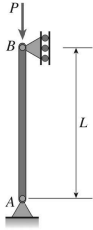
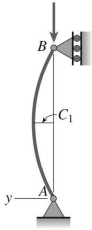
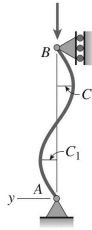
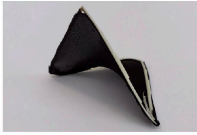
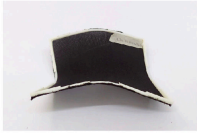

Given this explanation, it is possible to contrast the deformation of the 3D printings in lycra through the  $n$  parameter (buckling mode), that will define the number of curves that the printed figures will have when the textile is released. Through the static study of columns, specific combinations of extremes are analyzed, for their structural relevance and their mechanical feasibility. Considering two extremes, there are:

- Column with one end fixed and the other free
- Column with one end fixed and other hinged
- Column with both end hinged
- Column with both end fixed

Lycra Dupont as a textile material, its mechanical properties are measured in a non-standardized way. The simile to the young module in textile engineering is the comparison between the stretching of the fabric with the force applied to stretch it, is understood as the comparison between the stress and the strain of the material. (Goldade and Vinidiktova, 2017). Specifically, Lycra Dupont can be stretched up to 100% of its size in one direction, but in the other direction, it can be only stretched 75% of its size due to its fibre direction. This defines a stretched length criteria of considering its most unfavourable elasticity of the size of each sheet.

Understanding the key properties of the materials that give structure and form of the prototypes, deformations obtained were compared (Table 1) with the deflection curves named above. An adapted column buckling theory was used to predict the forms that were printed and then compared.

Table 1. Comparative table of prototypes and different modalities ( $n=1, n=2$ ) of the pivot-pivot configuration of column buckling theory.

$P < P_{cr}$	$P > P_{cr}$ $n=1$	$P > P_{cr}$ $n=2$
		
		

### 3.4. OUTPUT SIMULATED FORM

Initially, to mechanically simulate the static conditions of the prototypes, the base geometry of the membrane and input pattern were parameterized and the fixed vertices from the flat parametric surface were extracted. From this initial setup, a five-step computational definition was made (Figure 3):

Mesh and base points input for the printed figure (Figure 3, color magenta).

Mechanical and Young modules of each element. (Figure 3, color blue)

Anchor points from base points (Figure 3, color orange)

Stresses, tensions and deflections following column buckling theory with Karamba 3D solvers (Figure 3, color yellow)

Calculation of the deflection curves of the fabric (Figure 3, color cyan)

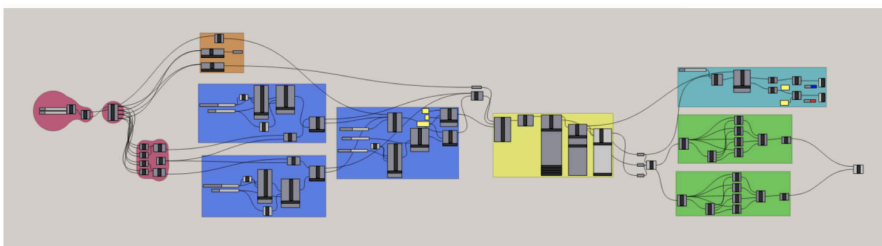


Figure 3. Grasshopper diagram of the simulator of the output simulated form. In colors divisions of elements in the code.

The definition starts with the selection of the finite elements that will

participate in the deformed body-defined from the basic parameterized geometry and the input pattern. Next, the single developable curves are generated from the base geometry; after that, mechanical and geometrical properties are defined in MatProps and Cross Section functions of Karamba3D plugin. In order to transform the developable curves to non-developable double curves, which in this case will be ABS beams pattern, using the Line to Beam component. The mechanical and physical properties of Lycra Dupont are given to the mesh, considering its contraction according to the predefined stretch distance.

The guiding key for the form-finding process within the simulator is the assignation of mechanical reactions to each anchor points of the input pattern, similar to the reactions they would have in a physical prototype. Based on initial prototypes, it was observed that there are mainly three types of lycra-supports (fixed, hinged and free) since their mechanical behaviour was relatable to the column buckling theory. These combinations will generate deformation in the simulator (Figure 4). Considering that the pivot type support generates parallel and perpendicular reactions, the fixed support generates the same reaction as the fixed one, added to moment or torsion reactions towards the centre of the bar. The free support generates reactions only on the axis towards which it is an external force applied (Gere, 2009).



Figure 4. Simulated outcomes generated using Grasshopper and Karamba 3D definition.

### 3.5. OUTCOME PHYSICAL FORMS

For the development of the outcome prototypes (Figure 5), tension, input shape, thickness and height of the print and the number of 'hinges' or segments of variations in height of the figure were varied to influence the performance of the outcome form relatable to critical pressure and inertia in theory of columns buckling. With small variations in the length of each beam, new equilibrium solutions are achieved (Kilian and Ochsendorf, 2005), for example, for three-dimensional networks, a spherical dome can become a conical shell by adjusting the length of each element.

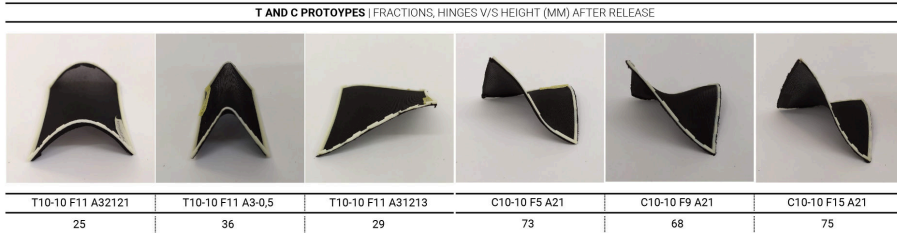


Figure 5. Comparison between outcome's physical prototypes varying in the number of hinges with the same thickness with the achieved height (mm) after tension was released. Prototypes name code: T or C(width-large (in cms)) F(number of segments) A(segment thickness pattern (in mm)) T prototypes: two parallel sides with the same thickness; the remaining sides with hinges with different thickness according to the pattern. C prototypes: same size and same thickness on four sides but with variable thickness and different hinge patterns. The last row shows the maximum height in mm achieved by the input pattern after the tension was released.

By varying the height of two of the sides of a squared printed pattern, the final outcome was deformed in only one direction. (T-prototypes) Even more, when segmenting the length of the pattern and giving each section a different height, thinner parts had a lower resistance to compression, a greater deflection and deformation of the output physical form.

The geometrical interaction between the textile tensile stress and the input form generated variable controlled outcomes that allows to pursue a functional final form. The development of a functional prototype (Figure 6) was possible due to the incorporation of the different behaviours of C and T prototypes mentioned above. Making possible to predict the outcome form and its geometrical assimilation of the input figure.



Figure 6. Evolution of a functional prototype. From a planar form (right) to the three-dimensional prototype (right) generated an increase in height after tension was released.

#### 4. Mechanical comparison between the digital and physical prototypes.

Printed patterns work as a continuous and closed geometry under the mechanical principle of deflected buckled columns, transmitting forces between them until they achieve a static equilibrium. Depending on the height and/or segment of a trace the energy will distribute until it finds its own stiffness balance.

As shown in the image above (Figure 7) the deflection principle finds its own

equilibrium by distributing forces all across the fabric, generating a deformation and resultant geometry. With an accurate printing over the textile, the outcome physical prototype will be structurally adapted keeping a force balance, similar to the simulated form.

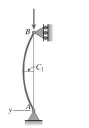
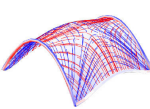


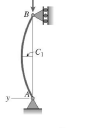
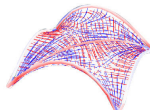

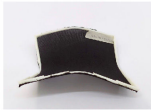
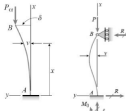
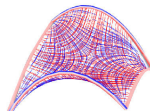

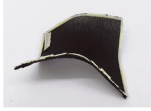
Mechanical Principle	Simulated		Outcome Physical form
	Stress Analysis	Baked	
			
			
			

Figure 7. Mechanical analysis comparison of the digital and physical output and outcome forms under the theory of columns.

The control of the outcome's curvature through the pattern section depends on the size of the segments of each pattern line, where smaller deformations are when fewer segments in the structure length. The behaviours of the physical prototypes are reciprocal with the simulated digital prototypes; therefore, the input behaviour can be projected without need to make physical prototype or by defining a pre-descriptive geometry.

## 5. Conclusions

Computation can contribute to understand and inform materials. Which only can be operated in the physical world, where material belongs. The idea of predefined forms questions the basis of creativity, which can only navigate within specific material constrains and production processes.

Developing an integrated research between physical and digital prototypes based on mechanical constraints, material strength can be considerably be optimized through geometry, decreasing the amount of embedded required energy of three-dimensional form. The input pattern through the force of the textile controls and adapts the embedded energy, generating a actuated transformation from a bi dimensional to tridimensional form, defined as a 4D printed.

As shown in prototype C10-10 F15 A21, this research reveals that by segmenting the printed bidimensional input pattern length its three dimensional achievement can increase considerable. This change of thickness and hinges gives a better resolution and control over the outcome physical form, opening new

exploration for design considering angle changes and straight elements, as show in initial further developments (Figure 8).

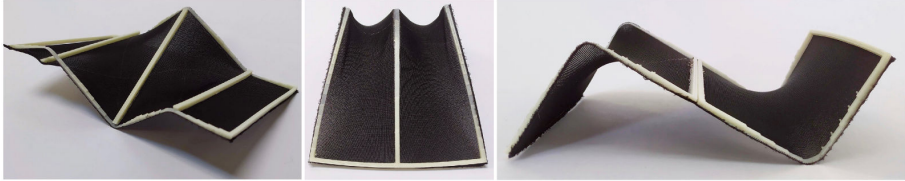


Figure 8. Experimental prototypes with rectilinear patterns and deformations.

This open new research questions based on the potential change of scale of the prototypes and outcome control to generate functional forms combining both curve and linear based forms in a continuous pattern with different resolution.

### Acknowledgments

Martín Campos, Tomás Peralta, Material Computation studio class from the School of Design from Pontificia Universidad Católica de Chile and Digital Futures PhD from Tongji University.

### References

- “Nervous System. Self forming structures: an exploration into 3D printing on pre-stretched fabric.” : no year given. Available from <<https://n-e-r-v-o-u-s.com/blog/?p=8011>>.
- J. Gere (ed.): 2009, *Mechanics of Materials*, Nelson Engineering.
- V. Goldade and N. Vinidiktova (eds.): 2017, *Crazing Technologies for Polyester Fibers*, Woodhead Publishing.
- Hensel, M. and Mengues, A.: 2008, Inclusive Performance: Efficiency Versus Effectiveness Towards a Morpho□Ecological Approach for Design, *AD Special Issue: Versatility and Vicissitude*, **78**(2), 54-63.
- Kilian, A. and Ochsendorf, J.: 2005, PARTICLE-SPRING SYSTEMS FOR STRUCTURAL FORM FINDING, *Journal of the International Association for Shell and Spatial Structures*, **46**, 77-84.
- T. Kostas (ed.): 2006, *Algorithmic Architecture*, Oxford: Elsevier Architectural Press.
- Leach, N. 2019, Discrete: Reappraising the Digital in Architecture, in G. Restin (ed.), *AD Magazine Discrete*, John Wiley & Sons Inc.
- Mengues, A.: 2018, *Digital Fabrication*, Tongji University Press.
- A. Mengues and S. Ahlquist (eds.): 2011, *Computational Design Thinking*, John Wiley & Sons Ltd.
- Oxman, N.: 2010, *Material-based Design Computation*, Ph.D. Thesis, MIT.
- Oxman, N. and Rosseberg, J.L.: 2007, Material-based design computation an inquiry into digital simulation of physical material properties as design generators, *International Journal of Architectural Computing*, **5**, 25-44.
- Sawhney, R. and Crane, K.: 2018, Boundary First Flattening, *ACM Transactions on Graphics (TOG)*, **37**, 13.
- Tibbits, S.: 2017, Active Matter, *MIT Press*, **1**, 351.
- Vivanco, T. and Yuan, P.: 2019, Programming Intelligence: consciousness of material algorithms, *International Conference on Computational Design and Robotic Fabrication*, Shanghai.

# HORIZONTAL FORMING IN ADDITIVE MANUFACTURING: DESIGN AND ARCHITECTURE PERSPECTIVE

ALEXANDER GEHT<sup>1</sup>, MICHAEL WEIZMANN<sup>2</sup>,  
YASHA JACOB GROBMAN<sup>3</sup> and EZRI TARAZI<sup>4</sup>  
<sup>1,2,3,4</sup>*Technion - Israel Institute of Technology*  
<sup>1</sup>*geht@campus.technion.ac.il* <sup>2,3,4</sup>*{wmichael|yasha|*  
*ezri.tarazi}@technion.ac.il*

**Abstract.** Extrusion based three-dimensional additive manufacturing technology forms objects by driving the material through a nozzle depositing a linear structure through vector-building blocks called roads. In a common 3-axis system, the roads are stacked layer upon layer for forming the final object. However, forming overhanging geometry in this way requires additional support structures increasing material usage and effective printing time. The paper presents a novel Horizontal forming (HF) approach and method for forming overhanging geometry, HF is a new extrusion-based AM approach that allows rapid and stable forming of horizontal structures without additional support in 3-axis systems. This approach can provide new design and manufacturing possibilities for extrusion AM, with emphasis on medium and large-scale AM. HF can affect the outcome's aesthetic and mechanical properties. Moreover, it can significantly accelerate the production process and reduce material waste. The present paper maps the influence of various parameters employed in the HF method, providing a deeper understanding of the printing process. Additionally, it explores and demonstrates the potential functional and aesthetic characteristics that can be achieved with HF for industrial design and architectural products.

**Keywords.** Additive manufacturing; Support; Horizontal forming (HF); Extrusion-based system; Fused granulate forming (FGF).

## 1. Introduction

Additive manufacturing (AM) is considered the next fabrication revolution, with its emphasis on customization, decentralization, and rapid production. In less than four decades since their introduction, AM technologies have made impressive progress. Nonetheless, issues associated with poor material properties, slow fabrication, expensive cost, and scaling constraints limit many AM approaches to rapid prototyping for early modeling, education and research fields.

One of the most popular types of AM technologies is extrusion-based modeling (3D Hubs 2018). In this technology, the material is driven through the nozzle and deposits in a linear structure through vector-building blocks called “roads”



(Bellini, Guçeri, and Bertoldi 2004). The roads are usually stacked layer upon layer (Figure 1, left) to form the final object. In this way, each new layer must be supported by the layer beneath it. Overhanging geometry over a certain degree (about  $60^\circ$ ) (Figure 1, middle), or free-space segments (Figure 1, second from right) can be very challenging, if not impossible.



Figure 1. Figure 1: Material deposition types, using extrusion-based AM.

The current research explores and develops an additional method for forming overhanging structures, in an attempt to expand the capabilities of complex models forming in 3-axis extrusion-based AM, with emphasis on fabrication speed and manufacturing processes.

The paper begins with a background section that presents several common methods of forming overhanging geometries and describes the benefits and drawbacks of each. The main part of the research is presented in the following section, which maps Horizontal Forming (HF) basic criteria such as horizontal printing distance and the material amount by various experiments in overlapping printing. The last part of the paper presents a software tool that generates a G-code tool path and several case studies that compare printing with a regular slicer and the new HF oriented software tool.

## 2. Background

### 2.1. COMMON APPROACHES TO OVERCOMING OVERHANGING GEOMETRY IN 3-AXIS MACHINERY

#### 2.1.1. Support structure

The most common approach to avoiding overhanging geometry failure is printing support structure. This is an additional structure generated under the overhanging geometry to prevent it from collapsing (Zhao and Xu 2019). Like a scaffold, it is a temporary structure, usually formed from the base up to the overhanging geometry. In some cases, when large areas of overhanging geometries are needed, the supports can become larger than the model itself in terms of volume, printing time, and amount of material used. As support is an additional structure, it required additional printing movements and increases the probability of failure. Moreover, removing the support is highly labor-intensive and time-consuming, and can damage the model's surface.

#### 2.1.2. Avoiding overhanging geometry

In some cases, complex shapes with large overhanging geometries are divided into several parts and printed in different orientations in order to avoid the need for support. As a result, the assembly process needs to be considered and integrated into the design, making the design and production more complex. Moreover, gaps

between parts can appear during the printing process, due to material deformation and the different printing orientations.

### *2.1.3. Freeform 3D printing*

Freeform is a technique of forming spatial structures without the need for support (Huang et al. 2016). It is based on a very slow printing process and material cooling. As a result, the extruded material solidifies in the course of the movement to create free-standing strands of material in space (Oxman et al. 2013). Although this method allows complex forming, it requires custom machinery adaptations and a high level of control over software and hardware (Molloy and Miller 2018). Moreover, the outcome of the freeform process tends to be less consistent with the design model, depending on material properties and printing parameters. Finally, as the material cools, fusion quality between the cross-sections can be poor.

## **3. Horizontal Forming**

Horizontal Forming is a new approach to creating overhanging structures using common, 3-axis machinery without relying exclusively on direct layering methods. HF is based on Fleximatter's method for fabricating hollow objects (Meshorer and Vasilevski 2017). HF based methods were developed especially for medium and large-scale fused granular fabrication (FGF) aiming to simplify and accelerate extrusion-based AM processes by cutting the need of support or infill at the manufacturing process.

The method comprises deposition of modeling material in parallel horizontal contours, wherein at least one of the contours is extruded horizontally above a three-dimensional region devoid of any solid support (Figure 1, right). The structure solidifies during the forming process and allows forming horizontal surfaces in mid-air without any support. HF provides new design complexity and can be more effective in material usage and manufacturing time, which are extremely important factors in manufacturing considerations (Austern, Capeluto, and Grobman 2018).

FGF may use industrial-grade, low-cost, and highly diverse materials. Moreover, this technology can be easily scaled up, for example by being mounted on a mobile platform, expanding the printing boundaries and providing almost limitless printing size (Keating and Wallace 2016). Thanks to simple machinery and affordable materials, this technology has a huge potential in the industrial and architectural design fields.

## **4. Research Aim**

The main aim of this research is developing a new approach (HF) to printing self-supporting horizontal structures and examining the effects of the overlap and material amount parameters on the performance of a new approach. The study was conducted in two phases. In the first, experimental phase, we defined and mapped the HF method parameters by examining the effect of overlap and material amount as the most significant parameters in this method (Meshorer and Vasilevski 2017). In this phase, we observed and analyzed the material's behavior and formation,

providing basic insights for developing the new approach as well as the database for future research.

In the second phase of the research a G-code path generator software tool was developed based on the data and conclusions from phase 1 experiments. The tool was tested in case study experiments that were designed to explore and demonstrate potential functional and aesthetic characteristics of HF from industrial design and architectural perspectives.

## **5. Phase 1: Mapping and Examination**

### **5.1. DESCRIPTION OF MACHINERY**

Initial testing was carried out with a medium-scale Fleximatter (850×750×1000 (X-Y-Z)) FGF system, using a 2mm nozzle. This technology was chosen given its ability to print medium-scale products and architectural fragments. Granulate ABS material was chosen as the most common and affordable industrial material for commercial objectives. For this study, we applied transparent ABS also known as MABS (methacrylate-acrylonitrile-butadiene-styrene (LG MABS TR557)). The raw material was mixed with pigments to provide immediate visual feedback, enabling us to examine contour fusion quality, as detached material leaves a white mark on the fused area (Bellehumeur and Li 2004) (Figure 5).

One of the most important HF parameters is contour overlap, defined as the distance between two adjacent contours (Figure 3, bottom). To define the overlapping distance range, we printed the same structure with overhanging geometry, observing the effect of the overlap distance. The overlap resolution was defined for the experiment as 0.1mm, with the experiment starting from zero overlap (no contact between contours), and reaching up to an overlap equal to nozzle diameter.

### **5.2. PHASE 1: EXPERIMENT**

The experiment's aim was to map and define the influence of various parameters on contour-overlap and material-amount on the printed result. Contour-overlap is defined as the distance between two adjacent contours (Figure 3, bottom). To define and map the printable overlapping distance range, we printed 200X50mm rectangle with 90 deg overhanging surfaces every 10mm (in the z-axis) with overlapping parameter increased by 0.1mm every following overhanging surface until the structure failed to form. The experiment started from zero overlap (no contact between contours) and reached up to an overlap equal to nozzle diameter (2mm). A rectangle modeled with varied rounded edges was used to observe forming behavior at round and sharp geometry.

To investigate the effect of the material amount on HF the process was done with different amounts of material. Material amount range defined between cross-section area of 1.196mm<sup>2</sup> that equivalent to a cross-section of 0.5mm layer height and 2.5mm road width up to 4.141mm<sup>2</sup>, equivalent to a cross-section of 2mm layer height and 2.5mm road width.

### 5.3. RESULTS

#### 5.3.1. Layer-on-layer vs. horizontal forming

The results show a significant difference between traditional layered roads (Figure 2A) and horizontal contour cross-section (2B), as the material forms under different conditions. Traditional layered road height is defined as that between the previous layer and the nozzle, providing constant boundaries due to the deposition process. While layer height is constant, the amount of extruded material affects road width. Both parameters affect the road cross-section shape, forming a symmetric road cross-section that can be calculated and predicted (Comminal et al. 2018).

Horizontal contours form, however, as the extruded material has enough overlap with the previous contour and fuses. Since the previous contour is the only boundary, the contour forms as an asymmetrical shape (Figure 2, right). Furthermore, predicting the contour cross-section is challenging as there is no material beneath the extruded layer and contour forming depends on material solidification, which is affected in turn by cooling and material characteristics. Unlike roads, contour width ( $C_w$ ) depends on nozzle diameter ( $N_d$ ) and overlap ( $O$ ) ( $C_w = N_d - O$ ). Our observations show that nozzle diameter limits the maximum contour width. Contour height is more complex to predict as it depends on material amount and solidification.

Based on the observation of the printed roads and contour cross-section shapes (Figure 2), it seems that the standard slicer used in the layer-on-layer method is unsuitable for working with the HF method, which requires a different approach due to the difference between roads and contours.

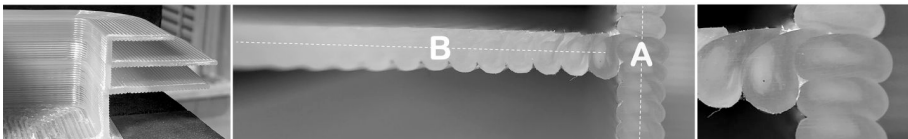


Figure 2. Figure 2: Layer on layer and horizontal forming cross-section. Left: Printed model with stable HF. Middle A: Roads cross-section. Middle B: Contour cross-section. Right: Cross-section close-up.

#### 5.3.2. Horizontal forming parameters

HF's success and mechanical characteristics depend on the overlap distance and material amount. The results of the different overlapping distances were classified into three main classes, based on contour fusion quality: "fail", "stable" and "over-overlap" (Figure 3): low overlapping distance will fail to form horizontal geometry due to low or non-fusion between two adjacent contours (Figure 6: overlap=0.0mm). Increasing the overlap will increase fusion quality providing a stable and constant horizontal structure since the extruded material will have enough surface to be attached to (Figure 6: overlap=0.2-0.5mm). Using stable HF parameters will enable forming a neck growth fusion providing a stable structure

(Bellehumeur and Li 2004).

There is a point of over-overlapping, however, where the material will accumulate excessively, and the designed geometry will be deformed, similarly to the over- extrusion effect in the layering method (Figure 4). It is complex to predict material deformation caused by over-overlapping, as in some cases, the material is not fully solidified, and the overhanging geometry bends up during the forming process (Figure 4, left). In other cases, with solidified geometry, the material starts to generate natural random patterns (Figure 4, middle). Still, other cases involve a combination of random patterns and bending (Figure 4, right) (O’Dowd et al. 2015).

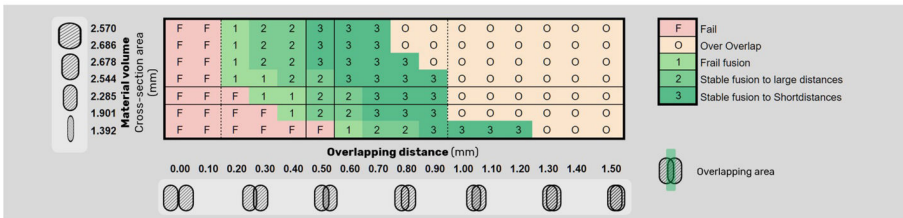


Figure 3. Figure 3: Mapping of the effect of overlapping and material amount. “F” refers to failure to fuse. “O” refers to over-overlapping. 1 - Frail contour fusion. 2 - Stable fusion for long HF. 3 - Stable fusion for short HF, after which it becomes over-overlapping.

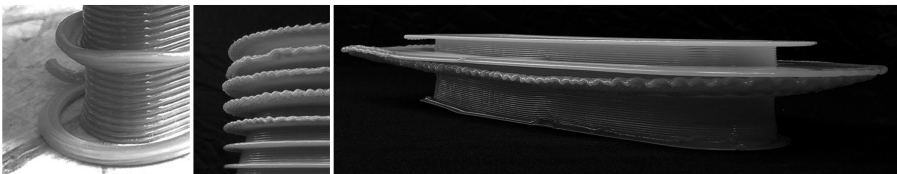


Figure 4. Figure 4: Over-overlapping parameters. Left: Material banding upward; Middle: random texture; Right: Material bending with random texture.

Stable fusion parameters, in this setup, have a range of around 0.6mm, providing a constant horizontal structure with differential fusion quality (Figure 3, 1-3). Parameters with low relative overlapping will form frail fusion (Figure 3, 1; Figure 4, left). Frail fusion can be used as a design and manufacturing tool: those areas can be used as a new opportunity to redesign material properties, 4D structures, or detachable areas (Tibbits 2014). For example, frail fusion areas can be set as an interface between the model and support structure )that can be easily removed( or be defined as foldable areas.

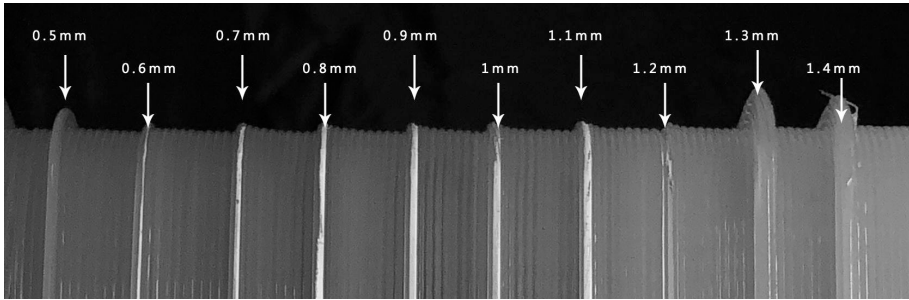


Figure 5. Figure 5: The white linear mark represents the fusion area between two contours after detachment. Left: 0.5mm overlap distance - providing frail fusion; contours were easily detached. Right: 1.3mm overlap distance - neck-growth fusion; impossible to detach manually.

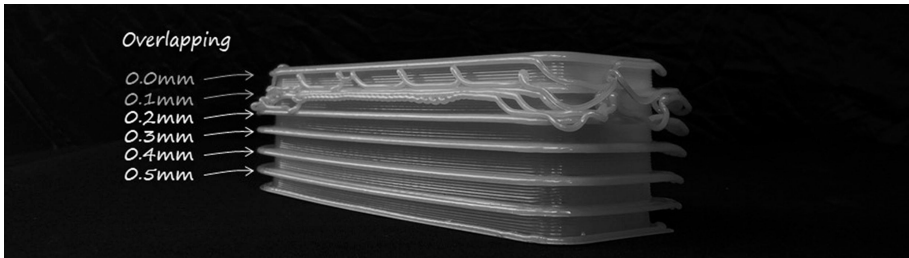


Figure 6. Figure 6: HF affected by overlapping parameters. 0.5mm overlap: stable forming; 0.0mm overlap: failure to form a horizontal structure.

### 5.3.3. Material effect

Common industrial materials have a shrinkage rate that adds complexity to the deposition process (Wang, Xi, and Jin 2007). Formed material continually deforms due to the deposition process. Forming horizontal geometry will take more time between two consecutive layers, and the layer with HF may shrink and deform while printed. Furthermore, as the layer has more overhanging contours, it will take more time to form, hence greater deformation. Additionally, as more contours are formed in the same layer, shrinkage forces will be stronger, leading to significant deformation; in some cases, a layer might fail to print due to the deformation of the previous one. Whereas forming failures due to material shrinkage can be predicted in the modeling stage, this is very complex due to the multiple parameters affecting deformation.

## 6. Phase 2: Case study - Freeform HF

Since the invention of AM, there has been a separation between the machinery (3D printer) and design tools. Technological advancements have concentrated on the manufacturing process, developing new materials, scale, and optimizing

the machinery performance. The gap between the machinery and CAD was bridged by third-party software, known as a slicer. Although the slicer makes the design model printable, it limits the technology's potential. As a result, most of extrusion-based AM parameters set as a constant parameter in the course of the printing process to simplify and ensure a stable and successful manufacturing process.

Yet, extrusion-based AM is a continuous process of material extrusion and machinery motion, which can be used similarly to a craft process, where the outcome is affected by the material's behavior and the motion of the tool. Tacit knowledge of expert operators can predict the effect of motion, material quantity, and temperature on the material's behavior. Having the designer's knowledge embodied in the technology allows designing unique artifacts just by having the vision of material behavior driven by the machinery. The most interesting part is to be able to translate this knowledge into a design tool everyone will be able to use (Bilotti, Norman, and Rosenwasser n.d.).

Next, we provide examples of applying freeform modeling rather than the slicer method using HF, and present other areas with potential for applying this method.

### 6.1. SLICER-GENERATED HF

The Fleximatter slicer uses 3D models to automatically generate paths for the printer and adds horizontal contours by generating offset contours at the required layer (model height). This method is effective in structures that require uniform horizontal reinforcement with horizontal ribs (Figure 7), forming horizontal support scaffolds for free-space objects and for other applications. However, this slicer generates horizontal structures only, as model offsets and the same overlap parameter are defined for the whole layer, without the ability to define variable overlapping within a single layer.

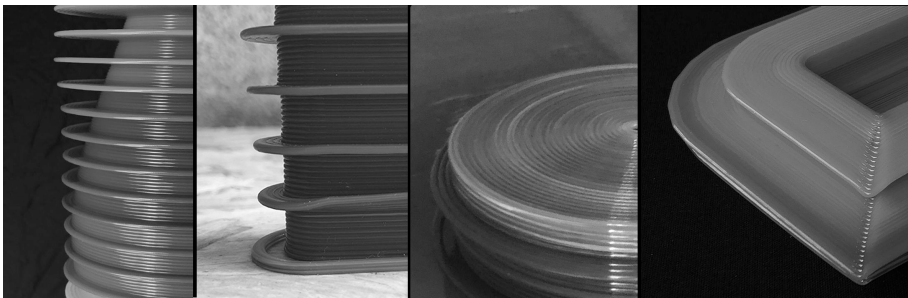


Figure 7. Figure 7: Offset contours at the required layer, having the same type-3 overlap parameter, which have become over-overlapping after a few contours.

### 6.2. HORIZONTAL FREEFORM

In order to control the overlapping parameters over the forming process, a G-code path generator software tool was developed. The tool allows defining the overhanging structure as a tool path, with full control of deposition motion and

direction. The tool was developed in Rhino and Grasshopper environments. It was based on the tested parameters from phase 1 and developed to fit the Fleximatter machinery.



Figure 8. Figure 8: HF design tool types.

The tool was used for generating several examples to explore the new possibilities for HF. The first example introduces local HF on the model surface - we were able to form horizontal contours on the specific areas of the model, without having to form an offset of the entire model, saving printing time. Using this method, we can reduce model damage caused by printing offset contour over the whole model. Moreover, we are able to control the shape and size of the structure.

The second example is based on fusion behavior driven by overlapping distance. Mechanical and aesthetic properties can be applied to the design model on the horizontal structure: Breaking point (Figure 8) - frail fusion contours can be set in a stable horizontal structure, providing a predicted breaking point as a design and manufacturing feature.

An additional example is a deferential HF (Figure 9). The overlap parameter can be applied in more complex shapes, controlling contour behavior between full fusion, frail fusion or fail areas to represent deferent aesthetics and functional properties, such as airflow, transference, and flexibility. This very basic tool helps us show a new way to think and design using this method. It is an important basis for future research.

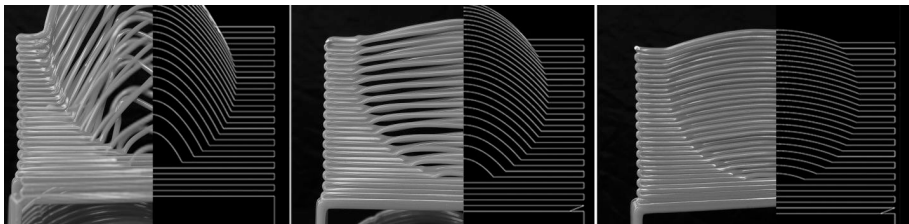


Figure 9. Figure 9: Material behavior affected by the overlap distance in the circle area. Left: 5mm overlap; Middle: 2.5mm overlap; Right: 1.6mm overlap.

## 7. Conclusion

The research explores the potential of horizontal forming (HF) for fabricating complex overhanging structures without the need for additional support or post-processing. Literature suggested that employing HF can accelerate the



manufacturing process and reduce material waste - advantages that are particularly critical in medium - and large-scale AM. The paper focused on mapping the overlap distance relative to extruded material volume and developing and examining the potential of a new software tool for HF, presenting new possibilities of using HF.

Mapping the effects of overlap distance and material amount allows predicting and programming the fusion type between contours, thus adding another layer of complexity to the HF method. The case study models demonstrated that the HF structures are stable for medium-scale products and architectural fragments.

FGF AM technology seems to have significant potential for desktop, large-scale and architectural manufacturing. Moreover, this method may be suitable not only for fused extrusion, but also when using other materials.

## References

- Austern, G., Capeluto, I.G. and Grobman, Y.J.: 2018, Rationalization methods in computer aided fabrication: A critical review, *Automation in Construction*, **90**(December 2017), 281-293.
- Bellehumeur, C. and Li, L.: 2004, Modeling of Bond Formation Between Polymer Filaments in the Fused Deposition Modeling Process, *Journal of Manufacturing Processes*, **6**(2), 170-178.
- Bellini, A., Güçeri, S. and Bertoldi, M.: 2004, Liquefier Dynamics in Fused Deposition, *Journal of Manufacturing Science and Engineering*, **126**(2), 237.
- Comminal, R., Serdeczny, M.P., Pedersen, D.B. and Spangenberg, J.: 2018, Numerical modeling of the strand deposition flow in extrusion-based additive manufacturing, *Additive Manufacturing*, **20**, 68-76.
- Huang, Y., Zhang, J., Hu, X., Song, G., Liu, Z., Yu, L. and Liu, L.: 2016, FrameFab: robotic fabrication of frame shapes, *ACM Transactions on Graphics*, **35**(6), 1-11.
- Hubs, initials missing: 2018, "3D Printing Trends Q1/2018". Available from <<https://f.3dhubs.com/tpeFNmNBD83pKJYnSHpne.pdf>>.
- Keating, S.J.: 2016, *From Bacteria to Buildings: Additive Manufacturing Outside the Box*, no thesis type given, no school given.
- Meshorer, Y. and Vasilevski, A.: 2017, "METHOD AND SYSTEM FOR FABRICATING HOLLOW OBJECTS". Available from <<https://patentimages.storage.googleapis.com/f3/28/e7/35f082462ab539/US20170274575A1.pdf>>.
- Molloy, I. and Miller, T.: 2018, Digital Dexterity, *ACADIA*, 266-275.
- O'Dowd, P., Hoskins, S., Walters, P. and Gelsow, A.: 2015, Modulated extrusion for textured 3D printing, *International Conference on Digital Printing Technologies*, 173-178.
- Oxman, N., Laucks, J., Kayser, M., Tsai, E. and Firstenberg, M.: 2013, Freeform 3D printing, *Green Design, Materials and Manufacturing Processes*, 479-483.
- Sabin, J.: 2018, Robosense 2.0, *ACADIA*, 276-285.
- Turner, B.N., Strong, R. and Gold, S.A.: 2014, A review of melt extrusion additive manufacturing processes: I. Process design and modeling, *Rapid Prototyping Journal*, **20**(3), 192-204.
- Wang, T.M., Xi, J.T. and Jin, Y.: 2007, A model research for prototype warp deformation in the FDM process, *International Journal of Advanced Manufacturing Technology*, **33**(11-12), 1087-1096.
- Zhao, P. and Xu, M.: 2019, *Lecture Notes in Electrical Engineering 543. Advances in Graphic Communication , Printing and Packaging*, S.

# KNIT CONCRETE FORMWORK

ABHIPSA PAL<sup>1</sup>, WI LEEN CHAN<sup>2</sup>, YING YI TAN<sup>3</sup>,  
PEI ZHI CHIA<sup>4</sup> and KENNETH JOSEPH TRACY<sup>5</sup>  
<sup>1,2,3,4,5</sup>*Singapore University of Technology and Design*  
<sup>1,2</sup>{abhpsapal.96|chanwileen}@gmail.com  
<sup>3</sup>yingyi\_tan@mymail.sutd.edu.sg <sup>4,5</sup>{peizhi\_chia|  
kenneth\_tracy}@sutd.edu.sg

**Abstract.** The manufacture of concrete funicular shells often relies on traditional formwork construction techniques to provide a sculptured cavity for the fluid material to occupy (Bechthold, 2004). While this enables a predictable geometric outcome, the extensive use of timber and/or steel to construct these formworks account for up to 60% of the total production cost of concrete and are discarded after the casting is complete (Lloret et al. 2014). Thus, we propose an alternative method to create prefabricated modular systems out of concrete casted in customised tubular knitted membranes. These perform as a network of struts that can be affixed onto 3D printed nodes of a singular design. Altogether, these components serve as a kit-of-parts that can be transported to site and assembled together to create shell geometries.

**Keywords.** Knitted Textile; Fabric Formwork; Concrete Casting.

## 1. INTRODUCTION

This paper demonstrates the design and fabrication of a modular system composed of prefabricated concrete struts that are cast within knitted tubular formwork and assembled together with 3D printed joints. In this scenario, we seek to capitalise upon the customisability of additive manufacturing methods (i.e. machine knitting and 3D printing) to create a kit-of-parts for the formation of shell-like frame geometries.



Figure 1. Lattice shell.

The fluid nature and structural properties of concrete have led to its prevalence as a construction material in the building industry. As such, concrete is used in the manufacture of planar and freeform geometries alike. However, the making of concrete forms usually entails the use of rigid formwork materials (e.g. timber and steel) which account for up to 60% of the total production cost (Loret et al. 2014). These are discarded after the casting is complete, further resulting in increased material waste.

In response, we propose the use of a strut-to-strut configuration of cylindrical concrete forms. These can be assembled into a network of beam-like components that can be interconnected to form shell-like geometries, inspired by the Funicular Funnel Shell typology (Rippman & Block, 2013). Each individual strut unit involves a bespoke textile machine-knitted out of Ultra-High-Molecular-Weight Polyethylene (UHMWPE) to serve as a flexible tubular formwork. We sew 3D printed interface nodes onto the edge of the fabric, enabling it to be linked to neighbouring strut nodes via a snap-fit joint. Lastly, we pretension the fabric tube with an adjustable jig, before casting it with concrete.

Thus, by integrating bespoke flexible membranes with an adjustable system, this potentially presents a sustainable alternative in the manufacture of complex forms in concrete. Such enables the formation of volumetric cylindrical geometries with varying diameters or lengths within a single jig. Thus, there is no reliance on traditional formwork making methods and this subsequently minimises the generation of waste.

For this paper, we focus primarily on the design of the knitted formwork with the aim to attain a physical model that has a good fidelity with its digital counterpart. Using CNC knitting technology, we investigated this objective by changing the input yarn materials and stitch patterns and recording the resultant geometry after concrete was cast into it. This was followed by a further refinement of the textile formwork to match our target geometry while incorporating 3D-printed snap fit joints. This cumulated in a 1:3 prototype with 3

interconnected struts. Furthermore, as part of a master's thesis, a building design was proposed for a full scale implementation of this fabrication method. This will also briefly demonstrate the computational tools employed in the design of this system.

## 2. LITERATURE REVIEW

Fabric formwork for concrete casting has been an ongoing research domain in both architecture practice and academia. In addition to minimising the amount of rigid formwork material, the use of fabric membranes for casting concrete brings about other advantages, such as facilitating the formation of curved forms.

Fabric concrete casting can be categorised into two groups: (i) open-faced moulds and (ii) closed moulds. The first type (i) employs the fabric membrane as a base that can be stiffened in place for more concrete to be applied upon it. Recent works include van Hennik & Houtmann's thin-walled concrete shells using pneumatic formwork (van Hennik, P. C., Houtman, R., 2008), Veenendaal's cable-net system (Veenendaal, D., Block, P., 2014) and Popescu's KnitCandela (Popescu, 2018). The second group (ii) involves concrete being poured into the cavity of a bounded fabric to solidify. Works that adopt this strategy are West's variable concrete truss (West, 2007), Yo\_cy's 'Cast Thicket' (Tracy, K., Yogiaman, C., 2014) and Culver & Sarafian's 'Fabric Forms' (Culver, R., Sarafian, J., 2016). We review the latter two built works which we find relevant to our proposal.

Yo\_cy's 'Cast Thicket' explores the principle of a fully cast-in-place installation consisting of multiple slender members. Yogiaman and Tracy assembled strips of polypropylene formwork with tabbed seams around internal steel bars, enabling the entire structure to be cast as a single piece with embedded reinforcement.

Culver & Sarafian's 'Fabric Forms' project takes a different approach through the use of robotic arms to form individual Y-shaped struts using stretched Lycra fabric. With one 'leg' secured onto a stationary jig and the other two affixed to 6-axis robotic arms, they poured concrete onto the internal cavity of the pretensioned formwork. The hydrostatic pressure from the concrete deformed the stretched elastic fabric in accordance with their simulated model. Upon curing, the physical 'Y' components were affixed together into a lattice space frame using 3D printed connectors that could be bolted together with their adjacent neighbours.

While both projects demonstrate successful formation of lightweight concrete elements using tensile membrane formworks, each reveals how the material interaction between the formwork and hydrostatic pressure from concrete influences the final outcome. 'Cast Thicket', due to the use of largely inelastic polypropylene sheets, experiences buckling of the surface when concrete is poured into the formwork. This causes geometric inaccuracies in the installation. On the contrary, the resultant geometry of 'Fabric Forms' is dependent on the interaction between the tensioned elastic Lycra fabric and the weight and hydrostatic pressure of the concrete. The interplay of material and forces introduces interesting geometric outcomes, but it is challenging to attain a target geometry without the

use of physics-based simulations.

Thus, we can see that it is vital to take into account the materiality of the fabric formwork in order to enhance the fidelity of the physical cast prototype. The capacity for the fabric to stretch needs to be stiff enough to resist the pressure exerted by the concrete, while also being adequately elastic to be pretensioned to minimise the effects of buckling. As such, we turn to a machine-knitted formwork of high performance yarns where we can customise its elasticity in different directions and also its initial shape. This tunability of both the fabric's structure and material will be explored more in the next section.

### 3. EXPERIMENTATION

In this research, we explored using CNC-knitting technology to alter the elasticity of our fabric formwork in the vertical (walewise) and horizontal (coursewise). This fabrication technology offers a stitch-by-stitch level of control to modify the yarn material, stitch pattern and loop lengths. We input these designs into a proprietary software which converts the code into machine instructions. The knitting machine reads the machine instructions and then knits a bespoke textile seamlessly in a single 'print'. For our experiments, we produced our samples on a 15-gauge Shima Seiki MACH2XS weft knitting machine.

Our goal was to create a relatively inelastic tube that could resist the hydrostatic pressure exerted by concrete yet could still be tensioned to prevent surface wrinkling. Thus, we decided upon a tubular jersey stitch pattern composed from UHMWPE yarns twisted with spandex and nylon to form a cylindrical cavity. This chosen stitch pattern coupled with the low extension of the yarn material resulted in a fabric that is stiff in the course-wise direction and could be stretched in the walewise axis.

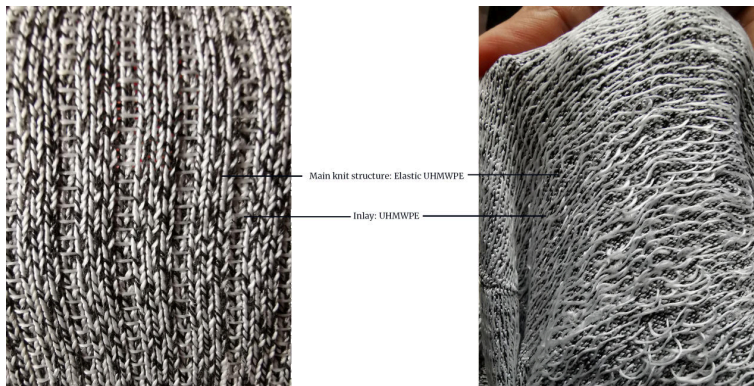


Figure 2. (Left) Outer face of knit mould, (Right) Inner face of knit mould.

#### 3.1. INITIAL TESTS AND PARAMETER VARIATIONS

In our first test, we knitted a tube of 65mm in diameter with the above-mentioned knitting parameters. We tensioned this upon a custom-made jig made from

threaded rods and MDF bases for the top and bottom plates. We affixed the fabric with 3D-printed nodes, with the top being open and the bottom being closed, and attached each end to the plates. This was done in such a way that the orientation of the fabric with its walewise axis in the vertical direction (i.e. parallel to the rods) and the coursewise axis parallel to the plates. Such a configuration resulted in the stiffer coursewise axis resisting bulging from the poured concrete.

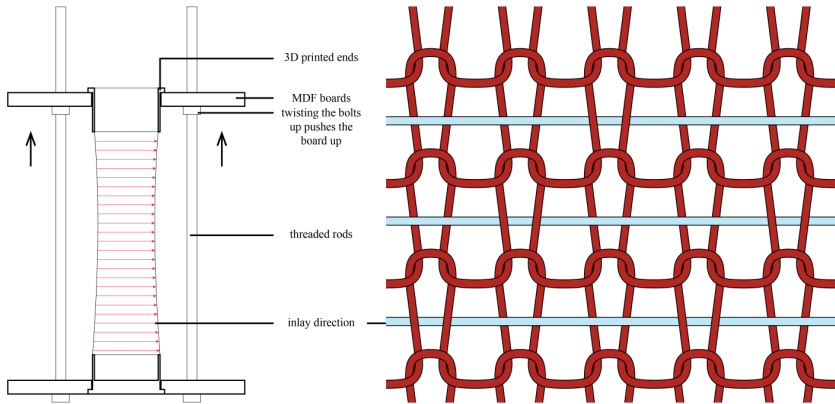


Figure 3. Knit tube being stretched.

In addition, we varied the knitting parameters and walewise stretch ratios. Specifically, these included inlays in the coursewise direction where a continuous UHMWPE yarn is woven in front of every alternate loop to restrict the extension in the coursewise axis. We hypothesised that this will be more effective in countering the effects of hydrostatic pressure. The walewise stretch factors were varied between zero stretch and the maximum of 1.5 times stretch. We believed that the stretching of the knit works together with the inlays to maintain the cylindrical form of the cast element, while preventing wrinkling of the surface.

In these casting attempts, we poured our concrete mix incrementally in small batches to prevent the tube from deforming excessively under the full weight of the concrete. This also meant that the bottom layers had time to harden and could therefore resist the load from the subsequent pours.

During the cast, we observed that water and small amounts of cement would seep out from the tube. This could be attributed to the porous nature of the knitted membrane structure despite a relatively tight knit. Our experiments also revealed that inlays are effective in restricting the expansion at the bottom half of the cylinders. Without the addition of inlays, the cylinder expands at the base and tapers three-quarters towards the top, which could be the result of the aforementioned hydrostatic pressure (see Fig. 4a). The walewise stretching also facilitates the control of the geometry where the bulging is negated while providing a consistent symmetrical geometry (see Fig. 4c,d). Thus, our subsequent casts utilised the parameters reflected in Fig 4d. The main knit structure is UHMWPE twisted with spandex and nylon.

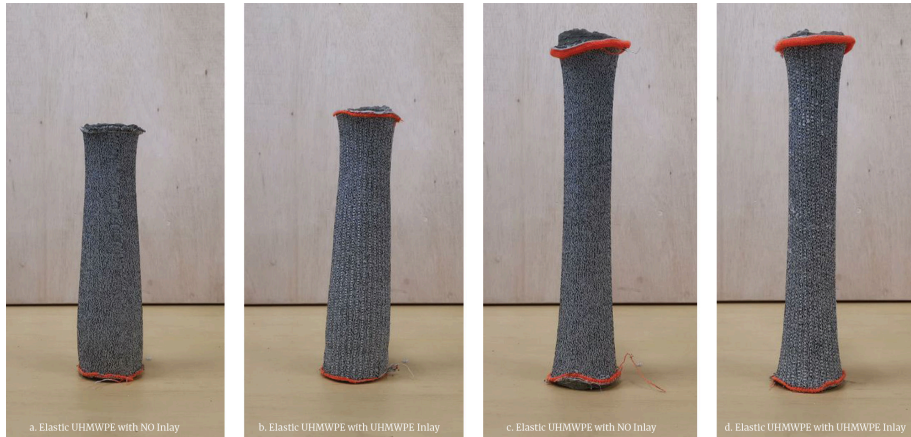


Figure 4. Experiments with inlays and stretch factors.

### 3.2. INTEGRATION WITH ADJACENT MEMBERS

Our next series of casts investigated connectivity with adjacent members. For this, we designed a strut configuration which consisted of 3 valences coming together at an intersection point. The struts were flared at their ends to interface with their neighbours and we performed this by modifying the textile's initial shape by narrowing and widening the perimeter edges. The concrete mix used was sand (64%), cement (23%), water (13%).

Our first design (see Fig. 5) presented a funnel shape on both the top and bottom of the knitted fabric, allowing the cast element to fit with the other members with a 120 degree angle. However, the design proved to be problematic due to the large cross-sectional profile at the flared regions, resulting in chunky ends with a narrow and thin central 'neck' which was prone to cracking.

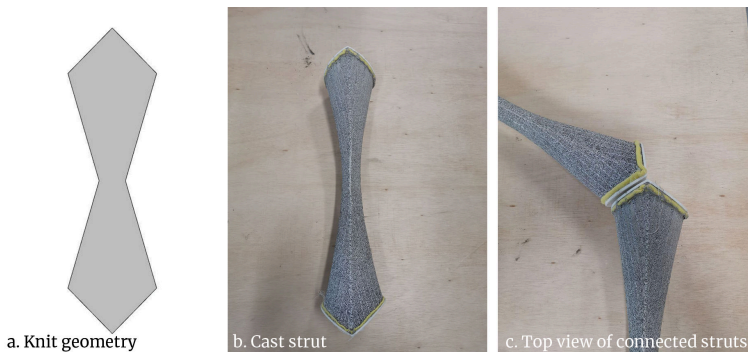


Figure 5. First flared funnel-like strut.

To fix the initial design, we edited the knit profile to reduce the large flared ends. The longer, sharp ends of the knit profiles were slightly shortened so that

the problem areas would be stiffer after tensioning; hence they would bulge less. We also straightened the knit profile which made the fabric more cylindrical. This will ensure that the smallest cross sections of each cast would not be too narrow.

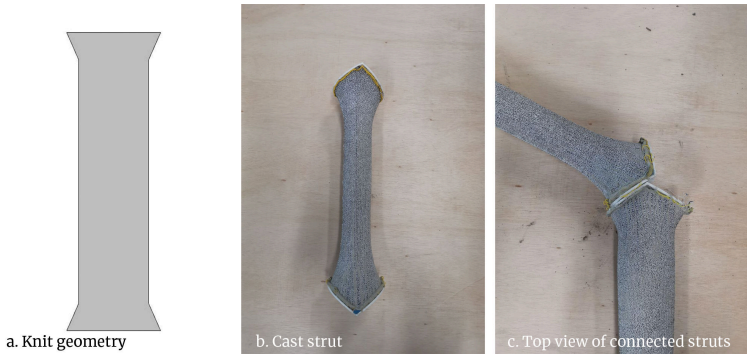


Figure 6. Refined cylindrical strut.

#### 4. Scale Prototype

Our experiments led to the making of a 1:3 scaled prototype model with three struts connected at a single intersecting point. We made the three struts out of the profiles in Fig. 6 and designed 3D printed joints that functioned as the interface between each strut member. The design of these 3D printed joints had curved indentations with holes that could be locked together with several steel threaded rods (see Fig. 7).

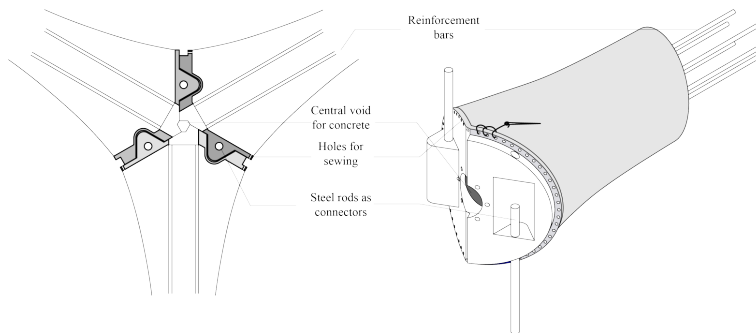


Figure 7. 3D printed joint and connector detail.

These joints also had additional functionalities where they acted as holders to position the embedded steel rods in place which serves as reinforcement. The edges of the joints consisted of tiny holes for the fabric to be sewn onto before casting was performed. Moreover, the joints also incorporated a central hole to pour the concrete into the internal cavity.



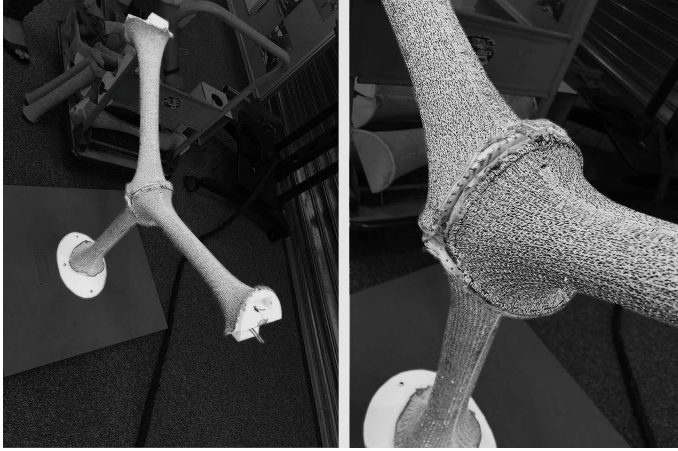


Figure 8. Scaled 1:3 prototype with 500mm length struts and having an overall size of 750x750mm.

#### 4.1. DESIGN PROPOSAL

The research gathered in the previous sections was implemented in a masters thesis project where this system of concrete struts was used to compose a funicular roof structure of a flower market based in India. Using planned circulation lines to derive the starting mesh, the roof was generated using a particle-springs simulation via the Kangaroo plug-in.

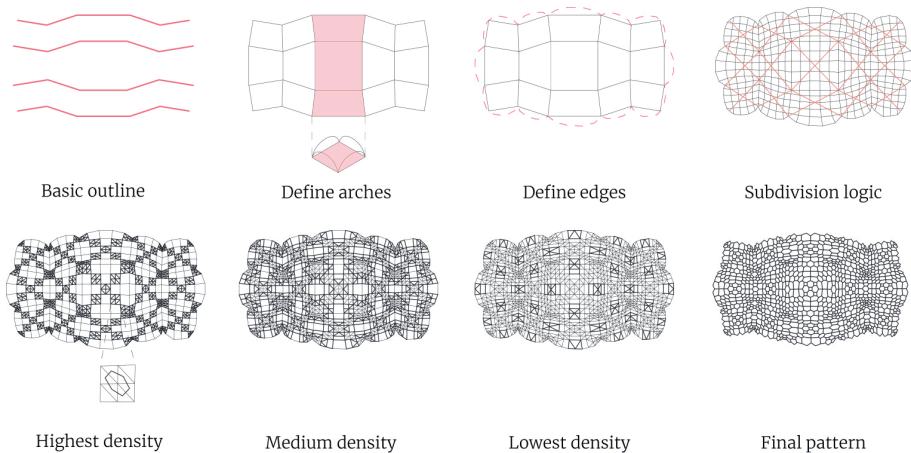


Figure 9. Mesh refinement for particle-springs simulation.

The starting mesh was further refined with the strut density being highest at the central axis and decreases in density away from this axis. The pattern is formed by connecting the centre of each mesh face, so a custom mesh was made to vary the pattern density. Using Weaverbird, a surface frame was made, which was

thickened and smoothed to create the final structure. We also chose a colour scheme that was relevant to the building context, given that it was a stay in place formwork that could be any colour.

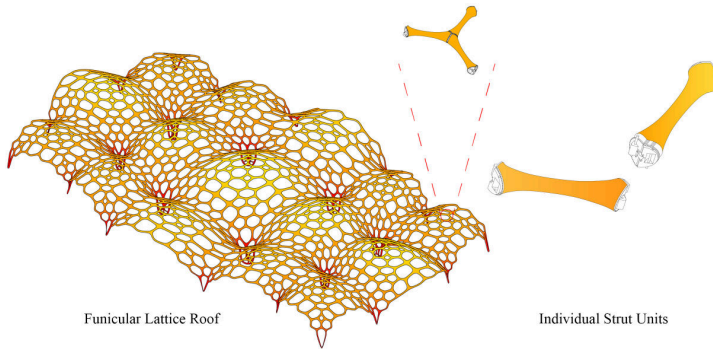


Figure 10. Proposed Lattice Roof Structure.

## 5. Discussion and Assessment

Our proposed fabrication system presents a method to create prefabricated strut elements with a single knitted fabric formwork on an adjustable tensioning jig. Thus, this has the advantage of making customisable strut members with a single bespoke fabric formwork. This also essentially breaks down the overall lattice structure into modular components that can be easily transported and assembled on-site.

The creation of individual strut components also overcomes the limitations of the knitting machine in terms of the maximum needle bed width of 1.5m. This potentially enables the creation of each member without the need for sewing to other pieces of fabric, especially when doing a large-scale single cast.

Additionally, our current research examines assessing our concrete struts quantitatively in terms of its structural performance. Using 4 point loading tests, we are examining the static and dynamic flexural stiffness of the tubular cast. These assessments look into the possibility of the outer textile contributing as a tensile component which works with the bonded concrete to improve its flexural properties. We hypothesize that the textile layer could also help in resisting the effects of creep since it is bonded with the concrete.

Another benefit is the haptic quality of the knitted fabric which alters the appearance of our concrete struts. The soft fabric contrasts with the hard appearance of bare-faced concrete and the fabric can be designed by altering the yarn colour and material. This provides an added layer of design over the aesthetics of the struts, which further enhances the spatial quality of the structure. However, an extra step of scrubbing off the concrete bits that bled out and hardened onto the surface was necessary to achieve a desirable finish.

## 6. Future Work

In summary, our proof-of-concept prototypes that present the possibility of creating new formal qualities and spatial configurations using fabric formwork. Our research proves, at a single strut scale that it is feasible to control the geometry of each strut and this therefore offers the potential to create relatively high fidelity physical models when compared to their digital counterparts. On a larger scale, these network lattice configurations show potential for making lightweight structural systems that could ease transportation and on-site assembly.

Future work would involve refining the connection details to accommodate non-planar strut arrangement as well as a higher valence. We also plan to test on 1:1 prototypes that assemble into overall funicular structural systems like arches or domes constructed out of multiple casted struts.

## References

- “Form Found Design” : no year given. Available from <<https://www.formfounddesign.com/fabric-forms>>.
- “KnitCandela - A flexibly formed thin concrete shell at MUAC, Mexico City, 2018” : no year given. Available from <<https://block.arch.ethz.ch/brg/project/knit-candela-muac-mexico-city>> (accessed 4 February 2020).
- Bechthold, M.: 2004, Surface Structures: digital design and fabrication, *ACADIA: Structures*.
- van Hennik, P.C. and Houtman, R. 2008, Textile Composites and Inflatable Structures II, in E. Oñate and B. Kröplin (eds.), *Pneumatic Formwork for Irregular Curved Thin Shells*, Springer, Dordrecht, 99-116.
- Lloret, E., Shahab, A.R., Linus, M., Flatt, R.J., Gramazio, F., Kohler, M. and Langenberg, S.: 2014, Complex concrete structures: Merging existing casting techniques with digital fabrication, *Computer-Aided Design*.
- Rippman, M. and Block, P.: 2013, Funicular Funnel Shells, *Design Modelling Symposium 2013*, Berlin.
- Tracy, K., Bell, B., Yogiama, C., Tessmer, L., McClellan, K., Vrana, A. and Verboon, E. 2014, Fabricate 2014, in F. Gramazio, M. Kohler and S. Langenberg (eds.), *Plastic-Cast Concrete: Fabrication as Applied Research*, UCL Press.
- Veenendaal, D. and Block, P.: 2014, Design process for prototype concrete shells using a hybrid cable-net and fabric formwork, *Engineering Structures*, **75**, 39-50.

# HYGRO-COMPLIANT: RESPONSIVE ARCHITECTURE WITH PASSIVELY ACTUATED COMPLIANT MECHANISMS

STELLA YI NING LOO<sup>1</sup>, DHILEEP KUMAR JAYASHANKAR<sup>2</sup>,  
SACHIN GUPTA<sup>3</sup> and KENNETH TRACY<sup>4</sup>  
<sup>1,2,3,4</sup>*Singapore University of Technology and Design*  
<sup>1</sup>*stella\_loo@mymail.sutd.edu.sg* <sup>2,4</sup>*{jayashankar|*  
*kenneth\_tracy}@sutd.edu.sg* <sup>3</sup>*sachin.sean.gupta@gmail.com*

**Abstract.** Research investigating water-driven passive actuation demonstrates the potential to transform how buildings interact with their environment while avoiding the complications of conventionally powered actuation. Previous experiments evidence the possibilities of bi-layer materials (Reichert, Menges, and Correa 2015; Correa et al. 2015) and mechanical assemblies with discretely connected actuating members (Gupta et al. 2019). By leveraging changes in weather to power actuated building components these projects explore the use of smart biomaterials and responsive building systems. Though promising the implementation of these technologies requires deep engagement into material synthesis and fabrication. This paper presents the design and prototyping of a rain responsive façade system using chitosan hygroscopic films as actuators counterbalanced by programmed compliant mechanisms. Building on previous work into chitosan film assemblies this research focuses on the development of compliant mechanisms as a means of controlling movement without over-complicated rotating parts.

**Keywords.** Passive Actuation; Responsive Architecture; Bio-polymers; 4D Structures; Compliant Mechanism.

## 1. Introduction

Previous research into passively actuated building systems has demonstrated the potential of responsive materials to transform how structures can interact with their environment. Integrating new material technologies into architectural assemblies is a profound challenge. The variation of the physicality of responsive structures brings forth considerations, complicating the structure and pulling it away from the industrial mantras of static inflexibility and mass standardization.

A previous study conducted on chitosan film-driven, rain actuated trusses found that large movements could be created within relatively little time (Gupta et al. 2019). Driven by the absorption, expansion, drying and shrinking properties of chitosan polymer films, the trusses could move through a 1-meter vertical range from dry-to-wet state in 5 minutes. To allow movement, 3D printed nodes were integrated into the carbon fiber structures. To further this work, the current

study replaces rotational hinges with compliant flexures which can be graded to create an enclosure surface. This change in approach allows for a single, additive manufacturing process to create a primary structure and hinging mechanism. By prototyping specially designed compliant mechanisms, the range of movement between and within each element in a hygro-compliant panel can be ascertained. This involved fabricating 1:1 prototypes of compliant flexures in a range of scales, from a single flexure to larger systems of compliance. Once the range of movement is determined that information can be used to grade the movement of panels to match a designed curvature.

Prototypes of discrete working hygro-compliant panels act as design constraint and guideline for the design of a tessellated, open-air façade system. The research identified wind-driven rain as a target area for application, with the responsive façade able to self-regulate between varying wet or dry weather situations experienced by a structure. The intention in this case was to render a scenario that could both imply the potential for use and articulate the aesthetic potential of the system. An exploration featured in the research shows the array of modular hygro-compliant panels making up the external surface of an outdoor pavilion, each of which enabled to react independently to its immediate environmental condition to provide a self-regulated, enclosed activity space. Along with the physical prototyping, the design gives a hint of the novel physicality and spatial potential of responsive systems.

## 2. Research Methodology

### 2.1. CHITOSAN BIOPOLYMER-ACTUATION MECHANISM

Chitosan is a deacylated form of chitin. Chitin, is a polysaccharide found in many living organisms such as crustacean exoskeleton, insect cuticles, surfaces of living organisms, etc. (Fernandez & Ingber, 2012). Chitosan is highly hygroscopic in nature and it can be converted into many physical forms such as nanoparticles, fibers, hydrogel, microsphere, etc. and so it is widely used in many such applications including food, agriculture, engineering, and medical. More recently, chitosan has also been utilized in the field additive manufacturing; to build a large-scale artifact (Sanandiya, Vijay, Dimopoulou, Dritsas, & Fernandez, 2018). This highlights that the material properties of chitosan could be tuned and used for any specific applications.



Figure 1. A simple schematic transformation of raw chitosan into thin films.

In this paper, the overall idea is to utilize chitosan's Hygroscopic swelling and use it as medium of transformation by incorporating in the architectural structures.

In a previous study (Gupta et al., 2019), chitosan was characterized and made into thin film with cotton fiber reinforcement as shown in Figure 1. The characterized chitosan films were then attached onto a truss system and tested in ideal condition to prove the applicability of the material in built structures. Results of the previous experiments demonstrated the shape change of the structure at considerable range of motion with respect to changing environmental conditions. It also proved that chitosan films have the ability to bear structural load with a tensile strength of up to 60 MPa and to use it in sustainable built environment (Jayashankar, Gupta, Sanandiya, Fernandez, & Tracy, 2019). As these experiments improved the confidence level of use of chitosan, a further study was conducted with 3D printed basic compliant mechanism structures (Jayashankar, Gupta, Loo, & Tracy, 2019), where the chitosan films had notably expanded up to 12.8% to its original length from dry to wet state and the actuation time was recorded to be less than 12 minutes. With these available data's, current research focusses on using chitosan films in the small-scale prototype: Hygro-Compliant Panel, with controlled actuation of movement and tested in an open space environment to get a complete insight of the working system.

2.2. COMPLIANT MECHANISM & GEOMETRICAL DESIGN EXPLORATION OF DIFFERENT COMPLIANT FLEXURES

Compliant mechanisms are modern design engineered mechanisms created by leveraging the materials properties to gain motion by the deflections of elastic member in order to avoid the rotating parts, and to replace the traditional hinges or revolute joints especially in machines and architectural structures. Compliant mechanisms are compact, friction & wear free with integrated functions and possess high reliability which could be adapted in any field to achieve a desirable controlled motion (Howell, 2001). However, it also comes with certain challenges such as limited rotation, dependency in materials properties and difficulty in design (Megaro et al., 2017). With these challenges, designing for controlled path or motion requires deep understanding and requires precise predictions of finite deformations. In this paper, we explored different compliant flexure designs and its potential to find its range of motion with varied material combinations to develop a small-scale prototype: Hygro-Compliant Panel.

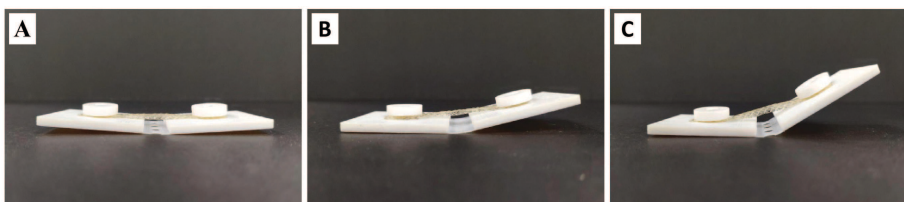


Figure 2. Preliminary tests of 3D printed compliant design (A) Sample assembled with wet chitosan films at flat condition (B) Sample starts to transform from wet state to dry state (C) Final dry state condition.

A preliminary sample had been designed and 3D printed following the

principles of compliant mechanism from the literature study (Howell, 2001). The sample was designed with two structural members connected by thin-walled compliance body with circular holes in order to reduce the stress involved and to improve the flexural stability. Wet chitosan films were then attached to the sample in flat position ideally at wet condition and the films transformation was recorded. Figure 2 shows the actuation of the assembly from wet to dry state. Furthermore, other flexural designs such as flexure from contour geometry, spring flexures, induced bending flexures were explored in the preliminary studies.

### 2.2.1. Flexures from contour geometry

To evaluate the rigidity and durability of the connection between continuous elements, a simple flexure with contoured geometry has been designed and tested. It is essential for the designed structure to withstand cyclic loading (stress, strains, forces, tensions, etc.) conditions at both wet and dry state. It can be noted from Figure 3(A), that simple flexures had a distinct point of weakness at various levels which should be avoided to improve the life of the compliant. The design: Single element model consists of continuous members of contour shaped compliant pivot geometries can be tuned to attain a wide variability of stiffness based on the desired requirements. The baseline configuration of the contoured surface should provide better manufacturability with increased controlling flexibility in a single direction array. Figure 3 (B-D) shows the assembly and actuation of single element model. In this model, the chitosan film was attached as a single membrane connecting the entire structure using the tapered 3D printed snap-fit fasteners. This model confirmed the actual range of motion from wet state to dry state by the contraction of chitosan film as per the design.

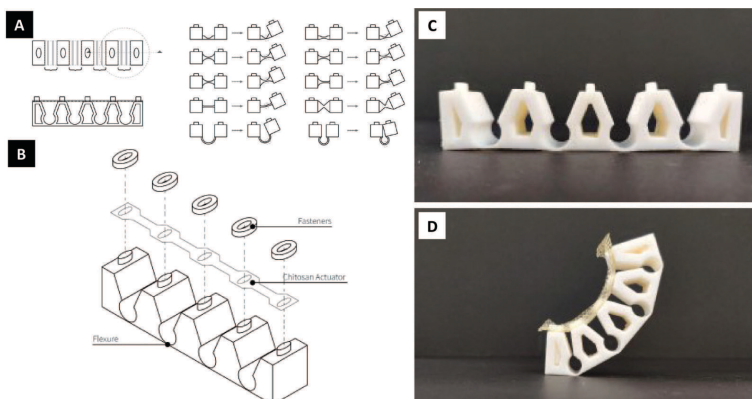


Figure 3. Design of Single element model (A) Contour geometry flexures and their start/end states (B) Assembly design (C) On a 3D printed truss system (D) Chitosan was assembled in wet state and allowed to dry with one end fixed to the floor.

2.2.2. Springy Flexures

In this phase, springy flexure derivatives were designed, 3D printed and tested. These ‘springy’ flexure designs comply with the principle of spring mass damping system which would allow elastic deformation even in a rigid structure. However, in this case, the flexures were designed to act up on in response to vertical oscillating force. (Calculations see: Jayashankar, Gupta, Loo, et al., 2019). Figure 4(A) shows the different flexure designs and range of movement and Figure 4(B) shows the bend angles and pre-bending in compliant flexures.

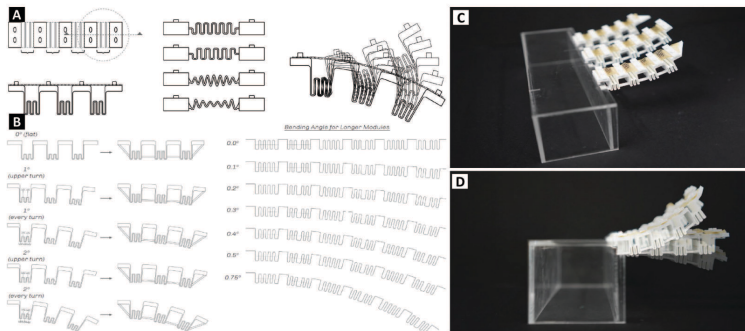


Figure 4. Feluxue design and testing (A) Springy flexure derivatives (B) Bend angles and pre-bending in compliant flexures; Testing of chosen compliant flexure (C) Isometric view of 3D printed flexure (D) Front view of the flexure during shape change.

At last, based on the observations from fundamental tests and previous studies, the models were 3D Printed in a pre-bent position (bending-induced) which would enable the chitosan film in tensions at wet condition and constantly pulling it into a taut position. This induced bending also allows us to ‘control the range of movement’ in the single compliant joint. As the mechanism itself possess energy due to induced bending, when the film gets wet, the actuation becomes expeditious. Figure 4(C) shows the isometric view of 3D printed compliant design flexures with chitosan films. A set of three individual members were 3D printed with the chosen design and tested for its compliance. Figure 4(D) shows front overlay view of three single member at dry and wet state. Finally, from all the primitive tests, the finest springy flexure design and its pattern has been adopted for prototyping the Hygro-Compliant panel.

2.2.3. Design Construction: A prototype of Hygro-Compliant Panel

The construction of a prototype is based on application-oriented design that would perform like an environmental smart-louvre. The individual compliant members are combined and designed as an elliptical flutter with fully covered layer of chitosan film to conceive movements in response to changing environmental conditions. The design consists of seven separable compliant members aligned in a series of array connected with chitosan films. In dry state, the compliant panel will appear like a horizontal slat and at wet state it will look like an angled louvre.



Figure 5(A) shows isometric & cross section of the panel at different states: wet state, intermediate state and dry state. The actuation (or movement of the entire structure) of hygro-compliant panel depends on the thermal and humid conditions, as if the environmental condition changes it allows the chitosan films to absorb or loose moisture from space. This phenomenon is also called hygroscopic swelling, which leads to an increase in length of the chitosan film. In addition to swelling, the strain energy stored in the complaint joint in the form of flexural bending and internal stress caused by pulling force (Gupta et al., 2019) gets mitigated and speeds up the transformation.

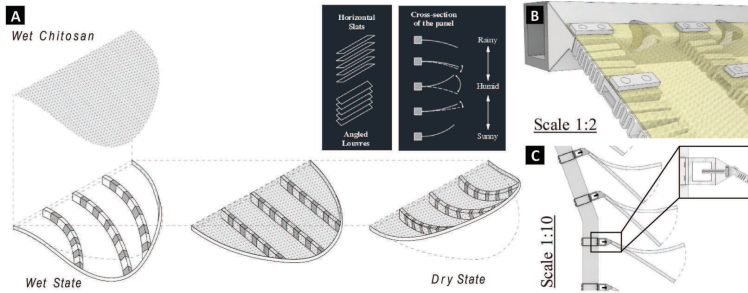


Figure 5. Schematic of panel design (A) Hygro-Compliant design (B) Chitosan film connection details (C) A set of aligned panels at 1:10 scale & panel joint connection.

The experiments in the above sections are at small-scale level when comparing to the real-world architectural facades. In a large-scale scenario, these hygro-compliant panels should be used in huge quantities in an enormous architecture and one design hypothesis is, will all compliant panels undergo transformation at the same time or not? Figure 5(B & C) shows the 3D design of compliant panel and its connections.

### 2.3. WIND-DRIVEN RAIN

Wind-driven rain is a condition whereby the path of falling rain is altered due to prevailing winds. In some cases when the wind is strong enough, rain falls at an angle larger than expected (at times almost parallel to the ground). Wind-driven rain becomes a significant issue not just to the durability of building facades (Foroushani et al., 2013), even challenging the ability of sheltered spaces to fulfill their purpose of providing *shelter*. Following this line of thought, the research simplified the problem to focus on creating a facade that would provide an ideal spatial condition regardless of the weather condition beyond its walls. A completely enclosed room would have to rely on other methods of cooling and ventilation. Common practice would see the insertion of louver systems or building overhangs, but this does not always create a balance between natural lighting, ventilation and wet weather protection (Figure 6).

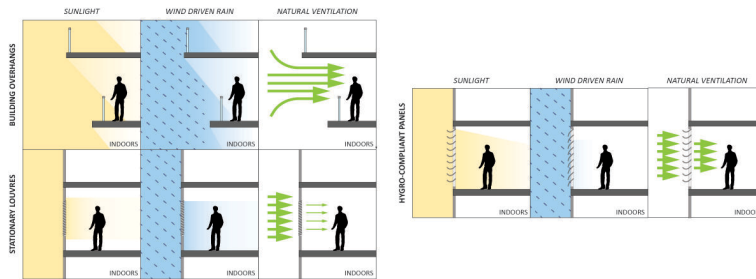


Figure 6. Diagrammatic comparison of using stationary overhangs and louvers vs. proposed responsive hygro-compliant panel system as strategies to combat Wind Driven Rains.

### 3. Fabrication & Testing

For fabrication the Prototype, the models were designed in Rhinoceros software and digitally manufactured using two different 3D printers (Stratysys fortus 450-mc & PolyJet J-750). From preliminary tests till the final prototype, we explored two different 3D printing technologies and two different materials: former being FDM-Fused Deposition Modelling and Polyjet; and latter being ASA-Acrylonitrile Styrene Acrylate and ABS-Acrylonitrile Butadiene Styrene. Initial samples were printed in both ABS & ASA and we noticed that the level of compliance in ASA is better than ABS because of its material and the technique of how it's produced. Even though, there is very little difference in strength between ABS & ASA, FDM produces the part with amplified ductility whereas Polyjet produces the part with increased brittleness which is the root cause for the complaint failure without any tests. Henceforth, the entire model were printed in ASA material with FDM technique and chitosan films were assembled at wet state. Figure 6 (A) shows the panel printed with FDM technique and films assembled.

Testings of the panel was done in a realistic environmental surroundings, an open space ideal location was chosen considering wind and weather to make sure there is no obstruction or other form of interactions with the prototype. The test begins by supplying water (assuming rain shower) and the actuation/shape change of the panel was initiated by the deposition of water particles on top of the chitosan films by a constant spraying of water for 30 minutes. The 30 mins time was identified from our previous studies and testing for the films to completely saturated (Jayashankar, Gupta, Loo, et al., 2019). However, the transformation was noticed after 4 minutes of continuous water spraying, but somehow the entire panel got saturated in less than 5 minutes. Followed by wetting cycle, drying cycle was carried out for next 30 mins. During drying, the films started to contract by curling upwards as the films get dehydrated and with the effect of pulling force induced in the films. The responses were documented through videography and the images were processed to obtain the percentage of shape change and compared with the actual design. Figure 7(B-E) shows the testing of hygro-compliant pane at different state.

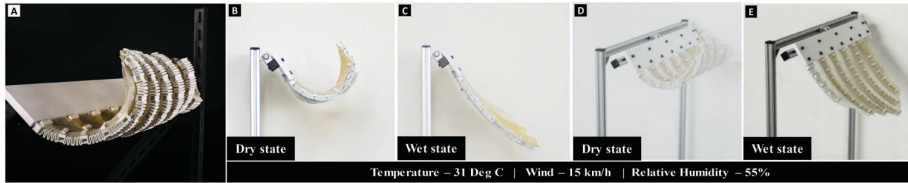


Figure 7. Hygro-compliant panel (A) 3D printed assembly with chitosan films (B) Front view at dry state (C) Front view at wet state (D) Isometric view at dry state (E) Isometric view at wet state.

#### 4. Results & Discussion

The hygro-compliant panel had performed well and indicated an acceptable level of transformation as expected. Three crucial parameters were observed from the test: (i) shape change; (ii) actuation time; and (iii) range of motion. Figure 8 shows the processed image of hygro-compliant panel.

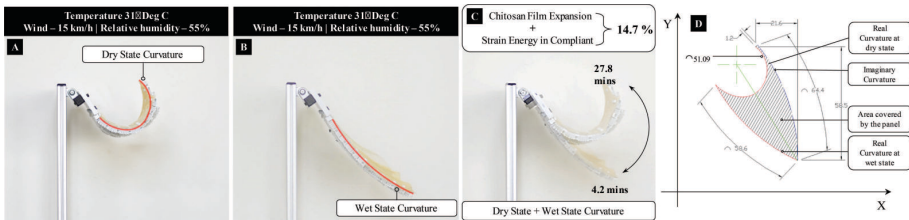


Figure 8. Hygro-Compliant panel (A) Dry state curvature (B) Wet state curvature (C) Overlay of dry & wet state curvature (D) Range of motion plot.

(i) Shape Change: The dynamic shape change of the panel was triggered by the chitosan film through absorption of water molecules which caused the panel to transform from dry state to wet state. The comprehensive expansion gained by the compliant panel was considerably higher than the previously reported studies [Gupta & Jayashankar]. The expansion went up to 14.7% as opposed to only 12.8% in previous studies, this increment should be from both chitosan film and the strain energy stored in the compliant due to induced bending. Hence, approximately 2% of expansion could be accounted by compliant joint but however, this should be confirmed by doing more number of cycles.

(ii) Actuation Time: Actuation time is the time taken by the panel to transform from dry state to wet state. From Figure 8(C), it took 4.2 mins for the films to get completely saturated whereas it took 27.8 mins to go back to dry state which is legitimate when comparing to the previous experiments.

(iii) Range of Motion: The range of motion is the area covered by the panel from dry state to wet state. As seen from the Figure 8(D), the plot shows the length of the arc, at dry state its 51.09 mm and at wet state its 58.6 mm. An imaginary border was plotted to discover the coverage area by the panel when travelled from dry to wet state. The approximate area was found to be 867.05 mm<sup>2</sup>

considering the curve shift error of 1.2 mm as the dry state curvature is typically a group of curves and needs advanced data interpretation for precise calculations. This coverage area or range of motion is particularly useful when designing for specific applications or aspect to consider for wind-driven rain especially if the rain at different angles.

**5. Architectural Scenario**

Architectural elements from the details researched above formed an overall visualization to address the scenario of a partially exposed outdoor pavilion in a rainy, equatorial city; leveraging the experiential potential of adaptive building skins. Massings were developed to mediate air flow, rain shedding and series of more or less exposed programmatic spaces (Figure 9). The hygro-compliant pavilion was designed to formally embody an urban park program navigating the constraints of the site and program while augmenting the performative, embodied experience of the proposals moving skin (Figure 10).

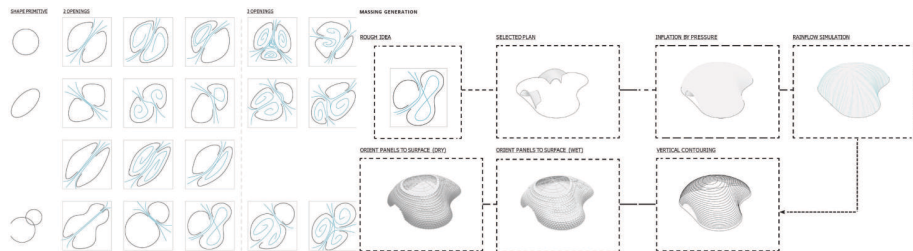


Figure 9. Massing studies.

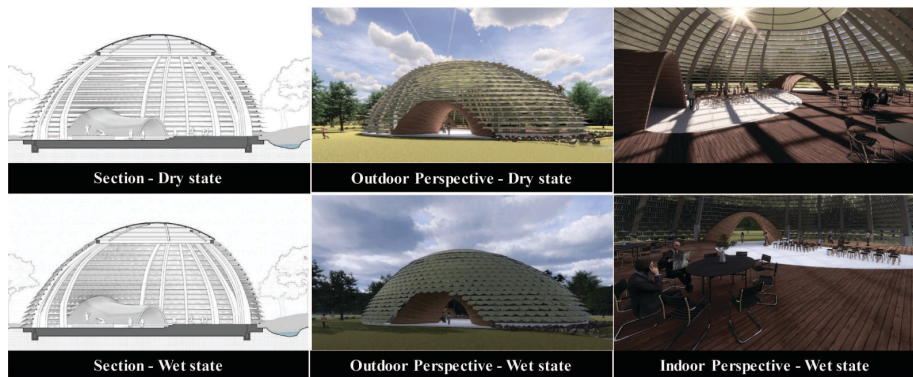


Figure 10. Hygro-Compliant pavilion (left to right- Section, outdoor & indoor perspective).

**6. Conclusion**

In this paper, an experimental analysis was carried to design and test a small-scale passive-complaint structures by leveraging the materials properties of chitosan

biopolymer and with basic compliant mechanism theories achieved through additive manufacturing technique. The experiment was successful and the most important parameters such as shape change, actuation time, and range of motion were evaluated. These results provided us with a greater insight on the working principle of compliant system and how these responsive architectures could be deployed in real time applications was portrayed using sample design: Hygro-Compliant pavilion.

To tackle the issue of making responsive architecture more sustainable, this paper touches on the topics of sustainable new materials, compliant movement mechanisms, and modern fabrication techniques. Amongst other hygroscopic materials, chitosan biopolymer stands out with faster actuation, ability to bear loads: more than 300 times its self-weight and its naturally biodegradable property. Instead of relying on conventional mechanical systems, the use of compliant mechanisms helps creating more robust movement similar to those in nature. The bending-active forms is a minor explored area of 'repeated shape forming' which could be used to design a fixed but responsive structure, that do not require re-programming for function - controlled sequential shape recovery.

## References

- Correa, D., Papadopoulou, A., Guberan, C., Jhaveri, N., Reichert, S., Menges, A. and Tibbits, S.: 2015, 3D-Printed Wood: Programming Hygroscopic Material Transformations, *3D Printing and Additive Manufacturing*, **2**(3), 106-116.
- Fernandez, J.G. and Ingber, D.E.: 2012, Unexpected Strength and Toughness in Chitosan-Fibroin Laminates Inspired by Insect Cuticle, *Advanced Materials*, **24**(4), 480-484.
- Foroushani, S.S.M., Hua, G. and Naylor, D.: 2013, Effects of Overhangs on the Wind-Driven Rain Wetting of a Low-Rise Building, *Proceedings of ASHRAE 2013*.
- Gupta, S.S., Jayashankar, D.K., D Sanandiya, N., G Fernandez, J. and Tracy, K.: 2019, Prototyping of chitosan-based shape-changing structures, *Proceedings of the 24th International Conference of the Association for Computer-Aided Architectural Design Research in Asia (CAADRIA)*, 441-450.
- Howell, L.L.: 2001, *Compliant mechanisms*, Wiley, New York.
- Jayashankar, D.K., Gupta, S.S., Loo, Y.N.S. and Tracy, K.: 2019, 3D Printing of Compliant Passively Actuated 4D Structures, *Proceedings of the 30th Annual International Solid Freeform Fabrication Symposiumth Annual International Solid Freeform Fabrication Symposium*.
- Jayashankar, D.K., Gupta, S.S., Sanandiya, N.D., Fernandez, J.G. and Tracy, K.: 2019, Fiber Reinforced Composite Manufacturing for Passive Actuators, *40th MATADOR International Conference on Advanced Manufacturing and Design*, 191.
- Megaro, V., Zehnder, J., B"acher, M., Coros, S., Gross, M. and Thomaszewski, B.: 2017, A computational design tool for compliant mechanisms, *ACM Transactions on Graphics*, **36**(4), 12.
- Reichert, S., Menges, A. and Correa, D.: 2015, Meteorosensitive architecture: Biomimetic building skins based on materially embedded and hygroscopically enabled responsiveness, *Computer-Aided Design*, **60**, 50-69.
- Sanandiya, N.D., Vijay, Y., Dimopoulou, M., Dritsas, S. and Fernandez, J.G.: 2018, Large-scale additive manufacturing with bioinspired cellulosic materials, *Scientific Reports*, **8**(1), 8642.

# CIRCULAR CONCRETE CONSTRUCTION THROUGH ADDITIVE FDM FORMWORK

ROBERTO NABONI<sup>1</sup> and GIULIO PAPARELLA<sup>2</sup>

<sup>1</sup>*CREATE, University of Southern Denmark (SDU) - Unit of Civil and Architectural Engineering*

<sup>1</sup>*ron@iti.sdu.dk*

<sup>2</sup>*Sapienza University of Rome - Department of Civil, Constructional and Environmental Engineering (DICEA)*

<sup>2</sup>*giulio.paparella@uniroma1.it*

**Abstract.** One of the major downsides of concrete construction is the difficulty to be adapted, modified and deconstructed. In this work, we look at the potential enabled by the use of Additive Formwork based on Fused Deposition Modelling, in order to design and manufacture structural elements which can be assembled and disassembled easily. We call this new typology of structures Circular Concrete Construction. The paper illustrates an integrated computational workflow, which encompasses design and fabrication. Technological aspects of the 3D printed formwork and its application in reversible node and strut connections are described, with reference to the material and structural aspects, as well as prototyping experiments. The work is a proof of concept that opens perspectives for a new type of reversible concrete construction.

**Keywords.** Circular Concrete Construction; Additive Formwork; Additive Manufacturing; Digital Fabrication.

## 1. Introduction

Concrete is the most used material in the world after water (Wangler et al. 2016) and by far the most used material in buildings. Concrete has good mechanical properties, is economically convenient and available in almost every country. It can be employed for a large variety of applications, across several scales, because of its capacity to adapt to any shape. Despite this intrinsic property, concrete construction is mostly limited by extrinsic factors, i.e. the employed formwork typology. Most constructions rely on reusable timber or metal formwork, to produce standard orthogonal building elements. Deviations from orthogonality in the design of concrete architecture, which is often the result of form and structural optimization, or the demand for advanced detailing are exceptions that require sophisticated approaches. The production of complex formwork is, in fact, impacting heavily on the overall construction cost (De Soto et al. 2018), and therefore largely avoided.

Advancements in digital fabrication have made it possible to develop approaches to the problem of complex concrete construction, by utilizing

subtractive techniques at a larger scale with the use of industrial robots. These approaches include the time-efficient but low-detail cut of foam blocks with a hot-wire or a hot blade (Søndergaard 2014; Søndergaard et al. 2016; 3XN et al. 2016; Brander et al. 2016), and the high-resolution but time-consuming process of milling.

In parallel to increasing ecological awareness, a recent wave of research has focused on the implementation of Additive Manufacturing (AM) to challenge the existing standards in complex formwork manufacturing. Potential advantages are in the near-zero material waste and the high level of geometric freedom (Aghaei-Meibodi et al. 2017). Moreover, AM allows for the easy integration of different functionalities within the formwork (Jipa et al. 2018). Fused Deposition Modelling (FDM) in particular offers specific advantages for construction applications, such as relatively high-resistance materials, the possibility for reuse and recycling of most plastics used for moulding, and a convenient ratio between precision and production time (Naboni and Breseghello 2018). To date, several projects have investigated FDM formwork for concrete, from early experiments (Peters 2014) to various applied work at Digital Building Technologies group at ETH Zurich (Jipa et al. 2017, Leshok and Dillenburger 2019), and at the CREATE group at the University of Southern Denmark (Naboni and Breseghello 2019), where new applications and levels of performance are targeted.

### 1.1. CIRCULAR CONSTRUCTION

The increased possibilities offered by FDM in forming concrete elements allow conceiving novel tectonic explorations. In this work specifically, we focus on one of the major limitations of conventional concrete buildings: the difficulty of modification and disassembly - which often leave no alternatives to demolition of buildings (Salama 2017). We introduce here the concept of Circular Concrete Construction (CCC), an approach to reversible and reusable structures which can be updated easily in time without waste generation. To achieve this, we propose an approach where the use of advanced FDM formwork is tested for the formation of reversible three-dimensional structures, made of dry-assembled struts and node joints. Specifically, we aim at proving the feasibility of using FDM to manufacture economically viable, intricate mould geometry, with sub-millimetre accuracy. In our approach, high precision moulds can be designed and produced with an automated design and fabrication process, including the detailing essential to embedding reversible features.

## 2. Methodology

This work involves various methods and a number of empirical experiments: it is introduced a specific material system for the formwork and the reversible node connections (i); this is initially tested and refined with a preliminary experiment (ii); subsequently, it is presented a computational workflow which automates the design and fabrication of complex concrete nodes (iii); lastly, is described a prototyping experiment in scale 1:1 which collects the previous methodological approaches into a physical artefact (iiii). The observations on this final experiment

include a functional test of reversibility, the fabrication ease and accuracy through 3D scanning, and an overall quality description for future implementations in constructions.

## 2.1. MATERIAL SYSTEM FOR REVERSIBLE CONNECTIONS

This work is fundamentally based on the possibility of producing complex concrete elements through the use of FDM-based moulds, which can be reused multiple times. The moulds are produced with commercial machinery using thermoplastic materials that can easily withstand the hydrostatic pressure of concrete for objects up to 500 mm in height. In this experiment, we employ PLA filament because of the high geometric stability during the printing process, and its strength which allows for a reduced amount of material. The mould parts are printed separately and joined together prior to the casting. The FDM mould is instrumental to the functional combination of the two actual construction materials: concrete and steel.

The utilized concrete is a high-resistance mix fluid enough to fit into thin complex elements. After several tests, a specific type of Ultra-High-Performance Fiber Reinforced Concrete (UHPRFC) was selected. The compound is a dry mortar based on a portland/micro silica cement, mixed with fine sand aggregates (less than 3 mm in diameter), and with the addition of short steel fibres (length 12 mm, diameter 0,4 mm). This material is characterized by compressive strength of 150 MPa, and 70-90 MPa achieved after curing for 24 hours (Hi-Con 2017). The steel fibres add strength, make the material ductile to prevent cracking and provide an effective anchorage to threaded reinforcing bars, which are used to ensure the reversibility connections between various parts while serving as rebar element.

## 2.2. PRELIMINARY EXPERIMENT

An initial experiment was developed to understand the material behaviour for the case of a four-directions node with a 34 mm diameter. The aim was to evaluate the optimal quantity of steel fibres in the UHPRFC when casting extremely narrow geometries. A formwork consisting of several parts was utilized: the external shell was subdivided into two parts, printed with a 1,4 mm wall thickness. External caps were printed for each axis, in order to confine the concrete poured into the formwork, and guarantee the precise embedding of steel nuts and threaded bars. The PLA node weighs about 800 grams and was printed in about 3,5 hours. This experiment was iterated with various quantities of steel fibres, which indicated an ideal ratio between the binder, steel fibres, water of 1/0,085/0,085 kg. With this proportion, the node was produced and easily connected to strut elements which were fabricated in a similar manner. Minor imprecisions were found in relation to the concrete shrinkage during the curing process, mostly at the interface zones among various parts (Fig.1).



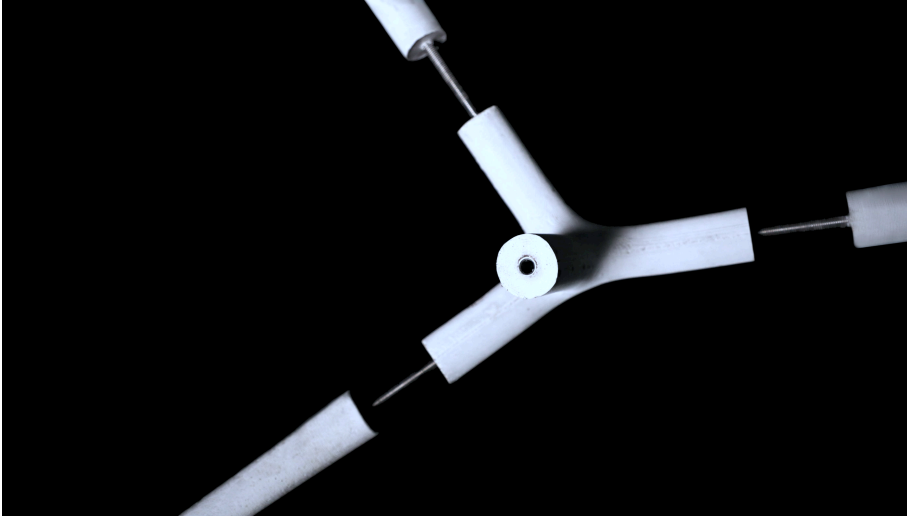


Figure 1. Preliminary experiment on node-strut reversible assembly.

### 2.3. INTEGRATED WORKFLOW FOR DESIGN AND FABRICATION

In order to streamline the process from design to production of the reversible concrete elements, it is developed a computational workflow which allows the automated preparation of moulding parts for nodes of any topology and complexity. In the first phase, a preliminary dimensioning of the structural elements is provided, taking into account a given geometry composed of simple intersecting segments which represent the axis of a joint connection, punctual loads applied in compression/tension, and the specific properties of the adopted structural material. With this data, a moment-resistant joint geometry is generated, with pre-dimensioned struts sections, which also takes into account the self-weight of each element.

In the second phase, the actual node design is generated utilizing tools for volumetric modelling to wrap a continuous node geometry with the determined sections and control various shape parameters. Subsequently, a refinement into a quadrilateral mesh is executed to obtain a mesh topology coherent with the overall node topology. The geometry is afterwards discretized parametrically.

The third workflow cluster focuses on the mould design for fabrication with 3D printing. An exact number of mould parts is here determined in coherence with the node topology, to allow an easy assembly and disassembly. The mould is oriented for the concrete casting process, and a supporting geometry is generated accordingly. Additional details are added to facilitate the referencing of the mould parts. An auxiliary positioner is also generated to hold the threaded rods in the correct position, both within the mould and to ensure accurate and easy welding of the steel elements. In this last phase, the G-codes for 3D printing are automatically generated taking into account the orientation of the parts for an optimal printing process (Fig.2).

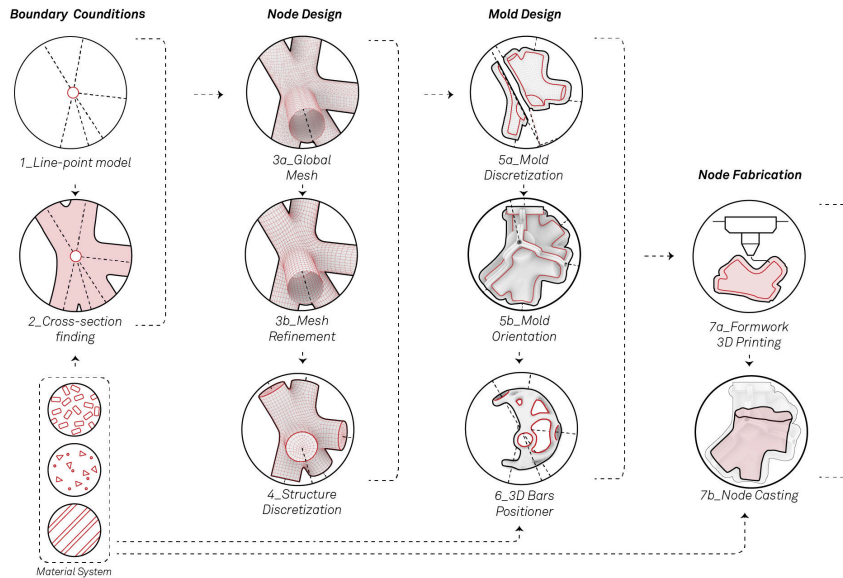


Figure 2. The scheme shows an overall design-to-fabrication workflow that has been implemented in this research.

## 2.4. PROTOTYPING EXPERIMENT

The above-described workflow is utilized for the design and manufacturing of an actual UHPFRC node for a lightweight concrete structure, prototyped in scale 1:1. The aim is testing the workflow, run assembly-disassembly tests in order to verify the initial hypothesis, and assessing the production accuracy. The node is a 6-axis connection, each with a diameter of 100 mm (Fig.3).

The overall node geometry is inscribed in a bounding box of approximately 350 mm by 300 mm by 300 mm for a total weight of 16,8 kg. Its formwork is characterized by a 5-piece moulding with a shell thickness of 4,9 mm. These parts have a 35 mm wide contact surface kept together by bolted connections.

Within the formwork, a welded piece with six threaded M8 struts is placed into position - this is previously welded with the use of a 3D printed positioner (Fig.4a). Threaded bars are connected to long nuts which will allow external parts to be connected afterwards.

The fabrication of the node required 2,2 kg of PLA and a printing time of 36 hours in total, using a nozzle diameter of 0,7 mm and a layer resolution of 0,2 mm (Fig.4b). The concrete mix was applied after a layer of releasing agent and exposed for a couple of minutes on a vibration table. After 48 hours, the mould parts are easily removed and cleaned for reuse - a total of three times in this experiment, without an observable reduction in functionality.

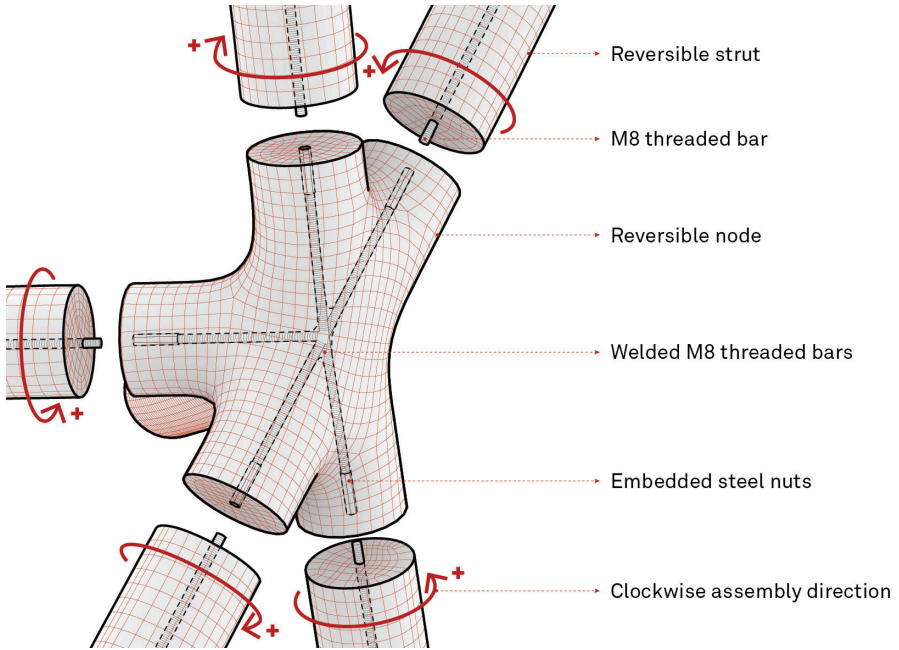


Figure 3. Schematic representation of a node-strut connection.

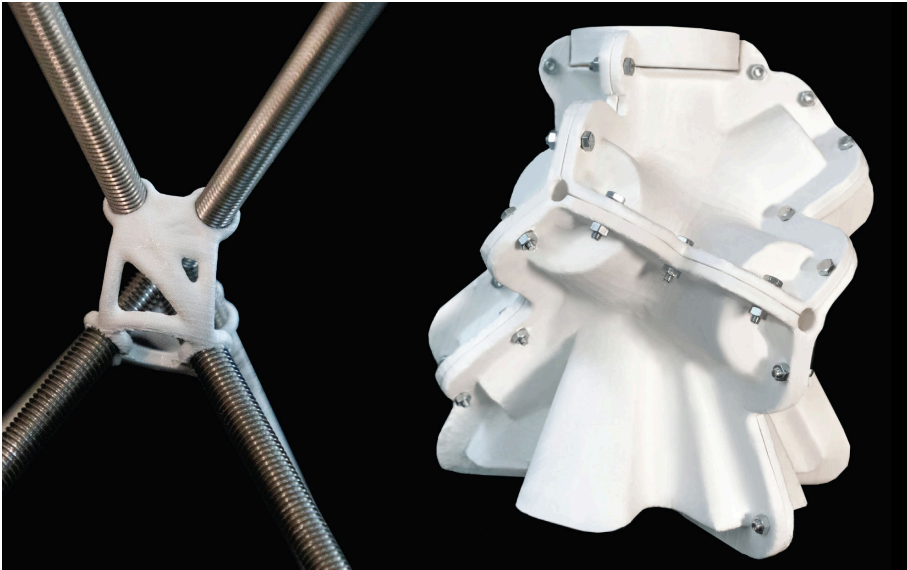


Figure 4. a) 3D printed fixture for an accurate welding process of the threaded rods which are placed within the node; b) 3D printed mould for a 6-axis node consisting of five assembled sub-parts which assure ease in demoulding process.

### 3. Results & Discussion

The experiment was successfully implementing a functional real scale prototype where the struts can be easily assembled and disassembled without the aid of complex machinery (Fig.5).

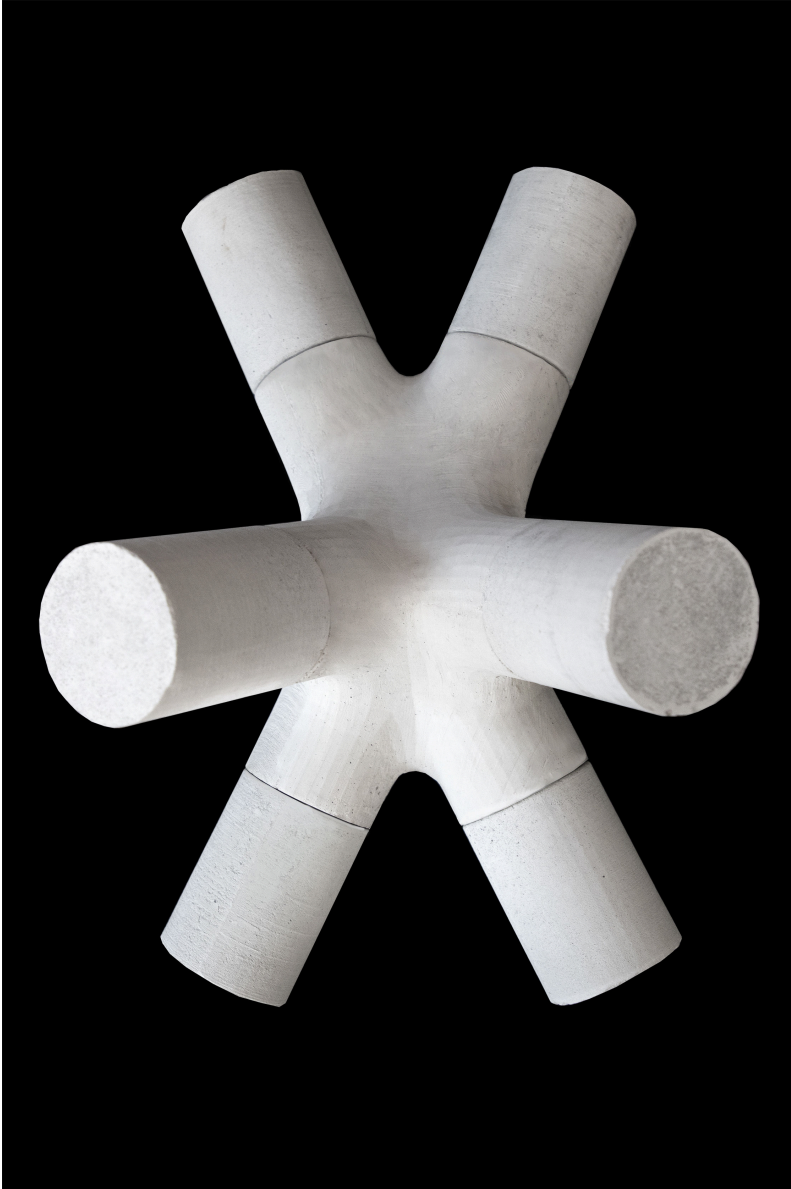


Figure 5. An assembly of a 6-axis node and the complementary struts.

In order to assess the precision of the prototyped node, we utilized an industrial metrology 3D scanner, from which we obtained a high-resolution point cloud. In the first analysis, we have compared the obtained point cloud data with the original geometry. This representation allows us to observe fine defects emerging from the fabrication process, such as the seams among assembled mould sub-parts, and local defects due to the evacuation of air embedded in the concrete mix, trapped within the non-transparent mould - which accumulates on the top surfaces of the volume (Fig.6a). An observation of the mesh model favours an intuitive understanding of the differential displacements within the node shape (Fig.6b). The areas with larger deviations from the original (max 6,7 mm) are localized in the top areas with horizontal orientation, due to volume reduction of concrete, as the air loss occurs during the curing period. 88,5% of the points are included in the deviation range of  $\pm 1$  mm.

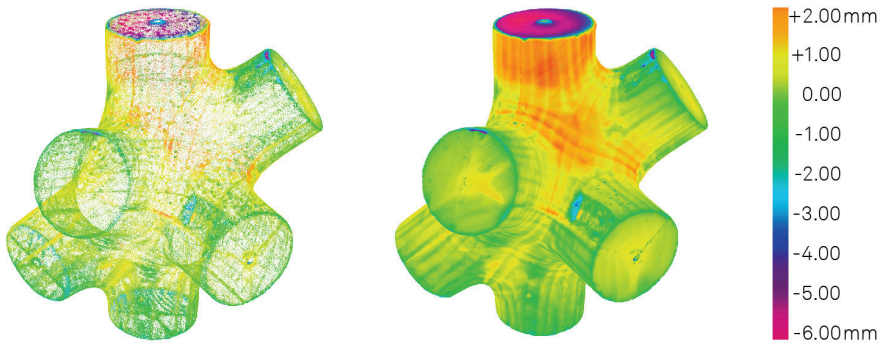


Figure 6. Points deviation analysis from the digital model to the 3D scanned one: a) points visualisation; b) mesh visualisation.

Furthermore, with an aim to provide the basis for a mechanical assessment of the node, one of the prototypes was oriented in the casting position and cut with a vertical plane, in order to investigate the internal organization of the steel fibres. We could observe an uneven distribution, with most of the fibres accumulated at the bottom areas of the geometry, in respect to the orientation adopted during the concrete pouring. This phenomenon requires further investigation in relation to the pouring process (Fig.7).



Figure 7. Analysis of the steel fibres distribution occurring through a vertical section of the node.

#### 4. Conclusions

This paper introduces and proves the feasibility of a novel approach to reversible concrete construction, enabled by the use of additive FDM formwork. The complexity enabled by this approach allows adding innovative formwork features, such as the use of advanced detailing for reversible connections. In parallel to the tectonic and manufacturing investigation, it is adopted a computational workflow for an easy and straightforward mould production starting from a simple line model, which can be easily utilized by non-expert designers. Next developments will look at controlling the reduction in the volume of concrete, and the fibre distribution in the volume, to ensure a superior production and mechanical quality. Future work will be directed at the implementation of such a system for large reversible concrete structures, segmented in modular components, whose formworks can be reused several times. Interesting perspective applications are in the field of temporary construction with considerable structural performances and in lightweight concrete structures which are designed to work mainly in compression.

#### Acknowledgements

This work was carried out at the CREATE Lab, a research infrastructure for digital fabrication at the University of Southern Denmark - Unit of Civil and Architectural Engineering, in cooperation with WASP Hub Denmark. The authors wish to thank

Hi-Con for in-kind support of concrete material, FILOALFA for in-kind support of 3D printing material. 3D Scanning of concrete elements was carried out at the SDU Prototyping Lab - Prof. Knud Bjørnholt.

## References

- “Hi-Con - CRC JointCast–Handling instructions UHPFRC” : 2017. Available from <<https://www.hi-con.com/concrete-blog/crc-jointcast-joints-that-are-small-strong-and-simple-1>>.
- Aghaei-Meibodi, M., Bernhard, M., Jipa, A. and Dillenburger, B. 2017, The smart takes from the strong., in A.E.A. Menges (ed.), *Fabricate*, UCL Press, 210-217.
- 3XN Architects, E.A.: 2016, *Bladerunner, 1st Edition*, KLS PurePrint, Denmark.
- Brander, D., Bærentzen, J.A., Clausen, K., Fisker, A.S., Gravesen, J., Lund, M.N., Nørbjerg, T.B., Steenstrup, K.H. and Søndergaard, A. 2016, Designing for hot-blade cutting: Geometric Approaches for High-Speed Manufacturing of Doubly-Curved Architectural Surfaces, in S.E.A. Adriaenssens (ed.), *Advances in Architectural Geometry 2016*, vdf Hochschulverlag AG an der ETH Zürich, Switzerland, 306-327.
- Jipa, A., Bernhard, M., Dillenburger, B., Ruffray, N., Wangler, T. and Flatt, R.: 2017, skelETHon Formwork 3D Printed Plastic Formwork for Load-Bearing Concrete Structures, *Proceedings of XXI Congreso de la Sociedad Ibero-americana de Gráfica Digital*, Concepción, Chile, 345-352.
- Jipa, A., Meibodi, M.A., Giesecke, R., Shammas, D., Leschok, M., Bernhard, M. and Dillenburger, B.: 2018, 3D-printed formwork for prefabricated concrete slabs, *Proceedings of the 1st International Conference on 3D Construction Printing*, 1-9.
- Leshok, M. and Dillenburger, B.: 2019, Dissolvable 3DP Formwork. Water-Dissolvable 3D Printed Thin-Shell Formwork for Complex Concrete Components., *ACADIA 19 - UBIQUITY AND AUTONOMY: Proceedings of the 39th Annual Conference of the Association for Computer Aided Design in Architecture.*, 188-197.
- Naboni, R. and Bresghello, L.: 2018, Fused Deposition Modelling Formworks for Complex Concrete Constructions, *Proceedings of Sigradi 2018, XXII Congress of the Iberoamerican Society of Digital Graphics*, São Carlos, Brasil.
- Naboni, R. and Bresghello, L.: 2019, Additive Formwork for Concrete Shell Constructions, *Proceedings of the IASS Annual Symposium 2019 - Structural Membranes 2019. Form and Force*, Barcelona, Spain.
- Peters, R.: 2014, Additive Formwork, *ACADIA 2014 - Design Agency: Proceedings of the 34th Annual Conference of the Association for Computer Aided Design in Architecture*, 517-522.
- Salama, W.: 2017, Design of concrete buildings for disassembly: An explorative review, *International Journal of Sustainable Built Environment*, **6**, 617-635.
- De Soto, B., Augusti-Juan, I., Hunhevicz, J., Joss, S., Graser, K., Habert, G. and Adey, B.: 2018, Productivity of digital fabrication in construction: Cost and time analysis of robotically built wall, *Automation in construction*, **92**, 297-311.
- Søndergaard, A.: 2014, Odico Formwork Robotics, *AD Architectural Design. Special Issue: Made by Robots: Challenging Architecture at a Larger Scale.*, **84**, 66-67.
- Søndergaard, A., Feringa, J., Nørbjerg, T., Steenstrup, K., Brander, D., Gravesen, J., Markvorsen, S., Bærentzen, A., Petkov, K., Hattel, J., Clausen, K., Jensen, K., Knudsen, L. and Kortbek, J. 2016, Robotic Hot-Blade Cutting. An Industrial Approach to Cost-Effective Production of Double Curved Concrete Structures, in D.E.A. Reinhardt (ed.), *RobArch2016 - Robotic Fabrication in Architecture, Art and Design 2016.*, Springer International Publishing, Switzerland, 151-164.
- Wangler, T., Lloret, E., Reiter, L., Hack, N., Gramazio, F., Kohler, M., Bernhard, M., Dillenburger, B., Buchli, J., Roussel, N. and Flatt, R.: 2016, Digital Concrete: Opportunities and Challenges, *RILEM Technical Letters*, **1**, 67-75.

# CAM AS A TOOL FOR CREATIVE EXPRESSION

## *Informing Digital Fabrication through Human Interaction*

OZGUC BERTUG CAPUNAMAN

<sup>1</sup>*Pennsylvania State University*

<sup>1</sup>*okc5048@psu.edu*

**Abstract.** Contemporary digital design and fabrication tools often present deterministic and pre-programmed workflows. This limits the potential for developing a deeper understanding of materials within the process. This paper presents an interactive and adaptive design-fabrication workflow where the user can actively take turns in the fabrication process. The proposed experimental setup utilizes paste extrusion additive manufacturing in tandem with real-time control of an industrial robotic arm. By incorporating a computer-vision based feedback loop, it captures momentary changes in the fabricated artifact introduced by the users to inform the digital representation. Using the updated digital representation, the proposed system can offer simple design hypotheses for the user to evaluate and adapt future toolpaths accordingly. This paper presents the development of the experimental setup and delineates critical concepts and their motivation.

**Keywords.** Computer-Aided Design (CAD) and Manufacturing (CAM); Human Computer Interaction; 3D Printing; Interactive Digital Fabrication; Robotic Fabrication.

## **1. Introduction**

Historically, the role of computers in design has been a topic of debate. Following the successful research efforts in automating the fabrication process starting in the 1940s, Computer-Aided Manufacturing (CAM) and Design (CAD) tools focused on liberating designers from arduous tasks of design. This shift echoed the Albertian definition of skilled craftsmen through the idea of computational tools as “perfect slaves” (Cardoso Llach 2015). What initially started as an aspiration to develop a collaborative partner to the human agent, soon was proven unable to capture and codify the informal and often subjective design process (Bazjanac 1975). Commercial efforts following the initial success of such systems shifted the course of CAD and CAM from creative endeavors to streamlined and representation-oriented tools (Cardoso Llach 2015).

In today’s context, different fields of design across different scales are increasingly adopting computer-aided tools, yet the majority of computer-aided systems fail to match up to the nonlinear process of design and to bridge



the gap between idealized digital representation and physical artifact (DeLanda 2001). Highly structured algorithms, black-boxed and generic implementations (Pinochet 2017) that these tools employ, impose designers a particular way of designing. This research addresses two significant drawbacks of contemporary computer-aided system implementations within the scope of creative and exploratory inquiries. The first is the problem of unidirectional processing of information. Primarily CAM tools heavily rely on the pre-programming of toolpaths which intrinsically limit users exploring the design space. This in turn results in inflexibility to reflect and iterate on ideas quickly within the fabrication process and increasingly excludes the human agent from the process altogether. Secondly, contemporary computer-aided systems often offer generic solutions to complex problems, failing to capture nuances in materials and techniques. These problems are often overlooked by non-expert users that lack the means to navigate these complex computational systems. These shortcomings limit the design space of the contemporary designer in the age of digital tools.

## 2. Related Work

There has been growing interest in facilitating conversational fabrication scenarios in different fields. One main area of interest has been exploring alternative interaction interfaces. In their paper which is often cited for coining the term interactive fabrication, Willis et al. propose alternative interfaces to control digital fabrication tools such as touch-based pointers (Willis et al. 2011). Pinochet presents gesture-based numeric control of a hot wire cutter to enable bodily interactions with digital fabrication tools (Pinochet Puentes 2015). Similarly, FormFab utilizes gestures to perform formative fabrication on PETG sheets (Mueller et al. 2019). Both On-The-Fly Print and RoMA, exemplify how real-time fabrication and design of low-fidelity wireframe artifacts in Augmented Reality environment is possible (Peng et al. 2016; Peng et al. 2018).

In another approach, researchers have been looking into how establishing a sensory feedback loop between digital representation and physical artifact can enrich the fabrication process. For example, Position-correcting router utilizes computer vision-based algorithms to continuously correct the position of a handheld router to match the digital template (Rivers et al. 2012a). Rivers et al. (2012b) extends the use of digital CAD data in clay sculpting using projection mapping to inform the user. Similarly, FreeD enables the use of digital CAD data as a guide to the user during the subtractive fabrication process using a handheld milling device (Zoran and Paradiso 2013). Bard et al. (2014) discuss how different approaches in real-time sensing can be used to update the digital representation to minimize discrepancies between representation and the artifact. Lastly, several projects have focused on methods of interaction with digital fabrication tools. Constructable employs turn-taking between human and machine agents to fabricate artifacts without digital interfaces (Mueller et al. 2013). Similarly, ReForm applies interactive turn-taking to build prototypes, allowing changes along the iterative design-fabrication workflow (Weichel et al. 2015).

### 3. Proposed Design-Fabrication Workflow

Building upon the existing body of work, this paper proposes an alternative interactive design-fabrication workflow and its implementation. It utilizes robotic 3D printing of clay, which enables hands-on manipulation of the object during the fabrication process by the users. This geometric manipulation is then captured using computer-vision based feedback loop to inform digital representation. Using the updated digital representation, the proposed workflow adapts and extrapolates future tool paths to continue fabrication. Throughout this process, human and machine agents take on different roles with varying levels of contribution to the process. By exploring this turn-taking approach, this research aims to explore computer-aided systems not as sole algorithm executors but instead as flexible facilitators of digital fabrication, capable of incorporating changes in the artifact and adapting accordingly.

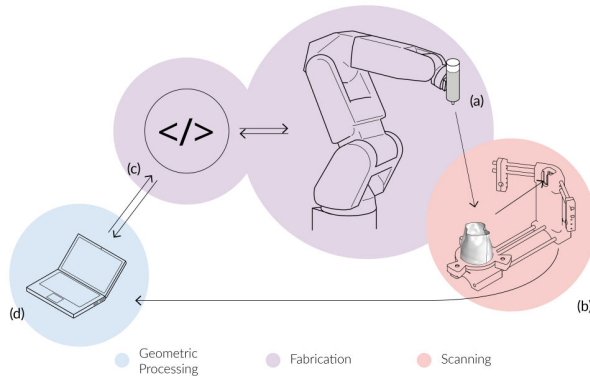


Figure 1. Subsystems of the proposed experimental setup: (a) Mechanical Paste Extruder, (b) Laser-Stripe Triangulation setup, (c) Live Communication Protocol, (d) Geometric Processing algorithms, and the Application.

This proposed workflow is mainly composed of five subsystems, illustrated in Figure 1, (a) a mechanical paste extruder to facilitate the fabrication of the object, (b) a laser-stripe triangulation scanning setup to update the digital representation of the artifact. Additionally, it incorporates (c) a real-time communication protocol which enables communication with the industrial robot arm, and developed (d) Grasshopper for Rhinoceros 6 script that performs tasks such as geometric reconstruction and tool path generation and (e) a Python 3.6 based application to coordinate the data flow between other subsystems.

Complementing the aim of this research to facilitate embodied material interaction, the physical artifact plays a crucial role as an interface between subsystems and a medium for transferring information. As an artifact engaged by both machine and human agents, the physical artifact can capture the design intention introduced by the human agent and constitute the foundation which machine agent can build upon. In addition to using the artifact as the primary medium, a wireless keypad has been integrated into the workflow. The role of this

keypad within the proposed workflow is mainly to address potential safety issues that can arise due to real-time control of the industrial robotic arm and to ensure no tasks are executed without the conscious decision of the user.

#### 4. Workflow Walkthrough

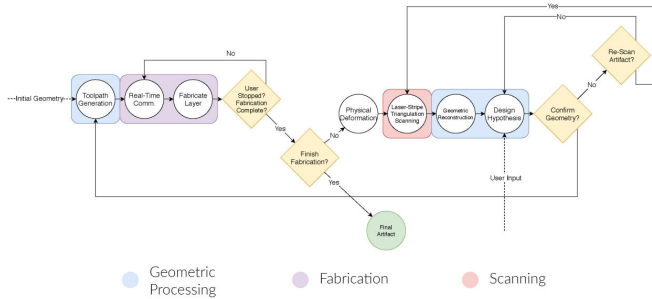


Figure 2. Proposed computational workflow flowchart.

The envisioned reciprocal interaction model for this experimental setup mainly consists of 3 computational stages; geometric processing, fabrication, scanning. The proposed design-fabrication workflow starts with the initiation of the application which ensures a robust communication between different subsystems using a virtual handshake. In the initial geometric processing stage, a slicing algorithm generates a series of toolpaths from the inputted geometry. Using the keypad, the user then initiates the fabrication stage. Target planes along the toolpath are sent to the robotic arm controller layer by layer. The fabrication process is carried out until all layers are fabricated or the user pauses the fabrication process any time after a sufficient amount of material is deposited for the user to modify. During the fabrication process, users can engage with the end-of-arm tool to tune the extrusion rate to accommodate for layer adhesion and inadequate material deposition.

Once the fabrication stage ends, the industrial robotic arm moves away from the fabrication environment for the user to safely manipulate the artifact by hand. Users are not necessarily restrained to any particular geometry, but best reconstruction results are obtained when the deviation in the surface curvatures are gradual. Once satisfied with the geometric deformation, the user can initiate scanning of the artifact and subsequent digital reconstruction. Following the digital reconstruction, the geometric extrapolation algorithm generates a design hypothesis using the surface tangency of the reconstructed surface. Using keypad inputs, the user can tune how compliant the design hypothesis is with the surface continuity of the digital reconstruction and generates extrapolated toolpaths once the user confirms the geometry. If the user does not wish to go any further, the workflow can be terminated. If continued, however, the workflow transitions back into the fabrication stage and another cycle of fabrication is initiated. Throughout the fabrication of the extrapolated layers, the user can end the fabrication if desired

or transition back to the physical deformation stage. The exemplified cycle can be repeated indefinitely as long as the artifact is within the bounds of the scanner and the artifact is structurally stable. Figure 3 shows instances from this process.



Figure 3. Stages of an exemplary use case scenario: (a) initiating the fabrication, (b) physical deformation of the artifact, (c) 3D capturing of the modified artifact, (d) user conforming design hypotheses, (e) user controlling the extrusion rate, (f) finished extrapolated geometry.

## 5. Implementation

The proposed design-fabrication workflow heavily relies on its subsystems to work synchronously within a low tolerance window. The hardware and software implementations have been significant in pinpointing the limitations and potentials of developed systems.

### 5.1. HARDWARE DEVELOPMENT

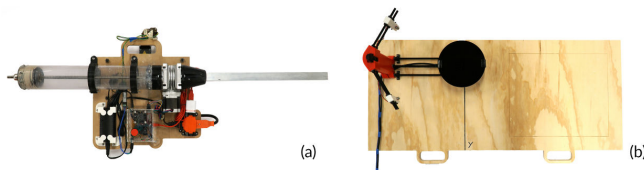


Figure 4. Assembled end-of-arm-tool and light-stripe triangulation scanner.

Within the scope of hardware implementations, the development of the end-of-arm tool and laser-stripe triangulation scanner, as shown in Figure 4, constitute the two most important subsystems. The designed and constructed mechanical assembly for clay deposition documented in this paper was based on an

open-source hardware project (Cera 2018). Many aspects of the mechanism such as the extrusion speed and the clay chamber volume, were modified in this implementation to accommodate fabrication with the industrial robotic arm better. Following the initial prototyping of the mechanical assembly, the control circuitry was implemented using an Arduino Nano microcontroller, which included necessary controls such as motor direction, extrusion speed and digital signal interfaces.

The other subsystem that required hardware development was the laser-stripe triangulation scanner. Aside from building and tuning the Ciclops 3D scanner kit, a significant modification was made to appropriate the hardware to the proposed workflow. Laser light sources were custom fitted with 3D printed mounts to intentionally occlude the light to only shine on the side that is closer to the camera by lowering the light source. This implementation aided the development of the geometric reconstruction algorithm. It eliminated the need to segment out readings from the inner surface of the artifact due to the hollow nature of the objects.

## 5.2. SOFTWARE DEVELOPMENT

Following the development of hardware subsystems, software implementations were carried out to control and regulate essential elements such as 3D scanning, processing of the scan data, toolpath generation, live communication with the industrial robotic arm and coordination between different phases of the proposed workflow.

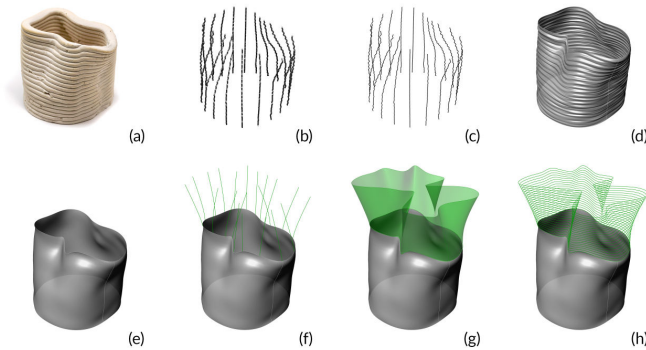


Figure 5. Steps of geometric processing from scan data to extrapolated toolpaths: (a) physical artifact, (b) point cloud, (c) lines generated from the point cloud, (d) high-resolution reconstruction, (e) simplified geometrical reconstruction, (f) extended section curves, (g) extended surface, (h) generated toolpaths.

Within the scope of this research, Horus library was used to communicate with the laser-stripe triangulation scanner hardware and to acquire geometric scan data (Horus 2019). Similarly, another open-source software, RobotExMachina (Garcia del Castillo 2019), was used to establish real-time communication with the ABB 6640. As a library based on .NET programming architecture, in order to integrate

it with other algorithms developed in Python 3.6, a Python wrapper developed by Garcia del Castillo and Bidgoli (2019) was used in the development of the real-time communication protocol. This library was modified to safely handle a large number of requests in order to eliminate connection interruptions.

In addition to open-source libraries used in this research, custom geometric processing algorithm was implemented as its steps shown in Figure 5. Instead of Horus's dense point cloud representation, the algorithm samples points at a sparser rate (b) and reconstructs profile curves (c). Since the laser-stripe triangulation technique inherently scans the object one section at a time perpendicular to the rotation plane, the algorithm reconstructs a NURBS surface (d) by using these curves as UV divisions. In order to circumvent any self occluding geometry, these curves were sampled by averaging readings from lasers placed on both sides of the camera. Using an adaptive resampling algorithm, these curves were smoothed (e) resulting low fidelity but relatively accurate representation of the global curvature of the artifact. Following the reconstruction of the target surface in NURBS definition, the geometric extrapolation algorithm utilizes the surface curvature to roughly estimate the geometry for future layers. Layers are extrapolated by extending scan curves (f) and the extrapolated surface (g) is reconstructed using a similar approach to how point cloud is processed and toolpaths are generated along this surface (h).

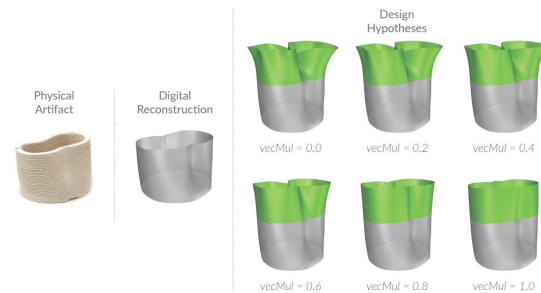


Figure 6. Generated design hypotheses for the given physical artifact with different compliance parameter values.

Furthermore, this algorithm also accommodates for user input to manipulate the design hypothesis. As implemented in the proposed experimental setup, the algorithm straightens extrapolated curves to match the World Z vector with a variable parameter. As a user-controlled parameter, this functionality allows users to select the desired curvature of the extrapolated surface. Once the user confirms the extrapolation of the surface, the algorithm generates the tool paths using the user-provided parameters. Since the workflow uses a 6-axis industrial robotic arm as a driving mechanism, the algorithm does not necessarily slice the object as planar curves but instead can accommodate for varying Z heights within each layer, which enables more complex geometries to be handled and fabricated.

## 6. Discussion

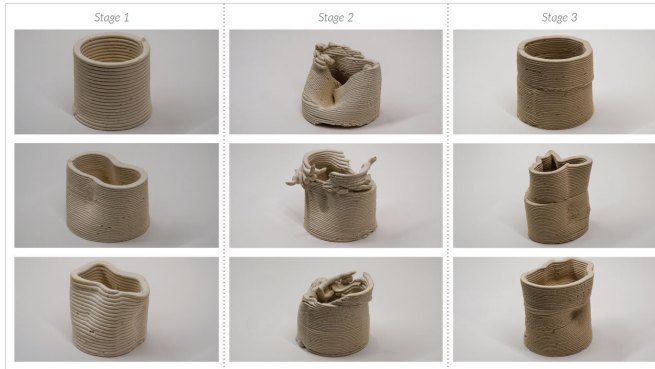


Figure 7. Experiment outcomes throughout different stages of the development.

As a tool for creative exploration, the proposed workflow enables a vast design space. Although this design space is still primitive in implementation, the proposed design-fabrication workflow provides an open-ended framework for creative inquirers. The proposed workflow encourages users to introduce design intentions through physical interaction with the fabricated artifact rather than optimized computational representation methods. It not only helps users build a better understanding of the material and the technique employed in fabrication but also presents an opportunity to refine the design iteratively. The initial design can change significantly during the design-fabrication process, allowing the user to develop design ideas as the workflow progresses.

The experimentation phase of this research focused on developing a keen understanding of the system's capabilities, pinpointing the limitations, and testing the proposed workflow for validity. Figure 7 above illustrates the consecutive stages of testing of the proposed system. Initial tests primarily focused on testing reliable fabrication of the artifact using paste additive manufacturing framework. The subsequent stage focused on geometrically extrapolating the physical artifact. Even though experiments conducted in this stage of development failed due to implementation inherent problems, the experimental setup could successfully capture different topologies and perform geometrical computation using the scan data. Once implementation problems were solved, the proposed system was able to continue the fabrication of the artifact using updated geometrical definition as a base to build upon.

Although the experimental setup detailed in this paper still relies on carefully orchestrated algorithms, it illustrates potentials of conversational interaction with computer-aided systems and integration of computational feedback loops. Throughout the testing of the proposed workflow, the experimental setup was successful at capturing geometrical intentions and at using this information to generate design hypotheses. By providing more control over execution of algorithms, the proposed workflow positions the user as an active agent within

the process. It encourages users to learn in action with materials and develop a deeper understanding of the problem. Moreover, it establishes a bi-directional flow of information beyond point-click-type interactions. The information flow between stages helps inform the digital reconstruction of the artifact throughout the workflow. This, in turn, enables the fabrication process to adapt accordingly to the current state of the artifact, capturing users' geometric design intentions.

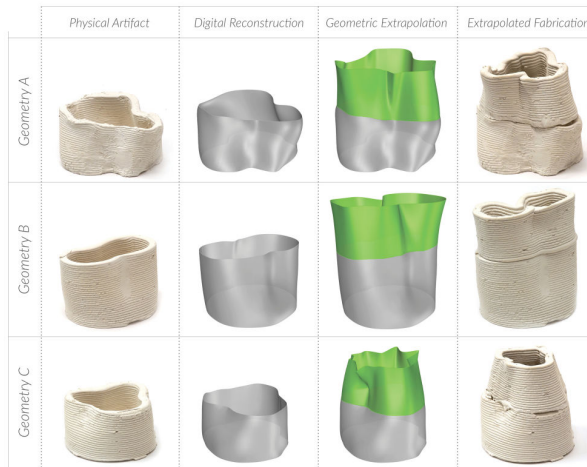


Figure 8. Processing of design hypotheses for three different geometries.

In addition, the proposed workflow also presents an alternative approach to how computation can be executed over physical mediums. It deliberately places the design-fabrication process away from well-established interfaces such as screens, pointing devices and keyboards, and executes computation with the material. Although the processing of information can be less accurate and more discrete at times due to system limitations, positioning the human agent as an active participant introduces ambiguity to the proposed workflow. Moreover, it provides promising evidence that such systems can capture design intention through computational feedback loops. Overall, the proposed design-fabrication workflow addresses the shortcomings detailed previously with varying degrees of success. The proposed experimental setup proved that once necessary calibrations for each subsystem are made and coordination in between these subsystems are established, it is capable of facilitating much needed human-machine dialogue and creative exploration with the use of computational systems.

### Acknowledgements

This research has been completed at the Carnegie Mellon University School of Architecture and partially funded by the Carnegie Mellon University Graduate Small project Help (GuSH) Research Grant. I would like to thank the valuable advising committee, Joshua Bard, Daniel Cardoso Llach and Mine Özkar, for their support, insight, and expertise that greatly assisted this research.



## References

- “Horus” : 2019. Available from <github.com/LibreScanner/horus>.
- Bard, J., Gannon, M., Jacobson-Weaver, Z., Jeffers, M., Smith, B. and Contreras, M.: 2014, Seeing is Doing: Synthetic Tools for Robotically Augmented Fabrication in High-Skill Domains, *Proceedings of the 34th Annual Conference of the Association for Computer Aided Design in Architecture*.
- Bazjanac, V. 1975, The Promises and the Disappointments of Computer-Aided Design, in N. Negroponte (ed.), *Reflections on computer aids to design and architecture*, Petrocelli/Charter, New York.
- Garcia del Castillo, J.L.: 2019, “RobotExMachina” . Available from <github.com/RobotExMachina/Machina-Bridge>.
- Garcia del Castillo, J.L. and Bidgoli, A.: 2019, “Machina - Python” . Available from <github.com/RobotExMachina/Machina-Python>.
- Cera, B.: 2018, “Mechanical Paste Extruder” . Available from <thingiverse.com/thing:3142561>.
- DeLanda, M. 2001, Philosophies of Design: The Case of Modeling Software, in J. Salazar (ed.), *Verb Processing: Architecture Boogazine*, ACTAR, Barcelona, 132-142.
- Cardoso Llach, D.: 2015, *Builders of the Vision: Software and the Imagination of Design*, Routledge, New York, NY.
- Mueller, S., Lopes, P., Kaefer, K., Kruck, B. and Baudisch, P.: 2013, Constructable: Interactive Construction of Functional Mechanical Devices, *CHI '13 Extended Abstracts on Human Factors in Computing Systems*, New York, NY, USA, 3107-3110.
- Mueller, S., Seufert, A., Peng, H., Kovacs, R., Reuss, K., Guimbretière, F. and Baudisch, P.: 2019, FormFab: Continuous Interactive Fabrication, *Proceedings of the Thirteenth International Conference on Tangible, Embedded, and Embodied Interaction*, New York, NY, USA, 315-323.
- Peng, H., Briggs, J., Wang, C.Y., Guo, K., Kider, J., Mueller, S., Baudisch, P. and Guimbretière, F.: 2018, RoMA: Interactive Fabrication with Augmented Reality and a Robotic 3D Printer, *Proceedings of the 2018 CHI Conference on Human Factors in Computing Systems*, New York, NY, USA, 579:1-579:12.
- Peng, H., Wu, R., Marschner, S. and Guimbretière, F.: 2016, On-The-Fly Print: Incremental Printing While Modelling, *Proceedings of the 2016 CHI Conference on Human Factors in Computing Systems*, New York, NY, USA, 887-896.
- Pinochet, D.: 2015, *Making Gestures : Design and Fabrication Through Real Time Human Computer Interaction*, Ph.D. Thesis, Massachusetts Institute of Technology.
- Pinochet, D.: 2017, Discrete Heuristics, *Computer-Aided Architectural Design. Future Trajectories*, Singapore, 306-326.
- Rivers, A., Adams, A. and Durand, F.: 2012, Sculpting by Numbers, *ACM Trans. Graph.*, **31**(6), 157:1-157:7.
- Rivers, A., Moyer, I.E. and Durand, F.: 2012, Position-correcting Tools for 2D Digital Fabrication, *ACM Trans. Graph.*, **31**(4), 88:1-88:7.
- Weichel, C., Hardy, J., Alexander, J. and Gellersen, H.: 2015, ReForm: Integrating Physical and Digital Design Through Bidirectional Fabrication, *Proceedings of the 28th Annual ACM Symposium on User Interface Software & Technology*, New York, NY, USA, 93-102.
- Willis, K.D., Xu, C., Wu, K.J., Levin, G. and Gross, M.D.: 2011, Interactive Fabrication: New Interfaces for Digital Fabrication, *Proceedings of the Fifth International Conference on Tangible, Embedded, and Embodied Interaction*, New York, NY, USA, 69-72.
- Zoran, A. and Paradiso, J.A.: 2013, FreeD: A Freehand Digital Sculpting Tool, *Proceedings of the SIGCHI Conference on Human Factors in Computing Systems*, New York, NY, USA, 2613-2616.

# **Generative, Algorithmic & Evolutionary Design/Techniques**



# ENABLING OPTIMISATION-BASED EXPLORATION FOR BUILDING MASSING DESIGN

*A Coding-free Evolutionary Building Massing Design Toolkit in Rhino-Grasshopper*

LIKAI WANG<sup>1</sup>, KIAN WEE CHEN<sup>2</sup>, PATRICK JANSSEN<sup>3</sup> and GUOHUA JI<sup>4</sup>

<sup>1,4</sup>*School of Architecture and Urban Planning, Nanjing University*

<sup>1</sup>*dg1436002@smail.nju.edu.cn* <sup>4</sup>*jgh@nju.edu.cn*

<sup>2</sup>*Andlinger Center for Energy and the Environment, Princeton University*

<sup>2</sup>*chenkianwee@gmail.com*

<sup>3</sup>*School of Design and Environment, National University of Singapore*

<sup>3</sup>*patrick@janssen.name*

**Abstract.** This paper presents an evolutionary design toolkit for performance-based building massing design optimisation. The toolkit is aimed to assist architects in exploring a wide range of building massing design alternatives guided by various performance objectives, thereby encouraging architects to incorporate evolutionary design optimisation for enriching design ideation at the outset of the design process. The toolkit is implemented in the Rhino-Grasshopper environment and includes components of a diversity-guided evolutionary algorithm and two pre-defined parametric models capable of generating a wide range of massing designs. The evolutionary algorithm can yield diverse design variants from the optimisation process and present more informative results with higher design differentiation. The pre-defined parametric models require minimal customisation from the architects. By using the toolkit, architects can readily explore high-performing building design with performance-based design optimisation with ease, and the coding-free optimisation workflow also streamlines the design process.

**Keywords.** Evolutionary design; building massing design; performance-based design; design process; design exploration.

## 1. Introduction

Over the last few years, there has been a focus shift from design optimisation to design exploration when using evolutionary design in architecture. Instead of purely maximising the performance of the design, the value of the information extraction from the optimisation and its role in boosting a performance-aware design process has become increasingly relevant to achieving a step change toward sustainable architectural design. Despite the increasing availability of

relevant know-how and tools related to evolutionary design, conducting such optimisation-based design exploration is still not trivial for most practitioners. On the one hand, parametric modelling of the design is typically time-consuming and technically challenging, which often results in an interruption to the design process (Nault, Waibel, Carmeliet, & Andersen, 2018). On the other hand, the feedback retrieved from the optimisation result is often limited due to the lack of design diversity in the result of optimisation (Wang, Janssen, & Ji, 2020).

In response to these challenges, we propose a coding-free evolutionary design toolkit to enable architects to undertake performance-based design optimisation and collect feedback from the optimisation result particularly for building massing design. The toolkit consists of two components. First, there are two pre-defined parametric models capable of generating a wide range of building massing designs beyond fixed topological configurations, which free the architect who carries out the performance-based optimisation from tedious parametric modelling. Second, the toolkit also includes a diversity-guided evolutionary algorithm that is aimed to enhance the design diversity in the optimisation result by increasing the genotypic differentiation in the design population. The two components allow the architect to quickly set up a task-specific evolutionary design system for performance-based design optimisation and exploring high-performing design solutions for design ideation and concept development.

To place this research into context, we first discuss the progress that has been made related to the evolutionary design tools. Then, we describe the proposed evolutionary design toolkit and present some design scenarios and associated results. We conclude by discussing the relative advantage of this toolkit and the possibilities for increasing the utility of optimisation-based design exploration in architecture.

### 1.1. EXISTING TOOLS FOR EVOLUTIONARY DESIGN

In the last decade, several evolutionary design and optimisation algorithm tools have been developed for performance-based building design optimisation. Popular tools include Galapagos, Octopus, and Opossum in Rhino-Grasshopper and Optimo in Revit-Dynamo. By using these tools, architects can set up a performance-based design optimisation system to search for high-performing solutions. However, establishing an optimisation system requires the architect to build up a parametric model for describing the design before running the optimisation process. For many architects who are not familiar with programming and coding, parametric modelling can be technically challenging and require considerable effort in setting up the parametric model. This technical barrier can to some extent be addressed by using visual programming tools for parametric modelling such as Grasshopper and Dynamo, which can free architects from coding. Even so, it is still challenging to use these tools to build up parametric models capable of producing substantial design differentiation over continuous design variations (Wang, Janssen, Chen, Tong, & Ji, 2019). As a result, the parametric models that get created are often only capable of generating very limited design differentiation, which makes the result of the optimisation predictable and less informing.

In order to address the challenge mentioned above, other researchers have proposed more integrated evolutionary design tools or workflows in recent years. Such evolutionary design tools and workflows typically integrate an evolutionary algorithm and pre-defined parametric models for generating simple building massings such as slab-/tower-type buildings and buildings with different footprint shapes (Natanian, Aleksandrowicz, & Auer, 2019; Nault et al., 2018; Xu et al., 2019). To use these tools or workflows, architects only need to customise the pre-defined parametric model by inputting constraints and preferences. These evolutionary tools and workflows do not require parametric modelling and associated coding and programming. As a result, the evolutionary design process based on these tools can be greatly streamlined. These tools and workflows are primarily aimed at the performance-based urban design optimisation, and the pre-defined parametric models are capable of generating diverse urban forms by varying permutations and combinations of different forms over multiple buildings.

Such coding-free and non-disruptive evolutionary design processes can also be used for performance-based design optimisation at the individual building level. However, for building design optimisation problems, the usage of these above-mentioned evolutionary design tools and workflows is limited. It is because the pre-defined parametric model embedded in these tools and workflows is typically unable to generate diverse building massings, which significantly confines the scope of design solutions for the optimisation process to explore (Nault et al. 2019). In order to address this issue, it is critical to develop pre-defined parametric models capable of generating diverse building designs with higher topological variability. Thus, we have proposed a parametric algorithm describing building design based on the subtractive form generation principle, which has proved to be effective for generating diverse building designs (Wang, Janssen, Chen, et al., 2019).

While the design process can be streamlined by providing pre-defined parametric models in the design tool, another problem is the lack of design diversity in the optimisation result. The evolutionary design tools and frameworks mentioned above are typically based on simple genetic algorithms. Such algorithms are typically poor in search efficiency and are only able to yield optimisation result within a family of similar solutions due to the genotypic similarity (Wang, Janssen, & Ji, 2020). This can undermine the type of design information and feedback that can be gained from the results. In order to enhance the information extraction, multi-objective optimisation is widely considered a means to reveal the trade-offs and compromises of the design problem by different design contestants. However, using multi-objective optimisation typically results in the reduction of search efficiency, and the contestants in the optimisation result are often too many. This can be overwhelming for architects, making information extraction very difficult (Yousif & Yan, 2018). In addition, with multi-objective optimisation, design variants must respond to multiple performance criteria. This can make the architectural implication related to each performance objective unclear.

To overcome the above weaknesses inherent in many evolutionary algorithms, we have proposed a hybrid evolutionary algorithm that can explore different

regions in the design space while only focusing on one performance objective (Wang, Janssen, & Ji, 2020). With the algorithm, the result of the optimisation can include a range of design variants that are both high-performing and that are also highly differentiated. This helps to clarify the architectural implications related to the performance factors and to enhance the feedback gained from the evolutionary design process (Wang, Janssen, Chen, et al., 2019).

## 2. Proposed toolkit and its implementation

### 2.1. OVERVIEW OF THE TOOLKIT AND APPLICATION WORKFLOW

The toolkit is developed to facilitate architects to carry out an explorative performance-based optimisation of building massing design aimed at various performance factors such as daylighting and passive solar energy while without additional programming required. The toolkit consists of the components of an evolutionary algorithm and two parametric models for generating building massing design. The toolkit was implemented in the Rhino-Grasshopper modelling platform to facilitate ease of use. In this platform, architects can establish an optimisation system by connecting the components of the parametric model (with the default colour scheme to Grasshopper components) and the evolutionary algorithm (with the same colour scheme, pink, to Galapagos component) to various building performance simulation tools such as *DIVA* and *Honeybee* (Figure 1).

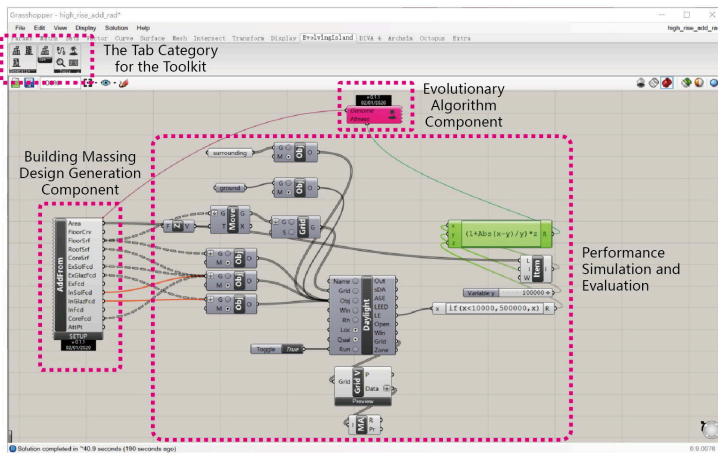


Figure 1. Example of a building massing design optimisation system established based on the toolkit.

With the system established (Figure 1), the architect first needs to adjust the selected parametric model via several user-defined parameters to generate building massings that satisfy the design setting. Second, the architect set the evolutionary algorithm and the simulation tool before running the optimisation process. While the design process is streamlined as no parametric modelling is

required, the optimisation system also has the merit of re-usability for different projects. For different projects, architects are only needed to adjust a few parameters to customise the set-up of the system as long as the performance criteria and the associated simulators remain the same.

## 2.2. PRE-DEFINED PARAMETRIC MODELS

The toolkit includes two pre-defined parametric models based on additive and subtractive form generation principles. As the two principles can schematically describe many passive building design strategies such as courtyards and stilts, the building massing generated by the two parametric models can help architects understand the performance implications related to those passive design strategies. The two models are also embedded with the rule abstracted from common architectural manipulation on the building massing design such as element regulation and alignment to ensure the generated design is feasible and meaningful. In addition, the architect can use several user-defined parameters to control the overall geometric features of the generated building massing design. Hence, the parametric models can play as a meta-model, which can derive various versioning task-specific models to generate satisfying building massing design simply by varying user-defined parameters.

For the parametric model based on the subtractive principle, it defines several cubic subtractive elements and creates the building massing design by removing the parts of these elements from a predefined maximal mass. The architect defines the dimension of the maximal mass, the maximum number as well as the size constraint of the subtracting elements. With different arrangements of the subtracting elements, the subtracted massing appears diverse topological configurations. In reverse, the one based on the additive principle creates the building design by accumulating and merging several cubic massing elements. Likewise, the architect defines the maximum number of massing elements, the maximal volume (spatial boundary) confining the massing elements, and the size constraint of the massing elements (Figure 2).

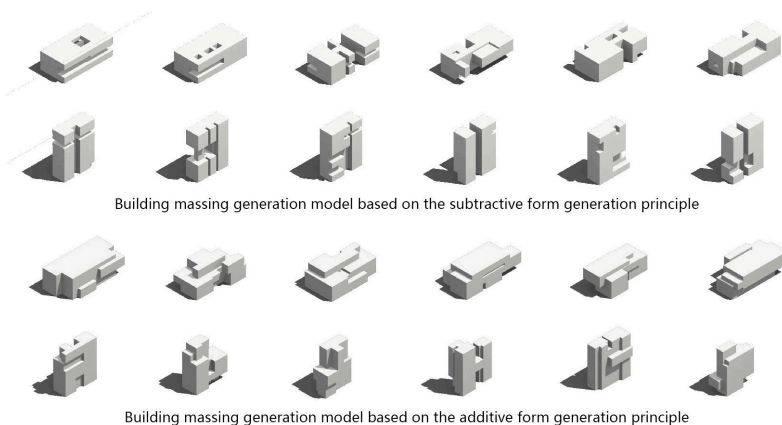


Figure 2. Examples of building massing design generated by the two parametric models.



### 2.3. DIVERSITY-GUIDED EVOLUTIONARY ALGORITHM

The toolkit includes an evolutionary algorithm integrating an island-model approach and a steady-state replacement strategy into a standard evolutionary algorithm, named SSIEA, for increasing diversity in the design population and improving the search efficiency. The island model allows the algorithm to launch multiple parallel search processes to evolve several “niching” subpopulations. Each subpopulation is guided to focus on a non-neighbouring region in the design space. The separation and multitude of subpopulations counteract the exploitative natural inherited in standard evolutionary algorithms and prevent the optimisation from ending up a set of neighbouring design solutions due to the genotypic similarity. In addition, the steady-state replacement strategy speeds up the optimisation process by increasing the evolutionary pressure on the whole optimisation process. Using the evolutionary algorithm can retrieve several high-performing solutions while having rich design diversity due to genotypic differentiation (Wang, Janssen, & Ji, 2020). The diversity in the result enhances the feedback from the optimisation, which facilitates architects to discover underlying compromises and trade-offs characterising the design problem.

### 2.4. SHOWCASE

In order to demonstrate the efficacy of the proposed evolutionary design toolkit, we first applied the toolkit into a case-study design task for exploring the building massing design responding to daylighting performance. In addition, the toolkit was used by two students in their design studio to design a 12-class kindergarten project, which allows the examination of the toolkit in a design scenario closer to reality.

For the first showcase, the design task describes a slab-type high-rise building surrounded by several high-rise buildings, and the quality of daylighting is set as the performance criteria to be investigated. As the surrounding buildings block a large amount of daylight from reaching the building, it presents a challenging design setting for achieving good daylighting performance (Figure 3). With the toolkit, we undertook optimisation based on the two parametric models to investigate how building design will be evolved to maximise the daylighting performance. The annual lighting energy consumption (LE) is taken as the performance indicator, which is calculated by DIVA, and the fitness evaluation is aimed to reduce LE. Moreover,  $45,000 \text{ m}^2$  is defined as the target gross area of the building. In response to the requirement of obtaining an acceptable gross area, the difference between the gross area of the generated building design and the target value is set as a penalty function in the fitness evaluation. The penalty function proportionally scales up the value of LE to punish the design variants failing to satisfy the gross area requirement.

For the optimisation process, we adopted six subpopulations to make the optimisation process to explore more regions in the design solutions space. In addition, the initial population was 300 (50 for each sub-population), and 130 generations were set for each optimisation process. In each generation, 36 offspring individuals were created and compared against their parents, and the total

iterations of design generations and performance evaluations for the optimisation process were 4,980.

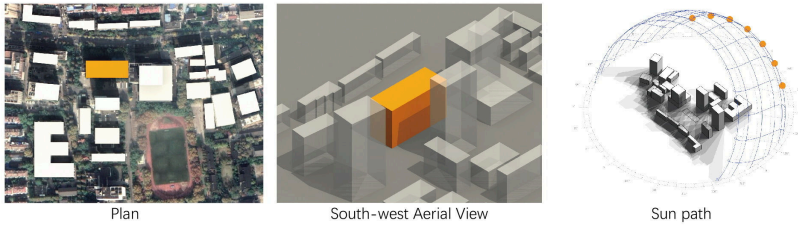


Figure 3. Design setting of the first showcase.

The second showcase is a 12-class kindergarten design (Figure 4). In this showcase, only the parametric model of the additive principle was applied, as the subtractive one is not suitable for generating design solutions with separated massing entities of classroom clusters. The gross area of the kindergarten is  $2,500\text{ m}^2$ , and the design was required to consider the arrangement of the classroom clusters, the outdoor playground, and other facilities such as kitchens and entrances. Two students chose the toolkit to explore design solutions in regard to the performance criteria of daylighting and passive solar heating. The students had no prior knowledge of computational design and building performance.

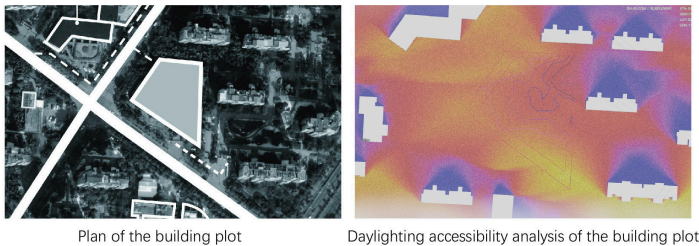


Figure 4. Design setting of the second showcase.

The period for the students to undertake the design optimisation lasted for three weeks (the overall period of the studio was eight weeks). As the students had no prior knowledge, we briefly introduced evolutionary optimisation and building performance to them while helping them to set up the optimisation system based on the toolkit in the first week. In the second and the third weeks, when the students became familiar with the toolkit and evolutionary optimisation, they began adjusting the setting of the parametric model and performance evaluation criteria according to the feedback from the previous optimisation result. After several trials, they extracted information from the optimisation result and developed their design concept based on the information.

### 3. Result

#### 3.1. SHOWCASE -1

The first row in Figure 5 shows the elite design solutions found by the evolutionary process based on the building massing generation model of the subtractive form generation principle. According to these solutions, three passive energy-saving strategies can be identified. These strategies can be effective in achieving good daylighting performance in this design setting. First, stilts appear in the Elite1 and Elite4. This strategy can help reduce the area on the lower floor levels, which is naturally poor in daylighting quality due to the daylight obstruction by surrounding buildings. Second, Elite2, Elite5, and Elite6 appear to be a high-rise tower-type building, which means that increasing the total height of the building can also improve daylighting performance. The increase in the building height can increase the proportion of floor area with fewer daylight obstructions by other buildings. In essence, these two strategies indicate that raising the major building mass in the vertical direction can improve the daylighting quality due to the reduction of the indoor space in the unfavorable under-daylit position close to the ground. Third, all elite solutions have jagged floors. This improves daylighting by increasing the facade surface and by creating gaps between the target building and other surrounding buildings.

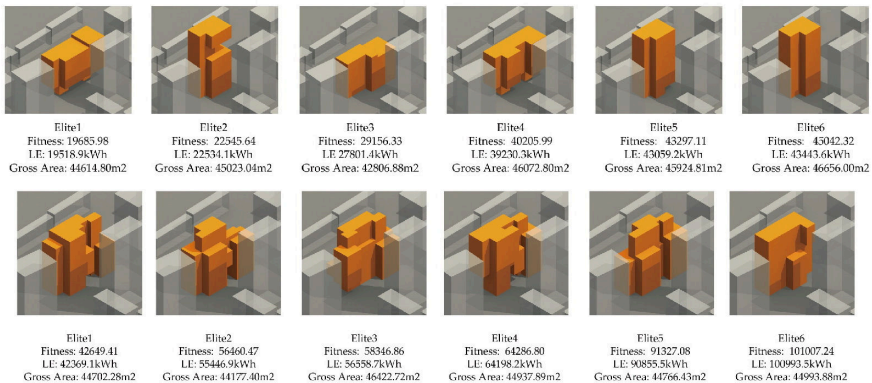


Figure 5. Elite design solutions in the optimisation result.

The second row in Figure 5 shows the elite design solutions found by the building massing generation model based on the additive form generation principle. Compared to their counterparts based on the subtractive form generation principle, these elite solutions share less similarity in the geometry. In general, Elite2, Elite3, and Elite4 show a stepped massing where a smaller mass sitting on a massive podium. Besides, stilts and jagged floor plans are also found among these elite solutions. These features also indicate the strategy in line with the strategy shown in the design variants based on the subtractive form generation principle that the building massing should be heightened to reduce the daylight obstruction by other surrounding buildings.

The reason why the result based on the additive generation model is different from the result based on the subtractive generation model is primarily due to an optional constraint imposed in the additive generation model. This constraint requires the building massing generated with at least half of the footprint to be occupied by the additive mass elements. The purpose of this constraint is aimed to avoid too many floating masses in the generated design. As a result, most of these elite solutions tend to have a large podium-like mass at the lower part of the building massing.

The above result shows that both parametric models can create diverse building massing designs to allow the architects to undertake an explorative performance-based optimisation. In addition, it should be mentioned that the effort and time required to establish the optimisation system for both optimisation processes are minor, as the two optimisation processes share most of the components in the system. The simple system establishing process may help architects focus on the optimisation process and exploring design solutions more deeply for solving the design problem.

### 3.2. SHOWCASE -2

In this paper, we present one student’s in-progress optimisation work and the corresponding final design in Figure 6. The general goal set by this student was to maximise daylighting performance. The student first examined two different orientations to generate the building massing of classroom clusters. By comparing the average daylighting quality, the student decided using a 45-degree rotated grid system as it can have a better average performance than that based on the north-south direction. Thereafter, the student selected several high-performing solutions and extracted the information from these. The student found the jagged massing and spacing are helpful for improving the daylighting performance (Figure 6-1). On this basis, the student re-arranged the mass elements taking other requirements into accounts, such as circulations and geometric order (Figure 6-2).

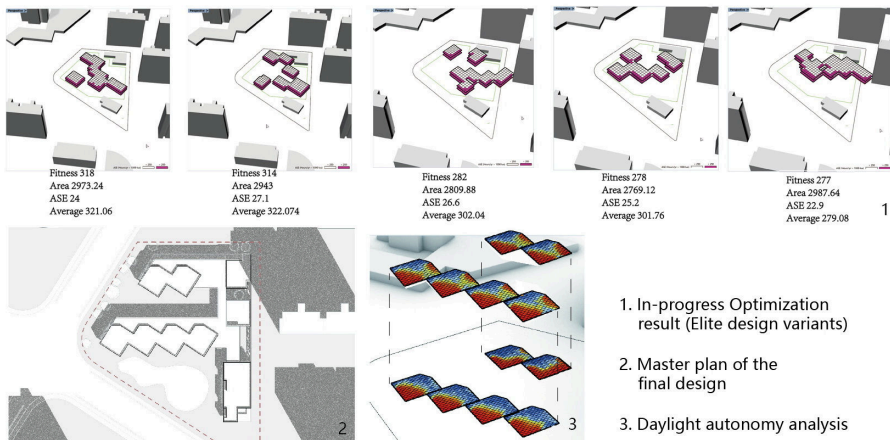


Figure 6. Elite design solutions in the optimisation result and the final design.

It may be noticed that the final design has marked differences from the optimisation result, which also points out a limitation of the toolkit. Indeed, the parametric model is primarily designed to generate single-entity building massing designs rather than the layout of multiple massing entities. Thus, the embedded rules and constraints may not be well suited to the kindergarten design. For such layout designs composed of predefined building massing entities, the building massing entity is typically not required to change in size, and the merging of two entities is also not appropriate.

#### 4. Conclusion and Discussion

This research proposes an evolutionary design toolkit aimed at optimisation-based design exploration for encouraging architects to collect feedback for enriching design ideation on the outset of the design process. By minimising the technical demand of utilising evolutionary design, the toolkit allows computational novices to undertake design optimisation with simple instructions. The two parametric models capable of generating adequate topological variability allow evolutionary optimisation to explore a broad range of design alternatives. Additionally, the feedback of the optimisation is enhanced by the genotypic differentiation obtained by using the hybrid evolutionary algorithm (SSIEA). The two showcases demonstrate how architects can extract useful information by using the toolkit, and how the information can positively affect the trajectory of the design process towards a desired environmental-friendly solution. Furthermore, while the optimisation system established by the toolkit yields entirely different result for the two showcases, the system used in the two showcases is *de facto* the same. Thus, this may open up a possible standardised approach to applying evolutionary design in conceptual architectural design, which architects can use in many routine design tasks for the initial concept development and design ideation.

#### References

- Natanian, J., Aleksandrowicz, O. and Auer, T.: 2019, A parametric approach to optimizing urban form, energy balance and environmental quality: The case of Mediterranean districts, *Applied Energy*, **254**(August), 113637.
- Nault, E., Waibel, C., Carmeliet, J. and Andersen, M.: 2018, Development and test application of the UrbanSOLVe decision-support prototype for early-stage neighborhood design, *Building and Environment*, **137**, 58-72.
- Wang, L., Janssen, P., Chen, K.W., Tong, Z. and Ji, G.: 2019, Subtractive Building Massing for Performance-Based Architectural Design Exploration : A Case Study of Daylighting Optimization, *Sustainability (Switzerland)*, **11**(24), 6965.
- Wang, L., Janssen, P. and Ji, G.: 2020, SSIEA: a hybrid evolutionary algorithm for supporting conceptual architectural design, *Artificial Intelligence for Engineering Design, Analysis and Manufacturing*, **34**, 1-19.
- Xu, X., Yin, C., Wang, W., Xu, N., Hong, T. and Li, Q.: 2019, Revealing urban morphology and outdoor comfort through genetic algorithm-driven urban block design in dry and hot regions of China, *Sustainability (Switzerland)*, **11**(13), 3683.
- Yousif, S. and Yan, W.: 2018, Clustering Forms for Enhancing Architectural Design Optimization, *23rd CAADRIA Conference: Learning, Adapting and Prototyping*, Beijing, 431-440.

# SPATIAL METAPHORS FOR MULTI-DIMENSIONAL DESIGN GALLERY INTERFACES

NAGHMI SHIREEN<sup>1</sup>, HALIL ERHAN<sup>2</sup>, ROBERT WOODBURY<sup>3</sup>  
and ALISSA N. ANTLE<sup>4</sup>  
<sup>1,2,3,4</sup>*Simon Fraser University*  
<sup>1,2,3,4</sup>{*nshireen|herhan|rw|aantle*}@*sfu.ca*

**Abstract.** With increased computing capabilities and large screen displays, the opportunity to support multiple designs in a single interface has recently become practical. Generating a large number of design alternatives is still a challenge but equally is to manage, review, understand and make-sense out of this multi-dimensional design space. Especially, when we consider the human cognitive limitations and the overly crowded informational displays. This research focuses on developing spatial metaphors based on the previous design literature and the findings from a study conducted to understand how to manage large design spaces with thousands of alternatives. We compare the existing design gallery systems used in practice with the spatial metaphors proposed in this paper. The goal is to develop a spatial structuring toolkit for interface designers of such tools.

**Keywords.** Design space exploration; spatial metaphors; multi-dimensional design space; gallery interfaces.

## 1. Introduction

Designers explore alternatives. Until recently, this exploration was mostly limited to a small number of alternatives ‘representing specific points in a multi-dimensional design space’ (Bradner et al., 2014). Designers also prefer to work with a continuously evolving design criteria discovered as the problem space revealed through iterations (Simon, 1973). They use the insights gained from each cycle of exploration to refactor the design problem and hence generate more alternatives to evaluate (Bradner et al., 2014).

With the availability of new computational design tools with generative capabilities, designers can create hundreds and thousands of alternatives. With these tools, designers iteratively generate alternatives from base model(s) and select a set of alternatives for further processing (Brown and Mueller, 2017). The cycle repeats until *satisficing* solutions are found (Simon, 1973). This is a cognitively intense process that can easily cause a cognitive choice-overload problem (Iyengar and Lepper, 2000). We contend that we should support this process with the tools equipped with presenting a gallery or a catalogue of design options (Brown and Mueller, 2017) to *review, understand, compare and evaluate* alternatives. For this, an investigation is needed to better understand

how designers can potentially review and make-sense of such a large design space of multi-dimensional, high performing, fully functional design alternatives. Parametric and generative systems have made it fairly easy for them to produce and optimize, but the next challenge remains, for not only how to visually represent these alternatives but also how to interact with and manage the alternatives. The results from our previous research (Shireen et al., 2017) tell us that filtering in such scenarios goes beyond mere selection. The new interfaces must include effective viewing and managing of alternatives along with supporting data analyzing strategies. The new features must focus on selection to make it an integral part of exploration workflow.

In our previous work (Shireen et al., 2017), we propose that the spatial structure of the task environment when working with alternatives determines how designers interact with a large number of alternatives. To accommodate the process of managing a large design space, designers develop spatial zones, make collections and arrangements within collections, compose spatial structures to support interactions with alternatives and collections, make visual clues, etc. (Shireen et al., 2019). As important these findings are, it is equally important to show how these findings can derive the development of new interfaces. Therefore, our next goal in this paper is to extend our previous research to develop a space-use taxonomy based on spatial structuring metaphors that can be later realized in different interface designs. We also look at the existing CAD tools and interfaces used in practice and research to develop a comprehensive understanding of spatial conjectures proposed by researchers from different fields. We aim to present interface designers and tool developers a toolkit of design exploration features focusing on spatial arrangements and structures.

Below, we introduce a literature review on design space exploration and tool support. This is followed by the description of the spatial metaphors we identified that we believe can guide development of novel interfaces for working with a large number of alternatives. We conclude with a discussion and future work.

## **2. Literature Review**

We have divided the literature review into two sections; design space exploration and human spatial cognition.

### **2.1. DESIGN SPACE EXPLORATION**

To review, compare and contrast the overall existing research describing Design Space Exploration (DSE), its techniques and interfaces, irrespective of design-space being spatially represented or not, we have classified DSE techniques and interfaces into four categories. These categories are based on the underlying/back-end representation used for exploration and the degree of automation, or in other words the degree of human-involvement in performing exploratory tasks. The four categories are Parametric Exploration (PE), History-based Exploration (HE), Genetic Exploration (GE) and Rule-based Exploration(RE), as shown in Figure 1.

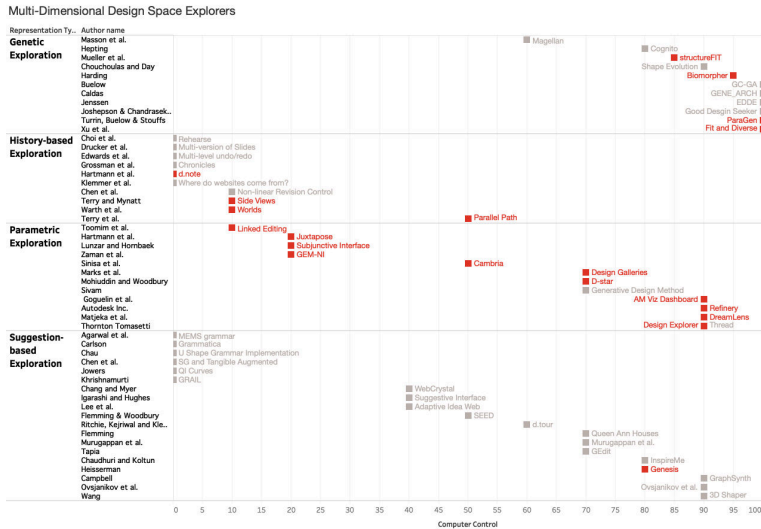


Figure 1. Design exploratory systems divided into four categories, highlighting the ones with mechanism to support simultaneous display and exploration of multiple design alternatives.

DSE has been a topic for research since 1970s, however it is not until recently the literature on simultaneous exploration of large design spaces has emerged. Among these, in *Parallel Path* (Terry et al., 2004), users can duplicate the current document along with its history, and can edit, backtrack variations in parallel or individually. Hartmann et al. (2008)’s *Juxtapose* provides interfaces for tuning parameters for run-time provision and exploration of computer programs. Similarly, Lunzer and Hornbæk (2008) proposes subjunctive interfaces with multi-dimensional data sliders with multiple handles, each representing an alternate input to a variable in content generation. *GEM-NI* (Zaman et al., 2015) and *Cambria* (Kolaric et al., 2014) allow editing multiple models in parallel by linking-unlinking geometries. *Cambria* uses collections and arranges them chronologically or arbitrarily.

With the increasing amount of data being used (as inputs) and produced (as output) using parametric design, there is a visible trend toward data-driven design exploratory systems. Most of these systems focus on visualization and interaction of a design space to steer the iterative cycles of exploration and optimization (Bradner et al., 2014; Brown and Mueller, 2017; Turrin et al., 2011; Joyce, 2015; Harding and Shepherd, 2017; Mueller and Ochsendorf, 2015). They address the exploration of design alternatives using data-driven, performance-based optimization strategies. Although these systems present valuable techniques in automating the generation and selection of the best candidate solution. However, our research agenda demands exploring systems with gallery-like interfaces. It is important for us to focus on systems and interfaces with gallery-like representations to understand the cognitive implications of spatial arrangements and structures used in those systems. The most prominent ones with gallery features are; *D-star* (Mohiuddin et al., 2017), *Design Explorer* and *Thread*



(Tomasetti, 2019), Dream Lens (Matejka et al., 2018), Refinery (Autodesk, 2019), ParaGen (Turrin et al., 2011), and StormCLOUD (Danhaive and Mueller, 2015).

The best part of the above systems, is the provision to manipulate design data to analyze and evaluate a design space for informed decision making. However the most notable short comings is their lack of functionality for recording design moves, reflection (Schön, 1983) and further exploration. They all provide a visual view of the design space presented spatially in a gallery-like environment, however, there is a lack of spatial operations that designers can perform on a gallery, to help *manage, review, record and reflect* on the design decisions within the gallery. The only system that stands out among them is D-star (Mohiuddin et al., 2017). It allows reflection on the generated design space by simultaneous editing. It provides novel alternative creation method through parallel coordinate interface. It also allows creating collections and performing parallel operations on alternatives and collections within a gallery. While we believe D-star is so-far potentially a spatially-structured design-space explorer, we still need to view it in light of human information processing, spatial cognition model and compare it with the spatial structure metaphors we propose in this paper.

## 2.2. HUMAN SPATIAL COGNITION

“Spatial cognition concerns the study of knowledge and beliefs about spatial properties of objects and events in the world” (Montello, 2001). Spatial properties include location, size, distance, direction, separation and connection, shape, pattern, and movement. From human cognitive perspective, these spatial properties play a vital role in human reasoning, processing, language, and action (Jackendoff, 1983). Many cognition scientists have used spatial metaphors to comprehend the abstract domains in our environment, and have driven lessons for variety of successful user interface designs.

The primary inspirations of our research come from Kirsh (1995)’s work. While Kirsh and other cognitive scientists (Lave, 1988; Hutchins, 1995) explore the use of space and spatial cognition within a everyday-use context, the majority of their work is based on watching experts carrying out routine tasks; such as chefs making food, supermarket staff arranging items, mechanics at work-shops assembling machinery and kids playing video-games or physical activities. While these observations are valuable, there is a need to question their universality when it comes to exploiting a spatial resource in helping to make a design decision. Previously we conducted a lab experiment (Shireen et al., 2017) to build upon this existing research literature within the context of large design spaces. Using the establish spatial cognition theory, we presented valuable findings regards to the spatial structures used by the participants of our study. We questioned the very notion of how spatial structuring in a goal-oriented design task can help simplify making a design selection, how can it help perceive a design situation and can simplify internal computation. Our goal in this paper is to extend our work and derive lessons from our observations for user interface design and develop a list of spatial metaphors.

### 3. Spatial Metaphors

Metaphors have become a prominent concept in HCI. They allow us to understand one thing in terms of another, without thinking they are the same. Over the past few decades, they have helped shape HCI and user interface design significantly. Through metaphors researchers map concepts in familiar source domains into computational target domains; e.g., digital folders on desktop, represent files on physical table.

In this paper, we have developed spatial metaphors based on the research findings from Shireen et al. (2017, 2019). By spatial metaphors, we mean mapping the physical spatial properties, patterns and structures observed in the study, into abstract components of user interface design. Based on the results from the study, we present three main spatial structures; divide, place and mark; each of which is sub-divided into further metaphors. ‘Divide’ refers to actions to create spatial structures using space as the main ingredient; ‘place’ corresponds to actions to support decision-making using spatial structures; and ‘mark’ refers to a visual indications or highlight of spatial structures to enhance and support human cognition and perception.

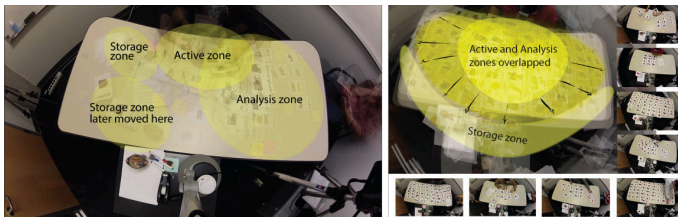


Figure 2. Left: The initial locations and rough boundaries of spatial zones. Right: Zones later into the design process, Shireen et al. 2017.

#### 3.1. DIVIDE

Divide is when we introduce a physical or logical ‘distance’ between any two or more elements. Human cognition works according to the law of proximity, i.e., elements that are closer to each other, are perceived as a group or a single unit (Gestalt principle).

When it comes to representing a gallery of thousands of design alternatives, distance, relative location-size-shape, connection and separation between every two designs, play a vital role in making sense of a gallery space. Owing to the fact that human perception works instantly and processes information way faster based on what an eye sees; this means looking at the big-picture influences humans to compose connections. In our previous study (Shireen et al., 2017) as well, we observed several divide-actions happening at multiple levels. Mainly there were two significant acts of dividing and partitioning; one that helped develop spatial zones onto the work-surface, and second that helped designers divide design variations into collections. Both types of actions were observed on the physical work-surface using spatial properties of the surface and design variations.

### 3.1.1. Divide Zones

Shireen et al. (2017) report three types of spatial zones developed by the participants of the study: active, analysis and storage zones. According to the qualitative analysis, these zones initially had tentative locations and loosely defined boundaries, but were continuously restructured and reconfigured depending on the design phase and the participant's personal preference. See Figure 2 and 3.

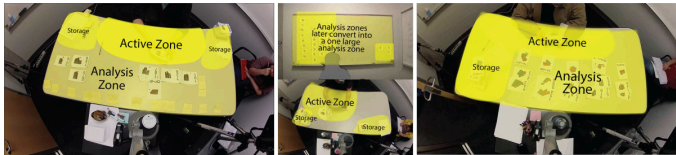


Figure 3. Spatial zones from Shireen et al., 2017.

Participants of the study kept changing the relative position, size, location and shape of the spatial zones throughout their process. Although the definition of a zone within the context of the study was related to one of the four primary tasks reported in the study, i.e., criteria building, testing, applying and reflection. However irrespective of its role, the creation and flexibility to adapt to the needs of the task is evident in a zone. If we map this behaviour into a digital interface design, we should expect space divisions to be dynamic, flexible and interchangeable. Knowing this, if we look at Dream Lens (Matejka et al., 2018), clearly we see the spatial distribution in terms of design-space visuals on left and design-space parameters on right, to help designer explore. However, one can imagine the need to enlarge or shrink one space or the other, while actively working with the design variations using Dream Lens interface. See Figure 4 Left. Similarly in Design Explorer (Figure 4 Right), the open source interface developed by Tomasetti (2019a) also provides its users with a default organization of spatial zones using three primary visualizations, i.e., design-space visuals (bottom half), the parallel coordinate filtering mechanism (top left) and scatter plot matrix (top right). It supports basic level of flexibility by allowing its users to remove one zone type at a time, while the rest of the two visualizations (zones) re-adjust themselves to cover the screen. However, It is hard to decide preemptively on the amount of screen-space users might need to visualize design data based on the task at hand. The same issue exists in the other design exploratory tools as well. In Table 1, we have compared these tools currently used in practice and research, to understand their use of divide metaphor.

### 3.1.2. Divide Designs

Dividing designs refers to organizing and composing the design space into collections. Based on human information processing system, our short-term memory has a limited capacity to hold and process information (Newell et al., 1972). Experiments in cognitive science literature confirms that this capacity is found to be 7 (+2) items or chunks of information. Consequently, it is natural

to organize items into manageable number of groups whenever we are faced with large number of items. This divide and organize strategy also helps our perception by making it easier to interpret, make-sense of, memorize and retrieve information at a later point in time with recognizable location, shape and size in space.

Likewise, in our previous experiment (Shireen et al., 2017), we report that ‘stacking’ was the most frequent action within the context of our study (Shireen et al., 2019). This stacking action implies a ‘collection’, especially when co-performed with visual marking and tagging. Even though the physicality of the experimental material did not allow much, our participants plotted cognitive informational cues (Kirsh, 1995) within their stacked designs. For instance, by stacking design-cards upside down to be perceived as ‘seen and rejected’, eliminating the need to remember and minimized the visual clutter on the work-surface. Another interesting mechanism reported in the study was to stack designs partially; affording a visual access to a design collection. This simplifies the visual perception by partially over-laying designs based on their visual weights and content. See examples in the Figure 5.

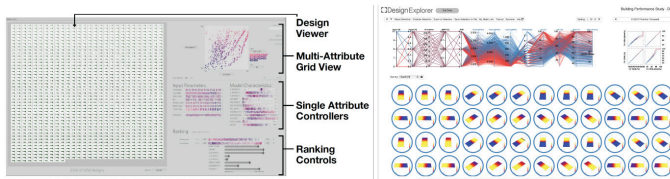


Figure 4. Left: Dream Lens interface. Photo published in Matejka et al.(2018).Right: Design Explorer interface. Photo taken from (Tomasetti, 2019a)’s open source web-link.

Table 1. Comparing existing design space exploration system for spatial divide metaphors.

System/Interface	Divide Zones	Divide Designs
Dream Lens	Non-flexible	No support
Design Explorer	Semi-flexible	No support
Refinery	Non-flexible	No support
D-star	Flexible	Supported
StormCLOUD	Non-flexible	No support

Now if we look at Dream Lens and Design Explorer once more with respect to *divide-designs* metaphor, we will notice that both of the interfaces have no support to even divide designs spatially, rest alone affording formal collections. See Table 1. The only system in the table that allows creating collections is D-star (Mohiuddin et al., 2017) See Figure 6 Left. Other than that, Cambria (Kolarić et al., 2014) also supports spatially-distributed nested design collections. See Figure 6 Right.

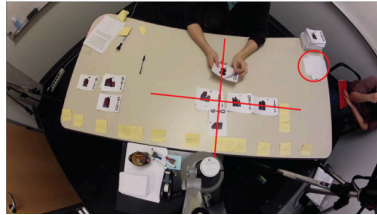


Figure 5. (Shireen et al., 2017) Notice the grid layout, spatial divide to represent groups and visually blocking designs from viewing.

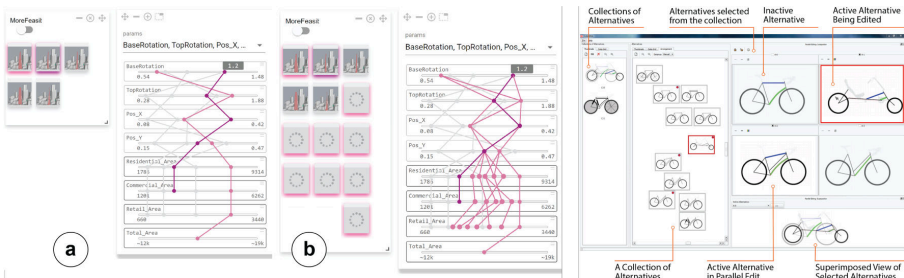


Figure 6. Left: D-Star interface by Mohiuddin et al., 2017. Right: Cambria interface by Kolaric et al., 2014.

3.1.3. Place and Mark

Place represents actions and structural affordances to position an alternative within a gallery. It supports human spatial cognition and perception by an interplay of location, size, orientation and shape. It is further divided into place-to-arrange, place-to-scan and place-to-compare.

Mark represents actions and structures to support adding a layer of information on top of existing data layers. Mark acts as an aiding device to code and highlight a substance of interest or of specific property. In our proposal, mark is further divided into four categories; bookmark, tags, notes and ranks/rate.

The detailed analysis of spatial -place and -mark metaphors are out of scope of this paper and are part of another publication. We do however provide a preliminary analysis of these two metaphors with respect to the existing design exploration systems. See Table 2 and 3.

Table 2. Comparing existing design space exploration system for spatial place metaphors.

System/Interface	Place to Arrange	Place to Scan	Place to Compare
Dream Lens	Automated	Supported	Supported
Design Explorer	Automated	Supported	Partially supported
Refinery		Supported	Supported
D-star	Manual and automated	Supported	Supported
StormCLOUD	Automated	Supported	Partially supported

Table 3. Comparing existing design space exploration system for spatial mark metaphors.

System/Interface	Visual Mark	Tags	Notes	Rank
Dream Lens	No support	No support	No support	Supported
Design Explorer	No support	No support	No support	Supported
Refinery	No support	No support	No support	Supported
D-star	No support	No support	No support	No support
StormCLOUD	No support	No support	No support	Supported

#### 4. Discussion and Future Work

In this paper, we present three spatial structuring metaphors based on the human spatial cognition in general and findings from our previous experiment in Shireen et al. (2017). The three metaphors are Divide, Place and Mark. We also look at existing research within the domain of representing large design space and examine the interfaces and systems currently in use. We compare a sample of these systems supporting large design spaces with respect to our proposed spatial structuring metaphors. Our preliminary findings indicate that although these new tools and systems provide novel interaction techniques to generate and analyze designs through graphic visualizations and other User Interface (UI) operations, they still lack in providing spatial affordances in their design gallery interfaces for users to effectively make-sense of the explored design space. Most of them have little to no-flexible support for spatial zones and spatial collections - highly needed features in any digital gallery system irrespective of its domain. None of the systems we examined provide bookmarking, highlighting, visual tagging or writing-notes operations to their design galleries. These Mark features are very important to reflect on the design space and have been the integral part of the design process as reported in Shireen et al. (2017) and previous design studies (Akin, 2001). Most of the currently-in-use systems support arrangements through automated sorting techniques and have no support for manual organization, division and placement of design alternatives. Almost all of them provide a mechanism to rank designs, which is great and well needed feature in a design gallery.

Our future work involves extending these spatial metaphors into interface mock-up implementations. The larger goal is to come up with a spatial structuring toolkit for interface designers of large-design-space gallery systems and show their usability.

#### References

- Akin, Ö 2001, Variants in design cognition, in C. Eastman, W. Newstetter and M. McCracken (eds.), *Design knowing and learning: Cognition in design education*, Elsevier, 105-124.
- Autodesk, I.n.c.: 2019, "Project Refinery Beta by Autodesk Inc." . Available from <<https://www.autodesk.com/campaigns/refinery-beta>>.
- Bradner, E., Iorio, F. and Davis, M.: 2014, Parameters Tell the Design Story: Ideation and Abstraction in Design Optimization, *Proceedings of the Symposium on Simulation for Architecture & Urban Design*, San Diego, CA, USA, 26:1-26:8.
- Brown, N. and Mueller, C.: 2017, Designing with data: moving beyond the design space catalog, *37th Annual Conference of the Association for Computer Aided Design in Architecture: Disciplines and Disruption, ACADIA 2017*, 154-163.
- Danhaive, R.A. and Mueller, C.T.: 2015, Combining parametric modeling and interactive

- optimization for high-performance and creative structural design, *Proceedings of IASS Annual Symposia*, 1-11.
- Harding, J.E. and Shepherd, P.: 2017, Meta-parametric design, *Design Studies*, **52**, 73-95.
- Hartmann, B., Yu, L., Allison, A., Yang, Y. and Klemmer, S.R.: 2008, Design as exploration: creating interface alternatives through parallel authoring and runtime tuning, *Proceedings of the 21st annual ACM symposium on User Interface Software and Technology*, 91-100.
- Hutchins, E.: 1995, *Cognition in the Wild*, MIT press.
- Iyengar, S.S. and Lepper, M.R.: 2000, When choice is demotivating: Can one desire too much of a good thing?, *Journal of Personality and Social Psychology*, **79**(6), 995.
- Jackendoff, R.: 1983, *Semantics and Cognition*, MIT press.
- Joyce, S.C.: 2015, Web based data visualisation applied to creative decision making in parametric structural design, *Proceedings of IASS Annual Symposia*, 1-12.
- Kirsh, D.: 1995, The intelligent use of space, *Artificial Intelligence*, **73**, 31-68.
- Kolarić, S., Woodbury, R. and Erhan, H.: 2014, CAMBRIA: a tool for managing multiple design alternatives, *Proceedings of the 2014 companion publication on Designing Interactive Systems*, 81-84.
- Lave, J.: 1988, *Cognition in practice: mind, mathematics and culture in everyday life*, Cambridge University Press.
- Lunzer, A. and Hornbæk, K.: 2008, Subjunctive interfaces: Extending applications to support parallel setup, viewing and control of alternative scenarios, *ACM Transactions on Computer-Human Interaction (TOCHI)*, **14**(4), 1-44.
- Matejka, J., Glueck, M., Bradner, E., Hashemi, A., Grossman, T. and Fitzmaurice, G.: 2018, Dream lens: exploration and visualization of large-scale generative design datasets, *Proceedings of the 2018 CHI Conference on Human Factors in Computing Systems*, 369.
- Mohiuddin, A., Woodbury, R., Ashtari, N., Cichy, M. and Mueller, V.: 2017, A Design Gallery System: Prototype and Evaluation, *Proceedings of the 37th Annual Conference of the Association for Computer Aided Design in Architecture (ACADIA)*.
- Montello, D.: 2001, *International Encyclopedia of the Social and Behavioral Sciences*, Oxford, Pergamon Press.
- Mueller, C.T. and Ochsendorf, J.A.: 2015, Combining structural performance and designer preferences in evolutionary design space exploration, *Automation in Construction*, **52**, 70-82.
- Newell, A. and Simon, H.A.: 1972, *Human problem solving*, Prentice-Hall Englewood Cliffs, NJ.
- Schön, D.A.: 1983, *The reflective practitioner*, New York.
- Shireen, N., Erhan, H. and Woodbury, R.: 2019, Encoding Design Process Using Interactive Data Visualization, *International Conference on Computer-Aided Architectural Design Futures*, 231-246.
- Shireen, N., Erhan, H., Woodbury, R. and Wang, I.: 2017, Making sense of design space, *International Conference on Computer-Aided Architectural Design Futures*, 191-211.
- Simon, H.A.: 1973, The structure of ill structured problems, *Artificial intelligence*, **4**, 181-201.
- Terry, M., Mynatt, E.D., Nakakoji, K. and Yamamoto, Y.: 2004, Variation in element and action: supporting simultaneous development of alternative solutions, *Proceedings of the SIGCHI conference on Human Factors in Computing Systems*, 711-718.
- Tomasetti, T.: 2019, "Design Explorer and Thread by CORE studio" . Available from <<http://core.thorntontomasetti.com/design-explorer/or.../thread>>.
- Turrin, M., Von Buelow, P. and Stouffs, R.: 2011, Design explorations of performance driven geometry in architectural design using parametric modeling and genetic algorithms, *Advanced Engineering Informatics*, **25**(4), 656-675.
- Zaman, L., Stuerzlinger, W., Neugebauer, C., Woodbury, R., Elkhaldi, M., Shireen, N. and Terry, M.: 2015, GEM-NI: A system for creating and managing alternatives in generative design, *Proceedings of the 33rd Annual ACM Conference on Human Factors in Computing Systems*, New York, NY, USA, 1201-1210.

# ARCHITECTURAL LAYOUT DESIGN THROUGH SIMULATED ANNEALING ALGORITHM

HAO ZHENG<sup>1</sup> and YUE REN<sup>2</sup>

<sup>1</sup>*University of Pennsylvania, Philadelphia, USA*

<sup>1</sup>*zhhao@design.upenn.edu*

<sup>2</sup>*University College London, London, UK*

<sup>2</sup>*yue.ren.19@ucl.ac.uk*

**Abstract.** Simulated Annealing is an artificial intelligence algorithm for finding the optimal solution of a proposition in an ample search space, which is based on the similarity between the physical annealing process of solid materials and the combinatorial optimization problem. In architectural layout design, although architects usually rely on their subjective design concepts to arrange buildings in a site, the judging criteria hidden in their design concepts are understandable. They can be summarized and parameterized as a combination of penalty and reward functions. By defining the functions to evaluate a design plan, then using the simulated annealing algorithm to search the optimal solution, the plan can be optimized and generated automatically. Six penalty and reward functions are proposed with different parameter weights in this article, which become a guideline for architectural layout design, especially for residential area planning. Then the results of several tests are shown, in which the parameter weights are adjusted, and the importance of each function is integrated. Lastly, a recommended weight and “temperature” setting are proposed, and a system of generating architectural layout is invented, which releases architects from building arranging work in an early stage.

**Keywords.** Architectural Layout; Simulated Annealing; Artificial Intelligence; Computational Design.

## 1. Introduction to the Simulated Annealing Algorithm

### 1.1. METROPOLIS ALGORITHM

Metropolis et al. (1953) firstly developed a method, especially running in computers, for finding the minimum or maximum value of a function, which may be complicated and hard to describe. Rather than recursively comparing values in the function and finding the direction of optimizing to reach the objective value, in the metropolis algorithm, there is a distinct possibility that the program will accept a worse result and its optimizing direction so that the optimizing process will not get trapped in a local optimum.

Figure 1 shows a minimum optimizing process. In the optimizing process, the current state  $x_n$  results in its value in the function  $f(x_n)$ . When the process moves



forward, the next state  $x_{n+1}$  results in its value in the function  $f(x_{n+1})$ , which is compared with the current value. If  $f(x_{n+1})$  is smaller than  $f(x_n)$ , such as  $f(x_2)$  compared with  $f(x_1)$ , the current state will move to  $x_{n+1}$  and waiting for the next loop.

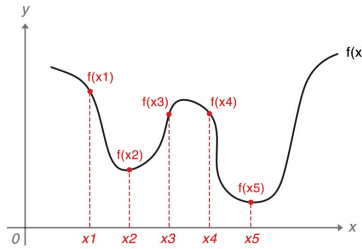


Figure 1. Optimizing Process of Metropolis Algorithm.

However, if  $f(x_{n+1})$  is greater than  $f(x_n)$ , such as  $f(x_3)$  compared with  $f(x_2)$ , in the metropolis algorithm, the program will calculate a probability of acceptance, which indicates whether the state will ignore the result and still move forward, as following:

$$p = \exp\left(-\frac{f(x_{n+1}) - f(x_n)}{T}\right) \quad f(x_{n+1}) \geq f(x_n) \quad (1)$$

Therefore ideally, with a proper setting of variable  $T$ , which is an inputted parameter controlling the updating possibility and frequency, the process will jump out of the local optimum  $f(x_2)$  and eventually reach the global optimum  $f(x_5)$ .

## 1.2. SIMULATED ANNEALING AND ITS APPLICATIONS

In the metropolis algorithm, the setting of variable  $T$  will primarily affect the accuracy and efficiency of the optimizing process. To find the best setup, Kirkpatrick, Gelatt, and Vecchi (1983) developed the Simulated Annealing Algorithm, changing the variable  $T$  into a process-related variable, which will decrease gradually so that the probability of accepting a worse result will become smaller and smaller, and finally reach a stable status without any acceptances of the worse outcomes. This process is similar to the physical annealing, where variable  $T$  acts as a temperature value to control the annealing rate, so it's called Simulated Annealing. The detailed procedure can be expressed as the following four steps:

(1) Set the starting temperature value as  $t_s$ , the ending temperature value as  $t_e$ , the function to update the  $T$  value as  $T_t$ , and the initial  $x$  value as  $x_0$ . Update the optimized  $x$  value  $x_{opt}$  by  $x_0$  and calculate  $f(x_{opt})$ .

(2) Apply a random change to  $x_{opt}$  and get  $x_n$ , then calculate  $f(x_n)$ .

(3) If  $f(x_n)$  is smaller than  $f(x_{opt})$ , update  $x_{opt}$  by  $x_n$ . If  $f(x_n)$  is greater than  $f(x_{opt})$ , calculate the probability of acceptance  $p(x_n, x_{opt})$ , then generate a random number  $p_n$  between 0 and 1. If  $p_n$  is greater than  $p(x_n, x_{opt})$ , update  $x_{opt}$  by  $x_n$ .

(4) Update the current  $T$  value  $t_n$  by  $T(t_n)$ . If  $t_n$  is greater than  $t_e$ , execute (2) and loop the procedure.

Thus, for any given objective function  $f(x)$ , the Simulated Annealing Algorithm can find the best way to approach the global optimum. Sen and Stoffa (1991) applied the Simulated Annealing Algorithm in engineering, minimizing the error energy between the data and theories in seismic waveform inversion. Abramson (1991) built a system to find the best solution for the school timetabling problem. Tracey, Clark, and Mander (1998) constructed an optimized data generation framework to find program flaws. Ekren and Ekren (2010) used the simulated annealing algorithm to optimize the size of the wind hybrid energy conversion system.

In urban, structure, and architecture fields, the Simulated Annealing Algorithm also has a wide range of applications. Hong (2011) built a model to achieve accurate forecasting of inter-urban traffic flow. Sonmez (2008) developed a method to optimize a structure to be lightweight, high-performance, and low-cost. AlHalawani et al. (2013) built a framework to produce a factored facade representation and a facade analysis algorithm with the help of Simulated Annealing. Yeh (2006) solved the facility layout problem in the interior design of a hospital by generating floor plans, while Michalek, Choudhary, and Papalambros (2002) developed a similar method to arrange rooms in a house.

### 1.3. PROJECT GOAL

Different from the previous research, this paper focuses on the Simulated Annealing Algorithm in arranging buildings in the site, especially for residential area planning, developing unique functions to describe the main aspects when designing the architectural layout, optimizing and making a balance between each design focus.

Through this research, we want to provide a useful tool for architects that the layout of the residential buildings can be generated by controlling the parameters of the design tendency, thus showing an example of translating design ideas and strategies into parameters with a more mathematical method.

## 2. Penalty and Reward Functions in Architectural Layout Design

### 2.1. PARAMETERS AND MEANINGS

To clarify the question and the working limit, parameters to represent the condition and the requirements of the design were proposed firstly (figure 2).

For the site, when designing, all parameters are already set and cannot be changed. Parameters include  $P_{ent}$  for the position of entrance,  $G_{bou}$  for the boundary geometry of the design area,  $A_{sun}$  for the local sunshine angle in the winter solstice, and  $G_{riv}$  for the geometry of the river or any landscape attractions. These four parameters stay constant and will be used to define penalty and reward functions.

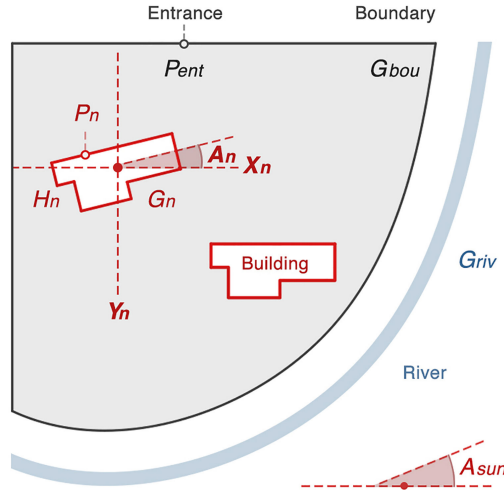


Figure 2. Parameters in an Architectural Layout Design.

Then for the buildings, which need to be placed into the site, parameters include  $G_n$  for the boundary geometry of each building,  $P_n$  for the entrance position of each building,  $H_n$  for the height,  $A_n$  for the rotating angle,  $X_n$  and  $Y_n$  for the relative position of each building. Among them,  $G_n$ ,  $P_n$  and  $H_n$  are pre-designed and should keep constant, while  $X_n$ ,  $Y_n$  and  $A_n$  are the main parameters, which will be fed into the Simulated Annealing Algorithm as  $x$  value for the objective function  $f(x)$ .

### 2.2. PENALTY FUNCTIONS

After defining all parameters, the objective function  $f(x)$  was developed as the weighted sum of 6 sub-functions. First, to avoid any glaring geometric errors for architectural design, two penalty functions were proposed (figure 3).

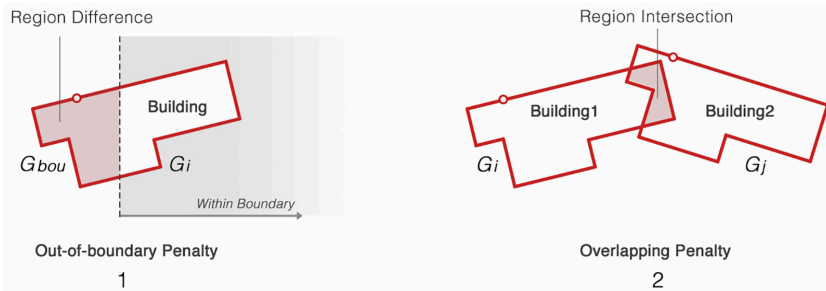


Figure 3. Penalty Functions.

One is called Out-of-Boundary Penalty, which means, when the geometries of buildings are partly or wholly outside the site boundary, a minus point will be

added into the objective function as the following formula:

$$f_1 = -k_1 \cdot \sum_{i=1}^n \text{Area}(\text{RegionDefference}(G_i, G_{\text{bou}})) \quad (2)$$

Also, when two buildings have an overlapping area, it doesn't make sense. Thus another penalty function is called Overlapping Penalty, to avoid the collision of buildings, as follows:

$$f_2 = -k_2 \cdot \sum_{i=1}^{n-1} \sum_{j=i}^n \text{Area}(\text{RegionIntersection}(G_i, G_j)) \quad (3)$$

In the two formulas,  $k_1$  and  $k_2$  are factors that adjust the order of magnitude, since the unit in these two formulas is  $m^2$ , which is different from the following formulas. And the proper settings of  $k_1$  and  $k_2$  will be discussed in the following pages.

### 2.3. REWARD FUNCTIONS

In addition to the penalty functions, 4 reward functions were also constructed, to guide the system to find the best solution (figure 4).

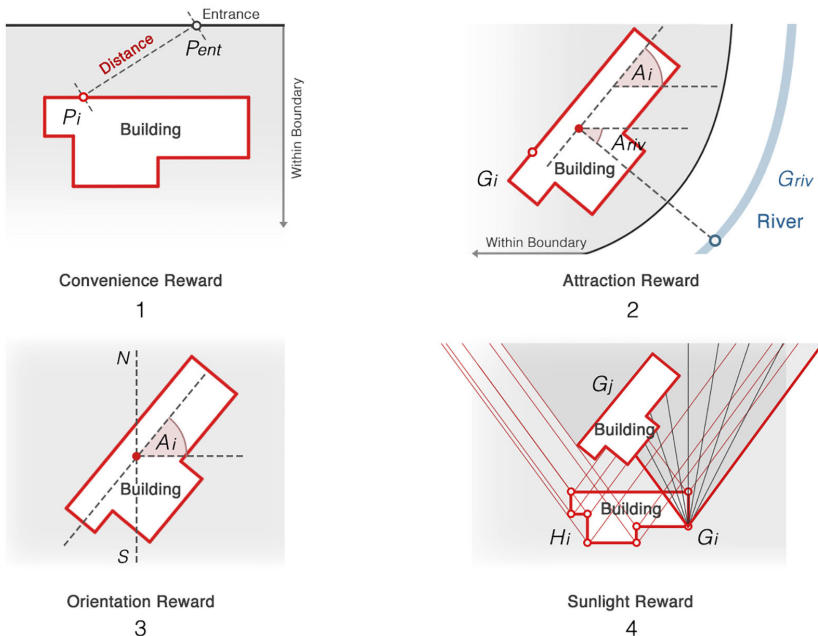


Figure 4. Reward Functions.

First, if the entrance of a building is close to the access of the site, the system will give a reward point to the function, because it will be convenient for the building users. It's called Convenience Reward, based on the following formula.

The shorter the distance between two entrances, the higher score it will gain. While  $k_3$  acts as a coefficient,  $l_3$  is a minimum limit for the distance, protecting  $f_3$  from becoming too large.

$$f_3 = k_3 \cdot \sum_{i=1}^n \frac{1}{\text{Maximum}(\text{Distance}(P_i, P_{\text{ent}}), l_3)} \quad (4)$$

Second, Attraction Reward was built, representing the landscape value in the site for each building. The system will find the closest point from the curve of the river to the center point of the building, and calculate the distance between two points. Then the angle between the normal of the river at that point and world vector X will be figured out as  $A_{\text{riv}}$ . By comparing  $A_{\text{riv}}$  with  $A_i$ , the orientation of the building facing the landscape will be evaluated. And the length of the boundary of the building will also be taken into account to represent the possible length of the area that the users can see the landscape from the building. Thus, the formula can be expressed as follows:

$$f_4 = k_4 \cdot \sum_{i=1}^n \frac{\text{Length}(G_i) \cdot (A_i + A_{\text{riv}})}{\text{Maximum}(\text{Distance}(G_i, G_{\text{riv}}), l_4)} \quad (5)$$

The third and fourth functions are both about sunlight. Since all buildings are initially modeled in the world coordinate, in which positive X unit towards the north and the balconies are always in the southern part of a building, the only face that can receive direct sunshine is the southern curve in the geometry. Therefore, the Orientation Reward was proposed, indicating that if the building is facing south as it originally is, an additional reward will be given to the evaluation function. The formula for the Orientation Reward is:

$$f_5 = k_5 \cdot \sum_{i=1}^n \left( \frac{\pi}{2} - A_i \right) \quad (6)$$

Also, there are always shadows for each building, which may block the sunlight of other buildings, the last reward function, Sunlight Reward, will be given to the evaluation function, if the buildings are exposed to the sunlight in most of the daytime. To calculate the worst period of receiving sunshine, the local sunshine angle in the winter solstice  $A_{\text{sun}}$  will be used to draw the boundaries of the shadows. Then by calculating the percentage of the area in the building, which is not covered by shadows in each period (7 am to 6 pm), the function will work adequately to feedback a reward number between 0 and 1, representing the overall condition of daylighting. The formula is:

$$f_6 = k_6 \cdot \sum_{i=1}^n \frac{\sum_{j=1}^n \frac{\sum_{t=7}^{18} \text{Area}(\text{RegionDifference}(G_i, \text{SunShadow}(G_j, H_j, A_{\text{sun}}, t)))}{\text{Area}(G_i) \cdot 12}}{n} \quad (7)$$

Lastly, by adding all 6 functions together, the final objective function is completed as follows:

$$f = f_1 + f_2 + f_3 + f_4 + f_5 + f_6 \quad (8)$$

### 3. Parameter Regulation

#### 3.1. FUNCTION WEIGHTS SETTINGS

Before inputting  $X_n$ ,  $Y_n$  and  $A_n$  to optimize the objective function  $f$ , there are 6 coefficients,  $k_1$ ,  $k_2$ ,  $k_3$ ,  $k_4$ ,  $k_5$  and  $k_6$  adjusting the weights of sub-functions. Different settings of these six parameters may result in totally different optimums, showing the design strategies from different design requirements. To find the best settings, several tests were carried out.

First,  $k_1$  and  $k_2$  were set as huge numbers, so that once the geometric error happens, the penalty functions will work in priority to drag the optimizing process back to the acceptable track.

Then, priority was given to different sub-functions by enlarging corresponding  $k$  value, to test the effect of each reward function. Figure 5 shows the generated results. The optimizing process starts from an initial status that all buildings are arranged in the center of the site, where  $X_n = 0.5$ ,  $Y_n = 0.5$ , and  $A_n = 0$ .

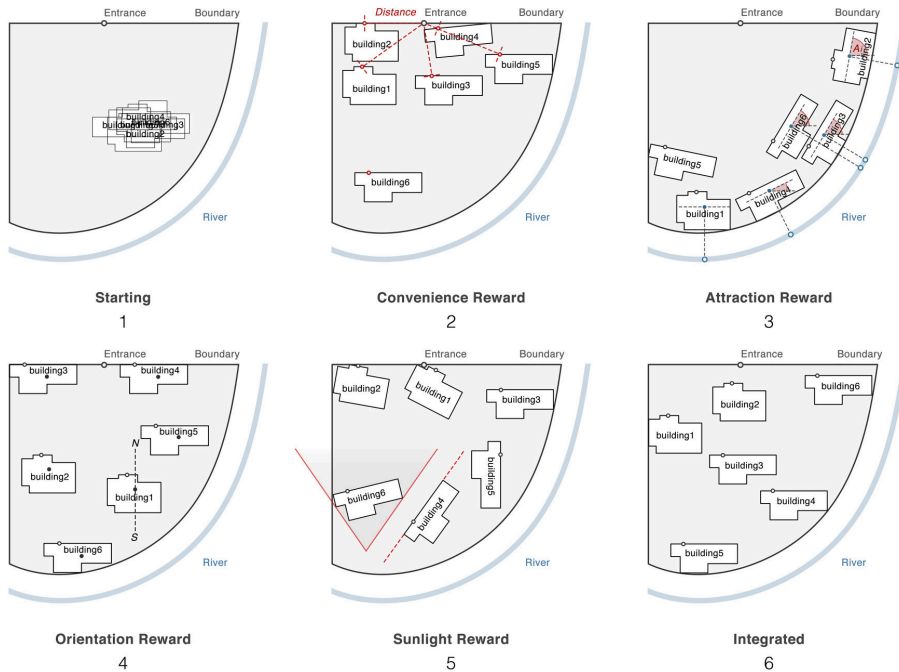


Figure 5. Generated Results with Different Parameter Weights.

In figure 2), with a more considerable  $k_3$  value for the Convenience Reward, the buildings gather near the entrance, but only building No.6 still stands far away from the entrance because of the bonus of not shadowing other buildings. In figure 3), the Attraction Reward acts as the primary role, so all buildings are placed along the river and facing toward the nearest points in the river. In figure 4), while the Orientation Reward forces all buildings to keep zero-rotated, other factors like the

attraction of landscape and entrance still work to construct the proper architectural layout. In figure 5), when the Sunlight Reward provides more bonus points, buildings tend to become more rotated and very precise in positions to avoid being covered by the shadows of other buildings. Especially for building No.4, it turns itself a lot to precisely match the boundary of the shadows from building No.6. In figure 6), a balanced consideration of parameter weights is applied to the objective function, so that all factors work together to generate a layout that, building No.2 follows the Convenience Reward, building No.5 follows the Attraction Reward, building No.1, No.3, and No.4 follow the Orientation Reward, and building No.6 follows the Sunlight Reward.

### 3.2. TEMPERATURE AND COOLING SETTINGS

With the integrated weight settings found in the previous tests,  $X_n$ ,  $Y_n$  and  $A_n$  were then inputted into the Simulated Annealing for optimizing. Galapagos in Grasshopper was used as the calculator to run the algorithm.

Mention before, in Simulated Annealing,  $t_s$  is the starting temperature value and  $T(t)$  is the function to update the temperature parameter, which is usually a recursive decreasing function as following:

$$T(t) = k_t \cdot t \quad (9)$$

In Galapagos,  $t_s$  and  $k_t$  can be given by the users as “temperature” and “cooling” to define how significant the initial probability of acceptance and the decreasing rate should be. Different settings may affect the efficiency of the optimizing process and the final result. Figure 6 shows the layouts of different settings after running the program for 5 minutes. Generally speaking, when  $t_s$  is equal to 100%, and  $k_t$  is equivalent to 0.95, the objective function  $f$  is more significant than other results.

Comparing the figures in each row, when  $k_t$  keeps the same, settings with more substantial  $t_s$  value will generate a better layout, whose  $f$  value is more significant. This phenomenon indicates that the optimizing process for an architectural plan is very complicated, it contains multiple locally optimal solutions, so the more significant initial probability of acceptance will help the process avoid being trapped in the early stage.

However, comparing the figures in each column, more considerable  $k_t$  value does not help to improve the results. For example, in figure 3), when  $k_t$  is equal to 0.99, which means the probability of acceptance almost keeps constant, the optimizing process runs very slowly. Hence, all buildings are still close to the initial status and stick together. Because the decreasing rate is too low, the optimizing process will keep accepting worse conditions and stay on a very superficial level, which is very inefficient. But if  $k_t$  value is too small, for example, 0.90, which means the decreasing rate is too large, the process will soon close its gate for accepting worse status, then be trapped in local optimal. Therefore, the experiments tell that the best  $k_t$  value is 0.95 for architectural layout optimizing. But if there is no limitation for the running time, the settings with more considerable  $k_t$  value should perform better.

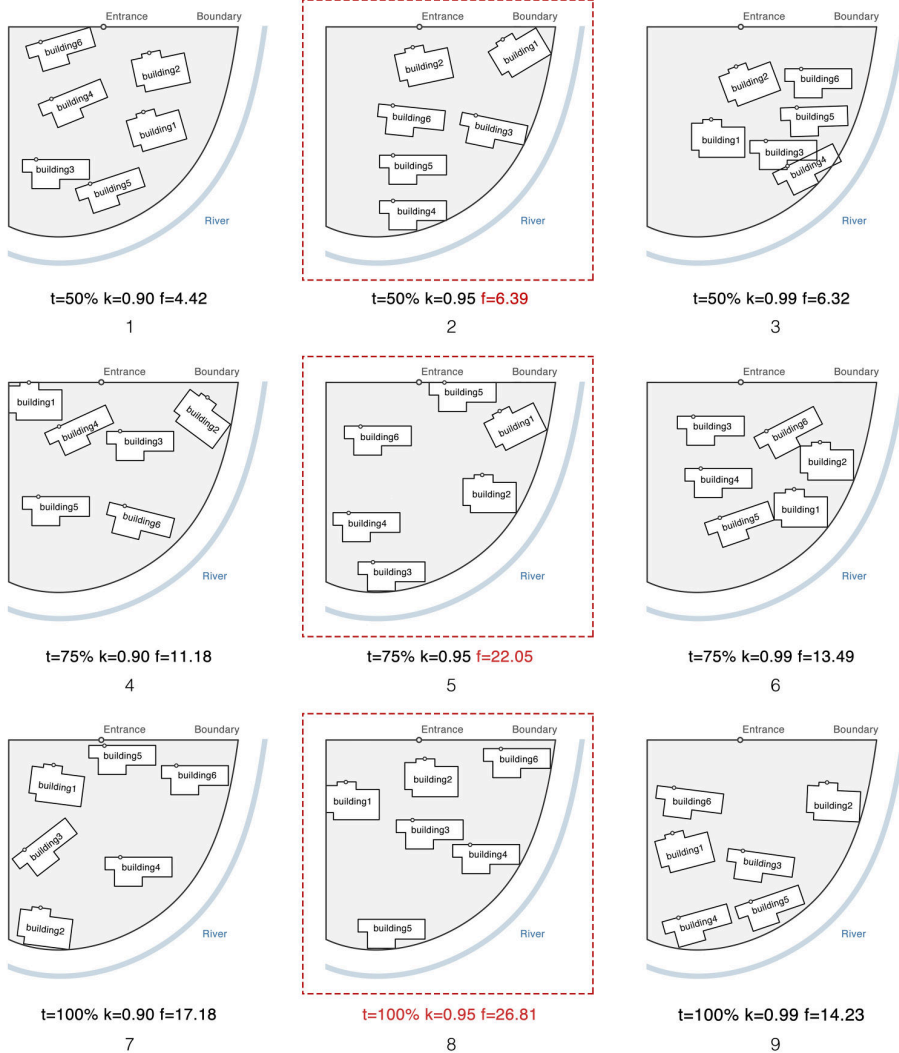


Figure 6. Layout Results with Different t and k Values.

#### 4. Conclusion

Simulated Annealing is a powerful artificial intelligence algorithm for finding the optimal solution based on the metropolis algorithm and the physical annealing process. Simulated Annealing can be applied to optimize architectural layout design, with customized penalty and reward functions and proper settings of parameter weights. Out-of-boundary penalty, overlapping penalty, convenience reward, attraction reward, orientation reward, and sunlight reward work together as the objective functions to guide the optimizing process. When running the



algorithm, proper settings of the “temperature” and “cooling” parameters in Simulated Annealing help avoid the local optimal to find the global optimal and increase the efficiency.

In the future, by setting the weights of the objective functions, architects can translate their design ideas and strategies into parameters, and efficiently use the Simulated Annealing to generate architectural layout design plans, which releases architects from building arranging work in an early stage.

## References

- Abramson, D.: 1991, Constructing school timetables using simulated annealing: sequential and parallel algorithms, *Management science*, **37** (1), 98-113.
- AlHalawani, S., Yang, Y., Liu, H. and Mitra, N.J.: 2013, Interactive Facades Analysis and Synthesis of Semi-□Regular Facades, *Computer Graphics Forum*, **32**, 215-224.
- Ekren, O. and Ekren, B.Y.: 2010, Size optimization of a PV/wind hybrid energy conversion system with battery storage using simulated annealing, *Applied Energy*, **87** (2), 592-598.
- Hong, W.: 2011, Traffic flow forecasting by seasonal SVR with chaotic simulated annealing algorithm, *Neurocomputing*, **74** (12-13), 2096-2107.
- Kirkpatrick, S., Gelatt, C.D. and Vecchi, M.P.: 1983, Optimization by simulated annealing, *science*, **220** (4598), 671-680.
- Metropolis, N., Rosenbluth, A.W., Rosenbluth, M.N., Teller, A.H. and Teller, E.: 1953, Equation of state calculations by fast computing machines, *The journal of chemical physics*, **21** (6), 1087-1092.
- Michalek, J., Choudhary, R. and Papalambros, P.: 2002, Architectural layout design optimization, *Engineering optimization*, **34** (5), 461-484.
- Sen, M.K. and Stoffa, P.L.: 1991, Nonlinear one-dimensional seismic waveform inversion using simulated annealing, *Geophysics*, **56** (10), 1624-1638.
- Sonmez, F.: 2008, Structural optimization using simulated annealing, *Simulated annealing*, **2008**, 281-306.
- Tracey, N., Clark, J. and Mander, K.: 1998, Automated program flaw finding using simulated annealing, *ACM SIGSOFT Software Engineering Notes*, **23**, 73-81.
- Yeh, I.: 2006, Architectural layout optimization using annealed neural network, *Automation in Construction*, **15** (4), 531-539.

# GENERATION OF PUBLIC SPACE STRUCTURE BASED ON DIGITAL MULTI-AGENT SYSTEM

*Taking the interaction between self-consensus “Stigmergy” particles and the old city area as an example*

ZHUOXING GU<sup>1</sup> and CHUNXIA YANG<sup>2</sup>

<sup>1,2</sup>Tongji University

<sup>1</sup>guzhuoxing@126.com <sup>2</sup>Yang\_arch@163.com

**Abstract.** In the study, the ant colony behavior was simulated to establish a parametric multi-agent system with independent consensus “Stigmergy” for interaction with the site. In the experiment, the initial points of the particles correspond to the key historical buildings, and the target points correspond to the important public space nodes. Edit and adjust the motion characteristics, search features, generation and disappearance characteristics of the simulated particles to obtain the main consensus particle swarm distribution and the distributed consensus particle swarm distribution. This form has a compliant or conflicting relationship with the existing urban environment. Using the contours of the self-consensus spatial form, the particle swarm density, and the pointing relationship between the particles and the building can provide a basis for the transformation and renewal of the existing urban environment, thus forming a spatial transformation strategy that more closely matches the user behavior in the space.

**Keywords.** Multi-agent system; Particle property construction; Stigmergy; Self-consensus particles; Public space structure.

## 1. Research on Complexity and Regional Urban Design

Since the 1960s, self-organization theory has been used to study the formation and development of complex systems, including living systems, social systems, and natural ecosystems. That is, under certain conditions, how does the system evolve from disorder to order automatically, from low-order to high-order. Bottom-up, spontaneity and emergence are the important basis of self-organization theory. (Andrasek 2016)

### 1.1. SYSTEM AND ENVIRONMENT-SWARM WISDOM

Manuel DeLanda outlined in “New Materialism”: the formation of matter is the process of the interaction, iteration, evolution, and gradual stabilization of real elements. The core idea is to focus on the establishment of material individuals. Individuals affect each other through various “rules”, and the final macroscopic

result of the group forms material. (Yang 2019) Delanda's research inspired urban design to focus on urban systems and operating mechanisms, rather than looking directly at physical space. Researchers look for factors that can act as agents of social activities or the urban environment, and then form "Swarm wisdom" through the interaction of individual elements, reflecting the operation, development and evolution of the city.(Reydon 2002)

In the 1980s, the wool experiment used the "wet grid" formed by the mechanical interaction of water molecules to make the wool's curved form closely integrate with the water environment. Compared with the L-system, the experiment achieves the simulation of "swarm intelligence" through the iterative interaction of individuals, which objectively reflects self-organization. (Weixin and Weiguo 2009) Coincidentally, in 2017, Kokkugia Architects used "swarm intelligence" as a design tool to realize self-organized urban system simulation and generate urban space. This "Swarm Urbanism" project builds a multi-agent system based on abstract social relations, energy, and information flow, and empowers agent particles to interact with information paths (stigmergy).

For urbanization, applying group logic can transform the concept of overall planning into an overall algorithm. Based on the calculation, iteration, and accumulation of urban elements, the evolution process of spatial form is not an empirical judgment and decision.( Weixin and Weiguo 2009) It is hoped that such a design method can speed up the matching of spatial forms and social relations, reach a more stable state, and reduce consumption and contradictions as much as possible.

## 1.2. SYSTEMS AND SYSTEMS-RECIPROCAL RECIPROCITY

Nurturing reciprocity in nature is a sustainable relationship, similar to a self-organizing process. In the 1990s, Gilles Deleuze and Félix Guattari's "Rhizome" concept extensively discussed the mutual adaptation and interaction logic of animal groups. Birth is the basis for the generation of group forms, and individual wisdom is the key to forming group wisdom. The evolution of this relationship is explained through the relationship between wasps and orchids. (Leach 2010) Individual plants need to communicate with each other, and insects should be used as their communication medium to encourage plants to produce sugar to attract wasps. The wasp approaches the orchid at a specific speed and direction, and decides how long to stay in the orchid according to its needs. In the end, the wasp gets food, and the orchid carries the information that needs to be transmitted to the wasp. Repeatedly, the relationship between the wasp and the orchid has reached a steady state, and the self-organizing relationship is reciprocal. Wasps and orchids are not only individuals with unique needs, but between the wasps and the wasps, and between the orchids and the orchids, they are groups of collective wisdom.

The focus of urban self-organization research is to treat urban elements and active people as intelligent groups and establish mutually beneficial relationships so that each can be optimized accordingly. The interaction between the crowd, the interaction between the crowd and the urban building space, functional layout, and natural environment does not follow a single logic. Crowds are attracted by

various functions or environments in the city, and their behaviours are changed because of various obstacles and alienation of needs. They constantly feedback and restrict each other, and eventually achieve some kind of reciprocity. (Chen 2003) Cities have affected the crowd, and the crowd has also affected the city. In the absence of strong external forces, the crowd and the city each take what they need in the process of interaction. Such principles are rarely mentioned in the study of urban dynamics. Therefore, constructing the interaction mechanism between the crowd and the city should also follow the principle of reciprocity, which reflects the macro emergence of the underlying logic.

## 2. Complex of historical protected areas

The swarm multi-agent system provides a medium for the study of urban complex dynamic systems between historically protected building groups. Through the translation of self-organized particle point information, the relationship between the public space scale, space connection, and space accessibility among building groups can be simulated. (Weixin and Weiguo 2009) The basic steps are as follows: First, establish the “personality” code of conduct of the particle swarm, so that the individual particles can move in space according to the rules established by the research, and the particles do not interfere with each other. Then, the interaction between the particle groups and the interaction between the particles and the site can be given special “rules”, and the parameters can be adjusted to obtain a specific particle group distribution pattern. Then, the information distribution during the self-organization process of the particle swarm is extracted, including space coordinates, velocity vectors, and force systems. Finally, combined with the wisdom of the designer, the results of particle swarm interaction with the site can be translated into physical space. Such as space size, enclosing interface, landscape form, etc., and then generate self-organizing characteristics of regional urban renewal space image.

Hengfu historical and cultural style area is the largest historical block in Shanghai. Formed in the first half of the twentieth century, it was originally a French Concession, which reflects the features of Shanghai’s modern residential and public places. The total area of Hengfu style area is 7.66 square kilometres, of which Xuhui area is 4.3 square kilometres. It has deep historical and cultural heritage and is the birthplace and bearing area of Shanghai’s cultural context. There are 950 outstanding historical buildings in the Hengfu style area, 1774 preserved historical buildings, and 2259 ordinary historical buildings. Including various styles of independent garden villas, new-style lanes, apartments and other residential buildings and elegant and sophisticated commercial office, cultural and entertainment, medical, education and scientific research, religion and other areas of public buildings.

This study selected historic buildings densest Fuxing Xi - Ferguson Lane - Hunan Road - Yongfu Road for the test area. In the construction of the simulation system, there are historical buildings such as Liangyou Apartment, Ke Ling Former Residence, Gu Zhutong Former Residence, Ba Jin Former Residence, Zhao Dan Former Residence, Yongfu Club, and many garden houses and apartments as important historical protection buildings. The relationship

between these historic buildings and public space has become an object worth optimizing. Therefore, based on the tight and tortuous urban space mechanism of its old city, its public space structure is optimized so that the outstanding historical building communities in the region can be closely connected, connected and accessible. In addition, optimizing the multiple spatial scales of its public space network to match more activity forms has become an update strategy that is more conducive to the area. Therefore, in this research scheme, an independent consensus particle swarm algorithm is used to make the main public space structure formed by particle consensus among outstanding historical buildings, in order to find a suitable main public space layout and scale. At the same time, the discrete scale and information transmission scale of the autonomous consensus particle swarm are adjusted to diffuse its organizational structure, form a richer roaming path, and optimize the level and structure of public space.

### **3. Construction of swarm multi-agent complex system**

The establishment of an autonomous consensus multi-agent system simulation medium can uniformly study the spatial scale of historical building communities, and the location information distribution and movement information of particle swarms can become the basis for the design of the shape. Multi-agent system has the characteristics of flexibility and intelligence, which can meet the needs of research. It uses multiple intelligent independent agents in local space to fully simulate group movements. The final group movement result is the result of interaction between each agent and the environment.(Gu 2017) As mentioned earlier, the use of autonomous consensus of swarm particles to generate public space is mainly divided into two key steps: 1) Shaping autonomous consensus particles and rules of movement, so that the swarm particle swarm can form ants nests, turtles Natural and continuous non-linear space mechanisms such as cracks; 2) Set the particle swarm starting point and passing point in the environment so that the public space system has the starting point and passes the necessary area.(Snooks 2016) Therefore, we can use a software platform with a multi-agent system to establish “particle swarms” and a simulation cellular matrix, thereby simulating the interaction between the autonomous consensus system and the external environment.

#### **3.1. SHAPING AUTONOMOUS CONSENSUS PARTICLES AND RULES OF MOTION**

Self-organizing algorithms originate from the concept of stigmergy in the biological world. It describes that the biological individual independently completes the next task by identifying the information and remnants left by other individuals, such as the information exchange of bee colonies and the movement of ant colonies. (Snooks 2016) This also inspired designers to establish indirect information inheritance among the particles of the multi-agent system, so that the particle movement follows, approaches, and finally integrates into a group “consensus” path. (Snooks 2016) In our multi-agent system space, the simulation cellular matrix in the previous article can be used as a unit for storing particle motion information. And record the particle’s motion information in the cell, and

then reserve the information to affect the subsequent particle’s motion. In this way, the trajectory and direction of the particles before and after will be coupled and inherited from each other, and a coherent, obvious and unified comprehensive path and movement mode will spontaneously appear. By adjusting the rate of birth and death of particles per unit time, the density of the entire particle group can be controlled. (Figure 1)

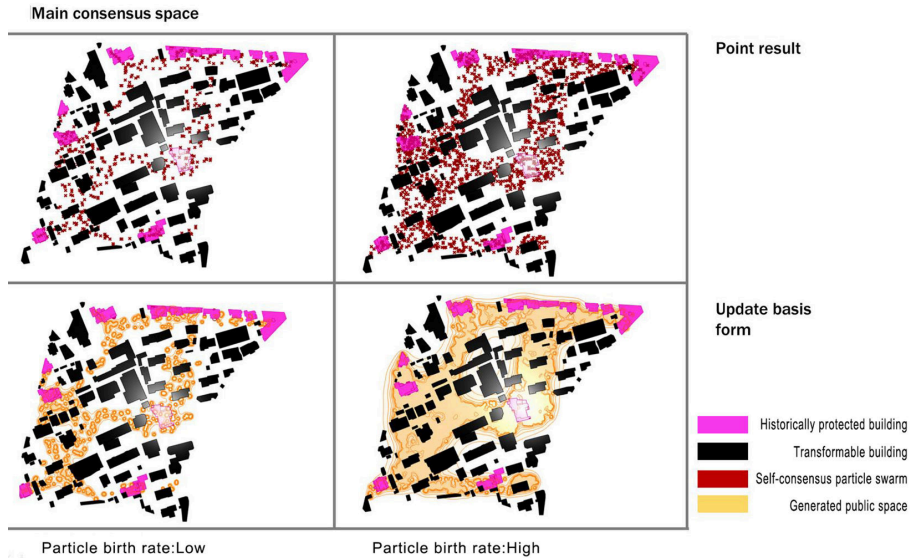


Figure 1. Generation of Main Consensus Space for Self-Consensus Particle Swarm.

Through the reservation information integration of the self-organizing information system (Stigmergy), the spontaneous and “intelligent” natural texture form will be obtained in the end. (Gu 2016) Reserved information in the particle capture space to affect its own motion. Therefore, by controlling the particle’s viewing angle width, capture range, influence factor  $p_{he}$  (the effect of reserved information on particle speed), particle speed and other parameters, it can affect the direction, density, and shape of non-linear texture, and perform graphic analysis. In addition, when we increase the calculation volume and calculation speed of the multi-agent system, increasing the number of agents will enable us to obtain rich natural shape simulations with huge amounts of information such as tree skins and soil cracks. In this way, autonomous consensus particles can form a continuous public space system with different scales.(Figure 2)

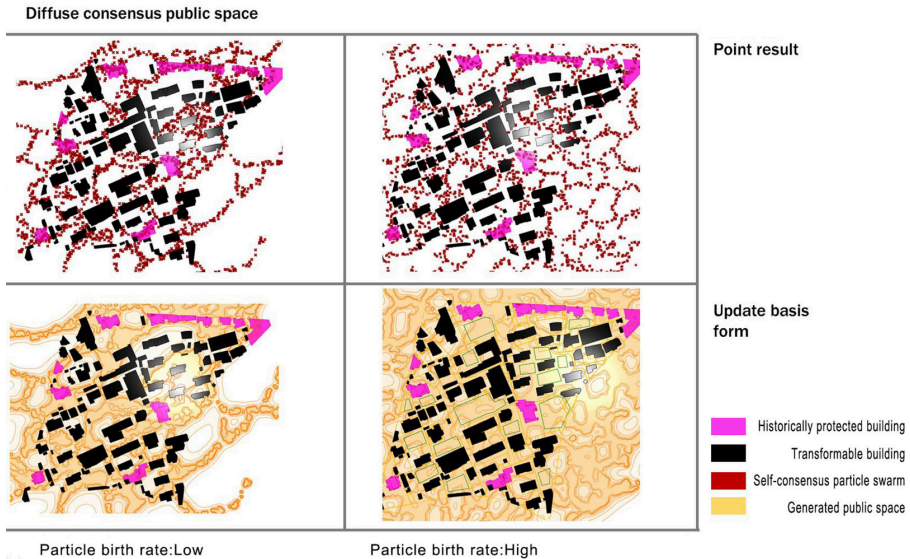


Figure 2. Consensus space generation for dispersive particle swarm.

### 3.2. APPLICATION OF PARTICLE SWARM STARTING POINT, PASSING POINT, AXIS

After the construction of autonomous consensus particle groups, we already have an agent system that matches the complex spatial structure of historical building communities. Next, we need to set the starting point, passing point, and destination point of the agent system space, so that the public space system is connected as a whole. In the Hengfu historical and cultural style area, we take outstanding historical buildings, preserved historical buildings, and former residences of celebrities as the main starting point and ending point, and try to use particle groups to find an optimized public space system between them. (Snooks 2016) At the same time, the research plot already has urban forms. These areas that can be reserved or rebuilt can coexist with autonomous consensus space. Looking for its reserved area and transformation area in the update plan, a new public space system can be formed eventually. It is worth mentioning that during the optimization of the space system, there are already fragmented public space sites in the study area, and their utilization rates are also different. They can be inducible factors in public space, allowing swarm particles to traverse them by autonomously seeking. Eventually, these original public space systems and autonomous systems were accommodated together, so that the renewal plan formed a good connection with the original space system.

The interaction between particle swarms and the environment can generate various types of swarm axes, of which the swarm axis and target axis are of great significance for space transformation. The particle swarm's own axis can reflect the distribution characteristics and distribution state of the particle swarm. For

example, in this case, the spatial axis of the main consensus particle group implies the possible distribution area of the main public space, and the distribution state of the diffuse particle group can also be referred to by its axis. And the connection between the particle swarm and the interactive target in the area can reflect the average distance between the group and the target, so as to lay the foundation for a reasonable planning partition. In this case, the shortest service path connection is obtained by integrating the shortest distance between the particle swarm and all targets, that is, the shortest path from each historical building to each point of the consensus space particle swarm. It is conceivable that for each point in the consensus public space, the closest historical building is the one with the closest walk and visual interaction. (Figure 3) Therefore, the architectural design and planning in this area can be carried out according to the needs of historical buildings.

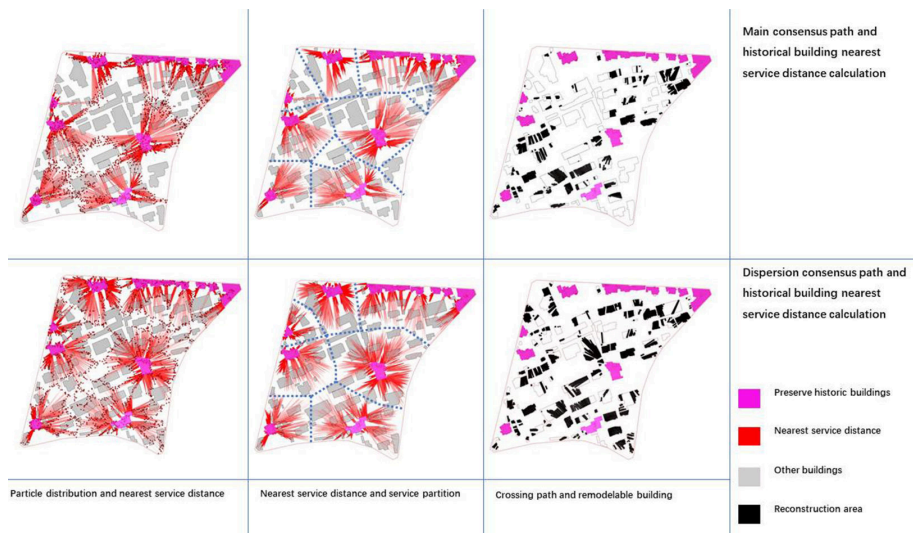


Figure 3. Consensus particle plane distribution and shortest distance application.

### 3.3. APPLICATION OF PARTICLE SWARM BOUNDARY AND DENSITY

In the process of morphological variation and development of the autonomous consensus particle swarm, the particle network structure can be induced to two types of concentrated particle shape and diffuse type by adjusting its movement rate, observation radius, particle birth and mortality and other variables (Figure 4). (Snooks 2016) Concentrated particle groups can quickly connect important historical building communities together. And bypass or pass the original building, making the public space that needs to be retained or added in the original urban mechanism is clearly visible, and other buildings that need to be retained or reduced are clear at a glance. In the end, a major public space was formed, and all important historical buildings in the area were communicated. A historical architectural cultural system was formed, laying the foundation for the unified



development of functions, unified culture and streamlined coordination. At the same time, dispersive particle swarms can form a walkable public space network with pleasant scales and winding paths. These networks can complement the main consensus space, providing multiple choices of space function, scale, and privacy. In the end, the autonomous consensus particle swarm can spontaneously form a complex public space morphological basis in the study area with the protection of the building community as the communication object.

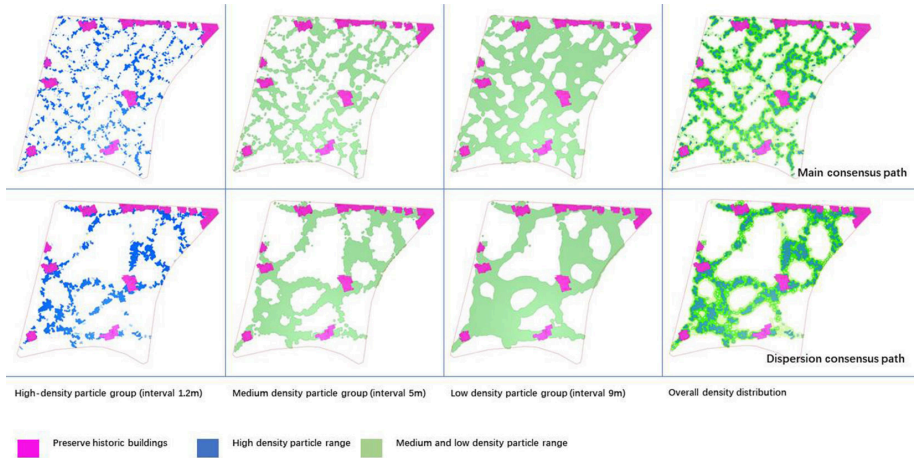


Figure 4. Consensus particle plane distribution and density application.

As a swarm system, the coordinate information and density information of particle swarms can be directly used by design and scientific researchers. For example, in this study, a density analysis is performed on the particle population, and its density is divided according to the scale of human activity. That is, the particle interval is 1.2 meters, 5 meters, 9 meters (Figure 5) and other states to correspond to different spatial scales of social activities, necessary activities, and spontaneous activities. It can also be considered as a space privacy planning. Areas with large particle densities are suitable for public activities, and their space privacy is low. Corresponding public infrastructure and landscape spaces should be set up. On the contrary, in areas with low particle density, more individual facilities and recreational spaces can be set up to provide users with a variety of choices while improving the privacy of public spaces. In the plane analysis diagram, we can see that the space system after the particle transition does not clearly separate the public and private spaces. The two are gradual transitions and contain each other, which is one of the inspirations that particle swarms bring to us.

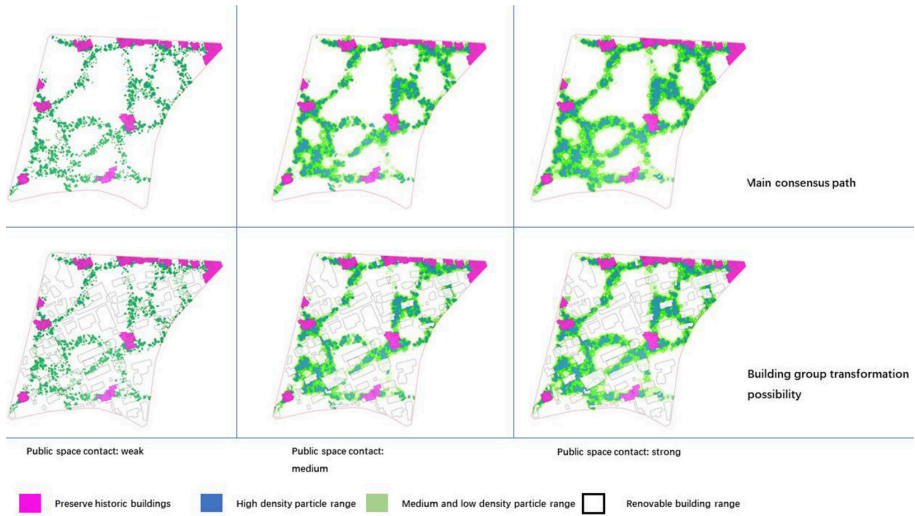


Figure 5. Plane public space of main consensus particles and its connectivity application.

In the distributed application of the main consensus particle swarm and the dispersive particle swarm, we can control its public space connectivity by adjusting its public space coverage radius. It can be seen in the map that the designer can control the division of space and connectivity by adjusting the particle radiation radius and the grouping of particle groups. And these parameters are freely combined, and based on the particle swarm density information, the space is controlled and reshaped according to special needs such as site functions, thereby giving the area space more possibilities for updating. (Figures 5 and 6)

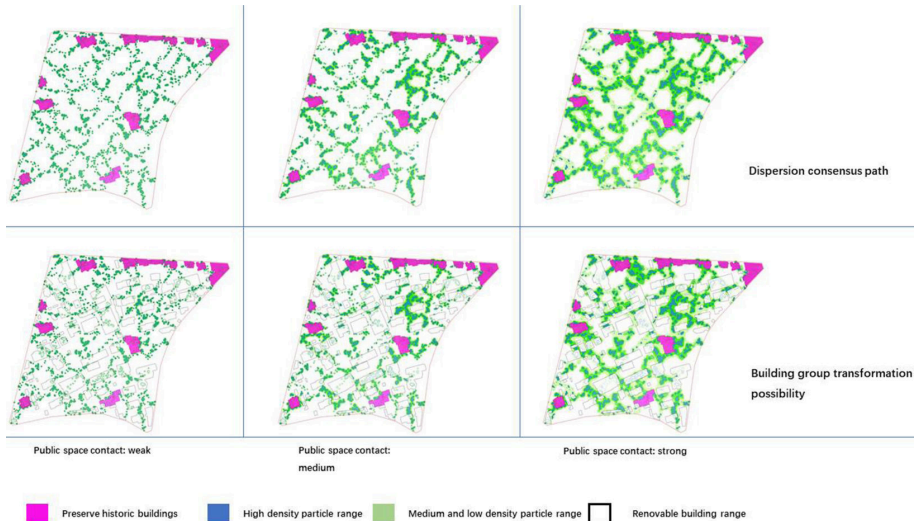


Figure 6. Plane public space with diffuse consensus particles and its connectivity application.

#### 4. Summary

In this study, an autonomous consensus is defined for the simulated particles through the swarm digital multi-agent system platform. The particle swarm interacts with the historical building community and the original public space of the site to communicate with the historical building group, forming a new public space generation basis and system. In addition, its particle motion information, coordinate information, group boundary, density, and the shortest distance to the interactive target can be transformed into a spatial structure system with the characteristics of a consensus network.

In general, the focus of this life shape strategy is to build a digital integrated platform to explore the form in a bottom-up manner. This is a departure from the traditional direct digital form of non-linear space. The use of an autonomous consensus algorithm increases the flexibility and complexity of the particle swarm, increases the uncertainty of the results and the difficulty of form finding control. And the design toughness of the multi-agent system is reflected. The particles do not run according to the precisely planned motion trajectory, but by adjusting their respective movement states, they finally form an organic continuous network form that can be identified. In addition, the particle swarm can construct a structural space based on the morphological information to solidify the simulation results. The network structure, space effect, and overall texture of the solidified result all reflect the characteristics of the consensus public space system of the historic building community in the site.

This study demonstrates the reorganization and fusion process of autonomous consensus particle swarms and historical building communities, and finally explores an operable morphogenesis strategy. Among the many digital form derivation methods, this is just the tip of the iceberg. We hope that the particle simulation methods and results presented in this article will help designers to see the benefits of digital design methods' forward-looking, toughness, openness, and uncertainty to the design process. This "bottom-up" form-finding method is worth exploring and using by designers.

#### References

- Andrasek, A.: 2016, "Xenocells: In the Mood for the Unseen.", *Architectural Design*, **86.6**, 90-95.
- Chen, Y.: 2003, Self-organization and self-organizing cities, *City Planning Review*, **27(10)**, 17-22.
- GU, Z., YAO, J. and YANG, C.: 2017, Research of Generation of Fluid Special Forms with Parametric Method, *Housing Science*, **12**, 15.
- Leach, N.: 2010, "Swarm Urbanism.", *Architectural Design*, **79**, 56-63.
- Reydon, T.: 2002, Emergence: The Connected Lives of Ants, Brains, Cities, and Software, *History & Philosophy of the Life Sciences*, **1**, 125-127.
- Snooks, R. and Jahn, G.: 2016, *Stigmergic accretion. Robotic Fabrication in Architecture*, Springer International Publishing.
- Weixin, H. and Weiguo, X.: 2009, "Form Finding" in Non-linear Architectural Design, *Architectural Journal*, **(11)**, 29.
- YANG, C., GU, Z. and YAO, Z.: 2019, Taking The Urban Renewal Design Of Shanghai Hongkou Port Area As An Example, *Proceedings of CAADRIA 2019*.

# ESCAPING EVOLUTION

## *A Study on Multi-Objective Optimization*

INÊS PEREIRA<sup>1</sup>, CATARINA BELÉM<sup>2</sup> and ANTÓNIO LEITÃO<sup>3</sup>  
<sup>1,2,3</sup>*INESC-ID, Instituto Superior Técnico, Universidade de Lisboa*  
<sup>1,2,3</sup>*{ines.pereira|catarina.belem|antonio.menezes.leitao}@tecnico.ulisboa.pt*

**Abstract.** The architectural field is currently experiencing a paradigm shift towards a more environmentally-aware design process. In this new paradigm, known as Performance-Based Design (PBD), building performance emerges as a guiding principle. Unfortunately, PBD entails several problems, for instance, building design is often associated with the simultaneous assessment of multiple performance criteria, which dramatically increases the complexity of the problem. In this vein, recent works claim that coupling optimization tools with PBD approaches allows for more efficient and optima-oriented strategies. This approach, known as Algorithmic Optimization, is based on the use of an optimization tool combined with a parametric model of a design to iteratively generate more efficient design alternatives. This paper focus on evaluating and comparing different classes of Multi-Objective Optimization (MOO) algorithms, namely, metaheuristics and model-based ones. In addition, in order to try to better understand the algorithms' suitability to different optimization problems, this research analyses two different MOO design problems.

**Keywords.** Performance-Based Design; Algorithmic Optimization; Multi-Objective Optimization.

## 1. Introduction

Prompted by environmental concerns and technological developments, the architectural field is currently experiencing a paradigm shift towards a more environmentally-aware design process. In this new paradigm, building performance emerges as a guiding principle, where analysis tools are used from the initial design stages to promote more informed design decisions - a paradigm known as Performance-Based Design (PBD) (Kolarevic and Malkawi 2005). Unfortunately, PBD entails several problems, namely, (1) even when parametric models are used, PBD frequently requires the tiresome manual generation and evaluation of different design alternatives; (2) it can be difficult to know a priori which design variations should be evaluated in order to ensure the optimality of the final design; and (3) building design is often associated with the simultaneous

assessment of multiple performance criteria, which dramatically increase the complexity of the problem.

In this vein, recent works claim that coupling optimization tools with PBD approaches can help circumvent the aforementioned problems, allowing for more efficient and optima-oriented strategies (Wortmann 2017; Belém and Leitão 2018). This approach, known as Algorithmic Optimization (AO), is based on the use of an optimization tool combined with a parametric model of a design to iteratively generate more efficient design alternatives.

Optimization has shown to benefit the architectural practices both in academic and industry worlds (Nguyen et al. 2014; Wortmann et al. 2015; Hamdy et al. 2016). However, most works often focus on Single-Objective Optimization (SOO) problems, failing to address the reality of the architectural context, which often requires the simultaneous optimization of multiple aspects, such as, structural behavior, lighting performance, thermal comfort, and costs. Additionally, most existing works on Multi-Objective Optimization (MOO) concentrate on studying just a particular class of metaheuristics algorithms, the Evolutionary Algorithms (EAs) (Hamdy et al., 2016; Evins et al., 2011), not exploring other promising algorithms like model-based or direct-search ones, or even other metaheuristics, such as Particle Swarm Optimization (PSO) algorithms (Wortmann et al. 2015).

This paper focus on addressing the limitations presented previously, by evaluating and comparing the performance of different classes of MOO algorithms, including both metaheuristics and model-based ones, since the latter have been showing promising results regarding SOO problems (Belém and Leitão 2018; Wortmann 2017). Moreover, to try to better understand the algorithms' suitability to different problems, this research analyses two MOO architectural design problems: (1) the optimization of an arc-shaped space frame's structural aspects, and (2) the daylight optimization of an exhibition space in Lisbon.

## **2. Optimization in Architecture**

Architectural problems usually involve dealing with multiple objectives that need to be contented simultaneously. Additionally, these objectives usually conflict with each other, meaning that the best solution regarding one of them is generally not the best solution for the others (Khazaii 2016). In this perspective, one of the main goals of a MOO approach towards a PBD is to find the best way to reconcile all these objectives (Kolarevic and Malkawi 2005). In addition, the computational resources required to perform the optimization prompt the need for more efficient algorithms, which can search for optimal solutions within the fewest evaluations possible. The following subsections contextualize architectural optimization and evidences the need for better performing and more diverse optimization tools.

### **2.1. MULTI-OBJECTIVE OPTIMIZATION**

One possible strategy to address MOO problems is to simplify them by combining the objectives in a single weighted function, and solving it as a SOO problem (Nguyen et al., 2014). Unfortunately, despite allowing users to handle MOO problems, this strategy does not consider the different trade-offs among the

potentially conflicting objectives, instead forcing architects to make an *a priori* decision regarding the importance of each objective. Conversely, Pareto optimization approaches attempt to address this limitation by postponing that decision until the end of the optimization process. This optimization approach treats all objectives as equally important during the search, making it more difficult to discern the quality of each solution. In fact, instead of a single solution, Pareto optimization approaches typically comprise a set of optimal solutions that represent the situations where it is impossible to improve an objective without deteriorating others. Such solutions are also called non-dominated, and together they comprise the Pareto front. On the other hand, the non-optimal solutions are called dominated, representing the ones that are worse than another solution at least in one objective and no better in any other, hence being dominated by a better solution. When confronted with non-dominated solutions, architects can compare the different design options according to different performance criteria, and, thus, make more informed decisions about the different compromises involved.

## 2.2. BLACK-BOX OPTIMIZATION

After modeling the optimization problem, it is up to the optimization algorithm to explore it and to find optimal solutions. While there seems to be no algorithm that outperforms all others for every problem, some algorithms do perform better for some particular problems (Wolpert and Macready 1997). In architecture, where simulations are very time-consuming, finding such algorithms is key to minimize the time complexity of optimization processes (Shi et al. 2016).

From the wide variety of existing optimization algorithms, only a subset of them can be used in practice due to the nature of the objectives, whose values are obtained via expensive simulations instead of being determined by analytical means. Since the latter are not available, optimization algorithms that explore information (e.g., slope, direction towards optima) about the objective functions' derivatives to guide the search more rapidly towards the optima cannot be used. Instead, the optimization process must be guided by algorithms that treat the objective functions as black-boxes for which no information is available except that obtained from previously evaluated solutions. For this reason, these algorithms are known as black-box optimization algorithms.

The set of black-box optimization algorithms encompasses algorithms with different underlying assumptions and properties, namely, (1) metaheuristics, which rely on randomization, and biological or physical analogies, (2) direct-search, which iteratively evaluate a set of candidate solutions, proposed by a deterministic strategy, selecting the best solution obtained up to that moment, and (3) model-based, which create approximations of the true objective functions based on previously evaluated solutions, optimize them, and then use the resulting solutions to iteratively refine the approximations (Wortmann and Nannicini 2016).

Despite the variety of black-box optimization classes, the architectural community seems to prefer EAs (Evins 2013; Hamdy et al. 2016) - a subclass of metaheuristics algorithms based on the evolution principles. A review over current optimization tools shows that the vast majority (e.g., Galapagos, Optimo, Octopus, Wallacei) only focus on EAs, with few exceptions, Goat and Opossum,

which support other algorithms, including model-based ones.

The need for optimization tools to offer a wider variety of algorithms is based on the idea that some algorithms may be more suitable for specific problems. Selecting the most efficient algorithm to address a MOO problem can greatly decrease the overall complexity of the optimization process, by reducing the number of simulations needed to find the optimal solution.

### **3. An Algorithmic Optimization Methodology**

The methodology this paper follows concerns: (1) the data collection for different MOO processes using a variety of optimization algorithms, taking advantage of an AO workflow inspired by Pereira et al. (2019); and (2) the evaluation and comparison of the optimization algorithms, according to different criteria, such as the quality and diversity of the Pareto Fronts.

The AO workflow enables the automation of MOO processes through the combination of parametric modeling with optimization algorithms and analysis tools: the MOO algorithm iteratively instantiates the parametric model by proposing new values for the parameters, then the resulting design variant is evaluated by the analysis tools, being the results sent back to the optimization algorithm. This process is repeated until a stopping criterion is satisfied, after which the optimization results are collected for visualization or, optionally, for later comparison with other algorithms' results.

Despite the lack of guidelines regarding the best way to compare MOO algorithms, most MOO literature seems to adopt a metric based on the volume of the dominated objective space, named hypervolume (While et al. 2006). This can be explained due to its guarantees for: (1) Pareto compliance, i.e., a set of solutions that completely dominates another necessarily yields a greater volume than the latter, and (2) any set of solutions that achieves the maximum possible volume is guaranteed to contain all non-dominated solutions. Additionally, the algorithms can also be compared in terms of their hypervolume per iteration, thus providing a way of comparing the algorithms' relative performance.

### **4. Evaluation and Results Discussion**

This research also aims at understanding the impact of the optimization problem in the algorithms' performance, by analyzing two different case studies, considering different performance objectives. Additionally, given that most MOO studies focus on the application of metaheuristics, more specifically on EAs, this paper extends the state-of-the-art by also benchmarking non EAs, including another subclass of metaheuristics, the PSOs, and a few model-based algorithms. Recent studies in building design, regarding SOO, have shown that model-based algorithms achieve good results in fewer evaluations, thus significantly reducing the overall optimization time (Wortmann 2017). Hence, testing similar algorithms in a MOO context may be crucial to bridge the gap that exists in building design, where MOO problems are often simplified to cope with time constraints.

Regarding the evaluation, we followed the Pareto Optimization approach to address two MOO case studies and we compared a total of 10 algorithms: 4

metaheuristics and 6 model-based. Due to the randomization inherent to all algorithms, we ran each algorithm three times and averaged the results. To compare algorithms, we used the hypervolume, whose values vary from 0 to 1, with values closer to 1 meaning the Pareto Front dominates a larger region of the objective space and is, in principle, more diverse. Moreover, we conditioned each algorithm to execute at most 195 evaluations, thus simulating the time constraints of most architectural projects. Except for the number of solutions evaluated per iteration, all algorithms ran with their default parameters. Regarding metaheuristics, they were set to evaluate 15 solutions per iteration, whereas model-based algorithms created the approximations of the objective functions by first evaluating 100 (in the first case study) or 75 (in the second one), hence leaving the other evaluations to be completed in the course of the optimization.

The algorithms are compared in two stages: (1) we compare the Pareto Fronts obtained for the three runs for each algorithm, by combining them in a single plot, thus providing an overview over the extent and the convergence of each algorithm, and (2) we compare the evolution of the Pareto Fronts with the number of evaluations, by computing the hypervolume per iteration. The following sections present the case studies and discuss their evaluation. The first one is a more theoretical problem, whereas the second one shows how real-life architectural projects can benefit from MOO processes.

#### 4.1. CASE 1: ARC-SHAPED SPACE FRAME

The first case study consists in the optimization of both the structural behavior and an ad-hoc measure of the irregularity of an arc-shaped space frame. To instil irregularities in the space frame, we introduced three attractors that cause a deformation in the shape of the truss, each of which is defined in terms of its fixed-radius cylindrical coordinates in the arc-shaped space frame. Each design variant is evaluated in terms of (1) the maximum displacement of the structure, computed with the Robot structural analysis tool, and (2) the sum of the Euclidean distances between the attractors. Both objectives are meant to be minimized, hence promoting the conflict between them: placing the attractors near each other will weaken the structure and, thus, increase the maximum displacement of the space frame. In fact, to reduce the maximum displacement, the attractors should be scattered across the space frame but this implies larger distances among the three attractors, thus worsening the second objective. Figure 1 illustrates three examples of the space frame structure.

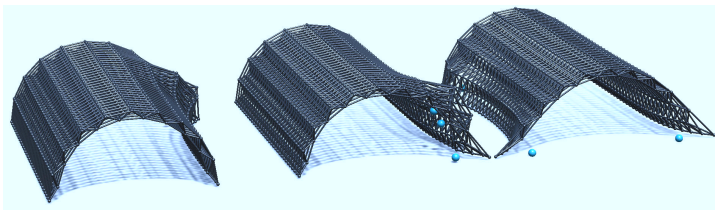


Figure 1. Three design variations of the space frame, with blue spheres as the attractors.



Figure 2 presents the results, combined over the three runs, for all the algorithms. Given that the true optimal solutions for this case are unknown and computationally difficult to identify, we considered a combined version instead, composed of the set of non-dominated solutions from all the evaluated ones. In this graph, it is possible to visualize that two PSO algorithms, namely SMPSO and OMOPSO, explored more extensively the objective space and are, therefore, capable of providing different valuable trade-offs. On the other hand, the EA SPEA2, together with the model-based algorithms, seem to have converged towards the same area, barely finding good solutions. Finally, despite diverging from previous algorithms, the EA NSGA-II and the model-based algorithm GPR\_SMPSO, were able to overcome that dense area and to explore larger regions of the objective space.

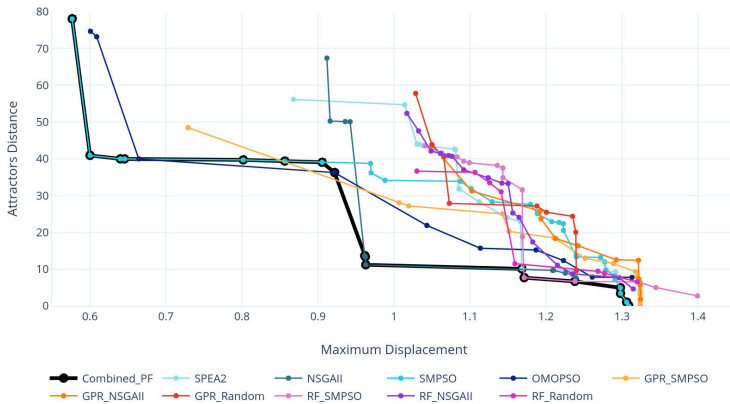


Figure 2. Space Frame: Pareto fronts for all tested algorithms. The combined Pareto front is formed by the non-dominated solutions from all the evaluated solutions.

The previous evaluation only provides us with a sense of the final results and is not really useful when we are interested in understanding how the algorithm evolves with the number of evaluations. Figure 3 shows the performance evolution for all tested algorithms, measured every 15 evaluations. As before, the PSO algorithms seem to attain better Pareto Fronts throughout the optimization process with the model-based GPR\_SMPSO approaching those results after 120 evaluations. It is noteworthy that, unlike metaheuristics, the first iterations of model-based algorithms are not guided, but instead random, and only after those evaluations does the search begin. Having this in mind, we can see that other than GPR\_SMPSO, all other model-based algorithms fail to improve much from the original Pareto Front, only outperforming the EA SPEA2. Contrastingly, the other EA, NSGA-II, outperforms most model-based algorithms.

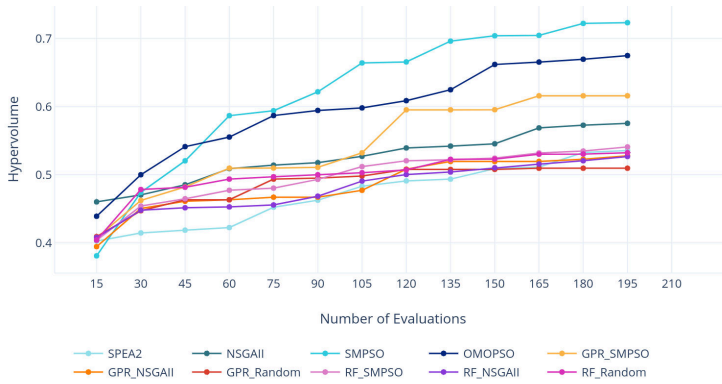


Figure 3. Space Frame: Average of the hypervolume per iteration for each of algorithm.

#### 4.2. CASE 2: BLACK PAVILION

The second case study is the optimization of a rectangular-shaped room intended for temporary art exhibitions. Located at the Black Pavillion in the Pimenta Palace, in Lisbon, the main daylight source of this room is a glazed curtain-wall that occupies half of the south façade and the entire east façade. As a way to balance and control the amount of daylight in the exhibition space, the architects intended to (1) add a rectangular skylight in the opposite side of the curtain-wall, and (2) change the curtain-wall material to a translucent one, in order to diffuse the light and avoid harsh shadows. The architects wanted to maximize the lighting conditions while minimizing the costs. Figure 4 shows a rendered image of the described exhibition space.



Figure 4. Rendered image of the exhibition area of the Black Pavilion.

To solve this MOO problem, we used (1) RADIANCE to compute the Spatial Useful Daylight Illuminance (sUDI) metric and, thus get a measure of the daylight performance, and (2) a cost function that takes into account the area of the new elements and the cost per unit area of the different materials needed. The length and width of the rectangular skylight, as well as the translucent materials applied to both skylight and curtain-wall were varied in the course of the optimization.

Similarly to the previous case, Figure 5 shows the combined results for the three runs of all the 10 algorithms. However, in this case the algorithms converged to the same area, thus making it very difficult to discern the quality of each algorithm. One possible reason for this, is that the design space considered for this problem is very small, allowing for each algorithm to rapidly converge towards the optimal region. In this case, while also not very conclusive, the assessment of the algorithms in terms of the hypervolume provides a different perspective over the evolution of the optimization processes. These results are depicted in Figure 6, and the GPR\_Random algorithm, a model-based one, immediately stands out as the worst algorithm. This can be explained by a poor approximation to the objective functions in one of the runs, which led to focusing on a specific region of the design space, thus trapping the optimization in that region.

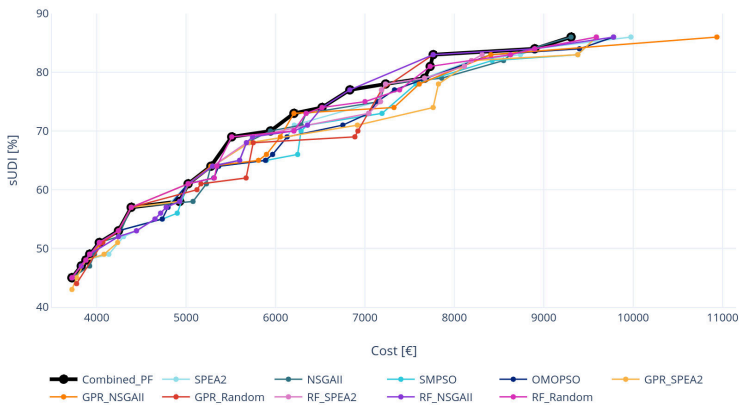


Figure 5. Black Pavilion: Pareto fronts for all tested algorithms. The combined Pareto front is formed by the non-dominated solutions from all the evaluated solutions.

Conversely to the previous case study, PSOs presented lower performance than EAs and the other model-based algorithms. Most algorithms seem to have stagnated after 120 evaluations, suggesting a small design space. It is also possible to observe that EAs actually performed reasonably well in this optimization problem, with NSGA-II having the best performance up until the 90-th evaluation, and with SPEA-2 recovering from a bad start and quickly finding optimal solutions and improving its Pareto Front. All other model-based algorithms behaved reasonably well, having achieved results as good as the EAs. However, only

the model-based algorithms based on Random Forests (RF) were able to improve immediately over the initial 75 evaluations, with the Gaussian Process Regression (GPR) only stepping up in later stages of the optimization.

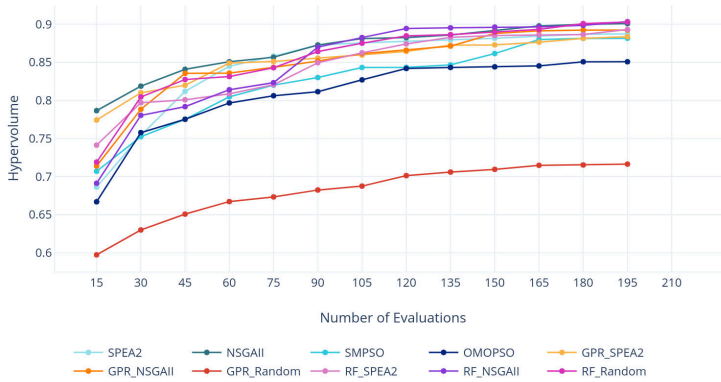


Figure 6. Black Pavilion: Average of the hypervolume per iteration for each of algorithm.

### 5. Conclusions

This paper focus on MOO, testing multiple MOO algorithms regarding two design problems with different objective functions. We set out to identify whether there are optimization algorithms that are best suited to solve specific problem types. To address this, we selected different classes of algorithms, both metaheuristics and model-based ones, and compared their performance in terms of the hypervolume, a metric that provides a perception on the quality and diversity of the results. Given the time-sensitiveness of most architectural projects, we also measured the performance evolution of each algorithm per iteration, thus allowing us to understand which algorithms more quickly approach optimal solutions. For the first case study, the PSO algorithms, which are a subclass of the metaheuristics algorithms, were the ones that showed a better performance. However, for the second case study, this subclass not only did not stand-out, but also were amongst the algorithms with the worse performance, being the EAs, in particular the NSGA-II, the ones who performed the best. Hence, our results suggest that no algorithm consistently outperforms all others in all problems, corroborating Wolpert’s No Free Lunch Theorem (Wolpert and Macready 1997). Moreover, the results show that the specificities of the optimization problem have an impact on how the MOO algorithms perform. Finally, as consequence of this research, we reinforce the need for architects to initially test a wide variety of algorithms, in order to understand which one(s) are better suited to solve their particular design problem. Only then, should they run the final optimization process, hot-starting them with the previous results.

## 5.1. FUTURE WORK

As future research, we plan to follow a different way of comparing the algorithms' performance, especially by giving each one the same set of initial solutions, so that results and conclusions are not affected by randomization. Moreover, design problems with larger number of variables and objectives will also be explored to compare the suitability of different classes of algorithms to higher-dimensional problems. An additional research question is raised by the need of solving optimization problems for which certain conditions on the variables cannot be violated. We plan to address this by studying existing techniques in constrained optimization.

## Acknowledgments

This work was supported by national funds through Fundação para a Ciência e a Tecnologia (FCT) with references UIDB/50021/2020 and PTDC/ART-DAQ/31061/2017.

## References

- Belém, C. and Leitão, A.: 2018, From Design to Optimized Design: An Algorithmic-Based Approach, *Proceedings of the 36th eCAADe Conference*, 549-558.
- Evins, R.: 2013, A Review of Computational Optimisation Methods Applied to Sustainable Building Design, *Renewable and Sustainable Energy Reviews*, **22**, 230-245.
- Evins, R., Pointer, P. and Vaidyanathan, R.: 2011, Multi-Objective Optimisation of the Configuration and Control of a Double-Skin Facade, *Proceedings of the 12th Conference of International Building Performance Simulation Association*, 1343-1350.
- Hamdy, M., Nguyen, A.T. and Hensen, J.L.: 2016, Performance Comparison of Multi-objective Optimization Algorithms for Solving Nearly-Zero-Energy-Building Design Problems, *Energy & Buildings*, **121**, 57-71.
- Khazaii, J.: 2016, *Advanced Decision Making for HVAC Engineers: Creating Energy Efficient Smart Buildings*, Springer.
- Kolarevic, B. and Malkawi, A.: 2005, *Performative Architecture: Beyond Instrumentality*, Spon Press.
- Nguyen, A.T., Reiter, S. and Rigo, P.: 2014, A Review on Simulation-Based Optimization Methods Applied to Building Performance Analysis, *Applied Energy*, **113**, 1043-1058.
- Pereira, I., Belém, C. and Leitão, A.: 2019, Optimizing Exhibition Spaces: A Multi-Objective Approach, *Proceedings of the 37th eCAADe Conference*, 53-62.
- Shi, X., Tian, Z., Chen, W., Si, B. and Jin, X.: 2016, A Review on Building Energy Efficient Design Optimization From the Perspective of Architects, *Renewable and Sustainable Energy Reviews*, **65**, 872-884.
- While, L., Hingston, P., Barone, L. and Huband, S.: 2006, A Faster Algorithm for Calculating Hypervolume, *IEEE Transactions on Evolutionary Computation*, **10**(1), 29-38.
- Wolpert, D. and Macready, W.: 1997, No Free Lunch Theorems for Optimization, *IEEE Transactions on Evolutionary Computation*, **1**, 67-82.
- Wortmann, T.: 2017, Opossum: Introducing and Evaluating a Model-based Optimization Tool for Grasshopper, *Proceedings of the CAADRIA Conference*, 283-292.
- Wortmann, T., Costa, A., Nannicini, G. and Schroepfer, T.: 2015, Advantages of Surrogate Models for Architectural Design Optimization, *Artificial Intelligence for Engineering Design Analysis and Manufacturing*, **29**, 471-481.
- Wortmann, T. and Nannicini, G.: 2016, Black-Box Optimization Methods for Architectural Design, *Proceedings of the CAADRIA Conference*, 177-186.

# TOWARDS A FINER HERITAGE MANAGEMENT

## *Evaluating the Tourism Carrying Capacity using an Agent-Based Model*

NAN BAI<sup>1</sup>, PIROUZ NOURIAN<sup>2</sup>, ANPING XIE<sup>3</sup> and  
ANA PEREIRA RODERS<sup>4</sup>

<sup>1,2,4</sup>*Department of Architectural Engineering and Technology, TU Delft*

<sup>1,2,4</sup>*{N.Bai|P.Nourian|A.R.Pereira-Rodgers}@tudelft.nl*

<sup>3</sup>*Department of Architectural Heritage, the Palace Museum*

<sup>3</sup>*anping\_xie@outlook.com*

**Abstract.** As one of the most important areas in the Palace Museum, Beijing, China, the Hall of Mental Cultivation had suffered from overcrowding of visitors before it was closed in 2016 for conservation. Preparing for the reopening in 2020, the Palace Museum decided to take the chance and initiate finer-grained tourism management in the Hall. This research intends to provide an audio-guided touring program by dynamically evaluating the Tourism Carrying Capacity (TCC) with the highlight spots in the Hall, to operate the touring program spatiotemporally. Framing an optimization problem for the touring program, an agent-based simulator, Thunderhead Pathfinder, originally developed for evacuation in the emergency, is utilized to verify the performance of the touring system. The simulation shows that the proposed touring program could precisely fit all the key requirements to improve the visitors' experience, to guarantee heritage safety, and to ensure more efficient management.

**Keywords.** Tourism Carrying Capacity; Agent-Based Simulation; Operations Research; Heritage Management.

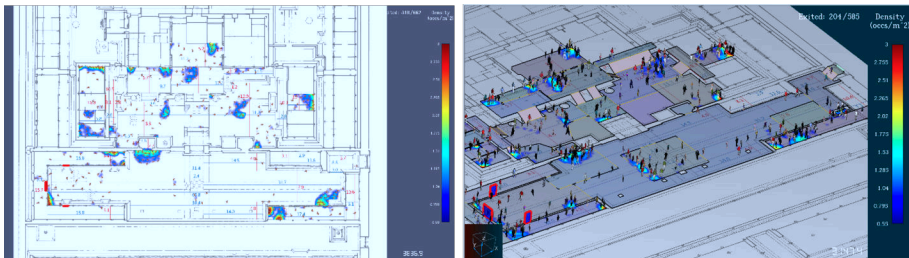


Figure 1. The simulation result as screenshots in Pathfinder software. Left: An instant density graph of the agents in the Hall; Right: The distribution of agents' movement in 3D.

## 1. BACKGROUND

Constructed in the early 17th Century, the Palace Museum (or The Forbidden City) in Beijing witnessed the rise and fall of Ming and Qing Dynasties. The palace was established as a museum in 1925, and was inscribed on the UNESCO world heritage list since 1987. Being one of the most important areas in the Palace Museum, Hall of Mental Cultivation (or Yangxin Palace) has served as the residential and working place for eight emperors in Qing Dynasty for more than 300 years (See *Figure 2d and 2e*). A major research project was initiated in 2016 on the Hall, intended to fully research on, conserve, restore, and further monitor the heritage site scientifically. Having been closed for conservation for 5 years, the Hall is planned to reopen in 2020 with special temporary and permanent exhibitions demonstrating the outcome of research and restoration, intended to celebrate the 600th anniversary of this grandiose heritage.

Before the conservation project started, the Hall of Mental Cultivation could have been visited by any visitor at any time, which led to a sensational overload of the area all over the year. As is shown in *Figure 2*, for 80% days of the year 2014-2015, visitors entering the Hall, the accessible area of which is only 1,000 m<sup>2</sup>, could reach 7,200 to 19,000 people per day, with 800 people staying in the Hall spontaneously. The Palace Museum has decided to set the daily reservation limit of visitors to 80,000 in June 2015, to improve the visitors' experience, to guarantee the safety of the heritage and to ensure more efficient management. Even after the limitation, the Hall of Mental Cultivation still could suffer from being visited by more than 20,000 people per day. Due to the overcrowding, the weakening of the heritage had been rather severe, urging for the conservation project (Zhang, Zhang, and Chen 2015).

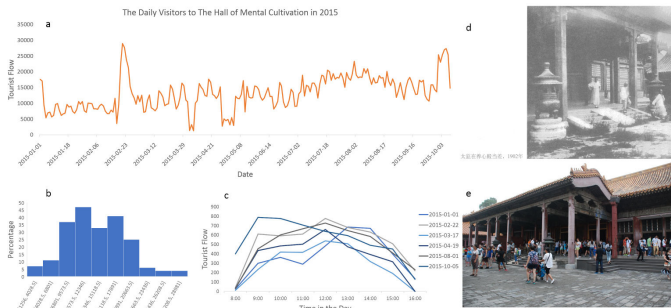


Figure 2. a) The number of daily visitors to the Hall of Mental Cultivation in 2015; b) the histogram showing the distribution of the daily visitors to the Hall in 2015; c) the instant visitors in the Hall for different time of the day in several typical days in 2015; d) the Hall in 1902; e) the Hall in 2015. SOURCE: a) to c) drawn by authors with the data of Department of Architectural Heritage, the Palace Museum; d) Lin J (2016), *Hundred Year Photograph in Ancient Beijing*. The Forbidden City Press; e) photo taken by Di Y from the Palace Museum.

Taking this chance of reopening the Hall after conservation, the Palace Museum intended to initiate an even finer-grained level of heritage management,

which could respond to the instant tourism condition and recommend optimal alternatives, both to the visitors and to the operators (Shan 2018). As a starting point, this research intended to provide an outline for the new touring program in the Hall of Mental Cultivation, which could balance the tourist flow spatiotemporally. Under such a condition, the traditional way to calculate the Tourism Carrying Capacity (TCC) statically has been updated with the aid of computer programming and agent-based simulation, in order to better fit and adjust the instant tourist dynamic.

## 2. CONTEXT

### 2.1. TOURISM CARRYING CAPACITY

Tourism Carrying Capacity (TCC) can be defined as “the maximum number of tourists that can be contained in a certain destination area”, considering both the issues of the negative impact of tourism on the site and the quality of the experience of tourists themselves (O’Reilly, 1986). This concept has been broadly applied in tourism site management around the world, by measuring the number of tourists in an area, usually compared as to the extent of the area occupied per person. However, some scholars such as (Mc Cool & Lime, 2001), argue that the numeric pursuit of TCC may rarely reflect the real issue, and that we should reformulate the question from being about a quantitative spatial limit to a question about an appropriate or an ‘acceptable condition’. It is also stated (Saarinen, 2006) that sustainable tourism should be based on a TCC according to the heritage site, tourist activities, and community perspective. Nevertheless, it is still common to trust on the TCC as a “magic number” in practice. In China, for instance, there is a set of defined TCC standards for the main tourism sites. And for the Palace Museum, it is 0.8-3.0  $m^2$  per person (China National Tourism Administration, 2014). For the past projects that we did in Palace Museum, we separated the TCC standard to two levels: 1) the maximum TCC relating to the first issue of impact on heritage, and 2) the suitable TCC pertaining to the perception and experience of visitors. Furthermore, for different sort of spaces, we also used different standards, for example, people in outdoor areas, psychologically, need a larger area per person compared to indoor areas.

In this paper, we follow the previous practice of two levels of TCC standards with different sorts of space, and we move one step further: the TCC would be measured spatiotemporally, i.e. along the dynamic process of touring, TCC should always be verified, leading to the “acceptable conditions” required for finer management.

### 2.2. AGENT-BASED SIMULATION IN URBAN STUDIES

As a bottom-up modelling approach for understanding and studying a complex system, an Agent-Based Model (ABM) or an Agent-Based Simulation (ABS) “allows one to simulate the individual actions of diverse agents, and to measure the resulting system behaviour and outcomes over time” (Crooks & Heppenstall, 2012). Due to its spatiotemporal nature and dynamics, ABMs have been broadly explored in urban studies as a tool to model the social phenomena and human



behaviour (Batty, 2001). Among other things, they are effective in mapping crowd movement patterns and detecting potential risks at spatial bottlenecks for pedestrians, e.g. (Du, Guo, & Jin, 2016) shows an application of an ABM in testing the effectiveness of congestion control measures with different strategies. Our approach is similar to the latter in the sense of formulating the problem mathematically and performing a crowd simulation. However, what sets our approach apart from existing approaches is our finer spatial and temporal scale as well as our focus on the entire tour program rather than only the peaks. In this paper, we use the Thunderhead Pathfinder 2019 software application, an agent-based egress and human movement simulator originally used for evaluating the ease of escaping emergencies in public buildings, as a tool for testing our mathematical formulation of the problem and the proposed touring program.

### 3. COMPUTATION

#### 3.1. TOURING PROGRAM ALTERNATIVES

At the starting point of the project, three alternative touring strategies were considered, namely free visit, human-guided tour and audio-guided tour, all of which have been applied for different areas of the Palace Museum. The free visit has been denied in the beginning by the operators, as it may go back to the situation before conservation easily, i.e. an overload of tourists, and it may not offer a meaningful experience for the visitors to take home. As for the other two options, they are both feasible to guide or even control the visitors spatiotemporally through a predesigned touring program (the highlighted spots are shown in *Figure 4*). However, while the human-guided option may lead to easier management on site, it also asks for more training costs and long-term running costs, such as the salaries for guides, which could be enormous. So, the computation here for the project focuses on the audio-guided individual visit program, which can be more economical and efficient for managers as well as comfortable for tourists.

#### 3.2. SPATIOTEMPORAL TOURING PROGRAM

In this section we propose the following sequence of deduction to compute the optimal touring program based on the constraints and objectives in reality:

For each individual visitor, their touring program follows the same sequence  $T_i$  values, denoting the ideal stay time at the  $i_{th}$  spot. However, for the  $j_{th}$  visitor, they may not follow exactly the allocated time. Therefore, the cumulative time spent for each visitor  $j$  at location  $i$ , denoted as  $M_{i,j}$  will differ after visiting  $i_{th}$  spot, according to the following equation, with some normally distributed error  $\epsilon_{i,j}$ :

$$M_{i,j} = M_{i-1,j} + T_i + \epsilon_{i,j}, \text{ where } : \epsilon_{i,j} \sim N(0, \sigma_i^2) \quad (1)$$

We can assume the lag time for any visitor to start the tour is the same value  $\tau$ . The  $j_{th}$  visitor will be staying at spot  $i$  within the range  $r = [\tau j + M_{(i-1,j)}, \tau j + M_{(i,j)}]$ , counting from the moment the first visitor started. At any moment in time denoted as  $t$ , the number of visitors staying at the spot  $i$  is the cardinality of the set of all visitors  $j$  that fulfil the following condition:  $t \in r$ .

The earliest and the latest persons who could still be present at the  $i_{th}$  space at time  $t$ , are respectively denoted as  $j_e$  and  $j_l$ , and can be found by solving the following equations:

$$t = \tau j_l + M_{i-1,j_l}, t = \tau j_e + M_{i,j_e} = \tau j_e + M_{i-1,j_e} + T_i + \epsilon_{i,j_e} \quad (2)$$

However, we only need to find the difference between these two ordinal indexes  $j_e$  and  $j_l$ , in order to find the capacity of the  $i_{th}$  spot as the number of visitors  $N_i$  which could be staying at spot  $i$  at any moment  $t$ :

$$N_i = j_l - j_e = \frac{T_i + \epsilon_{i,j_{\min}} + M_{i-1,j_{\min}} - M_{i-1,j_{\max}}}{\tau} \quad (3)$$

To make it easier for getting an initial draft touring program, we could assume that every visitor stays at the  $i_{th}$  spot, precisely following the allocated time, denoted as  $T_i$ , or that the deviations sum up to 0. Then the equation above could be simplified as  $N_i = \frac{T_i}{\tau}$ . We could then formulate the problem as maximizing the total number of daily visitors  $V$  as a function of the lag time  $\tau$ , the allocated times per spots  $T_i$ , and the daily opening time duration  $T_d$ , i.e. the manager can tune these three variables such that the overall throughput  $V$  could be maximized:

$$V(\tau, T_i, T_d) = \frac{T_d - \sum_i T_i}{\tau} \quad (4)$$

Subject to the following constraints, where  $A_i$  denotes the area of the  $i_{th}$  spot and  $C_i$  denotes the TCC standard capacity of that spot, and  $T_m$  means the minimum acceptable duration of visit:

$$N_i = \frac{T_i}{\tau} \leq \frac{A_i}{C_i}, \sum_i T_i \geq T_m \quad (5)$$

We can calculate the baseline allocated staying time  $T_i$  for each spot as  $T_i = \tau \frac{A_i}{C_i}$ ;

and compute the lag time  $\tau = \frac{T_m}{\sum_i \left( \frac{A_i}{C_i} \right)}$ .

The procedure above is probably an over-simplification biased towards considering the best-case scenario, i.e. a scenario in which all visitors precisely follow the tour within the allocated times, which clearly ignores the cumulative effect of the deviation  $\epsilon_{i,j}$ . In the real-world situation, this value could be very large in the worst-case scenario, so we do need a stochastic simulation model to verify the results.

As is suggested by the previous sections, we have set both the maximum and the suitable TCC standards differently for each highlighted spot according to their position (outdoor, roofed, and indoor) and importance. Bearing the issue of underestimation in mind, we choose to use the suitable rather than maximum TCC standard here, to give flexibility to the system.

The result of the computation is shown later in *Figure 4* as the mean staying time for each highlighted spot. The optimal lag time to start the tour  $\tau$  is 6 seconds, which leads to an overall daily number of visitors  $V$  being 4,200.

### 3.3. PEAK CONTROLLING FOR TOURIST FLOW

The result of computation leads directly to a dilemma here, i.e. the optimal lag time for people to start the tour  $\tau$ , is almost impossible to be implemented in practice: i.e. for operational reasons, it is only possible to admit tourists within a time-window, for example, if we issue a ticket for entry from 10:30 AM to 10:45 AM, the length of this time window will be 15 minutes, which is still far larger than the scale of  $\tau$ . If we assume that the inter-arrival of all the 150 people who reserve to enter the Hall in a reservation period follows a Poisson or exponential distribution, it may still cause peaks and valleys of the tourist flow, which is neither good for the heritages nor efficient for the managers. Thus, we could take one step backward: rather than ensuring the starting time of the entire tour with a lag time  $\tau$ , we could promise the frequency of entering the inner yard by setting several check-points in the outer yard to tune the flow gradually, like the water gates. Then the outer yard would function as a buffer zone to smoothen the peaks and valleys. Under such a principle, we could set a looser touring program for the highlighted spots in the outer yard, with relatively larger  $\sigma_i$ , i.e. wider span of likely error  $\epsilon_{i,j}$ , and thus give visitors more freedom to choose their own pace and explore the exhibitions themselves before entering the more deterministic space. The positions and the effects of each check-point are shown in *Figure 4*. The flow rate control could be realized by setting either an electric door or a brake at each entrance with a single adjustable operational frequency.

There is another issue that we have not discussed so far: if we designate a few check-points to smoothen the peak of tourist flow, then there will be queuing at these points and thus the check-points need to have the spatial capacity to hold people. For each check-point, we could allocate a queuing scheme for a time-window of 15 minutes. The inter-arrival times will follow an exponential distribution and correspond to the flow rate before and after the check-points. Theoretically, we could readjust the flow rate sequence and the number of staff needed handing out audio guide by computing the queue lengths and mean queuing times for each check-point according to Queuing Theory Models (Hillier & Lieberman, 2015, chapter 17), and/or Discrete Event Simulations (ibid, chapter 20) in Operations Research. However, in this research, we will achieve the goal, among the others, through an Agent Based Simulation Model.

## 4. SIMULATION

### 4.1. SIMULATION SETTINGS

We use the Thunderhead Pathfinder 2019 for running a crowd simulation to test our touring program. The assessment starts with manually setting input parameters for the model, which include the generation rate of the agents, the simulation length reflecting the real-world time range, the behaviour sequences of the different agent groups, the mean, variance, and probability distribution function of the staying pattern of the agents for each spots, and the entering directions and maximum flow rates of the gates. The output of the simulator includes a 3D animation showing the agents' movement and instant density along the simulation period all around the building, the route and staying time for all the agents (as is shown in *Figure 1*),

as well as the occupancy of all the rooms or subspaces and the count of bypassing agents through all the gates as a function of time.

For the first simulation, we set the parameters based on the results of previously estimated parameters. The generation rate of the agents into the system follows the theoretical arriving pattern, i.e. a Poisson distribution with a periodicity of 15 minutes. The simulation lasts for 7200 seconds with a status update timestep of 0.25 second, demonstrating the first half hour at the beginning of the day when the first groups are arriving, the last half hour during the end of the day when the last groups are leaving, and in between, at a typical hour when the system is in balance with arrivals and leaves. The agents follow a movement sequence as is suggested by the proposed touring program above, with mean staying time according to the allocated  $T_i$ , and the variance of the staying times of the individuals obeys a normal distribution  $N(0, \sigma_i^2)$ . The freedom while visiting the outer yard is larger than inner yard with a larger ratio of  $\frac{\sigma_i}{T_i}$ . In order to prepare for the real-world situation in the worst case, we allow 5% of the agents to behave abnormally, with significant longer staying times and larger variances at most of the spots. We also set the maximum flow rates of the check-point to test the effect of peak control on queuing.

#### 4.2. ADJUSTMENTS FOR THE TOURING PROGRAM

As we run the simulation with the initially proposed touring program based on estimated parameters, we can observe from the animation and the recorded data if the program is feasible. An infeasible program would result in the collapse of balance at certain spots, suggested by unbearable growth of the number of agents in the allocated space of that spot, which means long queues or even getting stuck for visitors and overload for the heritage. A touring program can be thus adjusted and improved to be more resilient to the possible worse cases by means of: 1) shortening the staying time  $T_i$  for the problematic spots, 2) narrowing or broadening the tolerance of variance  $\sigma_i^2$  for some regions, and/or 3) increasing the number of staff at the check-point where audio guides being handed out.

After several rounds of simulation and adjustments, we managed to keep the performance of our touring program in all spots reasonable at all time, meeting all the pre-set objectives, which will be discussed in the next section.

#### 4.3. VERIFICATION

Based on the discussion with the operator of the Palace Museum, we mainly needed to verify three management objectives with our agent-based simulation model for the touring programs: 1) not crossing the uncomfortable line of density based on tourism carrying capacity for any spot at any time; 2) the peak caused by arriving periodicity being finely controlled and smoothed along the tour; 3) no too long queues in any spot, especially for the check-points. With the results shown in Figure 3, we could demonstrate and explain that our touring program has fulfilled all of these objectives.

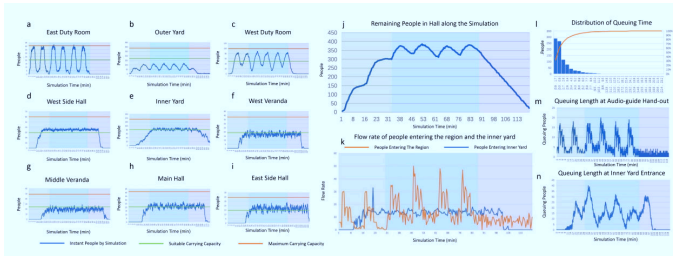


Figure 3. The results of the agent-based simulation in Pathfinder. Labels a) to i): The occurrence of agents at the space of each spot along the time-line; j) The overall number of visitors remaining in the building at any moment along the time-line; k) The flow rate of agents entering the system and entering the inner yard; l) The histogram showing the distribution of the total waiting times of the agents in the system; m) & n) The queuing status at the check-points.

In the *Figure 3a* to *3i*, we could see the simulated occupancy of each spot, with the green line showing the capacity of visitors  $\frac{A_i}{C_i}$  calculated with the suitable TCC standards, and the red line showing that with the maximum TCC standards. For all the six spots in the inner yard, the number of agents fluctuates around the suitable green line along the time-line, even for the two indoor spots in the outer yard, which are strongly influenced by the periodic peaks, the number of agents also never exceeds the maximum red line. For the spot shown in *figure 3b* which is the outdoor area in the outer yard, the number of agents is even lower than the green line all the time, which suggests that there is potential to add more activities here. The balanced overall visitors remaining in the region, as is shown in *Figure 3j*, ranges from 300 to 370 during the typical moments. The overall instant number of visitors also corresponds to the traditional method of TCC calculation, which would lead to 360 to 418 concerning only one single standard for the whole region and the overall accessible area. All the arguments here suggest that the touring program always fulfils the first objective of giving both the visitor a comfortable experience and the heritage site a bearable load. As shown in *Figure 3l* and *3m*, the queuing all around the region is also not an issue, as 90% of the agents in the simulation only queue for less than 3 minutes among their entire journey of 28-38 minutes. Even for the most severe part, where audio guides are being handed out, the queue length would be less than 20 people falling under 5 people in around 5 minutes, with 3 staff members working simultaneously. Concerning the longer queues at the entrance to the inner yard (*Figure 3n*), people can relax and enjoy exhibitions in the outer yard (*3b*), which is flexible enough as a buffer zone. The results also suggest that the touring program meets the third objective of lessening queues. As is seen also above in individual spots where the influence of the periodic peaks is being weakened along the touring sequence, the effect of peak control can be seen more directly from *Figure 3k*. The number of visitors going through the main gate follows the Poisson distribution with a cycle of 15min, which shows the peaks and valleys of the tourist flow. However, after several rounds of slowing down and smoothing by the check-points, the number

of people entering the inner yard remains more or less around a constant, which suggests that our peak control is successful as confirmed by the simulation.

The final touring program that fulfils all the objectives is shown in *Figure 4*, where the size of the circle visualizes the mean staying time at the spot, including the time spent with the audio guide and freely looking-around.

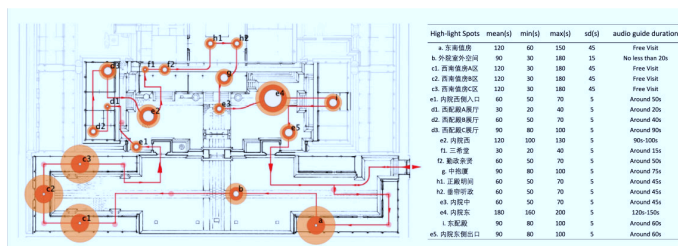


Figure 4. The final Touring Program after verifications and adjustments based on our Agent-based Simulation. Left: The touring route with the mean and variance of staying time on each spot denoted by circles and check-points as triangles; the glows around the circles demonstrate the variance of staying or the extent of freedom during the visit of that spot.

Right: The description of each spot.

## 5. DISCUSSION AND CONCLUSION

As is argued in the famous quote “All models are wrong but some are useful” (Box, 1979), our simulation model intends to provide a useful guideline to support and aid the real-world heritage management; but it is not meant to predict the individual trajectories of tourists within a heritage site. The simulation may reflect the reality poorly because of the various complicated attributes that we did not consider in this research. However, the model turns out to be insightful enough to guide the exhibition planning and the management program, both of which are yet to be realized. We intend to use tracking tools after the official reopening of the hall, in order to measure the actual use and validate/calibrate our model. Our proposed methodology is not meant to replace the existing feedback control procedures; instead, it is meant to provide insight as to how the system can be used at maximum capacity, to test the limits and make planning decisions. In real-time, the managers still do need to monitor the number of people exiting to decide whether they should let newcomers and latecomers in, and whether they should encourage or even nudge the visitors forward, in particular those who have been spending ‘too much time’ in a specific spot.

It can also be seen from our research, that the fineness and preciseness of the program, the difficulty of realizing the management and operation schemas, the objective of a high-quality memorable visiting experience, and the need for accepting as many visitors as possible, may be contradictory with each other. However, they are all critical and crucial from different angles. This methodology may not be able to solve all of these problems and fulfil the needs of everyone. It is, however, a starting point for heritage site managers such as those of the Palace

Museum to make a new step forward towards better and more efficient heritage management, trying to find a balance point to optimize the overall experience for the stakeholders involved: managers, operators, visitors, and the heritage site, while making some reasonable trade-off instead of imprecise compromises.

We presented the utilization of an agent-based simulation model for adjusting a touring program and gave a detailed example for the Hall of Mental Cultivation in the Palace Museum of Beijing for its reopening in 2020. The model is based on a relatively novel pursuit of estimating and verifying the Tourism Carrying Capacity from a dynamic perspective. The proposed touring program seems to meet the objectives of the visiting experience, heritage safety, and management efficiency, showcasing the effectiveness of the proposed methodology for better and finer heritage management. We have estimated the optimal staying times on a number of spots for a touring program and as elaborated in *Figure 3*, the simulation results agree with both the TCC standards and our engineered touring program. The results of the research are already approved by the department heads of the Palace Museum to be implemented for planning the future exhibition programs.

## ACKNOWLEDGEMENTS

The support of the Palace Museum and the HERILAND project funding (Marie Skłodowska-Curie grant agreement No 813883) and the suggestions of reviewers are gratefully appreciated.

## References

- C. China National Tourism Administration (ed.): 2014, *LB/T 034-2014 Guideline for measurement of carry capacity of scenic area (in Chinese)*, CNTA.
- Batty, M.: 2001, Agent-Based Pedestrian Modeling, *Environment and Planning B: Planning and Design*, **28**(3), 321-326.
- Box, G.E.P.: 1979, Robustness in the Strategy of Scientific Model Building, *Army Research Office Workshop on Robustness in Statistics*.
- Mc Cool, S.F. and Lime, D.W.: 2001, Tourism carrying capacity: Tempting fantasy or useful reality?, *Journal of Sustainable Tourism*, **9**(5), 372-388.
- Crooks, A.T. and Heppenstall, A.J. 2012, Introduction to Agent-Based Modelling, in A.J. Heppenstall, A.T. Crooks, L.M. See and M. Batty (eds.), *Agent-Based Models of Geographical Systems*, Springer, Dordrecht, 85-105.
- Du, S., Guo, C. and Jin, M.: 2016, Agent-based simulation on tourists' congestion control during peak travel period using Logit model., *Solitons and Fractals*, **89**, 187-194.
- Hillier, F.S. and Lieberman, G.J.: 2015, *Introduction to Operations Research Tenth Edition*, Mc Graw Hill Education, New-York.
- O'Reilly, A.M.: 1986, Tourism carrying capacity. Concept and issues, *Tourism Management*, **7**(4), 254-258.
- Saarinen, J.: 2006, Traditions of sustainability in tourism studies., *Annals of Tourism Research*, **33**(4), 1121-1140.
- Shan, J.: 2018, Practicing the Establishment of Research-Oriented Preservation Mechanism on Classic Architecture in the Forbidden City Notes on the Commencement of Research-Oriented Preservation Project of Hall of Mental Cultivation(Yangxin Palace) (in Chinese), *Architectural Journal*, **10**, 12-17.
- Zhang, X., Zhang, S. and Chen, H.: 2015, Research and Analysis of the Building Environment in the Conservation of Yang Xin Hall Area in the Palace Museum (in Chinese), *Traditional Chinese Architecture and Gardens*, -, 31-36.

# CONSTRUCTION OF ARCHITECTURAL FLOOR PLANS FOR GIVEN ADJACENCY REQUIREMENTS

KRISHNENDRA SHEKHAWAT<sup>1</sup> and PINKI PINKI<sup>2</sup>

<sup>1,2</sup>*Birla Institute of Technology & Science, Pilani-333031*

<sup>1</sup>*krishnendra.iitd@gmail.com* <sup>2</sup>*p20170003@pilani.bits-pilani.ac.in*

**Abstract.** For most of the architectural design problems, there are underlying mathematical sub-problems, they may require to consider for generating architectural layouts. One of these sub-problems is to satisfy adjacency constraints for obtaining an initial layout. But in the literature, there does not exist a mathematical procedure that can address any given adjacency requirements, i.e., there does not exist a tool for generating a floor plan corresponding to any given adjacency (planar) graph (there exist algorithms for constructing floor plans for planar triangulated graphs only). In this paper, we are going to present an algorithm that would generate a floor plan corresponding to any given planar graph. The larger aim of this research is to develop a user-friendly tool that can generate a variety of initial layouts corresponding to a given graph, which can be further modified by the architects/designers.

**Keywords.** Floor plan; Algorithm; Graph Theory.

## 1. Introduction

One of the primary task in most of the architectural design processes is to build a layout while satisfying the given adjacency constraints. It is easy to see that adjacency constraints need to be addressed using the mathematical tools only, in particular the graph theoretical tools. Even we can think of generating a layout only if we know there exists a layout for the given adjacency constraints (there may or may not exist a floor plan corresponding to a given adjacency graph). Hence, the generation of an initial layout can be seen as a difficult mathematical problem and if it is addressed, it can be a helpful tool for the architects.

In the literature, there exists a sufficient amount of work for the construction of floor plans based on graph theoretic approach. One of the initial works in this direction is given by Levin [8] in 1964. He gave an intuitive approach for mapping adjacency graphs to architectural floor plans. Then a lot of work has been proposed in this direction. This work can be categorized on the basis of rectangular floor plans and orthogonal floor plans. A brief overview of the construction of floor plans using graph theoretic approach is as follows:

In 1970, Grason [5] proposed a dual graph representation of a planar graph for generating a rectangular floor plan. In 1973, Steadman [17] produces all topologically distinct rectangular floor plans (illustrating all possibilities up to six



component rooms). In 1980, Baybars and Eastman [1] gave a systematic procedure for obtaining a floor plan for a given underlying maximal planar graph (MPG), where the boundary of the obtained floor plan is not necessarily rectangular (a graph is called *maximal* if no edges can be added to it without losing planarity). In 1982, Roth et al. [13] presented the construction of a dimensioned rectangular floor plan for a given planar triangulated graph (PTG). In 1985, Kozminski & Kinnen [7] developed the necessary and sufficient conditions for the existence of a rectangular floor plan for properly triangulated planar graphs (PTPG). Using the concepts of [7], in 1987, Bhasker & Sahni [2] gave a linear time algorithm for constructing a rectangular floor plan for bi-connected PTPG.

In 1990, Rinsma et al. [12] were the first ones to demonstrate the automated generation of an orthogonal floor plan corresponding to a given MPG. In 1993, Sun and Sarrafzadeh [18] found that there exist PTG for which rectangular floor plans do not exist, and for those PTG, there may exist a floor-plan having 0-CRM and 1-CRM (a  $k$ -concave rectilinear module, i.e.,  $k$ -CRM is a module with  $k$  bends). In the same year, Yeap and Sarrafzadeh [21] showed that if only 0-CRM and 1-CRM are allowed, there are PTG's that do not admit a floor-plan, i.e., 2-CRMs are sufficient and necessary for graph dualization floor-planning.

Using the concept of orderly spanning trees, in 2003, Liao et al. [9] gave a linear time algorithm for constructing an orthogonal floor plan for any  $n$ -vertex PTG which require fewer module types i.e., the algorithm uses only I-modules, L-modules (could be flipped horizontally), and T -modules, but Z-modules are not required.

In 2009, Eppstein et al [3] proved that a rectangular floor plan is area universal if and only if it is one sided (a rectangular floor plan is *area universal* if any assignment of areas to rooms can be realized by a combinatorial equivalent rectangular floor plan).

In 2011, Jokar and Sangchooli [6] introduced the concept of area of a face of a graph and used it for the construction of orthogonal floor plans, where the given graphs are maximal planar.

In 2014, Shekhawat [14] gave the enumeration of best connected rectangular floor plans. In 2015, Shekhawat [15] gave an algorithm for constructing plus-shaped floor plans. In 2018, Wang et al. [20] developed a prototype to regenerate well-known existing rectangular floor plans having an underlying graph as bi-connected PTPG. In 2019, Nisztuk et al. [11] developed an application, based on the evolutionary algorithms, for the automated generation of floorplans satisfying the given adjacency and dimensional requirements. But the proposed work does not cover the graphs for which it is not possible to construct floor plans with rectangular rooms only.

It can be observed from above discussion that most of the work done related to the existence and construction of a floor plan is restricted to planar triangulated graphs only, i.e., to the best of our knowledge, there does not exist an algorithm for checking the existence of a floor plan and for its construction corresponding to non-triangulated graphs (in 2019, Shekhawat et al. [16] gave an algorithm for constructing a floor plan for any given graph but for the algorithm, it is required to

have all generic rectangular floor plans and enumeration of generic rectangular floor plans for a large amount of rooms is computationally very demanding). Hence, we present an algorithm for generating floor plans for non-triangulated graphs (which can obviously be used for triangulated graphs).

## 2. Methodology

In this section, we present an algorithm for constructing a floor plan for a given planar adjacency graph. For a better understanding of the algorithm, we require the following terminologies.

A *planar graph* that can be drawn in a plane is called a *plane graph*, which divides the plane into connected components called *faces/regions*. The unbounded region is called the *external face*. Except for the external face, all other faces are *internal faces*. A planar graph  $G$  is said to be *triangulated* if all of its faces are triangular. If only interior faces are triangular, and the outer face is a cycle of length  $k$ ,  $k > 3$ , then  $G$  is called *internally triangulated*.

A *floor plan* corresponding to a graph  $G$  is a closed polygon in which every vertex of  $G$  is replaced by its component polygons called *rooms*. Two rooms in a floor plan are said to be *adjacent* if they share a wall or some part of it, where *wall* of a room refers to the edges forming its perimeter.

An ordering of a planar graph  $G_n$  whose vertices are denoted and ordered as  $v_1, v_2, \dots, v_n$  is a *canonical ordering* of  $G_n$  if the following conditions hold, when  $1 < k < n$ .

- $G_k$  is biconnected and internally triangulated.
- $(v_1, v_2)$  is an outer edge of  $G_k$ .
- Each vertex say  $v_{k+1}$  where  $k+1 \leq n$  must be adjacent to at least two vertices of  $G_k$  such that it forms a cycle having at least one edge that lies on the exterior face of  $G_{k+1}$ .

For example, the canonical ordering of graph in Figure 3(b) is shown in Figure 3(c).

*Horizontal Adjacency*: Two rooms are horizontally adjacent if and only if there is a horizontal line segment connecting them (see Figure 1).

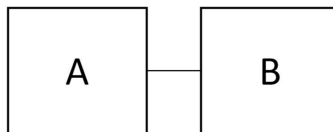


Figure 1. Horizontal Adjacency.

*Vertical Adjacency*: Two rooms are vertically adjacent if and only if there is a vertical line segment connecting them (see Figure 2).

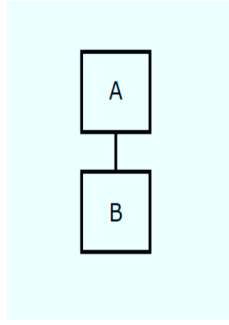


Figure 2. Vertical Adjacency .

A *2-visibility drawing* of a plane graph is a drawing where all the vertices are drawn as rectangular boxes and an edge is drawn either as a horizontal line segment or as a vertical line segment [4]. For example, in Figure 4 the steps of 2- visibility drawing of the graph in Figure 3(c) are illustrated.

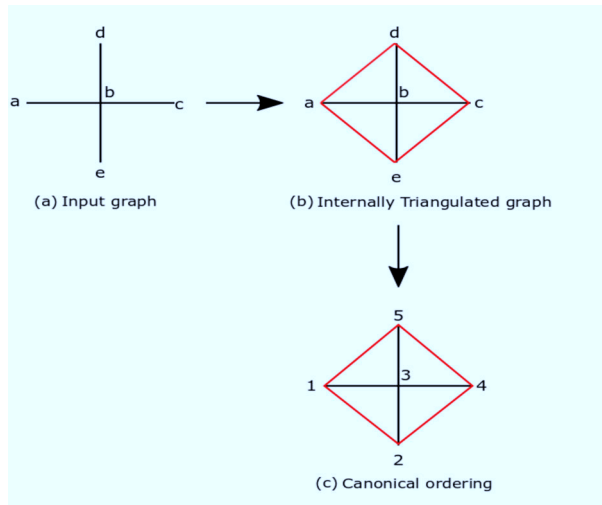


Figure 3. Triangulation of a given graph and canonical ordering of the triangulated graph.

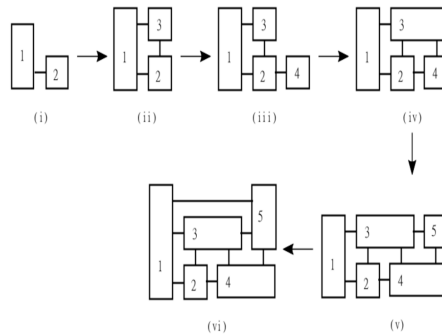


Figure 4. Obtaining a 2-Visibility drawing for the graph in Figure 3c.

### 2.1. ALGORITHM FLOORPLAN

**Input:** A planar graph  $G$  with its planar embedding.

**Output:** A Floor plan

**Procedure:**

#### 1. 2-Visibility Drawing of the given graph $G$ .

a) If  $G$  is not internally triangulated, add a minimum number of edges so that  $G$  would be internally triangulated.

**Example:** The graph given in Figure 3(a) is not triangulated however after adding the red edges it is transformed into a triangulated graph as shown in Figure 3(b).

b) Compute the canonical ordering of  $G$ , denoted as  $v_1, v_2, \dots, v_n$ .

i) Choose any edge on the outer face of  $G_n$  and mark its endpoints as  $v_1$  and  $v_2$ . Let the graph having only adjacent vertices  $v_1$  and  $v_2$  be called as  $G_2$ .

ii) **For**  $k=2:n-1$  **do**

iii) Choose  $v_{k+1}$  where  $k+1 \leq n$  in such a way it must be adjacent to at least two vertices of  $G_k$ .

iv) Add  $v_{k+1}$  to  $G_k$  such that it forms a cycle having at least one edge that lies on the exterior face of  $G_{k+1}$ .

**Example:** Start with any edge on the outer face of  $G$  and mark its endpoints as  $v_1$  and  $v_2$ . Let this graph be  $G_2$ . For  $k=2, k+1=3$  and  $3 \leq n$ . Hence,  $v_3$  must be located on the outer cycle of  $G_3$  and  $G_3$  is biconnected. Similarly, we obtain the canonical ordering of  $G$ , as shown in Figure 3(c).

c) Represent each vertex  $v_i$  of  $G$  by a rectangular box  $R_i$  where  $1 \leq i \leq n$ .

d) Place  $R_1$  and  $R_2$  of size  $1 \times 2$  and  $1 \times 1$  such that they must be horizontally adjacent as shown in Figure 4(a).

e) **For**  $i=3:n$  **do**

f) Consider every  $R_i$  of size  $1 \times 1$ .

g) Let  $R_{p_1}, R_{p_2}, \dots, R_{p_j}$  be the neighbors of  $R_i$  that are present in  $G_{i-1}$  and

are arranged in counterclockwise order where  $1 < j < n$ .

**Example:** In Figure 4(ii), For  $i=3$ ,  $R_3$  is of size  $1 \times 1$  and neighbors are  $R_1$  and  $R_2$ . In Figure 4(iv), the neighbors of  $R_4$  in counterclockwise order are  $R_1, R_3$  and  $R_2$ .

**h)** Place  $R_i$  above or to the right of its neighbors given in the drawing of  $G_{i-1}$  such that  $R_{p_1}, R_{p_2}, \dots, R_{p_{j-1}}$  is horizontally adjacent to  $R_i$  and  $R_{p_j}$  is vertically adjacent to  $R_i$ .

**Example:** In Figure 4(iii),  $R_3$  is drawn above  $R_2$  and to the right of  $R_1$  in such a way that it is horizontally adjacent to  $R_1$  and vertically adjacent to  $R_2$ . In Figure 4(iv),  $R_4$  is placed to the right of  $R_2$  and  $R_3$ . Here,  $R_4$  is horizontally adjacent to  $R_2$  but not to  $R_3$ .

**i)** Stretch each of the drawn rectangular boxes  $R_j$  to the right or upside such that they must be visible to  $R_i$  if  $v_j$  in  $G$  are adjacent to  $v_i$ .

**Example:** In Figure 3(c), vertices 3 and 4 are adjacent but in Figure 4(iii),  $R_4$  is not adjacent to  $R_3$ . Hence, stretch  $R_3$  to the right in such a way that it is vertically adjacent to  $R_4$ .

By following the above steps, we obtain a 2-visibility drawing of  $G$  as shown in Figure 4(vi).

**2. Horizontal Expansion**

Remove the horizontal line segments by expanding each  $R_i$  preferably from right to left to maintain the rectangularity of rooms. Alternate layouts can be obtained by expanding the boxes to their left.

**Example:** Horizontal expansion of a 2-visibility drawing of  $G$  is shown in Figure 5(b).

**3. Vertical Expansion**

Remove the vertical line segments by expanding  $R_i$  preferably from top to down to maintain the rectangularity of rooms.

**Example:** Vertical expansion of Figure 5(b) is shown in Figure 5(c).

For a further illustration of the algorithm, refer to Figures 6 and 7.

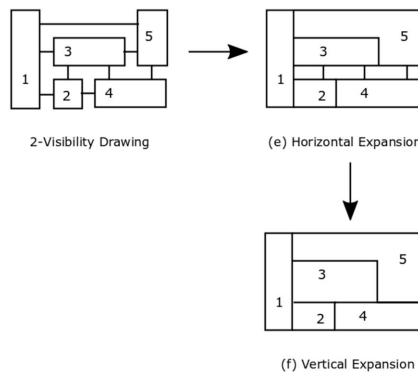


Figure 5. Obtaining horizontal expansion and vertical expansion from the 2-visibility drawing.

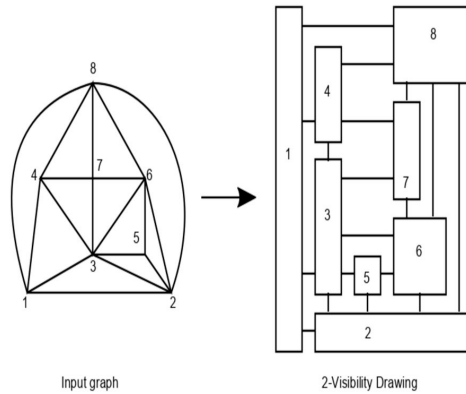


Figure 6. A planar triangulated graph  $G$  with its canonical ordering and its 2-visibility drawing.

### 3. Conclusion

We have known that architectural design is a multi-constraint problem and it cannot be addressed using the mathematical tools. At the same time, we can notice that there are some stages of architectural design where mathematicians can help designers, in particular, for developing an initial layout. In many cases, the initial layout needs to be developed while satisfying the given adjacency constraints, which mainly falls in the domain of graph theory. The problem of obtaining a floor plan for a given adjacency graph can be categorized into many mathematical sub-problems, where each one of them is quite difficult to handle. For example, how to identify the existence of a rectangular floor plan for a given adjacency graph. If it exists, how to construct it. If it does not exist, how to construct an orthogonal floor plan for the given graph. If there does not exist a floor plan for the given graph, how to transform the graph into a new graph for which a floor plan exists (for further details, about the use of graph theory in architectural design and related problems, refer to Nassar [10]). In the literature, there only exist few algorithms for constructing either a rectangular floor plan or an orthogonal floor plan for the given planar triangulated graphs, i.e., it is required to have an algorithm that can always generate a floor plan (either a rectangular floor plan or an orthogonal floor plan) for the given planar graph. To address this problem, we proposed an algorithm that generates rectangular and, if required, orthogonal floor plans from a given adjacency graph. It can be argued that the presented work is restricted to adjacency constraints only, whereas to have a floorplan with architectural meaning, at least dimensional constraints need to be considered. Recently, when given a rectangular layout, Upasani et al. [19] propose a method based on linear-optimization to adjust the geometric dimensional constraints of a given rectangular layout while keeping the topological adjacency

relations unchanged. This means that, once we can generate a layout, we can think of using a similar approach for addressing the dimensional constraints. Our ultimate goal is to build a general system for the automatic generation of floor plans, i.e., to provide architects with design aids, that is, algorithms that can generate good candidate solutions, taking adjacency requirements into account and that can be further improved and adjusted by them, to provide better solutions to the user.

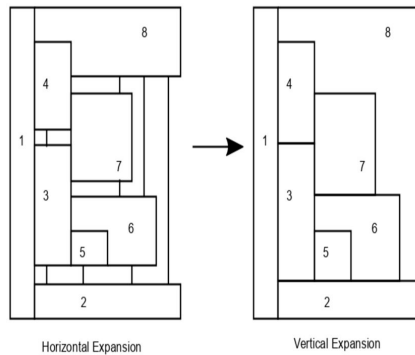


Figure 7. Obtaining horizontal expansion and vertical expansion from the 2-visibility drawing given in Figure 6.

## Acknowledgement

The research described in this paper is supported by BITS Pilani and is evolved as a part of the research project Mathematics-aided Architectural Design Layouts (File Number: ECR/2017/000356) funded by the Science and Engineering Research Board, India.

## References

- Baybars, I. and Eastman, C.M.: 1980, Enumerating architectural arrangements by generating their underlying graphs, *Environment and Planning B: Planning and Design*, **7(3)**, 289-310.
- Bhasker, J. and Sahni, S.: 1988, A linear algorithm to find a rectangular dual of a planar triangulated graph, *Algorithmica*, **3(2)**, 247-278.
- Eppstein, D., Mumford, E., Speckmann, B. and Verbeek, K.: 2012, Area-universal and constrained rectangular layouts, *SIAM Journal on Computing*, **41(3)**, 537-564.
- Fößmeier, U., Kant, G. and Kaufmann, M.: 1996, 2-visibility drawings of planar graphs, *In International Symposium on Graph Drawing*, Berlin, Heidelberg., 155-168.
- Grason, J.: 1970, A dual linear graph representation for space-filling location problems of the floor plan type, *Emerging methods in environmental design and planning*.
- Jokar, M.R.A. and Sangchooli, A.S.: 2011, Constructing a block layout by face area, *The International Journal of Advanced Manufacturing Technology*, **54(5-8)**, 801-809.
- Koźmiński, K. and Kinnen, E.: 1985, Rectangular duals of planar graphs, *Networks*, **15(2)**, 145-157.

- Levin, P.H.: 1964, Use of graphs to decide the optimum layout of buildings, *The Architects' Journal*, **7**, 809-815.
- Liao, C.C., Lu, H.I. and Yen, H.C.: 2003, Compact floor-planning via orderly spanning trees., *Journal of Algorithms*, **48(2)**, 441-451.
- Nassar, K.: 2010, New advances in the automated architectural space plan layout problem, *Proceedings Computing in Civil and Building Engineering*.
- Nisztuk, M. and Myszkowski, P.B.: 2019, Hybrid Evolutionary Algorithm applied to Automated Floor Plan Generation, *International Journal of Architectural Computing*, **17(3)**, 260-283.
- Rinsma, I., Giffin, J.W. and Robinson, D.F.: 1990, Orthogonal floorplans from maximal planar graphs, *Environment and Planning B: Planning and Design*, **17(1)**, 57-71.
- Roth, J., Hashimshony, R. and Wachman, A.: 1982, Turning a graph into a rectangular floor plan, *Building and Environment*, **17(3)**, 163-173.
- Shekhawat, K.: 2014, Algorithm for constructing an optimally connected rectangular floor plan, *Frontiers of Architectural Research*, **3(3)**, 324-330.
- Shekhawat, K.: 2015, Computer-aided architectural designs and associated covariants, *Journal of Building Engineering*, **3**, 127-134.
- Shekhawat, K. and Duarte, J.P.: 2019, A Graph Theoretical Approach for Creating Building Floor Plans, *In International Conference on Computer-Aided Architectural Design Futures*, Singapore, 3-14.
- Steadman, P.: 1973, Graph theoretic representation of architectural arrangement, *Architectural Research and Teaching*, 161-172.
- Sun, Y. and Sarrafzadeh, M.: 1993, Floorplanning by graph dualization: L-shaped modules, *Algorithmica*, **10(6)**, 429-456.
- Upasani, N., Shekhawat, K. and Sachdeva, G.: 2020, Automated generation of dimensioned rectangular floorplans, *Automation in Construction*, **113**, 103149.
- Wang, X.Y., Yang, Y. and Zhang, K.: 2018, Customization and generation of floor plans based on graph transformations, *Automation in Construction*, **94**, 405-416.
- Yeap, K.H. and Sarrafzadeh, M.: 1993, Floor-planning by graph dualization: 2-concave rectilinear modules, *SIAM Journal on Computing*, **22(3)**, 500-526.





# THE EVOLUTION OF CAADRIA CONFERENCES

## *A Bibliometric Approach*

TOMO CEROVSEK<sup>1</sup> and BOB MARTENS<sup>2</sup>

<sup>1</sup>*University of Ljubljana, Ljubljana, Slovenia*

<sup>1</sup>*tomo.cerovsek@gmail.com*

<sup>2</sup>*TU Wien, Vienna, Austria*

<sup>2</sup>*b.martens@tuwien.ac.at*

**Abstract.** This paper presents an analysis of the output, impact, use and content of 1,860 papers that were published in the CAADRIA conference proceedings over the last 20+ years (from 1996 to 2019). The applied methodology is a blend of bibliometrics, webometrics and clustering with text mining. The bibliometric analysis leads to quantitative and qualitative results on three levels: (1) author, (2) article and (3) association. The most productive authors authored over 50 papers, and the top 20% authors have over 80 % of all citations generated by CAADRIA proceedings. The overall impact of CAADRIA may be characterised by nearly 2,000 known citations and by the h-index that is 17. The webometrics based on CumInCAD.org reveals that the CAADRIA papers served over 200 k users, which is a considerable visibility for scientific CAAD output. The keywords most frequently used by authors were digital fabrication, BIM and parametric, generative, computational design. Notably, 90% of the papers' descriptors are 2-grams. This study may be useful to researchers, educators and publishers interested in CAAD.

**Keywords.** Bibliometrics; open source; text clustering; n-gram.

## **1. Introduction**

CAADRIA conference proceedings contain a history of contributions from the field of design creativity, technical and scientific excellence of the individuals committed to teaching and research in CAAD (Computer Aided Architectural Design). Notably, the number of CAADRIA conference papers steadily grew since the foundation of the association (see Fig. 1).

The total output of CAADRIA conferences is approaching 2,000 papers. This is a considerable body of design research knowledge, which is made freely available via the Open Access repository CumInCAD.org. However, the body of knowledge of published CAAD-research is by far too large to be manually reviewed. End users (eg teachers, researchers, practitioners) would appreciate assistance in review of contents, information retrieval and possibly content guidance.



Figure 1. Number of papers in CAADRIA conference proceedings per annum.

### 1.1. CONFERENCE AIM: RESEARCH SHARING PLATFORM

Conferences are one of the prevailing research sharing platforms that were introduced to allow for a researcher to inform others about his/her work, to get feedback from peers, to discuss, connect, and to be informed. A conference may be characterised by the theme, published call for topics, organisers & committees, time slot & frequency of organisation, its geographic location, delivery format, actual authors and participants.

The formulation of a conference theme along with the conference topics can be regarded as one of the very first “intellectual tasks” that a local conference host and PSC (Paper Selection Committee) has to setup. The “Call for Papers” will display the outcome of these efforts in detail and shall direct the subsequent steps, i.e., submission and review.

Geographic locations of CAADRIA conferences are changing from one country to another for several reasons. The most important reason is to maintain distributed presence in the geographical area covered by the association. This introduces some risks and opportunities as every year a new organising team is set up. Additionally, future organizers find it useful to observe preceding conference organisation work at an earlier stage (for example 1-2 years in advance to the “own” conference). A three-day-format is typical for the CAADRIA conferences and allows accommodations for a certain number of papers for presentation along with social events, aiming to boost opportunities for information exchange. However, on the one hand a PSC may and will have a higher permanency (appointment of members for more than one year). The number of presentation slots can be extended by way of multiple sessions. An extension or reduction of the duration is difficult, as travelling time is on the agenda as well as “out of office”-time (cost-benefit-ratio).

## 1.2. CONFERENCE RESULTS: OUTPUT & IMPACT

The body of participants is subject to change from year to year. Although some attendees are able to join on a frequent basis, others may submit from time to time their work to sibling CAAD-associations. It has to be noted that in case the submission does not lead to an accepted paper (i.e. for publication), in general the means to travel and to present onsite will be lacking. It is pleasing to see that efforts regarding young researchers lead to an ongoing "refreshment" of the participating audience.

The tangible result of a particular conference may be traced by way of the following two aspects: (1) The *output* of a conference may be measured in terms of availability, access and use of the published content. With the advent of digital technology, there are multiple information retrieval means that allow to keep hold on the output of conference proceedings; (2) The *impact* may be measured explicitly and implicitly. The most important and universally accepted measure of scientific impact regarding the created output is the so-called *h-index*.

## 2. Methodology

The content and use of CAADRIA conference proceedings are two main aspects analysed in this paper. The input to the analysis was derived from the CumInCAD.org repository. This repository contains over 10,000 papers stemming from different CAAD-associations. CumInCAD.org is organised as classical dublin-core compliant database with full texts. The study of CAADRIA-papers was conducted in the following steps:

- Data extraction from the CumInCAD repository;
- Analysis of the recordsets and descriptors;
- Cleaning and unifying of bibliographic entries;
- Extraction of topics from conference calls and paper keywords;
- Output of webometrics and extended bibliometric content analysis.

Extraction from the CumInCAD repository included 1,860 bibliographic records that were classified as CAADRIA conference proceedings. Analysis of the extracted recordsets and contained descriptors was performed to check against the consistency, completeness, organisation and formatting style. Cleaning of bibliographic records had to be conducted to be able to obtain relevant results. In the extraction of topics special attention was given to the n-grams, which (Wikipedia, 2019) defines: "*In the fields of computational linguistics means a sequence of n items from a given sample of text or speech*". In order to achieve a collated overview regarding utilised topical areas in the context of CAADRIA-conferences a compilation of "Calls for Papers" was gathered as well. With the exception of only three annual conferences (where this could not be traced back) a representative number of areas was accumulated, i.e. over 350. In this regard the question arises, which topical areas have emerged in the course of the conferences, as the listings in conference calls are dynamic by nature. For example, the current version of CumInCAD.org offers already an automated extraction of the field "keywords". However, automated cleaning of "stopwords" etc. - such as "de", "based", "using", "la" etc. - would make sense. (see Table 1).

Table 1. The automated extraction of most frequent terms in CumInCAD.org.

design (5295)	based (1054)	building (819)	study (508)
de (1787)	virtual (1031)	using (696)	modeling (506)
digital (1776)	computer (891)	space (610)	model (501)
architectural (1714)	urban (844)	information (606)	la (497)
architecture (1321)	system (825)	systems (521)	process (491)

Once the records were ready a detailed analysis of the contents, its use over CumInCAD.org along with text clustering was performed.

### 3. Bibliometric and webometrics analysis

The *quantitative* and *qualitative* metrics that are relevant for the analysis of the output of a conference may be divided into three levels: author, article and association (see Table 2). Only partial results are presented here.

Table 2. Overview on metrics for the conferences.

Level of metrics	Quantitative	Qualitative
Author-level	Number of authors Most frequent first author	Author h-index Number of citations
Article-level	Length - word count Number of images Number of references	Number of citations
Series-level	Number of events Frequency of events Cumulative duration	Series h-index Unique concepts Body of knowledge

While quantitative metrics are self explanatory, the qualitative metrics are more specific to scientometric analysis. It is assumed that the h-index and citations are a measure of quality (of author, article or proceedings), though they are quantitative by nature. The prevailing method of detecting the quality of the publication and its impact is the *h-index* (Cerovšek & Mikoš, 2014): h-index that was originally proposed by Hirsch in 2005 - is extendable, e.g. to research groups (Van Raan, 2006), institutions (Prathap, 2006), countries (Jacsó, 2009), and journals (Saad, 2006; Braun et al., 2006). There are advantages and disadvantages of the h-index (Costas and Bordons, 2007). The deficiencies of the h-index have led researchers to propose new forms of h-indices that are variations or extended versions of the original Hirsch h-index (Bornmann et al., 2008). These try to present the advantages of the newly proposed indices over the original ones for different purposes. In addition, the excellence of a researcher or research group can be determined with a combination of the easily computable h-index (from different sources/databases) and other scientometric indicators, such as citations; these combinations are intended to improve the overall ranking.

#### 3.1. RESEARCH OUTPUT AND ACCESS

The number of pages per conference paper is limited to ten pages and will hardly fall below six pages. This implies that the total number of published pages in the

context of CAADRIA conference will most likely exceed 10,000 pages by far and might amount close to 20,000 pages (see Fig. 2).

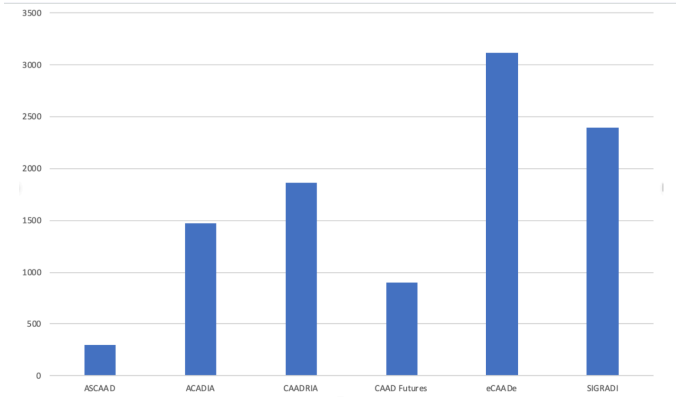


Figure 2. Output: Citations by association since 1981 (source: CumInCAD.org).

Table 3. Impact: Top authors at CAADRIA conferences (source: CumInCAD.org).

<b>Author</b>	<b>Role: First author</b>	<b>Role: Single author</b>	<b>Authorship: Not as first author</b>	<b>Total number of CAADRIA-papers</b>
Gero, John S.	18	4	30	48
Fukuda, Tomohiro	14	0	24	38
Fischer, Thomas	12	6	5	17
Herr, Christiane M.	11	4	5	16
Schnabel, Marc Aurel	11	3	29	40
Gu, Ning	10	0	14	24
Janssen, Patrick	9	2	19	28
Lin, Chieh-Jen	9	6	16	25
Nakapan, Walaiporn	9	3	5	14
Maher, Mary Lou	8	1	9	17
Martens, Bob	8	1	2	10
Kaga, Atsuko	8	0	24	32



Figure 3. Impact: Distribution of worldwide access (source: CumInCAD.org).

### 3.2. RESEARCH IMPACT

The research impact in terms of conference h-index shows that CAADRIA is one of the most successful conferences that are contained in the CumInCAD repository (Figure 4).

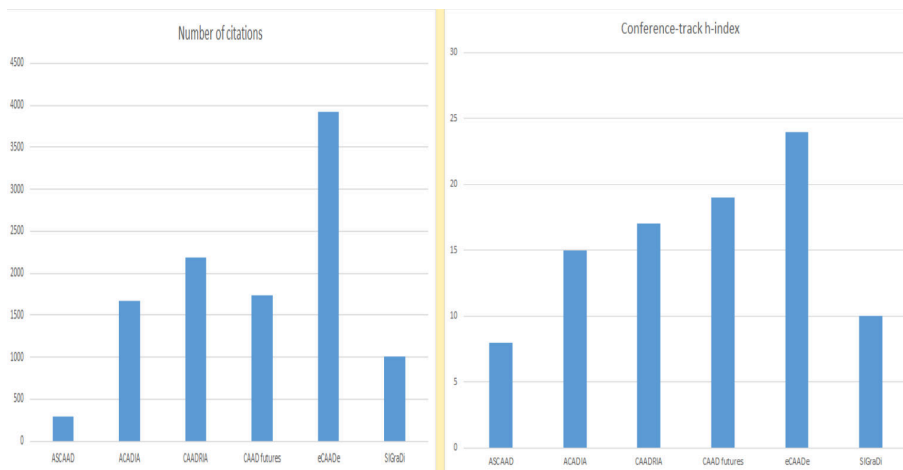


Figure 4. Impact: Number of citations and h-index per association (source: scholar.google.com).

**4. Content analysis**

The processing of CAADRIA proceedings consists of two techniques: n-grams analysis of the keywords and document clustering of bibliographic records.

**4.1. N-GRAM ANALYSIS**

The extraction of n-grams and their appearing frequency is of high interest as it seems a promising way to perform a pattern analysis. The Call for Papers from CAADRIA 2020 for example, displays several “bigrams”, such as Design cognition; Digital fabrication; Digital heritage. This observation applies also to preceding annual conferences.

The analysis starts with the extraction of n-grams and their appearing frequency from the calls and from bibliographic records. First of all, it allows potential submitters to identify whether the envisioned abstract might fit well (or not even hardly) within the academic field covered by the conference. It may also attract further submissions and forces submitters to roughly characterize the context of the abstract. After the whole review procedure is settled, the denotation of the conference session in the programme (and the proceedings) may again use the same listing of topical areas. The topical areas are also determined by the content of submitted and accepted publications.

Table 4. Analysis of topical areas (source: Call for Papers from CAADRIA conferences 1996-2020).

Gram (# of terms)	1	2	3	4	5	6
Frequency of topics	9	57	42	30	14	10

1-gram	2-grams (bigram)	3-grams (trigram)
Simulation (2) Culture (1) Environment (1) Ergonomics (1) Intelligence (1) Interoperability (1) Mechatronics (1) Sensing (1) Visualisation (1)	Collaborative Design (17) Knowledge representation (11) City Modelling (10) Virtual architecture (8) Design cognition (7) Virtual Reality (7) Interactive environments (6) CAAD Education (5) Design Creativity (5) Generative design (4) Generative Systems (4) Ubiquitous computing (4) Artificial Intelligence (3) Design Pedagogy (3) Environmental Simulation (3) Virtual Environment (3)	Human-computer Interaction (14) Computational design research (10) Computational design analysis (7) Case-based Reasoning (7) Sustainability and IT (7) Building Information Modeling (6) Virtual/augmented reality (6) Geographic Information System (5) Precedents and Prototypes (5) Digital design education (3) Prediction and Evaluation (3) Visualization & Animation (3)



Initial 350 n-grams were consolidated down to 162 unique items (Table 4). The largest group within this subset consists of bigrams (2-grams - word pairs, such as “Design cognition”) closely followed by trigrams (for example “Building Information Modelling”). It can be observed that occasionally the listing of the preceding Call for Papers was slightly adjusted. This is understandable, as these information packages are easy to gather and serve as a good starting point for adaptation.

Conference calls are based on experience, on-going research trends and expectations. However, if the keywords in the datasets are analyzed with the same focus the following aggregation was computed (Table 5).

Table 5. n-gram analysis of keywords of 1,860 CAADRIA papers (data source: CumInCAD.org).

Gram (# of keywords)	1	2	3	4	5	6	7
Frequency of papers	715	1605	621	132	34	6	3

1-gram	2-grams (bigram)	3-grams (trigram)
BIM (45) design (19) simulation (19) architecture (17) education (17) fabrication (15) pedagogy (12) collaboration (11) GIS (11) parametric (11) visualisation (11) computation (10) robotics (9) visualization (9) grasshopper (8) interaction (8) optimization (8) scripting (8) communication (7) generative (7) representation (7)	digital fabrication (72) parametric design (57) generative design (46) virtual reality (44) computational design (33) augmented reality (32) parametric modelling (29) robotic fabrication (17) 3D printing (16) collaborative design (16) design process (16) algorithmic design (14) form finding (14) machine learning (12) mixed reality (12) urban design (12) protocol analysis (11) shape grammars (11) ubiquitous computing (11) additive manufacturing (10) responsive architecture (10)	building information modelling (16) human computer interaction (15) building information model (6) computational fluid dynamics (5) architectural design optimization (4) data driven design (4) electronic design media (4) multi agent system (8) performance based design (4) 3D city modeling (3) agent based modelling (3) case based design (3) case based reasoning (3) collaborative virtual environments (3) computational design education (3) computer aided design (3) convolutional neural network (3) digital architectural design (3) human computer interface (3) internet of things (3) multi objective optimization (3)

#### 4.2. CLUSTERING ANALYSIS

A detailed presentation of the results of document clustering is beyond the scope of this paper. Therefore, only partial high level clustering results are presented.

Fig. 5 shows an example of visualisation of selected focus area. The analysis reveals several interesting developments in the context of cyber-physical relationship to architectural design. From static to dynamic parametric representations, evolution of grammars, to exploratory digital representations and direct connectivity and consumption of models in the material phase of a building project.



Figure 5. An example of results of partial clustering of titles from CAADRIA proceedings.

**5. Discussion and future developments**

It has to be noted that authors themselves define the keywords for their paper(s). This may be the reason that keywords sometimes may not be an accurate representation of the article contents, or the keywords are not used consistently. In addition, keywords are not always informative or may be even misleading. For example the use of terms like “grasshopper” or “generative” is not very entropic. Also the use of some very common n-grams, such as “computer aided design”,

may be too generic or/and may lose its importance over time with wide-spread use. The n-gram analysis may be heavily affected by the depiction of ongoing developments, which is much depending on the efforts of the acting conference chairs and/or paper selection committees.

The question may arise, what kind of contribution this type of research work potentially might deliver to the wider domain of architecture or design. In this regard the term “CAAD” (Computer Aided Architectural Design) contains the components “architecture” and “design”. However, design is not a standalone field, but directed in conjunction with “architecture”. Here again is the use of bigrams distinctive, i.e. “parametric design” / “generative design” / “computational design”.

Future developments may be grouped into three categories of changes: (1) Collaborative use with a substantial role of social media, submission and review changes, (2) Changes in distribution channels, (3) Issues of peer review and quality control, i.e. matching with already published entries (avoiding plagiarism issues)<sup>6</sup>. Is there still a strong need for paper-based versions as wide access to electronic forms is feasible? This could be regarded as a possible direction for future work.

## References

- “CumInCAD repository” : 2019. Available from <<http://papers.cumincad.org>> (accessed 11th December 2019).
- “Wikipedia” : 2019. Available from <<https://en.wikipedia.org/wiki/N-gram>> (accessed 11th December 2019).
- Bornmann, L., Mutz, R. and Daniel, H.D.: 2008, Are there better indices for evaluation purposes than the h index? A comparison of nine different variants of the h index using data from biomedicine, *Journal of the American Society for Information Science and Technology*, **59**(5), 830–837.
- Braun, T., Glänzel, W. and Schubert, A.: 2006, A Hirsch-type index for journals, *Scientometrics*, **69**(1), 169–173.
- Cerovšek, T. and Mikoš, M.: 2014, A comparative study of cross-domain research output and citations: Research impact cubes and binary citation frequencies, *Journal of Informetrics*, **8**(1), 147–161.
- Costas, R. and Bordons, M.: 2007, Advantages, limitations and its relation with other bibliometric indicators at the micro level, *Journal of Informetrics*, **1**(3), 193–203.
- Hirsch, J.E.: 2005, An index to quantify an individual’s scientific research output, *Proceedings of the National Academy of Sciences*, **102**, 16569–16572.
- Jacsó, P.: 2009, The h-index for countries in Web of Science and Scopus, *Online Information Review*, **33**(4), 831–837.
- Prathap, G.: 2006, Hirsch-type indices for ranking institutions’ scientific research output, *Current Science*, **91**, 1439–1440.
- Van Raan, A.F.J., Van Leeuwen, T.N., Visser, M.S., Van Eck, N.J. and Waltman, L.: 2010, Rivals for the crown: Reply to Opthof and Leydesdorff, *Journal of Informetrics*, **4**(3), 431–435.
- Saad, G.: 2006, Exploring the h-index at the author and journal levels using bibliometric data of productive consumer scholars and business-related journals respectively, *Scientometrics*, **69**, 117–120.

# OPTIMIZATION OF PUBLIC SPACE DESIGN BASED ON RECONSTRUCTION OF DIGITAL MULTI-AGENT BEHAVIOR

*–Taking the public space of the North Bund in Shanghai as an example*

CHUNXIA YANG<sup>1</sup> and ZHUOXING GU<sup>2</sup>

<sup>1,2</sup>*Tongji University*

<sup>1</sup>*Yang\_archi@163.com* <sup>2</sup>*guzhuoxing@126.com*

**Abstract.** This paper uses the digital software platform to build an intelligent multi-agent system. Through the classification of site elements, the Shanghai North Bund waterfront public space elements are classified into different systems such as transportation hub facilities, catering facilities, shopping facilities and leisure venues. The main population activities in this area are classified into different activities such as youth activities, elderly activities, and family activities through user behavior classification. Finally, the intelligent multi-agent particle swarm is built by the dynamic simulation component of grasshopper, and its individual behavior rules and group interaction rules are adjusted to form the crowd moving particle flow. The particle flow interacts with the classified site elements to derive a distribution pattern of population activity in different systems. Particle flow data information and particle distribution patterns after interactive simulation can be the support for urban design evaluation and optimization.

**Keywords.** Self-organizing system; Multi-agent system; Particle property construction; Urban design elements; Waterfront public space.

Shanghai Huangpu waterfront Public Space has been divided into five major sections of 45 kilometers of slow-moving space across the board. While various new waterfront spaces meet the public, we can't help but wonder whether there is any possibility of upgrading coastal space and facilities, whether there are more angles to observe the use of the built waterfront. The structure of the waterfront leisure public space of the Huangpu River has begun to emerge, and the basic infrastructure is basically equipped. Some local areas still have problems such as congestion or insufficient utilization, weak accessibility, and insufficient hydrophilicity.

## 1. Development status of behavioral simulation

In the study of environmental behaviour, at present, the basic method for helping people to interpret spatial elements under the framework of environmental behaviour is still observation. Researchers usually objectively record and observe

the user's natural performance in the environment. By recording specific data, they can compare and summarize law. Because of the limitation of this method, the research methods of environmental behaviour have withstood the test of reliability in three aspects: first, how to ensure objective rather than intrusive observation and judgment. No matter if we set up a camera at any ideal angle to observe the activist, there are more or less deviations and distortions in observation records.(Leach 2009) Therefore, is it possible to have a true top view that allows every activity to be analysed under absolutely fair conditions. Second, it is very difficult to classify activities and elements in complex systems, because each activity and space element are interrelated. If these elements can be analysed together as a hybrid, it is ideal. Third, between a space element and a user's behaviour, is it the space that determines the occurrence of the behaviour, or the behaviour's stress on the space to generate a new behaviour. However, in this study, because of the quantitative relationship between behaviour and spatial elements, this logical causality is ignored for the time being.

In the field of behavioural geography, Chai Yanwei summarizes the combination of behavioural individual behaviour and overall society, the combination of short-term behaviour and long-term behaviour, the combination of subjective initiative and objective constraints, the combination of quantitative research and qualitative research, and it establishes the relationship between behaviour and geographical space in the perspective of geography Research framework and methodology. (Chen 2003) Wang De and Zhu Wei of Tong ji University used the multi-agent system as a medium to talk about the quantitative simulation of the relationship between the business centre and the shopping needs of consumers, and finally obtained a new business centre and commercial scale judgment. (Zhu, Pang and Wang 2012) Yan Liu of the University of Queensland simulated the increase and decrease of real estate land value, and the investor's interest in the land plots, so as to preview the expansion of the city and try to construct a logical model of behaviour at the level of geographic research. In urban planning and geographic research, we often see the use of cellular automata or multi-agent models to simulate the spread and development of cities. The important key in each study is the behavioural elements that restrict or stimulate the urban land renewal, and how the evolutionary logic of these behavioural elements themselves is constructed.

## **2. Analysis and quantification of user behaviour in North Bund public space**

In this study, as the waterfront leisure space is extremely open, its main function is to provide a place for citizens to relax, entertain and relax. So we define elderly people who walk, family members who do leisure activities, and adults who exercise or walk alone as the three main groups of interest. The establishment and interaction of particle characteristics also revolves around the characteristics of these three groups of people. At the same time, the gender, age, occupation, and place of residence of the three types of population were analyzed and investigated. Because the freely moving children and aimless people have less uniform behaviour in this public activity space, and the proportion of these people in this space is not large, the main study population is included in the middle of

this study.

Before simulating the process, we need to give the particle swarm different attributes and unique ways of movement.(Weixin and Weiguo 2009) How to formulate different behavior rules needs to decompose, compare and quantify the various needs of users. In the statistical process, we mainly focused on the user’s preferences such as the type of transportation methods used by users to reach the site, the purpose of waterfront activities, who their peers are, and the attention of special areas. These preferences can help us design more diverse user particle swarms, each with their own unique laws of movement and purpose preferences, and help to obtain more realistic or more contrasting simulation patterns.(Figure 1)

In addition to selective preferences, users also have “implicit” behavioural habits differences in the venue. These habits play an important role in influencing behaviours without being reminded by the user, so they are of great significance for studying venue behaviour.(Gehl and Svarre 2013) Statistics on the habits of different user populations can better distinguish particle swarms and even individual particles, which depends on the multi-agent model structure and simulation accuracy. In the questionnaire, we added data surveys such as the time period of arriving at the waterfront, the frequency of arriving at the waterfront on weekdays, and the frequency of arriving at the waterfront during holidays.(Figure 1)



Figure 1. User behaviour decomposition.

### 3. Refinement of North Bund Public Space Elements

In the simulation process, information such as crowd attributes, crowd preferences, crowd habits, special points of interest can help edit proxy particles with unique attributes. After constructing a particle swarm, it is necessary to establish the space

environment in which it is active, and make the particle's activity flow match the space environment. In several articles by Zhu Wei and Wang De, we can see that its multi-agent particles enter the site through the entrance, adjust their own travel direction according to demand, and guide them to continue to move through path guidance points. (Zhu, Pang and Wang 2012) Therefore, in this experiment, we set up particle entrances and points of interest, and limit the range of particles' activities. The interaction between spatial elements such as entrances, boundaries, and public facilities and particles is set with reference to actual conditions to obtain more realistic simulation results.

According to the statistics of different user arrival methods in the survey, we use the plot near the subway station, bus station, and sidewalk entrance as the particle starting point. And according to the statistical preference settings, etc., the proportion of people at each starting point is calculated to determine its contribution to the number of people at the venue. In the simulation process, the interaction of the particle swarm is limited to the walkable area in the entire site, that is to say, we distinguish the walkable area from the non-walkable area, and the actual form of the public space in the area is obtained. This morphological boundary will squeeze or obstruct the particle's travel, making it possible to study the walking state and visual perception state of the user in the field. (Leach 2009) Based on surveys of points of interest, user preferences, and infrastructure preferences, we can determine the degree of demand for some infrastructure in public spaces, and set weights in the simulation software to distinguish the attractiveness of different venue facilities to users in order to obtain better simulation results. In addition, the weight setting based on survey data provides a basis for transformation, that is, in future research, we can intuitively judge the benefits of design by changing its weight. (Figure 2)

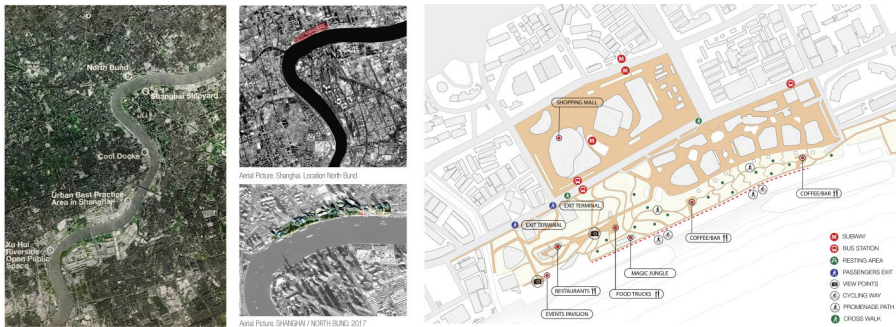


Figure 2. Public Space Site Elements.

#### 4. Interactive simulation and results analysis of user behaviour and public space elements

Based on the refinement of behavioural elements and public space elements of the North Bund, we divided the study target population into three types: the elderly, family active people, and adult active people, and determined the number of people

in the plot.(Gu, Yao and Yang 2017) The proportions are 24%, 36%, and 40% to ensure that the simulation can be as close as possible to the actual situation. And the three types of people have different preferences for the means of transportation to the venue, and different people have different preferences for activities in the venue. We mainly analyse the current relationship between waterfront public space and the flow of people by focusing on the three major waterfront activities in social activities, sports activities and functional areas.

#### 4.1. SIMULATION OF ELDERLY PARTICLE WATERFRONT PUBLIC SPACE ACTIVITIES

In the simulation of the elderly waterfront public space activities, the average moving speed of an adult person is set to 10, and we limit the maximum speed of the particles to 5 or less. In grasshopper's quelea plug-in, we have gathered parameters such as sight force, aggregation force, roaming force, collision prevention, discrete force, obstacle avoidance force, and recognition distance of neighbouring particles to control the particle motion personality, thereby shaping different particle swarms.(YANG, GU and YAO 2019) According to the survey results, we set the elderly's particles to have lower sight power and higher aggregation and roaming weights during social interaction activities. At the same time, the recognition distance of neighbouring particles is relatively long, which makes it easier for particle swarms to aggregate and interact. The particle swarm as a whole is slower, thereby simulating the social activities of the elderly in waterfront space. The particle swarm parameter settings in the interaction between sports activities and special venues are also the same. Through the matching of different weights, we get the elderly particle swarms in the waterfront space for sports facilities and special function plots.(Figure 3)

Before the simulation, the spatial elements of the North Bund were classified according to social venues, sports venues, and special event venues.(Gehl and Svarre 2013) Among them, the waterfront viewing platform is a social leisure venue that people yearn for, and it is also a special venue for resident activities. And some elderly people like to socialize in the activity gallery. Waterfront bars and port restaurants have also become the most common venues for social activities for older people. The elderly's physical activities usually take place on waterfront walks and traffic corridors. Dongyuan Plaza has become a special waterfront venue for middle-aged and elderly people in the North Bund.(Figure 4)

After the simulation, we can get the activity path relationship between the elderly's social activities, sports activities, special area functional activities and the entrance to the venue.(Gu, Yao and Yang 2017) It can be seen that in different needs, the optimal choice of the elderly's activity path is different, and the path distribution also appears relatively concentrated or scattered. Based on the overlay of the simulated activity path pattern, we can evaluate the intensity of the elderly's demand for this waterfront public space and propose appropriate renovation and update suggestions.



### 4.2. ADULT PARTICLE WATERFRONT PUBLIC SPACE ACTIVITY SIMULATION

It also collects data and organizes it. In the simulation of family crowd activities, the extreme speed of particle swarms is limited to a weight of 10 to 8. It is obvious that it is equivalent to the elderly and adult activities more quickly and conveniently. Because adults are more interested in sports and waterfront special functional areas, the weight of sight parameters in these two aspects is set relatively high.(Gu, Yao and Yang 2017) And the roaming power sets lower weight in the social and sports behaviours of adults, which shows that when adults have social needs and physical exercise needs, their purpose is very strong, they are more inclined to directly reach their destination to carry out activities . The survey data shows that when performing social activities and special function activities, the number of adults is large, so we set a higher weight in the parameter of the distance between adjacent particles to obtain a certain number of interactive particle groups. In sports particle swarm, this parameter is set to a low value, because most adults act alone when they exercise.(Figure 3)

Elderly particle swarm behavior weights				Adult particle swarm behavior weight				Family particle swarm behavior weights			
FORCE INSTANCES	SOCIAL	SPORTNESS	FUNCTIONALITY	FORCE INSTANCES	SOCIAL	SPORTNESS	FUNCTIONALITY	FORCE INSTANCES	SOCIAL	SPORTNESS	FUNCTIONALITY
Max Speed	8	4	4	Max Speed	8	10	8	Max Speed	8	8	8
View Force	0.2	0.8	0.8	View Force	0.5	0.8	0.7	View Force	0.2	0.8	0.5
Corner Force	0.7	0.9	0.7	Corner Force	0.6	0.9	0.7	Corner Force	0.6	0.9	0.7
Wander Force	0.8	0.2	0.8	Wander Force	0.2	0.1	0.8	Wander Force	0.8	0.2	0.8
Avoid Unaligned Collision	0.2	0.9	0.2	Avoid Unaligned Collision	0.7	0.9	0.2	Avoid Unaligned Collision	0.2	0.9	0.2
Separate Force	0.3	0.5	0.1	Separate Force	0.2	0.5	0.2	Separate Force	0	0.5	0.5
Avoid Obstacle	1	1	1	Avoid Obstacle	1	0.1	1	Avoid Obstacle	1	1	1
Get Neighbors in Radius r=0.3	0.7	0.2	0.7	Get Neighbors in Radius r=0.3	0.5	0.1	0.7	Get Neighbors in Radius r=0.3	1	0.2	0.3
<b>ATTRACTORS</b>				<b>ATTRACTORS</b>				<b>ATTRACTORS</b>			
Deck Viewpoint	0.4		0.1	Commercial Center	0.5			Commercial Center	0.7	0.1	
Event Pavilion	0.1			Event Pavilion	0.1			Event Pavilion	0.6		
Bar/Restaurants	1			Port restaurants			1	Port restaurants	0.9		
Bar/Restaurants	1			Bar/Restaurants	0.8			Bar/Restaurants	0.7		
Walking path		1	0.1	Bridge Viewpoint	0.1		0.6	Bridge Viewpoint	0.3		0.4
Promenade		1	0.3	Food Truck			0.5	Food Truck		1	
Winter Garden Plaza			0.4	Walking Path		0.3		Walking Path		0.8	0.4
				Magic Jungle			0.4	Magic Jungle			0.3
				Domus			1	Domus			0.8
				Winter Garden Plaza			0.6	Winter Garden Plaza			0.3

Figure 3. Classification and quantification of user behaviour (elderly, middle-aged, family).

In the setting of the weight of the venue elements, the social activities of adults occur more in the visits of commercial centres and bars, and in the bars and restaurants, the adult group will spend a lot of time. Similar to the elderly, the waterfront promenade and promenade are also the favourite physical exercise facilities for adults, but they are more inclined to carry out jogging and other physical exercises on the waterfront promenade.(Gu, Yao and Yang 2017) The adult group pays close attention to almost all special function venues in the venue, such as port specialty restaurants, bridge-viewing spots, food and beverage sales vehicles, jungle parks, Dongyuan Square, and so on. Therefore, the special purpose activities of the adult group in the venue are relatively abundant. (Figure 4)

We can see from the simulation results of the adults’ field activities that the paths of the fitness facilities are centralized and clear. The paths of social activities are relatively average and diverse, and there are also localized concentrations. The special function activity path is concentrated around each special function location. Therefore, we can reasonably combine social public spaces, so that social activity spaces are gathered in suitable places and separated from physical exercise paths. At the same time, the waterfront special function path, as the most abundant activities for adults in this space, can be combined with social interaction paths and

physical exercise paths to form a richer activity space system.

### 4.3. FAMILY CROWD PARTICLE WATERFRONT PUBLIC SPACE ACTIVITY SIMULATION

The family activity crowd combines the elderly, adults, and lively children, so we set the weight of its speed to 8 to get a particle swarm with medium speed. The activities of family-based people in public spaces are mainly fitness exercises and special functions, so the sight weights for these two types of activity points of interest are set higher. The particles of the family crowd are always aggregated in the family unit, so a high cohesive force is set so that the family activity particle cluster keeps a certain amount of aggregation. When doing physical exercises and venue-specific activities, the family crowd focuses on the family members of their peers. Therefore, we control the recognition distance of adjacent particles to a smaller range, so that particles interact less with particles outside the family.(Figure 3)

In the setting of the weight of the site elements, commercial centres, exhibition halls, restaurants, etc. are all places where family interactions occur. Compared with the elderly and adults, the family group will be more willing to spend time in physical centres such as commercial centres, fun jungles, and waterfront promenades.(Gu, Yao and Yang 2017) Because of children’s sake, they think that the fun of physical exercise is more important, and not all choose monotonous running. Special event venues such as bridge-viewing spots, promenades, waterfront promenades, and Dongyuan Square can also attract families to stay.(Figure 4)

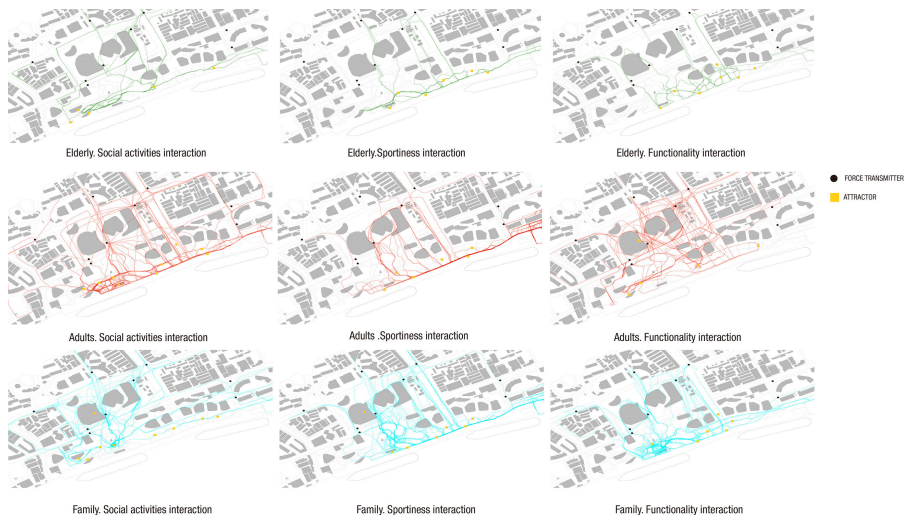


Figure 4. Particle Swarms and Site Elements Interaction Track.

In the final simulation pattern, we can find that the coverage of the activity path of the family group is the widest among the three groups, and the coverage of the

social activity path spreads more public space in the waterfront hinterland because there are more commercial centres here. The coastal water-viewing platforms, landscape squares, and bridge-viewing attractions are also favoured by families. Although the family-organized people do not have too many social interaction activities, they have diverse needs and long stays in the waterfront leisure space, forming a rich coverage of activities.

## 5. Post-simulation Evaluation and Strategy

### 5.1. COMPREHENSIVE ANALYSIS OF PARTICLE SWARM TRAJECTORIES

Through simulation, we can obtain the trajectory distribution of different people in the North Bund waterfront public space, that is, the elderly particle swarm trajectory distribution, the adult particle swarm trajectory distribution, and the family particle swarm trajectory distribution. By analysing the characteristics (density, trend, and shape) of its particle swarm distribution, the results can be evaluated for the effect of the corresponding crowd's activities in the local part of the site. In our simulation results, the trajectory distributions of the three types of particle swarms have similarities and differences.

First of all, from the perspective of commonality, the trajectory patterns of the three types of particle swarms show clear crowds of people in the venue. In the hinterland of the North Bund waterfront public space, there are two crowds of crowds, and the pattern is radial here. In the waterfront zone, crowds of people flow along the river. And in areas where the infrastructure is perfect, or where there are special crowds of special function sites, there are more gathering points, or the gathering scale is larger. Therefore, these meeting points of crowds are high probability points of crowd activity in the site, and they need to maintain good accessibility and visibility to ensure smooth traffic.(Figure 5)

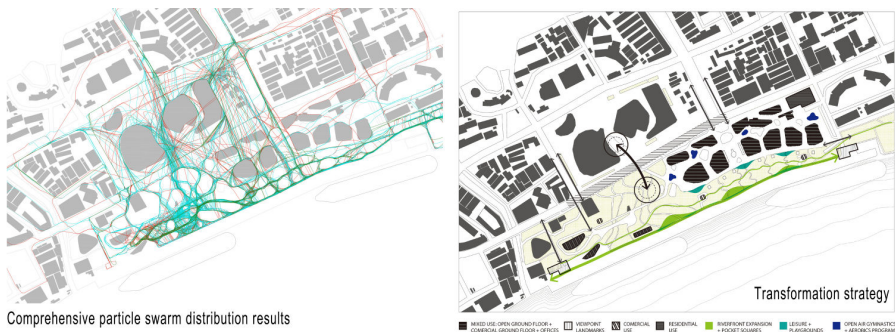


Figure 5. Particle Comprehensive Trajectory and Waterfront Space Reconstruction Strategy.

In terms of differences, the three types of particle swarms exhibit their own distribution characteristics. The family particle swarm has the largest area coverage in three aspects of social activities, sports activities, and special function activities, and its particle swarm trajectory has the most extensive correlation with different functions. This fully reflects the characteristics of the activities of family

groups in waterfront public spaces. The distribution of adult particle swarms is relatively clear and concentrated, while the trajectory distribution and connection in the bar and restaurant areas are the most. This fully reflects the place where adults' main social activities occur in the waterfront public space and its efficient exercise or viewing process. The trajectory of the elderly is concentrated in special areas, and physical exercise and viewing platforms have become their favourite places to stay.

## 5.2. PUBLIC SPACE PROMOTION STRATEGY AND SIMULATION VERIFICATION

Aiming at the simulation results and analysis conclusions, we can objectively put forward some transformation suggestions and carry out verification simulation. For example, the same concentrated area presented for different particle swarms can be regarded as a place where a large number of people gather, and its accessibility and visibility are particularly important.(Gu, Yao and Yang 2017) So we try to establish some convenient transportation to connect these areas. At the spatial level, these areas should also pay attention to the supporting arrangements of iconic landscapes, public recreation facilities, and public service facilities to ensure space efficiency. In different localized areas, we can adjust the space configuration according to the needs of different groups of people. The entrances and exits of commercial squares, bars and other facilities are closely integrated with the particle paths of families and adults to facilitate the use of the public. Set up more rest facilities and service facilities in the environment preferred by the elderly to improve the efficiency of service facilities. And in some areas with space potential but low usage rate, more crowd demands can be set in combination with particle swarm paths to improve space use efficiency and enrich user activities.(Figure 5)

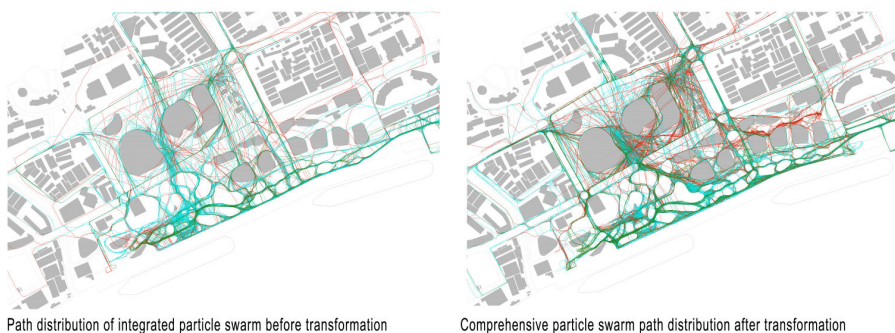


Figure 6. Comparison of particle trajectory before transformation and particle trajectory after transformation.

We can obtain a new public space strategy by adding, reducing, adjusting the form of space, and updating facilities such as service facilities.(YANG, GU and YAO 2019) Based on this new ideal space, we can use the original particle swarm parameters to perform the same simulation, and finally obtain the particle swarm

distribution for comparison and analysis. In this study, a new particle swarm distribution was obtained through limited space modification. We can find that increasing the number of accessible paths in the hinterland of the waterfront and the hydrophilic shoreline can make the distribution of people flow more uniform, and people's walking paths are more likely to be selected. Different types of people are concentrated in different demand sites. At the same time, the installation of service facilities attracts some activities in sites with low crowd density in reality, which makes the overall distribution of the pattern more even.(Figure 6)

## 6. Summary

In this research, a digital multi-agent system platform is used to define different population characteristics of the simulated particles, and the activity characteristics of the elderly, adults, and family groups are studied. And in the North Bund waterfront public space, it simulates and interacts with the spatial elements, thus forming the particle trajectory pattern left by different people interacting with the spatial elements. By analysing the density, distribution, connection relationship and other factors of the particle trajectory pattern, the effect of different people's activities in space is evaluated. Based on this analysis combined with urban design theory, a site update strategy to improve accessibility, visibility, and rich functional diversity is proposed to form a new public space. Finally, a comparison simulation was performed for the new public space to verify the reliability of the strategy. Different from the traditional urban design and reconstruction, this research is based on the crowd behaviour construction of the multi-agent system and the quantification of site elements, and directly studies the user behaviour and site elements to obtain intuitive judgment.

## References

- Chen, Y.G.: 2003, SELF-ORGANIZATION AND SELF-ORGANIZING CITIES, *City Planning Review*, **10**, 17-22.
- Gehl, J. and Svarre, B.: 2013, *How to study public life*, Island press.
- Gu, Z., Yao, J. and Yang, C.: 2017, Research of Generation of Fluid Special Forms with Parametric Method, *Housing Science*, **2017 (12)**, 15.
- Johnson, S.: 2002, *Emergence: The connected lives of ants, brains, cities, and software*, Simon and Schuster.
- Leach, N.: 2009, Swarm urbanism, *Architectural design*, **79(4)**, 56-63.
- Wei, Z., Yuqi, P. and De, W.: 2012, Travel Behavior Change after the Introduction of Public Bicycle Systems:A Case Study of Minhang District,Shanghai, *Urban Planning Forum*, **43(5)**, 76-81.
- Weixin, H. and Weiguo, X.: 2009, " Form Finding" in Non-linear Architectural Design, *Architectural Journal*, **2009 (11)**, 29.
- Yang, C. and Gu, Z.: 2019, Taking The Urban Renewal Design Of Shanghai Hongkou Port Area As An Example, *Proceedings of CAADRIA 2019*.

# A COMPARISON OF DESIGN IMPACT AND CREATIVITY IN THE EARLY STAGE OF COMPLEX BUILDING DESIGN PROCESSES

YUAN SUNG (KRIS) HSIAO

<sup>1</sup>(no affiliation)

<sup>1</sup>chris81413@gmail.com

**Abstract.** This paper applied empirical research, the evidence-based method, on the correlation between creativity and computing tools (parametric and nonparametric tools) for the design ideation stage of complex buildings like hospitals. The computer-based protocol analysis was set at observing two different groups of CAD architects worked in a small design task. Then the statistical tool, SPSS, was applied to explore the relationships of the different activities and the impact of design creativity on the design process. The research discovered that the numbers of idea generation had significant connecting to the parametric design process. Also, the users showed well-organised design decision making and better design cognition performance, such as strategical thought during the ideation stage. On the other hand, the nonparametric design users made fewer design ideas and did not appear clear ideation process in terms of some critical design decision making.

**Keywords.** Algorithmic design; Design creativity; Complex building design; Hospital; Design cognition.

## 1. Background

### 1.1. DESIGN COMPLEXITY AND PROBLEMS

Lawson (1990) suggests that design complexity has a significant relationship to its scale. For example, town planning must accommodate more complicated contexts such as housing, environmental policies, traffic, etc., in contrast to product design which might only consider materials, functions or shapes. The definition of design problems is obviously associated with the level of detail which is initially required by different scales of design. Also, design complexity connects to a variety of problems encountered such as urban-design or town planning needs to solve the problems of urban morphology associated with traffic congestion, parking problems, road accidents, etc. The wider design problems need to be solved in a systematic pattern through pre-organised relationships and an improved problem-solving process (Jones, 1970).

Alexander and Poyner (1967) examine design problems through an abstract model which suggests design, especially architectural design, should not only be decided by a geometrical structure. In other words, they think that architectural design deals with the problem in the complexity of environmental contexts but not

through geometrical arbitrariness. Geometric building blocks can never simply replace our environments; we architects should deeply consider the relationships between nature and function by utilising such building blocks to respond to the complex design problems.

## 1.2. DESIGN CREATIVITY

Hennessey and Amabile (2009) present creativity as an organised representation; an increasingly large concentric circle representing the major levels of the creative forces operating. The circle identifies the creativity level and relevant effects of culture or society and personality on the neurological aspect. They concluded that although there is much creativity research published in this area, the most important factor is how systematic and organised the interrelationship is between the creative impacts of the different forces or contexts. Also, the different backgrounds of the creators should not be checked as part of such a creativity test.

### *1.2.1. Measuring of design creativity and activity*

Torrance (1971) made an evaluation of creativity based on experimental findings from testing college students, using the Torrance Test of Creative Thinking. The results indicated that, in the ideation process, idea fluency (idea numbers), idea flexibility (idea types) and idea originality (uniqueness) have a significant relationship to the creative functioning of the subjects. Also, scores on design enjoyment and stimulation further support the expression of original ideas.

Guilford (1950) suggests there is a considerable relation between design behaviour, or design planning, and the performance of creativity. He particularly emphasises that an organised process including design synthesis and an evaluation process could help to improve the thought process in idea generation. In addition, the motivation and experience of designers are vital factors that could inspire novel ideas.

Runco and Chand (1995) concluded that creative behaviour connects the original product, idea and adaptive problem-solving activities. This is an insight into cognitive outputs. Their research suggests a two-tier model of creative thinking and presents the process as three main activities: problem-finding, ideation and evaluation. There are two additional sub-factors involved in the model: knowledge and motivation. Importantly, the entire process depends on interaction; the process shows the deep interrelation between those activities and the looping action optimises the cognitive process in creative cognition. Runco and Chand (1995) identify that thinking activity is an important information process.

## 1.3. DESIGN COGNITION

There are three important features of the cognitive process: memory, imagery and problem-solving. Firstly, memory provides an important feature of storing information from different situations; it means the ability to learn from the environment. Secondly, visual cognition contains two parts, one is image structure, and the other is image process. Kosslyn and Schwartz (1977) suggested

'Deep representation' which means images in the mind are not independent objects but are an associated mapping system. By literal encoding and propositional encoding, our brains store imagery as coded information then take action on it in different situations with related mental activities.

Lastly, problem-solving is a process to get an expected response from the given situation or goal (Hayes, 1991). This process could be seen as similar to the initial motivation for the design problem-solving process in many design theories. A different cognitive system could be defined and built into the problem-finding model for interaction. Problems input are broken down into several sub-problems in order to clarify the relationships. This interactive process is similar to the systematic or scientific design method of construction.

#### 1.4. PARAMETRIC DESIGN METHODOLOGY

The parametric design process offers variable attributes with mathematical or geometrical algorithms. The parametric model is created by values for parameters or variables and equations to establish the correlations between the objects or geometries (Barrios, 2006). Stavric and Marina (2011) summarised that since the parametric idea was created in 1990, two kinds of parametric designs have been defined: the first is architectural design using parametric conceptions, the second is architectural design using constructive parameters. In other words, conceptual parametric design means creating new computing objects (geometries) and operating them by using parametric values, a norm used in programs such as Grasshopper (a plug-in to Rhinoceros). On the other hand, constructive parametric design assembles the design elements by using a pre-set parametric system and integrates the relationships for building construction such as a procedure found in software packages such as Revit (Building Information Management/Modelling) and ArchiCAD.

Bentley and Corne (2002) introduced an idea for an evolutionary system of creativity including an algorithmic structure and parametric design definition; the system is used for iterative design evaluation that can finally generate the best solution to the design problem. They believe that creativity happens in a constant and structured evaluation and refinement process rather than picking up on an idea without giving the context. Therefore, this section focuses on the concept of the parametric design process and design examples to explore parametric design thinking and operations by providing backgrounds as well as investigating the creative potential of the design methods.

## 2. Research Methodology

### 2.1. RESEARCH HYPOTHESIS

The main research hypothesis can be stated as: '*Parametric design methodologies not only assist the architect in the management of design organization but also increase the potential of creativity at the early stages of complex building design process*'. A comparative study of parametric and nonparametric Computer-Aided Design (CAD) has been carried out in this research in order to gauge and understand different reactions to them as well as the potential creativity shown



during these CAD processes in hospital design/complex building.

## 2.2. RESEARCH SAMPLE AND DESIGN TASK

There were 30 participants selected for this study. All participants had around five years' experience in hospital design and the use of CAD; the participants were working at the time in Taiwanese hospital design firms. The participants were requested to propose a conceptual floor plan design, in 45 minutes, for the ground floor outpatient department of a hospital in Taiwan. The reason for selecting an outpatient centre design task rather than an inpatient project was the aim to test the CAD methodology for complex design integration and the user's reaction during the design problem-solving process.

The experimental work was applied to observe the on-going design behaviour when using different CAD methodologies for a pre-selected design task. The investigation used represents two stages of research methodology; the first is a computer-based protocol analysis and the second is based on the data of protocol analysis applying to statistical research with a software package, that is Statistical Package for the Social Sciences (SPSS). This investigation aimed to test the early design stages such as the ideation process rather than testing the entire design project.

## 2.3. MEASURING THE DESIGN PROCESS

The idea numbers produced in the design process use the definition of design intention, a single design idea, which follows Goldschmidt's (1991) definition: 'an act of reasoning which presents a coherent proposition pertaining to an entity that is being designed as a segment'. The other recorded transcripts were divided into four categories: Design Process, Problem Formulation, Design Cognition and Form Exploration. Each category presented a different aspect of the design. Through statistical comparison of the recorded behaviours and time-based investigation, the research further explored the impacts by numbers during the design process as well as discussing the relevant variables which were found in the design task.

## 3. Findings

### 3.1. CREATIVITY IN THE DESIGN IDEATION PROCESS

The result exhibits the descriptive statistics used for idea production associated with the performance of CAD in each group. The study summarises the results in Table1 and concludes that there was a statistical mean of 7 ideas generated in the algorithmic/parametric CAD process (Table1-A), compared to a mean of 1.5 to 2 ideas created by the nonparametric CAD activities (Table1-B). Table 1 percentiles also indicate that over 50 per cent of participants using Grasshopper developed at least 6 or 7 ideas in general (Table1-A1). On the other hand, of the participant's designing with AutoCAD of the nonparametric CAD, over 50 per cent could only generate 1 idea for the design task (Table1-B1). Moreover, if we check the value of the standard deviation (SD), we can measure the extent of dispersion of idea production in each of the design methods. The parametric

design method (Grasshopper) shows a 1.47 SD (Table1-A2) and the SD for the nonparametric design using AutoCAD is 0.73 (Table 9.1-B2). This result confirms that AutoCAD/nonparametric CAD was involved in idea generation but only where the data distribution is located within a small range; 1 to 2 (idea numbers).

Table 1. The creativity evaluation between the CAD ideation process.

Grasshopper	N		Valid	30
			Missing	0
	Mean		A	7.3000
	Std. Deviation		A2	1.46570
	Skewness			.283
	Std. Error of Skewness			.427
	Percentiles		25	6.0000
			50	7.0000
			75	8.0000
	AutoCAD	N		Valid
		Missing	0	
Mean		B	1.5000	
Std. Deviation		B2	.73108	
Skewness			1.135	
Std. Error of Skewness			.427	
Percentiles		25	1.0000	
		50	1.0000	
		75	2.0000	

Besides, the results of the independent samples test, T-Test (Table2), demonstrate there was a statistically significant difference ( $P < 0.05$ ) between the different CAD methods and idea production. The Eta squared,  $red = \frac{t}{t^2 + (N1 + N2 - 2)}$ , measured additionally shows that the effect size of these groups equalled 0.9, which strongly supports a large effect. This means if the architects switched design methods from nonparametric CAD (AutoCAD) to parametric/algorithmic CAD (Grasshopper), this could have an obvious and positive impact on their ability to produce a greater volume of ideas (shown by a large effect size of 0.9).

Table 2. T-Test shows a significant impact on the creativity of parametric CAD utilising.

		Equality of Variances		t-test for Equality of Means						
		F	Sig.	t	df	Sig. (2-tailed)	Mean Difference	Std. Error Difference	of the Difference	
									Lower	Upper
IdeaNumbers	Equal variances assumed	12.949	.001	19.395	58	.000	5.80000	.29904	5.20141	6.39859
	Equal variances not assumed			19.395	42.589	.000	5.80000	.29904	5.19676	6.40324

$$\text{Eta squared} = \frac{t}{t^2 + (N1 + N2 - 2)}$$

$$\rightarrow 0.9 = \frac{19.4^2}{19.4^2 + (30 + 30 - 2)}$$

.01= Small effect  
.06= Moderate effect  
.14=Large effect

During the design process, parametric design using the algorithmic method created an accumulated ideation process. Each design idea was generated with an associated algorithm or a group of algorithmic procedures and could be open-endedly connected to other ideas. The mathematically-based and associated algorithmic design ideas can be easily added to or modified using an absolutely

correct mathematical process with objective parameters such as scale, distance, angle, length and width. They increase the complexity and elaborateness of the design definition step-by-step and can complete the design problem-solving process with an appropriate solution.

Tedeschi (2011) suggests that a visually-based design process using Grasshopper certainly helps architects to target complex design problems; the node-diagram, also called a flow chart, visualises the design dependencies with instant effects on the design drawing. The second advantage of design ideation using an algorithmic approach is that 'An algorithm is a procedure for addressing a problem in a finite number of steps using logical if-then-else operations' (Terzidis, 2003). This indicates that algorithmic CAD defines every design action as a functional component; these components can be linked in a finite diagram, which means the architect never loses sight of the design process.

### 3.2. CREATIVITY IN THE DEVELOPMENT OF DESIGN COGNITION AND DESIGN BEHAVIOUR

This section extends the study of the ideation process into a pattern works of observing the design behaviours across the two types of CAD methods. The study provides a test of statistical correlation between design cognition, activities and the creativity indicator; the idea numbers as well as providing a mathematical regression equation for calculating the present, the expected time spent on the design actions and its influences on the production of ideas.

#### 3.2.1. *The parametric / algorithmic design method using Grasshopper*

Using the Pearson correlation test, three aspects were reported in the results. First, the synthesis ( $r=0.43$ ,  $p<0.01$ , 19 per cent of variance) and evaluation ( $r=0.96$ ,  $p<0.00$ , 93 per cent of variance) of the algorithmic CAD process showed a significant correlation with the production of idea numbers. In particular, the 93 per cent ( $r^2*100=y\%$ ) of variance between design evaluation and idea numbers indicated there was a significant relation between idea testing and idea production. This confirmed that the majority of the algorithmic design ideas had been supported by the design evaluation activity. Nigel (2011) suggests that an intensive engagement with idea testing is often found in innovative designers' processes.

Second, a strong correlation was also shown between problem identification ( $r=0.73$ ,  $p<0.00$ , 53 per cent of variance) and idea numbers meaning the mathematically-based design algorithms not only helped the architects in their design problem-solving processes but also improved the production of idea numbers. Jones (1970) highlights that mathematics is good not only for defining the design problem but also for optimising the design solutions.

Last, a close relationship between the design cognition process (cognitive memory:  $r=0.58$ , image:  $r=0.58$  and problem-solving:  $r=0.53$ ;  $p<0.00$ ) and idea numbers indicated that algorithmic design cognition operated well and have completely supported the design ideation process.

From the aspect of design cognition, we can ensure that the algorithmic

ideation contains an organised design strategy especially focused on the exploration of certain design problems and solutions rather than quickly targeting one specific answer to the design proposal. Mathematical thinking also extends the architect’s mental process through a series of mathematical problem-solving activities. For instance, the problem of travel efficiency needs to be identified as a mathematical process of distance calculation. Also, this design method is flexible in the process and can be tested and upgraded through the construction of a specific design algorithm that exhibits a cognitive design learning activity. As Nigel (2011) states, idea creativity means that ‘the clear, generative concept is not simply found in the problem as given, but is largely created by the designer; it is not a matter of recognising a pre-existing pattern in the data, but of creating a pattern that re-formulates the problem and suggests directions toward a solution’.

Design efficiency measures the time spent on individual design activities in relation to the number of ideas generated. The first of the scatter diagrams and relevant regression equation (Fig.1) provide further evidence of the relationship. For example, if the architects individually spent ten minutes (600 sec.) on design synthesis ( $6=4.48+1.7*0.001*600$ ), they were able to get around 4 to 6 relevant idea numbers.

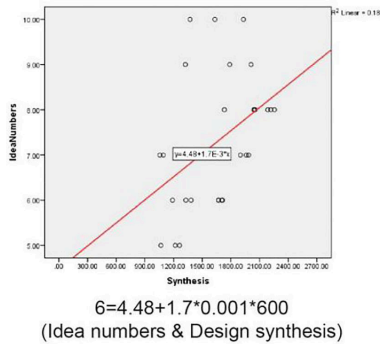


Figure 1. The scatter of parametric CAD design activity and idea numbers.

Besides, the regression test (Table 3) could further provided predictive calculations of the design performance between activities and ideas for future expectations. The prediction equation  $Z$  (idea numbers) =  $a(X)$  proposed design behaviour +  $C$  (constant value) confirms that if the architects were to engage in design synthesis ( $10.5=0.002*3000+4.478$ ) for 50 minutes (3000 sec.), the predicted idea numbers could be approximately 10 to 12, which means these design activities could support productive ideation.

Table 3. The predictable parametric design creativity by regression calculation.

Coefficients <sup>a</sup>						
Model		Unstandardized Coefficients		Standardized Coefficients	t	Sig.
		B	Std. Error	Beta		
1	(Constant)	4.478	1.135		3.947	.000
	Synthesis	.002	.001	.434	2.547	.017

a. Dependent Variable: IdeaNumbers

### 3.2.2. The nonparametric design method using AutoCAD

When it came to the nonparametric design process, the Pearson correlation found that idea numbers had a considerable relationship to design evaluation in 82 per cent of the variance,  $r = 0.9$  (large effects),  $p < 0.00$ . Medium effects between ideas and cognitive memory were also formed (13 per cent variance,  $r = 0.4$ ,  $p < 0.048$ ) as well as finding the form (18 per cent variance,  $r = 0.4$ ,  $p < 0.02$ ). Surprisingly, the idea generation of the nonparametric CAD process was not closely associated with the design synthesis or problem exploration. It meant the nonparametric CAD architects presented their idea assessment through their design experience rather than identifying their design process. Additionally, cognitive memory (CAD functions) and finding form were connected to idea production, which indicates the architects could have had some design prototypes in mind and directly presented them while they were engaging in the design project. That is to say, these AutoCAD/nonparametric CAD architects certainly employed a primary generator as their design method that is a conventional design ideation process representing design ideas arising from a pre-defined design concept (Darke, 1978). This design method has to be aligned with a pre-defined evaluation process, as Agabani (1980) argues in their proposal that evolutionary and revolutionary modification are essential processes in the early design stage of the primary generator. However, the primary generator design method is similar to an induction design process that creates a subjective design idea and forces the design process, including evaluation, to follow and support the main concept. The problem is that this method and the related design considerations can block idea generation due to its subjective design testing and the repeated utilisation of experience and memory of some typical form and layout prototypes, all of which may hinder design creativity. Regarding the cognitive design process, the correlation analysis revealed a similar pattern to the parametric design users. The cognitive memory had a significant correlation with cognitive image ( $r = 0.56$ ,  $p < 0.00$ ) and problem-solving ( $r = 0.49$ ,  $p < 0.01$ ). However, when it comes to the values of effect, the numbers were lower by about 32% and 24% when compared with around 80% and 81% for those same aspects in algorithmic design. This means the nonparametric design cognition had a weak connection between the cognitive stages, designers need more practices to reinforce their experience of designing problem-solving process.

However, the scatter diagram and the related regression equation (Fig.2) shows that when the AutoCAD architects spent ten minutes (600 sec.) on design evaluation, they could produce 4 ideas ( $4 = 1.14 + 4.78 * 0.001 * 600$ ). In addition, the regression test (Table 4) confirmed that if the architects were to

engage in design evaluation for around 50 minutes (3000 sec.), the prediction of idea numbers could be approximately 16 ( $16.4=0.005+3000*1.142$ ). These outcomes indicate how the evaluation of the design supported idea generation in the nonparametric CAD design process. Although the results for design evaluation show a productive impact on idea numbers, in reality, the percentile research shows 25 per cent of architects had spent less than two minutes (around 70 sec.) on design evaluation. The reason for this is simply that nonparametric design using AutoCAD cannot provide a valid objective design evaluation platform; the CAD program does not have any tools for the simulation of the geometrical functional and environmental performance of design ideas and functions. In addition, without the mathematics-based design ideation process, it is also difficult to engage in concept evaluation except for other extra forces such as technical assistance and engineering study.

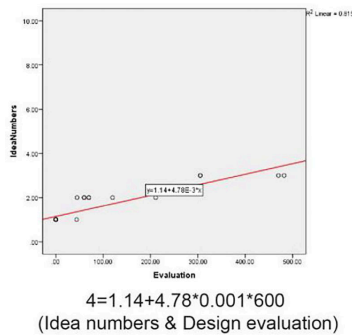


Figure 2. The scatter of nonparametric CAD design activity and idea numbers.

Table 4. The predictable nonparametric design creativity by regression calculation.

		Coefficients <sup>a</sup>			t	Sig.
		Coefficients		ed		
Model		B	Std. Error	Beta		
1	(Constant)	1.142	.067		17.104	.000
	Evaluation	.005	.000	.903	11.090	.000

a. Dependent Variable: IdeaNumbers

#### 4. Conclusions

Although there are some researches have discovered the parametric CAD provides positive design result in terms of idea generation and variation, there is very limited of them identified this result with strong evidence-based analysis such as percentage of impact and coefficients of effect size..etc. The research finds demonstrate the impact size on idea numbers and the related design behaviour showed that the parametric design produced impressive idea numbers, which is

an important indicator, according to Torrance's (1950) creativity identification system. Also, the calculation predicted that the longer the experience with using algorithmic CAD, the better the architects were able to produce more numbers of design ideas. On the other hand, the study discovered that the nonparametric CAD users produced limited idea numbers in their design process, even while using the same CAD tool. In addition, the correlation test of creativity in the design process and design behaviour further demonstrated that parametric/algorithmic CAD was well-organised with a systematic thought process and was focused on decision-making strategies through the activity of design synthesis and evaluation as well as the problem identification. This strategic thinking is akin to a scientist's thought processes, namely, being problem-focused and obliged architects to understand the design problem structurally and improved recognition of design problems through a process of algorithmic design definitions. By contrast, nonparametric design appeared to show disconnected design thinking when targeting particular design problems and an inability to think about all cognitive factors together. In addition, the time calculations on design performance using scatter diagram and linear regression analysis techniques suggested that nonparametric design analysis took too long and affected the problem formulation process in terms of both problem classification and problem identification. This was because the weaker design structure could not support the design synthesis process, which made the design context more complicated. Consequently, architects needed to spend more time on both the making of the design structure and the problem-solving process.

## References

- Agabani, F.: 1980, *Cognitive Aspects of Architectural Design Problem Solving*, Ph.D. Thesis, University of Sheffield.
- Alexander, C. and Poyner, B.: 1967, *The atoms of environmental structure*, Ministry of Public Building and Works.
- Barrios, C.: 2006, *Thinking parametric design: introducing parametric Gaudi*, Design Studies, London.
- Bentley, P. and Corne, D.: 2002, *Creative evolutionary systems*, Academic Press, San Diego.
- Darke, J.: 1979, The primary generator and the design process, *Design Studies*, **1(1)**, 36-44.
- Guilford, J.: 1950, Creativity, *American Psychologist*, **5(9)**, 444-454.
- Goldschmidt, G.: 1991, The dialectics of sketching, *Creativity Research Journal*, **4(2)**, 123-143.
- Hayes, N.: 1991, *Introduction to cognitive processes*, BPS, Leicester, England.
- Hennessey, B. and Amabile, T.: 2009, Creativity, *Annual Review of Psychology*, **January 2010**.
- Jones, J.: 1970, *Design methods*, Wiley-Interscience, London.
- Kosslyn, S. and Shwartz, S.: 1977, A simulation of visual imagery, *Cognitive Science*, **1(3)**, 1-6.
- Lawson, B.: 1990, *How designer think*, Architectural Press, Oxford.
- Nigel, C.: 2011, *Design thinking: Understanding how designers think and work*, Berg.
- Runco, M. and Chand, I.: 1995, Cognition and Creativity, *Educational Psychology Review*, **7(3)**, 243-267.
- Stavric, M. and Marina, O.: 2011, Parametric Modeling for Advanced Architecture, *International journal of applied mathematics and informatics*, **5(1)**, 9-16.
- Terzidis, K.: 2003, *Algorithmic architecture.*, Architectural Press, Oxford.
- Torrance, E.: 1971, Stimulation, enjoyment, and originality in dyadic creativity, *Journal of Educational Psychology*, **62**.

# FANTASTIC FACADES AND HOW TO BUILD THEM

SURAPONG LERTSITHICHAJ

<sup>1</sup>*Faculty of Architecture, Chulalongkorn University*

<sup>1</sup>*surapong@cuinda.com*

**Abstract.** As part of an ongoing investigation in augmented architecture, the exploration of an architectural facade as a crucial element of architecture is a challenging design experiment. We believe that new architectural facades when seamlessly integrated with augmented architecture, enhanced with multiple functionalities, interactivity and performative qualities can extend a building's use beyond its typical function and limited lifespan. Augmented facades or "Fantastic Facades," can be seen as a separate entity from the internal spaces inside the building but at the same time, can also be seen as an integral part of the building as a whole that connects users, spaces, functions and interactivity between inside and outside. An option design studio for 4th year architecture students was offered to conduct this investigation for a duration of one semester. During the process of form generations, students experimented with various 2D and 3D techniques including biomimicry and generative designs, biomechanics or animal movement patterns, leaf stomata patterns, porous bubble patterns, and origami fold patterns. Eventually, five facade designs were carried on towards the final step of incorporating performative interactions and contextual programs to the facade requirements of an existing building or structure in Bangkok.

**Keywords.** Facade Design; Augmented Architecture; Form Generation; Surface System; Performative Interactions.

## 1. Introduction

There has always been great fascination with architectural facades amongst architects since its invention over a century ago. Facades are usually designed to be visually attractive, showcasing a building's structural order and exploring many possibilities in form generations of the building mass. A facade usually sets the tone and identity for the rest of the building as it is the first visual element you perceive of a building. Today's architectural facades encompasses a variety of functionality and technological advancements throughout the process lifecycle of its design, construction and maintenance.

In terms of structure, facade fabrication has also developed from a simple rigid frame to a point-supported, double-skinned, and membrane-structured frame. Some structures provide flexibility for users and allow for facade panel movements depending on how users choose to manipulate them whether it be manually



operated (Storefront for Art and Architecture in New York) or automated by computers (Al Bahar Towers in Abu Dhabi). In addition to this, modern facades are becoming more energy-efficient, ecological conscience, electricity generating and a more intelligent element of the building, responding to the ever-changing environment and the needs of its users.

In the future, the design of these high performance facades will become extremely complicated to imagine and construct without the assistance of computer-aided technologies. Facades will also be much more effective with the development of new construction methods and new digital technologies that can offer customized interactivity to its users making future architecture always relevant and updated and possibly extending its lifespan.

## **2. Prelude to Augmented Architecture**

Referring to an ongoing investigation called augmented architecture, the project explores physical architecture that interactively responds to changes in human behavior due to new digital technologies such as the proliferation of digital devices, social media, embedded networks and intelligent surfaces (Lertsithichai, 2019). These digital technologies have great impact on the psychosocial aspects of a modern human life. New means of conducting activities have also changed due to digital technology and changes to physical architecture is no exception. Architecture of the future must respond to these changes and enhance the user experiences in order to remain relevant throughout its possible lifespan.

The most prominent element of a building is the facade which is multi-purposed in its function and tightly connected to meaning, identity and context of the urban fabric. While the lifespan of a typical building is around 50 years, many questions arise from how one can extend its use beyond the limitations of time. What role can a new type of architectural facade take to extend the buildings usage? How can new architectural facades be designed to respond to these challenges and become an integral part of new augmented architecture?

## **3. Fantastic Facades**

New architectural facades that are seamlessly integrated with augmented architecture, enhanced with multiple functionalities, interactivity and performative qualities are coined as augmented facades. These “Fantastic Facades” can be seen as a separate entity from the internal spaces inside the building but at the same time, can also be seen as an integral part of the building as a whole that connects users, spaces, functions and interactivity between inside and outside. For example, the moving facade of “One Ocean” thematic pavilion built for Expo 2012 in Yeosu, South Korea is seamlessly integrated into the building’s envelope. Inspired by nature, the prominent fish-gill like louvers on the building surface can open and close interactively as its main function is to control light conditions for internal spaces. While moving, it also creates animated patterns alongside its facade that can be viewed both from inside and outside the building. The choreography of this movement ranges from very subtle to waves spreading over the whole length of the building.

Another example is the BIX facade of the Graz Art Museum represents a singular fusion from architecture and new media. A combination of the words “big” and “pixels,” the facade is an acrylic glass skin of the eastern side of the building and consists of 930 fluorescent lamps whose brightness can be individually adjusted. the facade can also be used as a large screen for films and animations in what is referred to as a communicative display skin or a performative surface. As these examples show what is possible with current technologies, with further explorations in new technologies, new functions or new methodologies, what else could be done and how can one achieve this with a design approach?

#### **4. Facade Design Exploration**

To explore new fantastic facade designs, an option studio was offered to year 4 architecture students with an experimental design methodology that spanned one semester or 4 months. The challenge was to develop new types of facades for augmented architecture by following a controlled procedure that towards the end could bear various results. Referring to prior research in facade designs including performative building skin systems (Biloria & Sumini, 2009), adaptive surfaces, transformable structures and building envelopes (Lovell, 2010). The following process is how the studio approached facade designs.

##### **4.1. FACADE RESEARCH**

Starting with background research of existing facade designs in the past and new technologies of the future that may be applicable to facade designs. Over 12 case studies were selected and categorized into a building facade typology consisting of static (analog), dynamic (kinetic), interactive (adaptive) and hybrid (combinations). A static facade is built to be fixed with no kinetic movements of its facade elements. The design can be strictly functional responding to needs of its surrounding environment i.e. shading devices or with iconic forms and colors for visual stimuli. A dynamic facade is determined by its kinetic properties of its facade elements. Certain components could move mechanically with no electronic assistance, powered by wind or built with smart materials that change colors or form when exposed to heat or humidity. The interactive facade has features that can be controlled or pre-programmed electronically to interact with the environment or its users using a wide range of input sensors. Movements can be subtle and isolated, collective as a whole or transformative changing the appearance. Lastly, the hybrid facade or a combination of the aforementioned types. Some features of these facades can operate with or without power and can operate differently depending on the user. For the purpose of this research, students focused mainly on interactive and hybrid facades for further project references. Design insights of how surface forms are generated, how a structure is implemented and how the facade responds to users or its environment were analyzed and presented then shared online as reference during the following project proposals.

## 4.2. FORM GENERATION

After surveying existing façade designs, student are required to design new shapes and forms for the facade surface. Inspired by the concepts of biomimicry (Pawlyn, 2011), biomimetics and biomechanics (Benyus, 2002), a unique way to explore shape and form generation can be achieved through the study of natural order and designs (Thompson, 1942). While Thompson explores the growth of eggs, skeletons, crystals and other natural objects in terms of mathematics, economy and transformation, biomimicry explores a systems-based approach to innovation and design that mimics natural constructs. Students were encouraged to generate a new form or surface inspired by natural elements through an experiment with materials and structures using traditional or digital tools. The following are the inspirations and experimentation results.

### 4.2.1. Bubbles

Using soapy water bubbles structure as an inspiration of surface generation, the first group experimented with a process to recreate a bubble-like surface that is rigid and retains its organic shape. For the experiment, water-based gel balls roughly 1 cm in diameter, are placed in a glass tank and submerged in water. Melted aluminum is then poured into the mix filling in the gaps between the gel balls. The result is an aluminum structure with multiple holes that visually look similar to bubble inspiration (Figure 1).

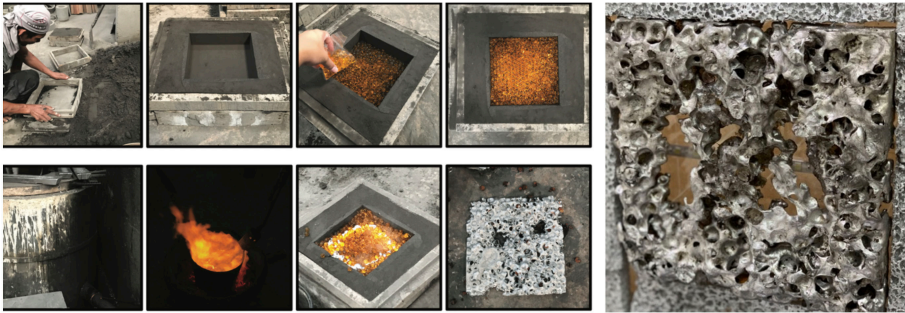


Figure 1. Form generations from bubble-like structures created by replacing gaps between gel balls with melted aluminum then left to cool down. The result is a porous surface with unique textures.

### 4.2.2. Biomechanics

The second group pursued the tracking movement of animal limbs and its joints as pivotal points to help generate interesting continuous line patterns. The 2D motions are then transferred into Grasshopper with 3D motions creating a three-dimensional surface pattern. Parameters such as radius, distance, angle of rotation are adjusted and tested until the best manageable 3D surface is generated (Figure 2).

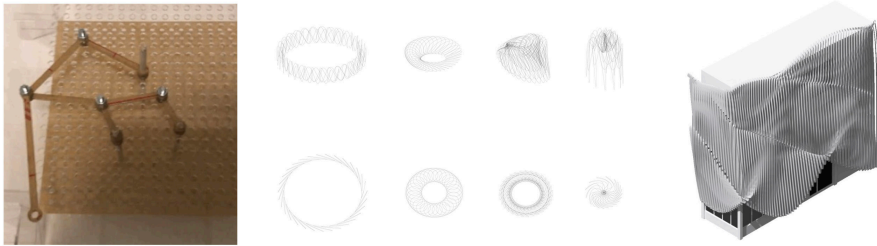


Figure 2. Physical biomechanical experiments using flexible pivotal structures can generate ambiguous but interesting 2D patterns. The same structure is reenacted in Grasshopper but modified to generate a continuous 3D surface.

4.2.3. Stomata

Inspired by the shape and pattern of a leaf stomata, the third group uncovered structural patterns of a leaf surface with stomata (Figure 3). A similar pattern is simulated with Grasshopper in 2D and combined with tree-like trunk sub-surface structures to create a unique 3D surface system.

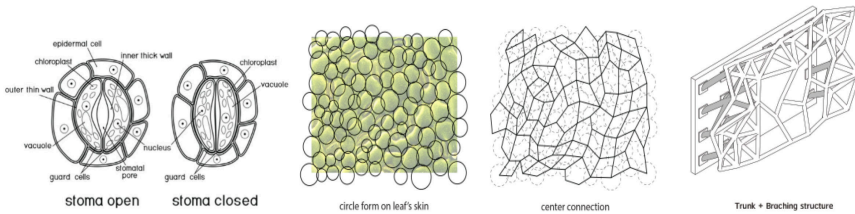


Figure 3. A stomata or an opening beneath a leaf surface (left), the mapping of the stomata points in 2D (center), and the combined 3D surface with a supporting framework.

4.2.4. Origami

The last group took inspirations from natural movements of a flower blooming, an sea anemone and the surface structure of Japanese origami. The 2D origami surface is curled into a cylinder, fixing one side and allowing the opposite side to open and close similar to a sea anemone. The combined shapes can form a functional building envelope to allow air ventilation into a building or respond to direct sunlight as a sunshade device.



Figure 4. The blooming of a flower and sea anemone (left) combined with origami folds (center) inspired this blooming flower-like form for a facade surface (right).

#### 4.3. SURFACE SYSTEM

Creating a unique surface usually requires a complex supporting structure that may not conform to industrial standards. The combination of a new surface and structure or a new surface system may need to look into inspirations from nature again. Nature has always been the best source of inspiration for designers and architects as a result of nature's billion years of evolution. Searching for answers from complex natural structures can help designers create a better and more efficient structure for a surface system. Therefore each surface proposed earlier, must design supporting structures that best fit the new form and combine them into a single scalable surface. The surface system can be considered as a modular surface system, a continuous or irregular surface system or a folded surface system depending on the economy of scale.

#### 4.4. PERFORMATIVE INTERACTIONS

Next, for the surface system to be functional and meaningful as a new architectural facade, performative interactions such as kinetic movements (Fortmeyer et al., 2014), digital information or visual displays to enhance user perception and experiences is an important progression for the design project (Telhan et al., 2010). The facade performance can be both functional or aesthetical but should always retain some meaning to its users and surrounding environment. Therefore, part of this requirement is for students to create a working prototype facade that can demonstrate its functionalities and performative interactions in specific scenarios. Simple Arduino starter kits were introduced to the studio along with various sensor inputs to provide a broad range of possible interactions for the facade prototypes.

#### 4.5. CONTEXTUAL PROGRAM

A building facade remains one of the most important exterior elements perceived by users in an existing context. One building facade may be suitable for a building located in a particular site and environment but may not be duplicated for another location. Differences in environmental features and culture impact the look and feel of a building facade. While the facade is an elegant external component that defines unique architectural aesthetics of the building, it also has the critical role related to sustainable performance and interior function of a building. Therefore,

students were asked to seek existing buildings or abandoned buildings and convert them into a functional architecture complete with a novel program. The new augmented facade that is to be incorporated into the building must align well with the proposed program and functions inside the building while considering the context of the site and site specific conditions in order for the building to fit in its urban fabric and not stand out alienated from its surroundings.

## 5. Facade Design Projects

After 4 months of experimentation, 8 facade projects were proposed complete with a surface system, performative interactions, a contextual program and a working prototype. Only 4 projects are highlighted here as the following.

### 5.1. ARTIFICIAL LUNG FACADE

The first project called the “Artificial Lung Facade” explored stomata patterns and applied a concept of breathable facades that could filter PM2.5 or fine particulate matter in the air as its main function and integrated it into facades of elevated skywalks where heavy traffic was present. The prototype incorporated a sensor that when PM2.5 is detected will activate and suck outside air into a closed chamber filled with layers of filters before returning only clean air (Figure 5). The project determined the production time and volume of fresh air required to purify the area and calculated the amount of surface area that the artificial lung would be installed on the existing skywalk facade.

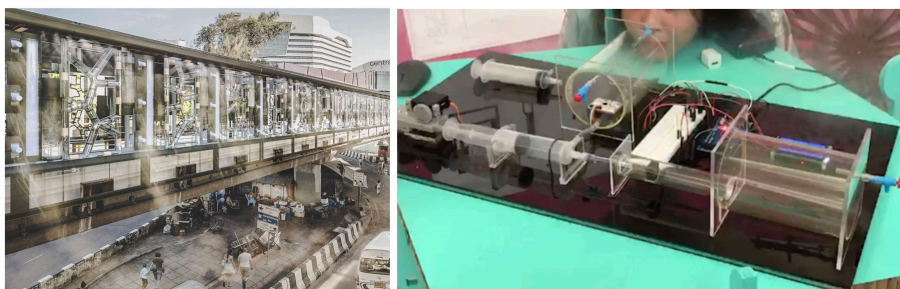


Figure 5. A rendering of the proposed artificial lung facade in a congested intersection (left), and the working prototype consisting of sensors, linked air chambers and air filters (right).

### 5.2. THEATER PERFORMANCE FACADE

The second project was a “Theater Performance Facade” for entertainment purposes fitted onto an old movie theater to revitalize its presence while preserving the building’s art deco style. The prototype included an array of interactive spinning flower shape patterns inspired by the ceiling decorations and programmed to activate during important times of the day or when ventilation is required. A prototype was built to demonstrate how the patterns could spin in various speeds and rotate clockwise or counter-clockwise to control air flow in or out of the theater (Figure 6).



Figure 6. Theater performance facade project using spinning flower shape patterns that double as visual performance elements and a ventilation fan.

### 5.3. SOUND ACTIVATED FACADE

The third project called the “Sound Activated Facade” was a redesigned factory building facade for an audio speaker manufacturer that could be used to test acoustic characteristics of their products. The prototype explored how sound waves could be translated into push and pull movements behind a grid facade covered with fabric and activated in real time through a Grasshopper plug-in. The prototype demonstrated how sound input to a laptop could interactively activate the servos behind the facade through Grasshopper in real time (Figure 7).

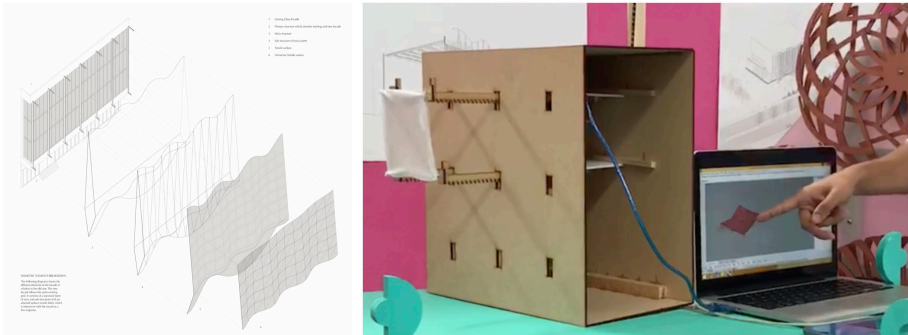


Figure 7. Mechanical pistons and fabric elements of the facade (left) and the demonstration of the real time interactivity of sound input towards the facade surface geometry (right).

### 5.4. EMOTION MAPPING FACADE

The last project is the “Emotion Mapping Facade” designed an interactive facade for an art and culture center that corresponds to visitor’s emotions towards displayed artworks. The prototype captured visitor’s facial expressions, analyzed the depth map and translated it into movement and color of a grid unit facade in real time. The prototype demonstrated how each unit can reconfigure its shape in

real time depending on readings of a video stream of a face through Grasshopper (Figure 8).

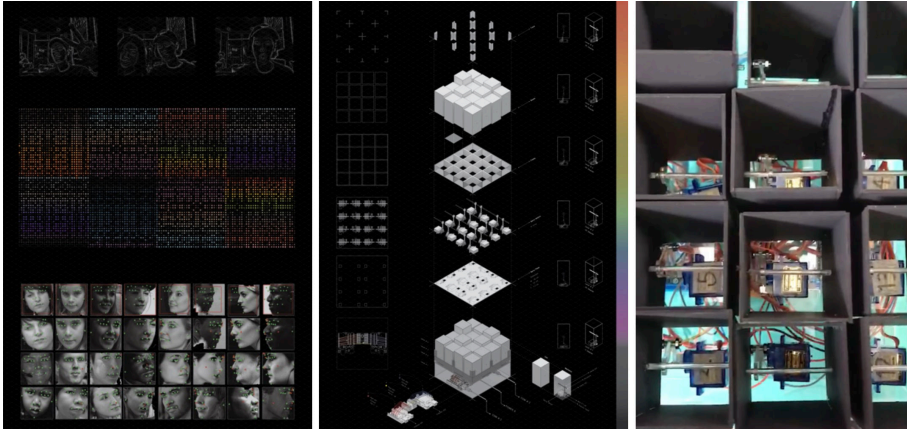


Figure 8. Mapping facial attributes with emotions (left), translating emotions into horizontal movements of façade pistons (center), and prototype model of interactive facade grid all of which are done in real time with Grasshopper (right).

## 6. Conclusion and Future Work

The investigation of fantastic facades within a design studio for architecture students is quite limited in terms of required time for implementation. The process of building a facade consisting of facade research, form generation, surface system, performative interaction, and contextual program requires a significant amount of time for refinement in each stage beyond a duration of 4 months. According to course feedback, the most productive and creative processes for students were the form generation and performative interaction processes. Students drew many inspirations from nature that could be applicable to unique form generations and discovered novel functionalities for an existing building through this process. They believe the experience can be applicable to their next design studio project and possibly their future practice. Unfortunately, little time was spent to investigate the use of building materials and its properties for form generation and performative interactions. Access to smart materials and construction materials was hindered by cost and size of materials. Also, the time spent to develop a working prototype for all projects was insufficient to showcase some features of the prototype in its entirety. This is due to the lack of experience in Arduino programming and building electronics of a few students.

As an open design studio, it is not realistic to determine whether the facade designs could possibly extend the lifespan of an existing building but rather to determine how the designs offer a new functionality (artificial lung facade) or supplementary use for the building in the near future (theater performance facade, sound activated facade) and enhance user experience towards a building (emotion mapping facade). Despite the limitation in time and investigative setbacks, two



projects (artificial lung facade and sound activated facade) were pursued further into a design patent registered by the university. Future directions for a continuous investigation of augmented architecture would look into transformable structures and spatial intelligence.

### Acknowledgements

The author would like to acknowledge the following students and assistants for their participation throughout the studio duration; Vedant Urumkar, Natcha Kikhoontod, Thanapon Harnpattanapanich, Thanakarn Srathongin, Natchapongtorn Gaesornsuwan, Atitep Rungkeeratikul, Panisa Kleosakul, Sarida Thanakarnjanasuth as well as guest reviewers; Michael Drinnan, Jaturon Kingminghae and Sorachai Kornkasem for their invaluable comments and suggestions. Lastly, the kind support and funding from the Faculty of Architecture, Chulalongkorn University in Bangkok, Thailand.

### References

- Benyus, J.M.: 2002, *Biomimicry: Innovation Inspired by Nature*, Harper Perennial.
- Biloria, N. and Sumini, V.: 2009, Performative Building Skin Systems: A Morphogenomic Approach Towards Developing Real-Time Adaptive Building Skin Systems, *International Journal of Architectural Computing*, 7(4), 643-676.
- Fortmeyer, R. and Linn, C.: 2014, *Kinetic Architecture: Designs for Active Envelopes*, Images Publishing Dist Ac..
- Lertsithichai, S.: 2019, Augmented Architecture: Interplay between Digital and Physical Environments., *Proceedings of CAADRIA 2019*, New Zealand, 353-362.
- Lovell, J.M.: 2010, *Building Envelopes: An Integrated Approach*, Princeton Architectural Press.
- Pawlyn, M.: 2011, *Biomimicry in Architecture*, RIBA Publishing.
- Telhan, O., Casalegno, F., Park, J., Kotsopoulos, S. and Yu, C.: 2010, Interaction design with building facades, *Proceedings of the 4th International Conference on Tangible and Embedded Interaction*, 291-294.
- Thompson, D.W.: 1942, *On Growth and Form*, Dover Publications.

# DOES ARCHITECTURAL DESIGN OPTIMIZATION REQUIRE MULTIPLE OBJECTIVES?

*A critical analysis*

THOMAS WORTMANN<sup>1</sup> and THOMAS FISCHER<sup>2</sup>  
<sup>1,2</sup>*Xi'an Jiaotong-Liverpool University*  
<sup>1,2</sup>*{thomas.wortmann|thomas.fischer}@xjtlu.edu.cn*

**Abstract.** This paper analyzes eight assumptions that underly the general consensus in the computer-aided architectural design community that multi-objective optimization is more appropriate for and more analogous to architectural design processes than single-objective optimization. The paper discusses whether (a) architectural problems are best formulated as multi-objective optimization problems, (b) architectural design optimization is only about negotiating tradeoffs, (c) multiple objectives require multi-objective optimization, (d) Pareto fronts represent design spaces, (e) Pareto fronts require multi-objective optimization, (f) multi-objective algorithms are efficient and robust, (g) evolutionary operators make multi-objective algorithms efficient and robust and whether (h) computational cost is negligible. The paper presents practical examples of combining multiple objectives into one and concludes with recommendations for when to use single- and multi-objective optimization, respectively, and directions for future research.

**Keywords.** Multi-objective optimization; Architectural Design; Scalarization; Pareto front; Evolutionary Optimization.

## 1. Introduction

Architectural Design Optimization (ADO) is a well-established research subject and practice in computer-aided architectural design (CAAD). A specialist technique for decades, the availability of parametric design platforms such as Grasshopper and optimization tools such as Autodesk Refinery make optimization increasingly accessible to broader communities of designers. ADO offers methods and tools to design more resource- and energy-efficient buildings with reduced life-cycle costs. Improving efficiency arguably is the most important challenge facing architects today as humans deplete global resources, pollute ecosystems, and cause rapid changes in climate. To inform applications of ADO in CAAD, we present a critical analysis of the related discourse. Specifically, we examine the long-standing consensus in the CAAD community that multi-objective optimization (MOO) is more analogous to architectural design processes than

single-objective optimization (SOO) and that, therefore, MOO is more appropriate for ADO than SOO. We identify eight (sometimes more, sometimes less explicit) assumptions underlying this consensus and challenge their rationales in light of experiences both published by others and made by ourselves.

## **2. “Architectural Problems are Multi-Objective Optimization Problems”**

The ADO literature often suggests that, since architectural design problems are characterized by multiple and conflicting goals, ADO problems are best formulated with multiple objectives. Radford and Gero (1980, p.76-77) introduce their seminal paper on (mostly) MOO as follows: “In single objective problems the aim is simply to identify the solution that gives the optimal value .... But buildings and their component systems are rarely designed with a single aim in mind”. Burry and Burry (2012, p.262) state that “architectural design is concerned with bringing things together”, which makes research on MOO “very pertinent”.

These statements conflate design and optimization as co-extensive. They also assume that design objectives can be enumerated and quantified at all stages of design processes. But complete formulations of design objectives are often next to impossible. While older, “analysis-synthesis” based design process models assume that design outcomes can be specified deductively from lists of requirements (Cross and Roozenburg, 1992), more recent, “co-evolution” based design process models assert that requirements are often identified during and through design processes and, to that extent, unknown in advance (Maher and Poon, 1996). Evins et al. (2012, p.5) furthermore argue that it is impractical to optimize “all sub-systems and variables simultaneously”. The impossibility of enumerating all objectives in advance, the invariability of objectives during optimization processes and the impracticality of simultaneously optimizing all objectives suggest that MOO is a deficient analogue of design processes.

Due to the exponential difficulty of MOO problems, standard MOO algorithms (MOOs) struggle to optimize more than three objectives (Emmerich and Deutz 2018). Do three objectives really make MOO particularly relevant for architectural design? Designers may sometimes be interested in optimizing one objective and sometimes multiple. A small survey of architectural designers that use optimization reports that “half of respondents ... typically optimize only a single objective, seven respondents ... two or three objectives, and two respondents more than three” (Wortmann 2019a, p.3). Out of five features for optimization tools, the respondents ranked the desirability of “multiple objectives” fourth, after “overview”, “choice” and “efficiency” and before only “interactivity”.

## **3. “Architectural Design Optimization is Limited to Negotiating Tradeoffs”**

A second assumption based on the multiple and sometimes conflicting goals that characterize architectural design problems is that all ADO problems are about negotiating tradeoffs between objectives. Radford and Gero (1980, p.77) give an introductory example where “the chosen solution may well be neither the minimum cost nor the minimum energy solution but some compromise between the two which offers the best balance of performance in both the objectives”. They

explain further that MOO is a good approach in such situations, because designers can choose a compromise solution without defining the relative importance of cost and energy in advance, and with additional, qualitative criteria in mind. Similarly, Evins et al. (2012, p.5) suggest that, in structural and environmental design, the “need for a holistic consideration of design and context” is best met with MOO and the consideration of tradeoffs.

The conflation of design and optimization in terms of tradeoffs is based on multiple assumptions discussed in this paper. This section focuses on the assumption that ADO is *limited to* negotiating tradeoffs. Empirical studies do not support this view: Bradner et al. (2014) find that designers often use optimization results as starting points for design development. Wortmann (2019a) finds that, among reasons for using optimization in design, “understanding tradeoffs” ranks second after “understanding what kinds of designs perform well, and why”. The view that ADO is concerned only with negotiating tradeoffs obscures other ways in which optimization can inform, rather than replace, design processes.

#### 4. “Multiple Objectives Require Multi-Objective Optimization”

A third assumption underlying dismissals of MOO in ADO is that multi-objective problems can only be addressed using MOOs. This assumption rejects the merger of multiple objectives into single ones through scalarization methods (such as weighted sums and products, penalty functions, and feasibility constraints). The rationale for this rejection is that relationships between multiple objectives cannot be known or understood in advance: Therefore, multiple objectives must not be combined *a priori*.

Mavrotas (2009, p.456) identifies two arguments against scalarization: (1) “It is very difficult for the decision maker to know beforehand and to be able to accurately quantify (either by means of goals or weights) his/her preferences” and (2) the decision maker “never sees the whole picture (the Pareto set) or an approximation of it”. Similar arguments are raised in the context of ADO (e.g. Radford and Gero 1980, p.79).

The following three sections present counterexamples where *a priori* definitions of design preferences and scalarization are possible. The argument that MOO is necessary and sufficient for designers to understand “the whole picture” is discussed in sections 5–7.

##### 4.1. WEIGHTED SUMS AND PRODUCTS

Weighted sums (1) and products (2) add or multiply objectives. Addition is possible when objectives have similar scales. Else one can normalize them to a scale from 0% to 100% (if the minimum and maximum for each objective is known) or multiply them. To express their relative importance, objectives can be multiplied with factors (i.e., weights) in weighted sums. In weighted products, weights can be expressed as exponents.

$$o = o_1 \cdot w_1 + o_2 \cdot w_2 + \dots + o_n \cdot w_n \tag{1}$$

$$o = o_1^{w_1} \cdot o_2^{w_2} \cdot \dots \cdot o_n^{w_n} \tag{2}$$

Daylight metrics often use a scale from 0% to 100%, as does utilization, a metric for structural design. Wortmann (2019b) uses an equally weighted sum of UDI and Daylight Glare Probability (DGP) to benchmark SOO algorithms and compares the resulting Pareto sets with results from a MOO algorithm that optimizes UDI and DGP separately.

#### 4.2. PENALTY FUNCTIONS

Upon closer examination, some MOO problems can be better formulated as SOO problems that are subject to constraints. Structural design optimization, for example, can be understood as the multi-objective problem of minimizing material cost while maximizing strength (Evins et al. 2012). But, typically, structural design does not maximize strength. Instead, it seeks to satisfy structural performance constraints. Structural design optimization can thus be better understood as a SOO problem of minimizing weight, subject to one or more performance constraints, i.e., of finding the lightest structure that is safe. This perspective is reflected in codes for structural design and minimizes material consumption. Structural optimization can be understood as the SOO problem of minimizing weight with one or more safety constraints, i.e., of finding the lightest structure that is safe.

Penalty functions – also known as soft constraints – add penalties to (single) optimization objectives. Penalties are zero when constraints are met. When a constraint is violated, the amount of the penalty represents the severity of the violation. Such “soft constraints” guide optimization algorithms to feasible solutions (i.e., solutions that meet the constraints).

$$o = o_1 + p_1 + \dots + p_n, p_n = \begin{cases} p_n & \text{if } o_n > c_n \\ 0 & \text{if } o_n \leq c_n \end{cases} \quad (3)$$

Wortmann (2019b) employs several penalty functions. The penalty terms for structures contain a square root that increases penalty violations smaller than one and decreases larger ones, with the intent to smoothen fitness landscapes for easier optimization. A penalty function that imposes visual uniformity demonstrates the utility of penalty functions for aesthetic design.

#### 4.3. FEASIBILITY CONSTRAINTS

Like penalty functions, feasibility constraints consider whether a design candidate violates one or more constraints. But instead of penalizing violations proportionally, feasibility constraints completely discard design candidates that violate them. This method guarantees that, when the optimization succeeds, the result is feasible. But, in the worst case, feasibility constraints can lead to failing optimization processes that do not find any feasible design candidates due to a lack of guidance for the optimization algorithm on how to move from unfeasible to feasible regions of the objective (decision) space.

The above counterexamples of scalarization demonstrate that, in design contexts, it is sometimes possible to reduce multiple objectives into one or to accurately quantify preferences, especially when they are expressed as – soft or hard – constraints. As such, proponents of MOO over SOO in the context of

ADO imply that most design objectives in architectural design are formulated better as optimization objectives than as constraints. In light of building codes that set standards (i.e., constraints) and conceptions of design that identify constraints as drivers for design exploration (Kilian 2006; Fischer and Richards 2014), this implication demands scrutiny. In (Wortmann 2019a), of the fifteen respondents that optimize multiple objectives, six use penalty functions, five use weighted sums, and only four use MOOs.

In some cases, close analyses of optimization objectives reveal that one is contained in the other – as for required materials and cost – or that a single metric combines two apparently separate objectives. For example, Useful Daylight Illuminance (UDI) combines daylighting and reducing excessive daylight and, in structural design, utilization combines stress and displacement. Such loss-less reductions in the number of objectives are advisable, since they result in a logarithmic reduction of the difficulty of optimization problems (Section 7).

## 5. “Pareto Fronts Represent Design Spaces”

To leverage optimization in architectural design processes, designers need to derive insights from optimization results (Wortmann and Schroepfer 2019). In the context of MOO, designers can visualize optimization results in the objective space by using Pareto front graphs (PFG) (Radford and Gero 1980). In a PFG, each orthogonal axis (i.e., dimension) represents an optimization objective, with the best values located at the origin. Design candidates are visualized as points with as many dimensions as there are objectives. In objective spaces that are characterized by one or more tradeoffs, the origin point cannot be reached (i.e., no design candidate is the best in all objective dimensions). Therefore, this point is called the “Utopia” point.

Design candidates that are non-dominated, i.e., design candidates that are not rivaled by design candidates that are better in one or more objectives without being worse in others, form a “front” in a PFG (a curve in a 2D PFG, a curved surface in a 3D PFG, etc.). By definition, design candidates do not fall below the Pareto front. Since accurate Pareto fronts are typically hard to find, the goal of MOO is to approximate them as closely as possible.

But PFGs do not represent design variables, and Pareto fronts do not constitute design spaces. Insights drawn from PFGs are limited to relationships between objectives. Relationships between variables and objectives, crucial for understanding why some design candidates perform well, are not represented in PFGs. Furthermore, PFGs do not represent other factors, such as the appearance of design candidates. Octopus, a popular MOO plugin for Grasshopper, aims to overcome the latter limitation by representing each point of PFGs as a three-dimensional shape (Vierlinger 2013).

Although relationships between variables and objectives are at least as relevant for designers as relationships between objectives, this is often not explicitly recognized in the ADO literature. Radford and Gero (1980, p.79) may be misinterpreted to suggest that PFGs present whole design spaces when they note that scalarization or “preference methods do not provide the context information

on the whole range of feasible solutions”. Similarly, Mavrotas (2009, p.456) states that, without MOO, the designer “never sees the whole picture”.

Another limitation is that standard PFGs are restricted to three dimensions, i.e., three objectives. Further objectives can be visualized as the points’ color, size, or shape. But this visualization decreases understandability because some objectives are represented spatially while others are not. Most PFGs display only two objectives, because two-dimensional graphs are easiest to display and understand, especially in print media. In short, PFGs provide a set of design candidates to choose from, which can be an advantage relative to SOO. But this set is neither representative of the design space nor necessarily representative of the objective space (Section 7).

## **6. “Pareto Fronts Require Multi-Objective Optimization”**

The preference of MOO over SOO also arises from the notion that MOO yields unique insights into tradeoffs between multiple objectives by visualizing optimization results as PFGs. Accordingly, and echoing a common position among researchers in ADO (e.g. Radford and Gero 1980; Evins et al. 2013), a reviewer for this paper’s abstract stated that MOO provides “invaluable” insights into such tradeoffs. This position is closely related to the assumption (discussed in Sections 2 and 3) that competing objectives are common in architectural design.

But the relationship between using MOO and gaining insights from PFGs is contingent: It is not mandatory to visualize MOO results as PFGs. Moreover, when multiple optimization objectives are recorded before being scalarized into a single one, PFGs can be produced and insights gained from only SOO. MOOs can, in principle, accurately approximate concave Pareto fronts, while weighted sums cannot. But this objection does not apply to sophisticated scalarization methods such as augmented Chebychev sums (Emmerich and Deutz 2018).

As such, one can study the efficiency of MOOs in terms of SOO by scalarizing multiple optimization objectives into a single one. (Scalarization is applied before optimization for SOO algorithms and after optimization for MOOs.) One can also study the efficiency of SOO algorithms in terms of MOO by plotting the PFGs resulting from optimizing a scalarization of multiple objectives. Wortmann (2017) compares the multi-objective HypE algorithm (Bader and Zitzler 2011) with several SOO ones on a daylight optimization problem. HypE outperforms several single-objective algorithms, but the single-objective RBFOpt (Costa and Nannicini 2018) finds a more accurate, though less diverse, PFG than HypE. These empirical results demonstrate that MOOs are neither necessary nor sufficient to find accurate PFGs.

## **7. “Multi-objective Algorithms are Efficient and Robust”**

Although the assumptions discussed in the preceding sections require that one can reliably find accurate approximations of Pareto fronts, this is not guaranteed. Inaccurate approximations might mislead designers instead of providing insights into tradeoffs. In the daylight and glare example presented in Wortmann (2017), the front found by the evolutionary MOO algorithm HypE suggests that UDI more

than 65% leads to a sharp increase in DGP, while the front found by the SOO algorithm RBFOpt shows a less sharp increase at 70%. In this scenario, a designer using HypE might choose a façade with less daylight quality to avoid glare, even though better design candidates exist.

It is thus critically important that the (evolutionary) MOOs employed (Evins 2013) and recommended (Evins et al. 2012) by the ADO literature are efficient and robust. Despite this importance, there is scant research on the performance of MOOs compared to SOO algorithms, especially on realistic, simulation-based problems. Many ADO papers that use MOO on such problems do not present benchmark results (Evins 2013), which makes it difficult to judge the efficiency and robustness of the employed algorithms.

A simulation-based MOO benchmark by Hamdy et al. (2016) concludes that better-performing MOOs require 1,400–1,800 optimization steps (i.e., simulations) to “stabilize” their results while “none of the tested algorithms could converge completely to the best Pareto front”. With 16 variables and two objectives the building energy optimization problems used in this study are relatively simple. Chiandussi et al. (2012) compare a MOO with a SOO and scalarization methods on an engineering design problem with seven variables, two objectives and two constraints. They conclude that “the large computational effort makes [the evolutionary MOO] generally not acceptable in usual [simulation-based] engineering problems”. Instead, they recommend  $\epsilon$ -constraints, a scalarization method. Emmerich and Deutz (2018) list the development of more efficient MOOs for simulation-based problems as a current research topic.

Beyond the (lack of) empirical results, there are more general reasons to suspect that (evolutionary) MOOs might not be very efficient: (1) As acknowledged by Radford and Gero (1980), the difficulty of optimization problems increases exponentially in the number of objectives. In addition, finding the optimum for simulation-based problems is challenging even in SOO (Waibel et al. 2019). (2) It is difficult to mathematically prove the effectiveness (i.e., convergence) of MOOs (Emmerich and Deutz 2018). This difficulty partially explains the, compared to SOO, smaller number of available algorithms and benchmark studies. (3) Most MOOs are evolutionary, but, at least in the single-objective case, most evolutionary algorithms tend to perform worse than other, less stochastic algorithms (Rios and Sahinidis 2013; Waibel et al. 2019; Wortmann 2019b). The effectiveness and robustness of MOOs thus is uncertain, especially for simulation-based problems with many variables and/or several objectives.

## **8. “Evolution Makes Multi-Objective Algorithms Efficient and Robust”**

Some architects equate “evolutionary” with “efficient and robust”, probably because the biological analogy implies sustainability, optimality and/or resiliency. For example, Makki et al. (2019) write that “morphological variation[s] of urban tissues, which evolve through the optimisation of multiple conflicting objectives, benefit significantly from the application of robust metaheuristic search processes”. In other words, existing urban tissues are good because they have



undergone a process of multi-objective “evolution”, and therefore one can use evolutionary MOO to generate them. Such associations with biological evolution have undoubtedly contributed to the popularity of evolutionary MOOs (Evins 2013), but are problematic for a least two reasons:

(1) Biological evolution might be better understood as the co-evolution of different species with each other and their environment, rather than a goal-oriented process that optimizes individual species relative to a fixed background (as is the case for ADO). In her critique of the (mis-)use of biological concepts in generative design, Cogdell (2019) writes that evolutionary algorithms “are more eugenic than new-Darwinian” because they reduce rather than preserve variety and because they “carry a teleology” and “Darwinian evolution does not”.

(2) Evolutionary algorithms to a certain extent reflect the “Modern Synthesis” of Mendelian genetics and Darwinian evolution from the first half of the 20th century, but not more recent revisions such as gene regulatory networks and epigenetic inheritance. Kumar and Bentley (2003) summarize: “Talk to any evolutionary biologist and they’ll tell you that the standard genetic algorithm (GA) does not resemble natural evolution very closely. While our GAs may evolve their binary genes, most biologists would be horrified to discover that concepts such as genotype and phenotype are so blurred in evolutionary computation that some researchers make no distinction between the two. Should you have the courage to go and talk to a developmental biologist, you’ll have an even worse ear-bashing. You’ll be told that development is the key to complex life”.

Similar arguments apply to swarm optimization and other algorithms that mimic natural processes. In short, evolutionary and other biologically-inspired optimization algorithms demonstrate that nature inspires working optimization algorithms. But arguing that optimization results must be good because they result from a biologically-inspired algorithm is to commit a naturalistic fallacy (Blok and Gremmen 2015).

## 9. “Computational Cost is Negligible”

According to Radford and Gero (1980, p.79), the value of insights that can be gained from MOO justifies the higher computational cost of MOO compared to that of SOO (i.e., the larger number of required simulations). But not all designers may accept this trade-off, especially in fast-paced concept design phases and when the accuracy of these insights is far from assured (Section 7).

There are two other assumptions why the concerns with algorithmic efficiency expressed in sections 7 and 8 might not matter: (1) The exponential increase of computational power in the second half of the 20th century will continue and eventually make computational cost inconsequential. (2) Parallel and cloud-computing provides a potential solution to the computational cost of MOO.

The first assumption is outdated: There now is a consensus among computer scientists that Moore’s Law is “dead”, or at least slowing down, due to quantum-physical limits in the miniaturization of silicone chips (Eeckhout 2017). Parallel and cloud computing (Janssen 2015) provide at best partial solutions, since they result in diminishing returns: Parallel optimization steps (e.g. one generation

of a genetic algorithm) allow only a wider, quasi-random search (i.e., exploration), but no deeper progress that benefits from previous steps (i.e., exploitation).

A more principled consideration is that SOO and MOO are by definition concerned with efficient search, because exhaustive search tends to be prohibitively expensive. If one accepts that efficient search of design spaces remains a need-and, in light of computing's increasing energy and CO2 burden, ethical responsibility-one should also accept that efficiency of optimization algorithms, and thus relative efficiency of SOO and MOO, matters.

## 10. Conclusion

The paper presents an example of a constant risk in computational design research and elsewhere: Mistaking a part for the whole. It presents eight challenges to the assumption that ADO requires MOO: (1) Optimization is a tool *for* rather than analogous *to* architectural design. (2) This tool is not only for understanding tradeoffs. (3) Scalarization, i.e., combining multiple objectives, can lead to better optimization results, i.e., more accurate PFGs. (4) PFGs do not replace representations of design spaces. (5) One can generate PFGs with SOO and scalarization. (6) MOO is exponentially more difficult than SOO and lacks efficient algorithms for simulation-based problems. (7) Evolutionary MOOs are not analogous to biological evolution. (8) The higher computational cost of MOO remains problematic.

Based on the role of optimization for architectural design (sections 2 and 3) and the discussions of scalarization and PFGs (sections 4, 5 and 6), we recommend the following: (1) Use MOOs only when it is important to understand tradeoffs between conflicting objectives. (2) Consider alternatives to MOO, such as scalarization with SOO algorithms. Making scalarization easier and more intuitive to use is a relevant direction for the development of future ADO tools.

Based on the exponential difficulty of MOO and the enduring challenge of computational cost (sections 7, 8 and 9), we recommend the following: (3) Use MOOs only when thousands or tens of thousands optimization steps are possible. (4) Research papers in ADO using MOO should more often provide benchmark results or other forms of validations, such as comparisons with SOO or, minimally, random search. Emmerich and Deutz (2018) offer guidance on performance assessment for MOO. (5) Developing and testing more efficient algorithms for simulation-based MOO is a relevant direction for future research.

## Acknowledgement

Informal discussions with John Gero and others have inspired parts of this paper.

## References

- Bader, J. and Zitzler, E.: 2011, HypE: An Algorithm for Fast Hypervolume-Based Many-Objective Optimization, *Evol Comput*, **19**(1), 45-76.  
Blok, V. and Gremmen, B.: 2016, Ecological Innovation: Biomimicry as a New Way of Thinking and Acting Ecologically, *J Agric Environ Ethics*, **29**, 203-217.

- Bradner, E., Iorio, F. and Davis, M.: 2014, Parameters tell the design story: ideation and abstraction in design optimization, *Proceedings of SimAUD*.
- Burry, J. and Burry, M.: 2012, *The New Mathematics of Architecture*, Thames & Hudson, London, UK.
- Chiandussi, G., Codegone, M., Ferrero, S. and Varesio, F.: 2012, Comparison of multi-objective optimization methodologies for engineering applications, *Comput Math Appl*, **63**(5), 912-942.
- Cogdell, C.: 2019, *Toward a Living Architecture?: Complexism and Biology in Generative Design*, Univ Of Minnesota Press, Minneapolis.
- Costa, A. and Nannicini, G.: 2018, RBFOpt: an open-source library for black-box optimization with costly function evaluations, *MPC*, **10**(4), 597-629.
- Cross, N. and Rozenburg, N.: 1992, Modelling the Design Process in Engineering and in Architecture, *Journal of Engineering Design*, **4**(4), 325-337.
- Eeckhout, L.: 2017, Is Moore's Law Slowing Down? What's Next?, *IEEE Micro*, **37**(4), 4-5.
- Emmerich, M.T.M. and Deutz, A.H.: 2018, A tutorial on multiobjective optimization: fundamentals and evolutionary methods, *Nat Comput*, **17**(3), 585-609.
- Evins, R.: 2013, A review of computational optimisation methods applied to sustainable building design, *Renew Sust Energ Rev*, **22**, 230-245.
- Evins, R., Joyce, S.C., Pointer, P., Sharma, S., Vaidyanathan, R. and Williams, C.: 2012, Multi-objective design optimisation: getting more for less, *Civil Eng*, 5-10.
- Fischer, T.: 2014, From Goal-Oriented to Constraint-Oriented Design: The Cybernetic Intersection of Design Theory and Systems Theory, *Leonardo*, **50**(1), 36-41.
- Hamdy, M., Nguyen, A.T. and Hensen, J.L.M.: 2016, A performance comparison of multi-objective optimization algorithms for solving nearly-zero-energy-building design problems, *Energ Buildings*, **121**, 57-71.
- Janssen, P.: 2015, Dexen: A scalable and extensible platform for experimenting with population-based design exploration algorithms, *AIEDAM*, **29**(4), 443-455.
- Kilian, A.: 2006, *Design Exploration through Bidirectional Modeling of Constraints*, Ph.D. Thesis, Massachusetts Institute of Technology.
- Kumar, S. and Bentley, P.J. 2003, Biologically Inspired Evolutionary Development, in A.M. Tyrell, P.C. Haddow and J. Torresen (eds.), *ICES 2003*, Springer Berlin Heidelberg, 57-68.
- Maher, M.L. and Poon, J.: 1996, Modelling Design Exploration as Co-Evolution, *Comput-aided Civil Infrastruct Eng*, **11**, 195-209.
- Makki, M., Showkatbakhsh, M., Tabony, A. and Weinstock, M.: 2019, Evolutionary algorithms for generating urban morphology: Variations and multiple objectives, *IJAC*, **17**(1), 5-35.
- Mavrotas, G.: 2009, Effective implementation of the  $\epsilon$ -constraint method in Multi-Objective Mathematical Programming problems, *Appl Math Comput*, **213**(2), 455-465.
- Radford, A.D. and Gero, J.S.: 1980, On Optimization in Computer Aided Architectural Design, *Build Environ*, **15**, 73-80.
- Rios, L.M. and Sahinidis, N.V.: 2013, Derivative-free optimization: a review of algorithms and comparison of software implementations, *J Glob Optim*, **56**(3), 1247-1293.
- Vierlinger, R.: 2013, *Multi-Objective Design Interface*, Master's Thesis, TU Wien.
- Waibel, C., Wortmann, T., Evins, R. and Carmeliet, J.: 2019, Building energy optimization: An extensive benchmark of global search algorithms, *Energ Buildings*, **187**, 218-240.
- Wortmann, T.: 2017, Model-based Optimization for Architectural Design: Optimizing Daylight and Glare in Grasshopper, *TAD*, **1**(2), 176-185.
- Wortmann, T.: 2019a, Architectural Design Optimization—Results from a User Survey, *2019 XJTU International Conference: Architecture across Boundaries*, Suzhou, CN, 473-483.
- Wortmann, T.: 2019b, Genetic Evolution vs. Function Approximation: Benchmarking Algorithms for Architectural Design Optimization, *JCDE*, **6**(3), 414-428.
- Wortmann, T. and Schroepfer, T.: 2019, From Optimization to Performance-Informed Design, *Proceedings of SimAUD*, San Diego, CA, 261-268.

# VISUAL MEETS TEXTUAL

## *A Hybrid Programming Environment for Algorithmic Design*

RENATA CASTELO-BRANCO<sup>1</sup> and ANTÓNIO LEITÃO<sup>2</sup>  
<sup>1,2</sup>*INESC-ID, Instituto Superior Técnico, Universidade de Lisboa*  
<sup>1,2</sup>*{renata.castelo.branco|antonio.menezes.leitao}@tecnico.ulisboa.pt*

**Abstract.** Algorithmic approaches are currently being introduced in many areas of human activity and architecture is no exception. However, designing with algorithms is a foreign concept to many and the inadequacy of current programming environments creates a barrier to the generalized adoption of Algorithmic Design (AD). This research aims to provide architects with a programming tool they feel comfortable with, while allowing them to fully benefit from AD's advantages in the creation of complex architectural models. We present Khepri.gh, a hybrid solution that combines Grasshopper, a visual programming environment, with Khepri, a flexible and scalable textual programming tool. Khepri.gh establishes a bridge between the visual and the textual paradigm, offering its users the best of both worlds while providing an extra set of advantages, including portability among CAD, BIM, and analysis tools.

**Keywords.** Algorithmic Design; Hybrid Programming Environment; Textual Programming; Visual Programming.

### 1. Introduction

Algorithmic Design (AD) is a method increasingly present in the architectural practice, which entails the creation of designs through algorithmic descriptions, allowing the designer to delegate repetitive tasks to the computer, accelerating the production process, reducing human errors (Burry, 2011) and allowing considerable cost savings (Woodburry, 2010).

However, designing with algorithms is a foreign concept to many (Terzidis, 2006) and, moreover, it requires representation methods that radically differ from those used in architecture (Maleki & Woodbury, 2013), thus creating a mismatch that is further exacerbated by the inadequacy of current Integrated Development Environments (IDEs). This hinders the adoption of AD, demotivating architects from its use and, thus, limiting the potential benefits.

### 2. Programming Paradigms

Given the advantages AD brings to the practice, many IDEs have been developed. Despite multiple attempts by different communities to develop means for

describing computation, two main paradigms stand out: (1) Visual Programming Languages (VPLs), which simplify the learning process but lack scalability (Bentrad & Meslati, 2011), i.e., as programs grow in complexity, they become hard to understand and navigate (Leitão, et al., 2012); and (2) Textual Programming Languages (TPLs), which scale better with larger programming projects but usually entail a steeper learning curve and are less attractive for the innate visual nature of architects (Sammer, et al., 2019).

## 2.1. VISUAL PROGRAMMING

In Visual Programming (VP), users can specify programs in a two or more-dimensional fashion (Zhang, 2007). Elements like spatial relationships, time, or visual expressions such as diagrams and sketches can all be used to convey the semantics of the instructions (Burnett, 1999). TPLs do not qualify as VP, since they are compiled or interpreted as long one-dimensional streams (Myers, 1990).

Strategies for VP include, for instance, concreteness (focus on particular instances) and explicitness (little inference required) - two features that make VP appealing at start by guaranteeing a smooth learning curve but which deter programmers from its use at large scales (Burnett, 1999). This lack of abstraction mechanisms has long led to the conclusion that the benefit of using VP is inversely proportional to the size and complexity of the problem (Whitley, 1997).

Furthermore, the efficacy of VP systems is intimately dependent on the context and task to be performed. Despite largely reducing their ideal field of application (Whitley, 1997), this also makes them an important puzzle piece to end-user programming in specific domains, which is the case of architecture. In proof of this stand languages like Grasshopper (GH), Dynamo or Generative Components, who have had stunning success among this community.

## 2.2. TEXTUAL PROGRAMMING

For general-purpose programming by professional programmers, Textual Programming (TP) is the appropriate and most favored choice (Myers, 1990). While VP diagrams tend to rapidly overflow the bounds of the screen (Nardi, 1993), TP, on the other hand, supports higher information density with abstraction and filtering mechanisms. The problem of TP lies in diametrically opposed concepts to those which lower VP's utility: the steep learning curve and the difficulty architects face in understanding AD programs and relating them to the building's concept.

The human brain is inherently visual and multi-dimensional (Zhang, 2007) and, despite the proven advantages of this approach, graphics are, in fact, closer to the user's mental representation of problems. Especially for non-expert or novice programmers, graphical representations make the programming task easier to understand (Myers, 1990). Specifically, in the architectural context, users must translate mental pictures into textual representations, which is a considerable challenge even for the most gifted (Boshernitsan & Downes, 2004). This suggests that textual programming alone also fails to satisfy our needs for all possible scenarios.

### 2.3. HYBRID PROGRAMMING

Hybrid programming solutions have also been developed, in an attempt to join the best of both worlds. Different classifications of hybrid programming consider both (1) programs that are created visually and then translated into an underlying textual language (Boshernitsan & Downes, 2004; Nardi, 1993), and (2) the use of VP environments to write textual code (Burnett, 2001). Within the specific domain of architecture, there are several examples of hybrid systems.

For the first case, there is Programming In the Model (PIM) (Maleki & Woodbury, 2013), whose interface offers three interactive live windows showing the model, the dependency graph (visual), and the script (textual). Users can write a program both in a VPL and a TPL and the tool converts between these paradigms: a twist on option number one. Unfortunately, this solution requires substantial computational power in order to scale.

Möbius (Janssen, et al., 2016) is a parametric modeler for the web and, although the authors consider this to be a VPL system, the interface is definitely hybrid. It presents a flowchart area where users develop networks of nodes and wires in an associative/data flow programming style. Each of these nodes corresponds to a set of procedures defined in imperative/code-block style. When run, the entirety of the program is converted into JavaScript for execution.

For the second case, and once more despite being considered a VPL, Dynamo provides users with the possibility to code in miniature text-scripting interfaces within the visual IDE as well, using DesignScript, the associative programming language at the heart of Dynamo and, more recently, Python.

## 3. Hybrid Programming Environment

Neither the visual nor the textual paradigm seem to suffice for the complex task of developing AD programs. Furthermore, current hybrid systems do not always succeed in gathering the best of both nor at providing the learning opportunity lying underneath. This research aims to provide architects with a programming tool they feel comfortable with, while allowing them to fully benefit from AD's advantages in the creation of complex architectural models. However, instead of developing new VPLs or TPLs, we rely on already established ones, facilitating the learning process. Thus, we present a hybrid solution that combines GH, a popular VP environment, with Khepri, a flexible and scalable textual programming tool - Khepri.gh.

### 3.1. TOOLS

Khepri (Sammer, et al., 2019) is a TP tool based on the idea that a single algorithmic description can be used to generate equivalent models in different backends, such as Computer-Aided Design (CAD), Building Information Modelling (BIM), analysis, and gaming applications. Khepri is currently implemented in Julia (Bezanson, et al., 2017), a modern programming language with a smooth learning curve, fast execution, and support for large-scale development.

GH is a well-known VP tool tightly integrated with Rhinoceros. As a VPL, GH

requires no prior knowledge of programming, which is a very attractive quality for architects with little scripting experience. However, as most VPLs, this one also lacks scalability, as the abstraction mechanisms that help manage complexity are at fault in this paradigm. GH offers several solutions to bypass this issue, which resort to textual programming, namely in C#, Visual Basic (VB) or Python.

### 3.2. IMPLEMENTATION

Khepri.gh's implementation is in many ways similar to GH's currently available textual scripting editors: users drag a blank Khepri component onto the canvas (Figure 1A), open up the editor box by double-clicking a component and develop Julia code within (Figure 1B); they can then save the new components onto a dedicated tab (Figure 1C).

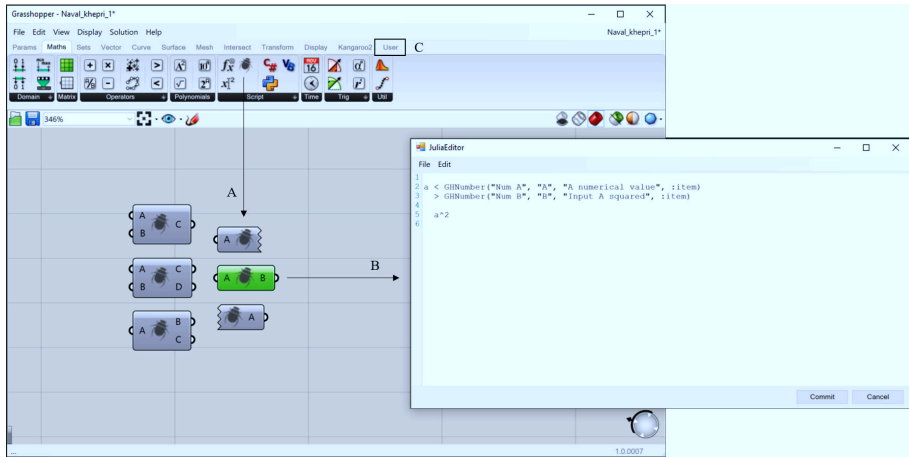


Figure 1. A – Khepri components on canvas with various inputs and/or outputs; B – Julia editor showing a component's code; C – User tab, where new components are saved.

However, while the C#, VB, and Python scripting editors only provide the features of each programming language unless other libraries are loaded, our implementation not only integrates the Julia language but also the Khepri programming tool from the start. This means, that besides the language primitives, users have access to the modeling primitives available in Khepri, which are transversal to the multiple backends.

### 3.3. PROGRAMMING STAGES

In order to better illustrate this workflow, we defined three main stages of program development where the differences between the typical GH approach and the Khepri.gh approach become visible. Phase one (1) includes *simple calculations*, the definition of mathematical functions, mapping locations, etc., all of which are typically achieved using native GH components. In the Khepri.gh workflow, these can also be done using Khepri components. Phase two (2) concerns the construction of more *abstract computations*, such as recursive and iterative

procedures, or high-order functions, which are typically implemented with the aid of textual scripts. Phase three (3) involves *geometry generation* and any other sort of operation realization in the connected applications. In GH’s case, this is usually done with native components, which provide immediate visual feedback in Rhinoceros and that can be baked in the end. In Khepri.gh, this stage would have to be done with Khepri components forcefully if the geometry is to be portable amongst backends.

Figure 2 presents a graphical representation of these three phases organized temporally according to the most common strategy of program development. The last phase is transversal to all others, as it regards the programming environment itself. In GH’s workflow, we are naturally using the IDE’s canvas to program through the entire process. With Khepri.gh’s, we are also given the possibility to visualize the entirety of the textual part of the program in a dedicated textual environment. This feature will be further discussed later on.

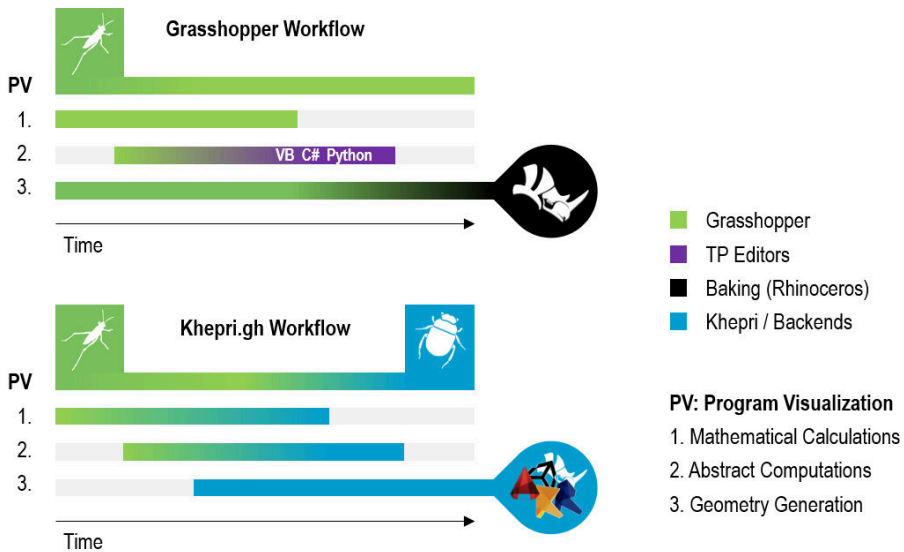


Figure 2. Workflow comparison, considering the three development stages, and the tools involved in the process (Grasshopper, Textual Programming (TP) editors, Rhinoceros, Khepri and its multiple backends).

#### 4. User-friendly Features

Khepri.gh’s implementation focuses on three main features designed to facilitate the coding task for non-expert programmers that, typically, find it difficult to understand complex programs and the impact of the changes applied to them: traceability, immediate feedback, and different code editing options.

To illustrate these features, in the ensuing subsections we present a project for a Nautical Center in Lisbon, a building projected onto the Tagus River. The Center is divided into three main blocks, anchored at the pier, which are then interconnected



by two other volumes lifted in the air above the boat launch ramps. Figure 3 shows rendered images of this project, along with a physical model. In the Khepri.gh model of the building, most of the geometrical constraints defining the shape of the three volumes are variable. Some of them can be seen in Figure 4.

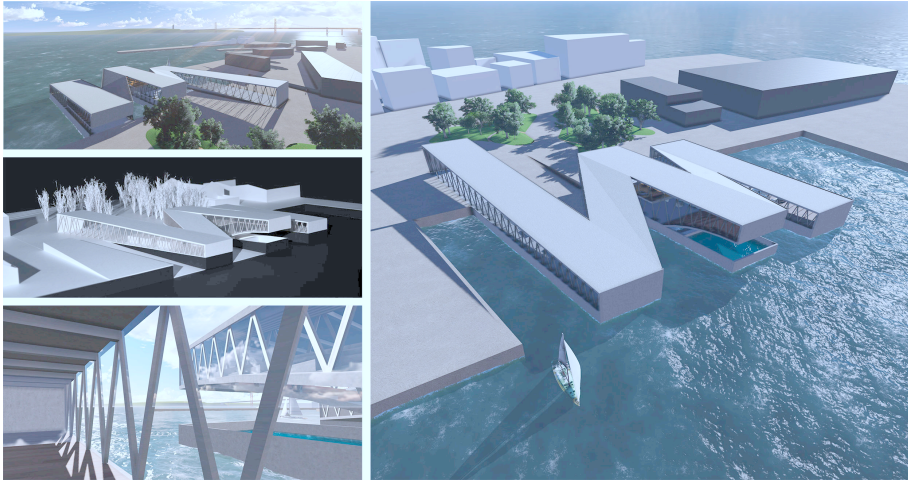


Figure 3. Case Study: Nautical Center renders and physical model.

#### 4.1. TRACEABILITY

Traceability entails the identification of which parts of the model correspond to which parts of the program, and vice-versa (Leitão, et al., 2014), a crucial correlation to understand, maintain, and debug the program. While GH presents unidirectional traceability, only relating program components to model elements, Khepri.gh supports bi-directional traceability and in multiple backends. Figure 5 shows the traceability feature in the AutoCAD and Unity backends.

#### 4.2. IMMEDIATE FEEDBACK

Immediate feedback is the ability to re-compute changes to the program's input or to the program itself in (near) real time (Rauch, et al., 2019), allowing designers to easily understand the program's behavior (Alfaiate, et al., 2017). GH immediately updates the geometry upon adding/changing components, Boolean toggles or sliders. Our solution extends this feature to the various backends but performance must be taken into consideration when dealing with complex models. Scale is already an issue for GH's optimized preview mode (i.e., non-baked geometry); even more so for Khepri.gh, which has to generate the geometry in the backends, a somewhat equivalent process to baking. This process is considerably faster in more performative backends, such as game engines, or using CAD tool's more performative view options, such as wireframe models. Figure 4 shows several variations of the Nautical Center generated by moving the project's sliders.

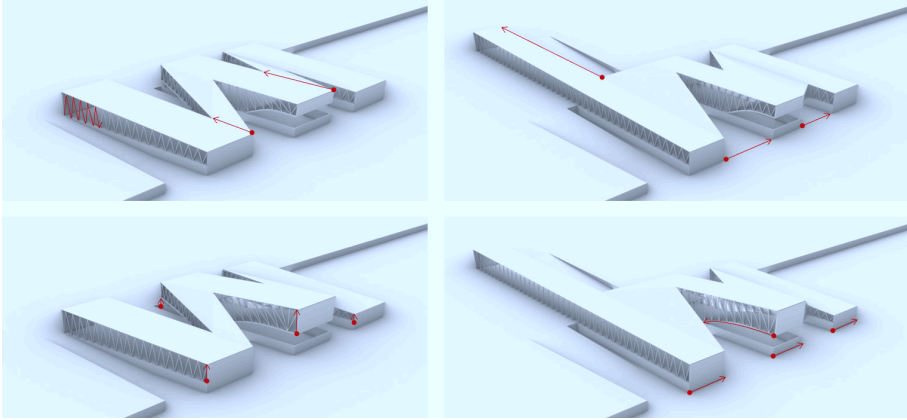


Figure 4. Screenshots from Rhino showing variations of the Nautical Center. The red arrows represent the variable parameters being changed in the model.

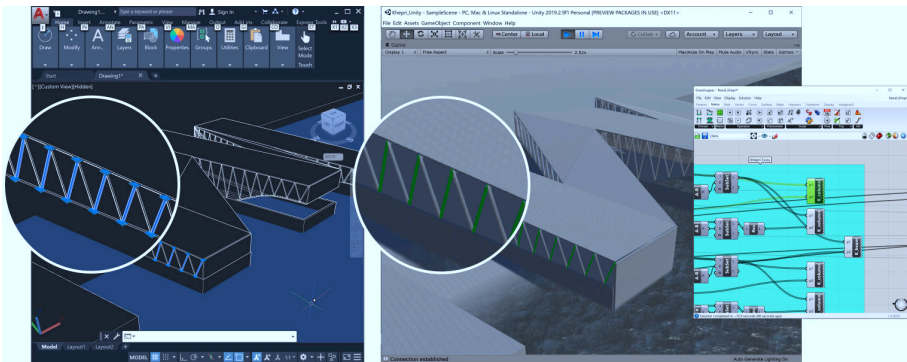


Figure 5. Traceability in different backends: GH program on the right showing the selected component, and respective representations automatically highlighted in AutoCAD, and Unity.

#### 4.3. CODE EDITING OPTIONS

Khepri.gh supports different code editing options (Figure 6). In the visual IDE the user can (a) manipulate existing GH components and (b) create new Khepri components, each one representing a parcel of code, using the textual programming editor available within GH. However, for more experienced programmers, (c) the code can also be accessed in a textual programming editor, such as Atom.

### 5. The Power of Abstraction

Having toured around the visual benefits of the proposed solution, we now peer into the advantages brought about by the textual paradigm.

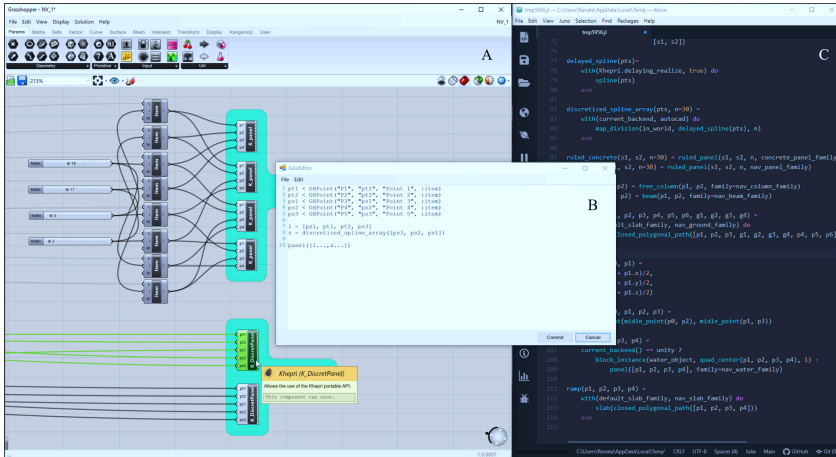


Figure 6. Code editing options: (a) visual, (b) textual within visual, and (c) full textual.

### 5.1. NO REPETITION

Following GH's native structure, VB, C# or Python scripting motivates the construction of standalone components, which both implement and execute operations. When reusing such components, the code is essentially duplicated and further changes to that structure must be performed in all similar components. Textual programming follows a different logic, where repetition is avoided at all costs for logic and organizational purposes. This makes the code structure more comprehensible and manageable, sparing the user the time-consuming and error-prone task of maintaining several versions of the same functionality.

Khepri.gh follows the textual logic in this issue, introducing a fundamental separation between function definitions and function calls. All components on canvas are processed on demand, with or without inputs, with or without specific modeling instructions. Users may gather function definitions, in one or more components, that can be used in all the others that call them, thus eliminating repeated definitions. When the user edits a definition component, the changes will have automatic repercussions in any other components dependent upon this one.

### 5.2. COMPLEXITY

The scalability issue inherent to VPLs affects many of the features that make these systems so appealing to users in earlier stages (Aish, 2003): both immediate feedback and program readability are compromised as complexity increases. For the first issue, GH cleverly offers a solution unsurprisingly inspired in the way TPLs deal with geometry generation: inputting numbers directly onto sliders instead of dragging them, or even disabling the solver as we edit the program, thus significantly reducing the number of times the model is recomputed.

For the second problem, the most obvious solution is abstraction: the possibility to encapsulate complex computations in much simpler program

structures, such as recursive and iterative first-order or higher-order functions. These mechanisms allow the development of more complex programs without resorting to the repetition of instructions. However, most VPLs, including GH, do not (directly) support these functionalities. Since Khepri.gh is built on top of the Julia language, any Julia functionality can be used from GH as well, meaning that the data that flows between components includes not only basic data structures, such as numbers and positions, but also functions, arrays, tuples, dictionaries, etc, and arbitrary combinations of these.

## 6. Discussing Transition

For all the advantages of abstraction, we get pulled further away from concreteness and explicitness, which helped smooth the learning curve of programming. The question then becomes: where should one draw the line between visual and textual? In this case, when should users shift from GH to Khepri components, relinquishing the ease of use in exchange for computational power? And should the answer somehow relate to one's programming capabilities?

To elaborate on this debate, we circle back to the scheme presented in Figure 2, where we defined three main phases of program development. After the presented experiments with the prototype, our own opinion reverts to the conclusion that phase (1) should be performed using mainly GH components by users with more experience using this IDE than any other. Provided they use Khepri components for phase (3) they will still benefit from the main advantages brought about by this approach. Users that find themselves limited by the existing GH components may also be motivated to learn how to create new Khepri components in phase (2). This solution is clearly the one where the least effort is required to program, and it represents a soft adaptation curve to Khepri's framework.

More experienced programmers may prefer to model Khepri components from the start. By developing phases (1), (2), and (3) on a Khepri base, users can access the entirety of their code in a textual programming environment as well, which provides a good incentive to the visual-to-textual transition. But, while developing Khepri components within GH's IDE, users can also benefit from the graphical properties provided by the environment, which facilitate the comprehension task.

In the end, we believe Khepri.gh can also serve as a smooth bridge for architects who wish to transition from the visual to the textual paradigm. The dichotomy between the two has for long represented a gap in the learning curve, with no visible progression from one to the other. Our solution thus also hopes to provide the means for expert VPL users to transition to the textual paradigm without having to restart the learning process from scratch. Having all of Khepri's operations available for use in a platform that architects feel comfortable using may help them get acquainted with the tool before switching to a textual IDE entirely.

## 7. Conclusion

Khepri.gh is a hybrid programming environment that combines Grasshopper, a popular visual programming environment, with Khepri, a flexible and scalable textual programming tool for algorithmic design. Exploiting the potential

of hybrid environments to serve as the middle ground between visual and textual programming languages, Khepri.gh provides users with a comfortable user-friendly visual interface while guaranteeing the portability, scalability, and complexity-handling mechanisms offered by the textual paradigm.

While the evaluation here presented focused mainly on Khepri's functionalities, as future work, we plan on further exploring the proposed benefits of the abstraction mechanisms provided by the Julia programming language within the Grasshopper environment.

### Acknowledgments

This work was supported by national funds through Fundação para a Ciência e a Tecnologia (FCT) with references UIDB/50021/2020 and PTDC/ART-DAQ/31061/2017.

### References

- Aish, R.: 2013, DesignScript: Scalable Tools for Design Computation, *Proceedings of eCAADe 2013*, Delft, The Netherlands, 18-20.
- Alfaiate, P., Caetano, I. and Leitão, A.: 2017, Luna Moth: Supporting Creativity in the Cloud, *Proceedings of ACADIA 2017*, Massachusetts, USA, 72-81.
- Bentrad, S. and Meslati, D.: 2011, Visual Programming and Program Visualization: Towards an Ideal Visual Software Engineering System, *Journal on Information Technology*, **1**(3), 56-62.
- Bezanson, J., Edelman, A., Karpinski, S. and Shah, V.B.: 2017, Julia: A Fresh Approach to Numerical Computing, *SIAM Review*, **59**(1), 65-98.
- Boshernitsan, M. and Downes, M.S.: 2004, Visual programming languages: A survey, *EECS Department, University of California, Berkeley*, 25.
- Burnett, M.: 2001, Visual programming, *Wiley Encyclopedia of Electrical and Electronics Engineering*, 275-283.
- Burry, M.: 2011, *Scripting Cultures*, John Wiley & Sons Ltd., United Kingdom.
- Jassen, P., Li, R. and Mohanty, A.: 2016, Mobius: A Parametric Modeller for the Web, *Proceedings of CAADRIA 2016*, Melbourne, Australia, 157-166.
- Leitão, A., Lopes, J. and Santos, L.: 2014, Illustrated Programming, *Proceedings of ACADIA 2014*, Los Angeles, USA, 291-300.
- Leitão, A., Santos, L. and Lopes, J.: 2012, Programming Languages For Generative Design: A Comparative Study, *International Journal of Architectural Computing*, **10**(1), 139-162.
- Maleki, M.M. and Woodbury, R.: 2013, Programming In The Model: A New Scripting Interface for Parametric CAD Systems, *Proceedings of ACADIA 2013*, Cambridge, Canada, 191-198.
- Myers, B.: 1990, Taxonomies of Visual Programming and Program Visualization, *Journal of Visual Languages & Computing*, **1**(1), 977-123.
- Nardi, B.A.: 1993, *A Small Matter of Programming: Perspectives on End User Computing*, MIT Press, Cambridge, USA.
- Rauch, D., Rein, P., Ramson, S., Lincke, J. and Hirschfeld, R.: 2019, Babylonian-style Programming - Design and Implementation of an Integration of Live Examples Into General-purpose Source Code, *Programming Journal*, **3**, 9.
- Sammer, M.J., Leitão, A. and Caetano, I.: 2019, From Visual Input to Visual Output in Textual Programming, *Proceedings of CAADRIA 2019*, Wellington, New Zealand, 645-654.
- Terzidis, K.: 2006, *Algorithmic Architecture*, Architectural Press, Oxon and New York.
- Whitley, K.N.: 1997, Visual Programming Languages and the Empirical Evidence For and Against, *Journal of Visual Languages & Computing*, **8**(1), 109-142.
- Woodbury, R.: 2010, *Elements of Parametric Design*, Routledge, Oxon.
- Zhang, K.: 2007, *Visual Languages and Applications*, Springer Science, New York.

# ALGORITHMIC GENERATION OF ARCHITECTURAL MASSING MODELS FOR BUILDING DESIGN OPTIMISATION

*Parametric Modelling Using Subtractive and Additive Form Generation Principles*

LIKAI WANG<sup>1</sup>, KIAN WEE CHEN<sup>2</sup>, PATRICK JANSSEN<sup>3</sup> and GUOHUA JI<sup>4</sup>

<sup>1,4</sup>*School of Architecture and Urban Planning, Nanjing University*

<sup>1</sup>*dg1436002@smail.nju.edu.cn* <sup>4</sup>*jgh@nju.edu.cn*

<sup>2</sup>*Andlinger Center for Energy and the Environment, Princeton University*

<sup>2</sup>*chenkianwee@gmail.com*

<sup>3</sup>*School of Design and Environment, National University of Singapore*

<sup>3</sup>*patrick@janssen.name*

**Abstract.** Using performance-based optimisation to explore unknown design solutions space has become widely acknowledged and considered an efficient approach to designing high-performing buildings. However, the lack of design diversity in the design space defined by the parametric model often confines the search of the optimisation process to a family of similar design variants. In order to overcome this weakness, this paper presents two parametric massing generation algorithms based on the additive and subtractive form generation principles. By abstracting the rule of these two principles, the algorithms can generate diverse building massing design alternatives. This allows the algorithms to be used in performance-based optimisation for exploring a wide range of design alternatives guided by various performance objectives. Two case studies of passive solar energy optimisation are presented to demonstrate the efficacy of the algorithm in helping architects achieve an explorative performance-based optimisation process.

**Keywords.** Parametric massing algorithms; performance-based optimisation; design exploration; solar irradiation.

## 1. Introduction

Parametric modelling incorporating evolutionary optimisation has been widely considered an efficient approach to facilitating architects to address complex energy optimisation challenges in sustainable building design. While this approach can technically solve performance-based building design problems by evolving design guided by various energy criteria, it also allows for an exploration of unknown design space, which may facilitate the discovery of unexpected

design solutions. The latter exercise can be referred to as *optimisation-based design exploration*, and its relevance in enhancing early-stage design ideation and overcoming design fixation has been increasingly acknowledged and upheld over the last decade.

Despite many successful applications in the literature, achieving a design exploration with meaningful and informative feedback from evolutionary optimisation is still challenging. Apart from the tedious optimisation process, the limited design space for the optimisation process to search often accounts for the unsatisfying result of such optimisation-based design exploration. The design space is limited as the result of the lack of diversity in the design space defined by the parametric model. Although there are a few complicated algorithms for parametric modelling to generate building design with higher differentiation, the implementation of such algorithms is often too challenging and time-consuming for architects to handle on the fly for each project. In order to address these challenges, it is essential to develop algorithms that can not only generate diverse building design alternatives but also be readily re-used to different design tasks. To this end, we propose two algorithms based on the additive and subtractive form generation principles (Simitch & Warke, 2014) for generating building massing design alternatives with high topological variability. Because these principles are the two most generic massing strategies in architecture, they can be adapted to different building design tasks with minimal customization. In this way, the algorithms can address the two requirements simultaneously.

To place this research in the context, we first discuss the progress that has been made related to the algorithms for parametric building design before going on to describe the proposed algorithms and present design scenarios demonstrating the efficacy of the algorithm. We conclude by discussing the effectiveness of the algorithm in supporting optimisation-based building design exploration.

### 1.1. ALGORITHM FOR PARAMETRIC BUILDING DESIGN

Describing design with explicit rules and parameters, parametric models can generate a large number of design variants by varying parameters. Sheikholeslami (2010) defines two types of design variant outcomes from parametric models. The first one is referred to as *design alternatives* which represent designs with “structurally different geometries”. The second one is referred to as *design variations*, in which the topological configuration of the generated building design remains fixed to the change in parameters. Most massing algorithms can be categorised into the second type of parametric models. Such algorithms are often used for representing a specific design concept. For example, a building block with a central internal courtyard is widely adopted in the building design optimisation for daylighting or passive solar energy. However, for the sake of design exploration, the invariant topological configuration of the building design variants significantly confines the scope of the design space, and, thereby, the opportunity of exploring other competitive design concepts is lost.

In order to widen the design space for exploration, a few researchers have developed algorithms for generating building massing design beyond a fixed topological configuration. The first approach is to include multiple parametric

schemes in one parametric model, and each scheme describes design with different topological configurations. The parametric model switches the schemes each time according to a regulatory parameter and generates solutions according to the selected parametric scheme (Chen, 2015). The second approach creates building massing by combining multiple smaller mass units. The mass unit typically has fixed or similar dimensions and shapes (Wang, Janssen, & Ji, 2019). Thus, the building design generated by this approach typically appears to be cellular-like massing. By arranging and re-arranging the mass units, the resulted building massing differs dramatically in terms of topological configuration, but it often comes with a large number of chaotic designs (Wang, Janssen, & Ji, 2019).

However, applying these two approaches in practice is time-consuming and technically challenging. The former requires the laborious creation of many parametric schemes, and the latter involves complicated constraint handling to ensure the generated design is feasible and legitimate. Furthermore, as the development of these algorithms is often subject to a large amount of task-specific knowledge, the re-usability of these algorithms to other design tasks is limited.

The task-oriented parametric modelling largely accounts for the lack of versatility and the limited re-usability of parametric models. Thus, peeling off the task-specific intentions while preserving generic domain knowledge and expertise into adaptable algorithms for repetitive tasks can allow for the generation of a broad range of preliminary design alternatives and, thereby, enable re-utilization. A relevant method is meta-modelling (Bernal, 2016; Harding & Shepherd, 2017), which captures the rules of parametric associative design. Recent efforts on meta-modelling aims at the automated generation of the parametric association of the nested sub-functions for differentiated design creation. However, due to the absence of architectural design knowledge, human intervention is still necessary, else the parametric model, randomly generated by computers, can be illegible.

Alternatively, we have proposed a parametric modelling approach to abstracting generic architectural massing strategies and developed an algorithm based on the subtractive form generation principle (Wang, Janssen, Chen, Tong, & Ji, 2019). The algorithms do not have a modifiable parametric association as other meta-modelling approaches do but can derive various versioning parametric models by specifying a set of user-defined parameters. Partly constrained by the user-defined parameters set by the architect, topologically varying building massing designs are generated according to different design settings while still complying with the subtractive form generation principle. In this study, we extend the research by including the additive form generation principle and compare the effectiveness of these two algorithms in supporting design exploration through performance-based optimisation.

## **2. Proposed Algorithm**

### **2.1. PARAMETRIC SCHEMAS FOR ARCHITECTURAL MASSING STRATEGIES**

In architecture, the additive and subtractive form generation principles are the two most commonly-adopted massing strategies, and most building designs can



be described by either of these two principles. Examples of the subtractive form generation principle include Simmons Hall at MIT in Boston, USA and Administration Building at XJTL University in Suzhou, China. For the additive form generation principle, examples include Ftown Building in Sendai, Japan and New Museum of Contemporary Art in New York, USA. Furthermore, these two principles also have a tight connection to many sustainable design strategies, such as courtyards, atriums, stilts, self-shading, and solar envelopes

The versatility and the connection to sustainable design strategies make these two principles suitable as generic parametric schemas for the performance-based optimisation in various design settings. The algorithm can delineate the design space reflecting the different sustainable design strategies through various design variants. By exploring the design space and evaluating the design variants against the performance criteria, the optimisation process, in fact, compares these strategies against one another and screens out the high-performing strategy. At the same time, architects can adjust the overall building features simply by defining the number and size of subtractive or additive massing elements and the behaviour of the elements when interacting with other elements. Thus, the algorithms satisfy the requirement listed in the previous section and can be re-usable in different design contexts.

## 2.2. GENERATIVE PROCEDURE OF THE ALGORITHMS

The research develops two algorithms respectively based on the two principles, and the core of the algorithms is to avoid commonly unwanted features, increase the diversity in the generated building massing design, and facilitate customisation by the architects. The core procedure of the two algorithms is similar. Thus, we first introduce the algorithm based on the subtractive form generation principle (*subtractive algorithm*) in detail. For the algorithm based on the additive principle (*additive algorithm*), only the major differences to the subtractive algorithm are pointed out.

### 2.2.1. Subtractive Algorithm

The subtractive algorithm creates building massing design by removing several parts from a maximal mass (Figure 1). The element defining the part being removed is referred to as the subtractive element (SE). By manipulating multiple SEs in different sizes and spatial positions, the maximal mass subtracted by these SEs can show vast different topological configurations. In this algorithm, the architect first defines the dimension of the maximal mass. By varying the dimension, the maximal mass can appear in different types of buildings such as high-/low-rise and deep-/thin-plan buildings. With the maximal mass defined, two types of SEs are defined. The first type is vertical SEs, and the second type is horizontal SEs. The vertical SEs tend to be tall and slender, which is aimed to cut through the maximal mass vertically to ensure features such as courtyards and atriums appearing in the building massing design. In contrast, the horizontal SEs are aimed to create features, such as stilts and stepped roofs. The architect defines the number of these two types of SEs, which can control the configurational

complexity of the generated building massing.

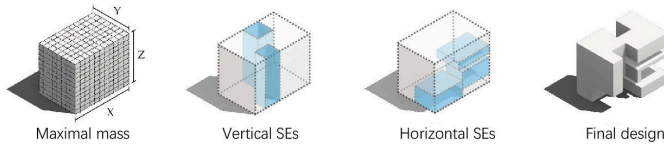


Figure 1. Relationship between the maximal mass and the two types of SEs.

Using parametric approaches can result in arbitrary size and placement of the SEs. First, the size of the SEs can be too large or too smaller, which may lead to infeasible building massing. Thus, the algorithm requires the architect to specify the size constraint to define the upper and lower size limits of the two types of SEs (Figure 2). In order to diversify the appearance of the parts removed from the maximal mass, two different operations are activated when the size constraint is violated. When the original size of a SE exceeds the upper size limit, the upper size limit is assigned to the SE. In contrast, when the original size is below the lower size limit, the SE is deactivated, and the corresponding part is not subtracted from the maximal mass.

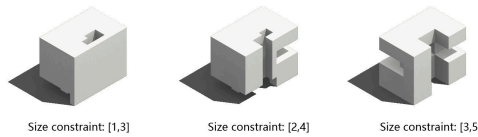


Figure 2. Size constraint.

Another problematic feature resulting from the arbitrary placement of SEs is that two SEs can be too close to one another or partly overlaps. When two SEs are close but not attach, it creates a space between the two SEs that may be too narrow to be of any use. This problem can also happen when a SE is close to the face of the maximal mass. Thus, the closest parallel faces of the two SEs or the face of the SE and the maximal mass are aligned to be co-planar (Figure 3-a,b). With the faces aligned, the two SEs are merged into a larger subtractive void in the maximal mass, or the SE creates an open void in the maximal mass. When two SEs partly overlap, it may create a subtractive void with small jagged faces. Thus, the algorithm also aligns the face of two overlapping SEs if they are close to one another to avoid this (Figure 3-c).

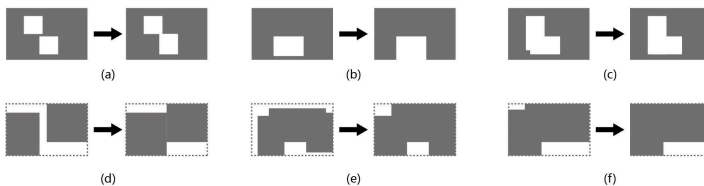


Figure 3. Alignment constraint.

With the size and alignment constraints, the algorithm can generate building massing with a broad topological variability from a building without any part removed to that with the largest number of parts permitted removed. In addition, the alignment constraint also enriches the diversity of the generated building massing. When two or more small SEs are merged into one large subtractive void, the algorithm can generate building massing either with several small parts removed or with one large part removed. Such diversity can reveal rich performance-related architectural implications. For example, the generated building massing can have a large courtyard or several smaller courtyards or light/air wells (Figure 4).



Figure 4. Example designs (randomly generated).

Lastly, the implementation of the algorithm also considers the gross area of the generated building massing as it is an important functional requirement in architectural design. As the accumulating occupied area by the SEs changes with varying parameters, the gross area of the generated building massing varies accordingly. It is important to ensure the gross area of the generated building massing satisfies the required value. Thus, this algorithm incrementally increases or decreases the dimension of the maximal mass in order to create the building massing with a gross area close to the required value (Figure 5-a).

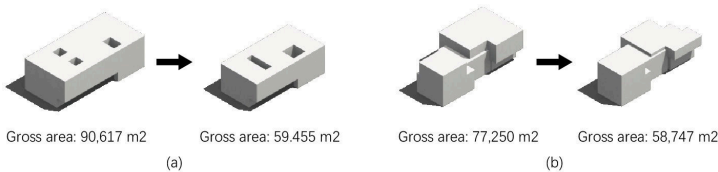


Figure 5. Gross area constraint (target area is 6,000 m<sup>2</sup>).

### 2.2.2. Additive Algorithm

The additive algorithm creates the building massing by accumulating several mass elements, which are referred to as *additive elements* (AE). The generative procedure can be viewed as the inverse operation of the subtractive algorithm. The maximal mass in the subtractive algorithm becomes a maximal volume (spatial boundary) in this algorithm to confine AEs. Similar to the subtractive algorithm, the size and alignment constraints are also applied in this algorithm to regulate the AEs for ensuring the rational space and geometric diversity in the generated building massing (Figure 3-d,e,f). Except for these shared procedures, there are two major differences in the additive algorithm from the subtractive one.

First, compared with the arbitrary behaviours of SEs, the arbitrary placement

of AEs is more likely to create chaotic designs such as floating masses and huge overhanging structures. In most cases, all AEs are floating when using the parametric approach. Thus, the algorithm iteratively lays down one of the floating AEs to the ground until half of the footprint of the predefined maximal volume has been occupied (Figure 6).



Figure 6. Floating constraint.

Second, the development of the additive algorithm also considers the requirement of the gross area but adopts another approach to adjusting the building massing. For the additive algorithm, all AEs are iteratively scaled up or down by 5% until the gross area of the building massing cannot get closer to the target value (Figure 5-b). At the same time, the maximal volume remains fixed, which is unlike the unchangeable maximal mass in the subtractive algorithm.

### 2.3. IMPLEMENTATION

The two algorithms were implemented in the Rhino-Grasshopper environment as two independent plug-in components. The components are integrated into an evolutionary design toolkit which also includes a diversity-guided evolutionary algorithm - SSIEA (Wang, Janssen, & Ji, 2020). The implementation in the Rhino-Grasshopper environment allows the two components as well as the component of SSIEA to be easily connected to other performance evaluation tools such as *DIVA* and *Honeybee*. As the two building massing generation components can be re-used in different design tasks, it also makes the established optimisation workflow re-usable as long as the performance criteria remain the same.

A graphic user interface (GUI) was also implemented in the algorithm components to facilitate the architect to input the user-defined parameters. In the GUI, the architect can specify the number of SEs or AEs and the constraints such as size limits. After inputting the user-defined parameter, the architect can generate several sampling design variants and receive timely visual feedback of the change in the user-defined parameters. As such, the architect can exclude the unwanted building features by parameter tuning before running the optimisation process.

### 2.4. CASE STUDY

For demonstrating the efficacy of the algorithms, two case studies of performance-based building design optimisation are presented (Figure 7). The design objects of two case studies are a high-rise slab type building and a middle-rise deep plan building located at the campus of Nanjing University in Jiangsu Province, China. This region is characterised as *cold-winter-hot-summer* climate, which results in heavy heating and cooling loads in winters and summers due to inadequate and excessive solar irradiation received. In this regard, the

optimisation is aimed to optimise the utility of passive solar energy by minimising incident solar irradiation in summers and maximising it in winters.

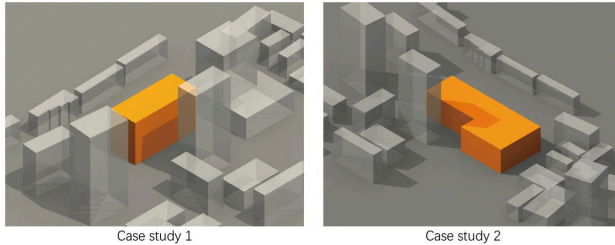


Figure 7. Case study design settings.

The objectives of minimising and maximising incident solar irradiation are formulated into a single-objective fitness function. The fitness is calculated by subtracting the amount of incident solar irradiation on facade surfaces in winters from that in summers. It is because the solar irradiation received in summers is always higher than that received in winters. Thus, for high-performing design variants, these variants receive lower solar irradiation in summers, while receiving higher of that in winters. Therefore, the difference between the two values tends to be small. In contrast, the design variants receiving unfavourable higher solar irradiation in summers and lower solar irradiation in winters have a large difference between the two values.

In addition,  $45,000 \text{ m}^2$  and  $100,000 \text{ m}^2$  are set as the target gross area of the building for the two case studies. The factor of the gross area is considered a penalty function in the fitness evaluation, which scales up the difference between the values of the incident solar irradiation received in summers and winters. As a result, the design variant that cannot satisfy the gross area requirement is punished by enlarging the difference of the incident solar irradiation values.

### 3. Result

#### 3.1. CASE STUDY 1

Figure 8 shows the results of the optimisation processes based on the two algorithms. The evolutionary algorithm used in the case study allows for yielding several distinct high-performing design variants. In this case study, the six highest-ranking design variants from each optimisation process are retrieved. Revealed by these variants, the optimisation process primarily identifies the building massing can achieve better solar avoidance in summers. It is because the building is surrounded by several high-rise buildings, which reduces incident solar irradiation in both seasons on the one hand. On the other hand, as the sun in summer afternoons can be on the north-west side of the target building, the building still receives intense incident sunlight on the summer afternoons, which can heat the building and increase the cooling load.

From the design variants generated by the subtractive algorithm, we can notice that these variants have a large stilt in the upper part of the building massing,

which self shades the facade to prevent overheating of the building (the first row in Figure 8). In contrast, the design variants generated by the additive algorithm typically have a narrow west facade which reduces the exposure to the fierce incident sunlight on summer afternoons. The narrow west facade also makes the design variants generated by the additive algorithm have better average fitness. The reduction in the gross area due to the narrow west facade is compensated by several overhanging structures or podiums which also self shade the building (the second row in Figure 8).

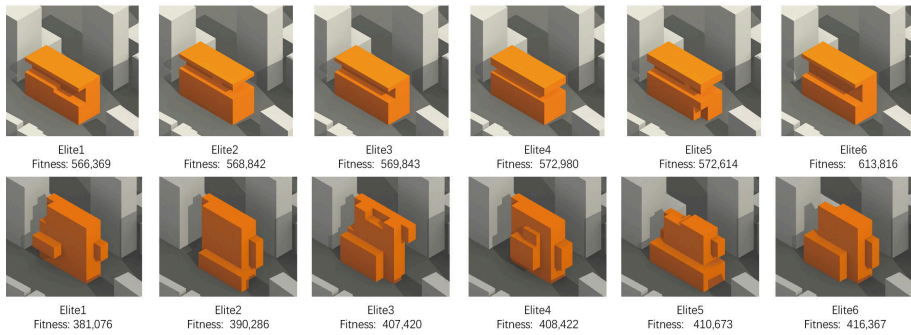


Figure 8. Optimisation result of case study 1.

### 3.2. CASE STUDY 2

Figure 9 shows the optimisation result of the second case study. The architectural implication related to the passive solar energy utility is similar to that unveiled in the first case study. Stilts and overhanging structures are the dominant features appearing in the design variants generated by both algorithms. Compared with the design variants of the first case study, the design variants generated by the two algorithms in this study share more similarities with regards to the strategy of self-shading. In addition, narrow west facades also appear in the design variants generated by the additive algorithm, which makes the average fitness of the design variant generated by the additive algorithm more desirable than those generated by the subtractive algorithm.

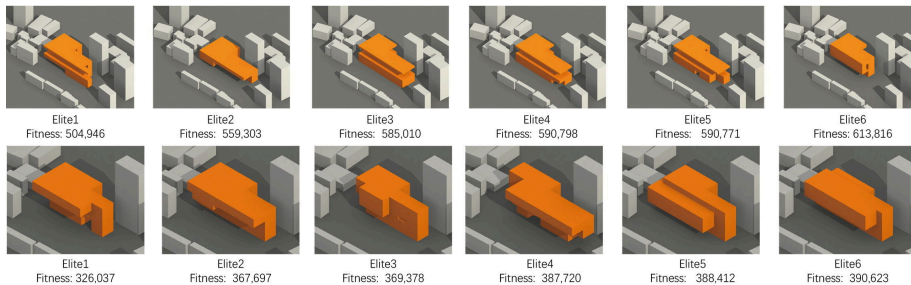


Figure 9. Optimisation result of case study 2.

#### 4. Discussion and Conclusion

The results of the optimisation based on the two algorithms unveil the architectural implication related to achieving good passive solar energy utilisation. The design variants have illustrated the appropriate and site-specific application of the self-shading strategy for the case study. However, due to the difference in the form-making procedure, the design variants generated by the two algorithms show different building features. In addition, in comparison with the two algorithms, the optimisation result based on the additive algorithm has design variants with higher design differentiation. The implication of self-shading shown in the optimisation results also provides a less conventional way to improve passive solar energy utilisation. Contrarily, this problem is typically addressed by adding external shading on buildings' facades. The case study highlights the potential of combining the proposed algorithms and performance-based optimisation for achieving an optimisation-based design exploration. Such exploration helps architects free from design fixation and stimulates design reflection and ideation, which makes the design of buildings become a more responsive and adaptive agent in shaping our future built environment.

To conclude, this study proposes two parametric massing algorithms to generate building massing with higher topological variability. The development of the algorithms aims to facilitate explorative performance-based optimisation in the early design stage of sustainable building design. The two case studies show that the algorithms can be adapted to different design settings with minimal customisation and generate task-specific solutions, which underlines the re-usability of the algorithms to various design tasks. The future research will consider providing higher geometric freedom in building massing generation in order to increase the versatility of the algorithms.

#### References

- Bernal, M.: 2016, From Parametric to Meta Modeling in Design, *Blucher Design Proceedings*, **3**(1), 579-583.
- Chen, K.W.: 2015, *Architectural Design Exploration of Low-Exergy (LowEx) Buildings in the Tropics*, Ph.D. Thesis, ETH Zurich.
- Harding, J.E. and Shepherd, P.: 2017, Meta-Parametric Design, *Design Studies*, **52**, 73-95.
- Sheikholeslami, M. 2010, Design space exploration, in R. Woodbury (ed.), *Elements of parametric design*. New York: Routledge, Routledge, 275-287.
- Simitch, A. and Warke, V.: 2014, *The language of architecture: 26 principles every architect should know*, Rockport Pub.
- Wang, L., Janssen, P., Chen, K.W., Tong, Z. and Ji, G.: 2019, Subtractive Building Massing for Performance-Based Architectural Design Exploration: A Case Study of Daylighting Optimization, *Sustainability (Switzerland)*, **11**(24), 6965.
- Wang, L., Janssen, P. and Ji, G.: 2020, SSIEA: a hybrid evolutionary algorithm for supporting conceptual architectural design, *Artificial Intelligence for Engineering Design, Analysis and Manufacturing*, **34**, 1-19.
- Wang, L., Janssen, P. and Ji, G. 2019, Utility of Evolutionary Design in Architectural Form Finding: An Investigation into Constraint Handling Strategies, in J. Gero (ed.), *Design Computing and Cognition*, Springer, 177.

# A METHOD FOR LOAD-RESPONSIVE INHOMOGENEITY AND ANISOTROPY IN 3D LATTICE GENERATION BASED ON ELLIPSOID PACKING

YAO LU<sup>1</sup>, EDA BEGUM BIROL<sup>2</sup>, COLBY JOHNSON<sup>3</sup>,  
CHRISTOPHER HERNANDEZ<sup>4</sup> and JENNY SABIN<sup>5</sup>  
<sup>1,2,3,4,5</sup>*Cornell University*  
<sup>1,2,3,4,5</sup>{yl3229|ebb75|cmj73|cjh275|jes557}@cornell.edu

**Abstract.** 3D lattice structures are gaining widespread application in multiple design fields. While the number of projects that utilize load-responsive inhomogeneous and anisotropic 3D lattices in design applications increase, accessible and effective algorithmic generation methodologies remain lacking. This paper addresses this gap by introducing a novel computational method for controlled load-responsive inhomogeneity and anisotropy in 3D lattice generation. The presented methods employ a responsive Ellipsoid Packing algorithm informed by the global tensor field of the packing geometry, followed by a Kissing Ellipsoids algorithm to generate the lattice. Load specific anisotropy and inhomogeneity in the ellipsoid packing process is achieved in response to the magnitude and directionality values of the global tensor field and specialized responsive lattices are easily generated. The proposed Ellipsoid Packing workflow is compared to various common lattice generation algorithms. Results show improvement in mechanical performance.

**Keywords.** 3D lattice; ellipsoid packing; bio-inspired; algorithmic design; ceramic brick.

## 1. Introduction

With increasing ease of fabrication through Additive Manufacturing Technologies (AMT), 3D lattice structures are gaining widespread application in architectural and design fields, as well as in fields such as biomedical and aerospace engineering. 3-Dimensional lattice structures offer advantages in these fields due to their ability to achieve high mechanical performance while maintaining a light weight (Niu et.al.2018).

Despite this increased ease of fabrication, “(...) there is relatively limited information available in the literature about designing large scale lattice structures (...) (Kantareddy, 2016)”. This gap is especially apparent as it pertains to random, inhomogeneous lattice structures and the pertaining generation and evaluation strategies. This paper aims to address this gap by exploring the advantages of inhomogeneity and anisotropy in 3 Dimensional lattice structures within architectural load-bearing applications. Inhomogeneity and anisotropy are



avored in natural load-bearing structures, such as the bone's trabecular lattice, and serve to achieve light weight and high mechanical performance. Within the context of bone's trabecular lattice, responsive inhomogeneity occurs as a result of thickening and thinning of trabecular struts in relation to high and low stress stimuli respectively. Anisotropy occurs through the adaptation of trabecular strut orientations parallel to the direction of pertinent compressive forces.

Establishing the anisotropic and inhomogeneous trabecular lattice structure as a natural precedent, the primary focus of this paper is to present detailed workflows of bio-inspired and responsive algorithmic lattice generation, whose manifestations can be realized at various scales through the employment of emerging AMT.

## 2. Background

Within the architectural field, various AMT including SLM (Selective Laser Melting), UV curing ceramic 3D printing, ceramic powder printing, and robotic extrusion have shown promise in realizing 3-dimensional lattice typologies and other load-bearing porous modules. In their paper *Responsive Spatial Print*, for example, Im and AIOthman present the potentials of real-time calibrated robotic extrusion as a means of fabricating "self-supporting spatial lattices" (Im, AIOthman, and Castillo, 2018). The PolyBrick series demonstrate the promise of ceramic powder printing (Sabin et.al 2014) and UV cured ceramic resin printing (Birol, Lu, Sekkin et. al. 2019) in the fabrication of load-bearing lattices. The realization of such projects consists of multiple phases including digital lattice generation, digital lattice thickening/meshing, and fabrication through the respective AMT. While the fabrication phase is making rapid progress in ease and accessibility due to recent developments in additive manufacturing technologies, preceding phases of digital lattice generation lack contained and accessible workflows for designer use. The outlined lattice generation algorithms aim to bridge this gap.

In introducing our lattice generation frameworks and possibilities, algorithmic generation processes, mechanical evaluations, and respective applications of various commonly used lattice typologies are outlined and compared to the proposed novel PolyBrick workflows and lattices. Hence, the paper not only compares the mechanical performance of generated lattice, but also tackles concerns about algorithmic efficiency and usability. Generated lattices are compared to commonly used periodic cellular lattices and various inhomogeneous anisotropic lattices from natural precedents. While uniform periodic lattice structures are advantageous in achieving high stiffness to mass ratio, it is difficult to introduce geometric specialization for heightened efficiency, allowing "unfavorable load cases like bending or shearing" (Reinhart and Teufelhart 2013) to occur. Inhomogeneous anisotropic lattice geometries break this constraint, differing from periodic cellular lattices in their specialized morphology. The bone's trabecular lattice is an important example of this, serving as a precedent for our outlined algorithms. As presented by several projects exploring applications of lattice structures in the architectural field (Reinhart and Teufelhart 2013) (Felder et al. 2016), the phenomenon of responsive morphology has immense potential in

rethinking and expanding the capacities of load-bearing lattice structures. While there are projects integrating load responsiveness and responsive directionality within design applications; accessible, effective and user-friendly algorithmic streamlining of this type of lattice generation remains lacking.

This paper introduces a novel computational method for controlled load-responsive inhomogeneity and anisotropy in 3D lattice generation. The primary focus of the proposed framework is presenting streamlined algorithmic processes of informed and responsive lattice generation. We particularly contextualize the advantages of inhomogeneity and anisotropy in 3-Dimensional lattice structures in architectural load-bearing applications. The introduced algorithm allows for a user-friendly process of inhomogeneous anisotropic load-bearing lattice generation facilitated through a custom Grasshopper plug-in. The algorithmic workflows presented expand upon PolyBrick 2.0's (Biol, Lu, Sekkin et. al. 2019) algorithmic processes and present a detailed account thereof.

### 3. Method

#### 3.1. LATTICE GENERATION ALGORITHM

##### *3.1.1. Ellipsoids as an intermediate parameter to control lattice morphology*

In our proposed processes for lattice generation, the trabecular bone is determined as a load responsive precedent of a 3D lattice geometry. The trabecular lattice is quantified by the morphological parameters of trabecular number, separation, length, and orientation (Bagi, Berryman, Moalli, 2011). In our workflow, these morphological quantifiers are algorithmically interpreted as controllable load response parameters. For this interpretation, ellipsoids are introduced as media. A number of ellipsoids are packed densely within a design geometry. Through a secondary algorithm, "Kissing Ellipsoids", the centroids of the touching ellipsoids are connected with a line segment. The morphological parameters of trabecular number, separation, and orientation are thus controlled by ellipsoid size, distribution, and orientation respectively, allowing the algorithm to interpret these major morphological features. The response condition is then introduced as a tensor field to inform ellipsoid packing parameters listed.

##### *3.1.2. Tensor field as a user input to inform Ellipsoid Packing*

The tensor field is the key input that establishes load-responsive inhomogeneity and anisotropy in the process of lattice generation. The tensor field is defined by a field of three orthogonal tensors at each point within the analyzed global design geometry. These points correspond to the "nodes" of the voxelized design geometry (Figure 2, left). For each ellipsoid packed in a design geometry with a corresponding tensor field, the three tensors interpolated at the ellipsoid centroid serve as a response condition in determining the length and orientation of semi-major, semi-median, and semi-minor axes (Figure 1).

The tensor field input can be generated in multiple ways. For processes outlined in this paper, ANSYS is used to apply Finite Element Analysis (FEA) to a user-determined design geometry under a set loading condition (Figure 2, right).

For each node, maximum, middle, and minimum principal stress directions are calculated as the three orthogonal tensors. In the responsive packing, areas of larger stress are packed with smaller ellipsoids. Ellipsoids' main axes are oriented to align with maximum principal stress direction.

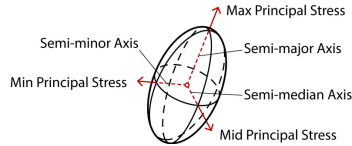


Figure 1. Semi-major, semi-median, semi-minor axis length aligned to and determined by tensor(stress) magnitudes.

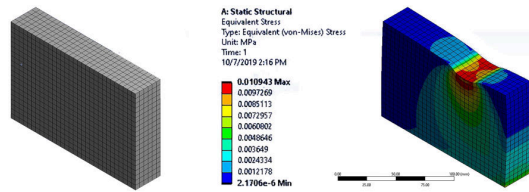


Figure 2. Left: Voxelized design geometry; Right: Finite Element Analysis by ANSYS.

### 3.1.3. Generation workflow

The Ellipsoid Packing and Kissing Ellipsoids algorithms are implemented using C#. The Ellipsoid Packing algorithm provides multiple adjustable inputs that serve as response factors in determining the lattice geometry. These inputs include boundary geometry, tensor field, maximum ellipsoid principal semi-axis length, minimum ellipsoid principal semi-axis length, pre-existing ellipsoids, and maximum iteration.

The lattice generation workflow starts with producing a tensor field for the boundary geometry with the assistance of ANSYS. The boundary geometry is first analyzed as a solid in ANSYS using a user-defined loading condition. Then, a CSV file containing the X, Y, Z coordinates of each node as well as key parameters evaluated at each node can be exported. As a convention of this workflow, the CSV file is exported in a format that contains maximum principal stress, middle principal stress, minimum principal stress, and Euler angles indicating the necessary angle of rotation to transform from the global coordinate system to each node's principal stress axis. Finally, the CSV file is translated to a tensor field.

Ellipsoid packing is initiated following the outlined process of tensor field generation. This consists of packing the design geometry with the associated tensor field with as many ellipsoids as possible. Simultaneously, the ellipsoids are scaled and rotated in accordance with the tensor field input.

The dense packing is realized by iteratively adding new ellipsoids and relaxing the existing ellipsoids. A user-defined input of an initial number of ellipsoids

is needed to begin the packing into the design geometry. To continue ellipsoid packing, collisions are checked between pairs of ellipsoids. This process is particularly complex and computationally expensive when applied to ellipsoid geometries because the ellipsoid collision point doesn't necessarily correspond to the line that connects the centroids as it does in spherical colliding. To simplify this process, the orientation difference of two colliding ellipsoids is assumed to be small, hence the collision point is still assumed to be in close proximity to the connection line. For each pair of ellipsoids, the summation of the two rim distances along the center connection line is calculated (Formula 1-3) and then compared to the centroid distance. When calculating the rim distance, a rotation transformation is applied to align the ellipsoid axes to the global 3D Cartesian coordinate system so that standard ellipsoid function can be used to simplify the calculation (Figure 3). If the sum of rim distances is greater than the centroid distance, they are determined to be colliding, otherwise not. If no collision is detected, indicating all the ellipsoids are fully relaxed within the boundary geometry, one more ellipsoid is added into the boundary geometry. If collisions are detected, a relaxation process is initiated and the colliding ellipsoids are moved away from each other by half of the overlap distance.

$$v_1 = \text{Normalize}(R_1(C_2 - C_1)) = (x_1, y_1, z_1) \tag{1}$$

$$v_2 = \text{Normalize}(R_2(C_2 - C_1)) = (x_2, y_2, z_2) \tag{2}$$

$$d_{rim_i} = \frac{1}{\sqrt{\left(\left(\frac{x_i}{a_i}\right)^2 + \left(\frac{y_i}{b_i}\right)^2 + \left(\frac{z_i}{c_i}\right)^2\right)}} \tag{3}$$

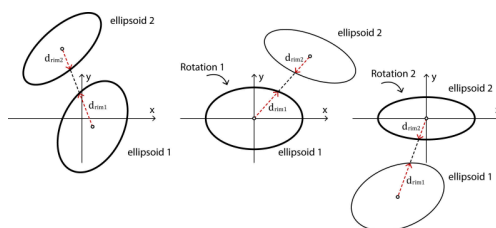


Figure 3. Left: A pair of ellipsoids in the global coordinate system; Mid: Transform the ellipsoids to the local coordinate system of ellipsoid 1; Right: Transform the ellipsoids to the local coordinate system of ellipsoid 2.

After the collision detection process is completed, the ellipsoid sizes and orientations are updated according to the tensors interpolated at the new centroid locations as a response to the tensor field. The three principal semiaxes of each ellipsoid are respectively aligned to the directions of the three tensors, and semi-axis lengths are determined by both the tensor magnitudes and user-decided maximum and minimum ellipsoid semi-axis lengths. Generally, an ellipsoid is expected to be smaller when the tensor magnitudes are higher, and is to be oriented towards the largest of the three tensors (Figure 4). In order to realize this, a

mathematical mechanism is designed. Each tensor is mapped to a semi-axis length inversely proportional to its magnitude, with the maximum and minimum magnitudes of the tensor field as a source range and the user-input maximum and minimum semi-axis lengths as a target range. Each mapped length is then assigned to the two ellipsoid axes orthogonal to the tensor (Formula 4-6). Of the two lengths that an ellipsoid axis receives this way, the smaller of these two, corresponding to the larger orthogonal stress, is chosen as the length of that semi-axis.

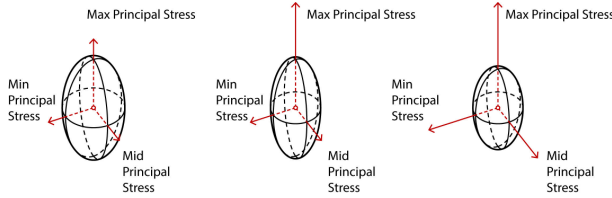


Figure 4. Larger tensor magnitude leads to a smaller ellipsoid.

$$l_x = \min \left( \frac{(t_y - t_{\min})(l_{\max} - l_{\min})}{t_{\max} - t_{\min}}, \frac{(t_z - t_{\min})(l_{\max} - l_{\min})}{t_{\max} - t_{\min}} \right) + l_{\min} \quad (4)$$

$$l_y = \min \left( \frac{(t_x - t_{\min})(l_{\max} - l_{\min})}{t_{\max} - t_{\min}}, \frac{(t_z - t_{\min})(l_{\max} - l_{\min})}{t_{\max} - t_{\min}} \right) + l_{\min} \quad (5)$$

$$l_z = \min \left( \frac{(t_x - t_{\min})(l_{\max} - l_{\min})}{t_{\max} - t_{\min}}, \frac{(t_y - t_{\min})(l_{\max} - l_{\min})}{t_{\max} - t_{\min}} \right) + l_{\min} \quad (6)$$

Ellipsoids are added and relaxed iteratively until boundary geometry is filled (Figure 5). When no more collisions are detected within the number of iterations, the packing process is finished and the last pack of ellipsoids is output. The 3D lattice is then generated through the Kissing Ellipsoids algorithm, which connects the centroids of the kissing ellipsoids(Figure 6). This algorithm allows for the adjustment of the number of struts by changing kissing tolerance (Formula 7).

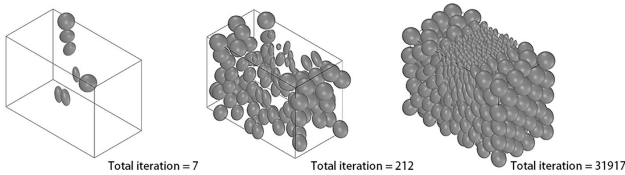


Figure 5. The pack of ellipsoids at different iterations.

Several optimization techniques are devised to improve the performance of the algorithm. When it comes to large-scale ellipsoid packing, looping over all pairs of ellipsoids for collision detection can be time-consuming and computationally expensive. To reduce the amount of required collision detection necessary during the packing iterations, the spatial partitioning technique is applied. The double of the maximum ellipsoid semi-axis length is used as the partition size, and the boundary is divided into voxels. Collision detection is only applied to a pair of

ellipsoids if one of them was moved during the last iteration. If no movement occurred in the ellipsoid pair in the previous iteration, no new collision detection is applied.

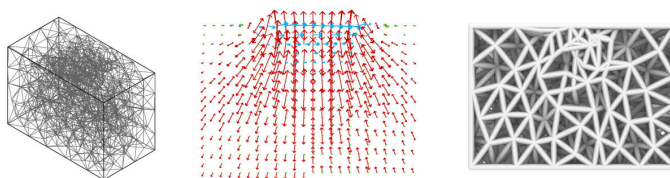


Figure 6. The lattice created by Kissing Ellipsoid algorithm and the comparison of the tensor field with the thickened lattice.

$$t_{\min}(d_{rim1} + d_{rim2}) < \|C_2 - C_1\| < t_{\max}(d_{rim1} + d_{rim2}) \quad (7)$$

### 3.2. COMPARATIVE STUDIES

#### 3.2.1. Qualitative comparison of algorithmic design

Control lattices for comparison include both cellular periodic lattices generated by Crystallon for grasshopper, and other inhomogeneous anisotropic lattice precedents such as Sphere Packing followed by 3D Voronoi by Alvin Huang (2016), Ellipsoid Packing with 3D Delaunay by Felder et. al (2016).

Crystallon works by applying adaptive voxelization to a set design volume. A 3D unit linework pattern is created and mapped into each voxel of the design volume. A 3D periodic cellular lattice is generated with each voxel containing the same unit. The main input parameters include design volume, voxel size, and unit pattern. Users can morph the voxels in some areas using point attractors or curve attractors to locally densify or loosen the voxel division and potentially respond to external factors like loading. However, attractors are not explicit and are difficult for users to manipulate. The inhomogeneity and anisotropy of the periodic cellular lattice highly depend on the topology of voxelization and the anisotropy of the unit.

Huang's method of Sphere Packing with 3D Voronoi is employed within the context of a chair design. The furniture geometry is analyzed with Karamba, a Grasshopper FEA plug-in. The calculated principal stresses are used to inform the sphere packing process, where areas of larger stress are packed more densely with smaller spheres. This is similar to the PolyBrick ellipsoid packing logics. The two algorithms differ, however, in the process of lattice generation. Huang uses sphere centroids as an input for a 3D Voronoi algorithm and therefore loses control of strut orientations. While this method is able to achieve load-responsive inhomogeneity, it doesn't have enough control over lattice anisotropy due to a lack of strut orientation control.

The method of Ellipsoid Packing with 3D Delaunay employed by Felder et al. and our proposed packing method are similar in their use of FEA informed Ellipsoid Packing to control lattice directionality. However, there are three important differences in the algorithmic designs. Firstly, in Felder's method,

Ellipsoid Packing is used to distribute lattice nodes and control inhomogeneity. The anisotropy is later achieved through a post-processing step, where struts not aligned with the stress field are removed. In our proposed Ellipsoid Packing algorithm, both anisotropy and inhomogeneity are controlled and enforced by dense packing. A second difference is the ways ellipsoids update in response to the stress field. In addition to aligning the ellipsoids to the stresses, Felder's method also tries to align the connection of the neighboring ellipsoids to the stresses. The lattice generation technique also shows a difference. In Felder's method, the lattice is generated by the 3D Delaunay triangulation algorithm, while our proposed method uses Kissing Ellipsoids.

### 3.2.2. Quantitative comparison of lattice mechanical performances

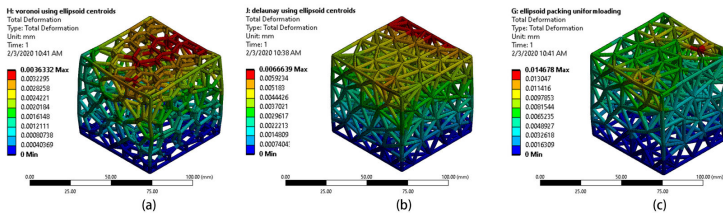


Figure 7. Part of the test lattices (a)3D Voronoi (b)3D Delaunay (c) Kissing Ellipsoids. Blue indicates zero deformation, red indicates the maximum deformation within each lattice.

Periodic cellular lattices, Sphere Packing with 3D Voronoi lattice, and Ellipsoid Packing with 3D Delaunay lattice are generated and tested with ANSYS (Figure 7). To begin the quantitative comparison, we generated lattices that had identical boundary sizes. When these line bodies were moved into ANSYS, they were all piped by the same radius, chosen to be 2mm. The total amount of force applied to each lattice is kept the same by dividing an arbitrary load of 1000N across the top face vertices of each lattice respectively. Controlling these parameters simplifies the post-processing of the axial force and directional displacement data because only lattice length is uncorrected for. Because some lattices have an overall longer length, meaning there was more material contained in the bounding box, they inherently perform better. To adjust for this, stiffness per volume is calculated using the maximum Y-direction displacement that occurs at the top face, the original height of the lattice, the total area of the top face piped vertices, and the 1000N uniform load. The maximum axial force and directional displacement data without this length correction are reviewed to get a general sense of the performance of the lattice.

## 4. Result

### 4.1. QUANTITATIVE COMPARISON OF LATTICE MECHANICAL PERFORMANCES

As the interest group, two ellipsoid packing lattices are tested, one generated with a uniform loading condition input and the other with a point loading input.

Figure 8 illustrates how our lattices perform in stress, deformation, and stiffness against the control lattices generated with different algorithms. An optimal lattice for load-bearing applications would minimize the highest stress found in a beam element, minimize the maximum deformation of the lattice, and maximize the stiffness because the forces would be most evenly distributed and protect the lattice well from breakage. Stiffness is essentially a combination of stress and deformation and by correcting for volume, we may consider the lattices independent of density. The ellipsoid packing lattices formed with uniform loading and point loading both show higher stiffness per volume ratios than a majority of the lattices tested, and outperform 11 and 14 lattices, out of the total 18 tested, respectively. The lattices each have a stiffness per volume of 172.7 kPa/m<sup>2</sup> and 197.9 kPa/m<sup>2</sup> respectively.

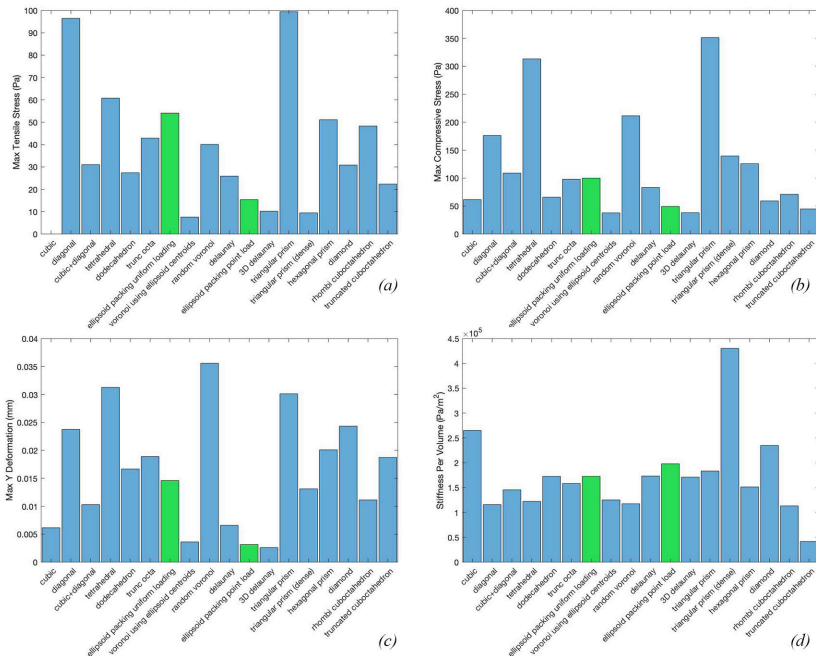


Figure 8. (a) Maximum Tensile Stress in one beam element. (b) Maximum Compressive Stress in one beam element. (c) Maximum deformation in the direction of the force application. (d) Stiffness per volume for each lattice. For a, b and c, lower value is more advantageous. For d, higher value is more advantageous.

## 5. Limitations and Conclusion

### 5.1. LIMITATIONS

In the quantitative comparison, we chose the piping radius of 2mm based on the expected physical dimensions of our physical prototypes. However, each individual lattice does have an optimal piping diameter to maximize performance.



Hence, we may not have chosen the ideal radius for the ellipsoid packing algorithm to demonstrate its full potential or we may have chosen a radius that causes other lattices to perform poorly. Therefore, our current results should only be considered on the scale of those prototypes. If we wanted to change the scale or extrapolate the results, more testing would be needed to explore the dependence between performance and piping radius. Additionally, the time and memory usage of different algorithms need to be compared for a better understanding of our method's computational performance.

## 5.2. CONCLUSION

In this paper, a new computational method based on ellipsoid packing is proposed for the generation of anisotropic and inhomogeneous lattice structures. In contrast with existing lattice generation algorithms, this method provides comprehensive control over both anisotropy and inhomogeneity and increases ease of generating specialized responsive geometries. For the next phase, a load-responsive strut thickening algorithm will be developed to create a complete lattice structure. Furthermore, the proposed method can be leveraged in architectural-scale projects with additional research of material and fabrication methods. Robotic clay extrusion is foreseen as a promising future trajectory to fabricate generated load-responsive lattice typologies at an architectural scale, contextualized as part of a wall design. Thus architectural advantages and potentials of proposed responsive 3D lattice algorithms will materialize.

## References

- Bagi, C.M., Berryman, E. and Moalli, M.R.: 2011, Comparative bone anatomy of commonly used laboratory animals: implications for drug discovery, *Comparative medicine*, **61**(1), 76-85.
- Biol, E.B., Lu, Y., Sekkin, E., Johnson, C., Moy, D., Islam, Y. and Sabin, J.: 2019, PolyBrick 2.0: Bio-integrative load-bearing structure, *Proceedings of the 36th Annual Conference of the Association for Computer Aided Design in Architecture*, Austin, 222-233.
- Felder, A.A., Lewis, H., Piker, D., Pereira, A. and De Kestelier, X.M.V.: 2016, Mechano-adaptive space frame generation based on ellipsoid packing, *Proceedings of IASS 2016 Symposium: Spatial Structures in the 21st Century*, Tokyo, Japan.
- Huang, A.: 2016, From Bones to Bricks: Design the 3D Printed Durotaxis Chair and La Burbuja Lamp, *Proceedings of the 36th Annual Conference of the Association for Computer Aided Design in Architecture*, Ann Arbor, 318-325.
- Im, H.C., AlOthman, S. and del Castillo, J.L.G.: 2018, Responsive Spatial Print: Clay 3D printing of spatial lattices using real-time model recalibration, *38th Annual Conference of Association of Computer Aided Design in Architecture*, 286-293.
- Niu, J., Choo, H.L., Sun, W. and Mok, S.H.: 2018, Numerical study on load-bearing capabilities of beam-like lattice structures with three different unit cells, *International Journal of Mechanics and Materials in Design*, **14**(3), 443-460.
- Sabin, J., Miller, M., Cassab, N. and Lucia, A.: 2014, PolyBrick: Variegated Additive Ceramic Component Manufacturing (ACCM), *3D PRINTING*, **1**(2), 78-84.

# REVISITING PACKING ALGORITHM

*A Strategy for Optimum Net-to-Gross Office Design*

BEATRICIA BEATRICIA<sup>1</sup>, ASWIN INDRAPRASTHA<sup>2</sup> and  
M. DONNY KOERNIAWAN<sup>3</sup>

<sup>1,2,3</sup>*School of Architecture, Planning and Policy Development, Institut  
Teknologi Bandung*

<sup>1,3</sup>{beatriciabeatricia|donnykoer}@gmail.com <sup>2</sup>aswin@itb.ac.id

**Abstract.** Net-to-gross efficiency is defined as the ratio of net area to a gross area of a building. Net-to-gross efficiency will determine the quantity of leasable building area. On the other side, the effectiveness of the spatial distribution of a floor plan design must follow the value of net-to-gross efficiency. Therefore in the context of office design, there are two challenges need to be improved: 1) to get an optimum value of efficiency, architects need to assign the amount and size of the office units which can be effectively arranged, and 2) to fulfill high net-to-gross efficiency value that usually set out at minimal 85%. This paper aims to apply the packing algorithm as a strategy to achieve optimum net-to-gross efficiency and generating spatial configuration of office units that fit with the result. Our study experimented with series of models and simulations consisting of three stages that start from finding net-to-gross efficiency, defining office unit profiles based on preferable office space units, and applying the packing algorithm to get an optimum office net-to-gross efficiency. Computational processes using physics engine and optimization solvers have been utilized to generate design layouts that have minimal spatial residues, hence increasing the net-to-gross ratio.

**Keywords.** Net-to-gross efficiency; packing algorithm; modular office area; area optimization; .

## 1. Background

In the disruptive era of the rental office market nowadays, net-to-gross efficiency is one of the significant factors in defining high-performance office design. The equilibrium state, among other factors such as energy efficiency, safety, and security, as well as service and amenities, is a performative factor that architects need to consider in a design process. Generative design methods can accelerate those processes by quickly generate numbers of layout designs that adhere to building codes and regulations in such a way that will be enabling the architect to focus on form and spatial exploration. This study focuses on revisiting the packing method and generative design as a computational strategy to develop

a procedure for generating maximum efficiency of office space layout. As the focus of the study is at the office space layout, the modular office space also being studied and analyzed based on local context and practices. Modular office space is our primary concern for generating office layout through packing algorithms and methodology. Meanwhile, the packing algorithm is an optimization method to pack objects into a defined convex space. In the context of this study, packing is a formal procedure to maximize the occupancy of definite objects into a closed boundary. In the packing problem, there are two aspects to be defined: 1) a convex region, two or three dimensions of space, and; 2) a set of objects that must be packed into the container where objects are not allowed to overlap. March (1971) was one of the first scholars to study the relation of architectural elements and combinatoric mathematics when he introduced a Product Set. Product Set is a combinatoric formula to generate combination configurations of two objects based on the type of conjunction relation of those objects. Dong, Fadel & Blouin (2005) studied method to solve packing problems by simulating the elastic movements of a set of packed objects using a physics engine emulating a rubber band that wrapped between objects. Based on the forces, objects translate, rotate, or deformed until maximum compactness is reached.

## **2. Case study on Conceptual Design Process**

### **2.1. RENTAL OFFICE SPACE**

To demonstrate packing and generative design tools that can be used to assist the design process, particularly on office design, a site in Central Business District in Jakarta has been selected as a case study. A preliminary study began by conducting a survey of office space units in rental offices building in Jakarta. A total of 18 rental office buildings in the Central Business District in Jakarta had been surveyed and the result shows the variation of office unit (module unit) offered by the 18 office buildings can be categorized into four major groups: 1) 50sqm-100sqm; 2) 100sqm-300sqm; 3) 300sqm-500sqm; 4) >500sqm. By then, we analyzed the preferable office unit based on direct observation and interview with building managers that resulted in seven range of office space size, that are 100-110sqm, 140-150sqm, 180-190sqm, 190-200sqm, 200-210sqm, 210-220sqm, 230-240sqm. The studies about office unit space took roles as the components that would be packed. The variation of rental office units of the 18 office buildings in Jakarta is depicted in Table 1.

Table 1. Rental Office Space Unit.

Office	Unit 1	Unit 2	Unit 3	Unit 4	Unit 5	Unit 6	Unit 7	Unit 8	Unit 9
1 District 8 Treasury Tower	318	143	141	133					
2 The East	303	294	290	288	279	270	250	232	
3 Menara Tandean	157	149	111	103	72	55			
4 Graha Makmur	195	188	146	144	116	109			
5 Wisma Barito Pacific 2	192	189	170						
6 The City Center Batavia	551	548	501	498					
7 18 Office Park	294	249	249	171	141	132			
8 Satrio Tower	221	217	191	186	165				
9 Lippo Thamrin Tower	351	339	193	190	155				
10 Gran Rubina Tower 1	259	205	200						
11 Menara Pertiwi	392	231	231	187	125	93			
12 Menara Prima	207	198	196	186	98	94	91	80	77
13 MNC Tower	427	261							
14 Unity Square Tower	259	248	234	141	131				
15 Menara BTPN	407	347	347	343	210	209			
16 Menara Palma Tower 1	237	212	186	124	112	107	105	104	
17 Centinental Tower	508	492	219	201					
18 Sudirman 7.8	311	280	249	245	238	217			

2.2. PROPOSED SITE

Our goal of the experiment is to develop a method for the design layout of modular office space with a maximum net-to-gross ratio. By considering office units obtained in the preliminary survey, we put them to the test of an office building design in an urban setting.

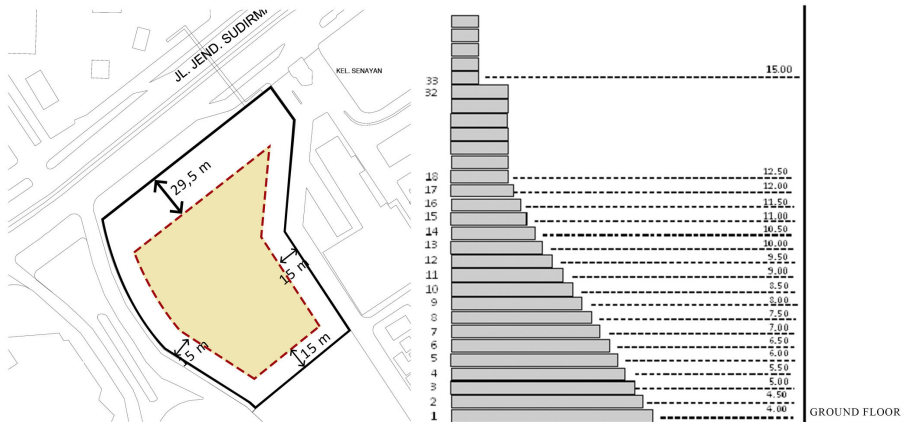


Figure 1. Building Setbacks and Free Distance Regulations.

The site is at CBD of Jakarta, Indonesia, with area 18,424sqm. Within the CBD, the local regulations mandate restrictions associated with a buildable area including maximum BCR:40%, Maximum plot ratio: 5.8, minimum Green Coverage Area: 30%, and maximum Basement Footprint Ratio: 55%. Besides, there are setbacks and Building Free Distance rules required, as depicted in Figure

1. This simulation resulted in the number of floors and a floor plate that would be become a closed boundary in the packing simulation.

### 2.3. MAXIMIZING ALLOWABLE TOTAL GROSS FLOOR AREA (GFA)

Given the estimated building footprint and total allowable area guided by local regulation, we established building core and central circulation area of 440sqm based on international standards (Chiara, D & Crosbie, J, 1980) and empirical data of the building core collected during field observation. The allowable building footprint delineated by the setbacks and Building Coverage Ratio as regulated. At this stage, the boundary of the building can be defined and can be controlled parametrically to adjust offset distances from the perimeter. Furthermore, maximum GFA was used to calculate the maximum height of the building. Evolutionary Solver has been used to find the optimum value of the floor slab area to achieve maximum GFA considering the total height of the building and floor to floor height. This method resulted in specific parameters such as Maximum GFA, Net Floor Area (sqm), Number of Floor, Floor Plate Area (sqm), Ratio of Achieved GFA and Allowable GFA and Net to Gross Area Ratio as depicted in Table 2 below:

Table 2. Optimization Result of Optimum Values.

	Gross Floor Area (sqm)	Net Floor Area (sqm)	Number of floors	Floor Plate Area (sqm)	Ratio with Allowable GFA	Net-to-Gross Ratio
1	105329,68	79770,01	58	1815,35	74,65%	76%
2	105393,56	92173,04	30	3512,43	86,26%	87%
18	106178,83	92958,31	30	3538,61	86,99%	88%
19	106190,66	85478,51	47	2258,69	79,99%	80%
29	106571,40	96876,35	22	4843,47	90,66%	91%
30	106573,04	94233,89	28	3805,50	88,19%	88%
31	106632,83	83276,58	53	2011,26	77,93%	78%
32	106634,35	92091,78	33	3230,66	86,18%	86%
33	106640,04	92538,15	32	3331,82	86,60%	87%
34	106873,63	95415,85	26	4109,84	89,29%	89%

The optimization process yields 40 data in which minimum efficiency (net-to-gross) is 76% and a maximum of 91%. Noted that the most suitable solution is the one with total GFA is near to the value of maximum allowable GFA= 106,859.2 sqm. We obtained three samples for a further process, which have an efficiency of 80%, 87%, and 91%, respectively, that has a positive correlation with the floor plate area. The 91% efficiency has a typical 4,843.47 sqm floor plate area with 22 floors. The conceptual building envelope resembles a site profile, as depicted in Figure 2.

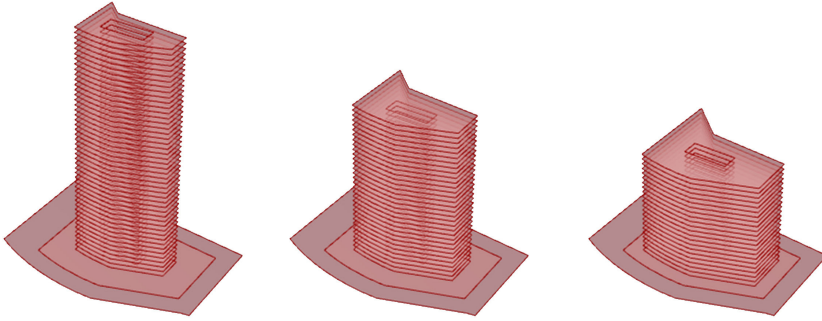


Figure 2. Conceptual Building Envelopes, (Left) Efficiency Factor 80%; (Middle) Efficiency Factor 87%; (Right) Efficiency Factor 91%.

#### 2.4. EVALUATION AND DETERMINATION OF OPTIMUM MODULAR OFFICE SPACE

We used the previous studies about preferable office unit space, which area are 100-110sqm, 140-150sqm, 180-190sqm, 190-200sqm, 200-210sqm, 210-220sqm, 230-240sqm for the experiment. We search in those categories the most efficient office area by utilizing the generative design of Evolutionary Solver based on the standard of proportional office space by Duffy (1976). An office area is defined by the length( $l$ ) and width( $w$ ) in which its  $l/w$  ratio determines the effectiveness of a bay office area. Duffy (1976) developed a relation between  $w/l$  ratio and a bay office area for determining office space by considering the Discount Factor. The Discount Factor is a coefficient of the residual area due to structural and utility elements located in an office area. The discount Factor value depends on the ratio as depicted in the diagram, and it defines the Effective Area as formulated as follows:

$$EffectiveArea = TotalArea - \left( TotalArea \cdot \left( \frac{Discount\ Factor}{100} \right) \right) \quad (1)$$

By using generative tools using the Evolutionary Solver, we took four parameters to search optimum area in each group: length ( $l$ ), width ( $w$ ) as *genome*, area as *fitness*, and Discount Factor coefficients following the area ratio indicated on the table above. Result of the optimization process then calculated with the Formula (1) returns the effective area of the group of 100-110sqm, 140-150sqm, 180-190sqm, 190-200sqm, 200-210sqm, 210-220sqm, and 230-240sqm as follows:

- a. Redefine unit profile

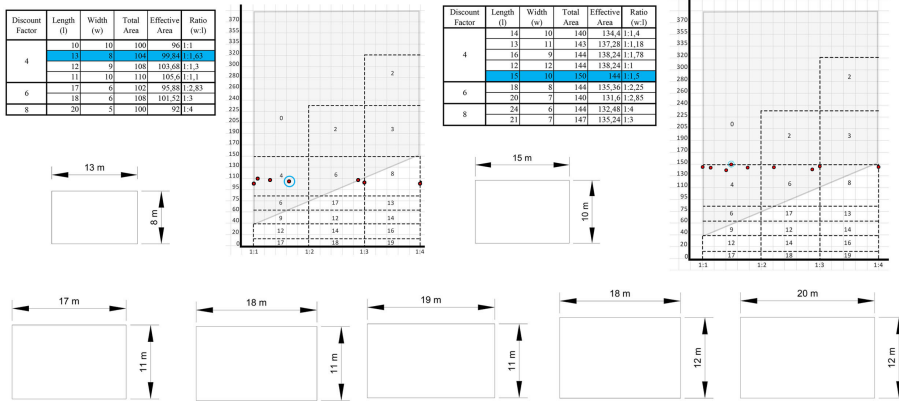


Figure 3. Optimization Result and Determination of the Dimension of Office Unit .

b. Office unit space

Evolutionary solver yields hundreds of variations of the solution in maximizing all units area, and by take into account the Discount Factors, we determine the most effective office area of each of units are: 104sqm (13m x 8m), 150sqm (15m x 10m), 187sqm (17m x 11m), 198sqm (18m x 11m), 209sqm (19m x 11m), 216sqm (18m x 12m), 240sqm (20m x 12m), respectively as depicted in Figure 3.

2.5. MINIMIZING SPATIAL RESIDUE OF FLOOR PLATE BY PACKING ALGORITHM

By the parameter geometry of floor plate boundary, building core, and office unit, we employed a packing algorithm based on Rubber Band methods with the main objective to maximize office unit space into the boundary of the floor plate and in accordance, minimize the residue area. Rubber Band method first was introduced in 2001 by Fadel and Sinha. By using the analogy of packing with rubber band character, which has flexibility and elastic force, units or components will be packed together to get the maximum compact configuration. This method also helps us to determine packing constraints, which are 1)compactness, to get maximum unit space area; 2)Collision, is an incident where the components collide each other; 3) Tolerance is a maximum space between components after the collision. These constraints are beneficial to develop the packing algorithm. The mechanism of packing simulation in the visual algorithm editor Grasshopper is described in Figure 4.

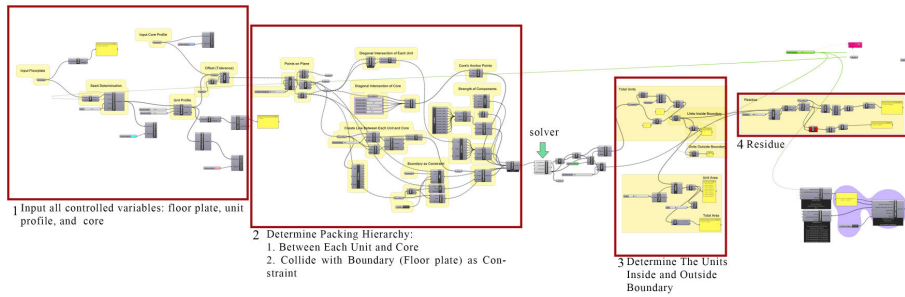


Figure 4. Overall Packing Algorithm.

### 2.5.1. Initiation

This stage is a set up the static location of boundary and building core, setting up the location of the point of reference of each office unit by its endpoint inside the boundary for packing simulation.

### 2.5.2. Packing Hierarchy

We defined the hierarchy rules the packing simulation as follows 1) centroid of each module is connected to the centroid of the building core; 2) equip the boundary with colliding property to prevent each module got overlapped and falls outside the boundary.

### 2.5.3. Packing Displacement

The packing simulation begins with each module moves and searching to fill in themselves inside the boundary by three displacements types: 1) translation: the connection between core and unit, employing the core as anchor or *attractor* force to produced vector inside each unit at the *centroid*. This vector creates a vector movement unit towards the core. Using building core as the *attractor* force, it pulls inside each module; 2) collision and rotation: this property embedded in boundary, and every time the unit collides with the boundary, they will bounce back with the possibility of deformation. Another possible movement when the collision occurred between objects is rotation; 3) deformation: deformation occurs when the module collide with each other or collide with the boundary. In each case, whenever there is a space available, each module will maintain its shape's integrity. Otherwise, the level of deformation of the unit will increase (Figure 5).



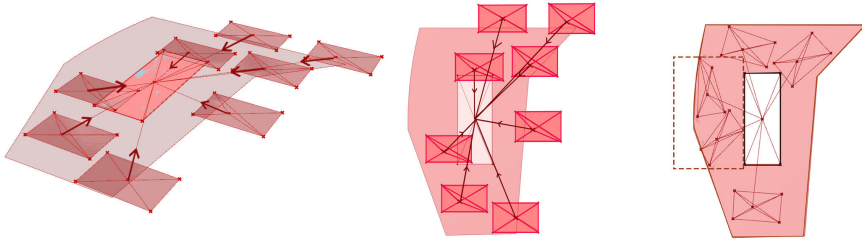


Figure 5. At Packing Simulation (Left) Translation and Rotation Toward Building Core and Fill the Boundary; (Right) Collision and Deformation.

### 3. Result of Packing Simulation

#### 3.1. PACKING WITH THE SAME UNIT

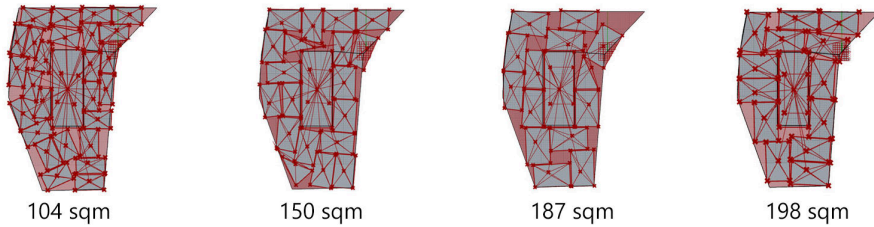


Figure 6. Packing Result of 104sqm, 150sqm, 187sqm, and 198sqm Office Unit.

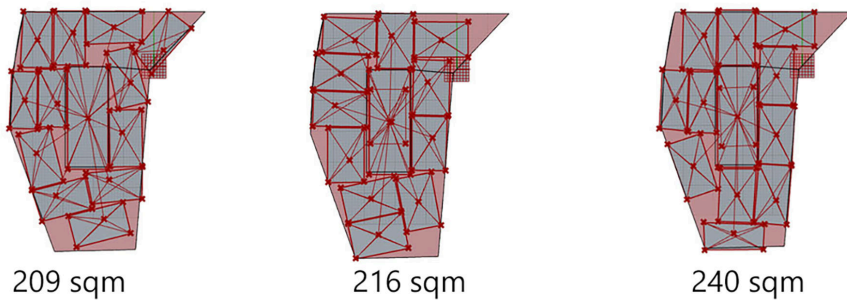


Figure 7. Packing Result of 209sqm, 216sqm, and 240sqm Office Unit.

Figure 6-7 depicted final result of the packing algorithm of each unit that implemented on the boundary area. Obviously the smallest unit (104sqm) has the most variation of its layout while the large unit (209sqm, 216sqm and 240sqm) has the least variation. The 150sqm unit has the most efficient net-to gross as it reaches

80.7% efficiency of 3,294sqm floor plate. The maximum area and maximum residual area produced by each packed unit is described in Table 3.

Table 3. Maximum Area and Maximum Residual Area of Packing Result.

Unit	No. of Variants	Maximum Area (sqm)	Residual Area (sqm)	Unit	No. of Variants	Maximum Area (sqm)	Residual Area (sqm)
<b>104</b>	27	2295	611	<b>209</b>	12	2256	670
<b>150</b>	19	2373	565	<b>216</b>	12	2239	653
<b>187</b>	15	2210	779	<b>240</b>	12	2325	613
<b>198</b>	14	2338	563				

### 3.2. PACKING WITH COMBINATION OF UNITS

Following the packing simulation of each unit, the simulation of the packing combination amount of each unit was based on the simulation's result. The number of each unit combination is 0,3,4,2,2,0 and 4 for the 104sqm, 150sqm, 187sqm, 198sqm, 209sqm, 216sqm, and 240 sqm respectively, of office units space. The purpose of packing combination units is to have more variants of units in a one-floor plate. The placement of each unit can randomly be located based on the seed's slider of the Evolutionary Solver. In this case, we used a constant five (5) as the seed for the random generator (Figure 8 and Figure 9).

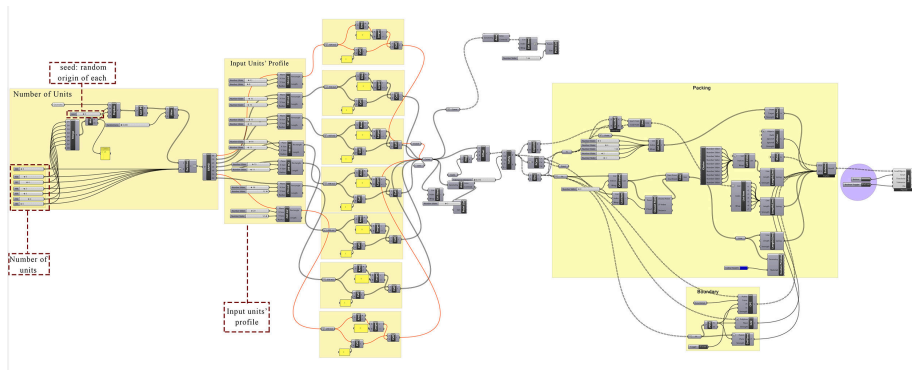


Figure 8. Packing Algorithm for The Combination of Units.

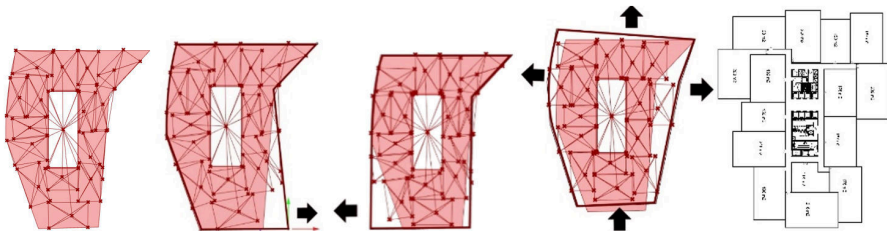


Figure 9. The Result of Packing for Combination Units.

The simulation of the packing combination will decrease the residual area because the amount of each unit is based on the previous simulation. After the simulation of the packing combination was achieved, the boundary needs to be stretched-out manually to get the maximum area. The final result of this simulation reached 84,43% value of net-to-gross efficiency with 3.294 sqm of floor plate area.

#### 4. Discussion

This study aims at applying the packing algorithm in defining space configuration to achieve optimum net-to-gross efficiency in rental office design. Rubber Band packing principles was used in this packing algorithm. This algorithm we used by utilizing physic engine Kangaroo in Grasshopper 3D emulated the rubber band methodology. As a proof of concept, we develop a methodology to generate a maximum net-to-gross, modular office space unit, and its spatial configuration. The final result of this study is a spatial configuration that can be available at the early stage of design. The division of a packing algorithm into two stages helps to decrease the residual area of a packing simulation. The application of this method gives advantages as well as disadvantages. By using this method, the designers only need to determine the number of modules and the size of units to generate office layout. The disadvantages that can be seen at the final results is, there are units that do not received natural lighting and some of them have reductions in unit area. The final result also shows the number of its efficiency is decreased to 84,43%. It is caused by the circulation component that had not been refined as a constraint in the packing simulation.

#### References

- Alajmi, A.I. and Wright, J.: 2014, Selecting The Most Efficient Genetic Algorithm Sets in Solving Unconstrained Building Optimization Problem, *International Journal of Sustainable Built Environment*, **3**(1), 18-26.
- Chiara, J.D.: 1980, *Time Saver Standards for Building Types*, McGraw-Hill.
- El Daly, H.M.T.: 2009, *Revisiting Algorithms in Architectural Design: Towards New Computational Methods*, Ph.D. Thesis, Ain Shams University Faculty of Engineering Department of Architecture.
- Dong, H., Fadel, G. and Blouin, V.: 2005, Packing Optimization by Enhanced Rubber Band Analogy, *ASME 2005 International Design Engineering Technical Conferences and Computers and Information in Engineering*.
- Duffy, F., Cave, C. and Worthington, J.: 1976, *Planning Office Space*, Architectural Press, London.
- Goldberg, D.E.: 1989, *Genetic Algorithms in Search, Optimization, and Machine Learning*, Addison-Wesley Longman.
- Keshav, A.: 2013, Effects of Core Design Form on Rentable Spaces of A High Rise Office Building., *The Relationship Between Structural System, Core and Rentable Spaces of a High Rise Office Building*, Bhopal, India.
- Leu, S.-S. and Yang, C.-H.: 1999, GA-Based Multicriteria Optimal Model for Construction Scheduling, *Journal of Construction Engineering and Management*, **126**(6), 420-427.
- M., F.G. and A., S.: 2001, Packing Optimization Using a Rubber band Analogy, *ASME, DETC*.
- Sev, A. and Ozgen, A.: 2008, Space Efficiency in High-Rise Office Building, *METU Journal of the Faculty of Architecture*, **26**(2), 69-89.

# THE TAIKOO SHING SUPERBLOCK: ADDRESSING URBAN STRESSES THROUGH SEQUENTIAL EVOLUTIONARY SIMULATIONS

MADISON RANDALL<sup>1</sup>, TINA KORDROSTAMI<sup>2</sup> and MOHAMMED MAKKI<sup>3</sup>

<sup>1,2,3</sup>*University of Technology Sydney*

<sup>1,2</sup>{*madison.m.randall|tina.kordrostami-1*}@student.uts.edu.au

<sup>3</sup>*mohamad.makki@uts.edu.au*

**Abstract.** The multiplicity of networks, connections and relationships that exist in every city - complex and varied - are inherent to the urban fabric. Variation within the built form is integral to ensure adaptability to environmental and climatic conditions imposed on cities over generations. This research aims to highlight the benefits of utilizing sequential evolutionary simulations, to arrive at a more resolved solution-set that addresses urban challenges of the Taiko Shing superblock in Hong Kong.

**Keywords.** Hong Kong; Urban; Sequential Simulations; Evolution; Computation.

## 1. Introduction

The utilisation of natural world principles for the design of urban tissues has been put forward as a more robust alternative for conventional approaches to urban planning by multiple authors and researchers throughout the late 20th and 21st centuries (Alexander, 1964; Batty, 2013; Marshall, 2008; Weinstock, 2010). Coupled with the rapid development of computational tools, the digital translation of biological evolutionary principles has allowed designers to approach complex design problems, comprised from multiple conflicting objectives, with a greater focus on localised relationships between the design variables; consequently bypassing the requirement of addressing the problem through a predominantly top-down approach.

Although the utilisation of an evolutionary system allows for the design optimisation of multiple conflicting objectives, the complexity of the design problem dictates the success rate of the evolutionary simulation in converging towards fit solutions, (Makki et al., 2018); at times forcing the simplification of the problem to allow for improved results from the simulation. An alternative to this is to divide the design problem and run multiple simulations, where the results of one simulation 'feeds' into the consequent simulation, allowing for greater efficiency when optimising the design problem.

In this context, the results presented will aim to highlight the benefits of utilizing sequential evolutionary simulations to arrive at a more resolved

solution-set that addresses urban challenges facing the Taikoo Shing Superblock in Hong Kong.

## **2. Context and Research**

### **2.1. TAIKOO SHING, HONG KONG**

Located within the suburb of Quarry Bay on Hong Kong Island, Taikoo Shing is an existing high-rise residential development comprising of sixty-one near-identical towers housing over thirty-five thousand people (Population Census, 2011). This urban superblock is representative of a heavy-handed top-down planning approach, designed as a solution to accommodate the exponentially increasing population density of Hong Kong. Upon analysis of the existing conditions, key environmental issues can be extracted as imperative to the foundation of an urban tissue in this setting. The projected growth of the population, the lack of sufficient open space for residents, the lack of apartment outlook and poor solar gain to apartments, all highlight areas that can be improved to provide an urban tissue that is more robust to an ever-changing context.

### **2.2. DENSITY + COMMUNAL OPEN SPACE**

As recorded in the 2011 Population Census, the total number of inhabitants for the Taikoo Shing superblock was 37,796 across approximately 18.15 ha of land. This equates to  $\sim 4.8\text{m}^2/\text{capita}$ . With the total population of Hong Kong estimated to increase from 7.07 million (2011) to 8.22 million people (2043); an increase of 0.4% per annum (Census and Statistics Department, 2017), it is vital that the infrastructure can accommodate this increase in population density. Environmental issues such as access to open space, solar and the outlook of apartments become progressively more apparent as the population continues to inflate. Highlighting that the prioritisation of one issue results in extremely poor outcomes for all other contributing concerns.

Currently, the existing development provides no access to private open space, and minimal access to communal open space. As per recommendations by the World Health Organisation,  $9\text{m}^2$  open space / inhabitant ratio (Maryanti et. al., 2016) should be provided in an urban context. The present condition provides  $2.9\text{m}^2$  per capita of communal open space, showcasing the severity of this design problem. As a result of the existing building typology, there is an imbalance between the requirements to accommodate an inflating population whilst maintaining global guidelines for equity in access to open space.

### **2.3. MULTI-SCALAR APPROACH**

Within the Taikoo Shing superblock, three fundamental relationships need to be addressed in order to successfully implement a resilient urban tissue. The first aspect of this multi-scalar understanding is the relationship of the Superblock to its surrounding context. This explicitly focuses on connections to existing networks, public facilities, distribution of people, and its reaction to site-specific conditions.

Secondly, within the scale of the Superblock, there is a rich relationship

between the block typologies. This level investigates functionality, distribution and scale of the blocks, and the impacts they have on each other.

Finally, the scale of an individual building needs to be assessed in regards to the podiums, the surrounding buildings, and within the tower form itself. Understanding what aspects of the form perform well, and could be maintained throughout the design stage.

Through breaking down these complex urban issues into different scales, it enables one to comprehend a design problem as a compilation of smaller design issues that can be addressed sequentially. Therefore, and in the context of utilising a multi-objective evolutionary algorithm to tackle the design problem, the utilization of sequential simulations allows a multitude of different relationships to be explored in greater detail. Through exploring two dependent, yet sequential evolutionary simulations, the algorithm can more directly explore the solution space for each simulation, thus allowing for a greater chance of convergence towards an optimal solution set.

### 3. Method

#### 3.1. EVOLUTIONARY STRATEGY

The evolutionary algorithm that will be implemented in this experiment is the *NSGA-2* developed by Deb et. al. (2000). *NSGA-2* is the driving algorithm behind the software *Wallacei*, a free plug-in written for *Grasshopper 3D* developed by Mohammed Makki, Milad Showkatbakhsh and Yutao Song (Makki et. al. 2018).

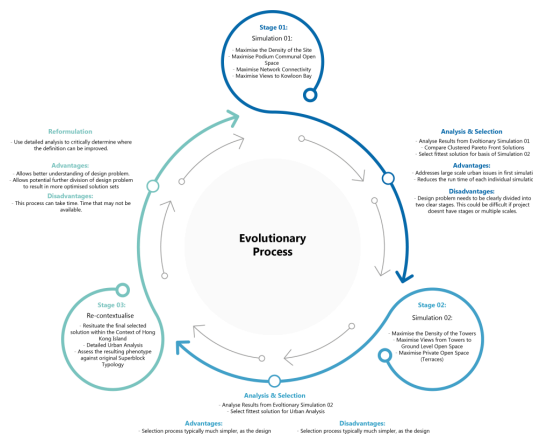


Figure 1. Evolutionary Workflow Diagram.

Through using a multi-objective evolutionary algorithm, in which the design objectives for the design problem have been identified, the experiment presented divides the formulation of the design problem into two simulations, the first and primary simulation addresses issues that are specific to the urban scale, while the secondary simulation focuses on issues within the scale of the block.

This approach of dividing the design problem (and thus the evolutionary

simulation) allows greater emphasis to be applied in resolving each stage individually, resulting in a more considered and improved design outcome. The pseudo code for the simulation is presented in Figure 01.

## 4. Experiment Setup

### 4.1. PRIMARY SIMULATION

#### 4.1.1. Parametric Definition

The foundation of the experiment is the existing site boundary and the primary/secondary road connections identified from studies of the existing site conditions (Figure 02). These existing conditions define the primary road connections, which in turn define the primary block structures which are consistent across all simulation outcomes. To assist in ‘randomising’ the location of the building forms, these static primary blocks are populated with rectangular regions ranging from 30.00-40.00m (Rx, Ry). Within each of these regions, a single point is created (Ptx, Pty) which acts as the centre point for the building forms.

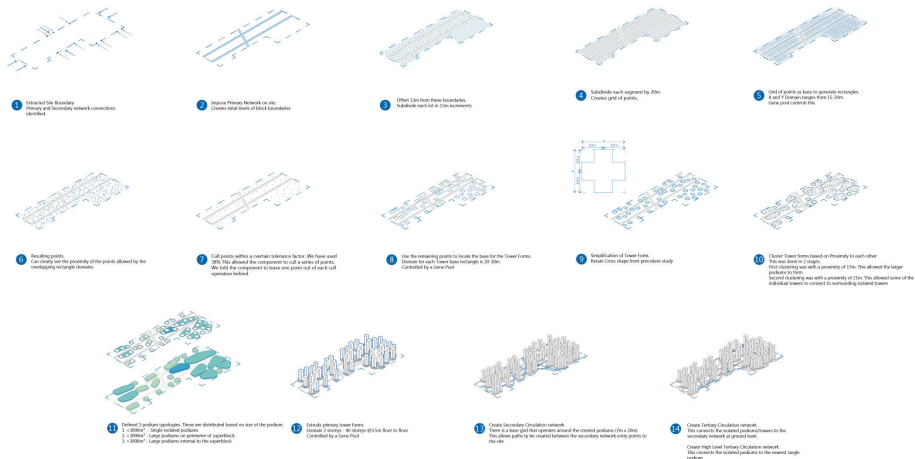


Figure 2. Construction of the Primary Parametric Definition.

To ensure there is a separation between the building forms, a culling operation has been introduced. This culls points within a tolerance of each other (38% for this experiment) leaving one point behind. The remaining network of points serves as the centre points for the preliminary building forms. The rectangular base size of the building forms is then generated using a gene pool (Bx, By) These building base plates are then clustered based on proximity to each other, resulting in podium forms that can range from a single isolated building to larger clusters of 5-6 buildings. These podiums are then sorted into three categories based on size (<3000m<sup>2</sup> - Single isolated podiums, >3000m<sup>2</sup> - Large podiums on the perimeter of the superblock, >3000m<sup>2</sup> - Large podiums internal to the superblock) These podium typologies are all extruded to a uniform height (3 storeys) as defined by studies of existing podiums.

The final stage of the primary simulation extrudes the tower footprints to various heights (H) whilst generating the secondary Networks based on a grid that goes around the created podiums and towers. This includes the tertiary street network which connects the isolated podiums to the secondary road network.

4.1.2. Fitness Objectives and Genes

Table 01 highlights the fitness objectives that the evolutionary simulation optimised for, as well as the variables (genes) modified by the evolutionary simulation which defined the superblock’s morphology.

Table 1. Fitness objectives and genes for the primary simulation.

Fitness Objectives				Genes			
#	Abbreviation	Objective	Definition	#	Abbreviation	Definition	Domain
1	V	Maximise Views from the Buildings to Kowloon Bay	This objective has been calculated by using a static curve representing the location of Kowloon Bay in relation to the site (for simplicity of the algorithm, the curve was divided into seven points, which serve as the points of interest) in which buildings were evaluated according to visibility to the bay.	1	R <sup>x</sup>	X length of the region in which the centre point for the building forms will be located	30.00m to 40.00m
2	D	Maximise Population Density across Taikoo Shing	From studies of the existing Taikoo Shing development, it has been calculated that the average apartment size is approximately 70m <sup>2</sup> , housing 3-4 people. This statistic was then applied to the calculated Gross Floor Area of the site to estimate the population density of the superblock.	2	R <sup>y</sup>	Y length of the region in which the centre point for the building forms will be located	30.00m to 40.00m
3	N	Maximise the Secondary and Tertiary Road Networks	This objective is calculated by measuring the accumulated length of all of the secondary and tertiary networks generated between secondary entry points to the site (Figure 03)	3	P <sup>x</sup>	X coordinate of building from centre point	0.00 to 1.00
4	SG <sup>r</sup>	Maximise Solar Gain to Communal Podiums	The solar analysis conducted in the experiments utilise three primary vectors, representing the sun’s position in the morning, midday and afternoon. Each point on the podium’s surface is calculated to either receive 100%, 66%, 33% or 0% of sunlight.	4	P <sup>y</sup>	Y coordinate of building from centre point	0.00 to 1.00
				5	B <sup>1</sup>	Building width	20.00 to 30.00
				6	B <sup>2</sup>	Building depth	20.00 to 30.00
				7	H	Extruded height of buildings	0 to 40 storeys

4.2. SECONDARY SIMULATION

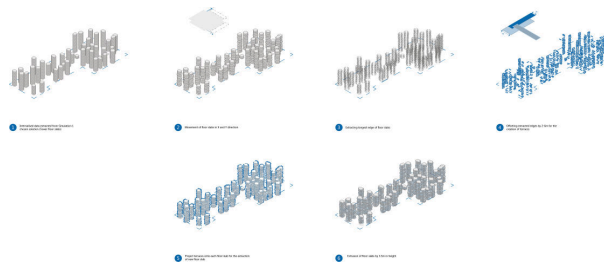


Figure 3. Construction of Secondary Parametric Definition.

4.2.1. Parametric Definition

This secondary simulation uses the extracted phenotype from the first simulation as the starting point (the selection process is described in the following sections). The tower floor plates from the selected outcome of the Primary Simulation are inputted as base phenotype for the secondary simulation. Each floor plate moves in the X and Y direction (Mx, My). While this process influences the outcomes for all objectives being optimised in this simulation (SGT, S and SGB) it has the most profound effect on (S) as the further the floor plate deviates from the original centre point of the building, the weaker or ‘less fit’ the solution becomes. This is countered by the requirement to optimise for (SGT) where the fitter solutions would have the most floor plate movement (Mx, My) contributing to



more extensive private terraces. The final stage of this simulation is the further offset of the building form to create the terraces (T). This gene has the most substantial impact on (SGT) as it significantly increases the area of the terraces, enabling greater solar gain to be achieved (Figure 05).

4.2.2. *Fitness Objectives and Genes*

Table 02 highlights the fitness objectives that the evolutionary simulation optimised for, as well as the variables (genes) modified by the evolutionary simulation which defined the superblock’s morphology.

Table 2. Fitness objectives and genes for the secondary simulation.

Fitness Objectives			
#	Abbreviation	Objective	Definition
1	SG <sup>T</sup>	Maximise Solar Gain to Private Terraces	The solar analysis conducted in the experiments utilise three primary vectors, representing the sun’s position in the morning, midday and afternoon. Each point on the podium’s surface is calculated to either receive 100%, 66%, 33% or 0% of sunlight.
2	S	Maximise Structural Integrity of Buildings	This objective optimises the centre of gravity of each tower by minimising the distance between the centre of each floor plate to the centre of the building’s bounding box.
3	SG <sup>B</sup>	Maximise Solar Gain to Building Facades	The solar analysis conducted in the experiments utilise three primary vectors, representing the sun’s position in the morning, midday and afternoon. Each point on the podium’s surface is calculated to either receive 100%, 66%, 33% or 0% of sunlight.

Genes			
#	Abbreviation	Definition	Domain
1	M <sup>X</sup>	Move floor plate in the X-Direction	-2.00m to 2.00m
2	M <sup>Y</sup>	Move floor plate in the Y-Direction	-2.00m to 2.00m
3	T	Terrace Depth	2.00m to 6.00m

4.2.3. *Algorithmic Setup*

The following settings (Table 03) have been applied within the *Wallacei* plugin for the *NSGA-2* evolutionary algorithm. The simulation was run on a consumer-grade PC, i7-8700 3.20GHz processor with 32.0 GB of RAM.

Table 3. Algorithm settings for both simulations.

Algorithm Settings	Simulation 1	Simulation 2
Generation Size	50	50
Generation Count	100	100
Population Size	5000	5000
Crossover Probability	0.9	0.9
Crossover Distribution Index	20	20
Mutation Distribution Index	20	20
Simulation Runtime	9hr 0min 40sec	7hr 10min 20sec

5. Experiment Results & Selection Process

5.1. PRIMARY SIMULATION

5.1.1. *Results*

Through reviewing the charts generated in *Wallacei* (Figure 04) it demonstrates that there are both successful and less successful aspects of this primary simulation. When analysing the Standard Deviation graph (SDG) in conjunction with the Standard Deviation Trendline (SDT), it illustrates that for the first three objectives (D, N, SGP), variation either stabilised or increased throughout the majority of the simulation’s runtime, however, convergence is observed across these three objectives in the final generations, indicating the algorithm localising towards an optima towards the end of the simulation.

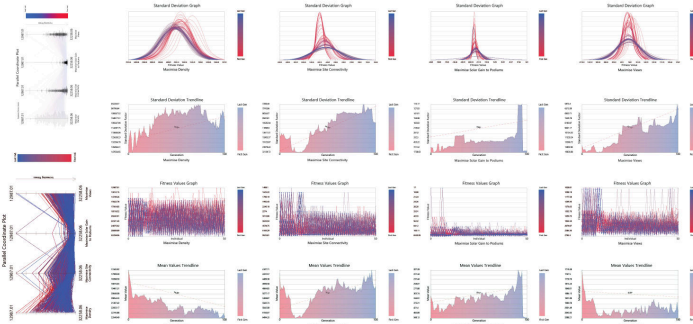


Figure 4. Primary Simulation Results (From top to bottom: Parallel Coordinate Plot, SDG, SDT, FVG and MVT).

Examining the Fitness Value Graph (FVG) concurrently with the Mean Values Trendline (MVT); an increase in fitness values indicates individual solutions that are fitter than previous generations. This pattern can be observed across objectives (V and D) where the MVT reflects fitter generations as the simulation progressed. However, with regard to objectives (N and SGP), and similar to the observations made in the SDT, the mean values across generations became less fit throughout the simulation, however, the mean value increased in fitness at the same stage where the variation across the generation began exhibiting signs of convergence. Through evaluating the outcomes of the charts, it indicates that the simulation optimised for some objectives better than others, while it seems that towards the end of the simulation’s run, the ‘weaker’ objectives exhibited better signs of convergence and fitness. This aspect of the design problem’s complexity highlights the applicability of EA’s, emphasizing that even through 5000 iterations of the design problem, there is observed a range of fit and less fit solutions. Most importantly, analysing the solution set across the entirety of the population is imperative as it exhibits patterns to the algorithmic run that are non-uniform throughout the simulation. Therefore, the process of selecting the fittest of these solutions then becomes imperative.

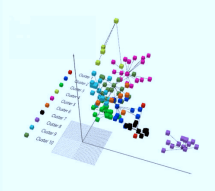
### 5.1.2. Selection Process

The selection process of the results from simulation 01 is fundamental to the success of the second simulation. Through the *Wallacei* plugin, a K-means clustering algorithm was applied to the Pareto front (the set of non-dominated or “optimal” solutions) of the population with a K-value of 10, in which the Pareto front was grouped into 10 clusters, and the centre of each cluster (i.e. the cluster’s best representative solution) was selected.

In order to determine which of the cluster centres was the fittest phenotype, a set of additional urban analytic criteria was conducted on each solution. The table below outlines the numerical urban data extracted from each phenotype (Table 04).

Table 4. Urban Analysis Table and K-means clustering of Pareto Solutions (Simulation 01).

		Cluster 1		Cluster 2		Cluster 3		Cluster 4		Cluster 5		Cluster 6		Cluster 7		Cluster 8		Cluster 9		Cluster 10	
		Gen. 45/Ind. 6	Gen. 51/Ind. 10	Gen. 57/Ind. 15	Gen. 63/Ind. 20	Gen. 69/Ind. 25	Gen. 75/Ind. 30	Gen. 81/Ind. 35	Gen. 87/Ind. 40	Gen. 93/Ind. 45	Gen. 99/Ind. 50	Gen. 105/Ind. 55	Gen. 111/Ind. 60	Gen. 117/Ind. 65	Gen. 123/Ind. 70	Gen. 129/Ind. 75	Gen. 135/Ind. 80	Gen. 141/Ind. 85	Gen. 147/Ind. 90	Gen. 153/Ind. 95	Gen. 159/Ind. 100
Solar Gain (Pushed)	Min (%)	10.0	10.0	10.0	10.0	10.0	10.0	10.0	10.0	10.0	10.0	10.0	10.0	10.0	10.0	10.0	10.0	10.0	10.0	10.0	10.0
	Max (%)	17.1	14.6	23.8	24	21.7	23.6	18.9	18.9	20.7	20.7	20.7	20.7	20.7	20.7	20.7	20.7	20.7	20.7	20.7	20.7
	Avg (%)	15.1	10.6	16.8	16.8	16.8	16.8	16.8	16.8	16.8	16.8	16.8	16.8	16.8	16.8	16.8	16.8	16.8	16.8	16.8	16.8
Solar Gain (Tweaked)	Min (%)	7.8	8.5	7.1	6.2	7.8	8.1	8.2	8	7.3	10	10	10	10	10	10	10	10	10	10	10
	Max (%)	18.4	17.6	18.4	20.4	18.4	21.5	18.7	21.6	19.5	23.2	23.2	23.2	23.2	23.2	23.2	23.2	23.2	23.2	23.2	23.2
	Avg (%)	17	16.8	20.2	20.8	19.4	20.5	20.9	21.8	19.4	21.7	21.7	21.7	21.7	21.7	21.7	21.7	21.7	21.7	21.7	21.7
Density and Programme	Residential (sqft)	176,463	102,212	738,885	762,728	680,890	664,144	611,391	111,794	714,847	413,717	413,717	413,717	413,717	413,717	413,717	413,717	413,717	413,717	413,717	413,717
	Commercial (sqft)	190,450	190,150	120,802	207,287	134,026	165,557	159,452	140,207	140,207	140,207	140,207	140,207	140,207	140,207	140,207	140,207	140,207	140,207	140,207	140,207
	Total (sqft)	366,913	292,362	859,687	970,015	814,916	829,699	770,843	252,001	855,054	553,924	553,924	553,924	553,924	553,924	553,924	553,924	553,924	553,924	553,924	553,924
Access to Views	Area (sqft)	9.2	10.6	9.6	8.5	10.6	9.9	9.9	9.7	9.7	10.6	10.6	10.6	10.6	10.6	10.6	10.6	10.6	10.6	10.6	10.6
	2-D POE	22.8	23.2	24.8	19.5	23.9	24.6	24.6	24.1	24.6	23.9	23.9	23.9	23.9	23.9	23.9	23.9	23.9	23.9	23.9	23.9
	3-D POE	48	46.4	46.4	75	65.2	65.2	65.2	65.2	65.2	65.2	65.2	65.2	65.2	65.2	65.2	65.2	65.2	65.2	65.2	65.2
Road Network Connectivity	No. Connections	149	190	300	300	118	112	420	300	248	340	340	340	340	340	340	340	340	340	340	340
	%																				



The selection process inherently has an aspect of subjectivity to it. The urban analysis conducted was ranked from one - six. This was applied as a tool to assist in determining which solution was to carry through to the second simulation. The selected solution (Gen. 95 Ind 38) was only the fittest for the Road Network Connectivity, however, it still showed strong results across the other analysis criteria. When reviewing the analysis, it was decided that a solution was not to be selected if it was severely detrimental to other analysis criteria. For this reasoning, Cluster 10 (Gen. 96 Ind. 19) was excluded from consideration, while it performed well for the Solar Access and access to view, it was at a severe cost to the density.

5.2. SECONDARY SIMULATION

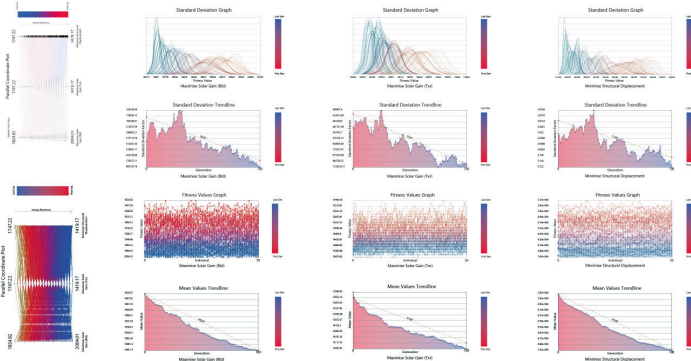


Figure 5. Secondary Simulation Results (From top to bottom: Parallel Coordinate Plot, SDG, SDT, FVG and MVT).

5.2.1. Results

Through reviewing the charts generated in *Wallacei* (Figure 05) it demonstrates that this secondary simulation was more successful than the primary simulation. This is due to the reduced complexity of the design problem being addressed within this simulation. Reviewing the (SDG) alongside the (SDT) clearly illustrates convergence across all objectives. The fitness values significantly increased throughout the course of the simulation, whilst simultaneously reducing variation in comparison to the earlier generations. The (FVG) and (MDT) charts also

re-iterate the above statements, reflecting a significant improvement of the fitness values as the simulation progressed.

5.2.2. Selection Process

The selection process for this simulation required a different approach than the first. There were only eight Pareto front solutions across the entire population set, each being located in the final generation. Instead of clustering the Pareto front, each of the Pareto solutions was extracted. Having all Pareto solutions located in the final generation is a further indication of convergence, also suggesting that there is very little variation between each of these solutions. When prioritising the objectives, weighting was applied to the size of the private terraces as it was the main objective for this simulation. Gen.99 Ind. 5 was selected as the fittest solution from the population set, as it had the largest m<sup>2</sup> of terraces. The terrace solar gain was comparable to Pareto Solution 3 which had the fittest values for that criteria. Similarly, with the building solar gain values, they were extremely close to the fittest values of Pareto Solution 4 (Table 05).

Table 5. Urban Analysis Table and Wallacei Objective Space(Simulation 02) .

		Pareto Solution 1		Pareto Solution 2		Pareto Solution 3		Pareto Solution 4		Pareto Solution 5		Pareto Solution 6		Pareto Solution 8	
		Gen. 99 Ind. 5	Gen. 99 Ind. 1	Gen. 99 Ind. 2	Gen. 99 Ind. 3	Gen. 99 Ind. 4	Gen. 99 Ind. 5	Gen. 99 Ind. 6	Gen. 99 Ind. 7	Gen. 99 Ind. 8	Gen. 99 Ind. 9	Gen. 99 Ind. 10	Gen. 99 Ind. 11	Gen. 99 Ind. 12	
Solar Gain (Building)	100%	7.36	7.36	7.14	7.55	7.53	7.51	7.53	7.34						
	66%	9.33	9.40	9.30	9.46	9.39	9.45	9.41	9.37						
	33%	20.66	20.56	20.64	20.53	20.70	20.59	20.80	20.63						
Solar Gain (Terraces)	100%	18.47	20.23	19.01	18.47	18.99	19.00	18.42	18.84						
	66%	30.84	30.31	31.33	31.24	29.72	30.65	30.69	30.46						
	33%	25.90	23.12	24.74	24.82	25.41	25.30	25.17	26.00						
Terraces	100%	23.5	24.34	24.72	24.37	25.88	25.16	25.48	26.7						
	Terrace (m <sup>2</sup> )	71,050	71,000	71,000	72,128	71,004	72,160	70,792	73,874						
	% of Floor Area	10.38	10.33	10.37	10.40	10.37	10.40	10.35	10.36						
Structural Displacement	Total Movement of Floor Plates (m)	1439.16	1432.76	1428.28	1423.83	1419.59	1422.00	1421.43	1419.72						

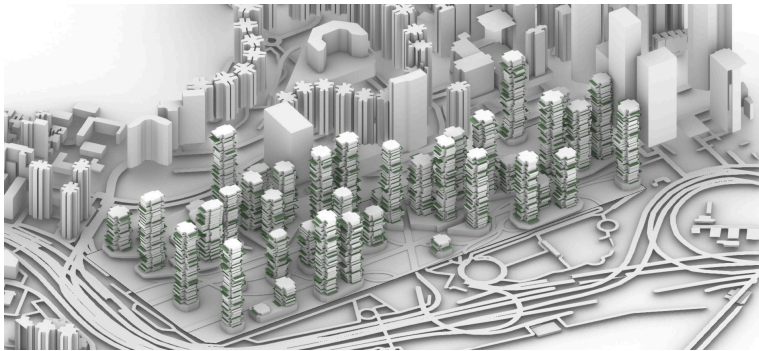


Figure 6. Selected Solution from Simulation 02 (Gen. 99 Ind. 5).

6. Conclusion and Discussion

In the experiments presented, the Taikoo Shing Superblock in Hong Kong was utilised as a case study to address demographic and environmental contextual stresses impacting the urban fabric. By no means is the evolved solution above

proposed as a replacement of the existing Taikoo Shing superblock; rather, it puts forward an alternative approach to designing a superblock that incorporates within it a greater degree of variation amongst the urban tissue, thus allowing for greater resilience towards contextual stresses. Therefore, and in the context of Hong Kong's growing population, adopting an approach of urban development that aims to optimise for multiple criteria (perhaps with preference of some criteria over others), serves as a more robust alternative to the conventional, top-down approach of the arrayed distribution of the same block across a given district.

Through the identification of multiple hierarchies of scale, it allowed for the definition and application of sequential evolutionary simulations as a method to better and more efficiently optimise for the design problem; and although the secondary simulation produced better results than the primary simulation, in applying sequential simulations, it highlighted the significance of selection and the analytic methods and reasoning associated with it. Additionally, It is imperative to note that the success rate of running multi-objective evolutionary algorithms is highly dependent on running multiple iterations of the same simulation, in which the design problem is continuously reformulated in order to achieve better results. Where the design problem of the above experiments has been reformulated multiple times, there remains the opportunity to further refine the design problem - specifically for the primary simulation

## References

- Alexander, C.: 1964, *A City is Not a Tree*, *no title given*.
- Batty, M.: 2013, *The New Science of Cities*, *The MIT Press*.
- Chang, Y.: Unknown, "NSGA-II algorithm flowchart" . Available from <[https://www.researchgate.net/figure/NSGA-II-algorithm-flowchart\\_fig2\\_283129353](https://www.researchgate.net/figure/NSGA-II-algorithm-flowchart_fig2_283129353)> (accessed 20th October 2019).
- Deb, K., Agrawal, S., Pratap, A. and Meyarivan, T.: 2000, A Fast Elitist Non-Dominated Sorting Genetic Algorithm for Multi-Objective Optimization: NSGA-II, *International Conference on Parallel Problem Solving From Nature.*, Springer, Paris, France, 849–858.
- Census and Statistics Department, initials missing: 2011, "2011 Population Census - Fact Sheet for Taikoo Shing in Eastern District Council District 2011" . Available from Census and Statistics Department<[https://www.census2011.gov.hk/pdf/fact\\_sheets/estates/C\\_61716e.pdf](https://www.census2011.gov.hk/pdf/fact_sheets/estates/C_61716e.pdf)> (accessed 1st December 2019).
- Census and Statistics Department, initials missing: 2017, "Hong Kong Population Projections 2017-2066 2017" . Available from Census and Statistics Department<<https://www.statistics.gov.hk/pub/B1120015072017XXXXB0100.pdf>> (accessed 4th December 2019).
- Makki, M., Showkatbakhsh, M. and Song, Y.: 2018, "Wallacei: An evolutionary and Analytic Engine for Grasshopper 3D" . Available from <<https://www.wallacei.com/>> (accessed 30th July 2019).
- Makki, M., Showkatbakhsh, M., Tabony, A. and Weinstock, M.: 2018, Evolutionary Algorithms for Generating Urban Morphology: Variations and Multiple Objectives, *Int. J. Archit. Comput.*, **0**, 1–31.
- Marshall, M.: 2008, *Cities Design & Evolution*, Routledge, London.
- Maryanti, M.R., Khadijah, H., Muhammad Uzair, A. and Megat Mohd Ghazali, M.A.R.: 2016, The urban green space provision using the standards approach: issues and challenges of its implementation in Malaysia, *WIT Transactions on Ecology and The Environment*, **210**, 369-379.
- Weinstock, M.: 2010, Emergence and the Forms of Cities, *Archit. Des.*, **80**, 118–121.

# AN INFORMED METHOD - VISUALIZATION FOR MULTI-OBJECTIVE OPTIMIZATION IN CONCEPTUAL DESIGN PHASE

ZHU SHUYAN<sup>1</sup> and MA CHENLONG<sup>2</sup>

<sup>1,2</sup>*School of Architecture, South China University of Technology; State Key Laboratory of Subtropical Building Science*

<sup>1,2</sup>{arzsylma.chenlong}@mail.scut.edu.cn

**Abstract.** The relationship of different performance objects may be very complicated that designers can't guarantee the improvement of one object don't affect the others. Multi-objective optimization algorithms provide Pareto optimal design solutions, but because of the nonlinearity introduced by the objective functions, the relationships in the objective space do not extend to the decision variable space and vice versa. Based on the design of building blocks and west facade in a practical project, the paper put forward a visualized method for optimization process of building performance, and combine the multi-objective optimization algorithm with the visualization of fitness landscape, so that architects can easily obtain the knowledge of complex relationships between building performance and building parameters. It is more conducive to obtain a design scheme which can balance the requirements of appearance and performance at the same time, and achieve the ultimate goal of improving the efficiency of design.

**Keywords.** Visualization; Multi-objective optimization; Fitness landscape.

## 1. Introduction

Building energy consumption has always accounted for a larger proportion of the world's continuously increasing energy consumption. At present building energy consumption even exceeds 33% of the total in China, simultaneously office buildings account for a large proportion. Therefore, the energy demand has become an important consideration during the whole design phase, but the inconvenience of using professional energy simulation tools has hindered the architects' intuitive consideration of building energy consumption in the early design stage of their project, which also has affected the optimization of building energy consumption.

In recent years, various plug-ins have been developed based on the Grasshopper platform in Rhinoceros, supporting architects to easily integrate building designs with various professional performance simulation software such as EnergyPlus, Radiance, Openfoam, etc. A variety of optimization plug-ins such as Galapagos, Octopus, Opossum make it possible for architects

to optimize building performance in the early design stages. Scholars such as Christoph Waibel, Kristoffer Negendahl, Kavan Javanroodi and others have used grasshopper in their related studies for buildings' performance optimization.

In most cases during conceptual design stage, a complex building performance optimization can be decomposed into several sub-tasks in which the number of performance target is small and there are only 2D or 3D variables. This low-dimensional data can directly be visualized by the use of 3D surface diagram or 3D point cloud diagram, at the same time, this visualization method can maximize the readability of the relationship between the data. We apply this method in the design process of a practical project and want to show a new design approach for architects.

## 2. Background

Table 1. The specific indicators of the office building.

	HEIGHT	TOTAL AREA	UPPER FLOORS
OFFICE AND CONFERENCE	24m<h<45m	58000	4-6

The project is the headquarter building of an big company, located in Shandong province, which belongs to the cold region of China. In urban design phase, the basic shape of building in the site has been specified. The building has four strip-type blocks arranged in parallel from east to west, which are connected by a north-south block to form a large office complex. The first and second floors include public service functions, and the upper floors are all for office and conference functions, the specific parameters are shown in Table 1. We attempt to make an optimization of the initial investment and later operational energy consumption of the building early from the concept design process. This complex optimization problem can be broken into several secondary optimization issues, including building volume settings and glass curtain wall optimization. At the same time, we need to notice that the main goal of the design practice is not to find out the ultimate performance optimization in every level, but to enable the architects using the tool which can help them intuitively understand the impact of current morphological operations on building performance, in addition, they can optimize the performance indicators of building as much as possible while guaranteeing its facade's artistic qualities.

## 3. Framework

### 3.1. SAMPLING

Based on grasshopper platform, a parameter space sampling is made. Compared with random sampling or grid sampling, Latin hyper-cube sampling (LHS) can ensure that the structure of the samples is similar to the overall structure. We use sampler tool of design-space-exploration tool set for sampling operation, in order to give full use of the CPU performance, IDF files are generated in batch

mode using Honeybee linking with EnergyPlus. Then the files are fed into Honeybee's batch energy calculation tool for parallel calculation, obtaining the target performance of each parameter combination.

### 3.2. GRASSHOPPER TO MATLAB

With the help of GH\_CPython, a data exchange interface is built. Sample data is sent to MATLAB through MATLAB API, meanwhile other input parameters can be set to determine which metamodel algorithm will be used for the fitting operations of subsequent data.

### 3.3. METAMODEL GENERATION AND VISUALIZATION

According to the parameters of the interface program, architects can decide which algorithm is used for generating the metamodel, so that they can choose ANN, RBF, Random Forest, Kriging, MARS and SVM modules. Besides, an automated framework is designed to filter out best metamodel with high  $R^2$  value. Taking ANN as an example, the candidate network structure is a single hidden layer neural network with 6-20 neurons or a double hidden layer neural network with 2-4 second hidden layers. First, different network structures are trained, then through the evaluation of new test data, a neural network that meets the maximum  $R^2$  value can be chosen as the best metamodel to predict a certain performance index. (Figure 1)

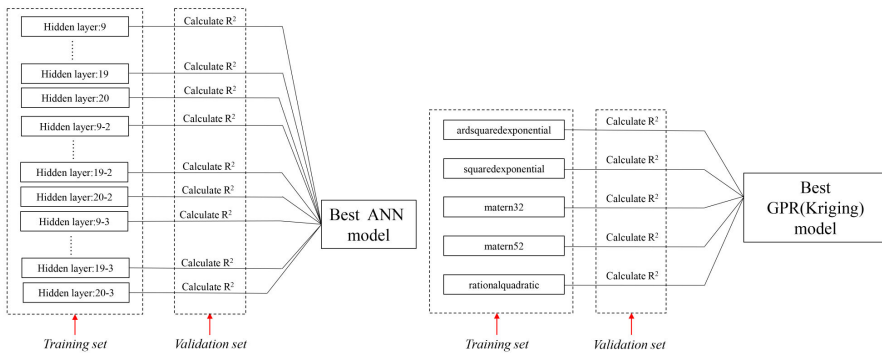


Figure 1. Automated optimal metamodel selection (left: ANN model, right: Kriging model).

A metamodel is used to perform grid sampling on decision variable space to obtain a function surface or three-dimensional point cloud that visualize the relationships of design parameters and building performance. The Z-axis value or the color of the sampling point represents the performance index (depends on whether the number of parameters is two or three). Multiple performance indicators are juxtaposed, and the viewing angles are synchronized, so that architects can accurately grasp the changing trend of each performance with different design parameters. (Figure 2)



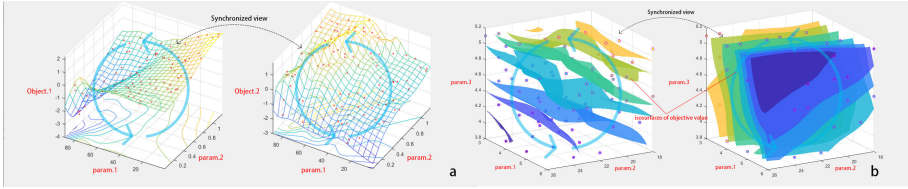


Figure 2. (a) Two-dimensional fitness landscape juxtaposition. (b) Three-dimensional fitness landscape juxtaposition.

### 3.4. DATA FEEDBACK INTERFACE

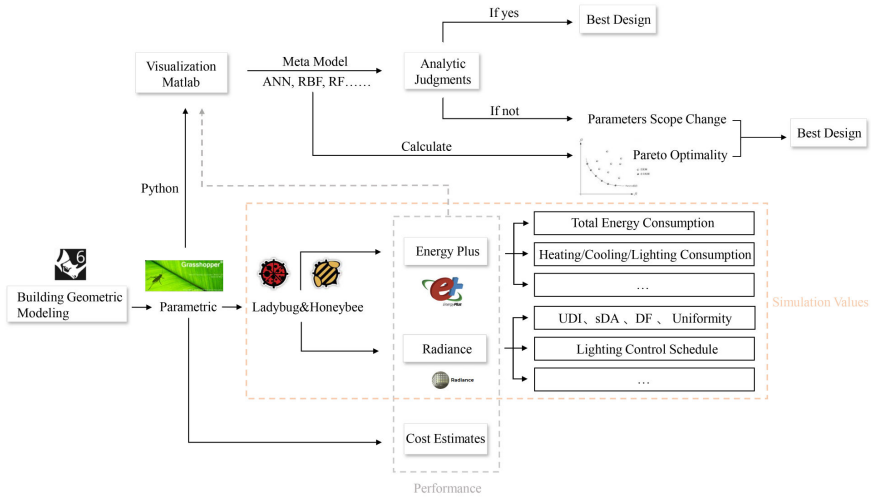


Figure 3. An overall framework based on parametric platform in design process.

Also, through customized GH\_CPython components, designers can input new design parameters to feed to the metamodel in MATLAB, and quickly get the predicted performance indicators in real time. How the interface is used depends on whether the designer can directly select test points based on the visualization results of the previous step. If the designer hopes to select only a more satisfactory value range based on the previous step and intends to perform multi-objective optimization on this basis, he can directly link this interface to an optimizer such as Octopus. The method successfully avoids the slower sampling process of the first step and can help quickly obtain approximate results of performance values. The approximate results are sufficient to meet the accuracy requirements of the conceptual design.

The framework shown in Figure 3 summarizes the whole process.

## 4. Case studies

### 4.1. VISUALIZATION OF ARCHITECTURAL FORM AND PERFORMANCE

From the perspective of the concept design, it's worth detailed study how the height and depth of the four east-west blocks influence the changes in the overall performance of the building. According to the national regulation, in order to reduce heating energy consumption as much as possible, buildings in northern cold regions should reduce the shape coefficient. How can this established regulation be reflected in specific building mass design? From the perspective of architects, intuitively, the depth of the building should be increased and the height of the building should be reduced to minimize the external surface area of the building, but it's not clear how much the changes of different parameter can impact the energy consumption. Considering that the northern buildings need more direct sunlight in winter, there should be enough distance between them. Meanwhile, it's also not certain whether the demand is contradictory to energy consumption or not. All these questions should be answered from building simulation analysis during the project design process.

#### 4.1.1. Design Task - One

The total area of each east-west block is set to 7,500 square meters, and there are three variables- the number of floors, building depth and building height . On this basis, the more the number of floors, the smaller the area of each floor, and the length of the building will be shortened with the same depth. Secondly, when all other things being equal, the higher the floor's height is, the more energy correspondingly increased. However. if considering the entire building mass, a higher height will also increase the total area of shadows between the building masses, potentially affecting the lighting effect. (Figure 4)

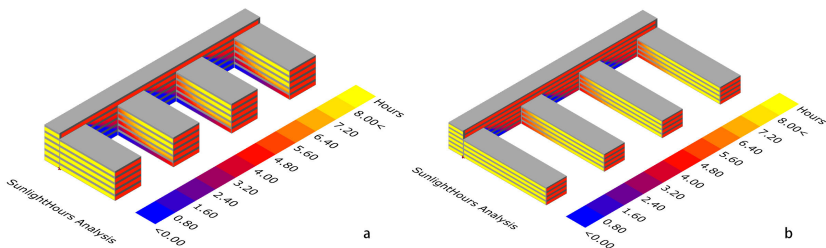


Figure 4. (a) 26m, 5 floors, 5.1 m/floor. (b) 21m, 4 floors, 3.9 m/floor. ( The first and second floors are not included in the analysis diagram. ) .

#### 4.1.2. Results Visualization

One hundred sampling points of the three parameters are simulated, the visualization results in MATLAB is shown below in Figure 5.

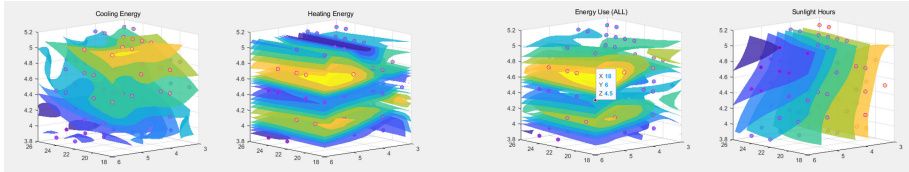


Figure 5. A series of three-dimensional point cloud diagrams.

From the visualization, it can be intuitively seen that the cooling energy consumption gradually increases with the increase of the building height and the decrease of the building depth, but has a weak correlation with the number of building layers. The relationship between heating energy consumption and other parameters is more complex. It is the largest when the height of the building is 4.8m or 4.2m, with the number of floors is 6, however the correlation with the building depth is weak; the trend of total energy consumption is the superimposed effect of the two; sunshine duration is negatively correlated with all the design variables.

The model construction and calculation have taken two hours in total. The performance visualization is simple, but instructive for the design process. After combining the above performance analysis results and building modeling requirements, our team finally choose a layer height of 4.5m, 6 floors and a depth of 18m to be the control parameters for further design.

## 4.2. PARAMETER OPTIMIZATION OF CURTAIN WALL ON WEST FACADE

### 4.2.1. Design Task - Two

During the design phase, part of the focus is the design of the west facade as the main facade. The final design is shown in the following Figure 6. It is hoped that the simple and repetitive facade elements can be used to create a whole building image. From the perspective of sun-shade, the west facade of the building is generally designed as a solid wall. Since the west facade of the project is directly facing the urban main road and represents the images of the headquarters, therefore, a zigzag glass curtain wall system is set up. The light getting in can meet the requirements of the internal office function while the office spaces are being protected from too strong sunlight by self-shielding. The inclination angle and extension distance of the zigzag glass curtain wall also affect the building skin investment cost, indoor lighting effect, cooling and heating energy consumption. However, architects do not have an intuitive impression of how each performance changes under different parameter combinations.

In consideration of limitations of the simulation time, the window units between the two column spans were selected for parameterization. Thereby the size and rotation angle of the window units were variables. The visualization performances are the material investment cost,  $UDI_{100\ 2000/60}$  value, cooling and heating energy consumption.

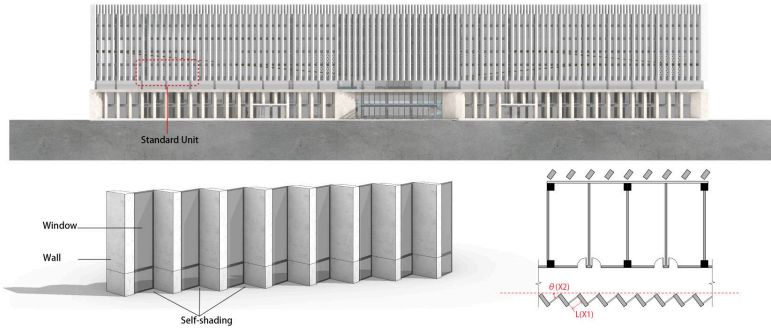


Figure 6. Standard unit of zigzag glass curtain-wall and analysis diagrams.

#### 4.2.2. Visualization Results

The rotation Angle ranges from -90 to 90 degrees, 100 combination samplings have been made, the batch simulation has taken 2 hours, and 4 juxtaposed visualization results are obtained. The results are shown as follows:

- Material Cost:

The general trend is that as the rotation angle approaches zero and the window length decreases, the cost gradually decreases. A curved surface with a V-shaped depression in the middle is formed, axial symmetry, and the lowest value may achieve when the window length is zero.

- $UDI_{100-2000/60}$  Value:

To consider multiple analysis points,  $UDI_{100-2000/60}$  is defined as the percentage of floor area (represented by the percent of analysis points) that receives the “useful” illuminances (i.e.100-2000 Lux) for at least a specified percentage of occupied hours. Nabil and Mardajevic proposed that the effective illuminance value range should be determined between 100-2000Lux. The percentage of occupied hours is initially set to 60% in this case.

The result shows that  $UDI_{100-2000/60}$  value decreases with the increase of the overhang distance, and a larger rotation angle implies more chance getting higher value; The fitness landscape forms a conical depression around point(0, 2.1), this is because the approximately flat wall and the wider window let excessive amount of beam light in; when the window size turns below 0.4m, the  $UDI_{100-2000/60}$  value sharply decreases as the inner space gets insufficient daylight.

- Energy Consumption:

It includes cooling and heating energy consumption; the cooling energy consumption decreases monotonically with the decrease of the window size and the rotate angle’s deviation value from around 10 degree, forming a convex surface; the fitness landscape of heating energy consumption turns to be complex, the value goes very high around the upper left corner, and in the mid-right place

around point(30,0.6) the landscape forms a shallow depression area.

Considering the optimization of the four target parameters, the less energy consumption, material cost and the more UDI is preferred. From the visualization, architects can get an overall understanding of the changing tendency with the change of parameters. One can easily get a knowledge that the window length should be short; The rotation value should better be around 30 degrees to obtain a better heating energy consumption while not affect the  $UDI_{100-2000/60}$  value and material cost so much. Based on the above analysis, combined with the corresponding appearance of the zigzag curtain wall, an angle of 30 degrees and the width of 0.7m are chosen as the final design parameters. Figure 7 below shows the final results for the four objectives.

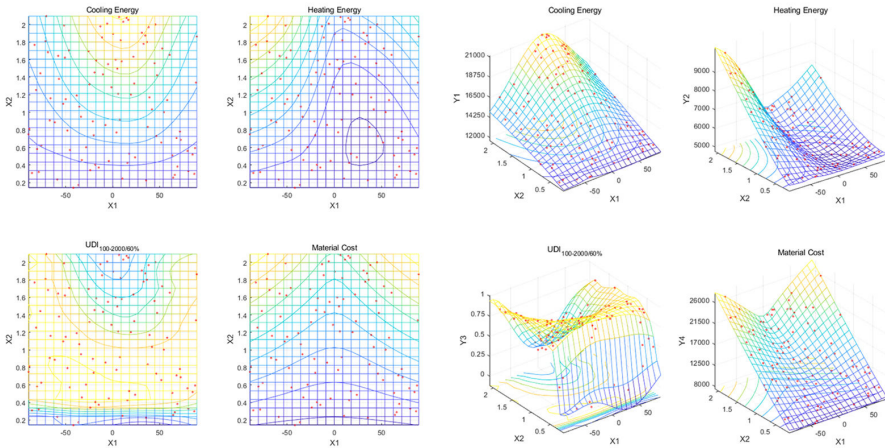


Figure 7. Visualization for the four objectives. (a: plan view, b: 3D view).

### 4.3. COMPARATIVE ANALYSIS

#### 4.3.1. Comparison with multi-objective optimization algorithm

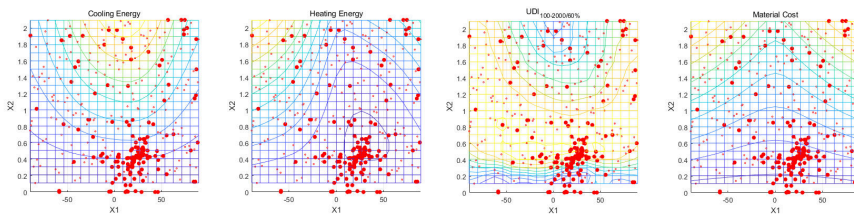


Figure 8. The sampling of a multi-objective optimization algorithm.

Constructing a multi-objective optimization algorithm for the second issue, and result of sampling which is visualized on the fitness landscape in Figure 8. Finally, the parameter combinations corresponding to the pareto front is close to the above

chosen area. But to achieve these points, many physical simulations must be done, which will take a long time. The crucial limitation is that the optimization method can't help architects to gain a holistic understanding of the design space. Since in the last generation and on the pareto front, most of the samples are in a small range compared with the whole design space.

4.3.2. Comparison with parallel plot

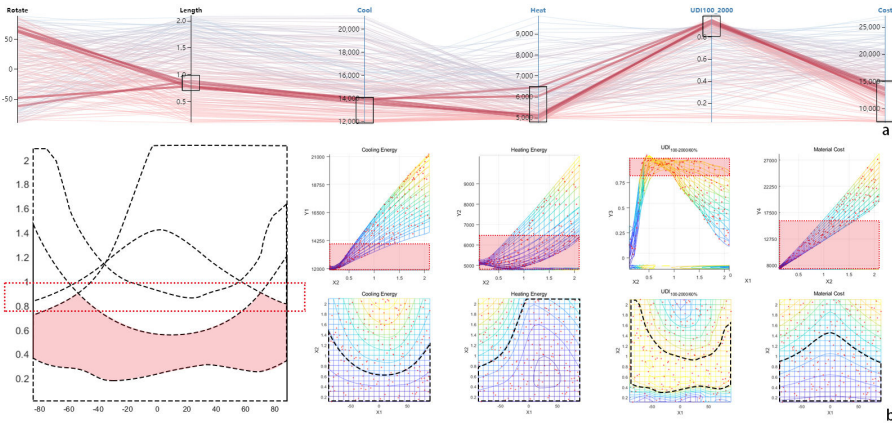


Figure 9. Comparison between (a) the parallel plot with (b) the three-dimensional surface plot

In normal conditions, with use of Design Explorer, through the Parallel plot designers can intuitively filter out better instances from a big number of samples. The performance of the scheme can be visualized and screened effectively even if the parameter space exceeds three (Figure 9-a). However, this method is a sparse sampling of the parameter space, which requires a very dense sampling data, otherwise, the potential optimal parameter combination is ignored. Also, the selection of parameter intervals is a tentative behavior, and it is not easy to know in which range there are matching parameters and whether a new unsampled parameter combination are more suitable or not.

In comparison, our research supplements the display of the parallel plot by including both the parameter range and the changing trend. The three-dimensional surface plot expresses the four different performances of the same combination of parameters, allowing designers to capture multiple performance trends at the same time (Figure 9-b). The juxtaposed display of the 3D surface plot can enable the designer to directly observe the undulating shape of the performance surface in the parameter space, and directly select the optimal parameter area based on this. Moreover, the range presented by the 3D surface plot is continuous and complete, and the changing trend of extreme values is expressed by the appearance of slopes and valleys, and there will be no omission of optimal values.

## 5. Conclusion

As part of the task to explore the correlation between architectural form and performance, the paper presented a methodology and a visualization platform to obtain and evaluate the impact of different design parameters and performance indicators on building form, focusing on the initial phase of architectural design.

Due to the new possibilities offered by Ladybug Honeybee and other simulation tools, various design performance of the building can be systematically evaluated, including daylight, energy demand and cost estimates, etc. However, the need for multi-target performance optimization in architectural design requires researchers to explore easier ways to achieve visual translation of performance parameters and better integrate into architectural design processes. This paper realizes the visualization of several building performance indicators by building a metamodel, so as to get the best solution quickly and effectively under multi-objective conditions. This method is then applied to two design tasks, one is to optimize the overall size of the building, the other is to optimize the shape of the zigzag curtain wall unit of the west facade. Further confirming the ease of use of this method, it is helpful for the architect to quickly capture the complex relationships between design parameters and multiple performance.

At present, the platform does not focus on obtaining accurate performance values, but rather provides architects with a powerful visualization tool to make them more confident in considering the key factors of building performance, and gain full control over what is beneficial to the operation of the building after completion. As the green building evaluation rules become more stringent, it is becoming more important to consider the key factors affecting building performance from the very beginning. Through the use of this new method, it is more convenient to design energy-saving and environmentally friendly buildings.

## References

- Christoph, W., Ralph, E. and Jan, C.: 2019, Co-simulation and optimization of building geometry and multi-energy systems: Interdependencies in energy supply, energy demand and solar potentials, *Applied Energy*, **242**, 1661-1682.
- Javanroodi, K., M.Nik, V. and Mahdavinejad, M.: 2019, A novel design-based optimization framework for enhancing the energy efficiency of high-rise office buildings in urban areas, *Sustainable Cities and Society*, **49**, 101597.
- Jonathan, N., Or, A. and Thomas, A.: 2019, A parametric approach to optimizing urban form, energy balance and environmental quality: The case of Mediterranean districts, *Applied Energy*, **254**(113637), 1-17.
- Nabil, A. and Mardaljevic, J.: 2005, Useful daylight illuminance: a new paradigm for assessing daylight in buildings, *Lighting Research and Technology*, **37**(1), 41-57.
- Nathan, B. and Caitlin, M.: 2017, Designing with Data: Moving Beyond the Design Space Catalog, *ACADIA*.
- Negendahl, K. and Rammer Nielsen, T.: 2015, Building energy optimization in the early design stages: A simplified method, *Energy and Buildings*, **105**, 88-99.
- Westermann, P. and Evins, R.: 2019, Surrogate modelling for sustainable building design - a review Energy Building, *Energy and Buildings*, **198**, 170-186.
- Yehsiang, H. and Borong, L.: 2015, Functional Relationship Between Lighting Energy Consumption and the Main Parameters for Double Atrium Offices, *Procedia Engineering*, **121**, 1869-1879.

# FROM GEOMETRICALLY TO ALGEBRAICALLY DESCRIBED HYPERBOLIC PARABOLOIDS

*An optimisation-based analysis of the Philips Pavilion*

THOMAS FISCHER<sup>1</sup> and THOMAS WORTMANN<sup>2</sup>  
<sup>1,2</sup>*Xi'an Jiaotong-Liverpool University, Suzhou, China*  
<sup>1,2</sup>*{thomas.fischer|thomas.wortmann}@xjtlu.edu.cn*

**Abstract.** In this paper, we present a procedure to derive algebraic parameters from geometrically described truncated hyperbolic paraboloid surfaces. The procedure uses parametric modelling and optimisation to converge on close algebraic approximations of hyperbolic paraboloid geometry through a successive breakdown of vast search spaces. We illustrate this procedure with its application to the surfaces of the 1958 Philips Pavilion designed by Le Corbusier and Iannis Xenakis. This application yielded previously unavailable parametric data of this building in algebraic form. It highlights the power of the parametric design and optimisation toolkit, both in terms of automated search and epistemological enablement.

**Keywords.** Parametric analysis; optimisation; ruled surfaces; hyperbolic paraboloid; geometry reconstruction.

## 1. Background

The Philips Pavilion designed by Le Corbusier and Iannis Xenakis for the 1958 Brussels World's Fair (Expo 58) stands out as an iconic early example of advanced, non-standard architecture based on doubly-ruled-surfaces (Treib, 1996). Despite having been realised without the aid of digital design tools, it prefigured recent computer-aided design and production strategies. Le Corbusier and Xenakis composed the pavilion as an arrangement of nine double-curved surfaces, which, for fabrication, construction, structural as well as aesthetic purposes, they rationalised as hyperbolic paraboloids, tessellated along straight ruling lines (Fischer, 2012, pp. 32–37). As illustrated in Figure 1, the hyperbolic paraboloid (or “hypar”) is a mathematically defined, double-curved surface resembling the “saddle” shape of a potato chip. Algebraically, the hyperbolic paraboloid is defined by Equation 1 (Vreedenburgh, 1958/59, p. 9).

$$z = \frac{y^2}{b^2} - \frac{x^2}{a^2} \quad (1)$$

As defined by Equation 1, hyperbolic paraboloids take up a standard orientation with their centroids located at the point of origin, and extend *ad infinitum*. In architectural applications, by contrast, hyperbolic paraboloid surfaces are subject



to geometric translations with regard to their spatial location and orientation and require the truncation of the surface areas of interest. The hyperbolic paraboloid owes its name to its property of intersecting with vertical planes along parabolas (shown second from the left in Figure 1) while intersecting with horizontal planes along hyperbolas (shown second from the right in Figure 1). It can be constructed from two parabolas (whose curvatures are defined by the parameters  $a$  and  $b$  in Equation 1), with one parabola translated along the other at a right angle, as shown in the second illustration from the left in Figure 1. Alternatively, it can be constructed as a grid of straight ruling lines between four corner vertices, as shown on the right in Figure 1 (see also Pottmann et al. 2007, p. 319). Consequently, albeit somewhat counterintuitively, the hyperbolic paraboloid is both doubly curved and doubly ruled.

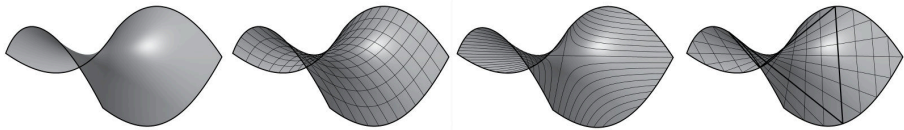


Figure 1. Hyperbolic paraboloid: surface, parabolas, hyperbolas, and ruling lines.

This rare geometric property is shared by the hyperboloid of one sheet and earned both surfaces a special status in the context of architectural design, as they afford the articulation of expressive, yet mathematically unambiguous forms that can be fabricated and assembled along straight guiding lines. The hyperbolic paraboloid shape arises naturally in tensile membranes and, if executed as a structural shell, performs well under compressive loads. Besides Xenakis and Le Corbusier, these architectural characteristics have also been harnessed prominently by Félix Candela and Antoni Gaudí (Sprague, 2013; Fischer et al., 2003). The affinity between the hyperbolic paraboloid and computer-aided and parametric architectural design has been examined extensively by Mark Burry (2002; 2005) and Jane Burry (2011a). Pertinent to the work presented here, Mark Burry (2011b, p. 115) applied local (*simplex* and *hill climbing*) optimisation algorithms to the parametric fitting of hyperboloids in the geometric reconstruction of Gaudí's *Sagrada Família* temple.

Xenakis's and Le Corbusier's design of the Philips Pavilion was based on a set of truncated hyperbolic paraboloid surfaces circumscribed by either straight – or at floor level curved – lines between 13 key points. The straight lines coincided with the centre lines of the pavilion's structural “ribs”. The left of Table 1 shows the coordinates of the 13 key points, based on a drawing by Xenakis (1958/59, p. 6, Figure 18). While this source drawing provides some elevation coordinates explicitly, we had to extract most of the point coordinates visually. The right of Table 1 relates the 13 key points to the surfaces of the pavilion. (To disambiguate the relationship of the surface labelled E by Xenakis to a structural rib that divides it, we describe the two divided surfaces separately as surfaces E and E\*.)

Xenakis rationalised the Philips Pavilion by tessellating its truncated hyperbolic paraboloid surfaces along suitably spaced ruling lines (Fischer, 2012,

pp. 33–34). Entrusted with the “mathematical translation” of Le Corbusier’s sketches (Capanna, 2015, p. 36), Xenakis (2008, p. 115) saw three potential methods to study and draw the form of the pavilion, which he referred to later as algebraic, geometric and experimental. He chose a combination of the latter two. Specifically, Xenakis (2008, p. 115) preferred geometric approximation over algebraic description due to its lower and visually controllable margin of error and its “evocative” quality. Xenakis (1958/59, p. 4, Footnote 2) commented on the algebraic option: “It is clear that it would hardly be convenient to define the hyper surfaces in terms of the numerical values of the coefficients in the appropriate equation of the surface.” Later, Xenakis (2008, p. 115) elaborated: “It is unthinkable to work with combinations of such forms with totally abstract algebraic functions. In a study like this, the subtleties of the curves and their dynamism can never be imagined through equations. This pavilion had to be pre-eminently successful on a plastic level. It was not determined by functions.” The inconvenience and unthinkability of describing the Philips Pavilion algebraically were, however, not only due to the demands of form-finding. They were also due to the extraordinary difficulty of identifying suitable algebraic parameters. The geometric and experimental translation of models into drawings was, according to Xenakis (1958/59, p. 4) “simple”. For this purpose, Xenakis devised a special-purpose tool consisting of two straight metal spokes connected by elastic strings. He explains that he positioned the tool such that the strings formed the ruling lines of a surface of interest, which then aided producing drawings and extracting coordinates (Xenakis, 1958/59, p. 4; 2008, p. 115).

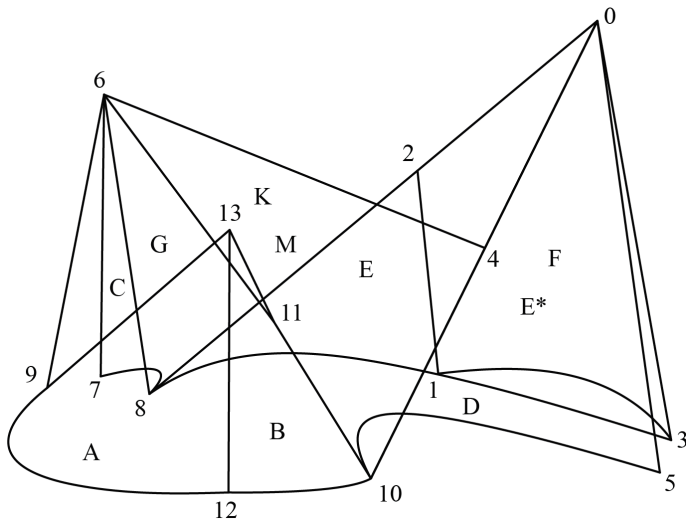


Figure 2. Key points (numbers) and surfaces (letters) of the Philips Pavilion.

In the following, we outline the analytical procedure by which we obtained algebraic parameters from the truncated hyperbolic paraboloid surfaces of the

Philips Pavilion (using surface A as an example) and provide a full set of algebraic parameters for all of the building’s surfaces. Figure 3 illustrates our procedure in broad strokes. It starts from a given, geometrically defined truncated hyperbolic paraboloid surface, ensures its description by four key points and a grid of ruling lines, then translates this grid of ruling lines into a network of perpendicularly arranged parabolas, from which, finally, the algebraic parameters are extracted. The development of our procedure was based on algebraic, geometric and experimental methods, relying on the use of Rhino, Grasshopper and Python scripting as well as on the Opossum (Wortmann, 2017) and Goat (Flöry, 2013) optimisation plugins for Grasshopper.

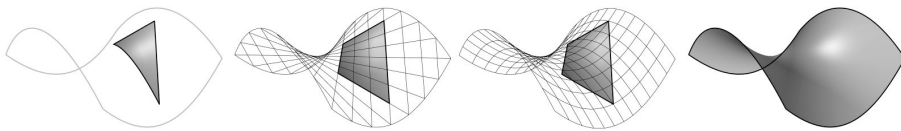


Figure 3. Inference of a hyperbolic paraboloid from a three-edged truncated area.

Table 1. Coordinates of key points (left) and surfaces (right) of the Philips Pavilion.

point	x	y	z
0	-14.788 m	23.532 m	20.500 m
1	-12.035 m	13.219 m	0.000 m
2	-9.338 m	14.860 m	12.945 m
3	-8.551 m	30.475 m	0.000 m
4	-5.050 m	22.355 m	9.603 m
5	-4.155 m	31.984 m	0.000 m
6	-3.219 m	-5.827 m	18.500 m
7	-0.951 m	-6.448 m	0.000 m
8	0.000 m	0.000 m	0.000 m
9	2.610 m	-7.419 m	0.000 m
10	3.532 m	21.318 m	0.000 m
11	6.709 m	19.003 m	8.000 m
12	8.511 m	16.814 m	0.000 m
13	10.771 m	21.141 m	13.000 m

surface	point 1	point 2	point 3	point 4
A	9	12	13	-
B	11	12	13	-
C	6	7	8	-
D	0	5	10	-
E	1	2	8	-
E*	0	2	3	-
F	0	2	3	-
G	6	9	11	13
K	0	4	6	8
M	4	6	10	11

**2. Locating the souterrain vertices and the corresponding ruling lines**

Our procedure requires truncated hyperbolic paraboloid surfaces to be described initially as grids of straight ruling lines. This, in turn, requires the four corner vertices of each such grid to be known. For surfaces G, K and M of the Philips Pavilion, all corner vertex coordinates can be gathered – explicitly or visually – from Xenakis’s (1958/59, p. 6, Figure 18) plan drawing. The remaining surfaces A through F intersect the ground plane along curved lines. One vertex of each of these surfaces lies at an unknown souterrain location (see the blank fields on the right of Table 1). Xenakis analysed the pavilion surfaces, including the souterrain portions of surfaces A through F, using the special-purpose tool described above, but, to the best of our knowledge, no records of the locations of the souterrain

vertices exist today. We located these vertices by modelling the topology of the ruling lines for each ground-intersecting surface, based on the three known vertices and a fourth, parametrically moveable vertex. For surfaces B and E\*, which intersect the ground plane while being circumscribed by four non-southern corner points, the procedure is slightly different and requires the parametric movement of the sought vertex along a southern extension of a circumscribing line defined by a “top” and a “bottom” vertex. Each moveable vertex was then driven by optimisation, using first the global RBFOpt (Opossum), second the global CMA-ES (Opossum) and third the local BOBYQUA (Goat) algorithms. The objective of this optimisation process was to minimise the deviation between the intersection of the grid of ruling lines with the ground plane and the corresponding base line provided in Xenakis’s (1958/59, p. 6, Figure 18) plan drawing, as illustrated in Figure 4. The coordinates of the southern vertices thus determined are shown on the left of Table 2, and their associations with surfaces A through F are shown on the right of Table 2. For surfaces G, K and M, this first step is unnecessary since their four corner vertices are known.

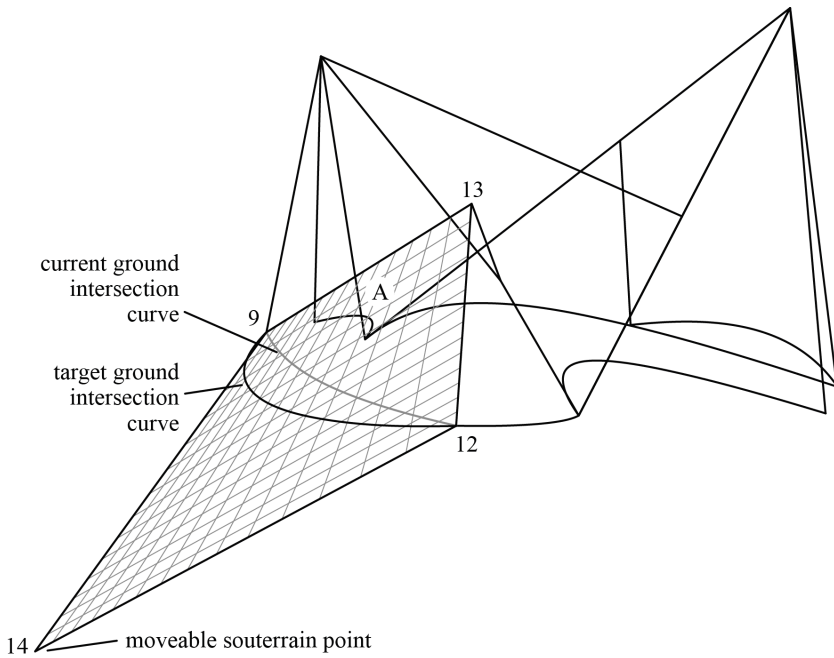


Figure 4. Determination of the southern geometry of surface A of the Philips Pavilion.

Table 2. Souterrain key points (left) and surfaces bisecting the ground plane (right).

point	x	y	z	surface	point 1	point 2	point 3	point 4
14	25.926 m	-13.067 m	-13.004 m	A	9	12	13	14
15	-1.328 m	24.859 m	-12.239 m	B	11	12	13	15
16	-11.595 m	-4.650 m	-18.469 m	C	6	7	8	16
17	12.958 m	-48.473 m	-68.047 m	D	0	5	10	17
18	-28.305 m	-64.827 m	-34.405 m	E	1	2	8	18
19	12.925 m	13.062 m	-1.239 m	E*	0	2	3	19
20	-80.401 m	-28.373 m	-328.121 m	F	0	2	3	20

Soraperra and Soraperra previously presented the souterrain portion of the pavilion, albeit without detailing the methods used and with somewhat different results (Sdegno, 2012, p. 172). The locations of some of the souterrain vertices raise questions about the scale of Xenakis's special-purpose tool. To pinpoint the souterrain vertex of surface F (the one furthest removed from the pavilion volume), at a likely model scale of 1:50, the tool would have had to extend across almost seven metres!

### 3. Extension of the grids of ruling lines

As a next step, it is advisable, and in many cases necessary, to extend the grid of ruling lines of each surface outwards as shown in Figure 5. Extended, each grid should reach well across its centroid, i.e. beyond the parabolic inflexion point in both directions of curvature. This extension was performed by first elongating the gridlines outwards and by then adding new grid lines across the elongated portions at equal intervals. This extension was a preparatory step to ensure long sequences of intersection points through the grid in the following section 4, including and extending well beyond either parabola's inflexion point in both directions to aid the analysis of the parabolic section lines in the subsequent section 5.

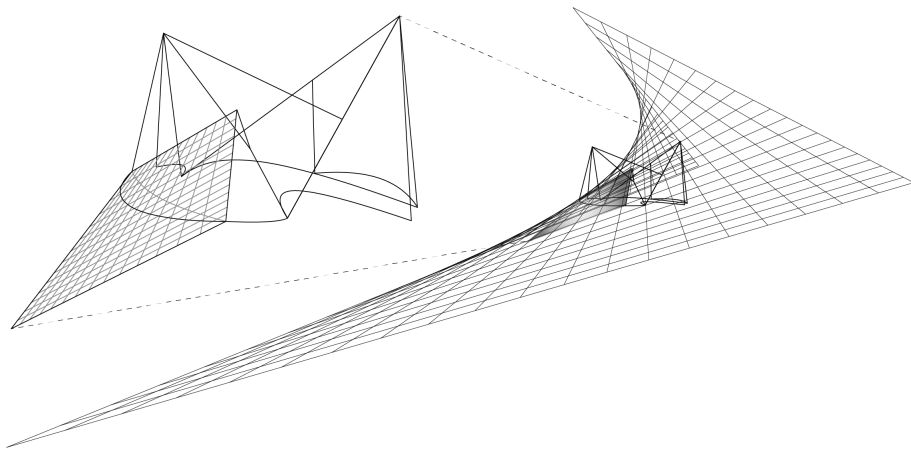


Figure 5. Extended grid of ruling lines of surface A of the Philips Pavilion.

#### 4. Identification of the parabolic section curves

As the hyperbolic paraboloid follows two, mutually orthogonal parabolic curvatures, any point on its surface is intersected by two mutually perpendicular parabolas. To identify these, two perpendicularly intersecting planes were rotated parametrically around the centroid of the four vertices of the surface of interest. Interpolated sequences of intersection points between the two mutually orthogonal planes and the grid of ruling lines were then translated along each other at a right angle to test how closely the resulting grid of interpolated intersection lines approximated the surface formed by the ruling lines. The centroid of the four vertices is a suitable centre for this rotation as it tends to yield long sequences of intersection points between the two planes and the extended grid of ruling lines. The two planes were rotated so as to minimise the compound distance between the grid of interpolated intersection lines and the extended grid of ruling lines using again the optimisation procedure described in section 2. Where this compound distance approached zero, the intersections between the two planes and the grid of ruling lines approximated two of the principal parabolas defining the sought hyperbolic paraboloid (see Figure 6).

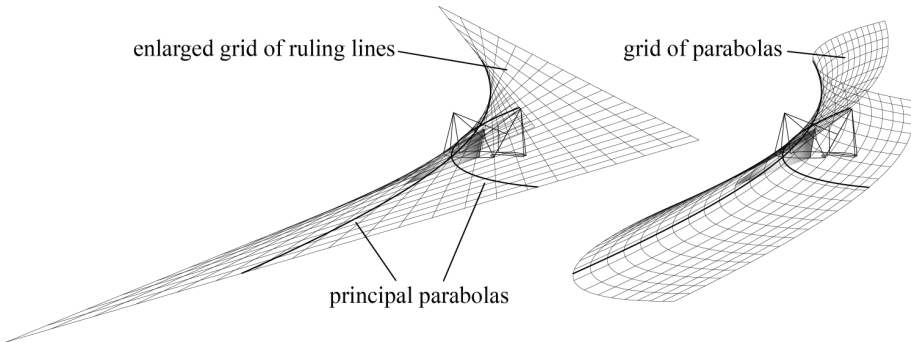


Figure 6. Identification of the parabolic section curves.

#### 5. Parabola analysis

The centroid of the hyperbolic paraboloid and its two hyperbolic curvatures ( $a$  and  $b$  in Equation 1) were then inferred from the two approximated parabolas. For this purpose, the inflexion point on each approximated parabola was found by moving three equally spaced points along the parabola while minimising the difference between the two outer points and the middle point, using the Goat optimisation plugin. The middle point thus approximated the inflexion point of the parabola. Both parabolas were then moved along each other such that their inflexion points coincided. This common inflexion point was the centroid of the sought hyperbolic paraboloid. Each of the two parabolas was then transformed such that its origin and orientation coincided with those of the coordinate system. A set of  $x/y$  coordinate samples was then taken from each parabola and used to calculate their quadratic coefficients using Numpy's *polyfit* function in Python.

## 6. Algebraic construction of the sought hyperbolic paraboloid

Using the two quadratic coefficients, a hyperbolic paraboloid was constructed algebraically according to Equation 1 shown above. This surface was then moved back from the origin of the coordinate system to the centroid identified in section 5 above and rotated to match the orientations of the two principal parabolas identified in section 4 (i.e. the reverse of the transformations described in section 5 was performed on the surface). The result matched the initial truncated hyperbolic paraboloid area (the pavilion surface in question) relatively closely. However, due to the accumulating limits in the precision of the optimisation steps as well as due to geometric and numerical inaccuracies affecting the procedure outlined above, the match could be closer. It was possible to improve this match substantially (28.5% error reduction for surface A, and 53.7% on average) by parametrically optimising the centroid location, orientation and quadratic coefficients of the hyperbolic paraboloid surface with the objective of minimising its deviation from the truncated hyperbolic paraboloid area given initially (again using the optimisation procedure described in section 2, but with very narrow variable ranges). The result for surface A of the Philips Pavilion is shown in Figure 7, and the resulting algebraic data for all the surfaces are given in Table 3.

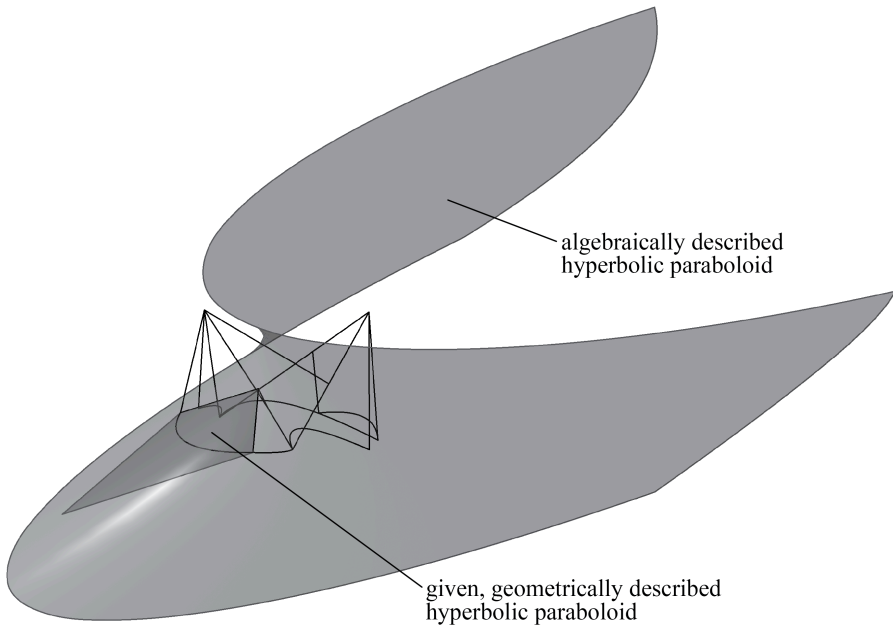


Figure 7. Algebraically described hyperbolic paraboloid approximating surface A of the Philips Pavilion.

Table 3. Algebraic parameters of all the surfaces of the Philips Pavilion.

surface	coefficients		centroid coordinates			rotations		
	a	b	x	y	z	xy	xz	yz
A	0.017 m	0.092 m	10.091 m	17.783 m	8.685 m	64.264 m	-1.930 m	-42.162 m
B	-0.538 m	-0.043 m	12.406 m	23.521 m	17.036 m	-42.803 m	-30.691 m	40.791 m
C	-0.010 m	-0.347 m	-2.758 m	-5.239 m	8.264 m	-19.217 m	5.115 m	88.693 m
D	-1.052 m	-0.038 m	-17.235 m	22.105 m	24.206 m	-90.430 m	46.731 m	-75.008 m
E	-0.301 m	-0.117 m	-10.447 m	15.980 m	16.822 m	-3.351 m	-69.434 m	28.549 m
E*	-0.025 m	-0.096 m	-9.008 m	12.747 m	9.435 m	-74.297 m	37.808 m	-20.529 m
F	-1.082 m	-1.043 m	-15.327 m	23.842 m	21.131 m	-9.706 m	-4.486 m	-2.176 m
G	-0.060 m	-0.219 m	5.861 m	14.195 m	10.218 m	41.151 m	-49.550 m	61.780 m
K	-0.371 m	-0.065 m	-5.877 m	11.778 m	12.826 m	-53.171 m	1.579 m	-101.620 m
M	0.086 m	0.209 m	4.266 m	21.132 m	-0.696 m	30.227 m	15.460 m	2.464 m

### 7. Discussion

In the absence of a method to directly calculate the algebraic parameters of hyperbolic paraboloids from truncated, geometrically defined hyperbolic paraboloid surfaces, we presented here a multi-step procedure for this purpose based on parametric modelling and computational optimisation. The multiple steps involved in this procedure were necessary due to three issues that, especially in combination, presented significant computational challenges. First, each of the algebraic hyperbolic paraboloid descriptions presented above involves eight parameters: quadratic coefficients  $a$  and  $b$ ,  $x$ ,  $y$  and  $z$  centroid coordinates, as well as rotation angles in three planes. The vastness of the search space between these eight parameters prohibits exhaustive searches (Fischer, 2019, p. 795). Second, due to the quadratic nature of hyperbolic paraboloid surfaces, small variations of the numerical parameters can result in significant changes of the corresponding surfaces. Third, we measured the closeness between each pair of given and candidate surfaces by calculating the compound distance between sets of points and the corresponding set of closest points on the given surfaces. This method can result in close numerical matches between significantly different hyperbolic paraboloid shapes.

We found the first two challenges to be mutually conflicting with regard to mathematical precision. Greater precision allows the closer algebraic approximation of target surfaces, but it also increases the search space. Modelling at the metre scale in Rhino, we used the maximum precision available in Grasshopper, i.e. six decimal places. (Values shown in Tables 1, 2 and 3 were rounded to three decimal places for visual clarity.) Nonetheless, our results offer close approximations of the target surfaces and may be improved upon by using greater computational precision. The third issue is prone to attract optimisation algorithms to numerous false local optima. From our perspective, the combination of all three challenges effectively prohibits global searches in a single step and necessitates the reduction of the overall search space in multiple consecutive steps as outlined above.

We investigated this multi-step procedure in verbal conversations, on paper and whiteboards and, most importantly, with the same parametric modelling and



optimisation toolkit with which we then applied the procedure to each of the surfaces of the Philips Pavilion. Throughout this investigation, we considered and tested numerous operations and strategies. The successful ones of these are outlined above. We did not record our path of enquiry towards this goal with its many dead-ends in full. For this, we have two explanations. First, we focused our attention on our goal of describing geometrically described hyperbolic paraboloid surfaces algebraically. Second, we explored numerous dead-ends that initially appeared promising but then turned out mistaken to extents not deserving to be recorded. In retrospect, however, many of these dead-ends were necessary to advance our overall enquiry. Without having recorded this enquiry in full, and despite its fixed goal, rational formality and precision, we remember it as akin to epistemic practices of design. In any case, we regard the algebraic approximation of hyperbolic paraboloid surfaces based on truncated, geometrically described surface areas, deemed “unthinkable” by Xenakis just some decades ago, as a testament to the power of the parametric design and optimisation toolkit, both in terms of automated search and epistemological enablement.

## References

- Burry, M.C.: 2002, Rapid prototyping, *Automation in Construction*, **11**(3), 313–333.
- Burry, M.C.: 2005, Homo faber, *Architectural Design*, **75**(4), 30–37.
- Burry, J.: 2011a, *Logic and Intuition in Architectural Modelling: Philosophy of Mathematics for Computational Design*, Ph.D. Thesis, RMIT University.
- Burry, M.C. 2011b, Architecture and practical design computation, in A. Menges and S. Ahlquist (eds.), *Computational Design Thinking, AD Reader*, Wiley, Chichester, 102–119.
- Fischer, T.: 2012, Geometry rationalization for non-standard architecture, *Architecture Science*, **5**, 25–46.
- Fischer, T.: 2019, Transcomputability, (Glanville’s Corollary of) Ashby’s Law of Requisite Variety, and epistemic processes, *Kybernetes*, **48**(4), 793–804.
- Fischer, T., Herr, C.M., Burry, M.C. and Frazer, J.H.: 2003, Tangible interfaces to explain Gaudi’s use of ruled-surface geometries, *Automation in Construction*, **12**(5), 467–471.
- Flöry, S.: 2013, “Geometry and Optimization”. Available from <[https://www.rechenraum.com/en/assets/downloads/goat/geometry\\_and\\_optimization.zip](https://www.rechenraum.com/en/assets/downloads/goat/geometry_and_optimization.zip)> (accessed 11 Dec 2019).
- Pottmann, H., Asperl, A., Hofer, M. and Kilian, A.: 2007, *Architectural Geometry*, Bentley Institute Press, Exton, PA.
- Sdegno, A. 2012, Ruled surfaces in Le Corbusier’s architectures, in M. Rossi (ed.), *Descriptive Geometry and Digital Representation: Memory and Innovation*, McGraw-Hill, New York, 167–175.
- Sprague, T.S.: 2013, Beauty, versatility, practicality: the rise of hyperbolic paraboloids in post-war America (1950–1962), *Construction History*, **28**(1), 165–184.
- Treib, M.: 1996, *Space Calculated in Seconds. The Philips Pavilion, Le Corbusier, Edgard Varèse*, Princeton University Press, Princeton, NJ.
- Vreedenburgh, C.G.J.: 1958/59, The hyperbolic-paraboloidal shell and its mechanical properties, *Philips Technical Review*, **20**(1), 9–17.
- Wortmann, T. 2017, Opossum. Introducing and evaluating a model-based optimization tool for Grasshopper, in P. Janssen, P. Loh, A. Raonic and M.A. Schnabel (eds.), *Proceedings of the 22nd CAADRIA Conference*, XJTLU, Suzhou, 283–292.
- Xenakis, I.: 1958/59, The architectural design of Le Corbusier and Xenakis, *Philips Technical Review*, **20**(1), 2–8.
- Xenakis, I.: 2008, *Music and Architecture: Architectural Projects, Text, and Realizations*, Pendragon Press, Hillsdale, NY.

# GENERATIVE MODELLING WITH DESIGN CONSTRAINTS

## *Reinforcement Learning for Object Generation*

YUTA AKIZUKI<sup>1</sup>, MATHIAS BERNHARD<sup>2</sup>, REZA KAKOOEE<sup>3</sup>,  
MARIRENA KLADEFTIRA<sup>4</sup> and BENJAMIN DILLENBURGER<sup>5</sup>  
<sup>1,2,4,5</sup>ETH Zurich  
<sup>1,2,4,5</sup>{akizuki|bernhard|kladefkira|dillenburger}@arch.ethz.ch  
<sup>3</sup>ETH Zurich, Lucerne University of Applied Sciences and Arts (HSLU)  
<sup>3</sup>kakooee@arch.ethz.ch

**Abstract.** Generative design has been explored to produce unprecedented geometries, nevertheless design constraints are, in most cases, second-graded in the computational process. In this paper, reinforcement learning is deployed in order to explore the potential of generative design satisfying design objectives. The aim is to overcome the three issues identified in the state of the art: topological inconsistency, less variations in style and unpredictability in design. The goal of this paper is to develop a machine learning framework, which works as an intellectual design interpreter capable of codifying an input geometry to form a new geometry. Experiments demonstrate that the proposed method can generate a family of tables of unique aesthetics, satisfying topological consistency under given constraints.

**Keywords.** Generative design; computational design; data-driven design; reinforcement learning; machine learning.

## 1. State of the Art

The trend of computational design in architecture has been widely spread now. Utilizing the power of computers, an entirely new design methodology emerged, which enabled architects to design unseen geometries. In computer science, a more radical design process has been explored, since generative adversarial networks (GANs) were proposed (Goodfellow et al. 2014). Originally, the method was only applicable to 2D image generation but soon became applicable to 3D object generation in voxel space (3D-GAN) (Wu et al. 2016), which is followed by further researches such as PointNet (Qi et al. 2017), a point-based 3D object generation. PointNet was used to generate chairs (Bidgoli and Veloso 2018). On the other hand, reinforcement learning (RL) is often used to train an agent to play games and to control robots. This algorithm has gathered attention since AlphaGo (Silver et al. 2016), made by DeepMind, beat one of the best Go players. The AlphaGo created an entirely new strategy in Go, which even professional Go players have never come up with. This suggests the possibility of a brand new design process in design, that is explored in this paper.

## 2. Problem Statement

Recently, the advances in deep neural networks are happening at a fast pace because of the rapid progress of computer hardware. Since then, artificial intelligence (AI) is widely applied to various fields and industries. In the field of architecture, computers are used to help architects and engineers design, analyze and optimize space and structures. Digital fabrication is pushing the boundaries of manufacturing in architecture in line with digital design, however, there is still additional human effort required to optimize design digitally or manually in order to achieve feasibility. On the other hand, there is a rapid progress in 3D object generation purely generated by AI in the domain of computer science, although fabrication of such complex geometries has not been explored. 3D-GAN and PointNet present a similar problem, as gaps are sometimes seen between voxels or points. This topological inconsistency derives from lack of semantic information of the target geometry and is one of the biggest challenges in 3D object generation especially in terms of fabricability.



Figure 1. Topological inconsistency as gaps in generated geometries through 3D-GAN (Wu et al. 2016).

Moreover, their output relies on voxels or points, which makes the outcome visually dense. Although new geometries are obtained through these algorithms, they often look similar and no other visual styles are to be expected. Furthermore, the latent vector is arbitrarily manipulated in the processes where designers cannot easily predict their consequences until they see the final results.

In this paper, RL is deployed in order to explore the potential of generative design satisfying design objectives. The aim is to overcome three issues identified in the state of the art: topological inconsistency, less variations in style and unpredictability in design. We aim at developing an ML framework which generates a novel geometry based on an input form following assumptions that fulfill fabrication and aesthetic goals.

## 3. Methodology

ML algorithms already surpassed humans in abstract strategy board games, not only Go, but also Chess and Shogi (Silver et al. 2017). This exemplifies the possibility that an ML algorithm is likely to design better objects satisfying design objectives than human, because the design is also an abstract and strategic process like board games.

In ML, there are three big paradigms: supervised learning, unsupervised

learning and reinforcement learning. Eigenchair (Hovestadt and Bühlmann 2014) and PointNet are classified as unsupervised learning which extrapolate geometric features only from input geometries. However, a particular objective is difficult to be fulfilled because designers cannot specify constraints there at all. Supervised learning is mainly used to predict or classify based on input-output pairs. GANs including 3D-GAN, are generally classified as semi-supervised learning, however the output image/geometry mainly relies on random values. This is why the results of GANs tend to become unpredictable.

Reinforcement learning, which is adopted in AlphaGo and is used in this research, is a process to train an agent to take the optimal action in order to maximize a specific value (reward), where this value can directly relate to geometric and architectural constraints. In other words, an agent decides on an action according to the current state of the environment and receives feedback from its environment whether the action is beneficial or not by the means of a reward. This algorithm is often used to train an agent to play a computer game (Volodymyr et al. 2013). In our approach, an analogy of game-playing is used to describe the design parameters. RL also allows control of a sequential process as a fabrication sequence, unlike the other ML strategies by tracking an agent’s movement history.

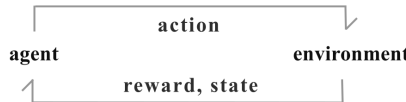


Figure 2. Brief diagram of reinforcement learning.

Table 1. Terminology in reinforcement learning.

Terminology	Description	Analogy in video game
Agent	A subject which is trained through the training.	Player
Environment	Overall system managing the training.	Game system
Action	Possible actions that the agent can take.	Jump, walk, etc.,
State	A scenario that the agent gets from the environment.	Screen
Reward	A numerical value received by the agent.	Coin, dead, etc.,
Step	One cycle that starts from an action till a feedback from the environment.	Every frame
Episode	All states between an initial-state and terminal-state.	One game play

In this game, an input geometry is given to define the boundaries of movement in the space of an agent. The goal of the agent is to generate a table tracking the trail of movement in the given space satisfying design and fabrication constraints. The agent moves inside the input geometry satisfying such constraints as well as staying inside the defined space as much as possible. The game is over, in other words, a new geometry is shaped, when the agent steps outside the input geometry. This setup of RL ensures the generation of a unified/sequential geometry because the output is a single stroke, which is difficult to achieve by the other ML strategies, while the fabrication sequence is also controlled.

## 4. Experiments

Before generating a 3D table, 2D experiments were executed to obtain the appropriate setup of RL for table generation because its design freedom in 3D space is generally higher than that in 2D space.

### 4.1. 2D EXPERIMENT

The goal in 2D space is to generate a section of a table as a binary image with one of the basic algorithms in RL, Deep Q Learning (DQN) (Volodymyr et al. 2013). DQN computes the next action from its current state. The possible actions are all discretized.

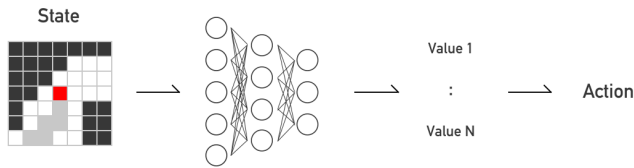


Figure 3. A discretized action space:  $N$  of independent  $Q$  values corresponding to each action are generated via DQN. The action with the bigger value is likely to be taken.

500 Binary images with  $64 \times 64$  resolution are used to train models where black and white pixels indicate inside and outside a table as an input, respectively. An agent draws a stroke inside the black area (see Figure 3) satisfying certain constraints given as reward and actions.

An agent can move to its closest 8 pixels, and its state is defined as a  $7 \times 7$  local window around it. In the window, pixels inside an input shape is filled in black, the pixels of its trail is filled in grey, and the rest are in white (see Figure 3). For the reward,  $+1$ ,  $-1$  are given when the agent steps on inside and outside the input geometry, respectively, in order to notify it that it should remain only inside the given input shape. In addition, a smaller negative reward of  $-0.5$  is given to the agent when the agent hits its trail, from which it can understand self-intersection is not a good manner but is better than going outside. The game is over when the agent hits its trail more than five times or goes to the outside.

Table 2. RL system setting in 2D.

<b>Actions</b>	8 actions of going to the nearby 8 pixels by a relative coordinate system
<b>States</b>	A $7 \times 7$ local window around the agent
<b>Rewards</b>	$+1$ for inside an input geometry, $-0.5$ for self-intersection, $-1$ for outside the input geometry

The state, a two-dimensional array as a grey-scaled image of the  $7 \times 7$  local window, is flattened into a vector to DQN, which returns an action where the agent ought to go under such a condition.

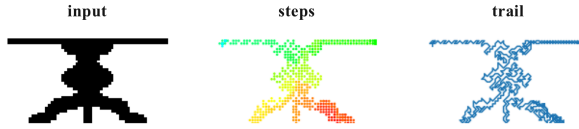


Figure 4. A table generation in 2D. left: an input geometry, middle: a movement history of the agent (the color gets green starting from red, as the step proceeds), right: a trail of an agent.

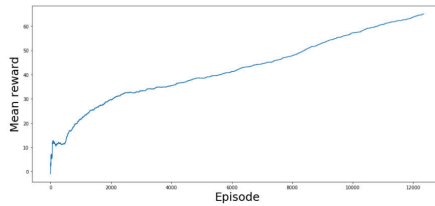


Figure 5. A mean reward transition during the training.

After the training, this agent becomes to fill the input shape as much as possible with a single stroke with a few self-intersections. In addition to that, it can even fill a chair whose geometry is not included in the training dataset, which means that the model achieves generalization in motion planning available for any shape.

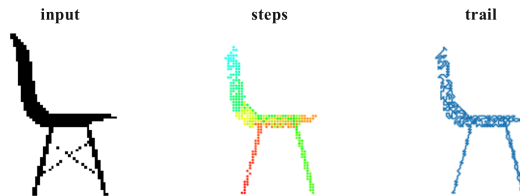


Figure 6. A path generation via Flexible pixel-wise model for a chair.

From this experiment, an agent to shape a geometry is successfully designed, although the constraint there is only an input geometry to prohibit the agent from deviating the initial shape, where the agent just can fill a shape with a single stroke. In 3D experiments, more strict design/fabrication constraints are introduced by designing actions and states to meet the intended purposes.

#### 4.2. 3D EXPERIMENTS

The scheme established in 2D is directly applied in 3D for the most parts, however there is a significant difference in action space, that is the number of possible actions. There are 8 pixels around an agent in 2D pixel space while there are 26 voxels around it in 3D voxel space. Obtaining many discrete and independent values is not reasonable so that discrete action space is replaced with continuous action space by introducing Twin Delayed Deep Deterministic Policy Gradients (TD3) (Fujimoto et al. 2018). TD3 outputs a vector of three values ranging from

-1 to 1 and the vector indicates where to go next as direction. The resolution here is 16x16x16 voxel space and a voxel window size as the state is 5x5x5 (See Figure 7). A thousand of 3D furniture mesh models are acquired through ShapeNet (Chang et al. 2015) and are converted into voxelized models. An agent here is also trained to stay inside an input geometry and to avoid self-intersection as much as possible while satisfying given design constraints to generate a new geometry.

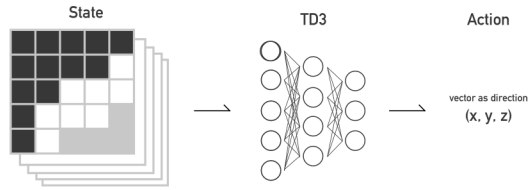


Figure 7. A continuous action space. Neural networks generate a series of continuous values.

#### 4.2.1. 6-Actions Model

An agent can go its 6 direct neighbor voxels, and a direction with the smallest angle with a vector obtained through TD3 is picked among the possible 6 directions. The game is over when the agent hits its trail more than five times or goes to the outside. The design constraint here is determined by the limited action set of horizontal and vertical movements, leading to an angular style.

Table 3. RL system setting in 6-actions model.

<b>Actions</b>	An agent can take 18 actions to place a LEGO block among a set of blocks
<b>States</b>	Same as Table 3
<b>Rewards</b>	+1 inside the input geometry, -1 outside the input geometry and for self-intersection

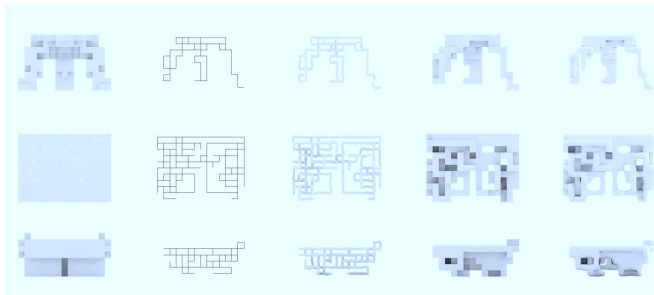


Figure 8. Object generation via 6-actions model - from left to right, input voxel geometries, voxels, pipes, and smoothed meshes.

The Figure 8 indicates that the intended angular style is achieved while the agent is staying inside the input geometry. In addition, all the geometries are

unified as a single object, which overcomes one of the issues of existing research, that is topological inconsistency.

4.2.2. 26-Actions Model

As another design constraint, the number of possible actions is increased to 26 from 6 by allowing diagonal movements, which makes less angular style. The other setup is exactly the same as the previous model.

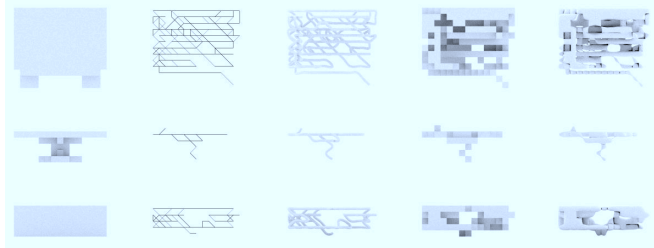


Figure 9. Object generation via 26-actions model - from left to right, input voxel geometries, voxels, pipes, and smoothed meshes.

Less angular geometries are produced by allowing diagonal movements. These two models validate that different design constraints can be realized according to action space design, nevertheless, these models sometimes generate imperfect tables due to the lack of the agent’s performance evaluation system, which is discussed in outlook section.

4.2.3. LEGO Block Model

The models so far focus on design perspective and do not have any fabrication constraints. In this model, LEGO blocks are introduced to make an agent consider a fabrication constraint. The objective here is to generate a LEGO table with a limited set of LEGO blocks. The agent adds a new LEGO block on or beneath the most recent block to prohibit branching, which makes it coherent as the previous models. A state is same as the previous model but for self-intersection because a new block cannot be placed where another block exists. There are three possible blocks: a unit block (a) and horizontal blocks of the length of two (b) and three (c) (seen in Figure 10). An agent designs a geometry only using these three types of blocks. Considering a unit LEGO block occupies a single voxel in space, a LEGO block is placed with the smallest angle with a vector from the agent’s current position to its farthest tip with a vector from TD3.



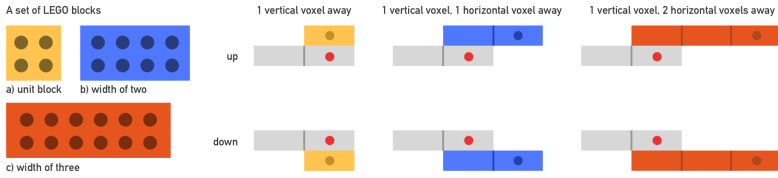


Figure 10. Possible LEGO blocks as action. Red dots indicate the agent's current position, from where a new LEGO block is placed.

Table 4. RL system setting in LEGO block model.

<b>Actions</b>	An agent can take 18 actions to place a LEGO block among a set of blocks
<b>States</b>	Same as Table 3
<b>Rewards</b>	+1 inside the input geometry, -1 outside the input geometry and for self-intersection

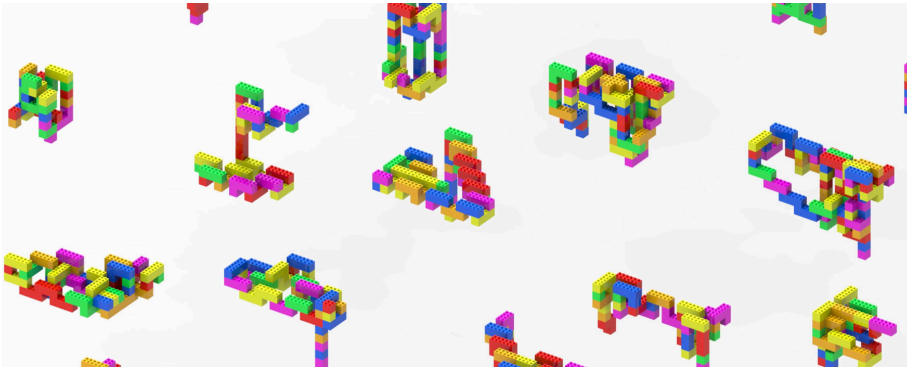


Figure 11. Object generation via LEGO block model.

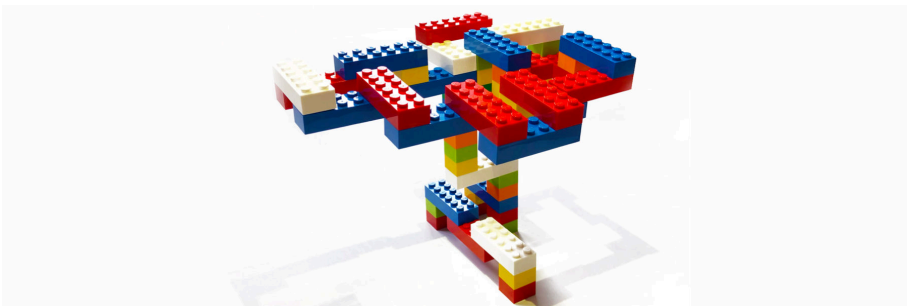


Figure 12. Assembled LEGO blocks.

The fabrication constraint here is to design a table with a set of LEGO blocks. The constraint is rather simple, yet the fabrication constraint is certainly satisfied

and a variety of tables are successfully generated. The better performance can be expected by introducing stricter constraints such as using LEGO blocks with more different shapes.

## 5. Conclusions

An agent can draw an object with a single stroke in 2D space, leading to a strategic learning behavior for any input shape. In 3D space, the trail of the agent materializes geometry as a continuous stroke satisfying design objectives. Designing action space appropriately, objects in the intended visual style are successfully produced. In the LEGO block experiment, a fabrication constraint of the modular system is implemented as a reward and action system in the algorithm, and a sort of geometries fulfilling the constraint are successfully achieved.

The experiments demonstrate that RL overcomes the issues identified in state of the art: topological inconsistency, less variations in style and unpredictability in design. This is brought by the three essential aspects of RL, action, state, and reward, which allows strict design constraints as well as design freedom. RL is validated as a promising methodology to codify the abstract concept of design. Computers are not merely a design assistant there. They are an independent design interpreter and designer in the game of design.

## 6. Outlook

In this paper, self-intersection is avoided as much as possible, though it increases the stiffness of a structure. How an agent interacts with its trail must be more elaborately controlled. In terms of stability, structural strength can also be evaluated as reward to achieve a stable and strong structure.

For action space, all the actions are mapped into discretized space in spite of getting continuous values from TD. If continuous values are directly used to navigate the agent, it can generate more visually-expressive objects, which provides more opportunities to explore in styles.

The 16x16x16 resolution in 3D space is so low that detailed objects cannot be generated. One possible solution is to introduce a wider window as state. There needs to be further researched, and this definitely increases the application opportunities of this methodology.

The LEGO experiment demonstrates that this approach is applicable to object generation with fabrication constraints of how blocks are assembled. This even can be extended to a robotic-fabrication-wise generative model where a robotic path is taken into consideration while fabrication.

Different types of constraints such as metal casting, lightweight structure and timber structure can also be feasible with this system.

Table 5. Fabrication methods and corresponding possible constraints in reinforcement learning.

Fabrication method	Possible constraints
LEGO	Possible actions are a set of available LEGO blocks.
Metal casting	Self-intersection is positively evaluated and the thickness of a geometry is getting thinner considering the metal flow.
Lightweight structure	Less steps are positively evaluated to go through the entire area of the input geometry.
Robotic assembly	If the agent steps on the area where a robot cannot access, a negative reward is given to punish such an action.
Aggregation	Possible actions are a set of modular units.

Finally, there is no way to evaluate the goodness of generated geometries so far. The current algorithm generates objects satisfying given constraints, however the algorithm does not know how good the result is. For instance, an output geometry is not uniformly distributed in the input geometry in some cases. To overcome such an issue, the distribution of the final geometry in its input geometry can be used to assess the goodness of the geometry as episodic reward. To establish a more reliable model, episodic reward must be given to the agent to notify the goodness of an overall geometry so that the agent can generate only “good” objects.

## References

- Bigdoli, A. and Veloso, P.: 2019, DeepCloud. The Application of a Data-driven, Generative Model in Design, *arXiv preprint arXiv:1904.01083*.
- Chang, A.X., Funkhouser, T., Guibas, L., Hanrahan, P., Huang, Q., Li, Z., Savarese, S., Savva, M., Song, S., Su, H., Xiao, J., Yi, L. and Yu, F.: 2015, Shapenet: An information-rich 3d model repository, *arXiv preprint arXiv:1512.03012*.
- Fujimoto, S., Hoof, H. and Meger, D.: 2018, Addressing Function Approximation Error in Actor-Critic Methods, *International Conference on Machine Learning*, 1582-1591.
- Goodfellow, I., Pouget-Abadie, J., Mirza, M., Xu, B., Warde-Farley, D., Ozair, S., Courville, A. and Bengio, Y.: 2014, Generative adversarial nets, *Advances in neural information processing systems*, 2672-2680.
- Hovestadt, L. and Bühlmann, V.: 2014, *EigenArchitecture*, Birkhäuser.
- Mnih, V., Kavukcuoglu, K., Silver, D., Graves, A., Antonoglou, I., Wierstra, D. and Riedmiller, M.: 2013, Playing atari with deep reinforcement learning, *arXiv preprint arXiv:1312.5602*.
- Qi, C.R., Su, H., Mo, K. and Guibas, L.J.: 2017, Pointnet: Deep learning on point sets for 3d classification and segmentation, *Proceedings of the IEEE conference on computer vision and pattern recognition*, 652-660.
- Silver, D., Huang, A., Maddison, C.J., Guez, A., Sifre, L., Van Den Driessche, G., Schrittwieser, J., Antonoglou, I., Panneershelvam, V., Lanctot, M., Dieleman, S., Grewe, D., Nham, J., Kalchbrenner, N., Sutskever, I., Lillicrap, T., Leach, M., Kavukcuoglu, K., Graepel, T. and Hassabis, D.: 2016, Mastering the game of Go with deep neural networks and tree search, *nature*, **529**(7587), 484.
- Silver, D., Hubert, T., Schrittwieser, J., Antonoglou, I., Lai, M., Guez, A., Lanctot, M., Sifre, L., Kumaran, D., Graepel, T., Lillicrap, T., Simonyan, K. and Hassabis, D.: 2017, Mastering chess and shogi by self-play with a general reinforcement learning algorithm, *arXiv preprint arXiv:1712.01815*.
- Wu, J., Zhang, C., Xue, T., Freeman, B. and Tenenbaum, J.: 2016, Learning a probabilistic latent space of object shapes via 3d generative-adversarial modeling, *Advances in neural information processing systems*, 82-90.

# A RECONFIGURABLE JOINT BASED ON EXTRUDED POLYHEDRONS

HUADONG YAN<sup>1</sup>, ZIYU TONG<sup>2</sup>, DAEKWON PARK<sup>3</sup> and HENG LU<sup>4</sup>

<sup>1,2,4</sup>*Nanjing University School of Architecture and Urban Planning*

<sup>1</sup>*mg1836028@smail.nju.edu.cn* <sup>2</sup>*tzy@nju.edu.cn*

<sup>4</sup>*childswim@gmail.com*

<sup>3</sup>*Syracuse University School of Architecture*

<sup>3</sup>*dpark103@syr.edu*

**Abstract.** An extruded polyhedron is a reconfigurable geometric shape based on the extrusion of each surface of a polyhedron along the normal direction. This paper introduces an extruded polyhedral joint that uses its own spatial structure to generate multiple states. The component primarily consists of an extruded polyhedron and is equipped with an optional adaptor to adapt to various situations. This research proposes that the formal deformations of a partially extruded polyhedron due to the instability of its own structure give it potential as a reconfigurable joint. To cope with the inevitable deformation of the extruded polyhedron branch cross-section during the overall deformation process, an adaptor - an indispensable component of the entire joint - is utilized at strategic branch locations. In addition, the reconfigurable methods and internal structure of the joints are discussed in detail. Finally, some practical application scenarios for connection components and their advantages in application scenarios are introduced.

**Keywords.** Extruded polyhedron; Adaptive joint; Transformation.

## 1. Introduction

Implementing adaptive features in artifacts and environments is beneficial. Foldable tables and chairs and interactive buildings are all designed to make the product play a role in different environments. (Li H, Hu R, Alhashim I, et al 2015, Nevatia R, Price K 2002) Among several strategies for creating flexible designs, utilizing an adaptive joint (i.e., reconfigurable joint) is an effective and reliable method.

In recent years, many achievements have been made in the study of geometric shapes and connection methods. Origami, as an ancient art form, has been introduced into this area of exploration. The extruded polyhedron described in this article can be regarded as a type of 3-dimensional origami structure. It was inspired by a modern origami technique called snapology, which can create a wide range of polyhedrons (Figure 1a) and extruded polyhedrons (Figure 1b) in a similar way to

a 2-dimensional origami structure. (Goldman F E 2017)The formal transformation of the 3-dimensional origami structure is also limited by the creases (i.e., folds). The different relationships between the creases are the source of diverse structural changes in space.

Scientific research on polyhedrons can be traced back to the ancient Greek era, from the earliest Platonic polyhedrons and Archimedean polyhedrons to the later Kepler polyhedrons, icosahedral polyhedrons, and other polyhedrons. (P.R.Cromwell 1999)With the deepening of research, the number of polyhedrons has increased tremendously. Many fields of research and design utilize polyhedrons, and the study of polyhedron morphology has always been guided by applications and functional demands.



Figure 1. Snapology.

In the field of structures, the most famous is a lightweight dome composed of triangular faces proposed by Richard Buckminster Fuller (Figure 2a). Fuller's original inspiration came from the icosahedron. This great invention made use of the principle of triangle stabilization. Fuller spheres composed of triangles are also stable. In 1967, at the Montreal World Expo, the American Pavilion was displayed in the form of a Fuller sphere. To date, the polyhedral dome structure is still the most widely used polyhedron in the field of architecture. Fuller's careful exploration of the stability of the polyhedron led to his great achievements in architecture. (Tarnai T , Iijima S , Hare J P , et al. 1993)

In the field of machinery, NASA has been studying the development and application of polyhedral robots since the early 21st century (Figure 2b). It is expected that polyhedral robots will replace traditional wheeled robots for space exploration. (Abrahantes M, Silver A 2008)However, contrary to the Fuller sphere utilizing the stability of triangles, polyhedral robots take advantage of the deformable features of the polyhedron.

Chuck Hoberman, from the Harvard Graduate School of Design, regards the extruded polyhedron as a reconfigurable component and focuses on the various deformation possibilities of the extruded hexahedron. An extruded hexahedron is a cell structure combined into a new material with a self-restructuring ability in the form of a 3D array (Figure 2c). Chuck Hoberman explained changes in the extruded hexahedron through formulas, which was the precedent for research on extruded polyhedrons. (Paik J 2017, Overvelde J T B, De Jong T A, Shevchenko Y, et al. 2016, Overvelde J T B , Weaver J C 2017)

From the above examples, we can understand some of the potential of this type of geometry in product development. However, until now, research

on polyhedron morphology has remained in a one-sided, decentralized state. There is no research that summarizes the evolution of the entire polyhedron group based on polyhedral forms. Inspired by research on polyhedrons at the Harvard University Graduate School of Design, this research explores various forms of polyhedrons, extracts representative polyhedrons, and conducts detailed morphological evolution studies. The main research objective of this paper is to characterize a reconfigurable hollow geometry based on a convex polyhedron extruded along the normal direction of each face of the polyhedron and to discuss its applications.

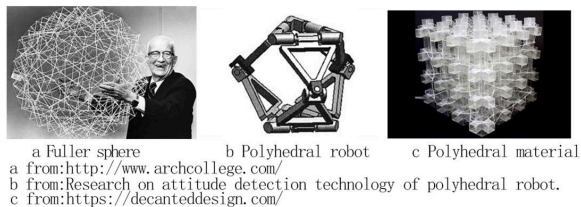


Figure 2. Polyhedral application.

## 2. Research Methodology

We classify the types of movements for each of the extruded polyhedrons, which can be divided into variable extruded polyhedrons and immutable extruded polyhedrons. Immutable extruded polyhedrons such as extruded regular tetrahedrons cannot undergo deformation, while variable extruded polyhedrons such as regular hexahedrons can switch between multiple states.

We chose a research object in the category of variable extruded polyhedrons. The variability of the extruded polyhedron is used to study its role in the field of modern architecture. Because the movement method of extruded polyhedrons is very complicated, it is difficult to build a movement model on a computer, so the entire experimental process adopts a traditional manual model. As the number of polyhedron faces and the number of single-sided edges increase, the materials and time consumed by the manual model increase exponentially. Considering the complexity of the study, some specific faces are selected in the simulation experiments to make relatively simple graphics. For example, triangles, quadrilaterals, pentagons, and hexagons are used to make extruded polyhedrons.

The main research on the deformation of the extruded polygon aims to confirm its potential as a connecting member. The variation of partially extruded polyhedrons is not suitable for a connecting member. Here, we perform a screening in a relatively simple way.

In the simulation, we found that the shape change of the extruded polyhedron is more complicated than traditional changes, such as rotation, distortion, and displacement. It is difficult to describe the formal characteristics of the movement that occurs during the change of the extruded polyhedron in a simple way. The way that polyhedrons are expressed using mathematical formulas is complex,

and with the increase in the number of polyhedrons, the logical difficulty of the mathematical expressions increases accordingly.

This article attempts to describe the deformation of the extruded polyhedron in a more understandable way. We take the relative positional relationships of points, edges, and faces as the basis for expression. We observe the evolution of the polyhedron to find the most descriptive relationship among the changes in the relationships between points, edges, and faces. This may be a point-to-point relationship description, an edge-to-edge relationship description, or a face-to-face relationship description.

In addition, during the experiment, we divided the branches of the extruded polyhedron (Figure 3a,b) into variable branches (Figure 3c) and fixed branches (Figure 3d). Sections change, while fixed branches do not. The purpose of the classification of branches is also to better express the deformation rules of the extruded polyhedron.

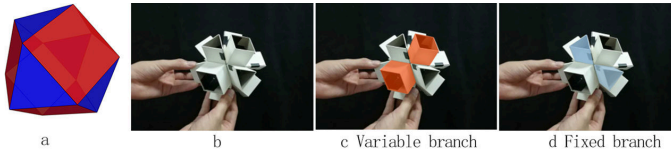


Figure 3. Polyhedral branches.

### 3. Extruded Truncated Octahedron

#### 3.1. ORIGINAL FORM

We study the deformation rules of extruded polyhedrons in groups of a dozen. Due to limitations of space, we take the extruded truncated octahedron as an example to illustrate our research method.

The truncated octahedron(Fig.4a,b,c) belongs to the category of Archimedes' polyhedrons. It consists of six regular tetragons and eight regular hexagons. This is precisely because its faces are all unstable quadrilaterals and octagons. When all the faces of the truncated octahedron are extruded, they show a very unstable state, and they cannot maintain a uniform extrusion polyhedron shape. It is disadvantageous to utilize this polyhedron as a connecting member.

Such a rich variety of forms is not truly beneficial in future practical applications. In contrast, too many form changes restrict the development of extruded polyhedrons for practical use. Here, we need some methods to limit the number of deformation modes of some overly abundant extruded polyhedrons. To limit the number of deformation modes of the extruded polyhedron and decrease this number to a controllable and usable range, we restrict discussion to the variable branch.

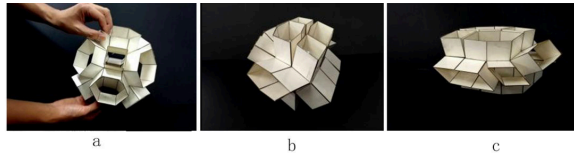


Figure 4. Flexible polyhedron.

### 3.2. RIGID LID

The variable branch is used as the geometric basis of extruded polyhedron motion. When a variable branch is artificially fixed, certain deformations are limited. A lid with a fixed shape added to a variable branch can play the role of a fixed branch. When considering the use of extruded polyhedrons in the future, the variable branch can be fixed in advance according to requirements.

During the research, we gradually increase the number of fixed branches of the extruded truncated octahedron and record the deformation of the extruded truncated octahedron in different states.

First, we fix the eight square faces. At this time, when the extruded truncated octahedron is pressed against a geometry with two opposing square sections as the stress points, we find that it had stability in this direction (Figure 5a), but there is still no stability when stressed along other directions (Figure 5b). Then, we experiment with the hexagonal branch as the starting point (Figure 5c, d). At first, the two opposite hexahedrons are still fixed (Figure 5e, f), and then the number of fixed faces increase gradually. When the four faces are fixed, the extruded truncated octahedron is in a relatively stable state (Figure 5g). When the five hexagons are fixed, the entire shape is completely stable (Figure 5h).

With the increase in the number of branches, even if an equal number of variable branches are fixed, because the positions of the variable branches are different, the possible deformation results will appear different.

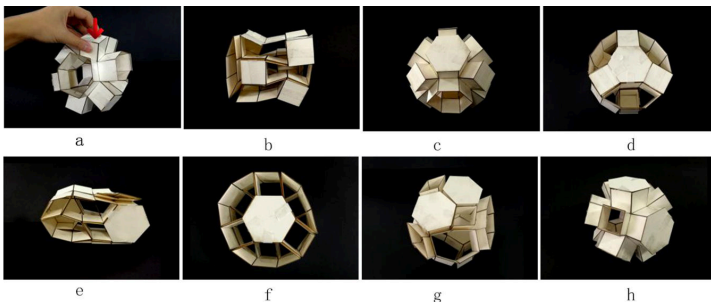


Figure 5. Rigid section.



### 3.3. IRREGULAR LID

Fixing the variable branch with a standard lid is a viable method for controlling extruded polyhedrons. Based on this method, we propose a new idea, which is to control the initial state of the extruded polyhedron by controlling the shape of the lid (Figure 6a) and then change all its subsequent manifestations.

We also carried out a simulation experiment using an extruded truncated octahedron, replacing the original square cover with a parallelogram with an included angle of  $45^\circ$ , and fixing the variable branch of the quadrilateral to a parallelogram.

After the variable branch, with its shape-changing ability, is fixed, the whole extruded truncated octahedron can obtain other controllable deformation results (Figure 6b, c).

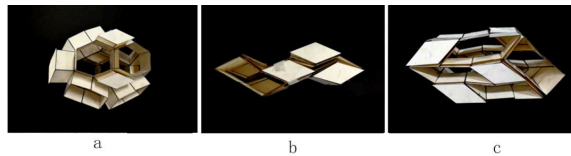


Figure 6. Irregular section.

### 3.4. THE CASE OF A RIGID LID

This time, we define the analysis of the extruded polyhedron motion in terms of the relationship between the central polyhedrons. The two selected hexagons are denoted as  $f_1$  and  $f_2$  (Figure 7a). The distance between the two opposite faces when the geometry is in the initial state (Figure 7b) is denoted as  $d$ . The cross-sections of the four extruded hexagons are gradually transformed into rectangles (Figure 7c), and when  $d$  is reduced to 0, the whole shape assumes another state: three legs on each side of the hexagon (Figure 7d).

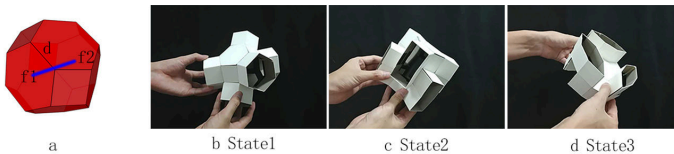


Figure 7. Case of a rigid lid.

### 3.5. THE CASE OF AN IRREGULAR LID

An irregular lid can give the extruded polyhedron a different initial shape and play a restricting role in the subsequent deformation process and the results of the extruded polyhedrons. We also used an extruded truncated octahedron as the research object, fixed all its quadrilateral faces to the parallelogram, and fixed a pair of hexagons in opposite positions to a rectangle so that the central polyhedron

would have oblique symmetry (Figure 8a).

We use the relationship of edges to describe the state change of the extruded truncated octahedron. The three lines L1, L2 and L3 are shown as state 1 when the three edges are in the same plane (Figure 8b). When the three edges form angles, the shape of the whole body splays and generates state 2 (Figure 8c).

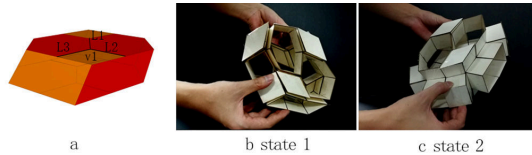


Figure 8. Irregular section.

### 3.6. OTHER EXTRUDED POLYHEDRONS

Besides extruded truncated octahedrons, there are many polyhedrons that have the potential to be joints. Figure 9 lists 4 kinds of extruded polyhedron prototypes.

These extruded polyhedrons also have one or more deformations. The method of change and control is similar to that of extruded truncated octahedron.

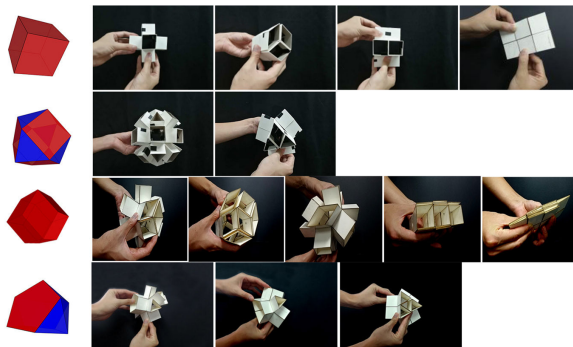


Figure 9. Other extrude polyhedron.

## 4. Component Processing

### 4.1. ADAPTOR

The first topic we need to address in the process of physical componentization is the contradiction between pure geometry and industrial products (i.e., how to connect joints with rods). The basic polyhedron itself, as a geometry, does not have the ability to interconnect with a member. The formation of the final component must be achieved with the assistance of a lid. Here, we propose the concept of a converter that helps extrude the polyhedron to finally achieve the goal of connecting members.

The whole converter is divided into two parts: the fixed end (Figure 10a) and

the terminal (Figure 10b). This idea originates from the idea of the terminal above. We use the lid as a fixed end, open a hole in the lid, and then set a custom terminal on it (Figure 10c).

A terminal as a joint can be a groove with any cross-section, and a rod can be nested into it to achieve a connection. Depending on the configuration of the structure, we can customize the form of the terminal and apply it in different scenarios.

The installation of the fixed end can be combined with the requirements of the extruded polyhedral motion while satisfying the requirements of stability and componentization.

It is worth mentioning that the irregular lid can sometimes play an unexpected role in the application of the process.

The fixed end and the terminal are independent of each other, and free combination of them can be used for many practical scenarios.

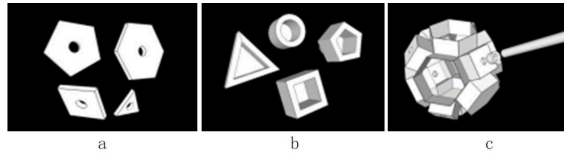


Figure 10. Adaptor.

## 4.2. INTERNAL STRUCTURE

The internal structure of an extruded polygonal component is composed of a rigid panel (Figure 11a,b) and a flexible connection (Figure 11c,d). The rigid panel plays a supporting role in the entire structure, and the flexible connection is the hardware foundation of the movement of the entire component. In this paper, rigid surfaces are divided into extruded surfaces and polyhedral surfaces according to their position. Connections are also divided into polyhedral connections and rigid surface connections.

The connecting part of a structure is the main position where a component is stressed, because there is an arbitrary angle at the connection site in the extruded polyhedron member. Its force will be extremely complicated, not only in terms of the type of force but also because multiple forces may act at the same connection site. For an entire assembly, it is difficult to strengthen connections in a controlled way due to the complexity of the forces. Therefore, if the use dictates a certain directionality, the cost of materials can be controlled in a targeted manner.

The required volume of materials of extruded polyhedrons also needs to be considered according to actual needs. We find that material in some branches can be saved. However, there is another layer to consider on the active branch. The rigid surface connection will have a reinforcing effect on the polyhedron connection. The connection of each branch plays a reinforcing role in the flexible connection of the whole extruded polyhedron. Therefore, when a polyhedral flexible connection requires higher strength, we can expand the length of the

branches. The longer the length of the branch, the stronger the polyhedral connection. In an actual production process, the directional extruded polyhedron component can be used where rigid connections are required. This will achieve the desired results with minimum cost.

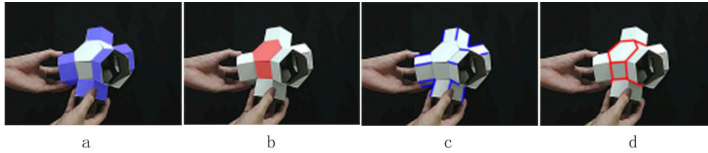


Figure 11. Extruded polyhedral structure.

### 5. Application

An application of extruded polyhedral joints can be a component of production, and its deformation is suitable for practical demands. We use fixed branches to obtain the deformation method we need according to the actual situation. It is also possible to combine two or more types of extruded polyhedrons to obtain more deformation possibilities.

Figure 12 demonstrates a deformable table. In this example, the extruded truncated octahedron component is the structural center of the entire deformable system. It is responsible for the performance of the entire table. The table can be expanded and shrunk freely through the deformation of the joint. According to the construction method shown in the previous chapter, the rod can also be freely installed and removed, and parts can be replaced. After properly adjusting the deformation angle and removing the table board, the structure can be used as a hanger.

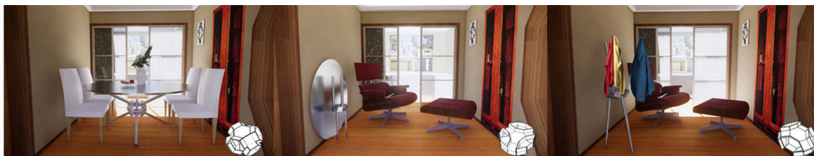


Figure 12. Application.

According to different application scenarios, a suitable constrained device is designed for the joints to control the deformation state. The constrained device is a part of the extruded polyhedron joints, and can be changed according to the specific requirements. Figure 13 demonstrates the constrained device used in this case.

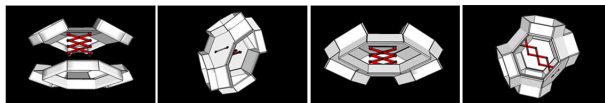


Figure 13. Constrained device.

## 6. Discussion and Conclusion

We discuss the deformation rules of extruded polyhedrons and the method of controlling their deformation. This research also makes use of the stated deformation rules to customize joints based on the requirements. Due to limitations of space, we only describe in detail the deformation of the extruded truncated octahedron and the process by which it becomes a joint. The deformation of extruded polyhedrons cannot be described by conventional rotation, displacement, etc. We can think of deformation as the evolution of a whole system. Extruded polyhedrons can achieve many complex deformations in some scenarios that current joints cannot without increasing the complexity of the system. There are many types of polyhedrons, and other kinds are worth studying, such as the extruded hexahedron mentioned in the application.

In the future, more scientific calculations will be necessary to mathematically support the theory of polyhedral components. The optimization of material consumption and optimization of structures are some aspects that can also be studied in depth.

## Acknowledgments

This research was supported by National Natural Science Foundation of China (51578277). We would like to thank Shuowen Chi, Shaojun Shi, and Wenxin Luo for their help in this study.

## References

- Abrahantes, M., Silver, A. and Littio, D.: 2008, Construction and Control of a 4-Terrahedron Walker Robot, *Southeastern Symposium on System Theory, New Orleans: University of New Orleans*, 343-346.
- Cromwell, P.R.: 1999, *polyhedron*, Cambridge University Press.
- Goldman, f. e.: 2017, Creating Polyhedra with Snapology, *Bridges 2017 Conference Proceedings*, 547-552..
- Li, H., Hu, R. and Alhashim, I.: 2015, Foldabilizing furniture, *ACM Trans. Graph*, **34**(4), 90:1-90:12.
- Nevatia, R. and Price, k.: 2002, Automatic and interactive modeling of buildings in urban environments from aerial images, *Proceedings. International Conference on Image Processing*, IEEE, 525-528.
- Overvelde, J. T. B., De Jong, T. A. and Shevchenko, Y.: 2016, A three-dimensional actuated origami-inspired transformable metamaterial with multiple degrees of freedom, *Nature communications*, **7**, 10929.
- Overvelde, J. T. B., Weaver, J. C. and Hoberman, C.: 2017, Rational design of reconfigurable prismatic architected materials, *Nature*, **541**(7637), 347-352.
- Paik, J.: 2017, Reconfigurable materials: Algorithm for architectural origami, *Nature*, **541**(7637), 296.
- Tarnai, T., Iijima, S. and Hare, J. P.: 1993, Geodesic Domes and Fullerenes, *Philosophical Transactions of The Royal Society A Mathematical Physical and Engineering Sciences*, **343**(1667), 145-153.

# BUILDING FROM WASTE CARDBOARD

*A Grammar for the Design and Fabrication of a Customized Modular House with Waste Cardboard and Wood-framed Panels*

JULIO DIARTE<sup>1</sup> and ELENA VAZQUEZ<sup>2</sup>

<sup>1,2</sup>*Penn State University*

<sup>1,2</sup>*{jcd40|emv10}@psu.edu*

**Abstract.** The project presented in this paper is part of a research project that investigates the reuse of waste cardboard as a building material for low-cost housing. The study combines craft-based production and digital-based tools. It implements a shape grammar formalism as a tool for structuring the design of a modular, customized house, including the generation of fabrication instructions for some building parts. In this paper, we present an implementation of the grammar for designing the floor plan of a single-story house.

**Keywords.** Material Reuse; Waste Cardboard Upcycling; Shape Grammars; Modular House; Sustainable Architecture.

## 1. Introduction

Waste corrugated cardboard is one of the most significant components found in the urban waste stream, and it is among the least valued recyclable materials. Waste cardboard is usually underutilized in developing countries where if it is not recycled for producing more cardboard, it ends up in landfills or dumpsters, increasing the impact of humans on the environment. In Asuncion, Paraguay—the case study for this project, for example, recycling rates are one of the lowest in the region—below 5% according to (IADB 2015); therefore, the implementation of novel and more sustainable methods for upcycling urban waste is critical.

Precedents of cardboard architecture occur in both research and practice. Since the 1940s, many investigations have analyzed and documented the many advantages and potential applications of cardboard products as building materials. Some of the most prominent studies can be found in (Eekhout et al. 2008; Pohl 2009; Salado 2011; Latka 2017). Following the same direction, in the last three decades, architects and structural engineers have experimented using cardboard products for humanitarian purposes—being the work of the Japanese architect Shigeru Ban the most noticeable in this area (Luna and Gould 2009). However, most of these works focused on using brand-new cardboard products, and little research has explored alternative applications of the waste cardboard that self-employed collectors recover from the streets in developing countries.

The project presented in this paper is part of a research that investigates alternative use of waste cardboard as a building material in developing parts of the world. The research includes: (a) experimental tools combining craft-based and digital-based methods for designing and prototyping building elements with waste cardboard—e.g., acoustic panels, concrete formwork molds, and wall panels (Diarte et al. 2019a, 2019b); and (b) hands-on work with waste cardboard collectors in Paraguay testing the feasibility of the workflow for building a prototype unit with panels made of waste cardboard and plywood (Diarte 2020).

This project aims to advance this research agenda and to continue building upon previous investigations on cardboard architecture by proposing a modular building system for housing that apply wall panels made of waste cardboard sheets and wood framing. The system uses shape grammars as a tool for (1) formalizing the design system of a customized modular house typology based on local precedents; (2) developing a structural system of the house; and (3) proposing a fabrication system that generates the fabrication instructions for producing the waste cardboard panels.

## **2. Practicalities of the Material**

The research focuses on the waste cardboard that is collected from the urban waste stream by self-employed collectors in the metropolitan area of Asuncion, Paraguay. Material parameters include variability of size, thickness, and quality. However, the project uses only the waste cardboard that not contaminated with food or medical waste, wet or torn. After selection, the sheets are organized by size and thickness and documented. A construction workshop held in Asuncion in August 2019 and published in (Diarte 2020) showed a high percentage of waste cardboard reuse—80% of reuse rate from a total 1.2 tons of collected waste cardboard—for building a prototype unit of 11.3 m<sup>2</sup> with panels made of waste cardboard sheets and plywood. This project follows the same criteria for material assessment.

## **3. Design Principles of the Modular House**

The definition of the archetype for this house was based on the “sausage-house” typology. This is a traditional urban house typology found in Asuncion that is a derivation of the porch-house. This typology has its roots in the Spanish colonial tradition, and its design and materiality have been successfully adapted to the climate and local culture, according to Gutierrez (1983) and Morra (2000). The typical floor plan of a sausage-house follows a succession of rooms containing the public and private areas along a corridor facing an interior patio. The depth and articulation of these spaces may vary in different cases, but in general, they are built in narrow and deep lots. Another reference used for defining the housing system was the regulation regarding the design of social housing in Paraguay. (SENAVITAT 2011).

The house developed for this project have three sub-systems: (a) the foundation or plate consisting of shallow foundations of reinforced concrete square footing or bricks masonry. The foundation or plate will help to adapt the house to moderate

slope situations and terrains with high humidity lifting the construction above the existent ground level; (b) the envelope, which consists of load-bearing and non-load bearing wall panels made of waste cardboard and wood frames and reinforcements; and (c) The roof made of conventional corrugated metal panels with wood or steel trusses. The shape grammar presented in this paper supports the design of the sub-system b.

The modularity facilitates adapting the house to different situations. The system works by addition or subtraction of modules, offering the alternative of customizing the floor plan of the house. However, the modules are limited to variations of squares and rectangles. This concept facilitates the production, transportation, assembly, and, more importantly, incremental construction that is critical in urban areas in developing countries. If the system, based on modular and dry construction, is easy to understand and practical to execute, the owners would be able to build using fewer resources and technical assistance compared to traditional masonry or concrete framing. An easy disassemble process could allow reusing the components and reducing waste in case of transformations or demolition.

**4. Methodology**

The project implements a shape grammars formalism as a tool for structuring the design and fabrication of the building parts for the envelope of the house using waste cardboard and wood frames. Shape grammar is a ruled-based algorithmic system used to create and understand designs through the computation of shapes and to define design languages (Knight 1989). This methodology has been extensively used to depict the construction logic of existing architectural elements as well as to generate new designs. The literature includes examples of modular systems (Duarte 1993), housing (Duarte 2005; Benros et al. 2011), masonry wall types (Vazquez 2017), among others. This project builds on this existing body of knowledge and proposes a novel application of shape grammars to describe the design and fabrication of cardboard architectures with the goal of upscaling a waste material. Table 1 illustrates the structure of the grammar for better understanding. This paper first describes the proposed shape grammars, and then we provide an initial validation of the grammar by an internal test through the design of a house.

Table 1. Structure of the Proposed Grammar.

	<b>Design Grammar</b>	<b>Rules</b>	<b>Fabrication Grammar</b>	<b>Rules</b>
	Lot Definition and First		Walls Reinforcement	
	1 Room Placement	0 and 1	Placement	8.1 to 10.5
Stage	2 Spatial and Structural		Wall Panels Floor Plan	
	Grid Design	2.1 to 2.8	Configuration	11 to 12.2
			Wall Panels Elevation and Doors/Windows	
	3 Function Definition	3.1 to 7.4	Placement	13.1 to 14.6
			Wall Panels	
	4		Construction Details	15.1 to 15.3



### 5. Modular Grammar

In *stage 1 of the modular grammar*, the designer defines the size of the lot and places the first room (rules 0 and 1). The local regulation does not allow a lot with less than 360 m<sup>2</sup> with few exceptions and establishes a width of between 10 m and 14 m. The program brief of this project includes a living room (12 m<sup>2</sup>), kitchen (8.5 m<sup>2</sup>), dining room (4.5 m<sup>2</sup>), bathroom (4 m<sup>2</sup>), master bedroom (15 m<sup>2</sup>), secondary bedroom (11 m<sup>2</sup>), bathroom (4 m<sup>2</sup>) and interior circulation (around 10% of the total surface). The next step is the placement of the first room in the lot. Rule 1 establishes specific parameters related to the size of the room—minimum width 2.5 m and maximum with 5 m—and its distance to the perimeters of the lot. For example, the minimum distance between the first room and the front limit is 3 m, and the minimum distance to the sides and back limits is 1.5 m.

*Stage 2 of the modular grammar* (rules 2.1 to 2.8) defines the spatial/structural grid of the house. This set of rules defines the spatial organization of the house. Stage 2 starts with the placement of the porch on the side of the first room and follows with the longitudinal growth of the house (rules 2.1, and 2.2). Lateral growth of the grid beside the placement of the porch is not allowed in this project. The rules also allow placing “gaps” in the grip to create small patios or to divide the house into two if necessary (rule 2.3). Rules 2.4 and 2.5 permit the designer to modify the grid by shrinking or enlarging a specific room. Rules 2.6 and 2.7 create subdivisions inside a room to give space for a corridor for internal circulation. Rule 2.8 integrates two adjacent spaces.

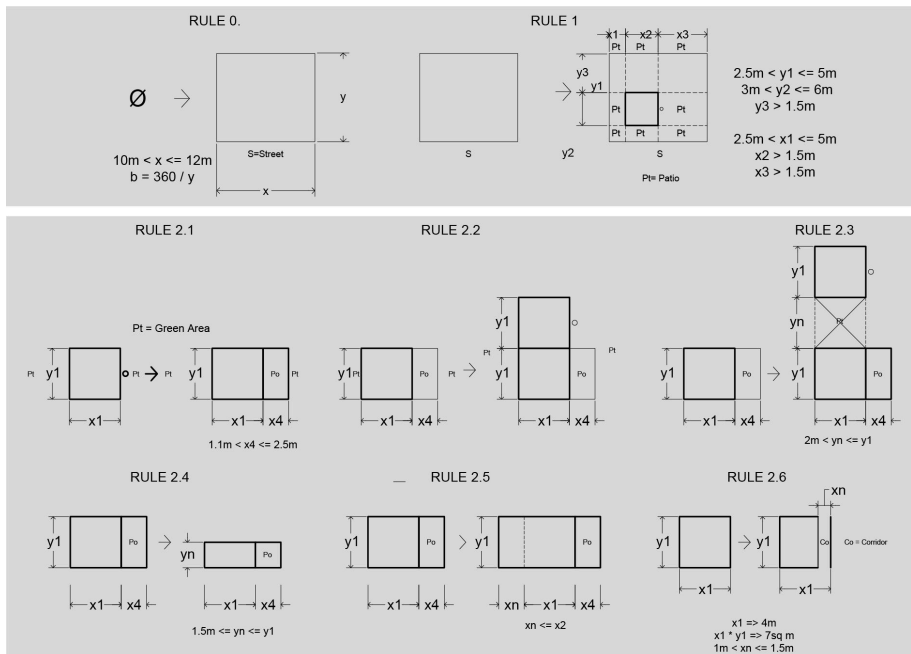


Figure 1. Partial rules for stages 1 and 2 of the modular grammar.

Stage 3 of the modular grammar includes rule 3.1 to 7.4 and deals with adding function to each one of the modules of the grid. This project considered five main functions: Living area (rules 3.1 and 3.2), kitchen (rule 4), dining area (rules 5.1 to 5.4), bedroom (rules 6.1 to 6.5), and service unit that includes the bathroom and laundry area (rules 7.1 to 7.4). The living area connects to the dining room and kitchen, and the bedrooms can be placed either in connection to the living or the kitchen. The service unit can be linked to a bedroom or a kitchen only. Take note that the porch goes along the house always, and eventually, part of it can be enclosed and transformed into a living extension, dining room, or bedroom extension.

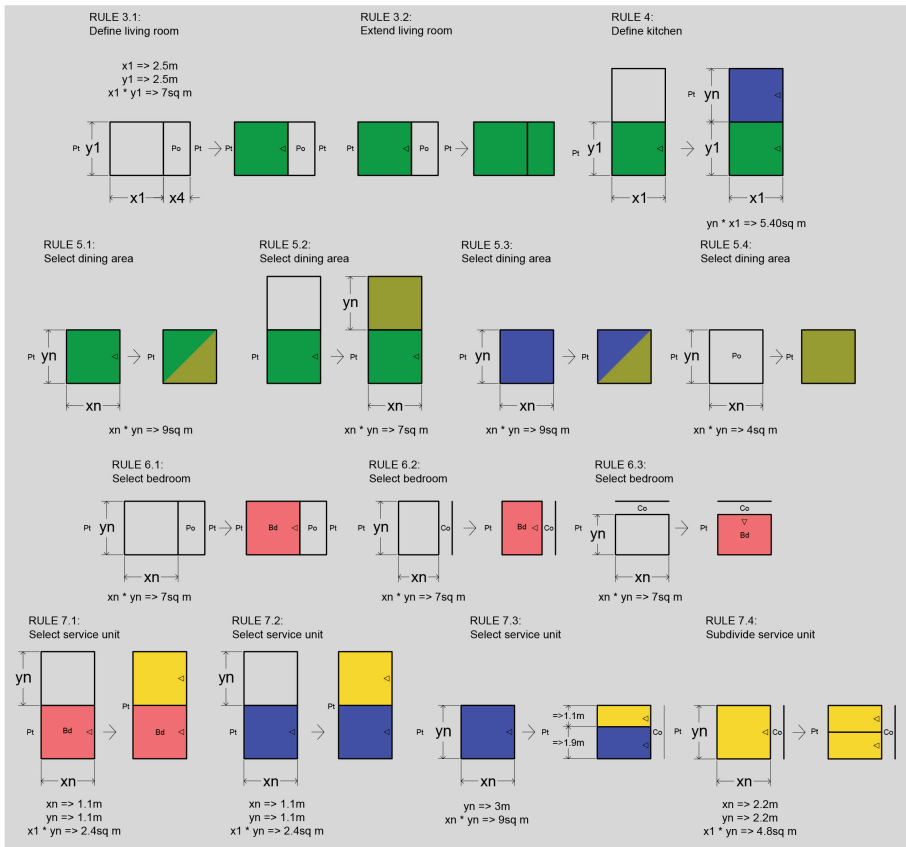


Figure 2. Partial rules for stage 3 of the modular grammar.

## 6. Fabrication Grammar

Stage 1 of the fabrication grammar focuses on the placement and definition of the columns for reinforcement (rule 8.1), definition of thicknesses of walls (rule 8.2), placement for doors (rules 9.1 to 9.5), and modification of the design of the

walls (rules 10.1 to 10.5). The size of the columns depends on the material used; however, each side of the column can vary between 10-30 cm. The columns are placed at the intersection of the segments that form a module. The thickness of the walls varies between 5-20 cm, depending on the function of the wall. For partition walls, the thickness is between 5-15 cm, and for load-bearing walls, the thickness is between 15-20 cm. The placement and position of doors are restricted by the size of the room and the location of the corridor next to the room. The modification of the walls allows the designer to integrate rooms to create larger spaces and to control the level of openness of the porch. The outcome of the first stage is a floor plan of the house showing the spatial and functional configuration.

*Stage 2 of the fabrication grammar* deals with the constructive part of the wall system. Rule 11, for instance, takes each segment of the wall between columns and subdivide it into panels. These panels can have thicknesses between 5-10 cm, 10-15 cm, and 15 and 20 cm. The thickness of the panel constrains its length, and this can vary between 0.25-0.50 m for the first category of walls, 0.50-1.0 m for the second category of walls, and 1-1.25 m for the third category of walls. Rule 12.1 and 12.2 control the placement and length of windows that can vary between 0.40-1.60 m wide and occupy the length of one or two panels. Stage 2 offers a detailed floor plan illustrating all wall panels of the house. Figure 3 shows some of the rules of stages 1 and 2.

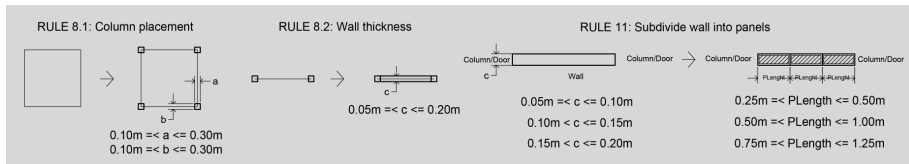


Figure 3. Partial rules for stages 1 and 2 of the fabrication grammar.

The rules in *stage 3* determine the elevation of each segment of the walls of the house. Rules 13.1 to 13.4 produce the elevation of columns, doors, and windows. The next group of rules (rules 14.1 to 14.6) take the floor plan of the panels given by the previous stage and produce the elevation of the frame that forms the panel. The dimensions of the frame vary depending on the condition of the panel. This project considered three situations: a panel between panels, the panel between a column and a panel, and the panel between columns. Constructively, the adjacent wall panels share vertical studs except when they are next to a window or door. Panels that are part of the windows or doors have their vertical studs.

*Stage 4* includes rules 15.1, 15.2, and 15.3. These rules advance the details for the manufacturing of the panels. The goal is to subdivide the panels into triangular profile tubes using sheets of waste cardboard. These tubes are glued together to form the cardboard panels that will be used to fill and reinforce the wood frames. The criteria for defining the dimension of the triangular profile tubes rely on the thickness of the panel. Rule 15.1 controls this configuration and then rules 15.2 and 15.3 places and multiply the profiles until completing the total length of the wall panel.

The *fabrication grammar* concludes with the application of the parametric grammar presented in (Diarte et al. 2019a). The parametric grammar takes the dimensions of the triangular profile tubes and determines the cutting, scoring, and folding patterns to produce the tubes for the cardboard panels. The parametric grammar, in combination with the modular and fabrication grammar, produce the instructions for the fabrication of the cardboard panels. Figures 5, 6, and 7 show the rules 13.1 to 15.3.

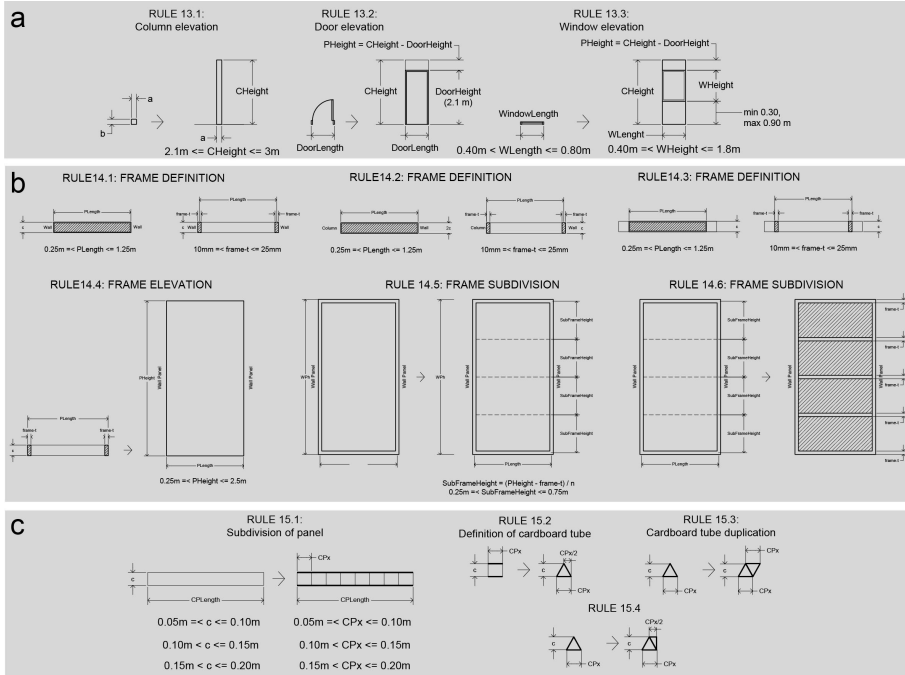


Figure 4. (a) Elevation rules (b) Frame design rules (c) Cardboard panel fabrication rules.

## 7. Results

The grammar was implemented to show possible design iteration generated with the rules. For this purpose, we produced the floor plan of a single-story house of 84.4 m<sup>2</sup> for a lot of 360 m<sup>2</sup>. The design follows some of the criteria found in the sausage-house typology, especially the linear organization of the rooms along a porch facing a patio. However, certain aspects differ from the precedent, for instance, the separation of the house from the left limit of the lot—to allow cross-ventilation of interior spaces—and the partial occupation of the porch for extending the bedroom or placing the dining room. The outcome represents a variation of the precedent within the language of the original typology.

Some features that could be improved in the *modular grammar* are the following: First, the integration of the rules for designing the structural/spatial grid with the assignment of functions. An alternative for doing this is by having a

library of pre-set spaces with the established minimum dimensions and in different configurations to help synthesize the design of the scheme for the floor plan. Second, the rules for modifying the grid can be useful for trained designers who use the grammar; however, it is not certain these rules can be helpful for non-designers who want to take advantage of the grammar for designing their own houses. Third, although the final floorplan presented in this paper can be considered satisfactory in terms of architectural qualities, the grammar does not prevent undesired outcomes, which is crucial for future computer implementation of the grammar. To control undesired outcomes is necessary to include more specific rules to restrict certain relations between spaces. Figure 8 illustrated the derivation of the rules of the *modular grammar*.

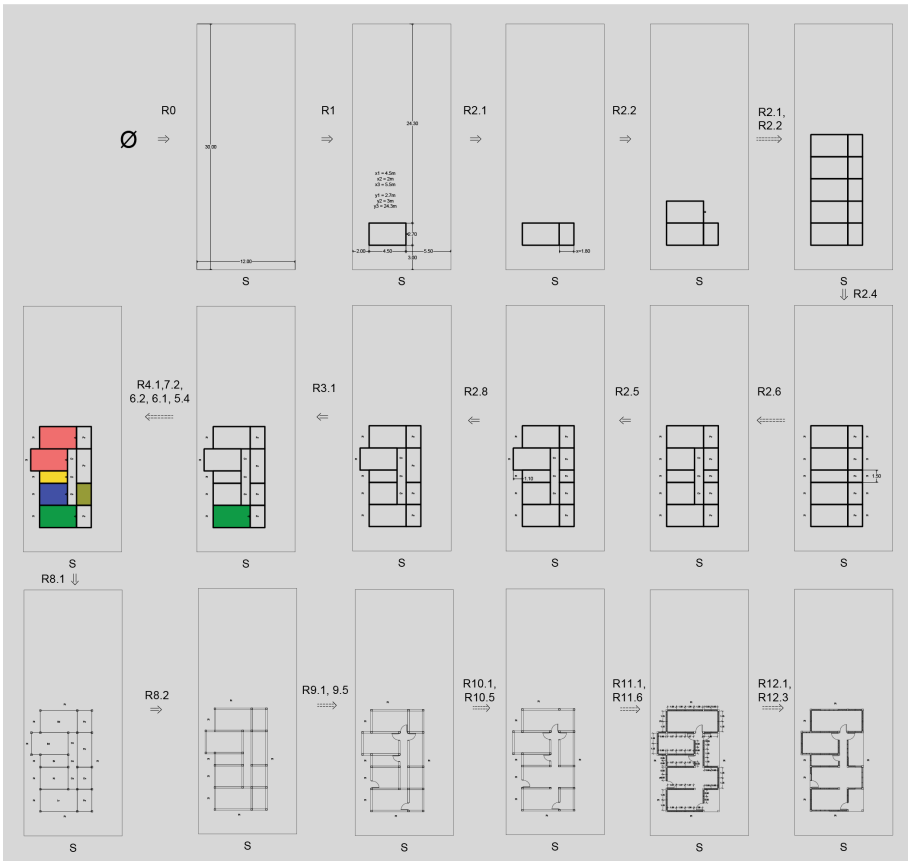


Figure 5. Derivation of rules of the modular grammar.

The *fabrication grammar* allowed for the definition of some construction details for the wall system and the outline of the facades, including wall panels, windows, and doors. The *fabrication grammar* also provided templates for cutting and scoring the sheets of waste cardboard. However, some details could be added

to the grammar. First, the grammar facilitated the design of the floor plan of the wood frames and offers the elevations for each wall but still needs more rules that depict more clearly fabrication instructions. Second, the design and fabrication criteria for the interior and exterior facing of the panels are not included in the grammar yet. Third, a step-by-step assembly instruction process needs to be included to make possible the actual production of the building parts. Four, although the integration of the parametric grammar produced in a previous study is useful and contributes substantially to this project, we still need to test the integration of both systems. Further work will investigate the integration of both tools in a single case study. Figure 9 shows the derivation of rules of the *fabrication grammar*.

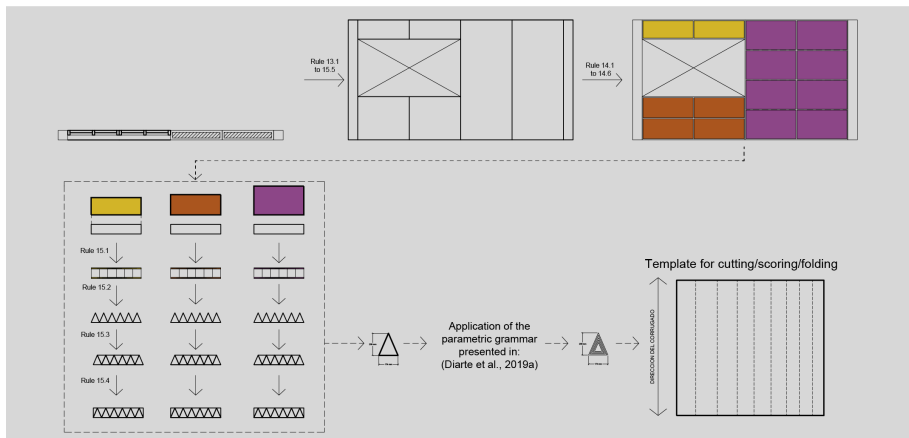


Figure 6. Derivation of rules of the fabrication grammar .

## 8. Conclusion

The work shown in this paper contributes to ongoing research aimed at developing tools and methods for upcycling waste corrugated cardboard. The outcomes include a grammar-based design tool for configuring modular houses and a set of rules for providing fabrication instructions for making wall panels made with wood and waste corrugated cardboard. Different types of rules were extracted in the proposed two-level grammar: design rules and fabrication rules.

The second section of this paper shows how the *modular grammar* and *fabrication grammar* can be implemented in the design of a house in the proposed typology. The proposed rules can conform to a rule-based generative system. However, further work will focus on testing the applicability of the grammar for different iterations of the typology and improving the fabrication instructions for the waste cardboard and wood-framed panels.

This project aims to contribute to providing methods for increasing the upcycling rate of waste corrugated cardboard in urban areas in low-income countries. We argue that waste corrugated cardboard—in combination with other

materials—can be reused as an alternative low-cost and sustainable building material for people who needs housing but cannot afford using only standard building systems. By formalizing a modular housing system with the grammar, we propose a novel way of reusing waste corrugated cardboard, in the form of hybrid wood-cardboard panels.

## References

- Benros, D., Granadero, V., Duarte, J.P. and Knight, T.: 2011, Automated Design and Delivery of Relief Housing : The Case of post-Earthquake Haiti, *Proceedings of the 14th International CAAD Futures Conference*, 1, 247-264.
- Diarte, J.: 2020, Tapping into Urban Recycling for Low-cost Building Alternatives: Experimenting Waste Cardboard Reuse in Architecture, *Proceedings of Divergence in Architectural Research 2020 Conference*, Atlanta.
- Diarte, J., Vazquez, E. and Shaffer, M.: 2019, Tooling Cardboard for Smart Reuse: A Digital and Analog Workflow for Upcycling Waste Corrugated Cardboard as a Building Material, *Computer-Aided Architectural Design. "Hello, Culture"*, Singapore, 384-398.
- Diarte, J., Vazquez, E. and Shaffer, M.: 2019b, Tooling Cardboard for Smart Reuse - Testing a Parametric Tool for Adapting Waste Corrugated Cardboard to Fabricate Acoustic Panels and Concrete Formwork., *Architecture in the Age of the 4th Industrial Revolution - Proceedings of the 37th eCAADe and 23rd SIGraDi Conference*, Porto, 769-778.
- Duarte, J.: 1993, *Order and Diversity Within a Modular System for Housing : A Computational Approach*, Master's Thesis, MIT.
- Duarte, J.P.: 2005, Towards the mass customization of housing: The grammar Siza's houses at Malagueira, *Environment and Planning B: Planning and Design*, **32**(3), 347-380.
- M. Eekhout, F. Verheijen and R. Visser (eds.): 2008, *Cardboard in Architecture*, IOS Press, Amsterdam.
- Gutierrez, R.: 1983, *Evolucion Urbanistica y Arquitectonica del Paraguay, 1537-1911*, Ediciones Comunerros, Asuncion.
- IADB, : 2015, "Solid Waste Management in Latin America and the Caribbean". Available from <<https://publications.iadb.org/handle/11319/7177e1xtbackslash#sthash.7bODjAHq.dpuf>> (accessed 3rd December 2019).
- Knight, T.: 1989, "Shape Grammars in Education and Practice: History and Prospects" . Available from <<http://www.mit.edu/~tknight/IJDC/>>.
- Latka, J.F.: 2017, *Paper in Architecture: Research by Design, Engineering, and Prototyping*, Ph.D. Thesis, The Delft University of Technology.
- I. Luna and L.A. Gould (eds.): 2009, *Shigeru Ban: Paper in Architecture*, Rizzoli International Publications, New York.
- Morra, C.: 2000, *Espacios intermedios*, Arquitrabe, Asuncion.
- Pohl, A.: 2009, *Strengthened corrugated paper honeycomb for application in structural elements*, Ph.D. Thesis, ETH Zurich.
- Salado, G.d.C.: 2011, *Painel de vedacao vertical de tubos de papelao: Estudo, proposta e análise de desempenho*, Ph.D. Thesis, Universidade de Sao Paulo.
- SENAVITAT, : 2011, "Reglamento de programas habitacionales" . Available from <<https://www.muvh.gov.py/descargasfonavis/Reglamento-Programas-Habitacionales.pdf>> (accessed 10th October 2019).
- Vazquez, E.: 2017, A grammar of Perforated Masonry Walls. A formal analysis of brick walls used for shading and ventilation in Paraguay, *XXI Congreso Internacional de la Sociedad Iberoamericana de Grafica Digital*, Sao Paulo, 544-551.

# FLOWUI: COMBINING DIRECTLY-INTERACTIVE DESIGN MODELING WITH DESIGN ANALYTICS

HALIL ERHAN<sup>1</sup>, MARYAM ZAREI<sup>2</sup>, AHMED M. ABUZURAIQ<sup>3</sup>,  
ALYSSA HAAS<sup>4</sup>, OSAMA ALSALMAN<sup>5</sup> and  
ROBERT WOODBURY<sup>6</sup>

<sup>1,2,3,5,6</sup>*Simon Fraser University*

<sup>1,2,3,5,6</sup>*{herhan|mzaree|aabuzura|oalsalma|rw}@sfu.ca*

<sup>4</sup>*Stantec Vancouver*

<sup>4</sup>*alyssa.haas@stantec.com*

**Abstract.** In a systems building experiment, we explored how directly manipulating non-parametric geometries can be used together with a real-time parametric performance analytics for informed design decision-making in the early phases of design. This combination gives rise to a design process where considerations that would traditionally take place in the late phases of design can become part of the early phases. The paper presents FlowUI, a prototype tool for performance-driven design that is developed in a collaboration with our industry partner as part of our design analytics research program. The tool works with and responds to changes in the design modeling environment, processes the design data and presents the results in design (data) analytics interfaces. We discuss the system's design intent and its overall architecture, followed by a set of suggestions on the comparative analysis of design solutions and design reports generation as integral parts of design exploration tasks.

**Keywords.** Non-Parametric Modeling; Performance-Driven Design; Design Analytics; Information Visualization.

## 1. Introduction

Designers use multiple computational tools throughout the life cycle of a design project. The tool selection and use are consistent with the task at hand and the level of design resolution at any given phase. An obvious challenge for designers is the limitation of tools for binding different design representations across them with varying levels of details. This challenge is emphasized when designers take advantage of divergent exploration of form by directly manipulating design geometries as if they are 'sculpting' in the early phases of design. They miss the advantage of using the capabilities of parametric modeling for computing performance data for informed exploration (Touloupaki and Theodosiou, 2017). On the other hand, designing using parametric modeling tools lacks the flexibility of using the sculpting features of directly interactive CAD tools. Analysis systems are used after the design is substantially developed and to validate the design



performance and to maximize the efficiency of an already established geometry (Anton and Tanase, 2016). In this paper, we present a system addressing this challenge as part of a larger research program focusing on how to bring design exploration with data analytics using interactive visualizations, in short, which we call this program *design analytics*.

In a system's building experiment with our industry partner, we developed a flexible prototype tool to simplify and develop a seamless workflow in moving between form-finding and performance analysis in design. The prototype system adapting this architecture, called FlowUI, receives pure geometric definitions of the design models that are under development; pulls desired performance data; computes select performance metrics; and presents the data through interactive visualizations for analysis and decision-making. This experiment also suggests system features for making a comparative analysis of design alternatives and their relative performances in this workflow. The FlowUI's interactive visualizations facilitate a comparison of alternatives considering calculated and target-performance metrics. Our initial observations and the feedback we received from our industry partner present encouraging evidence that applying the FlowUI's features in practice can improve design exploration.

Below, we first discuss the motivations of the study and development of FlowUI, its high-level requirements and the architecture. This is followed by the introduction of FlowUI's interfaces as an add-on for a directly-interactive geometric modeling tool, Rhinoceros 3D (McNeel, 1998) and interactive visualizations using Grasshopper's parametric capabilities for computing performance data from non-parametric models. We also present FlowUI's platform independent interfaces for data visualization, comparative analytics, and reporting. We conclude with our reflection on the potentials and limitations of the solutions we propose and future work.

## **2. Engaging Design Form-Sculpting with Data Analysis**

### **2.1. PARAMETRIC VS DIRECT MODELING OF DESIGN CONCEPTS**

The current parametric CAD tools have features to support the analysis of parametric designs' performance for informed decision making in the design development process (Danhaive and Mueller, 2015; Touloupaki and Theodosiou, 2017). However, taking advantage of these features requires a systematic parametric setup of a design model (Fu, 2018) that restricts the exploration of diverse alternatives from different designs. The designers working on concept development may not prefer parametric modeling to directly-modeling of geometric forms or lack the skills of using parametric tools (Zarei, 2012). In such cases, they use directly-interactive modeling tools like SketchUp or Rhino for sculpting forms, e.g. for mass-modeling or form exploration without committing to one parametric model. Directly-modified design models as geometric forms are preferred for their agility and low-effort for initial design setup (Hanna, 2012; Megahed, 2015). However, the analysis of non-parametric design models developed using directly-interactive modeling tools is highly limited (Weytjens et al., 2012; Soebarto et al., 2015): designers are required to take additional

data-processing steps that may hinder design exploration flow by reducing the chance of getting immediate performance feedback (Soebarto et al., 2015). Another disadvantage is that the models are built using purely geometric elements and the design performance details are only left to the designers' interpretation without further computational processing (Zapata-Lancaster and Tweed, 2016).

The literature covers form exploration using computational methods extensively. The notable different methods include Harding and Shepherd's (2016) Meta-Parametric Design that combines parametric modeling with genetic programming to widen design exploration with graph representation. In an earlier work, Bentley and Kumar (1999) explored the use of growth processes within evolutionary systems. For using non-manifold geometries for form and performance exploration, Jabi et al. (2018) propose hierarchical and topological representations of architectural spaces as part of parametric data flow models.

## 2.2. PERFORMANCE-DRIVEN DESIGN

Performance-driven design is gaining momentum mostly in the context of sustainability because it provides a shift from focusing only on form to emphasizing the balance between the traditional concerns of architectural design and building performances (Shi, 2010). This requires an agile analysis of performance metrics. However, the frequently used simulation programs such as EnergyPlus (Crawley et al., 2001) and Ecotect (Roberts and Marsh, 2001) require design models to be restructured for their computational format. Once a model is set up, the simulation program is called upon to analyze one or several select performance metrics. The simulation results are then analyzed. The designers modify the design based on the result of the analysis to improve their design. The process, in essence, is discrete and several modifications needed to achieve the desired outcome. However, the iteration is often not conducted fully in practice for many reasons among which it requires a sudden stop in design and computing design performances followed by form revision (Shi, 2010). Furthermore, these iterations are more appropriate in the late phases of design when most design decisions are already committed, which limits the divergent search.

## 2.3. TOOLS FOR PERFORMANCE-DRIVEN DESIGN

There are two categories of computational tools proposed to address the challenges above. In the first category, the tools work as an add-on on an existing design platform. These tools in general link a parametric definition to one or multiple performance computing modules, e.g. Ladybug for Grasshopper (Sadeghipour Roudsari and Pak, 2013) for environmental analysis. The design data may not be directly accessible through these tools and may require using external tools or set up to reveal the data. The second category provides interfaces that bring one or multiple add-ons together to allow designers to access the computed performance data from parametric models. *Reach* is an example of this category of tools (Wang and Steenblik, 2019). Both categories have a set of common restrictions: (a) they mainly require a well-defined model, which may not be preferred due to the cost of initial setup; (b) the add-ons used assume a complete set of inputs to be decided for computing design performances, which may not be available in the

earlier exploration phases. Hence, the iterative cycle of formation, performance computing, and analysis is rather prematurely executed. A change in the design, then, may require substantial revisions in the setup, which can limit the search to a few well-structured parametric models rather than an abundance of solutions. In addition, these tools fall short for directly working with design data available through other sources, e.g. program requirements in a spreadsheet. In addition, we believe that the most important bottleneck of these tools is that they continue to support single-state models that at any given time, only one design becomes the locus of attention of the designers. This hinders the comparative analysis of design alternatives explored along with their performance data hinting each alternative's potentials or drawbacks. Focusing on multiple alternatives together with their associated data helps designers to evaluate options as they are created.

### 3. FlowUI: Engaging Design with Data

The discussed challenges and bottlenecks of geometric or parametric modeling tools can be among the most salient ones faced by designers. We propose that we can overcome these challenges by tools that seamlessly support design decision-making in the early phases of design exploration and without creating an additional task layer. Our goal is to create a system solution to simplify the creation and evaluation of alternative design forms by learning from only relevant data to the task at hand. Below, we present the higher-level requirements, the conceptual architecture, and interfaces for this system, which we call FlowUI. The system attempts to provide a flexible and simple interaction combining directly-editable geometric models, visualization of design performances, association with external data, and dashboards for comparative analysis and reporting.

#### 3.1. DESIGN CRITERIA

The design criteria of FlowUI were developed over time with our partner from the AEC industry during a research collaboration. The criteria emerged through an iterative process where the requirements, system architecture, and interfaces evolved based on the feedback received from professional designers. Below are some of the high-level criteria highlighting the basic system features of FlowUI.

**Allow form-first exploration:** In practice, not all design cases prefer parametric modeling, but definitely almost all need to reveal at least some aspects of design information that are not obvious on the geometry. Sculpting design forms by moving between sketches and geometric modelers directly is a powerful combination for design ideation. This should be supported by continuously maintaining performance analysis. The goal is to enable accessing design data as early as possible without building a well-structured model. This is design-first interaction rather than emphasizing data and parameter.

**Incorporate program as input:** Designers should be able to associate their emerging design criteria with the design being explored and use the performance data computed for evaluating the form and the program. The program may include definition of the function types, the assignment of functions to building blocks, the definition of custom properties such as labels, floor heights, unit cost, etc.

The system should be able to visualize target values e.g. for budget constraints or usable areas. These values are externally defined and expressed as tentative targets that can change over the course of the design: if one source changes, the tool should propagate the change to maintain consistency between computed and target values without disturbing the design flow.

**Enable context definitions:** The context details can include site data, existing structures, desired view targets, location, environmental data, etc. The tool should allow designers to use this, possibly as non-parametric, information only when relevant and incorporate in computing performance values.

**Manage multiple design ideas:** This can be in the shape of: an effortless switching between design alternatives, recording and recreating different iterations on a design option, supporting a multi-state comparison and manipulation of design alternatives. The tool should coexist or refine the ability to explore alternatives in relation to their performance data. Any tool working with alternatives should also support the creation of a report on individual or compared alternatives for sharing with other stakeholders.

**Accommodate diverse design-analysis scenarios:** This can take the form of a flexible interface layout, the ability to constrain the performance calculations, and providing means for analyzing multiple aspects of an alternative at the same time. The tool should be configurable to enable different aspects of design as desired.

### 3.2. SYSTEM ARCHITECTURE AND DESIGN WORKFLOW

The system architecture of FlowUI is built on three functional modules: Design Modeling, Data Extraction, and Design Performance Analytics (Figure 1). The architecture specifies a structure for organizing the interfaces and their use considering the high-level requirements discussed above. The design exploration task workflow starts with creating design models as non-parametric geometries using the directly-interactive CAD tool. The Design Modeling module is a custom setup that enables defining the context, establishes custom attributes, and creates a layer structure where alternative solutions are stored and retrieved. Designers can associate a geometry by a program criterion, e.g. type of building function, in the Design Modeling module. Independent from the parametric modeling, designers can explore forms using manifold geometries in any technique, e.g. for changing geometry by pushing-pulling or using solid modeling operations.

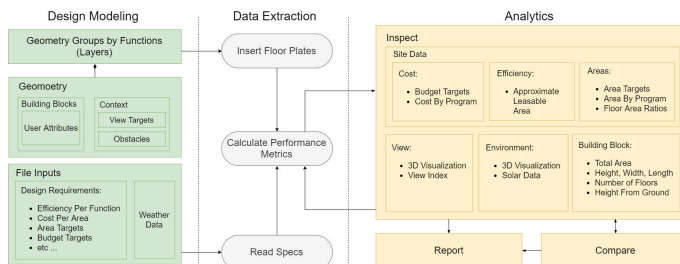


Figure 1. The architecture of FlowUI: non-parametric design modelling coupled with parametric data computing and supported by interactive data visualization dashboard.

The modeling setup directly links geometries to the Data Extraction module which recognizes the functions and program requirements associated with the geometries. This module has a parametric definition that can be extended to compute additional aspects of design when needed. The DE module is also linked to external data sources to retrieve design program data.

On the interfaces in the Design Analytics module, designers can select the relevant data for the task at hand to be computed and visually displayed. They include construction cost estimates, efficiency in area use, view quality, environmental metrics, etc. These visualizations are presented in a configurable dashboard layout (Figure 2) and assist designers to investigate each alternative as they are changed in the Design Modeling setup in Rhino. As part of the FlowUI ecosystem, we also developed two additional interfaces as design analytics of alternatives and reporting. These interfaces are used for further comparison and reporting of design alternatives in a Web browser outside of the FlowUI setup but are directly linked with the FlowUI Data Analytics module. These interfaces are further discussed below.

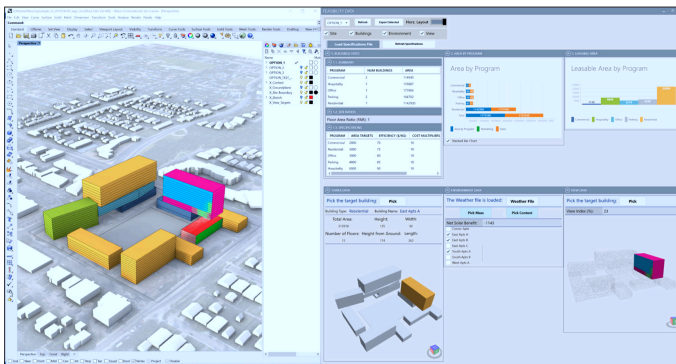


Figure 2. FlowUI interface: Directly sculpted massing model in Rhino analyzed and corresponding data is selectively presented in FlowUI's dashboard in real-time or on-demand.

### 3.3. FLOWUI TOOL FEATURES, INTERFACES, AND INTERACTION

FlowUI is a tool of performance-driven design aimed at mixed-use massing problems that have interrelated objectives and constraints channeled through form-finding. FlowUI provides immediate feedback about the performance of alternatives and enables comparison to design goals. The main components of the FlowUI interface are composed in the Data Analytics (DA) dashboard. They visualize the results of the performance calculation through textual and visual formats. The FlowUI DA dashboard can be arranged to be a vertical slice that occupies a small portion of the screen, or a horizontal mode that expands as needed in a multi-screen setting. The horizontal mode makes it possible to track all the performance visualizations simultaneously. The visualizations are organized in layers and change in response to changes in the modeling environment. Switching between design alternatives is performed on the dashboard that activates the

selected alternative in the Design Modeling.

The visualizations in the DA dashboard are three types: simple bar charts dedicated for showing the floor area and cost of each building function; 3D views visualizing different aspects of the design forms such as the view quality; the solar energy across the year, etc. The 3D views are built upon the user interaction with the geometry to enable a granular level of details. The tables show the design targets such as the sought floor areas and the budget limits, building dimensions, and floor areas. The DA dashboard responds automatically to changes in the modeled geometry, but it requires an on-demand update for the changes in the modeling module layer structure. This limits the frequency of updates in response to events that are less relevant for the task.

### 3.4. COMPARATIVE ANALYTICS AND REPORTING

However, a comparison can be the basis for the cross-pollination of design ideas. Comparisons can reveal the impact of the design form choices on the performance metrics. To enable comparative analysis, we retain the act of design exploration and use the FlowUI as a mediator through which satisfactory alternatives can be sent to an external environment to compare them against other alternatives or shared with other stakeholders. We studied a number of existing design explorer solutions proposed in the literature. These include interactive visualization dashboards for comparative analysis of design alternatives (Woodbury et al., 2017; Matejka et al., 2018; Tomasetti, 2019). While FlowUI output can be exported to be used with these systems, in FlowUI models are directly linked with data visualizations (Figure 2).



Figure 3. The interface design for the design analytics dashboard enabling comparison of alternatives based on the design and performance data.

Our ongoing development of a design analytics explorer interface (Figure 3) we combine visualizations showing design similarity along with their geometric forms and performance data. Although the main goal of the interface is to enable simplifying and exploring design spaces, selected solutions can be pushed back to FlowUI (Abuzuraiq and Erhan, 2020). On the FlowUI DA, the local version of the chosen alternative can be reactivated on-demand, and all the views on the DA are updated. Hence, the designer can study the chosen alternative in more details. This idea of ‘restoring’ an alternative from an external design analytics

context is borrowed from Woodbury et al. (2017). We extended their approach to non-parametric modeling of design alternatives.

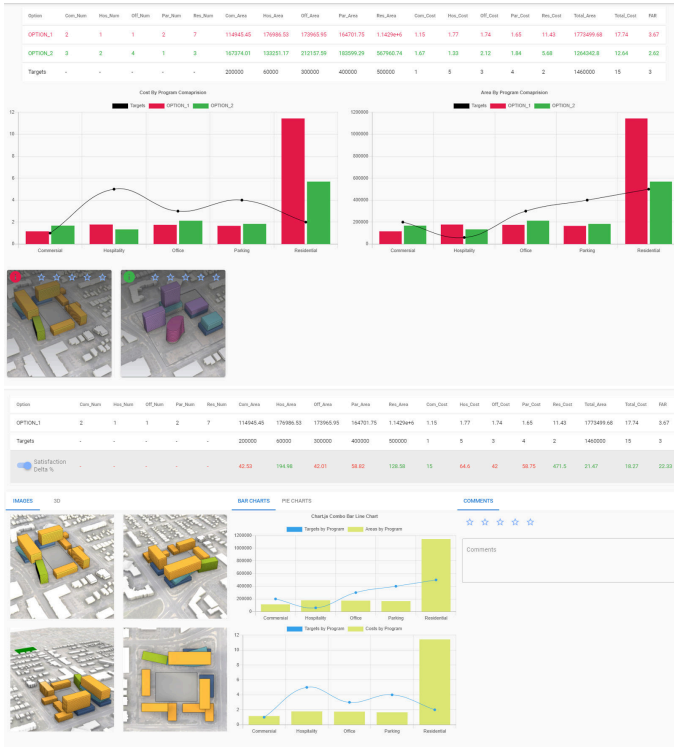


Figure 4. FlowUI Alternatives Reporting Tool. (Up) Two alternatives are compared side-by-side with their corresponding performance data visualized on a data table and bar graphs (Down) One alternative with views and corresponding data shown.

The FlowUI Alternatives Reporting Tool (ART) supports generating interactive reports that can be used to present and further study the selected alternatives. It relies on the data-sharing model of the FlowUI for retrieving select design alternatives for reporting that are updated on-demand. An important role of the ART is to help designers reflect in and share about their search process with other stakeholders. While the DA dashboard focuses on analytics, the ART focuses on reflection and presentation. It consists of three main visualizations. The first is an overview that displays alternatives in a juxtaposed layout for an overall evaluation. Its grid size and density can be adjusted by the designer to show alternatives in different multiples. The ART provides ranking and commenting functions for each alternative. The comparison visualization, the second view, shows multiple snapshot views or a 3D model of the design along with data graphs for a detailed evaluation of a set of selected alternatives (Figure 4 (Up)). The third view displays one alternative in detail with its form and performance data. The views are dynamically linked and support *highlighting* and *brushing* interactions

across the views. In this view, the stakeholders can comment and rank the solutions (Figure 4 (Down)). The stakeholders can decide what aspects of performance metrics are to be compared in this view and can generate printable reports.

#### 4. Reflection and Conclusion

The use of parametric modeling tools in the early phases of design is different than the later phases: the prior may use parametric definitions for form exploration and the latter for detailing structural elements for fabrication. Parametric models are labor-intensive to build and are rarely fully reusable, more so for complex and large projects. However, they also present computational capabilities that can reveal salient design aspects quickly. The directly-interactive CAD modelers provide agility for sculpting design geometries in the early phases of design and make a divergent, almost sketch-like, exploration possible. To take advantage of the benefits of both approaches, we proposed a systems approach supporting direct-modeling of geometries, performance computation by feeding design geometries to a parametric definition, and interactive visualization of design alternatives with their form and data. This aims to let designers work in a way that is familiar to them while leveraging real-time data analysis and reporting. The first functional iteration of the FlowUI shows the potentials for design exploration. However, it falls short for being practical to be used in a professional setting. Aside from its reliability, the system's fragmented modules should be better integrated in the workflow. We also think that there are opportunities for improving the overall workflow before we conduct a proper user testing. We plan to demonstrate the use of the prototype in a realistic design scenario borrowed from the industry. We think that our work on design analytics interfaces may make a positive change in the computational design task environments as the research matures and the prototypes become usable in time. For future work, we will conduct a series of case studies to test the FlowUI and ART's integration into the design workflow.

#### Acknowledgment

This research was supported by the MITACS Accelerate Program of Canada [IT12326] in partnership with the Boeing Company and Stantec Vancouver.

#### References

- Abuzurairq, A.M. and Erhan, H.: 2020, Many Faces of Similarity: A Visual Analytics Approach for Design Space Simplification, *25th International Conference on Computer-Aided Architectural Design Research in Asia: Design in the Age of Humans, CAADRIA 2020*.
- Anton, I. and Tănase, D.: 2016, Informed Geometries. Parametric Modelling and Energy Analysis in Early Stages of Design, *Energy Procedia*, **85**, 9-16.
- Bentley, P.J. and Kumar, S.: 1999, Three Ways to Grow Designs: A Comparison of Embryogenies for an Evolutionary Design Problem, *Proceedings of the Genetic and Evolutionary Computation Conference (GECCO 1999)*, Orlando, Florida, USA, 9.
- Crawley, D., Lawrie, L., Winkelmann, F., Buhl, W., Huang, Y., Pedersen, C., Strand, R., Liesen, R., Fisher, D., Witte, M. and Glazer, J.: 2001, EnergyPlus: Creating a New-Generation Building Energy Simulation Program, *Energy and Buildings*, **33**, 319-331.
- Danhaive, R. and Mueller, C.: 2015, Combining parametric modeling and interactive optimization for high-performance and creative structural design, *International Association*



- for Shell and Spatial Structures (IASS) Symposium*, **0**(20), 1-11.
- Fu, F. 2018, Chapter Six - Design and Analysis of Complex Structures, in F. Fu (ed.), *Design and Analysis of Tall and Complex Structures*, Butterworth-Heinemann, 177-211.
- Hanna, R.: 2012, Parametric tools in architecture: A comparative study, *Design Research*, **12**, 39-47.
- Harding, J. and Shepherd, P.: 2016, Meta-Parametric Design, *Design Studies*, **0**, 25.
- Jabi, W., Aish, R., Lannon, S. and Chatzivasileiadi, A.: 2018, Topologic: A Toolkit for Spatial and Topological Modelling, *36th annual Education and research in Computer Aided Architectural Design in Europe (eCAADe) 2018*, Poland, 9.
- Matejka, J., Glueck, M., Bradner, E., Hashemi, A., Grossman, T. and Fitzmaurice, G.: 2018, Dream Lens: Exploration and Visualization of Large-Scale Generative Design Datasets, *Proceedings of the 2018 CHI Conference on Human Factors in Computing Systems*, New York, NY, USA, 369:1-369:12.
- McNeel, R.: 1998, "Rhino3D (v6.0)". Available from <<https://www.rhino3d.com/>>.
- Megahed, N.A.: 2015, Digital Realm: Parametric-enabled Paradigm in Architectural Design Process, *International Journal of Architecture, Engineering and Construction*, **4**(3), 175-184.
- Roberts, A. and Marsh, A.: 2001, ECOTECT: Environmental Prediction in Architectural Education, *Architectural Information Management*, **0**, 342-347.
- Sadeghipour Roudsari, M. and Pak, M.: 2013, Ladybug: A parametric environmental plugin for grasshopper to help designers create an environmentally-conscious design, *Proceedings of BS 2013: 13th Conference of the International Building Performance Simulation Association*, **0**, 3128-3135.
- Shi, X.: 2010, Performance-based and performance-driven architectural design and optimization, *Frontiers of Architecture and Civil Engineering in China*, **4**(4), 512-518.
- Soebarto, V., Hopfe, C.J., Crawley, D. and Rawal, R.: 2015, Capturing the views of architects about building performance simulation to be used during design processes, *14th International Conference of the International Building Performance Simulation Association*, **0**, 7-9.
- Tomasetti, T.: 2019, "Design Explorer: an open source web interface for exploring multi-dimensional design spaces." . Available from <<https://github.com/tt-acm/DesignExplorer>>.
- Touloupaki, E. and Theodosiou, T.: 2017, Performance Simulation Integrated in Parametric 3D Modeling as a Method for Early Stage Design Optimization—A Review, *Energies*, **10**, 18.
- Wang, W. and Steenblik, R.S.: 2019, Bespoke Tools Providing Solutions for Contemporary Problems—Novel BIM practice for architects, *Proceedings of the 24th CAADRIA Conference*, **2**, 111-120.
- Weytjens, L., Attia, S., Verbeeck, G. and Herde, A.: 2012, The 'Architect-friendliness' Of Six Building Performance Simulation Tools: A Comparative Study, *International Journal of Sustainable Building Technology and Urban Development*, **10**(5390), 237-244.
- Woodbury, R., Mohiuddin, A., Cichy, M. and Mueller, V.: 2017, Interactive design galleries: A general approach to interacting with design alternatives, *Design Studies*, **52**, 40-72.
- Woodbury, R., Williamson, S. and Beesley, P.: 2011, Parametric Modelling as a Design Representation in Architecture: A Process Account, *Proceedings of the 11th International Conference on Computer-Aided Architectural Design Research in Asia. CAADRIA.*, **0**, 10.
- Zapata-Lancaster, G. and Tweed, C.: 2016, Tools for low-energy building design: an exploratory study of the design process in action, *Architectural Engineering and Design Management*, **12**(4), 279-295.
- Zarei, Y.: 2012, *The Challenges of Parametric Design in Architecture Today: Mapping the Design Practice (Master's Thesis)*, The University of Manchester, Manchester, England.

# THE MANY FACES OF SIMILARITY

## *A Visual Analytics Approach for Design Space Simplification*

AHMED M. ABUZURAIQ<sup>1</sup> and HALIL ERHAN<sup>2</sup>  
<sup>1,2</sup>*Simon Fraser University*  
<sup>1,2</sup>{aabuzura|herhan}@sfu.ca

**Abstract.** Generative design methods may involve a complex design space with an overwhelming number of alternatives with their form and design performance data. Existing research addresses this complexity by introducing various techniques for simplification through clustering and dimensionality reduction. In this study, we further analyze the relevant literature on design space simplification and exploration to identify their potentials and gaps. We find that the potentials include: alleviating the choice overload problem, opening up new venues for interrelating design forms and data, creating visual overviews of the design space and introducing ways of creating form-driven queries. Building on that, we present the first prototype of a design analytics dashboard that combines coordinated and interactive visualizations of design forms and performance data along with the result of simplifying the design space through hierarchical clustering.

**Keywords.** Visual Analytics; Design Exploration; Dimensionality Reduction; Clustering; Similarity-based Exploration.

### 1. Introduction

In the domains of design involving physical artifacts (e.g. architectural, mechanical and industrial design), the geometric forms of design alternatives and their performance are interrelated and equally important. Each presents information relevant to different design concerns. Generative design methods, including parametric design modeling, enable the creation of a large number of design alternatives. These methods can be augmented through tools that can estimate the performance of each alternative as they are created. This design process, guided with performance metrics, can be referred to as performance-based design (Shi, 2010). The combination gives rise to a design process where considerations that would traditionally take place at late design phases can now become part of the early formative phases. This warrants attention to research for systematically reviewing and building tools for interacting with and exploring design spaces considering design performance data beyond what design catalog systems currently offer (Brown and Mueller, 2017b).

An important artifact of this process that presents both opportunities and challenges for design is the large amount and different types of design data

involving both geometry and design performance. The field of Visual Analytics combines and leverages both interactive visualizations and data analysis for the sense-making of complex and abundant data (Thomas and Cook, 2006). We suggest that we are faced with a similar challenge in design decision-making when exploring design alternatives, as addressed by the visual analytics literature. Unlike data analysis, the main task in design is form-finding given design constraints and goals as part of a design brief. Focusing primarily on data may cause a lapse in this main task, while without data, design can be full of oversights.

For better supporting this process, in this research, we propose the use of design alternatives' form and performance similarity as a way for simplifying the design space and further investigating their affordances in an interactive data visualization setting. Although previous research (Beham et al., 2014; Erhan et al., 2015; Chen et al., 2015) were based on similar arguments, the conceptual justification that derived their solutions can be further expanded and applied to better demonstrate a seamless task integration between design exploration and data analysis, which we call 'design analytics'.

In this work, we build on the argument for design space simplification (Erhan et al., 2015; Brown and Mueller, 2017b) through the techniques of clustering and dimensionality reduction which expose and exploit the (dis)similarity between design alternatives. We further extend it by integrating the results of this simplification in a larger, interactive design analysis dashboard. We also find that this similarity-based simplification of the design space has many faces, in the sense that it can be achieved via varied means, represented in different ways and most importantly, has many potential applications for design space exploration. These applications include alleviating the choice overload problem, opening up new venues for interrelating design forms and data, creating visual overviews of the design space and introducing ways of querying alternatives through form-driven criteria. We create conceptual distinctions and remark about the use of design simplification by reflecting on the examples in the literature. Finally, we take this reflection one more step and present the first iteration in this line of research of a design analytics dashboard that combines the visual representations of design forms and performance data with similarity-based representations.

## 2. Information Visualizations: Key terms and Concepts

Visual Analytics combines interactive visualizations and data analysis. We address the use of both in design exploration. We will next introduce a few concepts from the information visualization literature next then proceed to data analysis in the form of data clustering and reduction in the next section.

**Key terms:** A view is a visual representation of some data (e.g. a scatterplot is a view representing two quantitative variables). Brushing is the act of highlighting elements on a view via user interaction. Multiple Coordinated Views (MCV) are views whose visual representations are changed in interactions (e.g. brushing, filtering) on the others. Multidimensional datasets are characterized by having multiple variables/metrics per record. For example, each design alternative is a single record and can be evaluated through multiple performance metrics.

**Overview then Detail-on-Demand:** To help us understand how data visualization tools can support the task of design exploration, we can be guided by the information-seeking mantra of “Overview first, zoom and filter, then details-on-demand” by Shneiderman (1996). In this work, we focus on the visual representations (also referred to as views) that provide an overview of information. We also consider the interactions between these views and on them. An overview view is a starting point for the exploration upon which the designer can focus their attention and attend to the details.

### 3. Design Space Simplification

Clustering and Dimensionality Reduction techniques group alternatives in a way that enables a hierarchy of choice and puts order into the design space.

#### 3.1. CLUSTERING

Clustering is the process of grouping items based on their similarity. The similarity between any two alternatives can be defined in terms of a subset (or all) of their associated data such as input parameters, performance metrics or their geometric features. The subsets chosen will highlight certain aspects of the two alternatives and possibly suppress others. For example, we may compute the similarity between two tower buildings based on the difference in their heights. While this will enable us to cluster together buildings of similar heights, buildings within the same cluster can vary with respect to other aspects such as their surface area, or energy usage. Hierarchical clustering techniques produce a tree where the leaves are individual alternatives. Similar alternatives belong to clusters which, in turn, belong to a smaller number of clusters and so on until the root of the tree is reached.

In recent works, we find a number of examples using hierarchical clustering methods that are performed for visualization purposes. In Erhan et al. (2015), design alternatives are compared based on the distances between their input parameters after which they are hierarchically clustered and visualized as a dendrogram tree. The system Cupid (Beham et al., 2014) is aimed at exploring the generative space of a geometry generator by categorizing the different shapes it can produce and understanding the relationship between the input parameters and these categories. Initially, the distance between alternatives is computed by directly comparing their geometry (average of minimum distances between their corresponding mesh vertices). Next, hierarchical clustering is performed using the calculated distances and clusters are visualized on both a hierarchical radial tree and a composite parallel coordinates plot. The two views are coordinated together through brushing. Chen et al. (2015) first cluster alternatives based on the similarity between their performance metrics and then, within each cluster, they are clustered again based on chosen quantitative architectural features. Furthermore, the work by Brown and Mueller (2017a) uses clustering techniques for identifying families of similarly performing design alternatives and illustrates their use in design space exploration.

### 3.2. DIMENSIONALITY REDUCTION

Dimensionality Reduction (DR) is a set of techniques that assists in analyzing multidimensional data by minimizing the variables under consideration or mapping the data into a new, smaller space. This is done for the purposes of simplifying or denoising the data while retaining any intrinsic patterns found in the multidimensional data. For example, in the context of parametric design models, a large number of parameters usually control the generated geometric variations leaving designers with the challenge of discerning the range of geometries that a parametric model can express. Harding (2016) proposed applying a DR technique to map design alternatives, through their input parameters, into a two-dimensional grid. As a result, the geometric variations can be more readily pronounced as we move along any of the two, newly synthesized dimensions. The technique used by Harding is called Self-Organizing Maps (SOM), first introduced by Kohonen (1982), and it aims at creating a spatial map whereas inputs that are similar in their original multidimensional space are close to each other on the resulting map.

The spatial map resulting from SOM have been used in different ways such as: Creating a visual structure that can be colored or extruded to represent performance data (Fuchkina et al., 2018; van Kastel, 2018), or can be augmented with visuals (e.g. thumbnails or 3D representations) to give an overview of the geometric variations in the design space (Harding, 2016; Fuchkina et al., 2018; van Kastel, 2018; Pan et al., 2019). Furthermore, when the number of design alternatives is more than the cells in the map, SOM can be used for clustering (Erhan et al., 2015).

## 4. The Many Faces of Similarity

The simplification of the design space through clustering or dimensionality reduction has a number of applications for design space exploration as can be construed by reflecting on the examples we surveyed. To present these applications in context, we first discuss the relation between design forms and their associated performance data. Followed by their implications on design data visualization. We also discuss salient issues in design exploration tools that could then be tackled through simplification.

### 4.1. FORM AND DATA VISUALIZATIONS OF DESIGN ALTERNATIVES

In design, the geometric forms and their performance data are interrelated and equally important. Each presents information on different aspects of the design alternatives. Therefore, we expect that the interactive visualization for design analysis should enable the exploration of form and performance data both independently from each other and also in unity. Given the mutual importance of design forms and their associated data, we find it useful to break down the components of Shneiderman (1996) taxonomy to focus on either design forms or data, e.g. an overview task is then performed on either a data or form overview.

A common visualization technique of multidimensional data is the parallel coordinates plot (PCP). The PCP can provide an overview of the data patterns and correlation between alternatives. The existing design exploration interfaces make use of PCPs extensively for providing an overview over data (Beham et al.,

2014; Abi Akle et al., 2017; Mohiuddin et al., 2018; Tomasetti, 2019). On the other hand, a grid of thumbnails in DreamLens (Matejka et al., 2018) or a radial tree visually representing clusters of similar forms in Cupid (Beham et al., 2014) provides an overview of the forms in the design space.

These visualizations can also be coordinated. For example, views of design forms in DreamLens and Cupid (a thumbnails grid and a radial tree respectively) are linked to the data views (a scatterplot and a PCP) via brushing. These are examples of Coordinated Multiple Views. The work by Javed and Elmqvist (2012) views (Javed and Elmqvist, 2012) identify a list of techniques for compositing these views. The aforementioned examples fall under Juxtaposed views. We also see other types of views' compositions (Nested) in the Design Space Explorer (DSE) (Fuchkina et al., 2018) and the thesis by van Kastel (2018).

In the Design Space Explorer (DSE) (Fuchkina et al., 2018), the design form views are nested in the data view. DSE creates a 2D hexagonal grid through SOM on which thumbnail images of forms are overlaid and the cells in the grid are colored based on the performance of the alternatives in each of these cells. In his thesis, van Kastel (2018) employs a similar technique of creating a combined overview but situates the visualization in a 3D digital environment where it encodes the design data geographically, e.g. by using soil layers, terrain variations, and water levels. By introducing this distinction between data and form views, whether they are juxtaposed or nested, we can clearly understand the kind of questions we can ask through interactions that link them. The left part of Figure 1 illustrates linking independent form and data views but can also be useful when thinking about combined views such as the ones in DSE or van Kastel's thesis.

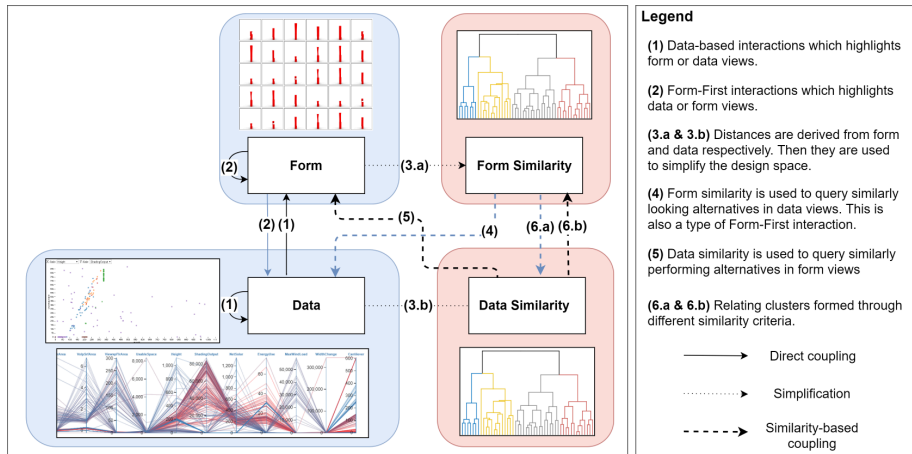


Figure 1. A conceptual model of the coupling of design data and forms in a visual analytics context. The Form and Data Similarity is derived by computing the distances between design alternatives. Examples of views for each are shown in the same colored block.

## 4.2. CALL FOR FORM-FIRST INTERACTIONS

We believe that the form overview visualizations in the systems discussed above can be further expanded to enable interactive form-driven queries that originate on these visualizations. This is analogous to the queries that are formulated on data overviews e.g. like brushing on parallel coordinates or scatterplot matrices. Examples of form-driven queries include: when a thumbnail in DreamLens is selected, then the point in the scatterplot associated with it is highlighted. Additionally, the chisel tool in DreamLens (Matejka et al., 2018) filters design alternatives by directly manipulating their superimposed forms. We also see an example in the radial tree in Cupid (Beham et al., 2014). Since the tree is created by clustering alternatives based on their geometric similarity, then brushing parts of that tree is essentially a form-driven query. We refer to these types of interactions, whether used for filtering or highlighting, as Form-First interactions. We expect that research into these interactions can open up new possibilities for supporting the explicit encoding of form-based design criteria.

## 4.3. SIMILARITY-BASED COUPLING OF FORM AND DATA

Although both DreamLens (Matejka et al., 2018) and Cupid (Beham et al., 2014) aim at visually representing design spaces, they show differences in how they enable interactions on them. The prior system implements a type of Form-First interactions on the raw 3D or 2D representations of the design forms through its ‘chisel’ tool. Cupid, on the other hand, first simplifies the design space through clustering and as a result, supports interactions on subsets of the design space. Both systems consider the visual similarity often found between generated design alternatives as an important factor in the design of their respective interactions.

We can refer to linking design forms and data in their raw format as direct coupling to distinguish it from the similarity-based coupling. Similarity-based coupling starts by computing the similarity between design alternatives. This computed similarity can be used implicitly or explicitly. An example of the implicit use can be found in DSE (Fuchkina et al., 2018), where it is possible to select an alternative on the SOM representation and highlight the thumbnails of alternatives that are visually similar to it. Explicit use of the similarity data starts by using it to simplify the design space through clustering or dimensionality reduction then visually represents their results as 2D maps, trees, or treemaps to name some. Interactions on the results of this simplification that then updates other data views can be referred to as an: explicit similarity-based coupling (ESC). An example of an ESC is the interaction on the radial tree in Cupid (Beham et al., 2014) which in turns highlights other data views in the system. Brushing on SOM representations (e.g. as in the DSE) that updates other views can also be considered an ESC. This is because of the similarity-preserving property of SOM, in that alternatives that are similar to each other are also closeby on the map.

These explicit representations can be used to provide an overview of the design space and to reduce the cognitive overload that can result from a large number of alternatives. Interacting with these representations enable us, depending on the clustering criterion, to either query the performance of alternatives with similar

forms or the appearance of similarly performing alternatives. An example of the first can be seen in (Beham et al., 2014), in the use of radar charts for visualizing derived properties of similar geometries (i.e. they belong to the same cluster). We can see examples of the latter in the works by Chen et al. (2015), as well as Brown and Mueller (2017a) where clustering was shown to allow querying the different geometric variations that exhibit similar performances. In Figure 1, we illustrate both Similarity-based coupling and Form-First interactions.

#### 4.4. A CASE FOR FORM-BASED SIMILARITY

The similarity between design alternatives can be computed in different ways depending on the aspects under comparison. If the similarity measured between alternatives correlate with their geometric or visual similarity, then we can refer to that as form-based similarity. Interactions that use form-based similarity, whether implicit or explicit, can be treated as Form-first interactions (which we argued for in Section 4.2). This applies to interactions with the results of both clustering and dimensionality reduction techniques that use form-based similarity data.

Form-based similarity can be computed by comparing input parameters if similar parameters also result in similar geometries. The applicability of this assumption is highly limited for design spaces with high complexity (Nagy et al., 2017) where the relationship between the input parameters and outputs is not predictable. Furthermore, in a design process that involves multiple generative design models, whether as iterations on a single model or resulting from a collaborative setting, we would like to be able to jointly explore them. Relying on the shared input parameters between them might not be possible or useful. Instead, we argue for comparing the geometric forms directly. This can be accomplished through shape similarity approaches which represent a geometric form (2D or 3D) numerically so that regular distance functions like the Euclidean distance can be used (Bustos et al., 2005). Alternatively, we can directly compare geometries by procedurally calculating the distances between their corresponding mesh vertices as is done in Cupid (Beham et al., 2014). In Figure 1, arrows (4) and (5) illustrate similarity-based coupling. Arrow (4) is also a type of Form-First interaction since it is initiated from a representation derived from form-related similarity.

### 5. First Design Iteration

Building on the arguments we outlined earlier, we describe our first design analytics dashboard prototype and the dataset we used to evaluate it.

#### 5.1. DATASET FROM A CASE STUDY

During a SmartGeometry (2018) workshop, a group of designers was asked to develop proposals for a mixed-use high-rise tower design. The tower is to be located in a downtown context and the necessary geographical and climate data was provided. Participants were provided with a common set of performance calculation modules that produced thirteen different metrics covering aspects such as floor areas per function, solar energy gain, and energy usage among others. Six designers submitted design alternatives generated by the parametric design models



they developed reaching a total of 250 alternatives. Each of the alternatives has a geometric form, performance metrics, and input values. For more details, the interested reader may refer to the case study by Erhan et al. (2020).

## 5.2. DESIGN DECISIONS

We developed a visualization dashboard to analyze the data mentioned above. We improved this dashboard to experiment with similarity-based exploration (Figure 2), which integrates Form and Data views along with Form and Data Similarity views. Here, we will motivate the choices made in terms of the views and the interactions between them with respect to the framework in Figure 1.

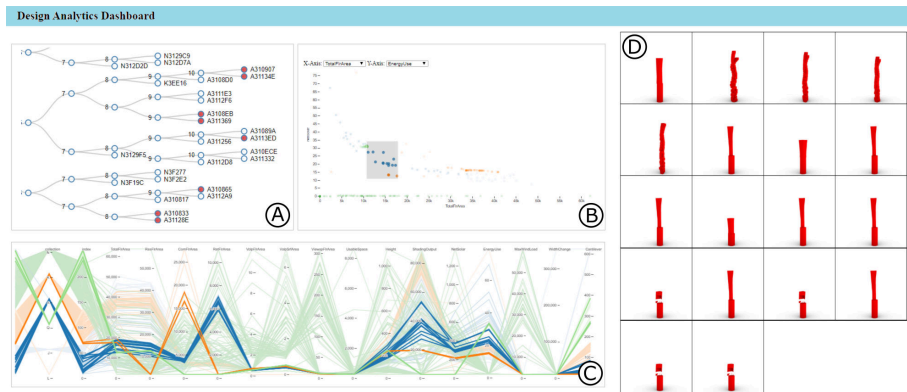


Figure 2. A: Dendrogram tree (Form or Data Similarity view), B: Scatterplot (Data view), C: Parallel Coordinates Plot (Data view), D: thumbnails grid (Form view).

### 5.2.1. Visualization Views

In this iteration, we have decided to provide both data and form views which are a parallel coordinates plot and a scatterplot as data views, and a grid of thumbnails as a form view. Dendrogram trees that represent hierarchies are chosen to present clusters in the design space with respect to either design forms or performance data. Because of the multidimensional nature of our performance data, we decided to use the parallel coordinates plot (PCP) as suggested by (Abi Akle et al., 2017). The PCP provides an overview visualization of performance data, enables filtering based on value ranges and can expose correlation patterns. In addition to the PCP, we have chosen to add a scatterplot chart to enable finding outliers and detecting a correlation between performance metrics. Since the design alternatives in our dataset come from multiple design models, we color the lines in the PCP and the scatterplot depending on the model they were generated from to facilitate inter-model comparison. We may also limit ourselves to a single model which then allows us to relate input parameters to performance metrics.

We have argued for design space simplification through dimensionality reduction and clustering. In this iteration, we decided to start our exploration

with hierarchical clustering. We chose to compute the distances between design alternatives in two ways: The first takes the euclidean distance between the performance metrics of each of the alternatives, and the second compares their geometry directly using Hausdorff distance (i.e. form-based similarity as per Section 4.4). Upon computing these distances we used them to create a hierarchical clustering of the alternatives. The resulting hierarchy tree can be visualized in a number of ways, including treemaps, dendrogram trees or radial trees, of which we choose an implementation of dendrogram trees that supports zooming and tree manipulations. The leaves in this tree are the design alternatives whereas the intermediate nodes are subclusters. Finally, not all aspects of a design can be quantified. It is then important for designers to have visual access to the design forms so that they could identify these qualitative features and compare the designs forms with each other. To support that, a grid of 2D/3D thumbnails is filled with the currently selected alternatives in the scatterplot or the dendrogram tree.

### 5.2.2. Interactions

The main design goal we have is to facilitate communication between the four views as they represent different aspects of the design data. In most of the cases, we have favored highlighting the other views when alternatives in one view are brushed. This is to maintain the context of these alternatives with respect to the unselected. A design decision was made to start the thumbnails grid with no form views and fill up the grid upon selection instead of filtering views down to the size of the selection. The latter approach was taken in DreamLens (Matejka et al., 2018). This enables an interaction whereas a rectangular brush can be moved on the scatterplot view (as in Figure 2, view B) gradually while updating the grid of thumbnails with the currently brushed alternatives only. This gradual movement demonstrates how geometric forms are changing in relation to changes in performance values. Finally, the dashboard currently supports form-first interactions in the form of highlighting alternatives in all data views when their thumbnails are hovered over.

## 6. Future Work and Conclusion

We had demonstrated a series of techniques and concepts relevant to exploring design spaces of computationally generated alternatives. These are derived by reflecting on and extending the literature of design space simplification and the patterns of their use. Finally, we presented the first iteration of a design analytics dashboard that instantiates some of the ideas discussed. In the future, we intend to continue iterating on and evaluating this dashboard and explore the practical and design-specific concerns surrounding similarity-based exploration.

## References

- “SmartGeometry” : 2018. Available from <[www.smartgeometry.org/inside-the-black-box](http://www.smartgeometry.org/inside-the-black-box)>.
- Abi Akle, A., Minel, S. and Yannou, B.: 2017, Information visualization for selection in Design by Shopping, *Research in Engineering Design*, **28**(1), 99-117.
- Beham, M., Herzner, W., Gröllner, M.E. and Kehrer, J.: 2014, Cupid: Cluster-Based Exploration of Geometry Generators with Parallel Coordinates and Radial Trees, *IEEE Transactions on*

- Visualization and Computer Graphics*, **20**(12), 1693-1702.
- Brown, N. and Mueller, C.: 2017a, Automated performance-based design space simplification for parametric structural design, *In Proceedings of IASS Annual Symposia*.
- Brown, N. and Mueller, C.: 2017b, Designing with data: Moving beyond the design space catalog, *Proceedings Catalog of the 37th Annual Conference of the Association for Computer Aided Design in Architecture, ACADIA 2017*, 154-163.
- Bustos, B., Keim, D.A., Saupe, D., Schreck, T. and Vranić, D.V.: 2005, Feature-based similarity search in 3D object databases, *ACM Computing Surveys (CSUR)*, **37**(4), 345-387.
- Chen, K.W., Janssen, P. and Schlueter, A.: 2015, Analysing Populations of Design Variants Using Clustering and Archetypal Analysis, *Real time-extending the reach of computation: eCAADe 2015; proceedings of the 33. International Conference on Education and Research in Computer Aided Architectural Design in Europe*, 251-260.
- Erhan, H., Abuzurairq, A., Zarei, M., Alsalman, O., Woodbury, R. and Dill, J.: 2020, What do design data say about your model? a case study on reliability and validity, *Proceedings of the 25th Int. Conference on Computer-Aided Architectural Design Research in Asia, CAADRIA*.
- Erhan, H., Wang, I.Y. and Shireen, N.: 2015, Harnessing Design Space: A Similarity-Based Exploration Method for Generative Design, *International Journal of Architectural Computing*, **13**(2), 217-236.
- Fuchkina, E., Schneider, S., Bertel, S. and Osintseva, I.: 2018, Design Space Exploration Framework-A modular approach to flexibly explore large sets of design variants of parametric models within a single environment, *Proceedings of the 36th eCAADe Conference*, 367-376.
- Harding, J. 2016, Dimensionality reduction for parametric design exploration, in F.G. Sigrad Adriaenssens (ed.), *Advances in Architectural Geometry 2016*, vdf Hochschulverlag AG.
- Javed, W. and Elmqvist, N.: 2012, Exploring the design space of composite visualization, *2012 IEEE Pacific Visualization Symposium*, 1-8.
- van Kastel, J.: 2018, *Visual Analytics for Generative Design Exploration: An interactive 3D data environment for a computational design system facilitating the performance-driven design process of a nearly Zero-Energy sports hall*, Master's Thesis, TUDelft.
- Kohonen, T.: 1982, Self-organized formation of topologically correct feature maps, *Biological cybernetics*, **43**(1), 59-69.
- Matejka, J., Glueck, M., Bradner, E., Hashemi, A., Grossman, T. and Fitzmaurice, G.: 2018, Dream Lens: Exploration and Visualization of Large-Scale Generative Design Datasets, *Proceedings of the 2018 CHI Conference on Human Factors in Computing Systems*, New York, NY, USA, 369:1-369:12.
- Mohiuddin, A., Ashtari, N. and Woodbury, R. 2018, Directly Interactive Design Gallery Systems: Interaction Terms and Concepts, in J.H. Lee (ed.), *Computational Studies on Cultural Variation and Heredity*, Springer, 15-32.
- Nagy, D., Villaggi, L., Zhao, D. and Benjamin, D.: 2017, Beyond Heuristics: A Novel Design Space Model for Generative Space Planning in Architecture, *Proceedings of the 37th Annual Conference of the Association for Computer Aided Design in Architecture, ACADIA 2017*.
- Pan, W., Sun, Y., Turrin, M., Louter, C. and Sariyildiz, I.: 2019, Design exploration of architectural geometries and structural performance for sports arenas based on SOM-clustering and structural performance simulation, *Proceedings of the Fourth International Conference on Structures and Architecture (ICSA 2019)*, 342.
- Shi, X.: 2010, Performance-based and performance-driven architectural design and optimization, *Frontiers of Architecture and Civil Engineering in China*, **4**(4), 512-518.
- Shneiderman, B.: 1996, The eyes have it: A task by data type taxonomy for information visualizations, *Proceedings 1996 IEEE symposium on visual languages*, 336-343.
- Thomas, J. and Cook, K.: 2006, A Visual Analytics Agenda, *IEEE Cmpt. Graph. Appl.*, **26**, 3.
- Thornton Tomasetti, C.S.: 2019, "Design Explorer". Available from <<https://github.com/tt-acm/DesignExplorer>>.

# **Simulation & Analysis**



# INFLUENCE OF UNCERTAINTIES IN ENVELOPE AND OCCUPANT PARAMETERS ON THE RELIABILITY OF ENERGY-BASED FORM OPTIMIZATION OF OFFICE BUILDINGS

CHUNXIAO WANG<sup>1</sup> and SHUAI LU<sup>2</sup>

<sup>1</sup>*Shenzhen University*

<sup>1</sup>*cxw@szu.edu.cn*

<sup>2</sup>*(no affiliation)*

**Abstract.** Building performance optimization is effective in finding optimal designs and improving building energy efficiency, but its reliability can be affected by uncertainties in input parameters. This paper conducts a reliability analysis on energy-based form optimization of office buildings under uncertainties in envelope and occupancy parameters. An optimization process involving Rhinoceros, EnergyPlus and genetic algorithms is first implemented. Then parametric studies of 644 scenarios involving 4 cities in different climates and 3 form variables are conducted. The results indicate that uncertainties in input parameters could lead to major unreliability of optimization results, including reductions up to 13% in energy saving achieved by optimization and descents up to 10% in energy efficiency compared with results before optimization. Moreover, the uncertainty in visual transmittance of windows is the most significant cause for the unreliability, followed by U-value of walls, while the uncertainty in occupant density and occupant schedule has limited influence. The results can help designers understand the uncertainty of which parameters should be controlled and to what extent optimization results can be trusted in various scenarios.

**Keywords.** Building Performance Optimization; Form Design; Building Energy Efficiency; Uncertainty Analysis; Office Building.

## 1. Introduction

### 1.1. RESEARCH BACKGROUND

Building performance optimization is a technique that employs optimization algorithms to generate designs based on simulation results and user-defined design objectives (Nguyen 2014). It is an efficient method to find the optimal or near-optimal design solutions compared with the conventional “trial-and-error” design methodology. Therefore, this technique has been widely used by designers and engineers, and also been intensively explored by researchers. The reliability of the results obtained from building performance optimization depends not only on the validity of simulation and optimization algorithms, but also on the accuracy of a number of input parameters as the boundary conditions, e.g., weather data,

material properties, and occupant behaviors (Bamdad 2018). Owing to lack of knowledge, design procedures, and the stochastic nature of certain parameters (Hensen 2011), uncertainties of some input parameters are inevitable, and thus modelers must rely on assumptions or default values, which could significantly affect the results of building performance simulation and optimization, and lead to problematic results.

The uncertainty problem of input parameters is even more crucial for the optimization of building forms. The design of building forms not only largely determines the appearance of buildings, but also plays an essential role in building performance. However, in the early design stage when building forms are designed, other issues such as material properties and service systems have not been fully determined yet. This leads to an even higher degree of uncertainty in the input parameters for building form optimization compared with the optimization of building envelope or service systems, which are designed during the later design phases. Therefore, the reliability of building form optimization under uncertainties of input parameters should be addressed.

## 1.2. STATE OF THE ART

There are numerous parameters that can affect a building's performance, including weather conditions, building forms, envelopes, service systems, operation, occupant behavior, etc. (Hensen 2011). Many such parameters have certain degrees of uncertainty. The sources of such uncertainties can be classified into three categories, namely, uncertainty in the physical parameters (the difference between the actual value and the theoretical value of a physical property), in the design parameters (the uncertainty and variations caused by the design process), and the scenario parameters (the uncertainty of the parameters that can be changed during a building's lifetime and thus cannot be accurately predicted in advance). Due to the uncertain nature of the input parameters, results generated through deterministic simulation with one set of assumed or default input parameters are actually an arbitrary sample from possible actual scenarios of a building (Hensen 2011). Therefore, performance gaps (the difference between the actual and predicted building performance) may occur.

Research in building performance optimization has been increasing rapidly during this decade (Nguyen 2014). Several studies on the reliability of building performance optimization have also been conducted and they mainly investigated the influence of different optimization algorithms. There are still certain aspects that should be further investigated: 1) The reliability of building form optimization under uncertainties should be better addressed because form design significantly influences the building energy efficiency and has a higher degree of uncertainty in the input parameters. 2) The influence of the uncertainty in design parameters should be further explored, as for form design in the early design stage, parameters related to the design tasks in later design procedures (envelopes, service systems, etc.) are normally not decided yet. 3) The influence of the uncertainties in individual input parameters should be better revealed to identify those parameters whose uncertainties can largely affect the reliability of building form optimization, allowing designers to reduce the degree of uncertainty in such parameters as much

as they can before starting the optimization.

### 1.3. OBJECTIVES OF THIS RESEARCH

This research aims to explore the reliability of energy-based form optimization of office buildings under uncertainties in the input parameters. Specifically, envelope parameters and occupancy parameters are investigated, the former of which incur uncertainties in the design parameters, which are significant in form design and have not been fully investigated in existing studies, whereas the latter represent uncertainties in the scenario parameters, the importance of which has often been underestimated by modelers (Hensen 2011).

## 2. Methods

### 2.1. PROBLEM STATEMENT

The problem of optimizing building form designs for minimum energy consumption can be stated as:

$$\min f(X, a_1, a_2, a_3...) \quad (1)$$

where  $f()$  is the optimization objective (energy consumption),  $X$  is a vector of form variables for optimization and represents form designs within feasible design spaces, while  $a_1, a_2, a_3...$  represent other input parameters that will not be optimized including envelope properties, service systems, weather and occupant behavior. If all input parameters are precise, the optimized form ( $X_t$ ) and the optimized value of energy consumption ( $E_t = f(X_t, a_1, a_2, a_3, \dots)$ ) by Optimization (1) can be regarded as the true optimal solution. During form design at the early design stage, however, uncertainties in some of the input parameters are inevitable so that modelers must rely on assumptions or default values. Supposing that  $a_1$  is an uncertain input parameter and different modelers could assume it to be  $a_1'$ ,  $a_1''$ ,  $a_1'''$ , etc., then the optimization problem is modelled as:

$$\min f(X, a_1', a_2, a_3...); \min f(X, a_1'', a_2, a_3...); \min f(X, a_1''', a_2, a_3...); \quad (2)$$

In Optimization (2), the optimized forms ( $X_{app1}, X_{app2}, X_{app3}, \dots$ ) are apparent optimal forms under assumed boundary conditions, instead of the true optimal form. Under real boundary conditions ( $a_1, a_2, a_3, \dots$ ), the energy consumption values of these apparent optimal forms are:

$$E_{app1} = f(X_{app1}, a_1, a_2, \dots); E_{app2} = f(X_{app2}, a_1, a_2, \dots); E_{app3} = f(X_{app3}, a_1, a_2, \dots); \dots \quad (3)$$

As  $X_{app1}, X_{app2}, X_{app3}, \dots$  are apparent optimal forms and may be different from the true optimal form ( $X_t$ ), their energy consumptions  $E_{app1}, E_{app2}, E_{app3}, \dots$  could be higher than  $E_t$ . This “performance gaps” are caused by input assumptions of the boundary condition parameter  $a_1$ . The higher the performance gaps are, the more influential the uncertainty in  $a_1$  is on the reliability of the building form optimization. For comparison, supposing that  $X_0$  is a base form, and its energy consumption under real boundary conditions is  $E_0$ , then the energy efficiency improvement achieved by optimization with precise input can be quantified by the improvement ratio:

$$P_t = (E_0 - E_t) / E_0 \quad (4)$$



Similarly, energy efficiency improvement achieved by optimization with assumed inputs of boundary conditions can be defined as:

$$P_{app1} = (E_0 - E_{app1}) / (E_0); P_{app2} = (E_0 - E_{app2}) / (E_0); P_{app3} = (E_0 - E_{app3}) / (E_0); \dots (5)$$

Then, the performance gaps caused by assumed inputs of the boundary condition parameter  $a_1$  are quantified by the performance gap ratio:

$$P_{gap1} = P_{app1} - P_t; P_{gap2} = P_{app2} - P_t; P_{gap3} = P_{app3} - P_t; \dots (6)$$

It is clear that the higher the performance gap ratios are, the more influence the uncertainty in  $a_1$  has, and the less reliable the results of building form optimization are under the uncertainty of  $a_1$ .

## 2.2. METHODOLOGY

To explore the reliability of energy-based form optimization of office buildings under uncertainties, a base case is first established (Section 2.3), and then form variables (as independent variables for optimization), optimization objective and uncertain boundary condition parameters are defined (Section 2.4). An optimization process is next implemented (Section 2.5), followed by parametric studies that define scenarios with different input of boundary condition parameters, locations and optimization variables. Optimized forms under each scenario are acquired, and the performance gaps caused by the uncertainty under different scenarios are calculated (Section 2.6).

## 2.3. BASE MODEL

A 3-story rectangular office building derived from a DOE benchmark model is defined as the base model (Figure 1), with a floor area of 1600m<sup>2</sup> and an aspect ratio of 1.5625 (i.e., 50m in length and 32m in width). The floor height is 4 m, the ceiling height is 3 m, and the window-to-wall ratio (WWR) of each façade is 0.33. The orientation is north-south facing. Parameters about envelope, service systems, occupancy and schedules are set as same as the recommended values for simulation of office buildings by Standard for Green Performance Calculation of Civil Buildings of China, and are in line with Design Standard for Energy Efficiency of Public Buildings of China. The U-Values of building envelope are: walls and ground, 0.35 W / (m<sup>2</sup>\*K); roof, 0.25 W / (m<sup>2</sup>\*K); windows, 2.0 W / (m<sup>2</sup>\*K). The visual transmittance of windows is 0.6. The power densities of lighting and equipment are 10 W / m<sup>2</sup> and 15 W / m<sup>2</sup>, while the occupant density is 10 m<sup>2</sup> / person. Lighting is under continuous dimming control together with daylighting, and the target illuminance is 300 lux. The set-point temperatures for heating and cooling are 20 oC and 26 oC, while the comprehensive COP for heating and cooling are 1.8 and 2.6. The air infiltration rate (ACH) is 0.3 h<sup>-1</sup> and the ventilation rate is 30 m<sup>3</sup> / h per person.

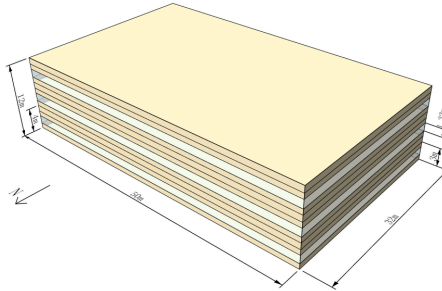


Figure 1. Base model in this research.

#### 2.4. VARIABLE DEFINITION

As this research focuses on building form optimization, three form variables are selected as the independent variables for optimization, namely aspect ratio (AR), window-to-wall ratio (WWR) and orientation (OR). These form variables can define possible variations of the base model, and their ranges and descriptions are shown in Table 1. For comparable results, other form characteristics are fixed as same as the base model.

Table 1. Form variables as independent variables for optimization.

Variable	Range	Description
Aspect Ratio (AR)	[1, 6.25]	Ratio of length to width. 1 stands for square (length=width=40m). 6.25 stands for a plan as narrow as 2 structural grids (16m in width).
Window-to-Wall Ratio (WWR)	[0.1, 0.75]	Ratio of window area to wall area. 0.1 stands for 0.4m-high bar windows. 0.75 stands for 3m-high French windows that reach ceiling.
Orientation (OR)	[0, 180]	Angle between building orientation and the north. 0 stands for north facing. 90 stands for west facing. [180, 360] excluded for symmetry.

The optimization objective is to minimize the annual total end-use energy consumption of the building, which includes energy for heating, cooling, lighting, fans, pumps and office equipment.

Four parameters related to envelope and occupancy are selected as the uncertain boundary conditions of optimization, namely U-Value of walls, visible transmittance of window glazing, occupant density and occupant schedule. The impacts of these four parameters on building energy efficiency and its simulation are widely proven. The range of each parameter is based on codes, standards and previous surveys of office buildings in China and in the world, and is set to be as wide as realistically possible. The range of U-Value of walls differs in different cities (four cities in different climates are investigated, namely Harbin, Beijing, Shanghai and Shenzhen), to be in line with buildings codes, while ranges for the rest three parameters are the same for all places. Ranges and sample values are listed in Table 2, and variations of occupant schedules are shown in Figure 2. Other

boundary conditions of optimization are fixed as same as the base model.

Table 2. Envelope and occupancy parameters as uncertain boundary conditions of optimization.

Parameter	Ranges	Sample Values
U-Value of walls - (U-Val)	[0.10,0.38] (Harbin); -	0.10, 0.16, 0.21, 0.27, 0.32, 0.38 (Harbin); -
	[0.15,0.5] (Beijing); -	0.15, 0.22, 0.29, 0.36, 0.43, 0.50 (Beijing); -
	[0.25,1] (Shanghai); -	0.25, 0.40, 0.55, 0.70, 0.85, 1.00 (Shanghai); -
	[0.25,1.5] (Shenzhen); -	0.25, 0.50, 0.75, 1.00, 1.25, 1.50 (Shenzhen); -
Visible Transmittance of Windows (Tvis)	[0.4, 0.85]	0.4, 0.49, 0.58, 0.67, 0.76, 0.85
Occupant Density (OcDens, people/m <sup>2</sup> )	[0.05, 0.25]	0.05, 0.09, 0.13, 0.17, 0.21, 0.25
Occupant Schedule (OcSche)	5 types (S1-S5), see Figure 2 for details	S1, S2, S3, S4, S5

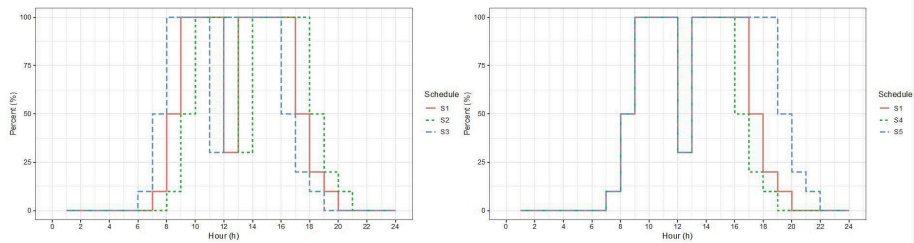


Figure 2. Variations of occupant schedules.

## 2.5. OPTIMIZATION PROCESS

Optimization is implemented by integrating Rhinoceros, Grasshopper, DIVA (a plug to Grasshopper that calls EnergyPlus), EnergyPlus (widely used simulation software for building energy) and Galapagos (an optimization engine based on genetic algorithm). A parametric model is first established in Rhinoceros and Grasshopper, which can generate various designs based on the base case and form variables. The energy consumption of designs is then calculated by EnergyPlus through DIVA. EnergyPlus is employed here as it is the most commonly used simulation software for building energy optimization. Finally, Galapagos is used here to find the optimal design with minimized annual total end-use energy consumption by genetic algorithm. Genetic algorithm is employed here due to its high efficiency and repeatability in achieving close-to-optimal solutions with a good diversity compared with other optimization algorithms.

## 2.6. PARAMETRIC STUDY

Parametric study is conducted to represent possible scenarios under the uncertainty of envelope and occupancy parameters. Sample values of each boundary condition parameter (as defined in Table 2), four major Chinese cities in different climate zones (namely Harbin, Beijing, Shanghai and Shenzhen, as mentioned in Table 2), and seven possible combinations of form variables for optimization (AR+WWR+OR, AR+WWR, AR+OR, WWR+OR, AR, WWR, OR, as defined in Table 1) are involved to deliver comprehensive results, and their combinations

result in 644 possible scenarios in total (4 cities \* 7 combinations of form variables \* (6+6+6+5) sample values of boundary condition parameters). Each scenario can represent one set of true boundary conditions and the optimal forms under each scenario are acquired. Then, for each scenario, the energy consumption of the base form ( $E_0$ ), of the true optimal form ( $E_t$ ), and of the apparent optimal forms ( $E_{app1}$ ,  $E_{app2}$ ,  $E_{app3}$ .....) are calculated by EnergyPlus. Then, the energy efficiency improvement ratios ( $P_t$ ,  $P_{app1}$ ,  $P_{app2}$ ,  $P_{app3}$ ...) and the performance gap ratios ( $P_{gap1}$ ,  $P_{gap2}$ ,  $P_{gap3}$ ...) are calculated as defined in Equation (4)-(6). The calculation results are presented in Section 3.

### 3. Results

The section reports the results of energy efficiency improvement by optimization with precise input ( $P_t$ ), performance gap caused by uncertain input ( $P_{gap}$ ), and energy efficiency improvement by optimization with uncertain input ( $P_{app}$ ). For conciseness, all form variables and uncertain input parameters are denoted in abbreviations as defined in Table 1 and Table 2.

#### 3.1. IMPROVEMENT BY OPTIMIZATION WITH PRECISE INPUT

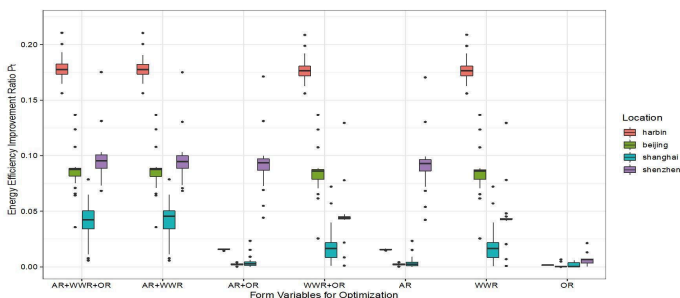


Figure 3. Distribution of improvement ratios by optimization with precise input ( $P_t$ ).

The energy efficiency improvement achieved by form optimization with precise input compared with the base form is first presented. The Box-Whisker plot in Figure 3 shows the distribution of the improvement ratios ( $P_t$ , as defined in Equation (4)) in different locations and with different combinations of form variables for optimization. In general, the energy efficiency improvement achieved by form optimization with precise input is remarkable for a majority of cases, and can be as high as more than 20%. This indicates the fact that building energy performance could be largely improved by appropriate form design. The overall improvement for cases in Harbin is the highest among all locations, where the median of the improvement ratio is more than 17.5%, as long as WWR is included in the form variables for optimization (i.e., AR+WWR+OR, AR+WWR, WWR+OR, WWR). Beijing and Shenzhen are the following locations, where the median of the improvement ratio is between 8% to 10%, as long as WWR (for Beijing) or AR (for Shenzhen) is included in the form variables for optimization respectively. The improvement for Shanghai is

lower than other locations, where the median of the improvement ratio is below 5% for all scenarios. In terms of different combinations of form variables for optimization, the improvement is minor regardless of locations if OR is the only form variable for optimization, while for all other combinations, the improvement could be remarkable (median>9%) depending on locations.

### 3.2. PERFORMANCE GAP BY UNCERTAIN INPUT

The energy performance gaps caused by the input assumptions of different uncertain boundary conditions are presented in this section. The distribution of the performance gap ratio ( $P_{gap}$ , as defined in Equations (6)) in different locations and with different form variables for optimization are shown in Box-Whisker plots (Figure 4). The performance gap ratio can be as high as 13%, which indicates that remarkable reductions in energy saving that should be achieved by form optimization could be caused by the uncertainty in boundary conditions. The distribution of performance gaps differs in different locations.

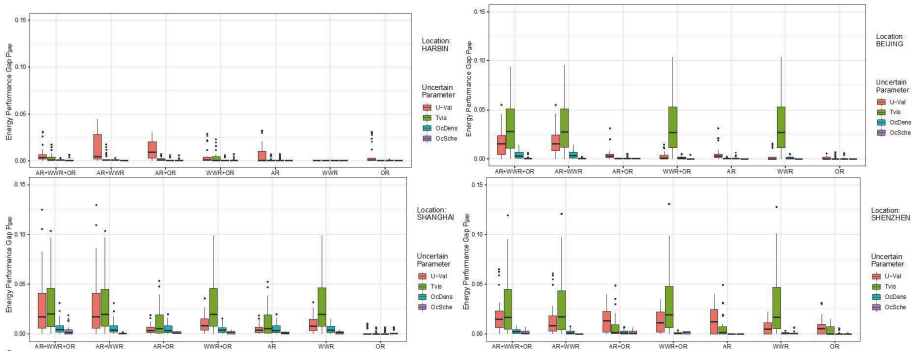


Figure 4. Distribution of the energy gap ratios ( $P_{gap}$ ).

For Harbin, the performance gaps are limited, with the median below 1% for all scenarios. Gaps >5% are not found, and gaps >3% are only caused by the uncertainty of U-val when some combinations of form variables are optimized (AR+WWR+OR, AR+WWR, AR+OR, AR, OR).

For Beijing, Shanghai and Shenzhen, the characteristics of performance gaps are similar. In terms of extreme cases, the performance gaps can be higher than 10% for all three cities (up to 13% for Shanghai and Shenzhen). The uncertainty of Tvis is the most significant cause for the performance gaps, with median gaps around 2% (Shanghai and Shenzhen) to 2.5% (Beijing) for scenarios where WWR is included in the form variables for optimization (i.e., AR+WWR+OR, AR+WWR, WWR+OR, WWR). Performance gaps >5% are also found in the aforementioned scenarios. The following significant cause is the uncertainty of U-Val, which could lead to performance gaps around 2% in terms of median for certain scenarios in all three cities. Performance gaps >5% are also found when AR+WWR+OR or AR+WWR are the form variables for optimization for all three cities, while gaps >3% can be found in some other scenarios. The uncertainty of

OcDens and OcSche results in much smaller performance gaps for all cities, as gaps >5% are not found and gaps >3% occur very seldom.

### 3.3. IMPROVEMENT BY OPTIMIZATION WITH UNCERTAIN INPUT

Based on Section 3.2, it is clear that uncertainties in some boundary condition parameters do cause major performance gaps compared with the energy efficiency achieved by form optimization with precise boundary conditions. Nevertheless, form optimization with uncertain boundary conditions is still beneficial if the building energy efficiency of the optimized form is higher than that of the form before optimization, i.e., the base form. However, if the energy efficiency of the optimized form could be even lower than the base form, careful attention must be paid to properly control the uncertainty of boundary conditions before conducting any form optimization. Therefore, the energy efficiency improvement achieved by form optimization with uncertain boundary conditions compared with the base form is also a crucial indicator of the reliability of building form optimization under uncertainty. The distribution of the improvement ratios ( $P_{app}$ , as defined in Equations (5)) in different locations and with different form variables for optimization are shown in Box-Whisker plots (Figure 5). The lowest improvement ratio approaches -10%, and this reveals that remarkable decreasing instead of increasing in energy efficiency compared with the base case could be caused by the uncertainty in boundary conditions. The distribution of the improvement ratios also varies in different locations.

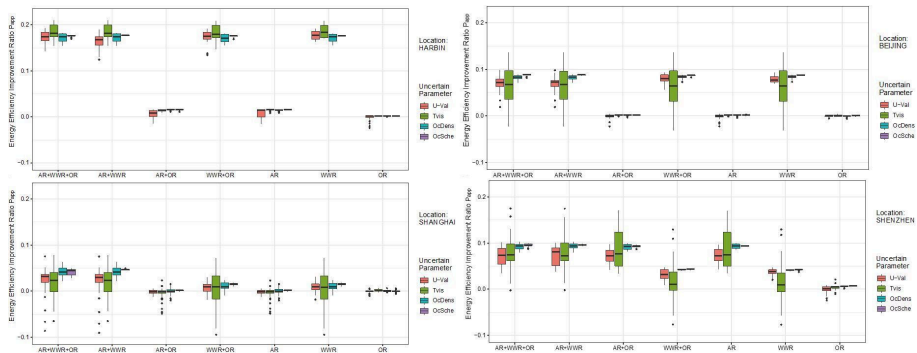


Figure 5. Distribution of improvement ratios by optimization with uncertain input ( $P_{app}$ ).

For Harbin, major energy efficiency improvement (median around 17.5%) can still be achieved by optimization even with the uncertainty of boundary conditions, as long as WWR is included in the form variables for optimization. For other combinations of form variables, the improvement ratios are limited, but the median values are still above 0. Moreover, no descent >3% is found for all scenarios. Therefore, it is generally safe to employ form optimization in Harbin even under the uncertainty of boundary conditions.

For Beijing and Shenzhen, the patterns are similar. The median improvement ratio is around 8%, as long as WWR (for Beijing) or AR (for Shenzhen) is included

in the form variables for optimization. For other combinations of form variables, the improvement ratios are limited, but the median values are still above 0. In Shenzhen, descents >5% of energy efficiency are only caused by the uncertainty of Tvis when WWR+OR or WWR are the form variables for optimization, while for Beijing, descents >3% are only caused by the uncertainty of Tvis with the same two combinations of form variables. Therefore, it is also safe to employ form optimization in Beijing and Shenzhen, as long as the uncertainty of Tvis is under control when WWR+OR or WWR are the form variables for optimization.

For Shanghai, the improvement ratio are rather low, with the medians below 5% for all scenarios. Moreover, descents >5% and >3% are found in various scenarios. The uncertainty of Tvis is the main cause, which leads to descents >5% (AR+WWR+OR, AR+WWR, WWR+OR, WWR) and >3% (AR+OR, AR) for all combinations of form variables for optimization except for OR alone. The uncertainty of U-Val also causes descents >5% when AR+WWR+OR or AR+WWR are the form variables for optimization. In short, employing form optimization with uncertain Tvis or U-Val could lead to decreasing instead of increasing in building energy efficiency, so careful attention must be paid to control the uncertainty before conducting form optimization.

#### 4. Conclusion

1) The uncertainty in boundary condition parameters could lead to major unreliability problems of energy-based form optimization of office buildings, including reductions up to 13% in energy saving achieved by optimization and descents up to 10% in energy efficiency compared with results before optimization.

2) The uncertainty in visual transmittance of window glazing is the most significant cause for the unreliability, followed by the uncertainty in U-value of walls, while the influence of the uncertainty in occupant density and occupant schedule is minor.

3) The influence of uncertainty in boundary conditions is limited in Harbin, without any reduction >5% in energy saving and descent >3% compared with results before optimization, while in Beijing, Shanghai and Shenzhen, the influence is more remarkable. The influence is generally large when WWR is included in form variables for optimization, while is generally small if OR alone is the form variable for optimization.

4) The results in this research can help designers understand the unreliability of form optimization of office buildings in various scenarios, so that they can better decide the uncertainty of which parameters to control, to what extent the results can be trusted, and even whether the optimizations are worth conducting.

#### References

- Bamdad, K., Michael, C.E. and Guan, L.: 2018, Building energy optimization under uncertainty using ACOMV algorithm, *Energy and Buildings*, **167**, 322-333.
- Hensen, J. and Lamberts, R.: 2011, *Building performance simulation for design and operation*, Spon Press.
- Nguyen, A., Reiter, S. and Rigo, P.: 2014, A review on simulation-based optimization methods applied to building performance analysis, *Appl Energy*, **113**, 1043-58.

# INSULATING WITH GEOMETRY

## *Employing Cellular Geometry to Increase the Thermal Performance of Building Facades*

CHELI HERSHCOVICH<sup>1</sup>, RENÉ VAN HOUT<sup>2</sup>,  
VLADISLAV RINSKY<sup>3</sup>, MICHAEL LAUFER<sup>4</sup> and  
YASHA J. GROBMAN<sup>5</sup>

<sup>1,5</sup>*Faculty of Architecture and Town Planning, Technion*

<sup>1</sup>*cheli@campus.technion.ac.il* <sup>5</sup>*yasha@technion.ac.il*

<sup>2,3,4</sup>*Faculty of Mechanical Engineering, Technion*

<sup>2</sup>*rene@technion.ac.il* <sup>3</sup>*rinsky@tx.technion.ac.il*

<sup>4</sup>*michael.laufer@campus.technion.ac.il*

**Abstract.** This paper presents the current stage of a study examining the potential of complex geometry concrete tiles to improve thermal performance in building envelopes. This stage focused on developing tile geometries and testing them using physical and digital CFD (Computational Fluid Dynamics) simulations. Tiles were developed taking two approaches: (i) developing variation from basic geometries (triangle, square, circle and trapezoid) and (ii) learning from natural envelopes. Following successful validation of experimental and numerical data, the designed tiles were tested using a digital simulation (Star-CCM+). The results show that for the examined configuration (flow perpendicular to the surface), a significant reduction of heat transfer rate occurs in most of the tested tiles. Furthermore, geometries that achieved the same thermal performance as the base-line flat tile saved up to 38 percent of the material.

**Keywords.** Complex Geometry; Microclimate; CFD.

## 1. Introduction

About 40 percent of the world's energy consumption accounts for buildings - mostly for heating and cooling interior spaces to achieve thermal comfort. This amount of energy can be significantly reduced by well insulating the building envelope. For many years, thermal insulation in buildings has been achieved by stacking layers of insulating materials creating a laminated orthogonal facade. However, this commonly used insulation method is not the only effective one: unique envelope geometries in nature are used, for example, by desert succulents and arctic animals to survive in harsh climatic conditions. Nature's approach to insulation demonstrates that not just the material itself, but also the organization of material in space, affects thermal performance. Due to the latest developments in CAD/CAM, the design and fabrication of complex geometries became achievable.



Today, computational tools enable the creation of almost every possible free-form, leading to a large interest in complex geometries. Much research has dealt with aesthetic and practical implementations of complex geometries, but not as much has dealt with its performative aspects. This paper presents the current stage of a study that aims to develop a new type of building envelope. The new envelope, inspired by nature is constructed from a simple material (concrete) and achieves its high performance through a combination of material properties and microclimate created close to its surface and within its cavities. A background section reviews architectural precedents in the field and the results of the previous stages of the study. The methods section describes the generation of basic and nature-based (bio-mimetic) geometry tiles and their examination by experiments and CFD simulations. The results section compares and discusses the measured values.

## **2. Background**

### **2.1. COMPLEX GEOMETRIES IN BUILDING ENVELOPES**

For many years, the implementation of complex geometries in architectural design was considered challenging due to technological limitations. One of the first architects to introduce complex geometries into the modern architectural discourse was Antoni Gaudi, who designed and built organic, highly intricate geometries. To describe his geometries he used diagrams, stereotomy and sculptures. In the mid-20th century, architects such as Eladio Dieste and Erwin Hauer developed some methods for the realization of complex surfaces (Hauer, 2004; Stanford, 2004). It wasn't until the 1990s, when architects such as Gehry Partners introduced computer-aided 3D modeling and manufacturing into the architectural discourse, that describing complex geometries became possible to all. In a parallel process, the ability to evaluate the performance of architectural forms was developed. Computational simulations, that emerged during the 1970s, brought the ability to calculate the expected performance of geometry rather than estimate or use rules of thumb. Today, the easy access to describing, evaluating and fabricating almost every form, enables the creation of high-performance, optimized complex geometries. Architectural precedents in the field of complex geometries can be divided into two types. The first aimed to answer aesthetical parameters with the creation of complex geometries, such as the architecture of Antoni Gaudi, Eladio Dieste and Frank Gehry. The second type of projects aimed to improve the performance of an element using geometry. Projects in this group are for example the Beijing National Aquatic Center by PTW Architects and KOL/MAC Architecture's INVERSAbrane building envelope.

### **2.2. THERMAL INSULATING WITH GEOMETRY**

Different studies demonstrate the impact of geometries on changing the airflow and thus improving thermal performance, from the macro-level of a city to the micro-level of building facade surfaces. large-scale studies show that air movement within the city depends on its morphology, its street design and orientation, and its form (Golany 1996). Another research examined the shape of domed roofs in Persian deserts and found that they created higher air velocities

over the vaulted section which enhanced heat transfer and kept interior spaces thermally comfortable (Golneshan and Yaghoubi 1990). In a micro-scale study, Montazeri examined the impact of balcony shapes on the airflow and showed that it can lead to very strong changes in wind pressure distribution due to the creation of multiple flow separation, recirculation and reattachment areas (Montazeri and Blocken 2013). Microscale investigations show that density and geometry of porosity affect the micro-scale flow patterns near porous screens and demonstrate the power of geometry in shaping air patterns (Hrynuik, Van Luipen, and Bohl 2012; Latifi Khorasgani et al. 2016). Based on these studies, we assume that changing the geometry of a flat façade tile can shape air patterns on the surface. The air patterns would potentially thicken the boundary layer and therefore lead to better insulating surfaces. Preliminary research (Grobman, 2013; Grobman and Elimelech, 2015) has validated the potential of basic shape cavities to improve the thermal resistance of a given concrete tile. A following paper (Hershovich et al., 2017) developed a methodology of employing computational fluid dynamic simulations for improving thermal resistance, based on validation in physical wind tunnel simulation. The following paper presents the results of an examination of the developed methodology on various types of façade concrete tiles geometries.

### 3. Methods

The current stage of the research focused on examination of different geometry tiles using physical and computational CFD simulations.

#### 3.1. DEVELOPING GEOMETRIES

Two main directions have guided the development of the tested geometries. The first one is based on a systematic approach. Since no study has been found defining specific geometries that improve thermal performance and following the results of the preliminary research (Grobman and Elimelech, 2015), we used basic geometries as a starting point. The first series included identical cavities in four shapes: rectangle, triangle, half-circle, and trapezoid, both in a round and rectangular section (commands revolve and sweep, Rhinoceros). The second series included the same shapes - this time as bumps protruding from the flat surface (Figure 1). In all cavities and bumps, the basic dimensions of diameter and depth were kept identical. The process of examining basic geometries is evolutionary: following the results and primary conclusions, the best performing geometries will be further developed and optimized.

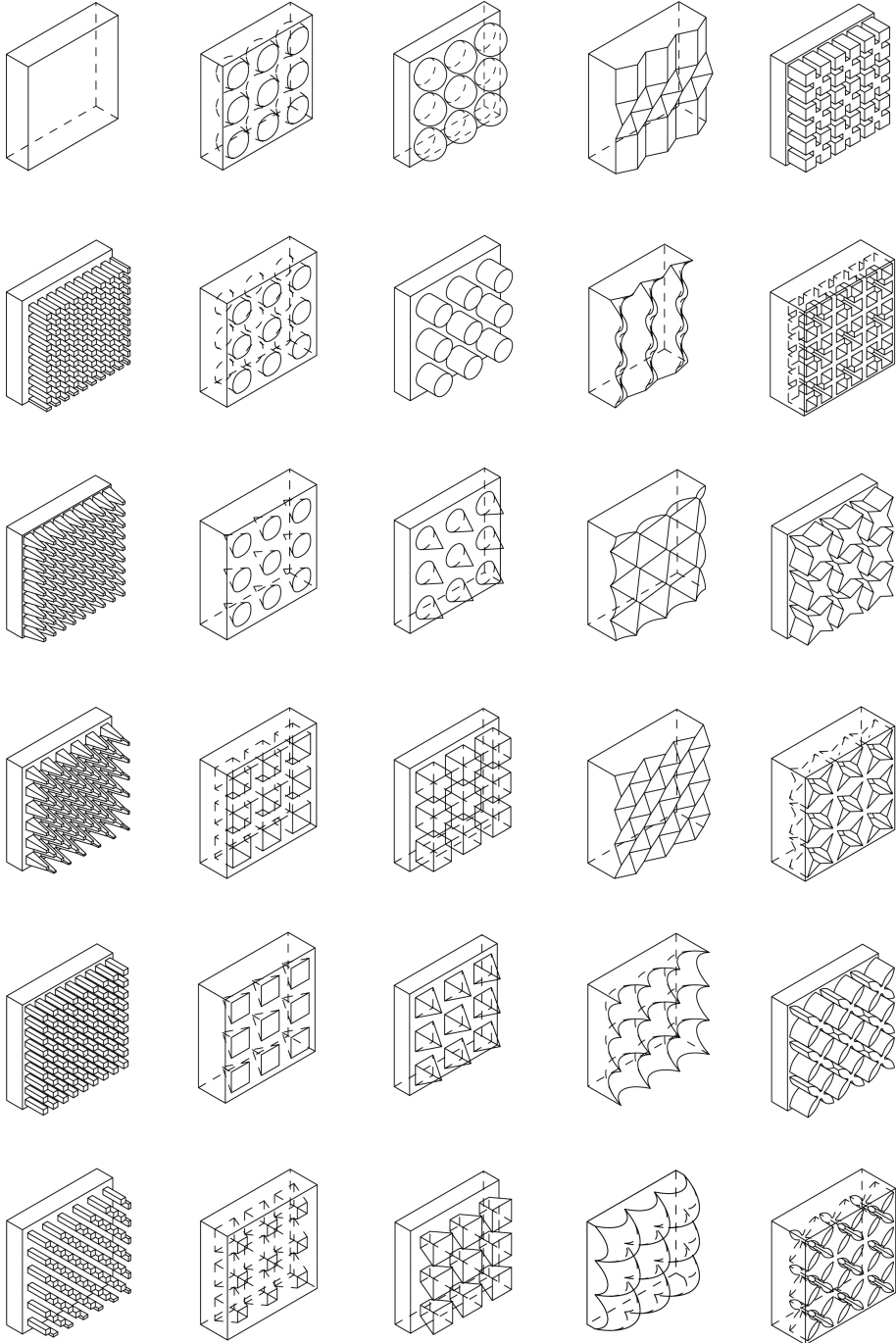


Figure 1. Tested tiles. From left to right, First row: Flat tile, Fur 1-5; Second row: Cavities 1-6; Third row: Bumps 1-6; Fourth row: Cacti 1-6; Fifth row: Sponges 1-6.

The other direction taken is learning from nature (biomimicry). Natural envelopes have been long optimized in an evolutionary process and thus efficiently perform to protect an inner space of a living creature from the outside environment. This direction was examined through three groups of envelopes: succulents, animal fur and sponges (Figure 1). For the succulent group, we picked cacti that live in harsh arid climatic conditions: *Oerocereus*, *Ferocactus*, *Mammillaria compacta*. Then we 3D scanned the chosen succulents (using an EVA scanner, ARTEC, 0.1mm accuracy) and imported the point clouds created as meshes into Rhinoceros. Measuring the exact dimensions, we created repetitive tile geometries based on the cacti textures (Figure 2). For the groups of animal fur and sponges, geometric abstraction has been used to create repetitive, comparable tiles (Figure 1). All the tiles are  $1.5 \times 20 \times 20 \text{ cm}^3$ , representing a real size  $7.5 \times 100 \times 100 \text{ cm}^3$  tile. 7 tiles of basic geometries were 3D printed (Z-Crop 350) for physical simulations.

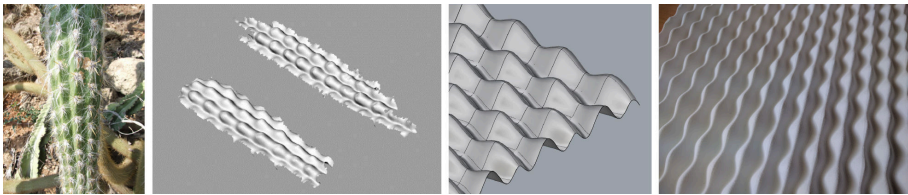


Figure 2. The process of creating geometric tiles based on cacti envelopes geometries. a - *Oerocereus* cactus, b - 3d scan converted to a point cloud mesh in Rhinoceros, c - an organized tile model, based on the exact proportions of the original scan, d - a 3d printed gypsum model.

### 3.2. WIND TUNNEL AND COMPUTATIONAL SIMULATION

A physical simulation was conducted at the Environmental Multi-Phase Flow Laboratory (EMPFL) at the Technion, Israel Institute of Technology. To model the flow on a building envelope, a set-up of a turbulent jet impinging on flat and sculptured 3d printed tiles was established (Figure 3). A detailed description of the set-up and the simulation process was presented in a previous paper (Hershovich et al., 2017). Seven 3D-printed tiles were tested: a flat tile (van Hout et al., 2018a), two tiles with large and small circular cavities (van Hout et al., 2018c, 2018b) as well as tiles with rectangular, triangular and trapezoidal cavities. Next, we performed simulations of the same tiles (3D modeled in Rhinoceros 5) using Star-CCM+ software package, defining the exact same parameters as in the physical wind tunnel simulation. Details are described in a previous paper (Hershovich et al., 2017). After comparing the experimental and numerical results, the digital simulation was validated as a reliable platform for further use. Digital simulations ran for 30 tile types: Flat tile, 12 basic geometries, 6 succulents, 5 animal fur, and 6 sponges.

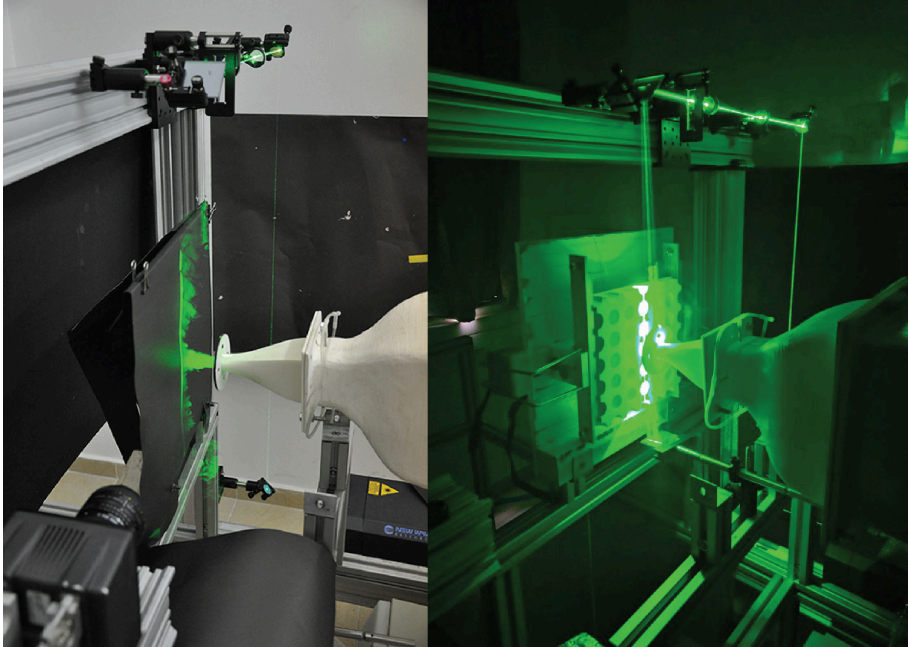


Figure 3. The experimental PIV setup (left) and flow visualization on a sculptured surface (right).

### 3.3. CONTROL SIMULATIONS

Besides 30 geometric tiles, a few control tiles were examined to validate the model assumptions. According to one of our assumptions, a perpendicular impinging jet flow on a surface provides the worst-case heat transfer scenario - where heat transfer rate through the material is highest. To validate this, the target surface (a flat tile) was positioned at an inclination of 45 degrees from the flow direction, while all other properties remained the same. The results showed that indeed the heat transfer rate is lower for a 45 degrees configuration.

## 4. Results

In total, 90 digital simulations were performed, measuring the heat transfer rate [W] in 30 tile types at three wind speeds: 1, 5, 10 m/s, corresponding to 1, 3 and 5 Beaufort numbers. The simulations aimed to examine the potential of complex geometry tiles to improve thermal performance (indicated by smaller values of heat transfer rate [W]) in comparison to a flat tile. Figure 4 presents the results for all tested tiles at the three different wind speeds, organized from smallest to largest. The figure provides a general overview of the different groups: the most significant improvement occurs in the group of animal fur, occupying the five smallest values in the graph. ‘Fur5’ provides the best results with on average an improvement of 22 percent, compared to the flat tile. Most of the geometries that

did not show any improvement belong to the groups of basic geometries (Cavities and Bumps). Within them, the bumps group occupies 4 out of the 5 largest values in the graph.

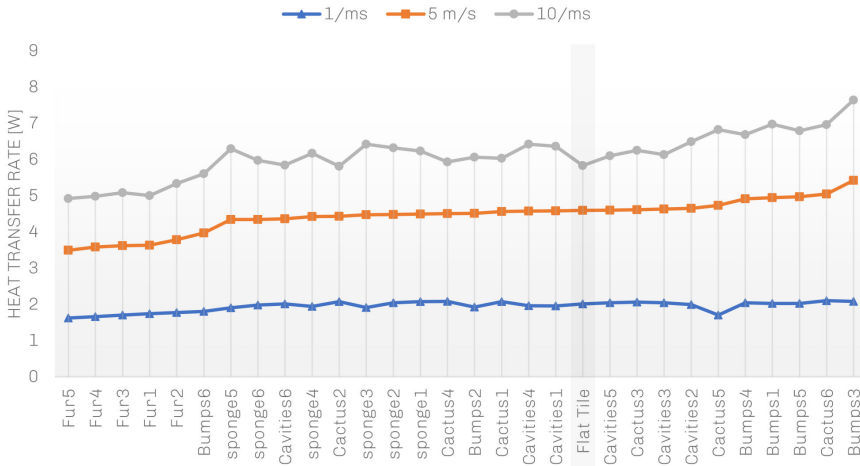


Figure 4. Heat transfer rate of tested tiles, sorted from smallest to largest results, according to a wind speed of 5m/s. .

Next, we examined the correlation between the heat transfer rate and the change in the exposed surface area in comparison to the flat tile (exposed surface ratio). A clear trend emerged for all wind speeds: as the exposed surface area ratio increases, the heat transfer rate decreases (Figure 5). This trend seems to contradict the common knowledge that the larger the surface area, the more heat it transfers. The most plausible explanation for the reduced global heat transfer is the enhanced capability of the sculptured surfaces to trap air inside cavities and increase the insulating properties of the tiles. The air serves as an insulator, a barrier, and limits heat transfer. Note that the group of animal fur is noticeably the best in trapping air, which may not come as a surprise when one considers how animals keep themselves warm. The “fur” tiles achieved the best results with relatively high surface area ratios.

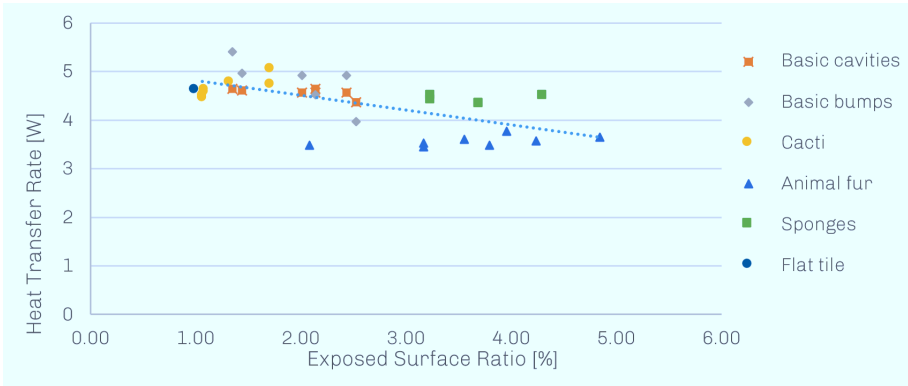


Figure 5. The relation between the obtained global heat transfer rate at a 5m/s wind speed to the exposed surface ratio (exposed surface area of a tested plate divided by the surface area of a flat tile).

Finally, to predict material savings, we looked at the tile volumes. We picked the tiles that achieved a similar result (+/- 0.05W) as the base-line flat tile for an average wind speed of 5 m/s (4.59 W) and compared their volume ratio (the tile’s volume divided by the flat tile’s volume). All the tiles that achieved a similar result as that obtained for a flat tile, had smaller volumes, varying between 0.90 (Cactus1, Cactus4) to 0.62 (Bumps2) of the original volume (Figure 6). Thus, these geometries achieved the same performance as the flat tile, while saving 10-38% of the material.

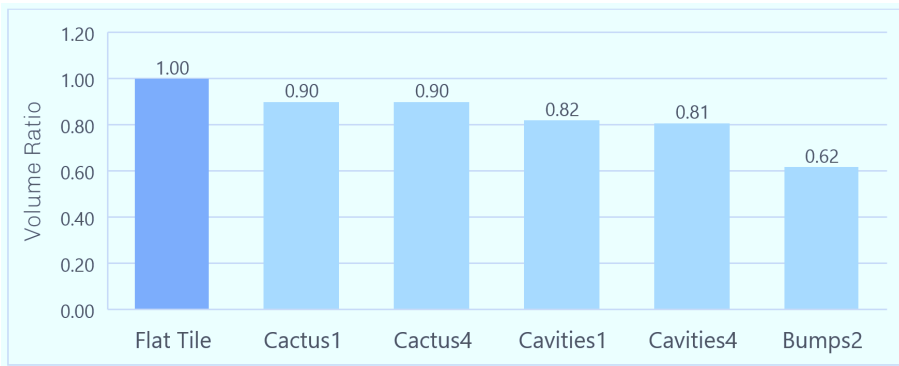


Figure 6. Volume ratio (tested tile volume divided by flat tile volume) of the tiles that reached a similar heat transfer rate (+/- 0.05W) as the flat tile for 5m/s. .

**5. Conclusion**

This paper presented the initial results of the current stage of a study examining the potential of complex geometry to reduce the heat transfer rate in concrete tiles. This stage focused on developing testing tiles and performing physical

and digital CFD simulations to examine their performance. Initial results show a reduction in heat transfer rate in most cases for the examined configuration, i.e. airflow perpendicular to the surface. The results were analyzed in relation to (i) the exposed surface area and (ii) the volume of the geometries. Surprisingly, a comparison of the exposed surface areas of the tiles showed that larger surface areas reduced the heat transfer rate in most cases. The most plausible explanation for this trend is that geometries with large surface areas are often those that have cavity geometries that facilitate trapping of air inside them. Evidence for this conjecture is depicted in Figure 7 that depicts a contour plot of the magnitude of the velocity vectors measured for a tile with trapezoidal cavities (Cavities 6). It can clearly be observed that the velocity inside the cavities is close to zero. Comparing the ratios of the sculptured tile volumes and the base-line flat tile revealed the same or even better performance can be achieved while saving material. Based on the results of the chosen geometries with the examined perpendicular flow, the main conclusion is that geometric manipulation in tiles has the potential to improve thermal performance as well as save material costs. Due to the complex nature of the airflow on an actual building envelope, the presented CFD simulations should be expanded in future research to examine wall-parallel airflow on the same geometries.

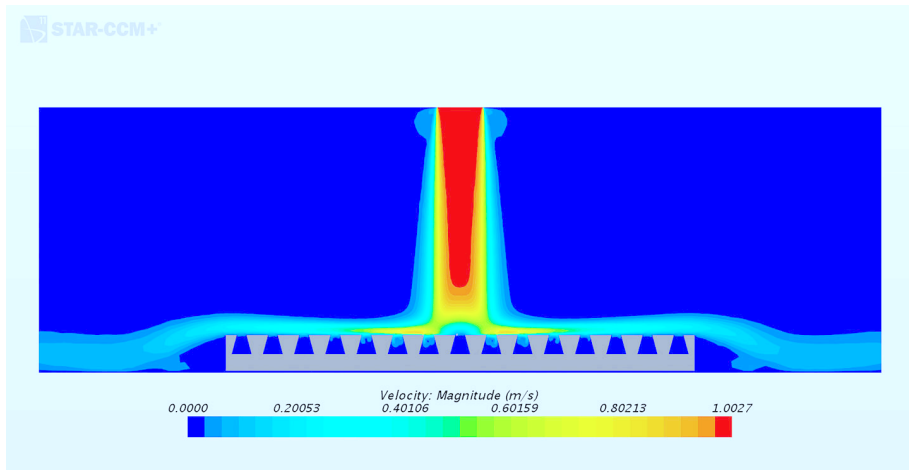


Figure 7. Contour plot of the velocity magnitude for tile 'Cavities6' at a wind speed of 5m/s (Reynolds Averaged Navier-Stokes simulation, Star-CCM+).

### Acknowledgments

The research was supported by the Israeli Ministry of Construction and Housing - grant number 2022402/2015.



## References

- Golany, G.S.: 1996, Urban Design Morphology and Thermal Performance, *Atmospheric Environment, Conference on the Urban Thermal Environment Studies in Tohwa*, **30 (3)**, 455-65.
- Golneshan, A.A. and Yaghoubi, M.A.: 1990, Simulation of Ventilation Strategies of a Residential Building in Hot Arid Regions of Iran, *Energy and Buildings*, **14 (3)**, 201-5.
- Grobman, Y.J.: 2013, Cellular Building Envelopes, *ICORD'13*, 951-963.
- Grobman, Y.J. and Elimelech, Y.: 2015, Microclimate on building envelopes: testing geometry manipulations as an approach for increasing building envelopes' thermal performance, *Archit. Sci. Rev.*, **59**, 269-278.
- Hauer, E.: 2004, *Erwin Hauer: Continua-Architectural Walls and Screens*, Princeton Architectural Press.
- Hershcovich, C., van Hout, R., Rinsky, V., Laufer, M. and Grobman, Y.J.: 2017, Microclimate on building envelopes: wind tunnel and computational fluid dynamic analysis of basic and complex geometries, *StimAUD 2017*, Toronto.
- van Hout, R., Rinsky, V. and Grobman, Y.J.: 2018, Experimental study of a round jet impinging on a flat surface: Flow field and vortex characteristics in the wall jet, *Int. J. Heat Fluid Flow*, **70**, 41-58.
- van Hout, R., Rinsky, V., Hershcovich, C. and Grobman, Y.J.: 2018, Outer shear layer characteristics of a radially expanding wall jet on smooth and dimpled surfaces, *Int. J. Heat Fluid Flow*, **72**, 304-316.
- van Hout, R., Rinsky, V., Sasson, N., Hershcovich, C., Tshuva, M. and Grobman, Y.J.: 2018, Axisymmetric jet impingement on a dimpled surface: Effect of impingement location on flow field characteristics, *Int. J. Heat Fluid Flow*, **74**, 53-64.
- Hrynyuk, J.T., van Luipen, J. and Bohl, D.: 2012, Flow Visualization of a Vortex Ring Interaction with Porous Surfaces, *Physics of Fluids*, **24 (3)**, 037103.
- Latifi Khorasgani, M., Prohasky, D., Burry, J., Moya Castro, R., McCarthy, J. and Watkins, S.: 2016, Breathing Skins for Wind Modulation through Morphology: Toward Integrating Turbulence Studies within Tectonic Scale for Design of Façade Components, *Associaion for Computer-Aided Architectural Design Research in Asia*, 219-28.
- Montazeri, H. and Blocken, B.: 2013, CFD Simulation of Wind-Induced Pressure Coefficients on Buildings with and without Balconies: Validation and Sensitivity Analysis, *Building and Environment*, **60 (February)**, 137-49.
- Stanford, A.: 2004, *Eladio Dieste-Innovation in structural art*, Princeton Architectural Press.

# ESTABLISHING A PREDICTION MODEL FOR BETTER DECISION MAKING REGARDING URBAN GREEN PLANNING IN A HIGH-DENSITY URBAN CONTEXT

JIA DING ZHONG<sup>1</sup>, MING CHUN CHAO, SARA<sup>2</sup> and JIN YEU TSOU<sup>3</sup>

<sup>1,2</sup>*Center for Housing Innovations, Chinese University of Hong Kong, Shatin, New Territories, Hong Kong, China*

<sup>1,2</sup>*{jiadingzhong|sarachao}@cuhk.edu.hk*

<sup>3</sup>*Department of Architecture and Civil Engineering, College of Science and Engineering, City University of Hong Kong, Hong Kong, China*

<sup>3</sup>*jytsou@cityu.edu.hk*

**Abstract.** This paper presents a prototype of a prediction model. The model helps to improve decision making regarding urban green patch planning. This process is achieved by the model predicting the response of thermal comfort conditions in an urban green patch to different planning decisions. This process is demonstrated via an investigation of variations in urban density. The model features a surface temperature mapping approach, which assigns surface temperature data acquired through field-measurement to solid surfaces in CFD simulations based on the shading state. Besides, trees are simulated in a systematic way, and the model combines CFD simulations with PET values, the processes of which are also demonstrated in this paper.

**Keywords.** Urban Green Planning; Decision Making; Thermal Comfort; CFD.

## 1. Introduction

As a deteriorated urban thermal environment poses threat to people's health, there has been a strong focus on protection of health against heat stress. The psychological well-being that is under the same threat should be also noticed. The improving effect of social interaction on psychological well-being has been documented by other scholars (Hartig et al. 2014; Ishii-Kuntz 1990). The use of "contacting with nature approach" to encourage social interaction in a high-density urban context, is also studied. Chao et al. (2018) performed an experimental study from which it was concluded that via participation in roof farming, people in a high-density urban context can gain more social interactions and improved psychological well-being. It has been reported a neighborhood park with ideal thermal comfort conditions can trigger its users to interact with others (Nikolopoulou and Steemers 2003). Based on these findings, an ongoing research aims to study how different planning decisions regarding neighborhood parks affect thermal comfort. Since in a high-density urban context,

the surrounding urban community has significant impacts on thermal comfort as well, the neighborhood park and the surrounding urban community are regarded as one urban green patch. Planning decisions regarding neighborhood park are the planning decisions in urban green patch.

To conduct a performance-based analysis of these interrelated planning decisions, a prediction model based on the Computational Fluid Dynamics (CFD) simulation technique is developed. Meanwhile, post-processing methods are developed to help decision-makers to understand how the thermal comfort condition responds to variations in the planning decisions.

This paper presents the processes in establishing a prototype of the prediction model that considers representative urban planning decisions in a high-density urban context and describes associated thermal comfort in Physiological Equivalent Temperature (Höppe 1999) values according to CFD simulations. The preliminary use of the model to facilitate decision making in urban green planning is also discussed.

## **2. Methodology**

### **2.1. ESTABLISHING THE PREDICTION MODEL**

To establish the prediction model, three major challenges have been tackled: 1) Identification and implementation of planning decisions; 2) Configuration of boundary conditions; 3) Calculation of PET values from CFD simulations. Each of the challenges is discussed as follows.

### **2.2. IDENTIFICATION AND IMPLEMENTATION OF PLANNING DECISIONS**

#### *2.2.1. Identify key planning decisions*

This paper uses site coverage and the plot ratio as key planning decisions to demonstrate how the prediction model operates. Site coverage and plot ratio control the spacing between adjacent buildings, which affects the wind flow pattern, and control the building height and massing, which affects interblock shading. Together, site coverage and the plot ratio can be described as urban density. Table 1 presents the 9 urban density scenarios to be investigated in a parametric study.

Table 1. Urban Density Scenarios.

Scenarios	Site Coverages	Plot Ratios
1.	50%	4.0
2.	50%	6.0
3.	50%	8.0
4.	70%	4.0
5.	70%	6.0
6.	70%	8.0
7.	90%	4.0
8.	90%	6.0
9.	90%	8.0

### 2.2.2. Implement planning decisions

The photographs shown in Figure 1 are of typical urban green patches in Hong Kong. To avoid site specific results, to facilitate parametric studies, and to increase the prediction model's calculation efficiency, a generic urban model is created based on the Hong Kong urban green patch geometry, as well as the typical urban morphology of Hong Kong.

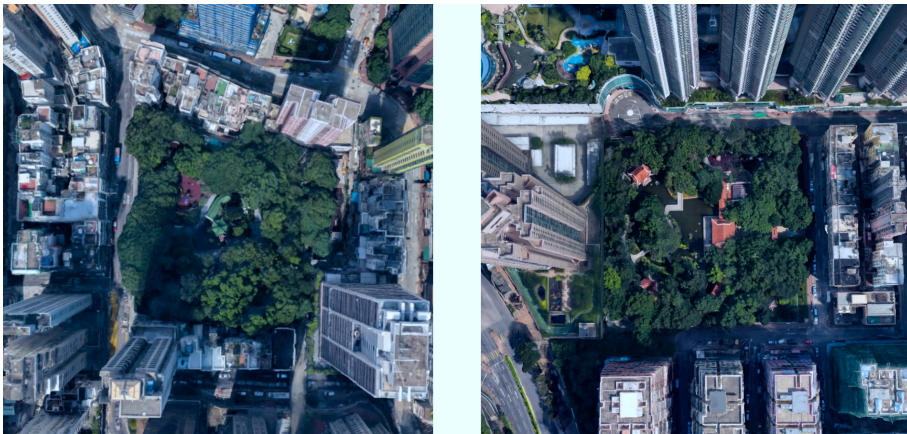


Figure 1. Green Patches in Hong Kong (Captured from Google Earth).

Figure 2 shows the generic urban model just created. The surrounding blocks represent actual buildings and the green block in the center represents the neighborhood park. Both of the buildings and the park are responsive to variations in planning decisions. For example, the green block may change to a combination of green and water body according to a different planning decision. Figures 3 and 4 demonstrate how the site coverage controls building spacing, and how the plot ratio controls building height.

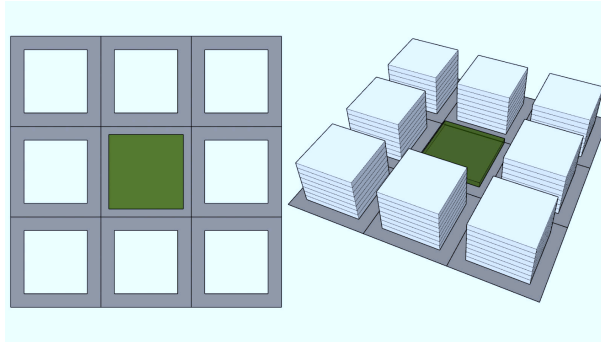


Figure 2. Generic Urban Model for Urban Green Patch.

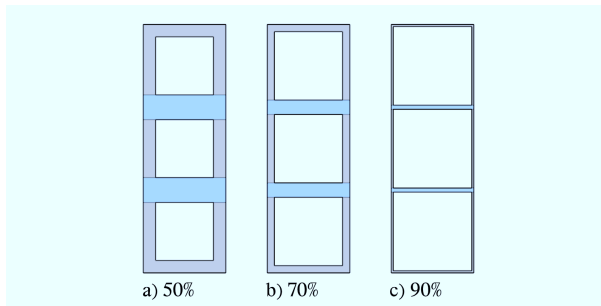


Figure 3. Building Spacing Changes Along Site Coverage Variation; Building Spacing is Highlighted in Blue.

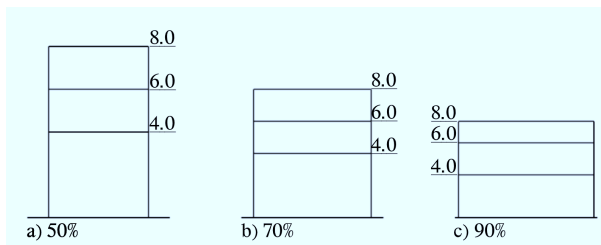


Figure 4. Building Height Changes Along Plot Ratio Variation Under Different Site Coverages.

## 2.3. CONFIGURATION OF BOUNDARY CONDITIONS

### 2.3.1. Simulate Trees

Trees have significant impacts on thermal comfort in the urban green patch. The developed prediction model can carry out simulations for three effects of trees,

namely, the shading effect, transpirational cooling effect, and aerodynamic effect. The approaches to simulating these effects are discussed as follows.

First, the shading effect is discussed. In PHOENICS, the material type of Foliage can be prescribed to tree-containing cells. Then, tree-containing cells become opaque to sunlight, and the shading effect of trees is thus simulated.

Second, the transpirational cooling effect is discussed. The group of tree-containing cells is regarded as porous media, which allows winds to penetrate but the properties of which are modified. To modify the thermal property of the wind, the volumetric cooling power developed by Gromke et al. (2015) is incorporated into each tree-containing cell. The volumetric cooling power is expressed as follows:

$$P_c = 250Wm^{-3} \cdot LAD \quad (1)$$

where  $P_c$  is the volumetric cooling power, and  $LAD$  is the leaf area density of the tree crown. The value for  $LAD$  is calculated via the following equation (2):

$$LAD = LAI/h \quad (2)$$

where  $LAI$  is the leaf area index that is prescribed by the user, and  $h$  is the average tree crown height. In this paper, the  $LAI$  value is 4.0, which represents a slightly dense tree crown, and the average tree crown height is 3m.

Third, the aerodynamic effect is discussed. There are generally two approaches to simulating the aerodynamic effect of trees (Buccolieri et al. 2018). One is the implicit method, which treats the aerodynamic effect as one of the urban surface's roughness components, the other is the explicit method, which treats the aerodynamic effect of trees more carefully. It has been found that the implicit method does not give reliable results (Salim et al. 2015). Therefore, the prediction model uses the explicit method. As in the previous step, the explicit method also regards the tree crown as porous media and prescribes source terms to tree-containing cells.

The source term to be incorporated into the momentum equation can be expressed as follows (CHAM 2019):

$$S_{d,i} = -\rho C_d LAD |U| u_i \quad (3)$$

where  $S_{d,i}$  is the source term for the drag effect,  $\rho$  is the density of air,  $C_d$  is the drag coefficient,  $LAD$  is the leaf area density given by Equation (2),  $|U|$  is the magnitude of the superficial velocity vector, and  $u_i$  is the superficial value of the Cartesian velocity along direction  $i$  (CHAM 2019).

The term  $C_d$  is an empirical constant and needs to be determined by the user. Buccolieri et al. (2018) summarized the  $C_d$  values used by other researchers. The value range is between 0.1 and 0.3, with 0.2 being the most commonly used  $C_d$  value. Since the choice of the  $C_d$  value is not the objective of this paper, a value of 0.2 is used for the prediction model.

The source terms to be incorporated into the turbulence transport equations can be expressed as follows (CHAM 2019):

$$S_k = C_d LAD \left( \beta_p |U|^3 - \beta_d |U| k \right) \quad (4)$$

$$S_\epsilon = C_d LAD \left( C_{4\epsilon} \beta_p |U|^3 \frac{\epsilon}{k} - C_{5\epsilon} \beta_d |U| \epsilon \right) \tag{5}$$

where  $S_k$  and  $S_\epsilon$  are the source terms to be incorporated into the  $k$  transport equation and the  $\epsilon$  transport equation, respectively. The terms  $\beta_p$ ,  $\beta_d$ ,  $C_{4\epsilon}$  and  $C_{5\epsilon}$  are empirical constants, the values of which need to be determined by the user (CHAM 2019). Buccolieri et al. (2018) summarized the sets of values for the empirical constants employed in different studies. They found no proof that any set of values was better off than others. Therefore, the set of values provided by Green (1992), the default option in PHOENICS, is employed in the prediction model.

Table 2. Empirical Values from Green (1992).

Empirical Constants	Green (1992)
$\beta_p$	1.0
$\beta_d$	4.0
$C_{4\epsilon}$	1.5
$C_{5\epsilon}$	1.5

### 2.3.2. Surface Temperature Mapping Based on the Shading State

Through the InForm interface of PHOENICS, the prediction model performs surface temperature mapping based on the shading state. Figure 5 below demonstrates how this process is achieved in PHOENICS. The yellow arrows represent sunlight, and the numbers are the LIT values. A cell that has an LIT value equal to 1 means that its nearest solid surface(s) is illuminated by the Sun. Solid surfaces near 0 LIT value cells are shaded. The colored cells are the three types of solid surfaces in our prediction model. Light grey cells are the building surface, dark grey cells are the artificial ground surface, and dark green cells are the natural ground surface. With the shading state being considered, each type of solid surface can be further divided into a sunlit surface or a shaded surface.

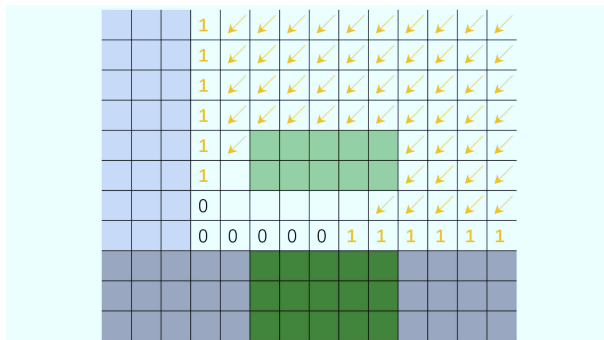


Figure 5. Achieve Surface Temperature Mapping Based on the Shading State in PHOENICS.

After finding the aforementioned 6 types of solid surfaces in the prediction model, the surface temperature at each solid surface is directly determined by data retrieved from longwave thermal infrared images. The retrieval process for the surface temperature at the artificial ground surface is demonstrated in Figure 6 as an example. After being determined for all the thermal images, the surface temperature at the artificial ground surface is determined by the mean value of all the values recorded.

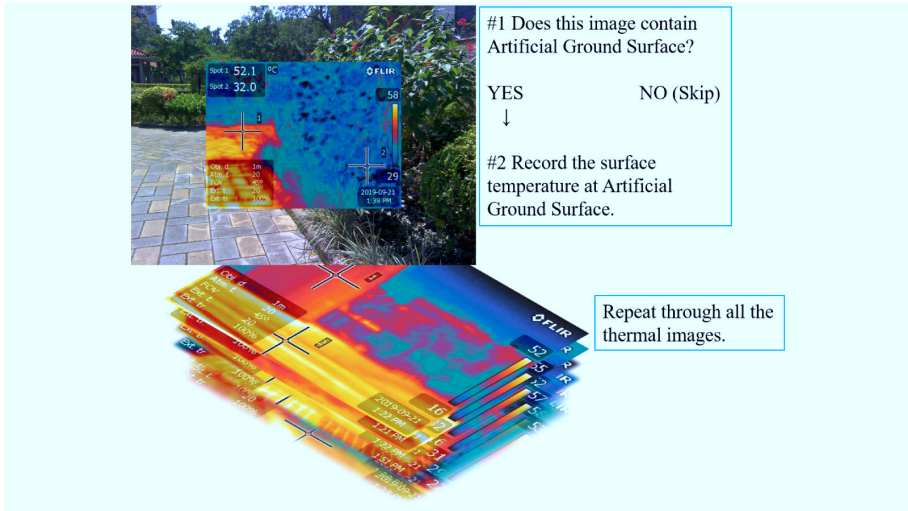


Figure 6. Surface Temperature Retrieval Process.

Figure 7 shows the mapping outcome when implemented in PHOENICS, where T3 is the term that describes the temperature in solids. The surface temperature retrieval results are listed in Table 3.

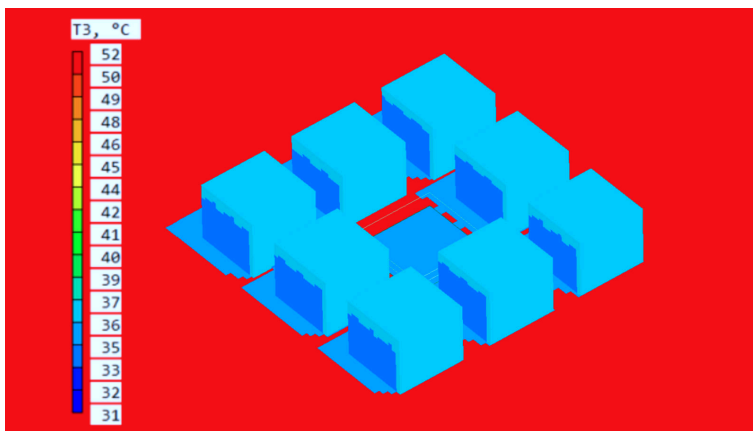


Figure 7. Mapping Outcome Based on Urban Density Scenario #1.



Table 3. Surface Types &amp; Temperatures.

	Building Surface	Artificial Ground Surface	Natural Ground Surface
Shaded	34.0°C	36.0°C	35.0°C
Sunlit	36.6°C	52.0°C	36.0°C

#### 2.4. CALCULATION OF PET VALUES FROM CFD SIMULATIONS

PET is a thermal comfort index that is a combination of different variables. Compared to air temperature, PET can reflect the actual thermal impact of different planning decisions on the human body, however, implementing PET calculations from CFD simulation outcomes is complicated, and the prediction model designs and establishes a data-processing workflow to solve this issue.

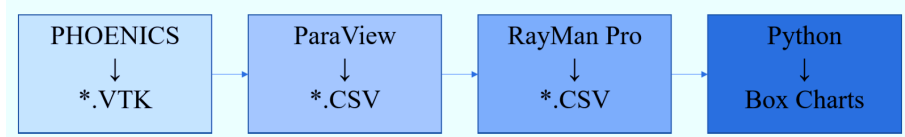


Figure 8. Data-processing Flowchart.

##### 2.4.1. Data Extraction

PET calculations are performed by RayMan Pro (Matzarakis et al. 2007; Matzarakis et al. 2010) for individual points. Figure 9 shows 28 monitoring points placed in the generic urban model for the PET calculation. Procedures to extract data at these monitoring points are: 1) Generate VTK file via PHOENICS; 2) Translate VTK file into CSV file in ParaView; 3) Delete data that is not on the monitoring points using a CSV reader.

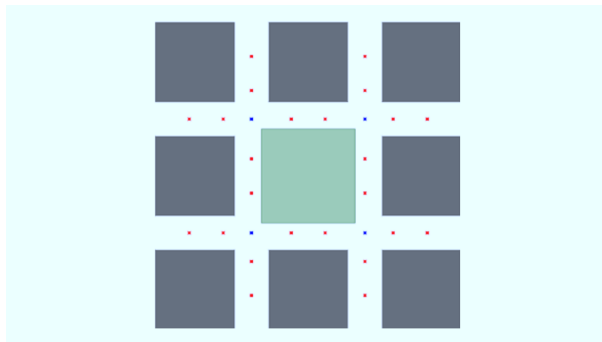


Figure 9. Distribution of Monitoring Points.

#### 2.4.2. PET Calculation

RayMan Pro requires the following value inputs to calculate PET, air temperature, relative humidity, wind velocity, mean radiant temperature, heat resistance of clothing, and activity of humans.

The values for air temperature, wind velocity, and the mean radiant temperature come from the aforementioned CSV file, while assumptions are taken for the other values. The relative humidity is assumed to be 80% at all the monitoring points to represent typical climate conditions in Hong Kong. The heat resistance of clothing is assumed to be 0.6 clo, which represents the common summer dress, and the activity of humans is assumed to be 90 W, which represents people standing calm.

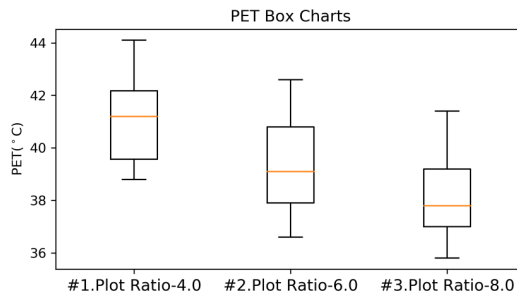


Figure 10. Some of the Prediction Results.

Box charts in Figure 10 above are some of the prediction results drawn with Matplotlib (Hunter 2007). There is a trend that, under the same site coverage of 50%, the increasing plot ratio can improve thermal comfort conditions in the urban green patch in a high-density urban context. Such a finding can be a reference to be used in decision making regarding urban green patch planning.

### 3. Conclusion & Limitations

This paper presents a prototype of the prediction model that aims to improve decision making regarding urban green patch planning in a high-density urban context. Variations in urban density are investigated in this paper, and the results are described in PET. For the CFD part, steady-state RANS simulations closed with the standard k- $\epsilon$  model are performed, and the surface temperatures are determined through a field-measurement.

The model is able to simulate different building settings, e.g. uneven building heights, various typologies, different orientations, etc. But in view of simulation result accuracy, the present model has a few major drawbacks that need to be addressed. First, the model ignores vehicle exhaust, which can be a significant source of heat stress. Second, the model adopts an assumption that the relative humidity is constant throughout the domain, which is not suitable for simulating water features. Finally, high albedo facade materials can be a cause for an oppressive pedestrian thermal environment, as the materials reflect a great amount of short-wave radiation towards pedestrians, but the model cannot yet simulate

short-wave radiation reflection.

The ongoing research also includes park surveys. Hopefully, the model can help study how different park designs or urban green patch design options affect users' thermal comfort (PET), thus supporting further studies related to social interaction and even psychological well-being in a high-density urban context.

## References

- Buccolieri, R., Santiago, J.L., Rivas, E. and Sanchez, B.: 2018, Review on urban tree modelling in CFD simulations: Aerodynamic, deposition and thermal effects, *Urban Forestry & Urban Greening*, **31**, 212-220.
- CHAM, initials missing: 2019, "The PHOENICS-VR reference guide; TR 326" . Available from <[http://www.cham.co.uk/phoenics/d\\_polis/d\\_docs/tr326/obj-type.htm#Foliage](http://www.cham.co.uk/phoenics/d_polis/d_docs/tr326/obj-type.htm#Foliage)> (accessed 21st November 2019).
- Chao, M.C., Tsou, K. and Tsou, J.Y.: 2018, Implementation of therapeutic landscapes through urban farm approach in high-density urban context: Hong Kong as an example, *Proceedings of The 8th Tropical and Subtropical Green Building Council Alliance Conference & The 9th Cross-Strait Green Building Technology Development Forum*, Hong Kong, China.
- Green, R.S.: 1992, Modelling turbulent air flow in a stand of widely-spaced trees, *PHOENICS Journal*, **5**(3), 294-312.
- Gromke, C., Blocken, B., Janssen, W., Merema, B., Hooff, T. and Timmermans, H.: 2015, CFD analysis of transpirational cooling by vegetation: Case study for specific meteorological conditions during a heat wave in Arnhem, Netherlands, *Building and Energy*, **83**, 11-26.
- Hartig, T., Mitchell, R., de Vries, S. and Frumkin, H.: 2014, Nature and health, *Annual Review of Public Health*, **35**(1), 207-228.
- Hunter, J.D.: 2007, Matplotlib: A 2D graphics environment, *Computing in Science & Engineering*, **9**, 90-95.
- Höppe, P.: 1999, The physiological equivalent temperature - a universal index for the biometeorological assessment of the thermal environment, *Int J Biometeorol*, **43**(2), 71-75.
- Ishii-Kuntz, M.: 1990, Social interaction and psychological well-being: comparison across stages of adulthood, *Int J Aging Hum Dev*, **30**(1), 15-36.
- Matzarakis, A., Rutz, F. and Mayer, H.: 2007, Modelling radiation fluxes in simple and complex environments - application of the RayMan model, *International Journal of Biometeorology*, **51**(4), 323-334.
- Matzarakis, A., Rutz, F. and Mayer, H.: 2010, Modelling radiation fluxes in simple and complex environments: basics of the RayMan model, *International Journal of Biometeorology*, **54**(2), 131-139.
- Nikolopoulou, M. and Steemers, K.: 2003, Thermal comfort and psychological adaptation as a guide for designing urban spaces, *Energy and Buildings*, **35**, 95-101.
- Salim, M.H., Schlünzen, K.H. and Grawe, D.: 2015, Including trees in the numerical simulations of the wind flow in urban areas: Should we care?, *J. Wind Eng. Ind. Aerodyn.*, **144**, 84-95.

# AN INVESTIGATION ON THE DEVIATION OF MICROCLIMATE SIMULATION BASED ON ENVI-MET

*Taking Suzhou Industrial Park as a Case Study*

HAINAN YAN<sup>1</sup> and GUOHUA JI<sup>2</sup>

<sup>1,2</sup>*School of Architecture and Urban Planning, Nanjing University*

<sup>1</sup>*dg1936002@smail.nju.edu.cn* <sup>2</sup>*jgh@nju.edu.cn*

**Abstract.** In this study, the applicability of ENVI-met was tested in the Suzhou Industrial Park (SIP). Eight selected parks in the core area of SIP were selected as samples for site measurement and simulation. Measurements were compared with estimated values derived from the ENVI-met model by the analysis of Root Mean Square Error (RMSE). Results showed that RMSE can properly represent simulation deviations and there was a significant positive correlation between the area of parks and relative humidity. During the daytime, the ENVI-met model overestimated air temperature and underestimated relative humidity, with no consistent simulation deviation for wind speed; During the nighttime, the simulation deviation of the ENVI-met model for the three climate parameters mentioned above did not show a consistent pattern. Consequently, this study considers that the ENVI-met model is not suitable for simulation at night time. The findings of this study will help researchers and planners recognize the limitations of the model and the accuracy of the results.

**Keywords.** ENVI-met; Microclimate; Deviation; Suzhou Industrial Park.

## 1. Introduction

With the help of computer-aided simulation, many studies on urban microclimate have emerged in recent years. There are many urban microclimate simulators based on computational fluid dynamics. Among these, ENVI-met has become a prevailing choice since it combines the outdoor wind field and thermal environment for comprehensive simulation analysis (Chen and Ng, 2012; Yang et al., 2012).

However, ENVI-met is developed for the cold climate in middle and high latitudes. Its accuracy under different climatic conditions needs to be investigated. And many parameters, such as the cell size of the simulation model or the update interval of the simulation, cannot be given with certainty. Furthermore, ENVI-met overlooks the effect of anthropogenic heat sources and cannot accurately describe the terrain of the site. As a result of these deficiencies, there must be deviations

between the simulation results and the actual microclimate of the site (Tsoka et al., 2018).

Validation with field measurement is an integral part of simulation-based studies. In terms of the accuracy of simulated data compared to measured values, the widely applied statistics involve difference metrics including Root Mean Square Error (RMSE), Mean Bias Error (MBE), the Mean Absolute Error (MAE) and the coefficient of determination R-Squared. Salata et al. (2016) verified the simulation deviation through field measurement in Rome, and the result showed that the values of R-Squared were 0.88 and 0.96 for air temperature and mean radiant temperature respectively, indicating a strong correlation between the measured value and the simulated value. In the study of Wang and Akbari (2015) carried out in Montreal, Canada, RMSE was selected to assess the discrepancy between the modeled and measured data. They further discovered that the discrepancy can be attributed to the disregard of cloud cover and the neglect of the influence of horizontal long-wave fluxes in the model. Nevertheless, the difference between measured and simulated data is not always attributed to ENVI-met, different parameter inputs can also result in simulation deviations. For example, if the data of the meteorological station far away from the measured site are taken as the input condition, a large deviation will occur.

This study took Suzhou as an example, which is a humid subtropical monsoon climate zone in China. Eight green spaces in the core area of the Suzhou Industrial Park (SIP) were selected as samples. Firstly, the microclimate factors of the site were measured. On this basis, ENVI-met was used for simulation. RMSE was used to analyze the overall deviation of ENVI-met simulation, and the simulation deviation trend for selected parks with different area sizes was revealed.

## **2. Experimental measurements on the field**

### **2.1. STUDY AREA AND FIELD MEASUREMENT**

The Suzhou Industrial Park (SIP) is located in the east of Suzhou ancient city. Over the past two decades, the urbanization process in this region has been rapidly promoted, and now it has been built into a high-density urban area. As the core area of the Suzhou Industrial Park, the Jinji Lake central business district was selected as the study area. As shown in Fig.1, eight parks were selected as survey samples. The selected parks are equally distributed on the east and west sides of the Jinji Lake, and the area of parks ranges from small to large, which is convenient for comparative analysis.

During on-site measurement, three measurement points were placed inside each park, and a reference control point was placed in an open area near the park. During the data processing stage, the data of the three measurement points were averaged to reflect the microclimate of the whole park. Measurement was conducted in August since this month had the hottest days throughout the year and sunny-cloudless weather often appears. Due to the lack of meteorological instruments, only one park can be measured at a time. The eight parks were measured in batches over a period of about half a month, from August 6, 2018 to August 24, 2018. Fig.2 lists the area of the park, the dates of measurement, and

the distribution of measurement points within each park.

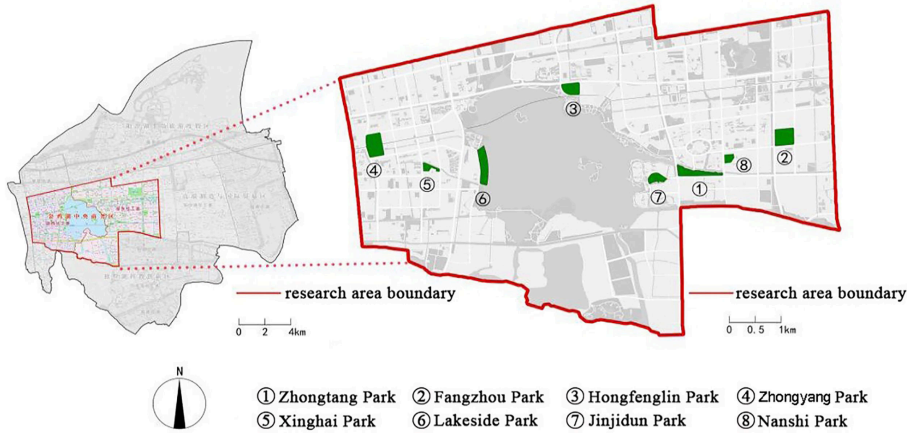


Figure 1. Study area and location of eight parks.



Figure 2. Measurement points and dates of selected parks.

## 2.2. EQUIPMENT USED FOR ON-SITE MEASUREMENT

The portable automatic weather stations (product model: FR-HWS) were used by the measurement of microclimate in summer. The performance parameters of the weather station are shown in Table 1. There were four weather stations in total, among which three were placed within the park green space and the other one was placed outside the park green space as a control measurement point. According

to a study conducted by Grimmond(2010), the weather measurement equipment should be installed at the standard observational height, which could vary from 1.25m to 2m. In keeping with this practice, the weather stations were installed at 1.5m above the ground level. The instrument recording interval was set to 10 minutes. The starting time of instrument measurement was set at 12:00 noon, and each measurement point was continuously measured for 24 hours. The position of the instrument was as far as possible to avoid the shadow of the building, reflective objects or the influence of heat sources such as air conditioners. The meteorological data released by Suzhou meteorological station were recorded synchronously during each measurement to verify the accuracy of microclimate measured data.

Table 1. performance parameters of the portable automatic weather station.

<b>Meteorological Data</b>	<b>Range</b>	<b>Resolution</b>	<b>Accuracy</b>
Air temperature	-50--50°C	0.1°C	±0.2°C
Relative humidity	0--100%RH	0.1%RH	±3%RH
Wind speed	0--45m/s	0.1m/s	± (0.3+0.03V) m/s
Wind direction	0--360°	3°	±5°
Air pressure	300--1100hpa	0.1hpa	±0.3hpa

### 2.3. MODEL CONFIGURATION

In this study, ENVI-met version 4.4.3 was used to achieve the research objectives (Bruse and Fler, 1998). The ENVI-met simulations were done at the same days of the field measurements. In order to guarantee the stability of the simulation process, the study adopted the boundary input conditions of the “Full Forcing” mode. The parameters of air temperature, relative humidity, and wind field came from the instrument of the control measurement point. The solar radiation data came from Suzhou meteorological station. The rest of the meteorological conditions remain default along the simulation period (e.g. cloud conditions and soil conditions).

Characteristics of the model domain in selected parks are presented in Table 2. To get more microclimate information concerning pedestrian height, the height of the cell was set at 0.5m in the 5 lowest grid cells. Additionally, a telescoping grid was used. Vegetation in the model domain was selected from the plant database of ENVI-met. The height, LAD and RAD attributes of the plant database were modified to approximate the planting in the study area. In order to compare with the measured data, three receptors were placed in each simulated area.

When the simulation is complete, the model produces many types of output parameters. In this study, air temperature, relative humidity, and wind speed were used as indicators to verify the accuracy of the simulation.

Table 2. Description of the model dimensions of selected parks.

Selected Park	Number of grid cells (x,y,z)	Size of grid cells (meter)(x,y,z)	Nesting Grids
Zhongtang Park	322,113,60	2,2,increasing with height	3
Fangzhou Park	171,130,30	2,2,increasing with height	3
Hongfenglin Park	180,123,30	2,2,increasing with height	3
Zhongyang Park	260,211,50	2,2,increasing with height	3
Xinghai Park	200,110,30	2,2,increasing with height	3
Hubin Park	100,206,30	2,2,increasing with height	3
Jinjidun Park	170,119,40	2,2,increasing with height	3
Nanshi Park	110,96,40	2,2,increasing with height	3

### 3. Results and discussion

#### 3.1. RESULTS OF ON-SITE MEASUREMENT

The values of air temperature, relative humidity and wind speed collected from three measurement points in each park were calculated on average to obtain the overall microclimate of each park green space. The meteorological parameters of each park were different, and they all showed a certain amount of fluctuation during the measurement period. The gradual decrease in average temperatures across the park green spaces can be attributed to the sequence of dates measured partially. As the measurement activity progressed, the hot weather gradually disappeared. As shown in Table 3, the average temperature ranged from 26.41°C (Jinjidun Park) to 31.72°C(Hongfenglin Park), the average relative humidity ranged from 70.14% (Hongjidun Park) to 80.21% (Zhongtang Park), and the average wind speed ranged from 0.02m/s (Fangzhou Park) to 0.61m/s(Xinghai Park). Fig.3 shows the measured air temperature, relative humidity, and wind speed respectively.



Table 3. Measured meteorological conditions in selected parks.

Selected Park	Mean meteorological parameters		
	Air Temperature (°C)	Relative Humidity (%)	Wind Speed (m/s)
Zhongtang Park	30.80	80.21	0.23
Fangzhou Park	30.39	76.50	0.02
Hongfenglin Park	31.72	70.14	0.07
Zhongyang Park	30.56	77.04	0.38
Xinghai Park	29.59	79.13	0.61
Hubin Park	29.11	77.93	0.45
Jinjidun Park	26.41	74.14	0.32
Nanshi Park	27.93	74.63	0.17

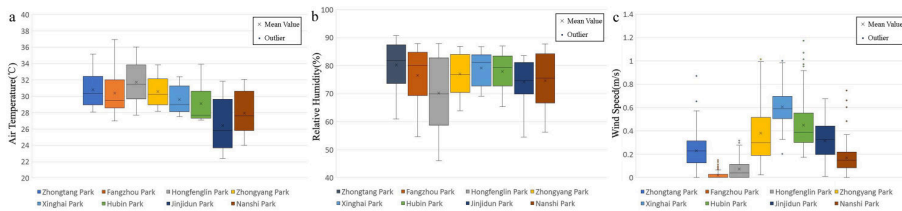


Figure 3. Measured (a) air temperature; (b) relative humidity and (c) wind speed in selected parks during the measurement period.

### 3.2. COMPARISON BETWEEN MEASURED & MODELED CLIMATE VARIABLES

In this section, RMSE is used to calculate the deviation between simulated and measured data to determine whether the deviation is within an acceptable range. Then the measurement time was divided into daytime (06:00-18:00) and nighttime (18:00-06:00) to evaluate the relationship between the simulated data and the measured data. In addition, in order to analyze the correlation between simulation deviation and park area, the selected parks were reordered by size.

#### 3.2.1. Analysis of the deviation by RMSE values

RMSE is one of the most reliable methods of error assessment and has been widely used in previous studies (Franks et al., 1982; Girard et al., 2018). According to the calculation formula of RMSE, the closer the value approaches zero, the higher the simulation accuracy is. In most of the observations in this study, RMSE values were at low levels.

As shown in Table 4, RMSE values for air temperature ranged from 0.95°C (Nanshi Park) to 2.13°C (Fangzhou Park), RMSE values for relative humidity

ranged from 4.68% (Nanshi Park) to 6.55% (Fangzhou Park), RMSE values for wind speed ranged from 0.05m/s (Fangzhou Park) to 0.32m/s (Nanshi Park). The Nanshi Park, with the smallest area, had the smallest simulation deviation in air temperature and relative humidity, and the largest simulation deviation in wind speed. On the other hand, the larger Fangzhou Park had the largest simulation deviation in air temperature and relative humidity, and the smallest simulation deviation in wind speed. From a comprehensive perspective, with the increase of the area of selected parks, the simulation deviation of ENVI-met on air temperature and relative humidity would increase, while the simulation deviation of wind speed had no obvious tendency.

This study further analyzed the correlation between simulation deviations of the area of parks and climate parameters, and the results showed that the correlation index between simulation deviations of relative humidity and park area was 0.729 ( $p < 0.05$ ), indicating that there was a significant positive correlation between the area of parks and relative humidity. The other two climate parameters (air temperature and wind speed) had weak correlations with the simulation deviation and failed the significance test.

Table 4. RMSE values between simulation data and measured data in selected parks.

Selected Park	Area (m <sup>2</sup> )	RMSE		
		Air Temperature (C°)	Relative Humidity (%)	Wind Speed (m/s)
Nanshi Park	25400	0.95	4.68	0.32
Xinghai Park	31500	1.44	5.27	0.26
Jinjidun Park	41400	1.47	5.7	0.15
Hongfenglin Park	72500	1.08	5.49	0.1
Hubin Park	86600	1.34	5.08	0.19
Zhongtang Park	94300	1.71	5.96	0.17
Fangzhou Park	107200	2.13	6.55	0.05
Zhongyang Park	137600	1.48	6.14	0.2

### 3.2.2. Analysis of the deviation during daytime (06:00-18:00) and nighttime (18:00-06:00)

As shown in Fig.4a, the ENVI-met evaluation results showed that the model underestimated air temperature for only one site with the smallest area (Nanshi Park) and overestimated for the rest seven sites during the daytime. Fig.4b showed the model generally underestimated relative humidity in all eight sites during the daytime. There was no obvious trend for the simulation deviation of wind speed (Fig.4c).

At nighttime, the simulation deviation of ENVI-met on air temperature, relative

humidity, and wind speed had no obvious consistency and trend, which may be caused by the disappearance of solar radiation at night (Fig.5a, Fig.5b, and Fig.5c).

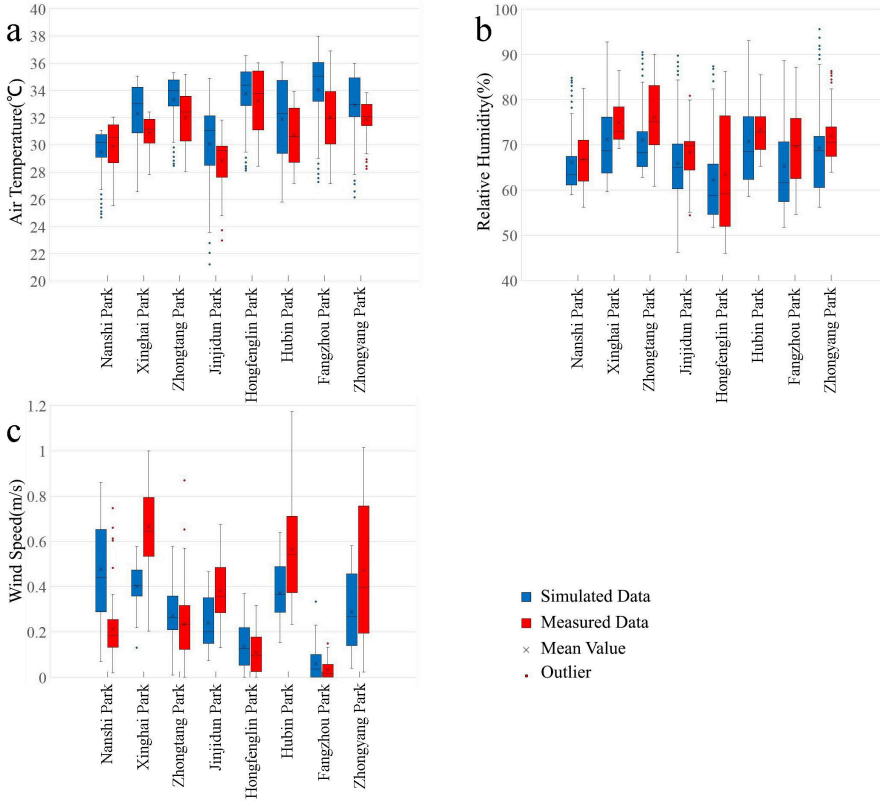


Figure 4. Comparison between measured & modeled climate variables of (a) air temperature; (b) relative humidity and (c) wind speed during daytime (06:00-18:00).

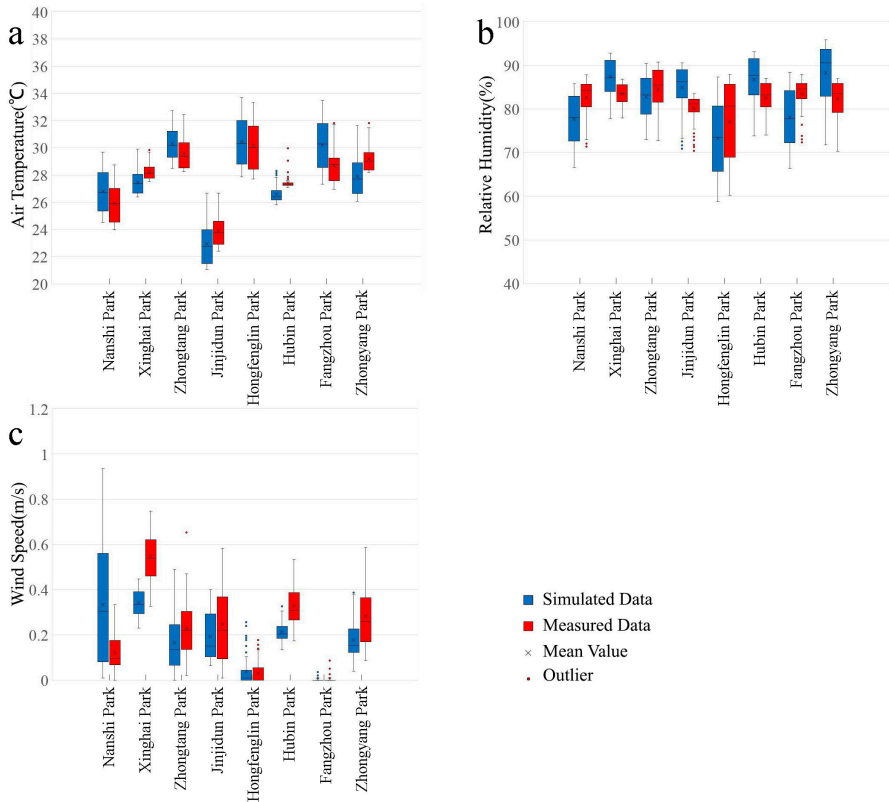


Figure 5. Comparison between measured & modeled climate variables of (a) air temperature; (b) relative humidity and (c) wind speed during nighttime (18:00-06:00).

#### 4. Conclusions

With the aid of ENVI-met, a holistic microclimatic modeling system, this paper aims to explore the simulation deviation of the software for the summer microclimate of Suzhou. The results showed that the RMSE maximum value of air temperature was 2.13°C, the RMSE maximum value of relative humidity was 6.55%, and the RMSE maximum value of wind speed was 0.32m/s. There are various reasons for software simulation deviations. Considering the specific situation of the site, this paper considers that the main reasons are as follows:

a) Potential inaccuracies in the input data regarding ground material, vegetation, and building height.

b) The radiation data obtained from the Suzhou meteorological station were too large, resulting in the model overestimating the air temperature during the daytime (06:00-18:00).

c) The incomplete modeling of the buildings around the selected parks in this

study resulted in the ENVI-met model not being able to reflect the real wind field, which partly led to the model's simulation deviations of wind speed.

The results of this study showed that there was no obvious consistency and regularity in the simulation deviation of ENVI-met at nighttime (18:00-06:00), which may be related to solar radiation factors. Related studies by Jamei et al., in Melbourne, also showed that the ENVI-met model was not suitable for simulation during nighttime (Jamei et al., 2019). Additionally, simulations of ENVI-met ran slowly and tended to consume a lot of time. The overall duration for running all eight simulations took approximately 20 days. This time-consuming process is the major challenge of ENVI-met in urban planning and design studies.

Based on above-mentioned conclusions, despite the ENVI-met model can be used as a forceful tool for urban climate analysis, it is important that researchers are aware of the limitations of the model and the accuracy of the results.

## References

- Bruse, M. and Fleer, H.: 1998, Simulating surface-plant-air interactions inside urban environments with a three dimensional numerical model, *Environmental Modelling & Software*, **13**(3-4), 373-384.
- Chen, L. and Ng, E.: 2012, Outdoor thermal comfort and outdoor activities: A review of research in the past decade, *Cities*, **29**(2), 118-125.
- Franks, I.M., Wilberg, R.B. and Fishburne, G.J.: 1982, Consistency and error in motor performance, *Human Movement Science*, **1**(2), 109-123.
- Girard, P., Nadeau, D.F., Pardyjak, E.R., Overby, M., Willemsen, P., Stoll, R., Bailey, B.N. and Parlange, M.B.: 2018, Evaluation of the QUIC-URB wind solver and QESRadiant radiation-transfer model using a dense array of urban meteorological observations, *Urban Climate*, **24**, 657-674.
- Grimmond, C., Roth, M., Oke, T., Au, Y., Best, M., Betts, R., Carmichael, G., Cleugh, H., Dabberdt, W., Emmanuel, R., Freitas, E., Fortuniak, K., Hanna, S., Klein, P., Kalkstein, L., Liu, C., Nickson, A., Pearlmutter, D., Sailor, D. and Voogt, J.: 2010, Climate and More Sustainable Cities: Climate Information for Improved Planning and Management of Cities (Producers/Capabilities Perspective), *Procedia Environmental Sciences*, **1**, 247-274.
- Jamei, E., Seyedmahmoudian, M., Horan, B. and Stojcevski, A.: 2019, Verification of a bioclimatic modeling system in a growing suburb in Melbourne, *Science of The Total Environment*, **689**, 883-898.
- Salata, F., Golasi, I., de Lieto Vollaro, R. and de Lieto Vollaro, A.: 2016, Urban microclimate and outdoor thermal comfort. A proper procedure to fit ENVI-met simulation outputs to experimental data, *Sustainable Cities and Society*, **26**, 318-343.
- Tsoka, S., Tsikaloudaki, A. and Theodosiou, T.: 2018, Analyzing the ENVI-met microclimate model's performance and assessing cool materials and urban vegetation applications-A review, *Sustainable Cities and Society*, **43**, 55-76.
- Wang, Y. and Akbari, H.: 2015, Development and application of 'thermal radiative power' for urban environmental evaluation, *Sustainable Cities and Society*, **14**, 316-322.
- Yang, X., Zhao, L., Bruse, M. and Meng, Q.: 2012, An integrated simulation method for building energy performance assessment in urban environments, *Energy and Buildings*, **54**, 243-251.

# RESEARCH ON SPATIAL DISTRIBUTION AND PERFORMANCE EVALUATION OF MASS SPORTS FACILITIES BASED ON BIG DATA OF SOCIAL MEDIA

*A Case Study of Harbin*

QI GUO<sup>1</sup> and HONGYUAN MEI<sup>2</sup>

<sup>1,2</sup>*School of Architecture, Harbin Institute of Technology; Key Laboratory of Cold Region Urban and Rural Human Settlement Environment Science and Technology, Ministry of Industry and Information Technology*

<sup>1</sup>871557387@qq.com <sup>2</sup>crystalguoqi1213@163.com

**Abstract.** The extensive application of Python script provides a new opportunity for the research on spatial distribution of mass sports facilities. The traditional way to obtain geography information of POI is by the crawler of API open platform, which needs accurate search content. Therefore, it is difficult to obtain the geography information of the mass sports facilities, which do not have specific category name. The paper took Harbin City in China as an example, combined the social network address text crawler and map websites crawler, accurately obtained the geographic information of mass sports facilities, and used ArcGIS to realize the visualization of the spatial distribution information. Combined with the information of Harbin population distribution, the paper evaluated the quantity spatial distribution and type spatial distribution of mass sports facilities by Lorenz curve and Global Moran's I, aiming to evaluate the health service performance of existing mass sports facilities and provide reference for the design and planning of sports facilities. The paper draws the conclusion that the distribution of mass sports buildings in Harbin is relatively average with the population distribution and the clustering of sports function types of mass sports buildings is obvious.

**Keywords.** Mass sports facilities; spatial distribution; crawler; Lorenz curve; Global Moran's I.

## 1. Introduction

Mass sports facilities are important urban public facilities to support physical activity. The rationality of its spatial distribution has a great impact on the sports participation. Humel (2002), Owen (2004) and Stralen (2009) have confirmed that the layout of mass sports buildings would promote residents' health. Andrew (2008) and T. Limstrand (2010) have pointed out that the quantity, type diversity, management and maintenance status of mass sports buildings are important factors

affecting the sports participation of residents. Therefore, the research on the spatial distribution and service performance of mass sports buildings has been paid attention by scholars in various fields. ZHOU (2018) studied the effect of the quantity, scale and location of urban green space on residents' physical activity. CAI (2018) evaluated the spatial distribution of sports facilities according to the quantity of sports facilities and their service area. TANG (2015), CHAI (2014) and WANG (2018) combined the quantity distribution with the population distribution to evaluate the social equity of spatial distribution. However, Chinese existing statistics of public sports facilities rely on the general survey of national sports venues conducted by the General Administration of Sport, and its data structure cannot fully reflect the current situation. The existing research relies on government data, which is regionally absent and slowly updated. Therefore, it is important to find a way to obtain the current accurate location and type of mass sports facilities.

GIS (Geography Information System) is widely used in the research on spatial distribution of sports facilities. However, the information of spatial distribution of sports facilities in urban areas cannot be accurately obtained either by field survey or by VGI (Volunteered Geography Information) and PPGIS (Public Participation Geography Information). With the wide application of Python web crawler, big data information obtained technology based on POI (Point of Interests) has been gradually applied to the research of urban spatial distribution. For instance XU Zhibang (2018) use POI data to analysis the fire station distribution, and Caihui Cui (2015) use POI data to analysis the retail spatial pattern in Zhengzhou. However, as mass sports facilities are different from parks, stations, hospitals and other defined POIs, the group don't have an accurate category name due to its complex constitution, and that makes the traditional methods of map searching and crawling have the problems of repeated search, deviation search and data cleaning. The paper takes Harbin mass sports facilities as the research object, crawling the fitness facilities address on social evaluation websites, using the combination of store address text crawler and longitude latitude crawler to obtain the big data of Harbin mass sports facilities. Combining with ArcGIS crawler of administrative boundary of Harbin, the paper analyzed and evaluated the quantity distribution and type distribution of mass sports facilities.

## **2. Method**

### **2.1. DATA OBTAIN METHOD**

#### *2.1.1. Data obtain method of geographic information for mass sports facilities*

The web crawler supported by Python script is the main method to obtain big data of urban geography information. The main process of web crawler contains data acquisition, data analysis, data extraction and data storage. You should judge if the information is located in HTML or XHR, import the response module to obtain the website data, use the "BeautifulSoup" or "Json" module to analyze the data, hierarchically extract the required data, and then use the CSV module to store the extracted data structurally.

According to this principle, the web crawler cannot get the information that





## 2.2. DATA ANALYSIS METHOD

### 2.2.1. Evaluation method of quantity spatial distribution

The paper used the Lorenz curve and Gini coefficient to evaluate the performance of the quantity spatial distribution. Loren curve is a statistical description tool invented by the American statistician M.O. Lorenz in 1907 to evaluate the fairness of national income distribution. Its horizontal axis is the cumulative percentage of allocated elements, and its vertical axis is the cumulative percentage of allocated resources. It is generally believed that the larger the curvature of Lorenz curve is, the more unbalanced the distribution is. In addition to economics, Lorenz curve and Gini coefficient are also widely used in the evaluation of equity in resource allocation. Set the cumulative ratio of resources as  $y$  and the cumulative ratio of allocation elements as  $x$ , then the points on the Lorenz curve can be calculated according to Formula 1 and 2. Gini coefficient is an evaluation index developed from Lorenz curve. The calculation formula of Gini coefficient is shown in Formula 3.  $r_k$  is the cumulative proportion of permanent population variable or geographical variable,  $k$  is the number of the  $k$ -th spatial unit, and  $S_k$  is the variable of mass sports facilities.

According to the Gini coefficient level stipulated by the United Nations Development Program, if the Gini coefficient is lower than 0.2, it means that the distribution equity is higher than the average level; if the Gini coefficient is between 0.2-0.29, it means that the distribution equity is relatively average; if the Gini coefficient is between 0.3-0.39, it means that the distribution equity is relatively reasonable; if the Gini coefficient is between 0.4-0.59, it means that the distribution equity gap is large; if the Gini coefficient is above 0.6, it means that the distribution is very unequal.

$$(x_0, y_0) = (0, 0), (x_1, y_1) = \left( \frac{1}{n}, \frac{I_1}{\sum_{j=1}^n I_j} \right) \quad (1)$$

$$(x_{n-1}, y_{n-1}) = \left( \frac{n-1}{n}, \frac{\sum_{j=1}^{n-1} I_j}{\sum_{j=1}^n I_j} \right), (x_n, y_n) = (1, 1) \quad (2)$$

$$G = 1 - \sum_{k=1}^n (R_k - R_{k-1})(S_k - S_{k-1}) \quad (3)$$

### 2.2.2. Evaluation method of type spatial distribution

The paper applied the statistics of the types of mass sports facilities, using spatial autocorrelation analysis to evaluate the sports types spatial distribution. Spatial autocorrelation analysis is a method of spatial statistical analysis. There is a correlation between spatial distribution data. In the category of space or event, this correlation is called autocorrelation. According to the autocorrelation of this spatial data, we can use the known types of mass sports buildings to determine whether there is clustering. In this study, the Global Moran's I index(M) is used to test whether the distribution of mass sports building types has spatial autocorrelation. The calculation formula is shown in Formula 4-6. The results

of global Moran's I index are in the range of [- 1,1]. If the index is greater than 0, the space is positively correlated, which means the space is clustered; if the index is less than 0, the space is negatively correlated, which means the space is decentralized. The significance of clustering and dispersion can be judged by Z value and P value, when P value is less than 0.05, and Z value is less than - 1.65 or greater than 1.65.

$$M = \frac{\sum_{i=1}^n \sum_{j=1}^n W_{ij}(X_i - X)(X_j - X)}{S^2 \sum_{i=1}^n \sum_{j=1}^n W_{ij}} \quad (4)$$

$$S^2 = \frac{1}{n} \sum_{i=1}^n (X_i - X)^2 \quad (5)$$

$$X = \frac{1}{n} \sum_{i=1}^n X_i \quad (6)$$

### 3. Results

#### 3.1. QUANTITATIVE SPATIAL DISTRIBUTION EVALUATION

The paper crawled the information of daily fitness places classified by popular comment website(www.dianping.com), and saved the data by names, positions, longitude and latitude coordinates, types and opening hours. We got 1512 mass sports facilities of Harbin in total. Through the development platform of GaoDe map, we crawled the information of administrative boundary coordinates, obtained the administrative area of Harbin central urban area, and connected it with mass sports facilities coordinates information to get the spatial distribution of Harbin mass sports facilities, which is shown in Figure 2. According to the public data of the 2018 statistical yearbook of Harbin City, we got the population data of different district in the central urban area. Through the geographical spatial association of ArcGIS, the quantity and type of mass sports facilities in different district of Harbin can be summarized. The result is shown in Table 1.

According to the cumulative percentage of the quantity, the cumulative percentage of the population and the cumulative percentage of the land, we can draw Lorentz curve to describe the distribution equity of the mass sports buildings. The per capita Lorentz curve is shown in Figure 3, and the average land Lorentz curve is shown in Figure 4. The Gini coefficient of Harbin is calculated according to Table1. After calculating, the Gini coefficient of quantity spatial distribution per capita in Harbin is 0.261, and the Gini coefficient of quantity spatial distribution per land is 0.6714. The quantity spatial distribution per capita in Harbin is relatively average, the Lorentz curve curvature is small, and the Gini coefficient is low, which is between 0.2-0.29. However, the quantity spatial distribution gap of mass sports facilities per land is wide, with large curvature of Lorentz curve and high Gini coefficient greater than 0.6.

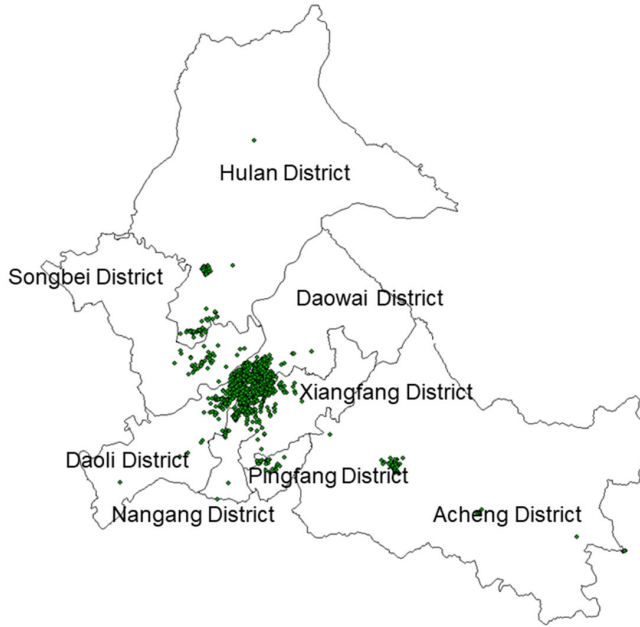


Figure 2. The location of mass sports facilities in Harbin and the geography boundary of Harbin.

Table 1. Quantity distribution of mass sports facilities in Harbin.

District Name	Land Area (Square Kilometres)	Population (Person)	Quantity of Mass Sports Facilities
Daoli District	479.2	755300	248
Nangang District	182.9	1023200	444
Daowai District	257	680800	155
Pingfang District	94	160700	30
Songbei District	736	211900	45
Xiangfang District	339.6	746500	172
Hulan District	2197	607900	109
Acheng District	2445	547000	64
Shuangcheng District	3112	774300	54

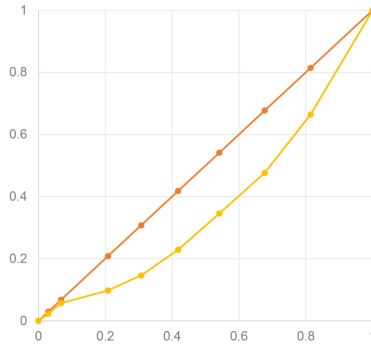


Figure 3. Lorenz Curve of the quantity of mass sports facilities per capita in Harbin.

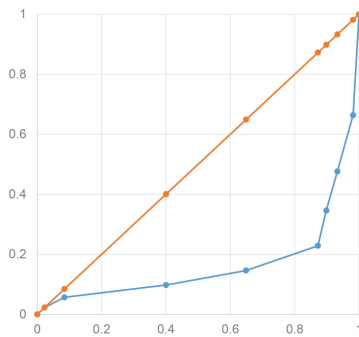


Figure 4. Lorenz Curve of the quantity of mass sports facilities per land in Harbin.

### 3.2. TYPE SPATIAL DISTRIBUTION EVALUATION

According to the statistics of the type of mass sports facilities, the types spatial distribution of mass sports facilities is shown in Figure 5. The existing facilities in Harbin are dominated by billiards, with the number of 41.67%. The number of professional sports venues such as basketball courts and badminton courts is relatively large, but the number of large sports venues such as football courts and tennis courts is small. The number of small confrontational venues such as boxing, taekwondo and karate is large. The number of billiards courts is much higher than that of professional venues. However, as a traditional sports event in Harbin, the quantity of skating rink, due to the complex equipment requirements, is far from enough.

The results of spatial autocorrelation analysis of Harbin mass sports building sport types are: Moran's index is  $0.062929 > 0$ , Z value is  $2.499672 > 1.65$ , P value is  $0.012431 < 0.05$ . Harbin mass sports building sport types are significantly clustered, which is shown in Figure 6.

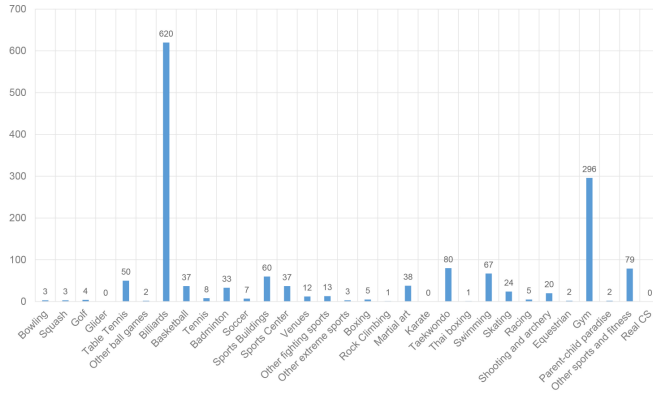


Figure 5. Comparison of types and quantities of sports court in existing mass sports facilities.

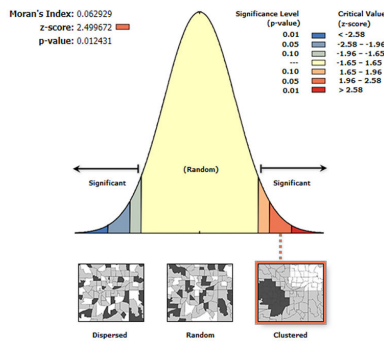


Figure 6. Global Moran's Index analysis of sports types in mass sports facilities.

#### 4. Discussion and Conclusion

Comprehensive analysis shows that the mixing degree of Harbin mass sports building is poor. The distribution and clustering of sports function types of Harbin mass sports buildings are obvious. Although it can ensure the quantity of supply, the selection type of sports is relatively single. It shows that the spatial distribution of mass sports buildings follows the population distribution and has strong service. However, the existing mass sports facilities have strong economic agglomeration and lack of public regional fair layout, which will lead to the supply of mass sports facilities in the process of urban expansion unbalanced.

Based on the data of 1512 public sports buildings' spatial location, sports types and supply subjects in Harbin, this study explores the service fairness, service quality and social spatial differentiation of the spatial distribution of mass sports facilities, aiming to improve the health service ability of sports facilities in Harbin. We can draw the conclusions as follows. First, although the distribution of mass

sports buildings in Harbin is relatively average with the population distribution, the regional distribution is extremely uneven, so the construction of health service facilities lags behind urban expansion. Second, the clustering of sports function types of mass sports buildings is obvious. Although the supply quantity can be guaranteed, the selection of sports function supply is relatively single, which cannot promote physical activities or guide mass sports participation behavior.

The innovation point of the research lies in the comprehensive statistics of the current situation of the existing mass sports facilities in Harbin, and promote the method of web crawler of specific POIs without accurate search content by social media. The method can also be applied to get the geography information of retails evaluation, house price, and so on. The application of big data in the investigation and spatial distribution of sports facilities, breaks through the regional restriction of the research on the spatial distribution of sports facilities caused by the lack of urban management data, avoids the sample interference caused by the artificial sampling, and provides reference for planning of sports facilities.

**AUTHOR COMMENTS:** Reviewer 1: The application of big data from social media in the research project introduced by the paper has reference value to other researchers. In addition to the experience of the application, a review and analysis on the effects of the technology would be very important. Reviewer 2: This paper gave a very detailed study on the spatial distribution and performance evaluation on mass sports building in Harbin and also provided some discussion about the result. Some improvement to the overall English writing is necessary or it is quite hard to understand what the author(s) is trying to convey. Overall structure and flow of the paper is quite clear though.

**REPLY TO THE REVIEWS:** We thank the referee for pointing out the problems of lacking progress of technology. We have implemented the referee's useful observations. Reviewer 1: Thank you for your comments. We have added a brief review and a brief effects analysis as the paper is already 10 pages. The main modify of the paper is as follows. First, we did the review about POI and spatial distribution, we pointed out that there were already papers done the research, like XU Zhibang (2018) and Caihui Cui (2015). The researchers have used the similar method to analyse the spatial distribution of fire station and retails. Second, we did the review about mass sports facilities and social media. Serdar Bilgi (2019) has proved that twitter comments can be used to research the sports facilities spatial distribution. Thirdly, we pointed out at the last paragraph that our method can be used to get the geographic information big data of the POI without accurate group names, such as retails evaluation and house price. Thank you for your comments. We have asked a native speaker in our institute to adjust the paper language. We would like to thank the referee once more for sparing the time to write the useful comments.

## References

- P. Buxton (ed.): 2018, *Metric Handbook: Planning and Design Data (Sixth Edition Published)*, Taylor and Francis, London.
- Chai, Y.W.: 2014, *TheFrontier of Space-Time Behavior Research*, Southeast University Press, Nanjing.

- Humpel, N., Owen, N. and Leslie, E.: 2002, Environmental factors associated with adults participation in physical activity: a review, *Am J Prev Med*, **22**(3), 58-69.
- Jin, Y.R., Yao, S.P. and Cai, Y.J.: 2015, Research on Leisure Sports Space-time Behavior of Urban Residents in Shanghai, *China Sport Science*, **35**(3), 12-19.
- Kaczynski, A.T., Potwarka, L.R. and Saelens, B.E.: 2008, Association of Park Size, Distance, and Features with Physical Activity in Neighborhood Parks, *American Journal of Public Health*, **98**(8), 1451-1457.
- Lai, D.J., Huang, J., Risser, J.M. and Kapadia, A.S.: 2008, Statistical Properties of Generalized Gini Coefficient with Application to Health Inequality Measurement, *Social Indicators Research*, **87**(2), 249-258.
- Limstrand, T.: 2010, Environmental characteristics relevant to young people, *Scandinavian Journal of Medicine & Science in Sports*, **18**(3), 275-287.
- Owen, N., Humpel, N., Leslie, E., Bauman, A. and Sallis, J.F.: 2004, Understanding environmental influences on walking: review and research agenda, *Am J Prev Med*, **27**(1), 67-76.
- Rycroft, R.: 2003, The Lorenz Curve and the Gini Coefficient, *Journal of Economic Education*, **34**(3), 296.
- Serdar, B., Ayse, G.G., Birgul, A., Himmet, K. and Ozge, O.: 2019, COMPLEXITY MEASURES OF SPORTS FACILITIES ALLOCATION IN URBAN AREA BY METRIC ENTROPY AND PUBLIC DEMAND COMPATIBILITY, *International Journal of Engineering and Geosciences*, **10**(4), 141-148.
- Van Stralen, M.M., de Vries, H., Mudde, A.N., Bolman, C. and Lechner, L.: 2009, Determinants of initiation and maintenance of physical activity among older adults: a literature review, *Health Psychol Rev*, **3**(2), 147-207.
- Tang, Z.L. and Gu, S.: 2015, An Evaluation of Social Performance in the Distribution of Urban Parks in the Central City of Shanghai: From Spatial Equity to Social Equity, *Urban Planning Forum*, **02**, 48-57.
- Wang, L. and Zhou, K.C.: 2018, Performance Assessment of Community Sports Facility Distribution from the Perspective of Healthy Equity: Case Study of the Central City of Shanghai, *Journal of human settlements in Western China*, **1**, 1-8.
- Zhibang, X.U. and Liang, Z.: 2018, Spatial optimization of mega-city fire station distribution based on point of interest data: a case study within the 5th ring road in Beijing, *PROGRESS IN GEOGRAPHY*, **37**(4), 535-546.
- Zhou, T., Koomen, E. and Van Leeuwen, E.S.: 2018, Residents' preferences for cultural services of the landscape along the urban-rural gradient, *Urban Forestry & Urban Greening*, **29**, 131-141.

# HOW TO SHARE A HOME

## *Towards Predictive Analysis for Innovative Housing Solutions*

DJORDJE STOJANOVIC<sup>1</sup> and MILICA VUJOVIC<sup>2</sup>

<sup>1</sup>*University of Melbourne*

<sup>1</sup>*d.s@unimelb.edu.au*

<sup>2</sup>*Universitat Pompeu Fabra*

<sup>2</sup>*milica.vujovic@upf.edu*

**Abstract.** Renewed interest in cohousing solutions is driven by the rapid population growth and a lack of affordable housing in many cities across the world. The home share has become more prevalent in recent years due to the cost benefits and social gains it provides. While it involves challenges primarily concerned with the usage of communal areas, the viability of this housing model increases with the advancement of technology enabling new tools for analysis and optimisation of spatial usage. This paper introduces a method of sensor application in the occupancy analysis to provide grounding for future studies and the implementation of advanced computational methods. The study focuses on the underexplored potential of the communal spaces and provides a method for the measuring of specific aspects of their usage. The study applies principles of mathematical set theory, to give a more conclusive understanding of how communal areas are used, and therefore contributes to the improvement of housing design. Presented outcomes include an algorithmic chart and a blueprint of a behavioural model.

**Keywords.** Cohousing; Housing share; Post Occupancy Evaluation; Machine Learning; Predictive Analysis.

### 1. Introduction

Cohousing is a housing model, where private dwellings and communal facilities are combined (McCamant and Durett 1988). The close-knit relationship between private and communal spaces is a vital characteristic of this housing typology. However, there is a stark defence between these two kinds of space. Private space is of a standard dwelling typology, whereas communal space can be anything and with many different roles. Private dwelling space is designed according to tested typologies, normative and regulations such as Apartment Design Guidelines for Victoria published by the Department for Environment, Land, Water and Planning (2017) in Australia. Communal space, on the other hand, is not so clearly defined. Its potential is not fully recognized in strategies, such as Housing Design



Guidelines (2018) published by the Department of Health and Human Services of Victorian Government concerned with public housing. In shared housing schemes, the communal space serves as an extension of the private domain and its use is subject to more dynamic occupancy patterns. Therefore, the role of communal space is open to interpretation. The focus of this study is on the usage of communal housing spaces, and the aim is to find ways to understand complex occupancy patterns arising from space-sharing to benefit both designers and occupants.

Conventional architectural analysis of three international and well-known housing precedents allows an initial insight into different roles of communal housing space (Figure 1). In Japan, four artists share communal space on the ground floor of a house, while their private studios are on the first floor (Ondesign Partners 2009). In Denmark, 54 families share a large communal dining room and an outdoor courtyard surrounded by individual units (Dorte Mandrup 2009). In the US, 55 micro homes share access to recreational facilities on the ground floor and a communal terrace of a multistorey building (nArchitects 2016). These three recently built projects offer themselves as testing grounds for the development of a methodology which can be applied across different scales and different time frames for in-depth occupancy evaluation.



Figure 1. Clockwise: Lange Eng Cohousing Community by Dorte Mandrup Architects 2009, Carmel Place by nArchitects 2016, and Yokohama Apartment by Ondesign Partners 2009.

## 2. Objective

The complexity surrounding the concept of communal space in housing is related to ownership, maintenance and social aspects, amongst other things. Typically, in a co-living arrangement, private units are owned individually, while communal spaces are owned jointly. The maintenance of the communal zones is delivered cooperatively by all residents. The regime of maintenance is agreed between occupants. It is not only based on a financial contribution toward corporate

fees but the active participation of occupants. Social aspects involve a sense of the community, which exceeds a single household. In addition to family bonds relevant to the design of individual housing units, housing share residents form both short and long-term bonds with other residents relevant to the design of communal areas. Therefore, this study establishes a way to measure specific aspects to expand understanding of how communal areas of housing share are being used.

In response to the topic of the conference RE: Anthropocene - Design in The Age of Humans, this paper introduces a novel method for design analysis of communal areas belonging to cohousing communities, relying on machine learning techniques. The research reported on is based on the interaction between architectural design, computation and mechatronics and contributes to the design methodology of cohousing solutions. The approach is based on data collection for through evidence-based understanding of shared usage of spaces and things.

The study aims to maximise opportunities arising from technological advances and utilise innovative ways of data collection to give more insight into occupants' behaviour. Post occupancy evaluations are demanding tasks and therefore infrequently conducted. Detailed research is rarely conducted after buildings are complete, and designers often remain uninformed of true implications of their decisions. The presented approach focuses on data collection and introduces temporal dimensions into the analysis process to help understanding how buildings are used. This study opens up the possibility to apply machine learning techniques in the design of communal housing spaces.

### **3. Previous research**

Numerous research efforts have identified the role of data mining in the understanding of the built environment. For example, data produced through occupancy scheduling has been valuable to the analysis of shared office space via machine learning techniques (Davis 2016). Similarly, machine learning algorithms are frequently used for the analysis of the built environment on a different scale. For example, Aschwanden (2016) has shown an application of learning algorithms to identify changing boundaries of the city's neighbourhoods based on geospatial and transportation data. Likewise, Panagoulia (2017) has identified the role of open data in identifying and evaluating the liveability of urban space. At the same time, data harvesting for housing analysis is challenging in its own right, and studies concerned with living spaces are still rare.

The departing point of the study is to establish what can be measured and what data is both available and relevant to better understanding of how communal housing areas are used. A wide array of techniques to measure specific aspects of space use has been tested, based on energy consumption, CO2 emission, and movement detection, radio-frequency identification (RFID) and many more. Occupancy analysis of office buildings, most commonly focus on data obtained through energy consumption to make conclusions on workplace optimisation. For example, Chang, W. K., and Hong, T. (2013) use lighting-switch data in statistical analysis and modelling of occupancy patterns in open-plan offices. In

the study by Cali et al. (2015), CO<sub>2</sub> level recordings were used to detect occupancy relevant to the validation of use in office and residential buildings. Other ways of collecting data for usage analysis include infra-red sensor application such as the one developed by Hashimoto et al. (1998) for detecting the number of people passing a wide door and their movement directions. A related application of sensors to capture “dynamic visuo-locomotive narrative experience” of building users is described in a study by Bhatt et al. (2016).

Reviewed techniques and technologies for measuring different aspects of space use are equally applicable to data gathering for occupancy analysis of communal housing spaces. The method described in the following chapters shows how data gathered by sensors can be turned into design intelligence for housing share solutions of different scales. Methodology for measuring and acquiring information on the usage of communal housing areas has not been described before. Moreover, the proposed method aims to provide a way to apprehend overall and qualitative aspects of space through usage, rather than to concentrate on specific and technical aspects of building performance.

The following chapter gives a more detailed description of the method for acquiring specific data sets and their overlapping to enable informed decision making in the design and use of communal housing areas. It gives an account of the network of sensors needed to harvest data and a blueprint of a behavioural model, including an algorithmic chart which demonstrates a specific information flow. The method identifies input data, way of data processing, and output information.

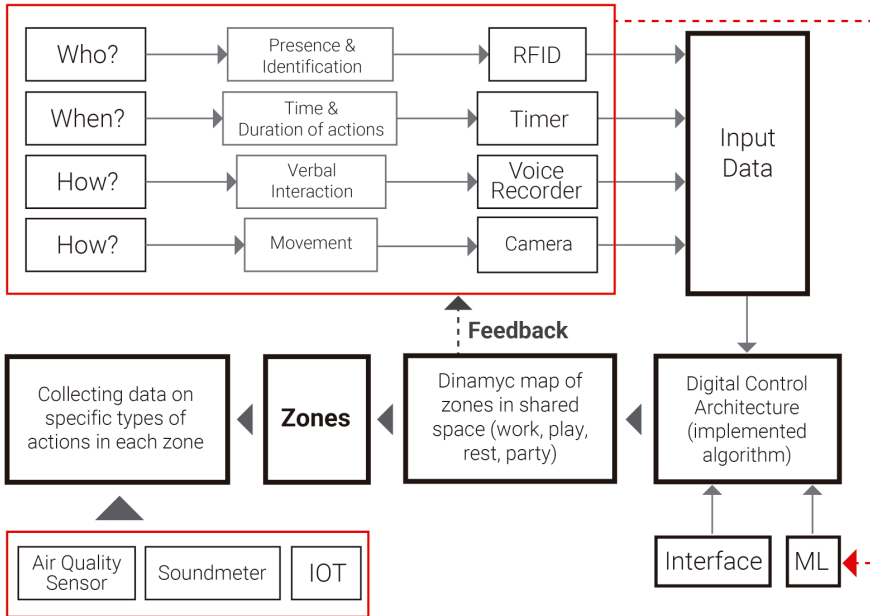
#### **4. Method**

The input data is divided into four categories, each representing a distinct initial entry point to feed the system with information. These categories are named: presence and identification of occupants, time and duration of activities, type of activity, and environmental conditions. The first group gives information on WHO is using communal space. It detects the presence of users in the specific areas of communal space and recognises their unique identification so that system knows not only where a resident is at any given time, but more importantly which resident is where. This will show if certain zones of communal areas are used more than others, but also if particular residents frequently populate them. The second group is concerned with WHEN is communal space occupied. It records the time of arrival and measures the amount of time spent by each user in an area. This is useful to establish peak usage times for certain areas, and to look for recurring instances in occupancy scheduling. The third group of entry data provides information on HOW is the space used. It establishes the type of activity performed by occupants through tracking the use of key furniture and appliances in an area. The fourth group monitors environmental conditions such as noise levels, air quality and temperature in an area. This category of entry information also helps to understand how space is used by measuring the environmental effects of the use in the area observed.

## 5. Structured data collection

The diagram (Figure 2) presents the flow of the information gathered by the network of sensory devices distributed in the communal space of housing share. For this study, it is assumed that this is a communal garden surrounded by individual housing units. The information provided by sensors is then processed according to the pre-defined algorithm to generate the output. There are two groups of sensors. The first group produces a general layer of information which is used to establish outcome categories. Presence, movement, interaction and time spent are measured using radio-frequency identification (RFID), camera, voice recorders and timers. There are four categories of the expected outcome, and they are named WORK, REST, PLAY and PARTY. Each category signifies the prevalent use of an area within the communal space of housing share. Also, the system defines the footprint of an area defined by the dominant use. The diagram contains a feedback loop which allows continual correction of the output based on the change of input data. The expected result is, therefore, a dynamic map which describes the actual change of areas defined by a dominant usage. In other words, the map changes according to the behaviour of occupants tracked through time. The information feedback enables reconfiguration of the initial map according to changes in the input, resulting in the dynamic occupancy mapping. The second group of sensors provides more detailed information on activities within established zones. This information is focused on the appliances/devices used (IOT), levels of noise (soundmeter) and quality of air (air quality sensor). For designers, this is a tool to understand spatial change through use over time, and for users, this is a way to plan the occupancy and use communal areas more efficiently.

**1st group of sensors** - Acquiring information for the dynamic map of zones



**2nd group of sensors** - Acquiring detailed information on types of actions and environmental conditions they are conducted in

Figure 2. The diagram of the information flow showing a feedback loop, and two groups of sensors.

## 6. The algorithm

The algorithm (Figure 3) gives a detailed description of the information flow based on the decision-making logic adjusted to one or more users. The system is, therefore, occupant centred. The movement and actions of occupants are tracked, and data sets gathered by different sensors are overlapped to establish activity zones. The zone is established when specific criteria are met, based on the proximity of users and correspondence between their actions. The size of the zone is directly proportional to the number of occupants.

The system is redundant, using both camera and RFID to detect people presence. The algorithm distinguishes individuals from groups based on their proximity. If the distance between two individuals is greater than two meters, they are not considered as a group. After this decision, the algorithm branches into two sections, making a differentiation between individual and group activities which form distinct but changeable spatial zones within the communal space. The individual zone is the area of the circle with a radius measuring two meters and its centre at the place where the occupant is. The group zone is defined as an area equivalent to the area of the circle. The radius of that circle is the number of occupants multiplied by the distance measured between them. In other words, the

more occupants there are in a group, the bigger the zone is. Once the boundaries of the zone are established, its type is defined according to variables related to the movement of occupants, their interaction, noise levels and age identification. The algorithm then relies on the set of defined conditions to differentiate between four zonal categories, named WORK, PLAY, REST, and PARTY. For instance, REST category is characterised with little movement and interaction, while PLAY or PARTY have plenty, and WORK zone is characterised with no movement and low noise levels. The naming of categories responds to the character of activities quickly establish through observation, but the algorithm also captures dynamics between zones and intensities of activities within each zone. The data is gathered every two minutes and the algorithm updates the map. Timestamps and RFID data are gathered and stored for further analysis. The diagram presents the first step in introducing the computer-supported analysis of communal housing spaces by providing replicable and easily automated steps for data processing.

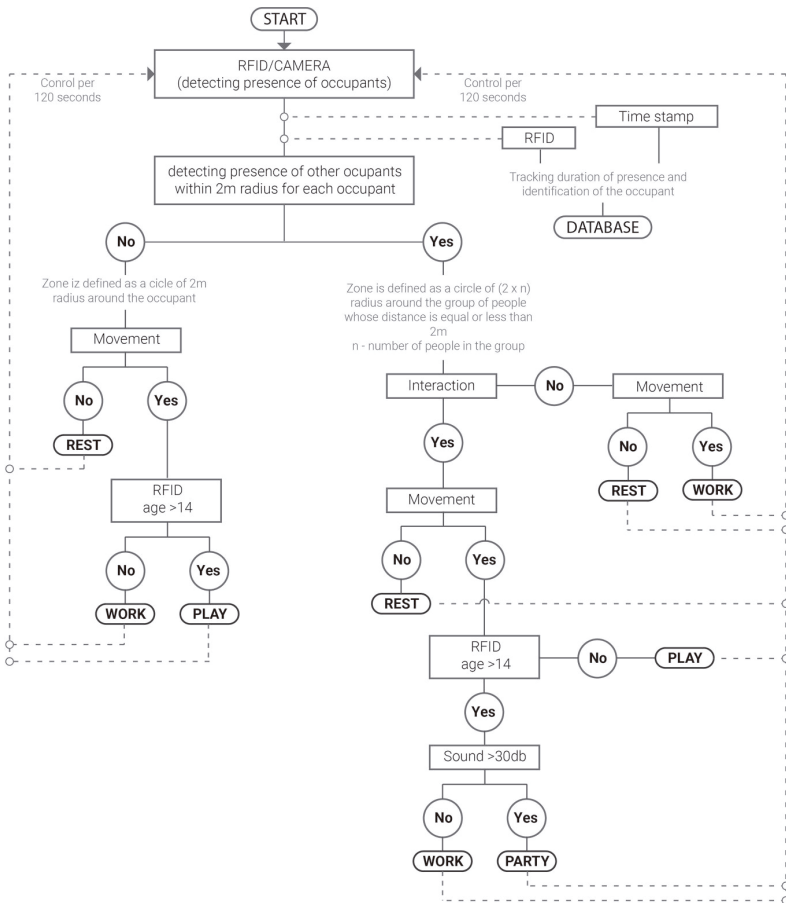


Figure 3. The algorithm showing data gathered by the network of sensors is overlapped to establish activity zones.

The algorithm is based on the principles of mathematical set theory, whereby objects, are being grouped into sets. The system recognises occupants as objects while areas established within the communal space are understood as sets. The type of the object is established according to the action performed by the user. When the activity and location of the user change, the output, which is the size of the thematic area, changes accordingly. The output is, therefore, a dynamic map representing sets which are exchanging objects and thus growing and shrinking over time.

## **7. Discussion**

The conceptual framework presented in this study demonstrate a way to collect data by electronic sensing in order to develop a better understanding of communal areas within collective housing. The proposed method enables designers to understand the usage of communal space across time, by tracking who is using communal areas, measuring when and establishing how is the space used.

The main advantage of the proposed occupancy analysis method is the ability to capture a large amount of information about the usage of communal areas over time. Computational techniques are employed to make sense of raw data. Instead of a static image, the expected result is a dynamic map showing fluctuations in occupants' behaviour over time. The presented time-based method enables designers to investigate and establish behavioural patterns and lends itself as a tool for predictive analysis in the design process.

The implications of joint ownership, cooperative maintenance, and changing social dynamics result with complexity, which is difficult to understand, to predict and to design for. The innovation in housing typology involving different forms of space share is, therefore, supported by the presented method for occupancy analysis. The method is applicable as a new tool for both the design and management of communal housing spaces. The presented occupancy analysis method will show if a specific area is underused, or if it is in high demand. The designer will be then able to make informed decisions if that area should be omitted, amended or expanded with architectural means. More importantly, the designer will be able to look comprehensively at the relationship between private units and communal spaces and take educated prediction on how to make this relationship more purposeful in future designs. At the same time, presented analysis method and a resulting visual map, could help occupants to predict if using a specific communal area at a specified interval would likely be a social occasion or a solitary opportunity. Children playing together would be an example when social interaction would be desired while reading a book in the garden would be the case when solitude is preferred.

The dynamic map is the very first layer of the information offered by the proposed system. It gives a visual overview of measured information. The system provides a tool for extracting precise information on how people use communal housing spaces and sets grounding for generating datasets for further research. For example, acquired information could give evidence if particular areas are used more often, if specific activities unfold at certain times and if owners of

individual units tend to use particular areas of communal space more often. Spatial components of activities intersect with temporal so that in the next phase of this research, information harvested over time and through the method described will form a database. Such a database provides training data for the model able to predict spatial implications of change in occupancy behaviour.

## 8. Conclusions

The development of housing typology involving different forms of space share is driven by the rapid population growth and a lack of affordable housing in many cities across the world. While housing share may be viewed as an affordable solution and an answer to the shortage of living space, it also involves challenges primarily concerned with ownership, maintenance and social aspects. These challenges have a significant impact on the overall quality of housing and the comfort of its residents, and more conclusive understanding of such complex behavioural patterns demands innovative analysis supported by computer science.

This paper gives an account of a post-occupancy evaluation method, based on the evidence obtained from the monitoring of shared use of things and spaces in the communal areas within collective housing. The presented research outcome includes an algorithmic chart which demonstrates a specific information flow based on who, when and how is using communal space. The presented result is a blueprint of a behavioural model, comprehended as a dynamic map showing occupancy changes over time.

The computational methods have become essential in architecture, through construction innovation, but also through analysis and optimisation of spatial usage. This paper shows how computational techniques can improve methods of post-occupancy evaluation and therefore contribute to better design and use of communal housing space. The number of recent cohousing projects has been developed for uniform social groups such as students, young professionals or senior citizens. A more conclusive understanding of behavioural patterns through computer-aided processes may help create new models centred on more profound ways of space sharing, so that they may become simultaneously attractive to occupants from different groups.

This paper provides grounding for future studies and the implementation of advanced computational techniques to understand how people use space. Further research will focus on the methodology for overlapping of acquired data sets to establish a framework for predictive and evidence-based architectural design

## References

- “Lange Eng Cohousing Community” : 2009. Available from Dorte Mandrup Architects<<https://www.dortemandrup.dk/work/lange-eng-cohousing-community>> (accessed 23rd November 2019).
- “Yokohama Apartment” : 2009. Available from Ondesign Partners<<http://www.ondesign.co.jp/city/housing/1/>> (accessed 08.11.2019).
- “Carmel Place Micro Housing” : 2016. Available from nArchitects<<http://narchitects.com/work/carmel-place/>> (accessed 5th November 2019).
- “Apartment Design Guidelines for Victoria” : 2017. Available from 6. Department for



- Environment, Land, Water and Planning<:https://www.planning.vic.gov.au> (accessed 8th November 2019).
- “Housing Design Guidelines” : 2018. Available from Department of Health and Human Services<https://dhhs.vic.gov.au> (accessed 8th November 2019).
- Aschwanden, G.: 2016, Neighbourhood Detection with Analytical Tools, *Proceedings of CAADRIA 2016*, 13-22.
- Bhatt, M., Suchan, J., Schultz, C., Kondyli, V. and Goyal, S.: 2016, Artificial intelligence for predictive and evidence-based architecture design, *Thirtieth AAAI Conference on Artificial Intelligence*, Phoenix, Arizona, 4339-4350.
- Cali, D., Matthes, P., Huchtemann, K., Streblov, R. and Müller, D.: 2015, CO2 based occupancy detection algorithm: Experimental analysis and validation for office and residential buildings, *Building and Environment*, **86**, 39-49.
- Chang, W.K. and Hong, T.: 2013, Statistical analysis and modelling of occupancy patterns in open-plan offices using measured lighting-switch data, *Building Simulation*, **6**, 23-32.
- Davis, D.: 2016, Evaluating Buildings with Computation and Machine Learning, *Proceedings OF ACADIA 2016*, 116-123.
- Gomez-Zamora, P., Bafna, S., Zimring, C., Do, E. and Vega, M.R.: 2019, Spatiotemporal Occupancy for Building Analytics, *Proceedings of eCAADe 2019*, 111-120.
- K, H., Kawaguchi, C., Matsueda, S., Morinaka, K. and Yoshiike, N.: 1998, People-counting system using multisession application, *Sensors and Actuators*, **66**(1-3), 50-55.
- McCamant, K. and Durrett, C.: 1994, *Cohousing: A Contemporary Approach to Housing Ourselves*, Ten Speed Press, Berkeley.
- Panagoulia, E.: 2017, The role of Open Data in identifying and evaluating the Livability of Urban Space, *Proceedings of eCAADe 2017*, Rome, 495-504.

# WHAT DO DESIGN DATA SAY ABOUT YOUR MODEL?

## *A Case Study on Reliability and Validity*

HALIL ERHAN<sup>1</sup>, AHMED M. ABUZURAIQ<sup>2</sup>, MARYAM ZAREI<sup>3</sup>,  
OSAMA ALSALMAN<sup>4</sup>, ROBERT WOODBURY<sup>5</sup> and JOHN DILL<sup>6</sup>  
<sup>1,2,3,4,5,6</sup>*Simon Fraser University*  
<sup>1,2,3,4,5,6</sup>{herhan|aabuzura|mzarej|oalsalma|rw|dill}@sfu.ca

**Abstract.** Parametric modeling systems are widely used in architectural design. Their use for designing complex built environments raises important practical challenges when composed by multiple people with diverse interests and using mostly unverified computational modules. Through a case study, we investigate possible concerns identifiable from a real-world collaborative design setting and how such concerns can be revealed through interactive data visualizations of parametric models. We then present our approach for resolving these concerns using a design analytic workflow for examine their reliability and validity. We summarize the lessons learnt from the case study, such as the importance of an abundance of test cases, reproducible design instances, accessing and interacting with data during all phases of design, and seeking high cohesion and decoupling between design geometry and evaluation components. We suggest a systematic integration of design modeling and analytics for enhancing a reliable design decision-making.

**Keywords.** Model Reliability; Model Validity; Parametric Modeling; Design Analytics; Design Visualization.

## **1. Introduction**

Parametric modeling tools adapting dataflow graphs have been widely used in many disciplines such as design, engineering, economics, natural sciences, etc. (Johnston et al., 2004; Sousa, 2012). They enable change propagation in and across models, exploration of variations, and multi-level interaction (Aish and Woodbury, 2005). Parametric models can be studied as computer programs and the activities to build them are akin to composing a program (Davis et al., 2011; Ko et al., 2011). This includes most aspects of parametric modeling from inserting a node and writing scripts to using APIs. It is essential that these models are reliable and perform as intended, and, like computer programs, they must be tested for their reliability and validity with a caveat that the testing methods should be unique for design modeling. Here, we use reliability as a criterion for determining if a given model performs without errors under changing conditions; and, for validity, if it produces expected designs with expected performance measures (Lyu, 1996). As

design information captured and used in design grows rapidly, it becomes almost impossible for the existing computational design ecosystem to assist designers in tracing their decisions in their design models. There is an important need to support traceability, reliability, and validity of complex design models in a collaborative environment (Marchenko et al., 2011).

A parametric model's reliability and validity can be affected by, first, the complexity of its intricate and changing structure (Erhan et al., 2010; Davis et al., 2011), and, second, the complexity of the process through which such models are built (Kasik et al., 2005; Ko et al., 2011). Their complexity increases parallel to the increase in their model's fidelity. The process complexity, on the other hand, can result from the involvement of different people in the modeling. These may be easily underestimated and must be considered to avoid undesirable outcomes. We contend that identifying and agreeing to sound practices for controlling parametric model reliability and validity is crucial. We conducted a case study demonstrating how the reliability and validity of parametric models can be tested in a realistic collaborative design case, and how such design models can be improved using the insight gained from the interactive data visualizations. We refer to the combination of computational design and visual data analytics as *design analytics*.

The next section provides a brief background on parametric modeling focusing on performance evaluation following which we describe our approach and the case study on how reliability and validity of such models can be tested and improved. Recent works, e.g. Matejka et al. (2018) and Fuchkina et al. (2018), have explored the use of interactive data visualizations for design space exploration. In the context of evaluating parametric models, the work by Beham et al. (2014) illustrates the use of interactive data visualization and analysis for the purpose of identifying invalid geometry, whereas the work by Nagy et al. (2017) demonstrates the use of heat-map visualizations for assessing the quality of the design space endowed by a parametric model (in terms of its scope and internal structure). In this study, we show how visualizations can facilitate debugging-like scenarios and motivate closer inspection of the parametric models in question. We conclude with recommendations for design teams and software developers to control complexities in parametric design models, and for this, the need for integration of design analytics throughout design workflows.

## 2. Background

### 2.1. PARAMETRIC MODELING AS PROGRAMMING

While graph-based parametric models share many similarities with imperative text-based programming, an important distinction arises from the fact that they make visual modeling possible using nodes and links and have an execution model adapting concurrency (Sousa, 2012). In addition, while inputs to a text program are seen as test cases to which the program must correctly react, inputs to a parametric model can be seeds for exploration. Designers, normally, have no obligation to maintain them or verify that they would work reliably with users' inputs as is the case with most other software.

## 2.2. PERFORMANCE EVALUATION IN DESIGN PHASES

Incorporating the performance metrics in design models from conceptual to the final stages of design has become a common practice (Shea, 2005; Anton and Tanase, 2016). For this, designers use parametric design tools with analysis tools, such as EnergyPlus, Radiance, Daysim, and OpenStudio. This combination allow designers to estimate the design performance as early as possible. However, they are assessment-oriented rather than focusing on dynamically supporting the decision-making (Touloupaki and Theodosiou, 2017). Nembrini et al. (2014) discuss the advantages of using a coding interface both to describe building form and conduct performance simulations. Their approach aims to address performance-related design questions at the early design stages. Architects use parametric modeling combined with various performance analysis software to influence form exploration in the early stages of design that may lead to more informed, efficient and meaningful solutions (Anton and Tanase, 2016).

## 3. Motivation and Approach

Generated design instances are to be evaluated in the context of a performance-driven design process (Shea et al., 2005; Anton and Tanase, 2016), where the reliability and validity of the models become more pronounced. The performance computation expects specific geometric fidelity and in specific data structures; any violation of this contract will result in unreliable or invalid outcomes. Considering these needs, the creators and users of parametric design should be aware of the importance of building reliable, scalable and reusable models as do their counterparts in the mainstream programming communities. The need for best practices when working with parametric models, especially when performance matters, is therefore a necessity and concepts such as Patterns for Parametric Design (Woodbury, 2010) can be part of the answer.

By generating alternatives, we not only explore the design space, but we simultaneously examine its behavior under various execution scenarios. When multiple designers work in parallel at a form-finding problem, we can expect more diverse forms and form-to-performance evaluations. To study this environment and explore the role of data and its visualization in a design realistic context, the case study we conducted focuses on experimenting with reliability and validity testing and improvement of the collaborative parametric design Setup created during SmartGeometry (2018).

## 4. Case Study: Collaborative Parametric Design of A High-Rise Building

This case study examines design data from different designers approaching the same design problem. The analysis of the data used design analytics methods. We applied this analysis to a sample of issues arising from the use of parametric modeling systems on complex design problems.

### 4.1. THE CASE STUDY CONTEXT

The case study is based on our observations of the process and a close study of the collaborative parametric design setup developed in SmartGeometry (2018)

‘Inside the Black Box’ group. The group comprised 19 participants who were designers, programmers, and visualization developers. The group worked on the design of a mixed-use high-rise building located in a city context with a range of real-world form and performance concerns, such as land-use, functional-spatial distribution, heat loss and gain, solar exposure, view quality, etc. The participants decided to focus on 13 performance criteria in their alternative solutions. One group of participants, who are professional designers, software developers, or parametric modelers, worked on developing the work environment setup, which is composed of performance evaluation, an inputs generator, and server-side data-sharing components (Figure 1). The five designers in the cluster developed six different proposals for the mixed-use high-rise tower design and generated alternatives. We then used their proposed alternatives in our case study.

#### 4.2. DESIGN ANALYTICS WORK ENVIRONMENT SETUP

Our design analytics work environment for testing reliability and validity (Figure 1) is consisting of the following components. First, a parametric model that specifies and generates geometries for alternatives design. The second component receives input parameters and changes input values algorithmically to automate serial generation of alternatives. Parametric design models are combined with a third component which includes parametrically defined context with site, view, geography, and the information regarding other structures around the site. The most complex part of this setup is the component where building performance measures are calculated. This is composed of in-house developed or third-party modules linked to the context and parametric model components. The setup is connected to a database on a dedicated Speckle (2019) server to store and retrieve form and performance data for each alternative, which are further analyzed using Tableau (2019) and our custom-designed set of design analytics tools.

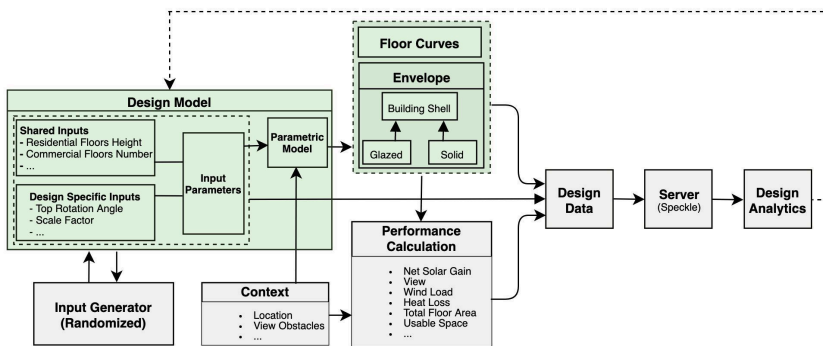


Figure 1. Work Environment Setup for Design Analysis: Design Model, Floor Curves and Envelope (developed by the designers and required for the Performance Calculation module).

We used data from 250 design alternatives generated using parametric models developed by workshop participants. The data associated with each alternative comprised: (a) the input parameters used to generate it; (b) the form and geometry;

(c) the 13 different performance values for, e.g. floor area by function, solar gain, cantilever areas, etc. Each alternative was denoted with a unique ID that includes an instance number and a symbol denoting the surname of the model developer.

#### 4.3. CHALLENGES AND PROBLEMS IDENTIFIED

The parametric models in the case study were complex. They presented many issues: they comprised multiple Grasshopper node clusters nested deep within other clusters; the dependencies between the nodes were difficult to trace; the logic of the dependencies was not obvious, etc. In addition, the modules (e.g. custom-script nodes) in the models were developed by different people that were not directly involved in this particular project. Therefore, the changes in the design models and the changes in the performance calculators might not have been synchronized. The inconsistencies due to versioning in the models increased the threat to reliability and validity of the work environment setup. For example, we identified that there were more than 10 different versions of the generator module created in the workshop. In addition, after creating visualizations of the initial data from 250 designs in Tableau (2019) and with our custom analysis tools, we discovered unexpected patterns on performance calculations. This motivated us to closely study the work environment setup and the models in it. For example, we questioned “what the trends in view quality are” and “how the different types of functions affect heat-loss”. These visualizations hinted to possible threats to the validity and reliability of the setup that were not obvious at the outset. Below we discuss some of the salient issues that we observed in the work environment setup.

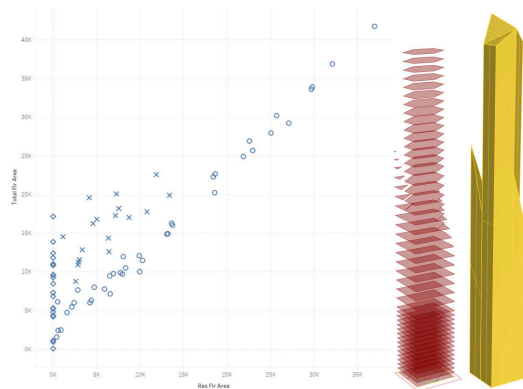


Figure 2. Left: Scatter plot of Total Floor Area vs. Residential Floor Area. Crosses show unexpected outliers. The vertical strip (diamonds) on the vertical axis are alternatives with no residential floors. Right: Floor planes showing segmentation.

**Unexpected Correlation.** The Total Floor Area (TFA) is the sum of the areas of the residential, commercial and retail floors of the building, hence we expect a correlation between each of them and TFA. Instead, as Figure 2 (Left) shows, we see that some of the alternatives do not follow the expected trend. At first, the reason was not clear. We looked at the parametric model that generated these

alternatives. This revealed that when a floor level comprised multiple floor plane segments, e.g. because of gallery openings in the floor, the module calculating TFA considered only the very first segment and ignored the remaining on the same floor level. A further investigation showed that this was due to a mismatch between the tree data structure containing the floor segments and the list data structure expected by the TFA module. This made TFA frequently smaller than the actual sum of the building floor areas. To verify this assumption, we contrasted alternatives close to the trend with outliers, finding that the outlying alternatives tended to have floor planes with more than one segment (Figure 2 (Right)).

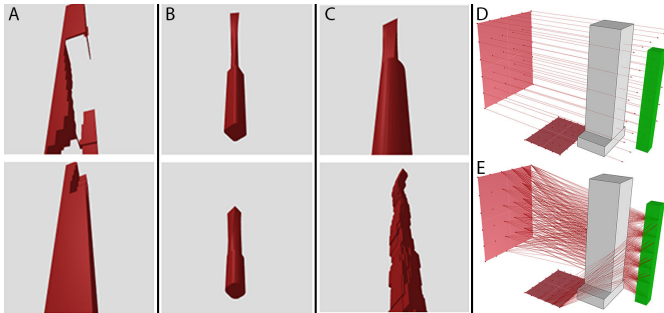


Figure 3. (Left) A: The same parametric model, similar view and height but the top alternative form is malformed. B: The same parametric model, similar view despite very different heights. C: Different parametric models, similar view and height despite differences in the building's shells. (Right) D: Original view calculation. E: Updated view calculation.

**View Calculation:** In comparing view qualities, we noticed that models with different sizes produced similar view quality values (Figure 3 A, B, and C) in unfamiliar units (degree/m<sup>2</sup>). Our close study showed the following: (1) In design practices, the view from a building should consider targets in multiple locations and directions. However, the view module was set to one target; (2) The module ignored the obstacles in the context; and, (3) The line of sights were projected from the target surface to the building, as opposed to from different points on the building to the target. In addition, this module used an arbitrary number of parallel projectors that ignored building size. After identifying these three issues in the original view module (Figure 3 D), we developed a new view approach (Figure 3 E) that projects view lines from different points at each floor in the building to multiple view targets and considering the obstacles in the context.

**Heat loss.** While studying heat loss values in the case study, two experts in our team recognized unexpected values in, which hinted at a possible problem with the calculations. The nested clusters calculating heat loss and heat gain of a building hid the logic and the data visualization showed unexpected results (Figure 4 (Left)), which, in turn, implied that the model might be invalid. Our first assumption was that the relevant module in the performance calculation, Heat Loss, was not working correctly. Therefore, we examined this module to find probable errors. We found the heat loss calculation used equations inconsistent with the standards: they were calculating heat loss due to transmission and

ventilation incorrectly. After updating the model with new formulae, we generated a new set of solutions to verify the updates.

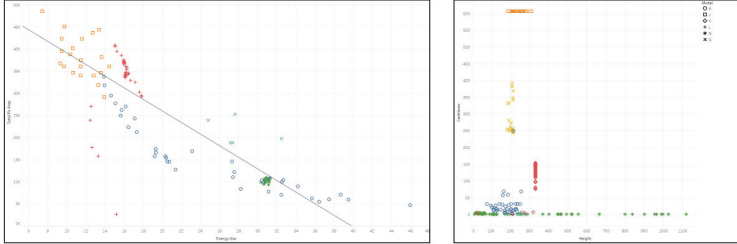


Figure 4. (Left) Plotting energy use vs total floor area, we expected energy use to be positively correlated with the total floor area. (Right) Scatter plot of building height versus cantilever area for 250 alternatives from six different design proposals.

**No Variation.** Figure 4 (Right) shows a scatter plot of the height versus cantilever area of the generated alternatives. This visualization helped us discover that alternatives generated by the model K do not vary in height, while those generated by model J do not vary in the cantilever area, contrary to what the designers intended. This flagged a problem in both models.

**Input Generator.** This module generates random values for each input parameter in its set range, from which the model generates a new alternative with the new input values. In the data, we noticed a discrepancy between the generated input values and alternatives. A close inspection showed that the generator module was making assumptions about the time that an alternative would take to be fully computed and prematurely generated new inputs values. However, reliably generating alternatives requires ensuring that the propagation solver finishes computing the current geometry and performance before a new cycle starts.

Table 1. The sample problems identified on the reliability and validity of models and the corresponding lessons derived when addressing them.

#	Lessons	Issues				
		Unexpected Correlation	Views	Heat loss	No Variation	Input Generator
1	Using Alternatives as Data	x	x		x	
2	The Need for Forms and Visualizations	x	x		x	
3	Matching Input to Performance Module Requirements	x				
4	Using Multiple Parametric Models	x	x			
5	Experts Required (early-stage involvement)		x	x		
6	Reproducibility for Revisiting Past Instances	x			x	x

### 5. Findings and Lessons Learnt

We noted a set of recurring issues and developed a set of solutions or approaches that can be used in addressing the issues in this case study. Table 1 below highlights



the mapping between these lessons and the sample issues we discussed above.

**Using Alternatives as Data.** When we work with a single design alternative at a time, we can only observe the problems that this alternative reveals. Observing a pattern as in Figures 2 and 4 is not possible unless we generate many alternatives and use a data visualization in which the pattern is visible. Data from the alternatives can cover a wide range of test cases demonstrating the model's behavior under a diverse sample of generated input.

**Need for Forms and Visualizations.** The quantitative performance evaluations and design forms (geometry) present two different aspects of design, complementing each other. Computed design evaluations capture only a fraction of the criteria that may be in action, while geometry at low fidelity can be misleading without further details. For example, the alternatives in Figure 3 (Left) had a similar view performance but the differences between them were only apparent by contrasting their forms. Similarly, the forms in Figure 2 explain the deviations in the Total Floor Area of some buildings.

**Matching Input to Performance Module Requirements.** Before starting the geometry modeling process, the designer needs to be aware of the requirements and limitations of the performance modules that are suitable for the task. This is so they can provide the right data structure or level of detail. The miscalculation of the Total Floor Area in Section 4.3 shows an example of passing the wrong data structure or so-called data type mismatch.

**Using Multiple Parametric Models.** For most of the parametric models, the Total Floor Area module worked properly but the expectations were violated for a single model that produced unexpected forms. This highlights the advantage of challenging the module's generality by subjecting it to different design models. Furthermore, when we work with multiple design models, we can learn about the nature of the forms that could achieve high values for given performance criteria. For example, Figure 4 (Right) shows that the forms generated by the model J had better cantilever areas than those of the rest.

**Experts Required (early-stage involvement).** While it is possible for a correlation pattern or an outlier to raise questions when observed in a data visualization, an expert knowledge is necessary for proper interpretation. Although nothing immediately catches our attention on the plots of heat loss against other performance criteria, an expert with experience in designing buildings in the same context as in the case study, might better identify the expected ranges of heat loss.

**Reproducibility for Revisiting Past Instances.** In general, designers reproduce an alternative to revisit and reevaluate it against new or updated designs. Achieving this requires retrieving both the input parameters and the model that was used to generate it. In our case study, due to the generator problem discussed in Section 4.3, the reported inputs could no longer be guaranteed to generate the same outputs. Furthermore, because of the dynamic nature of the design process, the parametric model is expected to change in time so that the reproduction is required. It is important then to save the full design model and the correct input values when an alternative is recorded. Re-creation of the design may be needed

for, for example, when investigating the source of an error, updating an alternative considering the new information about its performance, or improving form.

## 6. Conclusion and Discussion

Embedding performance calculation modules in each design module increases a parametric model's complexity and hence affects the models' reliability and validity. For example, each time a performance module changed in the case study, every model had to incorporate the new version, which interrupted the design process. On a practical side, the computing time taken by the performance modules in the model hindered the agility and rapid feedback into the design. Depending on the complexity of the model, the propagation of changes of one parametric model could take between 5 and 30 seconds. We also observed some software-specific issues when performance evaluators developed in a different computer on which the models built. To address these issues, we propose a new collaborative design Setup that decouples the design models from performance evaluation modules (Figure 5). We refactored the setup used in the workshop to separate the concerns and reduce its complexity: while a designer is working on an alternative, he or she can push the model to the server for evaluation. This eliminates embedding performance modules in the model, and hence, reduces complexity. The performance evaluation modules can function in a dedicated model without replication in each design model.

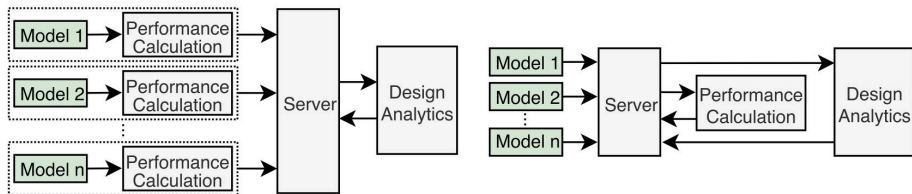


Figure 5. Original (Left) versus proposed (Right) architecture for the collaborative Setup.

The proposed Setup also integrates interactive design data analysis (design analytics tools) into the process. Designers may make better sense of their work when visual analytics is integrated into their workflow. They should be able to study form and geometry details along with performance data derived from design alternatives. The systems must make data available by mapping them on the model, in the model, or on separate visual data analytics interfaces as argued by Erhan et al. (2010). However, the workflow for creating and use of these data visualizations should not create an extra task layer in design.

The mismatch between the fidelity of the parametric models and the information required by the performance modules could be another source for errors. The performance modules should be flexible enough to handle varying input conditions. It is crucial to access different performance evaluation modules that are suitable for different levels of design abstraction. For example, calculating heat loss for a low-detail design model will require different input and rigor than a highly-detailed design model. The Setup should provide matching requirements

of performance modules with the fidelity of the design model.

As demonstrated through the case study, interactive visualization of design data can improve the reliability and validity of parametric modeling in a collaborative design setting. A bottleneck in achieving this is that parametric modeling and visual analytics are often discrete workflows. To alleviate this bottleneck, we need further and more systematic studies for exploring how the integration of these two workflows, i.e., parametric modeling and design analytics, can be further achieved.

### Acknowledgment

This research was supported by the MITACS Accelerate Program of Canada [IT12326] in partnership with The Boeing Company and Stantec Vancouver. We thank the SmartGeometry 2018 ‘Inside the Black Box’ cluster champions from Dialog Inc. and the participants for sharing their work with us for this study.

### References

- “SmartGeometry” : 2018. Available from <<https://www.smartgeometry.org>>.
- Aish, R. and Woodbury, R.: 2005, Multi-level interaction in parametric design, *Smart Graphics*.
- Anton, I. and Tănase, D.: 2016, Informed Geometries. Parametric Modelling and Energy Analysis in Early Stages of Design, *Energy Procedia*, **85**, 10-1016.
- Davis, D., Burry, J. and Burry, M.: 2011, Understanding visual scripts: Improving collaboration through modular programming, *Int. Journal of Architectural Computing*, **9**(4), 361-375.
- Erhan, H., Salmasi, N. and Woodbury, R.: 2010, ViSA: A Parametric Design Modeling Method to Enhance Visual Sensitivity Control and Analysis, *International Journal of Architectural Computing*, **8**, 461-483.
- Fuchkina, E., Schneider, S., Bertel, S. and Osintseva, I.: 2018, Design Space Exploration Framework, *Proceedings of the 36th eCAADe Conference*, 367-376.
- Johnston, W.M., Hanna, J. and Millar, R.J.: 2004, Advances in dataflow programming languages, *ACM computing surveys (CSUR)*, **36**(1), 1-34.
- Kasik, D.J., Buxton, W. and Ferguson, D.R.: 2005, Ten CAD Challenges, *IEEE Comput. Graph. Appl.*, **25**(2), 81-92.
- Ko, A., Abraham, R., Beckwith, L., Blackwell, A., Burnett, M., Erwig, M. and Scaffidi, C.: 2011, The state of the art in end-user software engineering, *ACM Comput. Surv.*, **21**, 1-21.
- Kolari’c, S.E.: 2017, CAMBRIA: Interacting with Multiple CAD Alternatives, *Computer-Aided Architectural Design. Future Trajectories*, Singapore, 81-99.
- Lyu, M.R.: 1996, *Handbook of software reliability engineering*, IEEE computer society press CA.
- Madkour, Y., Neumann, O. and Erhan, H.: 2009, Programmatic formation: practical applications of parametric design, *Int. Journal of Architectural Computing*, **7**, 587-603.
- Marchenko, M., Behrens, B., Wrobel, G., Scheffler, R. and PleBow, M.: 2011, A New Method of Visualization and Documentation of Parametric Information of 3D CAD Models, *Computer-Aided Design and Applications*, **8**(3), 435-448.
- Matejka, J., Glueck, M., Bradner, E., Hashemi, A., Grossman, T. and Fitzmaurice, G.: 2018, Dream Lens: Exploration and Visualization of Large-Scale Generative Design Datasets, *ACM SIGCHI Conference on Human Factors in Computing Systems*, 1-12.
- Nagy, D., Villaggi, L., Zhao, D. and Benjamin, D.: 2017, Beyond heuristics: a novel design space model for generative space planning in architecture, *Proceedings of Acadia 2017*.
- Nembrini, J., Samberger, S. and Labelle, G.: 2014, Parametric scripting for early design performance simulation, *Energy and Buildings*, **68**, 786-798.
- Sousa, T.B.: 2012, Dataflow programming concept, languages and applications, *Doctoral Symposium on Informatics Engineering*.

- Touloupaki, E. and Theodosiou, T.: 2017, Performance simulation integrated in parametric 3D modeling as a method for early stage design optimization: A Review, *Energies*, **10**, 10-3390.
- Woodbury, R.: 2010, *Elements of parametric design*, Taylor & Francis Group.



# OPTIMIZING TENSILE MEMBRANE ARCHITECTURE FOR ENERGY HARVESTING

HOYOUNG MAENG<sup>1</sup> and KYUNG HOON HYUN<sup>2</sup>

<sup>1,2</sup>*Department of Interior Architecture Design, Hanyang University*

<sup>1,2</sup>{roach555|hoonhello}@hanyang.ac.kr

**Abstract.** This paper identifies the correlation between the stiffness of a tensile membrane and wind-induced vibration. Here, a means by which to optimize the tensile membrane architecture and a harvester for the collection of energy from wind-induced vibration is proposed. Because its material property, the tensile membrane architecture is suitable for harvesting energy. While high stiffness is desired to ensure the stability of the tensile membrane architecture, the stiffness is negatively correlated with the energy collection. Thus, optimization considering the stiffness and the amount of harvestable energy in tensile membrane structures is conducted, broken down into the following tasks: 1) investigate the energy generator on the tensile membrane to combine a membrane type of architecture and wind energy harvesting; 2) set-up the computational environment with which to analyze the energy efficiency of the tensile membrane architecture; 3) visualize the resulting datasets to determine the relationship between the stiffness and the energy efficiency; and 4) define optimized tensile membrane architectures.

**Keywords.** Tensile Membrane Architecture; Design Optimization; Sustainable Architecture; Computational Design; Wind Energy Harvesting.

## 1. Introduction

At present, energy harvesting from vibrations is a notable subject and is part of the response to the global concern over energy and environmental issues (Abdelkefi 2016; Zhao and Yang 2018; Orrego et al. 2017). However, implementing wind-induced vibration-based energy harvesting techniques with a tensile membrane architecture has yet to be explored. Conventionally, vibration is a factor to be minimized in building structures, and doing so requires a refined analysis (BSI 2002). According to Stranghöner et al. (2016), tensile structures also require reduced wind-induced vibration to ensure their proper functioning and to prevent failure of the membrane. However, energy harvesting through generators requires vibration to maximize the amount of power generated. Moreover, the shape of the tensile membrane has a significant influence on the load paths for the pressure in these systems. The membrane must be prestressed to enhance the stiffness and to support material loads such as wind and snow. In this respect,

designers have explored various design concepts that are both structurally stable and aesthetically pleasing. Thus, it is crucial to find a balance between the amount of vibration and the degree of structural stability so as to maximize the energy harvesting performance while ensuring the serviceability of the tensile structure.

There are numerous related works on vibration-based energy harvesting through a membrane structure. A membrane-based energy harvesting device developed by Dong et al. (2015) had an adjustable resonant frequency of the membrane allowing the power output from vibration energy harvesting to be maximized. Allen and Smits (2001) investigated the feasibility of an “eel”-shaped piezoelectric membrane in underwater, aiming to maximize the strain energy and mechanical power. These studies concentrated on the development and evaluation of the efficiency of the generator itself. They focused on maximizing the amount of harvested energy, whereas shape optimization of the membrane was not considered. Therefore, the present paper aims to develop a method to simulate the energy harvesting performance and structural stability of a tensile membrane architecture depending on the shape and the membrane stiffness of the structure. To accomplish this, tensile membrane structure simulation software was developed with two major components. First, the proposed simulation software allows the generation of design variations based on three fundamental tensile structures: hyperbolic paraboloid (hypar), conic, and the barrel vault type. Second, the software estimates the amount of electrical power generated under various conditions, such as with different numbers of input sensors and different wind conditions. This paper focuses on developing a method to optimize the tensile membrane architecture for energy harvesting to assist designers when they make decisions about the design, including its form and the materials used.

## **2. Related Works**

### **2.1. TENSILE ARCHITECTURE**

Berger (1999) explained the advantages of a tensile structure, noting the “speed of construction, use of daylight, the reflection of heat from the sun, dispersal of interior sound, the beauty of the interior space and the excitement of the exterior sculpture.” Moreover, the high energy efficiency, possibility for daylight use, and heat-reflecting properties of a fabric structure can save energy and lower the general maintenance costs (Berger 1999). Tensile membrane structures offer efficient solutions that would not be possible with conventional building technologies. Tensile architectures have advantages in that they can be used in a variety of environments and may even be suitable for extreme environments such as that of the moon. Because the cost of transportation to the moon is extremely high, the structural materials must be as light as possible. The lunar structure must also be buildable with a minimum amount of manpower, as rapid construction lessens the time the workers are at risk. Tensile membranes meet these two requirements (Chow and Lin 1989). Therefore, the tensile structure is the optimal solution for the entire process of construction of a lunar structure, from logistics to installation. The soft architecture can be integrated with building systems or infrastructures and can act as an active building that communicates with

people with environmental or state information to which the architecture belongs (Davis 2011). Davis devised what is known as the sensing touch curtain, which uses electronics-embedded textile material programmed to glow or function as a type of insulation. It was shown that the tensile architecture can serve as not only a structure but also as an electronic medium of information.

The importance of the tensile membrane architecture is increasingly noted in modern urban environments. In contrast to conventional highly curved roof oriented membrane structures, recent developments have led to a wider range of shapes and uses. The tensile membrane structure is distinguished from other structures by its low self-weight, high flexibility, good deformability, and translucency. Given these properties, the membrane structure is an ideal option to express unique designs. When combined with other functions, such as electronics or software, it serves as a new medium for sharing information with the environment. In this paper, the membrane architecture and the vibration-based energy harvesting technique are combined to function as an energy generation method as well as an architectural structure.

## 2.2. ENERGY HARVESTING

In response to increasing carbon emissions and the limited supply of fossil fuels, vibration energy and the harvesting techniques have been widely researched. Vibration-based energy generation techniques can be utilized to harness electrical energy from wind, ocean waves, human motion and rain.

Membrane energy harvesting is commonly realized with piezoelectric, triboelectric and electromagnetic generators. These devices generate electric energy from the mechanical energy of fluttering, bending, folding, rubbing, stretching movements, vibration and/or pressure. The windbelt is a typical example of a power generation application that harvests energy from aeroelastic fluttering. One type, for example, uses a magnet attached to a flexible membrane to generate an induced electrical current with a coil fixed onto a supporting structure (Quy et al. 2016). Simple integration of the membrane and the anchoring support allows the use of triboelectric generators based on fluttering as well (Phan et al. 2017; Zhang et al. 2015). Rubbing and contact mechanisms are widely used in wearable generators. Triboelectric generators can harvest energy from human motions such as foot pressing, arm swinging or walking (Pu et al. 2015; Jung et al. 2014). The vibration of the membrane can be converted into applicable energy using a piezoelectric cantilever on the fabric or piezoelectric fibers embedded within a structure (Wei et al. 2013; Swallow et al. 2008). Stretching, folding or crumpling of the membrane can generate energy with the help of both triboelectric and piezoelectric components. Tensile membranes come in various types, examples of which include piezoelectric strap twining around an elastic core, a textile triboelectric nanogenerator with a 3D orthogonal woven structure, and a PVDF-based piezoelectric harvester attached onto a garment (Kim and Yun 2017; Dong et al. 2017; Yang et al. 2016). A wearable fabric device for water energy harvesting has been studied as well, in which triboelectricity is created by water droplets (Xiong et al. 2017). The papers described above provide evidence of successful membrane energy harvesting in various environments.



The tensile membrane architecture is open to the outdoor environment and the corresponding multi-ambient energy sources. This type of architecture utilizes a membrane material with a proven capacity to generate electrical energy. One important goal is to find an energy harvester suitable for the architecture that can also make use of wasted energy and thus contribute to green energy development. Existing structures can use attachment generators, while newly built structures can be composed of smart textiles or adequate generators depending on the environmental condition. This paper can help designers factor in new design considerations by suggesting membrane structures with energy harvesting capabilities.

### 2.3. DESIGN SUPPORT SYSTEM FOR OPTIMIZATION

Dream Lens was developed to explore large-scale generative design datasets (Matejka et al. 2018). Matejka et al. (2018) claimed that a large number of design solutions can be created with a generative design system by defining the goals, constraints or parameters. A parametric design with a limited condition can be used to create membrane architecture forms as well. Architects and engineers are able to make design decisions considering certain requirements, geometric forms and constraints, and desired materials for the most energy-efficient membrane architecture. Narangerel et al. (2016) explored building façade optimization for better daylighting performance. Parametric modelling and a multi-objective optimization algorithm were utilized to optimize the daylighting performance and BIPV efficiency. Datasets investigated with pre-defined design parameters were illustrated in a graph, and the three most outstanding alternatives were visualized.

In this paper, the parameters of the geometry of the tensile membrane architecture, the membrane stiffness and the wind are defined to find the optimized tensile membrane structure with the goal of stability of the structure and maximum amount of the harvested energy. The simulation results are presented in the form of graphs with an illustration of the optimized 3D model of the tensile membrane architecture. Providing such a design dataset will allow designers to make the optimal choices among various options.

### 3. Methodology

One of the aims of this paper is to determine the correlation between the stability of the structure and the performance of wind-induced vibration-based energy harvesting. The second goal is to help designers make decisions with visualized optimized design solutions and graphs with the two following objectives: the membrane stiffness and the amount of energy harvested. Simulations were carried out to achieve these goals. This study was conducted using Kangaroo, Grasshopper's plug-in, which is easy to use and widely used in relation to tensile structures for form-finding. Kangaroo has excellent accessibility, is capable of tests of wind actions on tensile structures, and allows real-time interaction. This makes Kangaroo a suitable tool for optimizing the tension and energy harvesting of membrane architectures in windy environments. While the average wind speed is constant at 1.7 m/s, the geometry of the membrane architecture changes by a

distance of 1 m inside the boundary of the 14m x 14m x 7m box as a variable in each simulation (Figure 1). Additionally, there is an interval of 500 kN/m starting from 1500 to 6000 kN/m in the other variable, i.e., the stiffness of membrane. The results considering these two objectives, stability and the amount of harvested energy, are organized and the optimized structures are visualized in this paper.

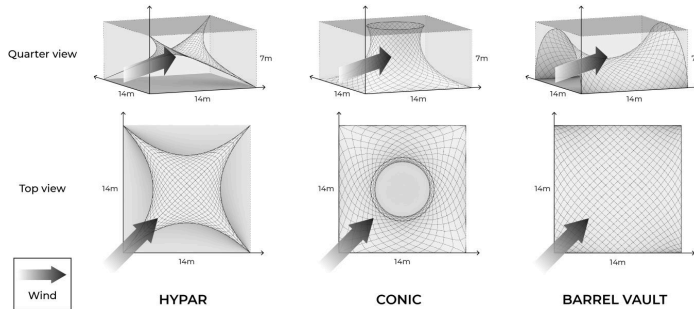


Figure 1. Hypar, conic and barrel vault types (arrows indicate the direction of the wind).

### 3.1. PARAMETERS

The three membrane structure types - the conic, hypar and barrel vault types - have different structural characteristics and main components affecting each structure (Bridgens and Birchall 2012). Analyses and optimization of these typical tensile forms were thus performed separately. The characteristics and parameters of the three forms considered in the experiment are as follows. A 14m x 14m x 7m boundary box is assumed, and all three aforementioned structures are formed inside the boundary zone. ‘Hypar’ features a geometry consisting of alternating high and low support points. The most basic form of the hypar type can take ‘Hypar 9’ in Figure 2 as an example which consists of two high points and two low points. More complex hypars can have a larger number of support points, but in this experiment, optimization was performed on a hypar with only four points, two of which are diagonally positioned and fixed onto the bottom. The other two non-fixed points are positioned in the 0-7m range along the z-axis. ‘Conic’ refers to a structure that consists of an upper ring shape and lower square supports. Regarding the conic shape, the membrane fails if the minimal surface and the desired shape are different (Bridgens and Gosling 2010). The ring height and radius are established by referring to the feasible bounds examined by Bridgens and Gosling. The radius is set within the range of 0-7m, the height between 0m and 7m and the radius is set to satisfy the feasible bounds. The Barrel Vault type consists of two parallel straight lines and elliptic curves at the end, anchoring the structure. The length of both straight lines is 14 m and the radius of each of the two ellipses is in the range of 0-7m. The distance between the two lines is fixed at 7m; therefore, if the radius approaches 0m, the barrel vault form would be similar to a flat panel. Design alternatives of the three tensile membrane architectures are visualized in Figure 2. Complete zero-height (flat) variables were not considered in this simulation, as they are unable to be referred to as hypar, conic or barrel

vault types.

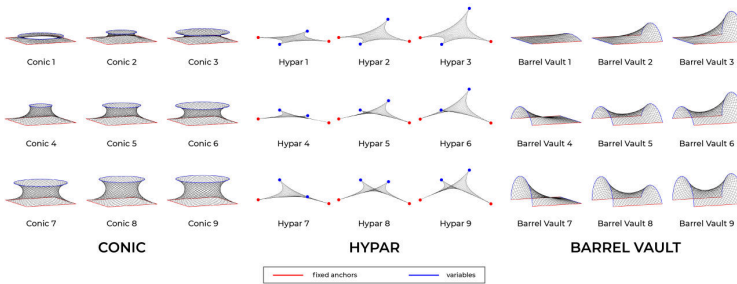


Figure 2. Design alternatives (fixed anchors are shown in red and variables are shown in blue).

The stiffness of the material is represented by the strength parameter of the Kangaroo solver. The Kangaroo solver regards the unit line object of a membrane surface as a spring. The spring follows Hooke's law; i.e., the strength of the spring is calculated as  $EA/L$ , where  $E$  is the Young's modulus,  $A$  is the cross-sectional area of the spring and  $L$  is the rest length (Piker 2014). The stiffnesses of the structural components, which are in this case polyester fabric and glass fiber fabric, are 25,200 N/cm and 54,720 N/cm, respectively; thus, the range of the stiffness was established according to real numbers from 1,500 kN/m to 6,000 kN/m (Uhlemann 2016).

### 3.2. WIND TYPE / GOALS

All simulations were conducted under the assumption that the surrounding ground conditions are negligible to focus on the geometry, stiffness and vibration of the membrane under the wind condition. The wind load applied to the membrane corresponds to the wind speed defined, by a sine function where the midline is at 1.7 m/s, the annual average wind speed in Seoul, with an amplitude level of 2 m/s. The wind speed thus has a maximum of 3.7 m/s and minimum of -0.3 m/s towards a fixed direction on the  $y=x$  graph (the boundary box is assumed to be located in the first quadrant). The wind speed can then be converted into the load in Pa, as the unit of time in the simulation differs from the actual time. The Kangaroo solver is used for the calculation according to its own iteration, which varies with different computer loads. The simulation begins once the membrane object is stabilized and ends after the applied wind speed draws a complete sine period twice.

The membrane is composed of a UV surface, on which power generators are assumed to be placed at the vertices of the surface. Each form has a different number of vertices: 613 for the hypar and barrel vault types and 800 for the conic type. Displacement and acceleration values are the obtained experimental results. The displacement is the sum of the distances travelled by all of the vertices during the simulation, and the acceleration is the sum of the number of vertices when the acceleration values exceed a defined value. Because the Kangaroo solver runs according to its own iteration, the defined value for measuring the acceleration is set to show the simulation results as clearly as possible.

The result of the experiment represents the movement of the assumed energy harvesters. In the literature, acceleration is not exactly proportional to the amount of energy generated but can be said to have the same direction (Saha et al. 2008). The optimum generator type differs according to the acceleration or displacement pattern, for which the designer will be able to select the harvester that matches their design based on the results of this experiment. In addition, by analyzing the resulting values of each vertex alone or together, the designer can choose the number and the position of generators for the highest efficiency in their design.

#### 4. Implementation Results

Figure 3 shows graphs of the results and the optimized forms, where the x-axis indicates the stiffness and the y-axis is the acceleration and displacement for the three tensile membrane structure forms. The stressed lines in Figure 3 indicate the values of the optimized alternatives. In the hyper and conic cases, alternatives Figure 3-b and Figure 3-d are the optimized options when stiffness is in 1500 kN/m and in the rest Figure 3-a, Figure 3-c and Figure 3-e have the largest acceleration and displacement values among the forms. An inverse relationship between the two axes: the stiffness and acceleration can be found in all three types and between the stiffness and displacement as well. Given the outcomes shown in Figure 3, it can be inferred that the amount of generated energy decreases as the material becomes stiffer. In a comparison between the two factors, the decline of the displacement grows steeper, resulting in logarithmic graphs, while the shapes of stiffness-to-acceleration graphs vary from nearly linear to logarithmic.

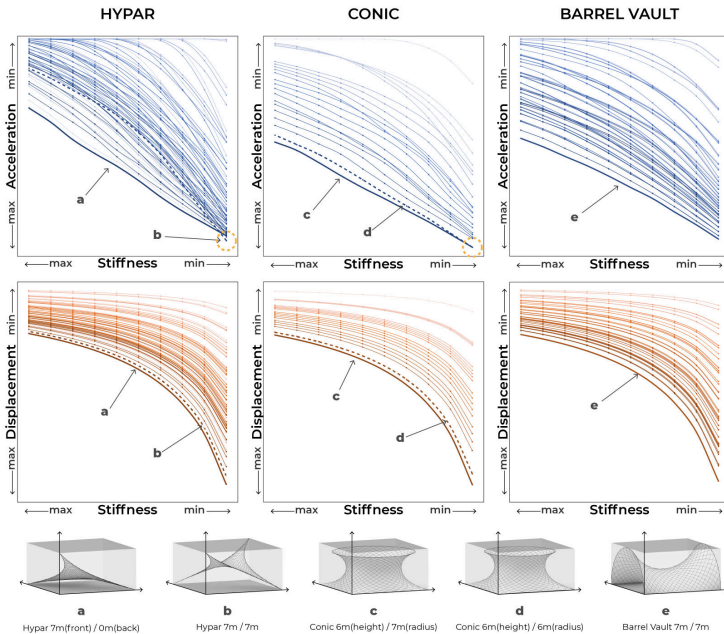


Figure 3. Results graphs and optimized 3D models.

The hypar was simulated with the combination of stiffness of 1500–6000 kN/m and a height of 0–7m. In the acceleration graph, outstanding values were achieved from hypar structures with anchors of the height of 7m and the form containing relatively tall anchors tend to be ranked highly. The remaining examples at the lower end are a combination of anchors with heights of 1–3m. Symmetrical forms such as the indication of a 0m / 7m anchored hypar and another 7m / 0m anchored hypar show minor differences in both the acceleration and displacement, demonstrating that the diametrical opposite directionality of the wind does not have a significant impact on the result. Additionally, the wind when blowing towards the inside of the hypar structure always scored slightly higher compared to when it was blowing towards the outside. Some of the forms show greater decreasing rates than others, indicating that it is desirable to use more flexible materials. The 7m / 0m anchored hypar has the most distinctive values of generated energy, while the 7m / 7m anchored hypar peaked at the 1500 kN/m material. Thus, the optimized structures are the two: 7m / 0m anchored hypar (Figure 3-a) at majority of stiffness value and 7m / 7m anchored hypar (Figure 3-b) at stiffness value around the 1500 kN/m. The displacement values indicate a clear hierarchy according to the geometric properties. The exception of an intersection between resulting graph lines did not occur. The displacement also shows larger variables when the wind blows towards the inside.

The conic simulation was conducted with variables according to the ‘feasible zone’ (Bridgens and Gosling 2010). A prominent feature of the conic type is that the height value has a strong influence on the results. Separation of the displacement results is done using blank gaps among curves of different heights. A greater height guarantees higher energy level, and with an equal height, a larger radius generates a higher energy level. Four different displacement values of the 2m height conic structures located on the upper side of the stiffness-to-displacement graph are barely distinguishable throughout the stiffness range. The optimized structures are the two: a height of 6m conic structure with a radius of 7m (Figure 3-c) at majority of stiffness value and a height of 6m conic structure with a radius of 6m (Figure 3-d) at stiffness value around the 1500 kN/m.

The highly ranked acceleration values of the barrel vault type clearly come from the radius of 7 m. The barrel vault is especially affected by a larger radius. The group of structures with higher radius values shows a definite upper position compared to those with lower values. Most of the results indicate a hierarchy compared to other structural forms. The barrel vault also shows higher acceleration values when the direction of the wind head is towards the inside. However, only a slight difference exists between the two symmetrical forms. The optimized structure is the 7m / 7m barrel vault (Figure 3-e), with the values of generated energy located on the top. The displacement graph is similar to the other structural forms. The variables of the 7m / 7m geometry are clearly at the very top.

Acceleration and displacement graphs are illustrated with the results of the simulations. The five optimized membrane forms and the correlation between the amount of energy harvested and the material stiffness are defined. Designers can utilize these graphs to select the shapes and materials of tensile membrane architectures.

## 5. Conclusion and Future Works

This paper proposes a new type of architecture that integrates energy harvesting with the tensile membrane architecture and then presents simulation results. Graphs of the integration results were visualized with the objective of maximizing the membrane stiffness as well as the amount of energy harvested. Low stiffness induces unstable vibration, which acts as an obstacle that may cause the tensile architecture to fail (Stranghöner et al. 2016). However, it can be harnessed as an option that ensures high energy efficiency if carefully handled. A limitation of this paper is that it does not fully cover the analysed features in terms of shear stiffness and/or serviceability, for example, to guide those building a tensile membrane architecture. However, focusing on the membrane stiffness without interference from features related to tensile failures proved effective to identify an obvious inverse correlation between the stiffness and energy efficiency. To the best of our knowledge, this is the first attempt to identify a correlation between wind-induced vibration-based energy harvesting and membrane stiffness levels. Future studies can involve factors that are analysed in actual tensile membrane architectures. Moreover, to overcome the limitation of using a simulation to verify the tensile deformation behavior and the wind, an experiment comparing computer simulation results with a scale model of an actual membrane structure with an energy harvester attached can be conducted. On the other hand, for greater convenience for the designer, a real-time simulation tool can be devised to allow an interactive decision-making process. Being able to observe the actual generated electrical power output by the material and selecting the electric generator with wind information will make the framework more intuitive. Fluid-structure interaction (FSI) programs can also be useful to supplement the calculation of real-world wind behaviors on membranes.

## Acknowledgement

This work was supported by the Ministry of Education of the Republic of Korea and the National Research Foundation of Korea (NRF-2019S1A5A8034285).

## References

- Abdelkefi, A.: 2016, Aeroelastic energy harvesting: A review, *International Journal of Engineering Science*, **100**, 112-135.
- Allen, J.J. and Smits, A.J.: 2001, Energy harvesting eel, *Journal of Fluids and Structures*, **Volume 15, Issues 3-4**, Pages 629-640.
- Berger, H.: 1999, Form and function of tensile structures for permanent buildings, *Engineering Structures*, **Volume 21, Issue 8**, Pages 669-679.
- Bridgens, B. and Birchall, M.: 2012, Form and function: The significance of material properties in the design of tensile fabric structures, *Engineering Structures*, **Volume 44**, Pages 1-12.
- Bridgens, B.N. and Gosling, P.D.: 2010, Importance of material properties in fabric structure design & analysis, *Symposium of the International Association for Shell and Spatial Structures*, Valencia, 2180-2191.
- Chow, P.Y. and Lin, T.Y.: 1989, Structural Engineer's Concept of Lunar Structures, *Journal of Aerospace Engineering*, **Volume 2**, Issue 1.
- Davis, F.: 2011, Sensing Touch Curtain: Soft Architecture, *SIGRADI 2011*.

- Dong, K., Deng, J., Zi, Y., W, Y.C., Xu, C., Zou, H., Ding, W., Dai, Y., Gu, B., Sun, B. and Wang, Z.L.: 2017, 3D Orthogonal Woven Triboelectric Nanogenerator for Effective Biomechanical Energy Harvesting and as Self-Powered Active Motion Sensors, *Advanced Materials*, **29**, 38.
- Dong, L., Grissom, M. and Fisher, F.: 2015, Resonant frequency of mass-loaded membranes for vibration energy harvesting applications, *AIMS Energy*.
- Jung, S., Lee, J.S., Hyeon, T., Lee, M. and Kim, D.H.: 2014, Fabric-Based Integrated Energy Devices for Wearable Activity Monitors, *ADVANCED MATERIALS*, **26**, Issue 36..
- Kim, M. and Yun, K.S.: 2017, Helical Piezoelectric Energy Harvester and Its Application to Energy Harvesting Garments, *Micromachines*, **8**, 4.
- Matejka, J., Glueck, M., Bradner, E., Hashemi, A., Grossman, T. and Fitzmaurice, G.: 2018, Dream Lens: Exploration and Visualization of Large-Scale Generative Design Datasets, *CHI Conference on Human Factors in Computing Systems*, **Paper No. 369**, 369.
- Narangerel, A., Lee, J.H. and Stouffs, R.: 2016, Daylighting Based Parametric Design Exploration of 3D Facade Patterns, *cuminCAD*.
- Orrego, S., Shoele, K., Ruas, A., Doran, K., Caggiano, B. and Kang, S.H.: 2017, Harvesting ambient wind energy with an inverted piezoelectric flag, *Applied Energy*, **194**, 212-222.
- Phan, H., Shin, D.M., Jeon, S.H., Kang, T.Y., Han, P., Kim, G.H., Kim, H.K., Kim, K., Hwang, Y.H. and Hong, S.W.: 2017, Aerodynamic and aeroelastic flutters driven triboelectric nanogenerators for harvesting broadband airflow energy, *Nano Energy*, **33**, 476-484.
- D. Piker (ed.): 2014, *Kangaroo 2 [computer software]*, ., United Kingdom.
- Pu, X., Li, L., Song, H., Du, C., Zhao, Z., Jiang, C., Cao, G., Hu, W. and Wang, Z.L.: 2015, A Self-Charging Power Unit by Integration of a Textile Triboelectric Nanogenerator and a Flexible Lithium-Ion Battery for Wearable Electronics, *advanced materials*, **27**, Issue 15.
- Quy, V.D., Sy, N.V., Hung, D.T. and Huy, V.Q.: 2016, Wind tunnel and initial field tests of a micro generator powered by fluid-induced flutter, *Energy for Sustainable Development*, **Volume 33**, Pages 75-83.
- Saha, C.R., O'Donnell, T., Wang, N. and McCloskey, P.: 2008, Electromagnetic generator for harvesting energy from human motion, *Sensors and Actuators A: Physical*, **147**, Issue 1.
- B.S.I. British Standard (ed.): 2002, *Eurocode. Basis of structural design*, CEN national Members.
- Stranghoner, N., Uhlemann, J. and Bilginoglu, F.: 2016, Prospect for european guidance for the structural design of tensile membrane structures, *Joint Research Centre (JRC) of the European Commission*.
- Swallow, L.M., Luo, J.K., Siores, E., Patel, I. and Dodds, D.: 2008, A piezoelectric fibre composite based energy harvesting device for potential wearable applications, *SMART MATERIALS AND STRUCTURES*, **17**, Number 2.
- Uhlemann, J.: 2016, *Elastic Constants of Architectural Fabrics for Design Purposes*, Thesis for: PhD, Advisor: Natalie Stranghöner, Kai-Uwe Bletzinger, Duisburg-Essen.
- Wei, Y., Torah, R., Yang, K., Beeby, S. and Tudor, J.: 2013, A screen printable sacrificial fabrication process to realise a cantilever on fabric using a piezoelectric layer to detect motion for wearable applications, *Sensors and Actuators A: Physical*, **203**, 241-248.
- Xiong, J., Lin, M.F., Wang, J., Gaw, S.L., Parida, K. and Lee, P.S.: 2017, Wearable All-Fabric-Based Triboelectric Generator for Water Energy Harvesting, *Advanced Energy Materials*, **7**, Issue 21.
- Yang, J.H., Cho, H.S., Park, S.H., Song, S.H., Yun, K.S. and Lee, J.H.: 2016, Effect of garment design on piezoelectricity harvesting from joint movement, *Smart Materials and Structures*, **Volume 25**, Number 3.
- Zhao, L. and Yang, Y.: 2018, An impact-based broadband aeroelastic energy harvester for concurrent wind and base vibration energy harvesting, *Applied Energy*, **212**, 233-243.

# PARAMETRIC MODELLING AND SIMULATION OF AN INDOOR TEMPERATURE RESPONSIVE ROTATIONAL SHADING SYSTEM DESIGN

JIAHUI CHENG<sup>1</sup>, ZHUOQUN ZHANG<sup>2</sup> and CHENGZHI PENG<sup>3</sup>

<sup>1,3</sup>*School of Architecture, The University of Sheffield*

<sup>1,3</sup>{JCheng17|c.peng}@sheffield.ac.uk

<sup>2</sup>*Department of Electrical & Electronic Engineering, The University of Sheffield*

<sup>2</sup>zzhang20@sheffield.ac.uk

**Abstract.** We present a digital design strategy for developing an intelligent rotational shading system responsive to changes in indoor temperatures. The strategy was first modelled with an Arduino-based physical prototype, identifying the concept of “mapping” between building indoor air temperature and rotational movement (angle) of external solar shading. A virtual parametric modelling approach was then followed to test three methods of mapping: linear, quadratic and logarithmic. The aim was to examine the performative differences exhibited by the three mapping methods in terms of the total comfort hours and estimated cooling energy demand during summer months. A typical cellular office in the Arts Tower of University of Sheffield was chosen for the parametric modelling (Rhino-Grasshopper) and environmental simulation (Honeybee-Ladybug) of horizontal and vertical rotational shading system design. The simulation shows that the horizontal shading system rotating according to the linear mapping methods achieve greater total comfort hours with lower cooling energy demand in the case of Arts Tower in Sheffield, UK.

**Keywords.** Indoor temperature responsive shading; temperature-angle mapping; parametric design; kinetic shading; overheating.

## 1. Introduction

Global warming is likely to induce significant heat stress on urban populations due to increased outdoor and indoor temperatures. Large-scale uptake of energy efficient building features that reduce cooling energy demand while maintain indoor thermal comfort could mitigate indoor heat stress in future climate. External or internal solar shading is widely used in buildings because it can moderate indoor environmental conditions. Active intelligent shading systems have been developed to be responsive to changing environmental conditions (Manzan and Clarich 2017). In this paper, we present a parametric modelling and simulation strategy for developing performative shading system design responsive to changes in indoor temperatures.



We follow a general principle that a medium-large non-domestic building integrated with smart solar shading can significantly increase thermal comfort of building users while reducing cooling energy demand during summer months. To explore the idea of indoor temperature responsive solar shading, we first built an Arduino-based physical computing prototype. The physical prototyping suggests a concept of “Temperature-Angle Mapping (TAM)” that an intelligent solar shading system may be modelled as a function that maps indoor air temperatures (obtained by indoor sensing) to rotational angles of shading blinds (delivered by motors). To further explore TAM more systematically, we then turned to parametric virtual modelling and simulation to define specific TAM methods and examine their performative implications. For the virtual parametric modelling and simulation, we used EnergyPlus, Honeybee, and Ladybug plug-ins (Crawley et al. 2008) (Ladybug tools LLC 2017) (Roudsari and Pak 2013).

## 2. Physical computing prototype

We take the 19-storey Arts Tower of the University of Sheffield as a test case scenario, and propose an intelligent automatic rotating shading system design that can respond to indoor temperature changes. This is considered a problem to be solved that, in present summertime, the manually operated Venetian blinds are often not applied in unoccupied rooms in the building, resulting in multiple overheated floors.

We first built a physical prototype using an Arduino-based physical computing platform. The basic working principle is to model a rotational shading system in response to real-time indoor temperature data collection via a temperature sensor installed in the room. The prototyping helped to clarify the correspondence between two values: (a) the sensed temperature, and (b) the rotation angle of louvre blades.

Two components were used in the prototyping: DHT11 temperature sensor and SG90 servo motor. DHT11 is suitable for the temperature measurement range of 0°C - 50°C, and the sampling frequency is once per second (Lady ada 2019). The rotation range of a SG90 servo motor is 0° - 180°, and the rotation speed can reach 0.1 second per 60-degree (Components101 2017). The shading panels and the servo motor were mechanically fixed to each other such that the shading panels rotate with the same angle as the servo motor.

Based on the Arduino platform, we produced a physical model of horizontal shading panels with linear mapping rotation method. The shading panels of this model can be driven by a servo motor, and respond to the real-time indoor temperature measured by the temperature sensor, and automatically rotate according to calculated linear mapping relationship between the rotation angle and the indoor sensing temperature.

To make the change of the rotation angle and the change of the indoor sensing temperature more visible in the experiment, an LCD screen was added to the Arduino platform to display the real-time indoor temperature measured by the temperature sensor. The physical model and circuit are shown as Figure 1.

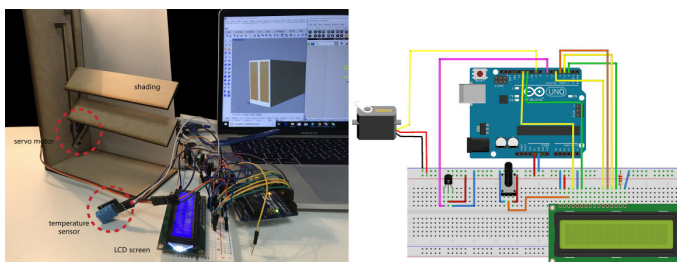


Figure 1. Physical model and Arduino circuit of temperature responsive rotational servo motor.

Through the prototyping, we observed that the key to the shading system design is to establish the relationship between sensing temperature and rotation angle of the shading blades. Also, for both horizontal and vertical shading, the opening and closing status of the shading system should be determined by (1) the higher indoor temperature, the larger the shading closing angle, and (2) the rotation angle should correspond to the sensing temperature on a one-to-one basis. So a simple “mapping” concept is that when the shading system is fully opened, the servo motor’s angle is defined as  $0^\circ$ , and positive motor rotation angles correspond to closing movement. It follows that the rotation angle of the servo motor can be obtained by a mapping function of an indoor temperature reading from the DHT11 sensor. In order to develop this mapping concept systematically, three mapping functions were selected to perform parametric modelling and simulation: linear, quadratic and logarithmic. These functions map indoor temperature values to blade rotation values which produce various indoor environmental conditions as performative indicators.

According to the Honeybee energy modelling and Ladybug thermal comfort assessment of a typical office room in the Arts Tower of Sheffield University, the maximum indoor temperature can reach  $36.24^\circ\text{C}$  (near  $37^\circ\text{C}$ ) in summer. But the most comfortable range of human indoor thermal comfort is between  $20^\circ\text{C}$  and  $22^\circ\text{C}$  (Morris 2018). Therefore, the shading system design for the Arts Tower should run automatically when the indoor sensing temperature is between  $22^\circ\text{C}$  and  $37^\circ\text{C}$ . When the indoor sensing temperature is lower than or equal to  $22^\circ\text{C}$ , the shading is fully opened, so that the room gets sufficient solar radiation heat. When the indoor sensing temperature reaches  $37^\circ\text{C}$ , the shading should be fully closed. Take linear horizontal shading system as an example, the key Arduino code is as follows:

```

lcd.setCursor(7, 0);
sensor_event_t event;
dht.temperature().getEvent(&event);
if (isnan(event.temperature)) {
    Serial.println(F("Error reading temperature!"));
}
else {
    temp=event.temperature;
}
srvDegree=round(map(temp, 22, 37, 0, 90));
    
```

```

srvDegree=constrain(srvDegree,0,90);
Serial.println(srvDegree);
myservo.write(srvDegree);

if (isnan(event.temperature)) {
  Serial.println(F("Error!"));
}
else {
  temp=event.temperature;
  lcd.print(temp);
}
lcd.setCursor(0, 1);

```

Specifically, for a horizontal shading system, the shading blades are defined as fully open when perpendicular to the window, and fully closed when rotated downward towards the window, and the rotation angle range is set  $0^\circ$ - $90^\circ$ . Three specific mapping methods are chosen for mapping the indoor sensing temperature range from  $22^\circ\text{C}$  to  $37^\circ\text{C}$  to the rotation angle range from  $0^\circ$  to  $90^\circ$ :

Linear mapping:  $A = 6 \cdot T - 132$

Quadratic mapping:  $A = \frac{6}{59} \cdot T^2 - \frac{2904}{59}$

Logarithmic mapping:  $A = \log_{e^{\frac{\ln(\frac{37}{22})}{90}}} \left( \frac{1}{22} \cdot T \right)$

For the vertical shading system, it is defined that the shading blades aligned south as fully open, and fully closed when rotated counter-clockwise to parallel to the window. Because the Arts Tower is oriented  $15^\circ$  south east, the rotation angle range is set  $0^\circ$ - $105^\circ$ . Three specific mapping methods were formulated as follows:

Linear mapping:  $A = 7 \cdot T - 154$

Quadratic mapping:  $A = \frac{7}{59} \cdot T^2 - \frac{3388}{59}$

Logarithmic mapping:  $A = \log_{e^{\frac{\ln(\frac{37}{22})}{105}}} \left( \frac{1}{22} \cdot T \right)$

The relationships between the rotation angle and the indoor sensing temperature horizontal shading and vertical shading are shown in Figure 2.

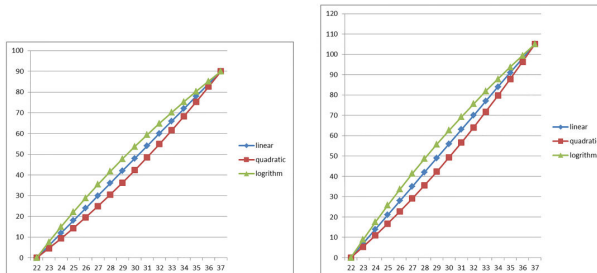


Figure 2. The proposed horizontal TAM functions and vertical TAM functions.

### 3. Parametric virtual modelling and simulation

In order to evaluate the environmental performance of the above Temperature-Angle Mapping (TAM) methods applied to the Arts Tower, we used three indicators: thermal comfort, cooling energy demand, and air temperature. A parametric design simulation workflow has been established to conduct the experiment in the following steps:

1. Create 3D models of typical rooms of Arts Tower by Grasshopper geometry components as building energy and thermal comfort modeling with Honeybee and Ladybug. Transform Grasshopper geometries into closed Honeybee zones, which can be used to simulation with Honeybee and Ladybug.
2. Add parametric models of rotational shading design to the room models. The degree of vertical or horizontal rotation is set as the primary parameter. The horizontal and vertical shading system design was modelled parametrically and linked to the TAM components in Grasshopper, which are shown in Figure 3.

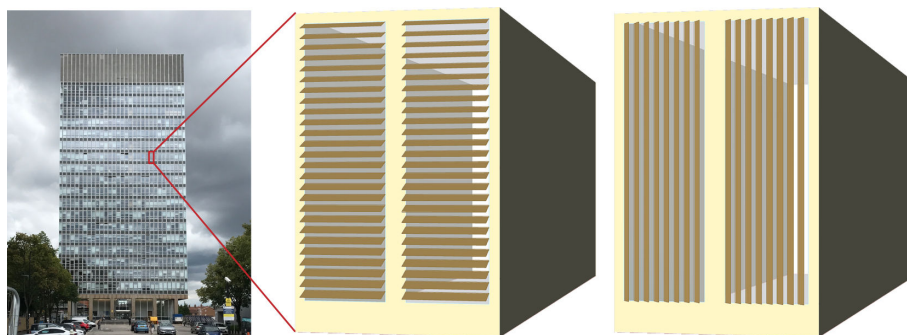


Figure 3. Arts Tower, typical room with horizontal and vertical shading system.

3. For each TAM method, four indoor sensing temperatures of 23°C, 27°C, 31°C, and 35°C were selected as the thresholds for running and comparing simulation results. Shading geometries are transformed into Honeybee context, which can be recognized as shading construction in simulation.

4. Honeybee material parameters are assigned to the walls, floors, windows and other components of typical room model. For example, the material of the window is a double glazed with an air space of 13mm, and the material of the wall is M11 lightweight concrete with a thickness of 100mm.

5. Load the Sheffield weather data (EPW) file as the basis for all simulation and analysis. As this study was mainly to address the problem of indoor overheating, the simulation period was set for summertime in Sheffield - from June to August. In order to obtain more detailed simulation results, the temporal unit was set hourly. The simulation outputs include temperature, humidity, and thermal load, and others. In this study, we used three indicators, simulation indoor temperature, total cooling energy demands, and total comfort hour percentage. Ladybug's psychometric module can then produce total comfort hours percent values for each duration of the simulation periods.

6. Visualize the results with Ladybug charts tools.

7. Repeat the above simulation and visualization processes for the six TAM methods and obtain the simulation results for comparison.

**4. Simulation results and discussion**

The simulation results are summarized in the table below:

**Table 1. Simulation results.**

		Without shading	Horizontal shading			Vertical shading																					
			linear mapping	quadratic mapping	logrithm mapping	linear mapping	quadratic mapping	logrithm mapping																			
Function			$A=6 \times T-132$	$A=(6+59) \times T^2-(2904+59)$	$A=89.9_{\ln(0.97^{220-96})} \times T^2-(1+22) \times T$	$A=7 \times T-154$	$A=(7+59) \times T^2-(3388+59)$	$A=89.9_{\ln(0.97^{220-96})} \times T^2-(1+22) \times T$																			
Diagram																											
Sensing temperature checkpoints & Angle		23°C 6°	27°C 30°	31°C 54°	35°C 78°	23°C 4.58°	27°C 24.92°	31°C 48.51°	35°C 75.36°	23°C 7.70°	27°C 35.45°	31°C 59.37°	35°C 90.38°	23°C 7°	27°C 35°	31°C 63°	35°C 91°	23°C 5.34°	27°C 29.07°	31°C 56.60°	35°C 87.92°	23°C 8.98°	27°C 41.36°	31°C 69.27°	35°C 93.78°		
Total comfort hour percentage (%)	Jun - Aug	17.57	17.89	17.71	17.75	17.62	17.89	17.66	17.75	17.71	17.93	17.66	17.66	17.57	17.44	18.03	18.30	17.57	17.35	17.75	18.30	17.57	17.48	18.25	18.30	17.57	
	Jun	14.44	14.44	14.44	14.86	14.72	14.30	14.72	15.00	17.71	14.30	14.44	14.44	14.58	14.03	14.17	14.72	14.44	14.03	14.17	14.44	14.44	14.03	14.31	15.14	14.44	
	Jul	16.80	20.03	19.22	19.63	20.02	19.22	19.62	20.03	19.35	20.03	19.35	20.03	19.89	18.95	19.89	18.95	19.89	18.95	19.89	18.95	20.16	20.03	16.80	16.80	16.80	16.80
Total cooling energy demands (kWh)	Jun - Aug	61.75	39.23	38.09	36.67	33.18	39.36	38.23	36.84	34.38	39.10	37.93	35.45	33.11	44.04	43.07	40.26	36.51	43.96	42.17	38.75	35.36	43.87	40.94	36.84	61.75	
	Jun	18.66	13.85	13.67	13.36	12.40	13.88	13.69	13.40	12.74	13.85	13.67	13.36	12.40	14.93	14.71	14.09	13.25	14.93	14.51	13.73	13.01	14.92	14.24	13.30	18.66	
	Jul	28.05	17.78	17.24	16.55	14.87	17.84	17.30	16.64	15.44	17.78	17.24	16.55	14.87	17.78	17.24	16.55	14.87	17.78	17.24	16.55	14.87	17.78	17.24	16.55	14.87	28.05
Simulation indoor temperature (°C)	Jun - Aug	max	36.24	34.63	34.54	34.40	34.02	34.64	34.53	34.41	34.15	34.62	34.53	34.26	34.02	34.96	34.78	34.42	36.24	34.98	34.81	34.52	34.24	34.97	34.71	34.35	36.24
		min	8.27	8.02	8.01	7.99	7.93	8.02	8.01	7.99	7.95	8.01	8.01	7.97	7.93	8.09	8.07	8.01	8.27	8.09	8.07	8.03	7.96	8.09	8.06	7.99	8.27
	Jun	max	36.24	34.63	34.54	34.40	34.02	34.64	34.53	34.41	34.15	34.62	34.53	34.26	34.02	34.96	34.78	34.42	36.24	34.98	34.81	34.52	34.24	34.97	34.71	34.35	36.24
		min	8.27	8.02	8.01	7.99	7.93	8.02	8.01	7.99	7.95	8.01	8.01	7.97	7.93	8.09	8.07	8.01	8.27	8.09	8.07	8.03	7.96	8.09	8.06	7.99	8.27
	Jun	max	34.96	33.21	33.13	32.99	32.57	33.22	33.14	33.01	32.72	33.20	33.12	32.84	32.56	33.60	33.44	33.06	34.96	33.61	33.47	33.16	32.83	33.61	33.37	32.97	34.96
		min	9.93	9.62	9.62	9.59	9.52	9.64	9.62	9.59	9.54	9.63	9.62	9.57	9.52	9.70	9.67	9.60	9.93	9.70	9.68	9.62	9.56	9.70	9.66	9.59	9.93
Jun	max	32.94	30.81	30.96	30.54	30.19	30.82	30.71	30.56	30.31	30.80	30.67	30.42	30.19	31.30	31.08	30.67	32.94	31.31	31.13	30.78	30.41	31.30	31.00	30.58	32.94	
	min	10.34	10.03	10.01	9.98	9.94	10.04	10.01	9.99	9.96	10.03	10.00	9.97	9.94	10.12	10.06	10.00	10.34	10.12	10.07	10.02	9.96	10.11	10.05	9.99	10.34	

**4.1. TOTAL COMFORT HOURS PERCENT**

During the entire summertime from June to August, the comfort hour percent of the current room was 17.57%. The simulation results of TAM-Horizontal show a slight increase of the comfort hour percent than without shading. In particular, the comfort hour percent at the 23°C of the logarithmic mapping reached 17.93%. As shown in Figure 4, the hours represented by the colour blocks in the wireframe with shading are significantly higher than those hours without shading. For a room fitted with vertical shading, the simulation results of TAM-Vertical at the 23°C show a lower percentage than without shading. Comparing the four threshold results, the horizontal shading system with the linear and quadratic mapping methods produce more indoor comfort hours.

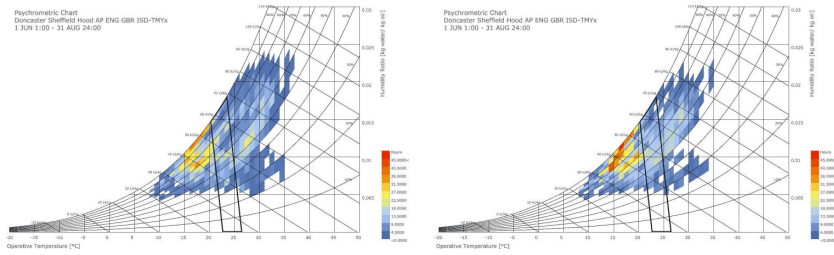


Figure 4. Comfort zones of rooms without shading system and with horizontal shading system at 23°C of logarithm mapping in June-August.

Monthly summer simulation results show that for the room without shading, the comfort hour percent in June, July, and August are 14.44%, 16.80%, and 20.70%, respectively. All simulation results for room with shading in June show no significant differences to room without shading. Only the comfort hour percent of the room with the TAM-Horizontal-Linear method was greater than that room without shading.

Both TAM horizontal and vertical produced more comfort zones in July. The comfort hour percent with shading at all thresholds are 2% - 4% higher than the percent without shading. As shown in Figure 5, the hours represented by the colour blocks in the wireframe with shading are significantly higher than those hours without shading. This suggests that such shading system design has a certain effect on regulating indoor thermal comfort during the hottest month of the year. Overall, the TAM-Horizontal linear and logarithmic methods produced more indoor comfort hours for the typical room in the Arts Tower.

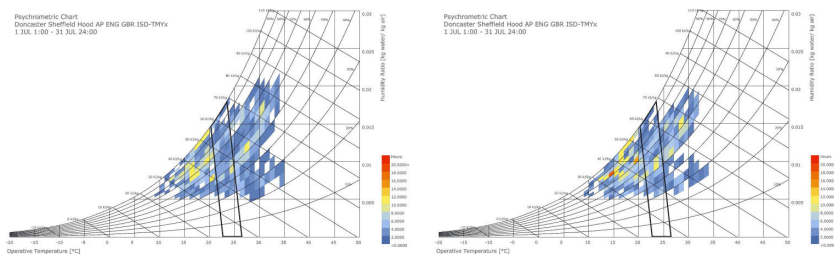


Figure 5. Comfort zones of rooms without shading system and with horizontal shading system at 23°C of linear mapping in July.

In August, the comfort hour percent of the typical room without shading reached 20.70%, which is much higher than other summer months. Contrary to the results in July, the comfort hour percent of room with shading was lower than without shading at all thresholds. One possible reason is that the shading produces more zones below the minimum value of comfort zone when blocking solar radiation in August in Sheffield.

4.2. TOTAL COOLING ENERGY DEMANDS

The total energy cooling demands of current typical room from June to August reaches 61.75kWh, the hourly result is shown in Figure 6. Shading systems greatly reduce this value by about 20kWh - 30kWh, which means shading systems can reduce cooling energy demand of one room by 20kWh - 30kWh. It can be seen from the data that total cooling energy demands of a room with horizontal shading is lower than that value of room with vertical shading. At 23°C, the total cooling energy demands of room with horizontal shading and vertical shading of linear mapping are 39.23kWh and 44.04kWh respectively, and hourly results are shown in Figure 7. Overall, the TAM-Horizontal linear and logarithmic methods produced more cooling energy demand reduction.

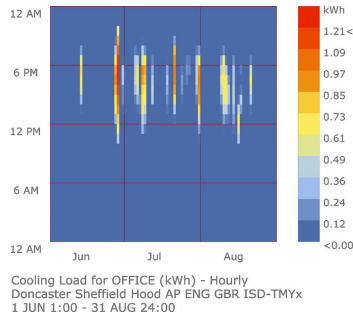


Figure 6. Cooling energy demands of room without shading system in June-August.

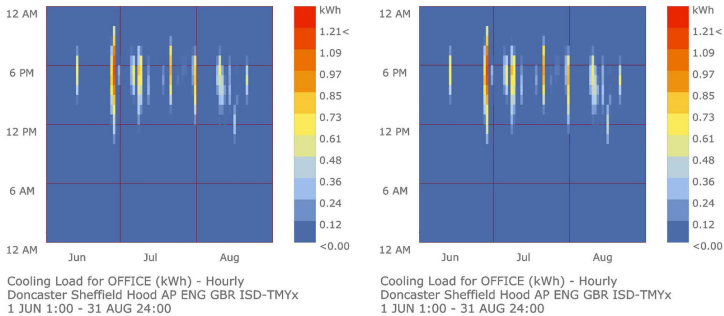


Figure 7. Cooling energy demands of rooms with horizontal and vertical shading system at 23°C of linear mapping in June-August.

Monthly results of total energy cooling demands are similar to the results of whole summer period. Shading system design can significantly reduce cooling energy demands, and horizontal shading can make a greater contribution than vertical shading. For the room without shading in July, the cooling energy demands is 28.05kWh, which is obviously higher than in June (18.66kWh) and in August (14.94kWh), which indicates that July is the hottest time in summer in Sheffield, and the shading system deployed in this period can play a greater role.

At 35°C, cooling energy demands of TAM horizontal and vertical with the linear method are 14.87kWh and 16.48kWh respectively, which indicated a reduction by about 50% compared to room without shading. As shown in Figure 8, the energy demands represented by the colour blocks are obviously lower than that value of room without shading system.

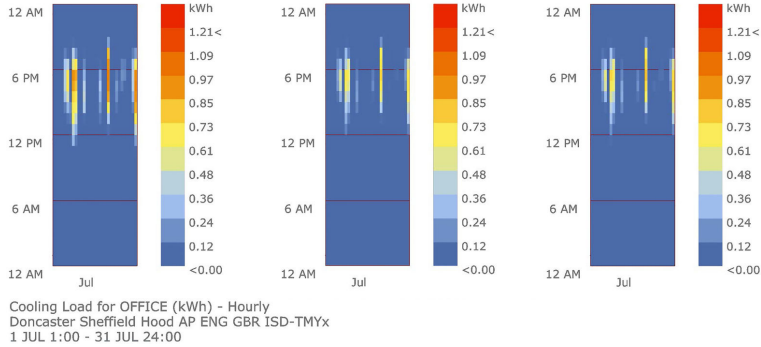


Figure 8. Cooling energy demands of rooms without shading system, with horizontal and vertical shading system at 35°C of linear mapping in July.

### 4.3. SIMULATED INDOOR TEMPERATURE

From June to August, the maximum simulated indoor temperature of the current typical room is 36.24°C. Horizontal shading and vertical shading reduce the maximum indoor temperature by about 2°C. Comparing the results of TAM-Horizontal logarithmic and without shading at 35°C, the diagram (Figure 9) shows that the highest temperature in red (room with shading) is clearly lighter than room without shading. Here the horizontal shading reduces indoor temperature by approximately 0.3°C more than the value of the vertical shading.

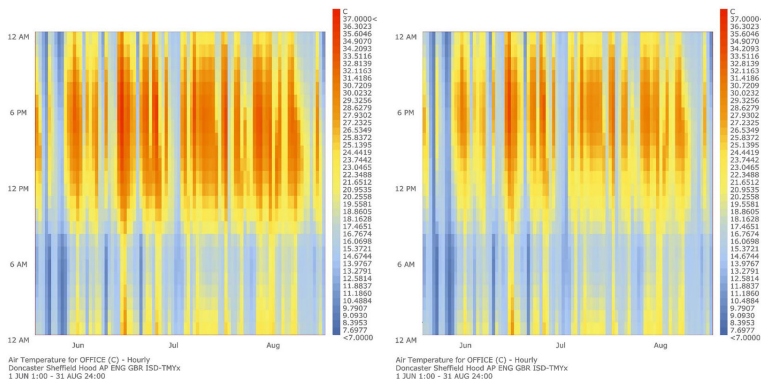


Figure 9. Simulation indoor temperatures of rooms without shading system and with horizontal shading system at 35°C of logarithmic mapping in June-August.



The maximum simulated indoor temperatures of room without shading in July and August were 34.96°C and 32.94°C respectively. Therefore, shading systems can be helpful to reduce indoor temperature in July and August; and the TAM-Horizontal linear and logarithmic methods produce greater effect on reducing indoor temperature in summer.

## 5. Conclusion and further work

To address the challenge of overheating in medium-large office buildings during summer months, we propose a parametrical modelling and simulation strategy for developing intelligent solar shading system design. Informed by an initial physical computing prototype modelling, we formulated a Temperature-Angle Mapping (TAM) concept for shading system design. The TAM concept was further developed into six methods and modelled parametrically. A typical office room of the Arts Tower at the University of Sheffield was selected as the test case site for implanting the TAM concept and methods. In conclusion, we show that the horizontal shading (TAM-Horizontal) with the linear mapping method appears optimal in terms of the total comfort hours obtained and cooling energy demand reduced.

Further work is required to verify the computational models of the adaptive shading system design through field measurement. The performance of fixed blinds (set once and forget) should be compared with the linear TAM horizontal mode, which is optimal, for a cost-benefit analysis of the adaptive system design. Also, the scope of the parametric modelling and simulation should be extended to include other factors such as lighting, relative humidity and occupants' behaviors which affect building users' comfort and work productivity leading to potential rebound effect. Future climate projection data should also be brought into the simulation to assess if the adaptive shading design is fit for the future.

## References

- "Servo Motor SG-90" : 2017. Available from <<https://components101.com/servo-motor-basic-s-pinout-datasheet>> (accessed 8th November 2019).
- "DHT11, DHT22 and AM2302 Sensors" : 2019. Available from <<https://learn.adafruit.com/dht>> (accessed 8th November 2019).
- "Honeybee" : 2019. Available from <<https://www.ladybug.tools/honeybee.html>> (accessed 5th July 2019).
- Crawley, D.B., Hand, J.W., Kummert, M. and Griffith, B.T.: 2008, Contrasting the capabilities of building energy performance simulation programs, *Building and Environment*, **43(4)**, 661-673.
- Manzan, M. and Clarich, A.: 2017, FAST energy and daylight optimization of an office with fixed and movable shading devices, *Building and Environment*, **113**, 175-184.
- W. Morris (ed.): 2018, *The American Heritage Dictionary of the English Language*, Houghton Mifflin Harcourt Publishing Company.
- Roudsari, M.S. and Pak, M.: 2013, Ladybug: a parametric environmental plugin for grasshopper to help designers create an environmentally-conscious design, *Proceedings of BS2013: 13th Conference of the International Building Performance Simulation Association*, Chambery, 3128-3135.

# RESEARCH ON COMMERCIAL SPACE VITALITY OF AIRPORT TERMINAL BASED ON 3D VISION FIELD SIMULATION OF PEDESTRIAN FLOWS

*Taking Guangzhou Baiyun International Airport Terminal 2 as a Study Case*

ZHICHAO MA<sup>1</sup>, YIQIANG XIAO<sup>2</sup> and XIONG CHEN<sup>3</sup>

<sup>1,2</sup>*South China University of Technology*

<sup>1</sup>*151010095@qq.com* <sup>2</sup>*yqxiao@scut.edu.cn*

<sup>3</sup>*Guangdong Architectural Design & Research Institute*

<sup>3</sup>*chgowy@163.com*

**Abstract.** In recent years, more and more large-scale terminal buildings have emerged. In the design and construction of the terminal, how to increase the non-aeronautical revenue of the terminal has become one of the difficulties and priorities. The commercial vitality is one of the important factors influencing non-aeronautical revenue of the terminal. There is a correlation between passenger flows and commercial space vitality. So it is necessary to analyze the impact of pedestrian flows on commercial space vitality. The commercial space vitality can be evaluated by the vision dwell time on the shop surfaces. This paper focused on the relationship between passenger flows and commercial space vitality at the terminal. We modeled and simulated the domestic mixed-flow hall of Baiyun airport terminal 2 in Massmotion. After the pedestrian 3D vision field simulation, Vision Time Maps were exported to assess the commercial space vitality. After comparing the survey results with simulation results, we can conclude that the mixing of multiple pedestrian flows can improve the commercial space vitality of the airport terminal.

**Keywords.** 3D vision field simulation; Airport terminal commercial space vitality; Guangzhou Baiyun International Airport Terminal 2; Pedestrian Flow.

## 1. Introduction

Airport terminal revenue generally consists of aeronautical revenue and non-aeronautical revenue. With the increase of population and economic development, the proportion of non-aeronautical revenue in terminal revenue is increasing rapidly (Graham, A, 2009). In the process of designing and constructing many new terminals, how to increase their non-aeronautical revenue has become one of the priorities. As an important factor that influences the non-aeronautical revenue of the airport terminal, the layout of the commercial space in the airport

terminal is also one of the main points when designing an airport terminal. On one hand, the commercial space design in the airport terminal should ensure the efficiency of passenger pedestrian flow; on the other hand, as the commercial space, it is necessary to increase its contact space and time with the passengers as much as possible. What people see when walking in the commercial area of the airport terminal has a direct impact on their shopping behavior, the commercial space vitality, the commercial planning, and the position of advertisements. By simulating passenger's dynamic three-dimensional vision field in the airport, passenger's vision focus and view time on surfaces can be obtained, which can be used to assess the commercial space vitality at the airport terminal.

This paper mainly studies how pedestrian flows influence the terminal commercial space vitality by pedestrian vision field simulation. We also proposed the application prospects of Massmotion in the pedestrian vision field simulation. The research is composed of 7 sections. The first section presents the background and significance of the research. In the second section, we describe the status quo of the researches on vision field simulation. The third section is focused on the research methods, including Massmotion simulation and the shop vitality survey. The fourth section shows the research area of Guangzhou Baiyun International Airport terminal 2. Before the results, the procedures of simulation model establishment are proposed. The main conclusion of this paper is that the mixing of multiple pedestrian flows can improve the commercial space vitality of the airport terminal.

## **2. Literature review: Pedestrian Vision Field Simulation**

In recent years, there has been more and more research on pedestrian vision field simulation in space cognition, sign design, and pedestrian pathfinding. In these studies, pedestrian vision field simulation is mainly divided into two types: two-dimensional pedestrian vision field simulation and three-dimensional pedestrian vision field simulation.

In terms of two-dimensional pedestrian sight simulation, the Space Syntax theory proposed by Hillier B is one of the mainstream researches (Hillier B, 1976). The visual analysis of Space Syntax theory has been widely used recently, including Visual Graph Analysis (VGA), Visual Fields Analysis, and Visual Integration (Al-Sayed K., 2014). Turner who studied Space Syntax for many years, applied Isovist Integration to the analysis of pedestrian flow in buildings and urban cities (Turner & Penn, 1999). On the basis of Isovist Integration, Turner further proposed the application of Visual Graph Analysis (VGA) to building space analysis and pedestrian vision simulation (Turner & Penn, 2001). In the subsequent research, many scholars used the VGA of Space Syntax to analyze two-dimensional pedestrian vision. For example, Othman, F presented Isovist and VGA could be applied to assess the visibility in urban space (Othman, F, 2019).

The visual analysis of Space Syntax has great advantages in two-dimensional space analysis. But it cannot obtain the three-dimensional vision focus and vision dwell time on surfaces during pedestrian walking. These contents are also significant for space design. Therefore, some researchers have proposed some

methods to make up for the shortcomings of Space Syntax. Psarras, S. combined the three-dimensional saliency with depth analysis of Space Syntax to model navigation behavior (Psarras, S., 2019).

In terms of 3D visual field simulation, the main researches were based on the model of view cone. Brandle N established a pedestrian vision field model by emitting N rays on the points of the pedestrian path (Brandle N, 2014). The value of the visibility was calculated as the amounts of rays intersecting with the surface in three-dimensional space. As defined in their vision model, the central field of view tangent to the pedestrian path was assigned a higher weight than the peripheral field of view. By this way, they illustrated that the central field of view was drawn more attention. JH Hwang, H Lee built a three-dimensional vision field model to study the privacy of Korean palace architecture by emitting rays from the observation point to the target interface on the Rhino 6 combined with Grasshopper (JH Hwang, 2017). Based on the research of JH Hwang, H Lee, Karoji G applied the model to simulate pedestrian flow in commercial spaces (Karoji G, 2019). Different from the previous view cone model, Brunnhuber, M. in his research considered the pedestrian field of view as an elliptical whose boundary was limited by the horizontal view angle  $\alpha$  and the vertical view angle  $\beta$  (Brunnhuber, 2019). In his research, this three-dimensional vision field model was applied to evaluate and improve the system of pedestrian vision guidance and signage in large buildings. By geometrically defining the view cone, Morrow proposed a pedestrian three-dimensional vision field simulation method based on Massmotion software (Morrow, 2014). This method based on the principle of the view cone calculated the time of each interface in the space viewed by pedestrian agents. In his paper, some experiments with the help of Massmotion software were conducted to test the approach to the simulation of agents' vision. This paper used Massmotion software to simulate the pedestrian vision field in the commercial space of the airport terminal based on the research of Morrow. This paper used Massmotion software to simulate the pedestrian vision field in the commercial space of the airport terminal based on the research of Morrow.

### **3. Methodology**

#### **3.1. SOFTWARE SIMULATION**

##### *3.1.1. Massmotion introduction*

The pedestrian flow simulation software used in this paper is Massmotion software. Massmotion is one of the most advanced software in simulating pedestrian movement and pedestrian behavior. It has been applied in many kinds of space including transportation architecture, commercial complex, and urban area. It can be used to research the crowd congestion, the crowd density, the capacity of the building, etc. Recently, more and more architectural design institutes have applied it to actual projects such as Beijing Daxing International Airport.

Massmotion is based on the social force model proposed by Helbing (Helbing, 1995). Compared with other social force model simulation software (Anylogic, SimWalk, etc.), Massmotion simulates the pedestrians' movement in real life

more accurately. Firstly, agents in Massmotion move toward their destination independently by observing the surrounding environment. Agents act according to the changes in the surrounding environment until they accomplish their tasks. Secondly, each agent's property can be defined to imitate passengers of the different traits (speed, age, size, etc.). Thirdly, users can assign different tasks to agents to simulate the pedestrians' behavior.

### 3.1.2. Software validation

Many scholars have verified the applicability of Massmotion software in the pedestrian movement. With a method of applying Massmotion software to the modeling and simulation of the Toronto Central Station and comparing the simulation results with the survey data, Morrow also verified the applicability of the software (Morrow, 2010). King D utilized Massmotion software to explore the impact of train arrival mode on pedestrian congestion. During his research, field survey data was collected to calibrate and verify the Massmotion simulation model (King D, 2013). Eric Riversa conducted evacuation drill observations on four buildings of different sizes, pedestrian numbers, and regional locations. Through the comparison of the results of the observation with those of Massmotion software simulation, the applicability of Massmotion software in pedestrian flow simulation on building exits was verified (Eric Riversa, 2014). Aucoin DR collected behavior data on two stadiums and verified their exit time under Massmotion's simulation model (Aucoin DR, 2014).

### 3.1.3. Principle of Massmotion 3D vision field simulation

As is shown in figure 1, a definition of pedestrian view cone was proposed by Morrow and was verified through his experiments by means of Massmotion software (Morrow, 2014). Agents in Massmotion have a certain range of vision field. They can observe their surroundings and other agents while walking. Simultaneously, the pedestrian's vision field range and view distance can be set up before the simulation. In Massmotion software, the selected objects can be computed through Vision Time Map. The value of vision time in Massmotion is time multiplied by the number of agents. That is to say, a vision time of 3 seconds may be produced by one agent looking at the surface for 3 seconds or three agents looking at the surface for 1 second. Vision Time Map shows the vision focus of agents in a 3D environment during their movements.

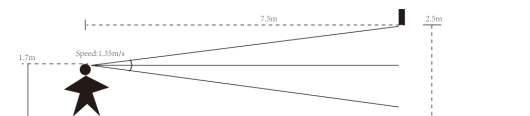


Figure 1. View cone model proposed by Morrow, E.

### 3.2. SITE INVESTIGATION AND DATA COLLECTION

Site investigations from 10:00 to 20:00 were conducted at the airport terminal on Thursday and Saturday of two weeks. The site investigations included the video data collecting and the shop vitality survey. Some videos were recorded by the camera to calculate the walking speed of passengers. And we counted the number of passengers entering each shop at one-hour intervals. The average number of passengers in a shopper day was used to assess the vitality of a shop.

### 4. Case study: Baiyun International Airport Terminal 2

We have selected the Baiyun International Airport Terminal 2 which was put into use in 2018 as the object of simulation in the research. The focus area of the research was the commercial space of the domestic mixed-flow hall on the second floor of the airport terminal. The following are the reasons why we chose this commercial space as the research area.

Firstly, in the process of designing Terminal 2, commercial space was one of the key considerations compared to Terminal 1. The designers intended to build the Terminal 2 into a non-traditional commercial complex to improve the terminal's non-aeronautical income.

Secondly, in order to expand the contact surface between commercial space and passengers, the commercial space of the domestic mixed-flow area was integrated with pedestrian flow. As shown in figure 2, there are several kinds of passenger flows (domestic departure flow, domestic arrival flow, and transfer flow) in the domestic mixed-flow hall. The mixing of multiple passenger flows in the domestic area is one of the highlights of the airport terminal.

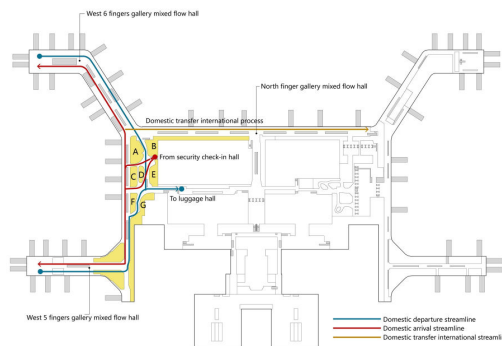


Figure 2. The research area and three kinds of pedestrian flows.

### 5. Simulation modeling

This section expounds the process of modeling the Terminal 2 of Baiyun International Airport in Guangzhou. The process of constructing the simulation model includes three parts: the establishment of a three-dimensional model in

Rhinoceros 6.0, the establishment of passenger activities, setting the value of related parameters.

### 5.1. ESTABLISHMENT OF THREE-DIMENSIONAL MODEL

In this paper, a three-dimensional model established by Rhinoceros 6.0 was imported into Massmotion software for analysis through the IFC file format. Massmotion's simulation scenes are mainly composed of barriers, floors, stairs, activities, links, agents, service facilities, and other elements. After the model is imported into Massmotion, we set the walls, pillars, and railings as barriers, and the stairs and the floor corresponded to the elements in Massmotion. Figure 3 shows the final three-dimensional model in Massmotion.

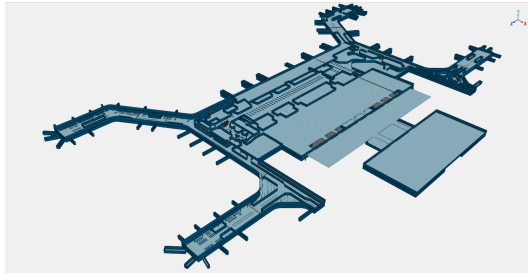


Figure 3. The Massmotion model of Guangzhou Baiyun International Airport Terminal 2.

### 5.2. ACTIVITY

In Massmotion, there are various activities such as Journey, Circulation, Vehicle, Evacuate, etc., which are used to simulate such actual events in real life. Vehicle can be used to simulate the departure or arrival of the passenger flow through the subway, airport flight, bus, etc. Therefore, we selected the Vehicle as an activity of simulation in this paper.

### 5.3. SETTING OF RELATED PARAMETERS

#### 5.3.1. Simulation period

In this paper, we set a passenger flow peak hour between 11:00 and 12:00 at Baiyun International Airport Terminal 2 as the simulation period.

#### 5.3.2. The number of agents simulated

According to the *Feasibility Study Report of Guangzhou Baiyun Airport Terminal 2*, the domestic departure number of passengers at a peak hour of Guangzhou Baiyun International Airport Terminal 2 is 8,949, including 2130 transit passengers. The domestic arrival number of passengers at a peak hour was 6,119. In the simulation, we respectively set the number of agents in three situations as 6819, 2130, and 6119.

5.3.3. Pedestrian walking speed

Werberich, B. R who illustrated a pedestrians’ route choice model for shopping behavior, applied the software Track to compute pedestrians’ data (Werberich, B. R, 2014). The pedestrian walking speed was calculated to 1.38m / s according to the video recorded at the airport terminal with the application of Track software. Therefore, the speed of agents was set to 1.38m/s in the simulation.

5.3.4. Pedestrian 3D vision field parameters

In Massmotion, it is possible to set the 3D vision field parameters of pedestrians, including the vision cone angle and the view distance. In this study, the view distance was set to 20 meters, and the vision cone angle was set to 30 degrees.

6. Results

6.1. PEDESTRIAN 3D VISION FIELD SIMULATION RESULTS

Three kinds of passenger flows (domestic arrival, domestic departure, and transfer) in the commercial area of the domestic mixed hall were simulated. We exported the Vision Time Map and analyzed the pedestrian 3D vision field in three kinds of passenger flows. The color corresponding to the value range of the vision time is shown in table 1:

Table 1. The value range corresponding to colors.

Color	Value range (s)
white	-∞-0
light yellow	0-10
brown yellow	10-20
bright yellow	20-40
light orange	40-80
bright orange	80-160
dark orange	160-320
red	320-∞+

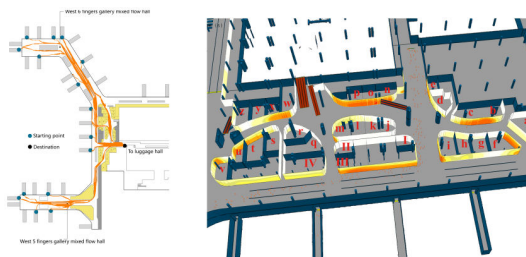


Figure 4. The domestic arrival flows map (left) and Vision Time Map of the domestic arrival flows (right).



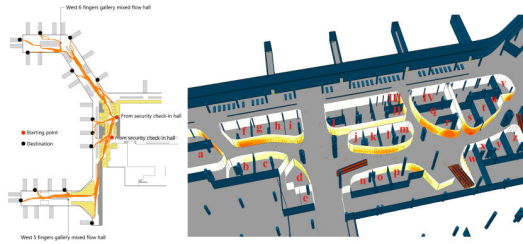


Figure 5. The domestic departure flows map (left) and Vision Time Map of the domestic departure flows (right).

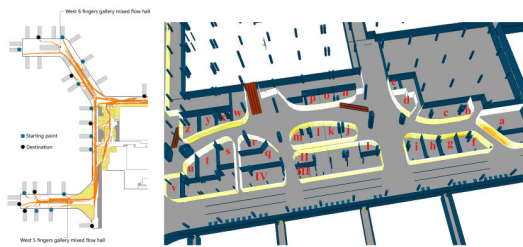


Figure 6. The transfer flows map (left) and Vision Time Map of the transfer flows (right).

By comparing with the 3 Vision Time Maps, we found that the view of agents when walking was more easily focused on the entrance and exit of commercial spaces. The corners between the shops were more likely to be viewed by agents for longer time, such as the corners of shop f, shop i, shop p, shop s. As was shown in figure 4, 6, there were three vision focuses of agents with the same location which was respectively on the surfaces of shop f, shop g, shop w. In figure 5, 6, three vision focuses with the same location remained respectively on the surface of shop a, shop f, and shop g. Little vision dwell time of agents in domestic departure flow was focused on shop b, n, o, w, x, where their vision dwell time in the domestic arrival flow was the longest. Compared with figure 4 and figure 5, there were obvious changes in the vision dwell time of shop j, k, l. Based on the changes in the vision dwell time on shops, it was illustrated that different flows had complementary effects on the visual focus of agents.

## 6.2. COMPARISON OF SIMULATION RESULTS AND SURVEY RESULTS

We compared the simulation results with the survey results in figure 7. In the simulation results, the shops with the highest vision time (above 160s) were: a, b, c, e, f, n, o, p, r, s, v, w. shops with low vision time (under 80s) were: h, j, y, z, A, B, D. By comparing with the survey results, we found that most of the shops with the highest vision time (shop a, b, c, e, f, n, p, r, v) had a higher average daily customer volume. The shops with the low vision time (shop h, j, y, z, A, B, D) had a lower average daily customer volume. Most shops with high commercial vitality had high vision time. That is to say, Massmotion's 3D vision field simulation can

predict the vitality of the terminal's commercial space well.



Figure 7. Comparison of vision focuses simulation results (left) with the commercial space vitality survey results (right).

## 7. Conclusion

We used Massmotion to simulate three kinds of passenger flows in the domestic mixed-flow hall of Guangzhou Baiyun International Airport Terminal 2. Through the comparison of the simulation results and survey results, we concluded that Massmotion's 3D vision field simulation of pedestrian flow has certain application prospects in airport commercial space organization, passenger flow arrangement, and space optimization of the terminal. Furthermore, compared with single pedestrian flows, the mixing of multiple pedestrian flows can improve the commercial space vitality of the airport terminal.

### 7.1. CONTRIBUTION

By using Massmotion, we proposed a dynamic 3D view simulation method based on pedestrian motion. In the process of design, human behavior and 3D view are often easily overlooked. This research can make up for the deficiencies in this area. Besides, this simulation method makes it possible for designers to analyze and test the three-dimensional building space layout, which provide strong support for seeking the optimal building space layout. At the same time, this research can also be combined with the POE (Post-Occupancy Evaluation) to evaluate and verify the space layout of the built environment, signage system, evacuation efficiency, etc.

### 7.2. APPLICATION

This research can be applied to the airport terminal design process and provide a reference for airport terminal design and expansion. In addition to evaluating and optimizing the commercial space in the terminal, this study can also be more broadly used to predict the privacy of the terminal space (e.g., nursery room,

medical rooms, offices, etc.), thereby assisting designers to optimize the functional layout of the airport terminal. The pedestrian dynamic 3D view simulation method proposed in this paper can also be beneficial to other types of architecture design, such as museums and hospitals. Vision focus of the pedestrian can be simulated by Massmotion, which will be a great use in the advertisement or signage placement.

## References

- Aucoin, D. R.: 2019, *The Use of Human Behaviour to Inform Egress Modeling in Stadiums*, Master's Thesis, York University.
- Brandle, N., Matyus, T., Brunnhuber, M., Hesina, G., Neuschmied, H. and Rosner, M.: 2009, Realistic interactive pedestrian simulation and visualization for virtual 3D environments, *15th International Conference on Virtual Systems and Multimedia*, 179-184.
- Brunnhuber, M., Schrom-Feiertag, H., Luksch, C., Matyus, T. and Hesina, G.: 2012, Bridging the gap between visual exploration and agent-based pedestrian simulation in a virtual environment, *the 18th ACM symposium on Virtual reality software and technology*, 9-16.
- Graham, A.: 2009, How important are commercial revenues to today's airports?, *Journal of Air Transport Management*, **15(3)**, 106-111.
- Helbing, D. and Molnár, P.: 1995, Social force model for pedestrian dynamics, *Physical Review E*, **51(5)**, 4282-4286.
- Hillier, B., Stansall, P. and Bedford, M.: 1976, Space syntax, *Environment and Planning B: Planning and design*, **3(2)**, 147-185.
- Hwang, J. H. and Lee, H.: 2017, 3D Visual Simulation and Numerical Measurement of Privacy in Traditional Korean Palace, *CAADRIA2017*.
- Karoji, G., Hotta, A. and Ikeda, Y.: 2019, Pedestrian Dynamic Behaviour Modeling-An application to commercial environment using RNN framework, *CAADRIA2019*.
- King, D., Srikukenthiran, S. and Shalaby, A.: 2013, Using Massmotion to Analyze Crowd Congestion and Mitigation Measures at Interchange Subway Stations: Case Of Bloor-Yonge Station in Toronto., *In Annual Meeting of the Transportation Research Board*, Toront: ARUP.
- Morrow, E.: 2010, MassMotion: simulating human behaviour to inform design for optimal performance, *The Arup Journal*, **1(45)**, 38-41.
- Morrow, E., Mackenzie, I., Nema, G. and Park, D.: 2014, Evaluating three dimensional vision fields in pedestrian micro-simulations., *Transportation Research Procedia*, **2**, 436-441.
- Othman, F., Yusoff, Z. M. and Rasam, A. A.: 2019, Isovist and Visibility Graph Analysis (VGA): Strategies to evaluate visibility along movement pattern for safe space., *In IOP Conference Series: Earth and Environmental Science*, 012-024.
- Psarras, S., Zarkali, A. and Hanna, S.: 2019, Visual Saliency in Navigation: Modelling Navigational Behaviour using Saliency and Depth Analysis., *International Space Syntax Symposium 2019*.
- Rivers, E., Jaynes, C. and Morrow, E.: 2014, Using case study data to validate 3D agent-based pedestrian simulation tool for building egress modeling, *Transportation Research Procedia*, **2**, 123-131.
- Turner, A., Doxa, M., O, D. and Penn, A.: 2001, From isovists to visibility graphs: a methodology for the analysis of architectural space, *Environment and Planning B: Planning and design*, **28(1)**, 103-121.
- Turner, A. and Penn, A.: 1999, Making isovists syntactic: isovist integration analysis, *In 2nd International Symposium on Space Syntax*, Brasilia.
- Werberich, B. R., Pretto, C. O. and Cybis, H. B. B.: 2016, Pedestrians' Route Choice Model for Shopping Behavior, *In ATT@IJCAI*.

# CREATIVITY INSPIRED BY ANALYSIS

*An algorithmic design system for designing structurally feasible façades*

INÊS CAETANO<sup>1</sup>, SARA GARCIA<sup>2</sup>, INÊS PEREIRA<sup>3</sup> and  
ANTÓNIO LEITÃO<sup>4</sup>

<sup>1,3,4</sup>*INESC-ID, Instituto Superior Técnico, Universidade de Lisboa*

<sup>1,3,4</sup>{*ines.caetano|ines.pereira|*

*antonio.menezes.leitao*}@*tecnico.ulisboa.pt*

<sup>2</sup>*INESC-ID*

<sup>2</sup>*sara.garcia@inesc-id.pt*

**Abstract.** Although structural performance has a crucial role in the overall design, its analysis is often postponed to later design stages. This largely occurs because analysis processes are time consuming and require the use of specific models and tools. This problem is then aggravated by the number of design variations that have to be analysed until an acceptable solution is found. However, the implementation of design changes at later stages is limited, as also is their impact on the solution's final performance. Fortunately, with algorithmic design, we can overcome these limitations, as it not only supports complex designs and facilitates design changes, but also automates the production of the specific models and their subsequent analysis and optimization. In this research we focus on buildings façades, proposing an algorithmic design system to support their design, structural analysis, and optimization.

**Keywords.** Performance-based Design; Algorithmic Design; Algorithmic Structural Analysis; Algorithmic Optimization; Façade Design.

## 1. Introduction

The architectural façade can be regarded as the building's skin as it separates the exterior from the interior spaces. Therefore, its design needs to consider several criteria, such as aesthetic, functional, structural, lighting, thermal, acoustic, and energetic. Of these requirements, structural performance plays a key role in ensuring the façade's feasibility and physical integrity, resisting to gravity, snow, wind, and seismic loads, among others. Unfortunately, only a few requirements are considered at early design stages, namely functional and aesthetical ones, being the others, including structural performance, typically postponed to later stages (Turrin et al. 2011), when the form is already delineated. This scenario largely results from the need to create specialized versions of the Design Model (DM), called the Analytical Model (AM), suiting each analysis tool; a process

that is not only time consuming, but also frequently inefficient, often involving redundant remodeling (Kolarevic 2003), and highly prone to information loss and the introduction of errors (Moon et al. 2011). To make the situation worse, this process has to be repeated every time the design changes. As a result, in practice, it is the engineers who make the AMs and, depending on the analysis results, suggest the architects the changes to the DMs. However, this back-and-forth process becomes potentially tiresome and may have costly impacts in the final design, as these changes get significantly expensive at latter stages (Anton and TĀnase 2016).

These limitations can be overcome by combining Algorithmic Design (AD) with analysis and optimization. AD uses algorithms to create and explore designs, supporting complex geometries, facilitating design changes, and automating repetitive tasks (Terzidis 2006). AD can automate the generation of AMs (Aguiar et al. 2017) by automatically repeating the analysis setup whenever a change is made to the design, while generating only the information required by the analysis tool. With AD, designers can integrate design analysis from early design stages and, thus, be aware of the design's performance, understand the impact of changes, and make more informed decisions. Moreover, at early stages, it is easier to incorporate the necessary changes to improve the design performance, allowing massive optimizations by simply making small design adjustments (Kolarevic 2003). On the other hand, AD and analysis can be coupled with optimization processes, a particularly useful combination when dealing with broad design spaces where manually analyzing all the design options becomes an unviable task. This approach follows performance-based design principles (Kolarevic 2003), in which, by considering performance criteria from early design stages, analysis is no longer a way of providing feedback, but a way of guiding the design process (Mueller 2014).

In this paper, we propose an AD System (ADS) for façade design, analysis, and optimization. The ADS contains several design strategies and algorithms suitable for multiple design scenarios and is coupled to different design and analysis tools, including a structural one. Moreover, the ADS can automatically produce with the same algorithm the DM and its corresponding AM, containing only the information needed for each specific analysis, updating both whenever the algorithm is changed. We evaluate the ADS in the design exploration, analysis, and optimization of a case study, a metal truss-like façade with glass panels. To this end, we use the AD tool *Khepri* and we take advantage of its portability between multiple design and analysis tools, in this case, between *AutoCAD* and *Robot*. The ADS presents the obtained results numerically and graphically, revealing the impact of changes in both the behavior and weight of the structure. In the end, the case study proves the ADS ability to produce and analyze different design variations, and to perform optimization processes by considering goals like structural performance and cost reduction, as in this case.

## 2. Related Work

### 2.1. STRUCTURAL ANALYSIS TOOLS

There are several analysis tools that simulate the behavior of a design in a real-world environment, while considering different criteria. Compared to manual analysis processes, these tools allow the automation of extensive calculations, speeding-up and improving the accuracy of performance evaluations. Also, these tools present the analysis results visually, making their understanding easier for designers, which therefore promotes a more conscientious qualitative appreciation of the results (Kolarevic 2003). Moreover, they also allow the analysis of buildings with more complex shapes, whose design and construction would be too laborious or even impossible with traditional methods (Mitchell 1998). Regarding structural analysis, we can find tools like *Robot*, *Tekla Structures*, *SAP2000*, *ETABS*, and *GSA Analysis*. A comparative study of these tools can be found in (Aguiar 2018).

However, analysis tools are not yet well-correlated with modeling tools, not only having a limited modeling capacity, but also requiring the introduction of extra set-up information, like materials and applied forces (Lee et al. 2015), which makes their use less suitable for conceptual design stages. Moreover, AMs often lack parametric features, which results in costly design changes and in the redoing of the analysis setup.

We can overcome these drawbacks by combining AD and structural analysis tools. *Karamba* (a structural analysis plugin for *Grasshopper*), *Geometry Gym* (a plugin to connect *Karamba* with *Robot*), and *GH2Robot* (a plugin to export *Grasshopper* models to *Robot*) are examples of such combination. Unfortunately, these tools do not easily automate the analysis setup, therefore hardly supporting multiple analyses (Aguiar 2018). Another drawback results from the scalability issues of the visual programming language used, i.e., *Grasshopper* (Leitão and Santos 2011), which hinders the analysis of more complex designs.

Textual programming languages (TPLs) do not suffer from scalability issues and are more flexible regarding the automation of different tasks. In this paper, we use the AD tool *Khepri*, which uses a TPL and is capable of generating, from the same algorithm, equivalent models in CAD and BIM tools. Moreover, it can also generate different AMs suiting the requirements of the supported analysis tools. As a result, it more easily handles the automation of single- and multiple-analysis processes, returning the results either graphically, in a modeling tool, or numerically, in a spreadsheet. Finally, *Khepri* can take advantage of the many optimization libraries that are available (Leitão et al. 2018), making it possible to automatically optimize designs according to multiple criteria. Differently from other well-established tools, *Khepri* is still being developed but it already supports all the features needed for the presented research.

### 2.2. FAÇADE STRUCTURAL ANALYSIS

AD and structural analysis are being increasingly applied in façades, whether they have visible structural elements (e.g., the diagrids systems of the *Hearst Tower* by Norman Foster and the *Morpheus Hotel* by Zaha Hadid), or not (e.g., the *Museu Soumaya* by FR-EE and the *Water Cube* by PTW Architects). We can find several

studies on this topic, namely the design curvature analysis of the *Museu Soumaya* (Sidelko 2013), the energy efficiency analysis of the *Institut du Monde Arabe* (Martinho et al. 2019), and the lighting analysis of the *Astana National Library* (Leitão et al. 2017). Regarding structural algorithmic analysis of façades, recent researches evidence the advantages of this approach, although not fully automating the analysis process: in the *Beijing Greenland Center*, even though the analysis and optimization processes of the origami façade used *Grasshopper* and *ANSYS* to produce a façade using 10% less material, these tools were used independently (Schultz and Katz 2018); Herr et al. (2018) used the *Grasshopper*'s plugin *Millipede* to algorithmically analyze the wool thread-inspired façade, however, they confirmed the results separately using *Oasis GSA Suite*.

### 3. Methodology

#### 3.1. WORKFLOW

The proposed ADS follows the workflow of Figure 1, which comprises the following steps: the designer develops an algorithm (A1), obtaining a design space (A2); this algorithm can generate designs in both CAD/BIM tools (B1), providing visual feedback to the designer (B2), or in an analysis tool to be automatically evaluated (C1). The analysis results can be returned by the algorithm (C2) and/or displayed in the modeling tool (C3), as well as used for optimization processes (D1), which require the production of multiple design variations (D2) to achieve an optimized design space (D3). Finally, the architect is presented with the set of acceptable design solutions, from which he then chooses the final design solution (E). To test this workflow, we develop a case study using the AD tool *Khepri*, the modeling tool *AutoCAD*, and the structural analysis tool *Robot*.

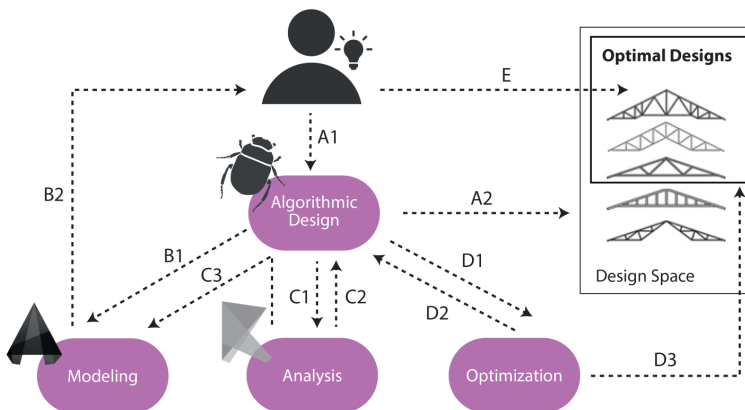


Figure 1. Workflow diagram: the designer creates an algorithm using *Khepri* (A1) and obtains a design space (A2); the designer uses *AutoCAD* (B1) to obtain visual feedback (B2) and *Robot* (C1) to analyze the design, receiving the results algorithmically (C2) and/or visually in the modeling tool (C3); to optimize the design (D1), the designer automates several analyses (D2), achieving a set of optimal solutions (D3) from which he then selects the final one (E).

### 3.2. CASE STUDY

The case study is the headquarters of the company *Channoine Cosmetics AG*, located in Vaduz, Liechtenstein, which was designed by Matthias Müller and engineered by Roschmann GMBH in 2009. The three-story building is about 15 meters high and has a rectangular cuboid shape. It has a double-skin façade, being the inner layer composed of aluminum and triple-glazed glass windows, and the outer layer made of a truss-like structure composed of stainless steel T-profiles and single-glazed glass panels. The truss-like structure forms asymmetrical rectangular pyramids, which have three of the four triangular faces subdivided (Figure 2). The heating and ventilation of the intermediate space between the layers helps the façade to be energy efficient.

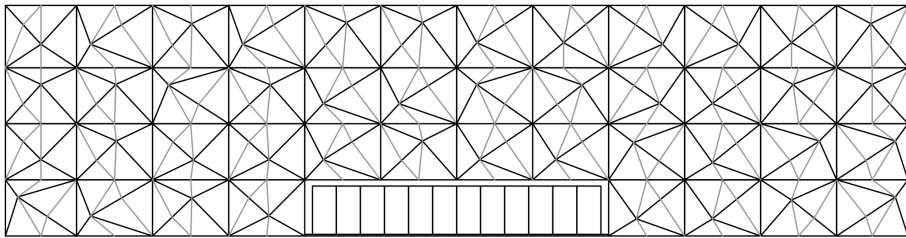


Figure 2. Front elevation (west façade) of the headquarters of Channoine Cosmetics AG (in grey: pyramid's subdivisions).

### 4. Evaluation

For the evaluation phase, we used the ADS to produce an AD model incorporating both the geometric and structural information of the case study, namely the buildings' overall dimensions, the floors' height, the material, height, and section radius of the truss pyramids, as well as the number of their subdivisions.

The use of structural analysis at early design stages allows the architect to be informed about the tendency his design has to deform under certain loads. We state that having a high degree of precision at these stages is not critical, as the design is still under development with many of its parameters ill-defined; a higher accuracy degree can be easily defined by engineers in latter stages of the design process. Therefore, we selected default materials (e.g., steel) and profiles (e.g., round) for the structural analysis of our case study.

Our ADS frees the designer from ensuring that the information described in the algorithm matches the requirements of both the design and analysis tools: while the geometrical model uses cylinders and spheres to represent the truss, the structural model uses a graph containing only the truss edges and vertices. Moreover, beyond geometric information, the ADS also adds to the algorithm the necessary data to setup the analysis, namely material properties, applied loads, and type of supports (fixed or non-fixed nodes). We applied two kinds of loads to each truss node, namely gravitational loads acting vertically, which are automatically calculated from the structure's self-weight, and wind loads acting horizontally.



Then, we produced several design variations of the case study and we analyzed their structural performance under identical loads. In this paper, we present eight of the examples explored using the ADS: the original truss structure with and without panel subdivisions (Designs A and B); the same truss structure but with bigger pyramids either randomly ranging their height from 1 to 4 times the original value (Design C) or doubling the size of their base (Design D); the truss with fixed-nodes only in its outer frame (Design E), with truss bars of smaller sections (Design F), with increased loads (Design G), and with a different material (Design H).

These variations resulted in design solutions with different amounts of material and therefore different weight and costs (e.g. Designs B and F), levels of natural daylight (e.g. Designs B and D), appearances (e.g. Designs C and H), and functional spaces (e.g. a double-height story in Design D, and a tall atrium in Design E). Figure 3 shows the Designs A, D, and H.

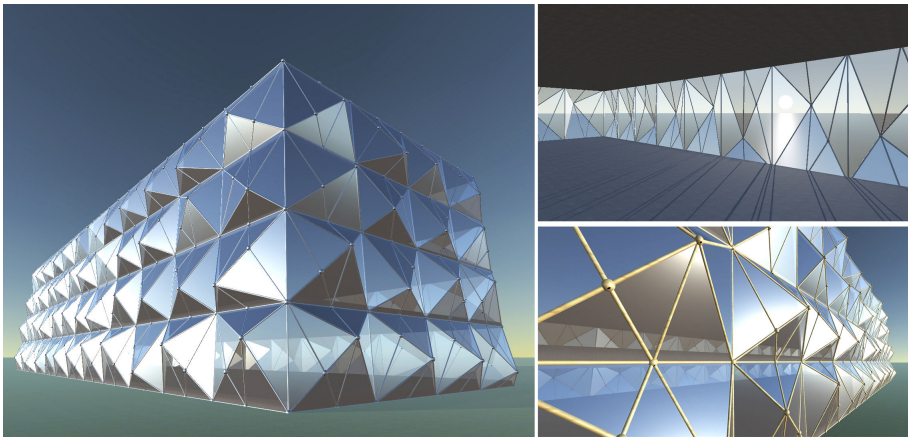


Figure 3. Renders of Design A (left), Design D (top right) and Design H (bottom right).

## 5. Results

The ADS presents the structural analysis results in two ways: (1) qualitative results, showing both the original and deflected structures in the CAD tool (Figure 4), and (2) quantitative results, returning the structure displacement and other structure-related information, including the bars' total weight (Table 1).

The analyses showed that the original truss structure (Design A) had little deformation, however, the solution without panels subdivisions (Design B) proved to improve the truss structural performance. Design C also revealed slight structural improvements, although the structure weight has also increased. Design D showed a slightly bigger structure deformation but a smaller weight. Design E evidenced a clear higher buckling, probably resulting from the removal of fixed supports, a scenario that was heavily aggravated with Design F. In Design G, the applied loads and, consequently, the structure's displacement doubled, but the solution with the worst structural performance was Design H, which used bamboo

as material and truss bars with an increased section.

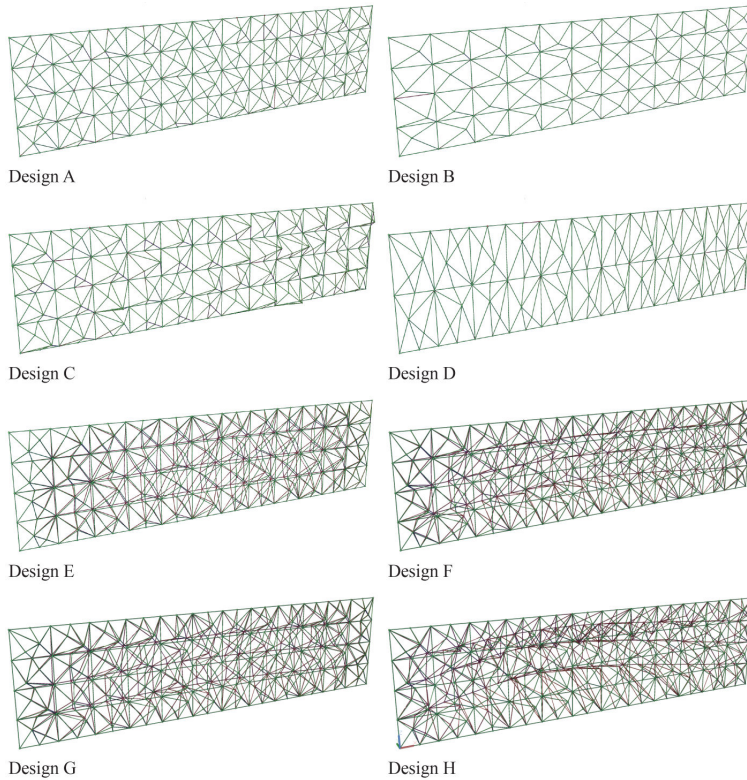


Figure 4. Designs A-H maximum displacement (in green: the original structure; in red: the deflected structure).

Table 1. Maximum displacement and bar weight of Designs A-H.

Design	Variation	Max. Displacement (m)	Max. Displacement (relative)	Bar Weight (Kg)	Bar Weight (relative)
A	Original case study	0.0017	0	4366	0
B	Remove subdivision elements	0.0005	-0.0012	3130	-1236
C	Pyramid's height [1.00,4.00]	0.0012	-0.0005	5125	+759
D	Double the floor's height	0.0068	+0.0051	3338	-1028
E	Remove inner fixed nodes	1.6633	+1.6616	4366	0
F	Halve the section radius in E	6.6975	+6.6958	1091	-3275
G	Double the load in E	3.3262	+3.3245	4366	0
H	Switch steel to bamboo in E	15.1506	+15.1489	4702	+336

To get a better perception of the deflection effects on the structure analyzed, the ADS provides the architect an animation of the structure displacement evolution

by gradually increasing the applied loads: Figure 5 shows three animation frames of the structural analysis of Design E, with the loads increasing from 0 to 200%.

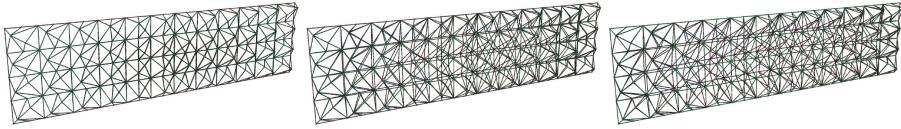


Figure 5. Three animation frames of the analysis of Design E, increasing the load from 0 to 200% (in green: the original structure; in red: the deflected structure).

We used the ADS to automate the structural analysis process and considered two goals: reduce both the structure displacement and cost, while experimenting four different materials (from M0 to M3). From the optimization algorithms available in *Khepri*, we selected the NSGA-II because it is commonly used in architectural problems, showing promising results (Belém and Leitão 2019). Figure 6 shows the Pareto front (i.e., the set of optimal solutions representing the trade-offs between the objectives) resulting from this optimization and three optimal designs, whose quantitative results are displayed in Table 2. Compared to the original truss, the results show that, to significantly improve the solution's structural performance, we need to select a more expensive material. Still, based on the Pareto front solutions, we can choose solutions in which the structural performance is slightly lower but have a much more acceptable cost. Note that, while in the previous analyses the parameters were set manually by the designer; with the ADS, they were automatically found by the optimization algorithm.

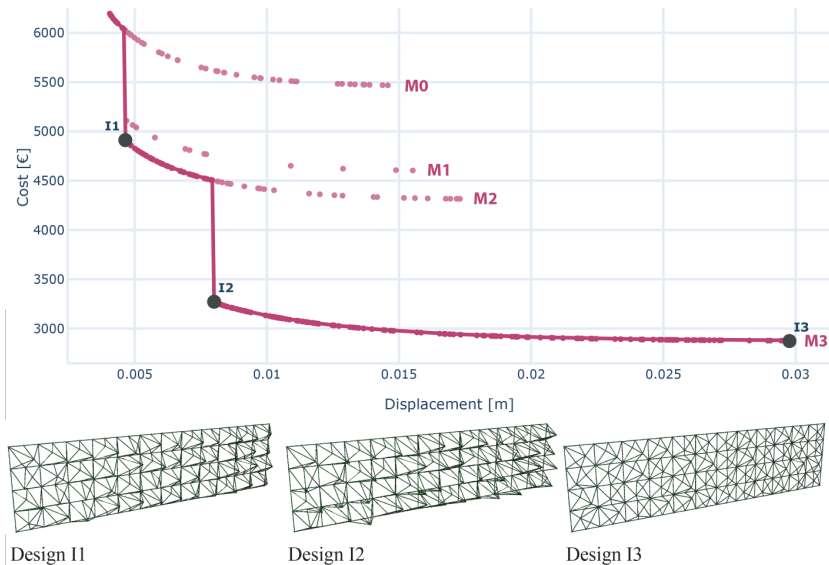


Figure 6. Optimization of Design I: Pareto front (above) and three optimal designs (below).

Table 2. Maximum displacement and bar weight of Designs I1-I3.

Design	Variation	Max. Displacement (m)	Max. Displacement (relative)	Bar Weight (Kg)	Bar Weight (relative)
I1	Pyramid's height 5.97, M2	0.0047	+0.0030	7700	+3334
I2	Pyramid's height 5.94, M3	0.0080	+0.0063	7676	+3310
I3	Pyramid's height 0.30, M3	0.0298	+0.0281	4183	-183

## 6. Conclusion

In this paper, we presented an Algorithmic Design System (ADS) for façade design, analysis, and optimization, and we focused on structural performance. The ADS allows the incorporation of structural analysis at early design stages, where changes in the design are easier, faster, and cheaper. Moreover, it allows architects to be more aware of how physical objects react to forces, promoting more informed design decisions, as well as to consider more unconventional designs that may have a good structural performance.

We evaluated the ADS with *Khepri*, an AD tool that, using the same algorithm, generates both geometric and analytical models, in the development of a case study: a pyramidal truss structure façade. We applied several design variations to the original truss by considering different criteria, namely structural, functional, and aesthetic. The analyses results considered for the evaluation were the structure displacement and weight, and these were presented numerically in a spreadsheet and visually in the design tool. The results revealed there is no single best solution but a set of solutions with the best trade-offs between architectural and structural requirements. In the end, this case study proved the suitability of the ADS to assist the designer with both the creative and design analysis processes.

For future work, we plan to improve the way results are presented to the architect, which includes (1) displaying the deflected structure using a color scale, (2) showing the maximum and minimum Von Mises stresses to inform the architect whether or not the structure surpasses the maximum allowable value, and (3) providing a recommender system to guide the designer with the selection of the parameters to change in order to improve the solution's performance. Also, we plan to extend the ADS with more types of structural analysis, e.g., seismic evaluation, as well as to include other kinds of structures and shapes.

## Acknowledgements

This work was supported by national funds through FCT, *Fundação para a Ciência e a Tecnologia*, under project UIDB/50021/2020 and PTDC/ART-DAQ/31061/2017, and by the PhD grant under contract of FCT with reference SFRH/BD/128628/2017.

## References

Aguiar, R.: 2018, *Integrating Structural Performance in Algorithmic Design*, Master's Thesis, Instituto Superior Técnico, University of Lisbon.

- Aguiar, R., Cardoso, C. and Leitão, A.: 2017, Algorithmic Design and Analysis Fusing Disciplines, *Disciplines & Disruption: Proceedings of the 37th ACADIA Conference*, MIT, Cambridge, Massachusetts, USA, 28-37.
- Anton, I. and Tănase, D.: 2016, Informed Geometries. Parametric Modelling and Energy Analysis in Early Stages of Design, *Energy Procedia*, **85**, 9-16.
- Belém, C. and Leitão, A.: 2019, Conflicting Goals in Architecture: A Study on Multi-Objective Optimisation, *Intelligent & Informed: Proceedings of the 24th CAADRIA Conference*, Victoria University of Wellington, New Zealand, 453-462.
- Herr, C.M., Lombardi, D. and Galobardes, I.: 2018, Parametric Design of Sculptural Fibre Reinforced Concrete Facade Components, *Learning, Adapting and Prototyping: Proceedings of the 23rd CAADRIA Conference*, Tsinghua University, Beijing, China, 319-328.
- Kolarevic, B.: 2003, Computing the Performative in Architecture, *Digital Design: 21th eCAADe Conference Proceedings*, 457-464.
- Lee, J., Fivet, C. and Mueller, C.: 2015, Modelling with Forces: Grammar-Based Graphic Statics for Diverse Architectural Structures, in M.R. Thomsen, M. Tamke, C. Gengnagel, B. Faircloth and F. Scheurer (eds.), *Modelling Behaviour*, Springer, Cham, Heidelberg, New York, Dordrecht, London, 491-504.
- Leitão, A., Castelo-Branco, R. and Cardoso, C.: 2017, Algorithmic-Based Analysis: Design and Analysis in a Multi Back-End Generative Tool, *Protocols, Flows and Glitches: Proceedings of the 22nd CAADRIA Conference*, Suzhou, China, 137-147.
- Leitão, A. and Santos, L.: 2011, Programming Languages for Generative Design: Visual or Textual?, *Respecting Fragile Places: Proceedings of the 29th eCAADe Conference*, University of Ljubljana, Slovenia, 549-557.
- Leitão, A., Sousa, S. and Loio, F.: 2018, SafePath: An Agent-Based Framework to Simulate Crowd Behaviors, *Computing for a Better Tomorrow: Proceedings of the 36th eCAADe Conference*, Lodz, Poland, 621-628.
- Martinho, H., Belém, C., Leitão, A., Loonen, R. and Gomes, M.G.: 2019, Algorithmic Design and Performance Analysis of Adaptive Façades, *Intelligent & Informed: Proceedings of the 24th CAADRIA Conference*, Victoria University of Wellington, New Zealand, 685-694.
- Mitchell, W.J.: 1998, Articulate Design of Free-Form Structures, *Artificial Intelligence in Structural Engineering*, **1454**, 223-234.
- Moon, H.J., Choi, M.S., Kim, S.K. and Ryu, S.H.: 2011, Case studies for the evaluation of interoperability between a BIM based architectural model and building performance analysis programs, *Proceedings of Building Simulation 2011: 12th Conference of International Building Performance Simulation Association*, Sydney, 1521-1526.
- Mueller, C.: 2014, *Computational Exploration of the Structural Design Space*, Ph.D. Thesis, Massachusetts Institute of Technology.
- Schultz, J. and Katz, N.: 2018, Origami-Inspired Facade Design: Parametric Studies for Architectural and Structural Efficiency, *Facade Tectonics 2018 World Congress*, Los Angeles, CA.
- Sidelko, J.: 2013, *Museo Soumaya: Facade Design to Fabrication*, Lulu.com.
- Terzidis, K.: 2006, *Algorithmic Architecture*, Architectural Press, Oxford, UK; Burlington, USA.
- Turrin, M., von Buelow, P. and Stouffs, R.: 2011, Design explorations of performance driven geometry in architectural design using parametric modeling and genetic algorithms, *Advanced Engineering Informatics*, **25**, 656-675.

# REPRESENTATION OF SOUND IN 3D

LI-MIN TSENG<sup>1</sup> and JUNE-HAO HOU<sup>2</sup>

<sup>1,2</sup>*National Chiao Tung University*

<sup>1,2</sup>{daffodils9966|jhou}@arch.nctu.edu.tw

**Abstract.** This study is based on Chladni figures and tries to spatially extend its representation of sound. The current Chladni figures only see parts of the sound. There should be more spatial representation of sounds because they are transmitted in space. This study explores how to capture and reconstruct invisible sound information to create three-dimensional forms. A series of steps are taken to record Chladni figures of different frequencies and decibels. Pure Data is used to generate sounds. The Chladni figures are captured in Grasshopper and converted into point clouds. These point clouds are processed by using different algorithms to produce layers of superimposed state from which 3D forms of sound can be generated and fabricated. Through the proposed methods of processing and representation, sound not only stays at the level of hearing, but can also be seen, touched, and reinterpreted spatially. With the spatial forms of sound, viewers no longer perceive sound through single but multiple states. This can help us comprehend sound in a vast variety of ways.

**Keywords.** Sound visualization; Form-finding; Spatial-temporal; Chladni figures; Cymatics.

## 1. Introduction

### 1.1. RESEARCH MOTIVATION AND CONTEXT

Sound is ubiquitous in our lives, but it is too common around us so that we are not particularly aware of its existence. We can only quickly perceive it by auditory organs. Therefore, how do diversities of sounds give everyone a particular sense? If we can “see” these disparate sounds, what do they look like? Most of us understand sounds through ears, but can’t we comprehend sounds in other ways? There are sound projects that will be depicted in the following.

#### *1.1.1. Chladni figures by Ernst Chladni in 1787*

In the field of visual sound, the study by Ernst Chladni called Chladni figures is the most typical. Drawing a metal plate with a violin bow until resonance will create nodes and antinodes at specific locations; thus, creating complex geometric patterns. It is the classic presentation of sound in 2D visualization. (Chladni 1787, Figure 1) Moreover, Hans Jenny, who is a physician and natural scientist, coined the term Cymatics to describe the typically acoustic consequences of sound

wave phenomena. (Jenny 1967) In 2002, John Stuart Reid started to develop the CymaScope scientific instrument, which can convert sound into visible geometric patterns. (Cymascope.com 2017) Therefore, people are also gradually inquisitive about several dimensions of sound visualization and try to create a series of 3D Chladni projects.

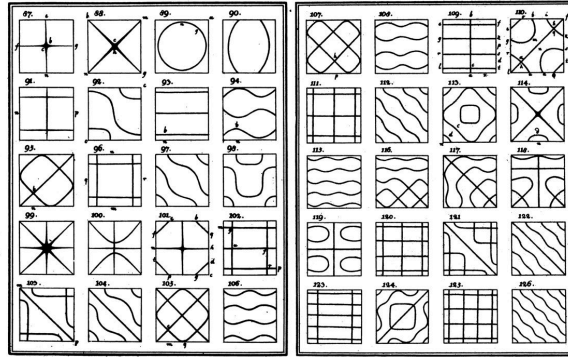


Figure 1. Chladni figures by Ernst Chladni in 1787 (Chladni 1787).

In the 3D Chladni research project, mathematical derivation and setting of conditional boundaries present the physics behind Chladni figures. With the advance of computer programs, the third dimension can further deduce from the physical and mathematical formulations of oscillation. In MATLAB, both a spectral and finite difference method is used to produce Chladni figures. Finally, images of 3D Chladni are created by employing Max / Msp / Jitter. (Skrodzki, Reitebuch and Polthier 2016) This method simulates the appearance of 3D Chladni with a numerical formula.

### 1.1.2. Kundt Tube by August Kundt in 1866

The acoustic equipment, Kundt's Tube, was invented in 1866 by German physicist August Kundt. The tube is transparent and encompasses some fine powders inside. The speaker at one end of the tube is responsible for emitting different frequencies, and the piston at the other end of it can be adjusted. When the length of the air column is some multiple of half wavelengths, the two opposite direction of waves create interference and produce standing waves. The fine powders are disturbed easily by the airflow back and forth, which shows how sound waves move between nodes. (Kundt 1866, Figure 2) With each difference in sound frequency, miscellaneous fluctuation patterns are produced. Viewers can immediately hear and see sound changes accordingly. Through the subtle variations in these sounds, different curved shapes are constructed. It makes us see a great diversity of sound surfaces in the spatial depth and width, and it can present sound in a three-dimensional space.

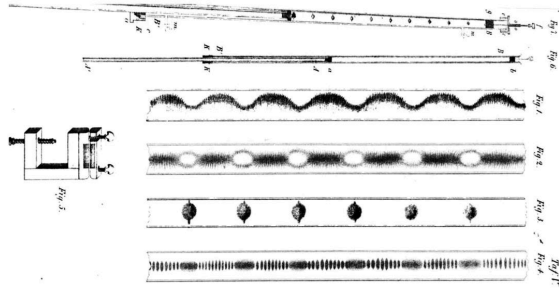


Figure 2. Kundt's Tube by August Kundt in 1866 (Kundt 1866).

### 1.1.3. Rubens' tube by Heinrich Rubens in 1905

The Rubens' tube was invented in 1905 by German physicist Heinrich Rubens. A row of small holes is drilled at a fixed distance on a long tube and sealed at both ends of the long tube. One end is connected to a speaker, and the other end is connected to flammable gas. If the length of a tube is equal to an integral multiple of the longitudinal wavelength, a standing wave will be formed, which will cause a change in the pressure of a gas in the tube. Because of variations in oscillating pressure, flammable gas will be released in distinct heights. Through each combination of varied flames, the positions between nodes and antinodes can be seen, which affect the sound shape produced. (Rubens and Krigar-Menzel 1905) (Gee 2009, Figure 3 left) In addition, a Danish science demonstrator group called Fysikshow displays the 2D Rubens' tube in 2014. (Nielsen and Muller 2014, Figure 3 right) Its presentation shows that sounds can be presented in multi-dimension. Due to an innovative alteration of creative medium and variable dimensions, this project conveys different appearances on sound expressiveness.

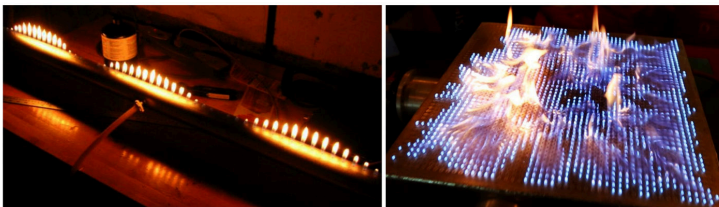


Figure 3. Rubens' tube in 1905 and 2D Rubens' tube in 2014 (Gee 2009 left; Nielsen and Muller 2014 right).

### 1.1.4. Cool Sound and Water Experiment by Brusspup in 2013

In this sound project, the first step is to make the rubber hose to connect the faucet and then pass down through the speaker. The next step is to hang the hose from the bottom of the speaker with approximately 1 to 2 inches and secure the hose to the speaker with tapes. The purpose is to ensure the hose actually contacts the speaker so that the speaker vibrates and triggers the hose. The last step is to set up



a camera at the end of the hose, play 24Hz audio, turn the faucet on, and shoot at 24 frames per second. The images will display water which seems to be frozen in space, and changes the original form. Through the changes of sound frequencies, when the frequency is adjusted to 23Hz, it looks like moving backward. However, when the frequency is adjusted to 25Hz, the water flow seems to move forward in slow motion. (Brusspup 2013, Figure 4) These phenomena make us see the visual representation that is transformed when the time information of sound is added. Therefore, each sound becomes a tangible entity. This project is a perfect conversion of digital media shooting and sound synchronization. It provides an advanced way to visualize sound.

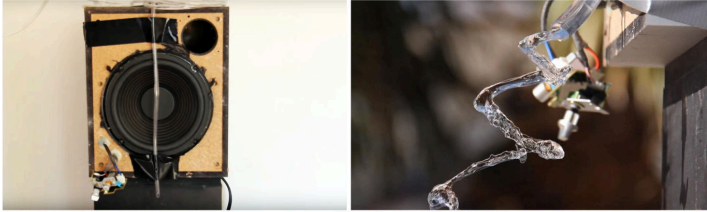


Figure 4. Cool Sound and Water Experiment by Brusspup in 2013 (Brusspup 2013).

## 1.2. RESEARCH PROBLEMS

This study is inspired by the above sound projects because they demonstrate that sounds are able to be visualized in space. Even though some projects are linear and vertical representations by directly presenting the waveforms of sound during vibration processes, each has its own distinctive characteristics of expression and different techniques, through which sounds are transformed into physical existence with visible appearances. Accordingly, this study is curious about Chladni figures, introduced in the first sound project, and how to represent them in 3D. In 2013, Ricky van Broekhoven produced a series of sound shapes projects by stacking frequency patterns and attempted to present 3D Chladni appearance. (Studiovanbroekhoven.com 2019) Therefore, this study combines the spatially expressed in projects one and two, the change of medium in project three, and the temporal of project four. Through sound capturing, images processing, and reconverting the fabricated medium, sound can be transformed into cymatic 3D.

To further understand cymatic 3D, this study investigates how to create invisible sound information to constitute a three-dimensional form. Most of the graphics constructed by Chladni figures exist in 2D, but the vibration of sound in space is a three-dimensional state. In sound shapes projects of Ricky van Broekhoven, he only stacked 2D frequency patterns, which lacked the conversion of different representations. As a result, this study attempts to present more possible states of cymatic 3D by recapturing the superimposing of cymatic 2D in different dimensions. The superimposing of diversified sound information can be more concrete to express the organic form of sound in space. This study tries to find out the possibility of sound in three-dimensional space by using a series of capture and representation techniques. By constructing a stereoscopic appearance

of sound, viewers can gain more experience in sound reception.

### 1.3. RESEARCH PURPOSES

This study is not intended to verify sound science or to justify the results of resonance experiments. Instead, we expand the possibilities of its representation by understanding sound and inspire people to observe sound information from different aspects. By creating an alternative way for people to perceive sound, three factors, including time, decibels, and frequency, are integrated to record the processes when sound is transmitted. Through interactive changes of these three elements, the innovative shape of sound can be constructed, which can help people imagine the sound space. Consequently, this study takes a series of slicing images under different decibel and frequency dimensional experiments. These sound images are imported into Grasshopper for taking points in them, and these points will perform geometric processing through feasible algorithms. Then, the 3D superimposed state of each slicing image is formed, and the shapes of sound variations are constructed in the fixed dimension.

## 2. Setup and Data Collection

### 2.1. EXPERIMENTAL SETUP

The experimental setup shown below is common for cymatics. (Grant 2009) In this study, sound is generated by Pure Data. The fulcrum is in the middle to fix a platform, and there is photographic equipment placed on top to record images. After preceding tests of diverse vibrating platforms, this study chooses to use a square aluminum plate with a size of 30x30x0.1 centimeters. Because square aluminum plates are extremely light and the measure is common, one fulcrum can stabilize it easily.

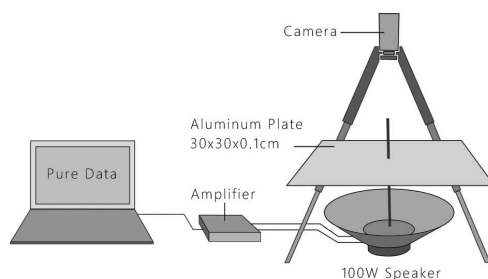


Figure 5. Setup System Diagram.

### 2.2. DATA COLLECTION PROCEDURES

There are three experiments for data collection and process. The main operations of this study mainly focus on the post-processing of recorded images. Therefore, Experiment One and Two will briefly describe data collection processes. First, Experiment One is fixed at the same decibel but different frequencies. The test frequency for this study is 100-400 Hz, and the process that the fine sand on the

aluminum plate gradually moved and gathered is recorded during vibrations. In addition, Experiment Two is fixed at the same frequency but different decibels. The test decibel is 0-83 dB. Finally, Experiment Three is the time strobe procedure for sound images that are collected from the above Experiment One and Two, which is described in the next third chapter.

### 3. Sound Images Processing

The following image post-processing flow chart is sound processing steps. After Experiment One and Two in the second chapter, the third chapter begins the post-processing of sound images. The slices of the sound images recorded during the vibration process are taken out at a specific time on the time axis by using Adobe Premiere. The images are sequentially inputted to Grasshopper in order to distinguish the color brightness and generate point clouds in each image. The images in different dimensions are successively superimposed to produce cymatic 3D multiple types.

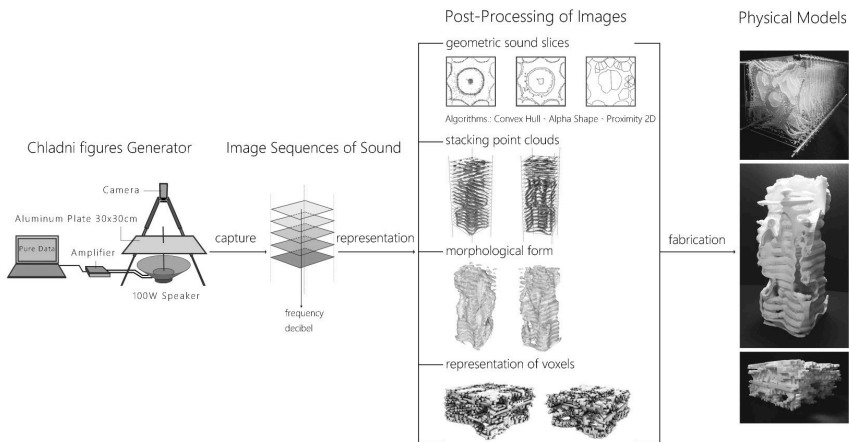


Figure 6. Sound Processing Steps.

#### 3.1. VISUALIZATION OF SOUND BY IMAGE SEQUENCES

The captured sound images are consecutively read into Grasshopper, and then Grasshopper's number slider can be used to scale images setting of the final output. Furthermore, Grasshopper's component image sampler is used to detect the grayscale value and brightness of the input images. Points of the images are outputted with the numerical value of the grayscale between 0-1. The distribution and density of points are determined according to these values. These selected points are superimposed to exhibit the outline of sound in 2.5D. Through a series of post-processing methods, it is more accurate and clear to see the subtle changes in the sound slices. The sound images are converted into point clouds according to the grayscale degree. It can control the numerical output of all parameters for subsequent processing and physical production.

3.2. VISUAL REPRESENTATION METHODS

Through the above Grasshopper process, these point clouds extracted from the images attempt to be presented in various algorithms. It is a creative way to reconstruct cymatic from using a geometric perspective. The following are the different geometric algorithm objects generated by the same sound slicing image. They are Convex Hull, Alpha Shape, and Proximity 2D. After analyzing the advantages and disadvantages of the following disparate algorithms, it is decided to use Proximity 2D first for subsequent 2.5D generation.

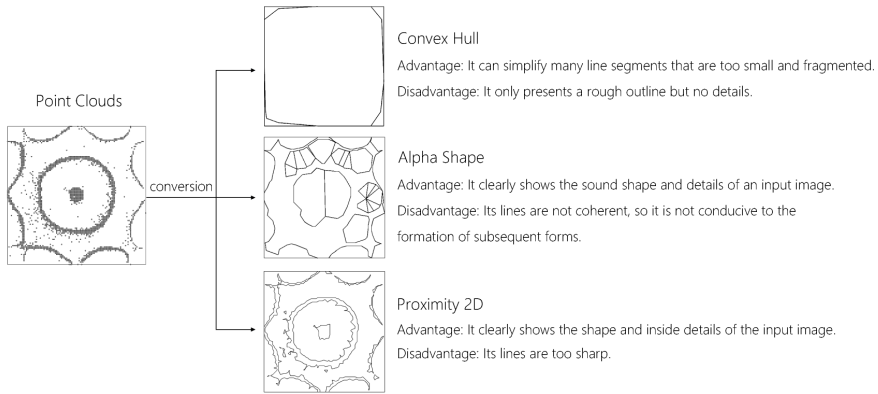


Figure 7. The picture shows the geometric representation of disparate algorithms.

4. Morphological Form of Sound

4.1. SLICING LAYERS OF SUPERIMPOSED STATES

The points taken out from the above post-processing are arranged according to the axial information. The axis can be frequency or decibel information, and it is transformed into an alternative form. As shown in Figure 8 below, the points of each slicing pattern are frequency 236 Hz to 272 Hz from the bottom to top, and the pattern changes every two Hz are superimposed.

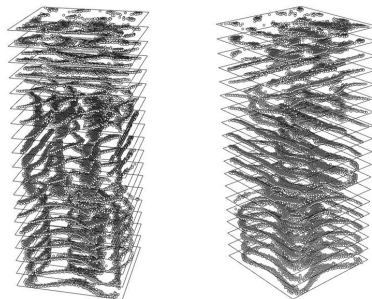


Figure 8. The picture shows that the frequency is 236 Hz to 272 Hz.

#### 4.2. VOLUMETRIC REPRESENTATION

Grasshopper's plug-in, Millipede, is a structural analysis and optimization tool for elemental frames or shells in 3D and 2D. (Michalatos 2014) Therefore, this study uses it to generate the morphology. The boundary of the form is set, and then point clouds arranged are inputted. According to the level of demandable details, the value of the data operation is determined. As shown in Figure 9 below, the left green part is a 3D model of sound frequency in the Grasshopper environment that connects all point clouds through Millipede. The right part shows a 3D virtual model of sound frequency.

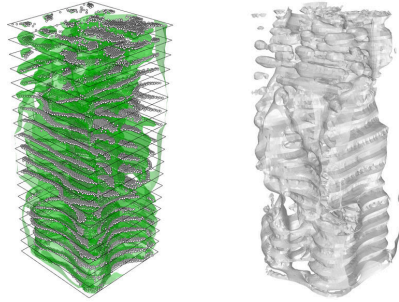


Figure 9. The Form of Sound Frequency.

#### 4.3. PHYSICAL FABRICATION

In the computer environment, forms can be adjusted quickly by setting different parameters. We can see the whole appearance of a model in advance and predict the representation of diverse fabrication. Because various forms of each sound have their characteristic representation, they can be constructed and modified in the 3D environment. Moreover, these forms are able to manufacture into touchable shapes by using a 3D printer.

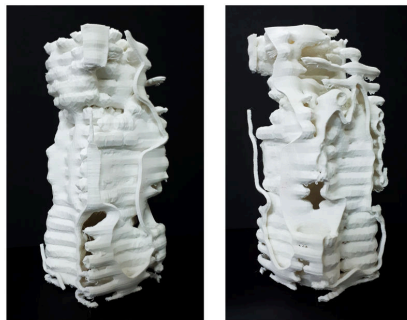


Figure 10. The Solid Model of Sound Frequency.

## 5. Conclusion

### 5.1. RESEARCH DISCUSSIONS

The images of sound have a special pattern because of plates in divergent shapes and material coefficients. However, reaching clear patterns are closely associated with frequency and decibel. After the experimental process in chapter two, the results revealed that the value of frequency and decibel have to match each other because decibels are related to energy and different frequencies also affect a multiple of the wavelength. For example, when the frequency emitted by the speaker causes the superposition of two propagating waves traveling in opposite directions to generate resonance, the entire energy will increase. The decibel value should be reduced so that fine sand will not shake out of the plate. In addition, when the destructive interference of two waves propagating in opposite directions, it means that energy is insufficient and decibel should be increased. The purpose of this study is to capture the patterns and process the images. Because of not using precise scientific instruments, the measurement of decibel generated by Pure Data has some numerical fluctuation. Then, the equilibrium of the plate also influences the accumulation and distribution of fine sand. These unexpected errors may happen during the vibrating experiment.

### 5.2. RESEARCH RESULTS AND CONTRIBUTIONS

In the researching process of 3D sound formation patterns, this study revisits sound image slices with different axial information in the spatial boundary. Capturing the sound appearances in the space makes the sound, image, and space create a connection among each other. The abstract sound can be transformed into a concrete entity. In the vibration setup, there are three variables: frequency, decibel, and time. These three variables can form the richness of sound. It is no longer just having a uniformity to understand sound; that is, it can be experienced in more sensory ways. Visualizing the shape of a sound and its three-dimensional appearance in space is no longer a dream but a reality that people can actually touch and feel it.

This study of sound representation can transform sound images into point clouds, shaping of different appearances, and make further production. As each representable method is tested separately; therefore, it can be performed in different combinations. This study attempts to find a visual process of sound from 2D to 3D through geometric representation mentioned in the previous chapter. This study finds out the way in which multiple sound messages are converted. It is a certain degree of visual representation of sound.

### 5.3. FUTURE DEVELOPMENT

Through the representation of sound in this study, it shows that sound can actually have more appearances and diversities. If this process is integrated with the Internet in the future, Chladni figures can be recorded immediately during vibration, transmitted to a computer to generate various shapes, and printed them out completely. Not only does it become a set of timely and interactive performing arts, but viewers can touch a change in the appearance of sound. Furthermore, in

the future, with the richness of sound information, it may allow designers to design space and devices through the use of sound shape. Variety methods or changes in the form of sound can make architects imagine the possibility of the unknown space and redefine the new spatial shape. As a result, this study gives rise to a new insight on cymatic 3D, as well as further research on other cymatic related topics.

## References

- “Brusspup” : 2012. Available from <<http://www.brusspup.com/>> (accessed 4th December 2019).
- “Millipede - Addon for Grasshopper” : 2014. Available from <<https://grasshopperdocs.com/addons/millipede.html>> (accessed 4th December 2019).
- “Home of the Cymatics” : 2017. Available from <<https://www.cymascope.com/cymascope.html>> (accessed 4th February 2020).
- “STUDIO VAN BROEKHOVEN” : 2019. Available from <<http://www.rickyvanbroekhoven.com/>> (accessed 4th February 2020).
- Chladni, E.F.F.: 1787, *Entdeckungen über die Theorie des Klanges*, Weidmanns Erben Und Reich, Leipzig.
- Gee, K.L.: 2009, The Rubens tube, *The Journal of the Acoustical Society of America*, **126**(4), 2294.
- Grant, E.: 2009, “Making sound visible through cymatics” . Available from TED Talks<[https://www.ted.com/talks/evan\\_grant\\_making\\_sound\\_visible\\_through\\_cymatics/transcript#t-86521](https://www.ted.com/talks/evan_grant_making_sound_visible_through_cymatics/transcript#t-86521)> (accessed 4th December 2019).
- Jenny, H.: 2001, *Cymatics: A Study of Wave Phenomena & Vibration*, Macromedia Press, 3rd edition, Epping, New Hampshire.
- Kundt, A.: 1866, Ueber eine neue Art akustischer Staubfiguren und über die Anwendung derselben zur Bestimmung der Schallgeschwindigkeit in festen Körpern und Gasen, *Annalen der Physik und Chemie*, **203**(4), 497-523.
- Nielsen, S. and Muller, D.: 2014, “The Pyro Board” . Available from <<https://www.youtube.com/user/Fysikshow/videos>> (accessed 4th December 2019).
- Oh, Y.J. and Kim, S.: 2012, Experimental Study of Cymatics, *IACSIT International Journal of Engineering and Technology*, **4**(4), 434-436.
- Rubens, H. and Krigar-Menzel, O.: 1905, Flammenröhre für akustische Beobachtungen, *Annalen der Physik*, **322**(6), 149-164.
- Skrodzki, M., Reitebuch, U. and Polthier, K.: 2016, August, Chladni Figures Revisited: A Peek Into The Third Dimension, *Bridges Conference Proceedings*, Jyväskylä, Finland, 481-484.

# IMMERSIVE SIMULATIONS OF ACOUSTICS FOR BUILDING ANALYSIS

*An Alternative Application of Unreal Engine as a Design Tool for Acoustic Environments*

MICHAEL YEOW<sup>1</sup>, KENNETH TRACY<sup>2</sup> and  
CHRISTINE YOGIAMAN<sup>3</sup>

<sup>1,2,3</sup>*Singapore University of Technology and Design*

<sup>1</sup>*michael\_yzw@outlook.com* <sup>2,3</sup>*{kenneth\_tracy|  
christine\_yogiaman}@sutd.edu.sg*

**Abstract.** This paper presents the exploration and analysis of alternative workflows in studying acoustics in architectural models, utilized in the development of the author's thesis project. Acoustic simulation software allows professionals to better understand the effects of different acoustic strategies on the overall aural experience of the space. These results are often presented as quantitative data, and auralisation programs cut back on visual representation for acoustic accuracy. The objective of this investigation is to explore the possibility of utilizing Unreal Engine as an acoustic simulation software that provides both quantitative data and an immersive understanding of the audio-visual experience of a space designed.

**Keywords.** Architectural Acoustics; Immersive Simulation; Unreal Engine.

## 1. Introduction

Advancements in digital technology have shifted industries away from analogue techniques towards automated and extensive software. The study of architectural acoustics has benefited from such progress, as acousticians nowadays are able to utilize a variety of programs at their disposal to best understand how their interventions affect the aural experience of the space. Although most of such programs possess an extensive amount of quantitative capabilities, few of such software provides a dynamic audiovisual experience that allows the user to critique designs from a qualitative perspective. Most auralisation tools present in software such as SONArchitect often support binaural simulations with flat coloured visuals of a basic model of the space being analysed (SONArchitect, n.d). This imbalance observed was key in leading the investigation to explore alternatives that value both the visuals and sounds of immersive representations of architectural spaces. Recent literature identify increasing opportunities for game engines to analyze and communicate acoustic performances of spaces (Gehron, et al 2019). Arnowitz



described that the experience should be compelling, enjoyable, and allow for designers to interact and explore in order to better understand the results of design decisions (Arnowitz 2017). The research is a proof-of-concept workflow between the game engine Unreal Engine, and Modeling software Rhinoceros that provides an immersive means of designing iteratively, discussing its relevance in the architectural profession, with further explanations on the procedures of setting up and analysing the virtual model. Written in C++, Unreal Engine offers a variety of template files for users to choose from depending on their needs and familiarity with programming. Plugins for Unreal Engine provide additional features for better visualization and representation of any virtual model. A key plugin for sound rendering is Steam Audio, which relies on physics-based sound propagation and Head-Related Transfer Function (HRTF) calculations to provide a more immersive audio-visual experience ('Steam Audio', n.d). The investigation will provide further insight into how the analysis of digital models using Unreal Engine with Steam Audio can provide a robust alternative for acoustic simulation and overall analysis of architectural designs.

## **2. Literature Review**

Acoustic principles and calculations have now been integrated into digital software to provide faster results for professionals to understand the effects of their design considerations on the acoustics of the space they are working on. There are two prominent methods that current acoustic simulation software often employs; utilizing the assumptions of geometrical acoustics or numerically solving the wave equation. The former is preferred amongst professionals because it requires less computational power and generates results at a greater speed. This comes at a cost of accuracy, as it does not consider the wave properties of sound, thereby less effective in delivering for lower frequency sounds. In contrast, wave-based calculations can give accurate results for sounds at all frequencies, but accounting for the complex nature of sound propagation effectively requires more computational power. It is also possible for some of the software available to adopt a hybrid model; utilizing geometrical acoustics for mid to high-frequency sounds and relying on wave-based calculations to solve for situations with low-frequency sounds (L.Savioja & U.P. Svensson, 2015). Steam Audio calculates and renders sounds in the Unreal Engine platform using two different methods; HRTF-based calculations for direct sound and raytracing for indirect sound. The former method accounts for the characteristics of the human ear, including boosting and attenuating different frequencies as well as enabling localization of the sound source (Potisk, T., 2015). This allows users to enjoy a binaural VR experience, in which depth could be perceived visually and aurally. Like most game engines, Unreal Engine with Steam Audio relies on raytracing to register visuals quickly, ensuring that games produced run smoothly without complex calculations for in-game sounds. The limitations of Unreal Engine as an accurate simulation software was kept in mind, and the investigation focused on the capabilities of Unreal Engine in providing an immersive and qualitative understanding of a building design.

### 3. Methodologies

It was key for this investigation to develop a virtual experience using Unreal Engine that represented real-life audio-visual experiences as closely as possible. A balance between attaining accurate results and lowering computational power had to be achieved as a result of deciding on key environmental settings. In addition, a set of commands that dictate the collection and analysis of data from gameplay was important to include in the simulation framework. The following paragraphs illustrate the parameters the author considered when setting up the model and developing tools to create an alternative method of simulating acoustic performances of spaces. Referencing the Steam Audio Plugin Documentation for Unreal Engine was important in ensuring that the virtual environment was suitable for acoustic simulation (‘Steam Audio Unreal Engine 4 Plugin’, n.d).

#### 3.1. SETTING ADJUSTMENTS AND IMPORTING MODELS

Utilizing a VR blueprint template as the base file for setting up the model instead of a C++ template is crucial for users who have little or no background in programming. A blueprint, or the Blueprints Visual Scripting system, is a visual scripting system that presents users with a node-based interface for determining object-oriented classes or objects within a virtual environment (‘Introduction to Blueprints’, n.d). The project settings, of which some are shown in Figure 1, had to be changed to ensure that the simulations carried out would yield more accurate results. For instance, the indirect spatialization was altered to HRTF to enable more realistic binaural VR visualizations. Meshes imported into the level are further assigned with two types of components; a Phonon Geometry component and a Phonon Material component. The former is responsible for registering the mesh as an object to account for Steam Audio calculations, whilst the latter allows the mesh to inherit material properties that affect indirect sounds experienced by the user. These properties include absorption and transmission coefficients that can be accordingly adjusted in custom material selection.

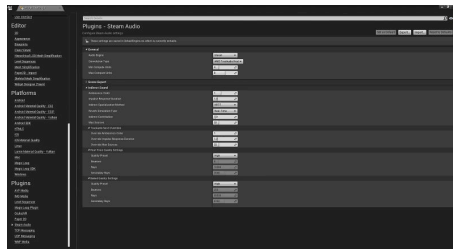


Figure 1. The interface for the Project Settings window.

#### 3.2. SIMULATION AND ANALYSIS

Once all sound sources are in place within the level, the level blueprint was edited to control how the player character obtains data from the gameplay, which could be exported seamlessly into external software for review. The level blueprint was

altered to include a character-centric logic that allowed users to control when and where they could collect audio data within the virtual environment. Parameters and conditions required for this logic included a component responsible for recording the sounds experienced during gameplay, a travelling path in which the player character can walk along whilst recording, as well as the player character's head orientation to capture the sounds rendered with the help of HRTF calculations. As shown in Figure 2, pseudocode chart was drafted to best illustrate how the components within the blueprint defined the simulation sequences. A series of locations are determined to ensure that the player character can move to these positions at the press of respective keys. A spline is drawn to establish a travelling path that the player character can move along at the press of a key to experience the virtual model. Upon the start of gameplay, recording of the in-game sounds starts. Players are given an option to explore different parts of the map or travelling along the aforementioned spline path with the aid of certain keys set in the level blueprint. Once gameplay has ended, the recording is subsequently saved as a wave file, which then can be exported into Adobe Audition and Grasshopper for further analysis. A sequence, or video recording of the gameplay, can also be initiated to obtain visuals for presentations and analysis. Sequencing gameplay from the preview interface was sufficient in providing convincing audio feedback whilst avoiding heavy rendering of lighting.

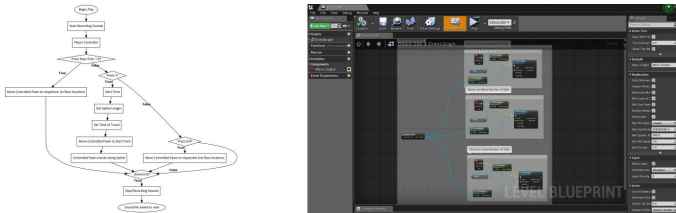


Figure 2. The pseudocode chart showcasing the character-centric logic of the simulation process, and the interface of the edited level blueprint.

### 3.3. SOUND SETUP

#### 3.3.1. Project Background

The investigation was carried out during the development of the author's thesis project, which explored how geometry and materials could help us control and design soundscapes within a building. In addition, the project attempted to understand how the conditions for altering geometry and materials of surrounding surfaces changed when designing exterior and interior spaces, as shown in Figure 3. These two types of spaces each have their own acoustic challenges, in terms of scale and enclosure. Such circumstances also gave rise to an opportunity to test the use of Unreal Engine in providing qualitative and quantitative analysis for both conditions. All sound sources included in the virtual model can be further altered by changing their spatialization, occlusion and reverberation settings for each type of sound file can further improve the realism of the virtual experience. HRTF Spatialisation Method and Bilinear HRTF Interpolation Method are the

preferred spatialization settings for all sound inputs so that all audio in gameplay is experienced binaurally. In the interest of replicating real-life conditions as accurately as possible, direct occlusion is enabled to account for geometry within the model placed between the player character and the sound source. Since sound decays across distance travelled, it is preferred to set the direct occlusion method to partial, which considers the distance from the source to the player character. This is especially important for accounting for the decay of sound pressure across distance. In addition, the frequency-dependent transmission is also enabled to the transmission of sound through objects is accounted for based on the frequency and material properties of each object.

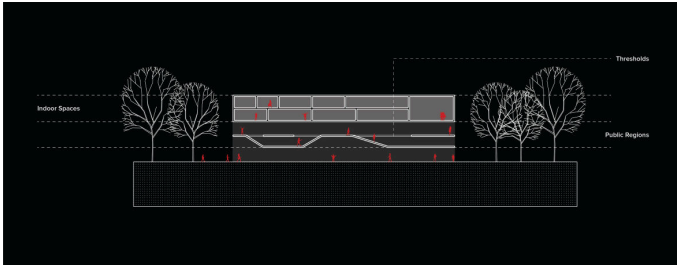


Figure 3. Conceptual section of the theatre, with the intention of designing exterior and interior soundscapes.

### 3.3.2. Exterior Soundscapes

The design intention of the semi-open ground floor of the building was to ensure that it was capable of hosting a series of performances without being excessively interrupted by the noises of the surrounding district. A reduction of physical barriers that disrupted the horizontal continuity of the public space was a key design direction. Based on the different programs and infrastructure around the site, the investigation concluded that traffic noise and park-related sounds would be the main contributors to the background sonic activity that should be accounted for during the design process of the theatre. A selection of roadside sounds and recordings of noises in the park were inserted into the virtual model as shown in Figure 4.

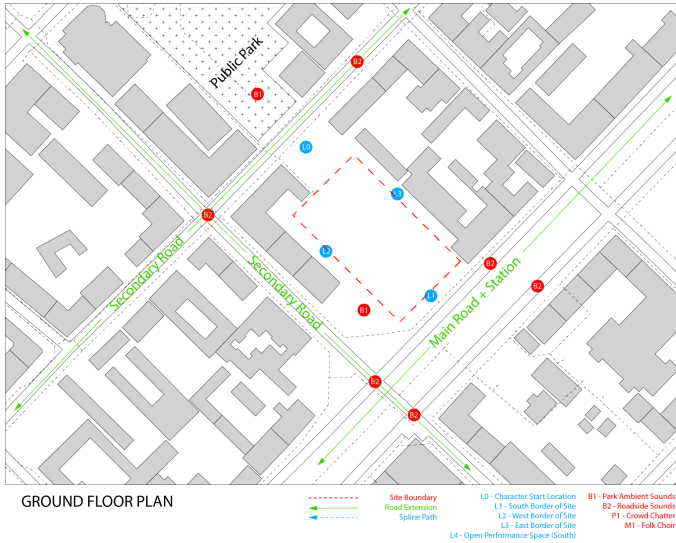


Figure 4. Plans of sound sources located in the virtual model, and the travelling path of the character during simulation.

### 3.3.3. Interior Soundscapes

Music practice rooms on the second floor of the building were to be categorised based on their reverberation times, rather than segregated based on performance type. This alternative means of classification would encourage musicians to explore different types of practice rooms, and their preferred choice of space may differ from the conventional types of rooms catered for their genre of music. As such, the music practice rooms were designed based on a range of reverberation times measured in different performance spaces, as shown in Figure 5. In Unreal Engine, sound sources are placed within the rooms to be tested, and the room locations are set in the level blueprint for users to access the spaces during gameplay, allowing users to record the sounds experienced within the rooms visited. The sound of a violin practice session was chosen and placed in multiple rooms so that users can compare the reverberation felt in each space from a qualitative perspective, simulating what it would be like for a violinist to try practicing in different rooms.

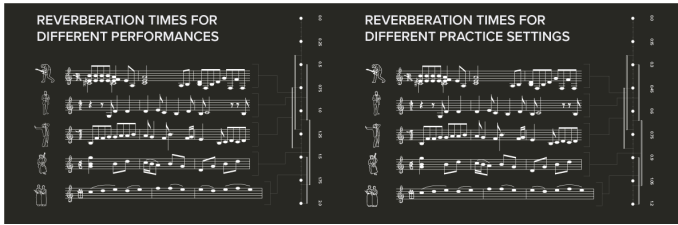


Figure 5. Range of reverberation times of performance spaces preferred by different musical genres in performances (left) and practice rooms (right).

#### 4. Design Parameters and Results

##### 4.1. DESIGN PARAMETERS

Based on the design considerations set for both exterior and interior conditions, the investigation sought to build a robust workflow of design and analysis processes involving the use of Grasshopper 3D and Unreal Engine respectively. Grasshopper 3D, a plug-in for Rhinoceros 6, allows the user to generate forms for both the exterior and interior spaces. Kangaroo 2, a live-physics engine plug-in, was used to design the envelope of the public space, whilst the design of the music practice rooms relied on Sabine’s formula for reverberation time to determine the shape and resolution of geometries mapped onto the surfaces of each interior space. These designs were exported into the Unreal Engine virtual model and analysed quantitatively and qualitatively, relying on post-processing in Adobe Audition and feedback about the audiovisual experience from colleagues. A flowchart representing this workflow is showcased in Figure 6.

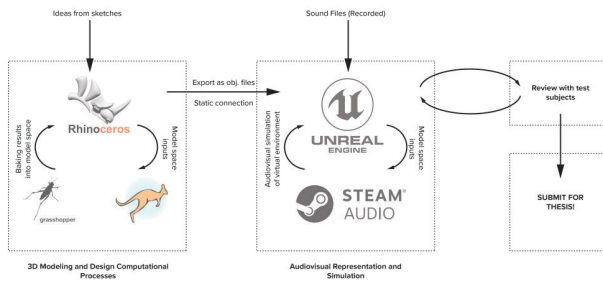


Figure 6. Flowchart representing the workflow carried out during the thesis’ investigation.

##### 4.2. OUTPUT FOR EXTERIOR SOUNDSCAPES

The investigation concluded from the simulation of aural conditions on-site based on a grid-like pathway across the area that more sound pollution would be

experienced at the south edge of the site, closest to the main road. Surrounding residential buildings help to shield the site from excessive noise pollution, and fewer sounds from the road and park can be experienced from the north edge of the site. In response to these observations, the design of the open space relied on the use of Kangaroo 2, which enables the sculpting of parabolic-like surfaces that are useful for augmenting music as well as scattering unwanted noises away from performance spaces. Ceilings above the allocated regions intended for musicians to perform would be raised, whilst areas closer to the north and south edges were lowered. These formal gestures were further tested for validation in Unreal Engine, which returned results that were positive. The noises from the surrounding roads and park could not be heard as much when one enters the semi-open public space, and music played below the high vaulted ceilings were augmented. Before and after scenarios were represented in drawings as shown in Figures 7 and 8.

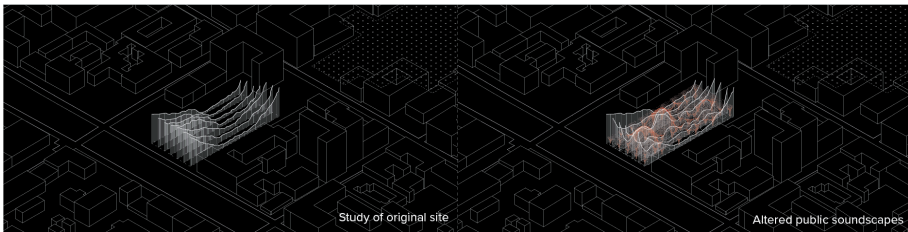


Figure 7. Existing aural conditions on site (left) and visualisation of soundscapes after intervention (right).

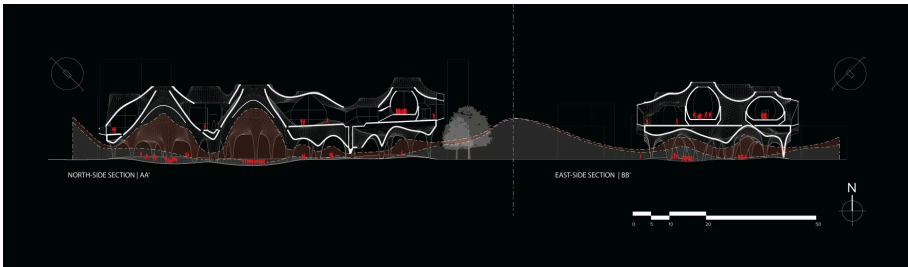


Figure 8. Sections of the building, showcasing the vaulted geometry of the ground floor envelope.

#### 4.3. OUTPUT FOR INTERIOR SOUNDSCAPES

Sabine's formula for reverberation time was inserted into a Grasshopper 3D script that determined the shape and dimension of the music practice rooms. The rooms had to be limited in size in order to fit within the established site boundary, which was also included in the Grasshopper 3D script. A selection of geometries to be mapped onto the interior surfaces of the music rooms was also taken into account when optimising the overall massing of the rooms to achieve the reverberation

time set for each of the spaces. These rooms were further evaluated in the Unreal Engine virtual environment, and colleagues were given the chance to comment on whether there were audible differences between music practice rooms with the same soundtrack being played. Based on the feedback from both Adobe Audition and test subjects, a series of rooms were selected to be arranged on the second floor of the building, as shown in Figure 9. These finalised designs were evaluated based on their aural performances as well as their spatial qualities.



Figure 9. Room designs categorised based on their surface geometry, materials and reverberation times.

#### 4.4. QUALITATIVE REVIEWS

An informal review of the virtual reality experience was conducted between myself and 25 other Master’s Thesis students in SUTD regarding the audiovisual experience created. These reviews were conducted across the design production period, and hence the responses to the legitimacy of the model vary. As shown in the info-graphic below, a large number of students were naturally impressed by the visuals that Unreal Engine could generate, and found the binaural effects of the experience convincing. Some expressed concerns regarding the glitches during the walk-through in the virtual environment. Students were quick to point out if the spaces created contributed excessively to loud and uncomfortable sounds, which aided the evaluation process of the different design iterations made over the course of the Master’s Thesis programme.

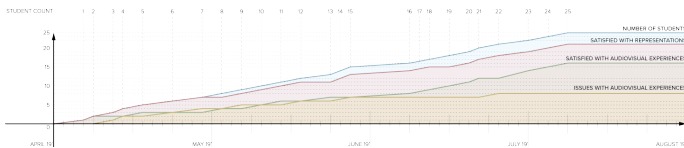


Figure 10. Infographic showcasing the responses of students who tested the virtual reality experience.

### 5. Conclusion

The setup of the model in Unreal Engine could have been further improved to deliver more accurate results if not for the limited computing power of the device used. Although the laptop on which the program was running has a Intel Core i7-7700HQ processor and a 8GB DDR4 2,400MHz RAM memory with 128GB M.2 SATA SSD, it had been in use for a few years and relied on a power adapter to remain switched on. With regards to the design parameters used, the assigning



of materials and their acoustic properties to meshes in the model would not be enough to provide a completely accurate representation of the aural experience on-site, as there are other factors such as wind speeds and humidity that are not accounted for during the simulation process. Conventionally utilised for developing games with smooth and stunning visuals, Unreal Engine lacks the rigidity of acoustic accuracy that can be found in conventional acoustic simulation software. However, the mechanisms behind its audiovisual rendering capabilities reaffirm its ability to provide approximate representations of architecture and their spatial qualities in a virtual model. Inviting external opinion to qualitatively evaluate the virtual model was also engaging and helpful in validating the work done using Unreal Engine, despite the number of willing participants being far from an ideal number. The Singapore University of Technology and Design (SUTD) has already tried and tested the use of Unreal Engine as a design tool and platform for representation of architectural studio work (ASD, 2019), showcasing potential as a mainstay software for educational purposes. To a designer new to acoustics, Unreal Engine provides a low-cost and interactive means of estimating the performance of their building designs. Its reliability as a tool for analysis could be useful as a platform for discussion between architects and other project consultants. Interactive representations of a given project made possible with Unreal Engine allow all parties involved to understand the issues and merits present during discussions, which aids in the communication of ideas and opinions about the project and how the team can move forward. The investigation hopes that marked improvements and developments of Steam Audio in the future could allow Unreal Engine to compete as a legitimate platform for qualitative and quantitative assessment of architectural acoustics.

## References

- “SONArchitect” : no year given. Available from <<https://www.sonarchitect.asia/>> (accessed 10th December 2019).
- “Steam Audio” : no year given. Available from <<https://valvesoftware.github.io/steam-audio/>> (accessed 10th December 2019).
- “Introduction to Blueprints” : no year given. Available from <<https://docs.unrealengine.com/en-US/Engine/Blueprints/GettingStarted/index.html>> (accessed 10th December 2019).
- “Steam Audio Unreal Engine 4 Plugin” : no year given. Available from <[https://valvesoftware.github.io/steam-audio/doc/phonon\\_unreal.html](https://valvesoftware.github.io/steam-audio/doc/phonon_unreal.html)> (accessed 10th December 2019).
- “ASD Core Studio 2 Exhibition ‘The Digital Archive’ featured on LIANHE ZAOBAO and Channel 8” : 2019. Available from <<https://asd.sutd.edu.sg/news-events/event/news/asd-core-studio-2-exhibition-digital-archive-featured-lianhe-zaobao-channel-8/>> (accessed 10th December 2019).
- Arnowitz, E., Morse, C. and Greenberg, D.: 2017, vSpline: Physical Design and the Perception of Scale in Virtual Reality, *Proceedings of ACADIA 2017*, Cambridge, MA, 110-117.
- Gehron, L., Chernick, A., Morse, C., Naumovski, S. and Ren, Z.: 2019, Sound Space, *Proceedings of ACADIA 2019*, Texas, Austin, USA, 346-351.
- Potisk, T.: 2015, Head-Related Transfer Function, *Seminar Ia, Faculty of Mathematics and Physics*, University of Ljubljana, Ljubljana, Slovenia.
- Savioja, L. and Svensson, U. P.: 2015, Overview of geometrical room acoustic modeling techniques, *The Journal of the Acoustical Society of America*, **138**, 708.

# **Virtual/Augmented/Mixed/ Interactive-Environments**



# VISUAL ATTENTION IN RETAIL ENVIRONMENTS

*Design Analysis using HMD based VR System Integrated Eye-Tracking*

NAYEON KIM<sup>1</sup> and HYUNSOO LEE<sup>2</sup>  
<sup>1,2</sup>*Yonsei University, Seoul, South Korea*  
<sup>1,2</sup>{ny.kim|hyunsl}@yonsei.ac.kr

**Abstract.** The goal of this study is to understand the spatial experience of users in retail environments in an immersive virtual reality setting. This study measures the visual attention and visual merchandising cognition of users via a quantitative method. The study was conducted to assess users' visual perception arising from the visual merchandising in-store environment during virtual reality experiences. The experiment was conducted using eye-tracking methodology in a virtual reality environment. After the experiment, participants responded to questionnaire surveys to assess visual merchandising cognition in retail environments. The experiment stimuli were provided in the virtual simulation of a retail store. During the experiment, each participant wearing a head-mounted display device was asked to experience the virtual retail space. The result shows the quantitative analysis of user behavior in the retail space and which design elements attract their attention. Unlike the precedent eye-tracking studies, this research analyzes visual attention during the spatial experience of retailing in its use of virtual reality technology. The approach and findings of this research provide useful information and practical guidelines to retailers and designers who are interested in improving the retail environment in consideration of customer visual attention and spatial elements.

**Keywords.** Visual Attention; Retail Environment; Eye-tracking; Virtual Reality; HMD (Head-Mounted Display).

## 1. Introduction

Today's retail market is changing more rapidly than ever before. The global e-commerce market has experienced accelerated growth in recent years. The rise of online shopping has caused offline stores to close and retail companies to go bankrupt. The speed and magnitude of this paradigm shift present challenges for the survival of traditional retailers. However, the opportunity exists for retailers to undergo a digital transformation. Offline retail stores have traditionally focused on driving sales but are now becoming centers which provide experiential value that customers cannot get online. Offline stores should be more than physical environments for the placing and selling of products; they should be more

oriented toward the customer experience. Retailers need to increase their efforts to attract the attention of customers and to optimize the in-store environment such that consumers can be better exposed to the visual perspective (Jang et al., 2018). It is important to add experiential value and understand the behavior and visual attention of consumers while they shop in a physical store. Contemporary shopping spaces are required to reflect customer interests and visual attention patterns. In the retail experience, visual merchandising creates the in-store environment to visually communicate with customers as well as to contribute toward driving sales. The physical retail spaces of evolved brands, such as flagship stores, are viewed as part of a marketing strategy for brand building.

There has been enormous growth in recent years in the use of neuromarketing methods to understand the customer experience at the point of sale. Previous studies were limited to measure visual attention on products by employing eye-tracking methodology to determine influences on consumer behavior and decision making (Kim and Lee, 2020). Eye-tracking methodology has been employed for evaluating marketing stimuli, such as packaging, or for evaluation of point-of-purchase marketing (P. Huddleston, Behe, Minahan, & Fernandez, 2015). However, there is a lack of research which evaluates visual attention on spatial design elements in retail environments. With the increased demand for experiential retail in physical stores amidst today's rise of online shopping, it is necessary to understand the in-store customer experience in retail environments.

This study aims to investigate where customers focus their attention and how they perceive visual merchandising in the in-store environment. The objective of this study is to measure visual attention and visual merchandising cognition in quantitative method. Using state-of-the-art technology, the experiment was conducted to assess users' spatial cognition arising from visual merchandising in a virtual reality (VR) environment. An eye-tracking method has been developed to take advantage of VR headsets to perceive a high level of realism in a VR setting. Head-mounted display (HMD) VR systems offer a high-quality immersive environment and interactive tools. They have the benefit of allowing control over the study environment in a VR setting for multiple tests, regardless of geographical location. We can observe exactly where the user's attention is focused, at all times, in real time. Scientific evaluation of various types of VR simulation design has a high potential for architectural research, but it is still in its infancy. For this reason, this study explores a novel approach to measure spatial behaviors and visual attention in naturalistic perception while providing a sense of presence via an immersive VR experience under full experimental control.

## **2. Theoretical Background**

### **2.1. EYE-TRACKING METHODOLOGY IN RETAIL ENVIRONMENT**

Eye-tracking methodology has been widely used in cognitive science, consumer behavior, psychology, and design analysis research and in evaluating design, visibility, usability, and advertisements. Since the 1990s, the eye-tracking method has been utilized in the field of human computer interaction in usability researches conducted on information sharing interfaces (Tonbuloglu, 2013). Through

tracking the user's gaze and eye movements, eye-tracking data can demonstrate what attracts a person's interest and where they get information. New VR technology offers new opportunities to research brand interaction and customer experience in retail environments. Recently, eye-tracking technology combined with a VR system has been used for the experimental study of an historical street design (Jeng & Zhang, 2018). However, advanced study in VR systems integrated with eye-tracking technology is still in the early stage of application to the built environment. Much synergy from the combination is expected to further experimental research to expose users to realistic visual stimuli, promoting a sense of presence in immersive settings. Eye-tracking has an intrinsic relation with VR, and the integrated system can provide more potential for eye-tracking research in VR environments (Jacob and Karn, 2003).

In this study, eye-tracking methodology is utilized in order to understand visual attention evoked from visual merchandising cognition in physical retail environments. Visual perception includes the various physiological components that give rise to the experience of vision. Recently, eye-tracking technology has also been used to examine the visual attention of consumers in online retailer environments. A recent study investigated the impact of various product photo features on the attention of online users through an eye-tracking experiment (Shin, 2019). In relation to retailing, the following literatures show the precedent studies which include search-choice process in the retail environment (P. T. Huddleston, Behe, Driesener, & Minahan, 2018). However, most of the literature in this area has been focused on the visual elements of product and package design. Unlike previous retailing studies, this study tackles the spatial experience and visual merchandising cognition perceived in in-store environments.

## 2.2. VISUAL MERCHANDISING COGNITION

Visual merchandising is both making merchandise attractive and selling merchandise through a visual medium (Pegler, 2012). Visual merchandising is a powerful tool for communicating visually with consumers and driving sales. Visual merchandising contributes to a brand's image and increases the likelihood that a customer will make a purchase. Many retailers utilize visual merchandising to maximize brand experiences in physical store environments. Visual merchandising is an important part of strategic product development planning and product sales methods for meeting consumer needs and driving them towards purchases.

Visual merchandising cognition is the visual perception of store characteristics associated with a brand image (Matthews, Hancock, Joseph, & Gu, 2013; Park, Jeon, & Sullivan, 2015). Research on how visual merchandising cognition affects brand attitudes and consumer purchase intentions has been limited (Park, Jeon, & Sullivan, 2015). Jeon & Park (2005) developed an instrument to measure visual merchandising cognition according to the dimensions of harmony, attractiveness, compatibility, trendiness, and functionality. Visual merchandising affects customer affective responses (Law, Wong, & Yip, 2012). According to Park et al. (2015), visual merchandising trendiness and attractiveness encompass a brand's aesthetic attributes and functionality describes a brand's utilitarian

attributes. The result shows that positive responses to visual merchandising are directly related to purchase intention (Park, Jeon, & Sullivan, 2015).

### 3. Methods

#### 3.1. EXPERIMENTAL PROCEDURES

This study was mainly conducted in two phases: an experiment and a post survey. The experiment was implemented using eye-tracking methodology in a VR setting and was conducted in a laboratory setting. After the experiment, participants were asked to respond to a survey regarding personal information, the sense of presence in the VR environment, and visual merchandising cognition in the in-store retail environment. The experiment protocol was reviewed and approved by the university's IRB for the protection of human subjects. The subjects were recruited on the university campus and randomly selected on a first-come basis. The condition is to fairly provide all subjects a first-time VR spatial experience of retail environment via headset display.

The visual stimuli were shown as the in-store environment of a global automobile retail company located in Seoul, South Korea. It is a standalone flagship brand showroom, which features a newly curated retail and cultural experiences, as well as exhibits. To create the interior and exterior architecture, 'Suh Architects' used 36,000 meters of steel pipes and anodized panels supplied by H motor group. The experiment stimuli were presented in the 360° virtual simulation of a retail space. The architectural images were modeled from a camera which can record 360° panoramic images with high-resolution. Ten architectural images from different perspectives were nominated initially, but after review with professionals, only two types of representative space were selected. The final selected images were modified using Adobe Photoshop CC properly for experimental stimuli use. For this study, we developed two types of 360° panoramic images for virtual simulation. Two spaces were distinguished by the price range of merchandise: high versus low. The one is a sales area for premium vehicles on the 3rd floor and the other is for economy compact vehicles on the 4th floor.

A total of six subjects went through calibration tests wearing an HMD VR integrated eye-tracking device, but only one subject failed. Finally, five subjects whose eye-tracking ratios were above 90% participated in this experiment. This is a preliminary study to observe and investigate individual user behavior and visual patterns in-depth. Nielson (2000) found that usability tests produce the best results when they are conducted with no more than five participants and that as many small such tests as can be afforded should be conducted. The subjects were aged in their 20s or 30s. Three were male and two were female. Two were students and three were office workers. They responded that they had previous experience using VR systems for games or entertainment only. All subjects were familiar with a global automobile brand, but they had not actually visited an automobile retail store. During the VR experience, all subjects responded that the immersive sense of presence caused them to feel as if they were in the physical store.

To benefit from eye tracking technology within the VR environment, there

are three main components that must be in place: VR content as visual stimuli, an eye-tracking enabled VR headset, and analysis software. For the experiment setup, it is required to create a setting for a VR environment. Cubical devices called 'base stations' set the extent of the implementation of a virtual space in the laboratory. The hardware used in this experiment was the 'HTC-Vive', manufactured by SMI (Senso Motoric Instruments, Germany). Integration of eye-tracking in the 'HTC-Vive' device enables controlled environments for naturalistic eye-tracking studies. Next, in order to collect the data from all subjects during the experiment, SMI experiment suite software for stimulus analysis, such as software development kit 'SDK (C/C++)', 'Experiment Center', 'BeGaze', 'Steam VR', 'Unity 3D', were installed on a laptop.

The HMD VR device enables collection of the user's gaze data simultaneously with the VR experience in real time. In particular, by simply setting start and end times for experiments, the user's raw eye data are synchronized with the time when the actual stimuli are presented. During the experiments, eye data transmitted from the HMD device is displayed on the laptop screen in real time, so that it is feasible for a researcher to check and manage the user's eye-tracking status as well as the progress of the experiments. Eye-tracking data is collected at 250 Hz binocular. Data include point of regard on the display (left and right eye, binocular), gaze base point, gaze vector, and inter-pupillary distance (pupil to pupil distance). Eye-tracking metrics including first fixation, total duration of fixation, and time to first fixation. In this study, participants were exposed to visual stimuli for 120 seconds and a total of 30,000 raw gaze data points from individual eye-tracking were collected. For all five participants' tracking, 150,000 raw data points in total were collected for analysis.

Each experiment was conducted individually with the researcher for a total time of approximately 30 minutes. As soon as a participant arrived at the experiment lab, the researcher explained the overall research procedure in person. All subjects were carefully informed of the step-by-step precautions of the experiment. In the experiment lab, the subject wore an HMD device with integrated eye-tracking. Each participant was taken through a calibration procedure prior to the experiment, then the experiment was conducted under researcher control. During the experiment, each participant wearing the HMD device was asked to look at two images of 360° virtual retail space for 120 seconds in total. Each image was shown for 60 seconds to collect eye-tracking data and visual attention patterns on each. After the experiment was complete, the participants were asked to answer survey questionnaires regarding demographics, the sense of presence of the VR experience, and visual merchandising cognition.

## 3.2. MEASURES

### 3.2.1. *Eye-tracking measures*

In this study, the researcher defined and classified the main spatial design elements as areas of interest in each image. Area of interest (AOI) means regions of a display that researchers define and classify by shape for which quantitative data can be calculated (Bergstrom & Schall, 2014). In this study, a researcher determined the



AOIs in each still image according to the spatial element composing the retail environment. The following introduces the basic AOI events that connect the data to stimulus space and key performance indicators (Bergstrom & Schall, 2014; Holmqvist, 2011). The details of key performance indicators of AOIs include: sequence, entry time, dwell time, hit ratio, revisits, revisitors, average fixation, first fixation and fixation count.

The analysis of participants' eye-tracking data and visual attention include fixation count, fixation duration, coordinates, gaze path, gaze pursuit and others. In addition, we analyzed AOIs of the in-store retail environment, including spatial components such as architectural elements and interior objects: floor, wall, ceiling, furniture, lighting fixture, and display object. Heatmaps were generated from eye movement data of average of all participants.

### 3.2.2. Visual merchandising cognition measures

Visual merchandising cognition is the visual perception of store characteristics associated with a brand image (Matthews, Hancock, Joseph, & Gu, 2013; Park, Jeon, & Sullivan, 2015). Jeon & Park (2005) developed an instrument that measures visual merchandising cognition according to the elements of harmony, attractiveness, compatibility trendiness, and functionality. In the study, the survey questionnaires shown in Table 1 were developed based on the literature review.

Table 1. Instrument of Visual merchandising cognition .

Variables	item	Scale
Harmony	• Harmonized floors, walls, ceilings in interior space	5 point Likert scale from "Strongly disagree"=1 to "Strongly agree"=5
	• Harmonized with your brand image with art display, fixtures, POPs etc.	
Attractiveness	• Creative image creation in display	
	• Make your products attractive through eye-catching techniques.	
Trendiness	• Introducing new trend through color display and design technique	
	• Delivering new trend using effective visual merchandising	
compatibility	• Visual merchandising elements are displayed in a consistent to communicate brand image.	
	• Use fixture, display objects, props that match the brand image.	
Functionality	• Consideration of sufficient corridor in the store layout	
	• Consider the functionality of spatial design	

## 4. Results and Discussion

### 4.1. ANALYSIS AND FINDINGS FROM EYE-TRACKING

During the VR experiment, all participants' behaviors were observed during the spatial experience in the retail environment. As an analysis of general spatial cognition, the following attention maps generated from eye-tracking show all participants' visual interest within the space. Red indicates a high intensity of visual attention. As shown in Figure 1, two attention maps represent the average data of all participants for two stimuli. In the first sales space for premium cars, people paid more attention to the premium lounge and the unique structural elements of the ceiling. In the lounge area, various components for the manufacture of premium cars are displayed to visually provide specific product information and brand communication to customers. In contrast, the economy

sales space has more efficient placement of different types of cars; participants paid more attention to the cars than the environment.

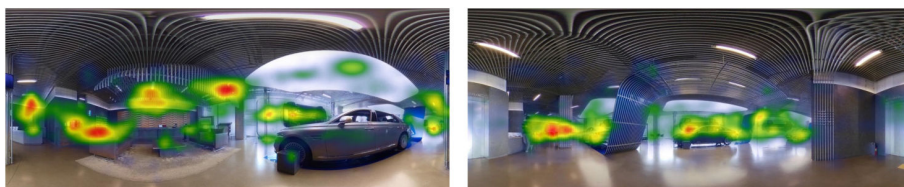


Figure 1. Heatmap of retail environment for premium cars(left) and for economy cars(right).

The following data represent an individual's spatial experience sequence. As an example, one participant (P04), who recorded the highest tracking ratio at 97%, is selected. Figure 2 shows how this individual behaved and look around the spatial element in sequence. The number of each spotted area indicates its position in the sequence.

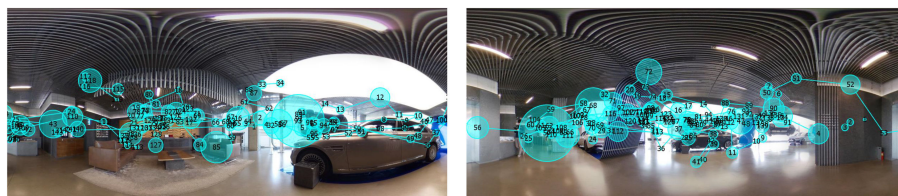


Figure 2. Scan path in retail environment for premium cars (left) and for economy cars (right).

In this study, we analyzed AOIs of the in-store retail environment including spatial components such as architectural elements and interior objects: floor, wall, ceiling, furniture, lighting fixture, and display object. The first experiment stimulus is the sales area for premium cars. As a result of averaging the eye-tracking of all participants, the fixation sequence of AOIs shows: (1) carpet- (2) ceiling- (3) furniture 2 - (4) furniture 3 -(5) furniture 1 - (6) lighting1 - (7) art wall - (8)wall - (9) floor - (10) display object. The first object in the fixation sequence shows 'carpet', and 'ceiling' is next. The carpet is in the premium lounge area where customers can consult with a salesperson. In addition, participants showed little interest in the display object. The second experiment stimulus is the sales area for economy cars. As a result of averaging the eye-tracking of all participants, the fixation sequence of AOIs shows: (1) ceiling - (2) wall 1 - (3) display object 1 -(4) lighting 1 - (5) floor - (6) display object 2 - (7) wall 2 - (8) pillar -(9) lighting 2 - (10) lighting 3. In this space, participants paid more visual attention to 'ceiling' and 'wall 1'. The last sequence of fixation shows 'lighting 3'. From all analysis of the two types of space, users show the least visual attention on the lighting fixtures, are the linear fluorescent light.

In addition, the total fixation time on each AOI events were measured. It is total amount of time that participants have spent looking at particular elements during entire experiment. Thus, if the dwell time on particular area is higher, the

interest of that element is higher. In the sales area for premium car, total fixation time shows from the longest to shortest: (1) ceiling- (2) wall - (3) lighting 1 - (4) furniture - (5)art wall - (6)floor - (7)display object - (8) furniture 2- (8) furniture 3- (9)carpet. In the sales area for economy cars, the result of total fixation time shows from the longest to shortest: (1) ceiling - (2)wall 1 - (3) floor - (4) display object 1 -(5) pillar - (6) wall 2 - (7)display object 2- (8)lighting 1 - (9) lighting 2 -(10) lighting 3. Figure 3 describes data from the key performance indicator analysis of AOI events: total dwell time, entry time, first fixation, average fixation, revisits, and fixation count.



Figure 3. KPI analysis: retail environment for premium cars (left) and economy cars (right).

The result shows that they paid little attention to carpet in the sales for premium car and lighting 3 in the sales of economy car. However, in both areas participants paid significant amount of attention to the architectural elements of unique industrial steel pipes on ceiling for the longest. It means people are interested in what is a common architectural element that conveys brand identity associated with automobile manufacture. Every detail within architectural elements should be designed to create synergy toward providing holistic brand experience. The physical retail environment should be utilized as part of a marketing strategy for brand building.

#### 4.2. ANALYSIS AND FINDINGS FROM VISUAL MERCHANDISING COGNITION

The survey of visual merchandising cognition is analyzed with the statistical software SPSS 24. Five instruments are measured to assess visual merchandising cognition: harmony, attractiveness, trendiness, compatibility, and functionality. Among the five variables of visual merchandising cognition, the average of participants' responses ranks them from highest to lowest as: 'attractiveness', 'harmony', 'trendiness', 'compatibility', 'functionality'. As a result, users generally felt the attractiveness of this space makes products appealing since it creates interesting spatial impression with eye-catching display. However, they perceived lower compatibility and functionality from visual merchandising cognitions. It means retailers and designers need to improve brand communication with customers in-store retail environment. For example, using fixtures, display

objects, and props which match the brand identity can help to enhance the brand image. Retailers also need to properly provide product information in each sales zone so that customers can easily find the information they want. In addition, the store layout also needs to be reconsidered to provide sufficient corridor for customer convenience.

From the findings of the eye-tracking experiment and the survey, in order to enhance the in-store retail environment, the brand image or product information that the retailer wants to deliver should be reflected and integrated into the particular spatial elements that the users looked at the most and the first time in sequence during the VR experiment. User experience-oriented design is required to reflect the user's interest and convenience by observing the user's behavior within the architectural space. The results of this study suggest that design communication between retailers and consumers should be further enhanced when creating spatial environments. In order for users to become familiar with products and brand images more quickly and easily, it is necessary to communicate brand identities through spatial elements with priority on areas to which consumers pay attention. Thus, the spatial experience eventually contributes to enhance brand image so customers can maintain a positive purchasing intention. This integrative study of eye-tracking analysis and survey on visual merchandising cognition can be the basis for building an evidence-based design to create a user-oriented retail environments.

## **5. Conclusion**

In this study scientific methods were used to quantitatively analyze the spatial design elements in which users are interested and to which they pay attention. The results show the quantitative analysis of where customers look in the in-store environment, how they behave with the space, and where they pay attention in AOIs. The approach and findings of this research provide useful information and practical guidelines to retailers and designers who are interested in improving retail environmental design in consideration of customer visual attention and spatial elements. This research assists designers in architectural design processes to engage user-oriented experiences. In addition, for retailers, this research can provide useful guidelines for applying visual merchandising related to the in-store environment.

Unlike precedent eye-tracking studies, this study uses a state-of-the-art technological system for a scientific approach to observe the user experience in real time within a VR setting. However, this study has a limitation in that it is a very basic preliminary study applied to one retail case with a small number of participants. Although the study needs further development, it has significance in demonstrating the protocol of experimental methodology using VR combined with eye-tracking technology. In future research, in addition to focusing on visual attention, pupillary response will also be studied and measured to investigate how users respond emotionally to the spatial experience. Further study may be extended to compare and analyze differences in user behavior patterns among different groups according to individual characteristics (e.g., gender, age, job status, product involvement).

Eye-tracking within VR creates more immersive research scenarios by enabling integrations based on gaze. It also opens up many opportunity apply to the evaluation of virtual simulation. VR experiments allow pre-evaluation of spatial simulations prior to construction in the real world. From the results of pre-testing the user experience, the final architectural design can be modified to fit customer needs and contribute to optimization of the design. Use of eye-tracking methodology within a VR environment contributes to a better understanding of how users navigate a space, what they actually look at, and how their attention is drawn to design elements. This is more powerful than relying on the intuition of designers or architects to optimize designed spaces. The implications of this study show many possibilities to enhance architectural design and its process in the future.

**Acknowledgments.** This work was supported by the National Research Foundation of Korea (NRF) grant funded by Korean Government (NRF-2017H1A2A1042750).

## References

- Bergstrom, J. R. and Schall, A. J.: 2014, *Eye tracking in user experience design*, Elsevier/Morgan Kaufmann.
- Huddleston, P. T., Behe, B. K., Driesener, C. and Minahan, S.: 2018, Inside-outside: Using eye-tracking to investigate search-choice processes in the retail environment, *Journal of Retailing and Consumer Services*, **43**, 85-93.
- Huddleston, P., Behe, B. K., Minahan, S. and Fernandez, R. T.: 2015, Seeking attention: an eye tracking study of in-store merchandise displays, *International Journal of Retail & Distribution Management*, **43(6)**, 561-574.
- Jacob, R. J. and Karn, K. S. 2003, Eye tracking in human-computer interaction and usability research: Ready to deliver the promises, in , *Mind*, Elsevier/Morgan Kaufmann, 573-605.
- Jakob, N.: 2000, *Why you only need to test with 5 users*, Nielsen Norman Group .
- Jang, J. Y., Beak, E., Yoon, S. Y. and Choo, H. J.: 2018, Store design: Visual complexity and consumer responses, *International Journal of Design*, **12(2)**, 105-118.
- Jeng, T. and Zhang, R. X.: 2018, Integration of virtual reality, 3-D eye-tracking, and protocol analysis for re-designing street space, *Proceedings of CAADRIA 2018*.
- Kim, N. and Lee, H. J. 2020, Evaluating Visual Perception by Tracking Eye Movement in Architectural Space During Virtual Reality Experiences, in T. Ahrum, R. Taiar, V. Gremeaux-Bader and K. Aminian (eds.), *Human Interaction, Emerging Technologies and Future Applications II. IHJET 2020. Advances in Intelligent Systems and Computing*, Springer, 302-308.
- Law, D., Wong, C. and Yip, J.: 2012, How does visual merchandising affect consumer affective response? An intimate apparel experience, *European Journal of marketing*, **46(1/2)**, 112-133.
- Park, H. H., Jeon, J. O. and Sullivan, P.: 2015, How does visual merchandising in fashion retail stores affect consumers' brand attitude and purchase intention?, *The International Review of Retail, Distribution and Consumer Research*, **25(1)**, 87-104.
- Pegler, M. M.: 2012, *Visual merchandising and display*, Fairchild Books., New York.
- Tonbuloglu, İ: 2013, Using Eye Tracking Method and Video Record in Usability Test of Educational Softwares and Gender Effects., *Procedia - Social and Behavioral Sciences*, **103**, 1288-1294.

# THE IMPACT OF MOVING THROUGH THE BUILT ENVIRONMENT ON EMOTIONAL AND NEUROPHYSIOLOGICAL STATE

*A Systematic Literature Review*

MITRA HOMOLJA<sup>1</sup>, SAYYED AMIR HOSSAIN MAGHOOL<sup>2</sup> and  
MARC AUREL SCHNABEL<sup>3</sup>

<sup>1,2,3</sup>*Victoria University of Wellington*

<sup>1</sup>*Mitra.Homolja@gmail.com* <sup>2,3</sup>*{SayyedAmirHossain.Maghool|  
MarcAurel.Schnabel}@vuw.ac.nz*

**Abstract.** Despite theoretical evidence about the capabilities of visual properties of space for manipulating inhabitants' emotions, a gap in knowledge exists for empirical studies in controlled environments. Interdisciplinary studies at the intersection of architecture, psychology, and neuroscience can provide robust guidelines and criteria for designers to engineer emotions. Due to the novelty of the field, the theoretical framework for such studies is not well established. Consequently, this paper presents a systematic literature review to find and synthesize recent relevant studies at this intersection. Based on these findings, we will investigate the impact of other visuo-spatial stimuli on emotions in a rigorous way. According to the theories of emotions, manipulation of emotions is linked to oscillations in physiological responses caused by exposure to sensory stimuli. Moreover, there is a consensus that human perception is action-oriented. Therefore, our review focuses on studies that employ biosensors as subjects move in physical or virtual environments.

**Keywords.** Neuroarchitecture; Brain Body Sensors; Virtual Reality; Physiological Response; Emotional Response.

## 1. Introduction

The qualities of spaces in the built environment impact profoundly on how we exist within them. Our perception of architecture and the built environment affects our physiological and emotional experiences of our immediate surroundings. There is a consensus that sensory stimuli in the built environment impact our feelings and emotions; however, the interrelation between architecture and the emotions it evokes is not yet fully understood. A gap exists in the knowledge at the intersection of architecture, psychology, and neuroscience. The intersection's relevance is gaining traction, but the conclusions on the matter are not straightforward, nor imminent. Moreover, there is an inherent need for architects to understand how their buildings impact the emotions of those who occupy them; for instance,

engineering people's emotional states when designing a memorial or a sacred building (Eberhard 2008). As Kahn states, "one may say that architecture is the thoughtful making of spaces. It is not the filling of areas proscribed by a client. It is the creating of spaces that evoke a feeling of appropriate use" (Kahn & Brillembourg 1992).

This paper is a part of a research project that aims to study the impact of variation in visuo-spatial variables on humans while they walk through built environments. We will utilize technologies, namely virtual reality and human body-brain sensors, to rigorously study the impact of the variation on subjective and objective emotional data gathered from human subjects. Our paper consists of a systematic literature review, where we identify existing research in the field of neuroarchitecture and environmental psychology. We intend to discuss contemporary empirical literature with the aim of presenting a compelling argument in favor of the need for further research in this field.

In order to understand the effects of spatial properties on human emotion, we have selected empirical studies that use subjective and objective measurements. Additionally, we identified studies that consider the importance of movement in the perception and experience of architectural space. We synthesise current literature to elucidate gaps in the existing knowledge and to establish our trajectory for research in this field.

## **2. Background**

Many researchers claim that we are at the beginning of a revolution in cognitive research and neuroscience; they suggest it is comparable to the Galilean revolution in physics (Robinson 2015). A growing body of research explores the impacts neuroscience can have on the field of architecture to offer designers novel possibilities for architecture with intent to impact people's short-term and long-term emotional states. A branch of science called neuroarchitecture is emerging from these studies (Banaei et al. 2017), where modern methodologies are employed from several disciplines into research in the architecture field.

Numerous studies have noted that emphatically measuring emotion is difficult; quantifying a very subjective emotive experience is an inherently complex task and subjective methodologies alone are argued to have limited effectiveness. Eberhard (2009) suggests that we can use metaphors to convey a part of emotions being experienced by our consciousness, but they are not the real experience of places. It emphasizes the importance of understanding subconscious neurophysiological reactions of experienced emotions. Neuroscience and psychology have developed a body of research which attempts to address the nature of primal responses to our surroundings; the James-Lange theory (James 1884), Cannon-Bard theory (Cannon 1927), Schachter-Singer theory (Schachter & Singer 1962), Facial Feedback theory (Lanzetta et al. 1976), all emphasize that external stimuli that trigger emotional responses are closely related to autonomous physiological responses.

Emotion is reflected in all modes of human communication such as word choice, tone of voice, facial expression, gestural behaviour, posture, skin

temperature and clamminess, respiration, muscle tension, and more (Picard et al. 2001). Picard et al. (2001) elaborate on how emotional recognition systems are most likely to be accurate when they combine "multiple kinds of signals from the user with information about the user's context, situation, goals, and preferences." They suggest "a combination of low-level pattern recognition, high-level reasoning, and natural language processing is likely to provide the best emotion inference" (Picard et al. 2001 p.1176). Consequently, we sought out studies that use any biosensors to measure biodata from subjects objectively.

Many have discussed the importance of the sense of movement in the architecture of historical buildings for evoking senses, such as a sense of awe. Barrie (1996) suggests that surface and textures, scale and distance of entrances, the shifting view as we move along the route, inclines and steps, our peripheral field of vision, and our empathy with the environment (reflected through decorations) are visuo-spatial factors that impact our emotions, and are the essential components of the experience of architecture.

Bruno discusses the interconnection between "sight" and "site" and "motion" and "emotion" while describing emotions in architecture and other arts (Bruno 2007). This means that studies concerned about emotion and architecture should approach architecture as an experience with a "duration" and a "path of movement". It stems from the notion that perception is action-oriented (Gibson 1966). By eliminating movement, studies may be limiting a real exploration of primal physiological responses (Schreuder et al. 2016). We elucidate a research trajectory which can build on existing knowledge in the field with the intention of addressing how movement in a controlled virtual test environment impacts on the physiological responses of participants.

### **3. Method**

#### **3.1. SEARCH PROCEDURE**

A systematic literature review was conducted in order to identify studies relevant to the search objectives and to identify the scope for future research. Due to the recently emerging research in regards to the built environment's impact on neurophysiological responses, the literature review's search terms, exclusion criteria and inclusion criteria required an iterative systematic approach to refine search terms and identify relevant material. There tends to be a discrepancy between recording objective measurements of physiological responses and correlating it as conclusive data of states of "emotion". Due to the limited amount of empirical research in the field, studies which used combined methods that recorded both subjective and objective human responses were considered for examination.

The following inclusion criteria were implemented to ensure the parameters of the literature search were relevant and within the scope of the review. Studies must include the use of objective and subjective methods of recording human physiological responses and experiences. Studies which reported empirical data were included, and studies which were purely theoretical were excluded after screening. The search was limited to investigations of physiological variables



related to the “built environment,” thus excluding social, cultural and behavioural factors and “clinical” studies. Studies should include some form of the virtual environment (VE) such as VR, CAVE, AR or XR as the controlled study environment, but the scope is open to physical spaces or other multisensory media (pictures, films, etc.). Studies should use monitoring equipment such as Electroencephalogram (EEG), Electrocardiogram (ECG), Functional Magnetic Resonance Imaging (fMRI), Galvanic Skin Response (GSR), or other for objective measurements. Studies should include questionnaires, surveys, Self-Assessment Manikins (SAM), Likert scales, verbal responses or other as a form of subjective self-evaluative response. Studies must have participants which are “human” and must exclude “animal” participants. Studies must exclude participants who are considered to be “children” or “elderly”. Due to the novelty of the field, in conjunction with technology’s rapid refinement, the search was limited to studies published between January 1st 2010 and January 1st 2020. Studies were limited to publications which were peer-reviewed. Studies were limited to publications in English.

### 3.2. ELECTRONIC SEARCH STRATEGY

Two electronic databases (ProQuest and Scopus) were identified as dependable directories for empirical studies as both provide advanced search option with the ability to refine inclusion and exclusion criteria. We used the advanced search option available in the electronic databases and implemented the eligibility criteria as was formerly established. Searches were conducted with an established set of keywords and refined through iterations. We screened results based on their titles and abstracts until the results which appeared were no longer relevant to the review. Citations were reviewed of articles which were deemed eligible in order to ensure other relevant referenced studies were identified.

### 3.3. SEARCH TERMS RATIONALE

A similar strategy was implemented for both ProQuest and Scopus and was adjusted to their individual syntax configurations and search restrictions. We identified three relevant groups of search terms: (1) keywords related to the experiments, stimuli, and design variables that are useful for finding studies related to architecture and the built environment; (2) keywords related to “methodologies” for studying human emotional and neurophysiological responses to those stimuli; and (3) keywords related to scientific terms for humans’ responses to external stimuli and the different ways that humans reveal their conscious and unconscious processes. Within each group, we used the “OR” function to expand the search result. Between the groups, we used the “AND” function to limit the number of search results, ensuring that each search result would have at least one keyword from each group of keywords. We searched for the most used keywords in the first search attempt and used them to refine the three groups of keywords. We reviewed those keywords, and the ones that were completely out of the scope of our research were selected. Those selected keywords constructed the fourth (4) keyword group consisting of terms which are to be excluded. It ensured the final results shows only the studies that include at least one keyword from each of the

first three groups and exclude keyword from the fourth group. Resulting in that many irrelevant results were removed from the search. A number of studies were identified via a manual search by examining references of existing studies, in order to mitigate electronic database bias and limitations. We used Google Scholar, and Researchgate websites to manually review the reference list of the selected papers. We explored the articles that have cited those selected papers using tools available on those two websites. It ensured relevant material which was not identified by electronic databases could be included.

### 3.4. MITIGATION OF BIAS

The literature review involves two people refining the method and the reviewing literature to mitigate individual bias. The method was further refined with the aid of two other researchers. Additionally, the search term effectiveness was counselled and filtered with the librarians in the Victoria University of Wellington Faculty of Architecture and Design.

## 4. Results

### 4.1. IDENTIFICATION OF RELEVANT STUDIES

Initially, 3208 results (2956 from ProQuest; 252 from Scopus) were identified based on the established search terms. After a number of iterations, the keyword group (4) consisting of terms which are to be excluded was applied to the databases, resulting in 660 results (545 from ProQuest; 115 from Scopus). After the screening of titles and abstracts and the addition of manually searched studies, a final 24 studies were identified and agreed upon by the authors. These studies underwent a full-text screening, thereby categorizing the main variables in each study in order to identify similar and juxtaposing trends.

Table 1. Details of selected studies which implement “natural walking” in controlled physical or virtual environment settings.

AUTHOR	YEAR	TEST SETTING	OBJECTIVE MEASUREMENT TOOLS	SUBJECTIVE MEASUREMENT	DATA ANALYSIS TECHNIQUE	MOBILE OR NON-MOBILE TESTS	INDEPENDENT VARIABLES
BANAEI ET AL.	2017	Virtual Reality using HMD	EEG 128-channel	SAM	ANOVA	Mobile	Various architectural styles
CHEN ET AL.	2018	Physical Urban Space	EEG / ECG / EMG / GSR	Interview and self-report of physiological state	Qualitative	Mobile	Properties of the surrounding environment
DJEBBARA ET AL.	2019	Virtual Reality using HMD	EEG 64-channel	SAM	ANOVA	Mobile	Size of entrance between two rooms
OJHA ET AL.	2019	Physical Urban Space	EEG / GSR	N/A	REP-Tree decision tree	Mobile	“Normal” VS “Aroused” physiological conditions
YIN ET AL.	2019	Virtual Reality using HMD	ECG / GSR / Eye Tracker / Pulse rate / Blood Pressure	Questionnaires	ANOVA	Mobile	Open space VS enclosed space
HORVAT ET AL.	2019	Virtual Reality using HMD	EEG 14-channel	N/A	Pearson's Correlation Coefficient	Mobile	Virtual environments with fearful images VS happy images

## 4.2. IDENTIFICATION OF STUDIES USING MOBILE NAVIGATION

Our particular interest lies in how moving through a space impacts on human physiological responses and, in turn, their perception of space. From our full-text screening, a number of studies enabled participants to be mobile in the test scenario. The factor leads to the removal of 18 papers, as only six studies tested participants navigating physical or virtual environments by natural walking (Banaei et al. 2017; Chen et al. 2018; Djebbara et al. 2019; Ojha et al. 2019; Yin et al. 2019; Horvat et al. 2018). These six studies (Table 1) form the basis of the discussion section of our paper.

## 5. Discussion

### 5.1. SUMMARY OF FINDINGS

The following is a summary and evaluation of the critical findings which were extracted from the relevant studies.

#### *5.1.1. Test environment independent variables*

By using mobile body-brain sensors on participants during walking, both Chen et al. (2018) and Ojha et al. (2018) use urban scale physical environments in an attempt to understand participants' physiological responses. Horvat et al. (2018) exposed participants to virtual environments with various pictures on a wall with the intent to evoke 'happiness' or 'fear' (Horvat et al. 2018). The study conducted by Djebbara et al. (2019) tested participants' physiological reactions to affordances in transitioning from 'easily passable' and 'non-passable' spaces, in which they argue that affordances in environments impact on the perception of that environment. Banaei et al. (2017) exposed participants to various architectural styles in virtual reality by using mobile brain-body imaging and electroencephalogram while walking. Similarly, Yin et al. (2019) investigated the impacts of open and enclosed spaces by monitoring ECG, GSR, eye tracking, pulse rate and blood pressure of participants. It is evident that there are a variety of valid approaches to studying the impact of architectural space on human physiological responses.

#### *5.1.2. Multisensory test and experiment settings*

Four studies reported using virtual reality environments as their experimental setting (Banaei et al. 2017; Djebbara et al. 2019; Yin et al. 2019; Horvat et al. 2018), allowing participants to inhabit the space through movement using head-mounted displays. Two studies (Chen et al. 2018; Ojha et al. 2019) conduct their experiments in physical urban spaces, where natural walking is included in the tests. All of the studies which utilise virtual reality as the controlled test environment only focus on the impact of visual stimuli (Banaei et al. 2017; Djebbara et al. 2019; Yin et al. 2019; Horvat et al. 2018). Among the ones that are conducted in a physical setting, one study (Ojha et al. 2019) considers the non-visual or multisensory experience of the environment by measuring factors such as the temperature. The signals which can be interpreted

in the built environment are a combination of multisensory information. The tests in physical settings which are multisensory are incapable of identifying the role of each sensory input on body and brain reactions due to the extensive number of variables influencing subjects in the physical tests, and inability to control those variables in a systematic way. In regards to the current technology, acquiring a suitable statistical method for understanding the impact of simultaneous change in environmental variables is necessary.

### *5.1.3. Comparing methods of data analysis*

Of the six selected studies, three used ANOVA (Banaei et al. 2017; Djebbara et al. 2019; Yin et al. 2019) as the mode of data analysis. REP-Tree (Ojha et al. 2019) and Pearson's Correlation Analysis (Horvat et al. 2018) were also implemented, with one study (Chen et al. 2018) using qualitative data analysis presented in diagrams. From this, it is evident that there is no standard for analysing data and predicting correlations; each study establishes its own parameters and explores the outcomes within the boundaries of its own scope. This means that individual case studies have different parameters and different baseline conditions, which inherently results in incompatible data. In experiments which use monitoring equipment such as EEG, ECG, fMRI and GSR, movement may cause noisy data, so is often avoided. Instead, most studies measure the physiological responses of people in static positions. It can be a limitation, as motion is a crucial part of making sense of any given haptic built environment. The majority of the six selected studies use Independent Component Analysis (ICA) to eliminate noise from raw EEG data recorded from the participants. ICA is a computational method for extracting underlying components from a multivariate signal. Hence, there is a way to mitigate the effect of movement in test scenarios; the inclusion of movement as a parameter in this field should continue to be explored in future studies. While all six studies have some form of objective data measurements such as EEG, ECG, EMG, GSR or fMRI, two studies (Ojha et al. 2019; Horvat et al. 2018) do not report any subjective self-reflection. There is undoubtedly a layer of information which can be gained from subjective self-reflection of experiences in the test environments. This inconsistency in procedure between studies makes it difficult to correlate data and make conclusions across studies.

### *5.1.4. Population sample sizes and demographics*

The selected studies had a range between 4 (Chen et al. 2018) and 30 (Ojha et al. 2019; Yin et al. 2019) participants. None of the studies reports equal numbers of male and female participants, with some disproportionately favouring one of the two groups (Horvat et al. 2018; Yin et al. 2019). Two studies failed to report on the participants' gender at all (Ojha et al. 2019; Chen et al. 2018). A larger sample of data needs to be acquired in order to see whether there is even potential in claiming that physiological responses are universal. However, by analysing these few subjects, the conducted tests have been able to show statistical significant differences in body and brain reactions of the participants. Additionally, the majority of studies suggest hiring subjects that do not have extensive knowledge in the field of architecture to minimise the effect of that factor on the response.

## 5.2. LIMITATIONS OF CURRENT METHODOLOGIES

Although a growing body of research has been published, this research field is still at the primary stages of its inception, which requires iterations of research. In future studies, more scientifically rigorous studies are needed to measure the effectiveness and accuracy of virtual reality for eliciting mental and emotional reactions akin to real-world scenarios. There is a general lack of evidence on realism within the simulations in virtual reality tests. This lack of immersion could create an element of disbelief in participants, altering the physiological reactions, and thus, the emotional responses. For example, the impact of the frame rate drop down in virtual reality setups that cause motion sickness is not discussed in the articles reviewed. Furthermore, many studies place participants in a passive role instead of an active one, and since perception is action-oriented, the way in which participants interact in the virtual environment can manipulate the body-brain interaction. By designing tests that engage people with activities in the physical or virtual environments, the outcomes may provide a more accurate dataset for understanding emotional responses. The limitations in the number of participants and the amount of data collected from them do not allow for the identification of direct interrelation between the built environment as a stimulus and the subjective and objective data of emotional reactions. A more rigorous approach is required to examine the way movement activates emotion in our experiences of built environments.

## 5.3. TRAJECTORY FOR INTENDED RESEARCH

Based on the discussion outlined above, we have identified a significant gap in the current research which requires a more robust body of evidence for conclusions to be made about the impact built environments have on emotion. We will focus on three less-investigated factors that we presume have a high potential to manipulate emotions: visual complexity, scale, and light. We argue that these factors have been utilised in the design of notable architectural buildings intuitively through history. Considering some theories of emotions which claim all emotions are capable of being mapped to a two-dimensional scale (Schachter & Singer 1962), we will investigate how characteristics of space can evoke various emotional states such as a sense of awe in humans. We assume that by maximising emotional arousal and pleasure levels, we will be able to elicit these emotions in users of a space. As an emotion which has been evoked from architecture for millennia, understanding awe could be the next step in understanding how architecture can elicit immense physiological and emotional responses. Central to the question of which characteristics of architectural space evoke awe and what features of architectural space can produce emotional arousal? Conversely, is there a way architects can remove stress from the environment by utilising virtual environments when designing the scenarios for inhabitants to experience?

We argue that using VR would be a solution for isolating visual stimuli for scientific investigations. Architectural texts suggest the importance of movement and motion in perception and emotion (Rasmussen 1964). In recent literature, only a small number of studies have tried to measure the emotional and physiological

responses of a built environment experience while participants are walking through those virtual or physical environments. By utilising VR, we will be able to measure and investigate the body and brain reactions of people that naturally walk in a controlled test setting. The majority of current studies suggest that multimodal biometric data and synchronisation between them contribute to the decoding the emotions of architectural experiences. Therefore, we will measure various biodata by acquiring simultaneous data from various biosensors such as EEG, GSR and Eye tracking. Our strategy for noise reduction in data includes using mathematical algorithms to eliminate noise and extract meaningful data from raw biodata. To study the interrelation between our interventions and high dimensional data gathered from biosensors, we will use advanced statistical methods such as machine learning classifications. Based on the Constructivist theory of learning, we learn through experience, which is a critical point in this matter. We have to consider that, as Piagetian theory of learning suggests (Piaget 1952), the brain may react to any external stimuli based on the culmination of all previous experiences. It means that a level of expectation in any test or experience can play an essential role in the emotional and physiological reactions. It also indicates the importance of the impact of short-term and long-term memories in future studies. We hope to investigate how expectations, or inversely, subversions of expectations in the built environment impacts physiological responses.

## 6. Conclusion

A small number of studies have emerged as a result of recent advancements in technology. These technologies pave the way for a better understanding of the interrelation between the built environment and the people who occupy it. Recent studies suggest that parameters such as open space versus enclosed space or even architectural style of an interior form can cause significant differences in neurophysiological reactions. Using portable and lightweight body-brain sensors have helped researchers to study the impact of external stimuli on people during move and stroll. It has brought a unique opportunity for researchers in the field of architecture to scientifically study emotion and come up with criteria and guidelines for the architectural design process. Moreover, modern statistical data analysis methods have helped those researchers to overcome the challenges of analyzing the raw and noisy biometric data. To conclude, since the field is still novel and anomalous, more studies need to be conducted in order to piece together the intricate way we perceive our built environment.

## References

- Banaei, M., Hatami, J., Yazdanfar, A. and Gramann, K.: 2017, Walking through architectural spaces: The impact of interior forms on human brain dynamics, *Frontiers in Human Neuroscience*, **11**, 1-14.
- Barrie, T.: 1996, *Spiritual Path, Sacred Place*, Shambhala.
- Bruno, G.: 2007, *Atlas of Emotion: Journeys in Art, Architecture, and Film*, Verso.
- Cannon, W.B.: 1927, The James-Lange theory of emotions: a critical examination and an alternative theory, *The American Journal of Psychology*, **39**, 106-124.
- Chen, Z., Schulz, S., Qiu, M., Yang, W., He, X., Wang, Z. and Yang, L.: 2018, Assessing affective experience of in-situ environmental walk via wearable biosensors for

- evidence-based design, *Cognitive Systems Research*, **52**, 970-977.
- Djebbara, Z., Fich, L., Petrini, L. and Gramann, K.: 2019, Sensorimotor brain dynamics reflect architectural affordances, *Proceedings of the National Academy of Sciences of the United States of America*, **116**(29), 14769-14778.
- J.P. Eberhard (ed.): 2008, *Brain Landscape: The Coexistence of Neuroscience and Architecture*, Oxford University Press.
- Eberhard, J.P.: 2009, Applying Neuroscience to Architecture, *Neuron*, **62**(6), 753-756.
- Gibson, J.: 1966, *The Senses Considered as Perceptual Systems*, Praeger.
- Horvat, M., Dobrinić, M., Novosel, M. and Jerčić, P.: 2018, Assessing emotional responses induced in virtual reality using a consumer EEG headset: A preliminary report, *41st International Convention on Information and Communication Technology, Electronics and Microelectronics (MIPRO)*, 1006-1010.
- James, W.: 1884, What is an Emotion?, *Mind*, **9**(34), 188-205.
- Kahn, L. and Brillembourg, C.: 1992, "Louis Kahn by Carlos Brillembourg [Architecture: Interview]" . Available from <<https://bombmagazine.org/articles/louis-kahn/>> (accessed 1st December 2019).
- Lanzetta, J.T., Cartwright-Smith, J. and Kleck, R.E.: 1976, Effects of nonverbal dissimulation on emotional experience and autonomic arousal, *Journal of Personality and Social Psychology*, **33**(3), 354-370.
- Ojha, V.K., Griego, D., Kuliga, S., Bielik, M., Buš, P., Schaeben, C., Treyer, L., Standfest, M., Schneider, S., König, R., Donath, D. and Schmitt, G.: 2019, Machine learning approaches to understand the influence of urban environments on human's physiological response, *Information Sciences*, **474**, 154-169.
- Piaget, J.: 1952, *The origins of intelligence in children*, W W Norton & Co.
- Picard, R.W., Vyzas, E. and Healey, J.: 2001, Toward machine emotional intelligence: analysis of affective physiological state, *IEEE Transactions on Pattern Analysis and Machine Intelligence*, **23**(10), 1175 - 1191.
- Rasmussen, S.E.: 1964, *Experiencing Architecture, Second Edition*, The MIT Press.
- Robinson, S.: 2015, John Dewey and the dialogue between architecture and neuroscience, *arg: Architectural Research Quarterly*, **19**(4), 361-367.
- Schachter, S. and Singer, J.: 1962, Cognitive, social, and physiological determinants of emotional state, *Psychological Review*, **69**(5), 379-399.
- Schreuder, E., Erp, J.V., Toet, A. and Kallen, V.L.: 2016, Emotional Responses to Multisensory Environmental Stimuli: A Conceptual Framework and Literature Review, *SAGE Open*, **6**(1), 1-19.
- Yin, J., Arfaei, N., MacNaughton, P., Catalano, P.J., Allen, J.G. and Spengler, J.D.: 2019, Effects of biophilic interventions in office on stress reaction and cognitive function: A randomized crossover study in virtual reality, *Indoor Air*, **29**(6), 1028-1039.

# VR UNMATCHED

## *Leveraging Non-experts as Co-Urban Designers*

MARC AUREL SCHNABEL<sup>1</sup> and SHUVA CHOWDHURY<sup>2</sup>

<sup>1,2</sup>*Victoria University of Wellington*

<sup>1</sup>*marcaurel.schnabel@vuw.ac.nz* <sup>2</sup>*shuva.chowdhury22@gmail.com*

**Abstract.** The recent development in Virtual Reality (VR) allows for novel engagement in participatory urban design. Despite that any design approach cannot include and address all items that are relevant or needed during a design process, social VR design instruments offer additionality via their real-time generation and visualisation possibilities that are unmatched in conventional realms. The research employs an anthropogenic approach to design research to engage end-users in the design process. An Immersive Virtual Environment (IVE) instrument ‘SketchPad’ allows laypersons to design successfully urban forms. SketchPad engaged laypersons in a meaningful design discussion and generations of urban spaces. The research discusses the findings of the experiments. The paper concludes with a reflection of how non-experts as co-designers can use IVE instruments to drive change of their neighbourhood proactively and to positively impact on the liveability of their neighbourhood.

**Keywords.** SketchPad; Co-design; Layperson; Design Participation; Urban Design.

### **1. Introduction**

Involving non-experts with an enhanced communication instrument in a design process brings their imagination to an understanding level of interpretation for themselves and the experts. In an urban design decision-making process, public participation is an established method to bring accountability (Healey 1998; Murray et al. 2009). However, due to the lack of a suitable design communication instrument, in most cases, the design ideas stay in assumption (Al-Kodmany 2001). Also, the lack of suitable visual information and instruments in the design process prevents the non-expert stakeholders from taking part in design with sufficient perceptual understanding of the design context. On the other hand, the conventional urban design process does not allow them to take part in the design ideation and generation stage. Therefore, the research speculates that an Immersive Virtual Environment (IVE) instrument called ‘SketchPad’ (Innes et al 2017; Innes 2018) can enable non-experts to actively take part in the early stage of an urban design process.



The research starts with understanding the urban design situations of a case study in Karori, a suburb of Wellington, New Zealand. A series of surveys and experiments are set up to investigate the scope of non-experts' active design ideation, generation and collaboration in neighbourhood design. The methodology incorporates a preliminary survey of urban design consultation, developing the VR instrument, engaging laypersons in IVE urban design, a survey on IVE experiment, an audio recording of the design conversation, transcribing recorded data, protocol analysis and expert evaluation (Figure 1). An extended report of the protocol analysis and the detail of the development of 'SketchPad' are published in Chowdhury and Schnabel (2019) and Innes (2018) respectively.

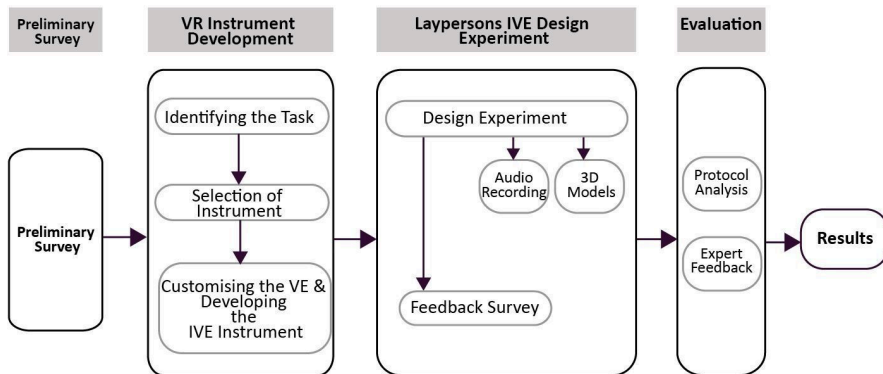


Figure 1. Research Methodology.

The results of the design experiment show that the Virtual Reality (VR) design setup provides effective perceptual affordance for laypersons to take design decisions on urban forms. The designers get into design discourse through the frequent insertion of design ideas and accepting one another ideas. The virtual perceptual environment is helping them to initiate new ideas and got into design discourse. It also shows that the design conversation extended beyond the task-related conversation, which indicates the continuity of the conversation was natural instilling flow. Occasionally, through the inclusion of jokes, the designers instigate new design ideas, which give opportunities to act socially with fellow design members. In the end, the research hypothesises that the design setup also can be useful to involve diverse stakeholders along with urban professionals in the discussion of urban design.

## 2. Using 3D Artefacts in IVE Design Collaboration

Traditional artefacts such as drawings, product samples, models, and now virtual artefacts as 3D models are used to mediate the journey of a building concept to the actual built form. Most often, these artefacts are produced for different purposes and obviously for people with different levels of understanding of the design and construction process. Luck (2007) argues that design practice using physical artefacts at the early stages of building design is appropriate for design

conversation, as it develops users' understanding of the design. The design conversation builds the user's confidence in the appearance of the design, rather than only by the ability of the artefacts to represent a future reality. The artefacts embody the current knowledge of the design in its present status, but during a conversation, it prompts discussion of ideas to modify the design. 'The act of interpretation' is acting as a part of the design process.

Design is a series of decisions which expose the relationships of geometries, materials and performance (Kan and Gero 2017). Designing as a cognitive activity entails the production of sequential representations of mental and physical artefact (Goldschmidt 2004). Designers always seek suitable means to construct imagination, express design concepts and turn the concept into visible artefacts (Chan 2011). Brown (2003) argues that the design representation is coupled with the content of the virtual environment, which involves perceptual experience, and the design generation of 3D artefacts involves direct manipulation of mental images. Abstract 3D artefacts represent instant design ideations and generations. The abstract format of the design representation instigates a meaningful urban design discourse between laypersons. It does not consider another format of design representation like paper-pencil methods, 3D models, or computer-generated images.

One of the prime factors in IVE assisted design collaboration is perceptual awareness (Maher 2011). Participants in the collaborative design process coordinate and inform their activities through peripheral awareness of the surrounding context and one another's activities. Designers move fluidly from individual working status to collaborative working status. IVE offers an active interaction with the design, therefore presenting an authentic feeling of being in the environment (Schnabel & Kvan, 2003). It leverages users to create, communicate and collaborate during the design process. Spontaneous generation of 3D artefacts in IVE enhances the design collaboration with acts of design actions and simultaneous discussion as reflections.

Portman, Natapov, and Fisher-Gewirtzman (2015) argues that the dimensions of immersion and interactivity of VR with 3D artefacts allow new possible ways of "exploration" which fits with the characterization of environmental planning and landscape architecture as a tool that enables going beyond, in some sense, existing reality. Such exploration empowers designers to express and explore their imagination with greater ease.

### **3. Experimental Procedure, Task and Participant**

An experimental setup is developed to facilitate design collaboration. In Figure 2, the design unit is formed between the two participants and how technology is used to facilitate the design, communication and socialisation - the first participant designs by being immersed in the environment via a Head-Mounted Display (HMD). The second participant experiences the whole scenario in real-time on the 80-inch display screen. All participants are local residents who were recruited through social media and poster billed in the neighbourhood. The in-situ experimental setup is shown in Figure 3.

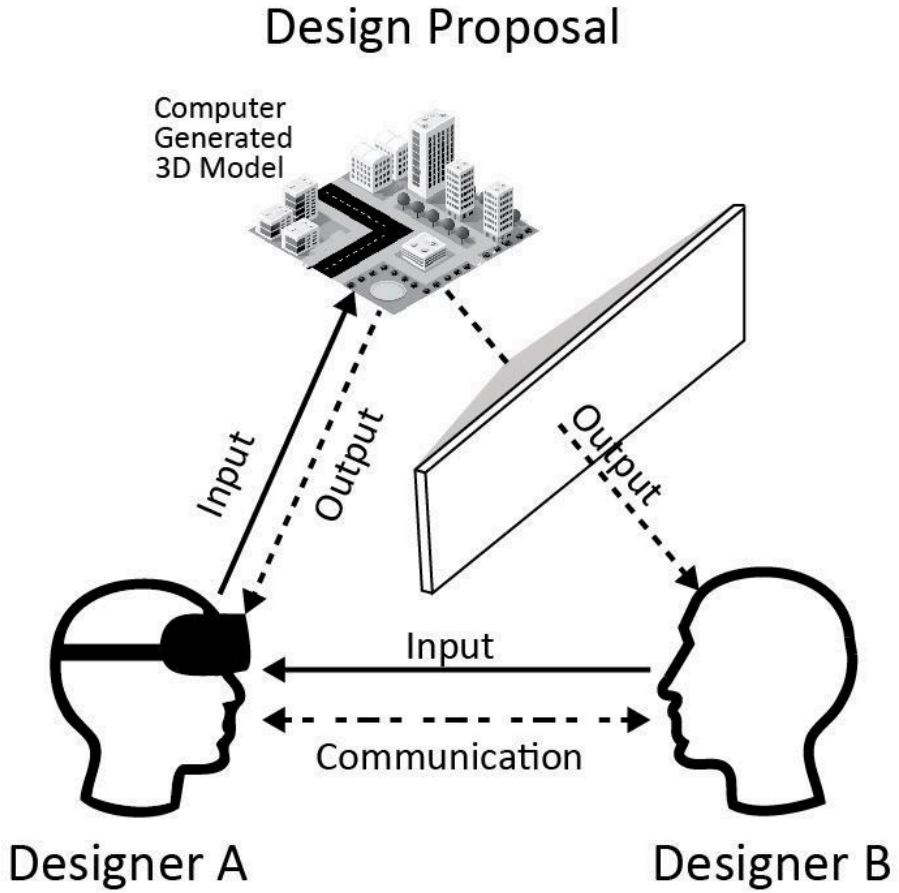


Figure 2. The design unit.

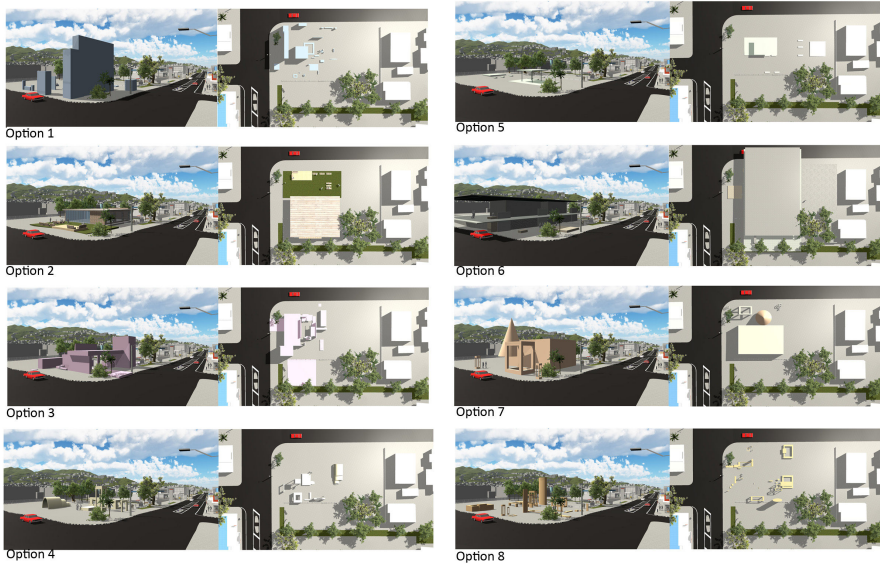


Figure 3. The in-situ experimental setup.

The design task was an actual and current urban development scenario of Karori. The participants were asked to design building blocks on an empty corner plot in Karori's Centre (Figure 4). The participants were introduced to the instruments and site conditions via a map laying out the urban conditions. The design conversations were recorded for protocol analysis, and the urban design proposals were saved for experts to evaluate. The total number of participants is 17. Figure 5 shows the generated design options.



Figure 4. Design experiments in Karori Community Centre. .



#### OUTCOMES

1. OPTION 1: MIXED-USE URBAN PARK – 2 PARTICIPANTS.
2. OPTION 2: OUTDOOR CAFÉ AND EVENT SPACE – 2 PARTICIPANTS.
3. OPTION 3: MIXED-USE URBAN PARK – 4 PARTICIPANTS.
4. OPTION 4: PLAYGROUND – 2 PARTICIPANTS.
5. OPTION 5: NIGHT-MARKET, FOOD STALL, COMMUNITY EVENT CENTRE – 2 PARTICIPANTS.
6. OPTION 6: MIXED-USE RETAIL SPACE AND CAFÉ – 3 PARTICIPANTS.
7. OPTION 7: PLAY CENTRE – 2 PARTICIPANTS.
8. OPTION 8: URBAN PARK – 2 PARTICIPANTS.

Figure 5. Generated design options.

## 4. Design Communication

The recorded conversation is transcribed to analysis the design conversation through protocol analysis. Based on Tsai et al. (2009), a coding scheme was developed to evaluate virtual design communication and collaboration. The four major categories of the scheme are i) Communication control, ii) Design communication, iii) Social communication and iv) Communication technology. Please refer to the details of the coding to Chowdhury and Schnabel (2019).

The result shows that there was clear evidence of successful design communication happened between the participants (Figure 6). Around 62.37%, 62.79% and 46.51% of the conversation respectively for Options 2, 4 and 7 happen about deriving the design concept. It indicates that the experiment facilitated the scope of collaborative design ideation. Similarly, frequent non-task-related of social communication took place that supports the presence of social communication (Figure 7). Almost 75.76 %, 16.67% and 80.52% of the conversation respectively for Option 2, 4 and 7 occur as non-task related social communication. It indicates the design actions generated by Designer A is successfully communicated to Designer B and vice versa leading to a meaningful

overall outcome.

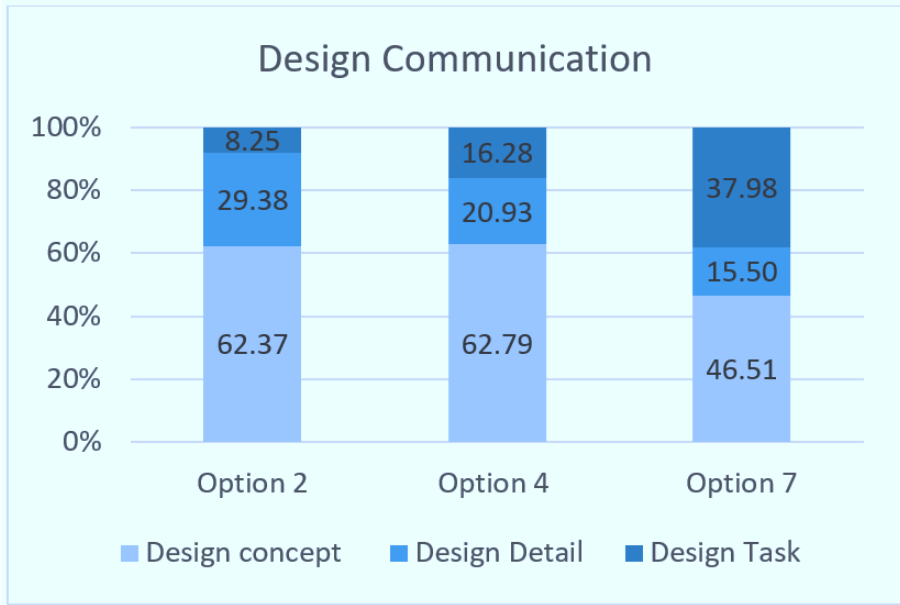


Figure 6. Design Communication.

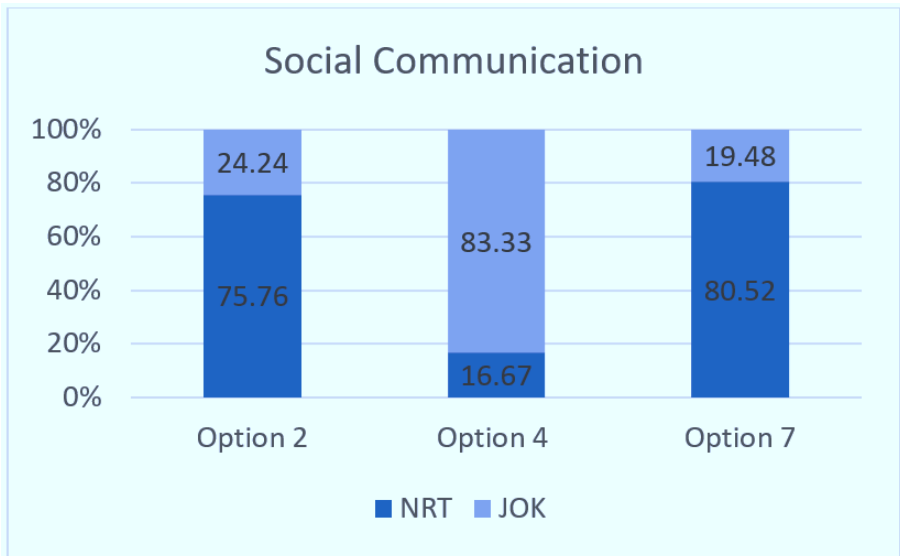


Figure 7. Social Communication.

## 5. Design Interaction

The IVE instrument SketchPad is designed to produce iterative 3D artefacts through design interaction and collaboration. Design imagination happens due to the contextual information, iterative production of 3D artefacts, and the user-friendly nature of SketchPad. The continuity of design production can be traced in the verbal conversation. The designers form internal mental models of themselves by interacting with the environment, with others, and with the artefacts of the technology. According to Norman (1988), such a process of mental modelling is one kind of interaction. In the line of Norman's concept, the employed immersive iterative 3D artefacts provide predictive and explanatory power for understanding the interaction.

The design discussion progressed when every action of a designer produced visual information and initiated the next level of design action. This can only be done if the design communication media provide continuous visual feedback to the designer. It informs successful design interaction. Following Fuchs et al. (2011) interaction techniques for 'Virtual Behavioural Primitives', the design interaction occurs in all of the four categories, where the designers observe, move, act, and communicate with others and also with the application for its virtual interface. It is the result of successful completion of the loop between "perception, cognition, and action." Also, this aligns with Brown (2003) arguments that interaction between the designer and graphical physical descriptions is a necessary part of an effective design process. Here, the designers' ability to produce urban forms meet the performance goals to a certain level including visual, technical, cultural, and social.

The employed VE design process reflects through action and negotiation between designers. According to Schön (1983), the design process is fluid and determined upon the designers' knowledge and experience, where designers continuously reflect on their strategies and actions to change the design situation. Design communication happens due to the presence of design interactions. It is the result of human-computer interactions, where the computer is producing 3D artefacts in the IVE and provides visual feedback of the design actions and initiates design discussion among designers. The assigned design tasks and limitation of the instrument helped the designers to formulate new design alternatives for Karori's centre.

## 6. Discussion

Through engaging non-experts, the research impacts on the perceptual affordance created through the interaction of virtual 3D artefacts, immersive, non-immersive visual information and verbal conversation. Participants actively take part in the design ideation and generation stage. In between their conversation, the computer produced 3D urban forms which provide visual feedback to continue the discourse. In contrast to Lefebvre, here the non-experts are designing in the abstract space, where they usually participate in concrete space (Luck, 2007). That means the VR instrument SketchPad is facilitating design participation, which is re-joining the scope of non-expert's role to the expert's role. The report of the protocol

analysis also shows that design communication happened regarding task-related design actions. It means the participants took design decision through their actions. Moreover, the experts' evaluation legitimises the design outcomes as products of meaningful design participation.

Conventionally, participatory design activities are dealt with urban professionals in a media either resembles a 'paper and pencil'-method, models or a non-immersive game-based virtual environment. On the contrary, the research shows that the end-users are actively and constructively involved in the discussion by being perceptually inhabited in the urban context. The IVE instrument Sketchpad and the anthropogenic experiment's set-up helped laypersons to decide on specific perceptual qualitative parts of urban form through collaboration. The research facilitates design discourse through visual and verbal interaction. The here presented participatory design setting empowers the participants to design building forms, shapes, textures and also their placements in the real contexts. So, end-users are acting as a co-designer together with experts of an urban design process. It seems the roles of designers and laypersons are coming to a level where the laypersons can create and propose design ideas through collaboration with lay- and expert-designers. The participatory mindset values people as co-creator in the design process. This participatory and anthropogenic design approach is bridging the gap between designers and users.

## References

- Al-Kodmany, K.: 2001, Visualization tools and methods for participatory planning and design, *Journal of Urban Technology*, **8**(2), 1-37.
- Brown, A.: 2003, Visualization as a common design language: connecting art and science, *Automation in Construction*, **12**(6), 703-713.
- C.-S. Chan (ed.): 2011, *Design representation and perception in virtual environments*, Springer.
- Chowdhury, S. and Schnabel, M.A.: 2019, Laypeople's Collaborative Immersive Virtual Reality Design Discourse in Neighborhood Design, *Frontiers in Robotics and AI*, **6**, pgs 97.
- Cross, N. and Cross, A.C.: 1995, Observations of teamwork and social processes in design, *Design Studies*, **16**(2), 143-170.
- Fuchs, P., Moreau, G. and Guitton, P.: 2011, *Virtual reality: concepts and technologies*, CRC Press.
- G. Goldschmidt (ed.): 2004, *Design representation: Private process, public image*, Springer.
- Healey, P.: 1998, Collaborative planning in a stakeholder society, *Town planning review*, **69**(1), 1.
- Innes, D.: 2018, *Virtually Handcrafted: An Investigation of Immersive Architectural Design Processes*, Master's Thesis, Victoria University of Wellington.
- Innes, D., Moleta, T. and Schnabel, M.A.: 2017, Virtual Inhabitation and Creation: A Comparative Study of Interactive 1:1 Modelling as a Design Method, *DADA 2017 International Conference on Digital Architecture: "Digital Culture"*, Nanjing, 402-408.
- Kan, J.W.T. and Gero, J.S.: 2017, *Quantitative methods for studying design protocols*, Springer.
- Luck, R.: 2007, Using artefacts to mediate understanding in design conversations, *Building Research & Information*, **35**(1), 28-41.
- M.L. Maher (ed.): 2011, *Designers and collaborative virtual environments*, Springer.
- Murray, M., Greer, J., Houston, D., McKay, S. and Murtagh, B.: 2009, Bridging top down and bottom up: Modelling community preferences for a dispersed rural settlement pattern, *European Planning Studies*, **17**(3), 441-462.
- Norman, D.A.: 1988, *The psychology of everyday things*, Basic books, New York.



- Portman, M.E., Natapov, A. and Fisher-Gewirtzman, D.: 2015, To go where no man has gone before: Virtual reality in architecture, landscape architecture and environmental planning, *Computers, Environment and Urban Systems*, **54**, 376-384.
- Schnabel, M.A. and Kvan, T.: 2003, Spatial understanding in immersive virtual environments, *International Journal of Architectural Computing*, **1**(4), 435-448.
- Schön, D.A.: 1983, *The reflective practitioner: How professionals think in action*, Basic Books, New York.
- Tsai, J.J.-H., Wang, X. and Huang, Y. 2009, Protocol Analysis of Collaborative Designs of Different Scales in Real and Virtual Environments, in N. Gu, M.J. Ostwald and A. Williams (eds.), *Computing, Cognition and Education: Recent Research in the Architectural Sciences*, ANZAScA, Australia, 233-245.

# URBAN WELLBEING, AS INFLUENCED BY DENSIFICATION RATES AND BUILDING TYPOLOGIES

*A Virtual Reality Experiment*

YAALA TROSSMAN HAIFLER<sup>1</sup> and  
DAFNA FISHER-GEWIRTZMAN<sup>2</sup>

<sup>1,2</sup>*Technion – IIT*

<sup>1</sup>*yaalat@campus.technion.ac.il* <sup>2</sup>*ardafna@ar.technion.ac.il*

**Abstract.** Urban morphology significantly impacts resident's wellbeing. This study examines the impact of urban environments on the sense of wellbeing, using virtual reality as a research tool. Participants were presented with simulated pedestrian movement through 24 virtual urban environments. The environments differed by density level, vegetation, and commercial activity. Participants assessed each alternative through structured questionnaires. The relationship between the participants' feelings and densification levels, vegetation, and commercial activity was analyzed. Densification levels independently predicted participant's wellbeing. An increase in density levels predicted a decrease in the participants' sense of belonging and wellbeing. At all levels of density, the presence of commercial activity predicted a higher sense of belonging. Density, vegetation and commercial activity had a significant impact on the participants' wellbeing. Extreme densification had a negative effect on the participants' feelings; but vegetation and commercial activity, especially at high-density levels, improved this feeling.

## 1. Introduction

Fifty-five percent of the world's population lives in urban localities; and it is expected that in two decades, more than 70% of the total population of the planet will be city dwellers (Fisher-Gewirtzman 2017). The link between urban planning practices and the wellbeing of inhabitants has been conclusively established in research (Martin and March 1972). Numerous studies have sought to identify the design principles which positively reflect user needs (Hawley 1963, Martin and March 1972, Rapoport 1977, Lynch 1984, Fisher-Gewirtzman and Wagner 2003, Fisher-Gewirtzman 2017). In densely populated areas, carefully considered architectural and urban design practice are critical tools for ensuring a quality living environment and broader wellbeing (Bardhan, Kurisu et al. 2015). However, it must be noted that urban morphology and dense residential developments-an inevitable consequence of population growth-have a complex relationship, an important role in shaping urban space (Cheng 2009).

Urban density has a crucial impact on various aspects of quality of life. It can adversely affect its residents (the perception of the historic city as noisy, dirty, crime-ridden, and an incubator of disease). But when carefully planned, the high density urban environment can facilitate significant quality-of-life benefits including educational facilities, cultural infrastructure, vibrant commercial activity, and livelihood opportunities (Carmon 1999). In addition, when balanced urban growth policies are in place, dense cities have the potential to support a higher quality of wellbeing (Bardhan, Kurisu et al. 2015). It is not enough to build new neighborhoods according to demand; emphasis must be placed on design and planning practice that acknowledges and complements urban wellbeing (Amir and Carmon 1996, Pedan 2014).

Density is defined in various ways, generally in relation to the ratio of the housing units to the land area. According to Fisher-Gewirtzman (Fisher-Gewirtzman, Burt et al. 2003), density has both quantitative and qualitative parameters. The latter are related to demand and convenience with respect to privacy, texture, color, odor, quality of life, nostalgia, and other physical and psychological aspects influencing perceptions of density. Gewirtzman agrees that existing methods of measuring density as a forecasting and evaluation tool is suitable for architectural planning at the macro, city and region levels; but with regard to dense urban environments, perceived density is equally influenced by the accumulated 3-D visibility from each viewpoint in a built-up environment (Fisher-Gewirtzman et al, 2003).

The effect of vegetation on perceived density and wellbeing has been examined in earlier research (Wolch, Byrne et al. 2014, Gilchrist, Brown et al. 2015) and found to increase the sense of wellbeing. However, the effect of commercial activity on wellbeing is yet to be examined, as too the interplay between vegetation, commercial activity, and density. The current study explores the impact of commercial activity (shops, cafes) and vegetation in urban environments on the wellbeing of residents.

Wellbeing is strongly influenced by urban planning (Martin and March 1972, Adkins, Dill et al. 2012), and extensive research has been directed toward defining the relevant factors (Hawley 1963, Lynch 1972, Martin and March 1972, Rapoport 1977, Fisher-Gewirtzman and Wagner 2003, Fisher-Gewirtzman 2017). In order to promote an overall high quality of life for residents, architectural design and urban design should incorporate such identified factors (Bardhan, Kurisu et al. 2015). The present study explores some features of the morphology of urban densified areas, and their effect on wellbeing. What aspects of general morphology promote a higher sense of wellbeing; what is the density threshold beyond which wellbeing is impaired; and how can planning practice contribute to general wellbeing, even in high-density environments?

Previous studies defined a framework that combined urban morphology, spatial human behavior, and the use of the VR lab as an effective research tool for analyzing complex urban situations (Natapov and Fisher-Gewirtzman 2016; Fisher-Gewirtzman 2018). The study presented in this paper is based on a behavioral experiment in virtual reality (VR) laboratory (Kuliga, Thrash et al. 2015, Portman, Natapov et al. 2015, Natapov and Fisher-Gewirtzman

2016, Shushan, Portugali et al. 2016, Kaya and Mutlu 2017, Fisher-Gewirtzman, 2018. Fisher-Gewirtzman, 2019 ). Design alternatives, differentiated by variable parameters (density, commercial activity, vegetation) for an urban environment were presented to research participants via a VR interface. The experiment was based on an existing case study, a Tel Aviv street undergoing urban renewal-and consequently, densification.

## 2. Objective

The principal objective of this research study is a consideration of the relationship between different forms of urban densification, vis-à-vis the wellbeing of subjects (potential residents), in an existing urban environment.

Research participants were asked to evaluate a number of virtual environments, characterized by differing levels of density, vegetation, and commercial activity, by means of a structured questionnaire.

The goal was to identify planning principles configuring spatial/geometric solutions responsive to the needs of potential residents, specifically the sense of wellbeing. Such principles can play a key role in the planning and design of existing urban environments undergoing densification, and the planning and design of urban environments in the future.

## 3. Research method

The research study comprised a controlled experiment in a visualization laboratory; statistical analysis of the results; and extraction of design criteria which could inform future densification processes, placing emphasis on the wellbeing of inhabitants. After approval by the Institutional Ethics Committee (obtained under study 1485/15), the experiment was conducted in the Virtual Reality Laboratory (VisLab) of the Faculty of Architecture and Urban Planning at the Technion.



Figure 1. The VizLab during an experiment.

The methodology was chosen on the basis of earlier research conducting laboratory experiments, and on the use of virtual reality to investigate space perception and behavior (Conroy-Dalton 2002, Portman, Natapov et al. 2015, Natapov and Fisher-Gewirtzman 2016, Fisher-Gewirtzman 2018). 76 students at the Technion-Israel Institute of Technology participated in the study. Their average age was 25.9 (5.2) years. 44 (59.5%) participants were female and 65 (86.7%) participants were single. Each participant spent approximately 45 min at

the VizLab.

Bloch Street, a medium-sized street currently experiencing significant urban renewal, was identified as a typical representation of urban densification and renewal processes in downtown Tel Aviv. Most of the buildings on Bloch Street were built during the 1950s and 1960s. They are characterized by a pillar-ed street floor plan facing the street, some housing several ground floor apartments and some with basements. The building form is characterized by several balconies around the building, some single dwelling units having up to 3 balconies. Typical street construction types are represented in the three-dimensional model of density X (existing condition), and will be presented in the section describing the 3-D models (see Figure 2)



Figure 2. Bloch St., Tel Aviv-actual and VR representations.

### 3.1. EXPERIMENT DESIGN:

The six densification alternatives are as follows (see Figure 3):

Scenarios were based on fixed parameters and variables. The constants were the street area and width; the variables were density levels, built morphology, considered in combination with the presence or absence of vegetation and/or commercial activity. 24 videos were prepared; these simulated pedestrian movement across the six densification modes, combined with the four vegetation and/or commercial activity options. The six densification alternatives are as follows (see Figure 3):

1. EXISTING CONDITION (X) (shown in the diagrams as A): The existing condition, used as a reference point for the other planning alternatives. Built-up volume was calculated in units of cubic meters.
2. DOUBLE HEIGHT (2X) (based on Israeli urban renewal principles, shown in the diagrams as B): Each building in the virtual model was added with 2 typical floors and on top of them 2 floors retreat backwards. This typical street style maintained the building's original characteristics.
3. MERGING ALL PLOTS (3X) (shown in the diagrams as C): All plots along the street were merged into one contiguous block. This morphology resembles that found in many European cities, and has no spaces between buildings.
4. MERGING 2 PLOTS + TOWERS (4X) (8 or 18 stories high, shown in the diagrams as D): Provides a varying street section.
5. MERGING ALL PLOTS + TOWERS (5X) (shown in the diagrams as E): Merging all the plots (3 above), interspersed with towers in order to increase density.

6. TOWERS (6X) (shown in the diagrams as E): This alternative is based on the merger of each 2 plots, creating towers of similar height in each combined plot. 18 stories high, this formed a sequence of towers along the street. This alternative presents the most extreme state of densification in the case study.

	NO VEGETATION NO COMMERCE	NO VEGETATION WITH COMMERCE	WITH VEGETATION NO COMMERCE	WITH VEGETATION AND COMMERCE	DENSITY LEVEL	MORPHOLOGY	VOLUME DESIGN
<b>A</b>					<b>X</b>	EXISTING CONDITION	
<b>B</b>					<b>2X</b>	DOUBLE THE HEIGHT	
<b>C</b>					<b>3X</b>	MERGING ALL PLOTS	
<b>D</b>					<b>4X</b>	MERGING 2 PLOTS + TOWERS	
<b>E</b>					<b>5X</b>	MERGING ALL PLOTS + TOWERS	
<b>F</b>					<b>6X</b>	TOWERS	

Figure 3. The alternative environments, outlining density levels, vegetation, and commercial activity.

### 3.2. THE QUESTIONNAIRES:

In order to identify the parameters influencing feelings of comfort and security, and the (hypothetical) attraction of the research subjects to a certain type of neighborhood, we sought to understand how they felt in each of the density options, combined with the commerce and vegetation options. We developed a questionnaire which assessed the individual's perceptions of these factors. The questionnaire comprised of 10 closed questions, rated on a scale of 1-7. The questions focused on a variety of topics: Belonging vs. Alienation; Vibrant vs. Boring; Dense vs. Spacious; Bright vs. Dark; Calming vs. Stressful

The questionnaire was made up of five pairs of meaningful questions, directed toward validating participants' perceptions and feelings (Nishio and Ito 2019). The questions were presented in random sequence, in order to increase the reliability of the answers.

The research environment: The experiment was conducted in a controlled environment at the (Vislab) Visualization Laboratory of the Faculty of Architecture and Urban Planning at the Technion. The laboratory is equipped with a 2.4x7.5-meter concave screen with a 75-degree viewing field, and three coordinated HD projectors which project a uniform and continuous image. The laboratory is used for research, and for teaching.

Course of the experiment: Participants attended the Visualization Laboratory

in groups of 3-8 per session. At the beginning of each session, participants completed a consent form, and were then given a brief description of the experiment. They were asked to imagine that they were moving to a new city, and were looking for a residential neighborhood to live in; sampling different residential neighborhoods, they were asked to report their impressions in each case.

### 3.3. ANALYZING THE EXPERIMENT RESULTS-

Continuous and categorical variables were described as mean (standard deviation) and proportion (%), respectively. First, univariate analysis was performed. A comparison of the continuous variables was performed using the Smirnov-Kolmogorov test. Subsequently, 3 ordinal regression models were fitted. The outcome of the models was Sense of Belonging, as rated by users on a Likert scale (1 - lowest, 7 - highest). The first model included level of densification, commerce and vegetation as explanatory variables only. In order to examine the interplay between the explanatory variables, the second model examined the bivariate interaction between densification, commerce and vegetation densification. Finally, the third model also considered the trivariate interaction between the factors. Multiple comparisons were corrected by controlling the false detection rate, in line with the Benjamini-Yekutieli method (Benjamini and Yekutieli 2001). The statistical analysis was performed using SAS (SAS Institute, Cary, USA). Statistical significance was set at  $p < 0.05$ .

## 4. Results

The greatest sense of belonging was expressed in the existing state (X), with commercial activity with and without vegetation. The lowest sense of belonging was recorded for 5X and 6X, without commerce and vegetation (Figure 5). High levels of sense of alienation were reported for all the environments without vegetation and commerce. A direct relationship was identified between densification and alienation; the highest values were reported for the X5 and X6 densification environments. High levels of alienation were reported for all the X6 densification (towers) alternatives.

The highest sense of calmness was reported for X, with commercial activity and no vegetation. The lowest sense of calmness was reported for the 6X and 5X densifications, without-commerce and or vegetation. Low levels of relaxation were also reported for 6X, with commerce and no vegetation.

The 5X and 6X densification environments, without vegetation or commerce, were reported as the most stressful environments. Variation X, in all its manifestations, was reported as the environment with the lowest levels of stress. Both 2X with vegetation and commerce and 4X with commerce and vegetation had similar values.

The highest perceived levels of density and crowdedness were reported for 5X and 6X, without commerce or vegetation. The lowest perceived levels of density were reported for X (benchmark densification level), without commerce and with or without vegetation. Similar values were reported for 2X and 4X, with vegetation and commerce.

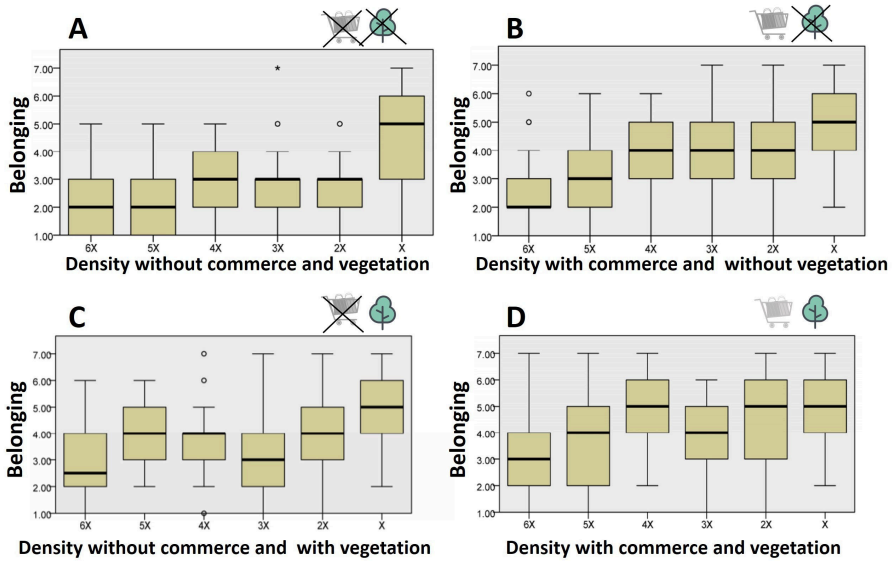


Figure 4. Sense of belonging distribution across alternative environments.

#### 4.1. MULTIVARIATE ANALYSIS - THE REGRESSION MODEL

Vegetation and commerce were found to be independent predictors of the sense of belonging (OR 3.31 and 4.9 respectively,  $p < 0.0001$ ).

Density level and vegetation interacted with each other. At densification levels 2X, 4X, 5X and 6X, the presence of vegetation independently predicted the sense of belonging. There was no interaction between densification and commerce. The presence of commercial activity was an independent predictor of the sense of belonging, regardless of the densification level.

In contrast, if the commercial activity was present in the model, vegetation only predicted a sense of belonging in the 6X densification environment. Without vegetation, commerce predicted a sense of belonging for all the densification levels except the benchmark X density level. In the presence of vegetation, commerce only predicted a sense of belonging for the 3X, 4X, and 6X densification levels.

In the absence of vegetation and commerce, the benchmark density level (existing state) X received the highest values for sense of belonging. There was no difference in sense of belonging for 2X-6X levels, all significantly lower than existing X ( $p < 0.001$ ).

### 5. Discussion

Our univariate analysis shows that densification levels had a significant effect on the different feelings that the participants were asked to rate (the pairs of sensations behaved inversely). As illustrated by Fisher-Gewirtzman, perceived density is inversely proportional to wellbeing (Fisher-Gewirtzman 2017). The results of



our univariate analysis support this assumption; but we also show, for the first time, that the relationship between densification levels and measures of wellbeing is complex. For example, the sense of calmness in the 2X-4X densification settings was similar and high compared to the 5X and 6X levels; similar results were recorded for the sense of illumination. It is possible to maintain a sense of wellbeing even at high levels of densification; however, there is probably a threshold beyond which this sense of wellbeing will be impaired. Future studies should explore this threshold with regard to urban models characterized by different morphologies. In addition, the presence of commerce and vegetation had a significant impact on the sense of belonging.

In order to identify the independent predictors of wellbeing, multivariate regression analysis was performed. The presence of vegetation and commerce predicted a high sense of belonging, regardless of levels of densification (OR = 3.32 and 4.9 respectively). These factors are known to reduce perceived density, and thus increase the sense of wellbeing (Cooper Marcus and Sarkissian 1986). However, an increase in densification levels predicted a lower sense of belonging. This result is supported by earlier studies, which showed that higher levels of density create higher levels of perceived density-which impairs the sense of wellbeing (Cooper Marcus and Sarkissian 1986, Natapov and Fisher-Gewirtzman 2016, Fisher-Gewirtzman and Polak 2019). The current study shows that the presence of vegetation or commerce increased the sense of belonging for all levels of densification, apart from densification X.

The interplay between all three factors was also examined. In the absence of commercial activity, vegetation increased the feeling of belonging, mainly at high density levels. However, when commerce was present, vegetation did not have any impact on the sense of belonging for any level of density other than the very highest. In the absence of vegetation, the presence of commerce did improve the sense of belonging; however, when there was vegetation present in the setting, this phenomenon was only observed at medium density levels. Future research should explore the possibly similar effects of vegetation and commerce on wellbeing. The presence of either seems to eliminate the effect of the other. When designing the street level of future developments, a designer can choose from either factor according the local requirements.

In an attempt to define the extent to which a city can be effectively densified under different vegetation and commerce conditions, the triple effect of all factors was examined. In the absence of vegetation and commerce, we found that-with the exception of the existing densification X-all other levels of density were rated as bestowing a low sense of belonging. Thus, the benchmark density level can be considered as the reference alternative. Without commerce but with vegetation, the 3X density level was rated significantly lower with regard to belonging values. This interesting result quite possibly stems from the monotony of this morphology option-an unvaried cross-section, with no spaces between the buildings. Finally, with vegetation and commerce present, densification up to 4X did not significantly affect the sense of belonging.

An interesting result of the study is that the 4X densification level had a tendency to engender higher belonging values, compared with lower density

levels. We hypothesize two possible reasons for this outcome. First, the cross-sectional variability and the change in the built-in morphology uniformity created an increased “interest” among the subjects. Second, spaces between buildings have a decisive effect on perceived density (Fisher-Gewirtzman and Wagner 2003).

In summary, our results highlight the need for urban planners to consider the delicate interplay between levels of density, vegetation and commerce, and their impact on the residents’ sense of wellbeing.

## 6. Conclusions

This study shows that density and the presence of vegetation or commercial activity in an urban environment have a significant impact on the wellbeing of the residents. The density level has a negative effect on residents’ feelings; but the introduction of vegetation and commercial activity can improve this, especially at the high density levels .

In addition, if commerce or vegetation are present, a setting can be densified up to a certain threshold (4X) and still maintain a positive sense of urban wellbeing. Given that the modern city is undergoing extensive densification-the consequence of population growth and increased urban habitation-the finding that density engineered through the introduction of mixed building heights and volumes, interspersed with spaces, can enhance the sense of urban wellbeing is significant. Our results showed that a street section constituted of buildings of different building with gaps between them contributed to the research participants’ (and potential dwellers’) sense of wellbeing.

This research is a milestone in establishing planning principles that can improve urban densification processes. It also opens a path for future research considering the influence of additional urban characteristics on the wellbeing of potential dwellers. An understanding of the wellbeing of urban dwellers, and the parameters that can influence this, will help urban designers and planners in creating better urbanized future environments.

The next stage of this study will examine high density urban morphologies and their effect on perceived density and wellbeing while maintaining the same build volume.

## References

- Amir, S. and Carmon, N.: 1996, New Immigrants in the Old Central Area of Haifa: Transitory Station or Urban Revitalization?, *Ofakim geography*, 7-25.
- Bardhan, R., Kurisu, K. and Hanaki, K.: 2015, Does compact urban forms relate to good quality of life in high density cities of India? Case of Kolkata, *Cities*, **48**, 55-65.
- Benjamini, Y. and Yekutieli, D.: 2001, The control of the false discovery rate in multiple testing under dependency, *Annals of statistics*, 1165-1188.
- Carmon, N.: 1999, Three generations of urban renewal policies: analysis and policy implications, *Geoforum*, **30**(2), 145-158.
- Cheng, V. 2009, Understanding density and high density, in E. Ng (ed.), *Designing High-Density Cities*, Routledge, London, 37-51.
- Conroy-Dalton, R.: 2002, Is spatial intelligibility critical to the design of largescale virtual

- environments?, *International Journal of Design Computing*, **4**.
- Fisher-Gewirtzman, D.: 2017, The association between perceived density in minimum apartments and spatial openness index three-dimensional visual analysis, *Environment and Planning B: Urban Analytics and City Science*, **44**(4), 764-795.
- Fisher-Gewirtzman, D.: 2018, Perception of density by pedestrians on urban paths: an experiment in virtual reality, *Journal of Urban Design*, 1-19.
- Fisher-Gewirtzman, D., Burt, M. and Tzamir, Y.: 2003, A 3-D visual method for comparative evaluation of dense built-up environments, *Environment and Planning B: Planning and Design*, **30**(4), 575-587.
- Fisher-Gewirtzman, F.-G.D.P.N. and Polak, N.: 2019, A learning automated 3D architecture synthesis model: demonstrating a computer governed design of minimal apartment units based on human perceptual and physical needs, *Architectural Science Review*, 1-12.
- Fisher-Gewirtzman, D. and Wagner, I.A.: 2003, Spatial openness as a practical metric for evaluating built-up environments, *Environment and Planning B: Planning and Design*, **30**(1), 37-49.
- Ford, L.R.: 1999, Lynch revisited: New urbanism and theories of good city form, *Cities*, **16**(4), 247-257.
- Gilchrist, K., Brown, C. and Montarzino, A.: 2015, Workplace settings and wellbeing: Greenspace use and views contribute to employee wellbeing at peri-urban business sites, *Landscape and Urban Planning*, **138**, 32-40.
- Hawley, A.H.: 1963, Community power and urban renewal success, *American Journal of Sociology*, **68**(4), 422-431.
- Kaya, H.S. and Mutlu, H.: 2017, Modelling 3D spatial enclosure of urban open spaces, *Journal of Urban Design*, **22**(1), 96-115.
- Kuliga, S.F., Thrash, T., Dalton, R.C. and Hoelscher, C.: 2015, Virtual reality as an empirical research tool—Exploring user experience in a real building and a corresponding virtual model, *Computers, Environment and Urban Systems*, **54**, 363-375.
- Lynch, K.: 1960, *The image of the city*, MIT press.
- Lynch, K.: 1972, *What time is this place?*, mit Press.
- Lynch, K.: 1984, *Good city form*, MIT press.
- Cooper Marcus, C.M.C.S.W.: 1986, *Housing as if people mattered*, Berkeley: University of California Press, Ltd.
- Martin, L. and March, L.: 1972, *Urban space and structures*, Cambridge University Press.
- Natapov, A. and Fisher-Gewirtzman, D.: 2016, Visibility of urban activities and pedestrian routes: An experiment in a virtual environment, *Computers, Environment and Urban Systems*, **58**, 60-70.
- Nishio, N.S.I.F.: 2019, Statistical validation of utility of head-mounted display projection-based experimental impression evaluation for sequential streetscapes, *Environment and Planning B: Urban Analytics and City Science*, 2399808318821693.
- Padan, P.Y.: 2014, "urban renewal Social aspects of planning" . Available from <<http://bimk.om.org/wp-content/uploads/%D7%93%D7%95%D7%97-%D7%94%D7%AA%D7%97%D7%93%D7%A9%D7%95%D7%AA-%D7%A2%D7%99%D7%A8%D7%95%D7%A0%D7%99%D7%AA.pdf>>.
- Portman, M.E., Natapov, A. and Fisher-Gewirtzman, D.: 2015, To go where no man has gone before: Virtual reality in architecture, landscape architecture and environmental planning, *Computers, Environment and Urban Systems*, **54**, 376-384.
- Rapoport, A.: 1977, *Human aspects of urban form*, Pergamon Oxford.
- Shushan, Y., Portugali, J. and Blumenfeld-Lieberthal, E.: 2016, Using virtual reality environments to unveil the imageability of the city in homogenous and heterogeneous environments, *Computers, Environment and Urban Systems*, **58**, 29-38.
- Wolch, J.R., Byrne, J. and Newell, J.P.: 2014, Urban green space, public health, and environmental justice: The challenge of making cities 'just green enough', *Landscape and urban planning*, **125**, 234-244.

# THE GUIDANCE SYSTEM OF GAMIFICATION AND AUGMENTED REALITY IN A MUSEUM SPACE

ZI-RU CHEN

<sup>1</sup>*Southern Taiwan University of Science and Technology*

<sup>1</sup>*zrchen@stust.edu.tw*

**Abstract.** Gamification is the application of game-oriented design approaches or game-inspired mechanics to otherwise non-game contexts. Mobile guiding system is the design process of information interactions. It is the integration of information design, interaction design, and sensorial design. The e-learning system of mobile guide is able to be loaded gamification concepts and let mobile learning interestingly, diversely, and validly. The problem of the research was if we combined the concept of gamification design into museum guide services with augmented reality for non-commercial purposes, it also provided the same benefits to the promotion of museum learning and knowledge, integrating mobile devices as navigation media. It would improve more users to participate in a museum and use the guide system actively, and then arise their interest and achievement. The result was to establish a preliminary model for developing a museum mobile guide system of gamification design and augmented reality.

**Keywords.** Gamification; Museum Learning; Multimedia Guided System; Augmented Reality.

## 1. Introduction

### 1.1. MUSEUM GUIDE AND GAMIFICATION

Nowadays, museums play the role of social education. It has a wealth of collections and related materials, and stimulates and encourages people to learn through educational programs, exhibitions, activities, etc. (Hooper-Greenhill, 1999) Lord et al. (1997) believed that informal education is the most successful in affective learning, which can change audience's attitude and interest, audience's use of guide, and affect their visiting experience and willingness to come again. Guide is frequently used by visitors in museums. Many museums and researchers like to explore what kind of guide method can improve learning motivation and effectiveness of visitors. In terms of guide device, currently, digital guide of personalized mobile is widely used. Such mobile guide can display multimedia, wireless communication and database technology with mobile device, and replace traditional printed material and guide manual (Yu, 2003). The mobile device is characterized by high portability and powerful computer functions. When combined with the easy-to-use mobile guide, it may interact with the display

content, allowing visitors to select their favorite exhibits at any time and at any place, and meeting different needs for experience activities.

In addition, previous research was pointed out that games can make people happy, make complicated things simple, and also change human behavior. Games can not only be used for entertainment or learning, but to change people's living habits, business behaviors, political and social activities, etc. Therefore, the design concept and application of "gamification" have received wide attention in recent years. The word "gamification" is generally defined as applying elements such as game thinking, game mechanism and design structure to non-game social activities and services (Deterding et al., 2011). Gamification is a phenomenon. Determining et al. (2011) explained that gamification is the use of game elements to perform certain activities with specific purposes in non-game situations. In 2015, New Media Consortium put forward some examples of gamification applied to museums, and believed that this trend could enhance visitors' viewing experience. It also pointed out that how to enhance the creative experience process is a major challenge for such guide design in the future (Johnson et al., 2015). The game system can stimulate users' emotions, promote better feeling and connection between people and technology interfaces (Roy et al., 2009). Besides, the integrated use of interactive technology and interactive design also involves the management of aesthetic experience (Locher et al., 2010).

## 1.2. AUGMENTED REALITY APPLIED IN GUIDE SERVICE

In recent years, the development of augmented reality technology has become mature and has begun to be applied in many different fields. There are increasing cases of introducing augmented reality application into museum guide experience. Such audience integration and immersion experience are different from the traditional display mode. They bring visitors sense of novelty and participation, and often become the highlight in the exhibition. Augmented reality may combine virtual and real worlds, and enable visitors to be in a three-dimensional environment to engage in real-time interaction with objects that cannot actually be brought to the exhibition environment, cannot be touched by visitors and must be enlarged. Such practice prolongs visitors' stay in front of exhibits, and connects knowledge the museum wants to convey with visitors' own experience (Guo, 2008). It is considered to serve as a communication medium between the museum and visitors (Hammady et al., 2016). The augmented reality in guide services uses image card identification and projection display to achieve the learning experience of integrated virtual and real scenes, adopts outdoor geographic information to achieve the purpose of action learning, and employs simple augmented reality tools to search virtual objects so as to innovate artistic display forms (Veenhof & Skwarek, 2010). Undoubtedly, the application of augmented reality in museums is of various possibilities and multiple creative expression potential, thereby triggering a range of studies on the application of augmented reality in museum guide experience, exhibition quality and learning results.

## 2. Problem and objective

In recent years, museum education has gained vigorous development. In light of the shortcomings in guide design in most museums, this study found that museum guides are mostly printed in writing, and multimedia video broadcasting and personnel on-the-spot interpretation and other ways are provided to convey exhibit information. However, most of the exhibits in the museum are of rich historical significance and profound knowledge background. If a museum provides different guide services and information content for different visitors, it will impose an excessive burden on manpower and material costs. In addition, traditional guide method can by no means achieve the best presentation and explanation effect for in-depth and detailed expertise of each exhibit. Also, professional but important exhibit information is often hard to understand, thereby depriving visitors of the motivations for further information, and preventing them from understanding the connotation of important cultural relics. Therefore, this study took the “Wood-frame Construction of Eastern Architecture Exhibition” of Ancient Machinery Research Center in Southern Taiwan University of Science and Technology as an example (refer to Figure 1.) to explore new possibility of museum guide planning and design through game-based design thinking and expanded reality application, and guide the public to re-recognize the museum learning mode.



Figure 1. The interior of “wood-frame construction of eastern architecture exhibition”.

## 3. Methodology and Steps

This study adopted case study, prototyping and user testing methods. Through case analysis, this study obtained the game elements, and made the prototype based on guide content planning, game elements and rules, system interface design, and prototyping of game guide system. Finally, the user testing was carried out to confirm feasibility of the prototype and explore the learning effect of application of game and augmented reality in museum guide.

### 3.1. CASE STUDIES: TO BUILD THE MODE AND FACTORS OF GAMIFICATION

Through the analysis of 5 gamification cases, this study took 6 game elements proposed by Zichermann and Linder (2013), including points, levels, trophies/badges/achievements, virtual goods, leaderboards and virtual gifts as the

analysis basis to extract elements that attract people in the game, and analysed the game-based design of the cases. The analysis results are applied to museum guide to propose design specifications or criteria of the game-based action application program. Please refer to Table 1 for the analysis framework.

Table 1. The analysis framework of gamification factors.

Game Elements		
Category	game mechanics	game dynamics
<b>Personal</b>	points	reward
	levels	status
	Trophies/badges/achievements	achievement
	virtual goods	self expression
<b>Social</b>	leaderboards	competition
	virtual gifts	altruism

### 3.2. PROTOTYPE IMPLEMENTATION: TO DESIGN A GUIDE SYSTEM

#### 3.2.1. exhibition themes selection

Above figure 1 shows the interior of “Wood-frame Construction of Eastern Architecture Exhibition”. There are various exhibits and display plans in the exhibition hall. In this study, 8 main exhibition themes were sorted out and used as exhibition contents of subsequent game-based guide plan. Please refer to graphical representation in Figure 2 and description in Table 2 for 8 exhibition themes and the guide plan.

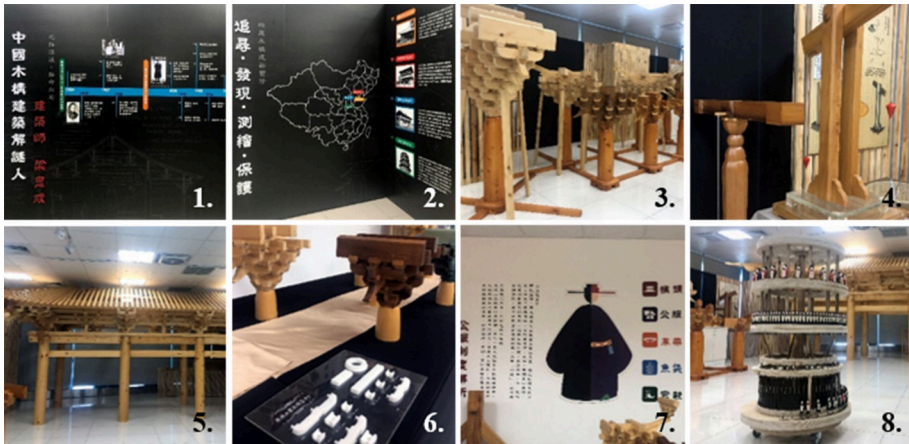


Figure 2. The display objects of eight main exhibition themes.

Table 2. The description framework of eight main exhibition themes.

<i>No.</i>	<i>Display Form</i>	<i>Exhibition Theme</i>	<i>Game element and rule planning</i>
1	display planes	<i>Timeline Wall</i>	multiple-choice game
2	display planes	<i>Moving Track</i>	multiple-choice game
3	1:3 physical models	<i>Dougong Group</i>	drag-moving game
4	physical models	<i>Calibration Instrument</i>	drag-moving game
5	a 1:3 physical model	<i>Wooden Construction</i>	silhouette-match game
6	1:6 DIY models	<i>Dougong Instruction</i>	silhouette-match assembling game
7	display planes	<i>Song Dynasty Costume</i>	pairs-matching game
8	a 1:6 physical model	<i>Timing Tower</i>	Story-driven game

### 3.2.2. USER INTERFACE AND FLOW DESIGN

According to the result of game elements and rules from case studies, the interface flow and usability design were carried out to plan. Refer to Figure 3 for part of the interface design. In terms of usability process design, as the museum guide discussed in this study focused on the interaction between visitors and exhibits, the "augmented reality" technology was adopted to achieve virtual-real integration. The guide experience was divided into "virtual scenes" and "real scenes". "Virtual scenes" refer to the guide information and game interactive content of exhibits provided in the application program, while "real scenes" refer to the contents of exhibits in the physical environment. The whole experience of guide/game was carried out simultaneously/alternately between virtual scenes and real scenes, so as to reach "creating innovative museum guide design and achieve "gamifying museum guide experience" proposed by this study, as seen in Figure 4.





Figure 3. The App and AR interface of museum guide prototype.

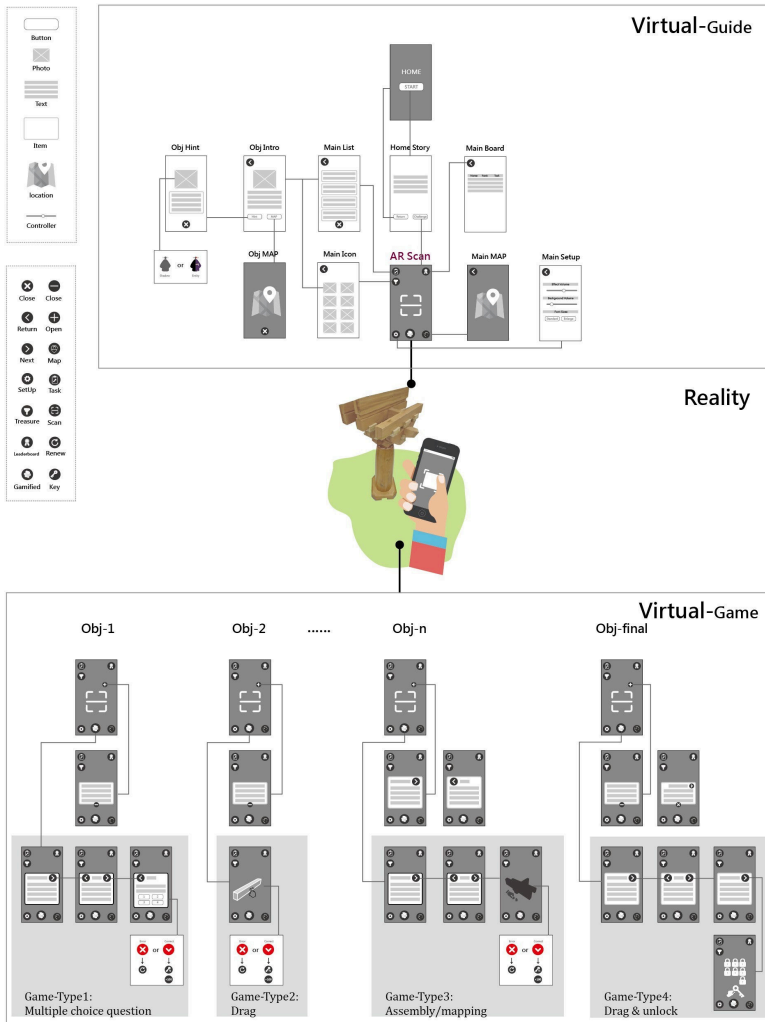


Figure 4. User interface flow of the museum guide.

### 3.2.3. *Prototype system implementation*

The system software in this study was developed by using a game engine, Unity. Unity is a cross-platform game development engine, with a hierarchical, comprehensive development environment, including visual editing, detailed attribute editor and dynamic game preview functions. It is also used to make games or develop game prototypes. Thus, it meets the needs of this study. The version adopted in this research is Unity 2018.2. 5f1. In addition, in the application of augmented reality technology, the Vuforia development kit was employed. Vuforia is a platform to assist in augmented reality technology. Producers can use its advanced computer vision to perform train on images. Currently, Vuforia has been integrated with the game development engine Unity.

As for the selection of hardware devices for guide, the technology of augmented reality can be applied to mobile devices such as smartphones or smart glasses. Considering of making more people get involved, smartphones are chosen as the platform for development. Finally, after the system is built, it is tested and used in the exhibition hall of “Wood-frame Construction of Eastern Architecture Exhibition” of Ancient Machinery Research Center, Southern Taiwan University of Science and Technology to ensure smooth implementation of the system, as shown in Figure 5.



Figure 5. User testing of museum guide system in the exhibition.

## 4. User testing

### 4.1. PARTICIPANT BACKGROUND

This study intended to explore whether the mobile application featuring gamification design and augmented reality technology in museum guide is helpful to the learning results of audience. It tested the feasibility of guide system and observed testers' system usage behavior. The total number of samples is 40, all of whom are college students aged 18 to 30 (15 males and 25 females). They were familiar with the user interface design and process in the mobile application program, but did not know the relevant knowledge of wooden buildings. The study hoped to know whether the subjects can successfully complete the exhibition experience through the guide App developed in this study.

## 4.2. THE ANALYSIS OF SYSTEM USAGE BEHAVIOR

### 4.2.1. Visiting time of each exhibit

The test results show that the average visiting time is 27 minutes 4 seconds. For the visiting time of 8 exhibits, please refer to Table 3. The average visiting time of 5 exhibits is about 3 minutes, namely “Moving Track”, “Dougong Group”, “Calibration Instrument”, “Song Dynasty Costume” and “Timing Tower”. Among all the exhibits, the one with the shortest visiting time is “Timeline Wall”. Most of the subjects passed through the game checkpoint of the exhibit in a very short time. The game was simple for most of the subjects, but some subjects deemed that there were too many words in this guide interface and they may sometimes ignore the important information.

The one with the most visiting time is No. 6. When visiting the exhibits of “Dougong Instruction”, as the game design was interaction between hands-on and exhibits, the subjects need to assemble the scattered Dougong components by observing the Dougong structure. Thus, they spent much time on this exhibit. Most subjects believed that such guide method was the most interesting, and they can understand the Dougong structure through the hands-on assembly process.

Table 3. The survey of visiting time of 8 exhibits.

<i>Exhibit No.</i>	<i>Shortest time of visit</i>	<i>Longest time of visit</i>	<i>Avg. time of visit</i>	<i>SD.</i>
<b>1</b>	00:00	05:24	01:43	01:17
<b>2</b>	00:23	04:56	02:09	01:08
<b>3</b>	00:43	07:14	02:10	01:23
<b>4</b>	00:27	08:26	02:54	01:47
<b>5</b>	01:30	13:57	04:17	02:34
<b>6</b>	01:04	16:11	07:01	03:41
<b>7</b>	12:11	09:05	03:38	02:00
<b>8</b>	00:00	07:04	03:13	01:31

### 4.2.2. game rule and achieving level

Each exhibit task in the guide system is a level. Subjects may obtain one key and up to 100 points when they beat a level, and 10 points will be deducted if they fail. If a subject beats a game task at the first time, he may get a golden key, and get a silver key when he didn't beat the task at the first time. Only one of the two keys can be obtained at each level. According to the experimental results, as shown in Table 4, only 5 subjects beat the level of No. 5 exhibit task. Many subjects pointed out the detection problem of image recognition resulted in the low passing rate. The final level is “Timing Tower”, which collect 7 keys to beat the level. There were only 5 subjects beat all of the levels. It can be known that the mobile guide application developed based on the gamification and augmented reality is

not easy for most subjects to master the system and game tasks in a short time (in about 30 minutes).

Table 4. The results of achieving levels of 40 subjects.

<i>Exhibit No.</i>	<i>Num. of golden keys</i>	<i>Num. of silver keys</i>	<i>Beating the level of subject numbers</i>
<b>1</b>	16	14	30
<b>2</b>	19	9	28
<b>3</b>	29	9	34
<b>4</b>	7	12	19
<b>5</b>	9	0	9
<b>6</b>	26	0	26
<b>7</b>	6	27	33
<b>8</b>	-	-	5

#### 4.3. THE RESULTS OF USER TESTING

According to the user tests, the study sorted out 3 major discussions, including suggestions on the application of augmented reality in guide system, suggestions on the application of gamification in the interface of augmented reality guide system, and suggestions on the design of game content. The explanations are as follows:

In terms of application of augmented reality to the guide system, it was difficult for subjects to eliminate problems encountered in the testing by themselves, and researchers were required to assist in handling such problems. It was suggested that the guide map of the system should display the number of detecting points on each exhibit, or added photos or illustrations of detected results to the guide system, which can reduce the detecting problems encountered by users during guide.

In terms of application of gamification to the interface of the augmented reality guide system, the experimental results showed that as subjects needed to use smart mobile phones for testing, they should be focused on both the mobile phones and the exhibits, and failed to carefully read the text introduction on the guide system. It was suggested that the text be presented in the form of voice or animation, which would make it easier for visitors to get involved in the situation when experiencing the exhibition.

In terms of game content design, the subjects preferred the game content with high feedback, such as the game level design of “Dougong Instruction” and “Song Dynasty Costume”. The interactive modes of hands-on operation and pairing make subjects felt fun in the guide process. Subjects pointed out that the question-and-answer mode and the way of finding components were boring. It was suggested that the user-friendly interactive mode with high feedback should be provided, so that visitors can have a good interactive experience when visiting the exhibition.

## 5. Conclusion

This study hoped to adopt prototyping to develop a guide application program that applies gamification concepts and augmented reality, and to obtain a preliminary design model of gamification for museum guide. Then, this study validated the feasibility of such model through user tests, and the display medium is an interface of mobile device. The preliminary result shows that the application of gamification in museum guide can extend the time of visiting exhibitions in a museum, and has significant effects on museum learning through questionnaires and interviews. It can be seen that gamification has a positive impact on the application of museum guide, and the related research may also be carried out in an in-depth manner.

## References

- Deterding, S., Khaled, R., Nacke, L. and Dixon, D.: 2011, Gamification: Toward a Definition, *Forthcoming in Gamification Workshop, CHI 2011*.
- Guo, S.W.: 2008, Preliminary Study on the Application of Augmented Reality in Museum Exhibition, *Technology museum review*, **12**(4), 25-37.
- Hammady, R., Ma, M. and Temple, N.: 2016, Augmented Reality and Gamification in Heritage Museums, *In: Marsh T., Ma M., Oliveira M., Baalsrud Hauge J., Göbel S. (eds) Serious Games.*, 181-187.
- Hooper-Greenhill, E.: 1999, *The educational role of the museum*, Routledge, London and New York.
- Johnson, L., Adams Becker, S., Estrada, V. and Freeman, A.: 2015, *NMC horizon report: 2015 higher education edition*, The New Media Consortium, Austin, Texas.
- Locher, P., Overbeeke, K. and Wensveen, S.: 2010, Aesthetic interaction: a framework, *Design issues*, **26**, 70-79.
- Lord, B. and Lord, G.D.: 1997, *The manual of Museum Management*, The Stationery Office, London.
- Roy, M., Hemmert, F. and Wettach, R.: 2009, Living interfaces: the intimate door lock, *In Proceedings of the third international conference on tangible and embedded interaction*, New York, 45-46.
- Veenhof, S. and Skwarek, M.: 2010, "Augmented reality art exhibition MoMA NYC" . Available from <<http://www.sndrv.nl/moma/>> (accessed 13rd December, 2019).
- Yu, S.C.: 2003, *Interaction Design of Personal Digital Mobile Guide Example of The Exhibition "Emperor Chien-lung Grand Cultural Enterprise" in National Palace Museum*, Master's Thesis, Yuan Ze University.
- Zichermann, G. and Linder, J.: 2013, *The gamification revolution: how leaders leverage game mechanics to crush the competition*, McGraw-Hill Education.

# MOBILE MIXED REALITY FOR ENVIRONMENTAL DESIGN USING REAL-TIME SEMANTIC SEGMENTATION AND VIDEO COMMUNICATION

*Dynamic Occlusion Handling and Green View Index Estimation*

DAIKI KIDO<sup>1</sup>, TOMOHIRO FUKUDA<sup>2</sup> and  
NOBUYOSHI YABUKI<sup>3</sup>

<sup>1,2,3</sup>*Osaka University*

<sup>1</sup>*kido@it.see.eng.osaka-u.ac.jp* <sup>2,3</sup>*{fukuda|  
yabuki}@see.eng.osaka-u.ac.jp*

**Abstract.** Mixed reality (MR), that blends the real and virtual worlds, attracted attention for consensus-building among stakeholders in environmental design with the visualization of planned landscape onsite. One of the technical challenges in MR is the occlusion problem which occurs when virtual objects hide physical objects that should be rendered in front of virtual objects. This problem may cause inappropriate simulation. And the visual environmental assessment of present and proposed landscape with MR can be effective for the evidence-based design, such as urban greenery. Thus, this study aims to develop a MR-based environmental assessment system with dynamic occlusion handling and green view index estimation using semantic segmentation based on deep learning. This system was designed for the use on a mobile device with video communication over the Internet to implement a real-time semantic segmentation whose computational cost is high. The applicability of the developed system is shown through case studies.

**Keywords.** Mixed Reality (MR); Environmental Design; Dynamic Occlusion Handling; Semantic Segmentation; Green View Index.

## 1. Introduction

The use of mixed reality (MR) has recently attracted attention in the architecture, engineering, and construction (AEC) field. MR is a technology that blends the real and virtual worlds (Milgram and Kishino, 1994). One target of MR in the AEC field is for consensus-building among stakeholders in environmental design. Stakeholders consist of experts such as architects and government, and non-experts such as residents, which means that there is a wide gap in the stakeholders' knowledge about environmental design. Then it is difficult for them to imagine a planned landscape appropriately. MR can produce a realistic landscape simulation by overlaying three-dimensional computer graphics (3DCG)

models of new structures on the target site. It is considered that this visualization can help stakeholders to grasp the project intuitively. Augmented reality (AR) is a similar concept to MR that overlays digital information on real space. However, the term of MR is used in our paper because MR was defined the merging of real and virtual worlds regardless of its ratio (Milgram and Kishino, 1994).

One of the technical challenges in MR is an occlusion problem, which occurs when virtual objects hide physical objects that should be rendered in front of virtual objects. When physical objects occlude virtual objects, the augmented image may cause user confusion related to depth perception and it is essential to handle occlusion for appropriate MR-based landscape assessment.

To solve this problem, the depth-based method and the model-based method have been widely presented. The depth-based method acquires the depth information of the occlusion target from a 3D sensing camera in real-time such as a RGB-D camera or a stereo camera, and compare the depth of the virtual objects with the acquired depth information to handle occlusion (Holynski et al., 2018). This method can handle occlusion dynamically in real-time, however, the range where a 3D sensing camera can obtain depth information is limited. Therefore, it is difficult to apply to occlusion problems in MR-based landscape simulation because occlusion targets can be far from a camera. The model-based method creates 3DCG objects of occlusion targets (occlusion models) in a real scene, and compare the depth of virtual objects with the occlusion models to handle occlusion (Inoue et al., 2018). However, this method can only apply to unchanged objects because of the pre-processing that reconstructs occlusion targets.

In our previous study, a MR system for landscape design simulation that performs real-time dynamic occlusion handling using semantic segmentation based on deep learning was developed (Kido et al., 2019). Semantic segmentation is a technique to link each pixel in an image to a class label. This system can extract only the area of occlusion targets in real-time and handle occlusion dynamically. Since real-time semantic segmentation processing involves heavy processing and needs a high-end computer, a framework was developed in which client device transfers image frames to a server, which performs semantic segmentation processing on those frames and sends processed frames back to the client. To realize the client-server communication in this system, a web application was developed and applied. However, the client-server communication system based on a web application is not a versatile method in terms of computer security. It is necessary to access the server computer for the use of the web application. If the web application was deployed to access from everywhere, the server computer has to be managed and secured and it takes a lot of care and cost.

Semantic segmentation is also effective for environmental assessment; one of the key elements of environmental design is greenery. The assessment of urban greenery in a planning and early design phase is effective for attractive environmental design because urban green spaces are vital components of healthy living and quality of life for residents in urban areas (Van Dillen et al., 2012). Cao et al. (2018) developed a real-time green view index (GVI) estimation system with semantic segmentation. GVI is defined as the ratio of the green area to the total area in the field of view of a person and can be used to evaluate the visual impact of

various planning and management practices on urban greening (Yang et al., 2009).

This study aims to develop a MR system for environmental design which involves two functions; one is real-time dynamic occlusion handling, and the other is the GVI estimation. Then, Internet-based real-time video communication technology is integrated into MR system to implement the client-server communication for semantic segmentation processing on a mobile device. This video communication technology enables to implement the client-server communication without especial management of the server computer in terms of computer security. And semantic segmentation and BIM-based approach are combined to estimate the GVI of the present and proposed landscape simultaneously.

## 2. Methodology

### 2.1. INTEGRATION OF A GAME ENGINE AND REAL-TIME SEMANTIC SEGMENTATION WITH VIDEO COMMUNICATION

A game engine software is widely used to develop a MR system because it provides many functions and user-friendly graphical interfaces. In our study, Unity game engine was used to develop a MR system to use OpenCV for Unity for occlusion handling, which is a plugin for Unity to implement image processing. To accomplish dynamic occlusion handling in MR and real-time GVI estimation, semantic segmentation processing is necessary to be integrated into Unity.

Figure 1 shows the communication flow of the live video and the segmentation video between the client-server in our proposed system. To realize the client-server communication over the Internet, WebRTC (Web Real-Time Communication), that enables web applications and sites to capture and optionally stream video media between browsers in real-time (Jennings et al., 2013), was adopted. WebRTC consists of several interrelated application programming interfaces (APIs) and protocols that work together to achieve real-time communication.

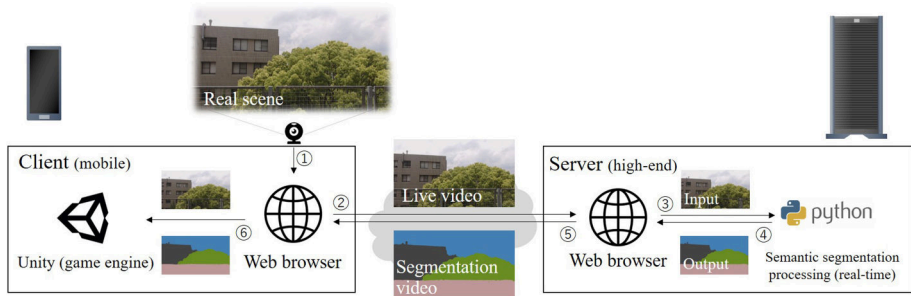


Figure 1. Integration of Unity game engine and semantic segmentation processing.

In our system, the packages of WebRTC were installed to both a client device and a server computer. When the communication with WebRTC is started, peer to peer (P2P) connection between the client-server needs to be established. At the timing of establishing a P2P connection, the stream data that is to be transferred



should be also specified. Then, a client device can specify the image frames acquired from a webcam connected to a client device as the stream data, however, a server computer doesn't have any data to transfer. Therefore, a canvas element that has no data was specified as the stream data in a server computer at first. After the P2P connection is established, processed frames were copied to the canvas element that was specified as the stream data and transferred to the client device (Figure 2).

Next, the video communication with WebRTC is optimized for real-time communication. If the network bandwidth is narrow, the quality of the transferred video can be low with video compression processing for real-time communication. However, this video compression processing may cause inaccurate semantic segmentation results because the transferred frames can be low-resolution. Thus, JPEG compression was conducted to the acquired webcam frames and they were transferred to the server to keep the quality of webcam frames in our system.

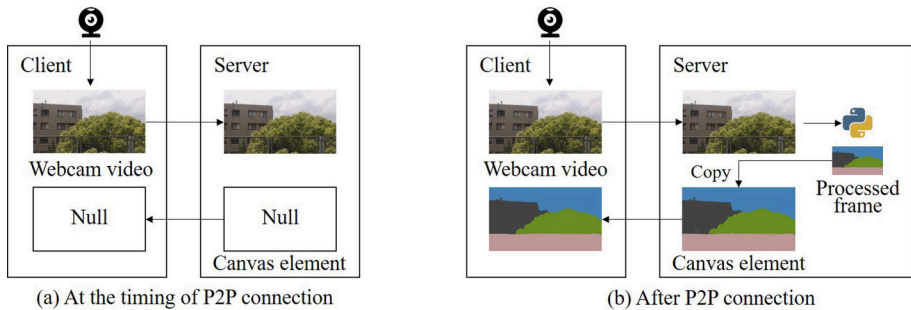


Figure 2. WebRTC communication in our system.

In a server computer, webcam frames were acquired on the web browser written in JavaScript and semantic segmentation processing was performed with Python. Thus, the communication between web browser (JavaScript) and Python is necessary to perform semantic segmentation processing on the received webcam frames. In JavaScript, Ajax (asynchronous JavaScript and XML) was used for JavaScript-Python communication. With Ajax, web applications can send and receive data from a server asynchronously without reloading the whole web page. In our system, webcam frames were transferred to Python with Ajax. In Python, flask was used for JavaScript-Python communication, which is a micro web application framework written in Python. In our system, webcam frames were received with flask and performed semantic segmentation processing, and sent processed frames back to JavaScript.

In a client device, webcam frames and semantic segmentation images in the web browser need to be transferred to Unity to develop a MR system. Since it is difficult to send those images from JavaScript to Unity directly, an intermediate server was developed at the localhost in a client device using flask. In JavaScript, Ajax was adopted to transfer those images to the intermediate server. In Unity, GET method in HTTP communication with www class was used to request the data and Unity received those images from the server.

## 2.2. SEMANTIC SEGMENTATION

In a server computer, semantic segmentation processing is conducted to transferred webcam frames. Recently, various frameworks of semantic segmentation based on deep learning have been proposed along with the advance of the computer vision field. Thus, this system was designed that the semantic segmentation framework is independent and can be replaced.

In our study, ICNet (Zhao et al., 2018) was adopted as a semantic segmentation framework considering its processing speed and accuracy. A dataset is also necessary to train the semantic segmentation framework. This system is assumed to be used for MR-based environmental assessment and needs to detect objects in the streetscape. Therefore, cityscapes dataset (Cordts et al., 2016), which was created for understanding urban scenes, was adopted for the training of ICNet. Labels and objects which can be detected in cityscapes dataset are shown in Figure 3.

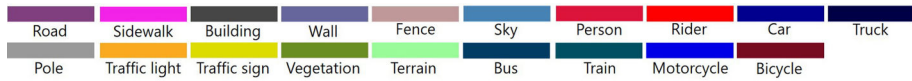


Figure 3. Labels which can be detected in cityscapes dataset.

## 2.3. DYNAMIC OCCLUSION HANDLING

Dynamic occlusion handling is implemented based on the method of our previous study (Kido et al., 2019). In this method, a mask image of occlusion targets was created with RGB value in a segmentation image. It was merged into an MR image that is rendered a 3DCG model and an MR layer with occlusion handling was created in real-time (Figure 4).

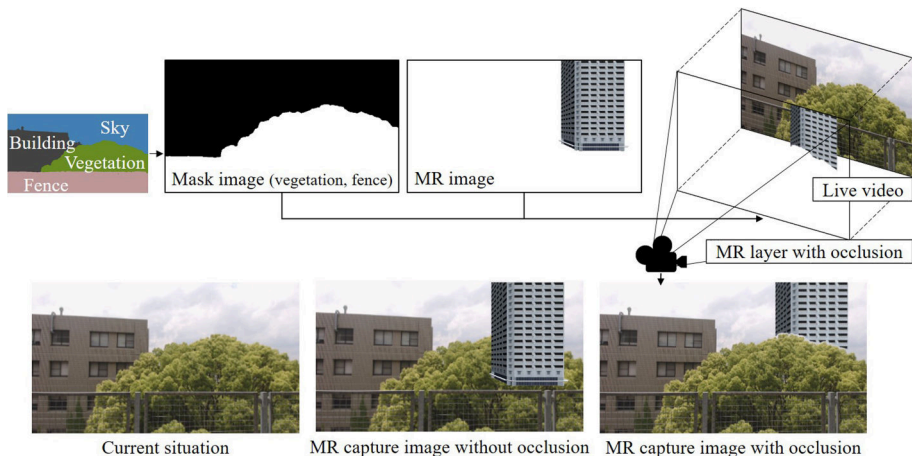


Figure 4. MR with occlusion handling using semantic segmentation.

## 2.4. GREEN VIEW INDEX ESTIMATION

This system estimates the GVI of the present and proposed landscape with MR simultaneously in real-time to facilitate the consensus-building based on the evidence-based design. In this system, the area of the vegetation and the terrain in the segmentation image is defined as green area according to Figure 3. The GVI of the present landscape is estimated by creating a mask image of a green area with a segmentation image. The GVI of the proposed landscape is estimated by the combination of a mask image of the proposed green area and a mask image of 3DCG models of planting (Figure 5). Then, planting models are given attribute information to create a mask image of only planting models.

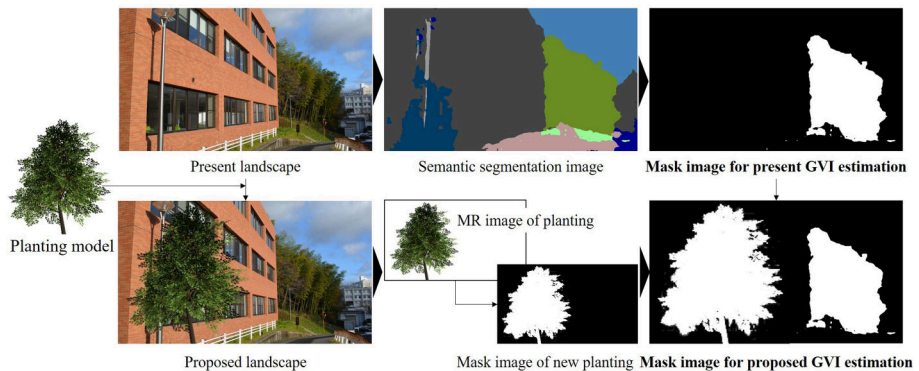


Figure 5. GVI estimation of present and proposed landscape.

To confirm the accuracy of the GVI estimation with our system, the accuracy rate was calculated using 20 images as the feasibility study. A part of the images and segmentation results are shown in Figure 6. The resulting accuracy rate was observed to be 93.3 % for our system. The previous GVI estimation system with semantic segmentation developed by Cao et al. (2018) achieved the accuracy rate of 96.3% and our results were less than the previous system by 3%. In the previous system, a dataset of the green areas was created by manual operation of the authors for the accurate GVI estimation. Thus, it is considered that an additional dataset of the green areas is necessary to improve the accuracy rate of the GVI estimation.

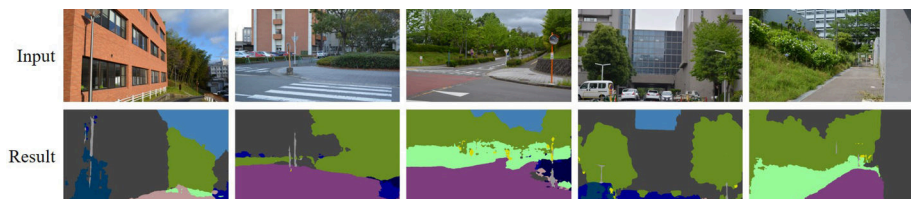


Figure 6. A part of images used for calculating the GVI estimation accuracy and the semantic segmentation results of the developed system.

### 3. Case study

To show the applicability of the developed system, two case studies were conducted; one was dynamic occlusion handling and the other was GVI estimation. In these case studies, Microsoft Surface Pro 6 which is a lightweight tablet computer with Intel Core i5-8250U of CPU, 8GB of RAM, and Intel UHD Graphics 620 of GPU was used as a client device, and a desktop computer with Intel Core i7-8700K of CPU, 32GB of RAM, and NVIDIA GeForce GTX 1080Ti 11GB of GPU as a server computer, and a Logitech HD Pro Stream webcam C920 was used. And also the SkyWay, which provides WebRTC communication platform, was used to conduct the client-server communication with WebRTC. Then, Internet communication speed was also measured with Fast.com which provides servers to measure the Internet communication speed. In MR, camera's position and orientation were computed using the method which solves the perspective n-points (PnP) problem and eliminates the outliers using the random sample consensus (RANSAC) method proposed by Inoue et al. (2018).

#### 3.1. DYNAMIC OCCLUSION HANDLING

In this case study, a MR-based landscape simulation was conducted to confirm the dynamic occlusion handling of our system. Figure 7 shows the arrangement and the measurement of a new building and the camera's position and orientation. Then, the viewpoint was set on the fourth floor of the M3 building in Osaka University. Vegetation and fence were defined as occlusion target in this case study. The webcam was panned in a horizontal direction in the range of the red dotted line of Figure 7 for 10 seconds. After 10 seconds, the webcam was tilted up for 10 seconds. The MR results are shown in Figure 8. Internet communication speed is shown in Table 1.

The results showed that the developed system can transfer the acquired webcam frames to a server computer with video communication over the Internet based on WebRTC, and the server computer implemented semantic segmentation processing on those frames and sent them to the client device, and dynamic occlusion handling was implemented. It is considered that this occlusion handling can help to conduct more appropriate MR-based landscape simulation. However, the processing speed of this system was about 4~5 frames per second (fps), which is insufficient for real-time processing.

#### 3.2. GREEN VIEW INDEX ESTIMATION

In this case study, MR-based planting design simulation was conducted with the GVI estimation of present and planned landscape. Figure 9 shows the arrangement and the measurement of a planting and the camera's position and orientation. The webcam was panned in a horizontal direction in the range of the red dotted line of Figure 9 for 10 seconds. The MR and GVI estimation results are shown in Figure 10. Internet communication speed is shown in Table 2.

The results showed that the developed system can estimate the GVI of the present and proposed landscape with MR simultaneously. However, it confirmed that the speed of the video communication was only 3 fps and the communication

speed is the important index.

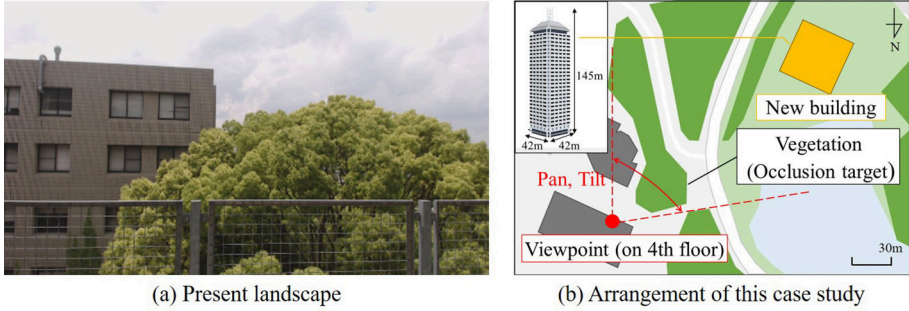


Figure 7. Present landscape and the arrangement of the case study for occlusion handling.

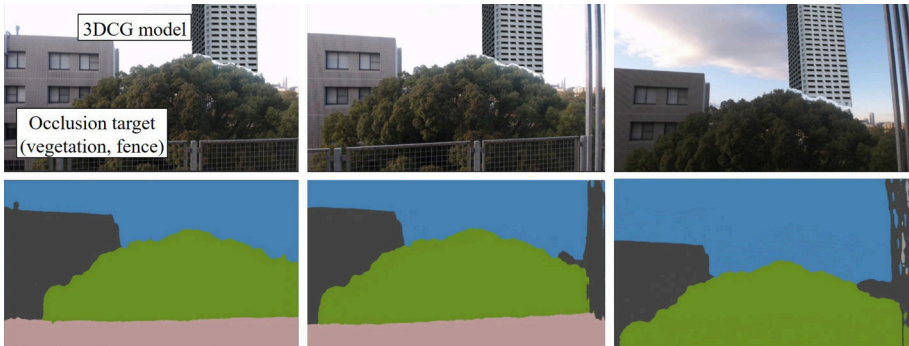


Figure 8. MR simulation with dynamic occlusion handling using the developed system: (Top) MR view with occlusion handling and (Bottom) semantic segmentation results.

Table 1. Internet communication speed in occlusion verification measured by Fast.com.

Communication	Speed [Mbps]
Brower (client)-Server (Provided by Fast.com)	Upload: 120, Download:122
Browser (server)-Server (Provided by Fast.com)	Upload: 714, Download: 900

### 3.3. DISCUSSION

In these case studies, we confirmed that this system can perform the client-server communication over the Internet, and dynamic occlusion handling and the GVI estimation were implemented. However, if the webcam acquires present surroundings against the sunlight, the acquired backlit frames can be rough and the accuracy of semantic segmentation can be low. Thus, it is preferable to use this system in cloudy weather or a venue where is not affected by the sunlight. It was also confirmed that this system can be affected by Internet communication speed.

This speed is important to implement client-server communication smoothly. And the communication latency was also appeared. The latency is also an important index and should be verified.

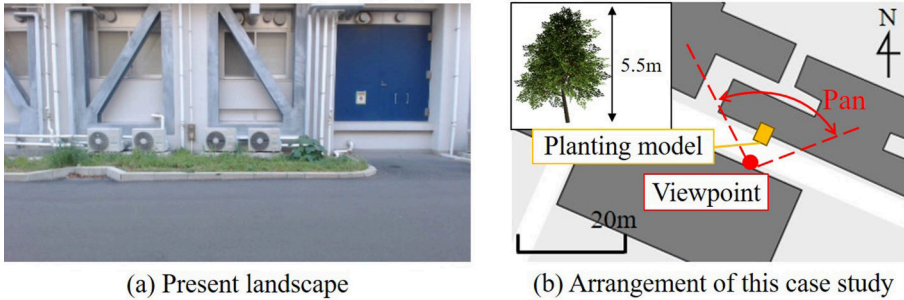


Figure 9. Present landscape and the arrangement of the case study for GVI estimation.

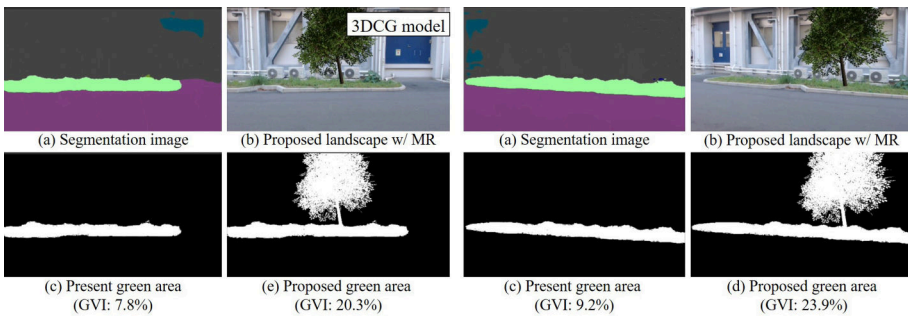


Figure 10. Planting simulation with MR and GVI estimation.

Table 2. Internet communication speed in GVI verification measured by Fast.com.

Communication	Speed [Mbps]
Browser (client)-Server (Provided by Fast.com)	Upload: 8.1, Download: 27.6
Browser (server)-Server (Provided by Fast.com)	Upload: 633, Download: 860

#### 4. Conclusions and future works

In our study, we developed a MR system which can handle occlusion dynamically and estimate the GVI of present and proposed landscape simultaneously for smooth consensus-building among stakeholders in environmental design. It was confirmed that the client-server video communication over the Internet was integrated into the MR system and the dynamic occlusion handling and the GVI estimation were implemented in real-time through the case studies. The contributions of this study are as follows:

- We integrated a MR system and real-time semantic segmentation framework based on deep learning whose computational cost is high on a mobile device using Internet-based real-time video communication.
- We implemented dynamic occlusion handling in MR-based landscape simulation even in the client-server communication over the Internet.
- We integrated a MR system and the GVI estimation using semantic segmentation. This has a potential for more smooth consensus-building among stakeholders by the accurate GVI estimation.

For future works, it is necessary to improve the processing speed of the MR system for an immersive landscape simulation. And also it is necessary to segment each instance to implement more accurate occlusion handling because semantic segmentation cannot distinguish the same category, which means that the vegetation area is detected only as vegetation. Thus, it is difficult to overlay the 3DCG model between the two objects whose category are same.

### Acknowledgement

This research has been partly supported by JSPS KAKENHI Grant Number JP19K12681.

### References

- “Fast.com” : no year given. Available from <<https://fast.com/ja/#>> (accessed 4th December 2019).
- “Skyway -Enterprise Cloud WebRTC Platform-” : no year given. Available from <<https://webrtc.ecl.ntt.com/>> (accessed 2nd December 2019).
- Cao, R., Fukuda, T. and Yabuki, N.: 2018, A Real-time Visual Environmental Evaluation System Using Image Segmentation: A Prototype for Green View Index, *Proceedings of the 41st Symposium on Computer Technology of Information, Systems and Applications*, 205-208.
- Cordts, M., Omran, S. and Ramos, S.: 2016, The cityscapes dataset for semantic urban scene understanding, *Proceedings of IEEE Conference on CVPR 2016*, 3213-3223.
- Van Dillen, S.M., de Vries, S., Groenewegen, P.P. and Spreeuwenberg, P.: 2012, Greenspace in urban neighbourhoods and residents' health: adding quality to quantity, *Journal of Epidemiology & Community Health*, **66**(6), e8.
- Holynski, A. and Kopt, J.: 2018, Fast depth densification for occlusion-aware augmented reality, *ACM Transactions on Graphics (TOG)*, **37**(6), 1-11, 194.
- Inoue, K., Fukuda, T., Cao, R. and Yabuki, N.: 2018, Tracking Robustness and Green View Index Estimation of Augmented and Diminished Reality for Environmental Design: PhotoAR+DR2017 project, *Proceedings of the 23rd International Conference on Computer-Aided Architectural Design Research in Asia (CAADRIA 2018)*, 339-348.
- Jennings, C., Hardie, T. and Westerlund, M.: 2013, Real-time communications for the web, *IEEE Communications Magazine*, **51**(4), 20-26.
- Kido, D., Fukuda, T. and Yabuki, N.: 2019, Development of a Semantic Segmentation System for Dynamic Occlusion Handling in Mixed Reality for Landscape Simulation, *Proceedings of the 37th eCAADe and 23rd SIGraDi Conference*, 641-648, 1.
- Milgram, P. and Kishino, F.: 1994, A Taxonomy of Mixed Reality Visual Displays, *IEICE Transactions on Information and Systems*, **E77-D**(2), 1321-1329.
- Yang, J., Zhao, L., McBride, J. and Gong, P.: 2009, Can you see green? Assessing the visibility of urban forests in cities, *Landscape and Urban Planning*, **91**, 97-104.
- Zhao, H., Qi, X., Shen, A. and Jia, J.: 2018, ICNet for Real-Time Semantic Segmentation on High-Resolution Images, *Proceedings of ECCV 2018*, 418-434.

## HOLONAVI

### *A study on User Interface for Assembly Guidance System with Mixed Reality in a Timber Craft of Architecture*

TAKAHARU SUZUKI<sup>1</sup>, HIKARU IKEDA<sup>2</sup>, ISSEI TAKEUCHI<sup>3</sup>,  
FUMIYA MATSUNAGA<sup>4</sup>, ERI SUMITOMO<sup>5</sup> and  
YASUSHI IKEDA<sup>6</sup>

<sup>1,2</sup>*Takenaka Corporation*

<sup>1,2</sup>{suzuki.takaharu|ikeda.hikaru}@takenaka.co.jp

<sup>3</sup>*Tsumiki Seisaku*

<sup>3</sup>issey@tsumikiseisaku.com

<sup>4,5,6</sup>*Keio University*

<sup>4,5,6</sup>{s17781fm|sumitomo|yasushi}@sfc.keio.ac.jp

**Abstract.** This paper introduces ideas to use Mixed Reality (MR) technologies in craftsman's work of architecture. One of the backgrounds of this study is emerging technology of Mixed Reality becoming much easier to use recently with new devices such as Microsoft HoloLens. Among many possible applications of this technique in architectural work, we particularly choose Japanese traditional timber joinery 'Kumiki' as a model case of complicated architectural work. We found that people need a certain sense of 3D recognition and knowledge about right order of assemble. That is what we can suggest for users with our MR guidance system named 'Holonavi' which can show appropriate information in 3D vision in real time. The aim of our research is to find useful knowledge about effective ways and sufficient information to guide users. As a conclusion, we found that guidance with MR technology gives users to have a recognition more effectively for take of right action when they are moving their viewpoint around the object and when they located in the range of reachable distance to the objects. It is the first achievement for use of 'Holonavi' to let people feel more fun to craft something by their hands aided by computer.

**Keywords.** Craftsman's work; Mixed Reality; Digital Construction; Augmented Reality; HoloLens.

## 1. Background

The technology of Augmented Reality has become widespread in recent years. In addition to AR or VR, Mixed Reality (MR) has been more familiar thanks to the development of affordable devices such as Microsoft HoloLens, and of open platforms such as Unity which application developer can use and access. MR



has been discussed in the context of architectural design by Schnabel et.al (2010) However these easier accessibility for the development of devices and platforms accelerate more application in industrial and construction field in recent years. Before our project in application of it for general methodology of instructions in assembly, we did investigate and referred prior projects and studies that utilize those technologies for construction.

“Augmented brickwork” (G. Jahn, et al. 2018) is a construction project of brick bench consists of multiple layers of curvature. A construction system of site fabrication such as cutting of bricks was designed with MR in order to materialize the smooth and continues curve surface. (See Figure.1)

Steampunk (S.Hahm et al. 2019) is a pavilion for Tallinn Architecture Biennale 2019. The special feature of this project is the hybrid structure of CNC Machining, 3D printing and handcrafting which is implemented by harmonization of human and digital devices (See Figure.1).

Honeycomb Lab and Takenaka Corporation jointly developed an application which assists construction with Hololens. By displaying information about component or mounting position in a real space, number of process of verification is shorten (See Figure.1).

MR is applied in those projects above especially for process of construction work. The guidance by Hololens mainly used for helping people to understand target form or position intuitively and interactively. It helps to have a vision of intricated design without using paper drawings. That could be helpful for traditional craftsmanship work such as Japanese timber joinery. In traditional assembly work, people used to understand processes of construction by exorcise with oral communication, and the assembly technique itself was tacit knowledge of some specific craftsman such as welder or shrine carpenter. In order to learn that kind of knowledge, it was common to be apprenticed to a master.

Those traditional techniques would be more general and be applied in unconventional ways through MR. Regarding a progress of technology in architectural construction, automated fabrication with less human labor have been main stream and it reduced complexity of design as a result.

Emerging tools like MR with computational modeling gives us new opportunity of craftsmanship with human data interaction instead of replacement of human effort from construction. Thus it deserves to get more knowledge about how human get effective inspiration for his work to create co-evolution with machine and information.

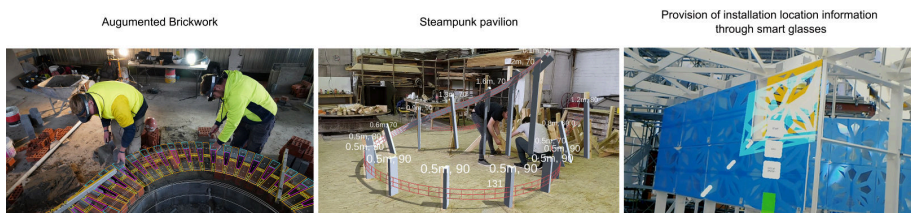


Figure 1. Reference project of construction with MR.

## 2. Research Topic

In the previous chapter, we studied background and existing projects for the investigation of the effectiveness of MR in terms of assembly process. If it is available to complement the guidance of assembly by MR, fabrication would become democratized where assembly of components is left to each craftsman. On the premise that those technology will be applied in the field of construction, we started from researching ‘Kumiki’ which is Japanese traditional timber construction system that requires complex process.

Kumiki is suitable system for this research because it is a traditional wooden joint in Japan and one of the typical joint systems. There have been many of examples of architecture which use Kumiki technique since long ago. In the timber construction process, it is proved that it is better to join only wooden pieces instead of using hardware to strengthen the structure. There are also many kinds of wooden joints designed in accordance with structure or way of joint, which represent traditional aesthetics and technique of Japanese architecture. These techniques are commonly applied for contemporary architecture and used by people under a new interpretation.

The most typical case is Kumiki toy which is produced for helping children to develop their ability to grasp three-dimensional shape or craftsman to understand the structure of joint. Indeed, it is a kind of training kit to learn how to join timbers in the traditional way. In this paper, we examine ‘Roppon-Kumiki’ which is one of the simplest Kumiki systems that consist of 6 timber components (See Figure 2). This Kumiki itself is considered as one of the techniques for assembling timber structure and is also commonly used.

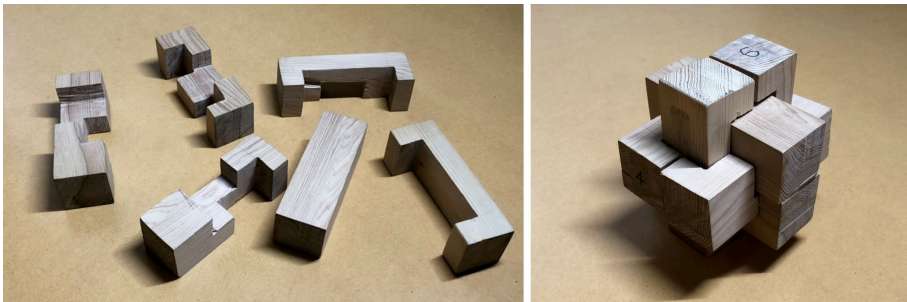


Figure 2. Roppon-Kumiki.

One of the most interesting aspects of Kumiki is the availability of both assembly and disassembly. This is reversible system that allows reconstruction because it does not use hardware such as nails nor screws; such disassemble availability would be the essence of timber architecture. It is constructed only by intersection of each component, and the most important process is the direction or order of the intersection. Those process are significant when it is assembled or disassembled. If there is even one mistake among the construction, the outcome would not be correct; the three-dimensional combination and the selection of component are essential.

Because of its complex geometry and the difficulty of the order of assembly, Kumiki is worth being investigated for the research of the assembly guidance system. This investigation would have the potential to apply the system to other approach such as furniture fabrication which has more variety of the direction of components.

### 3. Research Process

It is necessary to consider how to reutilize that traditional timber technique. This research does not aim only to hand down the skills of wooden joint by replacing it with MR. Attention is focused again on wooden architecture not only in Japan but also in the world, so there is a significant possibility of the application of the technique to timber structure which is strong against earthquake.

We proposed ‘Digital Woods’ which is a project to explore unconventional use of timber. It investigates architecture which metabolizes itself and also aims at construction of a system which controls information of timber used for architecture throughout the construction process and after completion (See Figure 3).



Figure 3. Digital Woods' .

Thus, wooden technique is expected to be applied to an innovative construction system which combines wooden and digital technology because it is easily processed with digital construction or digital fabrication. The assembly support system with MR enables not only to increase the number of components, but also to construct more complex architecture. It would change the way of monetization of building component and improve the range of the feasibility of construction technique.

On the basis of the research above, by making the use of the context such as Kumiki to apply the digital technology into wooden construction, traditional technique would be conserved and the possibility of creating unconventional type of architecture would be increased. We call this process as compound informatization by digital construction. The change of construction system itself expands the range of the ability of architecture, so there would be a great influence of this research on architecture in the future.

**4. Research Goal**

These are the list of tasks which are necessary to be solved for the development of our MR guidance system named ‘Holonavi’ which guides construction of Kumiki (See Figure 4).

1. Construction in correct order
2. Assembly in correct direction
3. Selection of correct component

Those tasks are self-evidently pointed out when we tried to assemble Roppon-Kumiki without any guidance as a first experiment. In this research, we will prove the efficient way of communication and information for the utilization of MR in Kumiki guidance (See Figure 4).

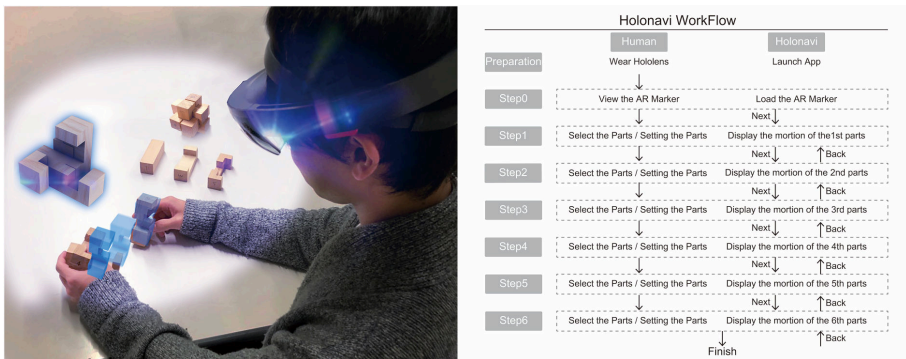


Figure 4. Holonavi.

**5. Reserach Method**

**5.1. ANALYSIS OF TWO-DIMENSIONAL MANUAL AND THREE-DIMENSIONAL IMAGING**

In order to develop better interface for MR guidance, we start from an investigation in previous technique to instruct assembly in graphical way such as printed manual. In many cases, it is difficult to let someone to be able to craft objects in their hand properly only with oral instruction and 2D drawings (See Figure 5). These skills are obtained by sufficient experience by themselves. MR for assemble guidance can be useful for training of inexperienced people or people who has disadvantages in language.

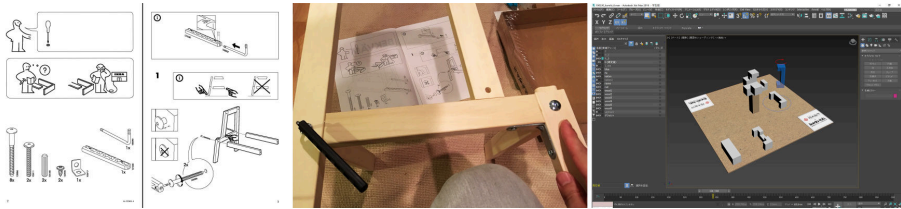


Figure 5. 2D manuals / 3D manuals.

We analyzed paper manuals of assembly and explored how to convert them into three-dimensional information (See Figure 6). After the evaluation of several types of paper manuals, there are factors which enable research subjects to understand better, and factors which seem to be unnecessary on the other hand. The efficient communication of graphical device or way of instruction were analyzed in order to achieve goals. We created three-dimensional image of that information and let the research subjects to experience it to understand the contents and assess the three-dimensional manual.

The visualization methods for assembling parts			
	Select the parts	Setting the parts	Motioning the parts
Give the parts a number	<input type="radio"/>		
Show example of the mistaken parts	<input type="radio"/>	<input type="radio"/>	
Show next state on separate window	<input type="radio"/>		
Enclose the parts with a circle	<input type="radio"/>		
Highlight the parts with color changed	<input type="radio"/>	<input type="radio"/>	<input type="radio"/>
Enlarged display		<input type="radio"/>	
Show the position fitted the parts		<input type="radio"/>	<input type="radio"/>
Fit the parts to the middle		<input type="radio"/>	
Use the specific Mark of the motion			<input type="radio"/>
Show last position of the parts			<input type="radio"/>
Show the before and after assembling the parts			<input type="radio"/>
Use another color with line			<input type="radio"/>
Connect two points of the parts with wire			<input type="radio"/>

Figure 6. Analysis of paper manuals.

### 5.2. DISPLAY ANIMATION IN HOLONAVI

By type canalization of existing assembling manual based on drawing, we have done experiment of similar methods in 3D vision to be evaluated by testers to compare to figure out its applicability. These experiments are applied to our system to demonstrate how it works and get feedbacks from public users.

There are some problems in the paper manuals such as picking the right component, instructing it to be in the correct direction, and instructing the procedure in correct order; which appeared also in three-dimensional manual. We examine those issue would be solved by assigning ID to each component in order to let people pick up a component initiatively with displaying only hologram of actual shape of it (See Figure 7).

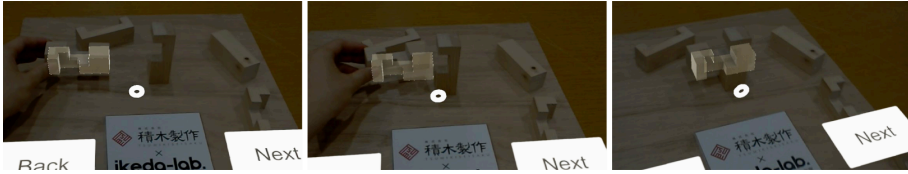


Figure 7. Animation in Holonavi.

## 6. Results

Through those experiments, we tried to get knowledge about better ways of MR interface. Technical issue appeared in the first trial where ArUco marker was stuck on a target component and suggests next hologram. We found that it is better to fix the target component for the sake of assembly in a similar way as actual construction.

The finding suggests that location-based AR can provide more stable condition of hologram without changing the display depending on the location of component. In addition, the research subjects can understand the output better because they were able to move around the component during assembly. Also, we found that the most efficient type of guidance information was animation of component itself which allows to complete the work rather than displaying diagrams such as arrows.

As the second trial, we fixed a marker in a field of vision and fixed a component on the assembly environment. In the first trial the research subjects needed to use both of their hands to assemble, but in this case, they became able to look at the hologram more stably (See Figure 8).

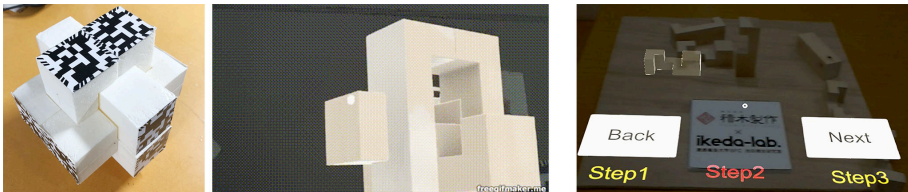


Figure 8. Marker on component / Marker on assemble environment.

## 7. Discussion and Conclusion

We applied Holonavi to the actual assembly. The result shows that Holonavi enables the assembly easy and correct. In other words, it makes fabrication which used to be impossible to be possible. Thanks to the 3D hologram display, people become able to grasp 3D objects who does not have the availability to do that only by 2D manuals. The availability is also covered with the assembly process where they can move and look around.

Some points still to be improved though. Many people are unfamiliar with the interface of Hololens, so the fact that they have to click a button when switching between steps takes a lot of time. They practiced in advance, but the finding shows

that there was a problem with this point because they needed to get used to it.

In terms of work progress, it was found that work would proceed even if it was wrong. If the subject himself / herself does not notice a mistake, the process proceeds to the next task and then returns. As long as they don't notice a mistake, the work will be left as it is, so it was disassembled because you didn't know the correct answer when you came back. This problem may be solved by requiring a mechanism that allows the computer to evaluate the resulting shape each time.

From the viewpoint of component selection, the subjects spontaneously select component by watching the moving animation. In this case, the correct part can be selected, but it depends on the subjects' ability of the selection, so it might not be said that it is possible to provide suitable guidance. However, there is a way to accurately capture objects with a 3D object authentication function of Vuforia (See Figure 9). It is possible to search for the correct part using the computational simulation, and even if it is a confusing part, it will be possible to search without errors.

There is also drawback in terms of device that subjects cannot see the target with close distance because of the narrow wide field of vision of Hololens. It is expected that this aspect will be improved in Hololens 2. In this research, it was solved by fixing a target component at the begging of the assembly; which enables the subjects to have certain distance between them and components.

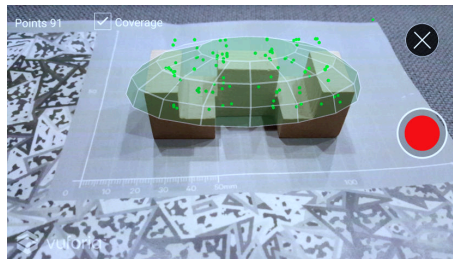


Figure 9. 3D object authentication in Vuforia .

## 8. Challenges and Prospects

After experimental operation and feedback from demonstration of Holo-Navi, we notice there are more potential in the current system than just to instruct the expected design in hologram correctly. If it is a tool to support human data interaction, we can develop some more further functions of it. The current system in Kumiki assembly is for single person, but it has potential to create collaborative communication through the system with multiple works. It is possible for a third person to recognize or grasp what another person figures out the workflow who works on this assembly. The construction work itself is based on group work, and in many cases, the work has been promoted by cooperation.

In addition, we understood that MR is more effective when dealing with large objects and causing physical movements rather than small objects in a hand. It is necessary to recognize how a worker can be physically affected by

using MR by handling something with a physical sense of scale. Furthermore, it can connect to interactive design with adaptive computational model that allows human intervention even in the process of construction. So next step of our research will investigate how effective the assembly work guidance is in the MR environment through experiments such as scaling up, multi-personalization and adaptive for human intervention (See Figure 10).

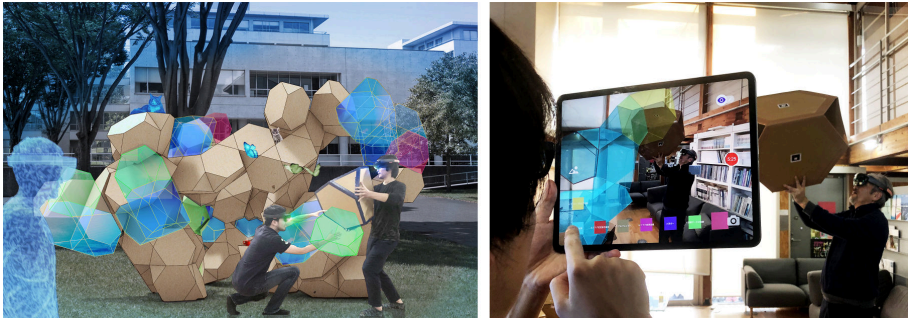


Figure 10. Future vision: Navigation of create space using Mixed Reality.

## Acknowledgment

This research project is supported by and collaborated with TsumikiSeisaku Co.Ltd.

## References

- “Steampunk, Intuitive Design Outwitting Computation, Is 2019 Tallinn Architecture Biennale” : 2019. Available from <<https://worldarchitecture.org/article-links/eezch/steampunk-intuitive-design-outwitting-computation-is-2019-tallinn-architecture-biennale-s-winner.html>> (accessed 11th December 2019).
- Bungbrakearti, N., Cooper-Wooley, B., Odolphi, J., Doherty, B., Fabbri, A., Gardner, N. and Haeusler, M.H.: 2018, HOLOSYNC - A Comparative Study on Mixed Reality and Contemporary Communication Methods in a Building Design Context, Learning, Adapting and Prototyping, *Proceedings of the 23rd CAADRIA Conference*, Volume 1, Tsinghua University, Beijing, China, 17-19 May 2018, 401-410.
- Chen, H., Lee, H., Swift, M. and Tang, J.: 2015, 3D Collaboration Method over HoloLens and Skype End Points, *Proceedings of the 3rd International Workshop on Immersive Media Experiences*.
- Chu, M., Jane, M. and Peter, E.D.L.: 2018, Integrating Mobile Building Information Modelling and Augmented Reality Systems: An Experimental Study., *Automation in Construction*, **85**, 305–16.
- Takenaka Corporation, : 2019, “Digital Design-Build Future design and construction technologies that realize EQ House” . Available from <[https://www.takenaka.co.jp/takenaka\\_e/eq\\_house/technology/index.html](https://www.takenaka.co.jp/takenaka_e/eq_house/technology/index.html)> (accessed 11th December 2019).
- Funk, M., Andreas, B., Liane, B., Thomas, K., Thomas, H. and Albrecht, S.: 2017, Working with Augmented Reality?: A Long-Term Analysis of In-Situ Instructions at the Assembly Workplace., *Proceedings of the 10th International Conference on Pervasive Technologies Related to Assitive Environment*, 222–9, Island of Rhodes, Greece: PETRA.



- Goepel, G.: 2019, Augmented Construction -Impact and opportunity of Mixed Reality integration in Architectural Design Implementation, [*Proceedings of the 39th Annual Conference of the Association for Computer Aided Design in Architecture*].
- ikedalab, initials missing: 2010, "Digital Woods for Timberize". Available from <[https://ikedalab.sfc.keio.ac.jp/digital\\_woods/](https://ikedalab.sfc.keio.ac.jp/digital_woods/)> (accessed 11th December 2019).
- Jahn, G., Newnham, C. and Beanland, M.: 2018, Making in Mixed Reality. Holographic design, fabrication, assembly and analysis of woven steel structures, *Proceedings of the 38th Annual Conference of the Association for Computer Aided Design in Architecture (ACADIA)*, Mexico City, Mexico 18-20 October, 2018, 88-97.
- Jahn, G., Newnham, C., van den Berg, N., Iraheta, M. and Wells, J.S.: 2019, Holographic Construction, *Design Modelling Symposium*.
- Kress, B.C. and William, J.C.: 2017, Towards the Ultimate Mixed Reality Experience: Hololens Display Architecture Choices., *Society for Information Display International Symposium Digest of Technical Papers 48*, 127-31.
- Ren, J., Yingying, L. and Zhicheng, R.: 2016, Architecture in an Age of Augmented Reality: Applications and Practices for Mobile Intelligence BIM-based AR in the Entire Lifecycle., *Proceedings of the International Conference on Electronic Information Technology and Intellectualization*, Guangzhou, China: ICEITI..
- M.A. Schnabel (ed.): 2009, *MIXED REALITIES: Framing Mixed Realities*, Mixed Reality In Architecture, Design, And Construction, Wang, Xiangyu; Schnabel, Marc Aurel (Eds.) 2009, XIV, ISBN: 978-1-4020-9087-5, pp. 3-11.
- Zeiba, D.: 11th October 2019, "A steampunk pavilion combines analog and digital technology". Available from <<https://techplus.co/a-steampunk-pavilion-combines-analog-and-digital-technology/>> (accessed 11th December 2019).

## SENSMOD

### *Computational Design through the lens of Henri Lefebvre's Spatial Theory*

ROBERT DOE

<sup>1</sup>Cardiff University

<sup>1</sup>doer1@cardiff.ac.uk

**Abstract.** Spatial productivity is the first of the elements comprising sensMOD, a student elective that implemented a methodology addressing the exigent need of our time for transformation in the architecture, engineering and construction (AEC) sector. The second and third elements of sensMOD are parts and interaction which focus attention on the nature of complexity and connectivity in our networked world. The paper proposes a methodology that was used to guide the teaching of an elective for third year architecture students at a UK university. Its wider purpose is to contribute to discussion concerning the dysfunctional state of an AEC sector that needs to consider its productivity as projections of wider networks of resource and energy relationships. Henri Lefebvre's spatial theory (1991) guides the narrative and formulation of sensMOD.

**Keywords.** Computational design; spatial productivity; modularity; interaction design.

## 1. Introduction

*Can change occur without expectation, without exploration of the possible and the impossible? (Lefebvre, 2014, p.27)*

This paper defines sensMOD, a student elective comprising a methodology used to guide the teaching of computational design principles and methods for a third year, RIBA accredited, BSc architecture elective at a UK university. Its premise is that the design and production of space by the global AEC sector needs overhauling because its buildings are responsible for 32% of global energy consumption. Stabilised global warming of 1.5°C requires new construction to be fossil-free and near-zero energy by 2020, with building emissions reduced by 80-90% by 2050 (IPCC, 2018). However, this paper does not examine the problem using the tools of scientific analysis but instead proposes a radical methodology, viewed through the lens of Lefebvre's spatial theory, that would transform the AEC sector. Accordingly, sensMOD considers space, parts and interaction as essential elements of the methodology, with each viewed from perspectives which are overlooked in conventional approaches to design and production. Space is examined as a phenomenological rather than abstract conception in accordance

to Lefebvre's notion of the production of space (1991) and with reference to Gaston Bachelard's reflections on the 'corner' in *The Poetics of Space* (1994). Parts are studied in relation to the whole with concepts borrowed from the manufacturing sector including slot, sectional and bus modularity, as described by Karl Ulrich (1995). Interaction, an essential element of the methodology that binds connectivity in space and between parts, is studied with reference to Malcolm McCullough's (2005) examination of pervasive computing and its influence on architecture.

A carefully chosen and disregarded 'corner' of the School of Architecture was the site for explorations by the students implementing sensMOD with the aim of developing an appropriate architectural intervention. The spatial realm was initially explored using 1st order modelling (Stasiuk, 2018) - sketches, observations, photos, videos and text - so that no predefined conventional representations would dominate and to limit the abstracting influence of computational design tools at this stage. The elements of parts and interaction combined 1st order modelling outcomes with 2nd order modelling techniques using the procedural method of parametric modelling with Rhino and Grasshopper, and computational modelling with Firefly and Arduino which included the use of scripting, sensors and actuators.

## 2. Space

*...the spider, for all its 'lowliness', is already capable, just like human groups, of demonstrating space and orienting itself on the basis of angles. (Lefebvre, 1991, p.173)*

Lefebvre alludes to the notion that through activity the living organism produces space that is networked to a field of activity that projects relationships into manifestations of the living organism. Accordingly, sensMOD challenges the notion that space derives from an analytical, centrally authored, hierarchical description of functions and adjacency relationships because it is a notion that supports interests which ignore decentralised, local activities and resource availability. Furthermore, this notion has encouraged architects to consider space as an analytical abstraction that is separate from behaviour. Instead, architects believe that the functional specificity of ordered spatial configurations will determine behaviour, as noted by Bryan Lawson who criticises architects lack of training in the ability to 'observe and evaluate buildings as social phenomena' (2001, p.200). Tim Ireland's study of sensory-based space extends Lefebvre's spatially oriented view of the world by focusing on the productive qualities of an 'archetypal organism-in-its-environment' which generate configurations in space (2015, p.383). Furthermore, Ireland promotes an architectural method of 'social' or 'projected geometry' implemented by computational modelling to configure spatial configurations and forms which he depicts as a fluid, decentralised and distributed intelligence arising from a 'cell-centric', agent-based strategy produced by the living organism (2015, p.389).

But the purpose of this stage of the methodology of sensMOD is to dwell in the realm of the phenomenon in all its manifestations and not be diverted by scientific

explorations. Returning to Bachelard's 'corner' the intent here is for the students to remain as long as possible in this '...sort of half-box, part walls, part door' where 'nothing is ever empty' and to continue to reflect on his notion that words are 'little houses' where we might go upstairs and withdraw or descend to the cellar to dream (1994, pp.137-147). The focus narrows to our interaction with space through our senses and the way that we affect the world through our capacity to affect - and to impart the idea, as alluded to earlier, that rather than planned the space of architecture is moving inexorably towards fluidity because function no longer commands attention as it once did. Indeed, as noted by William J Mitchell (2003, p.162), program and functional specificity have been eroded by 'continuous fields of presence' and the 'destabilisation of person-to-place relationships'. He goes on to assert that as a result of these processes we should be witnessing an architecture of,

*...continually reconfiguring clusters of spatial events characterised by their duration, intensity, volatility, and location. (Batty, M. 2002 in, Mitchell, 2003, p.163)*

The idea that connectivity matters more than functional adjacency relationships was propounded earlier by Nikolas Habraken in Supports (1961) and depicted in Cedric Price's Inter-Action Centre (Lobsinger, 2004). But the difference today is that connectivity is networked and reconfigured seamlessly and digitally, whereas these pioneers attempted to represent connectivity as a network of large-scale, reconfigurable physical relationships. This emphasis on networked seamlessness was developed by Lefebvre's *The Production of Space* (Lefebvre, 1991) originally published in 1974, which asserted that 'productive' space is correspondingly connected to a networked world. McCullough advanced the theme of connectivity imagining 'responsive place' instead of 'anytime - anyplace' with the additional insight that connectivity is 'inside of architecture' rather than 'instead of architecture' (2005, p.67). McCullough's description of interaction design connects with Lefebvre's field of phenomenology as they are both concerned with perceptions that are unrelentingly fluid and emergent yet sensuously responsive, hence he calls for,

*...interaction design to use the prospects of ambient, haptic and embedded interfaces as a way to reinvent computing. (2005, p.153)*

Correspondingly, Lefebvre had already noted that,

*...space...is first of all heard (listened to) and enacted (through physical gestures and movements). (1991, p.200)*

The notion of space as sensed and affected by our senses initiates the first stage of the methodology of sensMOD. The intention was to allow awareness of sights, sounds, touch and taste, and an interoceptive (i.e. inside) and proprioceptive (i.e. outside) sense of the body in space, to produce a response to a pre-existing spatial configuration in the School of Architecture. At the same time, the connected and networked nature of this productivity was introduced (Figure 1).

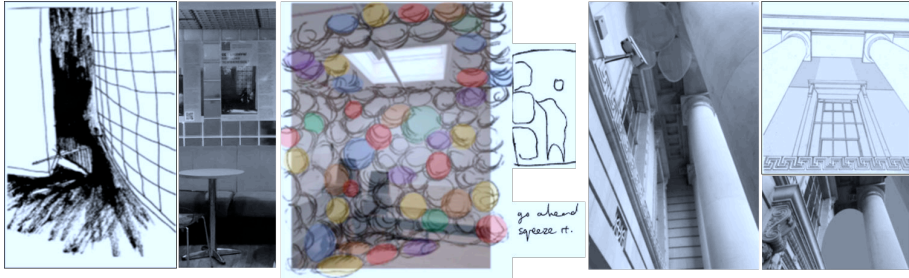


Figure 1. Development of concepts: Team 2 (SeeWhatHappens); Team 5 (Release); Team 9 (Airhead).

### 3. Parts

*...before the advent of the abstraction devised by human societies, information was no more distinct from material reality than the content of space was from its form: the cell receives material information in material form. (Lefebvre, 1991, p.178)*

Lefebvre verifies that nature's spatial envelope, the atom or the cell, has a boundary that is relative because its permeability must allow for the exchange of energy (food, air, excretion) and information (sensory data). Correspondingly, in human society boundaries are relative, that is permeable, but the envelope may also be closed for security or privacy reasons or to exclude outsiders. As Lefebvre observes, the spatiality of the office, or more generally the 'space of work', exemplifies relative or permeable boundaries,

*...as one network among others, as one space among many interpenetrating spaces, its existence is strictly relative. (1991, p.191)*

Thus, in this conception, atoms, cells and parts have permeability and porosity and they don't exist as independent entities but within connected wholes that produce and are the product of networked space and form. The part, like its function, is a relative concept and while it may be an atom, a molecule or a cellular complex, it may also be regionally defined as an arm or an office, but the common conditions of these parts are relativity of definition and connectivity. Furthermore, the bodily or holistic manifestation goes beyond these parts via networks as Lefebvre explains, again by reference to the office which manifests from these networks as the result of the 'gestures' and 'actions' of productive labour, divisions of labour, operation of markets and property relationships that are the ownership and management of the means of production (1991, p.191).

Therefore, the part was introduced to the students as a notional object which is relative rather than absolute, connected by networked links, and to enable the management and understanding of complexity. This facilitated further discussion of parts as modules that are responsive to sensory input and output. We utilised the manufacturing sector's concept of modular architecture which is different to architects' conceptions which include: the potentiality of the brick or block as a module, as demonstrated by Alfred Farwell Bemis (Bemis, 1936); the modular arrangement of standard components as exemplified by Rudolph Schindler and

Walter Segal (Broome, 1986; Schindler, 1946); the modularisation of parts as proposed by Konrad Wachsmann and Walter Gropius with their Packaged House of 1941-2 (Davies, 2005, p.23); and also recent examples of volumetric or modular containment (KieranTimberlake, 2017; SHoP, 2014). By contrast, for all scales of production in the manufacturing sector the concept of modularity has been refined by Ulrich (1995, pp.419-428) to include the strategies of slot, sectional and bus modularity (Doe & Aitchison, 2016) (Figure 2).

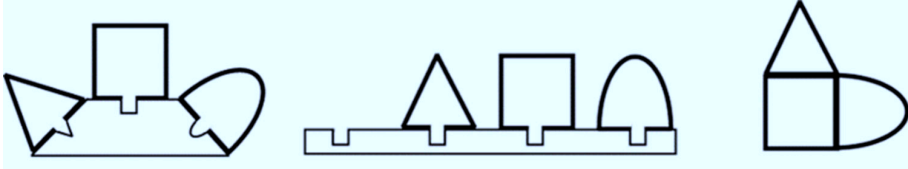


Figure 2. Slot, bus and sectional modular architecture strategies (Ulrich & Eppinger, 2016, p.188).

With slot modularity, each of the interfaces between components is of a different type from the others, so that the various components in the product cannot be interchanged e.g. a car radio whose interface is different to other components in the car. With sectional modularity, all interfaces are of the same type and there is no single element to which all the other components attach e.g. office partitions, computer systems. With bus modularity, there is a common bus to which the other physical components connect via the same type of interface e.g. expansion cards for personal computers, shelving systems. Thus, it's the interface, or point of connectivity, that defines the difference between these modular architecture strategies and the students were encouraged to nominate one or several of these in response to their spatial explorations and in the development of their architectural intervention (Figure 3). Rhino and Grasshopper seminars supported this approach by demonstrating how modularity can be interpreted as a 2nd order, parametric modelling method. But, as previously stated, the purpose was not to create specialised spaces or interventions that required supporting equipment, instead, as Mitchell suggests, the intention was towards,

*...creating flexible, diverse, humane habitats for electronically supported nomadic occupation. (Mitchell, 2003, p.162)*

This approach also confirmed that we are already carrying out our activities in connected, networked spaces where we determine function on the fly, and brought to awareness the realisation that it is now the 'software programmer' not the 'architectural programmer' who controls space use and 'thereby expresses power' (Mitchell, 2003, p.167).

The modular or component based element of the methodology advocated here is relevant and timely because it re-focuses attention towards the part and its interfaces where we can reconfigure spatiality using appropriate and adaptable materials, and where energy flows may be sensuously distributed and responsively networked in a decentralised way.

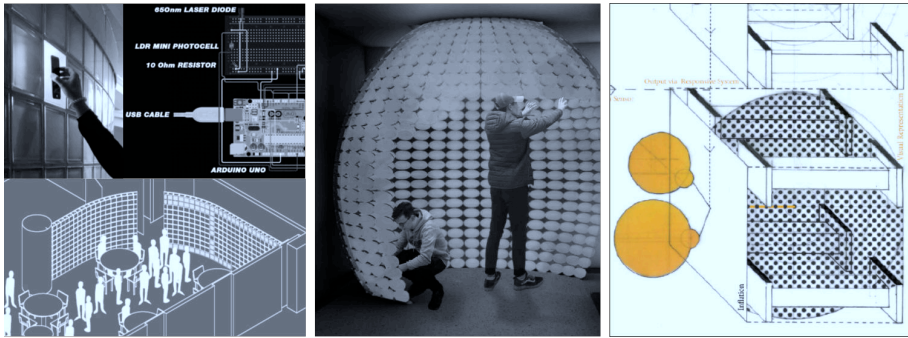


Figure 3. Development of prototypes: Team 2 (SeeWhatHappens); Team 5(Release); Team 9 (Airhead).

SensMOD counters the reproduction of homogeneity and its outcomes which are the creation of confounding places where formal geometry and visual spectacle dominates, leading to feelings of discomfort and unease. Instead, it reinforces Lefebvre's observations that the space of architecture should be produced in a distributed and decentralised way that acknowledges partiality and its interfaces, and that arises from our sensual capacity to hear, interact and enact through our 'physical gestures and movements' (1991, p.200).

#### 4. Interaction

*...life has been...an incessant diversification and intensification of the interaction between inside and outside. (Lefebvre, 1991, p.176)*

Lefebvre infers not merely to what passes through the permeable membrane of the cell, but is attesting to his enduring interest in space and his unusual awareness of his own body's sensuality with drives poetic desire to 'vivify' the body's 'rhythms and senses' (Lefebvre, 2014, pp. 34-35). Interaction is the key element of this relationship between the inside and outside of the part or module and, correspondingly, of the methodology of sensMOD. Concerning the importance of interaction, McCullough's enquiry into 'contextual computing' is instructive as it examines the phenomenological thinking that led to theories of 'embodiment', 'contextual perception' and 'situated action' (2005, p.178). In summary, this thinking explained that modern buildings' lack of responsiveness to place arose from their emphasis on the representation of abstractly geometric space. Essentially, this amounted to a failure to interact, but more poignantly Lefebvre, lamenting the influence of urban planners on architects' work, described such resultant non-places as '...the forgotten, obliterated location - of the architectonic work' (2014, p.3). These commentaries prompted further questions about intention, expression and implication which were relevant to the students' spatial explorations focussed around interaction:

- Intention. How can we make responsive modular interventions that renew and embody 'the joy of lived experience' (Lefebvre, 2014, pp.26-27)?
- Expression. If 'background experiences', rather than 'foreground objects'?

(McCullough, 2005, p.154), are the path to connection between interaction design and architecture, then how is this achieved?

- Implication. Is a responsive approach that uses ambient, haptic and embedded interfaces a way to ‘reinvent computing’ (McCullough, 2005, p.153), reinvent architecture, or both?

To answer these questions students explored ways of collecting sensory data to influence pattern, form and interaction using Grasshopper and Firefly, and examined how to use sensors and actuators with Arduino that were relevant to their initial responses to the spatial enquiry of their ‘corners’. With contributions from an artist working with light, DMX controls and other sensors, and an artist working with found objects, ‘upcycled’ e-waste, Arduino sensors and actuators the students were also introduced to ideas and methods by which spatially located, responsive modular interventions could be realised. The technical challenge of scripting using 2nd Order abstracted logic, territory unfamiliar in conventional architectural training and practice, was taken on by the students utilising the visual data flow graphs of Grasshopper and the imperative programming required to instruct Arduino’s microcontroller with its associated inputs and outputs.

Throughout these explorations the emphasis lay on spatial understanding, and on the process of design and production, rather than on the creation of a finalised representation or form. 2nd Order computational modelling was instead employed to enable spatial configurations to emerge - or in Lefebvre’s terms, for production to be ‘secreted’ from spatial practice (1991, p.38). The early explorations of the concept of the ‘corner’ guided students understanding of the patterns of activity that were of importance and that would embody ‘the joy of lived experience’, thus contributing delight for participants and passers-by. Rather than a centralised approach to design and making teams of four worked as distributed co-workers, sharing tasks and responsibilities. In such a setting, each team also represented all imaginary stakeholders’ interests, needs and desires from a technological, social, environmental, economic and political perspective, thus grounding the work and connecting these stakeholders via a network of relationships to their realised productions. And, rather than rigid, functionally specific spatial outcomes, the goal was to produce interaction bound, connected and distributed, spatially and partially responsive interventions that would be adaptable to quick, digitally driven change (Figure 4). Accordingly, and in recognition of the exigency to change the way that we design and produce buildings so that our limited resources and energy are utilised with appropriate care and attention, sensMOD’s radical approach aims to address the tacit norms of architectural practice and the AEC sectors’ dysfunctionality in general.



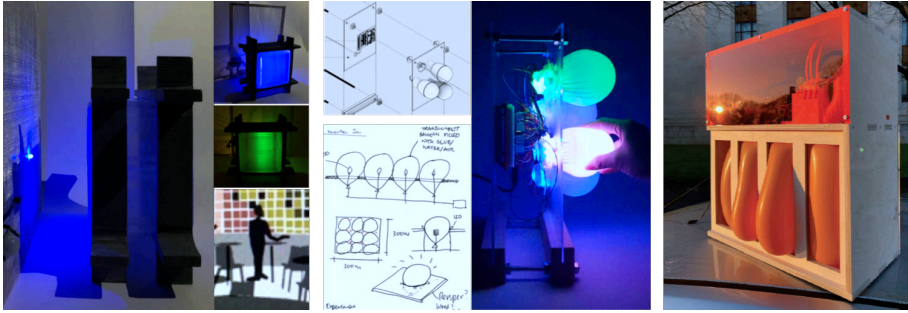


Figure 4. Development of final work: Team 2 (SeeWhatHappens); Team 5 (Release); Team 9 (Airhead).

## 5. Reflection and conclusion

*The architect (demiurge or hack) and limits of architecture (as specialised activity, aesthetic or technical) are secondary. It is a question of 'mankind' and its future. (Lefebvre, 2014, p.29)*

The methodology defined in this paper addresses the exigencies of Lefebvre's exhortation by reconfiguring the way that architects are trained to design and produce buildings. Additionally, as a responsive modular approach, sensMOD has included discussion of part to whole relationships, defined more broadly by Daniel Koehler (2019) as mereology which 'can gather the techniques of bonding, joining, interlocking, entangling and overlapping of parts' (Koehler, 2019, p.33). Mereology underpins the recently defined movement of 'discretism' which Mario Carpo also conflates with 'particled computation' (2017). Furthermore, the techniques which Koehler lists can be seen in Phillippe Morel's Bolivar Chair (2004) and Kengo Kuma's Kodama Pavilion, 'a new "democratic" way of construction' (Kuma, 2018). These techniques can be implemented using an aggregational computational method derived from a 'new kind of science', a notion first described by Stephen Wolfram (2002), and linked by Carpo to the design movement of discretism because the work of its proponents reflects,

*The inherent discreteness of nature... which is made of 'discrete chunks of matter' (Carpo, 2017, p.71)*

Clearly then sensMOD's methodology shares some of the attributes and characteristics of mereology and discretism but it is distinguished by its focus on interaction which links the production of space to activity and to projections beyond via networks of relationships, in accordance with Lefebvre's spatial theory.

The methodology of sensMOD has explored the possible and the impossible, aiming to instruct and inform in the field of academia, and to encourage discussion and urgently needed change in the AEC sector. What is possible is that architects could be trained to observe and evaluate buildings as social phenomena, using Lefebvre's way finding suggestions as a guide. What seems impossible is effecting change in the dysfunctional processes of design and production that the AEC sector engages in which ignore the limitations of resource and energy availability. A

methodology that considers parts and their interactions as projections of wider networks of resource and energy relationships attempts to bridge this gap in knowledge and understanding. Further research will examine the results arising from the implementation of sensMOD in the academic context and its wider implications for teaching and practice.

### Acknowledgements

My thanks to the 3rd year architecture students at the Welsh School of Architecture, DPM3, Elective 2, sensMOD, including Team 2 (Augusta Fiseryte; Ksenia Davydova; Erna Kuginyte; Miltiadis F Christodoulakos), Team 5 (Jamie Masters; Arnaud Latran; Anna Pavlou; Ke Chew) and Team 9 (Jan Stawiarski; Molly Hughes; Frank Brandon; Bo Tan) whose work is depicted, and also to artists Paul Granjon, Simon Fenoulhet and Leigh Davies for their collaborations with this elective.

### References

- Bachelard, G. 1994, Corners, in É Gilson and J.R. Stilgoe (eds.), *The Poetics of Space*, Beacon Press, 136-147.
- Bemis, A.F. 1936, Rational Design, in J. Burchard (ed.), *The Evolving House*, MIT Press, Cambridge, MA.
- Broome, J.: 1986, Special Issue: the Segal Method, *Architect's Journal*, **183**(45), 31-68.
- Carpo, M.: 2017, *The Second Digital Turn: Design Beyond Intelligence*, MIT Press, Cambridge, MA.
- Davies, C.: 2005, *The Prefabricated Home*, Reaktion Books, London.
- Doe, R. and Aitchison, M.: 2016, Facilitating change: the modular format in the design of prefabricated homes, *50th International Conference of the Architectural Science Association (ASA)*, 397-406.
- FullReport, I.: 2018, "Global Warming of 1.5°C". Available from <[https://www.ipcc.ch/site/assets/uploads/sites/2/2019/06/SR15\\_Full\\_Report\\_High\\_Res.pdf](https://www.ipcc.ch/site/assets/uploads/sites/2/2019/06/SR15_Full_Report_High_Res.pdf)>.
- Habraken, N.J.: 1999, *Supports: an alternative to mass housing*, Urban International Press, Gateshead, Tyne & Wear.
- Ireland, T.: 2015, The Spatiality of Being, *Biosemiotics*, **8**(3), 381-401.
- Koehler, D.: 2019, Mereological Thinking: Figuring Realities within Urban Form, *Architectural Design*, **89**(2), 30-37.
- Kuma, K.K.: 2018, "Kodama Pavilion". Available from <<https://kkaa.co.jp/works/architecture/kodama/>>.
- Lawson, B.: 2001, *The Language of Space*, Architectural Press, Oxford, UK.
- Lefebvre, H.: 1991, *The Production of Space*, Blackwell Publishing, Malden, MA.
- Lefebvre, H.: 2014, *Towards an Architecture of Enjoyment*, University of Minnesota Press, Minneapolis, MN.
- Lobsinger, M.L.: 2004, 'Out of the Box': Price-Rossi-Sterling and Matta-Clark, *Journal Of The Society Of Architectural Historians*, **63**(3), 384-386.
- McCullough, M.: 2005, *Digital Ground - architecture, pervasive computing, and environmental knowing*, MIT Press, Cambridge, MA.
- Mitchell, W.J.: 2003, *Me ++ : the cyborg self and the networked city*, MIT Press, Cambridge, MA.
- ProvingGround, P.G.: 2018, "Design Modeling Terminology". Available from <<https://provingground.io/2018/06/13/design-modeling-terminology/>>.
- Schindler, R.M.: 1946, Reference Frames in Space, *Architect and Engineer*, **165**(1), 10,40,44-45.

- SHopArchitects, S.: 2014, "461 Dean Street: b2 bklyn". Available from <<http://www.shoparc.com/projects/b2-bklyn/>>.
- Ulrich, K.: 1995, The role of product architecture in the manufacturing firm, *Research Policy*, **24**, 419-440.
- Ulrich, K. and Eppinger, S. 2016, Product Architecture, in , *Product Design and Development*, McGraw Hill Education, New York, NY.
- Wolfram, S.: 2002, *A New Kind of Science*, Wolfram Media, Champaign, IL.

# THE ASSOCIATION STUDY BETWEEN RESIDENTIAL BUILDING INTERFACE AND PERCEIVED DENSITY BASED ON VR TECHNOLOGY

*Taking 2 Enclosed Residential Districts of Guangzhou as Examples*

YAN LI<sup>1</sup>, HONGWU DU<sup>2</sup> and QING WANG<sup>3</sup>

<sup>1,2,3</sup>*the School of Architecture, South China University of Technology, Guangzhou, China*

<sup>1</sup>*1559930506@qq.com* <sup>2,3</sup>*{philipdu|lvorwang521}@126.com*

**Abstract.** As urban development enters the stock increment era, the demand of environmental quality in urban residential districts gradually improves, making the construction of livable residential environment an important direction of urban development. The improvement of livable environment is the inevitable result of this process and perceived density is an indispensable and important part. Among the statistical methods, preference study is the most commonly one to explore the subjective factors affecting preference. The experience of immersive virtual environment can provide a more appropriate analytical method better for traditional image selection. Different permeability of architectural interface has significant influences on the perception of space comfortability, crowding and fascination. In this paper, two existing enclosed residential districts are selected for case study. The factors closely related to perceived density, such as solid Wall, grille, glass, open space, greening, etc, are selected by using immersive virtual technology. Through the interviewees' evaluations of perceived density of the virtual environment, the relationship between building interface and the perceived density of the residential area will be established.

**Keywords.** Spatial Perceived Density; Virtual Reality Technology; Enclosed Residential District; Housing Interface; Association Study.

## 1. Introduction

With the gradually improved demand of environmental quality in urban residential districts, the 'soft dimension' construction of livable residential environment has become an important direction of urban development. The research of space perception in combination with new technology has rapid developments and breakthroughs, which provides a design and research basis for space construction in the psychological dimension and perception level. Many qualitative studies on perceived density have been carried out in the 1970s and 1980s, while less quantitative researches on related factors at the micro level can be found. In

addition, density indicators of urban development lack psychological, behavioral and emotional intervention factors.

This paper attempts to select two typical types of enclosed residential districts for simplified modeling in Guangzhou, China – multi-storey row enclosed residential district and high-rise point enclosed residential district – by taking building interface as a variable to optimize the research method of the preference of traditional photograph selection. Immersive virtual technology can provide more possibilities for excavating factors related to perceived density, to further explore the quantitative research on building interface changes and residents' perceived density, which can establish the correlation between them.

## **2. Research background and context**

High-density and vertical development is a common phenomenon in contemporary cities and neighborhoods, which can positively impact on social interaction but negatively impact on individuals and communities especially in the field of environmental psychology. The popularization of virtual reality technology has led to the development of immersive experience study, including the research of social psychology, visual perception, behavioral science and spatial cognition related to psychological cognition (Fisher-Gewirtzman, D. 2017; LU Yi. 2017; ZHEN S.H.,et al., 2019), as well as smart city (Sampaio et al., 2010; Jamei et al., 2017), public participation, space design practices and construction (Guan and Liang, 2015; Xu L.Q.,et al., 2019), which has reflected its perceived advantage. In addition, the experience of immersive virtual environment can make up for the static disadvantages of traditional picture-type selection method, and provides a more appropriate analysis method to explore the factors influencing the perception of preference.

### **2.1. DENSITY AND CROWD**

Density has become one of the important criteria for decision makers of different disciplines and specialties to implement policies and check results (Boyoko & Cooper, 2011). In the field of urban and architecture, density both reflects the physical size of space and the organization of surrounding environment. Professionals try to describe density in various ways that it becomes one of the most critical indicators in urban and architectural design. Density itself is a perceptual experience, including static and objective physical dimensions, as well as psychological and emotional social dimensions (Rapoport, 1975). Although density is mainly based on physical measurement dimension, it can objectively measure the distribution relationship between people and space, while crowding is a negative subjective experience of social and psychological overload caused by excessive density (Rapoport, 1975). Perceived crowding and perceived density are both subjective evaluations of density in a given environment (Eroglu et al., 2005), and have consistency in a certain context. To clarify the relationship between density and crowding, it is necessary to further distinguish physical density from perceived density, and perceived density from emotional density (isolation, suitability, crowding) (Rapoport, 1975; Alexander, 1993; Mousavinia

et al., 2019).

## 2.2. VISUAL PERCEPTION

Most of the information to understand the world is through vision, and the visual activity is highly selective. The process of visual perception is completed by actively selecting objects of interest and accumulating psychological experience. Visual Stimuli in the environment can affect people's perception and behavior, thus establishing the relationship mechanism of human-space (Gibson,1986). Evaluating perception density through visual perception is a key measure to study the relationship between spatial morphology and spatial perception (Varoudis, T & Psarra S, 2014), the development of new technology also provides new tools and entry points for visual perception research (Ryuzo OHNO, 2017;LU Yi, 2017; Fisher-Gewirtzman D, 2017, 2018). By using the visual elements in the spatial environment, the outward representation of mental activities can be carried out to further realize the correlation among the spatial perception, emotional changes and psychological activities.

## 2.3. PERCEIVED DENSITY

Perceived density refers to the perception and evaluation of the density of surrounding spaces, human and their activities (Rapoport, 1975; Churchman, 1999; Huang Y.R., Zhu P.D., 2016). Perceived density is the result combined with physical density, sociocultural factors, and individual cognitive factors (Figure 1) (Alexander, 1993), which focuses on how physical phenomena can be manipulated to increase or decrease the perceived density (Jacobs, Appleyard, 1987). Perceived density is also the result of the perception and evaluation in different ways by different people, environments, cultures and countries, and it emphasizes the interaction between individuals and environment (Cheng, 2010), which is a subjective phenomenon and influenced by many variables.

For any given physical density, differences in perceived density still exist due to different spatial configurations (Fisher- Gewirtzman et al., 2006). Since there is no direct causal relationship between the perceived density and other variables, it usually has a moderating effect on other things, or to be mediated or influenced by some variables. Therefore, most studies on perceived density are based on correlations (Huang Y.R. & Hu R.Z.,2015). The objective content of space environment is the basis of human spatial cognition, but it is not simply a mirror image or projection. The spatial images in the brain are constructed from the processed information which is projected into the whole sense organs of the body (Sack R D, 1980; Freundschuh S M, 1997). The concept of perceived density not only gives a deep insight into the key issues of density in spatial experience or cognition, but also opens up the research scope of spatial cognition. At the same time, it also criticizes the mechanical determinism only from "objective" indicators in architectural design, which blaze a trail for the subjective and dynamic architectural design.

From the perspective of human and environment, density mainly includes two aspects: perceived spatial environment – tends to acquire information between the

elements of physical space itself; perceived spatial density – the social interaction among actual, expected, and perceived sensory and behavior patterns, in which boundary properties play an important role (Rapoport, 1975). Therefore, the density issue needs to be paid more attentions to the boundary property and the relative permeability.

Interface is an effective way to reflect the connotation of architectural space environment. When it is used as a design vocabulary, it can transform abstract design concept into concrete space image and continue the sensitive value of space environment. Thus, the types, colors, materials and textures that beyond the interface itself can be generated, as well as further deepen people's cognition of space, architecture and city through visual perception.

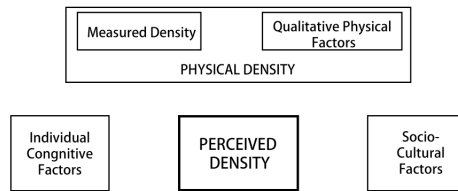


Figure 1. Perceived density-contributing factors (Alexander, 1993).

### 3. Experimental methods

#### 3.1. CONTEXT

In the 20th century, the researches of environmental behaviorists mainly focused on the fundamental paradigm of “space – perception – behavior”, which has been playing an important role in the field of architectural, urban design and landscape.

In recent years, technology of visual analysis tools have developed rapidly, including remote sensing based on GIS, GPS technology, physiological sensor technology based on interactive information technology, eye tracking technology etc. Effective recognition of the elements in human visual image data has begun to be applied in the study of spatial perception, behavior and built environment characteristics, and prediction research (Y. Ye, X.L. Dai., 2017). The data analysis of visual perception can establish a visual connection between the spatial perception of built environment and the psychological perception of human beings.

The layout pattern of modern residential districts has a significant change, from low-density enclosed layout to high-density development, and has gradually become one of the important modes of modern urban neighborhoods. Therefore, it is necessary to carry out specific research on the perceived density of residential forms in different development stages, so as to provide an effective basis for improving the human settlement environment.

### 3.2. CONSTRUCTION OF SAMPLE MODEL AND EVALUATION

In order to ensure pertinence and feasibility of the experiment, typical residential districts in Guangzhou were selected according to the experimental requirements, this can be the experimental model basis for the correlation study of perceived density. Simplifying the existing residential environment can construct a virtual environment model for comparative evaluation.

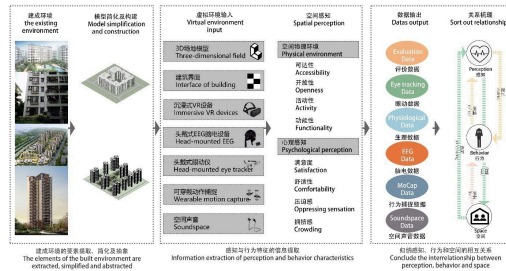


Figure 2. Structure pattern diagram for HEM in virtual reality and simulation environment.

The core of the study consists of three parts (Figure 2): (1) The virtual environment input. The tester will be connected by the wearable data collector that can establish visual and perceptible virtual residential space by inputting 360-degree immersive environment, 3D site model, residential interface, soundspace, photograph, video, et al. (2) The perception of the virtual residential space, includes the evaluation of physical environmental perception of the residential district, and the psychological perception evaluation at the micro level. (3) The output of data. Semi-structured interviews are conducted to get an in-depth understanding the reasons for the perceived density and the feelings of the residential environment.

Finally, the data output includes behavior observation data, motion capture data, eye movement tracking data, EGG data, facial expression recognition data, which are collected and analyzed by human machine environment (HEM) interaction platform. Together with the data collation and regression analysis after perceptual evaluation, they can establish the relationship between the residential perceived density and various factors in the micro-level, which can provide the optimization strategy for livable residential environmental design.

### 3.3. DATA COLLECTION SET

Data analysis includes pre-collection of real residential environmental problems, wearable devices' data collection, questionnaires, semi-structured interviews' data collection, and regression variance analysis. Preliminary data collection is intended to provide effective solutions to existing urban and architectural space problems with a problem-oriented approach. The ErgoLAB platform is used to summarize and collect the wearable information, establish the data set of the specific problem, and visualize the data. Finally, the quantitative data are used to establish the relationship between the physical indicators of spatial environment



and subjective perception.

### *3.3.1. Pre-collection of environmental problems in real settlements*

Through preliminary investigation, the universality of research objects, and the popularization of experimental results were determined, mainly including the data of layout form, physical density and greening rate of modern residential districts. This can summarize the existing problems in the living environment, as well as list and roughly classify the factors of the residential perceived density.

### *3.3.2. Physical Environment Measurement data collection*

The environmental data are collected in real and virtual scene, including the objective physical environmental data such as lighting, noise, volume ratio, density and greening rate, etc. It provides objective conditions for the subsequent analysis of subjective data such as emotion, psychology and behavior, and promotes the establishment of the relationship between objective environment and subjective data.

### *3.3.3. Wearable devices' data collection*

By making use of technologies like wearable data acquisition technology, wireless data transmission and other technologies, the psychological, physiological and behavioral changes of interviewees were recorded synchronously. Afterwards their behavior, cognitive load, fatigue, interest arousal, brain activity and other states were analyzed.

The wearable/portable eye tracking device provides individual visual changes, visual interests, gaze sequence, and duration of fixation within current interest to cross-analysis of eye tracking and behavior; The wearable physiological recording device collected multi-parameter physiological data of electrocardiographic (ECG), galvanic skin response (GSR), temperature, photo plethysmograph (PPG), heart rate (HR), etc. The wearable EEG device collects wireless data of individual head movement and position, providing raw data and real-time quantitative analysis, etc. The ErgoLAB HME interaction platform is used to meet the requirement of synchronization through collecting Experiment Design, Data Collection, Analysis and Statistics, Human Behavior and other multi-factor data, to achieve the targeted experiment and research continuity.

### *3.3.4. Questionnaires and semi-structured interviews' data collection and regression variance analysis*

By controlling the influencing factors of the residential perceived density, the interviewees were asked to select and evaluate the environmental preference of the virtual residential environment. Then semi-structured interviews were conducted as supplemented part of experimental results closer to people's real perception. Finally, the collected data were regressed to determine the correlation between the influencing factors and perceived density.

#### 4. Case study: the relationship between interface and perceived density

##### 4.1. SAMPLE MODEL AND CONSTRUCTION

According to the preliminary survey, typical examples of multi-storey row enclosed residential district and high-rise point enclosed residential district in Guangzhou–Lingnan Garden district and Vanke Donghui City district, were selected as the experimental model basis for the study to focus on the correlation between residential building interface and perceived density. Lingnan Garden district is a multi-storey residential with 6-7 floors, whose floor area ratio is 1.86 and a greening rate is 45%. Vanke Donghui City district is a high-rise residential area of 18-33 floors, with a plot ratio of 2.50 and a greening rate of 35%. These two layout patterns fully represent the current major residential forms in Guangzhou, and their simple architectural interface can provide ideal conditions for the controlled test of later design interface factor.

The experimental model of the multi-storey enclosed residential area is with 6 floors, and the high-rise point-enclosed district is with 33 floors (less than 100 m). The influence factors of building interface, which have relative permeability differences on perceived density: solid wall, grille, glass, open space, greening, etc., were selected and respectively put into the residential virtual environment model. Based on the total height of the building -“ H”, the height of the interface variables was set on the first floor, H/3, H/2, 2H/3 and the top floor. The experimental model was designed by controlling variables according to same interfaces in different positions or different interfaces in the same position. At the same time, the architectural details without affecting the correlative factors were added to ensure reach relatively realistic virtual environment scenes (Figure 3).

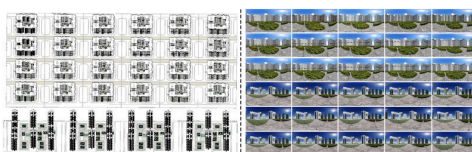


Figure 3. Construction of virtual environment test model and the part of virtual environment scenes in questionnaire.

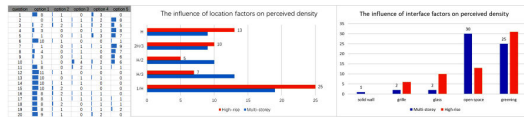
##### 4.2. EVALUATION AND RESULT OF VIRTUAL ENVIRONMENT

The model was transformed into 360-degree immersive virtual residential environment by software, and the respondents wear head-mounted VR devices to evaluate the perceived density of each group of virtual environments, and choose the lowest and highest density perception model of virtual environment. Semi-structured interviews was conducted to in-depth understand the reasons of the respondents’ perception of residential density. Two groups of questions were both applied to the multi-storey and high-rise point-enclosed virtual environments – same interfaces in different positions and different interfaces in the same position, with a total of 20 questions and 5 virtual scenes for each question.

Finally, the results of the questionnaire were digitized to determine the relationship between the impact factors of building interface and the perceived density of residential area.

Before submission of this paper, 12 individuals were interviewed. The results show that (Table 1):1) In multi-storey enclosed residential areas, the interface factor of low perceived density is gray open space> greening>glass=grille>solid wall, while in high-rise point-enclosed residential buildings is greening>gray open space>glass>grille>solid wall; 2) in multi-storey enclosed settlements, the position factor of low perception density is the first floor >H/3>H/2>2H/3>top floor, while in high-rise point enclosed settlements is the first floor>the top floor>2H/3> H/3>H/2.

Table 1. Questionnaire data, location and interface factors analysis.



### 5. Discussion

This study advocates the use of interactive and immersive virtual environment to establish the human-space-environment perception mechanism, using visual, auditory, behavioral, activity and other sensory systems to convey the perception data at the micro level in the residential environment, which can provide the basis for high-quality residential environment design. It can be seen from the results that both of interface factors and position factors have different effects on the multi-storey enclosure and the high-rise point-enclosed settlements. Gray open space and greening are more beneficial to reduce the perceived density both of multi-storey and high-rise point-enclosed residential areas. And the lower the interface position, the lower the perceived density in multi-storey row enclosed residential district, while in the high-rise point-enclosed residential area, the most effective interface position for decreasing perceived density is the first floor, followed by the top floor. The details are as follows:

Some clues related to the above results can be also found from the living preference of modern urban residents:

1)The high of residential building: Multi-storey residential area can provide more comfortable environment than the high-rise residential area, and has the absolute superiority to the reduction of spatial density perception. For example, In Singapore Interlace residential area, the multi-storey residential module forms the high-rise residential pattern, which provides a new direction for the modern urban residential morphology; 2)In terms of enclosed degree, the multi-storey is higher than the high-rise point residence, providing the inhabitant with a more comfortable living environment. The multi-storey enclosed residential district is consistent with the traditional Chinese courtyard pattern, and has strong ability to interact with the enclosed public environment, which is beneficial to the construction of the environment atmosphere and residents' sense of belonging;

3) Multi-storey residential areas are closely related to ground greening, and the demand of gray open space is higher than that of greening, which is also reflected in the perceived density. However, the distance between high-rise residential areas is far, and the self-evident of gray open space is lower than that of greening, which have highlighted the advantage of greening in reducing perceived density in high-rise residential areas. Therefore, different types of public space should be adopted in different residential models to provide more accurate and effective measures to create and manage the space environment.

In addition, during the interview, it was found that the perceived density was affected by varieties of factors, involving integrity, color, sunlight in the environment and even individuals' previous cognition of space. Besides, based on the consideration of control variables, this paper does not take environmental sound/noise as one of the influencing factors, but it is undeniable that the acoustic environment has a great influence on spatial perception.

## 6. Future work

In the later research work, more survey data will be used to establish the correlation regression variance analysis, and the study of relationship between perceived density and interface impact factors. Second, testing and verifying the correlation of variables, deepening the influence analysis of principal components will be conducted to obtain the results of the interface layout types and the location on perceived density of different enclosed residential areas.

Previous studies have found that the outcome of perception is influenced by many factors, especially subjective cognition. Although the correlation study of the factors affecting the perceived density has a tendency of subjective evaluation, with the continuous innovation of new technology, relevant technical methods can be conducted quantitative research on perception and behavior. Currently, we have established initial scientific research cooperation with human factors engineering enterprises, in order to provide systematic HEM synchronization technology and platform for later research. Therefore, we will make full use of the virtual immersive experience and augmented reality technology in the future, combined with HEM synchronization technology and wearable physiological acquisition instruments to record the subjects' fixation frequency and length, nerve activity, pressure, emotional changes, psychological comfort and other states in a specific environment. Color, time, sound and other factors will be involved in perceived density study to promote a more comprehensive quantitative study of spatial environment perception.

## References

- Alexander, E.R.: 1993, DENSITY MEASURES: A Review and Analysis, *ARCHIT PLAN RES*, **10**, 181-202.
- Boyko, C. T. and Cooper, R.: 2011, Clarifying and re-conceptualising density, *Progress in Planning*, **76**(1), 1-61.
- Cheng, B.K.: 2010, *Human Perception of Urban Density*, Ph.D. Thesis, University of Cambridge.
- Churchman, A.: 1999, Disentangling the concept of density, *Journal of Planning Literature*,

- 13**(4), 389–411.
- Eroglu, S.A., Machleit, K.A. and Barr, T.F.: 2005, Perceived retail crowding and shopping satisfaction: the role of shopping values, *Bus. Res.*, **58** (8), 1146–1153.
- Fisher-Gewirtzman, D.: 2017, The association between perceived density in minimum apartments and spatial openness index three-dimensional visual analysis, *Environment and Planning B: Urban Analytics and City Science*, **44**, 764-795.
- Fisher-Gewirtzman, D.: 2018, Integrating ‘weighted views’ to quantitative 3D visibility analysis as a predictive tool for perception of space, *ENVIRON PLAN B-URBAN*, **45**, 345-365.
- Fisher-Gewirtzman, D. and Wagner, I. A.: 2006, The spatial openness index: An automated model for three-dimensional visual analysis of urban environments, *JOURNAL OF ARCHITECTURAL AND PLANNING RESEARCH*, **23**(1), 77-89.
- Freundschuh, S.M. and Egenhofer, M.J.: 1997, Human Conceptions of Spaces :Implications for Geographic Information Systems, *Transactions in GIS*, **2**(4), 361-375.
- Gibson, J. J.: 1986, *The Ecological Approach to Visual Perception*, Psychology Press.
- Guan, C. and Liang, Y.: 2015, Application of Virtual Reality Technology in Library, *Advances in Social Science Education and Humanities Research*, **ISSS-15**, 254-257.
- Huang, Y.R. and Hu, R.Z.: 2015, Construction of the Concept of Residential Density, *Housing Science*, **2015**(03), 1-5.
- Huang, Y.R. and ZHU, P.D.: 2016, Study on the Correlation between Density Control and Perceived Density in Urban High-density Residential Areas, *Time+Architecture*, **2016**(06), 50-59.
- Jacobs, A. and Appleyard, D.: 1987, Towards an urban design manifest, *Journal of the American Planning Association*, **53**, 1112-1120.
- Jamei, E., Mortimer, M., Seyedmahmoudian, M., Horan, B. and Stojcevski, A.: 2017, Investigating the Role of Virtual Reality in Planning for Sustainable Smart Cities, *SUSTAINABILITY*, **9**(11), 1-16.
- Lu, Y., Guo, Z. and Ye, Y.: 2017, Three-dimensional Visibility Graph Analysis and Its Application, *Time+Architecture*, **2017**(05), 44-49.
- Mousavinia, S.F., Pourdehimi, S. and Madani, R.: 2019, Housing Layout, Perceived Density and Social Interactions in Gated Communities: Mediation role of territoriality, *SUSTAIN CITIES SOC*, 101699.
- Rapoport, A.: 1975, Toward a Redefinition of Density, *ENVIRON BEHAV*, **7**, 133-158.
- Ryuzo, O. and Translated by XU, S.C.: 2017, Possible Contribution of New Data Environment and New Analytical Techniques to Environment-behavior Studies, *Time+Architecture*, **2017**(06), 66-69.
- Sack, R.D.: 1980, *Conceptions of Space in Social Thought: A Geographic Perspective*, Macmillan International Higher Education.
- Sampaio, A. Z., Ferreira, M.M., Rosario, D.P. and Martins, O.P.: 2010, 3D and VR models in Civil Engineering education: Construction, rehabilitation and maintenance, *Automation in Construction*, **19**(7), 819-828.
- Varoudis, T. and Psarra, S.: 2014, Beyond two dimensions: Architecture through three-dimensional visibility graph analysis, *The Journal of Space Syntax*, **1**(5), 91-108.
- Wu, Z., Chen, C., Cai, Y., Lu, C., Wang, H. and Yu, T.: 2019, BIM-Based Visualization Research in the Construction Industry: A Network Analysis, *International Journal of Environmental Research and Public Health*, **16**(18).
- Xu, L.Q., Meng, R.X., Huang, S.Q. and Chen, Z.: 2019, Healing Oriented Street Design: Experimental Explorations via Virtual Reality, *Urban Planning International*, **34**(01), 38-45.
- YE, Y. and DAI, X.L.: 2017, Spatial Perception and Design Potentials in the Context of New Analytical Techniques and New Data, *Time+Architecture*, **2017**(05), 6-13.
- Zhen, S.H., Du, H.W. and Wang, Q.: 2019, Study on the Correlation Between Skycourt and Perceived Density of U Shape Urban Housing—An Example from the Grove of Vanke in Guangzhou, *Chinese Landscape Architecture*, **35**(9), 110-114.

# MULTI-SENSORY MATERIALITY

*Expanding Human Experience and Material Potentials with Advanced HoloLens Technologies and Emotion Sensing Wearables*

MARCUS FARR<sup>1</sup> and ANDREA MACRUZ<sup>2</sup>

<sup>1</sup>*American University Sharjah / Tongji*

<sup>1</sup>*mfarr@aus.edu*

<sup>2</sup>*Tongji University*

<sup>2</sup>*andrea.macruz@uol.com.br*

**Abstract.** What is the current state of human/material perception relative to advanced architectural technology? What sensory experiences are possible, and how are they designed and deployed? What happens when advanced HoloLens technologies are used in conjunction with wearable emotion-sensing technologies to connect people with deeper sensory experiences relative to materiality and space? Does this offer a heightened pedagogical perspective when teaching architecture? This paper responds to these questions by expanding on and critiquing a small scale digitally augmented project created in an academic setting. The project focuses on relationships between technology and human sensory experience relative to specific augmented and sensorial engagements. It employs an overlap of HoloLens technology to make and enhance the design experience and wearable emotion sensors to evaluate the human experience.

**Keywords.** Technology; Sensory; Materiality; Augmented.

## 1. Introduction

The work explores what it means to design spaces with high degrees of sensory feedback and potential. It is made in tandem with technology using Rhino, Houdini, Fologram, and HoloLens as a primary decision-making tools relative to the creation of space. The Rhino plugin Fologram extends the experience by offering a user an additional sensory experience while wearing the HoloLens headset or by using the iPhone app. To monitor and evaluate the reaction to the projects, users also wear emotion-sensing UpMood bracelets that collect biodata from the user and result in 11 different emotional states, stress level and BPM, every 1.5 to 3 mins. This project evaluates the use of these converging technologies as a way to improve our understanding of how we design for a deeper human experience. Through this process, the paper discusses user insight into emotional patterns and management. The resultant methodology and outcomes offer a new theoretical agenda for using technology in the architecture/teaching process and creates a conversation that critiques our current design process in academia.

With this small augmented installation, the paper follows the introductions of overlapping augmented reality into the design space by pairing emotional sensing wearables with Microsoft HoloLens technology as an extension to the traditional architecture/build workflow. The use of these technologies offers an expanded mode of inquiry relative to a host of architectural potentials, dialogue, critique and a deeper sense of concept development. This process also lends itself to teaching as a new pedagogical model whereby students and teachers can discuss project potential in real-time and in context relative to a given sensory-material scenario. The benefits include real-time simulation of scale, form, color, light, shadow, and the experimentation of these as they relate to a host of different material situations. Working in teams to share interactive experiences is also a profound advantage for teaching in the architecture profession.

Moving further, this paper documents and critiques the process and results from the projects, which took place in 2019, and explores these concepts relative to digital design and material interaction in the field of architecture and constructed environments. It begins by designing with typical parametric & computational software as an exercise, and then moves directly from the digital model to the process of construction. Instead, the project used Fologram to portray a full-scale hologram in a physical artspace as a digital projection or as an image on an iPhone. Its purpose is to engage people with multi-sensory experiences that force humans to re-evaluate and re-perceive our material world. Adding to the experience are additional sensory stimulations that can be experienced when wearing the HoloLens headset. These experiences are subsequently monitored in real-time by using emotion sensors that are designed to collect biodata from heart rate and contractions through a PPG sensor (i.e. photoplethysmogram - used to detect blood volume changes in the microvascular bed of tissue). Algorithms turn the data from human pulse waves into analytics to generate a discussion of interactive stress levels, heart rate, vitality levels, and emotions.

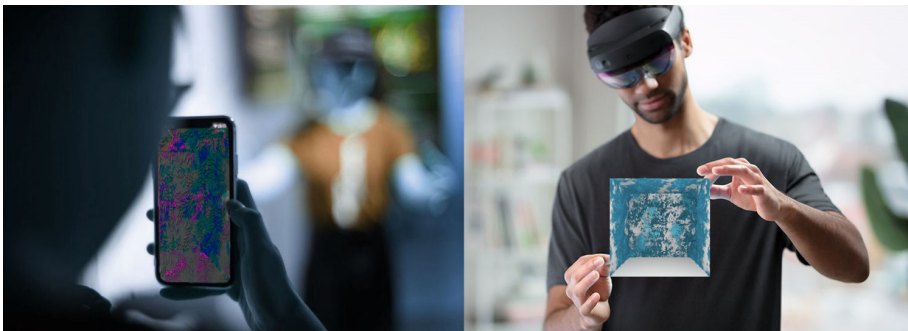


Figure 1. Fologram iPhone integration; Microsoft HoloLens augmentation.

Using this project as a vehicle, the paper goes on to theorize an agenda that is rather interested in supplementing our design process by new tools and advanced technologies that allow us to experiment in extremely informed ways relative to the perception of physical context. This heightened mode of inquiry proposes a new

way of looking at the process of designing full-scale projects by interacting with materials in a unique sensorial way. Because of this, it questions the relevance of current material conversations and proposes further discussions involving student, teacher, architect and client.

## 2. Sensory and Perception

“Materials are the flesh and bones of objects and buildings. Glass, Wood, and silicone breathe, shift, and sigh. A curtain or bench absorbs sound. Light bounces, reflects, and floods the periphery - light is not a thing, but it changes everything. Textures speak to the eye as well to the hand, incising flat surfaces with real or imaginary depth where the restless gaze can wander. Sensory design considers materiality across multiple dimensions, from the visible to beyond.” -Lupton, Ellen, Lipps, Andrea, “The Senses: Design Beyond Vision”, 2018.

In this project, it was important to understand materiality by creating a more compelling relationship with the potentials of sensory perception and technology in architectural space. To do this, the installation offers tactile, olfactory, and auditory interactions that enhance the aggregation of surface material and patterning on an otherwise normative architectural surface.

The surface patterning bends and flows along the course of 6.5 meters (1.8 meters height) meters offering a user the opportunity to come into contact with them along a particular path of circulation or as a random encounter. To contextualize the experience, salt crystals are used as the primary material reference. Salt and the generation of crystals by this material offers a alternate material palette that is extremely textural and has a unique interaction with light. This is extremely meaningful in that it embodies powerful symbolic associations with collective memory, ritual, landscape and purification. Because of our context, living and practicing in the desert, salt and sand are common materials that are very much a part of daily life in our region, however these materials are seldom used or explored in an architectural way.

With this experience, users can perceive the space differently, giving meaning and value to its physicality through embodied experiences and an expanded notion of spatial awareness. In this, the wall is occupying a physical and conceptual place in the space of architecture. It is given a new importance, one that is not merely structure or partition, but one that is designed to play a larger role in the experience of architecture, beyond the normative, beyond the visual. It is offering a fresh starting point for architecture by redefining the point of origin from one that is specifically for partition and structure, to one that is positioning itself within a broader set of human surface and sensory relationships. For us to revise and redefine our material perception, it is essential that our experience with material occurs deeply and intensely. This notion of materiality calls for an embodied response, and it calls for the architect to move beyond the current definitions of what it means to make a something as mundane as a wall.

The glorification of architecture is often presented through the concept of material craft, but not as often does it include the potentials of the “sensorial craft”. This is largely given to theory and speculation and rather than being



present in architectural space, and many times are presented in the form of art installations or gallery experiences. This paper argues that the need for sensorial craft is one that is intrinsic to human nature and also a part of material craft. Our relationships to touch, smell, sound and sight are, in fact, part of our search for a deeper understanding of place and meaning. The richness of this architecture is created with the encounter between the tangible aspects of architecture (brick, stone, glass, etc.) with the intangible (light, wind, sound, etc.).

What sensory experiences are possible, and how are they designed and deployed? In the book, *The Air From Other Planets, A Brief History of Architecture to Come*, author Sean Lally positions architecture as a discipline in need of a re-centering, arguing that instead of expanding on the traditional concepts of architecture as a container, the discipline should move to one that is more focused on concepts of energy and amplifications of spatial energies as the primary means of making decisions about space. He writes that the potential futures of design are already all around us, the physical and sensorial, and can be found in sensorial “microclimates, shadows, lighting, vegetation”, but there is a fundamental problem in the way architects design with this information because we are addicted to lines that represent walls, columns, and floors. The answer instead is to re-imagine what and how we draw and what sensorial feedbacks are already available to us, embracing the technologies that offer a heightened sense of place.

### **3. Touch, Sound and Smell**

The project achieved sensorial experiences through expanded notions of texture. To do this, a pattern 6.5 meters in length, was laser cut into 32 sheets of flat material and mounted to a wall. The paper material was mixed with different densities of salt to create the texture. The size and scale of this was important because it offered the users an opportunity to experience different densities and orientations of pattern and texture. The material was further covered with different densities of crystallization coatings, and salts that changed the weight, texture, and density of the surface. Further, layers of different colors were combined, creating contrasting light to the textures and new color interactions throughout the existing layers. This combination offered a noticeable sense of tactility and visual intricacy, not commonly found on wall surfaces.

In the book, *The Eyes of the Skin*, Juhani Pallasma asks the far-reaching question why, when there are five senses, has one single sense, sight, become so predominant in architectural culture and design. The book moves beyond concepts of phenomenology and discusses the need for deeper dimensions of human experience in architecture. The author goes on to write, “the flatness of today’s standard construction is strengthened by a weakened sense of materiality.” In most architecture, this flatness is pervasive, resultant of standardizations and ease of shipping and manufacturing. Many times decisions are made based on the materiality of convenience. This project, of course, critiques these decisions by asking new questions and asking for new responses.

This installation presents a comparison in contrast, combining the perception

of visual texture with the tactility of the physical. Because of this, as a user touches the surface, they feel the harsh tactility of the salt crystals, along with the softness of its visual texture.

Moreover, as Neal Leach questions in his book *Camouflage*, “If we have this natural urge to assimilate to our environment, what role might the environment play in facilitating that process?” In our process of assimilation, the identity of the self through differentiation and identification with the environment is enhanced when a multi-sensory approach takes place.



Figure 2. Tactile surface with salt; Installation with multi-sensory surface.

According to the legendary Randy Thom, Director of Sound Design at Skywalker Sound on why sound matters: “sound is important because it can tell us about character, place, and time. It’s important because it informs us and moves us in ways visuals can’t, and because certain combinations of sound and visuals can evoke what neither can do alone. It’s also potentially important because it can help to determine what we see.”

Sounds of nature are particularly interesting when their scale is amplified, or the sounds are transformed in a way that we are not used to listening to. Like that, we can perceive them differently, tending to fixate this experience in our head and helping us to build with a better accuracy a picture of places and events. This becomes a compelling feature for our installation in that the sound of salt crystallization was essential in forming a mental dialogue with the space. Crystallizing sound effects were edited through the online webpage [www.sodaphonic.com](http://www.sodaphonic.com), creating rigid, striking soundtracks. After this experience, our intent was that the visitors would be able to pay more attention to the sound properties of a determined material and that they would be able to relate more closely with sounds aligned with texture, color, and visual aspects in order to have a more holistic view of a specific material or architecture.

Kant also wrote in *Reflexionenzur Anthropologie*, “all the senses have their own descriptive vocabularies, e.g. for sight, there is red, green, and yellow, and for taste there is sweet and sour, etc. But the sense of smell can have no descriptive vocabulary of its own. Rather, we borrow our adjectives from the other senses, so that it smells sour, or has a smell like roses or cloves or musk. They are all, however, terms drawn from other senses.”

This philosophy illustrates why it was important that the installation experiment with virtual environments and real environments in a symbiotic way to help us to re-perceive materials through human sensorium. Smell, sound, and touch were used in this installation as a way to ground the visitors in the real environment, bringing the perception back to their body.

At the “Scent Fountain: Fear and Volatile Marilyn” at the Senses exhibition at the Cooper Hewitt Smithsonian Design Museum in NY, the visitors were instructed to touch the surface and smell the scent. A different scent accompanied each texture. One called Fear is electric, and cold while Volatile Marilyn is curvy and soft. It was a piece designed for visitors to experience the relationship between texture and smell proposed by Studio Joseph, Dmitry Rinberg, and Perfumer Christophe Laudamiel.

These examples point us toward the importance of combining smells, sounds, and textures in a holistic environment. These kinds of inclusive environments offer a broader spectrum of elements to the sensorium that can expand architecture’s role in our lives. Therefore, in the installation the smell of salt was combined with sound, texture, white color, and AR resulting in a compelling connection and a very integrated sensory experience.

#### **4. Augmentation**

According to Clark, as natural-born cyborgs, devices such as computers, smart phones, and other nonbiological constructs, props, and aids are becoming extensions of our minds that help us to solve problems related to survival. Many of these devices currently are portable, reliable, flexible, and personalized, increasing the extension of our minds. We therefore transform our reach, thought, and vision, upgrading the cognitive structure in our minds when we employ nonbiological devices. We create these supportive constructs, props, and aids, but they also re-create us. In the installation, new software and devices were used for design, construction and feedback which acted as an extended mind for us as designers to perceive differently. Also, its aim was to analyze how these devices help us to extend our perception, how they transform us, and what kind of environments are we going to create after this experience.

This process was significant in that it allowed for the exploration of new ways of thinking, making, and presenting spatial potentials that can affect the senses. But, beyond designing for senses, this project looks at what it means to not only evaluate a sensory experience but to heighten it with digital technology. This paper began by asking the question, “what happens when advanced technologies, such as those offered by Microsoft, HoloLens, are used in conjunction with physical architecture to connect people with deeper sensory experiences relative to materiality and space?” This augmented potential allows us to create a more rooted exploration of space, merging the physical with the digital, the buildable with the not yet buildable, the fabricated with unfabricated. The project was interested in augmented experiences rather than ones that were purely virtual, thus distinguishing between a computer-generated simulation and one that offered an augmented overlay of experience. It was also meaningful to allow this augmented

reality to be a part of how the project was measured through the UpMood wearable technology.

While VR, virtual reality, offers a complete immersion, such as entry into a different environment, a historical place, or a game world, the augmented experience, AR, offers an overlay onto the current physical installation, including additions to the scale, light, and potential materialities, combining real with unreal. These digital overlays are projected or layered along with the real world via glasses or iPhone monitors using Fologram. This technology is being used in many different industries beyond design as a means for translating complex tasks, teaching, delivering information, and promoting an idea of efficiency through technological assistance.

For this project, AR was used as a way to increase the perception of potential material enhancements. Using software such as Rhino and Houdini, an augmented version of the installation was created that expanded on the physical by growing, changing densities, colors, and increasing the size and scale of the patterns. As one interacts with the installation, they can also interact with the digital by using a Fologram linked cell phone device. It alters the perception of the original space and creates a stronger awareness of the potential of the original pattern sequences. Ultimately, this paper is interested in the overlaps of the architectural space, the sensory space, and the augmented space.

## **5. Evaluation Technology / Wearables**

In order to predict the potential overlap between the architectural, the sensorial, and the augmented, we worked with UpMood technologies to begin understanding how to measure and estimate how people might feel or respond in a given environment. To monitor and evaluate how people perceive certain criteria, users wore emotion-sensing bracelets when they visited the project. These collect biodata from the user and result in 11 different emotional states: calm, pleasant, unpleasant, happy, sad, excitement, anxious, confused, challenged, tense. This data was continuously fed into an App that revealed the different states back to the user. The evaluations and the use of these overlapping technologies acted as a way to gain insight into a more profound human experience. Through this process, the project addressed user insight relative to emotional patterns and management.

In the paper, *The Nature of Feelings: Evolutionary and Neurobiological Origins*, the author Antonio Damasio writes, “Survival depends on a homeostatic range”, and “feelings and experiences facilitate the learning of the conditions for homeostatic imbalances plus the anticipation of conditions. Feelings are mental experiences that accompany a change in the body state.” He goes on to write that, “external changes - displayed in the exteroceptive maps of vision or hearing (sensorium) are perceived, but largely not felt. It can trigger drives or emotions, causing a change in the body state, and subsequently felt.”

Homeostasis, the tendency towards a relatively stable equilibrium between interdependent elements, especially as maintained by physiological processes, is a big part of human survival, and is relevant to the theories of Damasio. Human survival depends on homeostasis, or the regulation of the body’s self-repair and

defense. The body can regulate itself without the person having a feeling, or “conscientious experience”. However, when the person does have a feeling, and therefore he/she is aware of it, it facilitates the learning of a change in body state for a better prediction of future situations and thus increases behavioral flexibility. With these concepts in mind, this installation tries to increase felt experiences, using the different stimuli to increase senses and also offer a recording of what a user felt to bring about potential self-awareness.

Wearing UpMood bracelets allowed us to monitor different emotional states in real time as we interacted with the project. What we found is that the technology can be sometimes accurate and sometimes surprising indicating that our heart rates change in different ways and can be highly situational. It was an interesting part of our experiments with this project because it allowed us to interact with a user in a way not normally accessed in architectural projects. The conclusions for these findings via UpMood wearable technologies indicate that stable peaks, highs and lows, in experience are crucial to accuracy and variance from person to person can differ. There can also be discrepancies between what the users “thought” they were feeling, and what the technology actually indicated. Fluctuation in experience will also affect the results.

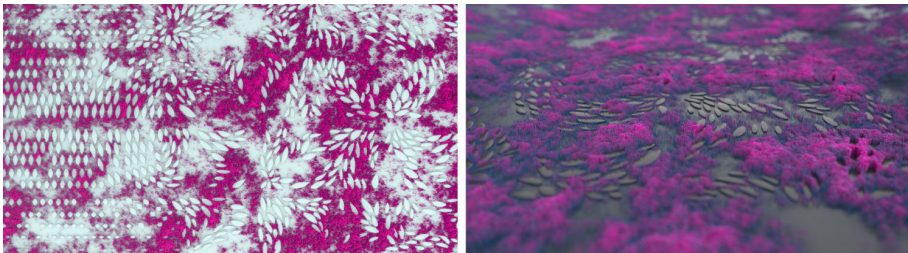


Figure 3. Augmented surfaces with salt crystallization.

## 6. Methodology

There is one profession and only one, namely architecture, in which progress is not considered necessary, where laziness is enthroned, and in which the reference is always yesterday.” Le Corbusier, “Towards a New Architecture”, 1923.

As discussed in the abstract, the methodologies used in this project are interested in looking toward the future, and creating a conversation about the potential of architecture relative to technology and the sensorial experience of a given space. The project involved the design and construction of a wall surface, the discussion of its material and sensorial qualities, and its virtual augmentation as a catalyst for new experiences. It employed digital technologies to help build, perceive, and evaluate the overall experience. The methods used in the project work with the existing paradigms of architectural design, but also speculate on a new agenda for current processes due to the use of new technologies in the process. Because of this, the project suggests a “re-centering” or a new starting point for how we can incorporate technologies into our design process as well as in our experience of a design project. Moving further, rather than designing

and then building and then experiencing, we believe that these activities have the potential to overlap more and inform each other in a real way throughout the course of a given design exercise in a way that moves beyond theory and offers both quantitative and qualitative results.

The methodology does not aim to provide solutions from the outset, but rather looks at using the process of augmented design and technology to inform solutions along the way, and then attempts to evaluate the potential impact of a set of sensorial experiences. Its aim was to build upon its own theoretical underpinnings, but is also interested in informing best practices and how this process can contribute or be applied to future projects.

As discussed in the initial abstract, the installation explored what it means to design spaces with high degrees of sensory interaction and feedback. The use of software assisted design also extended the experience and allowed us to evaluate how people were interacting with the project via technology. This offered insight into user attitudes and feedback. The wearable emotion sensors were used to collect biodata (interactive stress level, heart rate, vitality levels), and the associated algorithms turn the data from human pulse waves into analytics to generate a discussion of emotions.

The work allows for the overlapping of augmented reality into the design space by pairing emotional sensing wearables with augmented technology as an extension to the traditional design/build workflow and an extension of the material and spatial experience. The use of these technologies offers an expanded mode of inquiry relative the design process and outcome. While there are many critiques and areas still yet to be developed, we discovered a rich dialogue and a deeper sense of concept development in using this process.

One of the dialogue streams in this process that has yet to be expanded on is that it lends itself to teaching as a fresh pedagogical model whereby students and teachers can discuss project potential in real time and in context relative to a given sensory-material scenario. The benefits include real time facsimile of scale, color, form, light and shadow, and the experimentation of these as they relate to a host of different material situations.

## **7. Conclusion**

This paper documents and critiques the process of an installation that was designed to induce a sensory experience and ask questions about the capacity to design with technology and a wider taxonomy of choices that can impact our experience in architecture. It explores these concepts relative to digital design and augmented material interaction in the field of architecture and constructed environments. It started by employing typical parametric & computational software, thinking of the potentials between the digital and the real, and incorporated this potential by accepting the role of augmentation as a way to interact with architectural space. The purpose was to engage people with multi-sensory experiences that force humans to re-perceive our physical world. Adding to the experience are additional sensory stimulations of sound, touch, and smell that can be experienced in the augmented space.

The findings of this process come in the form of data collected by the wearable technology from user feedback. In the end, the data collection devices, while not as sensitive as we would have liked, offered a unique perspective to the way that a particular user felt as they interacted with the project. The outcomes imply that through research and design, stronger sensorial experiences can be used to increase awareness, perceptibility, and create new design conversations.

Using this project as a vehicle, the paper goes on to theorize an agenda that is interested in supplementing our design process by new tools and advanced technologies that allow us to experiment in extremely informed ways relative to the perception of physical context. This heightened mode of inquiry proposes a new way of looking at the process of designing full-scale projects by interacting with materials in a new sensorial way. Because of this, it proposes and questions the relevance of current material conversations and proposes new conversations involving student, teacher, designer, and client.

“There is much more to the experience of life than successfully meeting basic needs. Humans are emotional beings. We embrace concepts like beauty, awe and wonder, which contribute to the connection we have with each other and our environment. As practitioners who have the perspective, tools and intention to design a new reality for humanity, we need to pay attention to the emotional context and intention of our designs.” - Senova, Melis. “This Human: How To Be The Person Designing For Other People”, 2017.

## References

- Chang, A.: 2017, *The Tao of Architecture*, Princeton Architectural Press.
- Clark, A.: 2003, *Natural Born Cyborgs: Minds, Technologies, and the Future of the Human Intelligence*, Oxford University Press.
- Kant, I.: 1882, *Reflexionen Kants zur kritischen Philosophie. I*, Forgotten Books.
- Lally, S.: 2017, *The Air from Other Planets, A Brief History of Architecture to Come*, Lars Müller Publishers.
- Leach, N.: 2006, *Camouflage*, MIT Press.
- Lupton, E. and Lipps, A.: 2018, *The Senses: Design Beyond Vision*, Princeton Architectural Press, New York.
- Pallasma, J.: 1996, *The Eyes of the Skin*, Wiley.
- Sevona, M.: 2017, *This Human. How To Be The Person Designing For Other People*, Bis Publishers, Amsterdam.

# FENG-SHUI AND COMPUTATIONAL FLUID DYNAMICS (CFD)

## *Analyzing Natural Ventilation and Human Comfort*

BIN LI<sup>1</sup>, WEIHONG GUO<sup>2</sup>, MARC AUREL SCHNABEL<sup>3</sup> and TANE MOLETA<sup>4</sup>

<sup>1,2</sup>*South China University of Technology*

<sup>1</sup>*445453185@qq.com* <sup>2</sup>*whguo@scut.edu.cn*

<sup>3,4</sup>*Victoria University of Wellington*

<sup>3,4</sup>*{MarcAurel.Schnabel|Tane.Motela}@vuw.ac.nz*

**Abstract.** The paper explores the analogies between Computational Fluid Dynamics (CFD) and Feng-Shui by undertaking an analysis of natural ventilation in Jiangmen city, Southern China. Feng-Shui has been used to inform the orientation, layout, and design of buildings in China for thousands of years. The research questions if these concepts are still valid for contemporary building design. Noting that computational simulation methods such as CFD allow architects to analyse the natural ventilation of buildings, this paper provides a novel study that examines if Feng-Shui principles can be reconciled against contemporary design processes. The research simulates ‘community’, ‘block’, and ‘single courtyard’ via CFD study to confirm the scientifically measurable concepts of Feng-Shui have concerning natural ventilation. We conclude that Feng-Shui concepts enhance natural ventilation and subsequently makes a positive contribution to sustainable building and design.

**Keywords.** Human comfort; Natural ventilation; CFD; Feng-Shui.

## 1. Introduction

Design principles guided by Feng-Shui have informed building design in China for thousands of years. These principles are reported to relate to the building environment at a range of scales (Mak & Thomas, 2005). The concept of Feng-Shui has expanded globally; thus, we believe a reexamination of these tools is of importance and also timely due to development in CFD (Feuchtwang, 1974). The design principles found in Feng-Shui can be applied to orientation, layout, and design for the entire cycle of buildings (Mak, 1995; Lee, 1986). Several researchers have focussed how Feng-Shui impacts the location and spatial arrangement in architectural design (Knapp, 1986; Knapp, 1992; Lawrence & Raffestin, 1994; Kalland, 1996); our research, however, explores how Feng-Shui concepts can be used for architecture design to supply human comfort concerning natural ventilation. CFD is grounded on modern fluid dynamics which combines



numerical mathematics with computer science (Guo & Liu & Yuan, 2015 (a); Guo & Liu & Yuan, 2015 (b)). It can simulate the wind loads of urban environments and offer data to understand the performance of buildings concerning natural ventilation. The simulated and optimised building design of natural ventilation is reported to supply a better living condition for human comfort (Du & Mak, 2017). This research seats the CFD case study computational analysis in Jiangmen city as a case study. The natural ventilation of the ‘community’, ‘block’, and ‘single courtyard’ were not only analysed based on human comfort but also confirmed the rationale of the Feng-Shui concept for building design.

## 2. Methods

### 2.1. CFD MODEL

The simulation employed three different scales of the geometrical models to analyse. These are the ‘community’, ‘block’, and ‘single courtyard’ (Fig. 1). They are generated in Sketchup software according to the real physical space in Jiangmen city (Fig. 2). Subsequently, three different Sketchup files were imported to the Phoenix software for analysing.

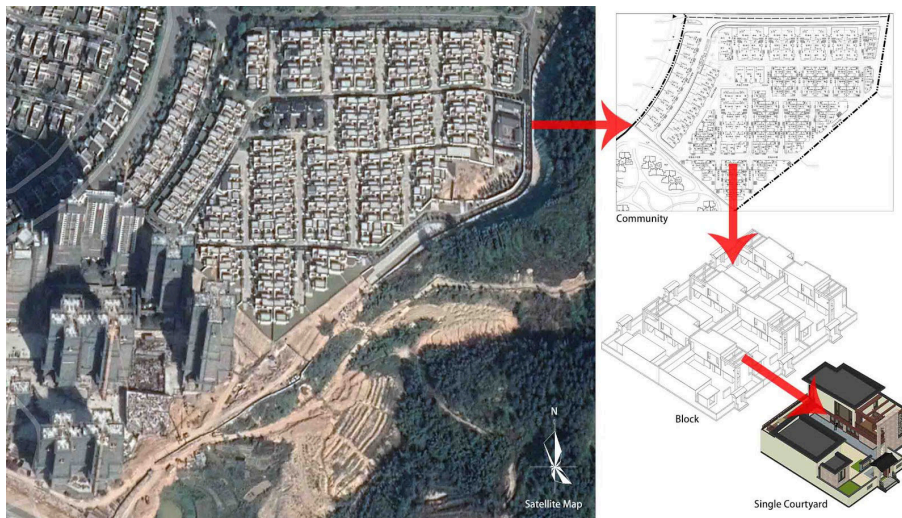


Figure 1. Three different scales of the geometrical models.

### 2.2. BOUNDARY CONDITIONS

The mean velocity profile for the inflow boundary was modelled as a power law, and the power-law exponent  $\alpha$  was determined by the object terrain category (Liu et al., 2017). Because of the object located in the suburb of Jiangmen city, the  $\alpha$  is 0.16. The average wind velocity is 2.3m/s in summer and 2.7m/s in winter. The wind direction is south southeast (SSE) in summer and north northeast (NNE) in winter, according to the Standard for Green Performance Calculation of Civil

Buildings (MOHURD, 2018).

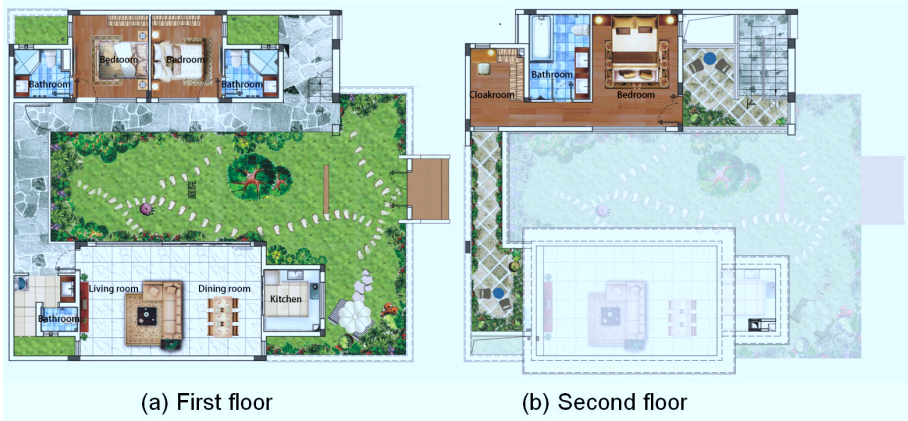


Figure 2. Basic model.

### 2.3. COMPUTATIONAL DOMAIN SIZE AND MESH GENERATION

The computational domain for models considered the site and surroundings. For the height of the computational domain, the blockage ratio should be below 3% (Jorg & Alexander, 2007; Tominaga et al., 2008). The boundary in the four horizontal directions should be a distance of at least  $5H_{max}$  (Jorg & Alexander, 2007; Scaperdas & Gilham, 2004). According to the Standard for Green Performance Calculation of Civil Buildings, the height to boundary above the object should be larger than  $5H_{max}$ , and the distance between object and wake region should be larger than  $10H_{max}$  for a realistic flow (MOHURD, 2018; Bartzis & Vlachogiannis & Sfetsos, 2004). The distance of  $5H_{max}$  for inflow,  $10H_{max}$  for outflow, and the height of  $5H_{max}$  beyond three objects were used. The model of summer simulation is shown in Figure 3. Moreover, the mesh generation was used object affects the grid and optimised by a hybrid grid scheme, which can adapt to the geometric structures very well.

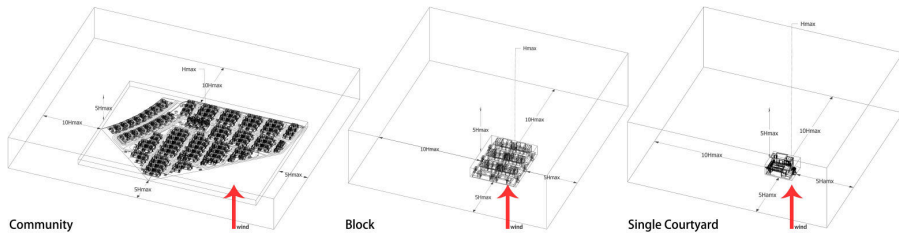


Figure 3. The model of summer simulation.

### 3. Results

#### 3.1. INITIAL RESULTS

The research explored conditions during summer and winter. Jiangmen city is in the Chinese ‘hot summer and warm winter’ climate zone. In summer, it is hot, and in winter, the building does not need heating (MOHURD, 2016). Therefore, natural ventilation is an essential measure for human comfort concerning indoor air quality and thermal comfort (Wang & Malkawi, 2019). In summer, strong natural ventilation will exhaust the excessive heat. In winter, reduced natural ventilation will provide a more comfortable living environment (He & Schnabel, 2016). According to the Assessment Standard for Green Building, the outdoor natural wind speed above 1.5m from the ground should be less than 5m/s in winter, and there should not exist calm wind zones in the main activity area in summer (MOHURD, 2019). The Standard of the Measurement and Evaluation for Efficiency of Building Ventilation shows indoor ventilation should flow from main rooms such as the living room and bedroom to functional rooms such as the bathroom (MOHURD, 2013).

The community simulation result showed the outdoor wind speed as being between 0.44m/s and 3.5m/s in winter. However, there are calm wind zones in summer, as highlighted in Figure 4. It is a problem since it is primarily caused due to the orientation of the community, which could be improved.

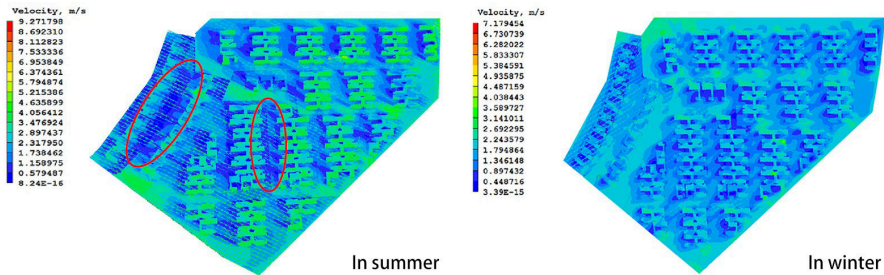


Figure 4. Outdoor wind simulation of community.

The block simulation result showed the wind speed as less than 5m/s in winter. Nevertheless, there are calm wind zones in the main rooms in summer, especially in the west of the block (Fig. 5 b). This problem is different from that in the community, which should focus on improving the layout of the block. As the other highlighted area shown in Figure 5 (a & d), there is also air pollution because of the bathroom in the upwind, which could be solved via a single courtyard layout.

The single courtyard simulation result showed that the indoor wind flows from bathroom to bedroom on the first floor, and the maximum wind speed in winter is 3.95m/s (Fig. 6). The winter wind speed meets the standard requirements. However, the wind flowing from bathroom to bedroom will cause air pollution. That is a problem with the design of a single courtyard layout.

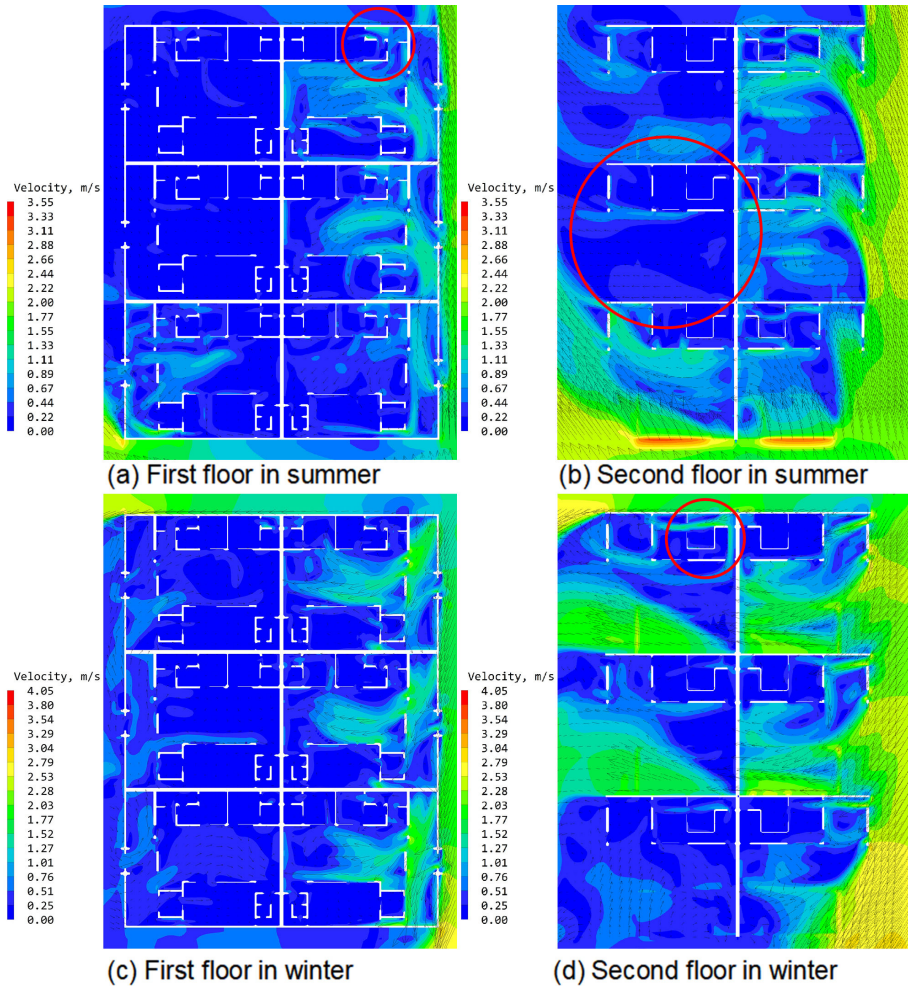


Figure 5. Wind simulation of block.

### 3.2. OPTIMIZED RESULTS

The challenges, as mentioned above, are the calm wind zones in the community during summer. The Feng-Shui principles for the community orientation prescribed that it should ‘Face South, with the Back to the North’. The building layout should be distributed. The building location should gradually raise with the site from south to north (Wang, 1998); because China is located in the northern hemisphere of the earth and eastern Eurasia. Most of the regions are affected by the southeast monsoon in summer and Siberian cold in winter. The community should face south with the back to the north orientation. Its location should also gradually raise with the site from south to north, which will achieve not only comfortable natural ventilation but also get better sunshine from the south. According to the

Feng-Shui philosophy regarding ‘community’, the optimised model of courtyards in this site is distributed. At the same time, the location of each building gradually rises from south to north. Then the optimised results showed that the outdoor wind speed is between 0.39m/s and 5.08m/s in summer, and between 0.36m/s and 3.28m/s in winter. The outdoor wind speed in summer is higher and in winter is lower than the initial results. The calm wind zones almost disappeared in summer, and the overall natural ventilation improved significantly (Fig. 7). The optimised community layout offers an improved comfortable wind environment.

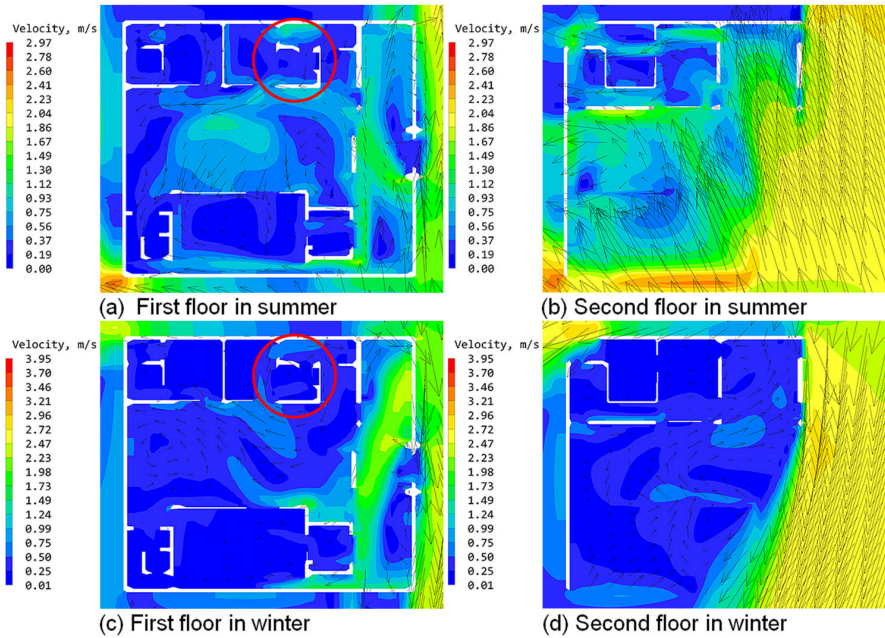


Figure 6. Wind simulation of single courtyard.

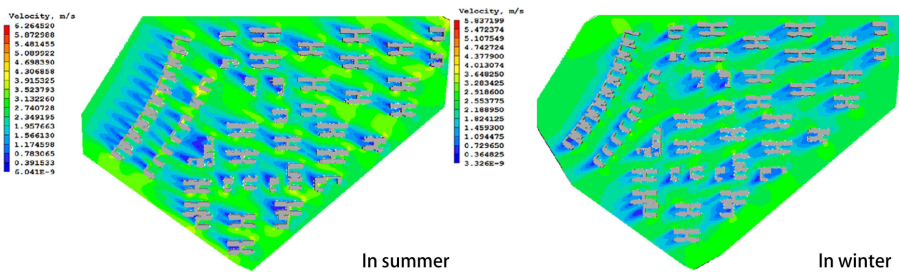


Figure 7. Optimized outdoor wind simulation of community.

In terms of block simulation, every single courtyard is attached back to back,

which causes a rise in indoor calm wind zones, especially in the west of the block. The local block construction is according to Feng-Shui concept, which requires the typical layout style for blocks to be detached from each other, whether for traditional or modern block layout. This kind of block layout can form ventilation alleys between blocks. It not only optimises natural ventilation but also improves the thermal pressure ventilation because the ventilation alleys are affected by block shadows (Guo & Liu & Yuan, 2015 (b)). The optimised result of natural ventilation in summer is between 0m/s and 2.48m/s. It is higher than the initial result of between 0m/s and 2.22m/s. The overall natural ventilation has been optimised even though calm wind zones still exist in the main rooms. The result in winter also optimized as 0m/s and 2.87m/s was reduced to 0m/s and 2.57m/s. The overall wind speed was lower than 5m/s (Fig. 8). This natural ventilation will give people a more comfortable environment.

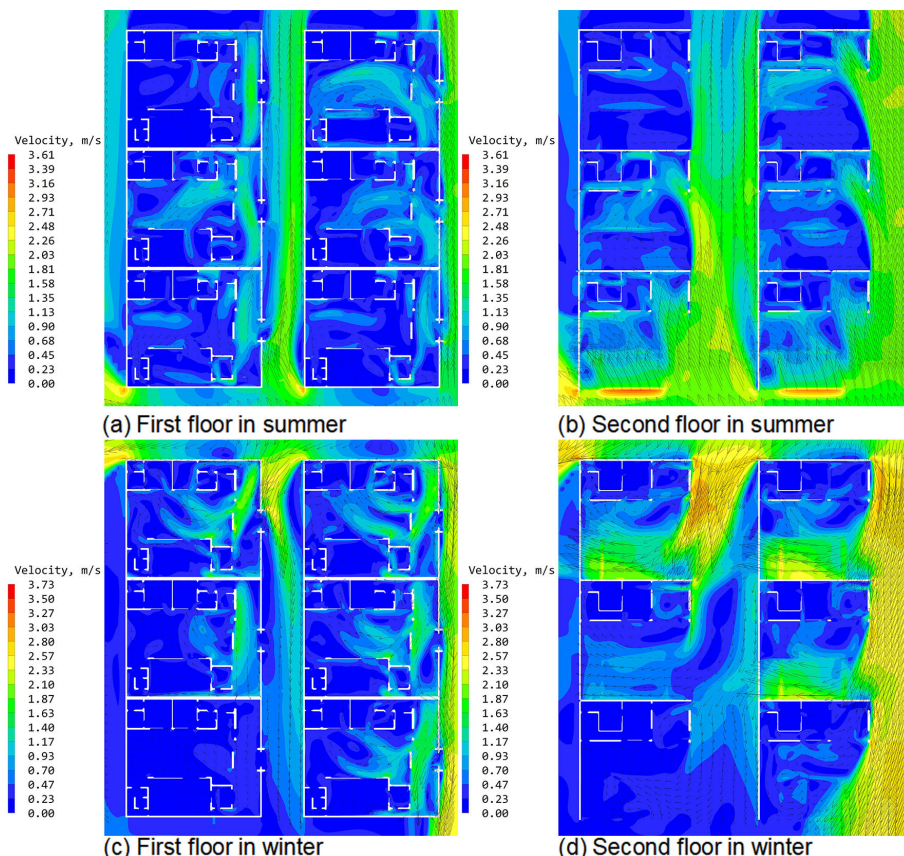


Figure 8. Optimized wind simulation of block.

The initial result of the single courtyard showed that the bathroom would pollute the air quality of the other rooms because the wind is blowing from the east, whether in summer or winter. According to Feng-Shui, the design of a house

should put the bathroom to the corner and in the downwind position (Yan, 2016). Therefore the design of the single courtyard should be optimised. The indoor wind should flow from main rooms to functional rooms, as shown in Figure 9.

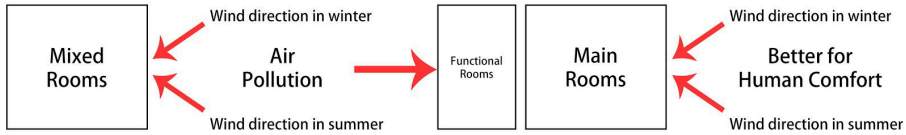


Figure 9. Single courtyard design diagram.

#### 4. Discussion

The three challenges to natural ventilation were described and analysed. These were 'community', 'block', and 'single courtyard'. The results showed that natural ventilation could be optimised according to Feng-Shui. In the community, the lighting surface orientation of facing south, and the foundation gradually raising with the site from south to the north offered higher wind speed in summer and lower wind speed in winter - resulting in improved human comfort. In the block, the layout of blocks is detached from each other. This way, more ventilation alleys are formed. Furthermore, the overall natural ventilation is optimised, whether in summer or winter. In the single courtyard, functional rooms such as bathrooms were designed to be put downwind of the building, subsequently solving the air pollution problem. All of our certified Feng-Shui principles have an architectural and building science value that can be applied in future architecture design. They also offer advantages for human comfort and provides support for other scholars' research (So & L, 2001; Jeffreys, 2000).

The research of CFD analysis only proved the value of natural ventilation based on Feng-Shui, which is only one part of the overall Feng-Shui philosophy relating to architecture design. The optimised community layout by raising the foundation with the site has only been simulated virtually, while the optimised result of block indoor natural ventilation in summer results in calm wind zones even though it is better than before. The computational simulation analysis for the optimised single courtyard was not designed to be a specific design. These issues need to be explored in future research.

#### 5. Conclusions

In this paper, the results of the 'community', 'block', and 'single courtyard' in Jiangmen city were simulated by the CFD method. The community's outdoor wind speed between 0.44m/s and 3.5m/s in winter, and there are calm wind zones in summer. The block simulation showed wind speed less than 5m/s in winter. There are calm wind zones in the main rooms in summer, especially in the west of the block. The indoor wind flowed from the bathroom to the other main rooms. The single courtyard simulation result showed that the indoor wind flows from bathroom to bedroom on the first floor, and the maximum wind speed in winter is

3.95m/s.

The ‘community’, ‘block’, and ‘single courtyard’ have been optimised according to the Feng-Shui concept. Community optimised result showed the outdoor wind speed between 0.39m/s and 5.08m/s in summer, and between 0.36m/s and 3.28m/s in winter. The wind speed in summer is higher and in winter is lower than the initial results. The calm wind zones almost disappeared in summer. Overall natural ventilation improved significantly. Block optimised result of natural ventilation in summer between 0m/s and 2.48m/s, and it is higher than the initial result between 0m/s and 2.22m/s. The overall natural ventilation has been optimised even though there are still exist calm wind zones in the main rooms. The result in winter also optimized from 0m/s and 2.87m/s reduced to 0m/s and 2.57m/s. The overall wind speed lower than 5m/s. The single courtyard optimised result showed that the bathroom layout in the house to the downwind position could solve air pollution according to Feng-Shui philosophy.

This research used CFD computational simulation method to analyse the natural ventilation of ‘community’, ‘block’, and ‘single courtyard’ in Jiangmen city, according to the human comfort required by relevant standards. The problems of initial results were found out. According to Feng-Shui philosophy, the optimised plans were built. Then the optimised results were analysed to show that the Feng-Shui wisdom has value for the fields of architecture and building science. We conclude that in the context of natural ventilation, CFD confirms that principles of Feng-Shui and its philosophy can contribute to natural ventilation and human comfort, ultimately improving architectural design and livability.

### Acknowledgment

This research was supported by the National Key R&D Program of China (Grant No. 2017YFC0702505); General Program of National Natural Science Foundation of China (No. 51678239); Science and Technology Program of Guangzhou, China (No. 201804020017).

### References

- Bartzis, J.G., Vlachogiannis, D. and Sfetsos, T.: 2004, Thematic Area 5: Best Practice Advice for Environmental Flows, *The QNET-CFD Network Newsletter*, **2**, 34-39.
- Ministry of Housing and Urban-Rural Development of the People’s Republic of China, M.: 2013, *The Standard of the Measurement and Evaluation for Efficiency of Building Ventilation*, China Architecture & Building Press.
- Ministry of Housing and Urban-Rural Development of the People’s Republic of China, M.: 2016, *Code for Thermal Design of Civil Building*, China Architecture & Building Press.
- Ministry of Housing and Urban-Rural Development of the People’s Republic of China, M.: 2018, *Standard for Green Performance Calculation of Civil Buildings*, China Architecture & Building Press.
- Ministry of Housing and Urban-Rural Development of the People’s Republic of China, M.: 2019, *Assessment Standard for Green Building*, China Architecture & Building Press.
- Du, Y. and Mak, C.M.: 2017, Effect of Lift-up Design on Pedestrian Level Wind Comfort Around Isolated Building under Different Wind Directions, *Procedia Engineering*, **205**, 296-301.



- Feuchtwang, S.D.R.: 1974, *An Anthropological Analysis of Chinese Geomancy*, White Lotus Co Ltd.
- Franke, J., Hellsten, A., Schlünzen, H. and Carissimo, B.: 2007, Best Practice Guideline for the CFD Simulation of Flows in the Urban Environment, *Cost Action*, **732**, 51.
- Guo, W.H., Liu, X. and Yuan, X.: 2015 (a), Study on Natural Ventilation Design Optimization Based on CFD Simulation for Green Buildings, *Procedia Engineering*, **121**, 573-581.
- Guo, W.H., Liu, X. and Yuan, X.: 2015 (b), A Case Study on Optimization of Building Design Based on CFD Simulation Technology of Wind Environment, *Procedia Engineering*, **121**, 225-231.
- He, H.Y. and Schnabel, M.A.: 2016, A CFD Analysis of Wall-effect Building Groups in a Curved Layout: A Study in Sha Tin, Hong Kong, *Proceedings of the 11th ISAI*.
- Jeffreys, P.: 2000, Feng-Shui for the Health Sector: Harmonious Buildings, Healthier People, *Complementary Therapies in Nursing and Midwifery*, **6**, 61-65.
- Kalland, A.: 1996, *Geomancy in a Japanese Community*, University of Pittsburgh.
- Knapp, R.G.: 1986, *China's Traditional Rural Architecture: a Cultural Geography of the Common People*, Honolulu: University of Hawaii Press.
- R.G. Knapp (ed.): 1992, *Chinese Landscapes: the Village as Place*, Honolulu: University of Hawaii Press.
- R. Lawrence and C. Raffestin (eds.): 1994, *Mythical and Ritual Constituents of the City*, London: F & FN Spon.
- Lee, S.H.: 1986, *Feng-Shui: Its Context and Meaning*, Ph.D. Thesis, Cornell University.
- Liu, S.M., Pan, W.X., Zhang, H., Cheng, X.L., Long, Z.W. and Chen, Q.Y.: 2017, CFD Simulations of Wind Distribution in an Urban Community with a Full-scale Geometrical Model, *Building and Environment*, **117**, 11-23.
- Mak, M.Y.: 1995, *Feng-Shui and Building Performance. Ecological Perspectives and Teaching Architectural Science*, Canberra: University of Canberra.
- Mak, M.Y. and Thomas, N.g. S.: 2005, The Art and Science of Feng-Shui—A Study on Architects' Perception, *Building and Environment*, **40**, 427-434.
- Scaperdas, A. and Gilham, S.: 2004, Thematic Area 4: Best Practice Advice for Civil Construction and HVAC, *QNET-CFD Netw. Newsl.*, **2**, 28-33.
- So, A.T. and Lu, W.Z.: 2001, Natural Ventilation Design by Computational Fluid Dynamics—A Feng-shui Approach, *Architectural Science Review*, **44**, 61-69.
- Tominaga, Y., Mochida, A., Yoshie, R., Kataoka, H., Nozu, T., Yoshikawa, M. and Shirasawa, T.: 2008, AIJ Guidelines for Practical Applications of CFD to Pedestrian Wind Environment around Buildings, *Journal of Wind Engineering and Industrial Aerodynamics*, **96**, 1749-1761.
- Wang, Q.H.: 1998, *Research of Feng-Shui Theory*, Tianjin University Press.
- Wang, B. and Malkawi, A.: 2018, Design-Based Natural Ventilation Evaluation in Early Stage for High Performance Buildings, *Sustainable Cities and Society*, **45**, 25-37.
- Yan, Y.: 2016, Application of Traditional Feng-Shui in Modern Interior Layout and Decor, *Art Panorama*, **9**, 109.

# A MACHINE-LEARNING DRIVEN DESIGN ASSISTANCE FRAMEWORK FOR THE AFFECTIVE ANALYSIS OF SPATIAL ENCLOSURES

ROHIT PRIYADARSHI SANATANI

<sup>1</sup>*Assistant Professor, Department of Urban Design, School of Planning  
and Architecture, New Delhi*

<sup>1</sup>*rohitsanatani@yahoo.co.in*

**Abstract.** There is a growing research direction that adopts an empirical approach to affective response in space, and aims at generating bodies of quantitative data regarding the correlations between spatial features and emotional states. This paper demonstrates a machine-learning driven computational framework that draws upon training data sets to predict the ‘affective impact’ of designed enclosures. For demonstration, it has been scripted as a Rhinoceros + Grasshopper based design tool that uses existing training data collected by the author. The data comprises of the spatial parameters of Enclosure Volume (V), Length/Width ratio (P) and Window Area/Total Internal Surface Area ratio (D) - and the corresponding emotional parameters of Valence and Arousal. The test values of these parameters are computed by defining the components of the test enclosure (walls, windows, floors and ceilings) in the script. Nonlinear regression components are run on the training datasets and the test input data is used to compute and display the real time predicted affective state on the circumplex model of affect.

**Keywords.** Affective Analysis; Affective Computing; Design Assistance; Machine Learning; Spatial Enclosures.

## 1. Introduction

The affective or emotional qualities of spatial enclosures have often been regarded as ‘intangible’ aspects of space beyond the scope of empirical inquiry. While it is well known that different ‘kinds’ of spaces affect us in different ways and elicit different emotional responses, architects have traditionally relied on intuition when engaging with design decisions pertaining to the affective domain. While there are well-established standards, models and design assistance tools for the design of other aspects of enclosures such as energy optimization, acoustics etc., there are few such supporting frameworks for the affective realm. Till recent years, a lack of empirical lines of inquiry into the affective qualities of spatial enclosures made it difficult for designers and architects to adopt a ‘scientific approach’ to the realm of emotional response in space. However, recent lines of inquiry have established frameworks for the systematic study of the correlations between specific attributes of the form of virtual enclosures, and corresponding emotional

response in occupants (Franz et al. 2003, Vartanian et al. 2013, Marín-Morales et al. 2018, Sanatani 2019). Challenges of generating parametrically controllable physical enclosures for experimentation have been overcome with advances in simulation technologies, and virtual reality systems. The rapid development and commercial availability of head mounted display driven VR apparatus have opened up new methodological possibilities for such research directions (Mazuryk and Gervautz 2010). Despite being an emerging line of inquiry, there is a growing body of data pertaining to the emotional impact of specific formal parameters or ‘features’ of spaces (such as geometric configuration, size, color, texture etc). Such studies directed specifically towards the effect of specific spatial parameters on emotional response has the potential to open up very valuable lines of enquiry into the correlations between the physical and the emotional realms within space. Most importantly, the body of empirical data generated can provide architects with strong rational grounding to design decisions pertaining to spatial experience.

The field of affective computing or ‘artificial emotional intelligence’ has seen rapid development since its inception two decades ago. Today, there are computational models and frameworks in place capable of recognizing emotional states based on facial expressions (Robinson and el Kaliouby 2009). Inquiries have been made into the correlations between features of photographs, and the corresponding emotional response and aesthetic judgment in observers (Datta et al. 2006). However it has only been in the past couple of years that affective computing has begun to be applied to the domain of spatial enclosures and architectural research (Marín-Morales et al. 2018). Such research directions have a strong potential to be taken forward in order to yield computational models for emotional response in space. The body of labeled empirical data gathered through such inquiries has immense potential to be used as training data for machine learning algorithms designed to ‘learn’ underlying patterns between spatial ‘features’ of enclosures and affective states in occupants. This can be taken forward to develop design assistance tools, which can employ machine-learning models to predict the emotional impacts of designed enclosures.

This paper demonstrates a computational framework for generating a design assistance model that predicts the emotional impact of a designed enclosure in real time based on specific spatial features, by applying non-linear regression algorithms to existing training data sets collected from prior experiments.

## **2. Quantifying affective response in space**

Any line of empirical inquiry focusing on emotional response in space must first adopt or synthesize a framework for the collection of objective and quantifiable data pertaining to one’s emotional state. While a number of models have been proposed as structures of human emotion, there have been two broad approaches towards structuring the affective realm.

Basic Emotion Theories/Discrete Theories maintain that there are sets of very basic and discrete human emotions, such as Joy, Disgust, Surprise, Fear, Anger and Distress (Ekman 1984), which cannot be broken down into simpler parts. These emotions lie within separate domains and are discrete in nature.

More recent schools of thought however opine that all emotions can rather be mapped on dimensional scales such as the Circumplex model (Russell 2003). The circumplex model consists of a three dimensional emotion-space with Valence (Pleasure-Displeasure) on the x axis and Arousal (Activation-Deactivation) on the y-axis. The z-axis of Dominance is also often used. According to this Dimensional Theory, a wide range of possible human emotions can be defined with respect to these basic dimensions. (Figure 1)

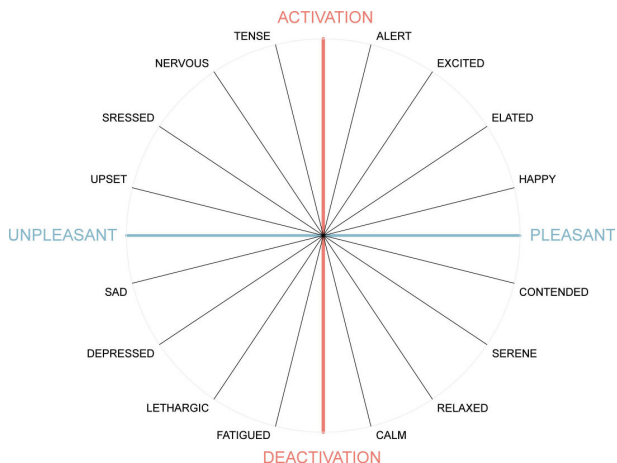


Figure 1. The Circumplex Model of Affect (Russell 2003).

One approach towards the objective recording of emotional response focuses on recording the physiological and biological indicators that accompany emotional response, such as facial expression, Electro Dermal Activity (EDA), Skin temperature (SKT), and Electrocardiography (ECG) (Kim et al. 2003). A large amount of emotional data collected for affective computing is in the form of such indicators. However, a number of methodological difficulties pertaining to the accuracy and relevance of such biological parameters as indicators of spatial affect have been highlighted in past studies (Hermund et al. 2019). Notably the sensitivity of the recording equipment to extraneous electrical signals, especially from the wearable VR systems is a factor that needs to be dealt with.

A second approach relies on one's own verbal assessment of his or her emotional response to any given stimulus (known as an 'affective appraisal'). Affective appraisals thus assume the accuracy and reliability of one's own conscious affective assessment. Bradley and Lang developed a language independent scaling method for recording appraisals known as the Self Assessment Manikin, which is now regularly employed in experiments for measuring a range of emotional stimuli. In this method, the two dimensions of human emotion (Valence and Arousal) are represented as pictorial scales. (Bradley and Lang 1994)

In one of the early studies enquiring empirically into the affective qualities of spatial enclosures in virtual reality, Franz, von der Heyde and Bulthoff studied the architectural parameters such as Total Window Area, Wall Openness Ratio,

Size of Single Window, Room Area, Room Length/Width etc. and their effects on spatial experience (Franz et al. 2003). Subjects were asked to rate parametrically altered variants of a designed virtual enclosure on a semantic differential scale with bipolar adjectives such as unpleasant-pleasant, boring-interesting, ugly-beautiful, arousing-calm etc. Notably, they found 'spaciousness' to be correlated more strongly to overall window area as compared to actual room area. The maxima for rated beauty corresponded to length/width and width/height ratio values which were very close to the golden ratio (Franz et al. 2003).

A related experiment by Shemesh, Bar and Grobman was directed towards testing the emotional responses of two sets of subjects - designers and non-designers - to different geometrical configurations of architectural space (smooth, curvy, symmetrical, asymmetrical etc) simulated in a visualization lab comprising of high-definition projection and motion sensors (Shemesh et al. 2015). A rating system comprising of the scales efficient, pretty, safe, pleasant, and interesting was used. The results indicated that both the groups appeared to prefer asymmetric spaces to symmetric ones. The non-expert group however found familiar spaces to be much more pleasant as compared to unfamiliar configurations. However the curved configuration (despite being unfamiliar) corresponded to a high degree of rated 'prettiness' and 'interestingness'. The round space however was more interesting and pretty to the expert group (Shemesh et al. 2015).

Outside the domain of spatial enclosures, McDuff et al synthesized a machine learning driven framework for predicting the affective states of individuals at their workstations (McDuff et al. 2012). They relied on labeled training data collected from five participants over two days. The independent variables or features logged included facial expression features decoded from a webcam stream, voice features decoded from microphone data, electro dermal activity (EDA), posture and file activity. The output data included Valence, Arousal and Engagement ratings normalized to produce discrete labeled classes corresponding to emotional states on the circumplex. A nearest neighbor classifier model was used to make predictions based on test data and the results were logged and displayed to the users.

Morales et al. applied statistical analysis and machine learning models to data sets correlating spatial parameters such as Geometry (Curvature, Complexity, Order), Color (Tone, Saturation, Value) and Illumination (Color temperature, Intensity, Position), and the corresponding biological indicators of heart rate variability and electro encephalic signals, collected through experiments conducted using HMD driven VR environments. Affective appraisals of the subjects were also recorded on dimensional emotion models using the self-assessment manikin (Marín-Morales et al. 2018). A support vector machine classifier algorithm was employed to predict the valence and arousal states of subjects with more than 70% accuracy. The methodology synthesized for these experiments show great potential to be adopted for focused research within the domain of spatial affect, and data collected through such experiments can be used as training data for machine learning algorithms to 'learn' underlying relationships between spatial features and emotional response.

### 3. The demonstrative training dataset

To demonstrate the computational framework presented in this paper, a pre-existing dataset has been adopted, which was collected through an earlier phase of empirical experimentation conducted by the author.

The experiments focused on deriving correlations between three spatial parameters or 'features', namely: (i) Area of glazing/Total internal surface area (**D**), which is the primary variable for daylight factor, (ii) Total volume of enclosure (**V**) (iii) Length/Width ratio of the enclosure (**P**) (Sanatani 2019).

Through three separate sets of experiments, 18 parametrically altered variants of an empty spatial enclosure corresponding to varying values of each of the three spatial parameters were presented to 50 subjects through a head mounted display (HMD) driven virtual reality system. Each of these scenes were spherical renders of field of view (FOV) 360° and resolution 4000x2000 pixels generated using Rhinoceros and Grasshopper3D, rendered using V-Ray for SketchUp and adapted for VR viewing through FullDrive VR (Sanatani 2019).

Subjects were asked to rate each space on the Self Assessment Manikin, the results of which were then converted into numerical Valence and Arousal scores on a -4 to +4 scale. Each set of experiments thus gave us two sets of 300 data points describing the variation in each of the dependent variables (arousal and valence) due to controlled variation of the independent variable (the spatial parameter being studied). The training dataset thus comprises of total of 900 data points each for Valence and Arousal.

A cursory analysis of the data revealed that daylight factor correlated very strongly with Arousal. Peak Valence values corresponded to a wall/window ratio of .03 an enclosure volume of 70 cu.m and a length:width range between 1:1 and 1:1.5. The golden ratio was not rated favorably (Sanatani 2019).

The dataset collected from these experiments has been adopted to demonstrate the computational framework and serve as training data for the machine learning algorithms to learn the predominant patterns.

### 4. The computational framework

#### 4.1. THE PLATFORM

The framework described in this paper has been developed on a Rhinoceros + Grasshopper platform, with the additional use of the nonlinear regression component provided for Grasshopper by the machine learning tools within the Lunchbox plugin. While this platform has been adopted for demonstration, it may be coded onto more appropriate platforms in the future. Existing python libraries (such as scikit-learn) can be employed for greater flexibility and control over the model. The framework also has potential to be developed as a separate plugin to Rhinoceros, or even as a standalone design assistance tool.

#### 4.2. THE FRAMEWORK

The computational design assistance framework presented in this paper comprises broadly of three parts or units and has been conceptually summarized in Figure 2.

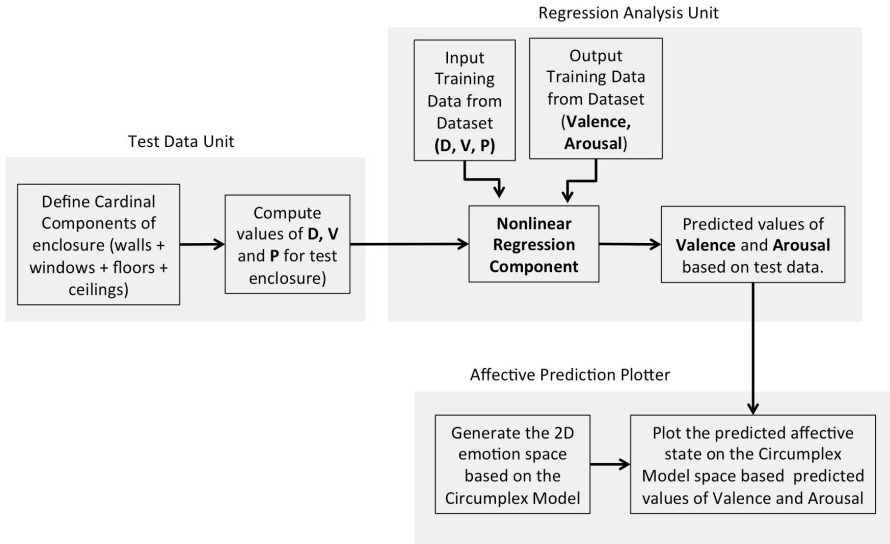


Figure 2. Conceptual representation of the design assistance framework.

The first part or the **test data generation unit** defines the cardinal components of the modeled test enclosure (such as walls, floor, roof, windows) into the Grasshopper script and subsequently computes the real-time values of the three spatial parameters (namely (D, V and P). Figure 3 shows a conceptual representation of the grasshopper script corresponding to this unit.

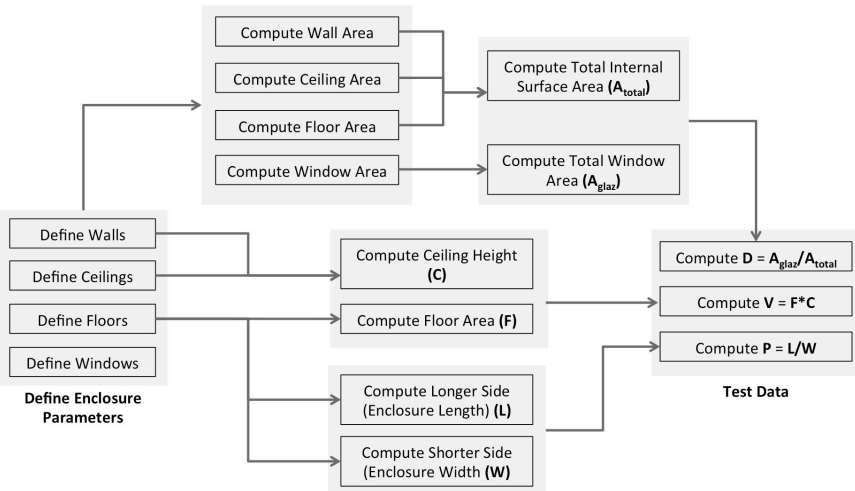


Figure 3. Conceptual script for the test data generation unit.

The second unit of the framework or the **regression analysis unit** runs the

main Multivariate Nonlinear Regression algorithm. The Nonlinear Regression component provided by Lunchbox for Grasshopper accepts the training data from the adopted dataset. The input training data is thus the 900 values of A, V and P respectively. The output training data for each set are the 900 corresponding values each of valence and arousal. There are thus two nonlinear regression components running i.e one for valence and one for arousal. These components output the real time predicted values of Valence and Arousal for the test enclosure.

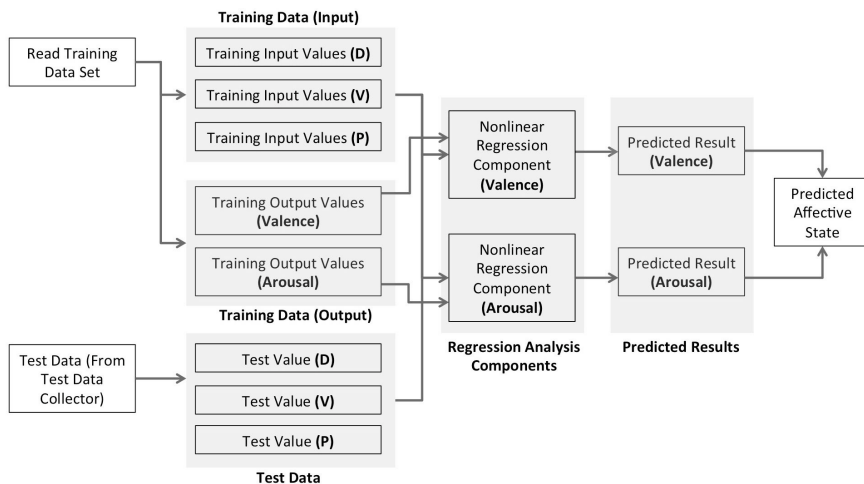


Figure 4. Conceptual script for the regression analysis unit.

The third unit of the computational framework or the **affective prediction plotter** generates the representative 2d affective space based on the circumplex model of affect in the Rhino modelspace. It then inputs the predicted values of valence and arousal from the previous unit and plots the predicted emotional state on the circumplex, thus allowing the designer to view real time shifts in affective states based on changes in spatial features made to the test enclosure.

Figure 5 and Figure 6 demonstrates the working of the tool. For a designed enclosure of  $V = 70.38$  cum,  $P = 1.0$  and  $D = .03$ , the nonlinear regression component predicts an affective state of Valence = +2.36 and Arousal = +1.95 and displays it as a point on the circumplex emotion space. When the spatial features of the enclosure are modified, changing the values of V, P and D to 428.43 cum, 2.15 and .0083 respectively, the shift in predicted affective state to Valence = -1.09 and Arousal = -.02 is reflected on the circumplex. This real time interface thus allows the designer to constantly monitor the affective implications of his design decisions pertaining to spatial features.



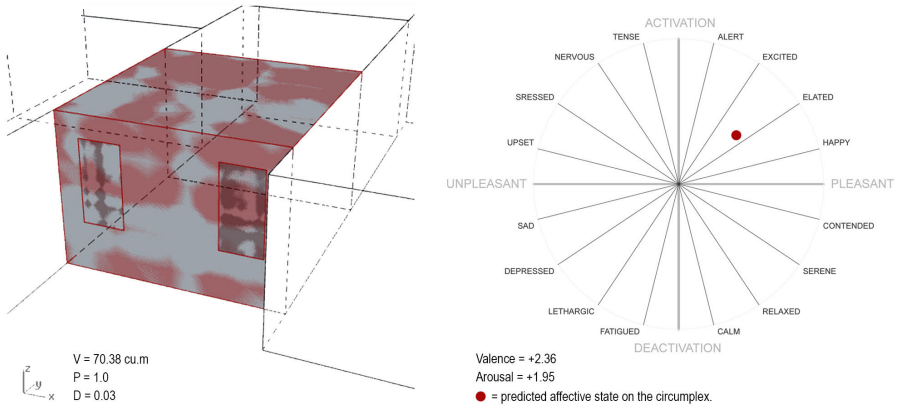


Figure 5. Predicted affective state for  $V = 70.38$  cu.m,  $P = 1.0$  and  $D = .03$ .

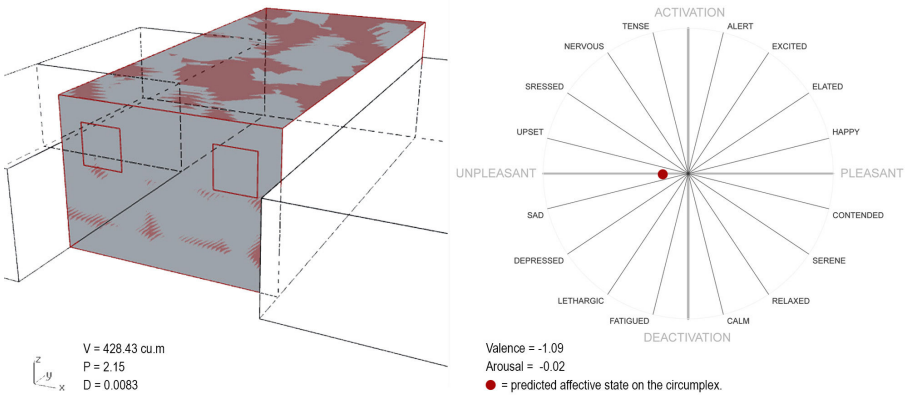


Figure 6. Shift in predicted affective state for  $V = 428.43$  cu.m,  $P = 2.15$  and  $D = .0083$ .

It may be mentioned here that the adopted demonstrative training data set has its limitations with respect to multivariate regression analysis. As discussed earlier, the data set was collected through 3 sets of controlled experiments corresponding to the three spatial parameters, with only a single parameter being varied in each set. For the multivariate regression model to have greater accuracy, the training data set should have data points corresponding to simultaneous variations in all the independent variables. For the current data set, three sets of bivariate regression analysis components will produce more accurate results. However, for demonstration of the framework, a multivariate model has been adopted, which can be applied to more appropriate datasets in the future.

## 5. Conclusion and future directions

The aim of this framework is to draw upon empirically derived training data in order to allow machine learning algorithms to learn underlying patterns in the ways in which specific formal attributes or ‘features’ of spatial enclosures impact affective states, thus allowing for real time predictive analysis of the affective qualities of enclosures during the design phase. As discussed earlier, while there are numerous design assistance and simulation tools for aspects of design such as energy performance or acoustic behavior, architects still rely primarily on their own intuitions when designing for the affective realm. While the field of affective computing has made rapid progress in applying quantitative and computational processes to make sense of the affective domain, this field has only very recently begun to foray into the world of architectural design. The framework presented in this paper aims to serve as a small yet firm step towards applying the processes of affective computing directly in the design process.

The demonstrative training data set drawn upon in this paper may be replaced by much larger and more accurate data sets, which will result in more accurate predictions. Moreover, such a framework has immense potential to be applied to occupant-specific datasets for algorithms to learn the affective patterns of the target occupant(s) in space, thus working towards the creation of tailor-made spaces that respond to the affective nuances of the individual(s). There are an incalculable number of spatial features that affect our emotional response in spaces, and this framework need to be expanded to include many more parameters such as color temperature, texture, geometry, opening configurations etc. which play vital roles in determining how the space makes us ‘feel’. In the age of big data, we have a plethora of new sources through which data pertaining to one’s emotional state may be obtained. It is hoped that data obtained through larger focused studies conducted in the future, or even through crowd sourced data collection systems, can plug into this framework and lead to the development of a design assistance tool that can aid architects in designing for the affective domain.

On a concluding note, one may reflect upon what such research directions will mean with respect to the role of the architect in the future. The advent of computer aided drafting tools has greatly reduced the time required in preparing architectural drawings and revisions. The advent of Building Information Modeling (BIM) systems has dramatically reduced the man-hours spent in coordination between consultants and compiling building related data. Rapid advances are currently being made in the field of automated floor plan generations based on preset constraints and design briefs (Nisztuk and Myszkowski 2019). It has often been argued that the one domain within which automation cannot replace the human mind is the domain of subjective phenomenological experience. Computers, it has been said, cannot ‘feel’ or design for ‘feelings’. The domain of affective computing however has been steadily proving otherwise. As discussed, algorithms are learning to predict what images and graphics will make people feel, and are also beginning to generate graphics that are intended to make people ‘feel’ certain ways. Where then, lies the role of the artist? Can we envision a future where algorithms are not only equipped to generate floor plans, but also design spaces that will make users ‘feel’? Where then, lies the role of the architect?

## References

- “Machine Learning with LunchBoxML” : 2017. Available from <<https://provingground.io/2017/08/01/machine-learning-with-lunchboxml/>> (accessed 11th December 2019).
- Bradley, M.M. and Lang, P.J.: 1994, Measuring Emotion: The Self Assessment Manikin and the Semantic Differential, *Journal of Behavioral Therapy and Experimental Psychiatry*, **29**, 49-59.
- Datta, R., Joshi, D., Li, J. and Wang, J.Z.: 2006, Studying Aesthetics in Photographic Images Using a Computational Approach, *European Conference on Computer Vision*.
- Ekman, P.: 1984, *Expression and the Nature of Emotion*, Lawrence Erlbaum Associates, Inc.
- Franz, G., von der Heyde, M. and Bulthoff, H.H.: 2003, An empirical approach to the experience of architectural space in VR, *DIGITAL DESIGN - 22nd eCAADe Conference*.
- Hermund, A., Jensen, M.M. and Klint, L.S.: 2019, The Neurological Impact of Perception of Architectural Space in Virtual Reality, *Virtually Real: Immersing into the Unbuilt. Proceedings of the 7th eCAADe Regional International Symposium. Aalborg University Press, Aalborg*.
- Kim, K.H., Bang, S.W. and Kim, S.R.: 2004, Emotion recognition system using short-term monitoring of physiological signals, *Medical & Biological Engineering & Computing*, **42**, 419-427.
- Marín-Morales, J., Higuera-Trujillo, J.L. and Greco, A.: 2018, Affective Computing in Virtual Reality: Emotion Recognition from Brain and Heartbeat Dynamics Using Wearable Sensors, *Scientific Reports*, **8**(1).
- Mazuryk, T. and Gervautz, M.: 2010, *Virtual Reality: History, Applications, Technology and Future*, Institute of Computer Graphics, Vienna University of Technology, Austria.
- McDuff, D., Karlson, A., Kapoor, A., Roseway, A. and Czerwinski, M.: 2012, AffectAura: An Intelligent System for Emotional Memory, *Proceedings of the SIGCHI Conference on Human Factors in Computing Systems*, Austin.
- Nisztuk, M. and Myszkowski, P.B.: 2019, Hybrid Evolutionary Algorithm applied to Automated Floor Plan Generation, *International Journal of Architectural Computing*, **17**, 260-283.
- Robinson, P. and el Kaliouby, R.: 2009, Computation of Emotions in Man and Machines, *Philosophical Transactions: Biological Sciences*, **364**(1535), 3441-3447.
- Russell, J.A.: 2003, Core affect and the psychological construction of emotion., *Psychological Review*, **110**, 145-172.
- Russell, J.A. and Pratt, G.: 1980, A Description of the Affective Quality Attributed to Environments, *Journal of Personality and Social Psychology*, **38**, 311-322.
- Sanatani, R.P.: 2019, An Empirical Inquiry into the Affective Qualities of Virtual Spatial Enclosures in Head Mounted Display driven VR Systems, *Virtually Real: Immersing into the Unbuilt. Proceedings of the 7th eCAADe Regional International Symposium. Aalborg University Press, Aalborg*.
- Shemesh, A., Bar, M. and Grobman, Y.J.: 2015, Space And Human Perception – Exploring Our Reaction to Different Geometries of Spaces, *Past, Present and Future of Digital Architecture, Proceedings of the 20th International Conference of the Association for Computer-Aided Architectural Design Research in Asia CAADRIA 2015*.
- Vartanian, O., Navarrete, G., Chatterjee, A., Fich, L.B., Leder, H., Modroño, C., Nadal, M., Rostrup, N. and Skov, M.: 2013, Impact of contour on aesthetic judgments and approach-avoidance decisions in architecture, *Proceedings of the National Academy of Sciences of the United States of America*, **110**, 10446 - 10453.

# USER-DRIVEN PARCELLATION OF HIGH-RISE UNITS FOR FUTURE URBAN HABITATION

*Participatory Computational Design Tools for Future Urban Habitation*

OLIVER HECKMANN<sup>1</sup>, MICHAEL BUDIG<sup>2</sup>,  
ZACK XUEREB CONTI<sup>3</sup>, RAY CHERN XI CHENG<sup>4</sup> and  
SKY LO TIAN TIAN<sup>5</sup>

<sup>1,2,3,4</sup>*Singapore University of Technology and Design*

<sup>1,2,3,4</sup>{oliver\_heckmann|michael\_budig|zackary\_xuereb|

ray\_cheng}@sutd.edu.sg

<sup>5</sup>*Harbin Institute of Technology (SZ)*

<sup>5</sup>lutiantian@hit.edu.cn

**Abstract.** Most residential high-rise apartments currently built to satisfy growing demands for housing, are predetermined and thus, are unable to respond to the increasingly diversifying forms of co-habitation. This research pursues alternative flexible approaches by building on Habraken's 'Open Building' paradigm, where permanent, polyvalent 'Support System' layouts are strategically designed to accommodate highly adaptable, user-driven 'Infill systems'. In this context, we adopt the participatory decision-making approach, by means of a computational framework that facilitates user-driven parcellations of entire buildings into apartments segments. The means is an algorithm that allocates numerous user-preference regarding size and position simultaneously - by searching for parcel permutations through a graph-syntax representation of floor plans. The research forms part of a larger project that aims to evaluate the resilience of mass housing for future uncertain demands.

**Keywords.** Participatory; generative; mass housing; open building.

## 1. Introduction

This paper presents a computational framework for parcelling residential units in mass housing high-rise projects, driven by simultaneous user wishes as an alternative to standardized mass housing strategies such as 'Build to Order' in Singapore and 'Standard Block' in Hong Kong. The research presented in this paper forms part of a larger project that aims to develop computational tools to evaluate the resilience of mass housing layouts for future uncertain demographics.

High-rise mass housing in growing cities fails to respond to the increasing diversification and unpredictability of forms of co-habitation. Unit layouts in residential mass housing high-rise projects are often predetermined by

the developers and planners based on user demands patterns from the past. Consequently, resulting floor plan layouts do not facilitate users to customize their acquisition according to their individual preferences, and as a result do not match the dynamics of shifting demographics (Wong 2010).

In response, this paper suggests an alternative approach to standardized mass housing approaches, based on the support and infill system methodology, within the ‘Open Building’ (OB) paradigm, developed by John Habraken (1961). The OB paradigm involves user-participants in the design loop of the building. An often referred to example for the OB paradigm is Molenvliet (Papendrecht, Netherlands 1977 - Arch: Van der Werf). This project was one of the first to test the paradigm of support and infill systems as a base framework to facilitate participatory design, where numerous meetings with high numbers of prospective tenants were necessary to moderate the parcellation (see right in figure 1). In a first phase: the entire complex was parcellated into units by coordinating multiple user wishes, simultaneously. In a second phase, individual units were jointly designed by users and architects.



Figure 1. Open building project in Molenvliet, Papendrecht, 1977, (Arch: Van der Werf) Left: phase 1, right: phase 2.

In the greater context of our project, we adopt a similar two-phase approach to mass-housing design through user participation. The first phase pertains to the parcellation of multiple units according to simultaneous size and position preferences. We interpret an OB-based support and infill system as a polyvalent pattern of adjacent spaces as a support system where infill elements act as agent of either connection or disconnection thus, produce new arrangements, without consequence to the structural integrity of the building. The second phase lies outside of the scope of this paper and is subject to subsequent research, where the polyvalency will facilitate new infill wall reconfigurations to accommodate new wishes expressed along the lifetime of the building.

### 1.1. INFILL SYSTEMS AND THE ‘OPEN BUILDING PARADIGM’

The concept of Open building for residential housing was proposed as a distinction of the built environment into two categories: a permanent support system as the only part for which an architect would still be in charge, and a flexible ‘infill system’ which would be entirely adaptable to individual user requirements during its entire life-cycle.

1.2. POLYVALENCE-BASED PARTICIPATION FOR MASS HOUSING

In projects like the first phase of Molenvliet, both the functional and topological flexibility of the pattern are enabled by the ‘Polyvalency’ of the entire pattern, defined by Hertzberger (1991) as “a form that can be put to different uses without having to undergo changes itself.” Neither the dimension of the individual cells nor their hierarchical relation with adjacent ones determine their appropriation. Furthermore, the pattern does not predetermine any division into hermetic apartment units and is thus open to a moderation of multiple user requirements regarding the size and form of their units.

In this context, we interpret the polyvalence of cell adjacency patterns as a configuration of cell-divisions, where potential connections between two adjacent rooms are represented as a configuration of on/off states. A figurative example (see figure 2) of such a rule-based adjacency configuration can be found in Mitchell’s application (1990) for the placement of doors and windows applied to Palladio’s Villa Malcontenta.

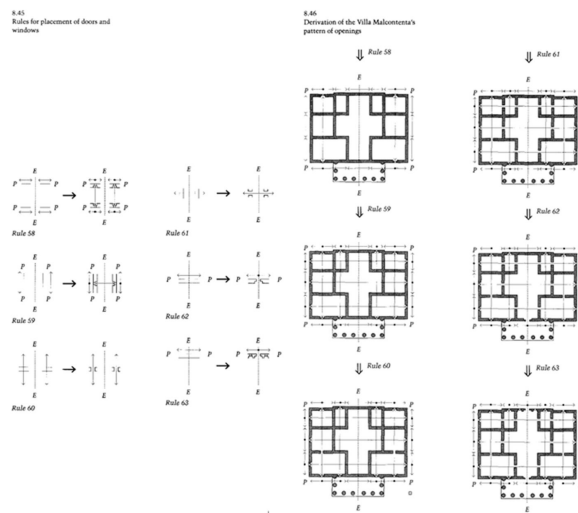


Figure 2. The logic of Architecture applied on Palladio’s Villa Malcontenta (Mitchell 1990).

In the 70s, Friedman (1975) and Negroponte (1975), respectively took advantage of topological descriptions to encode such rule-based spatial adjacencies into a graph syntax, that facilitated a computable format for the automatic generation of floor plans. Both applications suggest a participatory-driven approach where design generation was driven by user-inputted criteria. These early applications already start to indicate the notion of computational frameworks for user-driven parcellation.

More recent computational approaches to Habraken’s Open Building participatory approach include the work by Madrazo, Sicilia, González, and Cojo (2009) who present a collaborative web-based platform for the interaction of different ‘actors’ (client, architect, etc.). The platform facilitates the generation of

apartment layouts based on specified client preferences. The generative process adopts a graph-syntax based representation of floor plans. Building on this work, Lo, Schnabel, and Gao (2015) present ‘ModRule’ – a user-centric mass housing design platform that allows architects and future occupants to communicate throughout the design stages of mass housing buildings. Their system makes use of a ‘gamification’ methodology to facilitate a high-level accessibility to individuals with low architectural background.

Overall, the participatory-driven approaches described above focus on the generation of spatial arrangements at the local scale of the units. Instead, our research aims to address the cognitive challenge when it comes to simultaneously parcelling multiple user wishes at the scale of the high-rise building. Herr et al. (2005) discuss a generative approach to accommodate multiple demands of pre defined units according to market demand trends. In this paper we share a similar intention to Herr et al. (2005) but instead approach the parcellation of polyvalent floorplans as a search through a graph-based representation, is naturally representative of spatial relationships.

Our study builds upon a previous study (Heckmann et al. 2019) which suggested a support structure for a generic public housing high-rise type conceptually similar to the Molenvliet layout. Like Molenvliet the design study deliberately avoids to pre-determine apartment units such as in ‘Build to Order’ and thus allows flexible, user-responsive parcellations to accommodate diverse forms of co-habitation during the launch time of properties. With the inherent capability to divide or connect the generated parcels, the morphological pattern can also adapt to planned or unexpected changes in resident’s living situations.

## 2. Computational framework

The algorithmic workflow aims to generate an agglomeration of unit permutations that: i) maximise user preferences (unit size and position) while, ii) minimise invalid unit spatial arrangements. The overall workflow involves four main steps: specification of infill-based floor plan, encoding of layout as graph, algorithmic permutation search, and packing agglomeration. The following subsections describe each of the steps in figure 3.

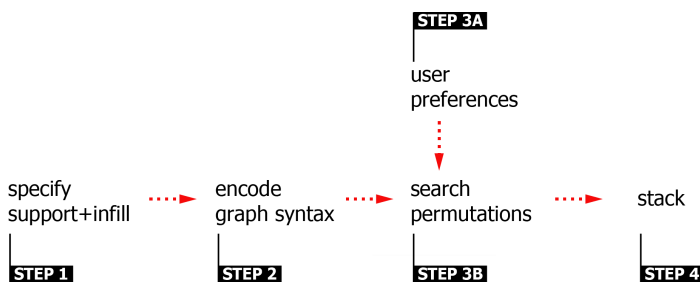


Figure 3. Overall computational workflow.

2.1. STEP1: SPECIFY SUPPORT AND INFILL SYSTEM

For this paper, we adopt a polyvalent floor plan (see figure 4) for a high-rise building based on an Open Building support and infill system from a precedent study (Heckmann, Budig, and Ng Qi Boon 2019).

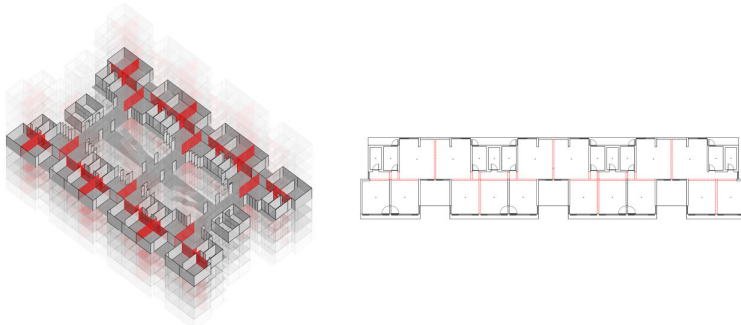


Figure 4. Polyvalent layout with specified support-infill system.

2.2. STEP2: ENCODE FLOOR PLAN GRAPH-SYNTAX

We adopt a syntax-based representation to encode a polyvalent floor plan in terms of the spatial adjacencies, similar to the approach described in Madrazo et al. (2009). In general, a space syntax aims to provide an objective representation of the continuous spatial layouts in a building (Hillier and Hanson 1989). More specifically, we adopt a convex map approach, because such a representation reflects directly, the polyvalence of OB-based layouts where, doorways in divisory walls can naturally be encoded as on/off states in a graph-based representation.

Each floor plan in the graph-based syntax is encoded as a graph data structure (see figure 5) where nodes represent enclosed spaces, while edges represent an adjacency between rooms. Each node is encoded with a *roomType* attribute to describe the function of the room. Possible room types include *hallway*, *normal* (living or bedroom), *kitchen*, *wet cell* and *storage*. Similarly, the edges are encoded with attributes to distinguish whether the room division is accessible or not (*isAccessible=True/False*).

In more detail, the *isAccessible* property is a flag to indicate whether the edge dividing the nodes (enclosed rooms) is traversable or not. On the other hand, the *isInfill* flag indicates whether wall is an infill partition or a load bearing partition. Figure 5 illustrates a simple graph example, showing a service hallway (node 1) accessible via nodes 2 and 3; whereas the toilet (node 4) is adjacent to both 2 and 3 but only accessible by 2.



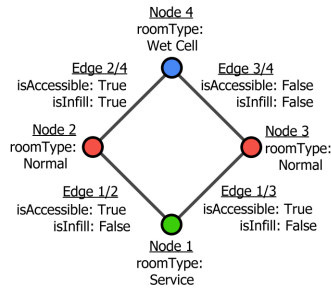


Figure 5. Simple graph-syntax layout example.

With the data structure in place, the floor plan was then encoded into a graph syntax (see figure 6). At the start of the algorithm, all the default edges are treated as accessible (*isAccessible=True*). Subsequently, infill walls are then turned on, once allocated nodes for units are determined. The goal here is to parcellise the layout for each floor of the building, based on floor location and unit specifications defined by the simultaneous user wishes.

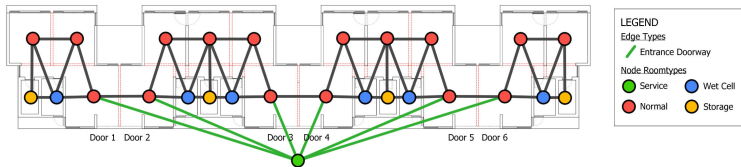


Figure 6. Floor plan layout represented as a graph-based convex map.

### 2.3. STEP 3A: USER PREFERENCE INPUTS

Each client is presented with a discretised representation of the building elevation in the form of a 2D matrix (see right in figure 7), similar to typical housing projects. In other words, each discretised 2D bin represents a region bounded by a range of preferable floors and an approximate preferred position on a floor (*left, middle, right*). The regions act as bins in a 2D histogram, where a client may assign a preferred unit configuration to one of the bins, from a set of predefined room arrangements (see left in figure 7). Subsequently, each bin is assigned with a frequency distribution that describes the distribution of preferred unit sizes for the respective region. For this case scenario, we generate synthetic user preferences composed of: unit size preferences derived from a normal distribution, preferred floor levels (see left in figure 7) derived from an empirical distribution of floor level preferences in Singapore public housing (Yuen et al. 2006), and floor wing position preferences derived from a normal probability distribution (see right in figure 7). Synthesised preference data serves as a proof of concept for subsequent work in which we adopt the parcellation algorithm to evaluate the resilience of layouts to adapt to future demographic trends.

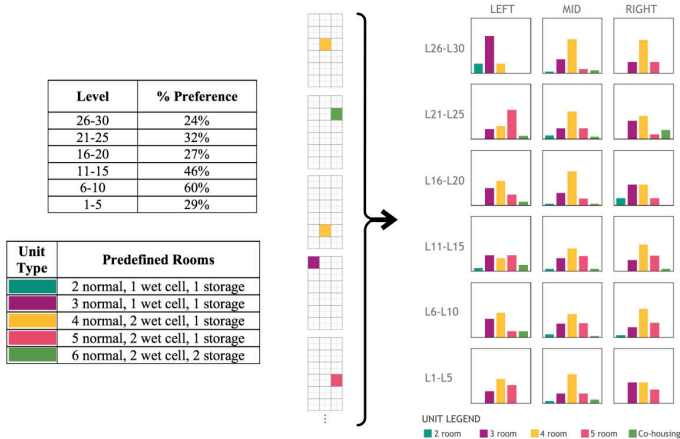


Figure 7. Predefined unit sizes and user preferred unit size and location distribution.

#### 2.4. STEP 3B: UNIT PERMUTATION SEARCH ALGORITHM

A custom algorithm was developed to search through the graph syntax representation of the polyvalent floor plan. The algorithm generates unit parcellations for each floor based on the user preferences of unit size and position assigned in step 2, by searching recursively through various traversal patterns through the graph topology of each floor (see figure 8).



Figure 8. Example of node traversal and unit allocation in the algorithm. Traversal path is shown in red; once it is defined as a unit (shown in purple), the algorithm tries the next path traversal for another unit.

In further detail, the algorithm interprets the unit size preferences for each bin into a list of check lists. Each check list indicates a set of node types (rooms) required to satisfy the corresponding unit size. For example, a unit size of 5 requires a 3 ‘normal’ nodes, 1 ‘wet cell’ node and 1 ‘storage’ node (see figure

7) to be satisfied. Once all checklists are determined, the algorithm traverses through the graph nodes on each floor level in search for valid units as per the list of position-sensitive checklists assigned to each floor level (see figure 8).

#### 2.4.1. Scoring

Each parcellation permutation is scored in order to identify the valid candidates from the possible set of permutations. In our approach we consider two scoring factors:

1. *white-space ratio*; a ratio of the number of unassigned spatial enclosures to the overall number of spatial enclosures. An unassigned enclosure is a space not allocated by the search algorithm in any of the unit. The search goal is to minimize this ratio.
2. *demand satisfaction*; the number units that satisfy the most preferred unit size from the preference frequency distribution of the respective elevation bin region. The search goal is to maximize this value.

#### 2.5. STEP 4: UNIT STACKING

The parcellation results for each floor layout of are processed iteratively and joined to form the elevation view visualization of the building. Figure 11 illustrates a schematic of the parcellised rooms facing the front elevation based on the synthesized demographic data from section 2.3.



Figure 9. Resulting elevation view of stacked unit parcels.

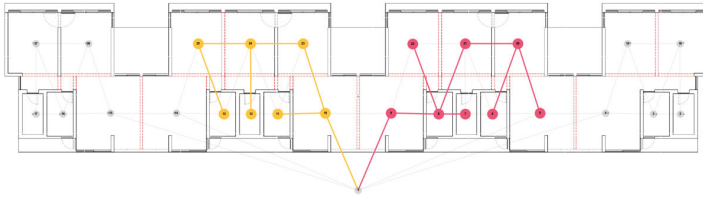


Figure 10. Resulting level 15 parcellation procedure.

The vacant parcellations in figure 9 and figure 10 result from exhausted demands on those locations. The vacant spaces are also an indirect outcome of the shape of the overall distribution of the preferred floor level ranges and floor positions.

Any remaining unallocated nodes from the first packing procedure are identified and it is determined whether further units can be ‘fit’ to these unclaimed nodes in a second search. Subsequently, any remaining nodes from the second process are considered as white-spaces and left unallocated. Figure 11 and figure 12 illustrate the result after attempting to assign these vacant parcellations.



Figure 11. Resulting elevation view of stacked unit parcels after filling. .

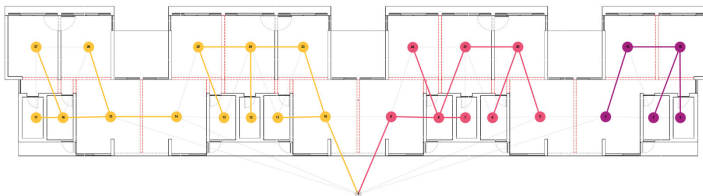


Figure 12. Resulting level 15 parcellation after filling procedure.

### 3. Conclusion and future work

In this research we presented a computational framework where polyvalent mass-housing building floor plans are encoded as a graph-based syntax representation to search for unit parcellations driven by simultaneous user wishes. We illustrated how the approach can serve as an alternative to standardized mass-housing approaches. In subsequent research we intend to integrate the computational framework within a web interface to facilitate user-preference inputs, for use during residential project launch. The presented parcellation method will be used to evaluate the resilience of floor plan layouts to be able to adapt to sequences of future user demand patterns, which are extrapolated from demographic models developed concurrently. The topological patterns will also be used to generate spatial models with which end-users may then co-design through a virtual-reality-based interface.

#### Acknowledgements

The presented work is part of the research project 'Next Residential High-rise' funded by the SUTD-MIT International Design Centre (Project No. IDG21800103). We would like to thank Lynnette Cheah (collaborator, Associate Professor, SUTD), Clement Lork, Jun Wen Loo, Amanda Qi Boon Ng (all researchers at SUTD) for their support

#### References

- Habraken, N.J.: 1961, *De dragers en de mensen - Het einde van de massawoningbouw*, Scheltema & Holkema NV.
- Heckmann, O., Budig, M. and Ng Qi Boon, A.: 2019, Next Generic Residential High-Rise - Flexible Housing Typologies and their Social and Environmental Sustainability, *CIB World Building Congress*, Hong Kong.
- Herr, C., Fischer, T., Wang, H. and Ren, W.: 2005, Demand-Driven Generative Design of Sustainable Housing for China, *Proceedings of the 5th China Urban Housing Conference*, Hong Kong, 703-710.
- Hertzberger, H.: 1991, *Lessons for Students in Architecture*, Uitgeverij 010 Publishers.
- Hillier, B. and Hanson, J.: 1989, *The social logic of space*, Cambridge university press.
- Lo, T.T., Schnabel, M.A. and Gao, Y.: 2015, ModRule: A user-centric mass housing design platform, *International Conference on Computer-Aided Architectural Design Futures*, 236-254.
- Madarazo, L., Cojo, A.M. and Sicilia, A.: 2009, Barcode housing system: Integrating floor plan layout generation processes within an open and collaborative system to design and build customized housing, *Proceedings of CAAD Futures 2009*, 656-670.
- Mitchell, W.J.: 1990, *The logic of architecture: Design, computation, and cognition*, MIT Press.
- Wong, J.F.: 2010, Factors affecting open building implementation in high density mass housing design in Hong Kong, *Habitat International*, **34**(2), 174-182.
- Yuen, B., Yeh, A., Appold, S.J., Earl, G., Ting, J. and Kurnianingrum Kwee, L.: 2006, High-rise living in Singapore public housing, *Urban Studies*, **43**(3), 583-600.

# A LIGHT-WEIGHT CAAD-VR BRIDGE

SHENG-FEN CHIEN<sup>1</sup>, CHIEH-I LIN<sup>2</sup> and KUAN-LING LIN<sup>3</sup>

<sup>1,2,3</sup>*National Cheng Kung University, Tainan Taiwan*

<sup>1</sup>*schien@mail.ncku.edu.tw* <sup>2,3</sup>*{N76071047|N76071055}@ncku.edu.tw*

**Abstract.** Virtual Reality (VR) has been proven an effective media for design communications. VR-enabled design environments allow laypersons to join in various stages of design process and achieve a wide range of participatory designs. However, most of these environments are developed for research purposes and not easily accessible to architects. This research aims to bridge the gap of VR hardware and design software to make VR easily accessible to architects. We develop a set of 4 use cases for implementing VR-enabled design environment: (1) Export Design Elements to VR; (2) Authorizing VR co-design environment; (3) Design Manipulation in VR; and (4) Output VR Objects to CAAD. A prototype has been implemented using HTC Vive and Unity to test these use cases. The data exchange between VR environment and CAAD environment is achieved through the JSON format. The prototype is tested by students in a graduate-level design studio with promising results.

**Keywords.** Virtual Reality; VR; VR-enabled CAAD; Use Case; JSON.

## 1. Introduction

Virtual Reality (VR) has been proven an effective media for design communications (e.g.: Donath and Regenbrecht 1995; Maver, Harrison and Grant 2001; Milovanovic et al. 2017). Furthermore, VR-enabled design environments allow laypersons to join in various stages of design process and achieve a wide range of participatory designs (e.g.: Achten, De Vries and Van Leeuwen 2001). However, these environments are developed for research purposes or specific organizations and are not easily accessible to architects and architectural students beyond the research groups or organizations.

Adopting VR environments in architectural design process have been very cumbersome. Af Klercker (2000) summarized that to be able to use VR effectively, designers have to simplify the geometry of CAAD (computer-aided architectural design) models by minimizing the amount of polygons, to plan the uses of textures and texture mapping carefully so as to match the level of details properly, to add proper shadows and physics properties to make scenes realistic, and to implement object behaviors (such as “door opening”) and player actions. The issues of having to readjust geometries and textures cause extra work for designers. In addition,

the issue of implementing object behaviors and player actions requires computer programming skills from designers. With the advances of computation and VR hardware, almost all issues have been addressed, except the “object behaviors and player actions” part, which is important in participatory design settings. An international working group for new virtual reality applications in architecture (Kobayashi et al. 2009) has demonstrated VR models and computational plug-in tools for VR software packages, but the adaptations of such tools are not widely spread.

Fast-forward to the present day, there are several commercial software products and services that have addressed or overcome CAAD-VR conversion issues. However, VR has not been widely adapted in architectural practices. Nor has it been a common medium in the architectural design education. Although the cost of VR hardware is reducing, the application of VR in the architectural design process seems to still be a heavy duty work. To employ a professional CAAD-VR service for daily design process is a “heavy” cost for small architecture offices and educational organizations. To develop in-house CAAD-VR integrations is a “heavy” burden for designers. We hope to find a light-weight (low in monetary cost and in workflow burden) approach to bridge the gap of VR hardware and design software to make VR easily accessible to architects and architectural students in their daily practices.

## **2. Approaches of CAD-VR Integration**

Approaches of CAD-VR integration can be categorized into three types based on the mode of data-coupling between CAD models and VR models. The first type, CAD-to-VR conversion, is a one-way conversion from a CAD model to a VR model; no data-coupling is maintained. This approach is suitable for presenting final design solution to clients and users. The second type, CAD-VR link, is a two-way conversion between CAD models and VR models; data-coupling is required to maintain consistency. This approach is suitable for design collaborations. The third type, VR-CAD system, is a VR-based CAD environment, in which CAD models are VR models.

### **2.1. CAD-TO-VR CONVERSION**

Whyte et al. (2000) have summarized and tested several conversion methods: a one-way “downstream” process that reduces complexity of CAD models and reduces workflow (e.g. see: Bourdakis 2001); a library-based approach to reuse VR models during conversion; a straightforward translation when models are small; and a database approach where building models are created in the central database and viewed through different applications (e.g. see: Ding et al. 2003). Pickersgill (2007) experimented with the VR game engine and reported the improved performance of VR system in handling complex geometries, textures, and interactivity. Yap, Taha and Dawal (2012) developed file conversion and translation mechanisms to allow for more effective translation of CAD models to VR models. With continuous improvement of VR software and conversion tools, Wolfartsberger (2019) is able to investigate VR-based engineering design review

using a straightforward file translation approach.

## 2.2. CAD-VR LINK

To support design collaborations in VR environment, a bridging system needs to encapsulate “design knowledge” so that proper attributes are associated with geometry that linked between VR geometry and CAAD geometry (see e.g., Achten, and Van Leeuwen 1999). Ding et al. (2003) used the database approach to link the CAD model with VR environment. Wang and Li’s research team (2010) created special purpose “virtual assembly models” to maintain the relationship between CAD models and VR models. Chotrov and Maleshkov (2013) added CAD model descriptions and CAD editing module in VR environment to achieve bidirectional synchronization of CAD and VR models. Lorenz et al. (2016) demonstrated a CAD to VR automatic conversion system that uses a shared “product model” to maintain bidirectional interaction.

To generalize, the bidirectional link (or automatic conversion) approach almost all involve using a shared model. The shared model may be implemented in a database or data server (Ding et al. 2003; Hawton et al. 2018; Kado and Hirasawa 2018). The share model may be implemented as an adaptor module to be attached or embedded within VR environment (Wang et al. 2010; Chotrov and Maleshkov 3012; Lorenz et al. 2016). The share model may be a platform that wraps the CAD system and VR system inside, such as BIM. Recently, BIM models are used as persistent data to drive displays in VR with manipulations of individual objects (e.g., Bille et al. 2014; Edwards et al. 2015; Nandavar et al. 2018; Lai et al. 2019). Bille et al. (2014), Nandavar et al. (2018) and Lai et al. (2019) together provide a comprehensive review of BIM-VR bi-directional data exchange projects.

## 2.3. VR-CAD SYSTEM

As early as 1995, Donath and Regenbrecht developed a VRAD-system. They defined “Virtual Reality Aided Design (VRAD) as Computer Aided Design using the methods of virtual reality” (Donath and Regenbrecht 1995). The system employed voxel space modeling methods. Do (2001) demonstrated the VR Sketchpad where objects are modeled in VRML. Fiorentino et al. (2002) created the Spacedesign, a mixed reality workspace for industrial design, that is based on a solid modeling kernel. VR-CAD systems have comprehensive geometric kernels under VR environments and often maintain construction history graphs (CHG) to support constraint-based CAD operations (Zhong, Mueller-Wittig and Ma 2003; Pang et al., 2006; Wang et al., 2010; Chotrov and Maleshkov 2013; Martin et al. 2017).

## 2.4. SUMMARY

With the advances of computer hardware and VR software, the CAD-to-VR conversion approach has become fairly easy and effective. Martin et al. (2017) stated that the main limitations in this approach is that it is impossible to directly create or modify CAD models in the VR environment. However, it is possible to add scripts in VR software to enable creation or modification of VR objects



and send outcomes to the CAD environment. The VR-CAD system approach is less feasible in that the modeling interface in VR is not as efficient as in CAD environment.

The CAD-VR link approach is the most favorable for implementing bidirectional interactions that support design collaborations. However, almost all projects reviewed are developed with serious computer programming work. As such, it is almost impossible for architects to duplicate the research effort even if some are open source projects. BIM-based CAD-VR link approach may have more commercial solutions, yet it is costly. The experimentation by Hawton et al. (2018) stands out in that free and open-source utilities are used to create bidirectional links between CAD and VR environment to allow for parametric design manipulations in VR. Further searches show that such setup may need very few programming skills and in a relatively short time (see: Horikawa 2019).

Milovanovic, et al. (2017) conducted a comprehensive survey of VR and AR applications in architectural design. They showed that VR/AR environments assist architectural design learning. They focused on “design critiquing” because the VR/AR is easier to be used as visualization environments. They reviewed SDAR system by Gu and Halici (2016) where users can create new shapes and scribble notes inside the virtual environment. They found cubes with markers work better than 3D pens. In VR, “a space” has to be modeled. It can be treated as a “void object” which in turn can be assigned attributes or behaviors. Pickersgill (2007) emphasized the use of “void objects”, indicating “game modeling” is actually very much inline with the real life.

### 3. CAAD-VR Bridge

To support designers using VR and creating design collaboration, we document the system requirements from user’s perspective using Use Cases (Jacobson et al. 1992). To prevent confusion, we define some CAD and VR terms.

- CAAD environment: the software that designers or architects use to conduct designs.
- Design model: the model of the CAAD environment that created by designers or architects as the outcome or temporary outcome of design.
- Design element: a part of the design model that can be manipulated in design collaboration.
- VR authoring tool: the software that designers or architects use to setup for creating the VR environment.
- VR environment: the packaged VR program that allows for interactive design collaboration.
- VR model: the model in VR authoring tool and VR environment that corresponds to the design model in CAAD environment. It may include behaviors attached to its components.
- Model component: a part of the VR model that may or may not have behavior attached.

### 3.1. USE CASES

From the literature survey and our own experience in the university settings, we concluded that VR in architectural design practices, as well as in architectural design educations, is most applicable and provides the best assistance in participatory design sessions and client/public communications. For the client/public communications, the CAD-to-VR approach, reviewed in the previous section, is sufficient. Therefore, we formulated the requirement of VR-based client/public communications in two use cases: first, *Export Design Elements to VR*; and second, *Authorizing VR Co-design Environment*. To support the participatory design, we need to employ the CAD-VR link approach. Two additional use cases, *Design Manipulation in VR* and *Output VR Objects to CAAD*, were formulated for the requirement.

#### 3.1.1. UC1: *Export Design Elements to VR*

When a designer (architect) wishes to co-design with potential users, or present to the client/public, the design products (buildings), the designer identifies appropriate design elements in a CAAD environment, prepares the CAAD model and exports the model to a VR authoring environment. Specifically, the designer's actions are:

1. Identify "design elements" to be manipulated in VR environment.
2. Prepare model: separate "design elements" from other elements (through layer arrangement or grouping).
3. Export the CAAD model to the VR project.

If the VR authoring environment cannot import the CAAD model directly, the step 3, instead, requires these actions:

- 3.a. Export the CAAD model to a VR modeling format (e.g., OBJ).
- 3.b. In the VR authoring environment, import the exported file.

The designer's goal is to obtain a VR model, properly representing the CAAD model, in a VR authoring environment. If the VR model shows up wrong in orientation, the designer should trace back to step 3 or 3.a and reconfigure the import/export setting to swap Y/Z axes. A VR authoring environment can simulate the VR environment with build-in functionality. Therefore, for client presentations, this use case may be sufficient already.

#### 3.1.2. UC2: *Authorizing VR Co-design Environment*

When a designer (architect) wishes to co-design with potential users, and the CAAD model is properly converted to a VR model in the VR authoring environment, the designer prepares VR scenes, defines a set of controls in VR authoring environment to support design manipulations, and authorizes the VR model. Specifically, the designer's actions are:

1. Check the correctness of geometry and texture of objects.
2. Assign appropriate controls to design elements.
3. Test run the VR model and verifies controls.

#### 4. Authorize the VR model (compile, build, and execute).

The designer's goal is to create a VR co-design environment. The co-design environment is a standalone application that the designer may bring to participatory design sessions.

##### *3.1.3. UC3: Design Manipulation in VR*

During a participatory design session, the designer invites participants (usually laypersons) as co-designers to discuss and adjust designs in VR. The designer sets up the VR system with the outcome from UC2. The co-designer navigates around the VR environment, examines and manipulates design elements, discusses with designers until they are satisfied. Specifically, the co-designer's actions are:

1. Navigate around the VR environment.
2. Identifies a design element.
3. Manipulate the selected design element.
4. Repeat steps 1 through 3 until satisfied.

Depending on the hardware setup, the VR environment may support single-person or multi-person interactions, i.e. designers and co-designers may work collaboratively in the VR environment.

##### *3.1.4. UC4: Output VR Objects to CAAD*

In a participatory design session, when the designer wishes to store the design back to the CAAD environment, the designer invokes an export design elements function in the VR environment, and checks for the updated model in the CAAD environment. Specifically, the designer's actions are:

1. Request the export of design elements in the VR environment.
2. Examine the CAAD model after the system exports design elements.

If the VR environment cannot export to the CAAD model directly, the step 2, instead, requires these actions:

- 2.a. Request the system to export design elements to a format that is acceptable to the CAAD environment.
- 2.b. Invoke appropriate function in the CAAD environment to import the output file and update the CAAD model.

The designer's goal is to obtain the updated CAAD model from the outcomes of VR co-design environment. It may be desirable that the updates of CAAD model to be instantaneous, or to be accessible from a remote site. These enables the possibilities of recording design alternatives during participatory design sessions, and/or conducting remote design participations.

## 3.2. SYSTEM DESIGN

Since our objective is to provide a light-weight solution, we want to minimize designers workflow and scripting time, as well as to increase the flexibility (Fig. 1). We plan to use off-the-shelf CAD-to-VR file transfer to support UC1. We envisage that designers will export CAAD models through proper file formats

(e.g. FBX), then import the files into VR authoring tools. For UC2, we plan to create behavior scripts of object manipulation (e.g. select, move, resize, duplicate) as library scripts so that designers may attach appropriate scripts to design elements/model components. For UC3, we hope the VR environment is portable, detached from CAAD environment, so that it can be easily brought to co-designers using various types of VR hardware. For UC4, we plan to provide scripts for outputting VR models and storing it in the JSON format. In addition, we will provide utility in CAAD environment to parse JSON formatted VR models back to design elements in CAAD models. Technically, we will develop a JSON parser for target CAAD environments, a set of object manipulation scripts, a model-to-JSON output script, and controller mapping scripts for target VR authoring tools.

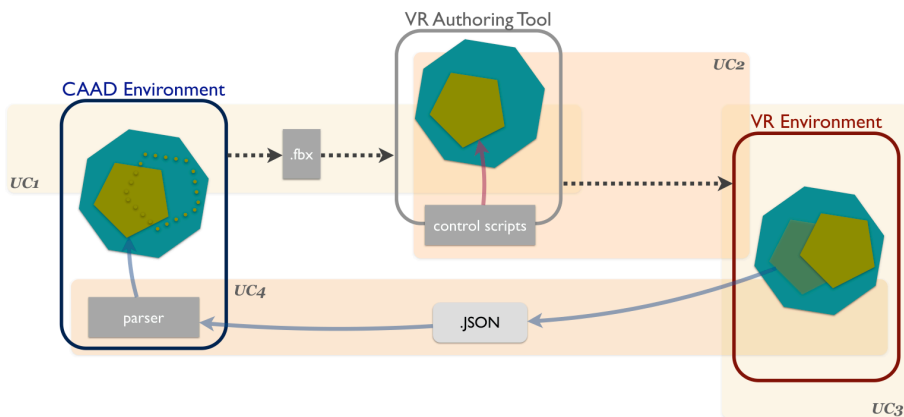


Figure 1. The framework of CAAD-VR bridge.

#### 4. Prototype

We have implemented a prototype to test these use cases. The CAAD environment is Rhino/Grasshopper. The VR authoring environment is Unity. The VR environment is VR Chat. The VR hardware is HTC Vive. The data exchange between the VR environment and the CAAD environment is achieved through the JSON format. We have implemented a JSON parser in Grasshopper. We have made a scripting library (assets) in Unity, which includes setting up controller (joystick and keyboard), move/scale/duplicate manipulation, and export to JSON. The prototype is tested by students in a graduate-level design studio.

Figure 2 illustrates the work of a student designer: he had designed a building block system and planned to test the system with friends. He organized building block units in Rhino and exported the model to FBX format. He imported the FBX file into Unity, and imported our assets. In Unity, he selected building block objects, tagged them with “DesignElement”, and dropped manipulation scripts onto objects (Fig. 2, left; a case of UC2). He completed the set up and export VR scenes to VR Chat. His friends were invited to his VR Chat room the played

with building blocks (Fig. 2, right; a case of UC3). He exported some VR models and tried to load them back using our parser script in Grasshopper. He encountered some errors and had to adjust the parser scripts several times. Nevertheless, he was able to get JSON files loaded and brought the co-design results back to Rhino. Figure 3 illustrates works of two student designers. One of them (Fig. 3, left) exported the whole CAAD models into Unity, added Unity built-in elements and controls. The other (Fig. 3, right) exported the CAAD model with several types of design elements into Unity, but scripted his own behaviors. The works of these students showed extreme variations of UC2.

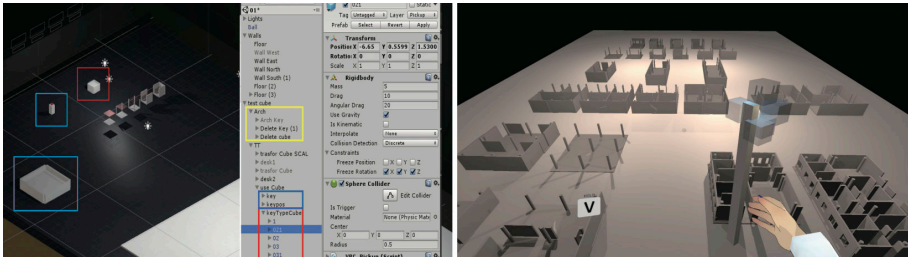


Figure 2. left: setting up controls in Unity; right: a co-design session in VR Chat.

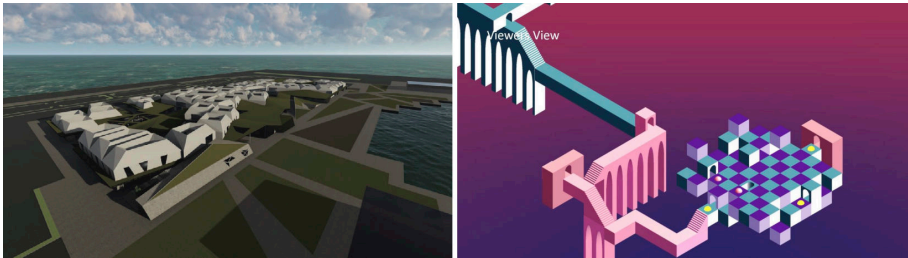


Figure 3. left: design work of Yen-Ning Hsu; right: design work of Cheng-Lin Chuang.

## 5. Discussion and Conclusion

Our prototype has been tried by four other student designers. They all reported that the workflow for each use case is easy. Among the use cases, the second one (UC2) the most difficult; they needed some time to learn the event control of Unity so that they can debug if things went wrong. For UC4, the JSON parser script is a solution template (rather than the solution) that needed to be adjusted according to the amount of their design elements. However, when the parser worked properly, if both the CAAD environment and the VR environment are running on the same computer, the output from the VR environment may produce almost instantaneous updates in the CAAD environment as though both environments were connected.

We have made deliberate decisions to specify our light-weight CAAD-VR bridge in four use cases. Learning from the literature and our prototyping, we have adjusted and refined these use cases to extensive details. These details may

work as step-by-step instructions for designers/architects who are interested in understanding CAD-VR integration steps. These details may work as guidelines for tech-affluent staff in design/architecture firms to implement inhouse solutions.

For architectural design presentation and collaboration, there are high-end commercial solutions for comprehensive, sophisticated VR interactions. For low cost solutions, current CAD environments provide fairly good VR conversions for walkthroughs, but no design interactions. Adding interactions in VR model is not an easy task. Adding design interactions in VR model has been a serious research issue where the solutions all require “heavy-weight” setup that is beyond architects or student designers. Our light-weight approach tries to fill the gap. We plan to revise our scripts to make them more robust and join the open source community.

### Acknowledgement

We thank IA Lab of NCKU Architecture for the access of HTC Vive systems. We also thank CL Chuang, YN Hsu, Y Hsing, YS Lin, and WL Wu for testing our prototype implementations and providing valuable feedbacks.

### References

- Achten, H.H. and Van Leeuwen, J.P.: 1999, Feature-Based High Level Design Tools - A Classification, *Proceedings of the Eighth International Conference on Computer Aided Architectural Design Futures*, Atlanta, USA, 275-290.
- Achten, H., De Vries, B. and Van Leeuwen, J. 2001, Computational Design Research: The VR-DIS Research Programme, in H. Achten, B. de Vries and J. Hennessey (eds.), *Design Research in the Netherlands 2000*, Eindhoven University of Technology, 155-163.
- Bille, R., Smith, S.P., Maund, K. and Brewer, G.: 2014, Extending Building Information Models into Game Engines, *Proceedings of the 2014 Conference on Interactive Entertainment*, New York, NY, USA, 22:1-22:8.
- Bourdakis, V.: 2001, On Developing Standards for the Creation of VR City Models, *19th eCAADe Conference Proceedings*, Helsinki, Finland, 404-409.
- Chotrov, D. and Maleshkov, S. 2013, Simultaneous Bidirectional Geometric Model Synchronization between CAD and VR Applications, in G. Bebis, R. Boyle, B. Parvin, D. Koracin, B. Li and F. Porikli (eds.), *Advances in Visual Computing*, Springer Berlin Heidelberg, Berlin, Heidelberg, 288-297.
- Ding, L., Liew, P., Maher, M.L., Gero, J. and Drogemuller, R.: 2003, Integrating CAD and 3D virtual worlds using agents and EDM, *Proceedings of the 10th International Conference on CAAD Futures*, 301-312.
- Do, Y.L.E.: 2001, VR Sketchpad: Create Instant 3D Worlds by Sketching on a Transparent Window, *Proceedings of the Ninth International Conference on Computer Aided Architectural Design Futures*, Eindhoven, 161-172.
- Donath, D. and Regenbrecht, H.: 1995, VRAD (Virtual Reality Aided Design) in the Early Phases of the Architectural Design Process, *Sixth International Conference on Computer-Aided Architectural Design Futures*, Singapore, 313-322.
- Edwards, G., Li, H. and Wang, B.: 2015, BIM based collaborative and interactive design process using computer game engine for general end-users, *Visualization in Engineering*, 3(1), 4.
- Fiorentino, M., De Amicis, R., Monno, G. and Stork, A.: 2002, Spacedesign: A mixed reality workspace for aesthetic industrial design, *Proceedings - International Symposium on Mixed and Augmented Reality, ISMAR 2002*, 86-96.
- Gül, L.F. and Halıcı, S.M.: 2015, Collaborative Design with Mobile Augmented Reality, *Complexity & Simplicity - Proceedings of the 34th eCAADe Conference*, Oulu, Finland, 493-500.

- Hawton, D., Cooper-Wooley, B., Odolphi, J., Doherty, B., Fabbri, A., Gardner, N. and Haeusler, M.H.: 2018, Shared Immersive Environments for Parametric Model Manipulation, *Proceedings of the 23rd CAADRIA Conference - Volume 1*, Beijing, China, 483-492.
- Horikawa, J.: 2019, "Load Grasshopper file with compute.rhino3d for Unity 3D". Available from Youtube Video<<https://youtu.be/ZBly3OUhSVg>> (accessed 10 December 2019).
- Jacobson, I., Christerson, M., Jonsson, P. and Övergaard, G.: 1992, *Object-Oriented Software Engineering - A Use Case Driven Approach*, Addison-Wesley.
- Kado, K. and Hirasawa, G.: 2018, Two-way Cooperation of Architectural 3D Cad and Game Engine, *Proceedings of the 16th ACM SIGGRAPH International Conference on VR Continuum and Its Applications in Industry*, New York, NY, USA, 22:1-22:4.
- Af Klercker, J.: 2000, Modelling for Virtual Reality in Architecture, *18th eCAADe Conference Proceedings*, Weimar, Germany, 209-213.
- Kobayashi, Y., Hawker, R., Terzidis, K., Narahara, T., Abdelhameed, W., Fukuda, T., Labarca, C., Calderon, C. and Jemtrud, M.: 2009, World8 International Working Group for New Virtual Reality Applications in Architecture, *Joining Languages, Cultures and Visions: CAAD Futures 2009*, PUM, 547-556.
- Lai, H., Deng, X. and Chang, T.Y.P.: 2019, BIM-Based Platform for Collaborative Building Design and Project Management, *Journal of Computing in Civil Engineering*, **33**(3), 05019001.
- Lorenz, M., Spranger, M., Riedel, T., Pürzel, F., Wittstock, V. and Klimant, P.: 2016, CAD to VR – A Methodology for the Automated Conversion of Kinematic CAD Models to Virtual Reality, *Procedia CIRP*, **41**, 358-363.
- Martin, P., Masfrand, S., Okuya, Y. and Bourdot, P.: 2017, A VR-CAD Data Model for Immersive Design, *Augmented Reality, Virtual Reality, and Computer Graphics*, Cham, 222-241.
- Maver, T., Harrison, C. and Grant, M.: 2001, Virtual Environments for Special Needs Changing the VR Paradigm, *Proceedings of the Ninth International Conference on CAAD Futures*, 151-159.
- Milovanovic, J., Moreau, G., Siret, D. and Miguët, F.: 2017, Virtual and Augmented Reality in Architectural Design and Education An Immersive Multimodal Platform to Support Architectural Pedagogy, *Future Trajectories of Computation in Design: CAAD Futures 2017*, Istanbul, Turkey, 513-532.
- Nandavar, A., Petzold, F., Nassif, J. and Schubert, G.: 2018, Interactive Virtual Reality Tool for BIM Based on IFC - Development of OpenBIM and Game Engine Based Layout Planning Tool, *Proceedings of the 23rd CAADRIA Conference - Volume 1*, Beijing, China, 453-462.
- Pang, Y., Nee, A.Y.C., Ong, S.K., Yuan, M. and Youcef-Toumi, K.: 2006, Assembly feature design in an augmented reality environment, *Assembly Automation*, **26**(1), 34-43.
- Pickersgill, S.: 2007, Unreal Studio: Game engine software in the architectural design studio, *Proceedings of the 12th International Conference on CAAD Futures*, Sydney, Australia, 197-210.
- Wang, Q.H., Li, J.R., Wu, B.L. and Zhang, X.M.: 2010, Live parametric design modifications in CAD-linked virtual environment, *The International Journal of Advanced Manufacturing Technology*, **50**(9), 859-869.
- Whyte, J., Bouchlaghem, N., Thorpe, A. and McCaffery, R.: 2000, From CAD to virtual reality: modelling approaches, data exchange and interactive 3D building design tools, *Assembly Automation*, **10**, 43-55.
- Wolfartsberger, J.: 2019, Analyzing the potential of Virtual Reality for engineering design review, *Automation in Construction*, **104**, 27-37.
- Yap, H.J., Taha, Z. and Dawal, S.Z.M.: 2012, A generic approach of integrating 3D models into virtual manufacturing, *Journal of Zhejiang University: Science C*, **13**(1), 20-28.
- Zhong, Y., Mueller-Wittig, W. and Ma, W.: 2003, Constraint manager for intuitive and precise solid modelling in a virtual reality environment, *Proc.SPIE*.

**Building/City/Region  
Information Modelling/  
Management**





## OGOS+

### *A Tool to Visualize Densification potential*

ANNA-MARIA CHATZI<sup>1</sup> and LISA-MARIE WESSELER<sup>2</sup>

<sup>1</sup>*HafenCity University Hamburg*

<sup>1</sup>*anna-maria.chatzis@hcu-hamburg.de*

<sup>2</sup>*Technical University Berlin*

<sup>2</sup>*l.wesseler@campus.tu-berlin.de*

**Abstract.** OGOS+ is a GIS data-based tool, which would offer urban planners, architects, and researchers visualisations of potential building mass in the form of 3D models. It compares the height of existing buildings to the maximum permitted height by German zoning law and calculates the potential building mass. To ensure minimum building footprints it only calculates the densification potential on top of existing buildings. It summarises information of the building potential for future utilisation. The goal is an increase of urban density achieved with micro interventions.

**Keywords.** Urban densification; City Information Modeling and GIS; Big Data and Analytics in Architecture.

## 1. Introduction

One third of the German population lives in cities, which are developing quickly. Due to the decrease of not occupied space, rents are increasing. In 2018 Berlin counted 3.6 Mio residents. Until 2030 this number will increase to 3.8 Mio. Berlin needs to supply 200 000 more people with a place to live, work, learn and move. After WWII most of Berlin was destroyed. The city got rebuild but its density is still beneath the density of 1940s Berlin. (Brichetti 2011; Haubrich 2016; Quantum 2017, Senat Stadtentwicklung 2018).

Developing inhabitable space in already developed inner-city areas could be a possible solution for Berlin's housing problem. By using already developed areas it would not be necessary to build new infrastructure from scratch. The costs of improving inner-city infrastructure is only one third compared to developing a new one. Inner-city densification would be an alternative to development in the periphery of the city. This is one way to minimise additional land sealing. Moreover, it is a possibility to bring work, living and leisure together more closely. Short distances can decrease traffic, emissions and save time. Disadvantages could be a decrease in livability and biodiversity due to higher buildings and less open space. Inhabitants of the area could be disturbed during construction processes and therefore could be opposed to changes in their neighbourhood. (Architektenkammer NRW 2009, BBSR 2014).



Open spaces for densification can be a gap between houses, patios and additional storeys on already existing buildings. Infills and buildings in patios are more versatile whereas an addition in storeys leaves the smallest building footprint. Large building projects are hard to get realised. Micro interventions could be easier to get permission for than huge development projects. Costly testing of zoning laws make smaller sites less lucrative. That is why an automatisations in zoning law testing could be beneficial. (Architektenkammer NRW 2009, BBSR 2014; Kim, & Clayton, 2010; Lobeck et al, 2016).

Previous studies have shown the potential of regulations for the design process. For example, Hugh Ferriss visualised possible building shapes considering safety issues for the city of New York in 1922. (Donath, & Lobos, 2008). A more recent study conducted by Kaisersrot and KCAP in 2007 visualised the maximal buildable space according to zoning regulations for their design proposal 'Neuplanung Umfeld Hauptbahnhof Zürich'. (Kaisersrot, & KCAP, 2007). OGOS+ takes up the approach of Zoning laws as design parameters. The tool tries to automatise the calculation of building regulations for a larger urban area.

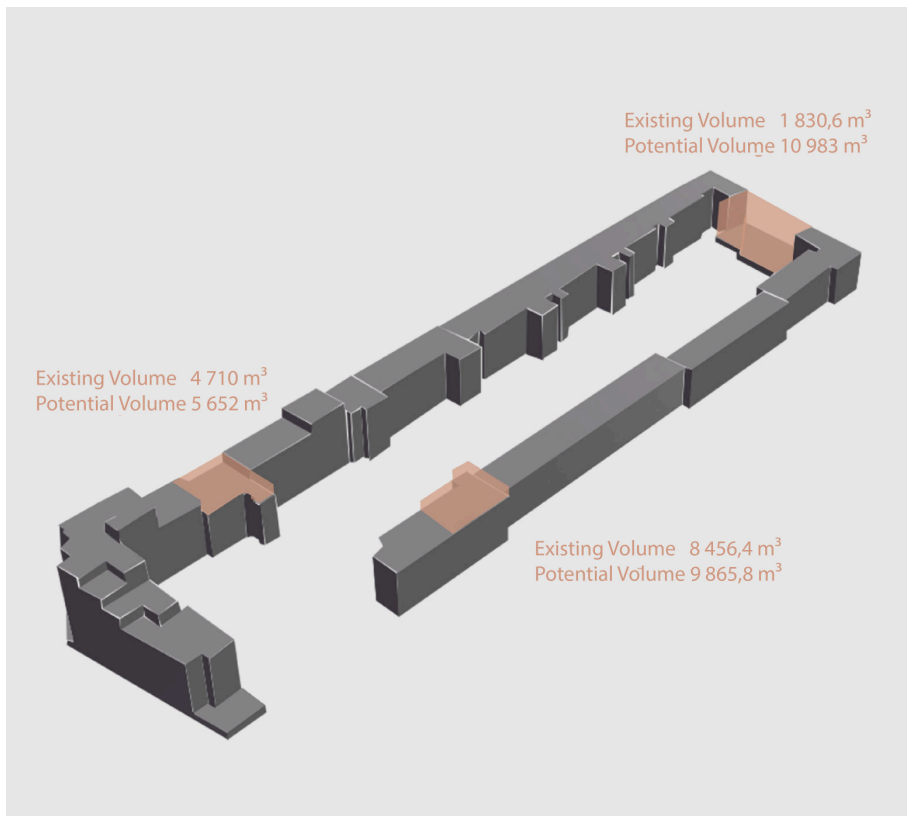


Figure 2. Findings.

## 2. Tool

### 2.1. PARAMETERS

OGOS+ uses various kinds of urban data as input for 3D visualisations of potential building masses. To work easier with all the data the input was organised into four categories [Figure 1].

The first input category is called ‘regulation parameters’. It contains the number of storeys allowed by regulations (development plan or BauGB), the existing kind of Land Use, and equations to determine distance space and the Floor Area Ratio (FAR). The second category contains all the OSM-data (OpenStreetMaps) such as Building Polylines, Plot Polylines, and the number of storeys of existing buildings. The third input category is ‘calculated parameters’. This category includes the Floor Area Ratio (FAR) of existing buildings, the FAR by regulations, distance spaces of existing buildings, distance space by regulations, the building and plot areas. All connexions of the parameters can be found in the German Zoning Law. The fourth input category contains parameters supplied by the user. It is crucial to acquire information regarding the chosen plot, the distances between public spaces and buildings, the current land use of adjacent plots and about the location of a building on its plot.

There is some data which was supposed to be obtained from the open geo data sets but was not included in it. That is why it was required to assign each plot and its corresponding building an ID manually. The ID is necessary to refer a geometry to its specific data set. Another issue is that meta data regarding storey heights is lacking in the geo data for Berlin. A generic storey height of three meters is therefore set for all buildings. Three meters are assumed as average storey height for Berlin. (Mäder, 2001).

### 2.2. INPUT SOURCES

#### 2.2.1. Regulations

German zoning law is divided into federal law such as ‘Baugesetzbuch’ (BauGB, Federal Building Code), ‘Baunutzungsverordnung’ (BauNVO, Federal Land Utilisation Ordinance) and state law, in this case ‘Bauordnung Berlin’ (BauO Bln, Building code Berlin) and development plans.

The city of Berlin offers an open data platform called ‘Berlin open data’. ‘Berlin open data’ offers Berlin GIS data and development plans. Development plans are available as PDF documents but not as statistical data. (Senatsverwaltung für Stadtentwicklung und Wohnen, n.d.).

#### 2.2.2. Open Street Map (OSM)

The required geo data was obtained via ‘OpenStreetMaps’ in form of OSM files. (OpenStreetMap, n.d).

### 2.2.3. *Plug-Ins for calculations*

Grasshopper (GH) was used for coding, Python for more flexibility in coding, Elk to utilise OSM data and Lunchbox to read Excel files, which contain additional data.

### 2.2.4. *Plug-Ins for user interface*

HumanUI was implemented to both gather data by the user and to visualise results. Human UI is a grasshopper plug-in to implement a user interface in the algorithm. (Food for Rhino, 2018c).

## 2.3. ALGORITHM

The algorithm aims to calculate all relevant distances to get the potential building mass. The user chooses a building and its corresponding plot. The algorithm detects the distances between the selected building polyline and the plot polyline ( $x$ ). Each building is assigned to a data sheet according to its ID number. The data in the list of the ID number is used in the calculations of the algorithm. The ID list contains data of the existing building (number of stories, FAR, area of building) and the regulations (number of storeys, FAR, land use). The number of storeys of the existing building and the number of storeys by regulation are multiplied by the storey height to define the height of the existing building and the height of the potential building mass according to the regulations. Each type of land use is associated with a constant. The result of the multiplication of the height of the existing building and the constant is the distance space of the existing building ( $y$ ). The multiplication of the height of the potential building mass and the constant is the distance space by regulation ( $z$ ). The user is required to provide some extra information. The user enters the land use of adjacent plots and the distance between public space and building ( $u$ ) into the user interface. The algorithm begins to repeatedly compare the factors ( $x, y, z, u$ ) to find the final potential building mass. There are three possibilities [Figure 3]. If the distance between the selected building polyline and the plot polyline is zero ( $x=0$ ), equal to or greater than the distance space by regulation ( $x \geq z$ ) then the height by regulation is usable. If the distance between the selected building polyline and the plot polyline is greater than zero and smaller than the distance space of the existing building ( $0 < x < y$ ) then the height of the existing building is already the maximum height that is allowed to build. If the distance between the selected building polyline and the plot polyline is less than the distance space of the existing building and bigger than the distance space by regulation ( $y < x < z$ ) then the user's answers are relevant. If the distance space by regulation is bigger than the distance between public space and building ( $z > u$ ) then the distance space by regulation is recalculated with the height of the potential building mass minus one storey height. This process is repeated until the distance space by regulation is less than the distance between public space and building ( $u \geq z$ ). That means that the height of the existing building is not equal to the height of the regulation and that a potential building mass exists. The potential building mass is visualized in the form of a 3D model. [Figure 2].

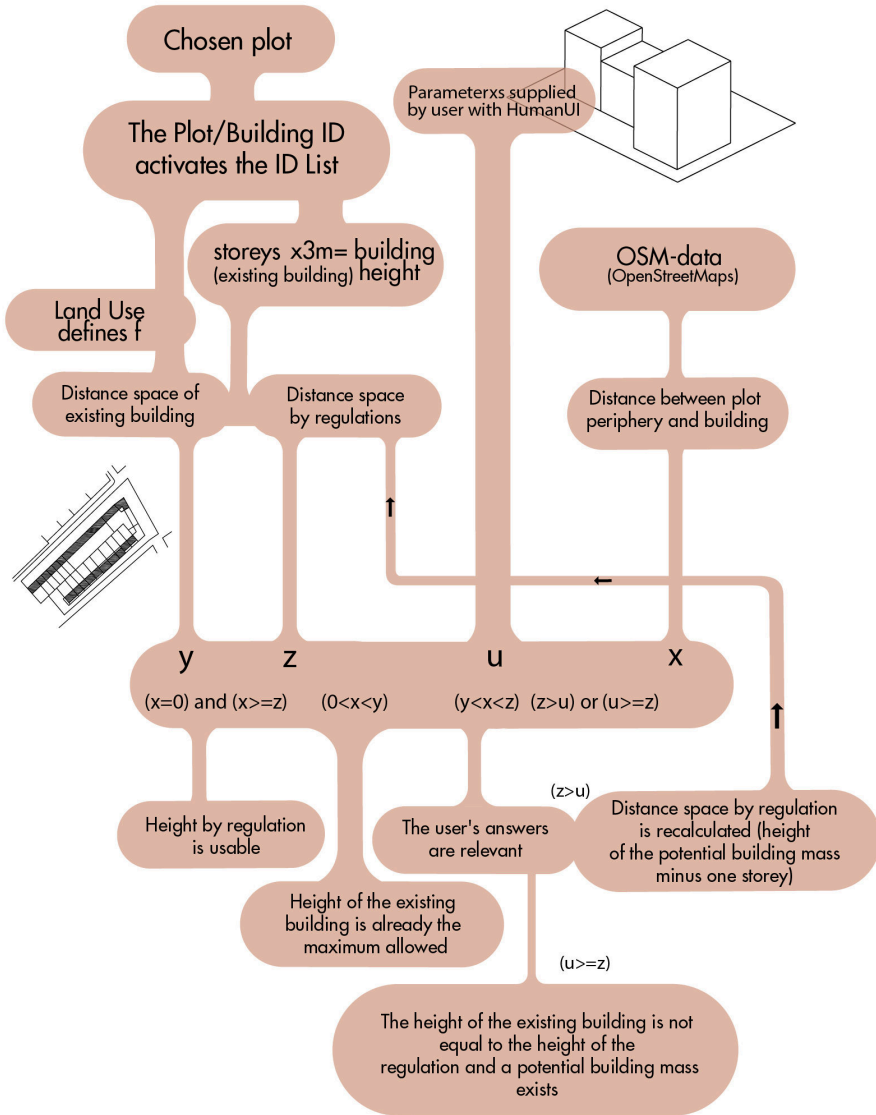


Figure 3. Workflow.

## 2.4. SPACIAL CASE

Not every plot has a development plan that contains information regarding the number of storeys allowed by regulation. In this case the algorithm analyses all the storeys of the buildings of adjacent plots to find the highest number of storeys of a building. This number defines the stories allowed by regulation (BauGB § 34). The highest number of storeys is set as number of storeys by regulation for all buildings in the block. The algorithm proceeds as described above.



Figure 4. Case Study.

## 2.5. CASE STUDY

Although, this tool can be applied for whole Berlin, three inner-city building blocks were selected as case studies [Figure 4]. Each building block meets different criteria. The algorithm was firstly applied and developed to a block with development plan [1]. It was important to pick a small block to understand and verify the gathered information. To confirm the results of the tool the calculations performed by the algorithm had to be done manually as well.

No development plan applies to the other two selected areas [2 + 3]. They were chosen to deal with special cases and to focus on emerging problems. In order to make the calculations for each case work the algorithm had to be altered several times.

## 2.6. USER INTERFACE

To navigate the tool a user interface is implemented. On the first tab, the user chooses a plot and the corresponding building. On the second tab, the chosen plot and building are shown, as are the distances between both. The second interface asks the user for the cardinal direction in which a public plot is located. On the second tab, the existing and potential building including the dimensions and storeys of the new volume are visualised. [Figure 5].



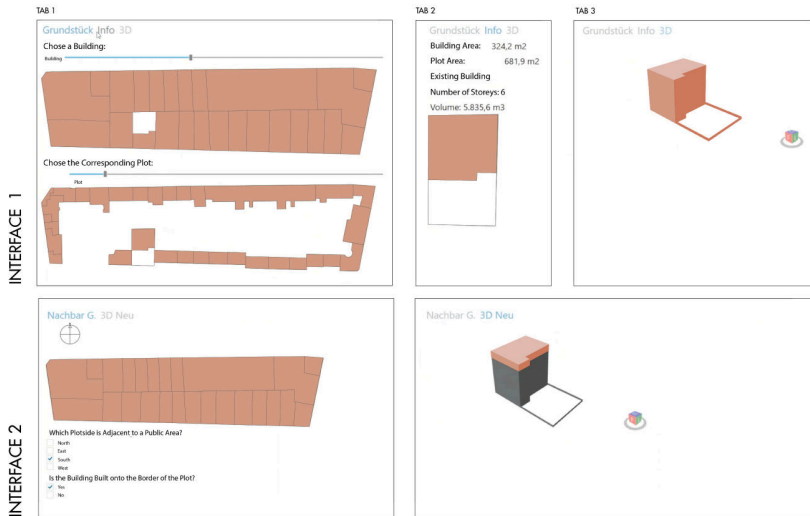


Figure 5. User Interface.

## 2.7. MANUAL

1. The user needs to download Rhino and Grasshopper.
2. The Grasshopper plugins (Human-Ui, gh-python-remote, lunchbox, elk) which can be found at [www.food4rhino.com](http://www.food4rhino.com) are required.
3. The plug-ins have to be link to Grasshopper.
4. The script needs to be downloaded.
5. One wants to open the file 'OGOS+.3dm' in Rhino and 'OGOS+.gh' in Grasshopper.
6. The Excel file 'OGOS+.xlsx' needs to be opened.
7. All data links are required to be updated.
8. A plot and corresponding building are chosen.
9. A few questions about the plot are required to be answered.
10. The potential building mass together with the existing building mass are visualised in form of a 3D model as is some additional information.

## 3. Conclusion

OGOS+ proposes a tool which uses open source data and German zoning law to calculate potential building mass. It gains to increase inner-city densification with as little soil sealing as possible.

While developing the tool we had some limitations. A generic test area in Berlin was chosen to reduce the required data. Berlin GIS data has some shortcomings in terms of additional information layers (e.g. function or height) and accuracy (e.g. overlapping lines). The documentation of Berlin zoning law had to be done manually and reimplemented into the tool with Excel files.

The tool works within the regulations of the German zoning law. It can be argued that this zoning system is not able to adapt to changes quickly (e.g. urban density factor) and make mixed-use development difficult. (BauNVO §1).

At the moment the tool can only be used to analyse one plot but not a block in total. The tool is not able to save the findings. In later versions, the user could filter the building potential for a specific kind of use and size and would be able to save the findings [Figure 6].

It is easier to get permission for smaller building projects. The time consuming testing of zoning laws effects the lucrativeness of smaller sites. Using the tool in the beginning of design processes could save time and labour in making analysis less costly and increase building development. (Donath, & Lobos, 2008; Grazziotin et al, 2004; Kim, & Clayton, 2010).



Figure 6. Prospect.

## References

- “Food for Rhino - Human UI” : 2018. Available from <<https://www.food4rhino.com/app/human-ui>> (accessed 3rd December 2019).
- “Food for Rhino - GH Python Remote” : 2018. Available from <<https://www.food4rhino.com/app/gh-python-remote>> (accessed 3rd December 2019).
- “Bauordnung für Berlin - BauO Bln 2005” : 2018. Available from <<http://gesetze.berlin.de/jportal/?quelle=jlink&query=BauO+BE&psml=bsbeprod.psml&max=true&aiz=true>> (accessed 3rd December 2019).
- “Food for Rhino - ELK” : 2018. Available from <<https://www.food4rhino.com/app/elk>> (accessed 3rd December 2019).
- “Food for Rhino - LunchBox” : 2018. Available from <<https://www.food4rhino.com/app/lunchbox>> (accessed 3rd December 2019).
- Architektenkammer, N.-W.: 2009, *Entwicklung der Innenstädte. Positionspapier der AKNW zur Nachverdichtung und Baulückenschließung*, Architektenkammer Nordrhein-Westfalen, Düsseldorf.
- Brichetti, K.: 2011, *Berlins neue Mitte*, Sutton Verlag, Erfurt.
- Bundesamt, F.J.: 1962, “Verordnung über die bauliche Nutzung der Grundstücke - Baunutzungsverordnung BauNVO (2017)” . Available from <<https://www.gesetze-im-internet.de/baunvo/>> (accessed 3rd December 2019).
- Bundesamt, F.J.: 2017, “Baugesetzbuch BauGB” . Available from <<https://www.gesetze-im-internet.de/bbaug/>> (accessed 3rd December 2019).
- Donath, D. and Lobos, D.: 2008, Massing Study Support, *Architecture in Computro 26th eCAADe Conference Proceedings*, Antwerpen, 101-108.
- Graziotin, P. C., Benamy, T., Sclovsky, L. and Freitas, C.M.D.S.: 2004, Cityzoom - A tool for the visualization of the impact of urban regulations, *Proceedings of the 8th Iberoamerican Congress of Digital Graphics*, Porte Alegre, Brasil, 216-220.
- Haubrich, R.: 2016, “Die Welt - Neue Wohnungen - wir müssen wieder bauen wie um 1900” . Available from <<https://www.welt.de/debatte/kommentare/article152736886/Neue-Wohnungen-wir-muessen-wieder-bauen-wie-um-1900.html>> (accessed 3rd December 2019).
- Kim, J. B. and Clayton, M. J.: 2010, Support Form-based Codes with Building Information Modeling – The Parametric Urban Model Case Study, *ACADIA 10: LIFE, On Responsive Information and Variations in Architecture*, New York, 133-138.
- Lobeck, M., Wiegandt, P.D.C.-C. and Wiese-von Ofen, D.-I.I.: 2006, *Entwicklung von umsetzungsorientierten Handlungsschritten zur Mobilisierung von Baulücken und zur Erleichterung von Nutzungsänderungen im Bestand in Innenstädten NRWs. Kurzfassung*, Geographisches Institut der Universität Bonn, Bonn.
- Mäder, K.: 2001, “Die Raumhöhe im Mietwohnungsbau” . Available from <[spurbreite.ch/download/raumhoehe\\_im\\_wohnungsbau.pdf](http://spurbreite.ch/download/raumhoehe_im_wohnungsbau.pdf)> (accessed 3rd December 2019).
- Bundesinstitut für Bau-, Stadt- und Raumforschung, B.: 2016, *Städtebauliche Nachverdichtung im Klimawandel. ExWoSt-Informationen 46/1-12/2014.*, BBSR Bundesinstitut für Bau-, Stadt- und Raumforschung, Bonn.
- Scharmanski, D.r. A. and Beneking, A.: 2017, Innenentwicklung als Chance für urbanes Wohnen, *Quantum Focus*, **26(4)**, 11, 16, 27.
- Senatsverwaltung, F.W.E.U.B.: 2018, “Berlin Open Data” . Available from <<https://daten.berlin.de/>> (accessed 3rd December 2019).

# DEVELOPMENT OF AN URBAN GREENERY EVALUATION SYSTEM BASED ON DEEP LEARNING AND GOOGLE STREET VIEW

YIXI XIA<sup>1</sup>, NOBUYOSHI YABUKI<sup>2</sup> and TOMOHIRO FUKUDA<sup>3</sup>  
<sup>1,2,3</sup>*Division of Sustainable Energy and Environmental Engineering,  
Graduate School of Engineering, Osaka University, Japan*  
<sup>1</sup>*yixi11900@gmail.com* <sup>2,3</sup>*{yabuki|fukuda}@see.eng.osaka-u.ac.jp*

**Abstract.** Street greenery has long played a vital role in the quality of urban landscapes and is closely related to people's physical and mental health. In the current research on the urban environment, researchers use various methods to simulate and measure urban greenery. With the development of computer technology, the way to obtain data is more diverse. For the assessment of urban greenery quality, there are many methods, such as using remote sensing satellite images captured from above (antenna, space) sensors, to assess urban green coverage. However, this method is not suitable for the evaluation of street greenery. Unlike most remote sensing images, from a pedestrian perspective, urban street images are the most common view of green plants. The street view image presented by Google Street View image is similar to the captured by the pedestrian perspective. Thus it is more suitable for studying urban street greening. With the development of artificial intelligence, based on deep learning, we can abandon the heavy manual statistical work and obtain more accurate semantic information from street images. Furthermore, we can also measure green landscapes in larger areas of the city, as well as extract more details from street view images for urban research.

**Keywords.** Green View Index; Deep Learning; Google Street View; Segmentation.

## 1. Introduction

With the growing consensus that nature and multi-functional ecosystems are intrinsic to sustainable cities. Decision-makers, designers and the broader public alike are looking to trees as urban keystone flora which provide natural infrastructure and services to reduce air pollution (Blum, 2017), mitigate heat island effects and support biodiversity (Laforteza et al., 2009), and even increase land value, improve aesthetics, improve human health.

City streets are a focal point of human activity in urban centers, citizens interact with the urban environment through the streetscape. Urban street greenery has long been recognized as an important urban landscape component (Bernhard E, 1910), and are closely related to people's physical and mental health (Bowler et al., 2010).

We know that 90% of the environment information received by people comes from vision, in the field of urban management, visual urban environmental management has become an inevitable approach to improve the quality of the urban environment. Most of the previous studies used field surveys, interviews, statistics, etc. to assess the amount of greening in the city to better understand the green level of the town. Since the 1970s, multi-scale remotely sensed (RS) has provided a new way to assess urban greening (Di et al., 2019), which can measure the urban greening environment on a larger scale. However, this method does have apparent limitations as they are obtained from a bird's eye view, while the pedestrian's typical view of greenery is from the profile aspect. Therefore, the urban green environment evaluated by multi-scale remote sensing images cannot accurately represent pedestrians' perception of urban green space.

To overcome these limitations, some researchers use street view images for assessing street-level, profile urban street greenery. Such as street view services on the web (e.g., Google, Tencent, Baidu), which allow researchers to virtually navigate through urban spaces composed of geo-tagged street-level images (Rundle et al., 2011). For instance, by taking these open-source images and stitching them together, Google Street View (GSV) images can create a 360-degree street view image, which can give people a feeling of "being there," quite similar to the images you see when driving, cycling or walking in the street.

The objective of this research is to develop an urban greenery analysis system based on a large number of street view images and deep learning algorithms to calculate the Green View Index (GVI) automatically. The next step is to demonstrate the performance of the system in estimating pedestrians' visual quality of street greenery. Discuss the relations of GVI with city greenery to find interactive applications in urban greenery planning and environmental management.

## **2. Literature Review**

### **2.1. USING STREET VIEW IMAGES IN URBAN STUDIES**

As we have known now, Google, Tencent, and Baidu are the three most representative providers of street view mapping service in the world. In addition to releasing street view map services for user browsing, they have released application program interfaces (APIs) for developers to customize web applications. The GSV image was a useful potential data source for urban studies, including 3D city model construction (Torii et al., 2009), commercial-entity identification (Zamir, et al., 2011), public environment audit (Edwards et al., 2013). And they are even used in layer interpretation for ground, pedestrians, buildings, and sky.

In addition to these new studies, Kelly et al. (2012) proposed a method to audit built environments by using GSV and also found it to be a very reliable method. In the field of urban planning, more and more researchers have used street view image as a tool to audit the urban environment and various environmental elements. However, most of the current work still based on manual observation of street view images. With the development of computer science and image recognition

technology, computer image technology that can automatically recognize pictures and extract sufficient information has become more and more mature. The combination of Street View images and computer image technology in urban planning can not only solve the time-consuming problems of traditional research methods but also help urban planners to audit our city from a new perspective.

## 2.2. USING GREEN VIEW INDEX (GVI) TO EVALUATE THE QUALITY OF ENVIRONMENT GREENERY

Greenery is always cited as an essential factor in the study of urban environmental quality. Since the 1950s, Olmsted has focused on urban park reform and street design in combination with the natural environment and living space. In the late 1980s, urban planners planned a large-scale green network to attract residents into the open space of the city. Another vital contribution of greenery is that there is to mitigate the effects of air pollution and urban heat island effects to a certain extent. Therefore, more research was on the functionality of greenery, and aspects of the visual impact or aesthetic have received less attention. According to some research by environmental psychologists, they believe that people's psychological feelings are closely related to the amount of green in their environment. And some researchers proposed that 90% of the information people receive in the environment comes from vision. In 1981, the National Institute of Environmental Studies of Japan proposed quantitative statistical analysis methods to identify the essential sources of stimulation that affect specific psychological changes and to identify environmental green areas that can generate positive subjective feelings. Later, the researcher of the institute officially proposed the concept of "green visible value" (Yoji Aoki, 1987), pointing out that the green visible value is the percentage of green in the human field of vision. Yoji Aoki (2006) summarized the research on visual greenery conducted in Japan since 1974, which confirmed the connection between the green quantity of the street and the psychological activities of people. This physical quantity will be a landscape evaluation factor for environmental greening.

After that, many researchers tried to measure green visible values by different methods to quantitatively evaluate the urban green environment. Yang et al. (2009) developed a way to assess the visibility of urban greenery through a combination of field surveys and manual photographing. However, this method relies heavily on human labor, which is laborious and prone to error. Li et al. (2015) proposed a way to estimate the green visible value by analyzing landscape images acquired by GSV. This method based on recognizing the green area in the images through Adobe Photoshop, which is pixel-based color recognition. However, it still requires a lot of human resources to complete. Li et al. (2015) further proposed a method to calculate GVI based on image recognition technology and GSV, which improved work efficiency significantly and combined the latest computer technology with urban planning. Liang et al. (2017) adopted computer vision methods based on SegNet to segment and quantify the proportion of visible landscape elements in an area using SVP datasets. Inoue et al. (2018) developed a new automatic GVI estimation system with the real-time estimation function. Gong et al. (2018) adopted another pixel-level semantic segmentation method,

namely, the Pyramid Scene Parsing Network (PSPNet), to extract sky, trees, and buildings from a panoramic street view picture dataset. And apply it to the analysis of urban streetscape greening in Hong Kong, China.

### 3. Proposed Method

#### 3.1. CRAWLING STREET VIEW IMAGES FROM GOOGLE MAPS

GSV is a free online street view map service provided by Google Maps and Google Earth Center. It offers several types of application programming interfaces (APIs) that allow users to crawl static images and 360° panoramas data. The parameters required by the API listed in Table 1, which includes the street view image size, location or location ID, horizontal and vertical angles, and the developer’s key.

Table 1. Parameters for the GSV crawling API.

Parameter	Description	Example
Size	The output size of the image in pixels	size=400x400 returns an image 400 pixels wide, and 400 high.
Location	Coordinates for confirming the Street View location	Location =34.80932445,135.5066877
Heading	The compass heading of the camera, accepted values are from 0 to 360	North: Heading = 0/360    South: Heading = 180 East: Heading = 90      West: Heading = 270
Pitch	The up or down angle of the camera relative to the Street View vehicle	Pitch = 0
Key	Developer’s key(Can be retrieved through the online application)	Key = Alza5yB5JNVNoTRH6XtSH8GD8hx9rd_-jJl_TQ

By importing the previously acquired street sample site data, we can obtain images of different vertical viewing angles of each site, covering 360° horizontal surroundings. Fig. 1 (a) shows an example of the requested GSV static image using Google API. Since the images, we crawled from GSV are views from ten directions taken from the same sampling point (Fig. 1 (b)). To get a panoramic view of the street view, we use the software Ptgui to stitch it into a 360° panoramic street view image (Fig. 2).



Figure 1. An example of the requested GSV static image using Google API (a) GSV images captured in six directions at a sample size in the study area (b).



Figure 2. GSV panoramas images made by PtGui.

### 3.2. USING GSV IMAGES TO CALCULATE GVI VALUES

Yang et al. (2009) defined a “Green View Index” to evaluate the visibility of urban greenery which was defined as the ratio of the total green area from four pictures taken at a street intersection to the entire area of the four pictures, using the following formula:

$$GVI = \frac{\sum_{i=1}^m Area_{g-i}}{\sum_{i=1}^m Area_{t-i}} \times 100\%$$

Figure 3. GVI values calculation formula.

Where  $Area_{g-i}$  is the total number of green pixels in the image taken in the  $i$ th direction for one intersection,  $Area_{t-i}$  is the total pixel number of the image taken in the  $i$ th direction. The parameter  $m$  is the number of pictures facing different directions in the horizontal plane. In this research, we will use the GSV images to measure GVI based on this formula.

### 3.3. GSV IMAGES SEGMENTATION BASED ON DEEP LEARNING

Li and Ratti (2018) proposed a method to identify the green and blue space from street view images using a sematic segmentation technique. With the development of artificial intelligence technology, deep learning performed well for image recognition tasks. Therefore in this research, we propose to use a full convolution neural network for semantic segmentation (i.e., the DeepLab V3) to segment the GSV images into common landscape objects (e.g., vegetation, sky). To train the network, we propose to use the collection of annotated images from the CityScapes Dataset, which contains a diverse set of stereo video sequences recorded in street scenes from 50 different cities, with high-quality pixel-level annotations of 50,000 frames in addition to a more extensive collection of 200,000 weakly annotated frames. By entering a Street View image into a trained network, we can obtain semantically segmented images, including vegetation, sky, buildings, and so on, that have been identified, as shown in Fig. 4.



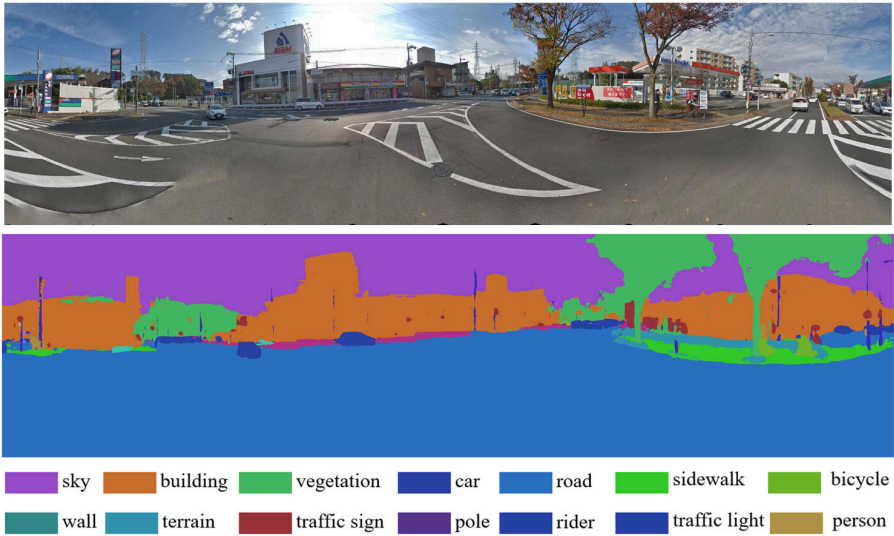


Figure 4. Image segmentation results.

## 4. Validation and Results

### 4.1. GVI SEGMENTATION OF GSV IMAGES

Fig. 5 shows the semantic segmentation results of four GSV images based on the system. Fig. 5(c) shows the initial vegetation classification results based on the system. Compared with the original GSV images (Fig. 5(a)), most of the green vegetation pixels in the GSV images were correctly delineated in the pre-classified image. To verify the accuracy of extraction results, we manually labeled the green plants of the original streetscape image through Adobe Photoshop software. Fig. 5(b) shows the results of the manually extracted green plants. The last column is the GVI value of these sampling sites calculated based on Formula(1). As for the accuracy of the image semantic segmentation results, we will demonstrate in the next article.

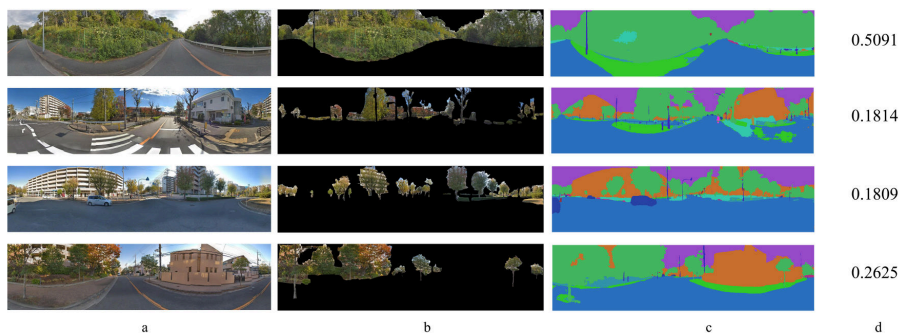


Figure 5. Green vegetation extraction results and references, (a) original GSV images, (b) manually extracted green vegetation, (c) segmentation result based on DeepLab V3, (d) GVI value obtained by our system.

Through semantic segmentation, we can automatically get the proportion of the images of the 19 categories shown in Table. 2. Including roads, buildings, vegetation, sky, cars, pedestrians, and so on. Using this data can help us assess urban landscape factors such as the GVI and Sky View Factor (SVF) (Cao et al., 2018).

Table 2. The categories of Semantic segmentation.

Number	Sort	Code	Type	Number	Sort	Code	Type
1	Road	0	flat	11	Sky	10	sky
2	Sidewalk	1	flat	12	Person	11	human
3	Building	2	construction	13	Rider	12	human
4	Wall	3	construction	14	Car	13	vehicle
5	Fence	4	construction	15	Truck	14	vehicle
6	Pole	5	object	16	Bus	15	vehicle
7	Traffic light	6	object	17	Train	16	vehicle
8	Traffic sign	7	object	18	Motorcycle	17	vehicle
9	Vegetation	8	nature	19	bicycle	18	vehicle
10	Terrain	9	nature				

#### 4.2. GVI ACCURACY VERIFICATION

To further verify the accuracy of the semantic segmentation, we randomly selected 100 images from the GSV images. By manually marking with Adobe Photoshop and automatically calculating using our system to obtain the GVI values of the 100 images. The scatter plot (Fig. 6) shows the relationship between the GVI values calculated using the proposed automatic classification system and the corresponding values calculated based on the reference data delineated manually using Adobe Photoshop. The GVI values are distributed near the 1:1 line, and the regression coefficient up to 0.9809, which indicates that the GVI values calculated using the two different methods were quite similar. Additionally, the root means square error (RMSE) is 0.018, which means that the GVI values calculated

automatically by the proposed system are of high accuracy. This verification of the GVI data indicates that the system can be used to evaluate the quality of urban greenery.

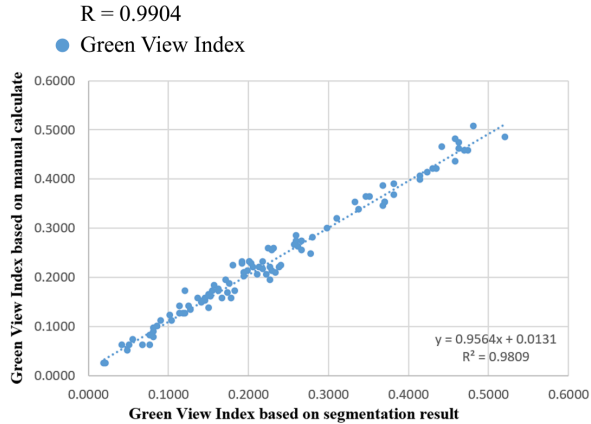


Figure 6. A scatter plot of green view index values calculated using the suggested automatic classification method vs the reference data delineated manually using Photoshop.

## 5. Conclusion and Future Work

Street greenery is a key factor affecting the urban landscape, and it is also an essential part of the urban ecosystem, which has a direct correlation with the physical health and mental health of urban residents. GSV images provided by Google, which had view angles similar to that of pedestrians on the street, were proposed to assess urban street greenery. From our research, using GSV images to assess visible street greenery based on deep learning is a flexible and effective method. In which the working time has been shortened, and the work efficiency has been improved, many processes can be automatically completed. Compared to the traditional method for assessing visible street greenery in cities, our study uses GSV images instead of manual photography. We can automatically download the street view images of the research area by parsing the URL using GSV image API. Automatic semantic segmentation of Street View images through deep learning and the GVI value is calculated. The whole process is automated and does not require excessive human intervention. However, the method proposed by us can not only provide a way to calculate the GVI values faster and more accurately, at a later stage we can combine with GIS to visualize the green visible index of urban streets and to show the greening level of the city more intuitively. With the increase in the number of countries and regions covered by Google Street View services, this method can be applied to more areas to assess visible street greenery. The urban greening evaluation system proposed by our research can help urban planners and managers better understand the impact of urban streetscapes on urban environmental perception.

Although we can calculate the GVI values of the city based on GSV images and deep learning instead of manual measurement, it still has some restriction concerns urgent to be resolved. The first is the accuracy of the image semantic segmentation could be further improved. In future research, we plan to label the training dataset by ourselves, then use that to train the existing model to obtain a more powerful subdivision framework and optimize the segmentation method. Secondly, because the acquisition time of GSV images does not agree, that street view images collected in batches may be taken in different seasons. However, with the development of Unmanned Aerial Vehicle (UAV) technology, and gradually applied to urban research, in future research we can combine the UAV system to detect and monitor the dynamic changes of street greening for urban landscape planning research.

Based on the street image and deep learning, this study developed an automatic evaluation system for urban street greening, showing the development direction of combining artificial intelligence with the urban landscape, which has inspired more aspects of urban research.

## References

- Aoki, Y.: 1987, Relationship between perceived greenery and width of visual fields, *J. Jpn. Inst. of Landscape Architects*, **51**, 1-10.
- Aoki, Y.: 2006, Trends of researches on visual greenery since 1974 in Japan, *Environmental Information Science*, **34**, 46-49.
- Bernhard, F.: 1910, *The care of trees in lawn, street and park*, H. Holt and company.
- Blum, J.: 2017, *Contribution of ecosystem services to air quality and climate change mitigation policies: the case of urban forests in Barcelona, Spain*, Apple Academic Press.
- Bowler, D.E., Buyung-Ali, L.M., Knight, T.M. and Pullin, A.S.: 2010, Urban greening to cool towns and cities: A systematic review of the empirical evidence, *Landscape and urban planning*, **97**, 147-155.
- Cao, R., Fukuda, T. and Yabuki, N.: 2019, Quantifying visual environment by semantic segmentation using deep learning: A Prototype for Sky View Factor, *CAADRIA 2019 24th Annual Conference of the Association for Computer-Aided Architectural Design Research in Asia*, Victoria University of Wellington, New Zealand, 623-632.
- Dí, S., Li, Z., Tang, R., Pan, X., Liu, H. and Niu, Y.: 2019, Urban green space classification and water consumption analysis with remote-sensing technology: a case study in Beijing, China, *International Journal of Remote Sensing*, **40**, 1909-1929.
- Edwards, N., Hooper, P., Trapp, G.S., Bull, F., Boruff, B. and Giles-Corti, B.: 2013, Development of a public open space desktop auditing tool (POSDAT): a remote sensing approach, *Applied Geography*, **38**, 22-30.
- Gong, F.Y., Zeng, Z.C., Zhang, F., Li, X., Ng, E. and Norford, L.K.: 2018, Mapping sky, tree, and building view factors of street canyons in a high-density urban environment, *Building and Environmental*, **134**, 155-167.
- Inoue, K., Fukuda, T., Cao, R. and Yabuki, N.: 2018, Tracking Robustness and Green View Index Estimation of Augmented and Diminished Reality for Environmental Design, *Proceedings of CAADRIA 2018*, Beijing, 339-348.
- Kelly, C.M., Wilson, J.S., Baker, E.A., Miller, D.K. and Schootman, M.: 2012, Using Google Street View to audit the built environment: inter-rater reliability results, *Annals of Behavioral Medicine*, **45**, S108-S112.
- Lafortezza, R., Carrus, G., Sanesi, G. and Davies, C.: 2009, Benefits and well-being perceived by people visiting green spaces in periods of heat stress, *Urban Forestry & Urban Greening*, **8**, 97-108.

- Li, X. and Ratti, C.: 2018, Mapping the spatial distribution of shade provision of street trees in Boston using Google Street View panoramas, *Urban Forestry and Urban Greening*, **31**, 109-119.
- Li, X., Zhang, C., Li, W., Kuzovkina, Y.A. and Weiner, D.: 2015, Who lives in greener neighborhoods? The distribution of street greenery and its association with residents' socioeconomic conditions in Hartford, Connecticut, USA, *Urban Forestry & Urban Greening*, **14**, 751-759.
- Li, X., Zhang, C., Li, W., Ricard, R., Meng, Q. and Zhang, W.: 2015, Assessing street-level urban greenery using Google Street View and a modified green view index, *Urban Forestry & Urban Greening*, **14**, 675-685.
- Liang, J., Gong, J., Sun, J., Zhou, J., Li, W., Li, Y., Liu, J. and Shen, S.: 2017, Automatic sky view factor estimation from street view photographs—A big data approach, *Remote Sensing*, **9**, 411.
- Rundle, A.G., Bader, M.D., Richards, C.A., Neckerman, K.M. and Teitler, J.O.: 2011, Using Google Street View to audit neighborhood environments, *American journal of preventive medicine*, **40**, 94-100.
- Torii, A., Havlena, M. and Pajdla, T.: 2009, From google street view to 3d city models, *2009 IEEE 12th International Conference on Computer Vision Workshops, ICCV Workshops*, Dresden, Germany, 2188-2195.
- Yang, J., Zhao, L., McBride, J. and Gong, P.: 2009, Can you see green? Assessing the visibility of urban forests in cities, *Landscape and urban planning*, **91**, 97-104.
- Zamir, A.R., Alexander, D. and Mubarak, S.: 2011, Street view challenge: Identification of commercial entities in street view imagery, *2011 10th International Conference on Machine Learning and Applications and Workshops*, Honolulu, HI, USA, 380-383.

# GEO-COMPUTATION FOR DISTRICT PLANNING

*An Agile Automated Modelling Approach*

PRADEEP ALVA<sup>1</sup>, HAN JIE LEE<sup>2</sup>, ZHUOLI LIN<sup>3</sup>,  
PALAK MEHTA<sup>4</sup>, JIELIN CHEN<sup>5</sup> and PATRICK JANSSEN<sup>6</sup>  
<sup>1,2,3,4,5,6</sup>*School of Design & Environment, National University of  
Singapore*  
<sup>1</sup>*akipaa@nus.edu.sg* <sup>2,3</sup>*{hanjie94|lin.zhuoli.94}@gmail.com*  
<sup>4,5</sup>*{palak\_mehta|chen.jielin}@u.nus.edu* <sup>6</sup>*patrick@janssen.name*

**Abstract.** This paper focuses on developing a novel geo-computational methodology for automating the generation of design options for district planning. The knowledge contribution focuses on the ability of the planners and designers to interact with and override the automated process. This approach is referred to as “agile automated modelling”. The approach is demonstrated through a case study in which three adjacent districts are generated with a total area of approximately 1300 hectares. An automated modelling process is implemented based on a set of core planning principles established by the planners. The automated process generates street networks, land parcels, and 3-dimensional urban models. The process is broken down into three steps and users are then able to intervene at the end of every step to override and modify the outputs. This aims to help planners and designers to iteratively generate and assess various planning outcomes.

**Keywords.** Geo-computation; procedural modelling; GIS; planning automation; neural network.

## 1. Overview

Geo-computation is at the evolving forefront of research and application. Geo-computational techniques contribute to essential management and processing of data to yield robust insights into the underlying patterns and provide reliable decision-support (Fischer et al. 1998, 2014; Openshaw 1998; Atkinson and Martin 2000; Stouffs and Janssen 2017; Thill and Dragicevic 2018). However, the process of building, displaying, communicating and enabling the addition of rule-based three-dimensional planning is still challenging (Marshall et al. 2019).

Geography has traditionally been forward-thinking regarding the development of algorithms for dealing with large and complex datasets in a timely fashion. The discourse on parallel computing in geography began in the 1990s, leading to the emergence of the subfield of geo-computation (Cheng et al. 2012). Geo-computation, as defined by Openshaw et al. (2000) is “concerned with

the application of a computational science paradigm to study all manner of geophenomena including both physical and human systems". Building on this, a greater focus needs to be placed on developing algorithms that are parallel in nature and can harness all types of parallelism. Turton and Openshaw termed "Thinking in Parallel" in 1998 but is yet to be fully adopted in the research community (Li et al. 2016).

For urban planners and designers, geo-computation can be applied in order to automatically generate large scale design proposals following various rules and guidelines. Such automated modelling approaches support rapid iterative virtual prototyping, in which a large number of design options can be generated and evaluated. However, automation also has its down-sides. Heumann and Davis (2019) hypothesize that the adoption of advanced automated processes in practice requires improving the experience for human designers as much as it requires focusing on improving the performance of algorithms. After observing the designer's workflow, they identify tasks that should be automated and propose methods for ensuring tools integrate into – rather than interrupt – existing processes.

We believe that in order to make automation useful for tasks such as planning, agile approaches have to be developed. In software development, the 'agile approach' is a human-centred software development method that can respond to rapidly changing end-user requirements through flexible iteration and gradual development (Martin, 2003). Agile automated modelling applies a similar approach to modelling design proposals. The aim is to allow designers to leverage high levels of automation while at the same time still maintain a high level of control over the outputs that are generated. We refer to this as *agile automated modelling*.

The approach encourages designers to create their own customised automated processes for generating design options by chaining together a variety of different GIS and 3D parametric modelling tools. However, for any automated process, there will always be special input cases in which the outcomes do not match the designer's expectations. Attempting to 'fix' such automated processes is very difficult, as the number of 'special cases' can be significant. Therefore, in the proposed approach we break the automated process into a series of smaller steps and allow the designer to intervene and to modify the outputs after each step. This approach has two key benefits for designers. First, the task of developing the automated generative processes is much easier, since all the special cases do not need to be resolved. Second, the ability to intervene and modify outputs gives designers a high level of control over the final output.

Following this philosophy, we have developed an agile automated modelling approach for district planning. The approach has been developed by working on a specific case study in Singapore. Section 2 gives an overview of the agile automated modelling approach and its application within the case study. Sections 3 and 4 briefly discuss future work and draw conclusions.

## 2. Agile-Automated Modelling Approach

The proposed agile automated modelling approach strives to create a synergetic relationship between the human designer and the automated processes. The aim is to create a process that is highly automated but that nevertheless gives the designer a high level of control at various points in the process. In the proposed approach, the human designer oscillates between two modes of working, which we refer to as ‘generating’ and ‘modifying’. In the generating step, the designer applies automated processes to generate large and complex datasets. In the modifying step, the designer will selectively modify those datasets to account for aspects that were not coded into the automated process. Finally, the modified output can then form the input into the next generating step, thereby creating an automation chain.

### 2.1. CASE STUDY

An agile automation modelling approach is tested with a case study in Singapore, generating three adjacent districts with a total area of approximately 1300 hectares. The district generation is conducted in a consecutive three-part geocomputation methodology (see Figure 1).

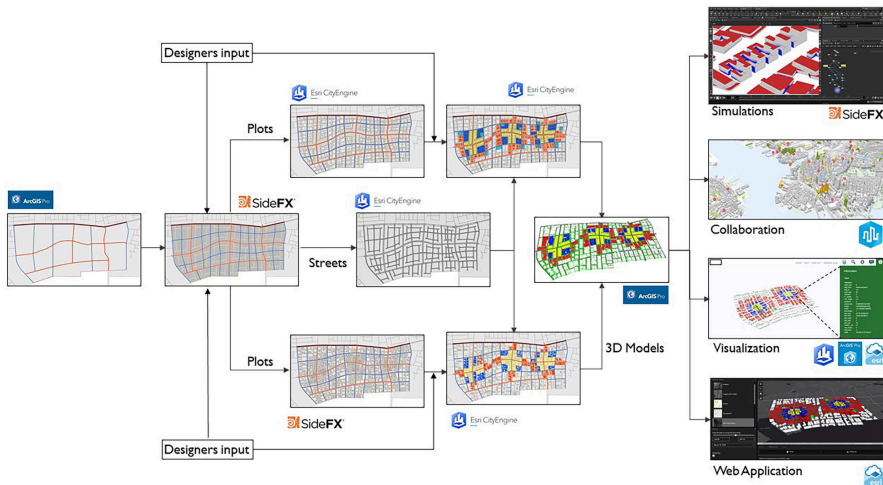


Figure 1. Overall workflow explaining the proposed agile-automation approach for district planning.

The three parts are: Part 1- Procedural Modelling using Houdini(SideFX), Part 2- Rule-Based Modelling using CityEngine and Part 3- Performative Modelling using various platforms. Procedural Modelling method starts with a district boundary, pre-existing conditions (roads) and guidelines to automate generation of street networks, plots (land parcels) and buildings. This is generated around nodes (primary and secondary) which are controlled by designers. At any point, a designer can intervene and modify the positions of these nodes. Eventually, gaining control over the output. The designer then takes the output of part-1 to



Rule-based modelling for developing a detailed model. The designer in part-2 gets further opportunities to explore many possibilities within this well-defined context before moving ahead. Finally, Performative modelling takes the generated district output of part-2 for further evaluation.

A district planning boundary definition is considered as a user-defined input. We have considered existing roads like CAT-1 (expressway) and CAT-2 (major arterial road) as inputs. Street widths and dimensions are pre-defined as per code of practice for road works by Land Transport Authority (LTA). Categories of roads are distinguished with varying widths and relationships to the development alongside it. The district is procedurally developed as per the district planning methodology which takes place on different levels, namely, precinct (800m), sub-precinct (400m), street and plot (see Figure 2). We connect these levels retaining an inter-dependency. This makes it easy for a designer to intervene and make any number of iterations.

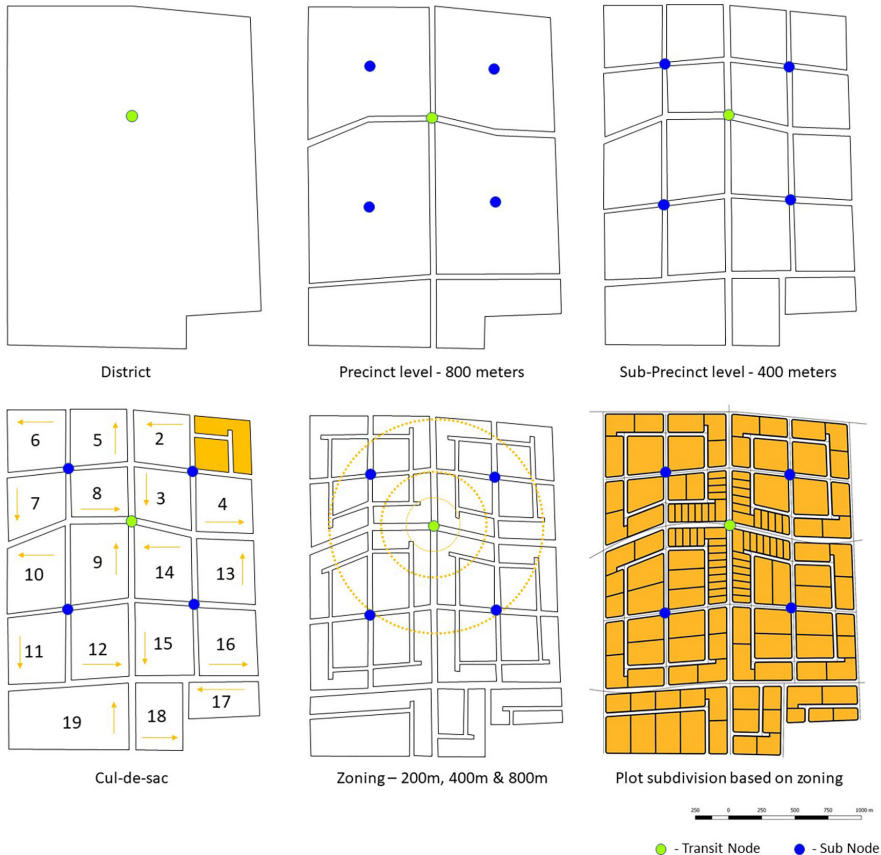


Figure 2. District planning methodology.

2.2. PROCEDURAL MODELLING

In the Procedural modelling method, Houdini (SideFX) software is used to create procedural modelling network for generating scenarios. Districts with roads, plots (land parcels) and buildings are generated as per the predefined planning principles. A district is generated around several urban nodes namely primary (major public transit node like mass rapid transit stations and bus interchanges) and secondary (identified sub-centres of portions of the district). The procedural modelling occurs in three major steps - a) Generating street networks b) Subdividing the plots and c) Identifying land use type. Subsequently, geometric data for roads, plots and buildings is created which carries processed information as attributes.

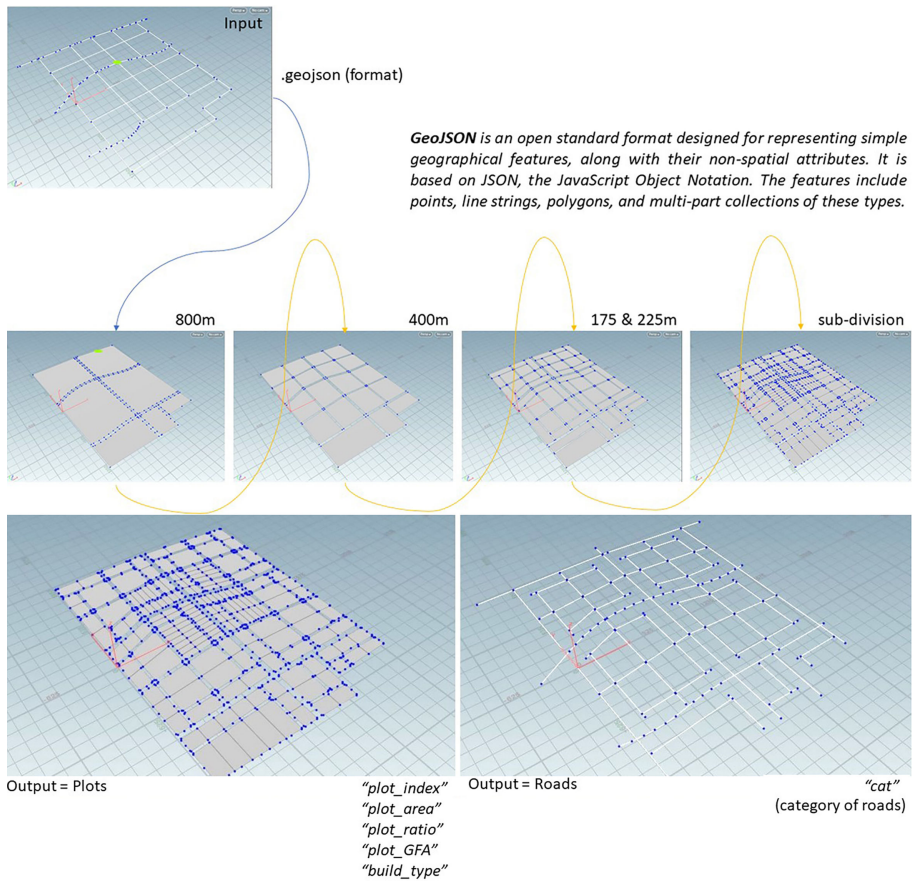


Figure 3. Houdini steps with input and output geometry.

With this information, incremental road centrelines are created. The distances between roads are generated following the planning principles. Clusters of land are formed following the road offsets and beyond the road reserve line as

defined by “LTA-code of practice”. Subsequently, plot subdivisions are applied onto clusters based on their distance to the primary node, land-use type, and minimum-maximum plot sizes (in terms of area and boundary length). Land use types are formulated as per plot proximity to the nodes. We have translated instructions from planning principles about mixed-use and amenity to create land-use type. Subsequently, buildings are extruded from each plot based on the specific plot ratio, gross floor area and land type assigned. Later, in the Rule-Based Modelling step, an alternative iteration is presented for building generation. The plot ratio and gross floor area are assigned based on the distance from the transit node.

Finally, the outputs of the Procedural Modelling step are generated separately as roads, plots, and buildings (see Figure 2). Each of these outputs carries additional information, stored as attributes attached to geometric entities. For instance, the road centrelines have the attribute “category\_of\_road”; the plot has “plot\_ratio”, “gross\_floor\_area”, “plot\_type” and “area”; and buildings have “elevation” and “total\_height”.

The input and output of the procedural modelling in Houdini is provided in the GeoJSON file format (.geojson). GeoJSON is an open standard format designed for representing simple geographical features, along with their non-spatial attributes. The features include points, line strings, polygons, and multi-part collections of these types. In our methodology, the inputs are the district boundaries and existing major road centrelines as line strings and primary-secondary nodes as points (see Figure 3). The outputs are road centrelines as line strings, and plots and building footprints as polygons. Using “JSON to Feature Tool” in ArcGIS Pro, we have converted these GeoJSON output files to ERSI file formats for subsequent use in CityEngine in Part-II.

### 2.3. RULE-BASED MODELLING

The Computer-Generated Architecture (CGA), is a unique programming language that is used to generate architectural 3D content. Based on the CGA syntax, the methodology was constructed complying with the existing guidelines established by local authorities for roads and plots. Street CGAs are applied on road centrelines to create detailed street models, incorporating pedestrian pathways, bus and cycling lanes, trees and vegetation, and street furniture and lighting. Similarly, plot CGAs are applied to generate building massing taking into account planning regulations and guidelines.

Through the specification of building parameters such as floor to floor height, several buildings in a plot can be tested iteratively by users with the “Inspector” tool in CityEngine. Buildings generated by CityEngine serve as alternative feedback to the part-I building output and aid in the specific plot descriptions.



Figure 4. 2D and 3D output generation of 3 Districts.

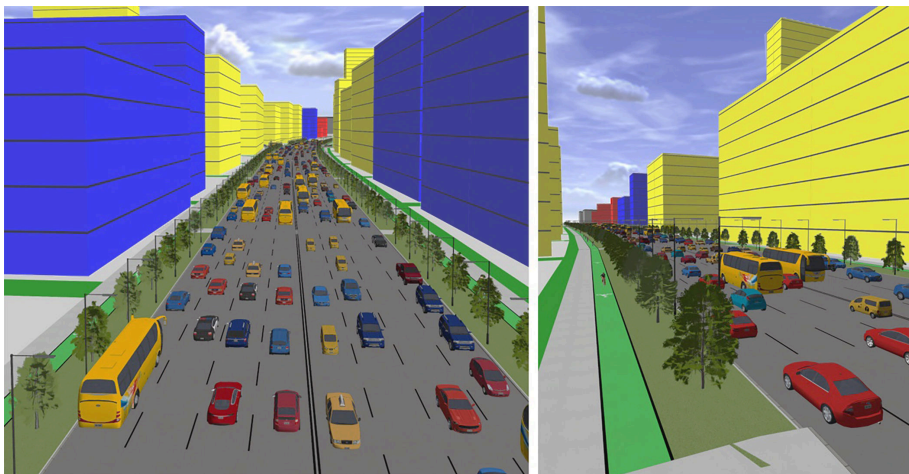


Figure 5. Detailed street models generated using CGA.

#### 2.4. PERFORMATIVE MODELLING

In the third part of our Geo-computation methodology, the generated 3D urban models are exported to various platforms (CityEngine, ArcGIS Pro, Houdini, WebGIS) for analysis and visualisation. This step helps designers to visualise the models and to further evaluate the models using a variety of analysis methods.

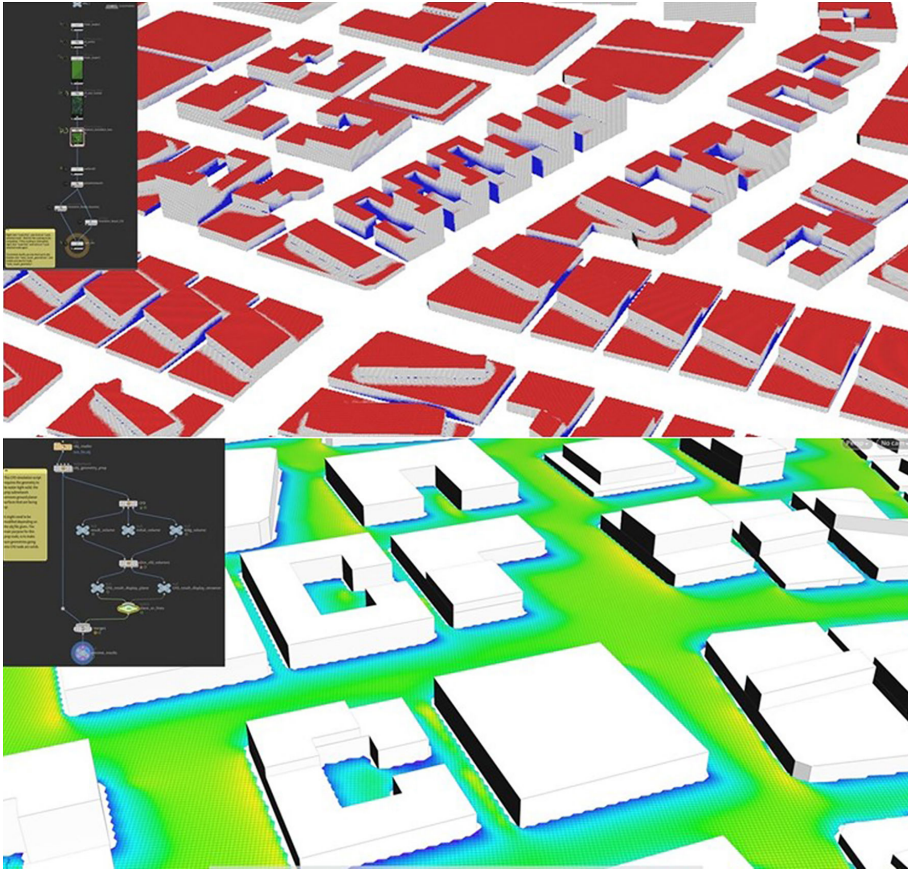


Figure 6. Solar radiance and wind simulation results in Houdini.

The CGA embedded model can be converted to a multipatch data type (feature in .gdb file geodatabase) in CityEngine. This 3D data with all attribute information is converted to CityGML (text format) using ArcGIS Pro. A CityGML file or .OBJ file can be taken to Houdini for running simulations like solar irradiance and CFD (Computational Fluid Dynamics) wind analysis for the buildings. CityGML can carry textures with attribute information and can be easily visualised back in GIS platforms. In our methodology, the simulation results are well documented in the files as we maintain our workflow, avoiding data loss. Figure 5 shows the results of the model simulations in Houdini. We also explore the possibility of using this

methodology to support planning using Form-Based Codes (FBC), i.e. regulating land development to achieve specific urban forms.

Using the CityEngine model export option of .3ws (CityEngine WebScene format), the model can be published on web platforms (see Figure 6), while ArcGIS Pro can publish the WebScene directly to ArcGIS Online. WebGIS platforms are used to visualise data with symbology and pop-ups for non-GIS experts. This step makes it easier to visualise, run a query and go through the urban prototype model for further evaluation.

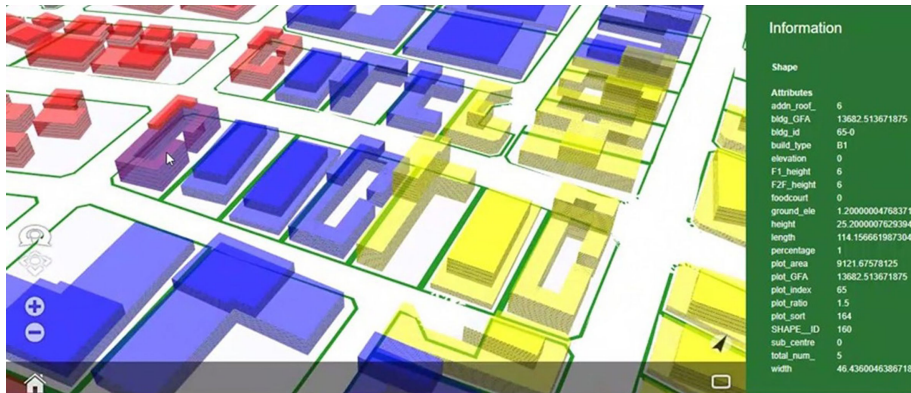


Figure 7. CityEngine webservice viewer.

### 3. Discussion

Overall, the research has resulted in the development of a geo-computational methodology for automating the generation of scenarios for district planning. The case study demonstrates how planning tasks can be seamlessly automated with an approach that is pragmatic and grounded with the designer's and the planner's involvement. A wide range of software was tested, with an aim to improve the ability of city planners and designers to interact with and override the automated procedures. The methodology enables users to combine the merits of the software together, improving the efficiency of the process and the efficacy of results. The research reports a methodology that helps users to iteratively generate and assess outcomes of planning tasks. The research also demonstrates an exploratory means to the planning process. With this exploratory path, there comes the question of standardization of planning principles. Although calibration is an essential part of the planning decision-making process, it is not covered here given the focus of this paper is on the methodology of automation.

### 4. Conclusion

The broader aim of this research is to develop a practice-oriented approach to create planning support systems, with the specific aim to improve the synergy between the tools and the workflows in practice. The research started by first mapping out end-to-end workflows that exist within planning practices. From

these workflows, a modular and flexible approach is derived and developed on top of an existing infrastructure that is already well established within the planning practices. The proposed *agile automated modelling* is demonstrated using a three-part geocomputation methodology - Procedural Modelling, Rule-Based Modelling and Performative Modelling. It enables the effective intervention of users which satisfies the requirements of flexible iteration and maintains a high level of control over the output.

Furthermore, the development of automation procedures needs to acknowledge the point of view of planners and designers. This requires further exploration of potential methods to provide this inclusivity in automation. Simultaneously, ways of visualising 3D data have to be evolved towards engaging dialogues among decision-makers who can think and plan for the complexities of future cities.

## References

- Alva, P., Janssen, P. and Stouffs, R.: 2019a, A spatial decision support framework for planning: Creating tool-chains for organisational teams, *Intelligent & Informed - Proceedings of the 24th CAADRIA Conference, 2019*, Victoria University of Wellington, New Zealand, 11-20.
- Alva, P., Janssen, P. and Stouffs, R.: 2019b, Geospatial tool-chains: Planning support systems for organisational teams, *International Journal of Architectural Computing*, **17(4)**, 336-356.
- Atkinson, P. M. and Martin, D.: 2000, *GIS and GeoComputation*, Taylor & Francis, London; New York.
- Cheng, T., Haworth, J. and Manley, E.: 2012, Advances in geocomputation (1996-2011), *Computers, Environment and Urban Systems*, **36(6)**, 481-7.
- Fischer, M.M.: 1998, Computational Neural Networks: A New Paradigm for Spatial Analysis, *Environment and Planning A: Economy and Space*, **30(10)**, 1873-1891.
- Fischer, M.M. and Nijkamp, P.: 2019, *Handbook of regional science*, Springer Berlin Heidelberg, Berlin, Heidelberg.
- Heumann, A. and Davis, D.: 2020, Humanizing Architectural Automation: A Case Study in Office Layouts, in C. Gengnagel, O. Baverel, J. Burry, M. Ramsgaard Thomsen and S. Weinzierl (eds.), *Impact: Design With All Senses*, DMSB 2019. Springer, Cham, Cham.
- Li, S., Dragicevic, S., Castro, F.A., Sester, M., Coltekin, A., Pettit, C., Jiang, B., Haworth, J. and Stein, A.: 2016, Geospatial big data handling theory and methods: A review and research challenges, *ISPRS journal of photogrammetry and remote sensing*, **115**, 119-133.
- Marshall, S., Hudson-Smith, A. and Farndon, D.: 2019, Digital participation – taking, *Town and Country Planning*, **88(1)**, 11-14.
- Martin, R.C.: 2003, *Agile software development: Principles, patterns, and practices*, Pearson Education., Upper Saddle River, N.J.
- Openshaw, S.: 1998, Towards a more computationally minded scientific human geography, *Environment and Planning A: Economy and Space*, **30(2)**, 317-32.
- Openshaw, S. and Abraham, R.J.: 2000, *Geocomputation*, New York: Taylor & Francis, London.
- Stouffs, R. and Janssen, P.: 2017, A Rule-Based Generative Analysis Approach for Urban Planning, in J.H. Lee (ed.), *Morphological Analysis of Cultural DNA, KAIST Research Series*, Springer, Singapore, 125-136.
- Thill, J. and Dragicevic, S.: 2018; 2017, *GeoComputational analysis and modeling of regional systems*, Springer International Publishing, Cham.

# IRRADIANCE MAPPING FOR LARGE SCALE CITY MODELS

HAN JIE LEE<sup>1</sup>, ZHUOLI LIN<sup>2</sup>, JI ZHANG<sup>3</sup> and  
PATRICK JANSSEN<sup>4</sup>

<sup>1,4</sup>*School of Design and Environment National University of Singapore*

<sup>1</sup>*hanjie94@gmail.com* <sup>4</sup>*patrick@janssen.name*

<sup>2</sup>*Gensler*

<sup>2</sup>*zhuoli\_lin@gensler.com*

<sup>3</sup>*Solar Energy Research Institute of Singapore*

<sup>3</sup>*ji.zhang@nus.edu.sg*

**Abstract.** This paper reports on the development of a geocomputational simulation workflow for the irradiance mapping of large scale city models. A fully automated workflow is presented, for importing CityGML city models, generating the simulation input models, executing the simulations, and aggregating the results. In order to speed up the overall processing time, the workflow uses parallel processing across multiple computers and multiple cores. Two case studies are presented, for Singapore and for Rotterdam.

**Keywords.** Integrated irradiance simulation; Solar potential assessment; Large scale urban 3D model; Houdini; Radiance.

## 1. Introduction

Irradiance measures the flux of radiant energy per unit area (Quaschnig 2003). Calculations of irradiance on building roof and facade helps planners and designers to understand the solar heat gain of the target buildings, and assess the potential of deploying photovoltaic (PV) systems to harness solar energy. In the Building Energy Efficiency R&D Roadmap published by Singapore National Climate Change Secretary (NCCS), out of 8,642 GWh of building electricity consumption, 60% were contributed by cooling (NCCS 2013). Relying more on cleaner sources of energy is crucial in the efforts to battle climate change (Merchant 2018). Singapore, for example, receives an average annual solar irradiance of 1,580kWh/m<sup>2</sup>/year (Singapore Business Review 2019) with low seasonal fluctuation, resulting in a high efficiency in the nation-wide deployment of Photovoltaic solar panels.

The goal of the workflow proposed in this paper aims to provide a solution for the simulation of a large scale city model. The workflow proposed in this paper has been tested with more than 150,000 buildings and millions of building surfaces, yet achieving detailed results. It has multithreading, pause and continue capability. When the software crashes, it can retain results produced and continue from where it stops. Ideally, the workflow should be able to show progress and output result



files building by building as they go through simulation handled by the lighting simulation software, Radiance ([www.radiance-online.org](http://www.radiance-online.org)).

CityGML, or City Geography Markup Language, is a type of file format for 3D models of cities (OpengEOSpatial 2019). For the proposed workflow, models written in the CityGML file format are used. Though city models in other file formats could be used too, the CityGML file format is preferred, as it is an open, standardised, XML-based format; has a small file size, easy to read, and is defined by various levels of details (LOD), serving different purposes.

In the practice of architecture and planning, the concept of LOD is often employed to minimise the need to show highly detailed model when the model is accessed for various purposes. In many cities, the local planning authorities often creates CityGML files of different LOD for urban planning and mapping. The higher the LOD, the more complex and detailed the building models become. Choosing the correct LOD model for simulation is crucial in order to achieve accurate results without compromising computational speed.

## 2. Simulation Tools

The current commonly used tools for irradiance simulation are mostly built upon the open-source software Radiance (Ward and Shakespeare 1998). While it works perfectly well for small clusters of buildings, the workflow would quickly be too computationally heavy if the model expands to urban scale.

### 2.1. RADIANCE

Radiance is a suite of validated programs widely used for lighting simulation. Within this suite of tools, the *rtrace* and *GenCumulativeSky* programs (Robinson 2011) were used as the engine for irradiance simulation. The *rtrace* program applies backward tracking techniques to compute radiance values at specific points within a model. The model includes geometric entities with material properties, describing the buildings and other objects in the scene to be simulated.

Using local irradiance data as input, the *GenCumulativeSky* program generates a file which describes the cumulative irradiance distribution for a specified time period across the sky hemisphere in discretized pattern according to Tregenza (1993) and the Perez luminance/radiance distribution model (1993). Combined with the *rtrace* program, this calculation file enables the simulation of annual cumulative irradiance for a given surface in just one go, rather than conducting the calculation on an hourly basis and aggregating the results afterward, leading to significant speedup of simulation without losing accuracy.

In this paper, a distinction is made between two types of geometric entities. On one hand, there are the geometric entities that make up the building being simulated, which we refer to as the *target building*. On the other hand, there are the geometric entities that make up the surrounding context, including other buildings, which we refer to as the *context geometry*. This context geometry acts as obstructions to the target building, possibly shading the building during certain times of the day or year. Note also that the target building is always included as part of the context geometry since it may be self-shading.

## 2.2. RADIANCE BASED TOOLS

There are many existing simulation tools that use Radiance as a simulation engine. However, most of these tools are designed for relatively small-scale building simulations. With an input model consisting of millions of polygons, Radiance would simply crash due to lack of memory. Even if enough memory could be obtained, the simulation would be highly inefficient as the whole city would be used as context geometry for each point being simulated.

The advantages and limitations of the existing methods and tools used for irradiance mapping have been compared and reviewed in previous studies (Jakubiec and Reinhart 2012; Melius, Margolis and Ong 2013).

Various plugins have been developed for existing 3D modelling platforms, linking to the Radiance simulation engine. Three such plugins were investigated. These were the Honeybee/Ladybug plugins for the Rhino3D Grasshopper platform developed by McNeel; the Diva tool, developed by Solemma LLC as a plugin for Rhino3D; and the OpenStudio plugin for SketchUp, developed as an Open Source project. In all cases, these existing plugins and 3D modelling platforms were found to be incapable of processing such a large dataset.

The input CityGML data set on its own already consisted (in the case of Singapore) of more than 150 thousand files organized into a particular folder structure. Once all the simulations had been run, more than a million files would be generated. What was required was a platform capable of processing such a data set in a highly scalable way. This included automating various processes:

- importing CityGML files from the folder structure,
- creating different representations of each building,
- saving these files back to the folder system,
- running the simulations and saving the simulation output files, and
- reading the simulations output files and creating various aggregated csv files containing the results.

Houdini is a procedural 3D modelling application developed by SideFX, primarily used in the movie industry (SideFX 2019). Due to the demanding requirements imposed by this industry, Houdini has been developed from the ground up with performance and scalability in mind. In March 2019, SideFX released Houdini 17.5, which included a new feature, *Procedural Dependency Graph* (PDG). PDG was developed to better scale and automate processes by distributing tasks across multiple CPUs (SideFX 2019). Although Houdini has no built-in support for running Radiance, the authors have developed a plugin that allows Houdini to run Radiance simulations.

In the irradiance mapping workflow, Houdini is used to process geometries and to run the simulation with the Radiance plug-in, while relying on PDG for its multithreading capability. Two Python plug-ins were developed for Houdini in order to support the irradiance mapping workflow; the first imported CityGML files into Houdini, while the second executed the Radiance simulation.

### 3. Proposed Workflow

A key strategy of the proposed workflow was the decomposition of the urban scale simulation into smaller building scale simulations. For each building in the model, a separate Radiance simulation was performed, with its own context geometry. The results of these smaller-scale simulations are later then aggregated back together again to generate the final result.

#### 3.1. VALIDATION

Prior to implementing the workflow, validation was conducted to verify the accuracy of irradiance simulation for an unobstructed upward-facing horizontal test surface, the annual total global horizontal irradiance (GHI) as simulated using the cumulative sky irradiance description and Radiance is very close to that calculated from the input file which is based on measured data recorded from the nine weather stations operated by SERIS, and the difference between them can be regarded as marginal.

#### 3.2. SIX STEPS

The proposed workflow consists of six steps as shown in *figure 1*.

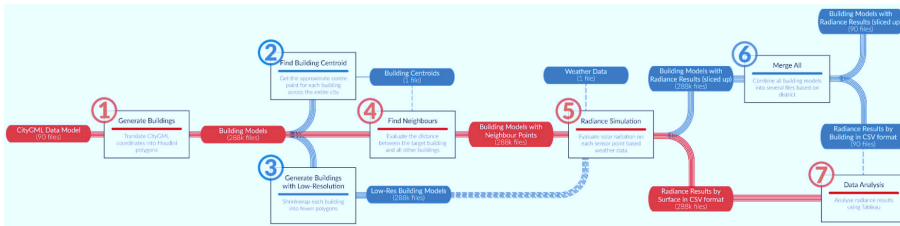


Figure 1. Workflow overview.

In step 1, the CityGML files were imported into Houdini and saved in the native *.bgeo* format. The geometry was imported with any additional attributes that are present. Geometries that were too small (<10m<sup>2</sup>) and broken geometries were marked and fixed, respectively.

In step 2, the building centroid of each building was calculated. This was used in deciding whether a building should be considered as the context of a target building and be included for the simulation. Buildings that were too far would have an insignificant influence in the simulated irradiance value, as its shading effect would be small, thus excluded. The building centroids were translated up in the z-direction to the full height of the building, as shown in *figure 2*. This allowed the shading angle to be taken into consideration. All building centroids were saved in a single file, and used to find the context geometry for each target building.

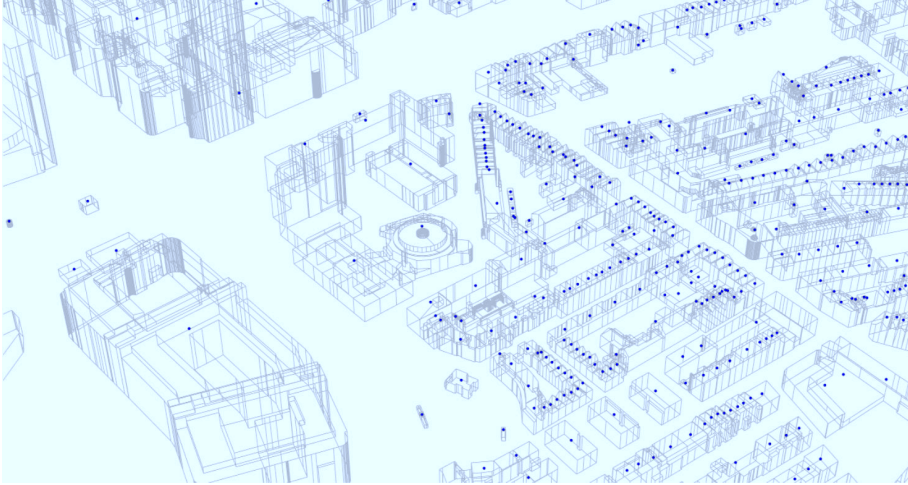


Figure 2. Building centroids with building geometries' outline.

In step 3, each building was converted into a low-resolution version to be used as context geometry. *figure 3* shows a building being “shrink-wrapped”. When the low-resolution building model is created, the volume of each of both low resolution and existing building model is measured and compared. The low-resolution building model is saved only when the volume of the low-resolution building model is less than 110% of the existing building model.

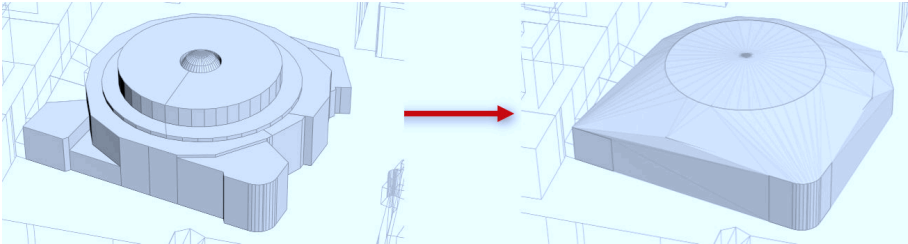


Figure 3. “Shrink-wrapping” a building.

In step 4, the context geometry for each target building was calculated. To accurately capture the impact of shading from the built environment on surface irradiance, neighbouring buildings within a given radius of the target building being simulated were retrieved from the database and imported into the model. When finding neighbours, each building centroid was measured against all other centroids across the entire city. Referring to *figure 4*, for “near” neighbouring buildings within 400 metres of the target building, they were included in the context geometry. Referring to *figure 5*, for “far” neighbouring buildings between 400 to 800 metres, the buildings are included or excluded based on the building height. As shown in *figure 6*, the angle from the edge of the “near” flat catchment to the measured building centroid (at the top) was more than 5 degrees, the building

was included. Buildings beyond 800 metres are excluded.



Figure 4. Buildings in context catchment area of less than 400m radius.



Figure 5. Buildings in context catchment area of 400-800m radius, excluding those with a centroid below 5 degrees.

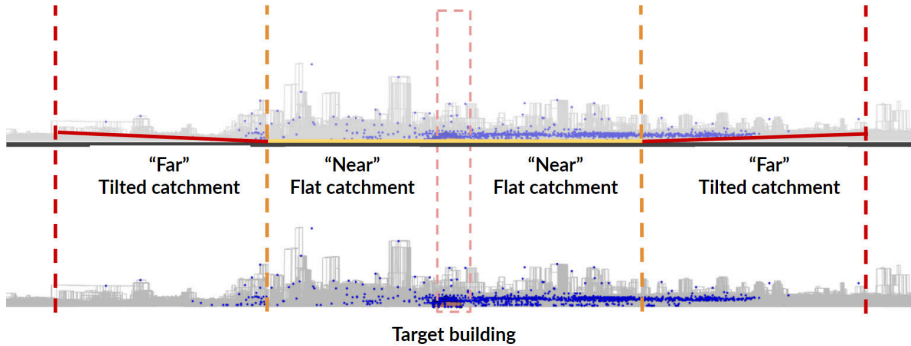


Figure 6. Sectional view diagram of context catchment area.

In step 5, the Radiance simulation is executed. Each target building with its surrounding geometry is loaded into Houdini. For “near” neighbouring buildings, the normal (LOD2) model was used. For “far” neighbouring buildings, the low-resolution model is used. Each surface on the target model was subdivided into patches of 3-by-3 metres. The surface subdivision operation is to ensure that irradiance is evenly sampled across every surface. A simulation input file is then generated for calculating the centroid of each surface patch. The simulation is then executed, using the centroid points, the neighbouring buildings models, and the cumulative sky model.

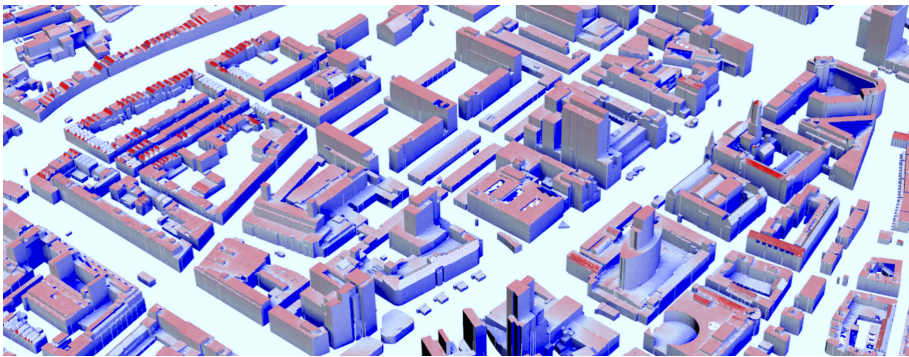


Figure 7. Rendered irradiance map on Rotterdam building facade.

Finally, in step 6, the simulation results are aggregated and processed. Each building is saved as an individual Houdini’s *.bgeo* model and a Comma Separated Value (*.csv*) file storing various attributes including irradiance. It then aggregates these models into larger files, allowing data of each district to be visualised.

#### 4. Results

The simulation workflow was applied on CityGML models of two cities: Singapore and Rotterdam. The Singapore model was created and provided by

the Singapore Land Authority (SLA); and it is not accessible for the public at the moment. Meanwhile, the Rotterdam model is available for public download.

#### 4.1. SIMULATION SETTINGS

For both models, LOD1 and LOD2 models were tested for simulation. The lack of roof geometry details on LOD1 model was unable to reflect the actual building roof, and thus generating less reliable results compared to the detailed roofs in LOD2 models. LOD2 model was eventually used for analysis targets, and LOD1 model for context geometries.

Surface subdivision size impacts the resolution of rendered radiation map and the simulation time. The smaller the size, the higher the resolution, and the longer the simulation time. Three settings of subdivision sizes of 1-by-1 metre, 3-by-3 metres, and 6-by-6 metres were tested. 3-by-3 metres were first tested as it ensures every floor has at least one measuring point. 1-by-1 metre was then tested as it is the typical resolution used in building-scale solar radiation simulations. 6-by-6 metre was tested as a low-precision option if simulation speed is the priority.

This variable affects the simulation time as the increase in resolution results in increase of number of test points. Since each point has to go through the same process regardless of the size of the surface, the simulation time will be proportional to the number of surface. The accuracy of value obtained for each test point would not be affected by the surface subdivision size. However, reducing number of test points might lead to less accurate simulation result for the entire building due to reduced resolution. 1-by-1 metre subdivision size produces 9 times of the number of surfaces compared to 3-by-3 metre. Yet, the overall building simulation result was similar to that of 3-by-3 metre setting. On the other hand, despite taking less simulation time, 6-by-6 metre surfaces hindered the potential to produce floor-by-floor PV potential data analysis. Hence, 3-by-3 metre was eventually used as it produces simulation points on every floor.

The first context catchment size used was 50 metre radius from building edge as “near”, and 50 to 150 metre radius from building edge as “far”. It produced accurate results in areas with mostly mid-rise buildings and consistent building heights, which is the characteristics of the sample data from SLA. However, it was too small for areas that has tall buildings and low sun angles.

For the same urban model, the simulation time increases as the number of surfaces in the set of context geometries increases. Expanding the overall context catchment size or the “near” context catchment size will both result in an increase in the number of context geometry surfaces. The effect of context setting on accuracy of results varies depending on the urban morphology, building height, and extreme sun angle. In general, the denser the city, the taller the buildings, or the higher the sun, the smaller the context could be. The principle of setting appropriate context catchment size is to ensure all possible shadow-casting objects are included. The best way to determine catchment size is to try a few settings for the same building.

## 4.2. SINGAPORE

The Singapore model was the first model that this workflow was implemented for. It was an iterative process that the workflow was constantly updated to respond to problems caused by messy 3D models. The dataset was given in the format of “one building per GML file”, and the geometry originated from Light Detection and Ranging (LiDAR) scans. Two LOD models were given: LOD1 in which the 3D models were extrusions of building footprint, and LOD2 in which the 3D models have more roof details.

The LOD2 model was used for simulation. However, the LiDAR-based model has significant amount of improperly defined quad surfaces that are non-planar. Initial mechanism to repair the geometries results secondary problems such as distorted geometries that were significantly different from the original geometry. The workflow then employed a more robust and primitive method of triangulation after rounds of iterations to prepare the geometry for simulation.

A context catchment size of 75 metre as “near”, and 75 to 250 metre as “far” was used for the Singapore model. This setting produced accurate results in the context of Singapore, where the sun angle is consistently high, and buildings are close to one another. The final simulation run on Singapore model of 156,000 buildings took 160 hours to complete on 36 2.6GHz cores.

## 4.3. ROTTERDAM

The Rotterdam model were in the format of “one district per GML file”, and three LOD models were given in the same GML file. While LOD1 and LOD2 has similar level of details as the Singapore model, Rotterdam model has LOD0 which geometry only contains the building footprint. The LOD2 model was used for simulation, while the LOD1 model was used as “far” context geometry. The workflow was implemented for Rotterdam model after finishing the Singapore model.

However, the context catchment size setting used in Singapore model was insufficient in the context of Rotterdam, primarily due to the low sun angle during winter. Hence, a bigger context catchment size of 400 metre as “near”, and 400 to 800 metre as “far” was employed for the Rotterdam model.

Due to the larger context catchment size used and greater number of buildings, despite having generally smaller buildings, Rotterdam model took longer time to complete. The entire workflow took 230 hours to finish for 200,000 buildings.

## 5. Conclusion

This paper reports an efficient, reliable and integrated simulation pipeline streamlined for city scale simulation as implemented and demonstrated in urban solar potential assessment for all building surfaces for Singapore and Rotterdam. The pipeline provides a solution to one of the primary technical bottlenecks faced by researchers and practitioners in urban studies, especially in large scale urban modeling, by achieving well balance between efficiency and accuracy. Other than offering the functions in assisting irradiance simulation efficiently, the pipeline also provides the possibility to embed the results back to CityGML database so



that the simulation outcomes can be retrieved by alternative software or platform for other analysis. The flexibility and scalability of the pipeline entails that it can be applied in cities around the world regardless of the local urban forms and irradiance conditions so that local solar potential can be assessed accurately and efficiently to support decision-making on policies to encourage deployment of solar PV. This pipeline is not limited to irradiance mapping exercises, but can also be tailored for similar large scale automation-based workflows in other fields.

### Acknowledgement

The authors would like to acknowledge the support from Singapore Land Authority (SLA) for providing access to the CityGML database of Singapore, and for the administrative support which facilitated the simulation work as reported in this paper. We also thank Solar Energy Research Institute of Singapore (SERIS) for leading the solar potential studies for Singapore.

### References

- “Singapore’s solar capacity to double over the next decade” : 2019. Available from Singapore Business Review <<https://sbr.com.sg/utilities/news/singapores-solar-capacity-double-over-next-decade>> (accessed 9th December 2019).
- “Procedural Dependency Graph” : 2019. Available from SideFX <<https://www.sidefx.com/products/pdg/>> (accessed 9th December 2019).
- “Houdini” : 2019. Available from SideFX <<https://www.sidefx.com/products/houdini/>> (accessed 9th December 2019).
- “CityGML” : 2019. Available from Opengeospatial <<https://www.opengeospatial.org/standards/citygml>> (accessed 9th December 2019).
- Boranian, A.P.B., Zakirova, B.Z., Sarvaiya, J.N.S., Jadhav, N.Y.J., Pawar, P.P. and Zhe, Z.Z.: 2013, *Building Energy Efficiency R&D Roadmap*, National Climate Change Secretariat (NCCS), Singapore.
- Gagnon, P., Margolis, R., Melius, J., Phillips, C. and Elmore, R.: 2016, Rooftop solar photovoltaic technical potential in the United States: A detailed assessment., *National Renewable Energy Laboratory, NREL/TP-6A20-65298*, 1-82.
- Jakubiec, J.A. and Reinhart, C.F.: 2012, Towards validated urban photovoltaic potential and solar radiation maps based on lidar measurements, GIS data, and hourly Daysim simulations., *SimBuild*.
- Melius, J., Margolis, R. and Ong, S.: 2013, Estimating Rooftop Suitability for PV: A Review of Methods, Patents, and Validation Techniques, *National Renewable Energy Laboratory*.
- Merchant, E.F.: 2018, “IPCC: Renewables to Supply 70%-85% of Electricity by 2050 to Avoid Worst Impacts of Climate Change” . Available from <<https://www.greentechmedia.com/articles/read/ipcc-renewables-85-electricity-worst-impacts-climate-change>> (accessed 9th December 2019).
- Perez, R., Seals, R. and Michalsky, J.: 1993, All-Weather Model for Sky Luminance Distribution - Preliminary Configuration and Validation, *Solar Energy*, **50**, 235-245.
- Quaschnig, V.: 2003, “The Sun as an Energy Resource” . Available from <<https://www.volker-quaschnig.de/articles/fundamentals1/index.php>> (accessed 9th December 2019).
- Robinson, D.: 2011, *Computer Modelling for Sustainable Urban Design: Physical Principles, Methods and Applications*, Routledge, London.
- Tregenza, S.: 1993, Daylighting Algorithms, *Energy Technology Support Unit*, **1350**, 1350-1993.
- Ward, L.G. and Shakespeare, R.: 1998, *Rendering with Radiance: The Art and Science of Lighting Visualization*, Morgan Kaufmann Publishers, Inc, San Francisco.

# FLÄVIZ IN THE REZONING PROCESS

*A Web Application to visualize alternatives of land-use planning*

WOLFGANG E. LORENZ<sup>1</sup> and GABRIEL WURZER<sup>2</sup>

<sup>1,2</sup>*TU Wien | 259-01 Digital Architecture and Planning*

<sup>1,2</sup>{wolfgang.lorenz|gabriel.wurzer}@tuwien.ac.at

**Abstract.** The rezoning process primarily deals with proposed changes on land-use and zoning plans. More and more often, the public is asked for its opinion and feedback. However, there are two main obstacles in today's practice: On the one hand land-use and zoning plans, in general, only define the potential of areas and so do proposed draft plans; they usually say nothing about the implementation of land-use in the built space. On the other hand, the untrained majority can hardly grasp the current form of representation as two dimensional plans with accompanying written information. In order to enable a wider public participation (and understanding), the authors present FLÄVIZ, a 3D visualization of potentials on land-use and zoning plans.

**Keywords.** Alternative land-use and Zoning plans; Three JS; Visual Representation.

## 1. Introduction

Land-use plans aim to define or guide the future evolution of cities. This influence the way citizens will live together in the future. Since local people are directly affected and know their neighborhood/needs best, public participation in project development becomes more and more important: In many cities, the public can examine, receive and discuss draft plans and related documentation at the municipality. The accompanying documents may include textual explanation of the proposed changes, a draft of the request for the municipal authorities, a statement of the advisory council for urban planning and design, an environmental report and other planning documents. However, typically, the proposed plan amendments are static; in most cases without any additional diagrams showing influences of dynamic aspects such as wind, noise, functional usage, pedestrian flow or pollution. Then again, the officials provide general planning material; in the authors case study region, Vienna, that includes a 3D map of existing buildings and the digital 3D terrain model, which can both be downloaded from the Open Government Data Portal [01]. However, this wealth of information is difficult to grasp without background knowledge: On the one hand, the overall regulation conditions (building regulations, standards and guidelines) are complex and, on the other hand, the impact of the planned changes is difficult to present. Our proposed application addresses both difficulties by using visualization and simulation.

According to Arpornwicharnop et. al (2007) the authors believe that the aim of land-use and regulations is to maintain the quality of life - which is influenced e.g. by population density, viewing and day lighting. At the same time, dealing with land-use and zoning plans means that diverging interests collide - 1) investors want a positive return (as quickly as possible), 2) local residents want to ensure that they will not suffer any negative consequences (e.g. no further deterioration of noise nuisance) and 3) the authority may simply be interested in solving the lack of housing. Hence, if there is a public interest to discuss and manage all these different interests, a common level of understanding is necessary. Additionally, zoning and land-use projects become better 1) if decisions can be tracked at all times (communication), 2) if citizens' opinions are taken into account (participation) and 3) if new plans can be tested beforehand (analysis). In order to achieve these objectives, adequate methods have to be developed that supports stakeholders, officials as well as the public. In short, a face-to-face discussion can only be achieved with an effective and easily comprehensible method for all participants. This will, finally, lead to a better quality of life.

## **2. Background**

The Web application FLÄVIZ is mainly related to two objectives: 1) the visualization of alternatives in a form everybody can quickly read and understand and 2) to provide feedback about alternatives in form of an objective comparison.

The first objective belongs to the group of support tools for discussions about land-use and zoning in order to communicate and facilitate understanding of decisions. This is especially important, because of the diverse audience, different knowledge, different educational qualification and not least because of emotional issues (Kellett et al. 1998). Basic requirements of such a tool, including site modeling, scenarios and feedback are discussed in Kellett et al. (1998). A different approach concerns prediction and forecasts of land-use changes. This include cellular automata as basis for a generic model of urban land-use dynamics (White et al 2000, Lau 2005) and agent-based models that model urban land-use change (Matthews 2007, Schwarz 2012). Good experience has been made with land-use/transport modeling - including, e.g., the analysis of air pollution and traffic noise (Moeckel et al. 2007) - although there still remains challenges to integrate them in practice (Moeckel et al. 2018). Another aspect deals with collaborative design itself in order to form an optimal layout that meets the highest demand of the community (Bai et. al 2018). The system described in Bai et. al (2018), e.g., collects the preference data of each user through interacting gaming which then serves as information for a self-adapting urban layout. Regarding the visualization of possible (urban land-use and zoning) changes it is obvious that web-based systems - such as ArcGIS [02] - have a big advantage, since they are available to everybody (who has access to the internet). ArcGIS Urban combines landscape information and city information models (context) with projects and (manually added) regulations, such as zoning and land-use codes (content). Building scenarios (e.g. building projects) are visualized in 3D enabling impact evaluations (e.g. shadow impact regulations).

The collaborative part of the first objective brings up another aspect. Thinking

about different file types of 3D terrain data, 2D hand sketches and simple block models, data exchange becomes relevant as well. In this context, Arpornwicharnop et. al (2007), e.g., propose a simulation software that concentrates on the information interchange by integrating a topological analysis tool, a constraint checking module and a geographical information process module (related to street name, street width and property number).

Concerning the first objective, FLÄVIZ provides the possibility to visualize proposed changes on land-use and zoning plans. The visualization is web-based, using JavaScript to select and analyze data. At the current stage of development, automation, exchange of additional data and interaction (for communication) are not yet implemented. Especially the possibility of exchanging notes seems to be an important task for the future.

The second objective of FLÄVIZ addresses quantities and qualities of alternatives; only a few of which have been implemented yet. In principle, quantities and qualities includes measurements such as incorporated in Modelur for SketchUp by AgiliCity company [03] - Modelur is a parametric urban design tool that 1) calculates important urban control values (including floor area ratio, built-up area, building height, number of stories, site coverage, number of apartments, required parking spaces and site coverage), 2) modifies buildings parametrically (adapting each building to already known zoning rules) and 3) warns if buildings are placed too close. However, feedback about alternatives should not only include urban control parameters but also additional information resulting from simulations. Other solutions are provided by Esri Inc. (Environmental Systems Research Institute), an international supplier of geographic information system (GIS) software. Preconfigured solutions for planning and community development includes, e.g., shadow impact analysis, flooding inquiry and calculation of solar relations [04]. Currently, FLÄVIZ only simulates sun/shadowing and wind. The feedback in both cases is given visually and not yet as a comparable number. Future work, nevertheless, will address other characteristic values as well.

FLÄVIZ not only uses 3D data of terrain and existing neighborhood, provided by the authority [05], but also for possible land-use (especially housing). Technically it is based on Java ThreeJS, using the standard data format 3DS - which reduces problems caused by exchange of different data formats. The primarily objective is not to predicting future developments, but to visualize jointly developed land-use alternatives (as 3D block models), giving quantity to certain objective criteria for each alternative (see figure 1). The 3D model serves as basis for certain simulations ranging from wind-simulation to analysis of shading, which complements the “standard” urban control values.

### 3. Method

Proposed changes on land-use and zoning regulations include two main objectives: 1) the dedication of an area (type of zoning; e.g. residential, industrial, commercial and open space; see figure 2 left) and, 2) the permitted construction class and housing type (e.g. 12-21m permissible building height, buildings aligned with

their neighbors; see figure 2 right). Both are specified as symbols, colors or numbers on a two dimensional plan, which makes it hard to understand for non-experts. Therefore, the proposed application visualizes the construction class and housing type in a 3D environment (partly including general regulations as well). This allows a broad public to understand the proposed changes.

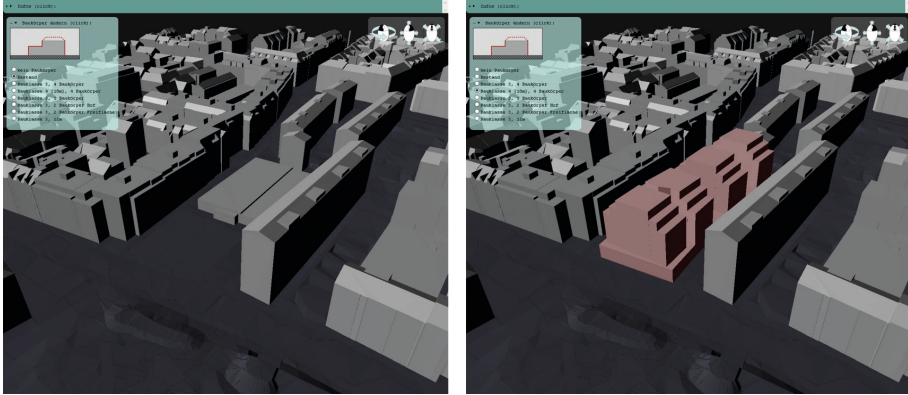


Figure 1. Possible visualization. Left: As-built model; Right: Algorithmically generated building structure for a specific construction class, housing type, including some regulations.

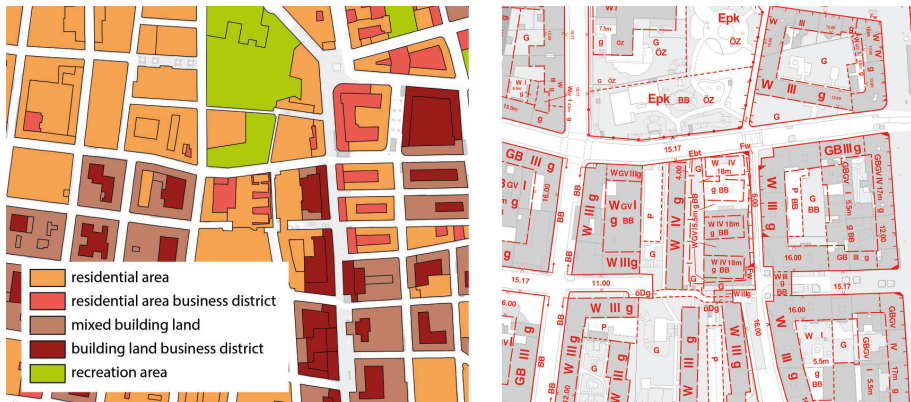


Figure 2. Zoning and land-use plan of Vienna (section); Left: zoning illustrated by color; Right: land-use regulations (maximal building height, building line and zoning).

Initially, FLÄVIZ loads the 3D terrain model and the current as-built model, which serves as basis for visualizing the inventory (see left in figure 1). The digital terrain model (DGM) contains the current terrain information for the entire city area of Vienna. DGM is provided by the open government Vienna in the following data formats: SHP (Shapefile, a geospatial vector format for data interoperability of GIS software products - contour lines or break lines), TIF (Tagged Image File Format, a raster graphics image format - one meter

raster), ASC (ActionScript Communication File - one meter raster) and DXF (Drawing eXchange Format). The open government Vienna also provides the building model LOD1 (Visicom Modelling Level of Detail 1), which contains all buildings of Vienna, depicted as prisms (about 200,000 buildings with more than 650,000 building volumes). LOD2, currently used by the web application, includes accurate roofs and architectural details and is provided as DXF (triangular transformation) and SHP (basic building model data from the “multipurpose map”).

With FLÄVIZ, the proposed and discussed zoning and land-use plan serves as basis for a maximum development on the building spot in question (see right in figure 1). In more detail, the maximum possible building volume is (at the moment manually) determined on the basis of the proposed construction class, the terrain profile and building regulations (proposed by the officials). Possible variations for construction classes and housing types (algorithmically or given by the residents) permits a real comparison between alternatives. Such variations may also include the density rate for buildings, number of buildings, distribution of buildings based on proposed building types and characteristics of the facade based on the intended use (not yet included). In the end, the user can easily switch between a given numbers of possible solutions. It is conceivable that within the maximum volume (defined by construction classes and housing types), building structures can be algorithmically generated, whereby regulation conditions are considered as well. This would give an even more realistic view on proposed changes.

In the current stage of development, users can only switch between predefined scenarios. The authors tested the application (related to a specific rezoning process) with local politicians, citizens and public authority staff. The first two groups in particular showed great interest, since, in most cases, they could not imagine the three dimensional impact. Such a reaction supports the assumption that already the three-dimensional visualization of proposed changes is helpful for decision makings (which is currently not the case). Since only two simulations are implemented yet and alternatives are predefined, the usability is intuitive (you see what you get: Changing the day and time affects the shadow). This might change when analysis becomes more complex (regarding input and calculation). Consequently, the user interface and interactivity have to be adapted. One possible direction might be to implement different user interfaces for different applications/groups of interest.

### 3.1. JAVA THREE JS

FLÄVIZ is a web application developed in Java Three.js using TDSLoader (3DS Max). Three.js uses WebGL and is a JavaScript library used to display 3D graphics in web browsers. The TDSLoader is a NodeJS wrapper for the TDSLoader library in order to convert 3D graphics to Three.js. While the terrain and existing neighborhood buildings (3DS) are loaded in any case, different alternatives for the spot in question are available in the form of a drop-down list. Each element of the list is defined by a specific unique value that refers to a specific 3DS model representing an alternative building development.

## 4. Simulation

It is conceivable that the model can serve as input for a simulation (e.g. of the building physics properties). This would mean that all given alternatives can be compared with each other on the basis of facts (e.g. solar radiation and shading or expected noise pollution; furthermore, predefined visual axes can be compared with all alternatives, in order to show possible negative influences on the overall urban planning). Subsequently, the calculated properties can be visualized on the building structures (e.g. heat map for solar radiation), whereby calculation methods and regulation foundations can be displayed in detail on request. At any time, the user has the opportunity to move freely in the three-dimensional model and to view it from all sides. It is also conceivable that any additional information can be directly attached to the structures (virtual sticky notes or comments).

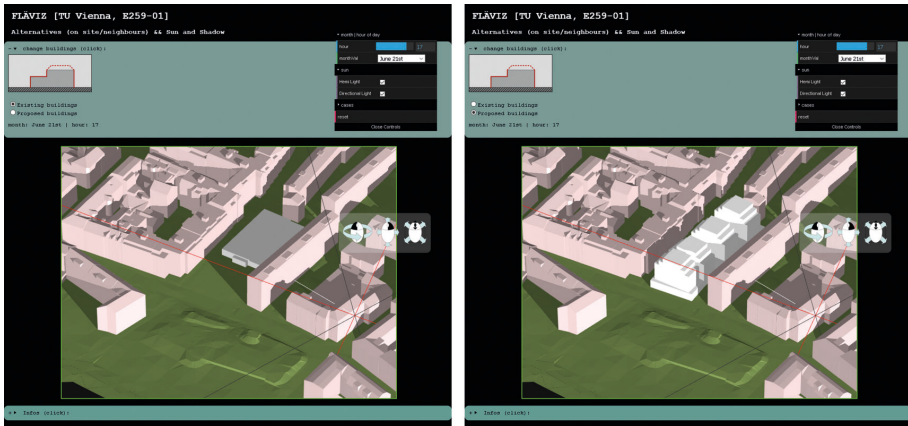


Figure 3. Shading and lighting for one and the same date and hour. Left: As-built model; Right: Proposed alternative construction.

### 4.1. LIGHTING AND SHADING

Since FLÄVIZ is based on Java Three.js, which already allows lighting and shadowing, it seemed obvious to implement this category first. The current version of the application allows to switch on and off two kinds of lights in order to light up the scene: a directional light and a hemisphere light (see Figure 3). However, only the directional light allows shading (the hemisphere light only gives a general light to the scene). For the moment, the settings are hardcoded and do not automatically react to the size of the scene (this includes the shadow map size and the shadow camera limits). Nevertheless, as shown in figure 3, differences between alternative constructions are immediately displayed in the scene, corresponding to the adjusted date and hour of the day. While the day of the year corresponds to a significant predefined date, the hour can be adjusted via slider. In future, the four main sun positions of the year (days of equinoxes and solstices) should serve as comparative values, reflecting the effects to the

surrounding area (facades of buildings as well as open space). The ratio of shaded areas to the overall facade is then an indicator for the impact of the proposed land-use and zoning change.

#### 4.2. WIND SIMULATION AND VOXELIZATION

For the wind simulation, it seemed appropriate to deal with a discrete world (i.e. split into cells) instead of a continuous one. That is not least because the authors made good experience with simulations of building effects in NetLogo (Wurzer et al. 2012; Wurzer et al. 2019), but also because it produces a considerable saving of time. NetLogo (Wilensky 1999) is a multi-agent programming language with an integrated modeling environment. It is most appropriate for simulation, where agents - the active entities within the simulation - operate in a discrete world consisting of  $n \times m \times o$  cells. The authors have shown that agent-based simulation (ABS) is able to compute and visualize dynamic factors in order to enable a quality assessment about multiple design variations (Wurzer et al. 2012). The key issue is that planning aspects can be evaluated by ABS, using simplified models. Simplification not only concerns the model itself but also the world that is discretized (turned into a grid). This leads to a similar environment of both, FLÄVIZ and the preceding models using NetLogo.

Technically, the transformation of the data set (continuous world) into a discrete world (boxes in a grid) is based on voxelization. Voxelization is a term from computer graphics and refers to a grid point in three-dimensional space that is well-defined by its coordinates (x, y, z). The position of a voxel (grid point) implicitly results from its relation to the other voxels. The process of voxelization is based on the decomposition of the geometry (stored in the “source” data format) into individual, continuously smaller triangles (Lorenz et al. 2015, Lorenz et al. 2016). A division algorithm decomposes each triangle until no cell of the world can be placed within the area of the remaining triangle. This ensures that cells within a triangle are detected as well. The advantage of a so-called voxelization lies in the analysis. It is thus possible that each cell contains additional storage of information about effects of certain criteria (e.g. the direction of light and intensity can be stored in each voxel, influencing the color of the voxel).

##### 4.2.1. *Prototype Simulation*

Changes to the zoning plan are comparable to the early stage planning. In both cases, decisions (should) depend on numerous influencing aspects such as wind, topology, flooding, visibility, circulation, parking facilities, development of the site and solar radiation, to name just a few (White ET. 1983). Urban planner may be either interested in evaluating current spatial configurations or they want to predict the behavior of future layouts that do not yet exist.

The prototype comes with a simulation of wind. It is the interplay of wind, temperature, humidity and rain that determines (micro-)climate. Therefore, the authors believe that sustainable building design is based on these decisive factors. Nowadays, sustainability is an important issue and, in the view of the authors, little noticed when dealing with proposed changes on land-use and zoning plans. For



instance, heat islands can be located in a city; however, the countermeasure is often limited to installations such as “artificial drizzle”. Wind simulations may be one small part of finding the optimal structural and zoning solution to avoid heat island at all. The simulation of wind also means to visualize wind pressure and to detect undesired turbulences. The authors made good experience with Lattice-Boltzmann cellular automaton for performing calculations of wind direction (Wurzer et al. 2012).

## 5. Discussion

The web-based 3D visualization of rezoning is a first step to allow the laypeople to read and understand proposed changes on land-use and zoning plans. Proposed changes can “easily” be implemented (by hand or algorithmically) and serve as alternatives for later comparison. At this point, the question arises: who is able to implement such alternatives and in what form. For the moment, the application uses the coordinate-system of the City Surveyor Vienna (which enables a consistent import of different digital maps - from the terrain to the buildings). All components including maps and buildings (and alternatives) are loaded in the file format .3ds, which is a common format used by the Autodesk 3ds Max 3D software. It retains the essential geometry, texture and lighting data. The advantage lies in its popularity as exchange format. However, one has to be able to create such a .3ds file and to place it on the right coordinates in the system. Therefore, one of the future questions deals with the implementation of a simple 3D drawing plug-in. This will allow untrained users to delete and draw simple building shapes. The other implementation of algorithmically based alternatives is even more difficult. The idea here is to implement (parts of) the building regulation, in order to find good and valid solutions. Good solution also means to define parameters that characterize a “good” solution. Since both implementations (by hand and algorithmically) require knowledge, “easily” refers to the data exchange by a trained person. So, for the moment, alternatives are hardcoded and selectable by a dropdown menu. This allows the user to switch through different scenarios. The benefit lies therefore in the comparability by the layperson and the simplicity in the data exchanged by a trained person (planner).

FLÄVIZ is a good basis for simulations acting on such variations in order to verify them with respect to hard facts (such as solar radiation, shadowing, viewing and so forth). The main advantage of the simulation model is the experiment in a non-existing environment instead of an already built-one: Paper is patient the environment is not! As mentioned in the introduction, FLÄVIZ addresses three groups of interest: investors (accomplish profitable investments), local residents (ensure quality of living) and the authority (solve the lack of housing). If citizen participation is desirable in the rezoning process (as it is propagated in many European cities), then, at first, a common level of understanding is necessary. This can be achieved by providing quality features based on calculable analysis (which means objectivity). That means, with simulation analysis, on the one hand citizens get a deeper understanding of the plan, and on the other hand investors can argue on facts (to reassure the residents). And, there is yet another advantage: the authority can test alternatives beforehand (before investors come into play): to

answer “what if” questions.

Local decision-makers already have the possibility of using commercial software that includes analysis tools for urban planning. E.g., ArcGIS Pro allows evaluating the shadow impact of proposed buildings on the surrounding. This is important in order to determine the additional shadow impact of a proposed development on a neighboring public park or school playground for any day in the year. [06] Some cities also provide a solar potential cadastre in order to display the energy potential of roof areas (energy potential affects the value of the property). However, this potential may change due to rezoning. Real estate appraisers may also be interested to determine visibility (to and from the building) in order to estimate the value of a proposed development. [07] For all of these considerations, the advantage of simulation lies in a quantitative and transparent assessment of the property in general (and of the effects on existing buildings/property in particular). However, available software so far implements only a few basic analysis tools. Last but not least, the relevance of the proposed simulation lies in a verifiable calculation, especially when different interests collide: diminish/prevent heat islands based on larger green areas (or the small inventions such as green facades) versus investment. Only calculations will show the real impact.

## 6. Outlook

Assuming that simulation models for many different factors are incorporated into the web application (shading, viewing, flooding, and so on) the question arises how they are weighted. In short: What counts more, e.g. shading or viewing? This is a question, the authors will deal with in the future. Another aspect concerns the input and output of the simulation models mentioned before, since planning issues and their evaluation often deals with fuzzy terms. This means to interpret the input and the output (in the ideal case turning it into a “comparable” number). Moreover, the implementation of other simulation models (apart from wind) will also be addressed in future work. Beside climate, described in this paper, other possible aspects concern 1) travel times, which deals with circulation, transport infrastructure and has influence on urban sprawl, 2) visibility to and from the site, which influences orientation in the city and well-being (especially if nature comes into play), 3) solar radiation and shading, which influences possible solar yield and natural cooling in the summer and 4) neighborhood context including 4a) social aspects, which goes hand in hand with demography or crime rate and 4b) noise and pollution, which may make costly noise protection walls obsolete.

In future work, it should be possible to generate possible zoning plan changes automatically, which are analyzed and simulated in the existing contexts. They can be stored on a web server and shared via link. The latter would allow discussions about different (previously calculated) alternatives.

## References

- “[01] Open Government Data (OGD)” : [01]. Available from <[open.wien.gv.at](http://open.wien.gv.at)> (accessed 5th September 2019).
- “[02] ArcGIS Urban” : [02]. Available from <[www.esri.com/en-us/arcgis/products/arcgis-urban/overview](http://www.esri.com/en-us/arcgis/products/arcgis-urban/overview)> (accessed 6th November 2019).

- “[03] Parametric Urban Design Software Tool” : [03]. Available from <modelur.eu> (accessed 6th November 2019).
- “[04] Preconfigured solutions for planning and community development” : [04]. Available from <www.esri.com/en-us/industries/state-local-government/solutions/community-development> (accessed 6th November 2019).
- “[05] Geodata Viewer of Vienna” : [05]. Available from <wien.gv.at/ma41/datenviewer/public/> (accessed 5th September 2019).
- “[06] ARCGIS Pro: Shadow Impact Analysis” : [06]. Available from <solutions.arcgis.com/local-government/help/shadow-assessment/> (accessed 29th January 2020).
- “[07] Visibility Assessment Event” : [07]. Available from <solutions.arcgis.com/local-government/help/visibility-assessment/> (accessed 29th January 2020).
- Arpornwicharnop, K., Pinyo, J. and Pizzanu, K.: 2007, Simulation Software Development for Urban Landscape Possibility Analysis, *Proceedings of CAADRIA 2007*, Nanjing (China) .
- Bai, N., Ye, W., Li, J., Ding, H., Pienaru, M.-I. and Bunschoten, R.: 2018, Customised Collaborative Urban Design - A Collective User-based Urban Information System through Gaming, *Proceedings of eCAADe 2018; Vol. 1*, Lodz (Poland), 419-428.
- Bauordnung, W.: 2018, *Bauordnung für Wien, LGBI 11/1930 idF 71/2018*, -, Vienna (Austria).
- Österreichisches Institut für Bautechnik, R.: 2019, *OIB-Richtlinie 3: Hygiene, Gesundheit und Umweltschutz*, Österreichisches Institut für Bautechnik, Wien (Austria).
- Kellett, R. and Girling, C.: 1998, Informing Public Participation in Neighborhood Scale Planning and Design, *Fourth Design and Decision Support Systems in Architecture and Urban Planning Maastricht, the Netherlands*, Maastricht (Netherlands).
- Lau, K.H. and Kam, B.H.: 2005, Cellular Automata Model for Urban Land-Use Simulation, *Environment and Planning B: Planning and Design*, **32**, 247-263.
- Lorenz, W.E. and Wurzer, G.: 2016, Flying Bricks - Algorithmic Design Studio, *Proceedings of eCAADe 2016, Vol. 1*, Oulu, 205-212.
- Lorenz, W.E. and Wurzer, G. 2015, NetLogo und Voxelisierung, in W.E. Lorenz, G. Wurzer and S. Swoboda (eds.), *flying bricks*, TUWien | Digital Architecture & Planning, Vienna, 9-18.
- Matthews, R.B., Gilbert, N.G., Roach, A., Polhill, J.G. and Gotts, N.M.: 2007, Agent-based land-use models: a review of applications, *Landscape Ecology*, **22**(10), 1447-1459.
- Moeckel, R., Llorca Garcia, C., Moreno Chou, A.T. and Okrah, M.B.: 2018, Trends in integrated land use/transport modeling: An evaluation of the state of the art, *Journal of Transport and Land Use*, **11**(1), 463-476.
- Moeckel, R., Schwarze, B., Spiekermann, K. and Wegener, M.: 2007, Simulating interactions between land use, transport and environment, *Proceedings of the 11th World Conference on Transport Research*, University of California at Berkeley.
- Schwarz, N., Kahlenberg, D., Haase, D. and Seppelt, R.: 2012, ABMland - a Tool for Agent-Based Model Development on Urban Land Use Change, *Journal of Artificial Societies and Social Simulation*, **15**(2)(8), 1-6.
- White, E.T.: 1983, *Site Analysis: Diagramming Information for Architectural Design*, Architectural Media Ltd, Tallahassee, Florida (USA).
- White, R., Engelen, G., Uljee, I., Lavalle, C. and Erlich, D.: 2000, Developing an Urban Land Use Simulator for European Cities, *Proceedings of the 5th EC-GIS Workshop*, Stresa (Italy), 179-190.
- Wilensky, U.: 1999, *NetLogo*, <http://ccl.northwestern.edu/net-logo>, Center for Connected Learning and Computer-Based Modeling, Northwestern University, Evanston, IL. (USA).
- Wurzer, G., Coraglia, U.M., Pont, U., Weber, C.h., Lorenz, W.E. and Mahdavi, A.: 2019, A Cell-Based Method to Support Hospital Refurbishment, *Applied Mechanics and Materials*, **887**.
- Wurzer, G., Lorenz, W.E. and Popov, N.: 2012, Meeting Simulation Needs of Early-Stage Design through Agent-Based Simulation, *Proceedings of eCAADe 2012*, Prague, 613-620.

# SPATIAL CHARACTERISTICS ANALYSIS OF URBAN FORM AT THE MACROSCALE BASED ON LANDSCAPE PATTERN INDICES

JUELUN ZHOU<sup>1</sup> and ZIYU TONG<sup>2</sup>

<sup>1,2</sup>*School of architecture and urban planning, Nanjing University, China*

<sup>1</sup>*mg1836032@smail.nju.edu.cn* <sup>2</sup>*tzy@nju.edu.cn*

**Abstract.** Spatial characteristics are significant for urban form studies. Because quantifying the urban form at the macroscale is difficult, most of the relevant studies neglect or simplify the diversity of urban built areas. Local climate zone (LCZ) classification systems can transform macro urban form into a theme map composed of different LCZ classes, and such LCZ maps represent an effective urban form mapping technique, especially for built areas. However, this method still fails to provide a quantitative representation of the spatial characteristics. In this paper, the LCZ map is treated as a matrix composed of different patches and landscape pattern indices are applied to quantify the urban form. Taking 8 Chinese cities as case studies, the results show that 4 landscape scale indices and 4 class scale indices can effectively quantify the spatial characteristics of the urban form, including the area, shape, aggregation, and diversity. The quantitative spatial characteristics can provide a reference for urban design and management.

**Keywords.** Landscape pattern indices; Local Climate Zones (LCZ); urban form.

## 1. Introduction

At the macroscale, urban form is classified into grids based on physical indicators, and the spatial characteristics of these grids (such as the number, shape and layout) are influenced by the human activity and urban environment and effect of urban social, economic and ecological factors (Jia et al., 2019; Lu, 2015). In current research, the spatial characteristics of urban form at the macroscale are quantified by a series of landscape pattern indices originating from ecology. The object of the landscape pattern indices is a patch, an area with the same continuous class of land use. Landscape pattern indices have three calculation scales: landscape, class and patch (Figure 1). These 3 scales separately reflect the spatial characteristics of the patches of the whole landscape, the patches of each landscape class and each individual patch. The landscape pattern indices can be simultaneously divided into 6 series of descriptive metrics: area, shape, aggregation, diversity, contrast and core area. The first four are independent of the buffer area and are selected in this paper (McGarigal et al., 2015).

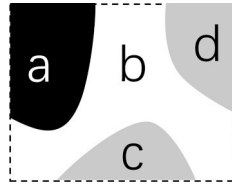


Figure 1. A landscape with 4 patches (a, b, c, d) and 3 classes (black (a), white (b), gray (c, d)).

Although originally concentrated in the natural environment, the landscape pattern can be used to research the ecological processes and attributes of cities (Jia et al., 2019). First, from the perspective of urban size, the shape of patches in mega cities is complex and the shape of patches in small- and medium-sized cities is simple (Jia et al., 2019). Moreover, landscape pattern indices can reflect the spatial structure within the city. From urban to rural, the degree of landscape diversity presents an inverted-U-shaped curve, and its highest value is in urban fringes (Weng et al., 2007). Second, urban landscape pattern indices are also related to urban land surface temperatures (LSTs). At the landscape scale, LSTs are positively correlated with the complexity of the patch shape and the degree of urban landscape diversity, and negatively correlated with the degree of aggregation (Azhdari et al., 2018). At the class scale, the total area and patch size of cooling land, such as grassland and woodland, have an important impact on LSTs. In addition, a more dispersed cooling land corresponds to a weaker surface cooling effect while a more dispersed warming land corresponds to a weaker surface warming effect (Rhee et al., 2014; Yin et al., 2015). However, in the current research on urban landscape pattern indices, land types are divided into construction land, industrial land, agricultural land and ecological land, which is a simple classification scheme that neglects or simplifies the diversity of the morphological characteristics of the urban built zones.

In the field of meteorology, the LCZ classification system established by Stewart and Oke (2012) provides a more detailed description of urban building zones via classifying the height, density and size of buildings, effectively divides urban form into 10 urban built classes and 7 land cover classes by the physical indicators based on the heat island strength at the macroscale, and generates the LCZ grid map (Bechtel et al., 2019; Wang et al., 2018). Shi et al. (2019) studied the relationship between urban landscape pattern indices and urban air quality based on LCZ classification, and they found that the concentrated distribution of compact high-rise, compact midrise and open high-rise buildings will hinder the diffusion of pollutants and reduce air quality. Therefore, at the macroscale, using the urban LCZ map to calculate landscape pattern indices is effective and provides detailed information for identifying building zones and urban form spatial characteristics.

In this paper, a spatial study of urban form at the macro form is performed, we use the LCZ classification system to provide a detailed classification on built areas and use landscape pattern indices to quantify urban spatial characteristics. Analyzing indices at both the landscape and class scale can differentiate the spatial characteristics of different cities and test the efficiency of each index, thereby providing a reference for urban form spatial studies at the macroscale.

## 2. Method

### 2.1. STUDY CASES AND LCZ MAP GENERATION

This paper selects 8 Chinese cities as the study cases (Figure 2): 5 cities in East China (Shanghai, Nanjing, Hangzhou, Suzhou and Hefei), 2 cities in South China (Hong Kong and Shenzhen) and 1 city in Central China (Wuhan). Each city is a mega city or a large city, their urban population is in the top 10% of all Chinese cities in 2015 (Jia et al., 2019) and their GDP in the top 5% of all Chinese cities. The selected center areas of the cities are mainly plain areas with a high built density, and some of them include water areas, such as rivers or oceans.

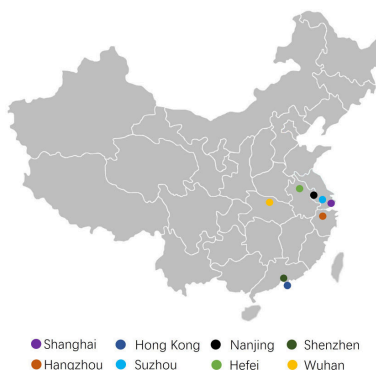


Figure 2. Locations of 8 cities in China.

Table 1. New LCZ classification – comparison with the original LCZ classification.

The new LCZ class	The original LCZ class	Land Use /Landscape Description
LCZ 1	LCZ 1	Compact high-rise (Mainly high-rise commercial office buildings and residential buildings)
LCZ 2	LCZ 2	Compact midrise (Mainly midrise residential buildings)
LCZ 3	LCZ 3, LCZ 7	Compact low-rise (Mainly the urban village area)
LCZ 4	LCZ 4	Open high-rise (Mainly high-rise residential buildings)
LCZ 5	LCZ 5	Open midrise (Mainly midrise residential buildings)
LCZ 6	LCZ 6, LCZ 9	Compact low-rise (Mainly villas and rural residence buildings and)
LCZ 8	LCZ 8, LCZ 10	Large low-rise (Mainly industrial plants and large public buildings)
LCZ A	LCZ A	Dense trees
LCZ B	LCZ B	Scattered trees
LCZ C	LCZ C	Bush scrub
LCZ D	LCZ D	Low plants
LCZ E	LCZ E	Bare rock or paved (Mainly Parking lot and square)
LCZ F	LCZ F	Bare soil or sand
LCZ G	LCZ G	Water

Based on the LCZ classification standards established by Stewart and Oke, the physical indicators of some grid zones in this study fall between the values of the two original classes; thus, to adapt the study cases, this paper renames the LCZ types according to 7 built classes and 7 land cover classes (Table 1).

Landsat 8 image data are used as the data source, and training areas are selected according to the new LCZ standards throughout the selected cities in Google Earth. Subsequently, local climate zone classification is performed to generate an LCZ map with a resolution of 100 m\*100 m using SAGA software version 7, a geographic information system software developed by the Dept. of Physical Geography in Hamburg. Then, a 5 km\*5 km urban center area in the LCZ map is identified for each city (Figure 3).

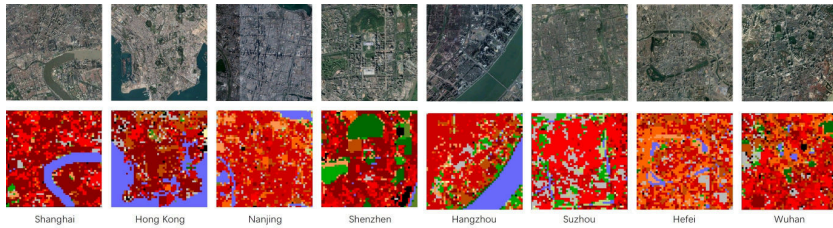


Figure 3. Satellite and LCZ map of each urban center.

## 2.2. CALCULATION SCALES AND INDICES SELECTION OF THE LANDSCAPE PATTERN INDICES

Fragstats software version 4 developed by McGarigal and Marks is used to analyze the landscape pattern indices of categorical maps. The software calculates the landscape indices of the LCZ maps by identifying the same continuous LCZ class grids as patches. The calculation scales include the landscape scale and the class scale. At the landscape scale, there are two sets of data. First, we calculate the indices that include all LCZ classes, which are called the all landscape pattern indices (with the suffix -(L)), reflecting the spatial characteristics of the entire urban center. Second, with 7 LCZ land cover classes as the background and 7 LCZ built classes as the objects, we calculate the indices called the built landscape pattern indices (with the suffix -(B)), reflecting the spatial characteristics of the building area. At the same time, the two sets of data are compared to reflect the characteristics of land cover classes, such as water and vegetation. For index selection, to avoid data redundancy, the dependent variables of each selected index are not identical. Referring to previous research and considering the study size and land use classification differences, this paper selects 5 landscape scale indices and 6 class scale indices from 4 basic metrics (Table 2).

## 3. Results

### 3.1. LANDSCAPE SCALE

As described in subsection 2.2, each index calculates the all landscape data and the built landscape data (Figure 4). AREA\_MN indicates the average area of patches in the landscape. In the all landscape, AREA\_MN(L) is [4.7 ha, 9.3 ha] and Shanghai has the largest average patch area. Compared with the all landscape and built landscape areas, the changes in Shanghai, Nanjing, Shenzhen, Hangzhou, Hefei and Wuhan are within 0.5 ha, and the built patch average area in Suzhou is

1.4 ha larger than that of the all landscape area. AREA\_CV indicates the area difference in patches in the landscape. In the all landscape area, AREA\_CV(L) is [226, 1093]; the patch area difference in Nanjing is the largest; and the area difference in Hefei and Wuhan is small. The AREA\_CV changes between the all landscape and built landscape areas are less than 87.

Table 2. Selected landscape pattern indices.

Index	Description Aspect	Meaning	Formula (Kevin et al.,2015)
The landscape scale			
AREA_MN	Area	Average of area for patches in the landscape	$AREA\_MN = \frac{\sum_{k=1}^n a_n}{10000n}$
AREA_CV	Area	Coefficient of variation of area for patches in the landscape	$AREA\_CV = \frac{\sqrt{\frac{\sum_{k=1}^n (a_n - AREA\_MN)^2}{n}}}{AREA\_MN}$
SHAPE_AM	Shape	Area weighted average of the shape index (SHAPE) for patches in the landscape	$SHAPE\_AM = \frac{\sum_{k=1}^n (a_n \frac{0.25p_n}{\sqrt{a_n}})}{\sum_{k=1}^n a_n}$
ENN_AM	Aggregation	Area weighted average of the Euclidean nearest-neighbor distance (ENN) for patches in the landscape	$ENN\_AM = \frac{\sum_{k=1}^n (a_n h_n)}{\sum_{k=1}^n a_n}$
SHEI	Diversity	Shannon's Evenness Index in the landscape	$SHEI = -\frac{\sum_{i=1}^m (P_i \ln P_i)}{\ln m}$
The class scale			
PLAND	Area	Area percentage of landscape for a certain class	$PLAND = P_i$
SHAPE_AM	Shape	Area weighted average of SHAPE for patches in a certain class	$SHAPE\_AM(i) = \frac{\sum_{k=1}^{ij} (a_{ij} \frac{0.25p_{ij}}{\sqrt{a_{ij}}})}{\sum_{k=1}^{ij} a_{ij}}$
CIRCLE_AM	Shape	Area weighted average of the related circumscribing circle for patches in a certain class	$CIRCLE\_AM(i) = \frac{\sum_{k=1}^{ij} [a_{ij} (1 - \frac{a_{ij}^2}{a_{ij}^2})]}{\sum_{k=1}^{ij} a_{ij}}$
PLADJ	Aggregation	Percentage of like adjacencies for grids in a certain class	$PLADJ = (\frac{g_{ii}}{\sum_{k=1}^m g_{ik}})(100)$
ENN_AM	Aggregation	Area weighted average of ENN for patches in a certain class	$ENN\_AM(i) = \frac{\sum_{k=1}^{ij} (a_{ij} h_{ij})}{\sum_{k=1}^{ij} a_{ij}}$
IJI	Aggregation	Interspersion and juxtaposition index for patches in a certain class	$IJI = \frac{-\sum_{k=1}^m l(\frac{e_{ik}}{\sum_{k=1}^m e_{ik}}) \ln(\frac{e_{ik}}{\sum_{k=1}^m e_{ik}})}{\ln(m-1)}$

$n$ = the number of patches in the landscape;  $m$ =the number of classes in the landscape; $a_n$ =the area of patch\_  $n$ , the unit is  $m^2$ ;  $h_n$ =the closest distance of patch\_  $n$  to the same class patch, calculating the center distance of the boundary patches in the two patches, the unit is  $m$ ;  $P_i$ = proportion of area of class\_  $i$  in the landscape;  $ij$ = the number of patches in class\_  $i$ ;  $a_{ij}$ =the area of patch\_  $ij$ , the unit is  $m^2$ ;  $p_{ij}$ = the perimeter of patch\_  $ij$ , the unit is  $m$ ;  $a_{ij}^2$ = the circumscribed circle area of patch\_  $ij$ , the unit is  $m^2$ ;  $g_{ik}$ =the number of class\_  $k$  grids surrounding class\_  $i$  grids;  $g_{ii}$ =the number of class\_  $i$  grids surrounding class\_  $i$  grids;  $h_{ij}$ =the closest distance of patch\_  $ij$  to the same class patch, calculating the center distance of the boundary patches in the two patches, the unit is  $m$ ;  $e_{ik}$ = the edge length between class\_  $i$  patches and class\_  $k$  patches, the unit is  $m$ .

SHAPE indicates the patch shape complexity, and its value is  $[1, +\infty)$ . When the patch is a square, SHAPE=1. In addition, a larger SHAPE indicates a more irregular patch. In the all landscape area, SHAPE\_AM(L) is [2.0, 5.6]; the patch shape of Shanghai and Nanjing is complex because of the high patch average area in Shanghai and the high patch area difference in Nanjing; and the shape is the most



regular in Hefei and Wuhan. A comparison between the all landscape and built landscape areas indicates that the patches are more irregular in the built landscape than the all landscape area, while Hefei and Wuhan present the smallest difference, at less than 0.1.

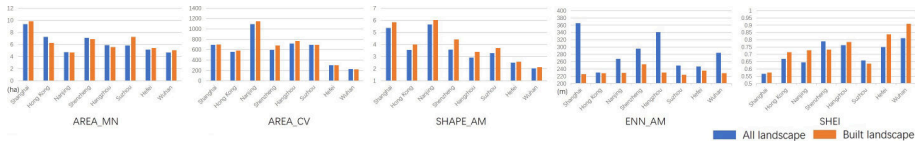


Figure 4. Landscape pattern indices for each urban center at the landscape scale.

ENN is the distance from a patch to the nearest same class patch. With the 100m grid size, the range of ENN is  $[200\text{m}, +\infty)$ . In the all landscape, ENN\_AM(L) is  $[230\text{m}, 366\text{m}]$ . The water and greening patches are scattered and small in the urban functional area and large in the nature area, and thus have larger ENN and area values than other classes. As a result, ENN\_AM(L) has a great relationship with water and greening. Shanghai and Hangzhou have high ENN\_AM(L); either city has a large independent water patch (the Huangpu River in Shanghai and the Qiantang River in Hangzhou), while their nearest water patches are small and scattered. Hong Kong has the lowest ENN\_AM(L) with close large water patches. In the built landscape, ENN\_AM(B) is  $[224\text{ m}, 253\text{ m}]$ ; Shenzhen is the highest, with a high area proportion of distributed patches.

SHEI describes the equitability of the area proportion of each class in the landscape, and the range is  $[0, 1]$ . When SHEI=0, the landscape contains only one landscape class; when SHEI=1, the areas of classes are the same. In the all landscape area, SHEI(L) is  $[0.57, 0.82]$  and Shanghai has the lowest class area distribution equitability. A comparison between the all landscape and built landscape areas indicates that the lowest change occurs in Shanghai at 0.01 while the largest change occurs in Wuhan at 0.10; thus, the landscape equitability of Wuhan is more obvious. At the landscape scale, although the description aspects are different, SHAPE\_AM is positively associated with AREA\_MN and AREA\_CV in the urban center. As a result, 4 indices (AREA\_MN, AREA\_CV, ENN\_AM, and SHEI) at the landscape scale can effectively quantify urban form.

### 3.2. CLASS SCALE

Nonexistent classes in each city are excluded from the statistical analysis (Figure 5). The meaning of SHAPE and ENN is provided in subsection 3.1. PLAND is determined by multiplying the area proportion by 100; and the distribution of PLAND is correlated with SHEI at the landscape scale. The highest value of PLAND is found for Shanghai's compact high-rise area (52.64). Shanghai has the most unevenly distributed class area with the lowest SHEI. The classes with the highest area proportion in each urban center are among the built classes; in Shanghai, Hong Kong and Shenzhen, the compact high-rise built class is the highest; in Nanjing, Hangzhou and Wuhan, the compact midrise class is highest; in Suzhou, the compact low-rise class is highest; and in Hefei, the open high-rise

class is highest. Except Hong Kong, Hefei and Wuhan, the area proportion of the highest class is greater than the second highest class by more than 20%. The proportion of Hong Kong's water area and Hefei's compact midrise are similar to that of the highest class. In Wuhan, the proportions of 2 high-rise classes, 2 midrise classes and the compact low-rise class are similar and the distribution of class area is the most even with the highest SHEI.

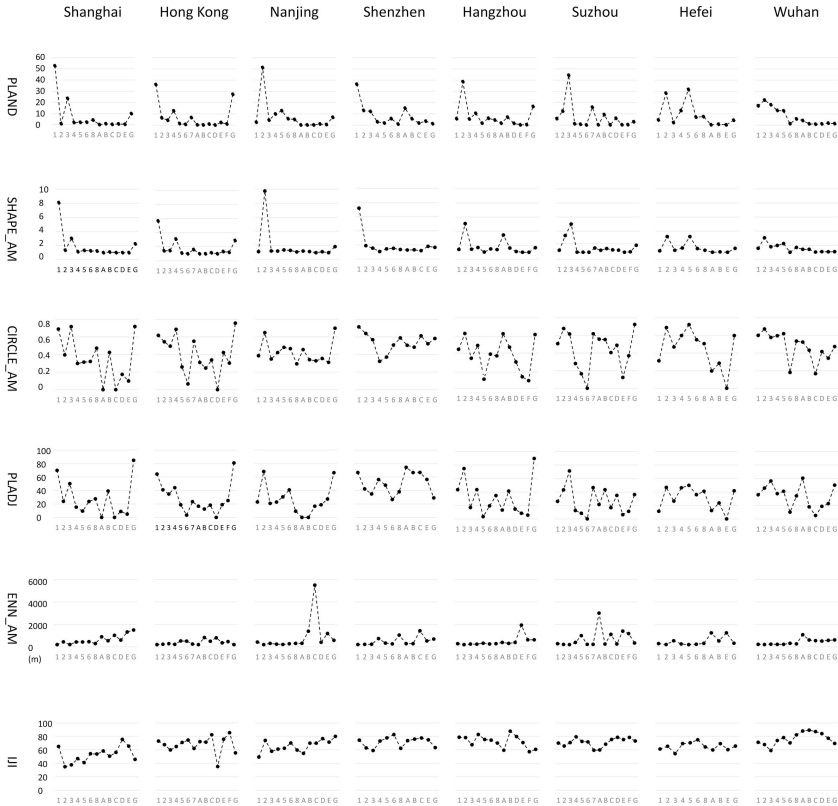


Figure 5. Landscape pattern indices of each urban center at the class scale.

The shape of the SHAPE\_AM graph is similar to that of PLAND. For most classes, the higher the area proportion is, the more irregular the patch shape is. In Shanghai and Nanjing, the patch shape is irregular at the landscape scale and the SHAPE\_AM of the highest area proportion class is greater than 8. In Wuhan and Hefei, the patch shape is regular at the landscape scale, the SHAPE\_AM of all classes is less than 4, and the average SHAPE\_AM value in Wuhan is the lowest.

CIRCLE expresses the similarity between a patch and a circle to indicate the compactness of the patch, and its value is [0, 1]. When CIRCLE=0, the patch is a circle, whereas a larger CIRCLE value indicates a more linear and elongated patch. In Fragstats, the CIRCLE value of the 1-grid patch is 0. The average CIRCLE\_AM of all classes in all cities is 0.44. In Shenzhen, the average

CIRCLE\_AM is the highest, and except for the open high-rise and open midrise classes, the CIRCLE\_AM values are larger than 0.44 because Shenzhen is mainly composed of classes with large patches and not 1-grid patches.

PLADJ is determined by calculating the average proportion of the same class grids around each grid in a class, and its value is [0, 100]. A higher PLADJ value corresponds to a more concentrated grid distribution. The data distribution of PLADJ in each city is similar to that of CIRCLE\_AM because a lower CIRCLE\_AM value corresponds to a greater number of 1-grid patches in the class and fewer similar grids around each grid. Moreover, when there are a few 1-grid patches, the value correlation between PLADJ and CIRCLE\_AM is poor, such as in Shenzhen. The average PLADJ of all classes in all cities is 31.7. In Shenzhen, because of the large-patch spatial characteristic and large area, the average PLADJ is the highest.

At the class scale, a high ENN\_AM value means that the patches are dispersed while a low ENN\_AM value has two cases: patches that are distributed equally and closely and patches that form closely clustered groups. In each city, ENN\_AM of the land cover classes is much higher than that of the built classes, which supports the finding that the all landscape ENN\_AM is mainly related to the land cover area. For the land cover classes, the bush shrub class of Nanjing, the dense tree class of Suzhou and the bare rock or paved class of Hangzhou are clearly dispersed. For the built classes (Table 3), the average ENN\_AM is 319 m. The open high-rise and large low-rise classes in Shenzhen and the open midrise clearly in Suzhou are clearly dispersed with ENN\_AM values that are 2-times higher than the average. In Wuhan and Hangzhou, the ENN\_AM values of 5 built class are lower than average; in the low ENN\_AM value cases mentioned above, the Wuhan patches distribution is the first and Hangzhou's is the other.

Table 3. ENN\_AM (m) of the built classes in each urban center.

CLASS	Shanghai	Hong Kong	Nanjing	Shenzhen	Hangzhou	Suzhou	Hefei	Wuhan
LCZ 1	200	202	429	204	284	287	295	224
LCZ 2	442	231	200	225	201	217	210	211
LCZ 3	206	284	309	236	248	202	542	242
LCZ 4	433	226	243	740	239	396	255	226
LCZ 5	432	529	218	337	322	998	203	224
LCZ 6	458	513	276	268	262	224	232	322
LCZ 8	290	252	306	1044	286	223	309	268

**Bold** means the value higher than 2 times of the average. Underline means the value less than the average.

IJI is used to measure the equitability of the patch edge length relative to other classes, and its value is (0, 100]; when IJI is close to 0, the patch is only contact with one other class; when IJI=100, patch edge length is equivalent between the patch class and the other classes and different class patches are concentrated. The average IJI of all classes in all cities is 67.9. In Wuhan, the average is the highest, meaning that the patches present the most equivalent contact with the other classes. In Shanghai, the IJI of 12 of 13 classes is less than 67.9, and the average is the lowest, meaning that that certain class patches present limited contact with the other classes and only contact specific classes

patches. At the class scale, SHAPE\_AM, ENN\_AM and PLAND can separately explain SHAPE\_AM, ENN\_AM and SHEI at the landscape scale; SHAPE\_AM and PLAND, CIRCLE\_AM and PLADJ present similar value distributions. As a result, 4 indices (PLAND, PLADJ, ENN\_AM and IJI) at the class scale can effectively quantify urban form.

#### **4. Conclusion**

This paper uses a detailed built classification scheme with the LCZ classification system and analyzes the landscape pattern indices of the urban center LCZ maps in 8 Chinese cities. The results show the urban form spatial characteristics of each city. Shanghai has the largest and most irregular patches and the most uneven area proportion of each landscape, and the layout shows an uneven length of each class in connection with other class; in addition, among each class, the compact high-rise class has the largest area with scattered water except for the Huangpu River. Hong Kong presents large water patches around land, the average area of land cover patches is much larger than that of built area, and the patch distances to the same class of the built class and the land cover class are similar; in addition, the compact high-rise and water classes have the largest area. Nanjing presents a smaller patch area but an irregular patch shape with large patch area differences, and the compact midrise class has the largest area. In Shenzhen, the large area-group characteristic leads to a high degree of grid aggregation and it also presents a large green area, and the compact high-rise class has the largest area. In Hangzhou, the Qiantang River is far away from the other small-area water patches; the number of the built classes with a concentrated distribution is the highest, and the compact midrise class has the largest area. In Suzhou, because of the historical and cultural protection, the study area is mainly of the compact low-rise class within the low-rise historical building class; the built patch area is much larger than that of the land cover area, and the equitability of the built class area is lower than that of the all landscape class. In Hefei, the patch area difference is small and the patch shape is regular and open high-rise and compact midrise classes have the largest area. In Wuhan, the patch shape and area present similar characteristics to that of Wuhan and the areas of high-rise, midrise and compact low-rise classes are similar and form the main city.

The analysis of each index shows that the urban form can be quantified based on different aspects. The shape indices are correlated with the area indices, with a larger area index at the landscape scale or a larger area proportion of most classes corresponding to a more irregular patch shape. In the landscape scale analysis, 4 indices (AREA\_MN, AREA\_CV, ENN\_AM, and SHEI) are effective and present clearly maximum values in all cities. However, the minimum AREA\_MN value is not clear. The built and the all area indices (AREA\_MN, ENN\_AM, and SHEI) can be used to compare the built and land cover areas, especially the ENN\_AM of the all landscape area, which mainly depends on the land cover area. In the class scale analysis, 4 indices (PLAND, PLADJ, ENN\_AM and IJI) are effective and can be used to differentiate each class and the city class construction. PLAND can quantify the area construction of each city, and PLADJ, ENN\_AM and IJI can differentiate aggregations based on grids, patch distances and patch edges.

The data distribution is similar between PLAND and SHAPE\_AM and between CIRCLE\_AM and PLADJ; however, the differences between these 2 pairs of parameters need further study.

To improve the accuracy of the landscape pattern indices for the LCZ map, further study is required. In the selected study zones, most of the indices are related to the size of the landscape, and whether comparisons can be performed between cities with different overall city area values is uncertain. The same selective square zones used in this paper might not contain all form information for a city and could reduce the accuracy of the urban form characteristics. For the studied indices, additional study cases are required to clarify the overall characteristics of each index and analyze the threshold values.

The urban form characteristic differentiation results and landscape pattern index values show that the LCZ classification system is suitable for macroscale studies of the spatial characteristics of urban form and can provide a reference for urban design, especially for built areas. In the future, the relationships between the LCZ landscape pattern indices and the urban climate, urban size and urbanization should be studied.

### Acknowledgments

This research was supported by National Natural Science Foundation of China (51578277) and Major Program of National Natural Science Foundation of China (51538005).

### References

- Azhdari, A., Soltani, A. and Alidadi, M.: 2018, Urban morphology and landscape structure effect on land surface temperature: Evidence from Shiraz, a semi-arid city, *Sustainable Cities and Society*, **41**, 853-864.
- Bechtel, B., Bechtel, P.J., Beck, C., Böhner, J., Brousse, O., Ching, J., Demuzere, M., Fonte, C., Gál, T., Hidalgo, J., Hoffmann, P., Middel, A., Mills, G., Ren, C., See, L., Sismanidis, P., Verdonck, M.L., Xu, G. and Xu, Y.: 2019, Generating WUDAPT Level 0 data – Current status of production and evaluation, *Urban Climate*, **27**, 24-45.
- Jia, Y., Tang, L., Xu, M. and Yang, X.: 2019, Landscape pattern indices for evaluating urban spatial morphology – A case study of Chinese cities, *Ecological Indicators*, **99**, 27-37.
- Lu, J.: 2015, Landscape ecology, urban morphology, and CBDs: An analysis of the Columbus, Ohio Metropolitan Area, *Applied Geography*, **60**, 301-307.
- McGarigal, K.: 2015, "FRAGSTATS HELP". Available from <<http://www.umass.edu/landeco/research/fragstats/documents/fragstats.help.4.2.pdf>> (accessed 30th August 2019).
- Rhee, J., Park, S. and Lu, Z.: 2014, Relationship between land cover patterns and surface temperature in urban areas, *GIScience & Remote Sensing*, **51**, 521-536.
- Shi, Y., Ren, C., Lau, K.K.L. and Ng, E.: 2019, Investigating the influence of urban land use and landscape pattern on PM2.5 spatial variation using mobile monitoring and WUDAPT, *Landscape and Urban Planning*, **189**, 15-26.
- Wang, T., Dong, J.J., Xu, S. and Tong, Z.: 2018, Comparative study of urban forms on macro scale, *The proceeding of the 26th International Conference on Geoinformatics*.
- Weng, Y.C.: 2007, Spatiotemporal changes of landscape pattern in response to urbanization, *Landscape and Urban Planning*, **81**, 341-353.
- Yin, C.Y., Shi, Y.S., Wang, H.F. and Wu, J.: 2015, Impacts of Urban Landscape Form on Thermal Environment at Multi-spatial Levels, *Resources and Environment in the Yangtze Basin*, **24**, 97-105.

# SPATIAL ELEMENTS OF COMMERCIAL STREETS AND PEDESTRIAN PERCEPTIONS VIA A MULTI-SCALE PERSPECTIVE

*An Analysis of Three Commercial Streets in the Old City of Guangzhou*

ZHEN ZHANG<sup>1</sup>, HONG WU DU<sup>2</sup> and YAN LI<sup>3</sup>

<sup>1,2,3</sup>*School of Architecture, South China University of Technology, Guangzhou, China*

<sup>1,3</sup>{1216820672|1559930506}@qq.com <sup>2</sup>philipdu@126.com

**Abstract.** After the large-scale construction of the city, the small-scale development has begun, which makes the optimization of the commercial street space more focused on the pedestrian perception experience of people. It can be seen that the spatial elements of the commercial street are closely related to the pedestrian perception of people. However, in the evolution of the old city of Guangzhou, due to the large-scale construction and road widening, the spatial scale is quite different. In addition, the space scale of the same commercial street also varies greatly in different historical periods. There are three types: large scale change, moderate scale change and small scale change, forming the diversity of spatial scale of the commercial street. Therefore, how to study the relationship between spatial elements of commercial street and pedestrian perception under the guidance of multi-scale has become the research value of this paper. The thesis selects three types of commercial street space and combines virtual reality technology to establish different commercial street scenes. Finally, through the virtual scene experience of interviewees, different commercial street space factors are scored, and then the coupling relationship is established to analyze the relationship between commercial street space factors and pedestrian perception.

**Keywords.** Multi-scale; Commercial street spatial elements; Pedestrian perception; Virtual Reality Simulation.

## 1. Research background

As a deeper content of urban substance form, the spatial scale is also an important basis for measuring urban characteristics. The disappearance of any level scale will cause the variation and disappearance of the commercial street space, which will have a very adverse impact on the continuation of urban characteristics. However, in the process of urban development, due to the continuous enhancement of human capacity for natural transformation and the failure of urban management and control, the scale of buildings in the old city is unimaginable, resulting in changes in the size of commercial streets at different levels. For example, some

commercial streets are large and wide, but the streets are too wide. Therefore, how to study the relationship between the space of commercial streets and the perception of pedestrians in various spatial scale environments has become an important topic in the spatial optimization of the old city (Figure 1).



Figure 1. A comparative picture of the old (left) and new (right) spatial scales in the old city of Guangzhou (Photo: Guangzhou Construction Archive).

## 2. Related literature research

### 2.1. RESEARCH ON STREET SPACE OF DIFFERENT SCALES

There are many types of research on the spatial elements of commercial streets in different dimensions. In urban design, the commercial street space is studied from three levels of city, block, and street according to different spatial dimensions. It is considered that if the commercial street space is closely related to the urban context, the spatial elements will become more and more complex and the spatial dimensions will be more and more diverse, consequently, the contents of the spatial elements of commercial streets are enriched (Zhang, 2010). Since the commercial street space is closely related to people's daily life, street space models can be established according to different levels of the spatial scale, and the space environment simulation of the place can be combined with green ventilation technology to provide the basis for the construction of commercial street spatial scene in this paper (Xiao & Lin, 2013). Furthermore, in the study of typical urban space, according to the spatial characteristics of inter-scale, for example, the comparison and analysis of Shenzhen's urban plan provide a good reference for the expansion of commercial street space elements (Luo, 2017). In the study of Kangbashi District, Ordos, it is believed that street spatial elements are closely related to human behaviour (Li, 2019). Nguyen-Ngoc et al (2015) explored how newly developed public spaces fail to address the needs of the public. Through the relevant researches, many papers have studied the street spatial elements from different spatial scales and provided relevant support and basis for the simulation of a commercial street space scene.

### 2.2. RESEARCH ON PEDESTRIAN PERCEPTION

In the research of related papers on pedestrian perception, the earliest research began in the 20th century with the research of environmental behaviour scholars in the field of architecture. Through the sequence of "space-perception-behaviour", the research on the pedestrian perception of people has been carried out.

Subsequently, many scholars study the relationship between pedestrian perception and street spatial environment. In the experiment of grouping urban design variables, the relationship between neighbourhood building environment and pedestrian behaviour elements are established. Combined with the related factors such as land mixed-use, suggestions for pedestrian space construction measures (Alfonzo, 2008) are put forward. This paper analyzes people's perception of pedestrian space in the street and explores the relationship between people's preference and space (Irvin et al, 2008) in smaller street spaces according to the choice of the pedestrian path and different people's preference for space. Through the review of this paper, the research on pedestrian perception depends more on street upon space to establish a connection, which makes it clear that there is a relationship between pedestrian perception and commercial street space. The major innovation of this paper is to simulate the scene space, establish the relationship between street spatial elements and pedestrian perception in the virtual environment, and realize the perception experience of human-computer interaction (Figure 2).

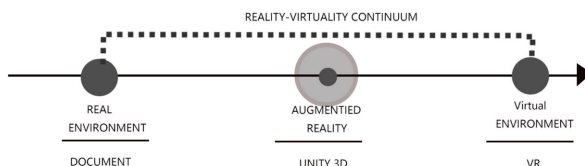


Figure 2. Virtual reality transmission process.

### 3. Research methods

Through the previous research and historical data review, the selected research objects involve different levels of street space scale, and the research has certain representatives. Subsequently, the commercial street space model is established, and the auxiliary VR technology is used as the technical support to realize the construction of human-computer environment interaction scene, and accordingly, the questionnaire is developed to record the psychological, physiological and behavioural changes of the interviewees. Analysis of their behaviour (López, 2007) determines the relationship between the spatial elements of commercial streets and pedestrian perception.

This paper is divided into three steps to construct the space scene of the commercial street. First and foremost, by combining with the spatial data of the commercial street, it establishes the SketchUp model. Furthermore, through the combination with the unity 3D, it constructs the scene and adds the corresponding environment settings (Handy, 1996). Last but not least, it allows different participants to be involved, experience the changes in the virtual street spatial scene, and record the changes of the interviewees' psychology and behaviour (Figure 3).



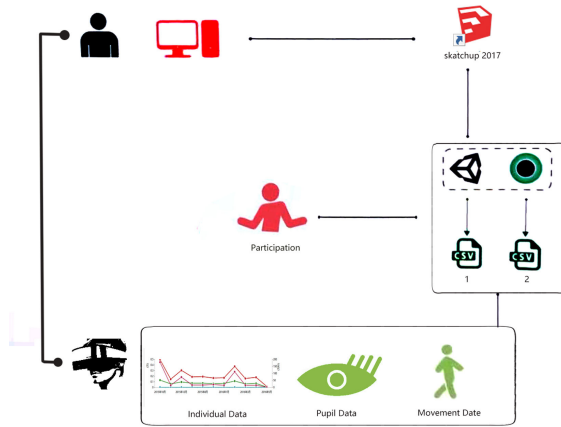


Figure 3. Research Framework .

#### 4. Case introduction

In the old city of Guangzhou, three commercial street spaces with different spatial scales are selected to study the spatial elements of the commercial street from the multi-scale perspective. Three different scales of commercial street space are the ‘Beijing Road Commercial Street’-space with traditional political, religious and cultural characteristics, the ‘Changdi Commercial Street’-space with characteristics of the Chinese republican area, and the ‘Zhuangyuanfang Commercial Street’-space with traditional cultural characteristics (Figure 4).

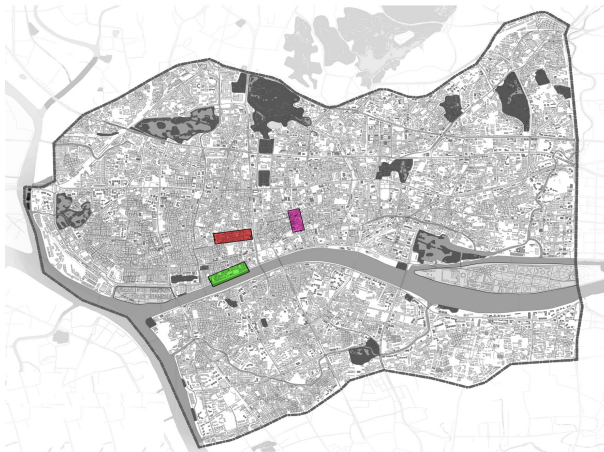


Figure 4. Location of three commercial street.

#### 4.1. BEIJING ROAD COMMERCIAL STREET SPACE

The spatial scale of Beijing Road Commercial Street varies greatly in different historical periods. For example, in the Qing Dynasty, the space of Beijing Road commercial street was called double door upper and lower street, which was the main commercial street in Guangzhou. During then, the width of the street space was about 10 meters, and there were two-story commercial buildings on both sides of the street. In the period of the Republic of China, due to the widening of roads and the construction of commercial streets dominated by arcades, arcades with three or four floors were formed. According to the review of the historical data, the width of streets and lanes rarely changed. The width of streets and lanes was controlled within the range of 2m to 6m. During that time, the height-width ratio of street space was about 1:1. In this paper, the spatial scale of the Beijing Road commercial street in different periods was studied. The comparative analysis is the basis of multi-scale commercial street space research (Figure 5).

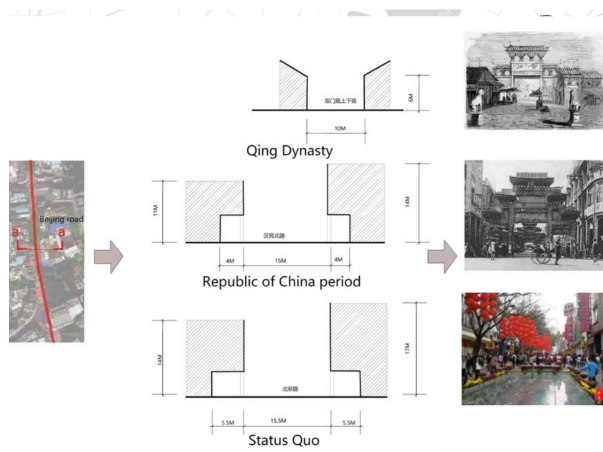


Figure 5. Spatial scale analysis of Beijing Road Commercial Street in different periods.

#### 4.2. SPACE OF CHANGDI COMMERCIAL STREET

As a representative of waterfront commercial street space, Changdi commercial street space has the characteristics of the Republic of China. In the historical evolution, the scale changes moderately. The width of the street is between 10m and 16m. Arcades are built on both sides of the street, with relatively large building scale, such as Aiqun building which contains 15 floors. The arcade is about 4.5m in width and the street is about 15m in width, making the street space narrow and high (Figure 6).

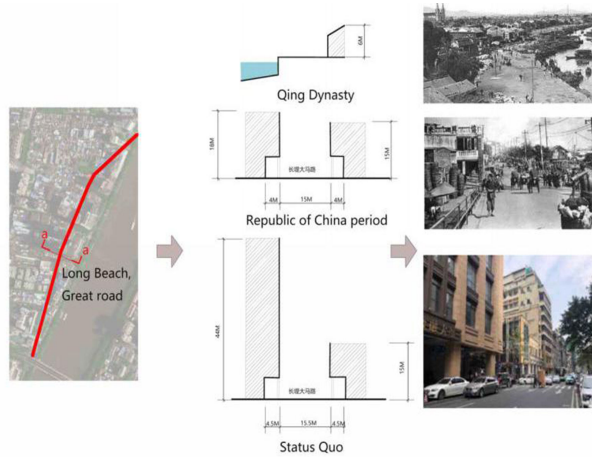


Figure 6. Spatial scale analysis of Changdi commercial street in different periods .

### 4.3. SPACE OF ZHUANGYUANFANG COMMERCIAL STREET

In the historical evolution of the space of the Zhuangyuanfang commercial street, it changes little in scale. The width of the street is about 6m and the buildings on both sides are mostly three floors, which represent most of the space scale in the street of the old city of Guangzhou and the scale is relatively pleasant (Figure 7).

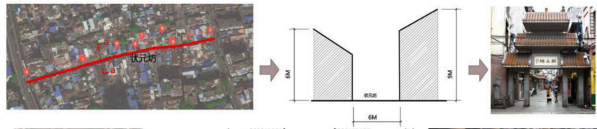











Figure 7. Spatial scale analysis of Zhuangyuanfang commercial street in different periods.

## 5. Research steps

### 5.1. MODEL ESTABLISHMENT

Three different types of commercial street space analysis make the characteristics of the commercial street space scene in different periods clear. First and foremost, the scene model is established through SketchUp, which provides the basis for the later research of pedestrian perception (Table 1).

Table 1. Commercial street spatial scene in different periods.

	Qing dynasty	Republic of China	Present situation
Beijing Road commercial street			
Changdi Commercial Street			
Zhuangyuan fang Commercial Street			

## 5.2. SCENE CONSTRUCTION AND REAL EXPERIENCE

In order to make the research more targeted and implementable, the virtual scene of the commercial street space is constructed. The research is mainly divided into three parts. First and foremost, the input of the scene is used to test the related objects (Gehl, 1996). Furthermore, it is used to establish a visual commercial street space and experience the virtual commercial street space, which mainly includes the perception evaluation of the scale, elements and satisfaction of the street space and the interview of the interviewees to deeply understand the interviewees' feelings on the commercial street space (Greenwald et al, 2001). Last but not least, it involves data processing. According to the interactive experimental data record of "human-machine environment", it analyzes the observed data, action capture data, expression recognition data, etc., as well as the collation of the relevant element data, establishes the relationship between the spatial elements of the commercial street and the pedestrian perception and puts forward the optimization strategy for the design of the commercial street space (Figure 8).



Figure 8. VR virtual scene construction .

## 5.3. SELECTION OF SPATIAL ELEMENTS OF COMMERCIAL STREETS

Due to the great difference in the spatial elements of the commercial street, the selected indicators are particularly important. To systematically evaluate all aspects of the commercial street space, especially how to quantify the spatial

environment of the commercial street, since different people have different feelings for the same environment which are totally different. While defining the objective indicators, there are likely to be deviations, such as the differences in the environment and the space. Therefore, this paper divides the relevant elements of commercial street space into two parts: on the one hand, the comprehensive objective elements of street space, such as whether to reach the commercial street space, public service facilities or other factors; on the other hand, the comprehensive perception elements of street space to better enhance the pedestrian perception experience, starting from the perception of urban residents in space, including the comfort degree of commercial street spatial environment and the management and operation elements, which are evaluated by the “behaviour perception” evaluation system (Figure 9).

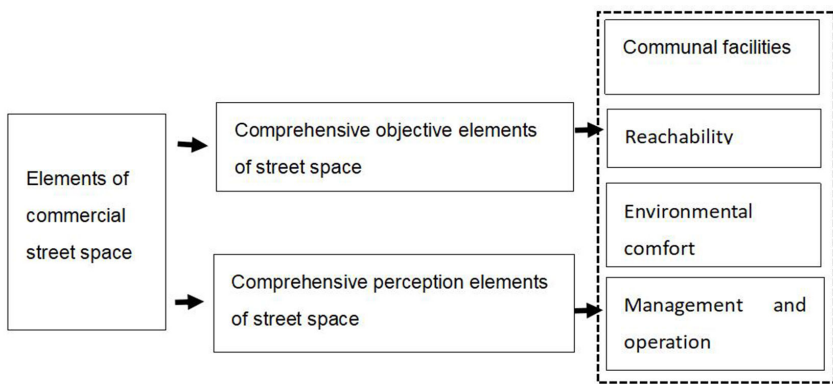


Figure 9. Spatial elements of Commercial Street .

#### 5.4. ESTABLISHMENT OF SPATIAL ELEMENT INDEX FOR COMMERCIAL STREET

Street spatial indicators are related to spatial environment level, location, layout mode, etc., and public facilities distribution quantity, service scope and other relevant indicators related to evaluation indicators which are extracted. According to the above classification of street space elements, it is made clear that “street space” is a place for different groups of people to recognize and study the space, analyze the living environment in-depth, and subsequently get the index elements and corresponding relationships at different levels (Table 2).

Table 2. Index composition of commercial street spatial elements.

First level index	Two level index
Communal facilities	Accessibility of health service facilities, surrounding supporting facilities
<u>Reachability</u>	Health service facilities, surrounding supporting facilities, facility accessibility road conditions, traffic mode, travel speed, traffic signs
Environmental comfort	Landscape sketch, environment comfort, space element, sight comfort
Management and operation	Environmental health maintenance level, greening maintenance level, facility operation maintenance level

In the above research, it is found that the commercial street space is the object of social evaluation in the research of environmental behavior and the street space is still the basic unit of urban space with clear scope and attributes to better reflect the availability of data. In society, from the perspective of human behavior characteristics, it is convenient to collect data through questionnaires and interviews for spatial units, to explore from the perspective of perception, to obtain the basic information required by typical market space, to establish corresponding indicator levels, and to form an evaluation system with different spatial levels and interdisciplinary intersection.

### 5.5. DISCUSSION

This paper introduces the preliminary research on the relationship between street spatial elements and pedestrian perception and clarifies the overall idea of the research. In the follow-up work, various people are invited to participate in the immersive experience and carry out the virtual experience. Moreover, participants are organized to come into the virtual reality, truly experience the changes of commercial street spatial elements. Correspondingly, a certain amount of data to complete the business research on the relationship between street spatial elements and pedestrian perception can be obtained and subsequently the related regression line equation can be established. Therefore, in-depth exploration can be conducted for the different commercial street space elements according to the coupling relationship. In the specific operation of the experiment, comparative experiments are divided into three groups, which are large scale evolution of commercial street space, moderate scale evolution of commercial street space and small scale evolution of commercial street space respectively. It also includes a comparative analysis of the same commercial street space in different periods to explore the relationship between the spatial elements of the commercial street and the pedestrian perception.

### 6. Conclusion

According to the previous research, under the virtual environment, the commercial street spatial scene is constructed and the commercial street spatial elements are defined meanwhile. In the virtual scene, the subjects are allowed to experience and pave the path for the next step. In addition, in the commercial street spatial scene, due to the diversity of selection factors, some elements will be overlapped, which increases the complexity of the article. In general, the research of this paper enriches the content of the commercial street space research.

## References

- Agrawal, A. W., Schlossberg, M. and Irvin, K.: 2008, How Far, by Which route and why? A Spatial Analysis of Pedestrian Preference, *Journal of Urban Design*, **13**, 81–98.
- Alfonzo, M., Boarnet, M. G., Day, K. and Anderson, C. L.: 2008, Te Relationship of Neighbourhood Built Environment Features and Adult Parents' Walking, *Journal of Urban Design*, **13**, 29-51.
- Gehl, J.: 1996, *The Life Between Buildings: Using Public Space*, Arkitektens Forlag, Copenhagen., **32**, 12-14.
- Greenwald, M. J. and Boarnet, M. G.: 2001, The Built Environment as a Determinant of Walking Behaviour: Analyzing Non-Work Pedestrian Travel in Portland, Oregon, *Center for Activity Systems Analysis, the University of California at Irvine*, **01**, 4.
- Handy, S.: 1996, Urban form and pedestrian choices: the study of Austin neighborhoods, *Transportation Research Record*, **1552**, 135 –144.
- Li, X. D.: 2019, Study on block size in Kang Bashi district of ordos, *Architecture and culture*, **10**, 57-58..
- Luo, J.: 2017, *Study on the evolution of urban plane pattern in Shenzhen based on multi-scale layers*, Master's Thesis, South China University of Technology.
- López, M. J. J. and Van Nes, A.: 2007, Space and Crime in Dutch Built Environments: Macro and Micro-Scale Spatial Conditions for Residential Burglaries and Thefts from Cars, *Proceedings, 6th International Space Syntax Symposium*, Istanbul Technical University., 14.
- Nguyen-Ngoc, M., Schnabel, M. A., Brand, D. D. and Moloney, J.: 2015, Use and Spatial Patterns of newly developed Public Squares in Urban Villages in Shenzhen, *Empowering Change: Transformative Innovations and Projects, 8th International Urban Design Conference*, Brisbane, 195-218.
- Xiao, Y. and Lin, H.: 2013, Study on the Spatial scale model of climate adaptability of Bamboo house in Guangzhou, *Southern architecture*, **02**, 82-86.
- Zhang, Y. I.: 2010, *Research on the scale of the commercial pedestrian block in the old city*, Master's Thesis, South China University of Technology.

# AUTOMATIC RECOGNITION AND SEGMENTATION OF ARCHITECTURAL ELEMENTS FROM 2D DRAWINGS BY CONVOLUTIONAL NEURAL NETWORK

YAHAN XIAO<sup>1</sup>, SEN CHEN<sup>2</sup>, YASUSHI IKEDA<sup>3</sup> and  
KENSUKE HOTTA<sup>4</sup>

<sup>1,2,3,4</sup>*Keio University, Japan*

<sup>1</sup>*yahanxiao@gmail.com* <sup>2,3</sup>*{cs0715|yasushi}@sfc.keio.ac.jp*

<sup>4</sup>*hottakensuke@keio.jp*

**Abstract.** The BIM modeling process is the most time-consuming aspect. This paper studies the possibility of applying the recognition and segmentation of architectural components by deep learning to assist automatic BIM modeling. The research has two parts: the first one is dataset preparing, that images with the labeled architectural components from an original CAD drawing are made for the network training, and second is training and testing, that a mature network which has been trained in hundreds of labeled images is used to make predictions. The utilization of the current study results is discussed and the optimization method as well.

**Keywords.** BIM; CAD drawings; Recognition and Segmentation; Convolutional Neural Network; Computer vision.

## 1. Background, related work, and meaning:

China's economic development in the past few decades has been very fast which is particularly obvious in the construction that sustainable urban development is required. While a digital model that contains all the information of a building or a project or even a city is a useful tool to achieve this goal. Therefore, building information modeling is not only needed for big new projects in core cities as it enables better regional planning, fire prevention, and disaster relief designing and so on, but also for modification projects as it contains the information like building's structure which is the main content in renovation mission.

In general, 3D modeling is a manual process (Horna, 2009) (Sigalov, 2017) whether according to the digital 2D of a new building or the remaining paper document of an old building, that consuming lots of time and labor. Then in this research, we used semantic segmentation technology in deep learning to recognize the architectural components in 2D drawings to assist automatic modeling.

Among the succeed automatic modeling research, lots of researchers have developed methods which are achieved by the algorithm for generating a 3D model from 2D drawings (including CAD and raster images) (Ren, 2018). In most cases, algorithms have been proposed and implemented in stand-alone toptype tools.



Only a few of them are accomplished within existing software that people who work in the AEC industry may already be familiar with, which still requires the collaboration of multiple tools (Lim 2018). However, those different methods have the similar framework of their processing structure and require some extra manual preparation work (Yin 2009), like transform the recognition target into a specific format, or clean up the 2D drawings and place the 2D geometry for different building elements onto separate layers (Lim 2018). Moreover, the common recognition target of 3D modeling is the standard 2D drawing, while the raster images are mostly for pattern, shape and topology-based space detection, which means the designing process is finished before the 3D modeling process.

The meanings of this research are:

1) It does not need to extract additional features such as grids lines and dimensions but be able to get good results directly through repeated data learning and image training.

2) it has a strong anti-interference ability and can better distinguish elements from the background automatically.

3) the model is light and more easily be applied to the different styles of drawings.

Experiments show that the convolutional neural network can effectively identify the more important architectural elements in CAD drawings and can segment them from irrelevant information, which can greatly save manpower to process CAD drawings. While the detection accuracy depends on the size and quality of the training set, and the training times as well.

## 2. Methodology

Deep learning is part of a broader family of machine learning algorithms that are based on learning data representations. It creates a more abstract high-level representation of attribute categories or features by combining low-level features to discover distributed features within data. In deep learning, a Convolutional neural network (CNN) (Geng, 2017) is the basis of image recognition that can distinguish the object in an image by learning the features and be commonly applied to analyzing visual imagery. They have applications in image and video recognition, self-driving systems (Siam, 2017), image classification, medical image analysis (Ronneberger 2015), and natural language processing. A convolutional neural network consists of an input and output layer, as well as multiple hidden layers, a series of convolutional layers with filters that process the feature data. A hidden layer has an activation function layer, commonly a RELU layer, and is subsequently followed by additional convolutions such as pooling layers. The semantic information passing through each hidden layer from the input to the output where the objects are categorized. Then by calculating the error or the loss between the predicted value and real value, the adjustment will be fed back from the last layer backward layer by layer to update the parameters. The forward process and the backward process is repeated until the whole model converge and a trained mature network is obtained. For detection tasks, the CNN network works well, but not competent for positioning tasks since it uses the bounding box for

detection and the size of the output image is changed.

Jonathan Long et al launched a new network in 2014 called fully convolutional network (FCN), a supervised deep learning network, which uses a convolutional neural network to transform image pixels to pixel categories. Unlike the convolutional neural networks, and FCN transforms the height and width of the intermediate layer features map back to the size of input image through the transposed convolutional layer which is basically another network but now with all convolution and pooling layers reversed so that the predictions have a one-to-one correspondence with the input image in spatial dimension. Given a position on the spatial dimension, the output of the channel dimension will be a category prediction of the pixel corresponding.

In this study, the outline and the categories of the elements on 2D drawings were obtained by the fully convolutional network. Elements on the floor plan, as the main target, were classified into 5 construction categories: wall, window, door, column, and stairs. Components' labels are attached manually on these 5 different elements on every training drawing. 300 planer drawings are trained and the parameters of the previously established deep learning network are adjusted during the process. Both the training and testing of the elements' classification and positioning were at the pixel level.

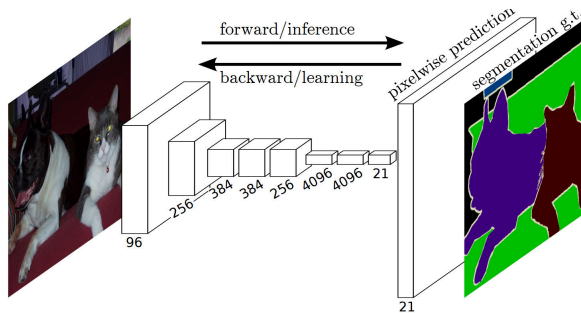


Figure 1. Segmentation network (from FCN paper).

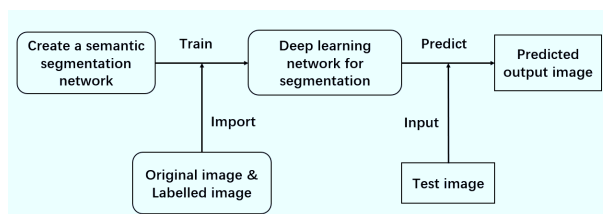


Figure 2. Research process.

### 3. Experiment

#### 3.1. IMAGE PREPARATION

To train an FCN network and get as much as accurate as possible, a suitable collection of images and the corresponding collection of pixel-labeled images are necessary.

A pixel-labeled image is an image in which every pixel value represents the categorical label of that pixel. In this research, we used a tool called label-me to segment images manually into 5 basic architectural components in 2D drawings: wall, door, window, stairs and column to get prepared. The label of the same components are given the same color, and the background label is black. Different types of buildings are included: residential buildings, education institutes, commercial buildings, and business buildings. In addition, the original images were standard black and white 2D print style which is better for training, and the size of each training image was unified to 1600\*1280 for the same reason, while the prediction accuracy will not be affected by this. At the last step, both 300 original images and their labeled mask images were prepared.

Colour	Representation
Yellow	Door
Green	Window
Red	Wall
Blue	Column
Purple	Stairs
Black	Background

Figure 3. Definition of the label color.

```
In[4]: VOC_COLORMAP = [[0, 0, 0], [128, 0, 0], [0, 128, 0], [128, 128, 0],
[128, 0, 128], [0, 0, 128]]
VOC_CLASSES = ['background', 'window', 'door', 'wall', 'column', 'stair ']
```

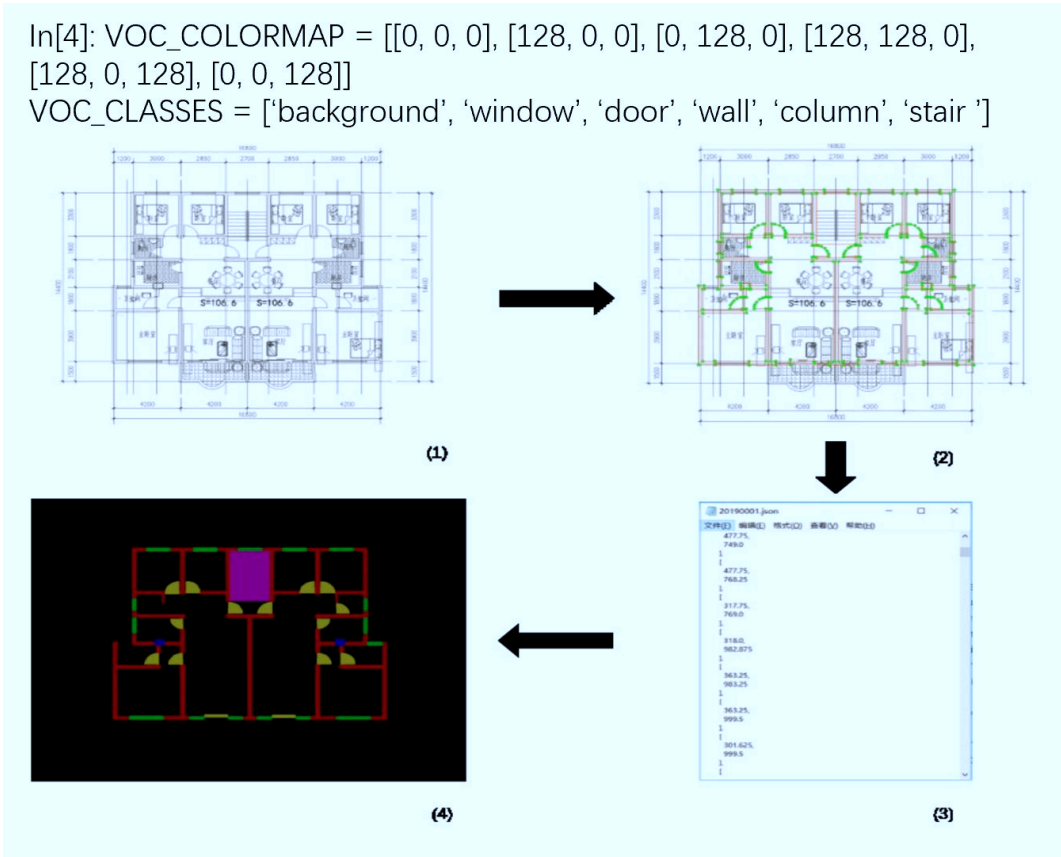


Figure 4. Dataset preparation.

### 3.2. SEMANTIC SEGMENTATION NETWORK BUILDING

Transfer learning is a machine learning method where a model developed for a task is reused as the starting point for a new model on a second task since deep convolutional neural network (He, 2016) models usually take days or even weeks to train on very large datasets. And it has three potential benefits:

- 1) Higher start. The initial skill (before refining the model) on the source model is higher than it otherwise would be.
- 2) Higher slope. The rate of improvement of skill during the training of the source model is steeper than it otherwise would be.
- 3) Higher asymptote. The converged skill of the trained model is better than it otherwise would be.

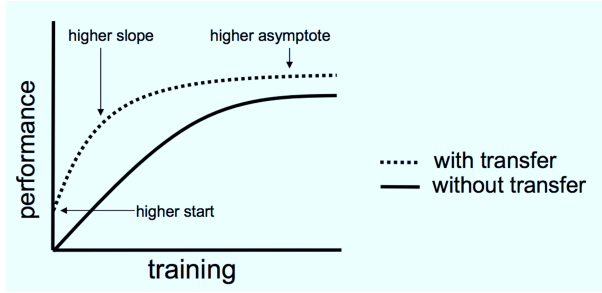


Figure 5. The learning rate of the transfer learning.

Therefore, a way to short-cut the training process is to reuse the model weights from a pre-trained model that was developed for the standard computer vision benchmark dataset. In this research, we used ImageNet and Residual Networks (He, 2016) to get a faster fitting rate and a mature FCN network as the basis.

Then we adjusted the parameters of the convolutional layers by supervised learning to figure out the labelled image. Supervised learning is the machine learning task of learning a function that maps an input to an output based on example input-output pairs. It infers a function from labeled training data consisting of a set of training examples. A supervised learning algorithm analyzes the training data and produces an inferred function, which can be used for mapping new examples.

After obtaining a mature FCN network, the feature map is available as well. Then it is up-sampled to obtain the same size as the input image, also the classification result is restored to the original image at the end.

### 3.3. SEMANTIC SEGMENTATION NETWORK TRAINING

The dataset of prepared original images and their paired labeled images were input into the semantic segmentation network (Liu, 2018) so that the training can be started.

Given an input of height and width of 320 and 480 separately, the forward computation of net will reduce the height and width of the input to 1/32 of the original. Then, transform the number of the output channels to the number of 6 different categories through the 1\*1 convolution layer. Finally, it needs to magnify the height and width of the feature map by a factor of 32 to change them back to the height and width of the input image. Recall the calculation method for the convolution layer output shape. Because  $(320-64+16*2+32)32 = 10$  and  $(480-64+16*2+32)32 = 15$ ,

$$\left[ \frac{Nh - Kh + Ph + Sh}{Sh} \right] \times \left[ \frac{Nw - Kw + Pw + Sw}{Sw} \right]. \quad (1)$$

The input shape is  $Nh * Nw$ ;

The convolution kernel window shape is  $Kh * Kw$

The total padding rows and columns are  $Ph$  and  $Pw$ ;

The stride of the height is  $Sh$ , and the width is  $Sw$ .

then construct a transposed convolution layer with a stride of 32 and set the height and width of the convolution kernel to 64 and the padding to 16. It is not difficult to see that, if the stride is  $s$ , the padding is  $s/2$  (assuming  $s/2$  is an integer), and the height and width of the convolution kernel are  $2s$ , the transposed convolution kernel will magnify both the height and width of the input by a factor of  $s$ . The hyperparameters in this research include 0.0001 learning rate, 10 epochs and SGD optimizing method.

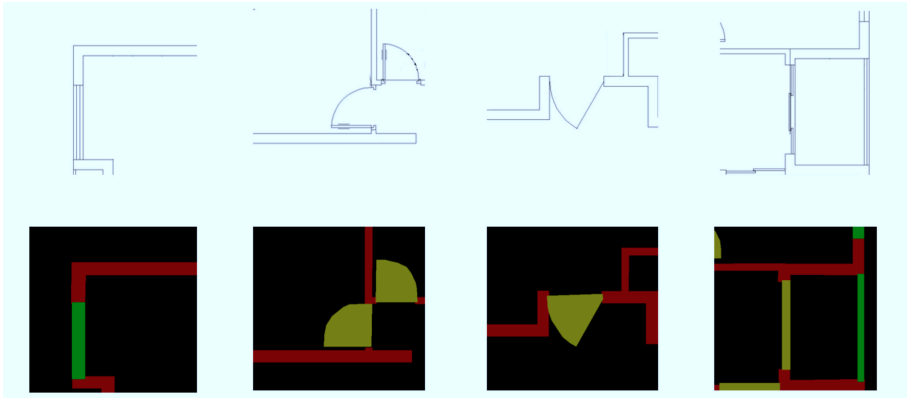


Figure 6. Training.

Then start to train the model. The loss function and accuracy calculation here is not fundamentally different from the image classification. Since the transposed convolutional channel has been used to predict the pixel class, the `axis = 1` (channel dimension) option is specified to `SoftmaxCrossEntropyLoss`. In addition, the model calculates the accuracy based on whether the prediction category of each pixel is correct.

### 3.4. EXPECTING RESULTS AND EVALUATING STANDARD

After training the network with the number of architectural drawings, the network will be expected to recognize the content of the testing picture and provide a visualization result of its recognition. Another expected result is the classification of the recognized objects. Since the different categories of the architectural element will be provided during the training process,

the recognized objects are expected to be classified into the right category. The evaluation factors include the categorization, the number and the completeness of the recognized architectural components. The last factor, which means the pixel loss condition, is specially imported in this research since it is vital for the component positioning in the future automatic modeling study.

### 3.5. SEMANTIC SEGMENTATION TESTING

After training 300 pairs of images, a customized FCN network with suitable parameters is became available. Then the network construction and training are

complete so the testing of architectural components recognition and localization can be started. Here we used ResNet152-V2, and set the Dropout percentage as 0.2, batch size as 2 and set 35 epochs.

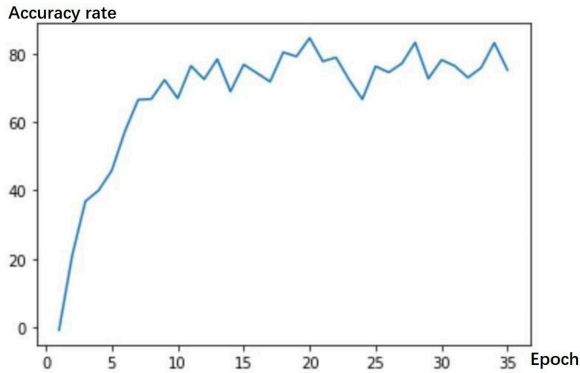


Figure 7. Accuracy rate and epoch.

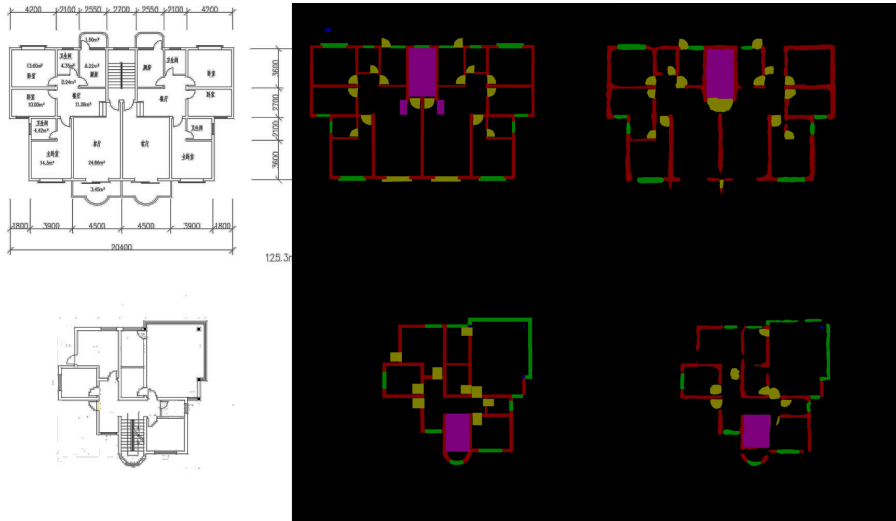


Figure 8. (Left) Original image; (Center) Labeled image; (Right) Predict result.

During the prediction, the input image should be standardized in each channel and be transformed into the four-dimensional input format required by the convolutional neural network. To visualize the predicted categories for each pixel, the predicted categories are mapped back to their labeled colors in the dataset.

The size and shape of the images in the test data set vary. Because the model uses a transposed convolution layer with a stride of 32, when the height or width of

the input is not divisible by 32, the height or width of the transposed convolutional layer output deviates from the size of the input image. In order to solve this problem, a solution that crops multiple rectangular areas in the image with heights and widths as integer multiples of 32 can be applied, and then perform forward computation on the pixels in these areas. When combined, these areas must completely cover the input image. Since a pixel is covered by multiple areas, the average of the transposed convolution layer output in the forward computation of the different areas can be used as an input for the SoftMax operation to predict the category.

For simplicity, the cropped area in which shape is 320\*480 from the top-left corner of the image will only be used for prediction. For the input image, the cropped area will be printout first, then comes to the predicted result, and finally, print the labeled category.

From the results we can see out of 5 categories of architectural elements can be accurately identified, they are window, door, wall, and stair. Because in some training images, the load-bearing wall and the column look very similar, they are all black filled, so the recognition of the column will be greatly affected, especially the dataset is small. For the categories that can be identified, the accuracy is still very high. There are elements in the place where the labels appear, and the colors are correct. And there are no such circumstances that a label appeared where there is no element exist.

#### **4. Conclusion and Future work**

In this research, we used a deep learning network for architectural components segmentation and categorization. The main goal to recognize the different architectural elements is to get the preparation for the automatic 3D model generating.

In order to get better training and prediction, we unified both the trained picture and tested picture size at 1600\*1280, and with the GTX 2080 Ti, 3.6 GHZ speed CPU, 32G RAM device processor, the prediction time for one image is less than one second. The appeared labels almost correspond to the element categories which can be seen from their colors, and the positions of the labels are also the same as the position of the elements. While the accuracy rate of recognition is 80% and the operating speed is fast. Therefore, the current stage that recognizes the element's type could be considered as successful. However, the pixel defection of the prediction is obvious and is more easily happens on the element in which the overall training amount is not enough and be similar to the others, like a column.

Therefore, to get a more precise and faster prediction, future work should include:

1) Optimize the network. There are many other options of the pre-trained network like SegNet which applied dilated convolution layers of different degrees of expansion to aggregate multi-scale background modules and improve front-end prediction and RefineNet which includes a component that can reuse multi-resolution features by upsampling lower resolution features. In the future, the goal is to get the network that may not be able to compete with other mature



networks but will be the most suitable one for this research.

2) Expand and diversify the dataset. Not only the amount of the dataset but also the types of drawings and elements should be diversified. The section plan and elevation plane should be included as well.

## References

- Castelo-Branco, R. and Menezes Leitão, A.: 2017, Integrated Algorithmic Design: A single-script approach for multiple design tasks, *Conference: eCAADe 35 - SchoCK (Sharing of Computable Knowledge)*.
- Geng, Q., Zhou, Z. and Cao, X.: 2017, Survey of recent progress in semantic image segmentation with CNNs, *Science China Information Sciences*, **61**, 51-101.
- He, K., Zhang, X., Ren, S. and Sun, J.: 2016, Deep Residual Learning for Image Recognition, *The IEEE Conference on Computer Vision and Pattern Recognition (CVPR)*, 2016.
- Horna, S., Méneveaux, D., Damiani, G. and Bertrand, Y.: 2009, Consistency constraints and 3D building reconstruction, *Computer-Aided Design*, **41**, 13-27.
- Joie, L., Janssen, P. and Stouffs, R.: 2018, Automated Generation of BIM Models from 2D CAD Drawings, *CADDRIA 2018*.
- Liu, X., Deng, Z. and Yang, Y.: 2018, Recent progress in semantic image segmentation, *Artificial Intelligence Review*, **52**, 1089-1106.
- Long, J., Shelhamer, E. and Darrell, T.: 2015, Fully Convolutional Networks for Semantic Segmentation, *The IEEE Conference on Computer Vision and Pattern Recognition (CVPR)*, 2015.
- Ren, H., Han, Y. and Sun, C.: 2018, Transdata: A Data Recording and Exchanging Plug-in for Architectural Computational Design, *CADDRIA 2018*.
- Ronneberger, O., Fischer, P. and Brox, T.: 2015, U-Net: Convolutional Networks for Biomedical Image Segmentation, *International Conference on Medical Image Computing and Computer-Assisted Intervention*.
- Siam, M., Elkerdawy, S., Jagersand, M. and Yogamani, S.: 2017, Deep semantic segmentation for automated driving: Taxonomy, roadmap and challenges, *2017 IEEE 20th International Conference on Intelligent Transportation Systems*.
- Sigalov, K. and König, M.: 2017, Recognition of process patterns for BIM-based construction schedules, *Advanced Engineering Informatics*, **33**, 456-472.
- Xuetao, Y., Wonka, P. and Razdan, A.: 2008, Generating 3D Building Models from Architectural Drawings: A Survey, *IEEE Computer Graphics and Applications*, **29**, 20-30.

# COMPUTATIONAL METHODS FOR EXAMINING RECIPROCAL RELATIONS BETWEEN THE VIEWSHED OF PLANNED FACILITIES AND HISTORICAL DOMINANTS

*Their integration within the cultural landscape*

KLARA CZYNSKA

<sup>1</sup>*West Pomeranian University of Technology, Szczecin, Poland*

<sup>1</sup>*kczyńska@zut.edu.pl*

**Abstract.** The article presents a methodology for the assessment of the impact of new buildings on the cultural landscape, in particular the exposure of historical landmarks. While using digital analysis and a 3D city model, the methodology examines reciprocal visual relations between historical and planned buildings. The following methods have been used: a) Visual Impact Size (VIS) which enables to determine a visual impact area and the degree of architectural facility domination in space; b) comparative analysis (cumulative viewshed) which enables to determine areas where viewsheds of new investment and historical buildings overlap; c) simulation of selected views from the level of human eyesight. The proposed landscape examination methodology has been presented using the case study of Katowice, Poland. The goal was to determine reciprocal relations between historical landmarks of the Silesia Museum and tall buildings planned in the vicinity. The study used a Digital Surface Model (DSM), a 3D city model. All simulations have been performed using software developed by the author (C++).

**Keywords.** Cumulative viewshed; digital cityscape analysis; historical dominants; visual impact; VIS method.

## 1. Introduction

The conservation of a historical urban landscape usually involves the designation of protected areas where so called Assets of Cultural Interest are the most important components of the cityscape and new investment should be subordinated regarding its form and materials used (O'Connor 2011). However, in the planning practice, such methods are frequently insufficient, especially in the context of a visual protection against the impact of tall buildings. Tall buildings have very large visual impact range and can be seen from kilometres away (Van der Hoeven, Nijhuis 2011). The use of 3D and computation methods enables to produce more advanced simulation and the protection of facilities that are important for the cultural heritage in cities.

The goal of the research presented in this article is to discuss the method that can support identification and planning of investment in terms of their impact on

the exposition of historical dominants. The method defines viewsheds (Danese et al. 2009) for historical facilities, which are components of a cultural heritage, and then the same for planned buildings. The study uses the Visual Impact Size (VIS) method (Czyńska 2015). The comparison of VIS analyses for a group of protected historical buildings and new ones enables us to identify exposure locations that can be loosely examined at the next stage through simulations using, e.g. height lines (Czyńska 2010). This enables to show the actual impact of planned buildings on the cityscape and their relationship to historical dominants.

## **2. Methods and materials**

### **2.1. 3D CITY MODEL**

The Digital Surface Model (DSM), or a 3D city model, of high resolution (grid size of 50 cm), is a basis for the study presented in the article. It consists of a regular cloud of points which contains all cityscape components, such as buildings, trees, bridges and overpasses, reflected with identical accuracy (for each element). Therefore, the DSM is a very good environment for visual analyses (Rubinowicz 2018). Nevertheless, the proposed method can also be applied using other city model formats, e.g. CityGML (Kolbe 2009). Its drawback, however, when compared with the DSM, is that it usually does not take into account trees despite of its major impact on the visibility of architectural facilities in space.

The study uses specialist C++ software which was developed with the involvement of the author and it is dedicated to complex computational tasks (e.g. visual analysis) for large urban areas. It is particularly important when examining tall buildings that may have their impact within the range of several kilometres. The algorithm has been optimized for enhancing the efficiency of processing data representing a digital picture of the city space. Although the study uses proprietary software, it is possible to conduct a similar process based on a standard specialist GIS software as well. In this case, the complexity of calculations due to the size of input data and computation time can be a limitation. Software applied in the study enables the emulation of the visibility field for an individual control point within 1.0 sq km and a mesh size of 0.5 m during approx. 48 s (4 core processor and 32GB RAM). The study always includes the full resolution DSM model. The precision of the model has relatively minor impact on the simulation time.

### **2.2. METHODS**

The examination of visual interactions between existing historical dominants and planned tall buildings necessitated a new suitable methodology. The methodology was based on the following: a) preparation of VIS maps for historical dominants; b) development of similar VIS maps for planned buildings; c) comparison of visual impact - cumulative viewshed; d) development of photographic documentation for selected vistas; e) preparation of simulations regarding the impact of tall buildings as seen from the human eye sight level using height lines.

In the study concerned, a key role was played by the VIS method which enables to simulate the viewshed of a building. The basics of the method stem from so called “reversed viewshed”, that is an area from which a target point is

visible (Caha 2017). Together with the visibility range, the method calculates the degree of domination of a facility in space, namely its domination or only partial visibility of a building. Each facility is represented by a single point (set in its centre) or a collection of control points (which enables to reflect facility in more comprehensive manner) (Caha 2017). Although the result has a continuous nature, i.e. the calculation leads to precise limit height values, the interpretation of findings is better once we limit the number of thresholds (depending on height of individual building). Usually, it is 8 to 10 different heights every 10-20 m. It depends, however, on the specific nature of the facility in question and the required precision of calculation.

As regards the research concerned, a major context in the theory of digital picture analysis comprise multiple viewshed (Kim, Rana & Wise 2004) and cumulative viewshed (Wheatley 1995). Multiple viewshed combines the total visibility for a number of points in space, while cumulative viewshed enables to obtain information about locations where visibility areas overlap for specific observation points. In this particular case, these are areas in which new investment influences the visibility of historical dominants. Cumulative viewshed maps are developed individually for each height examined in the VIS.

Locations where viewsheds of historical dominants and new buildings overlap are the exposure areas for which visualisations are developed simulating the level of a human eye sight. They show the actual impact of new buildings in the cityscape and their interaction with facilities that need to be protected. To extend the use of such simulations in the planning practice, instead of simulating the shape of an architectural facility, the methods uses three-dimensional height lines (Czyńska 2010). They provide information concerning impact depending on various heights of a planned building combined with its exposure, and help determine the view and maximum heights for the new building.

The VIS analysis does not take into account the distance from the facility in question. It results from major differences in the perception of high-rising buildings depending on the specific nature of the cityscape. Based on a number of examples worldwide, tall buildings can have their visual impact over a distance of several kilometres. A good example of the above, is a tall building in London, which disturbed one of strategic vistas of St Paul's Cathedral ("Skyscraper that 'destroys' view of St Paul's", 2016). The VIS method calculates the total possible range of visual impact. The result is then interpreted by an expert. Nevertheless, taking into account the distance is a question of the future development of the VIS method.

### **3. Katowice case study**

#### **3.1. RESEARCH PROBLEM**

The above methodology was used to analyse the impact of new tall buildings on a historical cityscape of Katowice, Poland, in particular facilities of a former mine in Katowice which comprise the Silesia Museum. Katowice is a city located in the largest industrial region in Poland. The history of the city has been associated with the mining industry. Traces of the cultural heritage can still be seen in the

landscape and as such should be protected. The Silesia Museum completed in 2012 (designed by Riegler Riewe Architekten) involved rehabilitation of buildings of a former coal mine (small red brick buildings). New museum facilities are hidden underground to highlight historical industrial facilities, including a winding tower and water tower. These are local dominants made of red brick and steel lettuce structure and subtle details. The architectural design of the Silesia Museum has won the recognition at the European level and it is now a major landmark of the city (see Figure 1a).

North of the museum planned is a new residential estate with tall buildings (investor: TDJ Estate, design: Medusa Group - see Figure 1b). In total, the plan includes 8 buildings exceeding the average height of other buildings in the immediate vicinity (from 38 m to 54 m above ground level). Considering cityscape conditions, configuration of land and exposition of valuable industrial heritage facilities, new tall buildings may significantly threaten the integrity of Silesia Museum dominants.

Therefore, the study aims to verify whether planned tall buildings impact the exposure of the dominants, and if yes, then in what way? What will be the character of the new neighbourhood? Will it dominate the cityscape? How many iconic vistas of the Museum will be changed by the new investment?

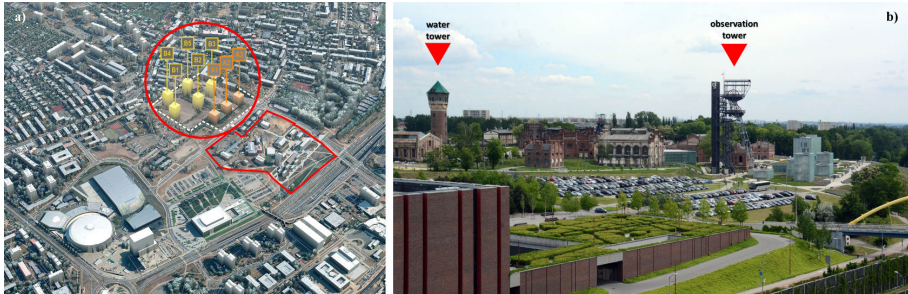


Figure 1. Historical dominants of Silesia Museum in Katowice and planned investment: a) visualisation of city including Museum and planned residential estate by TDJ-Estate (A1÷B5), b) historical dominants: observation tower and water tower.

### 3.2. APPLICATION OF COMPUTATIONAL METHODS

Cityscape analyses have been implemented based on digital height data covering an area of 25 sq km in Katowice. The DSM model was fitted onto a mesh of 50 x 50 cm. The model was revised and updated to eliminate technical errors and supplement changes in build-up environment of the city, i.e. demolition, new facilities etc. All visualisations and analyses have been developed using C++ dedicated software created partially by the author.

The first stage involved the development of VIS maps in various options: a) for observation tower; b) for water tower; c) for both historical dominants of Silesia Museum; d) for group of 3 planned residential buildings of smaller height; e) for group of 5 planned residential buildings; and f) for 8 new buildings. Each

map provides important and accurate information about the impact of particular buildings on the city space and their domination. The VIS analysis includes 7 identical levels for all facilities in question, i.e. 10, 20, 30, 40, 50, 60, 70 m. Each level is marked with a different colour which represents the domination of a given facility in space (red - major impact, blue - minor impact). A collective VIS map for historical dominants and collective VIS map for 8 new buildings are presented in figure below (see Figure 2).

Another stage involved the juxtaposing of impact areas for both historical dominants and the impact of eight tall buildings - a cumulative viewshed. A number of maps have been developed to show overlapping exposure areas, each for a different height between 10÷70 m above ground level (see Figure 3). The maps show three values: yellow - cumulative visibility of historical dominants; blue - aggregated visibility of new tall buildings; red - visibility of both historical dominants and planned buildings.

VIS maps (Figure 2) enable to examine all locations within a city from which specific facilities can be seen. The cumulative viewshed (Figure 3) presents interaction of viewsheds of protected historical facilities and new buildings. This helps to identify visibility points at which planned buildings can be a threat to the cityscape. At the same time, it is a starting point for field studies and the documentation of vistas. For the most important vistas, the study developed simulations of views from the human eye sight level showing the transformation of the cityscape after new buildings are completed, as well as their actual relationship with historical dominants. Particular simulations provide information important for planning of revisions to the height of planned buildings - enables to determine maximum height at which a given facility extends above the line of buildings in specific vistas. The study used multiple colour blocks placed in the cityscape of Katowice to mark the location and height of new buildings (see Figure 4). Colours used are identical as those in VIS analysis.

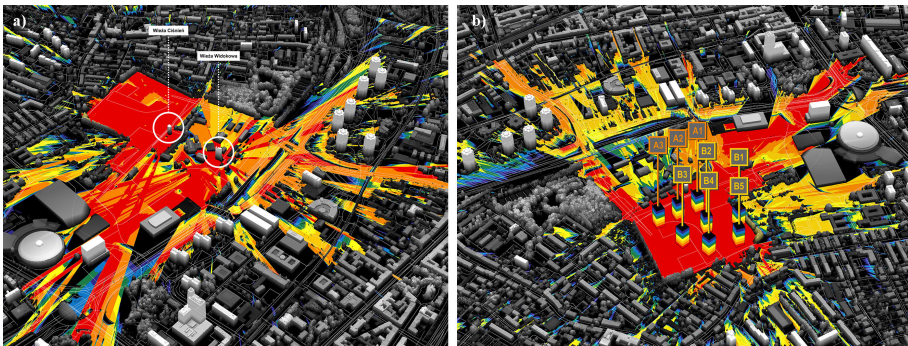


Figure 2. Cumulative VIS analyses for: a) historical dominants of Silesia Museum, b) 8 buildings planned by TDJ-Estate. Colours denote the power of building facility domination in space (red - major, blue - minor).

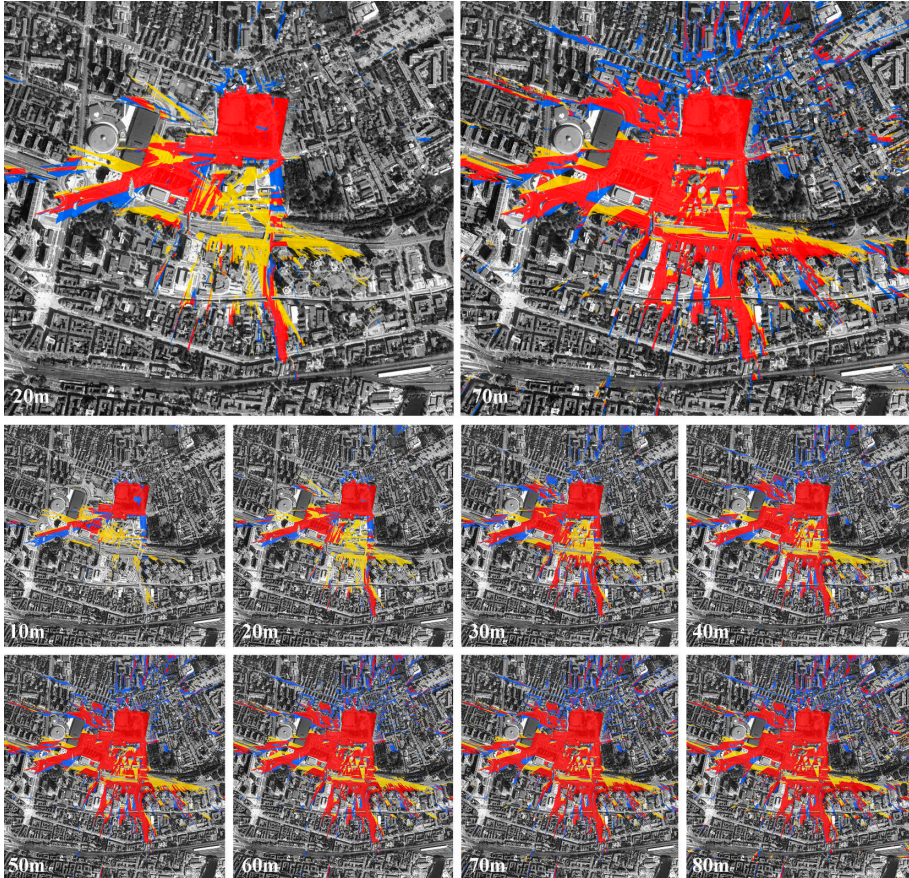


Figure 3. Cumulative viewshed - comparison of viewsheds of historical facilities (2 dominants) and planned buildings (8 facilities), at different levels. Red is used to mark areas of simultaneous visibility.

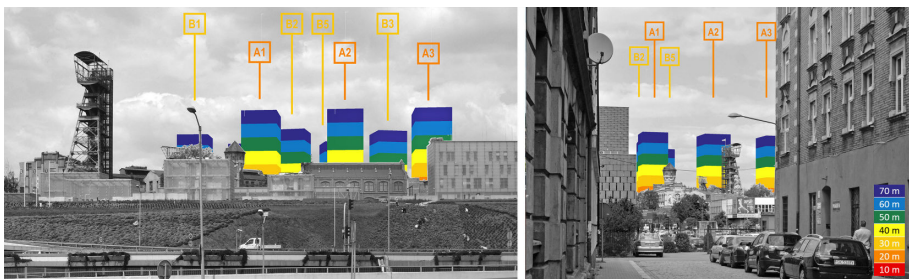


Figure 4. Sample simulations of vistas for new buildings using isovists (colours identical as in VIS analysis - height ranges every 10 m).

## 4. Results and discussion

### 4.1. INTERPRETATION OF RESULTS

The VIS analysis showed a broad visual impact of buildings planned in the vicinity of the Silesia Museum. A preliminary comparative VIS analysis for the investment planned and historical dominants indicates that those areas overlap to a considerable extent. It means that the vistas of historical Silesia Museum dominants will be irreversibly changed.

This has been confirmed by the cumulative viewshed analysis for specific heights (Figure 3). While examining a sequence of maps we could observe that the cumulative viewshed increased with the height of buildings planned. This enlarges the area marked red and reduces the visibility of dominants (yellow). It means that buildings planned will have a major impact on the exposure of historical facilities.

Cumulative viewshed results are presented in table below (see Table 1). Columns 2 and 3 show cumulative viewsheds: group A - for historical dominants; group B - for 8 new buildings. Column 4 refers to the common part with overlapping viewsheds of group A and group B. Columns 5 and 6, however, are the most important for the interpretation of results, since they show the degree of interference of new buildings with the facilities of the Silesia Museum.

The result corresponds with the initial intuitive perception. The majority of vistas (60 to 80%) with dominants of the Silesia Museum will be changed by the visual presence of new tall buildings (Table 1 - column no. 5). As many as 56 to 67% of vistas with planned buildings will include historical dominants as well (Table 1 - column no. 6). Although in the second instance there is no question of a reduced visual value of buildings planned, the question of how new buildings can fit into the cityscape, the Silesia Museum in particular, is debatable.

Table 1. Viewsheds of historical dominants and new tall buildings.

1	2	3	4	5	6
Height examined	Viewshed of hist. dominants	Viewshed of new buildings	Overlapping area	Interference of new building into vistas with hist. dominants	Presence of hist. dominants in vistas with new buildings
	<b>A</b>	<b>B</b>	<b>A∩B</b>	<b>(A∩B) / A</b>	<b>(A∩B) / B</b>
[m]	[thou. m2]	[thou. m2]	[thou. m2]	%	%
<b>10</b>	205.64	183.91	123.14	<b>59.9%</b>	<b>67.0%</b>
<b>20</b>	357.89	314.92	215.79	<b>60.3%</b>	<b>68.5%</b>
<b>30</b>	463.24	538.87	328.65	<b>70.9%</b>	<b>61.0%</b>
<b>40</b>	595.34	737.19	434.94	<b>73.1%</b>	<b>59.0%</b>
<b>50</b>	761.91	998.63	567.54	<b>74.5%</b>	<b>56.8%</b>
<b>60</b>	945.89	1295.71	727.73	<b>76.9%</b>	<b>56.2%</b>
<b>70</b>	1152.25	1620.18	915.79	<b>79.5%</b>	<b>56.5%</b>

Further conclusions can be drawn based on the simulation of selected views seen from the human eye sight level. In total, the study examined more than ten iconic vistas of the Silesia Museum from different directions (sample visualisation - see Figure 4). In the majority of viewsheds examined, new buildings can be seen



with historical facilities in the background. This means that their previous role in the cityscape as primary dominants is going to change. Those facilities will lose their initial integrity. They will no longer be observed against the background of the sky, and their delicate, partially transparent structure will be dominated by new buildings.

Partial results provide a lot of valuable information related to the cityscape of Katowice. They, however, need to be interpreted by an expert familiar with the specific nature of the cityscape, its morphology and history. Then it is possible to examine and interpret the meaning of particular visual impact.

A good example of the above is the viewshed of the Silesia Museum from Damrota Street. A narrow viewshed, shown in figure below (see Figure 5a), although in relation to the entire map poor, is de facto one of key and very iconic perspectives of Silesia Museum dominants. The axial composition of space ends with historical towers (see Figure 5b). The simulation shows the way new tall buildings interfere with the cityscape. Buildings can be seen once they reach the height of 30 m. Therefore, to reduce the visual impact of new buildings, it is necessary to reduce their height up to that level.

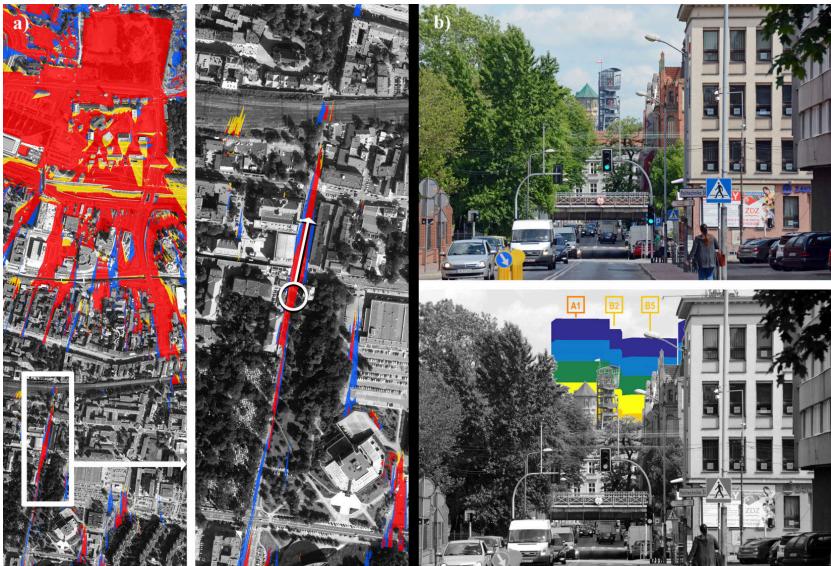


Figure 5. View from Damrota Street – example of axial visual impact with overlapping viewsheds of historical dominants and planned tall buildings: a) Cumulative viewshed, b) simulation from the human eye sight level.

#### 4.2. THE METHOD AND OTHER RESEARCH

The methodology comprises several techniques that can be useful while developing expert opinions on the impact of investment on the environment (Environmental Impact Assessment, or EIA) as regards the protection of cultural

heritage (Bond et. al. 2004). Such studies are usually based on viewshed analyses (Ozimek & Ozimek 2017). The theory related to measuring the viewshed has been developed for decades. With the development of computation capacity and accessibility of spatial data it is increasingly often used to analyse e.g. tall buildings. Van der Hoeven & Nijhuis (2011) have analysed a multiple viewshed for tall buildings in Rotterdam. The analysis, however, produced poor accuracy due to too small resolution of the 3D city model applied.

Apart from information whether a facility can be seen from a given location, an important aspect of the analysis is how powerful its exposure is. While examining a tall building in Trondheim, Rød and van der Meer (2009) determined angular values and the degree of domination of the facility in specific urban space. The VIS method, discussed in the article, determines domination by dividing a control point into height thresholds for which viewsheds are calculated. Results obtained are very accurate (up to 15 cm) in comparison to other studies published (Tabik 2012). It is possible due to the use of VIS dedicated software. The software enables to process DSM models at high precision level. It provides a full control over the viewshed calculation process.

Studies presented also involve the problem of a 3D visualisation of planned architectural facilities in the existing urban space. Falconer et.al. (2015) aims at making the designing process more interactive to produce a sustainable urban environment. The method of examining blocks of buildings (using height lines) is an attempt to expand the use of architectural concept visualisation (Pullar, Tidey 2001). It can be used in planning to determine the desired height of new buildings based on the analysis of their spatial context (Saedi et.al. 2019).

## 5. Conclusion

The study uses digital techniques in cityscape analysis to assess reciprocal visual relationship between historical facilities (protected) and new buildings planned. The proposed methodology is based on the visual impact analysis (VIS). VIS analyses are carried out separately for the group of historical dominants and the group of buildings planned, and then results of those analyses are compared in a measurable manner (cumulative viewshed). It enables to distinguish areas of exposure in which new facilities can interfere with the cityscape.

The application of the method is presented using the example of a case study of Katowice. Analyses covered 25 sq km of the city using a full precision DSM model (mesh of 0.5 m). Results of the VIS analyses and the cumulative viewshed analysis showed major impact of new buildings planned, since their viewsheds overlapped those of historical towers of the Silesia Museum (60-80%). Simulations developed for selected vistas confirmed that planned buildings could be seen with the museum in the background. The VIS method has enabled to identify a number of visual correlations also in distant locations and those that can hardly be determined intuitively. Selected vistas have been examined using height lines.

On the one hand, the cumulative viewshed analysis of historical and planned facilities enables to identify locations that need to be further examined in greater

detail. On the other hand, the overlap of viewsheds of historical and planned buildings is a measurable parameter which provides information about a possible risk of interference with the cityscape. The methodology can be used in planning practice in various cities including the use of other GIS software.

## References

- “Skyscraper that ‘destroys’ view of St Paul’s”: 2016. Available from <<https://www.architectsjournal.co.uk/news/outrageover-somskyscraper-that-destroys-view-of-st-pauls/10015058.article>> (accessed 3rd February 2020).
- Bond, A., Langstaff, L., Baxter, R., Wallentinus, H.-G., Kofoed, J., Lisitzin, K. and Lundström, S.: 2004, Dealing with the cultural heritage aspect of environmental impact assessment in Europe, *Impact Assessment and Project Appraisal*, **22**, 37-45.
- Caha, J. 2017, Representing buildings for visibility analyses in urban spaces, in I. Ivan et al. (ed.), *Dynamics in GIScience, Lecture Notes in Geoinformation and Cartography*, Springer International Publishing, 17-29.
- Czyńska, K.: 2010, Tall buildings and harmonious city landscape, *Space & Form*, **13**, 276-280.
- Czyńska, K.: 2015, Application of Lidar Data and 3d-City Models in Visual Impact Simulations of Tall Buildings, *International Archives of the Photogrammetry Remote Sensing and Spatial Information Science*, **XL-7/W3**, 1359–1366.
- Danese, M., Nole, G. and Murgante, B. 2009, Visual impact assessment in urban planning, in B. Murgante, G. Borruso and A. Lapucci (eds.), *Geocomputation and Urban Planning*, Springer-Verlag, Berlin Heidelberg, 133–146.
- Falconer, R. E., Isaacs, J. P., Gilmour, D. and Blackwood, D. J. 2015, Indicator Modelling and Interactive Visualisation for Urban Sustainability Assessment, in C. Silva (ed.), *Challenges, and Opportunities in Urban E-Planning*, PA: IGI Global, Hershey, 188-209.
- Van der Hoeven, F. and Nijhuis, S.: 2011, Hi Rise, I can see you! Planning and visibility assessment of high building development in Rotterdam, *Research in Urbanism Series*, **2**, 277–301.
- Kim, Y., Rana, S. and Wise, S.: 2004, Exploring multiple viewshed analysis using terrain features and optimisation techniques., *Computers and Geosciences*, **30**, 1019-1032.
- Kolbe, T. H. 2009, Representing and Exchanging 3D City Models with CityGML, in J. Lee and S. Zlatanova (eds.), *3D Geo-Information Sciences. Lecture Notes in Geoinformation and Cartography*, Springer International Publishing, Berlin Heidelberg, 15-31.
- Ozimek, A. and Ozimek, P.: 2017, Viewshed Analyses as Support for Objective Landscape Assessment, *Journal of Digital Landscape Architecture*, **2**, 190-197.
- Pullar, D. V. and Tidey, M. E.: 2001, Coupling 3D visualisation to qualitative assessment of built environment designs, *Landscape and Urban Planning*, **55**, 29-40.
- Rubinowicz, P.: 2018, Application of Available Digital Resources for City Visualisation and Urban Analysis, *Proceedings of the 36th eCAADe Conference 2018: Computing for a better tomorrow*, Łódź, Poland, 595-602.
- Rød, J. and van der Meer, D.: 2009, Visibility and dominance analysis: assessing a high-rise building, *Environment and Planning B: Planning and Design*, **36**, 698-710.
- Saeidi, S., Mirkarimi, S. H., Mohammadzadeh, M., Salmanmahiny, A. and Arrowsmith, C.: 2019, Assessing the visual impacts of new urban features: coupling visibility analysis with 3D city modelling, *Geocarto International*, **34**(12), 1315-1331.
- Tabik, S., Zapata, E. and Romero, L.: 2012, Simultaneous computation of total viewshed on large high resolution grids, *International Journal of Geographical Information Science*, **27**(4), 1-11.
- Wheatley, D. 1995, Cumulative viewshed analysis: a GIS-based method for investigating, in G. Lock and Z. Stancic (eds.), *Archaeology and Geographic*, Taylor and Francis, London, 171–186.

# SUSTAINABLE DEVELOPMENT OF A CITYSCAPE USING THE VISUAL PROTECTION SURFACE METHOD - OPTIMIZATION OF PARAMETERS FOR URBAN PLANNING

PAWEL RUBINOWICZ

<sup>1</sup>West Pomeranian University of Technology Szczecin, Poland

<sup>1</sup>pawel@rubinowicz.com.pl

**Abstract.** The article discusses computer techniques used to analyse a cityscape based on 3D models. The study focuses on the application of the Visual Protection Surface (VPS) method which enables to analyse the absorption capacity of a city as regards new investment while bearing in mind the goal of preserving a set of strategic views. The outcome of the process is a surface or a map which determines the maximum height of buildings. The goal of the study is to adjust VPS input to apply the method in urban planning. Analyses focused on the following VPS parameters: a) accuracy of 3D model, b) density of strategic views, and c) VPS resolution. They have been carried out based on the case study of Gdansk, Poland. The study shows which of the parameters are crucial for the quality of the outcome and time of the computation process. All simulations presented in the article have been developed based on the C++ program prepared by author.

**Keywords.** 3D city models; cityscape protection; computational urban analyses; urban heritage; VPS method.

## 1. Introduction

Research discussed in the article focuses on computer-aided techniques applied to analyse cityscapes while supporting urban and spatial planning. Considering the concept of the 'Anthropocene - the age of humans', the human impact on the Earth is multifaceted. However, we should always do our best to preserve development opportunities for future generations. Such a concept of sustainable development applies, inter alia, to the aim of preserving historical heritage of cities, on the one hand, and set directions of contemporary development and define the framework to fit new facilities into the existing urban structure on the other.

The research goal is to optimize input to the Visual Protection Surface (VPS) method described in the literature (Czyńska and Rubinowicz 2015). This applies in particular to the analysis of how 3D city model accuracy and other VPS parameters, influences the quality of results. The VPS is used in examining the absorption capacity of a city as regards new investment, including high-rising buildings. At the same time the assumption is that certain strategic views need to be protected, since they are fundamental for preserving cultural values of the cityscape. The

VPS generates a map of maximum building heights, indicating city development possibilities while preserving strategic views.

The research is expected to broaden knowledge about possibilities of using the VPS method in urban planning and determining of major input data quality parameters and their impact on VPS results. The VPS computation process is very complex and depends on a number of variables. The study includes analysis of the following VPS parameters: a) accuracy of 3D model, b) density of strategic views and c) VPS resolution. Simulations were carried out for the city of Gdansk, Poland. Case study and analysed VPS parameters are described in section 3. Results are presented in section 4 and discussed in section 5.

## **2. Method & materials**

### **2.1. VPS METHOD**

The protection of the cultural landscape concentrates on preserving valuable views, important for the identity and heritage of the city - referred to in the article as strategic views. The determination of such vistas and defining protection rules is the basis for a number of planning documents that regulate the policy of cityscape development in Europe and in the world (LVMF 2012, Vancouver Views 2011).

The VPS method is based on a digital analysis of the cityscape using 3D models. It enables to calculate the maximum height of new buildings in each section of the area examined. The main criterion for establishing the height limit is the protection of strategic views, so planned investment does not interfere, i.e. new buildings cannot be seen in protected skylines (Czyńska and Rubinowicz 2015). VPS results can be displayed as a 3D surface above the city or in the form of 2D maps where height limits are colour coded (see Figure 3e-f).

### **2.2. 3D CITY MODELS**

The study discussed in the article uses a 3D city model based on LiDAR data and processed to the Digital Surface Model (DSM) of 0.5m grid. The DSM is a point cloud placed on a regular mesh. It is the simplest possible structure to reflect the shape of the city and cover a massive volume of data. An advantage of the DSM is the completeness of the model, since it takes into account all elements of the cityscape. Terrain, buildings, infrastructure and tall green are reflected at the same constant accuracy. In the study concerned, DSM is treated as a 3D-Mesh (Rubinowicz 2019). Applied C++ software enables to examine visibility in vast city areas (up to 180 sq km) while preserving full DSM resolution. Moreover, the DSM grid 0.5m enables to project architectural details, geometry of roofs, towers etc. (see Figure 1).

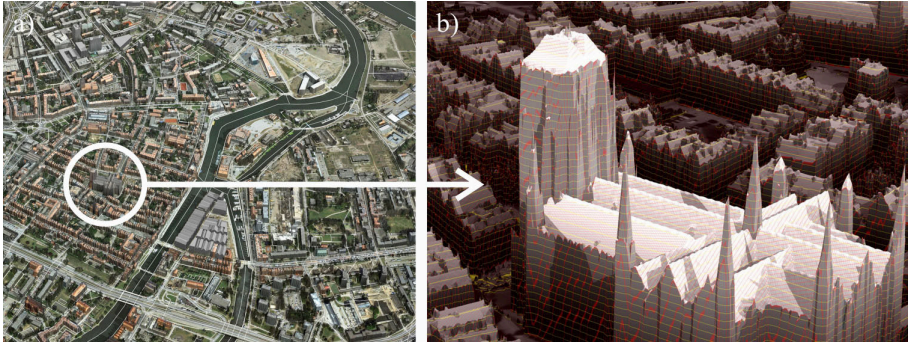


Figure 1. DSM Model of Gdansk, 0.5m grid as 3D-Mesh: a) visualisation of city centre using DSM and ortophotomap, b) zoom-in showing Basilica Church.

### 3. Case study & VPS parameters

#### 3.1. VPS APPLICATION FOR GDANSK

The study covers the city of Gdansk, Poland. The city has been implementing a large-scale investment in the area of the former shipyard (Lorens 2019). The surface area of the new development (district of Young City) is comparable to the area of the Gdansk Old Town. Plans also include tall buildings (see Figure 2) which may have a major impact on the cityscape. This applies, among others, to skylines seen from the Motława River, along viewpoints near the Spichrzów Island (see Figure 2). The possibility of using the VPS method for protecting panoramas has been proven by other studies (Rubinowicz 2019a). The example of Gdansk and panoramas from the Motława River is suitable for the study discussed in the article, which examine the accuracy of VPS maps and configuration of VPS input parameters: accuracy of 3D model, density of strategic views and VPS resolution. On the one hand, the optimisation of these parameters focuses on the shortening of time needed to generate VPS maps, and on the other hand, to obtain a relevant quality of the resulting simulation for planning purposes.

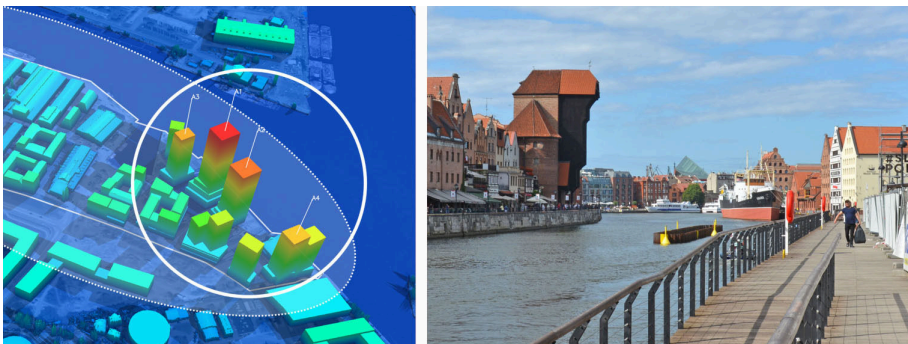


Figure 2. Investment planned in the Young City District of Gdansk (left) and panorama of the city from the Motława River as one of protected strategic views (right).

### 3.2. ACCURACY OF 3D MODEL

The first of VPS optimisation criteria examined in the article is the accuracy of the model. All simulations presented use DSM models of different resolution (grid: 0.5m, 1.0m, 2.5m, 5m, 10m, 20m). One may expect that the use of a very accurate DSM model of 0.5m grid (see Figure 1 & Figure 3a) produces a better VPS result than a simplified city model, e.g. 10m grid DSM (see Figure 3b). However, a very high resolution of the model can be a limitation for data processing by GIS software. The process of a VPS map generation necessitates an efficient Line-of-Sight analysis (Nutsford et al. 2015). Additionally, the use of relevant recurrence algorithms supports an efficient visibility analyses for very complex point clouds (Orlof et al. 2019, Rubinowicz 2019b).

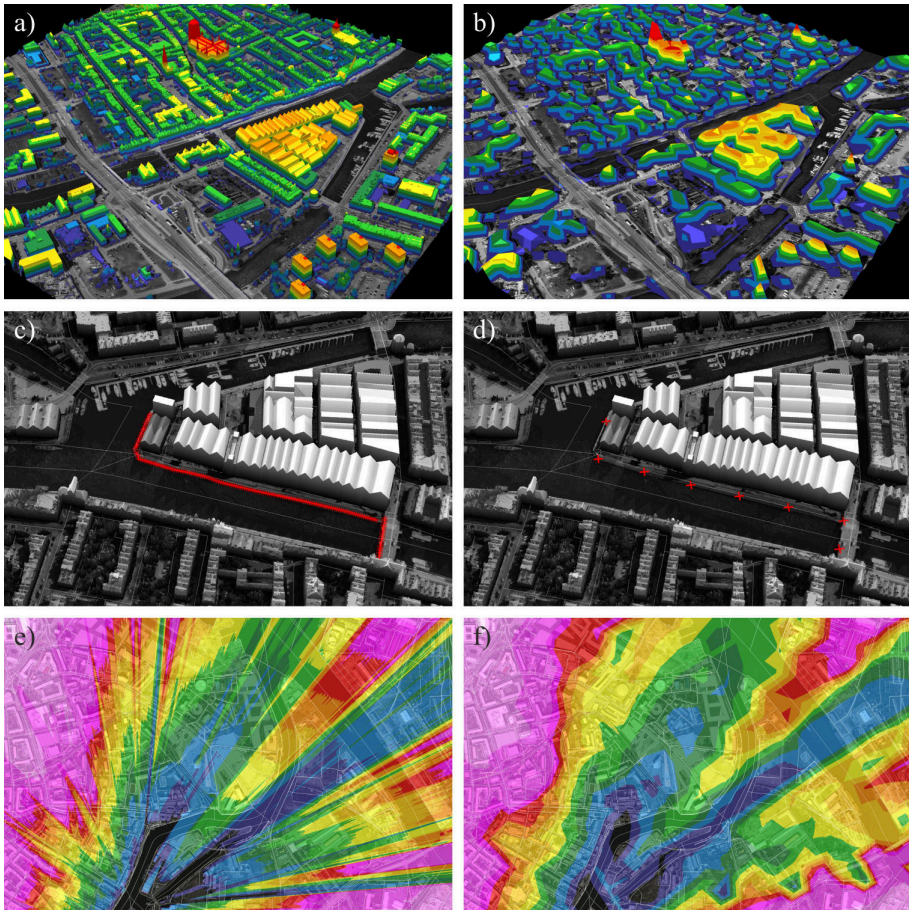


Figure 3. VPS input parameters examined: a) DSM 0.5m model; b) DSM 10m model; c) precise imaging of a series of sights (2.0m spacing of points); d) simplified imaging of sights (52.9m spacing of points); e) VPS map resolution of 1m; f) VPS map resolution of 100m.

### 3.3. DENSITY OF STRATEGIC VIEWS

The second criterion for the optimisation of the VPS is the adjustment of the density of strategic views for an appropriate presentation of the series of viewpoints. In the case study of Gdansk, protection measures concentrate on panoramas seen from boulevards along the Motława River - ca 0.37km. Thus, instead of individual view point, we examine their series that comprise a set of strategic views for the VPS. The smaller the distances between consecutive points in the series, the more accurate is the VPS result. To obtain the most precise result, the study adopted the distance of 2.0m between neighbouring points (see Figure 3c) - total of 185 points. Assuming 8 points (8 strategic views), the distance is ca. 52.9m (see Figure 3d).

### 3.4. VPS RESOLUTION

The third criterion for the optimisation of the VPS is the resolution of the VPS surface/map. The structure of VPS data is similar to that in the DSM (can be described in e.g. ESRI ASCII Raster format). Therefore, the VPS resolution can be approached in a similar fashion as in the DSM. To obtain possibly the most accurate result, the study used the VPS resolution of 1m. This means that for every point within 1m from each other (XY) in the area of the city examined we calculate the maximum height of buildings (see Figure 3e). The lowest VPS resolution was 100m. The imaging of the result necessitated the interpolation of heights determined (see Figure 3f). The VPS resolution has an exponential impact on the computation time. Therefore, the determination of an optimum VPS resolution, which produces a desired accuracy for planning, is particularly important.

## 4. Results

### 4.1. SIMULATION SCOPE

VPS analyses for Gdansk have been developed for the city area of 25 sq km (5km x 5km). The study includes 6 accuracy variations: DSM grid of 0.5m, 1.0m, 2.5m, 5.0m, 10.0m and 20.0m; 6 variations of strategic views density distribution: 2.0m, 4.2m, 6.6m, 13.7m, 28.4m and 52.9m and 6 VPS map resolutions: 1m, 2m, 5m, 10m, 25m and 100m. In total, 108 variations of VPS maps of different accuracy have been developed. The emulation time for these analyses varied significantly - from a fraction of a second to several hours. Parameters adopted had a major impact on the quality of results. The relationship between the emulation time and the quality of VPS results have been surprising in a number of instances. The analyses have been performed using the C++ software developed by authors and a 6-core PC I7-8700, 3.70GHz, 32GB RAM.

### 4.2. COMPARISON OF THE ACCURACY OF VPS MAPS

The analysis of various VPS variations was based on the most accurate simulation using the DSM model of 0.5m grid, while assuming the distribution of strategic views of 2.0m and the resolution of the VPS map of 1m. Their emulation time was 63148.6s (18 hours and 55 minutes). The result was used as a reference value



for assessing other less accurate VPS analyses. The process involved two stages: preliminary intuitive comparison of VPS maps, and then calculation of the average VPS error. Major differences have been noted in the distribution of inaccuracies of approximate VPS analyses (see Figure 4). Major height errors (in excess of 10m) were found in relatively small number of city areas (marked red). For the majority of areas in the city, the difference between the reference value and approximate results was relatively small - less than 3m (marked yellow).

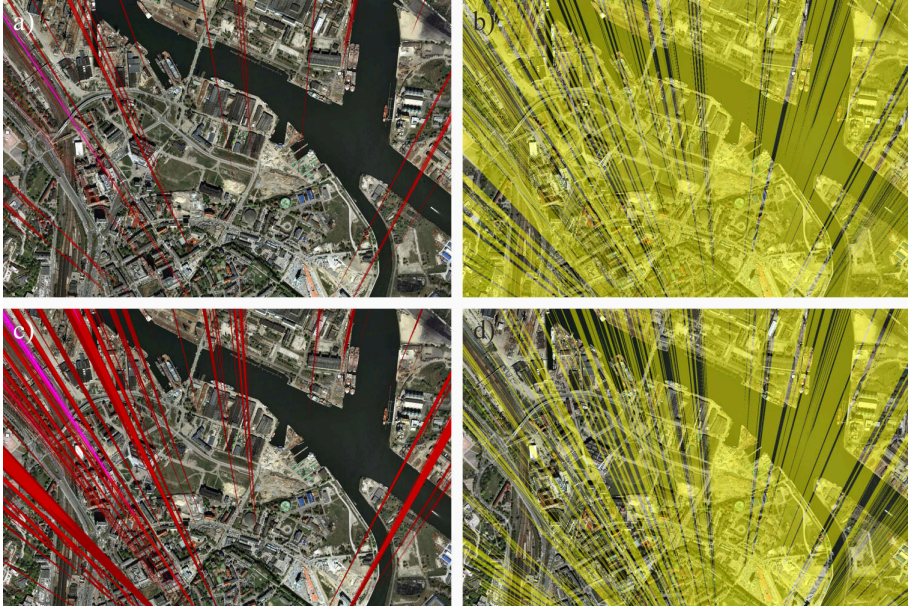


Figure 4. Comparison of the accuracy of VPS maps with a reference result: a-b) accuracy analysis for  $D = 4.2\text{m}$  (distance of strategic views) and VPS resolution 2m; c-d) accuracy analysis for  $D = 6.6\text{m}$  and VPS resolution 1m. Major height errors (in excess of 10m) – marked red and relatively small errors (less than 3m) – marked yellow.

### 4.3. COMPARISON OF THE ACCURACY OF VPS MAPS

The first group of VPS analyses includes 36 simulations at various densities of strategic views, defined by the minimum distance between viewpoints -  $D$  (from  $D = 2.0\text{m}$  to  $D = 52.9\text{m}$ ) and different resolutions of VPS maps (from 1m to 100m). Both parameters are crucial for the time needed to generate VPS maps. The time is directly proportional to the number of strategic views examined (reduced distance  $D$ ) and it increases exponentially with the VPS resolution (reduced grid). An average height error is from 0m (for reference VPS result of  $D = 2\text{m}$  and VPS resolution 1m) to 16.99m ( $D = 52.9\text{m}$  and VPS resolution 100m). For better clarity, results are presented as percentage figures to determine compliance with consecutive VPS simulations and the reference value (see Table 1). The table specifies also computing time needed. The most precise results are colour coded.

The study highlights major densities of strategic views and the possibility of reducing the VPS resolution to the level between 2.0m and 5.0m without any major quality loss.

Table 1. Optimization of VPS – density of strategic views (D) and VPS resolution.

	D = 2,0m	D = 4,2m	D = 6,6m	D = 13,7m	D = 28,4	D = 52,9m
VPS 1m	<b>100,00%</b> 68148,6s	<b>97,22%</b> 33521,1s	<b>94,30%</b> 20938,1s	<b>88,86%</b> 10011,1s	<b>84,66%</b> 5000,1s	<b>81,12%</b> 2869,1s
VPS 2m	<b>99,15%</b> 17051,1s	<b>96,80%</b> 8347,1s	<b>94,18%</b> 5217,4s	<b>88,75%</b> 2519,7s	<b>84,55%</b> 1243,0s	<b>81,01%</b> 725,7s
VPS 5m	<b>98,12%</b> 2740,1s	<b>96,19%</b> 1338,2s	<b>93,87%</b> 834,4s	<b>88,48%</b> 402,5s	<b>84,29%</b> 200,8s	<b>80,78%</b> 115,3s
VPS 10m	<b>97,20%</b> 683,0s	<b>95,49%</b> 336,1s	<b>93,37%</b> 209,8s	<b>88,08%</b> 100,4s	<b>83,90%</b> 49,8s	<b>80,42%</b> 28,7s
VPS 25m	<b>95,15%</b> 109,8s	<b>93,73%</b> 54,0s	<b>92,01%</b> 33,6s	<b>87,04%</b> 16,1s	<b>82,88%</b> 8,0s	<b>79,48%</b> 4,6s
VPS 100m	<b>88,40%</b> 6,9s	<b>87,53%</b> 3,5s	<b>86,58%</b> 2,2s	<b>82,67%</b> 1,0s	<b>79,39%</b> 0,5s	<b>76,47%</b> 0,3s

Table 2. Optimization of VPS – density of strategic views (D) and DSM grid size.

	D = 2,0m	D = 4,2m	D = 6,6m	D = 13,7m	D = 28,4	D = 52,9m
DSM 0,5m	<b>98,12%</b> 2740,1s	<b>96,19%</b> 1338,1s	<b>93,87%</b> 834,1s	<b>88,48%</b> 402,1s	<b>84,29%</b> 201,1s	<b>80,78%</b> 115,1s
DSM 1,0m	<b>96,35%</b> 2566,4s	<b>95,90%</b> 1307,1s	<b>94,78%</b> 815,5s	<b>89,72%</b> 393,7s	<b>85,52%</b> 194,9s	<b>81,67%</b> 115,0s
DSM 2,5m	<b>91,79%</b> 2156,3s	<b>93,67%</b> 1097,3s	<b>93,64%</b> 710,6s	<b>91,59%</b> 343,6s	<b>88,13%</b> 174,9s	<b>85,20%</b> 102,5s
DSM 5,0m	<b>87,73%</b> 1976,6s	<b>88,94%</b> 999,0s	<b>90,26%</b> 643,2s	<b>88,35%</b> 313,2s	<b>83,86%</b> 158,2s	<b>81,39%</b> 92,1s
DSM 10,0m	<b>69,86%</b> 1887,6s	<b>73,24%</b> 901,4s	<b>79,21%</b> 508,0s	<b>82,86%</b> 287,0s	<b>83,01%</b> 145,2s	<b>81,14%</b> 86,8s
DSM 20,0m	<b>54,28%</b> 1228,9s	<b>55,66%</b> 624,3s	<b>56,62%</b> 500,8s	<b>63,10%</b> 259,3s	<b>71,84%</b> 125,1s	<b>78,21%</b> 77,2s

#### 4.4. ACCURACY OF 3D MODEL

The second group of analyses applies to the assessment of the DSM model accuracy and its impact on the quality of VPS results (see Table 2). In total, the study includes 72 simulations in two variations: a) assumption of fixed VPS resolution of 5m, and b) VPS resolution of 2m. The accuracy of the DSM model varies between the DSM grid of 0.5m to DSM grid of 20.0m. As in previous analyses, different densities of strategic views have been used (from D = 2.0m to D = 52.9m). Results are presented in percentage values as in Table 1, which define the degree of compliance of consecutive VPS simulations with the reference VPS

result. Results shown in the Table 2 apply to the VPS 5m analysis and are similar to those of VPS 2m. The lowest accuracy of the model does not have a major influence on the VPS generation time. The use of DSM models 0.5m and 1.0m grid produces satisfactory results, whereas less precise DSM models do not allow to reach reliable VPS results.

## 5. Discussion

### 5.1. SUMMARY & EVALUATION OF RESULTS

The goal of the study was to optimize input data for the application of the VPS method in urban planning. It turned out to be more complex than it was previously thought, and thus analyses focused on one case study only, i.e. the protection of Gdansk panoramas seen from the Motława River. The study showed two relationships that were important for the VPS in general.

Firstly, a key factor decisive regarding the accuracy of the VPS result is the distribution of strategic views examined (reflecting the series of viewpoints, as in Gdansk case study, or other distribution of viewpoints on viewing location e.g. on squares).

Secondly, a high resolution of VPS about 1.0m is not necessary to obtain a desired quality of the analysis. An interpolation of heights from the VPS of a lower 2.0m to 5.0m resolution enables to obtain sufficiently good results that can be used in urban planning, and at the same time, they can be computed much faster.

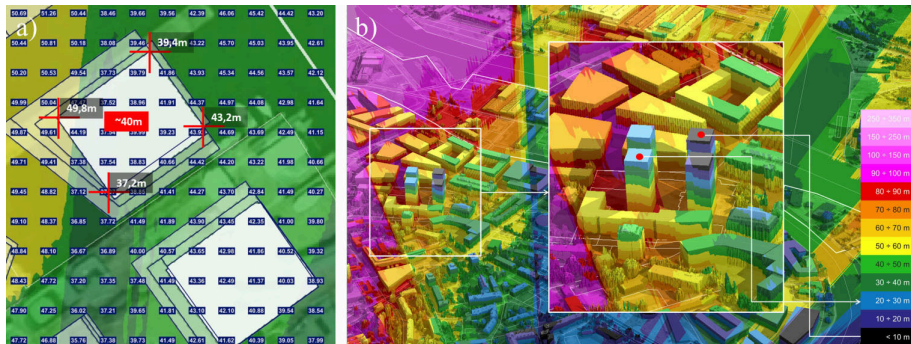


Figure 5. Application of VPS: a) determination of maximum heights of a sample planned facility; b) VPS 3D visualisation showing possibility of elevating of the existing building.

### 5.2. A GLANCE AT THE USE OF VPS IN URBAN PLANNING

VPS builds our knowledge about the impact of new investment on the cityscape. A relevant accuracy of VPS (discussed in article) determines the application of the method in the planning process. The Gdansk case study (based on full resolution VPS) helps to determine precise height limits for new buildings. This applies not only to the height of a new building but also to particular sections of its shape (see Figure 5a). VPS also enables to analyse a possibility of increasing the height of

existing building facilities or replacing them with new taller buildings (see Figure 5b). Nevertheless, VPS results do not determine planning decisions. They enable, however, to examine new investment projects that may have a potential impact on the cityscape and the implementation of which requires further analysis (e.g. analysis using VIS method, Czyńska 2018).

### 5.3. PERSPECTIVES OF VPS

The cityscape is a value that needs to be protected and deserves responsible approach. The VPS method may support a complex planning process by using digital techniques and 3D models. Thus, it refers to a number of other scientific studies (Guney at al. 2012, Yusoff et al. 2014). It is also related to a broader research area involving visual analyses and the use of isovist 3D in urban planning (Suleiman at al. 2013). A distinguishing feature of VPS is the possibility of analysing viewing places using dozens or hundreds view points (strategic views or vistas). Often, a small shift of the observation point to a side may reveal completely new spatial relations in a city. Further studies designed to adjust VPS to the needs of urban planning should take into consideration analyses of other cities and other examples of the cityscape conservation, as well as other types of 3D models, such as CityGML (Kolbe and Gröger 2003). The VWEM method may support the process of identifying strategic views (Czyńska and Rubinowicz 2019).

### 5.4. GUIDELINES FOR APPLICATION OF VPS FOR OTHER CITIES

The study focused on the City of Gdańsk. Although the optimization of VPS parameters is subject to a further analysis, preliminary results enable to apply the VPS method in other cities in Europe and in the world. The study shows that a key factor determining the quality of VPS results is a high density of strategic views - at least 6m. Previous VPS analyses for the protection of cityscapes of Dresden (Rubinowicz, Czyńska 2015), the distance was 50m and it was too large to obtain results of desired accuracy needed in urban planning. The VPS resolution of ca 5.0m provides sufficient approximation of the VPS map. The abovementioned parameters provide guidance for further VPS application in other cities and for the implementation of the method in urban planning.

## 6. Conclusion

In the majority of planning documents in the world, the conservation of the landscape concentrates on preserving vistas that are important in terms of city's identity and culture. The protection of strategic views brings limitations primarily to the height of new buildings. The VPS method, discussed in the article, enables to examine mutual relations between various elements and it produces a plane or a map determining maximum heights of new buildings.

Studies presented in the article focused on adjusting the VPS method and taking into consideration two major criteria: the VPS emulation time and the accuracy of results. Both criteria are crucial for the use of VPS in urban planning. Analyses focused on the Gdansk case study and the use of LiDAR / DSM data. They primarily focused on 3 parameters: accuracy of 3D model, density of strategic

views and the VPS resolution. In total, the study provided 108 VPS analyses using C++ software developed by author.

The study shows that the key factor decisive regarding the quality of the VPS result is the distribution of strategic views examined, which precisely reflect viewing place (high density of viewpoints) and the high VPS resolution is not necessary to obtain relevant quality of the analysis, which has a major impact on the time needed for computation.

## References

- “Vancouver Views – Implementation of “Vancouver Views” and Opportunities for Higher Buildings in the Downtown” : 2011. Available from <<https://vancouver.ca/docs/planning/final-council-report.pdf>> (accessed 6th December 2019).
- “LVMF – London View Management Framework” : 2012. Available from <<https://www.london.gov.uk/what-we-do/planning/implementing-london-plan/planning-guidance-and-practice-notes/london-view-management>> (accessed 6th December 2019).
- Czyńska, K.: 2018, High precision visibility and dominance analysis of tall building in cityscape – on a basis of Digital Surface Model, *Proceedings of the 36th eCAADe Conference*, Łódź, Poland, 481-488.
- Czyńska, K. and Rubinowicz, P.: 2015, Visual protection surface method: Cityscape values in context of tall buildings, *Proceedings of the 10th International Space Syntax Symposium 2015*, London, 142:1-142:10.
- Czyńska, K. and Rubinowicz, P.: 2019, Classification of cityscape areas according to landmarks visibility analysis, *Environmental Impact Assessment Review*, **76**, 47-60.
- Guney, C., Girginkaya, S. A., Cagdas, G. and Yavuz, S.: 2012, Tailoring a geomodel for analyzing an urban skyline, *Landscape and Urban Planning*, **105**(1-2), 160-173.
- Kolbe, T. H. and Gröger, G.: 2003, Towards Unified 3D-City-Models, *Proc. of ISPRS Commission IV Joint Workshop on Challenges in Geospatial Analysis, Integration and Visualization*, Stuttgart.
- Lorens, P.: 2019, Shaping the New Face of the Imperial Shipyard in Gdańsk, *Space & Form*, **40**, 151-170.
- Nutsford, D., Reitsma, F., Pearson, A. L. and Kingham, S.: 2015, Personalising the viewed: Visibility analysis from the human perspective, *Applied Geography*, **62**, 1-7.
- Orlof, J., Ozimek, P., Łabędź, P., Widłak, A. and Nytko, M.: 2019, Determination of Radial Segmentation of Point Clouds Using K-D Trees with the Algorithm Rejecting Subtrees, *Symmetry*, **11**, 1451.
- Rubinowicz, P.: 2019, Protection of the waterfront panoramas based on computational 3D-analysis, *Proceedings of the 37th eCAADe / SIGraDi Conference 2019*, Porto, 325-332.
- Rubinowicz, P. 2019, Visualisation of DSM as 3D-Mesh for Urban Analyses, in L. Cocchiarella (ed.), *Advances in Intelligent Systems and Computing*, Springer, Cham , 1013-1022.
- Rubinowicz, P. and Czyńska, K.: 2015, Study of City Landscape Heritage Using Lidar Data and 3d-City Models, *Int. Arch. Photogramm. Remote Sens. Spatial Inf. Sci.*, **XL-7/W3**, 1395-1402.
- Suleiman, W., Joliveau, T. and Favier, E.: 2013, A New Algorithm for 3D Isovist, *Proceedings of 15th International Symposium on Spatial Data Handling Geospatial dynamics, geosimulation and exploratory visualization*, Bonn, 157-173.
- Yusoff, N. A. H., Noor, A. M. and Ghazali, R.: 2014, City Skyline Conservation: Sustaining the Premier Image of Kuala Lumpur, *Procedia Environmental Sciences*, **20**, 583-592.

# ENVIRONMENTAL PERFORMANCE-BASED COMMUNITY DEVELOPMENT

*A parametric simulation framework for Smart Growth development in the United States*

JONG BUM KIM<sup>1</sup>, BIMAL BALAKRISHNAN<sup>2</sup> and  
JAYEDI AMAN<sup>3</sup>

<sup>1,2,3</sup>*University of Missouri Columbia*

<sup>1,2,3</sup>*{kimjongb|balakrishnanb|ja2qm}@missouri.edu*

**Abstract.** Smart Growth is an urban design movement initiated by Environmental Protection Agency (EPA) in the United States (Smart Growth America, 2019). The regulations of Smart Growth control urban morphologies such as building height, use, position, section configurations, façade configurations, and materials, which have an explicit association with energy performances. This research aims to analyze and visualize the impact of Smart Growth developments on environmental performances. This paper presents a parametric modeling and simulation framework for Smart Growth developments that can model the potential community development scenarios, simulate the environmental footprints of each parcel, and visualize the results of modeling and simulation. We implemented and examined the proposed framework through a case study of two Smart Growth regulations: Columbia Unified Development Code (UDC) in Missouri (City of Columbia Missouri, 2017) and Overland Park Downtown Form-based Code (FBC) in Kansas City (City of Overland Park, 2017, 2019). Last, we discuss the implementation results, the limitations of the proposed framework, and the future work. We anticipate that the proposed method can improve stakeholders' understanding of how Smart Growth developments are associated with potential environmental footprints from an expeditious and thorough exploration of what-if scenarios of the multiple development schemes.

**Keywords.** Smart Growth; Building Information Modeling (BIM); Parametric Simulation; Solar Radiation.

## 1. Smart Growth and its impact on environmental performances

Smart Growth has advocated sustainable community development by using strong design controls with design-based planning regulations (Borys, et al., 2017). These design controls have a relationship with energy performances. Smart Growth regulations have rapidly substituted conventional land use and zoning regulations.

However, forecasting the impact of Smart-Growth regulations on sustainability is still challenging.

Buildings are inarguably a key variable of energy consumption and the sustainable built environment. In planning and resource management, measuring energy use and predicting energy demand are significant steps. Building stock modeling has been rigorously investigated to calculate energy performances of existing buildings (Dascalaki, et al., 2011), evaluate new retrofit plans (Sandberg, et al. 2016), and estimate the potential energy savings and CO<sub>2</sub> emissions (Ballarini, 2014). These studies are based upon the dataset of existing buildings, which has a limitation to envision future development.

Over the decades, urban regulations have implicitly shaped our built environment (Talen, 2012). Land use and zoning in the United States have controlled the distribution of building use to achieve the safety and security of neighborhoods. In 2005, Environmental Protection Agency (EPA) created the Smart Growth Implementation Assistance (SGIA) program to advocate reform of conventional land use and zoning (US EPA, 2013). Since its adoption, public and private sectors have performed various economic analyses to understand the impact of Smart Growth such as Pro-forma analysis, potential financial feasibility, and parking demand simulation. However, the potential impact of Smart Growth regulations on environmental performances has not been fully investigated. Understanding the impact of Smart Growth regulations on energy performances will be a significant step towards sustainable community development.

## **2. Parametric BIM-SIM framework for Smart Growth**

The research aims to analyze and visualize the impact of Smart Growth developments on environmental performances. This paper presents a parametric modeling and simulation framework for Smart Growth developments that can model the potential community development scenarios, simulate the environmental footprints of each parcel, and visualize the results of modeling and simulation. To do so, we conducted (1) an analysis of Smart Growth regulations, (2) parametric modeling in Building Information Modeling (BIM), (3) software prototyping for parametric simulation, and (4) a usability test of the proposed framework.

### **2.1. METHODOLOGY**

Our strategy is to integrate parametric BIM, energy simulation (Solar radiation in this paper), Virtual Reality (VR), and software development. These technologies are rapidly evolving. We have explored varying methods for urban simulations that can be integrated with parametric modeling and BIM. Largely, we have explored four approaches in view of the communication and data exchange between BIM and parametric simulation.

- BIM + BIM API programming (Revit + Revit API + Revit Energy Simulation)
- BIM + BIM visual programming (Revit + Dynamo + Dynamo energy simulation)
- Parametric modeling + visual programming (Rhino + Grasshopper energy

- simulation)
- BIM + visual programming (Revit + Grasshopper energy simulation)

They vary in many aspects, but we focused on (1) the available energy simulation modules, (2) the use of BIM database and the parameters, (3) reliability for a large set of simulations, and (4) a seamless communication between BIM and energy simulation.

## 2.2. PROTOTYPING PROCESS

This paper presents our recent prototype development based upon the fourth approach by using Revit, Grasshopper, Rhino.Inside, and Ladybug. Figure 1 explains the workflow of Parametric BIM-SIM framework. First, we identified required information for parametric modeling from Smart Growth regulations (A1). For parametric BIM modeling, we used Autodesk Revit (A2). For software prototyping (A3, A4), we used Visual Programming with Python and Application Programming Interface (API). For the energy simulation, we performed solar radiation simulation by using open source simulation modules for Grasshopper.

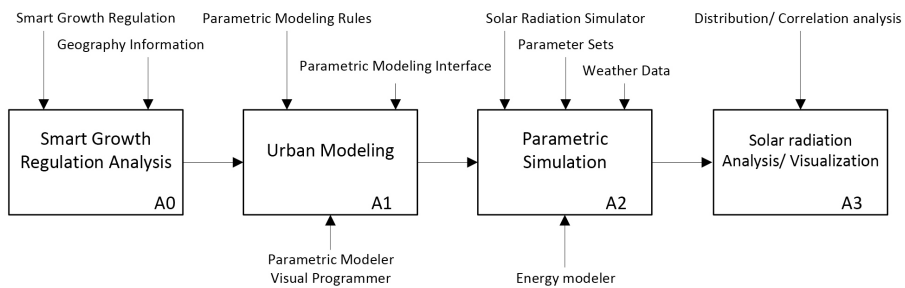


Figure 1. A workflow of Parametric BIM-SIM framework.

## 3. Case Study of Two Smart Growth Regulations

### 3.1. SMART GROWTH REGULATION ANALYSIS

For implementation, we performed a case study of two Smart Growth regulations of Columbia Unified Development Code (UDC) in Missouri and Overland Park Downtown Form-based Code (FBC) in Kansas City. Overland Park FBC has six-focused districts and we implemented Overland Park Downtown district.

Columbia Unified Development Code (UDC) is a Smart Growth regulation adopted in 2017 to achieve economic and sustainable development in Downtown District of Columbia, Missouri. Columbia Downtown is adjacent to University of Missouri Columbia, Columbia College, and Stephens College. Historical buildings, civic centers, locale retails, and new mid-rise apartments coexist in the district. The UDC controls zoning, use, platting/subdivision design, streetscape design, building use, and building configurations. In this paper, we analyzed the design-related provisions from the forth section, Form control of Downtown Columbia.



Overland Park FBC was developed for downtown revitalization. In the mid-2000s, the City of Overland Park experienced a growing economic decline in the old downtown corridor along Metcalf Avenue. For the downtown revitalization, the city adopted the Vision Metcalf Plan in 2008 and identified a long-term vision. According to the progress report, the Metcalf vision plan drives \$270 million new development, redevelopment, and tenant upgrades, which is approximately 14% of the city's total growth (City of Overland Park, 2018, 2017). In 2011, the city adopted Form-Based Code (FBC) to foster coherent visual character, mixed-use development, walkable public realm, and transit-oriented design. FBC had a significant revision in 2019. We focused on the Downtown Form District, one of the six districts of Metcalf Plan.

The two regulations have similar formats and styles in their provisions. Overland Park is 140 miles west from Columbia, so they have similar weather conditions. On the other hand, they have different urban block typologies: Columbia downtown is based on the grid-system, but Overland Park has non-uniform block typologies along the historical corridor, the Metcalf Avenue.

In our case study, we selected key sections and provisions that control urban morphology and building typology. The main selected components are Regulating Plan, Building Envelope Standards (BES), and Architectural Standards. While two cases use their own naming conventions in the regulations, their structures and the provisions styles are similar or identical. It enabled us to formulate a standard parameter set for our parametric modeling and simulation. In our previous research, we successfully imbedded a comprehensive set of Smart Growth regulations into the object parameters in BIM such as transect types, storefront types, building use, building dimensions, parking requirements, and construction costs. In this paper, we demonstrate the parametric BIM and solar radiation simulation, so limited parameters are included in our implementation.

### 3.2. PARAMETRIC URBAN MODELING IN BIM

We created district models in parametric BIM by using Regulating Plan, BES, and Architectural Standards in Smart Growth regulations (Figure 2). BES provides regulation variables about building section configuration such as height, use, and key building components that can affect the potential energy performances. The general modeling process is illustrated in Figure 2. First, we mapped parcel information from Regulating Plan to the individual parcel objects. Next, we determined the location of building objects based upon the Required Building Line (RBL) in Smart Growth Regulations. The sectional configurations of individual objects were formulated based upon the Building Envelope Standards. Last, we parameterized the provisions related to the building dimensions as BIM object parameters and their behavior. For modeling, we used Autodesk Revit.

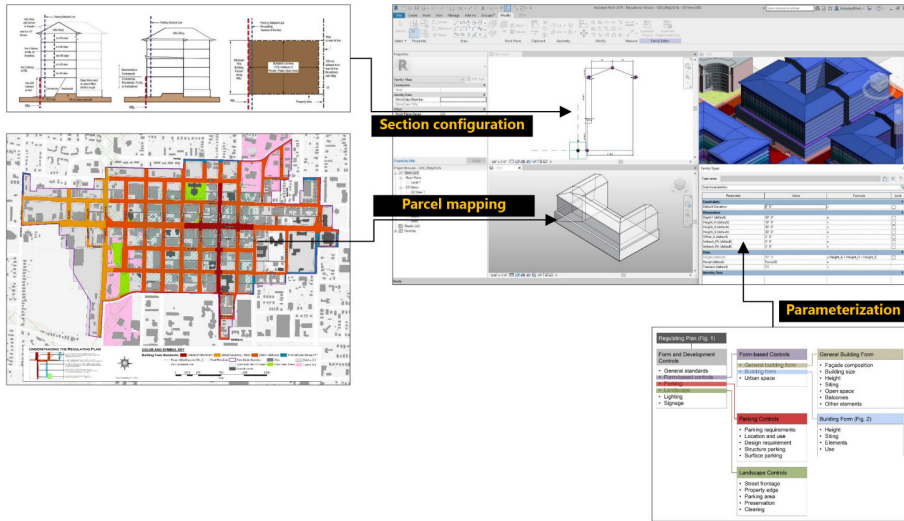


Figure 2. Parametric urban modeling for Smart Growth.

### 3.3. PARAMETRIC BIM-SIM INTERFACE

Our objective in parametric simulation is to integrate BIM and solar radiation simulation for testing a large number of development scenarios. Since our district model represents flexible buildable volumes identified in Smart Growth regulations, we prioritized the capability of handling a large number of parameter values throughout the software prototyping process. Figure 3 presents the major process of our parametric BIM-SIM workflow.

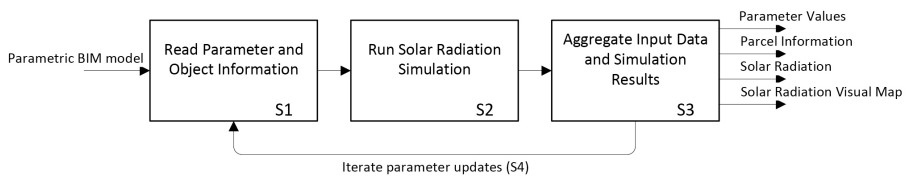


Figure 3. Parametric BIM-SIM Workflow.

For our software prototyping, we used Revit, Grasshopper, Rhino.Inside (Robert McNeel, 2019), Ladybug (Roudsari, 2013), and Colibri (CORE studio, 2017). The first step is to load a visual programming interface from Revit. We used Rhino.Inside, an open-source plug-in that allows running Rhino and Grasshopper in Revit. It enables users to access BIM information, extract subsets of object information, update BIM parameters, and execute performance simulations through Grasshopper platform. This approach made it possible to handle rich semantics and BIM information with various visual programming modules of Grasshopper. For solar radiation simulation, we used Ladybug,

an open-source simulation interface using legacy simulation engines such as EnergyPlus, Radiance, and Daysim. For weather information, we used TMY3 data of Columbia, MO (724450) and Kansas City, Kansas (724460). To simulate a large number of parameter sets, we used Colibri, a Grasshopper plug-in that can iterate a range of input values, export the simulation results, and produce the solar radiation renderings. In sum, we developed the prototype in a flexible way so that users can have full access to the parameters, design the simulation iterations, and customize output data.

Three main simulation phases illustrated in Figure 3 are creating inputs for solar radiation (S1), executing simulation (S2), and exporting simulation results (S3). Figure 4 is a screenshot of the Grasshopper script that performs these tasks.

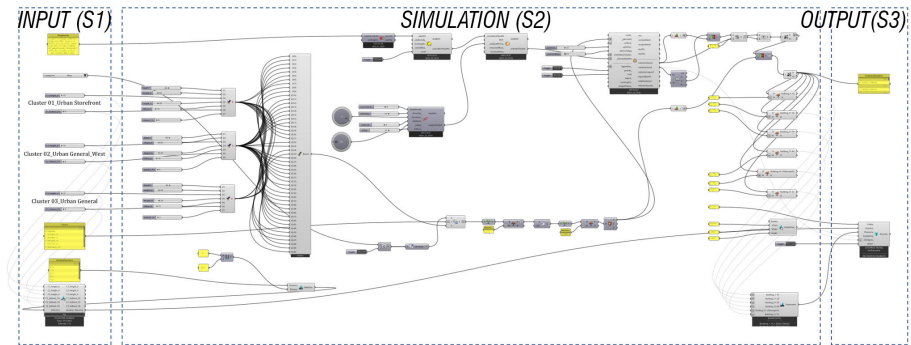


Figure 4. Software Prototype for Solar Radiation Analysis.

GenCumulativeSky node in Ladybug calculates the amount of radiation for different sky patches, providing an overall projection of the local sky condition. We fed Revit geometry information into Ladybug and set up the sky matrix information for individual parcels (Figure 2). Then, we assigned the optimal sensor grid on the object surfaces in consideration of simulation time and accuracy.

Besides that, simulation iterations are significant for understanding the association of Smart Growth regulations and energy performances. We used Colibri Iterator to manipulate parameter values and Colibri Aggregator to export simulation results. The current simulation output includes the parcel information, input regulation variables, building object information (volume and surface area), solar radiation values (sensor, surface, building object, and parcels), and solar radiation renderings.

For each case, we run 216 simulations at the summer solstice based on the weather data. To handle a large number of simulation iterations, we tested three parameters: transect type, building height, and setback. Transect is a zoning classification method in Smart Growth regulation to promote cohesive design by using specific design requirements such as building height, use, building components. For example, Columbia UDC has three Transect types of Urban Store Front, Urban General, and Urban General-West. We clustered individual parcels by using the Transect types and assigned three types of building height and two

types of setback. These parameter sets were connected with Colibri notes and the application executed 216 simulations in a single run. Table 1 shows the parameter sets for the simulation iterations.

Table 1. Parameter sets for simulation iterations.

Parameter inputs	Values (feet)	Transect Types	Iterations
Building height	20, 40, 60	3	3 x 3 x 3
Setback	0, 5	3	2 x 2 x 2
<b>Total Number of Iterations</b>			<b>27 x 8 = 216</b>

In our experiment, the simulation for two cases of 432 iterations spent about 12 hours by using Intel Xeon 3.2 GHz processor, 32GB memory, and 4GB graphics. The run time was sensitive to the number of sensors assigned to each surface.

Figure 5 presents color-coded renderings of solar radiation levels generated from the Ladybug and Colibri plugins. The solar radiation of the top surface is consistent across the parcels, but vertical surfaces present a wide range of colors.

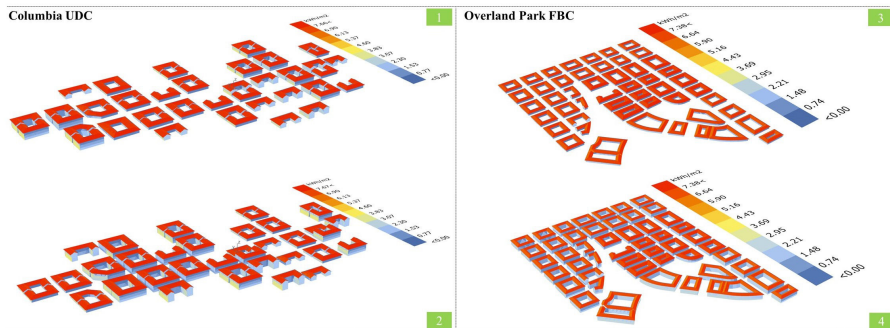


Figure 5. Solar radiation renderings of two cases.

The whisker plots in Figure 6 shows the distribution of solar radiation of individual sites, including maximum, minimum, and median values. We observed that some parcels have more variations than others do, which means the solar radiation differs across the parcels. When comparing two Smart Growth regulations, the variations across the parcels were noticeable. This random distribution makes it ambiguous to predict the energy performances not only of each parcel but also of the entire community development. Still, this impact of Smart Growth on sustainability is not addressed in the planning stage.

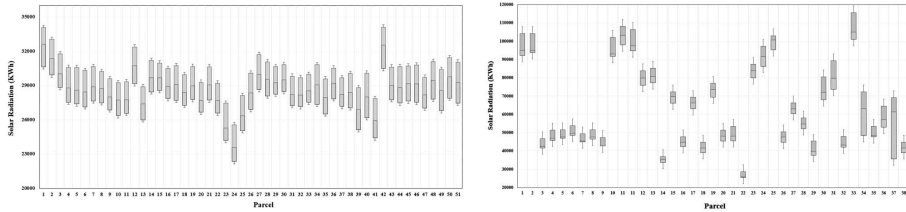


Figure 6. Whisker plots of a parcel-level solar radiation distribution (left: Columbia UDC; right: Overland Park FBC).

### 3.4. VISUALIZATION AND USABILITY TESTING

The last step of our experiment was a usability test at the immersive visualization lab, which is in progress. Figure 7 shows our pilot test at our visualization lab.



Figure 7. A pilot test at the visualization lab.

The research team consists of faculty members, graduate researchers, and a sustainable manager of City of Columbia. Users loaded the district model to Revit, run Rhino.Inside, and call the software prototype in Grasshopper. Then, users assigned the range of parameter values and executed solar radiation simulation. For visualization, we opened Enscape plug-in from Revit and projected streetscapes and illuminance renderings through VR headsets. For VR, we used Oculus Quest and HTC Vive Pro. In the test, users were able to walk through the streetscape to see the abstract building façades and the potential outdoor spaces. The illuminance view in Enscape provided a time-series visualization of solar availability of the built environment. The system operator and the sustainable manager discussed the what-if scenarios and updated the parameters by using a visual programming interface.

#### 4. Findings and Discussion

In this research, we investigated a parametric BIM and simulation method that can analyze and visualize the impact of Smart Growth developments on environmental performances. This paper presented the parametric BIM-SIM framework and software prototype development. The prototyping method enabled us to use rich semantics and parametric modeling capabilities in BIM for Smart Growth regulation modeling.

Parametric in BIM was significant in our implementation. Once we parameterized the range of provision allowances as BIM parameters, such as a minimum and a maximum building height, it enabled us to calculate the impact of building geometry on the potential solar radiation. The simulation module generated not only parcel-level solar accessibility but also surface-level solar radiation of individual building objects. The simulation iteration allowed us to generate a large number of simulation results that consist of information on potential urban morphologies and the regulation variables of Smart Growth.

The main challenges in urban simulation are handling the level of scale of urban model, the level of detail of individual building objects, and the simulation computing capacities. Still, managing a large number of simulations is challenging in view of simulation time and system reliability (Quan, 2014, Reinhart, 2016). We tested limited parameters and each case has less than 50 parcels. In our simulation, each simulation spent 1.5 minutes, but it is not fast enough when considering the large scale of urban blocks and the extensive number of regulation variables. In VR, the synchronization between our software interface and BIM took a couple of seconds. Then, Enscape projected the updated development scenario later. The time lack for synchronization was recognizable, but any file conversion or data exchange was not required. As we described in a previous research paper, Revit material and visibility settings were not fully compatible with Enscape, which deteriorated the quality of VR-based navigation. The other limitation in simulation visualization is that the illuminance rendering in VR is an automatically generated view from Enscape engine, which is not associated with the simulation results our prototype produced. In this research, we used multiple software environments to implement our framework. More accessible user interfaces will be able to eliminate software dependencies for performance-based community development.

**Acknowledgments.** This research was supported by Richard Wallas Faculty Incentive Grant and Research Council Grant of University of Missouri Columbia

#### References

- “Codes That Support Smart Growth Development” : 2013. Available from US EPA<<https://www.epa.gov/smartgrowth/codes-support-smart-growth-development>>.
- “Unified Development Code” : 2017. Available from City of Columbia Missouri<<https://www.como.gov/community-development/planning/development-code-update-project/>>.
- “Vision Metcalf - City of Overland Park, Kansas” : 2018. Available from City of Overland Park Planning and Development Services<<https://www.opkansas.org/city-services/planning-development/long-range-planning/special-area-studies/vision-metcalf/>>.
- “Smart Growth America” : 2019. Available from Smart Growth America<<https://smartgrowthamerica.org/our-vision/what-is-smart-growth/>>.

- “Municipal Code” : 2019. Available from City of Overland Park<<http://online.encodeplus.com/regs/overlandpark-ks/doc-viewer.aspx#secid-7098>>.
- C.F., R. and C.C., D.: 2016, Urban building energy modeling – A review of a nascent field - ScienceDirect, *Building and Environment*, **97**, 196-202.
- E, T.: 2012, *City Rules: How Regulations Affect Urban Form - Emily Talen - Google Books*, Washington DC, USA: Island Press.
- E, D., P, D., C, B. and S, K.: 2011, Building typologies as a tool for assessing the energy performance of residential buildings – A case study for the Hellenic building stock - ScienceDirect, *Energy & Buildings*, **43**, 3400-3409.
- H, B., E, T. and M, L.: 2017, “Form-Based Codes? You’re not alone. PlaceMakers”. Available from <<http://www.placemakers.com/how-we-teach/codes-study/>>.
- I, B., S.P, C. and V, C.: 2014, Use of reference buildings to assess the energy saving potentials of the residential building stock: The experience of TABULA project - ScienceDirect, *Energy Policy*, **68**, 273-284.
- N.H., S., I, S., O, H. and R, D.: 2019, Dynamic building stock modelling: Application to 11 European countries to support the energy efficiency and retrofit ambitions of the EU - ScienceDirect, *Energy and Buildings*, **132**, 26-38.

# FOUR APPROACHES FOR INTEGRATION OF DIGITAL BIM PRACTICES IN AEC PROJECTS

GILLES HALIN<sup>1</sup>, VERONIKA BOLSHAKOVA<sup>2</sup>,  
ELODIE HOCHSHEID<sup>3</sup>, HENRI-JEAN GLESS<sup>4</sup> and SIALA AIDA<sup>5</sup>

<sup>1</sup>UMR CNRS MAP. Lorraine University, France

<sup>1</sup>*gilles.halin@univ-lorraine.fr*

<sup>2</sup>UMR CNRS MAP

<sup>2</sup>*bolshakova.veronika@gmail.com*

<sup>3,4</sup>UMR CNRS MAP. School of Architecture of Nancy, France

<sup>3,4</sup>*{elodie.3h|hj.gless}@gmail.com*

<sup>5</sup>UMR CNRS MAP. Carthage University, Tunisia

<sup>5</sup>*aida.saila@gmail.com*

**Abstract.** The newest information and communication technologies bring a major shift to the AEC sector and foster it towards the new digital globalized economy. The last decades witnessed many changes in the AEC industry brought in by digital tools and by the adoption of Building Information Modeling/Management (BIM). The changes had influenced the common practices of design, construction and management, they have also fostered new digital practices into AEC. Innovative digital project management becomes a base element of an effective BIM project management. The project teams' collective competencies and skills contribute to design development and value engineering of the project. In this context, four approaches: BIM adoption, agile BIM, 4D digital decision-making, qualitative requirements to BIM, which are resulting from the research are presented in this article whose objective is to assist and facilitate the integration of digital in AEC specific professional practices.

**Keywords.** Digital Practice; BIM Process; Adoption; 4D; Agility.

## 1. Introduction

The last decades witnessed many changes in the AEC industry brought in by digital tools and by the adoption of Building Information Modeling/Management (BIM). The changes had influenced the common practices of design, construction and management, they have also fostered new digital practices into AEC. Innovative digital project management becomes a base element of an effective BIM project management. In this context, four research approaches are presented in this article, with an objective is to assist and facilitate the integration of digital in AEC specific professional practices.

Since BIM is a collaborative innovation, the research has mainly focused on understanding implementation in project teams, neglecting that BIM has also a



great impact on every firm of AEC project. The first approach, presented in part 2, focuses on the adoption steps and organizational changes that firms face when they are adopting BIM. It proposes an online tool to help architecture firms understand the steps in a process of BIM adoption and the stages of its implementation. In following part 3, the approach focuses on integration of the agile software engineering practices into design activities in French architecture firms to improve: communication, group cohesion, and client integration. Four agile practices have been identified and adapted for architecture project design. The next part presents the third approach, it describes a collaboration practice issue to the adoption of an nD BIM in a project: the collective decision-making with 4D BIM. This research explores the use of natural user interfaces (NUIs) and proposes touchable tool for the meetings (synchronous collaboration sessions). The tool improves interactions between the un-trained users and the 4D BIM. The last approach focuses on a new digital design practice that allows us to consider and implement the program spaces requirements in BIM process. The goal is to support the design of BIM models that meet better the project program requirements and optimize design time. This approach is based on a semantic model describing project spaces, it encompasses: qualitative spatial requirements, a process and a tool.

These four approaches are the result of mutual thinking on the integration of digital practices into AEC projects. Approaches are based on different surveys, on different pedagogical or professional experiments, which are supporting and validating the proposed methods, and tools foster their integration into a collaborative BIM process.

## **2. BIM adoption and implementation in architecture firms**

Architects are at the heart of design and construction process and are often at the origin of the first digital mock-up of the project. In France, architectural firms are generally very small and rarely ready to go through BIM implementation. While more and more companies are interested in BIM, many are afraid to adopt this innovation. Some firms found BIM avoidance strategies, despite the increasing demands from clients for BIM deliverables. Some firms do not want to implement BIM practices, others do not wish to do so but do not know how to operate. So it seems essential to carry out work on the adoption of BIM in architectural firms to respond two main objectives: (1) build a better understanding of the adoption of BIM in architectural firms and (2) provide tools, methods, and documentation that will help companies that want to implement BIM.

During an exploratory work in 2016, we identified that there was no BIM implementation guide adapted to SMEs. In these guides, implementation is very often understood as setting up BIM in a project team that is already operational on BIM processes. We studied BIM implementation as the first setting up of BIM in a firm, which refers to micro BIM adoption (Succar and Kassem 2015).

Semi-directive exploratory interviews were conducted with fifteen architects at the beginning of the project. These interviews allowed us to identify four BIM-reaction profiles within the architect's population : (1) firms who regularly use BIM on a large part of their project, (2) those who work with traditional

processes and don't want to change to BIM (Succar and Kassem 2015), (3) those who work with traditional processes and want to implement BIM, and (4) firms that have several processes coexisting (Hochscheid and Halin 2019b). Situation 1 is quite rare in France, and Situation 2 allowed us to identify BIM avoidance strategies.

A BIM-specific literature review allowed us to identify a gap : the difference between diffusion, adoption and implementation was not explicit (Hochscheid and Halin 2019a). This distinction led us to focus on the five-stages BIM adoption process found in the diffusion of innovation theory (Rogers 2003). During the adoption process, a company goes through five main stages: awareness, intention, decision, and, once the adoption decision is taken, companies go through implementation and confirmation stages ((Hochscheid and Halin 2019a). Decision of adoption (DoA) seems to be a turning point in the adoption process. Before the DoA, companies focus on decision while after the DoA, they are concerned about the practical problems and the success of the implementation. The BIM adoption process model allowed us to distinguish the factors that influence the decision to adopt (decision factors) from the factors that influence implementation (implementation factors).

In BIM adoption scientific literature, factors that influence BIM adoption are rarely placed on the adoption process. It has led to a confusion: factors that intervene before and after DoA are not differentiated and are often reduced to factors that influence decision do adopt BIM. Implementation factors have been little studied, as if decision to adopt necessarily leads to the success of the implementation. We defined a framework for studying factors that influence the process of adopting BIM and specifically those on implementation to help the company understand how to avoid failure. It has been identified that implementation factors can be of four different types: internal context of the firm, external context, BIM and change characteristics (implementation strategies and change management) (Hochscheid and Halin 2019c).

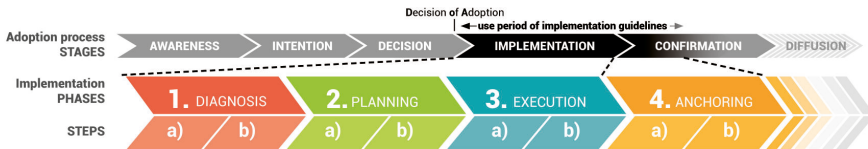


Figure 1. BIM adoption process with the four-phases guidelines for implementation.

Identification of adoption factors has been useful for the elaboration of a survey we diffused to 30,000 architects via the French Institute of Architects (CNOA) and we collected 892 valid responses. The results are not yet published but this survey will allow us to get to know the French architectural firms better, to identify their digital practices, their reaction to the BIM, factors that influenced them to decide to adopt the BIM and the BIM implementation practices that they put in place.

The final part of this work focuses on developing a method to assist firms to implement BIM. A action research based on the observation of four architecture firms during BIM implementation has been put in place. These experiences

allowed us to test implementation strategies and to observe how firms react to BIM implementation. Based on an in-depth literature review, interview results, survey results, and action research, we proposed guidelines to help companies to develop their personalized implementation plan (Hochscheid et al. Halin 2019b). This method covers the last two steps of the adoption process (implementation and confirmation) and comprises four main phases: diagnosis, planning, implementation and anchoring (Figure 1). The first three phases refer to a disruptive change, whereas the anchoring phase refers to an incremental change. We developed a web application that tools this method and gives access to architecture firms in an interactive and playful way.

### 3. A BIM-Agile method in Architectural design project

According to Patrick MacLeamy's curve, BIM technology increases design work, (Kensek 2014) and it also changes digital and collaborative practices. By emphasizing the design work, BIM technology brings more tasks and decision-making, its implementation obliges designers to early coordination. This creates mistrust among the project actors, and rigidifies collaboration. In software engineering and HCI design sectors, agile methods are being applied to answer similar challenges (Womack and Jones 2003). Thus, we have oriented our research towards collaborative practices to improve collaboration and consequently exchanges within a group in order to solve these problems.

Agile methods are specific management methods that involve the client into the decision-making process and follow three fundamental rules: team collaboration, continuous improvement and change acceptance (Beck et al. 2001). We hypothesize that the implementation of agile practices into design activities will improve project team communication and coordination and project quality. We identified four agile practices in software engineering and HCI design, and then experimented and adapted them to architecture design.

The **design matrix** is an collaborative online tool that obliges design team to complete a table which is linking the program (inputs) and the architecture designers intentions (outputs). The table of the design matrix contains in rows the program elements of the project (an entrance hall, a living room or a meeting room) and in columns the stakes (concept, keywords or materials). Collaboratively, the designers fill each cell and write their architecture intentions. The design matrix is thus positioned as an intermediate object, like a dashboard in which all design information is recorded. Also it is essentially a tool to assist designers therefore each cell does not need to be filled.

**Micro poker** is a card game inspired by poker planning (Kniberg 2015), an agile practice used in Scrum or XP methods in which designers will ask themselves questions about how to perform BIM tasks (complexity, duration, urgency or relevance) and then show the tasks estimates using game cards. To answer these questions, each player selects a card from a set of four cards, with several scales of estimates on every card: numerical, colour, magnitude, chance (see Fig. 3). We avoid the phenomenon of cognitive anchoring, known as the "first speaker". Thus, a player cannot influence others by showing his card first. First players

choose their cards, next ones with the most extreme card values start a debate. The objective is to reach a consensus by allowing all players to express themselves and thus to develop collective group consciousness.

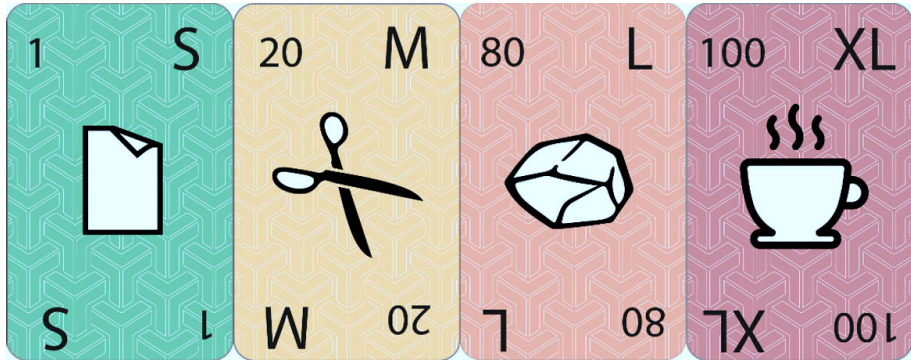


Figure 2. Set of a micro poker deck.

The **stand-up meeting** is a practice mainly used in the Scrum method (Kniberg2015). It involves regularly convening the design team and measuring the progress. Each person, answers three questions: what did I do yesterday, what will I do today, what problems am I facing? The meeting should be short and give the global vision of team’s work while allowing mutual assistance and solutions. It is held standing to avoid comfort and shorten meeting duration.

The **BIM-agile coach** is a practice inspired by the agile coach (Kniberg 2015). This is a person outside the design team whose role is to ensure that the BIM collaboration is applied properly, and that the team has all the necessary to advance the project. His approach must resemble to a client representative, a person who envisions clients’ needs to be responsive. Thus, the BIM-agile coach can be a person who will lead the stand-up meeting, play the role of the game leader at the micro poker or check the correct fill up of the design matrix. This person maybe the project manager of a project.

These four practices were tested at an architecture design workshop with multidisciplinary student teams. The workshop survey results show that BIM-agile practices improve communication and coordination among design actors (Gless et al.2019).

#### 4. Digital tool support for a synchronous collaboration and decision-making with 4D BIM

- 4D BIM uses and project development phases

4D BIM binds a virtual 3D model of the project with time and resources related information, and it occurs mostly at a pre-construction phase of project progress. Projects with 4D BIM use usually offer an improved cost and error control, whilst making scheduling and coordination more efficient during the digital project management. During the last two decades, various studies have been conducted

and often concluded that the 4D BIM adoption rate stays relatively low (Gledson and Greenwood, 2017). Often, the main use of 4D BIM is for visualization of a construction project, however, the other uses have not been fully integrated into common practices for now (Guerriero et al., 2017).

To ample the general study of BIM uses, (Guerriero et al. 2017) propose the 4D BIM uses: Scheduling, Clash Detection, Safety Management, Site Layout & Environment Management, Constructability Management, Monitoring, and Visual communication as a core use. We propose the 4D BIM uses potential introduction and implementation by project development phases in correlation with the project LOD. Table 1 below presents a scheme for the proposal.

Table 1. Project phases and model LOD, 4D BIM use potential introduction.

PROJECT DEVELOPMENT PHASE				
Project identification	Pre-design	Pre-construction	Construction	Operation & Maintenance
Program	Schematic design Design development	Construction documentation	Fabrication	
BIM MODEL LOD				
Conceptual	Approximate	Precise	Detailed	Recorded
TIME MANAGEMENT				
4D BIM uses	4D Scheduling			
	4D Clash Detection			
			4D Safety Management	
			4D Site Lay-out, Environment Management	
			4D Constructability Management	
				4D Monitoring

Naturally, through project progress, the project information and task complexity augments as well as augments a number of professionals involved in the project development.

- 4DCollab research project and a new digital tool support for a collective decision-making

Digital nD information and tools form the core of a sociotechnical system. The core is encompassed by cooperation, collaboration and professional culture established by project stakeholders A continuity of digital information flow is important for efficient exchanges and collaboration. To maintain the digital continuum at the meetings (synchronous collaboration sessions SCS), a research team of 4DCollab ([www.4dcollab-project.eu](http://www.4dcollab-project.eu)) project aims to design a new collaborative 4D-based decision-making tool. Where the 4D represents more complex information than a 3D, thus, it provides a perspective on questions of an efficient and adapted to the 4D BIM uses visualization of the nD project information. We propose to implement a digital synchronous collaboration tool (a multi-touch table and software) at the meetings. The tool unites the stakeholders' attention to the same documents, and also offers democratic interactions with the interface through natural user interactions (NUI). In addition, NUI offers the ease of access and low appropriation time with a tool. It fosters collaboration and the 4D BIM uses convergence with the ease of interactions. The research project team chose a user-centred approach to adapt the future prototype to AEC needs and to different types of meetings.

- Groundwork steps to the prototyping of 4D-based decision-making support tool

4DCollab team has run a series of experiments with AEC professionals, who have used a multi-touch table and 4D simulation for SCS on a task proposed by the experiment. Also, the pedagogic experiments complete the SCS observations (Bolshakova et al., 2019). These let to better understand and identify the specific needs of the users. In addition, we have assembled relevant to 4D BIM uses the stakeholders' roles and documents in correlation to a decision-making type. These concepts are united in an SCS model where a Collaboration Group Persona concept becomes a base of the multi-user cantered approach for the prototyping (Bolshakova et al., 2019), it helps to adapt the user interactions and visualization to the use cases, and completes the social part of sociotechnical system. On a technical side, a semantics for linking data from 4D BIM to digital collaborative tool fulfils the digital continuity of the documents flow (Boje et al., 2019).

### **5. Integration of qualitative spatial requirements in BIM process practices**

Architecture design is based on spatial requirements determined at an early stage of design process. The requirements are either quantitative geometrical constraints (e.g. length, width, ceiling height, etc.), either qualitative constraints (e.g. accessibility, relation between spaces, relative disposition to each other, visibility, communication, etc.). These qualitative spatial requirements (QLSR) are fundamental to guide the designer on project shaping, and they are useful to evaluate a conformity of designed BIM models to a requested program. However, current BIM practices do not consider the QLSR, since they are based on standards, which transform all building information into mainly quantitative data. Currently, only constructive information is taken into account during design (Siala and al. 2016) and the QLSR are still partially known by design teams who have to check the program many times to retrieve the necessary information to verify their model conformity through project evolution. This activity is a significant time-waste, especially in highly collaborative projects where a data absence causes errors.

This research focuses on integration of QLSR into current BIM practices to allow designers to consult and check compliance of BIM-based models throughout the design process. First a content analysis work on architecture program documents corpus identified the most relevant QLSR. The corpus encompasses a selection of program studies of various public building projects (e.g. a school group, a media library, etc.) and programming guides (e.g. a hospital, a museum, etc.), in order to collect the types of qualitative requirements. This allowed to identify five types of QLSR including: accessibility requirements (e.g. access type, characteristic and constraints), topology requirements (e.g. space arrangement constraints, type of the relationship between spaces, type of distribution) and comfort requirements (e.g. lighting type, ventilation type, acoustic, thermal and safety constraints). These are not taken into account by current BIM tools and formats (Siala and al. 2017). Also the analysis identified the most frequently used qualifiers of spatial requirements.

Based on this work, we have developed a new approach to integrate QLSR

into BIM practice. It is built on a new process and a new space model. The space model considers and organises information on the identified QLSR. It includes the latest IFC specifications and represents a possible evolution of the standard. It contains information about the project spaces in both design and programming phase. Figure 5 shows this new model of QLSR. The process is based on the programming and the design phases. It involves two actors, the architect and the programmer (actor in charge of architecture programming) and adopts Autodesk Revit as a BIM tool and its visual programming plug-in Dynamo. This process has three steps; QLSR digital input in a Revit relevant format, their integration into Revit, and the checking of models' compliance.

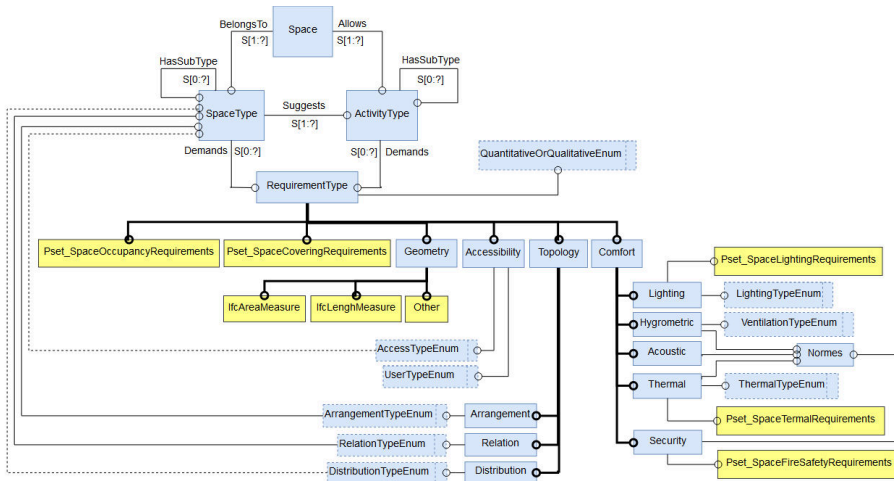


Figure 3. Extract from the proposed space model: the requirements model.

In the input step, a pre-filled spreadsheet has been prepared to allow a programmer to link the requirements with the requested rooms by selecting them from predefined values lists (according to the specified space model). Thus, the programmer provides the designer a programming study and a qualitative requirements spreadsheet file. In the integration step, before starting the designer adds those requirements to Revit by an execution of the spreadsheet exploit script.

When having all the QLSR on Revit, the designer does the design respecting the requirements visible in the rooms' constraint list. For the checking step, the designer can verify his model compliance to the required program, through the rooms' visualization according to each requirement parameter using a colour code (green: compliant/red: non-compliant) ensured through a set of scripts defined on a set of checking rules to verify: proximity of rooms, contiguity, distribution (vertical and horizontal), relation between rooms, accessibility, natural lighting, natural ventilation, etc. In this approach, the designer works only with the BIM design tool.

This approach was tested at a pedagogical experiment in real design situations and it was confronted with the usual design approach. The experiment

shows that the approach not only allows to produce BIM models more in line with the program requirements but also to optimize the design time. This approach must now be experimented on a larger scale to determine how this new BIM practice should be improved for adoption by AEC professionals.

## 6. Conclusion

Each of these four approaches contributes to the integration of BIM technology into AEC specific professional practices. The first one reveals that taking the adoption decision of BIM technology in a firm is not sufficient to succeed a real integration. The implementation factors must be taken into account. The second approach, on the other hand, shows that the use of agile practices in project management can facilitate the integration of new tasks resulting from the integration of BIM. The last two approaches identify new practices that has emerged with the integration of BIM. The collective decision-making with 4D requires relevant and AEC adapted digital tools and supports, which allow project actors: to access and manipulate all the digital information from a BIM model; to integrate the results of decision-making into the same BIM model. The last approach proposes a collaborative BIM practice that improves programmer and architect interactions by integrating qualitative requirements into the BIM model through the use of relevant processes and tools. The integration of BIM technology and, more generally, emerging digital technologies, into existing or new AEC practices still require more studies and research, which will be defining appropriate methods (models, tools and processes) and will be validated by experimental approaches for more efficient adaptation and adoption.

## References

- Beck et al., K.: 2001, "Manifesto for Agile Software Development" . Available from <<http://a-gilemanifesto.org>> (accessed december 2019).
- Boje, C., Bolshakova, V., Guerriero, A., Kubicki, S. and Halin, G.: 2019, Semantics for linking data from 4D BIM to digital collaborative tool, *Frontiers of Engineering Management*, **online**, nn.
- Bolshakova, V., Guerriero, A., Carvalho, H. and Halin, G. 2019, Collective Decision-Making with 4D BIM: Collaboration Group Persona Study, in I. Mutis and T. Hartmann (eds.), *Advances in Informatics and Computing in Civil and Construction Engineering*, Springer International Publishing, Cham, 455-462.
- Bolshakova, V., Halin, G., Guerriero, A. and Besançon, F.: 2019, Collaboration tool for 3D and 4D models: A pedagogical experiment applied to wooden construction, *Proceedings of CIBw78 2019*, Newcastle, University of Northumbria, 21-31.
- Gledson, B. J. and Greenwood, D.: 2017, The adoption of 4D BIM in the UK construction industry: an innovation diffusion approach, *Engineering, Construction and Architectural Management*, **24**(6), 950-967.
- Gless, H.J., Halin, G. and Hanser, D. 2019, Towards a BIM-Agile Method in Architecture Design Assessment of a Pedagogical Experiment, in I. Mutis and T. Hartmann (eds.), *Advances in Informatics and Computing in Civil and Construction Engineering*, Springer, Cham, 397-404.
- Guerriero, A., Kubicki, S., Berroir, F. and Lemaire, C.: 2017, BIM-enhanced collaborative smart technologies for LEAN construction processes, *International Conference on Engineering, Technology and Innovation (ICE/ITMC)*, *IEEE*, 1023-1030.



- Hochscheid, E. and Halin, G.: 2019a, Generic and SME-specific factors that influence the BIM adoption process: an overview that highlights gaps in the literature., *Frontiers of Engineering Management*, **On line**, 1-12.
- Hochscheid, E. and Halin, G.: 2019b, Micro BIM adoption in design firms: Guidelines for doing a BIM implementation plan, *Proceedings of Creative Construction Conference 2019 (CCC2019)*, Budapest, Hungary.
- Hochscheid, E. and Halin, G.: 2019c, A framework for studying the factors that influence the BIM adoption process, *Proceedings of CIBw78 2019*, Newcastle, England, UK.
- Kensek, K.: 2014, *Building Information Modeling*, Routledge.
- Kniberg, H.: 2015, *Scrum and Xp from the Trenches: How We Do Scrum*, Lulu Press, Morrisville.
- Rogers, E. M.: 2003, *Diffusion of Innovations*, Simon and Schuster.
- Siala, A., Halin, G., Allani-Bouhoula, N. and Bouattour, M.: 2016, Toward Space Oriented BIM Practices, *Proceedings of eCAADe 2016*, Oulu, Finland.
- Siala, A., Halin, G. and Bouattour, M.: 2017, Architecture space quality, from virtual to physical, *Proceedings of 5th eCAADe Regional International Symposium*, Cardiff, Wales, UK.
- Succar, B. and Kassem, M.: 2015, Macro-BIM adoption: Conceptual structures., *Automation in Construction*, **57**, 64-79.
- Womack, J. and Jones, D.: 2003, *Lean Thinking: Banish Waste and Create Wealth in Your Corporation*, Free Press, New York.

## Index of Authors

### A

Aagaard, Anders Kruse 1-125  
 Abdelmohsen, Sherif 1-163  
 Abuzuraiq, Ahmed M. 1-475, 1-485,  
 1-557  
 Agra, Rocío 2-233  
 Aida, Siala 1-883  
 Akizuki, Yuta 1-445  
 Alsalman, Osama 1-475  
 AlSalman, Osama 1-557  
 Alva, Pradeep 1-793  
 Aman, Jayedi 1-873  
 van Ameijde, Jeroen 2-283  
 An, Keyao 2-601  
 Antle, Alissa N. 1-265  
 Araújo, Gonçalo 2-101

### B

Bai, Nan 1-305  
 Balakrishnan, Bimal 1-873  
 Banon, Carlos 1-153  
 Bar-Sinai, Karen Lee 2-223, 2-243  
 Beatricia, Beatricia 1-405  
 Belém, Catarina 1-295  
 Bernhard, Mathias 1-445  
 Birol, Eda Begum 1-395  
 Bissoonauth, Chitraj 2-213  
 Blasetti, Ezio 2-661  
 Bolshakova, Veronika 1-883  
 Brown, Andre 2-163, 2-173  
 Bruce, Caitlin 1-135  
 Budig, Michael 1-751, 2-303  
 Bui, Do Phuong Tung 2-323  
 Burry, Mark 2-51

### C

Caetano, Inês 1-599  
 Capunaman, Ozguc Bertug 1-243  
 Carroll, Stan 1-65  
 Castelo-Branco, Renata 1-375  
 Cerovsek, Tomo 1-325  
 Chai, Hua 1-55  
 Chan, Wi Leen 1-213  
 Chang, Teng Wen 2-273  
 Chang, Teng-Wen 1-105  
 Chao, Sara, Ming Chun 1-517

Chatzi, Anna-Maria 1-773  
 Cheah, Lynette 2-303  
 Chen, Chen-cheng 1-13  
 Chen, Chun-Yen 1-105  
 Chen, Jielin 1-793  
 Chen, Kian Wee 1-255, 1-385  
 Chen, Sen 1-843  
 Chen, Xiong 1-589  
 Chen, Zi-Ru 1-671  
 Cheng, Celine 1-85  
 Cheng, Jiahui 1-579  
 Cheng, Ray Chern Xi 1-751  
 Chenlong, Ma 1-425  
 Chia, Pei Zhi 1-213  
 Chien, Sheng-Fen 1-761  
 Cho, Dahngyu 2-719  
 Choi, Jungsik 2-719  
 Choi, Seok-won 1-35  
 Chow, Ka Lok 2-283  
 Chowdhury, Shuva 1-651  
 Chuang, I-Ting 2-61  
 Chun, Hwiwon 2-589  
 Co, Dominic Lim 2-465  
 Crolla, Kristof 2-313, 2-509  
 Czysnska, Klara 1-853

### D

Dai, Sida 2-559  
 Das, Avishek 2-293  
 Davidova, Marie 2-203, 2-333  
 De Sá, Danilo Pico 2-183  
 Dezen-Kempter, Eloisa 2-183  
 Diarte, Julio 1-465  
 Dias, Ulisses 2-183  
 Dill, John 1-557  
 Dillenburger, Benjamin 1-183, 1-445  
 Doe, Robert 1-701  
 Doherty, Ben 2-699  
 Döllner, Jürgen 2-539  
 Du, Hong Wu 1-833  
 DU, Hongwu 1-711  
 Du, Mengzeshan 1-173  
 Dunn, Kate 2-363  
 Dąbrowska-Żóltak,  
 Karolina 2-415

- E**
- Eftekhar, Nik 1-183
- Erhan, Halil 1-265, 1-475,  
1-485, 1-557
- Ezzat, Mohammed 2-111
- F**
- Farr, Marcus 1-721
- Fehrenbach, Joshua 2-435
- Feng, Shiyu 1-173
- Fida, Aysha 1-75
- Fingrut, Adam 2-343
- Firth, Charlotte 2-363
- Fischer, Thomas 1-365, 1-435,  
2-213
- Fisher-Gewirtzman, Dafna 1-661
- Fuji, Takaaki 2-31
- Fukuda, Tomohiro 1-681, 1-783
- Furusho, Genki 2-611
- G**
- Gao, Letong 2-549
- Gao, Xinrui 2-253
- Garcia, Sara 1-599
- Gardner, Nicole 2-489
- Gaudilliere, Nadja 2-499
- Geht, Alexander 1-203
- Ghandi, Mona 2-121
- Glaetzer, Timm 2-375
- Gless, Henri-Jean 1-883
- Goepel, Garvin 2-313, 2-509
- Graham, Jeremy 2-631
- Grobman, Yasha J. 1-507
- Grobman, Yasha Jacob 1-203
- Gu, Zhuoxing 1-285, 1-335
- Guo, Qi 1-537
- Guo, Weihong 1-731
- Guo, Xiangmin 2-263
- Guo, Zhe 1-13
- Gupta, Sachin 1-223
- H**
- Haas, Alyssa 1-475
- Haeusler, M. Hank 2-363, 2-489,  
2-631
- Hagedorn, Benjamin 2-539
- Halin, Gilles 1-883
- Han, Yoojin 2-691
- Hassab, Ahmed 1-163
- He, Peijun 2-81
- Heckmann, Oliver 1-751, 2-303
- Hernandez, Christopher 1-395
- Herr, Christiane M. 2-213, 2-569
- Hershovich, Cheli 1-507
- Herthogs, Pieter 2-81
- Higgs, Baptiste 2-699
- Hirasawa, Gakuhito 2-611
- Hoban, Nicholas 2-455
- Hochscheid, Elodie 1-883
- Holguin, Jose Rafael 2-41
- Holmes, Tyler 2-435
- Holzer, Dominik 2-351
- Homolja, Mitra 1-641
- Hotta, Akito 2-31
- Hotta, Kensuke 1-843, 2-31
- Hou, June Hao 2-519
- Hou, June-Hao 1-609
- van Hout, RENÉ 1-507
- Hsiao, Chi-Fu 1-105
- Hsiao, Yuan Sung (Kris) 1-345
- Hu, Wei 2-651
- Huang, Jeffrey 2-71
- Huang, Weixin 2-549
- Hudert, Markus 2-303
- Hung, Wei-Tse 2-425
- Hyun, Kyung Hoon 1-569, 2-589
- I**
- Ikeda, Hikaru 1-691
- Ikeda, Yasushi 1-691, 1-843
- Indraprastha, Aswin 1-405
- J**
- Janssen, Patrick 1-255, 1-385,  
1-793, 1-803,  
2-323
- Jayashankar,  
Dhileep Kumar 1-223
- Jensen, Mads Brath 2-293
- Ji, Guohua 1-173, 1-255,  
1-385, 1-527
- Johnson, Colby 1-395
- Joyce, Gabriella 2-405
- K**
- Kado, Keita 2-611

- |                         |               |                          |               |
|-------------------------|---------------|--------------------------|---------------|
| Kakooee, Reza           | 1-445         | Lo, Tian Tian            | 1-751, 2-253, |
| Kalo, Ammar             | 2-445         |                          | 2-263         |
| Karakiewicz, Justyna    | 2-41          | Loh, Paul                | 2-351         |
| Kawagishi, Noboru       | 2-31          | Loo, Stella Yi Ning      | 1-223         |
| Kido, Daiki             | 1-681         | Lorenz, Wolfgang E.      | 1-813         |
| Kieffer, Lynn Hyun      | 1-125         | Lork, Clement            | 2-303         |
| Kim, Jinsung            | 2-719         | Lu, Heng                 | 1-173, 1-455  |
| Kim, Jong Bum           | 1-873         | Lu, Ji Rong              | 2-273         |
| Kim, Jun Sik            | 2-529         | Lu, Ming                 | 2-395         |
| Kim, Nayeon             | 1-631         | Lu, Shuai                | 1-497         |
| Kimm, Geoff             | 2-51          | Lu, Yao                  | 1-395         |
| King, Madison           | 2-363         | Lu, Yi-Heng              | 2-425         |
| Kladeftira, Marirena    | 1-445         | Luo, Qi Huan             | 1-145         |
| Kleiss, Michael         | 2-559         | Luo, Yue                 | 2-549         |
| Koerniawan, M. Donny    | 1-405         |                          |               |
| Koh, Immanuel           | 2-641         | <b>M</b>                 |               |
| Kordrostami, Tina       | 1-415         | Ma, Zhichao              | 1-589         |
| Kramer, Krystal         | 2-455         | Macruz, Andrea           | 1-721         |
| Krishnamurti, Ramesh    | 2-671         | Maeng, Hoyoung           | 1-569         |
| Kvan, Thomas            | 2-41          | Maghool,                 |               |
| Kwon, Hyunchul          | 1-183         | Sayyed Amir Hossain      | 1-641         |
|                         |               | Makki, Mohammed          | 1-415         |
| <b>L</b>                |               | Martens, Bob             | 1-325         |
| Lange, Christian        | 2-465         | Martin Iglesias, Rodrigo | 2-233         |
| Larsen, Niels Martin    | 1-125         | Martinho, Helena         | 2-101         |
| Laufer, Michael         | 1-507         | Marzęcki, Waldemar       | 2-579         |
| Lee, Ching-Han          | 1-105         | Matsunaga, Fumiya        | 1-691         |
| Lee, Han Jie            | 1-793, 1-803  | McIennan, Sam            | 2-163         |
| Lee, Hyunsoo            | 1-631, 2-691  | McMeel, Dermott          | 2-333         |
| Lee, Jin-Kook           | 2-719         | Mehta, Palak             | 1-793         |
| Leitão, António         | 1-295, 1-375, | Mei, Hongyuan            | 1-537         |
|                         | 1-599, 2-101  | Melnyk, Virginia         | 1-115         |
| Lertsithichai, Surapong | 1-355         | Meng, Leo Lin            | 2-489, 2-631  |
| Leschok, Matthias       | 1-183         | Mezencio, Davi Lopes     | 2-183         |
| Lesna, Joanna Maria     | 2-385         | Miranda, Erica De Matos  | 2-183         |
| Li, Andrew              | 2-153         | Moleta, Tane             | 1-731, 2-163, |
| Li, Bin                 | 1-731         |                          | 2-173         |
| Li, Yan                 | 1-833         | Mulder, Hugo             | 2-143         |
| LI, Yan                 | 1-711         |                          |               |
| Liang, Manchen          | 2-549         | <b>N</b>                 |               |
| Lin, Che-Wei            | 2-425         | Naboni, Roberto          | 1-233         |
| Lin, Chieh-I            | 1-761         | Nakamura, Yusuke         | 2-611         |
| Lin, Kuan-Ling          | 1-761         | Ng Qi Boon, Amanda       | 2-303         |
| Lin, Zhuoli             | 1-793, 1-803  | Nicholas, Paul           | 2-385         |
| Liu, Chenjun            | 1-23          | Nourian, Pirouz          | 1-305         |
| Liu, Chi                | 1-145         |                          |               |
| Liu, Chuan              | 2-681         | <b>O</b>                 |               |
| Liu, Yige               | 1-55          |                          |               |

Ok, Jeongbin	1-135	Shireen, Naghmi	1-265
Ortner, Frederick Peter	2-71	Shuyan, Zhu	1-425
<b>P</b>		Son, Kihoon	2-589
Pal, Abhipsa	1-213	Sprecher, Aaron	2-223, 2-243
Pang, Yu-Hsuan	2-425	Stefanescu, Dimitrie	1-95
Papadonikolaki, Eleni	1-95	Stojanovic, Djordje	1-547
Paparella, Giulio	1-233	Stojanovic, Vladeta	2-539
Park, Daekwon	1-173, 1-455	Stouffs, Rudi	2-153
Park, Hyoung-June	2-133	Su, Xia	2-549
Patt, Trevor Ryan	2-91	Sumitomo, Eri	1-691
Pei, Wanyu	2-263	Sun, Chengyu	2-651
Pelosi, Antony	1-85, 2-405	Suzuki, Takaharu	1-691
Peng, Chengzhi	1-579	Sweet, Kevin	1-135, 2-529
Pereira Roders, Ana	1-305	<b>T</b>	
Pereira, Inês	1-295, 1-599	Takeuchi, Issei	1-691
Peters, Brady	2-455	Tam, Mark	2-445
pinkie, Pinki	1-315	Tan, Ying Yi	1-213
Poinet, Paul	1-95	Tarazi, Ezri	1-203
Poustinchi, Ebrahim	2-435	Taseva, Yoana	1-183
Pung, Derek	2-323	Teng, Teng	2-475
<b>R</b>		Tessmann, Oliver	2-375
Randall, Madison	1-415	Tian, Jieren	2-11
Raspall, Felix	1-145, 1-153	Toh, Hui Ping	1-153
Ratoi, Lidia	2-465	Tomarchio, Ludovica	2-81
Ren, Yue	1-275, 2-601, 2-621, 2-681, 2-709	Tong, ZiYu	1-823
Rhee, Jinmo	2-671	Tong, Ziyu	1-455, 2-21
Rinsky, Vladislav	1-507	Tracy, Kenneth	1-223, 1-619, 2-445
Rogers, Maria	2-173	Tracy, Kenneth Joseph	1-213
Rubinowicz, Pawel	1-863	Trapp, Matthias	2-539
Rushton, Hannah	2-193	Trossman Haifler, Yaala	1-661
<b>S</b>		Tseng, Li-Min	1-609
Sabin, Jenny	1-395, 2-475	Tsou, Jin Yeu	1-517
Sanatani, Rohit Priyadarshi	1-741	Tu, Chun Man	2-519
Schnabel, Marc Aurel	1-641, 1-651, 1-731, 2-163, 2-173, 2-193	Tuncer, Bige	2-81
Shaked, Tom	2-223, 2-243	<b>V</b>	
Shekhawat, Krishnendra	1-315	Valencia, Antonia	1-193
Shen, Jiaqi	2-681	Vazquez, Elena	1-465
Sheng, Yu-Ting	2-425	Velooso, Pedro	2-671
Sheth, Urvi	1-75	Vivanco, Tomas	1-193
Shin, Eunseo	2-719	Voto, Cristina	2-233
		Vujovic, Milica	1-547
		<b>W</b>	
		Wang, Chenxi	2-549
		Wang, Chunxiao	1-497

Wang, Joann	1-45	Zhang, Hang	2-661
Wang, Likai	1-255, 1-385	Zhang, Ji	1-803
WANG, Qing	1-711	Zhang, Yuchun	2-549
Wang, Shih-Yuan	2-425	Zhang, Zhen	1-833
Wang, Sihan	1-145, 1-153	Zhang, Zhuoqun	1-579
Wang, Weiyi	1-173	Zheng, Hao	1-275, 2-601, 2-621, 2-681, 2-709
Wang, Xiang	1-13		
Wei, Jingxuan	2-601	Zhong, Jia Ding	1-517
Weizmann, Michael	1-203	Zhou, JueLun	1-823
Wesseler, Lisa-Marie	1-773		
Wibranek, Bastian	2-375		
Wietschorke, Leon	2-375		
Wojtowicz, Jerzy	2-415		
Woodbury, Robert	1-265, 1-475, 1-557		
Wortmann, Thomas	1-365, 1-435		
Wrona, Stefan	2-415		
Wu, Yi Sin	2-273		
Wurzer, Gabriel	1-813		
<b>X</b>			
Xia, Xinyu	2-21		
Xia, Yixi	1-783		
Xiao, Kai	1-13		
Xiao, Yahan	1-843		
Xiao, Yiqiang	1-589		
Xie, Anping	1-305		
Xu, Qiaoliang	2-173		
Xu, Weishun	1-145		
Xuereb Conti, Zack	1-751		
<b>Y</b>			
Yabuki, Nobuyoshi	1-681, 1-783		
Yan, Chenyun	1-13		
Yan, Hainan	1-527		
Yan, Huadong	1-455		
Yang, Chunxia	1-285, 1-335		
Yeow, Michael	1-619		
Yogiaman, Christine	1-619		
Yoon, Jungwon	1-35		
Yu, Chuanfei	2-11		
Yuan*, Philip F.	1-55		
Yuan, Philip F.	1-193, 2-395		
<b>Z</b>			
Zarei, Maryam	1-475, 1-557		
Zavoleas, Yannis	2-203		
Zhang, Guo Li	1-145		



# RE: ANTHROPOCENE

Design in the Age of Humans

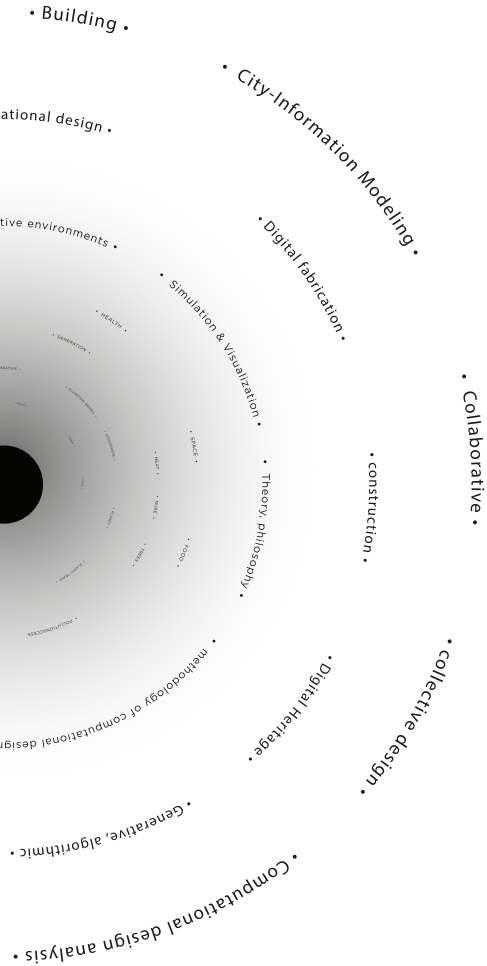
International Program in Design and Architecture (INDA)  
Faculty of Architecture, Chulalongkorn University

What if we are already in the Anthropocene epoch where the function of the Earth system is being impacted by human activities? What if our actions indeed are significant enough to have a critical force on the Earth as a system? The term Anthropocene (the Age of Humans) has gained increasing recognition as a description of a crucial geological stage of our planet as we face the consequences of our own events on the earth's ecosystem. While we are beginning to address the predominant challenges of sustainability and ecology, the environments we built have also shaped our behaviours.

To celebrate CAADRIA's 25th Anniversary, we challenge ourselves with these questions, asking what we want our future to look like, in the next 25, 50, or even 100 years? If human creations are substantial enough to start a new geological epoch, what does this imply for our explorations of the realm of computational design, and how will advanced technologies shape our futures? With the theme RE: Anthropocene, we challenge ourselves to REgard this new geological age as the main meaningful site for exploration into the future, REthink what our planet could become, REvisit our actions and behaviours to foster the REsponsibilities for the planet existence, and perhaps & importantly, REspond to whatever magnitudes happen to the built-environments and other planetary beings.

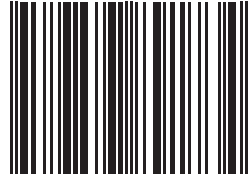


CHULALONGKORN  
UNIVERSITY



© 2020 All rights reserved and published by the Association for  
Computer-Aided Architectural Design Research in Asia (CAADRIA)  
Hong Kong, China

ISBN 978-988-78917-3-4



9 789887 891734 >